Inorganic Reactions and Methods

Volume 18

Inorganic Reactions and Methods

Inorganic Reactions and Methods

Volume 18

Formation of Ceramics

Founding Editor

J. J. Zuckerman

Editor

Jim D. Atwood

WILEY-VCH

New York · Chichester · Weinheim · Brisbane · Singapore · Toronto

Library of Congress Catalog Card Number: 85-15627
ISBN 0-471-19202-3

Contents of Volume 18

How to Use this Book

1. Organization of Subject Matter

1.1. Logic of Subdivision and Add-On Chapters

This volume is part of a series that describes all of inorganic reaction chemistry. The contents are subdivided systematically and so are the contents of the entire series. Using the periodic system as a correlative device, it is shown how bonds between pairs of elements can be made. Treatment begins with hydrogen making a bond to itself in H_2 and proceeds according to the periodic table with the bonds formed by hydrogen to the halogens, the groups headed by oxygen, nitrogen, carbon, boron, beryllium and lithium, to the transition and inner-transition metals and to the members of group zero. Next it is considered how the halogens form bonds among themselves and then to the elements of the main groups VI to I, the transition and inner-transition metals and the zero-group gases. The process repeats itself with descriptions of the members of each successive periodic group making bonds to all the remaining elements not yet treated until group zero is reached. At this point all actual as well as possible combinations have been covered.

The focus is on the primary formation of bonds, not on subsequent reactions of the products to form other bonds. These latter reactions are covered at the places where the formation of those bonds is described. Reactions in which atoms merely change their oxidation states are not included, nor are reactions in which the same pairs of elements come together again in the product (for example, in metatheses or redistributions). Physical and spectroscopic properties or structural details of the products are not covered by the reaction volumes; the latter are concerned with synthetic utility based on yield, economy of ingredients, purity of product, specificity, etc. The preparation of short-lived transient species is not described.

While in principle the systematization described above could suffice to deal with all the relevant material, there are other topics that inorganic chemists customarily identify as being useful in organizing reaction information and that do not fit into the scheme. These topics are the subject of eight additional chapters constituting the last four volumes of the series. These chapters are systematic only within their own confines. Their inclusion is based on the best judgment of the Editorial Advisory Board as to what would be most useful currently as well as effective in guiding the future of inorganic reaction chemistry.

1.2. Use of Decimal Section Numbers

The organization of the material is readily apparent through the use of numbers of headings. Chapters are broken down into divisions, sections, and subsections, which have short descriptive headings and are numbered according to the following scheme:

1. Major Heading
1.1. Chapter Heading
1.1.1. Division Heading
1.1.1.1. Section Heading
1.1.1.1.1. Subsection Heading

Further subdivision of a five-digit "slice" utilizes lower-case Roman numerals in parentheses: (i), (ii), (iii), etc. It is often found that as a consequence of the organization, cognate material is located in different chapters but in similarly numbered pieces, i.e., in parallel sections. Section numbers, rather than page numbers, are the key by which the material is accessed through the various indexes.

1.3. Building of Headings

1.3.1. Headings Forming Part of a Sentence

Most headings are sentence-fragment phrases which constitute sentences when combined. Usually a period signifies the end of a combined sentence. In order to reconstitute the context in which a heading is to be read superior-rank titles are printed as running heads on each age. When the sentences are put together from their constituent parts, they describe the contents of the piece at hand. For an example, see 2.3 below.

1.3.2. Headings Forming Part of an Enumeration

For some material it is not useful to construct title sentences as described above. In these cases hierarchical lists, in which the topics are enumerated, are more appropriate. To inform the reader fully about the nature of the material being described, the headings of connected sections that are superior in hierarchy always occur as running heads at the top of each page.

2. Access and Reference Tools

2.1. Plan of the Entire Series (Front Endpaper)

Printed on the inside of the front cover is a list, compiled from all 18 reaction volumes, of the major and chapter headings, that is, all headings that

are preceded by a one- or two-digit decimal section number. This list shows in which volumes the headings occur and highlights the contents of the volume that is at hand by means of a gray tint.

2.2. Contents of the Volume at Hand

All the headings, down to the title of the smallest decimal-numbered subsection, are listed in the detailed table of contents of each volume. For each heading the table of contents shows the decimal section number by which it is preceded and the number of the page on which it is found. Beside the decimal section numbers, successive indentations reveal the hierarchy of the sections and thereby facilitate the comprehension of the phrase (or of the enumerative sequence) to which the headings of hierarchically successive sections combine. To reconstitute the context in which the heading of a section must be read to become meaningful, relevant headings of sections superior in hierarchy are repeated at the top of every page of the table of contents. The repetitive occurrences of these headings is indicated by the fact that position and page numbers are omitted.

2.3. Running Heads

In order to indicate the hierarchical position of a section, the top of every page of text shows the headings of up to three connected sections that are superior in hierarchy. These running heads provide the context within which the title of the section under discussion becomes meaningful. As an example, the page of Volume 1 on which section 1.4.9.1.3 "in the Production of Methanol" starts, carries the running heads:

1.4. The Formation of Bonds between Hydrogen and O, S, Se, Te, Po
1.4.9. by Industrial Processes
1.4.9.1. Involving Oxygen Compounds

whereby the phrase "in the Production of Methanol" is put into its proper perspective.

2.4. List of Abbreviations

Preceding the indexes there is a list of those abbreviations that are frequently used in the text of the volume at hand or in companion volumes. This list varies somewhat in length from volume to volume; that is, it becomes more comprehensive as new volumes are published.

Abbreviations that are used incidentally or have no general applicability are not included in the list but are explained at the place of occurrence in the text.

2.5. Author Index

The author index is compiled by computer from the lists of references. Thus it tells whose publications are cited and in that respect is comprehensive. It is not a list of authors, beyond those cited in the references, whose results are reported in the text. However, as the references cited are leading ones, consulting them, along with the use of appropriate works of the secondary literature, will rapidly lead to the complete literature related to any particular subject covered.

Each entry in the author index refers the user to the appropriate section number.

2.6. Compound Index

The compound index lists individual, fully specified compositions of matter that are mentioned in the text. It is an index of empirical formulas, ordered according to the following system: the elements within a given formula occur in alphabetical sequence except for C, or C and H if present, which always come first. Thus, the empirical formula

for	$Ti(SO_4)_2$	is O_8S_2Ti
	$BH_3 \cdot NH_3$	BH_6N
	Be_2CO_3	CBe_2O_3
	$CsHBr_2$	Br_2CsH
	$Al(HCO_3)_3$	$C_3H_3AlO_9$

The formulas themselves are ordered alphanumerically without exception; that is, the formulas listed above follow each other in the sequence BH_6N, Br_2CsH, CBe_2O_3, $C_3H_3AlO_9$, O_8S_2Ti.

A compound index constructed by these principles tells whether a given compound is present. It cannot provide information about compound classes, for example, all aluminum derivatives or all compounds containing phosphorus.

In order to open this route of access, as well, the compound index is augmented by successively permuted versions of all empirical formulas. Thus the number of appearances that an empirical formula makes in the compound index is equal to the number of elements it contains. As an example, $C_3H_3AlO_9$, mentioned above, will appear as such and, at the appropriate positions in the alphanumeric sequence, as $H_3AlO_9^*C_3$, $AlO_9^*C_3H_3$ and $O_9^*C_3H_3Al$. The asterisk identifies a permuted formula and allows the original formula to be reconstructed by shifting to the front the elements that follow the asterisk.

Each nonpermuted formula is followed by linearized structural formulas that indicate how the elements are combined in groups. They reveal the connectivity of the compounds underlying each empirical formula and serve to distinguish substances which are identical in composition but differ in the arrangement of elements (isomers). As an example, the empirical formula $C_4H_{10}O$

might be followed by the linearized structural formulas $(CH_3CH_2)_2O$, $CH_3(CH_2)_2OCH_3$, $(CH_3)_2CHOCH_3$, $CH_3(CH_2)_3OH$, $(CH_3)_2CHCH_2OH$ and $CH_3CH_2(CH_3)CHOH$ to identify the various ethers and alcohols that have the elemental composition $C_4H_{10}O$.

Each linearized structural formula is followed in a third column by keywords describing the context in which it is discussed and by the number(s) of the section(s) in which it occurs.

2.7. Subject Index

The subject index provides access to the text by way of methods, techniques, reaction types, apparatus, effects and other phenomena. Also, it lists compound classes such as organotin compounds or rare-earth hydrides which cannot be expressed by the empirical formulas of the compound index.

For multiple entries, additional keywords indicate contexts and thereby avoid the retrieval of information that is irrelevant to the user's need.

Again, section numbers are used to direct the reader to those positions in the book where substantial information is to be found.

2.8. Periodic Table (Back Endpaper)

Reference to periodic groups avoids cumbersome enumerations. Section headings in the series employ the nomenclature.

Unfortunately, however, there is at the present time no general agreement on group designations. In fact, the scheme that is most widely used (combining a group number with the letters A and B) is accompanied by two mutually contradictory interpretations. Thus, titanium may be a group IVA or group IVB element depending on the school to which one adheres or the part of the world in which one resides.

In order to clarify the situation for the purposes of the series, a suitable labeled periodic table is printed on the inside back cover of each volume. All references to periodic group designations in the series refer to this scheme.

Preface to the Series

Inorganic Reactions and Methods constitutes a closed-end series of books designed to present the state of the art of synthetic inorganic chemistry in an unprecedented manner. So far, access to knowledge in inorganic chemistry has been provided almost exclusively using the elements or classes of compounds as starting points. In the first 18 volumes of **Inorganic Reactions and Methods**, it is bond formation and type of reaction that form the basis of classification.

This new route of access has required new approaches. Rather than sewing together a collection of review articles, a framework has had to be designed that reflects the creative potential of the science and is hoped to stimulate its further development by identifying areas of research that are most likely to be fruitful.

The reaction volumes describe methods by which bonds between the elements can be formed. The work opens with hydrogen making a bond to itself in H_2 and proceeds through the formation of bonds between hydrogen and the halogens, the groups headed by oxygen, nitrogen, carbon, boron, beryllium and lithium to the formation of bonds between hydrogen and the transition and inner-transition metals and elements of group zero. This pattern is repeated across the periodic system until all possible combinations of the elements have been treated. This plan allows most reaction topics to be included in the sequence where appropriate. Reaction types that do not arise from the systematics of the plan are brought together in the concluding chapters on oxidative addition and reductive elimination, insertions and their reverse, electron transfer and electrochemistry, photochemical and other energized reactions, oligomerization and polymerization, inorganic and bioinorganic catalysis and the formation of intercalation compounds and ceramics.

The project has engaged a large number of the most able inorganic chemists as Editorial Advisors creating overall policy, as Editorial Consultants designing detailed plans for the subsections of the work, and as authors whose expertise has been crucial for the quality of the treatment. The conception of the series and the details of its technical realization were the subject of careful planning for several years. The distinguished chemists who form the Editorial Advisory Board have devoted themselves to this exercise, reflecting the great importance of the project.

It was a consequence of the systematics of the overall plan that publication of a volume had to await delivery of its very last contribution. Thus was the defect side of the genius of the system revealed as the excruciating process of extracting the rate-limiting manuscripts began. Intense editorial effort was required in order to bring forth the work in a timely way. The production process had to be designed so that the insertion of new material was possible up to the very last stage, enabling authors to update their pieces with the latest

developments. The publisher supported the cost of a computerized bibliographic search of the literature and a second one for updating.

Each contribution has been subjected to an intensive process of scientific and linguistic editing in order to homogenize the numerous individual pieces, as well as to provide the highest practicable density of information. This had several important consequences. First, virtually all semblances of the authors' individual styles have been excised. Second, it was learned during the editorial process that greater economy of language could be achieved by dropping conventionally employed modifiers (such as very) and eliminating italics used for emphasis, quotation marks around nonquoted words, or parentheses around phrases, the result being a gain in clarity and readability. Because the series focuses on the chemistry rather than the chemical literature, the need to tell who has reported what, how and when can be considered of secondary importance. This has made it possible to bring all sentences describing experiments into the present tense. Information on who published what is still to be found in the reference lists. A further consequence is that authors have been burdened neither with identifying leading practitioners, nor with attributing priority for discovery, a job that taxes even the talents of professional historians of science. The authors' task then devolved to one of describing inorganic chemical reactions, with emphasis on synthetic utility, yield, economy, availability of starting materials, purity of product, specificity, side reactions, etc.

The elimination of the names of people from the text is by far the most controversial feature. Chemistry is plagued by the use of nondescriptive names in place of more expository terms. We have everything from Abegg's rule, Adkin's catalyst, Admiralty brass, Alfven number, the Amadori rearrangement and Adurssov oxidation to the Zdanovskii law, Zeeman effect, Zincke cleavage and Zinin reduction. Even well-practiced chemists cannot define these terms percisely except for their own areas of specialty, and no single source exists to serve as a guide. Despite these arguments, the attempt to replace names of people by more descriptive phrases was met in many cases by a warmly negative reaction by our colleague authors, notwithstanding the obvious improvements wrought in terms of lucidity, freedom from obscurity and obfuscation and, especially, ease of access to information by the outsider or student.

Further steps toward universality are taken by the replacement of element and compound names wherever possible by symbols and formulas, and by adding to data in older units their recalculated SI equivalents. The usefulness of the reference sections has been increased by giving journal-title abbreviations according to the *Chemical Abstracts Service Source Index*, by listing in each reference all of its authors and by accompanying references to patents and journals that may be difficult to access by their *Chemical Abstracts* citations. Mathematical signs and common abbreviations are employed to help condense prose and a glossary of the latter is provided in each volume. Dangerous or potentially dangerous procedures are high-lighted in safety notes printed in boldface type.

The organization of the material should become readily apparent from an examination of the headings listed in the table of contents. Combining the words constituting the headings, starting with the major heading (one digit) and continuing through the major chapter heading (two digits), division heading (three digits), section heading (four digits) to the subsection heading (five digits), reveals at once the subject of a "slice" of the plan. Each slice is a self-contained unit. It includes its own list of references and provides definitions of unusual terms that may be used in it. The reader, therefore, through the table of contents alone, can in most instances quickly reach the desired material and derive the information wanted.

In addition there is for each volume an author index (derived from the lists of references) and a subject index that lists compound classes, methods, techniques, apparatus, effects and other phenomena. An index of empirical formulas is also provided. Here in each formula the element symbols are arranged in alphabetical order except that C, or C and H if present, always come first. Moreover, each empirical formula is permuted successively. Each permuted formula is placed in its alphabetical position and cross referenced to the original formula. Therefore, the number of appearances that an empirical formula makes in the index equals the number of its elements. By this procedure all compounds containing a given element come together in one place in the index. Each original empirical formula is followed by a linearized structural formula and keywords describing the context in which the compound is discussed. All indexes refer the user to subsection rather than page number.

Because the choice of designations of groups in the periodic table is currently in a state of flux, it was decided to conform to the practice of several leading inorganic texts. To avoid confusion an appropriately labeled periodic table is printed on the back endpaper.

An enormous debt of gratitude toward all our authors is to be recorded. These experts were asked to prepare brief summaries of their knowledge, ordered in logical sequence by our plan. In addition, they often involved themselves in improving the original conception by recommending further refinements and elaborations. The plan of the work as it is being published can truly be said to be the product of the labors of the advisors and consultants on the editorial side as well as the many, many authors who were able to augment more general knowledge with their own detailed information and ideas. Because of the unusually strict requirements of the series, authors had not only to compose their pieces to fit within narrowly constrained limits of space, format and scope, but after delivery to a short deadline were expected to stand by while an intrusive editorial process homogenized their own prose styles out of existence and shrank the length of their expositions. These long-suffering colleagues had then to endure the wait for the very last manuscript scheduled for their volume to be delivered so that their work could be published, often after a further diligent search of the literature to insure that the latest discoveries were being cited and that claims for facts now proved false were eliminated. To these

co-workers (270 for the reaction volumes alone), from whom so much was demanded but who continued to place their knowledge and talents unstintingly at the disposal of the project, we dedicate this series.

J. J. ZUCKERMAN
Norman, Oklahoma
July 4, 1985

Volume 18 is the final volume of *Inorganic Reactions and Methods*, completing the series. We have retained the format, style and nomenclature for consistency. Thus, the current group numbering (1–18) has not been used, but the older I–VIII with A and B was retained. The periodic table used is provided on the back inside cover to avoid confusion. Volume 18 provides one of the applications of inorganic reactions, the formation of ceramic materials. The formation of ceramics is an old area that has important new applications highlighted in this volume. The authors of this volume have shown exemplary patience and cooperation – thank you! A special thank you to Mary Atwood for her efforts in bringing this volume to completion.

JIM D. ATWOOD
Buffalo, New York
November 19, 1998

Editorial Consultants to the Series

Professor H. R. Allcock
Pennsylvania State University

Professor J. S. Anderson
University of Aberystwyth

Professor F. C. Anson
California Institute of Technology

Dr. M. G. Barker
University of Nottingham

Professor D. J. Cardin
Trinity College

Professor M. H. Chisholm
Indiana University

Professor C. Cros
Laboratoire de Chemie du Solide du C.N.R.S.

Dr. B. Darriet
Laboratoire de Chemie du Solide du C.N.R.S.

Professor E. A. V. Ebsworth
University of Edinburgh

Professor J. J. Eisch
State University of New York at Binghamton

Professor J. R. Etourneau
Laboratoire de Chemie du Solide du C.N.R.S.

Professor G. L. Geoffroy
Pennsylvania State University

Professor L. S. Hegedus
Colorado State University

Professor W. L. Jolly
University of California at Berkeley

Professor C. B. Meyer
University of Washington

Professor H. Nöth
Universität München

Professor H. Nowotny
University of Connecticut

Dr. G. W. Parshall
E.I. du Pont de Nemours

Professor M. Pouchard
Laboratoire de Chemie du Solide du C.N.R.S.

Professor J. Rouxel
Laboratoire de Chemie Minérale au C.N.R.S.

Professor R. Schmutzler
Technische Universität Barunschweig

Professor A. W. Searcy
University of California at Berkeley

Professor D. Seyferth
Massachusetts Institute of Technology

Dr. N. Sutin
Brookhaven National Laboratory

Professor R. A. Walton
Purdue University

Dr. J. H. Wernick
Bell Laboratories

Contributors to Volume 18

Professor C. L. Aardahl
University of Washington
Department of Chemical Engineering
Seattle, WA 98195-1750
(*Sections* 17.2.5–17.2.5.5.9)

Professor David A. Atwood
Department of Chemistry
Chemistry/Physics Building 125
University of Kentucky
Lexington, KY 40506
(*Sections* 17.3.8.2–17.3.8.4)

Dr. Robert J. Eagan
Dept. 0100
Sandia National Laboratories
P.O. Box 5800
Mail Stop 0513
Albuquerque, NM 87185-0513
(*Sections* 17.3.3–17.3.3.6)

Dr. Dennis F. Elwell
Magnum Defense Incorporated
5 Autry
Irvine, CA 92618
(*Sections* 17.2.4–17.2.4.4)

Professor Richard B. Fair
Department of Electrical and Computer Engineering
Duke University
Durham, NC 27708
(*Sections* 17.2.6–17.2.6.5)

Dr. Brian Fitzpatrick
Optical Semiconductors, Inc.
8 John Walsh Boulevard
Suite 421
Peekskill, NY 10566
(*Sections* 17.3.8.5–17.3.8.6.15)

Professor Ronald S. Gordon, Head
Department of Materials Science and Engineering
College of Engineering
Virginia Polytechnic Institute and State University
213 Holden Hall
Blacksburg, VA 24061-0237
(*Sections* 17.3.7–17.3.7.5)

Professor Eugene E. Haller
Lawrence Berkeley Laboratory
University of California
Bldg. 2, Rm. 205
Berkeley, CA 94720
(*Sections* 17.3.8–17.3.8.1)

Professor H. R. Harrison*
(*Sections* 17.3.9–17.3.9.3.3)

Professor Jurgen Michael Honig
Purdue University
Department of Chemistry
1393 Herbert C. Brown Laboratory of Chemistry
West Lafayette, IN 47907-1393
(*Sections* 17.3.9–17.3.9.3.3)

* Deceased.

Dr. Orville Hunter, Jr.
816 Bucks Run
Columbia, MO 65201
(*Sections* 17.3.6–17.3.6.3.3)

Dr. David W. Johnson, Jr.
Lucent Technologies
Bell Labs Innovations
Room 1F-206
700 Mountain Avenue
P.O. Box 636
Murray Hill, NJ 07974-0636
(*Sections* 17.2.2–17.2.2.5)

Professor Angus Kingon
North Carolina State University
Department of Materials Science and Engineering
Raleigh, NC 27695-7919
(*Sections* 17.3.11.1–17.3.11.4)

Dr. Ronald E. Loehman, Manager
Advanced Materials Laboratory
Sandia National Laboratories
P.O. Box 5800
Albuquerque, NM 87185-1349
(*Sections* 17.3.3–17.3.3.6)

Dr. Robert E. Newnham, Associate Director
Alcoa Professor of Solid State Science
The Pennsylvania State University
251-A Materials Research Lab.
University Park, PA 16802-4801
(*Sections* 17.3.11.1–17.3.11.4)

Professor Jacque I. Pankove
Solid State Physics
Materials Science Engineering
Campus Box 425
University of Colorado
Boulder, CO 80309-0425
(*Section* 17.3.8.7)

Professor Mohamed N. Rahaman
University of Missouri-Rolla
Department of Ceramic Engineering
1870 Miner Circle
Rolla, MO 65401
(*Sections* 17.2.3.1–17.2.3.5.4)

Dr. Zhifeng Ren
State University of New York
University at Buffalo
Department of Chemistry
Natural Sciences Complex
Buffalo, NY 14260-3000
(*Sections* 17.3.10–17.3.10.2.6)

Professor J. W. Rogers, Jr.
Department of Chemical Engineering
University of Washington
Box 351750
Seattle, WA 98195-1750
(*Sections* 17.2.5–17.2.5.5.9)

Professor Massoud T. Simnad
Center for Energy and Combustion Research
University of California-San Diego
La Jolla, CA 92093
(*Sections* 17.3.12.1–17.3.12.5)

Dr. David A. Thompson, Director
Strategic Planning
Corning Incorporated
Corning, NY 14831
(*Sections* 17.3.2–17.3.2.7.3)

Professor Peter Albert Thrower
Reedcroft
Staithe Road
LUDHAM
Gt. Yarmouth, Norfolk
NR29 5 AB
UK
(*Sections* 17.3.4–17.3.4.7)

Professor Jui Wang
State University of New York
University at Buffalo
Department of Chemistry
Natural Sciences Complex
Buffalo, NY 14260-3000
(*Sections* 17.3.10–17.3.10.2.6)

Dr. Ernest G. Wolff
Department of Mechanical
Engineering
Oregon State University
Corvallis, OR 97331
(*Sections* 17.3.5–17.3.5.6)

Inorganic Reactions and Methods

Volume 18

Inorganic Reactions and Methods, Volume 18
Edited by J. J. Zuckerman, Jim D. Atwood

17. The Formation of Ceramics

17.1. Introduction

Ceramics is a forgotten area of inorganic chemistry. A quick scan of textbooks on inorganic chemistry found ceramics listed in the index of only one. Despite the lack of coverage, ceramics manufacture remains a major industrial application of inorganic chemistry with products ranging from bricks to superconductors. The dictionary definition of ceramic "Engineering materials and products made from inorganic chemicals by high temperature processing. They are resistant to chemical attack, can range from semiconductors (now superconductors) to insulators and include refractories, glasses, cement and cement products, vitreous enamels, abrasives, pottery, china, porcelain, clay wares, alumina, etc." show the breadth of products and the placement in inorganic chemistry. The terms used in formation of ceramics (grog, cladding, flux reaction, etc.) are also not common in the inorganic literature. Techniques for forming ceramics frequently are more of an art than science. The following material on formation of ceramics highlights the art and science involved and provides an excellent source for the inorganic chemist to gain an appreciation of ceramic formation.

(JIM D. ATWOOD)

17.2. Ceramic Preparative Methods

17.2.1. Introduction

Preparation of ceramics involves high temperature rearrangement of bonds from a starting mixture. Frequently the mixture is solids where particle size, mixing, etc., become very important to the nature of the ceramic. In other cases a vapor of correct stoichiometry is decomposed to give the ceramic. In either approach, the removal of impurities is important to the ceramic properties. The following sections describe the important parameters for preparation of ceramic materials.

(JIM D. ATWOOD)

17.2.2. Preparation of Powders for Ceramic Processing

Ceramic powder characteristics are important because the purity of the powder sets the maximum purity level of the final processed ceramic part, and the particle size and size distribution play major roles in defining the microstructure and properties of the final parts. Both the purity and the microstructure of sintered ceramics influence the properties of ceramic materials, including mechanical, thermal, electrical, and magnetic properties and chemical corrosion resistance.

This section addresses the need for ceramic powder preparation and gives an overview of the methods. Several reviews categorize ceramic powder preparation techniques[1-4].

(D. W. JOHNSON, JR.)

1. D. W. Johnson, Jr., *Advances in Ceramics, 21*, American Ceramic Society, Westerville, OH, 1987, p. 3.
2. D. W. Johnson, Jr., in *Advances in Powder Technology*, G. Y. Chin, ed., ASM International, Metals Park, OH, 1981, p. 23.
3. D. E. Niesz, *Proceedings of the 45th Porcelain Enamel Institute Technical Forum*, American Ceramic Society, Westerville, OH 1987, p. 159.
4. K. Akio, *J. Surf, Sci. Soc. Jpn., 8*, 316 (1987).

17.2.2.1. Purity, Particle Size Uniformity, and Small Particle Size

For many traditional ceramics such as structural elements (tiles, bricks, etc.), whitewares, (tableware, sanitaryware, etc.), and common refractories, the raw materials are naturally occurring minerals, and moderate levels of impurities are tolerated. More specialized technical ceramics such as electronic ceramics (substrates, electronic packages, capacitors, inductors, etc.) or high performance structural ceramics (silicon carbide, silicon nitride, etc.) demand low or controlled levels of impurities and make use of higher purity powders often made by more specialized techniques.

Inorganic Reactions and Methods, Volume 18
Edited by J. J. Zuckerman, Jim D. Atwood

17.2. Ceramic Preparative Methods

17.2.1. Introduction

Preparation of ceramics involves high temperature rearrangement of bonds from a starting mixture. Frequently the mixture is solids where particle size, mixing, etc., become very important to the nature of the ceramic. In other cases a vapor of correct stoichiometry is decomposed to give the ceramic. In either approach, the removal of impurities is important to the ceramic properties. The following sections describe the important parameters for preparation of ceramic materials.

(JIM D. ATWOOD)

17.2.2. Preparation of Powders for Ceramic Processing

Ceramic powder characteristics are important because the purity of the powder sets the maximum purity level of the final processed ceramic part, and the particle size and size distribution play major roles in defining the microstructure and properties of the final parts. Both the purity and the microstructure of sintered ceramics influence the properties of ceramic materials, including mechanical, thermal, electrical, and magnetic properties and chemical corrosion resistance.

This section addresses the need for ceramic powder preparation and gives an overview of the methods. Several reviews categorize ceramic powder preparation techniques[1–4].

(D. W. JOHNSON, JR.)

1. D. W. Johnson, Jr., *Advances in Ceramics, 21*, American Ceramic Society, Westerville, OH, 1987, p. 3.
2. D. W. Johnson, Jr., in *Advances in Powder Technology*, G. Y. Chin, ed., ASM International, Metals Park, OH, 1981, p. 23.
3. D. E. Niesz, *Proceedings of the 45th Porcelain Enamel Institute Technical Forum*, American Ceramic Society, Westerville, OH 1987, p. 159.
4. K. Akio, *J. Surf, Sci. Soc. Jpn., 8*, 316 (1987).

17.2.2.1. Purity, Particle Size Uniformity, and Small Particle Size

For many traditional ceramics such as structural elements (tiles, bricks, etc.), whitewares, (tableware, sanitaryware, etc.), and common refractories, the raw materials are naturally occurring minerals, and moderate levels of impurities are tolerated. More specialized technical ceramics such as electronic ceramics (substrates, electronic packages, capacitors, inductors, etc.) or high performance structural ceramics (silicon carbide, silicon nitride, etc.) demand low or controlled levels of impurities and make use of higher purity powders often made by more specialized techniques.

The particle size and size distribution characteristics of a ceramic powder are dictated by the application. For traditional ceramics, the source of the fine particles (ca. 1 μm) that impart the rheological characteristics needed in forming, and the reactivity necessary for sintering, are often obtained from naturally occurring small particle minerals, usually clays. With most ceramic processing, a preponderance of small particles leads to poor packing and thus relatively large shrinkages during drying and sintering. Therefore, it is desirable to incorporate a distribution of particle sizes. Close-packed monosized spheres have a packing density of 74%, even though this level of packing would be difficult to achieve in particulate systems. If smaller particles are then placed into the interstices between the monosized spheres, the packing density is increased. An extreme example can be found in the brick and refractory industry, where grog, a sintered and crudely crushed product, is mixed with the starting powders to reduce shrinkages during processing.

In higher grade ceramics, grog is not used, since it would adversely affect the microstructure of the sintered parts. The starting powders do, however, have a distribution of particle sizes, and the processing shrinkages are controlled through methods such as dry pressing or the addition of organics, which facilitate high packing densities.

In principle, the high surface area afforded by very fine particles is desirable for sintering because a minimization of surface free energy is the driving force for densification. In practice the processing of very fine particles ($\ll 1$ μm) leads to problems with handling and forming. Only with careful forming will the particle packing density be high enough or uniform enough to yield a sintered part having a dense, uniform microstructure. The packing difficulty exists because with very fine particles, surface forces predominate and lead to agglomerates that pack nonuniformly. This can be overcome only by careful dispersion of the particles in a fluid system.

Fine particle powders are useful for several reasons:

1. For systems in which a low sintering temperature is needed, the reactivity of fine powders can be of use (see above).
2. Some ceramic applications (e.g., smooth surface substrates, high strength ceramics) require fine grains, which cannot be achieved unless the starting particles are smaller than the desired final grain size in the sintered parts.
3. Fine particles are desirable for ceramic pigments, where particle sizes on the order of the wavelength of light are most effective in scattering light.

(D. W. JOHNSON, JR.)

17.2.2.2. Comminution Techniques

In comminution, the oldest and most widely used technique for ceramic powder preparation, large pieces or particles are reduced in size by crushing or grinding. Preparing powders by comminution is frequently referred to as the conventional process. In conventional powder preparation, starting powders are mixed and calcined to move toward chemical homogeneity and phase formation. The calcined material is then ground to break the large particles and aggregates formed during calcining as well as to promote further chemical homogeneities.

The first stages of comminution for large pieces of raw material involve machines such as jaw crushers, roll crushers, and hammer mills. These heavy devices reduce the

particle size to the millimeter or submillimeter range, where further grinding operations can be initiated.

The most common grinding devices for submillimeter particles are ball mills[1,2]. These are closed cylindrical containers ranging in volume from less than a liter to several cubic meters, and partly filled with milling media (usually spheres or short cylindrical pellets ranging in size from a few millimeters to 10 cm, depending on the mill size and the nature of the material to be ground). The material to be ground is placed in the jar with the milling media, and the ball-to-ball or ball-to-container impacts during mill rotation cause fragmentation of the particles.

Ball mills can be used either wet or dry. In wet milling, which is often preferred, the powder to be milled is added to water, alcohol, or another liquid to make a slurry. Dispersing agents such as tetrasodium pyrophosphate are often added in small quantities to minimize the volume of liquid needed and to prevent agglomeration of particles. For dry milling, grinding aids such as stearates are also used to minimize packing of particles in the corners of jars and to reduce the fracture energy of the material to be ground.

The mill size is dictated by the size of the charge to be milled, with 20–25% of the mill volume available for the charge. The size of the milling media (balls) depends on the size and hardness of the charge as well as the density of the milling media. Large balls provide high impact energies, whereas small balls provide large numbers of lower energy impacts. The smallest media consistent with the size of particles to be ground should be used.

The choice of mill jar material and milling media depends on cost and impurity considerations. Ball milling inevitably leads to wear of the mill and media, which is a potential source of contamination. In some cases this is minimized by using a noncontaminating materials (e.g., Al_2O_3, for grinding Al_2O_3 or aluminates, steel for grinding Fe_2O_3 or ferrites). Many mills are lined with polymers to minimize contamination from the jar. The use of polypropylene or polyethylene jars for laboratory-sized batches is common. Liners for large mills are made of steel, porcelain, natural flint rock, or alumina. Milling media include flint pebbles, porcelain, alumina, zirconia, steel, or tungsten carbide balls (listed in order of ascending density).

Mill rotation speeds are set such that the balls are lifted nearly to the top of the jar before tumbling to the bottom. As a rule, about 50–75% of the critical speed or the speed at which the media are held to the walls by centrifugal force is appropriate. The critical speed (in rpm) can be calculated as $273/\sqrt{r}$, where r = jar radius (cm).

The time of milling depends on the degree of fineness desired; overlong milling, however, leads to excessive contamination due to wear. Comminution theory[3] relates particle size and distributions to the work imparted from the mill. The theories require certain constants to be determined. In practice, size and size distribution after milling are obtained by a powder characterization technique.

Ball mills are useful in grinding particles to the 1–10 μm range, with low milling rates for the smaller sizes. More rapid grinding can be achieved by means of mills in which the jar containing the media is vibrated to cause large numbers of ball-to-ball collisions. Attrition mills, where the slurry of particles to be milled is mixed with coarser grinding media in a container into which a rotating paddle of various designs is place, allow even more rapid grinding of fine particles[4,5]. This technique is used in the paint industry for grinding and dispersion of pigments. The reaction of Ti with N_2 during milling to form TiN is typical of chemical reactions that can occur during ball milling[6].

A comminution technique that minimizes contamination is the fluid energy mill or jet mill[3]. The particles are entrained in high velocity streams of fluid (generally gases such

as air or steam). Two or more streams of fluid intersect, and the particles are fractured upon impact with each other. One potential problem involves segregation by density of particles in a multicomponent system during the air classification step.

(D. W. JOHNSON, JR.)

1. *Handbook of Ball Mill and Pebble Mill Operation*, Paul O. Abbe, Little Falls, NJ, 19.
2. Y. N. Kryuchkov, *Steklo Keram., 8*, 14 (1995).
3. C. Greskovich, in *Ceramic Fabrication Processes*, F. F. Y. Wang, ed., Academic Press, New York, 1976, p. 15.
4. L. Y. Sadler, D. A. Stanley, D. R. Brooks, *Powder Technol., 12*, 19 (1975).
5. J. L. Hoyer, *Am. Ceram. Soc. Bull., 67*, 1663 (1988).
6. J. Secondi, R. Yavari, *J. Phys. IV, 3*, 1287 (1993).

17.2.2.3. Solution Preparation

Solution preparation of ceramic powders is often thought to be a speciality technique for small lots of high purity ceramic materials. High quality powders can be (obtained, and solution technique are chosen to produce many of the powders used in the ceramic industry in large quantities. A major example is Al_2O_3, most of which is produced when the mineral bauxite is dissolved in an alkaline solution and hydrated oxides are precipitated from the solution[1].

Solution techniques offer the advantage of high chemical purity, controlled fine particle sizes, and a high degree of chemical homogeneity on an atomic or molecular level (due to the dissolving of the metal species in a liquid). A goal of the various techniques is to preserve as much of this homogeneity as possible. Some of these techniques are reviewed elsewhere[2,3].

The first step is preparation of the solution. Aqueous solutions are prepared by dissolving either soluble salts in solvents (usually water) or metals in acids. For multicomponent systems, the mutual solubility of the various components must be considered. For example, a solution for lead zirconate cannot be prepared from lead nitrate and zirconium sulfate, both of which are soluble in water, because lead sulfate, which is insoluble, will precipitate. A solution of nitrates of both cations is satisfactory.

The next step is that of solvent removal, which categorizes solution preparation techniques[4,5]. The most important processes are discussed in the subsections that follow. The final step is thermal decomposition of the salts (discussed in 17.2.2.5).

(D. W. JOHNSON, JR.)

1. W. H. Gitzen, ed., *Alumina as a Ceramic Material*, American Ceramic Society, Columbus, OH, 1970.
2. W. E. Rhine, H. K. Bowen, *Ceram. Int., 17*, 143 (1991).
3. P. Cousin, R. A. Ross, *Mater. Sci. Eng. A, A130*, 119 (1990).
4. D. W. Johnson, Jr., P. K. Gallagher in *Ceramic Processing Before Firing*, G. Onoda, Jr., L. Hench, eds., Wiley, New York, 1978, p. 125.
5. D. W. Johnson, Jr., *Am. Ceram. Soc. Bull., 60*, 221 (1981).

17.2.2.3.1. Coprecipitation.

Coprecipitation is used when close control of composition or high chemical homogeneity is desirable in the formation of multicomponent compounds or solid solutions.

Inorganic Reactions and Methods, Volume 18
Edited by J. J. Zuckerman, Jim D. Atwood

as air or steam). Two or more streams of fluid intersect, and the particles are fractured upon impact with each other. One potential problem involves segregation by density of particles in a multicomponent system during the air classification step.

(D. W. JOHNSON, JR.)

1. *Handbook of Ball Mill and Pebble Mill Operation*, Paul O. Abbe, Little Falls, NJ, 19.
2. Y. N. Kryuchkov, *Steklo Keram., 8*, 14 (1995).
3. C. Greskovich, in *Ceramic Fabrication Processes*, F. F. Y. Wang, ed., Academic Press, New York, 1976, p. 15.
4. L. Y. Sadler, D. A. Stanley, D. R. Brooks, *Powder Technol., 12*, 19 (1975).
5. J. L. Hoyer, *Am. Ceram. Soc. Bull., 67*, 1663 (1988).
6. J. Secondi, R. Yavari, *J. Phys. IV, 3*, 1287 (1993).

17.2.2.3. Solution Preparation

Solution preparation of ceramic powders is often thought to be a speciality technique for small lots of high purity ceramic materials. High quality powders can be (obtained, and solution technique are chosen to produce many of the powders used in the ceramic industry in large quantities. A major example is Al_2O_3, most of which is produced when the mineral bauxite is dissolved in an alkaline solution and hydrated oxides are precipitated from the solution[1].

Solution techniques offer the advantage of high chemical purity, controlled fine particle sizes, and a high degree of chemical homogeneity on an atomic or molecular level (due to the dissolving of the metal species in a liquid). A goal of the various techniques is to preserve as much of this homogeneity as possible. Some of these techniques are reviewed elsewhere[2,3].

The first step is preparation of the solution. Aqueous solutions are prepared by dissolving either soluble salts in solvents (usually water) or metals in acids. For multicomponent systems, the mutual solubility of the various components must be considered. For example, a solution for lead zirconate cannot be prepared from lead nitrate and zirconium sulfate, both of which are soluble in water, because lead sulfate, which is insoluble, will precipitate. A solution of nitrates of both cations is satisfactory.

The next step is that of solvent removal, which categorizes solution preparation techniques[4,5]. The most important processes are discussed in the subsections that follow. The final step is thermal decomposition of the salts (discussed in 17.2.2.5).

(D. W. JOHNSON, JR.)

1. W. H. Gitzen, ed., *Alumina as a Ceramic Material*, American Ceramic Society, Columbus, OH, 1970.
2. W. E. Rhine, H. K. Bowen, *Ceram. Int., 17*, 143 (1991).
3. P. Cousin, R. A. Ross, *Mater. Sci. Eng. A, A130*, 119 (1990).
4. D. W. Johnson, Jr., P. K. Gallagher in *Ceramic Processing Before Firing*, G. Onoda, Jr., L. Hench, eds., Wiley, New York, 1978, p. 125.
5. D. W. Johnson, Jr., *Am. Ceram. Soc. Bull., 60*, 221 (1981).

17.2.2.3.1. Coprecipitation.

Coprecipitation is used when close control of composition or high chemical homogeneity is desirable in the formation of multicomponent compounds or solid solutions.

Inorganic Reactions and Methods, Volume 18
Edited by J. J. Zuckerman, Jim D. Atwood

as air or steam). Two or more streams of fluid intersect, and the particles are fractured upon impact with each other. One potential problem involves segregation by density of particles in a multicomponent system during the air classification step.

(D. W. JOHNSON, JR.)

1. *Handbook of Ball Mill and Pebble Mill Operation*, Paul O. Abbe, Little Falls, NJ, 19.
2. Y. N. Kryuchkov, *Steklo Keram., 8*, 14 (1995).
3. C. Greskovich, in *Ceramic Fabrication Processes*, F. F. Y. Wang, ed., Academic Press, New York, 1976, p. 15.
4. L. Y. Sadler, D. A. Stanley, D. R. Brooks, *Powder Technol., 12*, 19 (1975).
5. J. L. Hoyer, *Am. Ceram. Soc. Bull., 67*, 1663 (1988).
6. J. Secondi, R. Yavari, *J. Phys. IV, 3*, 1287 (1993).

17.2.2.3. Solution Preparation

Solution preparation of ceramic powders is often thought to be a speciality technique for small lots of high purity ceramic materials. High quality powders can be (obtained, and solution technique are chosen to produce many of the powders used in the ceramic industry in large quantities. A major example is Al_2O_3, most of which is produced when the mineral bauxite is dissolved in an alkaline solution and hydrated oxides are precipitated from the solution[1].

Solution techniques offer the advantage of high chemical purity, controlled fine particle sizes, and a high degree of chemical homogeneity on an atomic or molecular level (due to the dissolving of the metal species in a liquid). A goal of the various techniques is to preserve as much of this homogeneity as possible. Some of these techniques are reviewed elsewhere[2,3].

The first step is preparation of the solution. Aqueous solutions are prepared by dissolving either soluble salts in solvents (usually water) or metals in acids. For multicomponent systems, the mutual solubility of the various components must be considered. For example, a solution for lead zirconate cannot be prepared from lead nitrate and zirconium sulfate, both of which are soluble in water, because lead sulfate, which is insoluble, will precipitate. A solution of nitrates of both cations is satisfactory.

The next step is that of solvent removal, which categorizes solution preparation techniques[4,5]. The most important processes are discussed in the subsections that follow. The final step is thermal decomposition of the salts (discussed in 17.2.2.5).

(D. W. JOHNSON, JR.)

1. W. H. Gitzen, ed., *Alumina as a Ceramic Material*, American Ceramic Society, Columbus, OH, 1970.
2. W. E. Rhine, H. K. Bowen, *Ceram. Int., 17*, 143 (1991).
3. P. Cousin, R. A. Ross, *Mater. Sci. Eng. A, A130*, 119 (1990).
4. D. W. Johnson, Jr., P. K. Gallagher in *Ceramic Processing Before Firing*, G. Onoda, Jr., L. Hench, eds., Wiley, New York, 1978, p. 125.
5. D. W. Johnson, Jr., *Am. Ceram. Soc. Bull., 60*, 221 (1981).

17.2.2.3.1. Coprecipitation.

Coprecipitation is used when close control of composition or high chemical homogeneity is desirable in the formation of multicomponent compounds or solid solutions.

Coprecipitation is applicable to a wide range of compositions and uses simple equipment. Therefore, it is often chosen for laboratory preparation of reactive ceramic powders.

Many ceramic powders are based on the precipitation of single component materials from solution. The example of Al_2O_3 has already been noted, but most of the high purity powders such as metal carbonates used in the electronic ceramics industry are prepared from soluble salts in solutions. High quality Fe_2O_3 powder, used by the pigment and magnetic ceramic industries, is prepared by precipitation from iron sulfate or chloride solutions.

The most common coprecipitation technique makes an intimate mixture of the insoluble salts by massively exceeding the solubility coefficients of all the cations as quickly as possible for nearly quantitative precipitation. This requires that the solution containing the desired cation ratio be introduced by dropping or spraying into an excess of the precipitant. This mixture is homogeneous on a scale not obtainable by conventional mixing. The preparation of homogeneous, fine particle $BaFe_{12}O_{19}$ powder for permanent magnets, for example, makes use of aqueous $FeCl_3$ and $BaCl_2$ in water[1]. This is poured into a NaOH solution, after which the precipitate is washed to remove unwanted Na ions. Heating this to 925°C gives highly coercive barium ferrite, indicative of fine particles.

Examples of this type of coprecipitation encompass such diverse fields as nuclear ceramics[2], electrooptic ceramics[3], superconducting oxides[4,5], stabilized ZrO_2[6], and sulfide powders[7]. In the production of low loss MnZn spinel ferrites[8], the metals are dissolved in sulfuric acid, which is mixed with an NH_4OH–$(NH_4)_2CO_3$ solution. Proper adjustment of the pH and hydroxide–carbonate ratio prevents Zn complexing, and quantitative precipitation occurs. After filtering, drying, and calcination, the powder is used to make magnetic cores having lower losses than those obtained by means of conventional preparation techniques.

Hydroxide precipitations can be difficult to use because of gelation during washing to remove electrolytes; carbonates or oxalates are often used instead.

In some cases the conditions are particularly advantageous for controlling composition or maintaining homogeneity. If a precursor compound exists that has the desired cation ratios, it can be precipitated, and the composition will be independent of the cation ratios in the starting solution. The homogeneity will be on an atomic scale within this precursor compound [e.g., the preparation of $BaTiO_3$ by precipitating $BaTiO(C_2O_4)_2 \cdot 4H_2O$[9]. If no precursor compound of the exact composition exists, a solid solution precursor composition may. Again, homogeneity is assured on an atomic scale, but composition must be controlled by solution concentration and precipitation conditions (e.g., in the use of divalent metal oxalates for the preparation of ferrites)[10].

Special forms of coprecipitation include the digestion of precipitated hydroxides to form the desired oxides without having to decompose the usual hydroxide precursor to the oxide. For ferrites, this is an air oxidation, because the iron is added as a divalent ion and is oxidized during the digestion to trivalent ion in the ferrite (e.g., in Zn ferrites)[11]. Zn and Fe(II) sulfate solutions are added to a sodium hydroxide solution that is digested and oxidized with bubbled air to give crystalline ferrites. The technique gives regular cubic crystallites[12]. These techniques are used for other ceramic powders such as $BaTiO_3$[13].

Hydrothermal conditions represent an extension of the digestion technique that permits the use of temperatures exceeding 100°C for aqueous solutions yielding well-formed crystals[14] or powders[6,15–17].

Ceramic powders of exceptional purity with very fine particle sizes (ca. 10 nm) have been prepared by precipitation of hydrolyzed oxides from high purity alkoxides[18]. Yttria-stabilized zirconia is prepared by mixing high purity zirconium and yttrium isopropoxides in *n*-hexane, with water added dropwise to precipitate the oxides quantitatively[19]. The homogeneity of the oxides results in stabilized cubic ZrO_2 at very low temperatures. Cyclic organoaluminum amides are used to prepare nonoxides such as sulfides[7] and AlN[20].

An unusual precipitation uses a molten salt as solvent. For the preparation of lead zirconate titanate[21], TiO_2, ZrO_2, and excess PbO are mixed with a NaCl–KCl mixture and reacted at 1000°C. Lead zirconate titanate is less soluble in the molten salts than is TiO_2 or ZrO_2 and precipitates. Finally, the salt and excess PbO are leached out using an acetic acid solution.

Liquid drying[22] involves dissolving soluble salts in water and adding this solution to a massive amount of another solvent in which the desired components are relatively insoluble. This technique is used to produce ferrite powders or pyrite solid solutions by dissolving the sulfates in water and adding this solution to 10 times their volume of acetone. The precipitate is filtered, dried, and heated in H_2S to form the pyrites[23].

Supersaturation of solutions to precipitate ceramic powders is attained by means of supercritical fluids. This technique, termed rapid expansion of supercritical solutions (RESS), is reviewed elsewhere[24].

Coprecipitation using electrolytic decomposition of metal anodes in solution as a source of ions[25] produces NiZn ferrite from Ni, Zn, and Fe anodes in a sodium sulfate solution at 80°C. Cation ratios can be controlled by adjusting currents through the three anodes.

A type of precipitation and digestion that produces spherical particles has potential in producing sintered ceramic materials, since the uniformity of packing possible with discrete monosized particles can allow low temperature sintering. Monodispersed silica spheres[26] are produced by adding tetraalkylsilicate (e.g., tetraethylsilicate) to a mixture of alcohol (e.g., methanol), water, and NH_3. The spheres form after agitation for about 10 minutes or more. Depending on conditions, the sphere sizes range from $\sim$ 0.1 to 2 μm in diameter. The field of monodispersed metal (hydrous) oxides has been reviewed elsewhere[27–29], showing that a wide range of metal oxides such as Al_2O_3, Fe_2O_3, Fe_3O_4, CuO, ZnO, V_2O_5, NiO, and TiO_2 is produced in monodisperse form.

(D. W. JOHNSON, JR.)

1. W. Roos, *J. Am. Ceram. Soc., 63*, 601 (1980).
2. D. T. Rankin, G. A. Burney, P. K. Smith, R. D. Sisson Jr., *Am. Ceram. Soc. Bull., 56*, 478 (1977).
3. G. Haerting, *SAMPE J., 23*, 9 (1987).
4. E. R. Vance, *Key Eng. Mater., 66–67*, 461 (1992).
5. E. R. Vance, *Ceram. Int., 16*, 361 (1990).
6. J. Lin, J. Duh, *J. Am. Ceram. Soc., 80*, 92 (1997).
7. P. N. Komptu, S. H. Risbud, *Prog. Cryst. Growth Charact. Mater., 22*, 321 (1991).
8. A. Goldman, A. M. Laing, *J. Phys. (Paris) Colloq., 1*, 297 (1977).
9. W. S. Clabaugh, E. M. Swiggard, R. Gilchrist, *J. Res. Natl. Bur. Stand., (U.S.), 56*, 289 (1956).
10. P. K. Gallagher, F. Schrey, *J. Am. Ceram. Soc., 47*, 434 (1964).
11. T. Kanzaki, J. Nakajima, Y. Tamaura, T. Katsura, *Bull. Chem. Soc. Jpn., 54*, 135 (1981).
12. M. I. Mendelson, *J. Am. Ceram. Soc., 59*, 219 (1976).
13. S. S. Flaschen, *J. Am. Chem. Soc., 77*, 6194 (1955).
14. A. A. Van Der Giessen, *Klei. Keram., 20*, 30 (1970); *Chem. Abstr., 72*, 114604S (1970).
15. W. J. Dawson, *Am. Ceram. Soc. Bull., 67*, 1673 (1988).

16. D. R. Biswas, *J. Mater. Sci., 24*, 3791 (1989).
17. D. Hennings, *Br. Ceram. Proc., 41*, 1 (1984).
18. R. F. Hill, J. Lee, L. C. Montgomery, *Euro-Ceramics, 1*, 1 (1989).
19. K. S. Mazdiyasni, C. T. Lynch, J. S. Smith II, *J. Am. Ceram. Soc., 50*, 532 (1967).
20. F. C. Sauls, L. V. Interrante, *Coord. Chem. Rev. 128*, 193 (1993).
21. R. H. Arendt, J. H. Rosolowski, J. W. Szymaszek, *Mater. Res. Bull., 14*, 703 (1979).
22. R. E. Jaeger, T. J. Miller, *Am. Ceram. Soc. Bull., 53*, 855 (1974).
23. R. J. Bouchard, *Mater. Res. Bull., 3*, 563 (1968).
24. J. W. Tom, P. G. Debenedetti, *J. Aerosol Sci., 22*, 555 (1991).
25. R. M. Glaister, N. A. Allen, N. J. Hellicar, *Proc. Br. Ceram. Soc., 3*, 67 (1965).
26. W. Stober, A. Fink, E. Bohn, *J. Colloid Interface Sci., 26*, 62 (1968).
27. E. Matijevic, *Acc. Chem. Res., 14*, 22 (1981).
28. S. K. Milonjic, *Mater. Sci. Forum, 214*, 197 (1996).
29. G. L. Messing, *J. Ceram. Soc. Jpn., 99*, 1036 (1991).

17.2.2.3.2. Sol-Gel.

The term "sol-gel processing" has become very popular and often refers to the preparation of thin films or bulk objects as well as powders; the subject has been reviewed extensively[1–5].

The sol-gel process was first used[6] for the preparation of silicates used in phase equilibrium studies. Often the sol-gel process makes use of a concentrated hydrous sol, a colloidal dispersion of (hydrated) oxide particles produced by controlled precipitation. It is also a precipitation process that makes use of immobilization of ions in a gel or glassy structure.

The sol formation step can be carried out by precipitating a hydroxide with ammonia, which is then washed and dispersed as a sol by peptizing the slurry while controlling the pH. A 3.5 M zirconia sol, prepared by dispersing zirconium hydroxide in a dilute acid and then adding calcium or yttrium salt solutions, produces Y_2O_3-stabilized ZrO_2[7].

The gelling step can take place by removal of some of the water or by increasing the pH. In the case of microsphere formation, the sol is first formed into droplets. For dehydration, these droplets are fed into a column of dehydrating liquid such as a higher alcohol, which removes water from the droplets and yields gel spheres. If gelation is to be effected by an increase in pH, an ammonia donor such as hexamethylenetetramine is added to the sol. The sol is introduced into a hot organic fluid, which causes evolution of NH_3 within the sol, leading to gelation. Such gelation methods are used to prepare titania-based ceramics such as TiO_2, $CaTiO_3$, and TiC[8].

Examples of the sol-gel process for ceramic powder preparation include titanate and aluminates[9], cuprate superconductors[10], ceramic packaging materials[11], and $BaTiO_3$[12].

Not all gel processes involve preparation of a sol. Gels can also be prepared by polymerization of hydrolyzed metal alkoxides or by direct precipitation of a colloidal gel from a solution of alkoxides. Chemically homogeneous silicates, for example, are prepared by dissolving tetraethyl orthosilicate in ethanol and adding nitrates of other metals[13]. This solution is hydrolyzed with water to form a gel, which is dried and calcined. Transparent, porous Al_2O_3 is prepared by hydrolyzing and polymerizing aluminum isopropoxide and heat treating to 500°C[14]. Polymerized and colloidal gels are also used for low temperature preparation of glasses[15].

Homogeneous ceramics are also prepared by means of precursor materials. The simplest case is the dehydration without crystallization of highly soluble salts such as

Inorganic Reactions and Methods, Volume 18
Edited by J. J. Zuckerman, Jim D. Atwood

16. D. R. Biswas, *J. Mater. Sci., 24*, 3791 (1989).
17. D. Hennings, *Br. Ceram. Proc., 41*, 1 (1984).
18. R. F. Hill, J. Lee, L. C. Montgomery, *Euro-Ceramics, 1*, 1 (1989).
19. K. S. Mazdiyasni, C. T. Lynch, J. S. Smith II, *J. Am. Ceram. Soc., 50*, 532 (1967).
20. F. C. Sauls, L. V. Interrante, *Coord. Chem. Rev. 128*, 193 (1993).
21. R. H. Arendt, J. H. Rosolowski, J. W. Szymaszek, *Mater. Res. Bull., 14*, 703 (1979).
22. R. E. Jaeger, T. J. Miller, *Am. Ceram. Soc. Bull., 53*, 855 (1974).
23. R. J. Bouchard, *Mater. Res. Bull., 3*, 563 (1968).
24. J. W. Tom, P. G. Debenedetti, *J. Aerosol Sci., 22*, 555 (1991).
25. R. M. Glaister, N. A. Allen, N. J. Hellicar, *Proc. Br. Ceram. Soc., 3*, 67 (1965).
26. W. Stober, A. Fink, E. Bohn, *J. Colloid Interface Sci., 26*, 62 (1968).
27. E. Matijevic, *Acc. Chem. Res., 14*, 22 (1981).
28. S. K. Milonjic, *Mater. Sci. Forum, 214*, 197 (1996).
29. G. L. Messing, *J. Ceram. Soc. Jpn., 99*, 1036 (1991).

17.2.2.3.2. Sol-Gel.

The term "sol-gel processing" has become very popular and often refers to the preparation of thin films or bulk objects as well as powders; the subject has been reviewed extensively[1–5].

The sol-gel process was first used[6] for the preparation of silicates used in phase equilibrium studies. Often the sol-gel process makes use of a concentrated hydrous sol, a colloidal dispersion of (hydrated) oxide particles produced by controlled precipitation. It is also a precipitation process that makes use of immobilization of ions in a gel or glassy structure.

The sol formation step can be carried out by precipitating a hydroxide with ammonia, which is then washed and dispersed as a sol by peptizing the slurry while controlling the pH. A 3.5 M zirconia sol, prepared by dispersing zirconium hydroxide in a dilute acid and then adding calcium or yttrium salt solutions, produces Y_2O_3-stabilized ZrO_2[7].

The gelling step can take place by removal of some of the water or by increasing the pH. In the case of microsphere formation, the sol is first formed into droplets. For dehydration, these droplets are fed into a column of dehydrating liquid such as a higher alcohol, which removes water from the droplets and yields gel spheres. If gelation is to be effected by an increase in pH, an ammonia donor such as hexamethylenetetramine is added to the sol. The sol is introduced into a hot organic fluid, which causes evolution of NH_3 within the sol, leading to gelation. Such gelation methods are used to prepare titania-based ceramics such as TiO_2, $CaTiO_3$, and TiC[8].

Examples of the sol-gel process for ceramic powder preparation include titanate and aluminates[9], cuprate superconductors[10], ceramic packaging materials[11], and $BaTiO_3$[12].

Not all gel processes involve preparation of a sol. Gels can also be prepared by polymerization of hydrolyzed metal alkoxides or by direct precipitation of a colloidal gel from a solution of alkoxides. Chemically homogeneous silicates, for example, are prepared by dissolving tetraethyl orthosilicate in ethanol and adding nitrates of other metals[13]. This solution is hydrolyzed with water to form a gel, which is dried and calcined. Transparent, porous Al_2O_3 is prepared by hydrolyzing and polymerizing aluminum isopropoxide and heat treating to 500°C[14]. Polymerized and colloidal gels are also used for low temperature preparation of glasses[15].

Homogeneous ceramics are also prepared by means of precursor materials. The simplest case is the dehydration without crystallization of highly soluble salts such as

nitrates. This can be achieved by cooling the solution to form a supercooled liquid (a glass) and then dehydrating the glass at low temperatures. Organic polyfunctional acids (e.g., citric, malic, tartaric, glycolic, lactic acid) are also used[16]. Nitrate solutions and the organic acids are mixed and dehydrated slowly to give a viscous, glassy structure. This material can be dehydrated without crystallization or segregation and results in a degree of chemical homogeneity rivaling that of the original solution. Citric acid is commonly used and the method is sometimes termed the citrate process. The final step involves removal of the organic molecules by thermal oxidation; care must be exercised to avoid excessive temperatures from oxidation of the citrates[17].

(D. W. JOHNSON, JR.)

1. M. E. A. Hermans, *Powder Metal. Int., 5*, 137 (1973).
2. D. W. Johnson, Jr., *Am. Ceram. Soc. Bull., 64*, 1597 (1985).
3. R. Roy, *Science, 238*, 1664 (1987).
4. R. C. Mehrotra, *Struct. Bonding (Berlin), 77*, 1 (1992).
5. H. Dislich, *Glastech. Ber., 62*, 46 (1989).
6. R. Roy, *J. Am. Ceram. Soc., 49*, 145 (1956).
7. J. L. Woodhead, in *Science of Ceramics*, Vol. 4, G. H. Stewart, ed., British Ceramic Society/ Henry Blacklock, Manchester, England, 1968, p. 105.
8. J. L. Woodhead, in *Science of Ceramics*, Vol. 9, K. J. DeVries, ed., printed in Great Britain by Sherwin Rivers, Cobridge, Stoke-on-Trent, Staffordshire, for Netherlandse Keramische Vereniging, 1977, p. 29.
9. P. Cousin, R. A. Ross, *Mater. Sci. Eng. A, A130*, 119 (1990).
10. S. X. Dou, H. K. Liu, C. C. Sorrell, K. Song, M. H. Apperley, S. J. Guo, K. E. Easterling, W. K. Jones, *Mater. Forum, 14*, 92 (1990).
11. E. M. Rabinovich, *J. Electron. Packag., 111*, 183 (1989).
12. D. Hennings, *Br. Ceram. Proc., 41*, 1 (1984).
13. D. M. Roy, R. Roy, *Am. Mineral., 39*, 957 (1954).
14. B. E. Yoldas, *Am. Ceram. Soc. Bull., 54*, 286 (1975).
15. S. P. Mukherjee, *J. Non-Cryst. Solids, 42*, 477 (1980).
16. C. Marcilly, P. Courty, B. Delmon, *J. Am. Ceram. Soc., 53*, 56 (1970).
17. L. Koppens, in *Science of Ceramics*, Vol. 8, made and printed by Sherwin Rivers, Cobridge, Stoke on Trent, Staffordshire, for the British Ceramic Society, 1976.

17.2.2.3.3. Freeze-Drying.

The freeze-drying method[1] is one of solvent volatilization, but it differs from the common solvent evaporation techniques in that the solvent is sublimed from the solid state. A solution, prepared by means of soluble salts or by dissolving metals in acid, is frozen and the solid solvent, usually water in the form of ice, is sublimed away giving the dried salts. The process gives high surface area powders of excellent chemical homogeneity.

The object of the freezing step is to immobilize the metal cations quickly to prevent segregation. At the same time, an ice phase must be present for sublimation. Thus during freezing the water is crystallized, leaving behind the resultant hydrated salt phases, which are homogeneous. The absence of a liquid phase during drying preserves this homogeneity.

One simple freezing technique[1] forces the liquid under pressure into a swirling bath of refrigerated hexane. Hexane is chosen because aqueous solutions are immiscible, and the freezing point is below that of a dry ice–acetone mixture, the refrigerant used. The liquid stream leaving the nozzle breaks into droplets whose size depends on the nozzle diameter and the hydraulic pressure used. A 0.25 mm nozzle with a pressure of 20 kPa

Inorganic Reactions and Methods, Volume 18
Edited by J. J. Zuckerman, Jim D. Atwood

nitrates. This can be achieved by cooling the solution to form a supercooled liquid (a glass) and then dehydrating the glass at low temperatures. Organic polyfunctional acids (e.g., citric, malic, tartaric, glycolic, lactic acid) are also used[16]. Nitrate solutions and the organic acids are mixed and dehydrated slowly to give a viscous, glassy structure. This material can be dehydrated without crystallization or segregation and results in a degree of chemical homogeneity rivaling that of the original solution. Citric acid is commonly used and the method is sometimes termed the citrate process. The final step involves removal of the organic molecules by thermal oxidation; care must be exercised to avoid excessive temperatures from oxidation of the citrates[17].

(D. W. JOHNSON, JR.)

1. M. E. A. Hermans, *Powder Metal. Int., 5*, 137 (1973).
2. D. W. Johnson, Jr., *Am. Ceram. Soc. Bull., 64*, 1597 (1985).
3. R. Roy, *Science, 238*, 1664 (1987).
4. R. C. Mehrotra, *Struct. Bonding (Berlin), 77*, 1 (1992).
5. H. Dislich, *Glastech. Ber., 62*, 46 (1989).
6. R. Roy, *J. Am. Ceram. Soc., 49*, 145 (1956).
7. J. L. Woodhead, in *Science of Ceramics*, Vol. 4, G. H. Stewart, ed., British Ceramic Society/ Henry Blacklock, Manchester, England, 1968, p. 105.
8. J. L. Woodhead, in *Science of Ceramics*, Vol. 9, K. J. DeVries, ed., printed in Great Britain by Sherwin Rivers, Cobridge, Stoke-on-Trent, Staffordshire, for Netherlandse Keramische Vereniging, 1977, p. 29.
9. P. Cousin, R. A. Ross, *Mater. Sci. Eng. A, A130*, 119 (1990).
10. S. X. Dou, H. K. Liu, C. C. Sorrell, K. Song, M. H. Apperley, S. J. Guo, K. E. Easterling, W. K. Jones, *Mater. Forum, 14*, 92 (1990).
11. E. M. Rabinovich, *J. Electron. Packag., 111*, 183 (1989).
12. D. Hennings, *Br. Ceram. Proc., 41*, 1 (1984).
13. D. M. Roy, R. Roy, *Am. Mineral., 39*, 957 (1954).
14. B. E. Yoldas, *Am. Ceram. Soc. Bull., 54*, 286 (1975).
15. S. P. Mukherjee, *J. Non-Cryst. Solids, 42*, 477 (1980).
16. C. Marcilly, P. Courty, B. Delmon, *J. Am. Ceram. Soc., 53*, 56 (1970).
17. L. Koppens, in *Science of Ceramics*, Vol. 8, made and printed by Sherwin Rivers, Cobridge, Stoke on Trent, Staffordshire, for the British Ceramic Society, 1976.

17.2.2.3.3. Freeze-Drying.

The freeze-drying method[1] is one of solvent volatilization, but it differs from the common solvent evaporation techniques in that the solvent is sublimed from the solid state. A solution, prepared by means of soluble salts or by dissolving metals in acid, is frozen and the solid solvent, usually water in the form of ice, is sublimed away giving the dried salts. The process gives high surface area powders of excellent chemical homogeneity.

The object of the freezing step is to immobilize the metal cations quickly to prevent segregation. At the same time, an ice phase must be present for sublimation. Thus during freezing the water is crystallized, leaving behind the resultant hydrated salt phases, which are homogeneous. The absence of a liquid phase during drying preserves this homogeneity.

One simple freezing technique[1] forces the liquid under pressure into a swirling bath of refrigerated hexane. Hexane is chosen because aqueous solutions are immiscible, and the freezing point is below that of a dry ice–acetone mixture, the refrigerant used. The liquid stream leaving the nozzle breaks into droplets whose size depends on the nozzle diameter and the hydraulic pressure used. A 0.25 mm nozzle with a pressure of 20 kPa

yields droplets about 0.3 mm in diameter. The droplets are directed into the vortex of the swirling hexane, where they are separated from each other and rapidly frozen. The frozen spheres settle to the bottom and are subsequently removed.

Another freezing technique involves spraying the solution directly into liquid N_2[2]. The lower temperature could promote more rapid freezing, but this potential advantage is offset by poor thermal contact of the solution with the liquid N_2, due to an insulting layer of gas around the solution droplets. A pneumatic rather than hydraulic nozzle can also be used to disperse the solution into a fine aerosol whose droplets can be frozen quickly because of their small size. This technique is less manageable because it is difficult to separate the fine aerosol droplets from the gas before freezing.

Another variant of the freezing process allows a continuous freezing method[3], where a solution is injected through nozzles into the bottom of a chilled Freon bath that is denser than the frozen droplets. Thus, the droplets rise through the refrigerated liquid, freeze, and are skimmed from the surface continuously. To prevent freezing of the solution in the nozzles, two immiscible Freon liquids are used, with the denser liquid at the bottom being heated to prevent freezing at the nozzle and the less dense liquid refrigerated above it. The interface between the two liquids prevents rapid heat transfer between the liquids. Droplets of narrow size distribution can be made, and the mean size can be varied by modifying the pressure and the nozzle size. This freezing technique can be used to produce sphere sizes up to several millimeters.

The drying step in freeze drying makes use of the principle that when the partial pressure of water vapor is below the triple point of the ice in the system, the ice will sublime rather than melt. For pure water, the triple point is approximately 530 Pa and 0°C.

Commercial freeze-dryers have a vacuum chamber, with product shelves that can be heated or cooled and a cooled condenser. In a typical operation the frozen salt is introduced in trays onto cooled shelves to prevent melting. The chamber is evacuated by means of a mechanical vacuum pump, usually to a pressure of less than 100 Pa. The condenser coils are cooled to about -50 to -60°C, and the product shelf is then gently heated. The condenser coils trap water as ice rather than inefficiently pumping the large volumes of water vapor generated. The heated product shelves provide the needed heat of sublimation to the frozen material.

Maintaining a total pressure below 100 Pa in the chamber and a condenser temperature below 50°C is not technically difficult. The partial pressure of water at -50°C dew point is about 4 Pa, well below that of the triple point. For thick powder beds that receive a rapid heat input from the shelf, the local partial pressure of water can rise owing to the kinetics of transporting the water vapor through the powder bed to the condenser. Under sufficiently severe conditions, the vapor pressure will exceed that of the triple point, causing melting. Infrared heaters minimize this problem, since the rapid heating occurs on the surface of powder beds, where the water vapor is easily transported away from the ice.

Simple laboratory freeze-dryers can be constructed from vacuum bell jars and cold traps or from an evacuated glass apparatus consisting of two connected vertical legs, one containing the sample and the other immersed in liquid N_2 to act as a cold trap.

The solubility of salts in water affects the freezing and drying steps. If the salt is sparingly soluble, then large quantities of water must be sublimed to dry the salt, an expensive process that may lead to excessively dusty powder. On the other hand, if the salt is highly soluble, ice crystals will not precipitate during the freezing step; rather, the

solution will be cooled to a glass, which can be dehydrated to give powders of superb chemical homogeneity. This process, however, is not as rapid as normal freeze drying. In such a glassy system the viscosity depends only on the temperature of the solution. Therefore, to maintain rigid glasses, the product shelf must be kept as low as -20 to -30°C. Under these conditions the ΔT between the shelf and condenser is low and the partial pressure of water over the product is low, both of which slow the drying process. Nitrate salts are usually very soluble and can be quenched to glasses easily, but sulfate salt solutions usually freeze to ice–salt mixtures that can be easily freeze-dried in the normal fashion.

After drying, the salt maintains the shape of the frozen solution: usually spheres derived from freezing solution droplets. After decomposition of the salts, the oxide particles remain aggregated into spherical shapes with low bulk densities (< 5 vol% solid) depending on the solution concentrations used. These aggregates consist of chained crystallites radiating from the center of the sphere[4]. The radial texture derives from the freezing step, where ice crystals nucleate at the sphere surface and grow radially toward the center, precipitating salt crystallites similarly oriented. The chained aggregate structure is common to many of the powders derived from solution techniques.

The chemical homogeneity of freeze-dried powder is demonstrated by showing that $MgAl_2O_4$, freeze-dried from sulfate forms the spinel phase at temperatures lower than those associated with powders formed by conventional mixing of the oxides[1]. The use of freeze-drying for ceramic powder preparation ranges from uniformly doped NiO catalysts with Li_2O[5] to Mg-stabilized β-Al_2O_3 powders prepared for ionic conductors[6]. Solvents other than water are also used for freeze-drying[7]. Freeze drying as a powder preparation technique is compared with other methods for aluminates and titanates[8] and similarly compared for cuprate superconductors[9].

(D. W. JOHNSON, JR.)

1. F. J. Schnettler, F. R. Monforte, W. W. Rhodes, in *Science of Ceramics*, Vol. 4, G. H. Stewart, ed., the British Ceramic Society, printed in Great Britain by Henry Blacklock & Co., Manchester, England, 1968, p. 79.
2. V. V. Mirkovich, T. A. Wheat, *Am. Ceram. Soc. Bull., 49*, 724 (1970).
3. H. A. Sauer, J. A. Lewis, *AIChE J., 18*, 435 (1972).
4. D. W. Johnson, F. J. Schnettler, *J. Am. Ceram. Soc., 53*, 440 (1970).
5. A. C. C. Tseung, H. L. Bevan, *J. Mater. Sci., 5*, 604 (1970).
6. K. Kuribayashi, P. S. Nicholson, *Mater. Res. Bull., 15*, 1595 (1980).
7. D. B. Hibbet, A. C. C. Tseung, *J. Mater. Sci., 14*, 2665 (1979).
8. P. Cousin, R. A. Ross, *Mater. Sci. Eng. A, A130*, 119 (1990).
9. S. X. Dou, H. K. Liu, C. C. Sorrell, K. Song, M. H. Apperley, S. J. Guo, K. E. Easterling, W. K. Jones, *Mater. Forum, 14*, 92 (1990).

17.2.2.3.4. Solvent Evaporation.

In contrast to sublimation in freeze-drying, evaporation of a solvent is straightforward but may lead to less homogeneity: for example, if a multicomponent solution is slowly evaporated, the various constituents crystallize nonuniformly. Thus, the goal of evaporative techniques is to break the solution into small droplets to minimize the volume over which segregation can take place as well as to maximize the surface area for evaporation and then evaporate the solvent as rapidly as possible to quench in the homogeneity of the solution.

A simple method of achieving this type of evaporation is to spray the solution from a pneumatic nozzle onto a heated plate[1]. The equipment is inexpensive and, depending

Inorganic Reactions and Methods, Volume 18
Edited by J. J. Zuckerman, Jim D. Atwood

solution will be cooled to a glass, which can be dehydrated to give powders of superb chemical homogeneity. This process, however, is not as rapid as normal freeze drying. In such a glassy system the viscosity depends only on the temperature of the solution. Therefore, to maintain rigid glasses, the product shelf must be kept as low as -20 to $-30°C$. Under these conditions the ΔT between the shelf and condenser is low and the partial pressure of water over the product is low, both of which slow the drying process. Nitrate salts are usually very soluble and can be quenched to glasses easily, but sulfate salt solutions usually freeze to ice–salt mixtures that can be easily freeze-dried in the normal fashion.

After drying, the salt maintains the shape of the frozen solution: usually spheres derived from freezing solution droplets. After decomposition of the salts, the oxide particles remain aggregated into spherical shapes with low bulk densities (< 5 vol% solid) depending on the solution concentrations used. These aggregates consist of chained crystallites radiating from the center of the sphere[4]. The radial texture derives from the freezing step, where ice crystals nucleate at the sphere surface and grow radially toward the center, precipitating salt crystallites similarly oriented. The chained aggregate structure is common to many of the powders derived from solution techniques.

The chemical homogeneity of freeze-dried powder is demonstrated by showing that $MgAl_2O_4$, freeze-dried from sulfate forms the spinel phase at temperatures lower than those associated with powders formed by conventional mixing of the oxides[1]. The use of freeze-drying for ceramic powder preparation ranges from uniformly doped NiO catalysts with Li_2O[5] to Mg-stabilized β-Al_2O_3 powders prepared for ionic conductors[6]. Solvents other than water are also used for freeze-drying[7]. Freeze drying as a powder preparation technique is compared with other methods for aluminates and titanates[8] and similarly compared for cuprate superconductors[9].

(D. W. JOHNSON, JR.)

1. F. J. Schnettler, F. R. Monforte, W. W. Rhodes, in *Science of Ceramics*, Vol. 4, G. H. Stewart, ed., the British Ceramic Society, printed in Great Britain by Henry Blacklock & Co., Manchester, England, 1968, p. 79.
2. V. V. Mirkovich, T. A. Wheat, *Am. Ceram. Soc. Bull., 49*, 724 (1970).
3. H. A. Sauer, J. A. Lewis, *AIChE J., 18*, 435 (1972).
4. D. W. Johnson, F. J. Schnettler, *J. Am. Ceram. Soc., 53*, 440 (1970).
5. A. C. C. Tseung, H. L. Bevan, *J. Mater. Sci., 5*, 604 (1970).
6. K. Kuribayashi, P. S. Nicholson, *Mater. Res. Bull., 15*, 1595 (1980).
7. D. B. Hibbet, A. C. C. Tseung, *J. Mater. Sci., 14*, 2665 (1979).
8. P. Cousin, R. A. Ross, *Mater. Sci. Eng. A, A130*, 119 (1990).
9. S. X. Dou, H. K. Liu, C. C. Sorrell, K. Song, M. H. Apperley, S. J. Guo, K. E. Easterling, W. K. Jones, *Mater. Forum, 14*, 92 (1990).

17.2.2.3.4. Solvent Evaporation.

In contrast to sublimation in freeze-drying, evaporation of a solvent is straightforward but may lead to less homogeneity: for example, if a multicomponent solution is slowly evaporated, the various constituents crystallize nonuniformly. Thus, the goal of evaporative techniques is to break the solution into small droplets to minimize the volume over which segregation can take place as well as to maximize the surface area for evaporation and then evaporate the solvent as rapidly as possible to quench in the homogeneity of the solution.

A simple method of achieving this type of evaporation is to spray the solution from a pneumatic nozzle onto a heated plate[1]. The equipment is inexpensive and, depending

on the temperature of the heated plate, solvent evaporation may be very rapid; however, the powder may aggregate or stick to the heated plate.

Spray-drying of the solution is a straightforward technique for evaporating solvent from solution droplets. Spray-drying is commonly used in the ceramic industry for drying slurries of particles, and the same equipment can be used to produce powder from solutions. The solution is atomized using either a centrifugal disk or a two-fluid nozzle. The droplets are sprayed into a moving heated airstream, where they dry before they contact the walls of the chamber. Cyclones are used to collect the powder. This technique has been used to prepare powder for ferrites of very high density[2], β-Al_2O_3[3], and titanate ceramics[4,5].

In an extension of the spray-drying technique called spray roasting[6], evaporative decomposition of solutions (EDS)[7,8], spray pyrolysis[9], or aerosol pyrolysis[10], the temperature of the heated chamber is high enough to decompose the dried salts after the solvent has evaporated. Nitrate salts are used because of their low decomposition temperatures. The technique eliminates the problems of handling dried nitrate powders, which can be hydroscopic. These methods are used to prepare chalcogenide powders[11,12] and barium titanate[13].

Another solvent evaporation process is fluidized-bed drying of solutions[14]. Here the solution is atomized and injected into a heated bed of fluidized particles, where the solution is dried and, if the temperature is high enough, nitrates are decomposed. The technique is continuous and has a high throughput for the size of the equipment, but maintaining stable fluidized beds is difficult under conditions that enable the agglomerates to grow as solution is introduced.

An evaporative technique that maintains stable solution droplets during evaporation makes use of an emulsion of the solution and an immiscible liquid. The process is termed emulsion drying or, if the matrix liquid is kerosene, the hot kerosene process[10,15]. A dispersing surfactant, is used to emulsify the solution with the matrix liquid, and dehydration is achieved by means of a vacuum drying process or a heated matrix liquid such as kerosene. After drying, the salts are flocculated and separated from the matrix liquid. These powders, particularly those dried slowly under vacuum, are not as homogeneous as those made by other evaporative processes such as spray-drying, but they are better than those obtained by conventional mixing. For long drying times, the technique depends on a fine dispersion of the solution in the matrix liquid to maintain good chemical homogeneity.

(D. W. JOHNSON, JR.)

1. R. Roy, *Int. J. Powder Metall. 6*, 25 (1974).
2. J. G. M. DeLau, *Am. Ceram. Soc. Bull., 49*, 572 (1970).
3. W. Baukal, H. P. Beck, W. Kuhn, R. Sieglen, *Power Sources, 6*, 655 (1977).
4. J. Thomson, Jr., *Am. Ceram. Soc. Bull., 53*, 421 (1974).
5. P. Cousin, R. A. Ross, *Mater. Sci. Eng. A, A130*, 119 (1990).
6. T. Akashi, T. Tsuji, Y. Onoda, in *Sintering and Related Phenomena*, G. C. Kucznski, N. A. Hooton, C. F. Gibbons, eds., Gordon & Breach, New York, 1967, p. 747.
7. D. M. Roy, R. R. Nevrgaonkar, T. P. O'Holleran, R. Roy, *Am. Ceram. Soc. Bull., 53*, 421 (1977).
8. G. L. Messing, S. Zhang, G. V. Jayanthi, *J. Am. Ceram. Soc., 76*, 2707 (1993).
9. A. Gurav, T. Kodas, T. Pluym, X. Xiong, *Aerosol Sci. Technol., 19*, 411 (1993).
10. G. L. Messing, *J. Ceram. Soc. Jpn., 99*, 1036 (1991).
11. C. M. Vaughan-Forster, W. B. White, *J. Am. Ceram. Soc., 80*, 273 (1997).
12. D. S. Albin, S. H. Risbud, *Adv. Ceram. Mater., 2*, 243 (1987).

13. D. Hennings, *B. Ceram. Proc., 41*, 1 (1989).
14. A. A. Jonke, E. J. Petkus, J. W. Loeding, S. Lawroski, *Nucl. Sci. Eng., 2*, 303 (1957).
15. P. Reynen, H. Basties, *Powder Metall. Int., 8*, 91 (1976).

17.2.2.4. Vapor Phase Techniques

Vapor phase techniques make use of the nucleation of particles from the vapor phase. Large-scale industrial examples are the preparation of fumed SiO_2 and TiO_2 by the flame hydrolysis of $SiCl_4$ or $TiCl_4$. The processes are categorized according to the following reaction mechanisms: multicomponent reaction of vapor species, decomposition of vapors, and direct vaporization–condensation. These methods are well suited for the preparation of unaggregated powders because individual crystallites are nucleated from the vapor and are well separated from each other during the growth stage, but the powder must be separated from large volumes of gas using filters or electrostatic precipitators. Complex compositions are difficult to form in the vapor phase. The use of plasma and lasers in vapor phase methods has been reported[1–4].

(D. W. JOHNSON, JR.)

1. W. E. Rhine, H. K. Bowen, *Ceram. Int., 17*, 143 (1991).
2. D. R. Biswas, *J. Mater. Sci., 24*, 3791 (1989).
3. P. R. Taylor, *Adv. Performance Mater. 1*, 35 (1994).
4. A. M. Hart, B. C. Peters, J. H. Plonka, H. James, W. H. Werst, Jr., J. M. Macki, *Chem. Eng. Prog., 85*, 32 (1989).

17.2.2.4.1. Reactions in the Vapor Phase.

Powders can be formed by the reaction of at least two gas phase reactants[1]. Metal chlorides are often used because of their high volatility, for example:

$$SiCl_4 + 2H_2O \longrightarrow SiO_2 + 4HCl \quad \text{(a)}$$

$$TiCl_4 + 2H_2O \longrightarrow TiO_2 + 4HCl \quad \text{(b)}$$

Powders made in large quantities by flame hydrolysis are intentionally agglomerated to aid in separation from the gas phase[2]. A fluid energy mill as described in 17.2.2.2 is used if deagglomerated powder is desired.

Another simple gas phase reaction is oxidation of chlorides (e.g., in the production of TiO_2)[3].

$$TiCl_4 + O_2 \longrightarrow TiO_2 + 2Cl_2 \quad \text{(c)}$$

Submicrometer monodisperse cubic particles of TiO_2 are produced.

Vapor reaction methods are of interest for producing refractory carbides and nitrides, which are difficult to obtain by solution processes. The following reactions are used in the production of silicon nitride[4,5]:

$$3SiCl_4 + 4NH_3 \longrightarrow Si_3N_4 + 12HCl \quad \text{(d)}$$

and silicon carbide[6]:

$$SiCl_4 + CH_4 \longrightarrow SiC + 4HCl \quad \text{(e)}$$

Inorganic Reactions and Methods, Volume 18
Edited by J. J. Zuckerman, Jim D. Atwood

13. D. Hennings, *B. Ceram. Proc., 41*, 1 (1989).
14. A. A. Jonke, E. J. Petkus, J. W. Loeding, S. Lawroski, *Nucl. Sci. Eng., 2*, 303 (1957).
15. P. Reynen, H. Basties, *Powder Metall. Int., 8*, 91 (1976).

17.2.2.4. Vapor Phase Techniques

Vapor phase techniques make use of the nucleation of particles from the vapor phase. Large-scale industrial examples are the preparation of fumed SiO_2 and TiO_2 by the flame hydrolysis of $SiCl_4$ or $TiCl_4$. The processes are categorized according to the following reaction mechanisms: multicomponent reaction of vapor species, decomposition of vapors, and direct vaporization–condensation. These methods are well suited for the preparation of unaggregated powders because individual crystallites are nucleated from the vapor and are well separated from each other during the growth stage, but the powder must be separated from large volumes of gas using filters or electrostatic precipitators. Complex compositions are difficult to form in the vapor phase. The use of plasma and lasers in vapor phase methods has been reported[1–4].

(D. W. JOHNSON, JR.)

1. W. E. Rhine, H. K. Bowen, *Ceram. Int., 17*, 143 (1991).
2. D. R. Biswas, *J. Mater. Sci., 24*, 3791 (1989).
3. P. R. Taylor, *Adv. Performance Mater. 1*, 35 (1994).
4. A. M. Hart, B. C. Peters, J. H. Plonka, H. James, W. H. Werst, Jr., J. M. Macki, *Chem. Eng. Prog., 85*, 32 (1989).

17.2.2.4.1. Reactions in the Vapor Phase.

Powders can be formed by the reaction of at least two gas phase reactants[1]. Metal chlorides are often used because of their high volatility, for example:

$$SiCl_4 + 2H_2O \longrightarrow SiO_2 + 4HCl \quad \text{(a)}$$

$$TiCl_4 + 2H_2O \longrightarrow TiO_2 + 4HCl \quad \text{(b)}$$

Powders made in large quantities by flame hydrolysis are intentionally agglomerated to aid in separation from the gas phase[2]. A fluid energy mill as described in 17.2.2.2 is used if deagglomerated powder is desired.

Another simple gas phase reaction is oxidation of chlorides (e.g., in the production of TiO_2)[3].

$$TiCl_4 + O_2 \longrightarrow TiO_2 + 2Cl_2 \quad \text{(c)}$$

Submicrometer monodisperse cubic particles of TiO_2 are produced.

Vapor reaction methods are of interest for producing refractory carbides and nitrides, which are difficult to obtain by solution processes. The following reactions are used in the production of silicon nitride[4,5]:

$$3SiCl_4 + 4NH_3 \longrightarrow Si_3N_4 + 12HCl \quad \text{(d)}$$

and silicon carbide[6]:

$$SiCl_4 + CH_4 \longrightarrow SiC + 4HCl \quad \text{(e)}$$

Inorganic Reactions and Methods, Volume 18
Edited by J. J. Zuckerman, Jim D. Atwood

13. D. Hennings, *B. Ceram. Proc., 41*, 1 (1989).
14. A. A. Jonke, E. J. Petkus, J. W. Loeding, S. Lawroski, *Nucl. Sci. Eng., 2*, 303 (1957).
15. P. Reynen, H. Basties, *Powder Metall. Int., 8*, 91 (1976).

17.2.2.4. Vapor Phase Techniques

Vapor phase techniques make use of the nucleation of particles from the vapor phase. Large-scale industrial examples are the preparation of fumed SiO_2 and TiO_2 by the flame hydrolysis of $SiCl_4$ or $TiCl_4$. The processes are categorized according to the following reaction mechanisms: multicomponent reaction of vapor species, decomposition of vapors, and direct vaporization–condensation. These methods are well suited for the preparation of unaggregated powders because individual crystallites are nucleated from the vapor and are well separated from each other during the growth stage, but the powder must be separated from large volumes of gas using filters or electrostatic precipitators. Complex compositions are difficult to form in the vapor phase. The use of plasma and lasers in vapor phase methods has been reported[1–4].

(D. W. JOHNSON, JR.)

1. W. E. Rhine, H. K. Bowen, *Ceram. Int., 17*, 143 (1991).
2. D. R. Biswas, *J. Mater. Sci., 24*, 3791 (1989).
3. P. R. Taylor, *Adv. Performance Mater. 1*, 35 (1994).
4. A. M. Hart, B. C. Peters, J. H. Plonka, H. James, W. H. Werst, Jr., J. M. Macki, *Chem. Eng. Prog., 85*, 32 (1989).

17.2.2.4.1. Reactions in the Vapor Phase.

Powders can be formed by the reaction of at least two gas phase reactants[1]. Metal chlorides are often used because of their high volatility, for example:

$$SiCl_4 + 2H_2O \longrightarrow SiO_2 + 4HCl \quad \text{(a)}$$

$$TiCl_4 + 2H_2O \longrightarrow TiO_2 + 4HCl \quad \text{(b)}$$

Powders made in large quantities by flame hydrolysis are intentionally agglomerated to aid in separation from the gas phase[2]. A fluid energy mill as described in 17.2.2.2 is used if deagglomerated powder is desired.

Another simple gas phase reaction is oxidation of chlorides (e.g., in the production of TiO_2)[3].

$$TiCl_4 + O_2 \longrightarrow TiO_2 + 2Cl_2 \quad \text{(c)}$$

Submicrometer monodisperse cubic particles of TiO_2 are produced.

Vapor reaction methods are of interest for producing refractory carbides and nitrides, which are difficult to obtain by solution processes. The following reactions are used in the production of silicon nitride[4,5]:

$$3SiCl_4 + 4NH_3 \longrightarrow Si_3N_4 + 12HCl \quad \text{(d)}$$

and silicon carbide[6]:

$$SiCl_4 + CH_4 \longrightarrow SiC + 4HCl \quad \text{(e)}$$

Tungsten carbide from tungsten chloride, methane, and hydrogen is another example of nonoxide ceramic powder preparation[7]. The reaction of the vapors takes place in heated tubes, dc plasmas or rf plasmas. The preparation of fine particles for high sintering reactivity is important in these nonoxide ceramics, which are otherwise difficult to densify.

The preparation of multicomponent powders from gases is not widely used because control of composition is difficult. However solid solutions such as Al_2O_3–Cr_2O_3[8] and Al_2O_3–TiO_2[9] are prepared by oxidation of halides. High purity SiO_2 powders doped with up to 14 wt% Al_2O_3 are prepared[10] by vaporizing metal particles in an Ar plasma and reacting the vapors with O_2. Elementary particles are typically 100 nm in diameter.

Another vapor phase method involves reacting a solid particulate phase with a gas to form particles. One method[11] is the self-propogating high temperature synthesis (SHS) method. Also used for making sintered bodies, SHS can be used in reacting particles with the gas phase. An example of combustion synthesis involves forming ceramic carbide powders[12].

(D. W. JOHNSON, JR.)

1. M. I. Boulos, *IEEE Trans. Plasma Sci., 19*, 1078 (1991).
2. L. J. White, *Ind. Eng. Chem., 51*, 232 (1959).
3. Y. Suyama, A. Kato, *J. Am. Ceram. Soc., 59*, 146 (1976).
4. S. F. Exell, R. Roggen, J. Gillot, B. Lux, in *Fine Particles, Second International Conference*, W. E. Kuhn, ed., Electrochemical Society, Princeton, NJ, 1974, p. 165.
5. D. L. Segal, *Trans. J. Br. Ceram. Soc., 85*, 184 (1986).
6. Y. Okabe, J. Hojo, A. Kato, *J. Less-Common Metals, 68*, 29 (1979).
7. J. Hojo, T. Oku, A. Kato, *J. Less-Common Metals, 59*, 85 (1978).
8. R. McPherson, *J. Mater. Sci., 8*, 859 (1973).
9. M. S. J. Gani, R. McPherson, *J. Aust. Ceram. Soc., 8*, 65 (1972).
10. R. Tueta, M. Braguier, J. Canteloup, *Am. Ceram. Soc. Bull., 57*, 1135 (1978).
11. R. Pampuch, J. Lis, L. Stobierski, *Sci. Ceram., 14*, 15 (1988).
12. R. Pampuch, L. Stobierski, *Ceram. Int., 17*, 69 (1991).

17.2.2.4.2. Vapor Decomposition.

Vapor decomposition is a powder preparation technique useful in a few cases when a vapor phase precursor exists (often an organometallic compound) which can be decomposed to the desired composition[1,2]. The vapor decomposition usually takes place at elevated temperatures. Single component oxide powders of high purity can be prepared by vapor decomposition of metal alkoxides; for example, ZrO_2 is prepared by pyrolyzing zirconium tetra-*t*-butoxide[3].

$$Zr(OR)_4 \longrightarrow ZrO_2 + 2ROH + \text{olefin} \qquad \text{(a)}$$

The decomposition is complete by 300°C, and the ZrO_2 powder (mean particle size 5 nm) is collected by means of an electrostatic precipitator. Nonoxide ceramic powders such as SiC are prepared by the decomposition $(CH_3)_2SiCl_2$[4] and CH_3SiH_3[5].

(D. W. JOHNSON, JR.)

1. J. Chaiken, *Appl. Organomet. Chem., 7*, 163 (1993).
2. R. McPherson, *J. Aust. Ceram. Soc., 17 (N-1)*, 2 (1981).
3. K. S. Mazdiyasni, C. T. Lynch, J. S. Smith, *J. Am. Ceram. Soc., 48*, 372 (1965).
4. O. DePous-Battelle, *Ceram. Int., 13*, 283 (1978).
5. W. Boecker, H. Hausner, *Ber. Dtsch. Keram. Ges., 55*, 233 (1978).

Inorganic Reactions and Methods, Volume 18
Edited by J. J. Zuckerman, Jim D. Atwood

Tungsten carbide from tungsten chloride, methane, and hydrogen is another example of nonoxide ceramic powder preparation[7]. The reaction of the vapors takes place in heated tubes, dc plasmas or rf plasmas. The preparation of fine particles for high sintering reactivity is important in these nonoxide ceramics, which are otherwise difficult to densify.

The preparation of multicomponent powders from gases is not widely used because control of composition is difficult. However solid solutions such as Al_2O_3–Cr_2O_3[8] and Al_2O_3–TiO_2[9] are prepared by oxidation of halides. High purity SiO_2 powders doped with up to 14 wt% Al_2O_3 are prepared[10] by vaporizing metal particles in an Ar plasma and reacting the vapors with O_2. Elementary particles are typically 100 nm in diameter.

Another vapor phase method involves reacting a solid particulate phase with a gas to form particles. One method[11] is the self-propogating high temperature synthesis (SHS) method. Also used for making sintered bodies, SHS can be used in reacting particles with the gas phase. An example of combustion synthesis involves forming ceramic carbide powders[12].

(D. W. JOHNSON, JR.)

1. M. I. Boulos, *IEEE Trans. Plasma Sci., 19*, 1078 (1991).
2. L. J. White, *Ind. Eng. Chem., 51*, 232 (1959).
3. Y. Suyama, A. Kato, *J. Am. Ceram. Soc., 59*, 146 (1976).
4. S. F. Exell, R. Roggen, J. Gillot, B. Lux, in *Fine Particles, Second International Conference*, W. E. Kuhn, ed., Electrochemical Society, Princeton, NJ, 1974, p. 165.
5. D. L. Segal, *Trans. J. Br. Ceram. Soc., 85*, 184 (1986).
6. Y. Okabe, J. Hojo, A. Kato, *J. Less-Common Metals, 68*, 29 (1979).
7. J. Hojo, T. Oku, A. Kato, *J. Less-Common Metals, 59*, 85 (1978).
8. R. McPherson, *J. Mater. Sci., 8*, 859 (1973).
9. M. S. J. Gani, R. McPherson, *J. Aust. Ceram. Soc., 8*, 65 (1972).
10. R. Tueta, M. Braguier, J. Canteloup, *Am. Ceram. Soc. Bull., 57*, 1135 (1978).
11. R. Pampuch, J. Lis, L. Stobierski, *Sci. Ceram., 14*, 15 (1988).
12. R. Pampuch, L. Stobierski, *Ceram. Int., 17*, 69 (1991).

17.2.2.4.2. Vapor Decomposition.

Vapor decomposition is a powder preparation technique useful in a few cases when a vapor phase precursor exists (often an organometallic compound) which can be decomposed to the desired composition[1,2]. The vapor decomposition usually takes place at elevated temperatures. Single component oxide powders of high purity can be prepared by vapor decomposition of metal alkoxides; for example, ZrO_2 is prepared by pyrolyzing zirconium tetra-*t*-butoxide[3].

$$Zr(OR)_4 \longrightarrow ZrO_2 + 2ROH + \text{olefin} \qquad \text{(a)}$$

The decomposition is complete by 300°C, and the ZrO_2 powder (mean particle size 5 nm) is collected by means of an electrostatic precipitator. Nonoxide ceramic powders such as SiC are prepared by the decomposition $(CH_3)_2SiCl_2$[4] and CH_3SiH_3[5].

(D. W. JOHNSON, JR.)

1. J. Chaiken, *Appl. Organomet. Chem., 7*, 163 (1993).
2. R. McPherson, *J. Aust. Ceram. Soc., 17 (N-1)*, 2 (1981).
3. K. S. Mazdiyasni, C. T. Lynch, J. S. Smith, *J. Am. Ceram. Soc., 48*, 372 (1965).
4. O. DePous-Battelle, *Ceram. Int., 13*, 283 (1978).
5. W. Boecker, H. Hausner, *Ber. Dtsch. Keram. Ges., 55*, 233 (1978).

Inorganic Reactions and Methods, Volume 18
Edited by J. J. Zuckerman, Jim D. Atwood

17.2.2.4.3. Direct Vaporization Condensation.

While all vapor techniques depend on a condensation step, the direct vaporization techniques begin with the desired composition and evaporate or sublimate the material. This is straightforward and allows a diversity of compositions to be used[1], but excessively high temperatures are demanded to vaporize refractory ceramics. Various heating methods used[2], including dc arcs, dc plasmas, rf plasmas, and electron beam heating. These techniques are not popular for large-scale production or routine laboratory powder preparation.

Spherical particles of TiO_2 are prepared by condensing vapors of $TiCl_4$ or titanium ethoxide as uniform-sized aerosol droplets on AgCl nuclei[3]. The aerosol is subsequently hydrolyzed to give TiO_2 spherical particles of narrow size distribution with model diameters ranging from 0.06 to 0.6 μm.

(D. W. JOHNSON, JR.)

1. A. Gurav, T. Kodas, T. Pluym, Y. Xiong, *Aerosol Sci. Technol., 19*, 411 (1993).
2. D. W. Johnson Jr., *Am. Ceram. Soc. Bull., 60*, 221 (1981).
3. M. Visca, E. Matijevic, *J. Colloid Interface Sci., 68*, 308 (1979).

17.2.2.5. Thermal Decomposition

Thermal decomposition is a broad category for powder preparation that impacts on the other techniques discussed and is an important method in its own right. High purity Al_2O_3 is prepared by thermal decomposition of ammonium aluminum sulfate, and pigment and electronic grade Fe_2O_3 are prepared by thermal decomposition of iron sulfates and chlorides. Decomposition of soluble salts has the advantages of allowing purification of the salts in solution and can make use of industrial wastes such as pickling liquors.

Thermal decomposition[1,2] also plays an important role in the conventional ceramic powder process, which makes use of starting materials such as metal carbonates that decompose during calcining, exposing reactive surfaces, which in turn aid in phase formation and chemical homogenization. Thermal decomposition is an important final step in solution preparation techniques. Precipitated hydroxides, carbonates, or oxalates are decomposed to oxides. Freeze-drying yields dried salts such as sulfates, which must be thermally decomposed to oxides. Similarly, many solution techniques use nitrates, which are decomposed as part of the process or in a separate step.

Illustrative of the diversity of the technique, small amounts of spinel ferrites such as $MnFe_2O_4$, $CoFe_2O_4$, and $NiFe_2O_4$ are prepared by thermally decomposing the pyridine or pyridine-1-oxide complexes of the metal nitrates by heating to 500°C[3]. Well-crystallized ferrites are observed after heat treatment to 1000°C. Potassium β-Al_2O_3, a compound usually synthesized by ion exchange of K for Na in sodium β-Al_2O_3, is prepared by thermal decomposition of a potassium trioxalatoaluminate, $K_x(NH_4)_{3-x}[Al(C_2O_4)_3] \cdot 3H_2O$ ($0.091 \leq x \leq 0.333$) at 1200°C[4]. Yttrium iron garnet is prepared by decomposition of coprecipitated hydroxides and carbonates of yttrium and iron[5] at temperatures in the range of 200–800°C. These powders have better sintering properties than those made by conventional mixed oxides calcined at 1200°C.

The kinetics of decomposition of salts for the preparation of ceramic powders[6,7] reveal the minimum time–temperature conditions necessary for complete decomposition.

Inorganic Reactions and Methods, Volume 18
Edited by J. J. Zuckerman, Jim D. Atwood

17.2.2.4.3. Direct Vaporization Condensation.

While all vapor techniques depend on a condensation step, the direct vaporization techniques begin with the desired composition and evaporate or sublimate the material. This is straightforward and allows a diversity of compositions to be used[1], but excessively high temperatures are demanded to vaporize refractory ceramics. Various heating methods used[2], including dc arcs, dc plasmas, rf plasmas, and electron beam heating. These techniques are not popular for large-scale production or routine laboratory powder preparation.

Spherical particles of TiO_2 are prepared by condensing vapors of $TiCl_4$ or titanium ethoxide as uniform-sized aerosol droplets on AgCl nuclei[3]. The aerosol is subsequently hydrolyzed to give TiO_2 spherical particles of narrow size distribution with model diameters ranging from 0.06 to 0.6 μm.

(D. W. JOHNSON, JR.)

1. A. Gurav, T. Kodas, T. Pluym, Y. Xiong, *Aerosol Sci. Technol.*, *19*, 411 (1993).
2. D. W. Johnson Jr., *Am. Ceram. Soc. Bull.*, *60*, 221 (1981).
3. M. Visca, E. Matijevic, *J. Colloid Interface Sci.*, *68*, 308 (1979).

17.2.2.5. Thermal Decomposition

Thermal decomposition is a broad category for powder preparation that impacts on the other techniques discussed and is an important method in its own right. High purity Al_2O_3 is prepared by thermal decomposition of ammonium aluminum sulfate, and pigment and electronic grade Fe_2O_3 are prepared by thermal decomposition of iron sulfates and chlorides. Decomposition of soluble salts has the advantages of allowing purification of the salts in solution and can make use of industrial wastes such as pickling liquors.

Thermal decomposition[1,2] also plays an important role in the conventional ceramic powder process, which makes use of starting materials such as metal carbonates that decompose during calcining, exposing reactive surfaces, which in turn aid in phase formation and chemical homogenization. Thermal decomposition is an important final step in solution preparation techniques. Precipitated hydroxides, carbonates, or oxalates are decomposed to oxides. Freeze-drying yields dried salts such as sulfates, which must be thermally decomposed to oxides. Similarly, many solution techniques use nitrates, which are decomposed as part of the process or in a separate step.

Illustrative of the diversity of the technique, small amounts of spinel ferrites such as $MnFe_2O_4$, $CoFe_2O_4$, and $NiFe_2O_4$ are prepared by thermally decomposing the pyridine or pyridine-1-oxide complexes of the metal nitrates by heating to 500°C[3]. Well-crystallized ferrites are observed after heat treatment to 1000°C. Potassium β-Al_2O_3, a compound usually synthesized by ion exchange of K for Na in sodium β-Al_2O_3, is prepared by thermal decomposition of a potassium trioxalatoaluminate, $K_x(NH_4)_{3-x}[Al(C_2O_4)_3] \cdot 3H_2O$ ($0.091 \leq x \leq 0.333$) at 1200°C[4]. Yttrium iron garnet is prepared by decomposition of coprecipitated hydroxides and carbonates of yttrium and iron[5] at temperatures in the range of 200–800°C. These powders have better sintering properties than those made by conventional mixed oxides calcined at 1200°C.

The kinetics of decomposition of salts for the preparation of ceramic powders[6,7] reveal the minimum time–temperature conditions necessary for complete decomposition.

However, in decomposing salts such as sulfates where stable oxysulfates exist, traces of sulfur can persist at temperatures even above 1200°C. Decomposition reactions often follow kinetic models of a sphere or cylinder, where the reaction interface moves at constant velocity from the spherical or cylindrical surfaces inward.

(D. W. JOHNSON, JR.)

1. D. A. Young, *Decomposition of Solids*, Pergamon Press, Oxford, 1966.
2. D. R. Biswas, *J. Mater. Sci.*, *24*, 3791 (1989).
3. R. T. Richardson, *J. Mater. Sci.*, *15*, 2569 (1980).
4. T. Takahashi, K. Kuwabara, H. Ohyanagi, *J. Appl. Electrochem.*, *11*, 77 (1981).
5. K. R. Nair, *Am. Ceram. Soc. Bull.*, *60*, 626 (1981).
6. D. W. Johnson Jr., P. K. Gallagher, *J. Am. Ceram. Soc.*, *54*, 461 (1971).
7. D. W. Johnson Jr., P. K. Gallagher, *J. Phys. Chem.*, *75*, 1179 (1971).

17.2.3. Densification of Ceramic Powders

17.2.3.1. Introduction

Because of their strong chemical bonds, bulk ceramics are most efficiently fabricated by means of densification of powders. The fabrication process involves two main stages: (1) consolidation of the powder to form a porous, shaped article (the "green" body), also referred to as *forming*, and (2) heating of the shaped powder form to produce a dense article, referred to as *firing* or *sintering*. The final product commonly consists of a relatively dense *polycrystal* with some residual porosity (Fig. 1). The microstructure, which

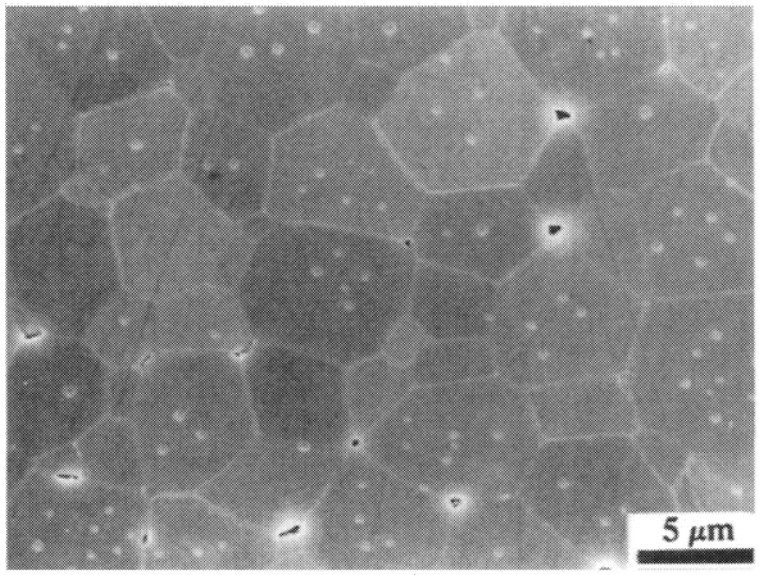

Figure 1. Microstructure of a polycrystalline ceramic showing grains (crystals), grain boundaries, and pores.

Inorganic Reactions and Methods, Volume 18
Edited by J. J. Zuckerman, Jim D. Atwood

However, in decomposing salts such as sulfates where stable oxysulfates exist, traces of sulfur can persist at temperatures even above 1200°C. Decomposition reactions often follow kinetic models of a sphere or cylinder, where the reaction interface moves at constant velocity from the spherical or cylindrical surfaces inward.

(D. W. JOHNSON, JR.)

1. D. A. Young, *Decomposition of Solids*, Pergamon Press, Oxford, 1966.
2. D. R. Biswas, *J. Mater. Sci.*, *24*, 3791 (1989).
3. R. T. Richardson, *J. Mater. Sci.*, *15*, 2569 (1980).
4. T. Takahashi, K. Kuwabara, H. Ohyanagi, *J. Appl. Electrochem.*, *11*, 77 (1981).
5. K. R. Nair, *Am. Ceram. Soc. Bull.*, *60*, 626 (1981).
6. D. W. Johnson Jr., P. K. Gallagher, *J. Am. Ceram. Soc.*, *54*, 461 (1971).
7. D. W. Johnson Jr., P. K. Gallagher, *J. Phys. Chem.*, *75*, 1179 (1971).

17.2.3. Densification of Ceramic Powders

17.2.3.1. Introduction

Because of their strong chemical bonds, bulk ceramics are most efficiently fabricated by means of densification of powders. The fabrication process involves two main stages: (1) consolidation of the powder to form a porous, shaped article (the "green" body), also referred to as *forming*, and (2) heating of the shaped powder form to produce a dense article, referred to as *firing* or *sintering*. The final product commonly consists of a relatively dense *polycrystal* with some residual porosity (Fig. 1). The microstructure, which

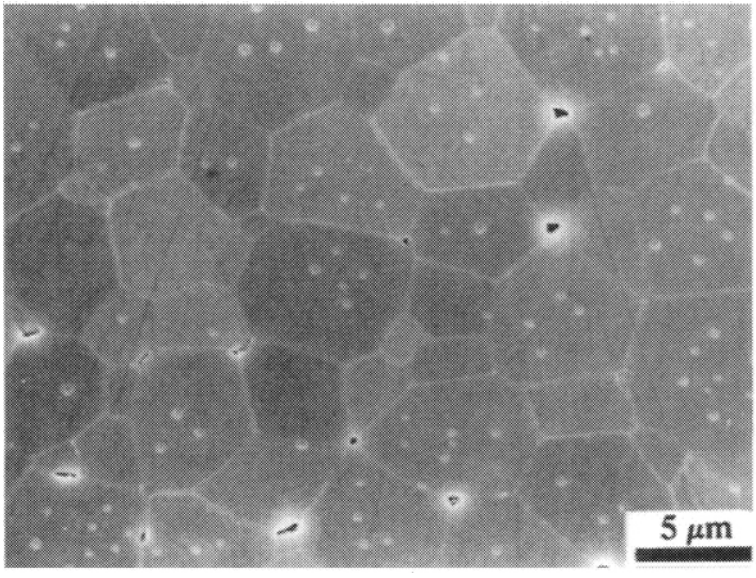

Figure 1. Microstructure of a polycrystalline ceramic showing grains (crystals), grain boundaries, and pores.

controls the engineering properties, generally is the most important feature of the fabricated material. The term *microstructure* refers to the nature, quantity, and distribution of the phases (including porosity) in the ceramic. The achievement of a controlled microstructure forms the primary goal of the fabrication process. Many properties tend to improve with high density and fine grain size and thus a dense, fine-grained microstructure is required for many advanced applications.

Close attention must be paid to each processing step in the fabrication route if the very specific properties required of many ceramics are to be achieved. Each step has the potential for producing in the body undesirable microstructural *flaws*, which can limit the properties and reliability of the item. The powder characteristics and the forming method control the particle packing of the green body which, in turn, has a significant influence on the microstructural evolution during the firing stage. Large variations in the packing density lead to microstructural heterogeneities (e.g., large voids) during firing, which can provide sources of failure in the fabricated article.

The following sections outline the processes and reactions for control of the microstructure in ceramics for the forming and firing stages. Liquids and organic additives are commonly used as processing aids during the forming step, and these must be removed prior to firing. The drying and binder removal steps must also be considered because they can provide serious limitations for microstructural control. The approach used here is to highlight the key principles and parameters. The practical details of the methods are not described, but key references are given appropriately in the text.

(M. N. RAHAMAN)

Further Reading

M. N. Rahaman, *Ceramic Processing and Sintering*, Marcel Dekker, New York, 1995.
R. J. Brook, ed., *Processing of Ceramics*, Vols. 17A and 17B: *Materials Science and Technology*, VCH, Weinheim, 1995.
R. M. German, *Sintering Theory and Practice*, Wiley, New York, 1996.

17.2.3.2. Forming

The common methods used for forming ceramic powders into a porous, shaped article are summarized in Table 1. The specific method to be adopted will depend in each case on the shape and size of the green body as well as on the manufacturing cost. However, for each method, an important partical consideration is the extent to which the parameters can be manipulated to control the packing uniformity and packing density of the green body. For high density in the fired article, uniform particle packing and a high packing density are desirable. Geometrical particle packing concepts provide a useful basis for understanding the structure of the green body[1,2].

While forming methods are the focus of the present section, two factors have a significant effect on the ability to control the geometry and structure of the green body: the use of additives that are commonly polymeric and the stability of colloidal suspensions.

Additives serve a variety of functions in forming[3], which may be divided into four categories: binders, plasticizers, dispersants (also referred to as deflocculants), and lubricants.

Binders are organic substances consisting of long chain molecules. They serve to improve the strength of the green body, to provide plasticity to a powder system during

Inorganic Reactions and Methods, Volume 18
Edited by J. J. Zuckerman, Jim D. Atwood

controls the engineering properties, generally is the most important feature of the fabricated material. The term *microstructure* refers to the nature, quantity, and distribution of the phases (including porosity) in the ceramic. The achievement of a controlled microstructure forms the primary goal of the fabrication process. Many properties tend to improve with high density and fine grain size and thus a dense, fine-grained microstructure is required for many advanced applications.

Close attention must be paid to each processing step in the fabrication route if the very specific properties required of many ceramics are to be achieved. Each step has the potential for producing in the body undesirable microstructural *flaws*, which can limit the properties and reliability of the item. The powder characteristics and the forming method control the particle packing of the green body which, in turn, has a significant influence on the microstructural evolution during the firing stage. Large variations in the packing density lead to microstructural heterogeneities (e.g., large voids) during firing, which can provide sources of failure in the fabricated article.

The following sections outline the processes and reactions for control of the microstructure in ceramics for the forming and firing stages. Liquids and organic additives are commonly used as processing aids during the forming step, and these must be removed prior to firing. The drying and binder removal steps must also be considered because they can provide serious limitations for microstructural control. The approach used here is to highlight the key principles and parameters. The practical details of the methods are not described, but key references are given appropriately in the text.

(M. N. RAHAMAN)

Further Reading

M. N. Rahaman, *Ceramic Processing and Sintering*, Marcel Dekker, New York, 1995.
R. J. Brook, ed., *Processing of Ceramics*, Vols. 17A and 17B: *Materials Science and Technology*, VCH, Weinheim, 1995.
R. M. German, *Sintering Theory and Practice*, Wiley, New York, 1996.

17.2.3.2. Forming

The common methods used for forming ceramic powders into a porous, shaped article are summarized in Table 1. The specific method to be adopted will depend in each case on the shape and size of the green body as well as on the manufacturing cost. However, for each method, an important partical consideration is the extent to which the parameters can be manipulated to control the packing uniformity and packing density of the green body. For high density in the fired article, uniform particle packing and a high packing density are desirable. Geometrical particle packing concepts provide a useful basis for understanding the structure of the green body[1,2].

While forming methods are the focus of the present section, two factors have a significant effect on the ability to control the geometry and structure of the green body: the use of additives that are commonly polymeric and the stability of colloidal suspensions.

Additives serve a variety of functions in forming[3], which may be divided into four categories: binders, plasticizers, dispersants (also referred to as deflocculants), and lubricants.

Binders are organic substances consisting of long chain molecules. They serve to improve the strength of the green body, to provide plasticity to a powder system during

TABLE 1. FEED MATERIALS AND SHAPES OF THE GREEN BODY FOR THE COMMON CERAMIC FORMING METHODS

Forming Method		Feed Material	Shape of Green Body
Dry or semidry pressing	Die compaction	Powder or free-flowing granules	Small simple shapes
	Isostatic pressing	Powder or fragile granules	Larger, more intricate shapes
Casting of a concentrated suspension	Slip casting	Free-flowing slurry with low binder content	Thin intricate shapes
	Tape casting	Free-flowing slurry with high binder content	Thin sheets
Plastic deformation of a mixture	Extrusion	Moist mixture of powder and binder solution	Elongated shapes with uniform cross section
	Injection molding	Granulated mixture of powder and solid binder	Small intricate shapes

forming (e.g., extrusion and injection molding), or to provide flexibility of the formed material (e.g., tape casting). Compared to binders, *plasticizers* are usually lower molecular weight organic substances. The plasticizer molecules disrupt the chain alignment and reduce the van der Waals bonding between adjacent polymer chains of the binder. They act to reduce the binder viscosity in forming (e.g., in injection molding) or to increase the flexibility of the formed material (e.g., tapes). *Dispersants* are either inorganic or organic substances. They act to stabilize a suspension against flocculation and so play a key role in the casting methods (slip casting and tape casting). *Lubricants* are used to reduce the friction between the particles of the feed material or between the particles and the die during consolidation.

The selection of additives, particularly for methods employing a high concentration of additives, is a vital step in the forming process. An understanding of the chemical, mechanical, and rheological properties of the additives is important for the forming step. The thermal decomposition characteristics are also important because in almost all partical systems, the additives must be removed prior to densification of the body during the firing step. The use of binders that decompose to produce a material having the same composition as the ceramic powder (e.g., Si_3N_4) has been investigated[4]. However, the high cost of such binders limits their use in industrial applications.

Techniques for the achievement of *colloid stability*[5,6] provide considerable benefits for control of the packing density and packing uniformity of the green body in the forming methods that involve the casting of suspensions. Because of the need to control shrinkage during drying and firing, the suspensions used for the forming of ceramics are fairly concentrated ($\sim$20–50 vol % of particles). They are commonly referred to as *slurries*.

In aqueous solvents (commonly used in slip casting), stabilization of the suspension is achieved by electrostatic repulsion[7]. Stabilization can be controlled by means of inorganic electrolytes (acids, bases, or salts) through adsorption of charged ions on the surfaces of the particles. In organic solvents (widely used in tape casting), polymeric dispersants are generally assumed to produce stabilization by steric repulsion[8]. High

molecular weight organic polymers that either adsorb or chemically bond onto the surfaces of the particles provide the most effective stabilization. The use of ionic polymers (referred to as *polyelectrolytes*) as dispersants is increasing steadily[9]. Adsorption of the ionized polymer molecules onto the particle surfaces is believed to produce stabilization predominantly by electrostatic repulsion for larger interparticle distances (greater than ~20 nm). At shorter distances, steric stabilization becomes dominant.

(M. N. RAHAMAN)

1. D. J. Cumberland, R. J. Crawford, *The Packing of Particles*, Elsevier, New York, 1987.
2. R. M. German, *Particle Packing Characteristics*, Metal Powder Industries Federation, Princeton, NJ, 1989.
3. D. J. Shanefield, *Organic Additives and Ceramic Processing*, Kluwer Academic Publications, Boston, 1995.
4. K. B. Schwartz and D. J. Rowcliffe, *J. Am. Ceram. Soc., 69*, C106 (1986).
5. J. W. Goodwin, ed., *Colloidal Deispersions*, The Royal Society of Chemistry, London, 1982.
6. F. F. Lange, *J. Am. Ceram. Soc., 72*, 3 (1989).
7. R. J. Hunter, *Foundations of Colloidal Science*, Vols. 1 and 2, Oxford University Press, Oxford, 1995.
8. D. H. Napper, *Polymeric Stabilization of Colloidal Dispersions*, Academic Press, New York, 1983.
9. J. Cesarano III, I. A. Aksay, A. Bleier, *J. Am. Ceram. Soc., 71*, 250 (1988).

17.2.3.2.1. Pressing of Dry or Semidry Powders.

Pressing of dry or semidry powders in a die (*die pressing*) is one of the most widely used forming methods in the ceramic industry. It allows formation of relatively simple shapes rapidly and with accurate dimensions. However, the agglomeration of relatively dry powders and the nonuniform transmission of the applied pressure during compaction lead to significant variation in the packing density of the green body. To minimize the density variation, die pressing is used for relatively simple shapes (e.g., disks) with a length to diameter ratio of less than 0.5–1.0.

Die pressing involves the simultaneous compaction and shaping of a powder in a rigid die. The overall process consists of filling the die, compacting the powder, and ejecting the compacted material. The agglomeration of fine powders (particle size < 5–10 μm) limits their flow properties and hinders the efficient filling of the die. In industrial practice, where fast pressing rates and reproducible properties of the pressed article are required, it is often necessary to form the powders into granules (e.g., by spray-drying) prior to pressing[1].

The compaction process is a complex many-body problem[2]. However, it can be divided into two stages. After die filling, the initial structure of the powder will, in general, contain large voids with sizes on the order of the particle (or granule) size or greater, and voids that are smaller than the particle (or granule) size. The first stage of compaction involves reduction of the large voids by sliding or rearrangement of the particles or granules (Fig. 1). In the second stage, the small voids are reduced by fracture of the particles. In the case of relatively soft ceramics (e.g., NaCl), plastic flow can also lead to a reduction of the small voids. The particles also undergo elastic compression in the second stage.

The dependence of the density of the powder compact on the applied pressure is commonly used to characterize the compaction stage. Because of the complex nature of

Inorganic Reactions and Methods, Volume 18
Edited by J. J. Zuckerman, Jim D. Atwood

molecular weight organic polymers that either adsorb or chemically bond onto the surfaces of the particles provide the most effective stabilization. The use of ionic polymers (referred to as *polyelectrolytes*) as dispersants is increasing steadily[9]. Adsorption of the ionized polymer molecules onto the particle surfaces is believed to produce stabilization predominantly by electrostatic repulsion for larger interparticle distances (greater than ~20 nm). At shorter distances, steric stabilization becomes dominant.

(M. N. RAHAMAN)

1. D. J. Cumberland, R. J. Crawford, *The Packing of Particles*, Elsevier, New York, 1987.
2. R. M. German, *Particle Packing Characteristics*, Metal Powder Industries Federation, Princeton, NJ, 1989.
3. D. J. Shanefield, *Organic Additives and Ceramic Processing*, Kluwer Academic Publications, Boston, 1995.
4. K. B. Schwartz and D. J. Rowcliffe, *J. Am. Ceram. Soc.*, *69*, C106 (1986).
5. J. W. Goodwin, ed., *Colloidal Deispersions*, The Royal Society of Chemistry, London, 1982.
6. F. F. Lange, *J. Am. Ceram. Soc.*, *72*, 3 (1989).
7. R. J. Hunter, *Foundations of Colloidal Science*, Vols. 1 and 2, Oxford University Press, Oxford, 1995.
8. D. H. Napper, *Polymeric Stabilization of Colloidal Dispersions*, Academic Press, New York, 1983.
9. J. Cesarano III, I. A. Aksay, A. Bleier, *J. Am. Ceram. Soc.*, *71*, 250 (1988).

17.2.3.2.1. Pressing of Dry or Semidry Powders.

Pressing of dry or semidry powders in a die (*die pressing*) is one of the most widely used forming methods in the ceramic industry. It allows formation of relatively simple shapes rapidly and with accurate dimensions. However, the agglomeration of relatively dry powders and the nonuniform transmission of the applied pressure during compaction lead to significant variation in the packing density of the green body. To minimize the density variation, die pressing is used for relatively simple shapes (e.g., disks) with a length to diameter ratio of less than 0.5–1.0.

Die pressing involves the simultaneous compaction and shaping of a powder in a rigid die. The overall process consists of filling the die, compacting the powder, and ejecting the compacted material. The agglomeration of fine powders (particle size < 5–10 μm) limits their flow properties and hinders the efficient filling of the die. In industrial practice, where fast pressing rates and reproducible properties of the pressed article are required, it is often necessary to form the powders into granules (e.g., by spray-drying) prior to pressing[1].

The compaction process is a complex many-body problem[2]. However, it can be divided into two stages. After die filling, the initial structure of the powder will, in general, contain large voids with sizes on the order of the particle (or granule) size or greater, and voids that are smaller than the particle (or granule) size. The first stage of compaction involves reduction of the large voids by sliding or rearrangement of the particles or granules (Fig. 1). In the second stage, the small voids are reduced by fracture of the particles. In the case of relatively soft ceramics (e.g., NaCl), plastic flow can also lead to a reduction of the small voids. The particles also undergo elastic compression in the second stage.

The dependence of the density of the powder compact on the applied pressure is commonly used to characterize the compaction stage. Because of the complex nature of

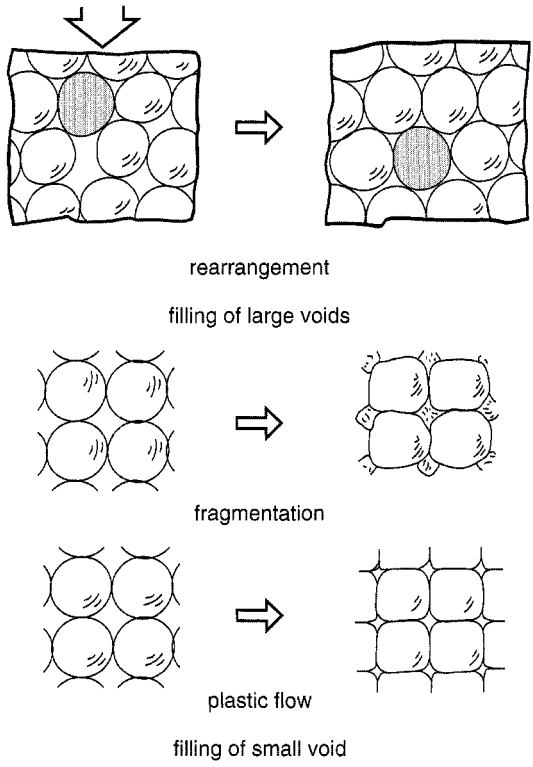

Figure 1. Mechanisms of compaction of particles or granules in a die. (Reprinted from R. J. Brook, ed., *Concise Encyclopedia of Advanced Ceramic Materials*, copyright (© 1991, p. 114, with kind permission from Elsevier Science Ltd.)

the compaction process, theoretical analysis is difficult. A number of empirical compaction equations have been developed to describe the experimental data. However, none have been found to be generally applicable, and the equations have been criticized as being merely curve fitting. One equation that has the advantage of simplicity and is as good as any of the others is:

$$p = \alpha + \beta \ln\left(\frac{1}{1-\rho}\right) \tag{a}$$

where p is the applied pressure, ρ is the relative density, and α and β are material constants.

The most severe problem in compaction is that the applied pressure is not transmitted uniformly to the powder because of friction between the powder and the die wall. To characterize the problem, the distribution in density in a powder compact has been measured by several methods, including microhardness, X-ray radiography, and quantitative microscopy. Another approach has been to use finite element and other techniques in calculating the stress distribution, hence the density distribution, in a powder

compact[2]. In a third approach, model experiments have been performed to study the dependence of the friction at the die wall on key parameters of the process[3].

In the ejection of the compact, the release of pressure is accompanied by a slight expansion of the powder compact (referred to as *strain recovery, strain relaxation, or springback*), consisting of an instantaneous elastic component as well as a time-dependent plastic component. A large amount of strain recovery can lead to defects, such as delamination and microcracks. The amount of strain recovery increases with increasing applied pressure and, generally, with higher binder content. The problem of defects is commonly alleviated by a trial-and-error approach involving changes in the pressure and binder content as well as reduction in the rate of release of the pressure.

Isostatic pressing is the application of a uniform hydrostatic pressure to the powder contained in a flexible rubber container. The method alleviates many of the problems associated with die pressing but is used less often industrially because of the greater difficulties of automation. Compared to die pressing, the more uniform transmission of pressure to the powder and the higher pressure capability can be used to produce a more uniform and higher packing density in the green body.

(M. N. RAHAMAN)

1. K. Masters, *Spray Drying*, 4th ed., Wiley, New York, 1985.
2. D. Bortzmeyer, in *Ceramic Processing*, R. A. Terpstra, P. P. A. C. Pex, A. H. de Vries, eds., Chapman & Hall, New York, 1995, pp. 102–146.
3. S. Strijbos, A. Broese van Groenou, P. A. Vermeer, *J. Am. Ceram. Soc.*, *62*, 57 (1979).

17.2.3.2.2. Casting of Concentrated Suspensions.

The forming methods based on the casting of slurries consist of slip casting and tape casting. Both methods require a relatively stable slurry with the highest concentration of particles but with viscosity low enough for the slurry to be poured during casting. The selection of additives and the formulation of the slurry are vital steps in the methods. The application of scientific principles has been hampered because many additive formulations have been treated as proprietary information. Furthermore, many slurry formulations have been developed on a trial-and-error basis.

A major difference between the two methods is the process by which the liquid is removed from the slurry. In slip casting, the liquid is removed by capillary suction provided by a porous mold. In contrast, the liquid is removed by evaporation in tape casting. In most tape casting processes, the liquid is nonaqueous because the higher volatility allows faster evaporation.

(i) Slip Casting. In slip casting, a slurry is poured into a microporous plaster of Paris mold (Fig. 1). The porous mold provides a capillary suction pressure of ~ 0.1–0.2 MPa, which draws liquid from the slurry into the mold. A consolidated layer of particles, referred to as the *cast* (or cake), forms on the walls of the mold. When the cast has become sufficiently thick, the surplus slurry is poured out and the mold and cast are allowed to dry. Normally, the cast shrinks away from the mold during drying and can be easily removed.

As shown in Figure 1, the filtrate (liquid) passes through porous media of two types: the consolidated layer (the cast) and the porous mold. The flow of liquid through a porous medium is described by Darcy's law which, in one dimension, can be written

Inorganic Reactions and Methods, Volume 18
Edited by J. J. Zuckerman, Jim D. Atwood

compact[2]. In a third approach, model experiments have been performed to study the dependence of the friction at the die wall on key parameters of the process[3].

In the ejection of the compact, the release of pressure is accompanied by a slight expansion of the powder compact (referred to as *strain recovery, strain relaxation, or springback*), consisting of an instantaneous elastic component as well as a time-dependent plastic component. A large amount of strain recovery can lead to defects, such as delamination and microcracks. The amount of strain recovery increases with increasing applied pressure and, generally, with higher binder content. The problem of defects is commonly alleviated by a trial-and-error approach involving changes in the pressure and binder content as well as reduction in the rate of release of the pressure.

Isostatic pressing is the application of a uniform hydrostatic pressure to the powder contained in a flexible rubber container. The method alleviates many of the problems associated with die pressing but is used less often industrially because of the greater difficulties of automation. Compared to die pressing, the more uniform transmission of pressure to the powder and the higher pressure capability can be used to produce a more uniform and higher packing density in the green body.

(M. N. RAHAMAN)

1. K. Masters, *Spray Drying*, 4th ed., Wiley, New York, 1985.
2. D. Bortzmeyer, in *Ceramic Processing*, R. A. Terpstra, P. P. A. C. Pex, A. H. de Vries, eds., Chapman & Hall, New York, 1995, pp. 102–146.
3. S. Strijbos, A. Broese van Groenou, P. A. Vermeer, *J. Am. Ceram. Soc.*, *62*, 57 (1979).

17.2.3.2.2. Casting of Concentrated Suspensions.

The forming methods based on the casting of slurries consist of slip casting and tape casting. Both methods require a relatively stable slurry with the highest concentration of particles but with viscosity low enough for the slurry to be poured during casting. The selection of additives and the formulation of the slurry are vital steps in the methods. The application of scientific principles has been hampered because many additive formulations have been treated as proprietary information. Furthermore, many slurry formulations have been developed on a trial-and-error basis.

A major difference between the two methods is the process by which the liquid is removed from the slurry. In slip casting, the liquid is removed by capillary suction provided by a porous mold. In contrast, the liquid is removed by evaporation in tape casting. In most tape casting processes, the liquid is nonaqueous because the higher volatility allows faster evaporation.

(i) Slip Casting. In slip casting, a slurry is poured into a microporous plaster of Paris mold (Fig. 1). The porous mold provides a capillary suction pressure of ~ 0.1–0.2 MPa, which draws liquid from the slurry into the mold. A consolidated layer of particles, referred to as the *cast* (or cake), forms on the walls of the mold. When the cast has become sufficiently thick, the surplus slurry is poured out and the mold and cast are allowed to dry. Normally, the cast shrinks away from the mold during drying and can be easily removed.

As shown in Figure 1, the filtrate (liquid) passes through porous media of two types: the consolidated layer (the cast) and the porous mold. The flow of liquid through a porous medium is described by Darcy's law which, in one dimension, can be written

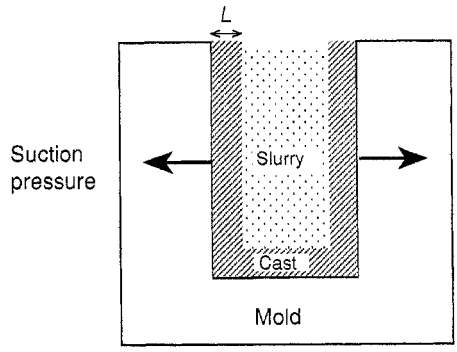

Figure 1. Slip casting in a porous mold.

as follows:

$$J = \frac{K(dp/dx)}{\eta_L} \tag{a}$$

where J is the flux of liquid, dp/dx is the pressure gradient in the liquid, η_L is the viscosity of the liquid, and K is the permeability of the porous medium. As indicated by equation (a), a pressure gradient is essential for flow to occur. It is found by assuming a force balance across any plane of the cast. By solving Darcy's law, the thickness of the cast L is given by[1]:

$$L^2 = \frac{2Hpt}{\eta_L} \tag{b}$$

where the function H depends on the properties of both the consolidated layer and the mold. It is defined by:

$$H = \frac{1}{(V_c/V_s - 1)\left[\frac{1}{K_c} + \frac{(V_c/V_s - 1)}{P_m K_m}\right]} \tag{c}$$

where V_c is the volume fraction of solids in the cast, V_s is the volume fraction of solids in the slip, P_m is the porosity of the mold, and K_m and K_c are the permeabilities of the mold and cast, respectively.

For a given system of mold and slurry, the function H is constant, and equation (b) predicts that the thickness of the cast, L, is proportional to $t^{1/2}$. The rate of consolidation therefore decreases with time, and this limits the usefulness of the slip casting route to a certain thickness of the cast (typically a few centimetrs). The rate of consolidation also depends on the viscosity of the filtrate η_L and the capillary suction pressure p. As outlined earlier, the microstructural uniformity of the green body is of great importance. A flocculated slip leads to the production of a cast with a fairly high porosity and with density variations. A well-dispersed slip containing no agglomerates and stabilized by electrostatic or steric repulsion leads to the formation of a fairly dense cast with better microstructural uniformity. In practice, the fairly dense cast formed from a well-dispersed slip has a low permeability, hence a low casting rate. For industrial operations where

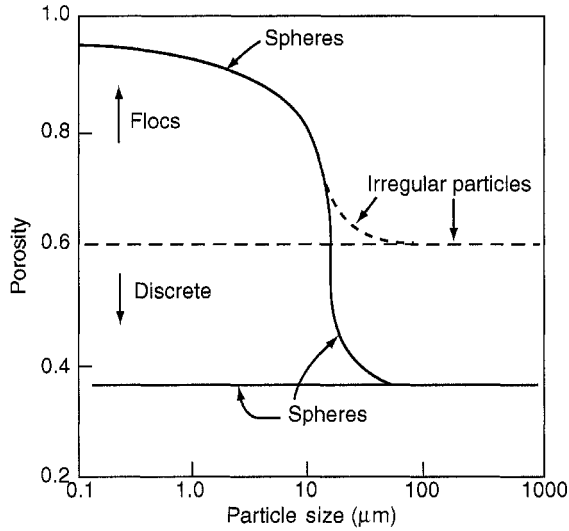

Figure 2. Schematic diagram showing the effects of particle size, shape, and degree of flocculation on the porosity of the cast produced in slip casting.

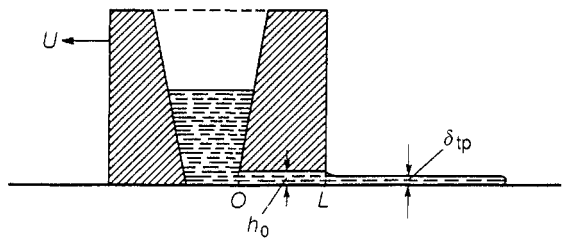

Figure 3. Section of a tape casting unit. (After Ref. 2.)

such low casting rates are uneconomical, the slip is only partially deflocculated. In addition to the degree of dispersion of the slip, other parameters such as the size, size distribution, and shape of the particles can also influence the process. Figure 2 summarizes, schematically, the effects of some of these variables on the packing density of the cast.

(ii) Tape Casting. In tape casting, also referred to as the *doctor blade process*, the slurry is spread over a surface covered with a removable sheet of plastic (e.g., cellulose acetate) by means of an adjustable doctor blade that is mounted in a frame with a reservoir for the slurry (Fig. 3). During drying, the tape adheres to the carrier surface so that the shrinkage occurs in the thickness.

The principles of fluid dynamics have been used to analyze the flow behavior of the slurry during the casting of the tape[2]. Assuming that the slurry can be treated as

a Newtonian viscous fluid, the thickness of the dry tape δ_{tp} is:

$$\delta_{tp} = \frac{\alpha\beta}{2}\frac{\rho_w}{\rho_{tp}} h_0\left(1 + \frac{h_0^2 \Delta p}{6\eta UL}\right) \tag{d}$$

where α (< 1) and β (< 1) are correction factors, ρ_w and ρ_{tp} are the densities of the slurry and the dry tape, respectively, h_0 is the height of the doctor blade, Δp is the pressure difference, η is the viscosity of the slurry, U is the velocity of the doctor blade relative to the casting surface, and L is the thickness of the doctor blade (Fig. 3). For $\eta > 10P$, the tape thickness is almost independent of the velocity, U, even for small velocities. The analysis indicates that a fairly rapid casting operation can be maintained without any deleterious effects on the thickness of the tape.

Equation (d) describes the effects of the physical and geometrical parameters on the thickness of the tape. While an understanding of these factors is useful, the success of the tape casting process, as outlined earlier, depends critically on the selection of additives and the formulation of the slurry[3]. Homogeneous mixing of the components and the removal of particle agglomerates and entrapped gases from the slurry are two practical factors that influence the success of the process. In addition, careful attention is necessary to ensure drying of the tapes and removal of a significant amount of additives during binder burnout without cracking, warping, or inhomogeneous shrinkage.

(M. N. RAHAMAN)

1. F. M. Tiller, C.-D. Tsai, *J. Am. Ceram. Soc.*, *69*, 882 (1986).
2. Y. T. Chou, Y. T. Ko, M. F. Yan, *J. Am. Ceram. Soc.*, *70*, C280 (1987).
3. R. E. Mistler, in *Ceramic Processing*, R. A. Terpstra, P. P. A. C. Pex, A. H. de Vries, eds., Chapman & Hall, New York, 1995, pp. 147–173.

17.2.3.2.3. Plastic Deformation of Powder Mixtures.

Plastic deformation of a moldable powder–additive mixture is employed in a number of forming methods. Of these, extrusion and injection molding are receiving much interest. Extrusion of a moist clay–water mixture is used extensively in the traditional ceramic industry for forming components with a regular cross section (e.g., cylinders, tiles, bricks). It is also used as a forming method for some oxide ceramics in advanced applications (e.g., catalyst supports, capacitor tubes, electrical insulators). Injection molding of a powder–binder mixture is a potentially useful method for the mass production of ceramic articles with complex shapes. However, the removal of a high concentration of binder prior to firing of the formed article remains a limiting step for thicknesses greater than $\sim$1 cm. Application of extrusion and injection molding to the forming of ceramic powders has benefited considerably from the principles and technology developed in the plastics industry. Extruders and molding machines used in the plastics industry are employed with modification for ceramic systems (e.g., hardening of the contact surfaces).

Two basic requirements must be satisfied for plastic forming to be successful. First, the mixture must flow plastically (above a certain yield stress) for formation of the desired shape. Second, the shaped article must be strong enough to resist deformation under the force of gravity or under stresses associated with handling. These two requirements are particularly important in extrusion, where the powder mixture contains a limited amount of binder and the shaped article must be dried after forming. As in casting methods, the

Inorganic Reactions and Methods, Volume 18
Edited by J. J. Zuckerman, Jim D. Atwood

a Newtonian viscous fluid, the thickness of the dry tape δ_{tp} is:

$$\delta_{tp} = \frac{\alpha\beta}{2}\frac{\rho_w}{\rho_{tp}} h_0\left(1 + \frac{h_0^2 \Delta p}{6\eta UL}\right) \qquad \text{(d)}$$

where α (< 1) and β (< 1) are correction factors, ρ_w and ρ_{tp} are the densities of the slurry and the dry tape, respectively, h_0 is the height of the doctor blade, Δp is the pressure difference, η is the viscosity of the slurry, U is the velocity of the doctor blade relative to the casting surface, and L is the thickness of the doctor blade (Fig. 3). For $\eta > 10P$, the tape thickness is almost independent of the velocity, U, even for small velocities. The analysis indicates that a fairly rapid casting operation can be maintained without any deleterious effects on the thickness of the tape.

Equation (d) describes the effects of the physical and geometrical parameters on the thickness of the tape. While an understanding of these factors is useful, the success of the tape casting process, as outlined earlier, depends critically on the selection of additives and the formulation of the slurry[3]. Homogeneous mixing of the components and the removal of particle agglomerates and entrapped gases from the slurry are two practical factors that influence the success of the process. In addition, careful attention is necessary to ensure drying of the tapes and removal of a significant amount of additives during binder burnout without cracking, warping, or inhomogeneous shrinkage.

(M. N. RAHAMAN)

1. F. M. Tiller, C.-D. Tsai, *J. Am. Ceram. Soc.*, *69*, 882 (1986).
2. Y. T. Chou, Y. T. Ko, M. F. Yan, *J. Am. Ceram. Soc.*, *70*, C280 (1987).
3. R. E. Mistler, in *Ceramic Processing*, R. A. Terpstra, P. P. A. C. Pex, A. H. de Vries, eds., Chapman & Hall, New York, 1995, pp. 147–173.

17.2.3.2.3. Plastic Deformation of Powder Mixtures.

Plastic deformation of a moldable powder–additive mixture is employed in a number of forming methods. Of these, extrusion and injection molding are receiving much interest. Extrusion of a moist clay–water mixture is used extensively in the traditional ceramic industry for forming components with a regular cross section (e.g., cylinders, tiles, bricks). It is also used as a forming method for some oxide ceramics in advanced applications (e.g., catalyst supports, capacitor tubes, electrical insulators). Injection molding of a powder–binder mixture is a potentially useful method for the mass production of ceramic articles with complex shapes. However, the removal of a high concentration of binder prior to firing of the formed article remains a limiting step for thicknesses greater than $\sim$1 cm. Application of extrusion and injection molding to the forming of ceramic powders has benefited considerably from the principles and technology developed in the plastics industry. Extruders and molding machines used in the plastics industry are employed with modification for ceramic systems (e.g., hardening of the contact surfaces).

Two basic requirements must be satisfied for plastic forming to be successful. First, the mixture must flow plastically (above a certain yield stress) for formation of the desired shape. Second, the shaped article must be strong enough to resist deformation under the force of gravity or under stresses associated with handling. These two requirements are particularly important in extrusion, where the powder mixture contains a limited amount of binder and the shaped article must be dried after forming. As in casting methods, the

selection of additives and the formulation of the mixture are critical steps in the forming process.

(i) Extrusion. In extrusion, the requirements for plastic forming can be satisfied by three different approaches: manipulation of the characteristics of the powder–solvent system, addition of fine particles of an inorganic phase that is compatible with the powder composition, and addition of a polymeric binder system. A combination of a fine second phase and a polymeric binder is also used in a few systems.

In the first approach, commonly used for plastic forming of clay–water mixtures, the plasticity arises from two main factors: particle-to-particle bonding (due to the charged particle surfaces and intervening charges) and surface tension effects (due to the presence of water). The second approach is applicable to powder systems in which surface charges and surface tension do not play a significant role (e.g., coarse particles). An example is the addition of boehmite (AlOOH) particles to a coarse Al_2O_3 powder system. In the third approach, a binder system is incorporated into the powder–solvent mixture to provide the required plasticity. Binders that produce a rapid increase in the viscosity of the solvent with increasing binder concentration (often referred to as *high viscosity* binders) are commonly used in extrusion. Methyl cellulose binders can display the property of *thermal gelling* (i.e., marked change in the rheological behavior with temperature), which has been used to great advantage to closely control the rheological behavior of the system during mixing and extrusion.

The flow pattern of the powder mixture through the extruder influences the quality of the shaped article. The rheology of concentrated ceramic suspensions can be divided into four classes: ideal plastic, Bingham, shear thinning, and shear thickening (dilant).

Bingham-type behavior is widely observed and forms a useful approximation for theoretical analysis. The pressure variation and velocity profile for plastic flow of a Bingham-type material in a cylindrical tube have been analyzed[1]. A characteristic feature of the velocity profile is the occurrence of *differential flow* with a central plug. The velocity, which is constant with radius in the central plug, decreases with radius between the central plug and the inner wall of the tube. In more extreme situations there may be *slippage flow* or *complete plug flow*, in which the velocity of the material through the extruder is independent of the radius of the tube.

Attempts have been made to relate the extrusion pressure and the strength of the green body to the water content of the plastic mixture. For a wide range of clays, the extrusion pressure p has been observed to depend on the water content w according to the equation:

$$p = A \exp(-\alpha w) \tag{a}$$

where A and α are parameters that depend on the clay composition. The parameter α can be related experimentally to the degree of flocculation of the clay. An equation with the same functional form was derived theoretically using the principles of soil mechanics[2]. The principles of soil mechanics have also been used to derive an equation for the strength of the extruded material with water content and with the consolidation pressure[2].

A variety of flaws can occur in the shaped article, and their elimination is a primary concern[3]. Commonly, a practical approach involving modifications of the formulation of the powder mixture, the extrusion parameters and the die design is used to reduce the problems associated with the formation of flaws.

(ii) Injection Molding. The formation of a green body by injection molding[4,5] can be divided into two main steps: formulation of the mixture and molding in the die cavity to produce the form. In formulation of the mixture, the required rheology is imparted to the system by means of organic additives consisting of at least three components: a *binder*, a *plasticizer*, and a *processing aid* (*lubricant* or *dispersant*). The binder controls the rheology of the system during mixing and forming, as well as the strength of the molded article and the binder burnout characteristics. Because thermoplastic polymers flow in a highly viscous manner when heated and do so reversibly on being heated and cooled, they have commonly been preferred as the major binder. However, waxes and thermosetting resins have also been used. The plasticizer is used to improve the flow characteristics or to reduce the glass transition temperature during mixing and molding. It may also extend the temperature range of the binder removal step. The processing aid may serve as a lubricant during mixing or as a dispersant for the powder.

The volume fraction of the powder that can be incorporated in the mixture depends on the particle size and the particle size distribution. It is an important parameter because it controls the particle packing density of the green body. For a dry powder, the maximum packing fraction V_m increases with the width of the size distribution. However, to achieve flow during forming, the particles are separated by a layer of polymer so that the actual volume fraction, V, in the mixture is 5–10% less than V_m. The particle size effect arises because for fine powders (commonly used for the production of ceramics), the thickness of the adsorbed polymer layer increases with decreasing particle size. Homogeneous mixing of the constituents is important for reducing flows during forming as well as during binder removal and firing. The presence of agglomerates in the powder, a common problem, is alleviated by the use of mixers operating at a high shear rates.

Ceramic powder formulations used in injection molding correspond to polymer systems that are highly filled with a finely divided, hard, brittle phase. In view of the many variables of the molding process, it may be more useful to consider the complications introduced into the molding of an unfilled polymer by the presence of the high volume fraction of ceramic phase in the mixture. In filling the mold cavity, flow behavior and stress distribution would be more complex, particularly in regions with sharp angles. After mold filling, the melt must be cooled. Because of the ceramic phase, the filled system will have a higher thermal diffusivity, which will lead to a faster cooling rate of the molded article. The solidified layer will have a higher elastic modulus than the unfilled polymer and will resist deformation. Faster cooling will lead to the development of thermal stresses that cannot be relaxed easily because of the stiffness of the solidified layer. As a result, residual stresses will build up in the article. The filled polymer will be prone to formation of internal flaws and cracks. Careful modification of process variables is required to alleviate the problem of residual stresses.

(M. N. RAHAMAN)

1. E. Buckingham, *Proc. ASTM, 21*, 1154 (1921).
2. M. A. Janney, in *Ceramic Processing*, R. A. Terpstra, P. P. A. C. Pex, A. H. de Vries, eds., Chapman & Hall, New York, 1995, pp. 174–211.
3. G. C. Robinson, in *Ceramic Processing Before Firing*, G. Y. Onoda, L. L. Hench, eds., Wiley, New York, 1978, pp. 391–407.
4. R. M. German, A. Bose, *Injection Molding of Metals and Ceramics*. Metal Powder Industries Federation, Princeton, NJ, 1996.
5. B. C. Mutsuddy, R. G. Ford, *Ceramic Injection Molding*, Chapman & Hall, New York, 1996.

Inorganic Reactions and Methods, Volume 18
Edited by J. J. Zuckerman, Jim D. Atwood

17.2.3.3. Drying

Moist green bodies produced by the forming methods described earlier must be dried prior to binder burnout and firing. An understanding of the key parameters is essential for conducting the drying step economically and for the control of defects (e.g., cracking or wraping) during the drying step[1].

(M. N. RAHAMAN)

1. G. W. Scherer, *J.Am. Ceram. Soc., 73*, 3 (1990).

17.2.3.3.1. Physical Principles of Drying.

Experimentally, drying curves (Fig. 1) show two distinct regions: a constant rate period (CRP), which is followed by a falling rate period (FRP). In the CRP, the evaporation rate is constant and shrinkage of the article occurs. At the end of the CRP, shrinkage stops and the FRP begins.

When evaporation starts, the temperature of the surface of the body drops because of a loss of heat due to the latent heat of vaporization of the liquid. However, heat flow to the surface from the atmosphere quickly establishes thermal equilibrium. The temperature of the surface becomes steady (and is refered to as the *wet-bulb temperature*). The rate of evaporation during the CRP can be described by:

$$\dot{V}_E = H(p_W - p_A) \qquad \text{(a)}$$

where p_W is the vapour pressure of the liquid at the surface, p_A is the ambient vapour pressure, and H is a factor that depends on the temperature, the velocity of the drying atmosphere, and the geometry of the system.

Initially, the system consists of a granular solid in which the particles are surrounded by a layer of liquid. For green bodies formed by extrusion and tape casting, the pores will

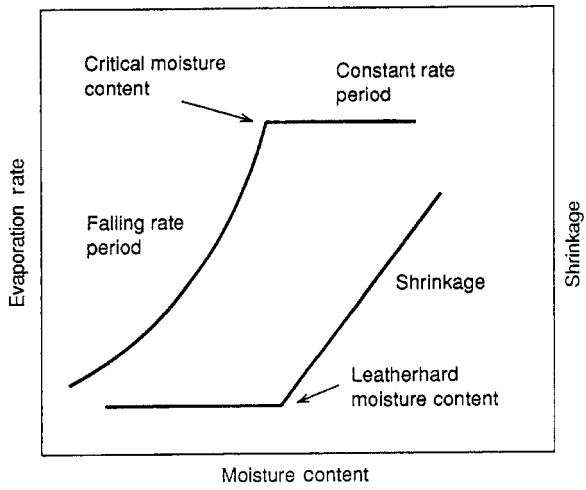

Figure 1. Schematic diagram showing evaporation rate and shrinkage as functions of the moisture content for the drying of a granular solid.

Inorganic Reactions and Methods, Volume 18
Edited by J. J. Zuckerman, Jim D. Atwood

17.2.3.3. Drying

Moist green bodies produced by the forming methods described earlier must be dried prior to binder burnout and firing. An understanding of the key parameters is essential for conducting the drying step economically and for the control of defects (e.g., cracking or wraping) during the drying step[1].

(M. N. RAHAMAN)

1. G. W. Scherer, *J.Am. Ceram. Soc., 73*, 3 (1990).

17.2.3.3.1. Physical Principles of Drying.

Experimentally, drying curves (Fig. 1) show two distinct regions: a constant rate period (CRP), which is followed by a falling rate period (FRP). In the CRP, the evaporation rate is constant and shrinkage of the article occurs. At the end of the CRP, shrinkage stops and the FRP begins.

When evaporation starts, the temperature of the surface of the body drops because of a loss of heat due to the latent heat of vaporization of the liquid. However, heat flow to the surface from the atmosphere quickly establishes thermal equilibrium. The temperature of the surface becomes steady (and is refered to as the *wet-bulb temperature*). The rate of evaporation during the CRP can be described by:

$$\dot{V}_E = H(p_W - p_A) \qquad \text{(a)}$$

where p_W is the vapour pressure of the liquid at the surface, p_A is the ambient vapour pressure, and H is a factor that depends on the temperature, the velocity of the drying atmosphere, and the geometry of the system.

Initially, the system consists of a granular solid in which the particles are surrounded by a layer of liquid. For green bodies formed by extrusion and tape casting, the pores will

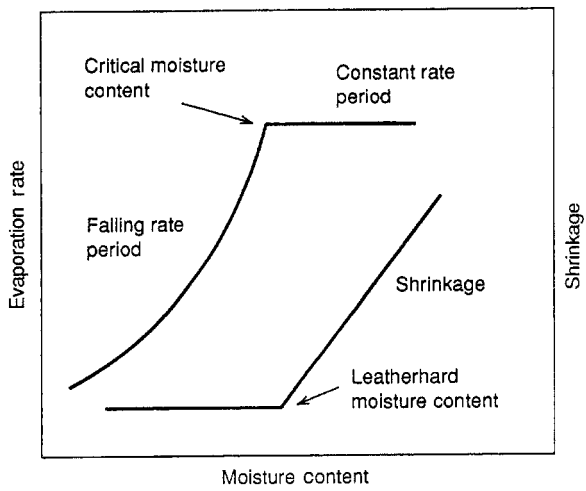

Figure 1. Schematic diagram showing evaporation rate and shrinkage as functions of the moisture content for the drying of a granular solid.

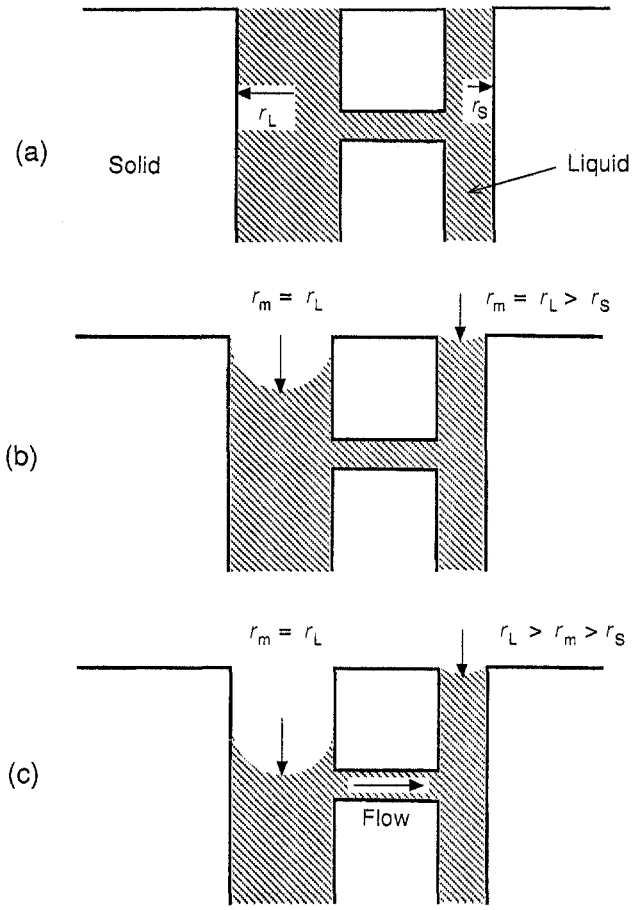

Figure 2. Evaporation and liquid flow during drying. The large pore empties first, while the liquid meniscus is maintained at the surface of the small pore; then the small pore empties.

also be filled with liquid. As an approximation, we will assume that the pores are cylindrical. As evaporation starts, a dry surface region is created and the liquid stretches to cover the dry region (to reduce the free energy of the system). A hydrostatic tension develops in the liquid, the magnitude of which is related to the radius of curvature, r, of the meniscus:

$$p = -\frac{2\gamma_{LV}}{r} \tag{b}$$

where γ_{LV} is the surface tension of the liquid. The tension in the liquid is balanced by compressive stresses on the solid phase. The compressive stresses cause the body to contract, and the *liquid meniscus remains at the surface.* As drying proceeds, the particles achieve a denser packing and the body becomes stiffer. The liquid meniscus at the surface

deepens [i.e., r in equation (b) becomes smaller], and the tension in the liquid increases. The particles, surrounded by a thin layer of bound water, eventually, touch, and shrinkage stops. This forms the end of CRP.

When shrinkage stops, further evaporation drives the meniscus into the body and the rate of evaporation falls (i.e., the FRP begins). The point at which the rate starts to fall is the critical moisture content. In the initial part of the FRP (sometimes referred to as the first FRP), most of the evaporaation occurs at the exterior surface. Contiguous pathways exist along which liquid can flow to the surface. At the same time, some liquid evaporates in the pores and the vapour diffuses to the surface. Eventually, a stage is reached when the liquid near the outside of the body becomes isolated into pockets. Flow to the surface stops, and the liquid is removed (predominantly by diffusion of the vapor). This stage is sometimes referred to as the second FRP.

In practice, the pores do not have the same radius. Let us consider a model in which interconnectaed pores of two different radii are present (Fig. 2a). Even though the pores have different radii (r_L and r_S), initially liquid evaporates from them at the same rate so that the radii of the menisci (r_m) are equal. As evaporation proceeds after shrinkage has stopped, a point is reached at which the radius of the menisci is equal to the radius of the large pore, (i.e., $r_m = r_L$: Fig. 2b). Further evaporation forces the liquid to retreat into the large pore. However, the radius of the meniscus, r_m, will continue to decrease in the samll pore, and the capillary tension will suck liquid from the large pore (Fig. 2c). In this way the large pore empties first and small pore remains full of liquid. After the large pore has been emptied, the small pore starts to empty. The same principles apply to a distribution of pore sizes and pore shapes. Thus, considerable redistribution of the liquid occurs during drying. Furthermore, the evaporation front is not expected to move uniformly into the body. Instead, pore channels first develop deep into the body as liquid from the larger pores is drawn into the smaller pores.

(M. N. RAHAMAN)

17.2.3.3.2. Drying Defects.

Cracking and warping during drying are caused by differential strain due to pressure gradients in the liquid and inhomogeneities in the body produced by imperfect forming operations. If the tension p in the liquid is uniform, there is no differential stress in the solid phase. However, when p varies through the thickness, the body tends to contract more where p is high and the differential strain causes wraping or cracking.

For a cylindrical pore of radius a, the maximum tension in the liquid occurs when the radius of the meniscus is small enough to fit in the pore; that is, when r in equation (b) (17.2.3.3.1) is:

$$r = \frac{a}{\cos\theta} \tag{a}$$

where θ is the contact angle. If the evaporation rate is high, the tension in the liquid can reach its maximum value at the surface while the average tension in the interior of the body is still small. The total stress at the surface of the body is then:

$$\sigma = \frac{2\gamma_{LV}\cos\theta}{a} \tag{b}$$

For clay–water mixtures with a particle size in the 0.5–1 μm range, assuming $\theta = 0$, $\gamma_{LV} = 0.07\,J/m^2$, and the pore size equal to half the particle size gives $\sigma_x \approx 0.5\,MPa$. Unfired ceramics containing little binder are very weak, and this stress is high enough to cause cracking.

During the constant rate period, the boundary condition at the surface of body is given by[1]:

$$\dot{V}_E = \frac{K}{\eta_L} \nabla p \Big|_{surface} \tag{c}$$

where V_E is the evaporation rate, K is the permeability of the body, η_L is the viscosity of the liquid, and ∇p is the pressure gradient in the liquid. According to equation (c), a fast evaporation rate leads to high ∇p. To avoid cracking or warping, the body must be dried slowly. However, the "safe" drying rates may be so slow that the drying times needed are prohibitively extensive. To increase the safe drying rates, a few procedures can be used. According to equation (c), for a given V_E, ∇p decreases with higher K and lower η_L. According to one form of the Karman-Kozeny relation[2], the permeability can be estimated from:

$$K = \frac{D^2(1 - V_c)^3}{36\alpha V_c^2} \tag{d}$$

where D is the particle size, V_c is the volume fraction of solids in the dried material, and α is the Kozeny constant ($=5$ for many ststems), which defines the shape and tortuosity of the flow channels. According to equation (d), K increases roughly as the square of the particle size or the pore size. One approach is to use larger particle size or to mix a coarse filler with the particles. However, this approach is often impractical because it can lead to a reduction of the densification rate in the firing stage. Another approach, based on a decrease in η_L is used practically in "high humidity drying," where the process is carried out at slightly elevated temperatures ($\approx 70°C$) and high ambient humidity in the drying atmosphere. Increase in the temperature leads to a decrease in η_L (by a factor of ≈ 2) and also increases the rate of drying. However, the increase in the drying rate is counteracted by increasing the ambient humidity [see equation (b), (17.2.3.3.1)]. In this way a reasonable drying rate is achieved while keeping ∇p small.

Even if the moist body is dried uniformly and at a safe rate, inhomogeneities produced by imperfect forming operations can still lead to cracking and wraping. As indicated earlier (see Fig. 1 in 17.2.3.3.1), regions with higher moisture content (above the leatherhard value) undergo higher shrinkage. Differential shrinkage due to moisture gradients is a common source of cracking and wraping. Gradients in the particle size caused, for example, by preferential settling can also lead to differential shrinkage. In this case, the coarser particles settle at the bottom while the finer ones settle at the top. The top of the body with the finer particles will be expected to undergo a larger shrinkage.

(M. N. RAHAMAN)

1. G. W. Scherer, *J. Am. Ceram. Soc.*, *73*, 3 (1990).
2. J. Dodds and M. Leitselement, in *Physics of Finely Divided Matter*, Vol. 5: *Procedures in Physics*, N. Boccara, M. Daoud, eds., Springer-Verlag, Berlin, 1985, pp. 56–75.

Inorganic Reactions and Methods, Volume 18
Edited by J. J. Zuckerman, Jim D. Atwood

17.2.3.4. Binder Removal

The process of binder removal, also referred to as *debinding*, is a critical step in ceramic processing, particularly in the case of forming methods such as tape casting, extrusion, and injection molding, where the binder content is relatively high. Ideally, we would like to remove the binder completely without disrupting the packing of the particles or producing new defects in the body. Residual contaminants such as carbon and inorganic ions and defects such as cracks and large voids create additional problems in the control of the microstructure during the firing stage.

Binder removal can be accomplished by *thermal decomposition* or by *dissolutiion*. In ceramics, the thermal decomposition method is commonly used and will be considered here. The process is referred to as *thermal debinding* or, more simply, as *binder burnout*. In thermal debinding of ceramic green bodies, both chemical and physical factors are important. Chemically, composition of the binder determines the decomposition temperature and the decomposition products. Physically, the removal of the binder is controlled by heat transfer into the body and mass transport of the decomposition products out of the body.

In practice, binder system may consist of three or four additives that differ in their volatility and chemical decomposition. Furthermore, interactions between the binder and the particle surfaces may alter the decomposition kinetics of the pure polymer[1]. In view of its complex nature, a detailed analysis of thermal debinding is not useful. Instead, we consider the basic features of the process for a simplified system consisting of a powder compact with a single binder [e.g., a high molecular weight thermoplastic polymer such as poly(methyl methacrylate), poly(propylene), or poly(vinyl butyral)].

(M. N. RAHAMAN)

1. S. Masia, P. D. Calvert, W. E. Rhine, H. K. Bowen, *J. Mater. Sci.*, *24*, 1907 (1989).

17.2.3.4.1. The Process of Thermal Debinding.

The process of thermal debinding can be divided into three stages. Stage 1 involves the initial heating of the binder to a softening point ($\sim$150–200°C for a long chain termoplastic binder). Chemical decomposition and binder removal are negligible in this stage, but a number of the physical processes that occur can have important consequences for control of the shape and structural uniformity of the body and formation of flaws. These processes include shrinkage, deformation, and bubble formation.

In stage 2 (covering a temperature range on the order of 200–400°C), most of the binder is removed by evaporation and chemical decomposition. Appreciable capillary flow of the molten polymer can accompany the evaporation process. The nature of the decomposition reactions depends on the chemical composition of the polymer and on the atmosphere. In inert atmospheres, chain scission and depolymerization reactions lead to the formation of smaller chain segments or monomers, which reduce the viscosity and enhance the evaporation rate. In oxidizing atmospheres, oxidative as well as thermal degradation occurs, leading to production of a high percentage of volatile, low molecular weight compounds such as water, carbon dioxide, and carbon monoxide.

Inorganic Reactions and Methods, Volume 18
Edited by J. J. Zuckerman, Jim D. Atwood

17.2.3.4. Binder Removal

The process of binder removal, also referred to as *debinding*, is a critical step in ceramic processing, particularly in the case of forming methods such as tape casting, extrusion, and injection molding, where the binder content is relatively high. Ideally, we would like to remove the binder completely without disrupting the packing of the particles or producing new defects in the body. Residual contaminants such as carbon and inorganic ions and defects such as cracks and large voids create additional problems in the control of the microstructure during the firing stage.

Binder removal can be accomplished by *thermal decomposition* or by *dissolutiion.* In ceramics, the thermal decomposition method is commonly used and will be considered here. The process is referred to as *thermal debinding* or, more simply, as *binder burnout.* In thermal debinding of ceramic green bodies, both chemical and physical factors are important. Chemically, composition of the binder determines the decomposition temperature and the decomposition products. Physically, the removal of the binder is controlled by heat transfer into the body and mass transport of the decomposition products out of the body.

In practice, binder system may consist of three or four additives that differ in their volatility and chemical decomposition. Furthermore, interactions between the binder and the particle surfaces may alter the decomposition kinetics of the pure polymer[1]. In view of its complex nature, a detailed analysis of thermal debinding is not useful. Instead, we consider the basic features of the process for a simplified system consisting of a powder compact with a single binder [e.g., a high molecular weight thermoplastic polymer such as poly(methyl methacrylate), poly(propylene), or poly(vinyl butyral)].

(M. N. RAHAMAN)

1. S. Masia, P. D. Calvert, W. E. Rhine, H. K. Bowen, *J. Mater. Sci., 24*, 1907 (1989).

17.2.3.4.1. The Process of Thermal Debinding.

The process of thermal debinding can be divided into three stages. Stage 1 involves the initial heating of the binder to a softening point ($\sim$150–200°C for a long chain termoplastic binder). Chemical decomposition and binder removal are negligible in this stage, but a number of the physical processes that occur can have important consequences for control of the shape and structural uniformity of the body and formation of flaws. These processes include shrinkage, deformation, and bubble formation.

In stage 2 (covering a temperature range on the order of 200–400°C), most of the binder is removed by evaporation and chemical decomposition. Appreciable capillary flow of the molten polymer can accompany the evaporation process. The nature of the decomposition reactions depends on the chemical composition of the polymer and on the atmosphere. In inert atmospheres, chain scission and depolymerization reactions lead to the formation of smaller chain segments or monomers, which reduce the viscosity and enhance the evaporation rate. In oxidizing atmospheres, oxidative as well as thermal degradation occurs, leading to production of a high percentage of volatile, low molecular weight compounds such as water, carbon dioxide, and carbon monoxide.

Finally, in stage 3, the small amount of binder still remaining in the body is removed by evaporation and decomposition at temperatures above $\approx 400°C$. The highly porous nature of the body facilitates removal of the binder. However, the atmosphere will, to a large extent, control the amount of binder residue remaining in the body.

(M. N. RAHAMAN)

17.2.3.4.2. Models for Thermal Debinding.

Thermal degradation, as outlined above, leads to production of volatile, low molecular weight products throughout the binder phase and the removal of the binder by evaporation of a liquid. Binder removal by this mechanism may be quite similar to the drying of a moist granular material considered above (*17.2.3.3.1*). Considerable redistribution of the liquid occurs, and the evaporation front does not move uniformaly into the body[1]. Instead, pore channels first develop deep in the body as liquid from the larger pores is drawn into the smaller pores.

In oxidative degradation, the reaction occurs at the polymer–gas interface, which recedes into the body as degradation proceeds. The reaction products are gaseous and must be removed by diffusion or permeation through the porous outer layer. The mean free path of the gaseous reaction products determines whether diffusion or permeation controls the transport of the gases through the porous outer layer. For the model shown in Fig. 1, and assuming that the binder is removed isothermally as a single-component vapor that is low in molecular weight, the time for removal of the binder depends on several parameters, as summarized in Table 1 for diffusion and permeation control[2]. In both cases, small particle size and low porosity reduce the rate of binder removal. However, small particle size and low porosity enhance densification during the firing step. A conflict therefore exists between rapid removal of the binder and the achievement of high densification.

One solution of the conflict might involve the use of a sintering aid to enhance densification during firing. Table 1 also indicates that a low ambient pressure or a vacuum serves to reduce the time for binder removal. A vacuum, however, does not lead to oxidative degradation. Furthermore, temperature control and transport of heat are

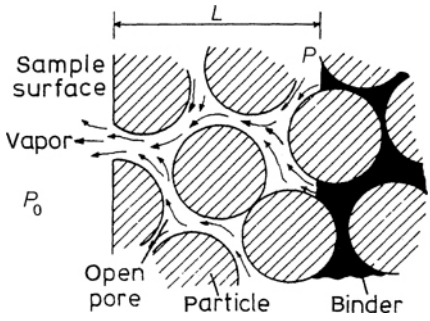

Figure 1. Model for thermal debinding by oxidative degradation where the binder–vapor interface is at a distance L from the surface of the compact. (After Ref. 2.)

TABLE 1. EFFECT OF PROCESS VARIABLES ON THE TIME FOR THERMAL DEBINDING BY OXIDATIVE DEGRADATION

Process Variable	Diffusion Control	Permeation Control
Powder particle size	D^{-1}	D^{-2}
Porosity of green body	P^{-2}	$(1 - P^2)/P^2$
Thickness of green body	H^2	H^2
Viscosity of gaseous product		η
Pressure drop	$(p - p_0)^{-1}$	$p/(p^2 - p_0^2)$

Source: From Ref. 2, reprinted by permission of the Metal Powder Industries Federation.

poor in a vacuum. The use of an oxidizing gas at reduced ambient pressure may provide adequate degradation as well as good thermal transport.

(M. N. RAHAMAN)

1. M. J. Cima, J. A. Lewis, A. D. Defoe, *J. Am. Ceram. Soc.*, *72*, 1192 (1989).
2. R. M. German, *Int. J. Powder Metall.*, *23*, 237 (1987).

17.2.3.5. Firing

In the firing stage the porous shaped article is heated to produce the desired microstructure. The changes occurring during this stage may be fairly complex, depending on the complexity of the starting materials. In the ceramic literature, two terms are used to refer to this heating process: *firing* and *sintering*. Generally, the term *firing* is used when the changes occurring are fairly complex, as in the production of many traditional (clay-based) ceramics from a mixture of starting materials. In less complex cases, the term *sintering* is used. We will not emphasize the distinction between the two terms and will use them interchangeably.

The simplest case of sintering is for a pure, single-phase powder (e.g., α-Al_2O_3).The porous powder compact is heated to a temperature that is typically 0.5–0.9 of the melting temperature (e.g., in the range 1350–1650°C for Al_2O_3: mp = 2073°C). The powder does not melt; instead, atomic diffusion in the solid state produces joining of the particles and reduction in porosity (i.e., densification) of the body. This type of sintering is referred to as *solid state sintering*. While the microstructural changes are not simple, the understanding of solid state sintering is considerable.

A common difficulty in solid state sintering is that duffusion may be so slow that high densities are difficult to achieve. One solution is application of pressure to the body during heating, giving the method of *pressure sintering* (hot pressing is a common example). Another solution is use of an additive that forms a small amount of liquid phase between the grains at the sintering temperature. This method is referred to as *liquid phase sintering*.

Our approach to the firing stage will be to consider the physical principles of solid state sintering and then to consider how the sintering process is influenced by the key process variables, including the application of an external pressure and the presence of a liquid phase.

(M. N. RAHAMAN)

Inorganic Reactions and Methods, Volume 18
Edited by J. J. Zuckerman, Jim D. Atwood

TABLE 1. EFFECT OF PROCESS VARIABLES ON THE TIME FOR THERMAL DEBINDING BY OXIDATIVE DEGRADATION

Process Variable	Diffusion Control	Permeation Control
Powder particle size	D^{-1}	D^{-2}
Porosity of green body	P^{-2}	$(1 - P^2)/P^2$
Thickness of green body	H^2	H^2
Viscosity of gaseous product		η
Pressure drop	$(p - p_0)^{-1}$	$p/(p^2 - p_0^2)$

Source: From Ref. 2, reprinted by permission of the Metal Powder Industries Federation.

poor in a vacuum. The use of an oxidizing gas at reduced ambient pressure may provide adequate degradation as well as good thermal transport.

(M. N. RAHAMAN)

1. M. J. Cima, J. A. Lewis, A. D. Defoe, *J. Am. Ceram. Soc.*, *72*, 1192 (1989).
2. R. M. German, *Int. J. Powder Metall.*, *23*, 237 (1987).

17.2.3.5. Firing

In the firing stage the porous shaped article is heated to produce the desired microstructure. The changes occurring during this stage may be fairly complex, depending on the complexity of the starting materials. In the ceramic literature, two terms are used to refer to this heating process: *firing* and *sintering*. Generally, the term *firing* is used when the changes occurring are fairly complex, as in the production of many traditional (clay-based) ceramics from a mixture of starting materials. In less complex cases, the term *sintering* is used. We will not emphasize the distinction between the two terms and will use them interchangeably.

The simplest case of sintering is for a pure, single-phase powder (e.g., α-Al_2O_3).The porous powder compact is heated to a temperature that is typically 0.5–0.9 of the melting temperature (e.g., in the range 1350–1650°C for Al_2O_3: mp = 2073°C). The powder does not melt; instead, atomic diffusion in the solid state produces joining of the particles and reduction in porosity (i.e., densification) of the body. This type of sintering is referred to as *solid state sintering*. While the microstructural changes are not simple, the understanding of solid state sintering is considerable.

A common difficulty in solid state sintering is that duffusion may be so slow that high densities are difficult to achieve. One solution is application of pressure to the body during heating, giving the method of *pressure sintering* (hot pressing is a common example). Another solution is use of an additive that forms a small amount of liquid phase between the grains at the sintering temperature. This method is referred to as *liquid phase sintering*.

Our approach to the firing stage will be to consider the physical principles of solid state sintering and then to consider how the sintering process is influenced by the key process variables, including the application of an external pressure and the presence of a liquid phase.

(M. N. RAHAMAN)

17.2.3.5.1. Principles of Solid State Sintering.

The system consists of a porous body in which, initially, the particles may be considered to be in point contact. For sintering to occur, a *thermodynamic* requirement must be satisfied: the free energy of the system must decrease. However, the *kinetics* of matter transport must also be taken into account: diffusion must be fast enough for the desired changes to be accomplished within reasonable times. The *driving force* for sinstering is the reduction in surface free energy of the particles. The surface energies of ceramics are $\sim 1\ J/m^2$ and are only weakly dependent on temperature and composition[1]. More generally, sintering can be considered to be a *chemical diffusion process* in which the driving force is a reduction in the *chemical potential* of the system.

Matter tends to move from regions of positive (convex) curvature to regions of negative (concave) curvature, thereby leading to the filling of the necks between the particles. In crystalline materials, the plane of contact between the particles (grains), referred to as the *grain boundary*, has a specific energy, γ_{gb}, called the *grain boundary energy*. This reflects the failure of crystal planes in the adjacent particles to match exactly. During sintering, part of the energy decrease due to the decrease in surface area of the particles goes into creating a new grain boundary area. The grains also have a tendency to grow by migration of the boundaries, to reduce the energy associated with the grain boundaries, As outlined later, *grain growth* can seriously limit the density.

Matter transport occurs by several mechanisms or paths. The four main mechanisms for crystalline ceramics are shown in Figure 1 for two particles. The easiest mechanisms are *surface diffusion* and *vapor transport* (evaporation/condensation). Both

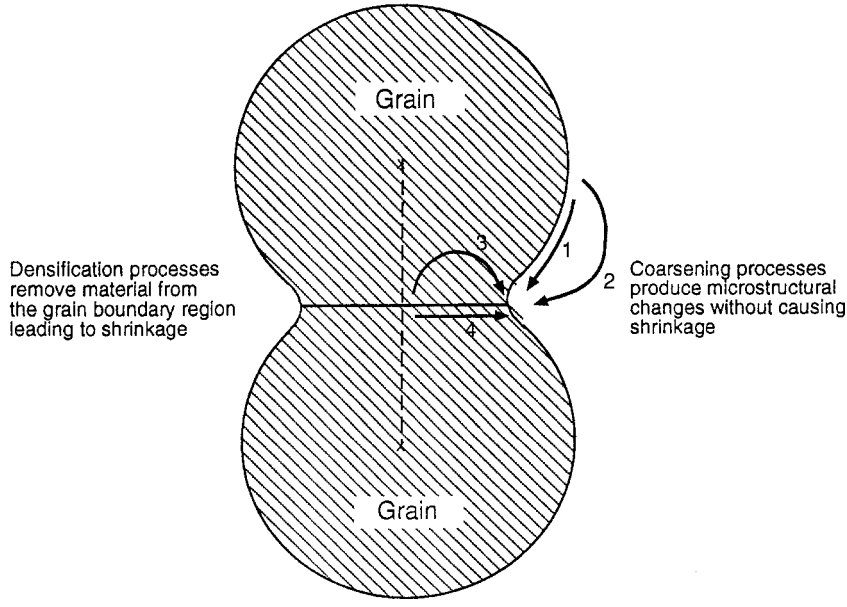

Figure 1. Schematic indication of the distinction between densifying and nondensifying mechanisms during the sintering of ceramic powders. Mechanism 1: Surface diffusion; 2: vapor transport; 3: lattice diffusion; 4: grain boundary diffusion.

mechanisms involve transport of matter from the surface of the particle to the neck, thereby reducing the surface energy. However, neither mechanism leads to densification because each one simply rearranges matter on the surfaces of the pores without reducing the volume of the pores. Surface diffusion and vapor transport produce *coarsening* of the microstructure (i.e., the particles, necks, and pores become larger). Other mechanisms (e.g., *lattice diffusion* and *grain boundary diffusion*) lead to *densification* of the body because they take matter from the contact region between the particles (the grain boundary) and deposit it into the pores, thereby reducing the pore volume.

(i) Competition Between Densification and Coarsening. A central issue in the sintering of ceramics is the relationship between densification and coarsening of the microstructure. Both processes lead to a reduction in the free energy of the powder system. However, the coarsening mechanisms (surface diffusion, vapor transport, and grain growth) also lead to a reduction in the driving force for densification. This relationship is sometimes expressed by the statement that sintering involves a competition between densification and coarsening. As shown in Figure 2(a), the domination of the densifying diffusion processes favors the production of a dense body. When coarsening processes dominate, the production of a highly porous body is favored [Fig. 2(b)]. An understanding of the key variables that influence the rates of the densifying and coarsening mechanisms is fundamental for controlling the microstructure during sintering.

(ii) Interaction Between Pores and Grain Boundaries: Thermodynamics. The thermodynamic aspects of the interaction between pore surfaces and grain boundaries must be considered because they control whether a pore will shrink or coarsen. The equilibrium pore shape is dictated by the surface energy γ_{sv} and the grain boundary energy γ_{gb}. As shown in Figure 3a, balance of forces at the junction where the surfaces of the pores meet the grain boundary leads to:

$$\cos\left(\frac{\psi}{2}\right) = \frac{\gamma_{gb}}{2\gamma_{sv}} \qquad \text{(a)}$$

where ψ is the dihedral angle. The pore surface in Figure 3a is concave (negative curvature), and since it moves toward its center of curvature, the pore will shrink. However, as shown in Figure 3b, when the pore is surrounded by a large number of grains (i.e., the *pore coordination number* is large), the balance of forces at the junction dictates that the pore surface will become convex (positive curvature). In this case the pore will grow (or become metastable).

In general, whether a pore shrinks depends on the dihedral angle and the pore coordination number[2]. For a given dihedral angle, large pores are expected to have large pore coordination numbers and will be difficult to shrink. These pores will very likely lead to residual porosity in the fired article. The importance, emphasized earlier, of controlling the particle packing during the forming step is clear.

(iii) Interaction Between Pores and Grain Boundaries: Kinetics. One consequence of the presence of grain boundaries, as outlined earlier, is that the grains will tend to grow to reduce the grain boundary area. Grain growth occurs by atom diffusion across the boundary so that the boundary migrates toward its center of curvature. In general, the larger grains (i.e., above a critical size) grow, while the smaller grains shrink and

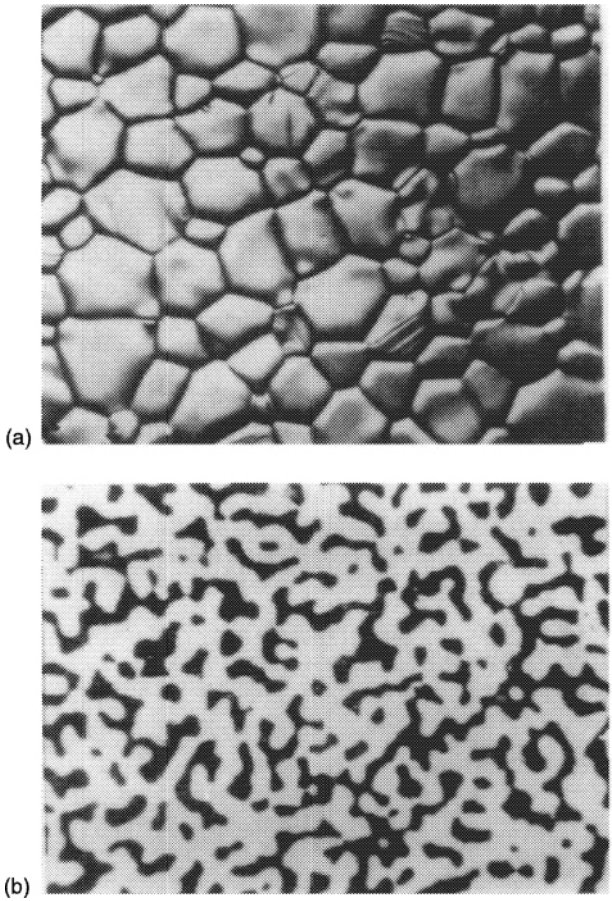

Figure 2. (a) The surface of an alumina ceramic from which all porosity has been removed during sintering; the microstructure consists of grains and the boundaries between them. (b) The sintering of silicon results in the formation of a continuous network of solid material (white) and porosity (black). The microstructural change is not accompanied by any densification. (Reprinted from R. J. Brook, ed., *Concise Encyclopedia of Advanced Ceramic Materials*, copyright (© 1991, p. 4, with kind permission from Elsevier Science Ltd.)

eventually disappear. The number of grains therefore decreases so that the average grain size increases.

A migrating boundary will apply a force on any pore situated at the boundary and will try to drag it along. As illustrated in Figure 4, the force causes the pore to change its shape. The leading surface of the pore becomes less strongly curved than the trailing surface. The difference in curvature causes a flux of matter from the leading surface to the trailing surface. The result is that the pore attempts to move with the boundary. Two situations can be visualized: either the pore remains attached to the migrating boundary

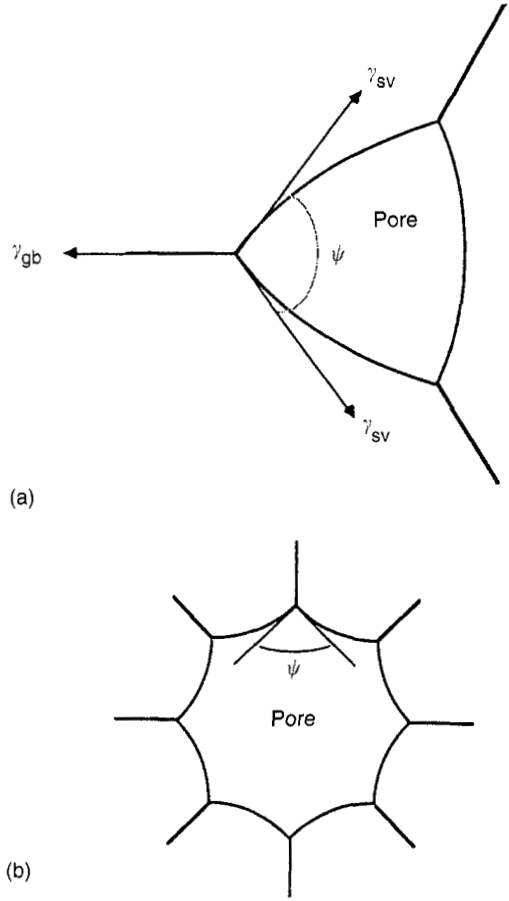

Figure 3. Pore stability is determined by the dihedral angle and the pore coordination number. (a) The pore with concave surfaces will shrink while (b) the pore with convex surfaces will grow (or become metastable).

(referred to as *attachment*) or the boundary breaks away, leaving the pore behind (*separation*).

The occurrence of attachment or separation depends on the mobility of the pores and boundaries. For a pure, single-phase material, the boundary mobility M_b is controlled by atom diffusion across the boundary[3]:

$$M_b = \frac{D_a \Omega}{kT\delta_{gb}} \tag{b}$$

where D_a is the atomic diffusion coefficient, Ω is the atomic volume, k is the Boltzmann constant, T is the absolute temperature and δ_{gb} is the thickness of the grain boundary region. As indicated in Figure 4, matter transport from the leading surface to the trailing

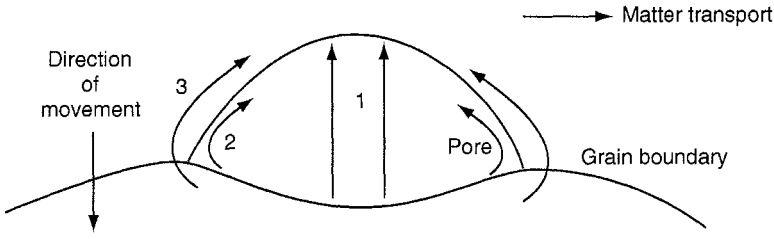

Figure 4. Possible transport paths for a pore moving with grain boundary: 1, vapor transport; 2, surface diffusion; and 3, lattice diffusion.

surface of the pore can occur by three separate mechanisms: vapor transport, surface diffusion, and lattice diffusion. For a model system with nearly spherical pores, the pore mobility M_p depends on the appropriate diffusion coefficient D for matter transport and the pore radius r[3]:

$$M_p = \frac{AD\Omega}{kTr^m} \tag{c}$$

where A is a constant and m depends on the matter transport mechanism: $m = 3$ for vapor transport and lattice diffusion and $m = 4$ for surface diffusion. According to equation (c) fine pores are highly mobile and are better able to remain attached to the boundary.

Whether a pore remains attached to the boundary or becomes separated is vital to microstructural control during sintering. Pores that become separated are difficult to shrink: in some cases the matter transport path has been eliminated (e.g., diffusion along the grain boundary), whereas at other times the rate of matter transport is very slow as a result of a large increase in the matter transport path. In general, separated pores remain as residual porosity in the sintered article and must be avoided if high density is a requirement.

(iv) Control of Grain Growth (coarsening). Rapid grain growth is detrimental to high density because it increases the diffusion distances for matter transport into the pores and also leads to separation of the pores from the boundaries. For powders with a wide distribution of sizes that have not been consolidated in a uniform manner, some form of grain growth control is necessary if the normal requirements of high density and small grain size are to be achieved.

The most effective approach involves the use of dopants that are incorporated into the powder to form a solid solution[3]. Examples of systems that have successfully used the dopant approach include Al_2O_3 (0.025 atom % Mg as dopant), $BaTiO_3$ ($\sim$1 atom % Nb), and CeO_2 (3–6 atom % Y). The effectiveness of the dopant is believed to depend on its ability to segregate at the grain boundaries, presumably by a space charge mechanism[4,5]. A mechanism in which the dopant cations (the solute) exert a drag on the moving boundary is believed to be responsible for inhibition of grain growth[6].

Another approach, which is less widely used, involves the use of fine, inert precipitates at the grain boundaries. An example is the use of 10–15 vol % ZrO_2 particles to control the grain growth of Al_2O_3. The precipitates inhibit grain growth by means of a pinning mechanism[7].

(v) Models. Theoretical analysis and experiments performed during the past 50 years or so have provided an excellent *qualitative* understanding of sintering in terms of the driving force, the mechanisms, and the effect of primary processing variables such as particle size, temperature, and applied pressure. However, the models are far less successful at providing a *quantitative* description of sintering for most systems of interest. Two factors responsible for this lack of success at the quantitative level are the available database and the complexity of the microstructural evolution in real powder compacts. The available data are commonly inadequate to predict the sintering rate under a given set of conditions. Because of the complexity of the sintering process, the models assume drastic simplifications of the microstructure. The models also ignore coarsening (grain growth), which is treated separately by grain growth models.

(vi) Models for Sintering. The main approaches used in the theoretical analysis of sintering consist of scaling laws, analytical models, and numerical simulations. The scaling laws[8] do not assume a specific geometrical model. Instead, they assume that the geometrical changes remain similar. The laws consider the effect of change of scale (e.g., particle size) on the rate of matter transport for individual mechanisms. The dependence of the rate on the particle (or grain) size G is given by:

$$\text{rate} \sim \frac{1}{G^m} \tag{d}$$

where $m = 4$ for surface diffusion and for grain boundary diffusion, $m = 2$ for vapor transport, and $m = 3$ for lattice diffusion. Since the densification rate varies as $1/G^4$ for grain boundary diffusion and as $1/G^3$ for lattice diffusion, the grain boundary path is favored for fine particles. Since, however, the rate of coarsening by surface diffusion also varies as $1/G^4$, grain boundary diffusion and surface diffusion are expected to be in competition during the sintering of fine particles.

The analytical models assume a simplified, idealized geometry and, for each mechanism, the diffusional flux equations are solved analytically to provide equations for the sintering kinetics. They also assume uniform packing and no grain growth. Even with the simplifications introduced, a single geometrical model cannot adequately represent the entire process. The sintering process is therefore conceptually divided into three sequential stages: the *initial* stage, the *intermediate* stage and the *final* stage[9]. Each stage represents an interval of density (or time) over which the geometry is considered to be well defined. In the initial stage, the pores are continuous and the necks grow by any of the mechanisms shown in Figure 1. There is also a few percent of shrinkage. The model is based on a two-sphere geometry (Fig. 1). In the intermediate stage, the model consists of polyhedral grains (14-sided, i.e., *tetrakaidecahedral*) with continuous, cylindrical pores along the edges. It is assumed that when the pores shrink to reduce their cross- section, densification occurs. Eventually, the pores become isolated and pinch off, leaving isolated pores. This marks the end of the intermediate stage. The intermediate stage normally covers the major part of the sintering process and is considered to end at a density of 0.9–0.95 of the theoretical density. The final stage model consists of tetrakaidecahedra with isolated, spherical pores at the grain corners. The pores are assumed to shrink continuously, ultimately disappearing altogether.

Equations for neck growth in the initial stage have been derived for each mechanism. While the neck growth equations were critical to the early development of sintering theory, their usefulness in practical sintering is limited. The predicted dependence of the

densification rate on the primary processing variables (temperature, particle size and applied pressure) is far more useful. For any stage of the process, the diffusional flux equations can be solved to give a densification rate equation of the form[10]:

$$\frac{1}{\rho}\frac{d\rho}{dt} = \frac{HD\Omega}{G^m KT}\left(p_a\phi + \frac{\alpha\gamma_{sv}}{r}\right) \qquad \text{(e)}$$

where $(1/\rho)d\rho/dt$ is the densification rate, H is a constant (that depends on the geometry of the model and the mechanism), Ω is the atomic volume, p_a is the applied stress, ϕ is a density-dependent term, α is a constant that depends on the geometry of the pores ($\alpha = 1$ for the initial and intermediate stages, $\alpha = 2$ for the final stage), γ_{sv} is the specific surface energy, G is the grain size, k is the Boltzmann constant, T is the absolute temperature, and r is the pore radius. The diffusion coefficient D and the grain size exponent m take on their appropriate values for a given mechanism: $D = D_l$ and $m = 2$ for lattice diffusion, $D = D_{gb}\delta_{gb}$ and $m = 3$ for grain boundary diffusion, where δ_{gb} is the grain boundary thickness.

For a given microstructure, equation (e) predicts that the densification rate will increase almost exponentially with T (owing to the strong Arrhenius dependence of D on T). For diffusional mechanisms, the rate increases linearly with applied pressure. Assuming that the pore radius scales linearly as the grain size, during sintering ($p_a = 0$), the densification is predicted to vary as $1/G^3$ for lattice diffusion and as $1/G^4$ for grain boundary diffusion (as also predicted by the scaling laws discussed earlier).

In practice, more than one mechanism operates during sintering. While sintering with *concurrent mechanisms* has been treated by the analytical models, the problem is better solved by *numerical simulations* that allow the use of more realistic geometries[11]. The approach has not achieved popularity, however, perhaps because the calculations can be fairly complex. *Sintering maps* have been constructed to show the dominant mechanisms as functions of the temperature and density[12]. The construction employs the sintering equations derived in the analytical models and data for the material parameters in the equations. Because of the inadequacy of the database and the drastic simplifications of the models, the applicability of the maps is very limited. However, they have proved useful in visualizing conceptual relationships between the various mechanisms and changes in the sintering behavior under different conditions of temperature and particle size.

(vii) Models for Grain Growth. Grain growth in ceramics is generally divided into two types: *normal* grain growth and *abnormal* grain growth, which is sometimes referred to as *exaggerated* or *discontinuous grain growth*. In normal grain growth, the average grain size increases with time but the grain size distribution remains fairly self-similar. In abnormal grain growth, a few large grains grow rapidly at the expense of the smaller grains, so that the distribution changes with time. In porous ceramics, abnormal grain growth is accompanied by breakaway of the boundaries from the pores and, as outlined earlier, must be avoided if high densities are to be achieved.

Although grain growth in porous systems is more relevant to sintering, it is useful to start with the less complex situation present in fully-dense ceramics. Normally grain growth in dense materials has been analyzed by a number of different approaches[13]. One of the earliest models[14] considered the diffusion of atoms across an isolated boundary under the driving force of the grain boundary curvature. *Mean field theories* consider the change in size of an isolated grain embedded in a matrix that represented the average

effect of the whole array of grains[13]. The early model[14] and the mean field theories ignore the topological requirements of the space-filling array of grains in a real system. Topological analysis of grain growth has been carried out[15]. More recently, the use of computer simulations has shown a remarkable ability to provide realistic pictures of grain growth and to provide a good fit to experimental data[16].

The grain growth models predict a kinetic equation of the form:

$$G^m - G_0^m = kt \tag{f}$$

where G is the grain size at time t, G_0 is the grain size at $t = 0$, and k is a temperature-dependent rate constant. For the early model[14] and for the mean field theories, $m = 2$ (i.e., parabolic growth kinetics), while the topological model predicts $m = 3$. The value $m = 2.44$ has been obtained in one set of simulations[16]. In practice, m values ranging from 2 to 4 have been observed.

In porous powder compacts, grain growth is limited in the initial stage of sintering, but surface diffusion and vapor transport can result in coarsening of the microstructure. The growth rate increases in the intermediate stage but is most pronounced in the final stage when the pores pinch off and become isolated. A model consisting of a nearly spherical pore on an isolated grain boundary has been used to analyze normal grain growth. As outlined earlier, the kinetic interaction between the pore and the boundary determines the conditions for pore attachment and breakaway. The kinetics of normal grain growth can be described by equation (f), where the exponent m (2–4) now depends on the mechanism of pore motion and the extent of the drag produced by the pores on the boundaries[3]. Experimentally, the value $m = 3$ has been observed most often.

(M. N. RAHAMAN)

1. Y.-M. Chiang, D. P. Birnie III, W. D. Kingery, *Physical Ceramics*, Wiley, New York, 1997.
2. W. D. Kingery, B. Francois, in *Sintering and Related Phenomena*, G. C. Kuczynski, N. A. Hooton, C. F. Gibbon, eds., Gordon & Breach, New York, 1967, pp. 471–498.
3. R. J. Brook, in *Treatise on Materials Science and Technology*, Vol. 9: *Ceramic Fabrication Processes*, F. F. Y. Wang, ed., Academic Press, New York, 1976, pp. 331–364.
4. K. Lehovec, *J. Chem. Phys.*, *21*, 1123 (1953).
5. J. Frenkel, *Kinetic Theory of Liquids*, Oxford University Press, Oxford, 1946.
6. J. W. Cahn, *Acta Metall.*, *10*, 789 (1962).
7. C. S. Smith, *Trans. AIME*, *175*, 15 (1948).
8. C. Herring, *J. Appl. Phys.*, *21*, 301 (1950).
9. R. L. Coble, *J. Appl. Phys.*, *32*, 787 (1961).
10. R. L. Coble, *J. Appl. Phys.*, *41*, 4798 (1970).
11. P. Bross, H. E. Exner, *Acta Metall.*, *27*, 1013 (1979).
12. M. F. Ashby, *Acta Metall.*, *22*, 275 (1974).
13. H. V. Atkinson, *Acta Metall.*, *36*, 469 (1988).
14. J. E. Burke, D. Turnbull, *Prog. Met. Phys.*, *3*, 220 (1952).
15. F. N. Rhines, K. R. Craig, *Metall. Trans.*, *5A*, 413 (1974).
16. M. P. Anderson, D. J. Srolovitz, G. S. Grest, P. S. Sahni, *Acta Metall.*, *32*, 783 (1984).

17.2.3.5.2. Experimental Observations of Solid-State Sintering.

The complex nature of the sintering process in real powder systems coupled with the drastic simplifications assumed in the models means that quantitative testing of the sintering models is seldom meaningful. Nevertheless, the models clearly indicate the parameters that must be controlled to promote densification. Because of the strong

Inorganic Reactions and Methods, Volume 18
Edited by J. J. Zuckerman, Jim D. Atwood

effect of the whole array of grains[13]. The early model[14] and the mean field theories ignore the topological requirements of the space-filling array of grains in a real system. Topological analysis of grain growth has been carried out[15]. More recently, the use of computer simulations has shown a remarkable ability to provide realistic pictures of grain growth and to provide a good fit to experimental data[16].

The grain growth models predict a kinetic equation of the form:

$$G^m - G_0^m = kt \tag{f}$$

where G is the grain size at time t, G_0 is the grain size at $t = 0$, and k is a temperature-dependent rate constant. For the early model[14] and for the mean field theories, $m = 2$ (i.e., parabolic growth kinetics), while the topological model predicts $m = 3$. The value $m = 2.44$ has been obtained in one set of simulations[16]. In practice, m values ranging from 2 to 4 have been observed.

In porous powder compacts, grain growth is limited in the initial stage of sintering, but surface diffusion and vapor transport can result in coarsening of the microstructure. The growth rate increases in the intermediate stage but is most pronounced in the final stage when the pores pinch off and become isolated. A model consisting of a nearly spherical pore on an isolated grain boundary has been used to analyze normal grain growth. As outlined earlier, the kinetic interaction between the pore and the boundary determines the conditions for pore attachment and breakaway. The kinetics of normal grain growth can be described by equation (f), where the exponent m (2–4) now depends on the mechanism of pore motion and the extent of the drag produced by the pores on the boundaries[3]. Experimentally, the value $m = 3$ has been observed most often.

(M. N. RAHAMAN)

1. Y.-M. Chiang, D. P. Birnie III, W. D. Kingery, *Physical Ceramics*, Wiley, New York, 1997.
2. W. D. Kingery, B. Francois, in *Sintering and Related Phenomena*, G. C. Kuczynski, N. A. Hooton, C. F. Gibbon, eds., Gordon & Breach, New York, 1967, pp. 471–498.
3. R. J. Brook, in *Treatise on Materials Science and Technology*, Vol. 9: *Ceramic Fabrication Processes*, F. F. Y. Wang, ed., Academic Press, New York, 1976, pp. 331–364.
4. K. Lehovec, *J. Chem. Phys.*, *21*, 1123 (1953).
5. J. Frenkel, *Kinetic Theory of Liquids*, Oxford University Press, Oxford, 1946.
6. J. W. Cahn, *Acta Metall.*, *10*, 789 (1962).
7. C. S. Smith, *Trans. AIME*, *175*, 15 (1948).
8. C. Herring, *J. Appl. Phys.*, *21*, 301 (1950).
9. R. L. Coble, *J. Appl. Phys.*, *32*, 787 (1961).
10. R. L. Coble, *J. Appl. Phys.*, *41*, 4798 (1970).
11. P. Bross, H. E. Exner, *Acta Metall.*, *27*, 1013 (1979).
12. M. F. Ashby, *Acta Metall.*, *22*, 275 (1974).
13. H. V. Atkinson, *Acta Metall.*, *36*, 469 (1988).
14. J. E. Burke, D. Turnbull, *Prog. Met. Phys.*, *3*, 220 (1952).
15. F. N. Rhines, K. R. Craig, *Metall. Trans.*, *5A*, 413 (1974).
16. M. P. Anderson, D. J. Srolovitz, G. S. Grest, P. S. Sahni, *Acta Metall.*, *32*, 783 (1984).

17.2.3.5.2. Experimental Observations of Solid-State Sintering.

The complex nature of the sintering process in real powder systems coupled with the drastic simplifications assumed in the models means that quantitative testing of the sintering models is seldom meaningful. Nevertheless, the models clearly indicate the parameters that must be controlled to promote densification. Because of the strong

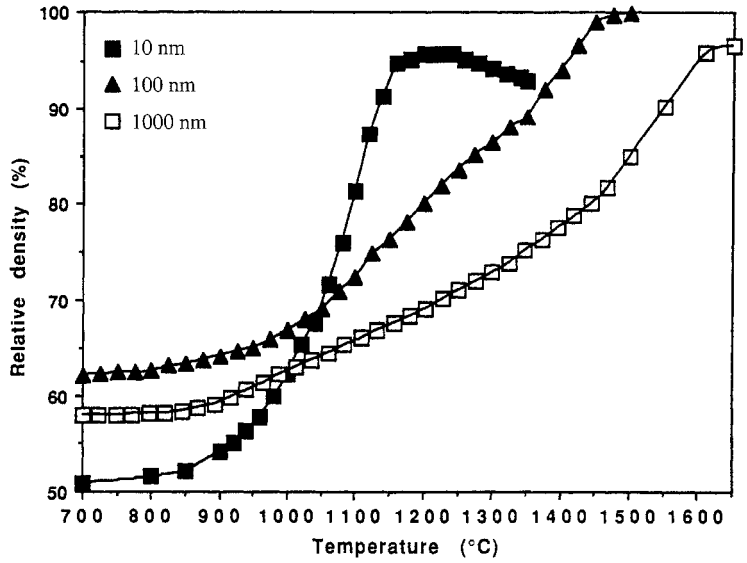

Figure 1. Data showing the effect of particle size on the densification of cerium oxide powder compacts during sintering at a constant heating rate of 10°C/min.

dependence, particle (or grain) size is a primary variable [equations (d) and (e) (17.2.3.5.1)]. The use of fine particles and the consequent increase in the densification rate have resulted in the lowering of the sintering temperatures of many ceramics by several hundred degrees (Fig. 1). Because of competing coarsening processes and nonuniformity in the particle packing, however, the observed benefit of fine particle size is generally not nearly as great as that predicted by the models.

The use of pressure sintering, of which hot pressing is the most common technique, can provide conditions that are closer to the assumptions in the models. The applied pressure enhances the densification process but has almost no effect on the coarsening process. Pressure sintering therefore provides the conditions under which densification dominates and the competing coarsening processes are relatively insignificant. The use of hot pressing has revealed a nearly linear dependence of the densification rate on applied pressure, as predicted by equation (e) (17.2.3.5.1).

The models predict an Arrhenius dependence of the densification and coarsening (grain growth) rates on the sintering temperature, and this dependence is commonly observed. In practice, an increase in the sintering temperature does not always lead to an increase in the final density because the rate of the competing coarsening processes also increases. An optimum sintering temperature is commonly found, above which the final density decreases.

While the observed dependence of the densification rate on particle size, applied pressure, and temperature follows qualitatively the predictions of the sintering models, factors such as particle packing, sintering atmosphere, and heating schedule can have a decisive effect on the sintering process.

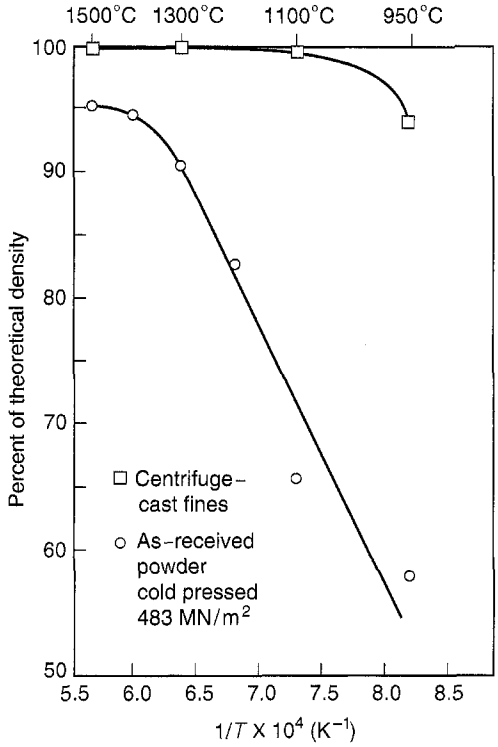

Figure 2. Effect of particle packing on the densification of yttria-stabilized zirconia powder compacts during sintering for 1h at various temperatures. The compact with the more homogeneous packing (formed by centrifugal casting of a fine, agglomerate-free powder) reaches a significantly higher density than a compact formed by die-pressing of 2.9 μm agglomerates. (After Ref. 1.)

(i) Effect of Particle Packing. The sintering models assume uniform particle packing. However, the packing in real systems is never uniform, particularly when the compact is formed from dry or semidry powders. Fine powders are prone to agglomeration, which leads to nonuniform packing in the green body and to reduced densification rates and residual porosity in the sintered body. According to the principles outlined earlier, dense, uniform particle packing leads to an enhancement in sintering because the matter transport paths (the contacts between the grains) are maximized for a minimum pore volume. One of the clearest demonstrations of the effect of packing was for the sintering of yttria-stabilized zirconia[1]. A fine powder (crystallite size 8–12 nm) synthesized by the hydrolysis of alkoxides was used to prepare a suspension, and the agglomerates were allowed to settle. The fine particles in the supernatant were then used to prepare compacts by gravitational settling in a centrifuge. After drying, the compact had a density of 0.74 of the theoretical density (i.e., equal to that for close-packed, uniform spheres). As shown in Figure 2, sintering for 1 h at 1100°C produced almost theoretical density. In comparison, compacts prepared from the as-received powder reached a

density of only 0.95 of the theoretical after sintering for 1 h at 1500°C. Additional studies of the effect of particle packing were reported[2,3].

(ii) Effect of Sintering Atmosphere. The sintering models assume an ideal sintering atmosphere that does not inhibit the sintering process. However, the atmosphere can have a dramatic effect on the rate of sintering and the ability to achieve high density with a controlled grain size. The important effects of the sintering atmosphere can be divided into two areas: gas solubility in the solid phase (particularly when the gas is trapped in isolated pores in the final stage of sintering) and chemical reactions with the powder system (particularly when the volatility, oxidation states, and defect chemistry can be modified.

In the final stage of sintering when the pores just become isolated, the pressure of the gas trapped in the pores is equal to the pressure of the atmosphere. The final density achieved in subsequent sintering is dependent on the solubility of the gas (i.e., its ability to diffuse into the solid and escape into the atmosphere). At one extreme, when the gas is very soluble in the solid, the densification rate is unaffected by the gas in the pores because rapid gas diffusion in the solid can occur during shrinkage. At the other extreme, for an insoluble gas, shrinkage of the pores leads to compression of the gas and an increase in the pressure. When the gas pressure becomes equal to the driving force for sintering, shrinkage stops. The final, limiting porosity is given by:

$$P_L = P_0\left(\frac{p_0 r_0}{2\gamma_{sv}}\right)^{2/3} \tag{a}$$

where P_0 is the porosity ($\sim$0.08–0.10) when the pores become isolated, p_0 is the gas pressure in the atmosphere (10^5 N/m^{-2} for atmospheric pressure), r_0 is the radius of the pores when they become isolated, and γ_{sv} is the specific surface energy ($\sim$1 J/m^{-2}). The limiting porosity is predicted to decrease with decreasing pressure of the sintering atmosphere and with decreasing particle (or grain size), assuming that the pore size scales as the initial particle size. Sintering in a vacuum eliminates the problem of trapped gases but is not practical for many systems that are prone to decomposition.

At some intermediate solubility, the kinetics of the gas diffusion to the surface of the solid can control the rate of final stage densification. At some lower solubility, the diffusivity in the gas is low enough to prevent escape of gases to the surface of the solid, whereupon only diffusion of gas between neighboring pores takes place. In this case, there is a net diffusion of gas from the smaller pores (higher chemical potential) to the larger pores (lower chemical potential). Because of the higher gas pressure in the smaller pores, transfer of gas leads to expansion of the larger pores. The density of the body goes through a maximum, as sketched in Figure 3.

Information on the diffusivity of gases in ceramics is normally not available, so it is difficult to predict the effects of a given gas trapped in a solid. However, diffusion of the smaller molecules (e.g., H_2 or He) will be easier than that for the larger molecules (e.g., Ar or N_2). Sintering in a vacuum, whenever it can be used, eliminates the problem of trapped gases. The significance of gases in pores was investigated[4] in the sintering of MgO^- doped Al_2O_3 to theoretical density. Complete elimination of porosity was possible in H_2, in O_2, or in vacuum but not in He, Ar, or N_2 (and, therefore, not in air).

Chemically, the sintering atmosphere can lead to a variety of effects, including evaporation of volatile constituents from the solid, decomposition of the solid, enhanced

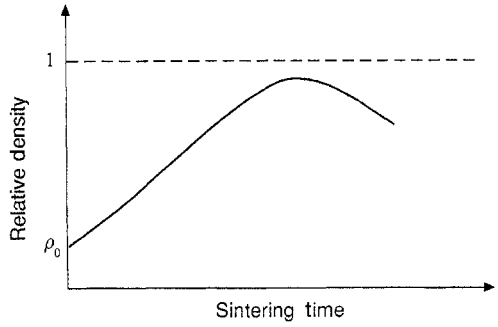

Figure 3. Schematic diagram showing the densification of a powder compact in a gaseous atmosphere that is only slightly soluble in the solid. The density goes through a maximum as a result of sintering with the trapped gas in the pores.

vapor transport, and changes in the atomic oxidation number of atoms, defect chemistry, and stoichiometry.

The evaporation of volatile constituents (e.g., Na or Pb) can occur during sintering, thereby making it difficult to control the chemical composition, hence the microstructure. A common solution is to encapsulate the green body in a powder of the same composition. The partial pressure of the vapor in the surrounding powder limits the evaporation of the volatile constituent from the body. Encapsulation in a powder is also commonly used to limit decomposition of the body. Another solution commonly used for the sintering of Si_3N_4 is raising the N_2 gas pressure in the atmosphere (1–2 Mpa).

Vapor transport, as outlined earlier, leads to coarsening of the microstructure and to a reduction in the driving force for densification. The effects of enhanced vapor transport have been clearly demonstrated through the sintering of several oxides in reducing atmospheres[5]. For example, the sintering of Fe_2O_3 in air for 5 h at 1000°C produced a density of $\sim$95% of the theoretical value. In comparison, sintering in an atmosphere of 10% HCl produced almost no increase in the green density ($\sim$47%).

The sintering atmosphere can influence the oxidation number of atoms, particularly in the transition elements. Changes in the oxidation number produce changes in the properties of the compound which can alter its sintering behavior. The oxides of Cr form a classic system in which control of the oxidation number has been vital to improving the sintering behavior[6]. The oxidation number of the Cr atom changes readily from + 6 in an atmosphere with a high O_2 partial pressure to + 4, + 3, + 2, and finally 0 as the O_2 partial pressure decreases. Each oxidation state, except the + 3 state, corresponds to an oxide with a high vapor pressure.

In the sintering of Cr_2O_3, which is the oxide of most technological interest, the O_2 partial pressure in the atmosphere must be at the value required to maintain the Cr atoms in the + 3 oxidation state. The O_2 partial pressure ($\sim 10^{-12}$ atm) can be determined readily from an Ellingham diagram. Sintering at this O_2 partial pressure produces the maximum density ($\sim$99% of the theoretical value). In comparison, sintering in O_2 partial pressures in the range of 10^{-9} to 1 atm produced a density of below 75%. The ferrites are an important class of magnetic ceramics where both the oxidation number and stoichiometry must be controlled to produce the desired properties[7].

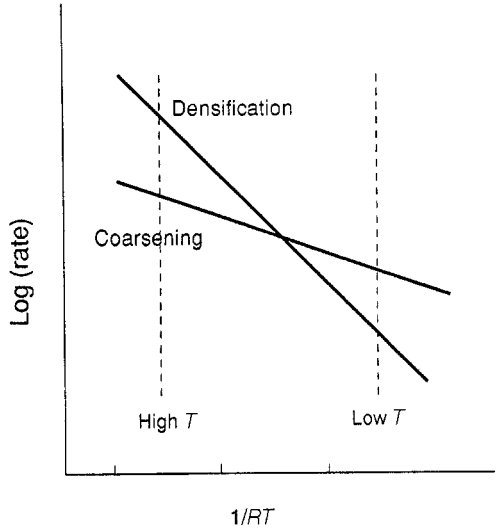

Figure 4. When the densification mechanism has a higher activation energy than the coarsening mechanism, a fast heating rate to high firing temperatures (rapid sintering) can lead to the production of high densities.

(iii) Effect of Heating Schedule. The models assume that the sintering temperature is constant (i.e., isothermal sintering) and that it is reached instantaneously. In practice, because of the thermal mass of the furnace and the low thermal conductivity of many ceramics, the body must be heated at some reasonable rate to the desired sintering temperature. The heating schedule, consisting in the simplest case of the heating rate and the isothermal sintering temperature, provides another important parameter that can be manipulated to control the final microstructure.

As outlined earlier, the coarsening mechanisms (surface diffusion and vapor transport) are expected to dominate at lower temperatures, while the densifying mechanisms (grain boundary diffusion and lattice diffusion) are expected to dominate at higher temperatures. Assuming that the activation energy for coarsening is lower than that for densification, high sintering temperatures lead to an enhancement of the ratio of the densification rate to the coarsening rate (Fig. 4). Furthermore, the faster the body is heated through the low temperature region (where the ratio is unfavorable), the more the extent of coarsening is reduced. According to these principles, rapid heating to a high enough temperature can provide favorable conditions for achievement of high density with controlled grain size[8]. The validity of these principles has been well demonstrated in the rapid sintering (fast firing) of Al_2O_3 and $BaTiO_3$. However, the rapid sintering approach has not been successful for MgO, a system for which the conditions are believed to be unfavorable. In practice, the low thermal conductivity of most ceramics limits the rapid sintering approach to small or thin articles. For large articles, the initially higher surface temperature leads to densification of a surface layer that later hinders the densification of the interior.

(M. N. RAHAMAN)

1. W. H. Rhodes, *J. Am. Ceram. Soc., 64,* 19 (1981).
2. E. A. Barringer, H. K. Bowen, *J. Am. Ceram. Soc., 85,* C199 (1982).
3. T.-S. Yeh, M. D. Sacks, *Ceram. Trans., 7,* 309 (1990).
4. R. L. Coble, *J. Am. Ceram. Soc., 45,* 123 (1962).
5. D. W. Readey, *Ceram. Trans., 7,* 86 (1990).
6. P. D. Ownby, G. E. Jungquist, *J. Am. Ceram. Soc., 55,* 433 (1972).
7. T. Reynolds III, in *Treatise on Materials Science,* Vol. 9: Ceramic Fabrication Processes, F. F. Y. Wang, ed., Academic Press, New York, 1976, pp. 195–215.
8. R. J. Brook, *Proc. Br. Ceram. Soc., 32,* 7 (1982).

17.2.3.5.3. Pressure Sintering.

The term *pressure sintering* refers to sintering with an externally applied pressure. The two techniques used for the fabrication of ceramics are *hot pressing*, where the pressure is applied uniaxially to the powder in a die[1], and *hot isostatic pressing*, where the pressure is applied isostatically by means of a gas[2]. In practice, because of the high fabrication costs, pressure sintering is used when high density coupled with fine grain size must be guaranteed. The method is particularly useful for powders that cannot be adequately densified by sintering. Examples include highly covalent bonded nonoxide ceramics (e.g., Si_3N_4 and SiC) and fiber-reinforced composites.

The sintering mechanisms outlined earlier also operate during pressure sintering. However, for the commonly used pressures (e.g., 25–50 Mpa in hot pressing and 100–200 MPa in hot isostatic pressing), the coarsening mechanisms can be neglected because they are relatively unaffected by the pressure while the densifying mechanisms are significantly enhanced [equation (e), (17.2.3.5.1)]. The applied pressure can also activate new mechanisms. *Rearrangement* of the particles contributes to densification in the initial stage but is difficult to analyze theoretically. Dislocation motion can occur for a few ceramics in the initial stages of densification; for commonly used pressures, however, diffusion is still the dominant mechanism for matter transport.

In hot pressing, *grain boundary sliding* is necessary to accommodate the grain shape changes that occur during diffusional transport. Diffusional transport and grain boundary sliding are not independent mechanisms. They occur sequentially, so that the slower mechanism controls the rate of densification. Furthermore, because the pressure is applied uniaxially in hot pressing, the microstructure may develop some *texturing*, exhibiting preferential orientation of the grains or enhanced grain growth in the direction perpendicular to the pressing direction (Fig. 1). In hot isostatic pressing, grain boundary sliding is unnecessary and texturing is absent.

Commonly, the applied pressure is much greater than the driving force for sintering, and as a result, equation (e) of (17.2.3.5.1) becomes:

$$\frac{1}{\rho}\frac{d\rho}{dt} = \frac{HD\Omega}{G_m KT}(p_a\phi)^n \tag{a}$$

where the exponent n depends on the mechanism of densification. Since pressure sintering corresponds to the situation in which coarsening processes are relatively insignificant, the comparison of experimentally derived values for the exponents m and n with the theoretical values can provide valuable information about the mechanism of densification. For the possible mechanisms in pressure sintering, the theoretical values of the exponents are as follows: lattice diffusion, $m = 2$, $n = 1$; grain boundary diffusion,

Inorganic Reactions and Methods, Volume 18
Edited by J. J. Zuckerman, Jim D. Atwood

1. W. H. Rhodes, *J. Am. Ceram. Soc., 64,* 19 (1981).
2. E. A. Barringer, H. K. Bowen, *J. Am. Ceram. Soc., 85,* C199 (1982).
3. T.-S. Yeh, M. D. Sacks, *Ceram. Trans., 7,* 309 (1990).
4. R. L. Coble, *J. Am. Ceram. Soc., 45,* 123 (1962).
5. D. W. Readey, *Ceram. Trans., 7,* 86 (1990).
6. P. D. Ownby, G. E. Jungquist, *J. Am. Ceram. Soc., 55,* 433 (1972).
7. T. Reynolds III, in *Treatise on Materials Science,* Vol. 9: Ceramic Fabrication Processes, F. F. Y. Wang, ed., Academic Press, New York, 1976, pp. 195–215.
8. R. J. Brook, *Proc. Br. Ceram. Soc., 32,* 7 (1982).

17.2.3.5.3. Pressure Sintering.

The term *pressure sintering* refers to sintering with an externally applied pressure. The two techniques used for the fabrication of ceramics are *hot pressing*, where the pressure is applied uniaxially to the powder in a die[1], and *hot isostatic pressing*, where the pressure is applied isostatically by means of a gas[2]. In practice, because of the high fabrication costs, pressure sintering is used when high density coupled with fine grain size must be guaranteed. The method is particularly useful for powders that cannot be adequately densified by sintering. Examples include highly covalent bonded nonoxide ceramics (e.g., Si_3N_4 and SiC) and fiber-reinforced composites.

The sintering mechanisms outlined earlier also operate during pressure sintering. However, for the commonly used pressures (e.g., 25–50 Mpa in hot pressing and 100–200 MPa in hot isostatic pressing), the coarsening mechanisms can be neglected because they are relatively unaffected by the pressure while the densifying mechanisms are significantly enhanced [equation (e), (17.2.3.5.1)]. The applied pressure can also activate new mechanisms. *Rearrangement* of the particles contributes to densification in the initial stage but is difficult to analyze theoretically. Dislocation motion can occur for a few ceramics in the initial stages of densification; for commonly used pressures, however, diffusion is still the dominant mechanism for matter transport.

In hot pressing, *grain boundary sliding* is necessary to accommodate the grain shape changes that occur during diffusional transport. Diffusional transport and grain boundary sliding are not independent mechanisms. They occur sequentially, so that the slower mechanism controls the rate of densification. Furthermore, because the pressure is applied uniaxially in hot pressing, the microstructure may develop some *texturing*, exhibiting preferential orientation of the grains or enhanced grain growth in the direction perpendicular to the pressing direction (Fig. 1). In hot isostatic pressing, grain boundary sliding is unnecessary and texturing is absent.

Commonly, the applied pressure is much greater than the driving force for sintering, and as a result, equation (e) of (17.2.3.5.1) becomes:

$$\frac{1}{\rho}\frac{d\rho}{dt} = \frac{HD\Omega}{G_m KT}(p_a\phi)^n \tag{a}$$

where the exponent n depends on the mechanism of densification. Since pressure sintering corresponds to the situation in which coarsening processes are relatively insignificant, the comparison of experimentally derived values for the exponents m and n with the theoretical values can provide valuable information about the mechanism of densification. For the possible mechanisms in pressure sintering, the theoretical values of the exponents are as follows: lattice diffusion, $m = 2$, $n = 1$; grain boundary diffusion,

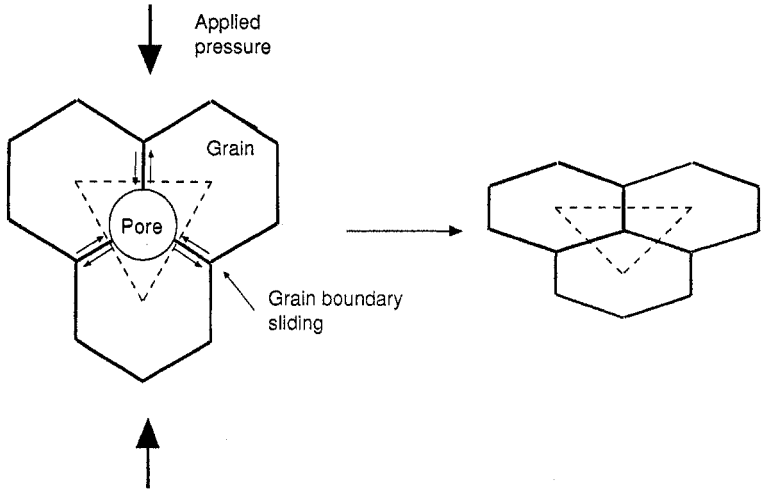

Figure 1. Development of microstructural texture that can occur during hot pressing: the grains are flattened in the direction of the applied pressure. For matter transport by diffusion, grain boundary sliding is necessary to accommodate the change in grain shape.

$m = 3$, $n = 1$; dislocation motion, $m = 0$, $n \geq 3$; and grain boundary sliding, $m = 1$, $n = 1$ or 2.

(M. N. RAHAMAN)

1. M. P. Harmer, in *Concise Encyclopedia of Advanced Ceramic Materials*. R. J. Brook, ed., Pergamon Press, Oxford, 1991, pp. 222–225.
2. E. Arzt, in *Concise Encyclopedia of Advanced Ceramic Materials*. R. J. Brook, ed., Pergamon Press, Oxford, 1991, pp. 215–219.

17.2.3.5.4. Liquid Phase Sintering.

Liquid phase sintering is a fairly common type of sintering, particularly for industrial systems. It is important for powders that are difficult to densify by solid state sintering. In the process, a mixture of two powders (the major component and an additive) is heated until melting of the additive or reaction of the additive with a small part of the major component results in the formation of a liquid. In most systems, chemical reaction between the particles of the major component and the liquid phase is relatively insignificant, and the surface tension of the liquid provides the driving force for densification. Furthermore, the liquid phase commonly persists throughout the sintering stage (Fig. 1). When compounds form, the effects of the chemical forces must be taken into account. In a few systems, the liquid plays a transient role in that it aids the densification process but disappears prior to the end of the sintering stage. Compared to solid state sintering, the additional phase makes liquid phase sintering more difficult to analyze. However, many features of the process are well understood.

Assuming that the liquid wets and spreads to cover the solid surfaces, the particles will be separated by a liquid bridge. Compared to solid state sintering, the liquid

Inorganic Reactions and Methods, Volume 18
Edited by J. J. Zuckerman, Jim D. Atwood

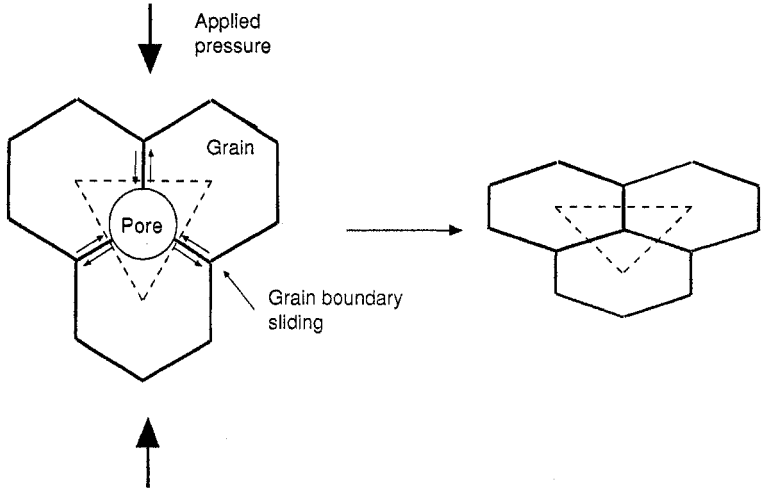

Figure 1. Development of microstructural texture that can occur during hot pressing: the grains are flattened in the direction of the applied pressure. For matter transport by diffusion, grain boundary sliding is necessary to accommodate the change in grain shape.

$m = 3$, $n = 1$; dislocation motion, $m = 0$, $n \geq 3$; and grain boundary sliding, $m = 1$, $n = 1$ or 2.

(M. N. RAHAMAN)

1. M. P. Harmer, in *Concise Encyclopedia of Advanced Ceramic Materials*. R. J. Brook, ed., Pergamon Press, Oxford, 1991, pp. 222–225.
2. E. Arzt, in *Concise Encyclopedia of Advanced Ceramic Materials*. R. J. Brook, ed., Pergamon Press, Oxford, 1991, pp. 215–219.

17.2.3.5.4. Liquid Phase Sintering.

Liquid phase sintering is a fairly common type of sintering, particularly for industrial systems. It is important for powders that are difficult to densify by solid state sintering. In the process, a mixture of two powders (the major component and an additive) is heated until melting of the additive or reaction of the additive with a small part of the major component results in the formation of a liquid. In most systems, chemical reaction between the particles of the major component and the liquid phase is relatively insignificant, and the surface tension of the liquid provides the driving force for densification. Furthermore, the liquid phase commonly persists throughout the sintering stage (Fig. 1). When compounds form, the effects of the chemical forces must be taken into account. In a few systems, the liquid plays a transient role in that it aids the densification process but disappears prior to the end of the sintering stage. Compared to solid state sintering, the additional phase makes liquid phase sintering more difficult to analyze. However, many features of the process are well understood.

Assuming that the liquid wets and spreads to cover the solid surfaces, the particles will be separated by a liquid bridge. Compared to solid state sintering, the liquid

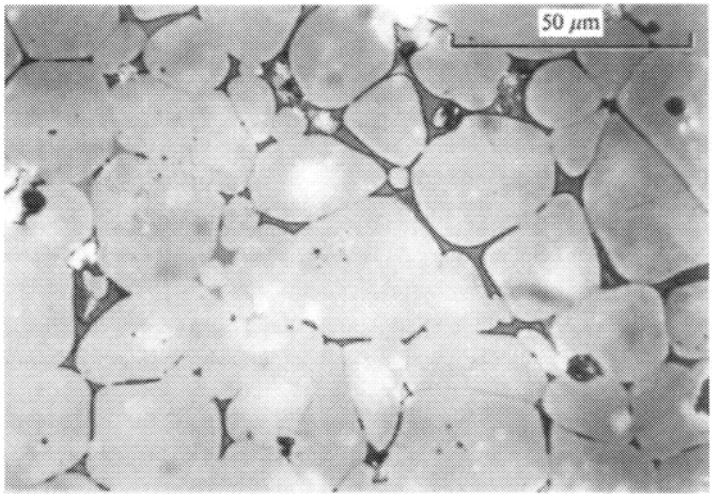

Figure 1. Microstructure of a ceramic produced by liquid phase sintering showing rounded grains, some residual porosity, and the intergranular glassy phase resulting from the liquid phase. (From R. W. Davidge, *Mechanical Behavior of Ceramics*, copyright © 1979, p. 14. Reprinted with the permission of Cambridge University Press.)

enhances densification by two main mechanisms. First, particles can arrange more easily under the capillary force of the liquid because the friction between them is significantly reduced. Second, the faster diffusion through the liquid phase provides a path for enhanced matter transport.

As sketched in Figure 2, liquid phase sintering occurs in stages[1]. During heating of the mixed powders, solid state sintering can lead to considerable densification prior to formation of the liquid. Subsequent densification depends on the amount of liquid as well as on the properties of the solid–liquid interaction. However, three stages are commonly encountered. With formation of the liquid, densification by *rearrangement* of the particles occurs rapidly. The rearrangement stage, regarded as the first stage, is accompanied by considerable *liquid redistribution* to lower the free energy of the system[2]. If the liquid volume is sufficient to fill the pores within the particulate structure, full densification can be achieved by rearrangement alone. The liquid content is low (< 5 vol %) in most systems, however, and other processes are required to achieve high density.

As the increased viscosity of the densifying system causes rearrangement to slow, the solubility of the solid in the liquid and diffusion through the liquid dominate, giving rise to the second stage referred to as *solution–precipitation*. The solid phase dissolves at the solid–liquid interfaces with a higher chemical potential (e.g., the surfaces of small grains), diffuses through the liquid, and precipitates at the interfaces with a lower chemical potential (e.g., the surfaces of large grains). The net result is densification accompanied by Ostwald ripening in which the average grain size increases. Depending on the amount of liquid, *grain shape accommodation* may also occur, allowing the growing grains to pack more efficiently.

In the final stage, densification is very slow because of the large diffusion distances and the rigid skeleton of contacting solid grains. Microstructural coarsening by the

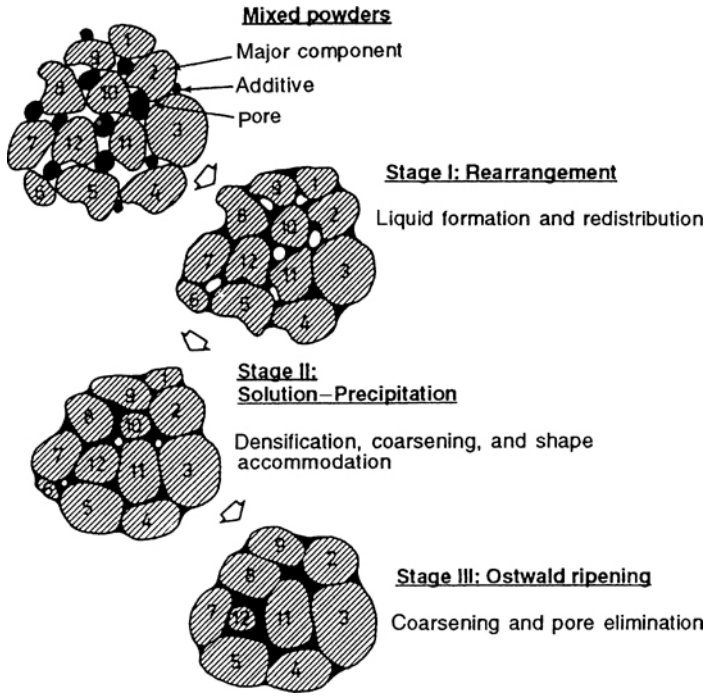

Figure 2. Schematic diagram illustrating the three stages of liquid phase sintering, with the dominant mechanisms and processes for each stage. (After Ref. 1.)

Ostwald ripening process dominates. Furthermore, enlargement of residual pores containing trapped gases leads to swelling of the compact if the final stage is too prolonged.

(i) Kinetic and Thermodynamic Factors. Kinetic and thermodynamic factors control the behavior of the system during sintering. Wetting of the solid by the liquid is an important factor in liquid phase sintering. The degree of wetting is usually described in terms of the *contact angle* θ, shown in Figure 3 and defined by:

$$\gamma_{sv} = \gamma_{sl} + \gamma_{lv} \cos \theta \qquad \text{(a)}$$

where γ_{sv}, γ_{sl}, and γ_{lv} are the specific energies of the solid–vapour, solid–liquid, and liquid–vapor interfaces, respectively. A liquid with *good wetting* characteristics (*small* contact angle) provides a compressive capillary force on the particles, thereby aiding rearrangement to minimize the energy of the system and providing a bonding force on the particles that holds them together. In contrast, a *poor wetting* liquid (*large* contact angle) causes *swelling* of the powder compact.

Spreading is the process in which the liquid distributes itself to cover the surfaces of the particles. It is important in the early stage of liquid phase sintering because the liquid normally forms in isolated regions of the compact. A spreading liquid has a contact angle of zero.

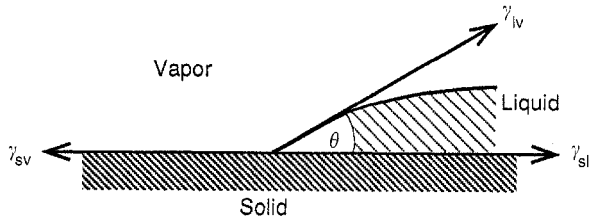

Figure 3. Wetting behavior between a liquid and a solid showing the balance of interfacial tensions for a liquid with a contact angle of θ.

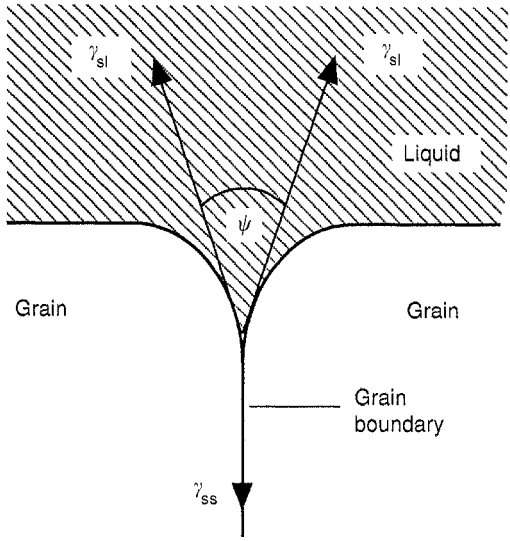

Figure 4. The definition of the dihedral angle ψ for a liquid in contact with the corners of the grains.

Another key parameter is the *solubility* of the solid in the liquid. The common requirement is for the solid to be soluble in the liquid but for the liquid to have a low solubility in the solid. This requirement leads to a liquid that persists during sintering. A high liquid solubility in the solid leads to a transient liquid phase and swelling of the compact during heating.

The *dihedral angle* is another important parameter. As shown in Figure 4, it forms where a grain boundary intersects the liquid. It is defined by a force balance:

$$2\gamma_{sl}\cos\left(\frac{\psi}{2}\right) = \gamma_{ss} \tag{b}$$

where γ_{ss} is the specific grain boundary energy. The dihedral angle influences the shapes of the liquid and the grains[3]. Figure 5 shows the shape of the liquid at the junction

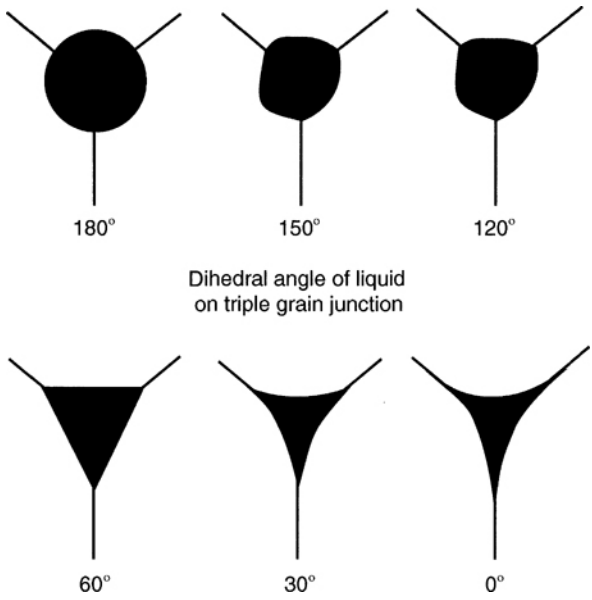

Figure 5. Effect of the dihedral angle on the idealized shape (in two dimensions) of the liquid phase at the corners of three grains. (After Ref. 1.)

between three grains. For $\gamma_{ss}/\gamma_{sl} > 2$, the dihedral angle is zero degrees and the liquid completely penetrates the grain boundaries. The grains are therefore separated by a liquid layer, and the system may lose its rigidity if the capillary force is not high enough. At the other extreme, for a large dihedral angle, there is only little penetration of the grain boundaries, and densification by solid- state diffusion becomes important.

(ii) Processing and Microstructural Parameters. Several processing and microstructural parameters also have a significant effect on liquid phase sintering. For a given system, a *fine particle size* is beneficial because it leads to an increase in the capillary stress exerted by the liquid on the particles, hence to an enhancement of the driving force for sintering and the cohesion of the particulate system. A fine particle size also leads to an increase in the solubility of the solid in the liquid.

To control the homogeneity of the final microstructure, it is important to have *uniform particle packing* in the green body, a property that results in the production of pores with a narrow distribution of sizes; *homogeneous mixing* of the major component and the liquid-producing additive is necessary, as well. After formation of the liquid, minimization of the free energy of the system dictates that the pores be filled sequentially (smallest pores first, largest last). With heterogeneous packing, the filling of the largest pores later in the sintering process produces regions that are enriched in the liquid. Inhomogeneous mixing leads to an inhomogeneous liquid distribution such that there is no driving force for redistribution of the liquid.

The volume of liquid phase, controlled by the amount of liquid-producing additive or by the temperature in eutectic systems, controls the extent of densification in the

rearrangement stage, as outlined earlier. For further densification by the solution–precipitation mechanism, the rate is expected to increase with higher liquid content because the volume of matter transported into the pores is higher. However, coarsening is also expected to decrease with higher liquid content because the diffusion distance for coarsening is increased.

(M. N. RAHAMAN)

1. R. M. German, *Liquid Phase Sintering*, Plenum Press, New York, 1985.
2. T. M. Shaw, *J. Am. Ceram. Soc.*, *69*, 27 (1986).
3. C. S. Smith, *Trans. AIME*, *175*, 15 (1948).

17.2.4. Crystal Growth from Melts and Solutions

Single crystals are required for applications that make use of their unique optical or crystallographic properties or which would be adversely affected by grain boundaries. Typical applications are as lasers and frequency doublers, gemstones, and lenses. For some applications glasses are acceptable, but the disorder in an amorphous structure results in greater scattering of electromagnetic energy. Only rarely is a single crystal ceramic required for an application above 1200°C. However, the hardness, heat resistance, low thermal conductivity, and optical transparency associated with ceramics are useful properties.

The growth of a single crystal often starts with a small seed crystal, which is selected for its crystallographic qualities (relative absence of inclusions, chemical impurities, and physical defects such as dislocations, twins, and stacking faults). Conditions must then be chosen that permit growth, while maintaining good quality and avoiding the formation of new crystals. It may not be possible to use a seed crystal, especially when novel materials are crystallized. The formation of the solid from the fluid phase then occurs by spontaneous nucleation, and the main experimental requirement is that relatively few nuclei should form; if this condition is not achieved, the product will be multicrystalline, rather than consisting of large crystals. Most measurements or applications require about 1 cm^3 of crystal, and some use much larger volumes. While useful measurements can be made on small crystals, the production of material less than about 1 mm^3 is considered to be synthesis rather than crystal growth.

During growth of a crystal the solid–liquid interface should maintain a regular shape. Ideally, the interface should be flat or slightly convex toward the liquid. The solid normally rejects impurities into the melt, and these tend to accumulate ahead of the interface and depress the local melting point. Thus, if crystallization occurs too rapidly, the interface breaks down into a cellular structure, with impurities trapped inside the crystal. The condition for stable growth of a solid–liquid interface is the subject of theoretical and experimental investigations. In its simplest form, the condition for stable growth can be expressed by the constitutional supercooling criterion[1]:

$$v < \frac{GKD}{mn(1-K)} \tag{a}$$

where v is the linear growth rate, G the temperature gradient at the solid–liquid interface, K the segregation coefficient of the impurity, m the slope of the liquidus curve, n the concentration of the impurity in the bulk liquid, and D the diffusion coefficient of the impurity.

Inorganic Reactions and Methods, Volume 18
Edited by J. J. Zuckerman, Jim D. Atwood

rearrangement stage, as outlined earlier. For further densification by the solution–precipitation mechanism, the rate is expected to increase with higher liquid content because the volume of matter transported into the pores is higher. However, coarsening is also expected to decrease with higher liquid content because the diffusion distance for coarsening is increased.

(M. N. RAHAMAN)

1. R. M. German, *Liquid Phase Sintering*, Plenum Press, New York, 1985.
2. T. M. Shaw, *J. Am. Ceram. Soc.*, *69*, 27 (1986).
3. C. S. Smith, *Trans. AIME*, *175*, 15 (1948).

17.2.4. Crystal Growth from Melts and Solutions

Single crystals are required for applications that make use of their unique optical or crystallographic properties or which would be adversely affected by grain boundaries. Typical applications are as lasers and frequency doublers, gemstones, and lenses. For some applications glasses are acceptable, but the disorder in an amorphous structure results in greater scattering of electromagnetic energy. Only rarely is a single crystal ceramic required for an application above 1200°C. However, the hardness, heat resistance, low thermal conductivity, and optical transparency associated with ceramics are useful properties.

The growth of a single crystal often starts with a small seed crystal, which is selected for its crystallographic qualities (relative absence of inclusions, chemical impurities, and physical defects such as dislocations, twins, and stacking faults). Conditions must then be chosen that permit growth, while maintaining good quality and avoiding the formation of new crystals. It may not be possible to use a seed crystal, especially when novel materials are crystallized. The formation of the solid from the fluid phase then occurs by spontaneous nucleation, and the main experimental requirement is that relatively few nuclei should form; if this condition is not achieved, the product will be multicrystalline, rather than consisting of large crystals. Most measurements or applications require about 1 cm^3 of crystal, and some use much larger volumes. While useful measurements can be made on small crystals, the production of material less than about 1 mm^3 is considered to be synthesis rather than crystal growth.

During growth of a crystal the solid–liquid interface should maintain a regular shape. Ideally, the interface should be flat or slightly convex toward the liquid. The solid normally rejects impurities into the melt, and these tend to accumulate ahead of the interface and depress the local melting point. Thus, if crystallization occurs too rapidly, the interface breaks down into a cellular structure, with impurities trapped inside the crystal. The condition for stable growth of a solid–liquid interface is the subject of theoretical and experimental investigations. In its simplest form, the condition for stable growth can be expressed by the constitutional supercooling criterion[1]:

$$v < \frac{GKD}{mn(1-K)} \qquad \text{(a)}$$

where v is the linear growth rate, G the temperature gradient at the solid–liquid interface, K the segregation coefficient of the impurity, m the slope of the liquidus curve, n the concentration of the impurity in the bulk liquid, and D the diffusion coefficient of the impurity.

Equation (a) neglects heat flow in the solid, and a more complete perturbation treatment[2] gives the condition for stable growth:

$$\frac{G_L}{v} + \frac{L}{2\lambda_L} < \frac{mK(1-K_0)n\bar{\lambda}S}{DK_0} \qquad \text{(b)}$$

where G_L is the temperature gradient in the liquid, L the latent heat, λ_L the thermal conductivity of the liquid, $\bar{\lambda} = (\lambda_S + 2\lambda_L)/2\lambda_L$, with λ_S the thermal conductivity of the solid, K_0 the phase diagram value of K, and S a stability function with values $\sim 0.8 \pm 0.1$. Equations (a) and (b) work for crystal growth from an impure melt, but neglect of the stabilizing effect of the surface energy leads to discrepancies between experimental and theoretical values of the maximum stable growth rate from solution. Crystals grown from solution are normally faceted, and the high surface energy associated with the facets has a strong stabilizing influence on the growth. Perturbations of a faceted interface involve the development of higher energy surfaces, so the perturbations tend to decay to restore the plane surface[3].

The conditions for stable growth of a crystal are closely associated with segregation of dopants or impurities. Crystal growth theory includes an expression[4] for the effective segregation coefficient K, for a crystal growing from a medium in which the dopant distribution is characterized by a boundary layer of thickness δ:

$$K_{eff} = \frac{K_0}{K_0 + (1-K_0)\exp(-v\delta/D)} \qquad \text{(c)}$$

with other symbols defined above. This equation describes semiquantitatively the variation of dopant concentration in the crystal with growth rate v and with changes in rotation rate ω, which change the boundary layer thickness, δ ($\delta \propto \omega^{-1/2}$).

The choice of a method for crystal growth entails consideration of several factors. Growth from the melt is preferable, since growth rate is fastest and contamination problems with solvents are avoided. When melt growth is not possible or desirable, solution growth is often the choice, although vapor growth is used for growth of crystals in the form of thin films. Vapor growth can occasionally give larger and more perfect crystals than growth from the liquid (of, e.g., silicon carbide)[5]. Recrystallization from the solid state is used rarely: the recrystallization of polycrystalline material on seeds of yttrium iron garnet ($Y_3Fe_5O_{12}$) is an example[6].

More detailed descriptions of crystal growth from liquids are found in reviews[7–9].

(DENNIS ELWELL)

1. W. A. Tiller, K. A. Jackson, J. W. Rutter, B. Chalmers, *Acta Metall. 1*, 428 (1953).
2. W. W. Mullins, R. F. Sekerka, *J. Appl. Phys. 35*, 444 (1964).
3. H. J. Scheel, D. Elwell, *J. Electrochem Soc., 120*, 818 (1973).
4. J. A. Burton, R. C. Prim, W. P. Slichter, *J. Chem. Phys. 21*, 1987 (1953).
5. Yu. M. Tairov, V. K. Tsvetkov, *J. Cryst. Growth, 52*, 146 (1981).
6. V. A. Timofeeva, L. M. Belyaev, N. D. Ursulak, A. V. Belitsky, A. B. Bykov, V. M. Prilepo, *J. Cryst. Growth, 52*, 633 (1981).
7. J. C. Brice, *The Growth of Crystals from Liquids*, North Holland, Amsterdam, 1973.
8. J. C. Brice, *Rep. Prog. Phys., 40*, 567 (1977).
9. J. C. Brice, *Prog. Cryst. Growth Charact., 1*, 244 (1978).

17.2.4.1. Growth from Melts

Crystal growth from the melt is preferable to the alternatives, provided there are no adverse factors. Melt growth is more rapid (typically, by one to two orders of magnitude),

Inorganic Reactions and Methods, Volume 18
Edited by J. J. Zuckerman, Jim D. Atwood

Equation (a) neglects heat flow in the solid, and a more complete perturbation treatment[2] gives the condition for stable growth:

$$\frac{G_L}{v} + \frac{L}{2\lambda_L} < \frac{mK(1 - K_0)n\bar{\lambda}S}{DK_0} \qquad \text{(b)}$$

where G_L is the temperature gradient in the liquid, L the latent heat, λ_L the thermal conductivity of the liquid, $\bar{\lambda} = (\lambda_S + 2\lambda_L)/2\lambda_L$, with λ_S the thermal conductivity of the solid, K_0 the phase diagram value of K, and S a stability function with values $\sim 0.8 \pm 0.1$. Equations (a) and (b) work for crystal growth from an impure melt, but neglect of the stabilizing effect of the surface energy leads to discrepancies between experimental and theoretical values of the maximum stable growth rate from solution. Crystals grown from solution are normally faceted, and the high surface energy associated with the facets has a strong stabilizing influence on the growth. Perturbations of a faceted interface involve the development of higher energy surfaces, so the perturbations tend to decay to restore the plane surface[3].

The conditions for stable growth of a crystal are closely associated with segregation of dopants or impurities. Crystal growth theory includes an expression[4] for the effective segregation coefficient K, for a crystal growing from a medium in which the dopant distribution is characterized by a boundary layer of thickness δ:

$$K_{\text{eff}} = \frac{K_0}{K_0 + (1 - K_0)\exp(-v\delta/D)} \qquad \text{(c)}$$

with other symbols defined above. This equation describes semiquantitatively the variation of dopant concentration in the crystal with growth rate v and with changes in rotation rate ω, which change the boundary layer thickness, δ ($\delta \propto \omega^{-1/2}$).

The choice of a method for crystal growth entails consideration of several factors. Growth from the melt is preferable, since growth rate is fastest and contamination problems with solvents are avoided. When melt growth is not possible or desirable, solution growth is often the choice, although vapor growth is used for growth of crystals in the form of thin films. Vapor growth can occasionally give larger and more perfect crystals than growth from the liquid (of, e.g., silicon carbide)[5]. Recrystallization from the solid state is used rarely: the recrystallization of polycrystalline material on seeds of yttrium iron garnet ($Y_3Fe_5O_{12}$) is an example[6].

More detailed descriptions of crystal growth from liquids are found in reviews[7–9].

(DENNIS ELWELL)

1. W. A. Tiller, K. A. Jackson, J. W. Rutter, B. Chalmers, *Acta Metall. 1*, 428 (1953).
2. W. W. Mullins, R. F. Sekerka, *J. Appl. Phys. 35*, 444 (1964).
3. H. J. Scheel, D. Elwell, *J. Electrochem Soc., 120*, 818 (1973).
4. J. A. Burton, R. C. Prim, W. P. Slichter, *J. Chem. Phys. 21*, 1987 (1953).
5. Yu. M. Tairov, V. K. Tsvetkov, *J. Cryst. Growth, 52*, 146 (1981).
6. V. A. Timofeeva, L. M. Belyaev, N. D. Ursulak, A. V. Belitsky, A. B. Bykov, V. M. Prilepo, *J. Cryst. Growth, 52*, 633 (1981).
7. J. C. Brice, *The Growth of Crystals from Liquids*, North Holland, Amsterdam, 1973.
8. J. C. Brice, *Rep. Prog. Phys., 40*, 567 (1977).
9. J. C. Brice, *Prog. Cryst. Growth Charact., 1*, 244 (1978).

17.2.4.1. Growth from Melts

Crystal growth from the melt is preferable to the alternatives, provided there are no adverse factors. Melt growth is more rapid (typically, by one to two orders of magnitude),

but it requires more power than solution techniques and may involve problems of contamination from precious metal crucibles. This section describes the experimental techniques of crystal growth from the melt, with examples of ceramic materials grown by these techniques.

(DENNIS ELWELL)

17.2.4.1.1. Pulling from the Melt.

The technique of pulling from the melt is the most popular for crystal growth of silicon for the semiconductor industry and for large crystals of refractory oxides. A typical arrangement is shown in Figure 1, and examples of crystals grown by this method are listed in Table 1. Lithium niobate crystals and wafers grown by pulling from the melt are shown in Figure 2.

Fluid flow within the melt has a crucial effect on crystal quality. If the crystal is stationary, the dominant convection pattern is upward flow of material at the crucible walls and radial flow inward at the surface (type I). Rapid rotation of crystal causes material to be thrown radially outward at the surface, and opposes the thermal convective flow (type III). These flow patterns are shown in Figure 3. In the intermediate regime, where the two flows are of comparable rates, a more complex surface pattern is observed, labeled type II. The crystal–liquid interface is convex toward the melt in type I flow and planar in type II, a condition that is used for the growth of large crystals of gadolinium gallium garnet[1].

Among the problems facing crystal growers are dislocations, facets, striations, and nonstoichiometry.

(i) Dislocations. These result from thermal stresses in the crystal, and their incidence depends on the shape of the growth interface. Control of the interface is especially crucial during the shouldering period, when the diameter is increasing from the seed to the required value, which is maintained constant until the final stages of growth. Dislocations may propagate from the seed to the crystal, but this can be minimized by reducing the diameter to a small value prior to increase to the final diameter, (e.g., 10 cm diameter gadolinium gallium garnet crystals can be grown free from dislocations).

(ii) Facets. Ideally, crystals grown from the melt are not faceted, but take the shape of an isotherm at the solid–liquid interface. The presence of facets (low index crystallographic faces) causes local strain because the faceted area differs in lattice parameter from that of the nonfaceted region[2], owing to a difference in impurity or point defect concentration or a difference in stoichiometry. The occurrence of facets can be eliminated by adjustment of the growth conditions, (e.g., the crystal rotation rate).

(iii) Striations. Regular changes in composition of the crystal with distance along the pulling axis occur as a result of periodic changes in the instantaneous rate of crystal growth. Such changes may result from an asymmetric temperature distribution, which leads to variations in interface temperature at the rotation rate. Alternatively, periodic or irregular changes in temperature may be due to unstable convection within the melt. Convective effects such as temperature oscillations in the melt can be reduced by the use of baffles[3].

(iv) Nonstoichiometry. Rarely is the solid composition that melts congruently (i.e., without change in composition) the stoichiometric composition in which the constituents

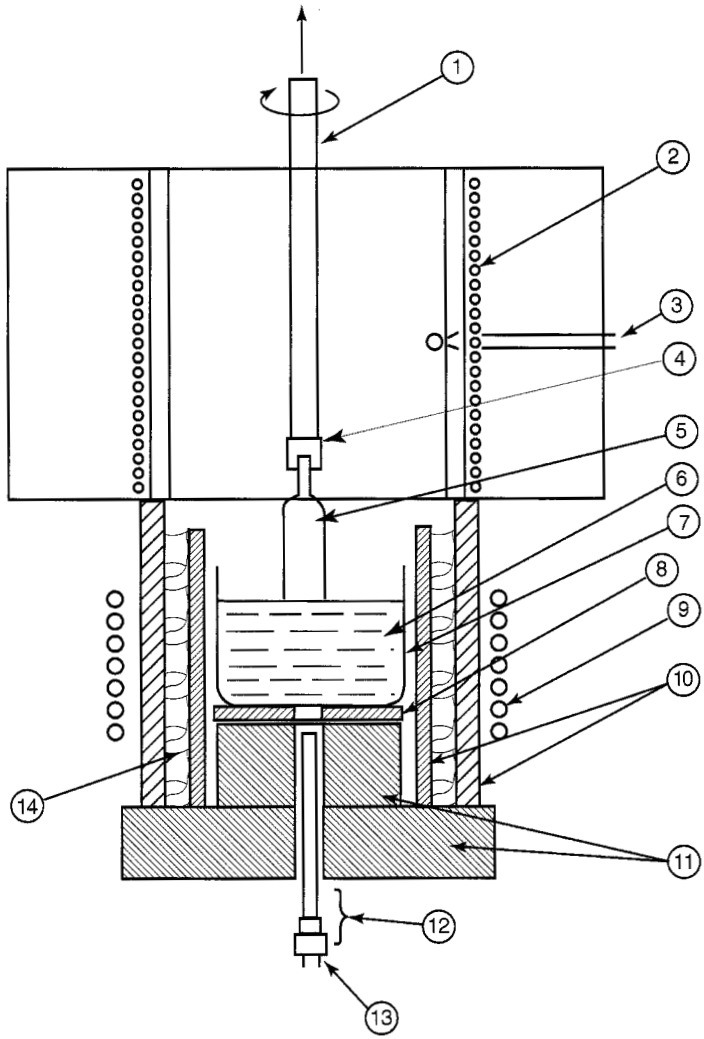

Figure 1. Schematic diagram of furnace used to pull lithium niobate crystals: 1, alumina pull rod; 2, after heater; 3, temperature control signal to auxiliary controller; 4, Pt seed holder; 5, $LiNbO_3$ crystal; 6, $LiNbO_3$ melt; 7, Pt crucible; 8, alumina plate; 9, rf coil; 10, alumina tubes; 11, firebricks; 12, sapphire rod–radiation pyrometer; 13, temperature signal to main controller; 14, Fiberfrax insulation. (Courtesy W. L. Kway.)

are present in exact whole-number ratios. Typically, the crystals grown by melt solidification differ from the ideal composition. For example, gadolinium gallium garnet grows as $Gd_{3.03}Ga_{4.97}O_{12}$, rather than $Gd_3Ga_5O_{12}$. The starting melt should have the congruently melting rather than the ideal composition; otherwise, the composition of the melt, and the crystal, will change as crystal growth proceeds. Crystal properties may vary

Table 1. Materials Grown by Pulling from the Melt

Material	Melting Point (°C)	Crucible	Applications
Al_2O_3	2037	Molybdenum	Laser, gemstone
$Gd_3Ga_5O_{12}$	1825	Iridium	Substrates
$LiTaO_3$	1650	Iridium	Nonlinear optics
$MgAl_2O_4$	2100	Iridium	Substrates
$MnFe_2O_4$	1500	Iridium	Magnetic
$NaBa_2Nb_5O_{15}$	1450	Platinum	Nonlinear optics
$Y_3Al_5O_{12}$	1975	Iridium	Laser, gemstone
$LiNbO_3$	1260	Platinum	Nonlinear optics

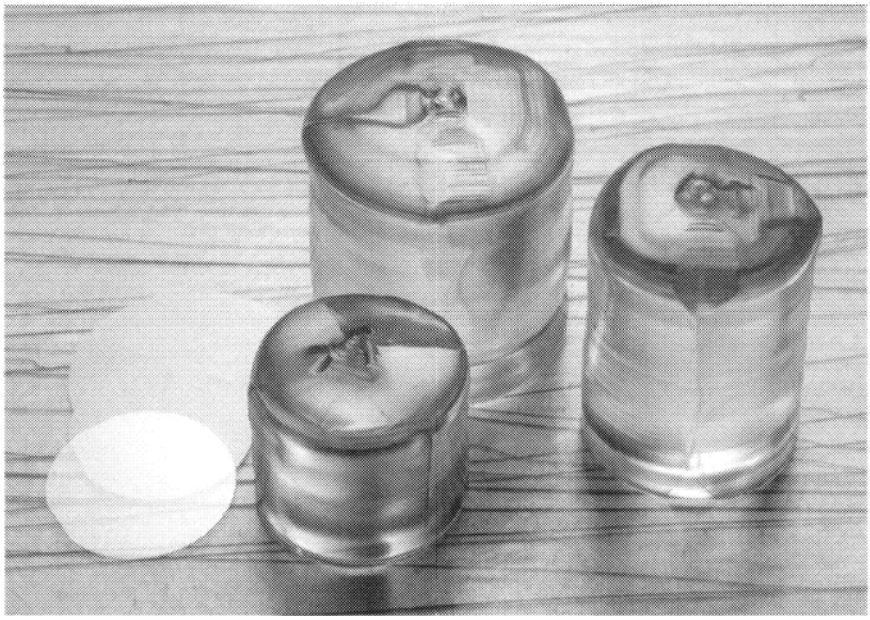

Figure 2. Crystals of lithium niobate up to 10 cm in diameter grown by pulling from the melt. (Courtesy P. Bordui, Crystal Technology.)

with changes in stoichiometry (e.g., in lithium niobate, $LiNbO_3$). Crystals of a specific composition away from the congruently melting (e.g., the composition with a phase-matching temperature of 130°C for CO_2 laser radiation[4]), can be grown from the incongruently melting starting composition, but to minimize the spread in properties owing to variation in axial composition, samples must be cut across the crystal rather than along the axis.

The growth of large crystals of constant diameter requires automatic diameter control, which uses continuous weighing either of the crystal or of the crucible containing the melt. A typical diameter control system is shown schematically in Figure 4. Weighing the melt has several advantages: the reading is not influenced by rotation of the crystal,

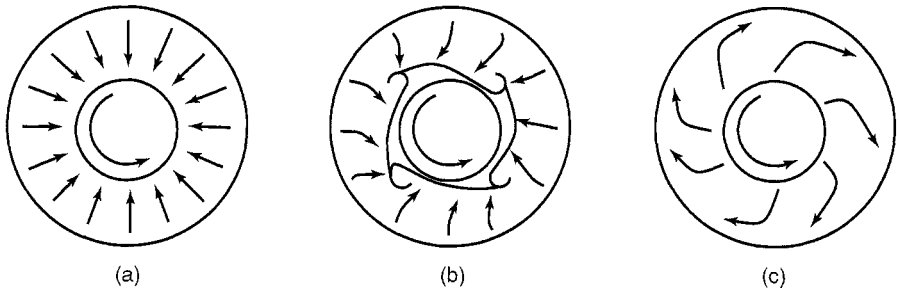

Figure 3. Convective flow patterns in melts as seen on the surface: (a) slow crystal rotation, (b) moderate rotation, and (c) fast rotation. (From Ref 1.)

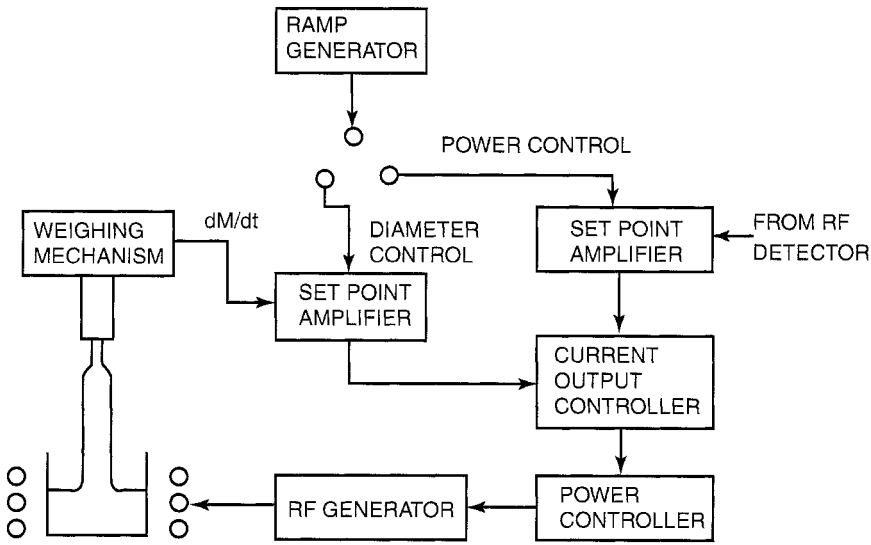

Figure 4. Schematic diameter control system. (After Ref. 1.)

and melt weighing systems are easier to install. However the assembly that is weighed, including the crucible support, is of substantially greater mass than that of the crystal, so there is some loss of sensitivity. In addition, erroneous weight readings can occur owing to levitation of the melt when rf heating is used, and this effect changes with time as the rf input power changes. Weighing the crystal gives higher sensitivity, but constructing a system that is not influenced by crystal rotation is difficult. An alternate method of diameter control utilizes radiation detectors that sense the extra thermal radiation from the meniscus around the crystal, in comparison with that from either the plane liquid surface or the crystal itself. Optical detectors are less versatile. For example, if a detector is located at some fixed distance from the crystal axis to control a set diameter, operator skill is required during the important state of shouldering as the diameter is increased

from that of the seed. The reflection of a laser beam from the meniscus is also used in achieving control. Optical techniques suffer from problems of condensation of evaporating species on the detector or other optical components.

(DENNIS ELWELL)

1. C. D. Brandle, in *Crystal Growth: A Tutorial Approach*, W. Bardsey, D. T. J. Hurle, J. B. Mullin, eds., North Holland, Amsterdam, 1979, p. 189.
2. B. Cockayne, J. M. Roslington, A. W. Vere, *J. Mater. Sci.*, *8*, 382 (1973).
3. J. C. Brice, *The Growth of Crystals from Liquids*, North Holland, Amsterdam, 1973.
4. R. L. Byer, Y. K. Park, R. S. Feigelson, W. L. Kway, *Appl. Phys. Lett.*, *39*, 17 (1981).

17.2.4.1.2. Directional Solidification.

Pulling from the melt and several of the other methods described are examples of directional solidification, but are best described and better known by the terms used. Directional solidification includes techniques in which a melt contained in a crucible is solidified in a temperature gradient, either by moving the crucible through a temperature gradient or by programmed reduction of the temperature (gradient freezing). Seeding may be used but is often difficult, since the crucible may be opaque and direct observation inside a fused silica crucible is of limited value at high temperatures where the image is dominated by thermal radiation. The only successful method of seeding at high temperatures (unless a long seed is available) utilizes thermocouples to measure the local temperature in the region of the seed. Seeding is desirable, especially for systems in which the melts supercool by several tens or even hundreds of degrees. The nucleation of the solid phase here is rapid and uncontrolled, so that much of this solid must be remelted to remove the damaged region. Unseeded growth is carried out in crucibles having long capillary tubes in the lower region. This region enhances seed selection, since most crystallites grow at an angle to the crucible axis; the probability is, therefore, strong that a single crystallite will survive at the end of the capillary and provide the seed for the remainder of the crystal.

In directional solidification, growth occurs in close contact with the crucible, and if the expansion coefficient of the crucible material differs from that of the crystal, severe stresses may be induced during cooling, especially when the expansion is anisotropic[1]. The advantage is that the crucible may be sealed to permit the growth of crystals of volatile materials. It has also been used for refractories that do not require a sealed crucible, as in the examples shown in Table 1[2].

TABLE 1. CERAMIC MATERIALS GROWN BY DIRECTIONAL SOLIDIFICATION

Material	Melting Point (°C)	Growth Rate (mm/h)	Crucible
Al_2O_3	2037	6	Molybdenum
$FeAl_2O_4$	1790	10	Iridium
$Gd_3Ga_5O_{12}$	1825	2	Iridium
$YFeO_3$	1685	2	Platinum
$Y_3Al_5O_{12}$	1975	2	Molybdenum

Inorganic Reactions and Methods, Volume 18
Edited by J. J. Zuckerman, Jim D. Atwood

from that of the seed. The reflection of a laser beam from the meniscus is also used in achieving control. Optical techniques suffer from problems of condensation of evaporating species on the detector or other optical components.

(DENNIS ELWELL)

1. C. D. Brandle, in *Crystal Growth: A Tutorial Approach*, W. Bardsey, D. T. J. Hurle, J. B. Mullin, eds., North Holland, Amsterdam, 1979, p. 189.
2. B. Cockayne, J. M. Roslington, A. W. Vere, *J. Mater. Sci.*, *8*, 382 (1973).
3. J. C. Brice, *The Growth of Crystals from Liquids*, North Holland, Amsterdam, 1973.
4. R. L. Byer, Y. K. Park, R. S. Feigelson, W. L. Kway, *Appl. Phys. Lett.*, *39*, 17 (1981).

17.2.4.1.2. Directional Solidification.

Pulling from the melt and several of the other methods described are examples of directional solidification, but are best described and better known by the terms used. Directional solidification includes techniques in which a melt contained in a crucible is solidified in a temperature gradient, either by moving the crucible through a temperature gradient or by programmed reduction of the temperature (gradient freezing). Seeding may be used but is often difficult, since the crucible may be opaque and direct observation inside a fused silica crucible is of limited value at high temperatures where the image is dominated by thermal radiation. The only successful method of seeding at high temperatures (unless a long seed is available) utilizes thermocouples to measure the local temperature in the region of the seed. Seeding is desirable, especially for systems in which the melts supercool by several tens or even hundreds of degrees. The nucleation of the solid phase here is rapid and uncontrolled, so that much of this solid must be remelted to remove the damaged region. Unseeded growth is carried out in crucibles having long capillary tubes in the lower region. This region enhances seed selection, since most crystallites grow at an angle to the crucible axis; the probability is, therefore, strong that a single crystallite will survive at the end of the capillary and provide the seed for the remainder of the crystal.

In directional solidification, growth occurs in close contact with the crucible, and if the expansion coefficient of the crucible material differs from that of the crystal, severe stresses may be induced during cooling, especially when the expansion is anisotropic[1]. The advantage is that the crucible may be sealed to permit the growth of crystals of volatile materials. It has also been used for refractories that do not require a sealed crucible, as in the examples shown in Table 1[2].

TABLE 1. CERAMIC MATERIALS GROWN BY DIRECTIONAL SOLIDIFICATION

Material	Melting Point (°C)	Growth Rate (mm/h)	Crucible
Al_2O_3	2037	6	Molybdenum
$FeAl_2O_4$	1790	10	Iridium
$Gd_3Ga_5O_{12}$	1825	2	Iridium
$YFeO_3$	1685	2	Platinum
$Y_3Al_5O_{12}$	1975	2	Molybdenum

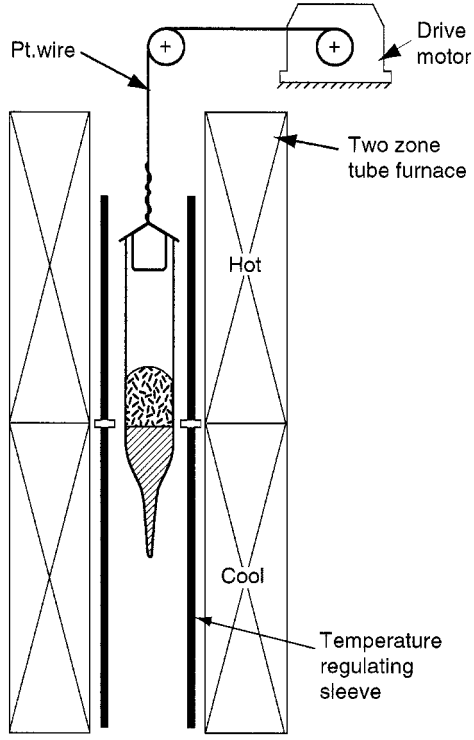

Figure 1. Arrangement for crystal growth by the Bridgman method. (Courtesy of R. K. Route.)

From the interface stability conditions outlined in 17.2.4, a steep temperature gradient is required for stable growth. This is achieved in the moving crucible technique by use of a two-zone furnace with the temperature profiles adjusted to produce a steep gradient at the division between the two sets of windings (see Fig. 1). As in the case of pulling from the melt, control of the interface shape is crucial for achieving good quality crystals. The interface shape is governed by heat flows within the system (see Fig. 2)[1]. If the net heat flux at the solid–liquid interface is inward from the furnace, the interface shape is convex toward the liquid; conversely, if the heat flow at the interface is radially outward, the interface shape is concave. A plane interface can be achieved only if the heat flow through the liquid is the same as that through the crystal. Crystals of low dislocation density can be grown only if the interface is planar or slightly convex. A simplified but useful treatment of the theory of the interface shape is available for both the moving crucible variant[3] and gradient freezing[4].

The interaction with the container, especially the stress generated during cooling, makes pulling from the melt preferable for most ceramic materials. If volatility is a problem, temperature gradient growth is preferred to gradient freezing, since a steep temperature gradient can be maintained in the critical region of the furnace where growth occurs.

(DENNIS ELWELL)

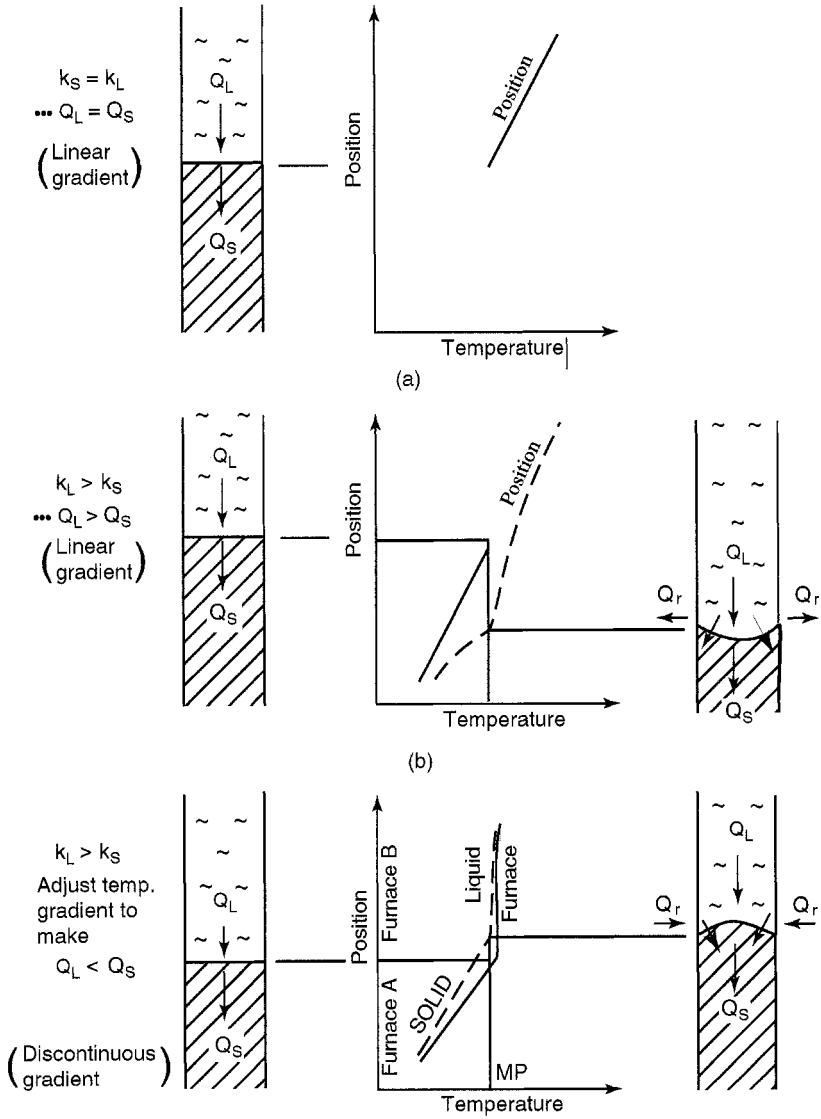

Figure 2. Dependence of interface shape on heat flows Q_L (through liquid), Q_S (through solid), and Q_R (radial heat flow) depending on temperature distribution in furnace; K_L and K_S are thermal conductivities of liquid and solid, respectively. (From Ref. 1.)

1. R. S. Feigelson, R. K. Route, *J. Cryst. Growth, 49*, 261 (1980).
2. J. C. Brice, *The Growth of Crystals from Liquids*, North Holland, Amsterdam, 1973.
3. C. E. Chang, W. R. Wilcox, *J. Cryst. Growth, 21*, 135 (1974).
4. C. E. Chang, V. F. S. Yip, W. R. Wilcox, *J. Cryst. Growth, 22*, 247 (1974).

Inorganic Reactions and Methods, Volume 18
Edited by J. J. Zuckerman, Jim D. Atwood

17.2.4.1.3. Controlled Heat Removal.

A closely related technique for crystal growth involves cooling a stationary melt by moving the temperature field[1]. Large crystals of alkali halides are grown[2], but it is difficult to maintain a large temperature gradient toward the end of the crystallization process when heat is being removed through a thick layer of insulating crystal. Seed crystals can be placed over a helium-cooled heat exchanger to achieve sensitive control over the temperature gradient throughout crystallization[3]. In this way large (25 × 15 cm) cylindrical crystals of Al_2O_3 having low dislocation densities are produced. This heat exchanger method is used to grow large, high quality crystals of $Y_3Al_5O_{12}$[4]. This little-used method could be employed to grow large crystals of other ceramic materials.

(DENNIS ELWELL)

1. J. C. Brice, *The Growth of Crystals from Liquids*, North Holland, Amsterdam, 1973.
2. J. Strong, *Phys. Rev.*, *36*, 1663 (1930).
3. D. Viechnicki, F. Schmid, *J. Cryst. Growth*, *26*, 162 (1974).
4. J. L. Caslavsky, D. Viechnicki, *J. Cryst. Growth*, *46*, 601 (1979).

17.2.4.1.4. Float Zone Growth.

The growth of crystals by the passage of a molten zone between a seed crystal and a polycrystalline feed rod (Fig. 1) is a method of crucible-less growth. It is of value for

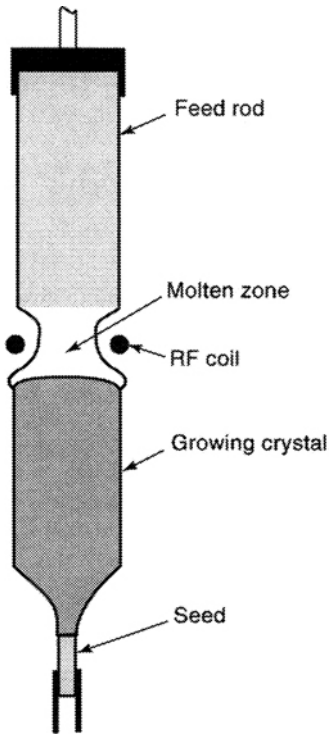

Figure 1. Schematic system for floating zone growth.

Inorganic Reactions and Methods, Volume 18
Edited by J. J. Zuckerman, Jim D. Atwood

17.2.4.1.3. Controlled Heat Removal.

A closely related technique for crystal growth involves cooling a stationary melt by moving the temperature field[1]. Large crystals of alkali halides are grown[2], but it is difficult to maintain a large temperature gradient toward the end of the crystallization process when heat is being removed through a thick layer of insulating crystal. Seed crystals can be placed over a helium-cooled heat exchanger to achieve sensitive control over the temperature gradient throughout crystallization[3]. In this way large (25 × 15 cm) cylindrical crystals of Al_2O_3 having low dislocation densities are produced. This heat exchanger method is used to grow large, high quality crystals of $Y_3Al_5O_{12}$[4]. This little-used method could be employed to grow large crystals of other ceramic materials.

(DENNIS ELWELL)

1. J. C. Brice, *The Growth of Crystals from Liquids*, North Holland, Amsterdam, 1973.
2. J. Strong, *Phys. Rev.*, *36*, 1663 (1930).
3. D. Viechnicki, F. Schmid, *J. Cryst. Growth*, *26*, 162 (1974).
4. J. L. Caslavsky, D. Viechnicki, *J. Cryst. Growth*, *46*, 601 (1979).

17.2.4.1.4. Float Zone Growth.

The growth of crystals by the passage of a molten zone between a seed crystal and a polycrystalline feed rod (Fig. 1) is a method of crucible-less growth. It is of value for

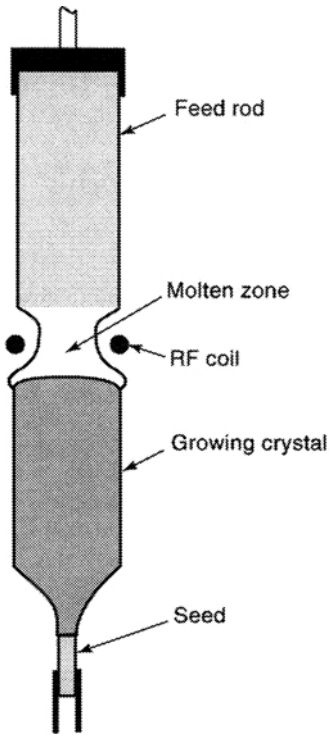

Figure 1. Schematic system for floating zone growth.

reactive materials that are contaminated by the crucible, or for highly refractory materials for which an inert crucible may not exist. Since the molten zone is held in place by surface tension only, its thickness must not exceed a critical amount, depending on the material.

The preferred heat sources to produce the molten zone depend on the melting point and on the optical and electrical properties of the material. In heating, the power is supplied to a single turn rather than by a coil. An electric arc or high intensity lamp may also be used as a heating source with a mirror system to focus the beam onto the crystal to form the molten zone. An ellipsoidal mirror system is preferable to parabolic, and temperatures up to 2800°C are achieved when a xenon arc lamp is used[1]. Lasers are convenient and stable heat sources that do not require a mirror system[2]. A platinum strip can be placed through the sample to ensure that the molten zone is produced simply by resistive heating[3]. If the material is conducting, electron bombardment may be used as a heating source, as for LaB_6[4].

The floating zone method is widely applicable and that can be applied for refractory materials such as $VC_{0.8}$, which melts at 2700°C[5]. The absence of a crucible is an advantage. Drawbacks include the difficulty in controlling the zone unless the heating source is well stabilized, and of growing large diameter crystals of good quality (because the radial temperature gradient tends to increase with crystal diameter, setting up strains that lead to dislocations). However, dislocation-free crystals of semiconductor silicon can be grown by this method.

(DENNIS ELWELL)

1. M. Kitazawa, N. Nagashima, T. Mizutani, K. Feuki, T. Mukaibo, *J. Cryst. Growth, 39*, 211 (1977).
2. B. Cockayne, D. B. Gasson, N. Forbes, *J. Mater. Sci., 5*, 837 (1970).
3. D. B. Gasson, *J. Sci. Instrum. 42*, 575 (1965).
4. M. Aono, C. Oshima, T. Tanaka, E. Bannai, S. Kawai, *Jpn. J. Appl. Phys. 49*, 2761 (1978).
5. W. Precht, G. E. Hollox, *J. Cryst. Growth, 3/4*, 818 (1968).

17.2.4.1.5. Flame Fusion Method.

The flame fusion process was the first method to give crystals of acceptable size for commercial applications from the melt, namely ruby crystals for use as gemstones.

In the earliest version two torches are used with powder fed through a tube into the hot zone[1]. The main improvement involves feeding hydrogen and oxygen through coaxial tubes, with the powder fed through the oxygen by a vibrator or hammer acting on a container located above the furnace (Fig. 1a). The powdered material falls into the oxyhydrogen flame and forms tiny droplets, which are condensed onto a ceramic pedestal. Initially a cone of polycrystalline material is formed, and the tip of the cone reaches the hot zone and melts to form tiny crystals. Operator skill is necessary to select one of these to form the seed from which the crystal will develop (Fig. 1b). The temperature may be adjusted by changing the hydrogen-to-oxygen ratio, and the powder flow rate can also be changed as the crystal diameter is increased. Once the crystal has reached a constant diameter, the growth process can continue without attention, and a single operator can produce crystals in many furnaces simultaneously in modern plants used for crystal growth of Al_2O_3 and $MgAl_2O_4$ (Fig. 1c).

After heating arrangements reduce the temperature gradients and so reduce the strain, which is normally severe in crystals grown by this method. Dislocation densities

Inorganic Reactions and Methods, Volume 18
Edited by J. J. Zuckerman, Jim D. Atwood

reactive materials that are contaminated by the crucible, or for highly refractory materials for which an inert crucible may not exist. Since the molten zone is held in place by surface tension only, its thickness must not exceed a critical amount, depending on the material.

The preferred heat sources to produce the molten zone depend on the melting point and on the optical and electrical properties of the material. In heating, the power is supplied to a single turn rather than by a coil. An electric arc or high intensity lamp may also be used as a heating source with a mirror system to focus the beam onto the crystal to form the molten zone. An ellipsoidal mirror system is preferable to parabolic, and temperatures up to 2800°C are achieved when a xenon arc lamp is used[1]. Lasers are convenient and stable heat sources that do not require a mirror system[2]. A platinum strip can be placed through the sample to ensure that the molten zone is produced simply by resistive heating[3]. If the material is conducting, electron bombardment may be used as a heating source, as for LaB_6[4].

The floating zone method is widely applicable and that can be applied for refractory materials such as $VC_{0.8}$, which melts at 2700°C[5]. The absence of a crucible is an advantage. Drawbacks include the difficulty in controlling the zone unless the heating source is well stabilized, and of growing large diameter crystals of good quality (because the radial temperature gradient tends to increase with crystal diameter, setting up strains that lead to dislocations). However, dislocation-free crystals of semiconductor silicon can be grown by this method.

(DENNIS ELWELL)

1. M. Kitazawa, N. Nagashima, T. Mizutani, K. Feuki, T. Mukaibo, *J. Cryst. Growth, 39*, 211 (1977).
2. B. Cockayne, D. B. Gasson, N. Forbes, *J. Mater. Sci., 5*, 837 (1970).
3. D. B. Gasson, *J. Sci. Instrum. 42*, 575 (1965).
4. M. Aono, C. Oshima, T. Tanaka, E. Bannai, S. Kawai, *Jpn. J. Appl. Phys. 49*, 2761 (1978).
5. W. Precht, G. E. Hollox, *J. Cryst. Growth, 3/4*, 818 (1968).

17.2.4.1.5. Flame Fusion Method.

The flame fusion process was the first method to give crystals of acceptable size for commercial applications from the melt, namely ruby crystals for use as gemstones.

In the earliest version two torches are used with powder fed through a tube into the hot zone[1]. The main improvement involves feeding hydrogen and oxygen through coaxial tubes, with the powder fed through the oxygen by a vibrator or hammer acting on a container located above the furnace (Fig. 1a). The powdered material falls into the oxyhydrogen flame and forms tiny droplets, which are condensed onto a ceramic pedestal. Initially a cone of polycrystalline material is formed, and the tip of the cone reaches the hot zone and melts to form tiny crystals. Operator skill is necessary to select one of these to form the seed from which the crystal will develop (Fig. 1b). The temperature may be adjusted by changing the hydrogen-to-oxygen ratio, and the powder flow rate can also be changed as the crystal diameter is increased. Once the crystal has reached a constant diameter, the growth process can continue without attention, and a single operator can produce crystals in many furnaces simultaneously in modern plants used for crystal growth of Al_2O_3 and $MgAl_2O_4$ (Fig. 1c).

After heating arrangements reduce the temperature gradients and so reduce the strain, which is normally severe in crystals grown by this method. Dislocation densities

are typically 10^5–10^6 cm^{-2} compared with 10^3 cm^{-2} or less for crystals pulled from the melt, and flame-fusion-grown crystals often contain tiny bubbles of trapped gas. In addition to the temperature distribution, the powder feed is important in achieving good quality crystals, and a free-flowing form is essential.

The flame fusion method is used to grow sapphire crystals for bearings and similar applications, and tons of Al_2O_3 are crystallized annually, particularly in factories in Switzerland, France, Czechoslovakia, China, Japan, and Russia. Ruby, sapphire, and

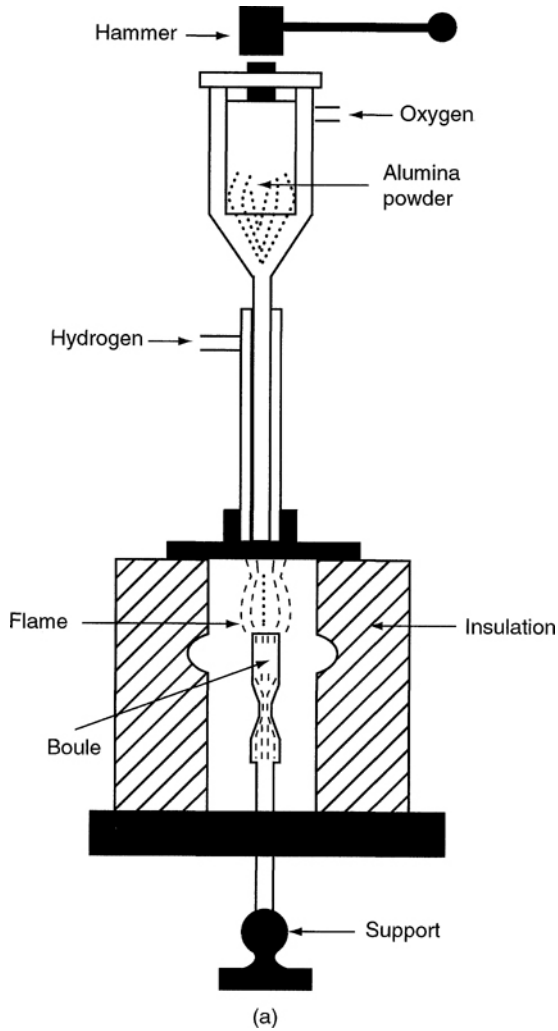

Figure 1. (a) Schematic diagram of crystal growth by the flame fusion method. (b) Stages of development of undoped Al_2O_3 and Cr-doped (ruby) crystals. (c) Furnace room used for Al_2O_3 production by H. Djevahirdjian Company at Monthey, Switzerland. (Courtesy of V. Djevahirdjian.)

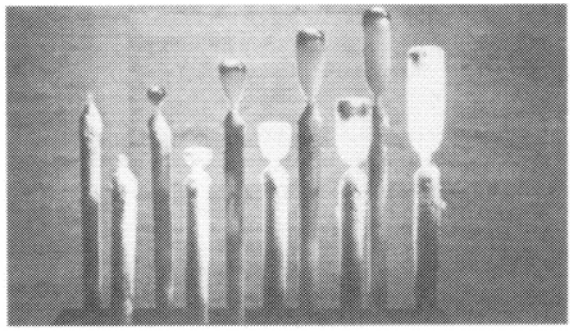

(b)

(c)

Figure 1 (*Continued*).

Table 1. Materials Grown by the Flame Fusion Process

Material	Melting point (°C)
Al_2O_3	2037
Al_4SiO_8	1900
Cr_2O_3	2275
Mg_2SiO_4	1898
Mg_2TiO_4	1840
$SrTiO_3$	2050
TiO_2	1925
Y_2O_3	2410

spinel crystals are also used extensively as gemstones. The process was used to grow crystals of rutile, TiO_2, and strontium titanate, $SrTiO_3$, also for the gem industry[2]. The tendency of these materials to lose oxygen during growth, because of the reducing nature of the flame, leads to the use of the three-tube burner, the third tube serving to provide an oxidizing atmosphere. Table 1 lists materials[3] grown by this method. A well-designed furnace is described[4], as is the extensive Russian work on flame fusion growth of Al_2O_3[5].

The highest melting material that can be grown by the flame fusion method is determined by the maximum temperature of the flame. A plasma torch may be used as an alternative heat source[6] for materials that decompose in a hydrogen–oxygen or coal gas–oxygen flame.

(DENNIS ELWELL)

1. K. Nassau, R. Crowningshield, *Lapidary J.*, *23*, 114, 313, 440 (1969).
2. D. Elwell, *Man-Made Gemstones*, Ellis Horwood, Chichester, 1979.
3. R. Falckenberg, in *Crystal Growth*, Vol. 2, C. H. L. Goodman, ed., Plenum Press, New York, 1978, p. 109.
4. J. G. Bednorz, H. J. Scheel, *J. Cryst. Growth*, *41*, 5 (1977).
5. L. M. Belyaev, ed., *Ruby and Sapphire*, Nauka, Moscow, 1974; transl. National Bureau of Standards, Githersburg, MD, 1980.
6. T. B. Reed, *J. Appl. Phys.*, *32*, 2534 (1961).

17.2.4.1.6. Skull Melting.

An alternative method for growing crystals of reactive high-melting materials is the skull melting technique in which the molten charge is surrounded by powder of the same

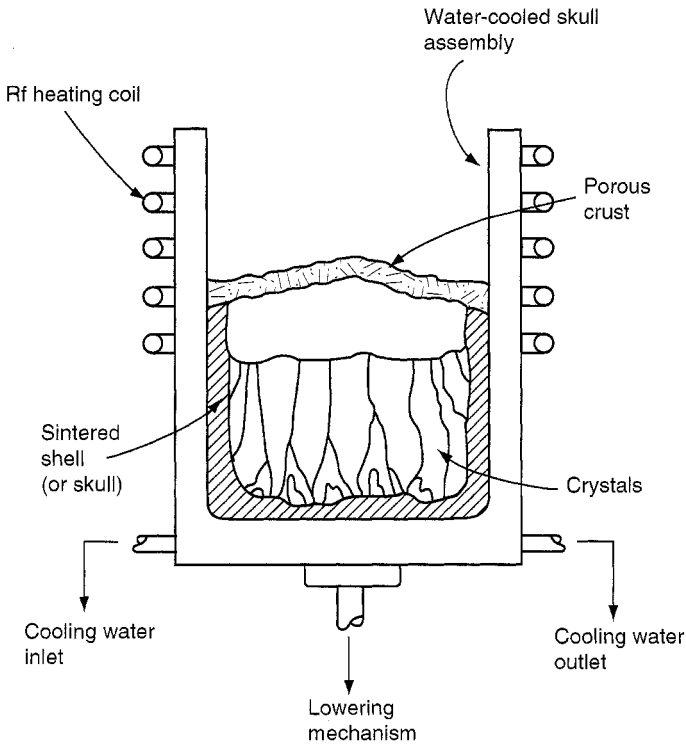

Figure 1. (a) Small-scale arrangement used for skull melting, showing distribution of crystals after cooling. (b) Small Crystal of cubic zirconia grown by skull melting. (Courtesy of J. F. Wenckus, Ceres Corporation.)

Inorganic Reactions and Methods, Volume 18
Edited by J. J. Zuckerman, Jim D. Atwood

The highest melting material that can be grown by the flame fusion method is determined by the maximum temperature of the flame. A plasma torch may be used as an alternative heat source[6] for materials that decompose in a hydrogen–oxygen or coal gas–oxygen flame.

(DENNIS ELWELL)

1. K. Nassau, R. Crowningshield, *Lapidary J.*, *23*, 114, 313, 440 (1969).
2. D. Elwell, *Man-Made Gemstones*, Ellis Horwood, Chichester, 1979.
3. R. Falckenberg, in *Crystal Growth*, Vol. 2, C. H. L. Goodman, ed., Plenum Press, New York, 1978, p. 109.
4. J. G. Bednorz, H. J. Scheel, *J. Cryst. Growth*, *41*, 5 (1977).
5. L. M. Belyaev, ed., *Ruby and Sapphire*, Nauka, Moscow, 1974; transl. National Bureau of Standards, Githersburg, MD, 1980.
6. T. B. Reed, *J. Appl. Phys.*, *32*, 2534 (1961).

17.2.4.1.6. Skull Melting.

An alternative method for growing crystals of reactive high-melting materials is the skull melting technique in which the molten charge is surrounded by powder of the same

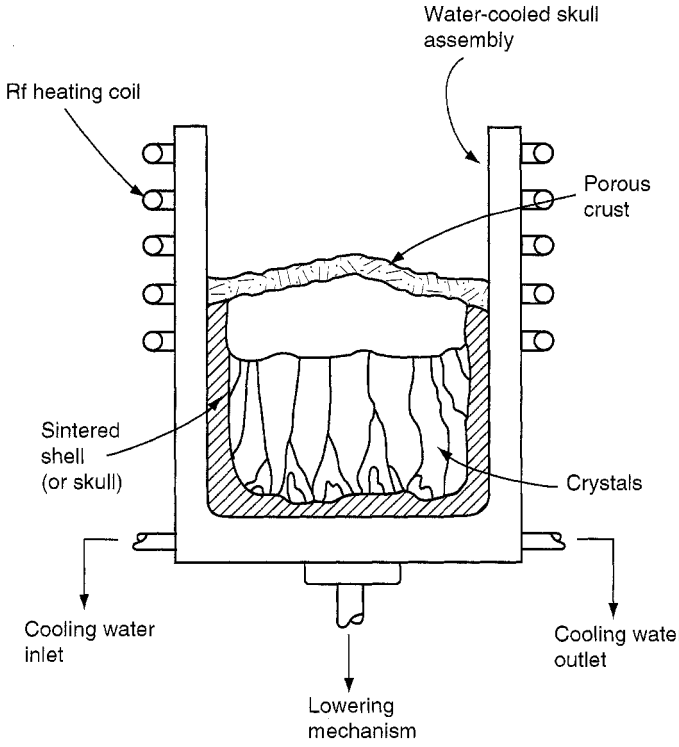

Figure 1. (a) Small-scale arrangement used for skull melting, showing distribution of crystals after cooling. (b) Small Crystal of cubic zirconia grown by skull melting. (Courtesy of J. F. Wenckus, Ceres Corporation.)

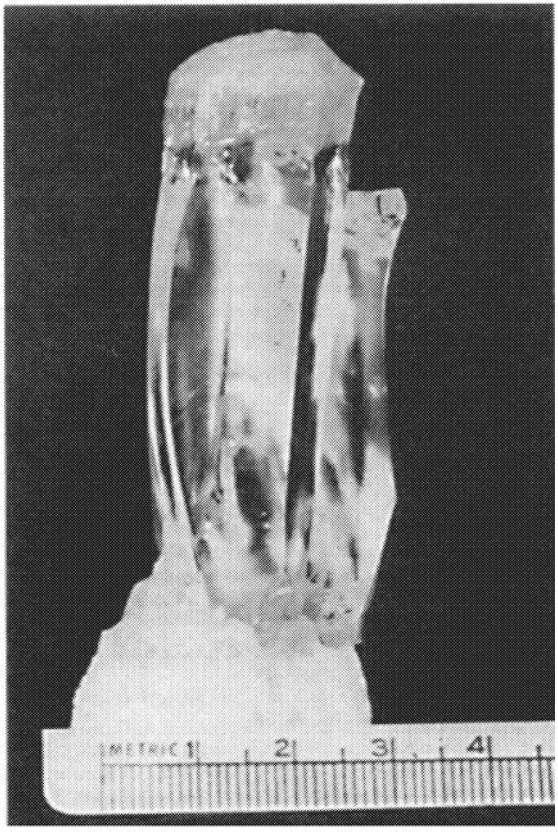

(b)

Figure 1 (*Continued*)

composition. The method involves melting by an rf field, confining the melt in a solid shell of the same material, and growing crystals by directional solidification[1]. This method is not suited to crystal growth of metals, since the small difference in electrical conductivity between the solid and liquid leads to rapid disappearance of the solid phase once most of the system has melted. Since, however, a powder of ceramic material is almost opaque to rf, direct heating of a material with conductivity that increases with temperature forms a melt surrounded by a powdered shell. Preheating of a refractory material (e.g., by an arc lamp) may be required until the conductivity reaches a value at which heating can produce and maintain the molten core.

For the container to be to transparent to rf radiation, it must be sectioned to avoid circular currents. A typical arrangement used for the growth of the cubic phase of zirconia is shown in Figure 1a. The growth of cubic zirconia for gem applications is a commercially important use of the skull melting technique. Melting is facilitated by including metallic zirconium in the ZrO_2 charge; this acts as a coupling medium for the rf

TABLE 1. EXAMPLES OF MATERIALS CRYSTALLIZED IN A COLD CONTAINER

Material	Melting Point (°C)
$CaHfO_3$	2700
$CaZrO_3$	2345
$LaAlO_3$	2100
MgO	2880
$SrTiO_3$	2038
Ta_2O_5	1877
Y_2O_3	2410
ZrO_2	2690

Source: Ref. 1.

power in the low temperature region, but oxidization occurs as the temperature rises to the point at which the oxide becomes conducting. Crystal growth is performed by slowly cooling the melt in a temperature gradient. Since seeded growth is not practical, several crystals grow in each run, but individual crystals grow up to many centimeters in diameter (Fig. 1b). Pure zirconia melts at 2690°C and is one of the more refractory materials to crystallize in a cold container. Commercial growth involves charges of several hundred kilograms. Other examples are listed in Table 1.

(DENNIS ELWELL)

1. V. I. Aleksandrov, V. V. Osiko, A. M. Prokhorov, V. M. Tatarintsev, in *Current Topics in Materials Science*, Vol. I, E. Kaldis, ed., North Holland, Amsterdam, 1978, p. 421.

17.2.4.1.7. Shaped Crystal Growth.

Crystals of specific cross-sectional shape can be grown by inserting an inert shape into the top of the melt to form a melt column of the desired shape. This process has been reviewed[1]. The melt column is then solidified by contact with a seed crystal, which is pulled vertically at a rate that is fast in comparison with pulling from the melt (see 17.2.4.1). Shaped crystal growth attracts attention for growing sapphire not only as filaments but also in shapes such as tubes, sheets, and narrow-bore tubing, all in single crystal form. These shaped crystals are now grown using a die strongly wetted by the molten alumina, with capillary flow used to transport the melt to the solid–liquid interface region. This edge-defined, film-fed (efg) method is used to produce silicon sheets for solar cells in addition to sapphire sheets for bar code readers in supermarkets, and so on. "Edge-defined" refers to the use of a die to determine the diameter and shape of the crystal to be pulled (see Fig. 1). It is this use of a die to control the crystal shape, rather than attempting to shape the melt column, that distinguishes the efg approach. The process may be made continuous by use of a self-filling technique to maintain a constant melt volume as the crystal is grown.

A molybdenum die is normally used for sapphire growth and rhenium for spinel, $MgAl_2O_4$. Sapphire plates are grown over 15 cm in width, and many small ribbons can be produced simultaneously from a single furnace[2].

(DENNIS ELWELL)

Inorganic Reactions and Methods, Volume 18
Edited by J. J. Zuckerman, Jim D. Atwood

TABLE 1. EXAMPLES OF MATERIALS CRYSTALLIZED IN A COLD CONTAINER

Material	Melting Point (°C)
$CaHfO_3$	2700
$CaZrO_3$	2345
$LaAlO_3$	2100
MgO	2880
$SrTiO_3$	2038
Ta_2O_5	1877
Y_2O_3	2410
ZrO_2	2690

Source: Ref. 1.

power in the low temperature region, but oxidization occurs as the temperature rises to the point at which the oxide becomes conducting. Crystal growth is performed by slowly cooling the melt in a temperature gradient. Since seeded growth is not practical, several crystals grow in each run, but individual crystals grow up to many centimeters in diameter (Fig. 1b). Pure zirconia melts at 2690°C and is one of the more refractory materials to crystallize in a cold container. Commercial growth involves charges of several hundred kilograms. Other examples are listed in Table 1.

(DENNIS ELWELL)

1. V. I. Aleksandrov, V. V. Osiko, A. M. Prokhorov, V. M. Tatarintsev, in *Current Topics in Materials Science*, Vol. I, E. Kaldis, ed., North Holland, Amsterdam, 1978, p. 421.

17.2.4.1.7. Shaped Crystal Growth.

Crystals of specific cross-sectional shape can be grown by inserting an inert shape into the top of the melt to form a melt column of the desired shape. This process has been reviewed[1]. The melt column is then solidified by contact with a seed crystal, which is pulled vertically at a rate that is fast in comparison with pulling from the melt (see 17.2.4.1). Shaped crystal growth attracts attention for growing sapphire not only as filaments but also in shapes such as tubes, sheets, and narrow-bore tubing, all in single crystal form. These shaped crystals are now grown using a die strongly wetted by the molten alumina, with capillary flow used to transport the melt to the solid–liquid interface region. This edge-defined, film-fed (efg) method is used to produce silicon sheets for solar cells in addition to sapphire sheets for bar code readers in supermarkets, and so on. "Edge-defined" refers to the use of a die to determine the diameter and shape of the crystal to be pulled (see Fig. 1). It is this use of a die to control the crystal shape, rather than attempting to shape the melt column, that distinguishes the efg approach. The process may be made continuous by use of a self-filling technique to maintain a constant melt volume as the crystal is grown.

A molybdenum die is normally used for sapphire growth and rhenium for spinel, $MgAl_2O_4$. Sapphire plates are grown over 15 cm in width, and many small ribbons can be produced simultaneously from a single furnace[2].

(DENNIS ELWELL)

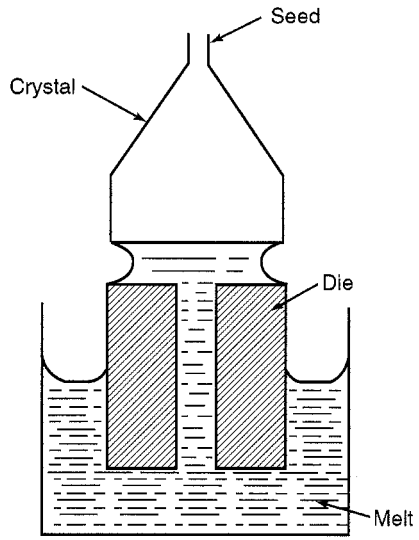

Figure 1. Arrangement for the growth of shaped crystals by the method. (After Ref. 2.)

1. P. I. Antonov, S. P. Nikanorov, *J. Cryst. Growth, 50,* 3 (1980).
2. H. Labelle, *J. Cryst. Growth, 50,* 8 (1980).

17.2.4.1.8. Fiber Growth.

The efg process can produce crystals in the form of fine fibers, but the range of materials grown successfully by this process is small. Single crystal fibers are also grown by controlled downward flow of a melt through a capillary terminated by a shaper immediately above the solid–liquid interface. A roller stabilizes the location of the solid fiber and controls its rate of movement[1]. In the extrusion technique a melt is pushed by nitrogen gas through a nozzle that determines the size and shape of the crystal. This method is used to grow silver bromide fibers 0.35–0.75 mm in diameter[2].

Refractory materials are subject to problems in the choice of container materials, and a float-zone method of fiber growth is more widely applicable. An approach that is particularly successful is a small-diameter version of a bulk crystal growth technique known as pedestal pulling. In this float-zone growth variation, a polycrystalline rod of the material to be crystallized is used to support the molten zone and a crystal of smaller diameter is pulled from this zone. In the apparatus shown diagrammatically in Figure 1a, the molten zone is produced by a laser beam that is split to provide heating from two or more directions. This beam splitting reduces the temperature inhomogeneity; but rotation of the feed rod is still desirable to reduce the azimuthal temperature gradients. Figure 1b illustrates pulling of single crystal fibers of circular cross section by this technique, at rates of several centimenters per minute. This technique is applied to Al_2O_3,

Inorganic Reactions and Methods, Volume 18
Edited by J. J. Zuckerman, Jim D. Atwood

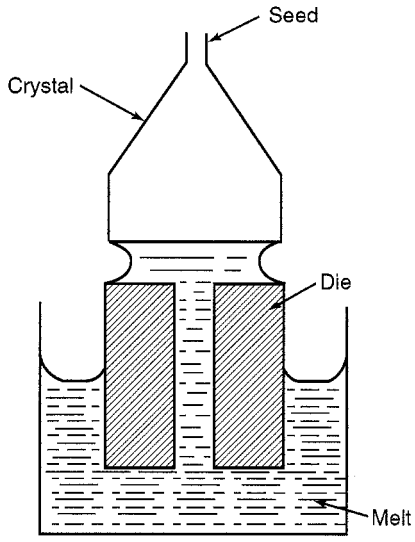

Figure 1. Arrangement for the growth of shaped crystals by the method. (After Ref. 2.)

1. P. I. Antonov, S. P. Nikanorov, *J. Cryst. Growth, 50,* 3 (1980).
2. H. Labelle, *J. Cryst. Growth, 50,* 8 (1980).

17.2.4.1.8. Fiber Growth.

The efg process can produce crystals in the form of fine fibers, but the range of materials grown successfully by this process is small. Single crystal fibers are also grown by controlled downward flow of a melt through a capillary terminated by a shaper immediately above the solid–liquid interface. A roller stabilizes the location of the solid fiber and controls its rate of movement[1]. In the extrusion technique a melt is pushed by nitrogen gas through a nozzle that determines the size and shape of the crystal. This method is used to grow silver bromide fibers 0.35–0.75 mm in diameter[2].

Refractory materials are subject to problems in the choice of container materials, and a float-zone method of fiber growth is more widely applicable. An approach that is particularly successful is a small-diameter version of a bulk crystal growth technique known as pedestal pulling. In this float-zone growth variation, a polycrystalline rod of the material to be crystallized is used to support the molten zone and a crystal of smaller diameter is pulled from this zone. In the apparatus shown diagrammatically in Figure 1a, the molten zone is produced by a laser beam that is split to provide heating from two or more directions. This beam splitting reduces the temperature inhomogeneity; but rotation of the feed rod is still desirable to reduce the azimuthal temperature gradients. Figure 1b illustrates pulling of single crystal fibers of circular cross section by this technique, at rates of several centimenters per minute. This technique is applied to Al_2O_3,

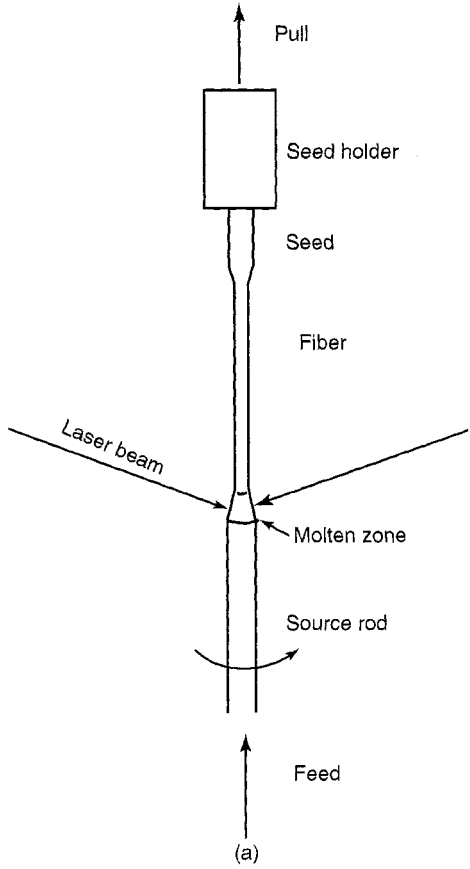

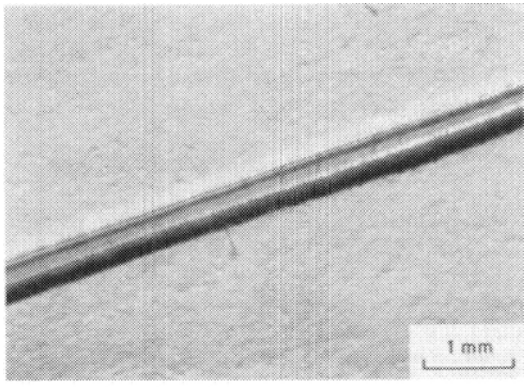

Figure 1. (a) Arrangement used for fiber pulling. (After Ref. 3) (b) Cross section of 100 μm diameter fiber grown by the pedestae pulling method. (Courtesy of M.M. Elweu.)

$CaSc_2O_4$, $GdMoO_4$, $LiNbO_3$, Bi superconductors, and $Y_3Al_5O_{12}$, and laser action has been demonstrated in a fine $Y_3Al_5O_{12}$ (Nd) fiber.

(DENNIS ELWELL)

1. Y. Mimura, Y. Okamura, Y. Komazawa, C. Ota, *Jpn. J. Appl. Phys., 19*, 269 (1980).
2. T. J. Bridges, J. S. Hasiak, A. R. Strnad, *Opt. Lett., 5*, 85 (1980).
3. C. A. Burrus, L. A. Coldeen, *Appl. Phys. Lett., 31*, 383 (1977).

17.2.4.1.9. Arc-Fusion Method.

In the arc fusion method, a large powder charge (typically 60 kg) is inserted into an insulated enclosure and a molten core is produced at the center by striking an arc between carbon electrodes. The melt is then solidified by slow reduction of the current between the electrodes, and the resulting mass may contain large crystals, although nucleation is uncontrolled.

This method is used commercially to grow crystals of MgO, and single crystals weighing up to 300 g are produced[1]. The crystals are of poor crystallographic quality, since they are grown rapidly and are subject to severe stresses during cooling. Crystals of other refractory oxides such as BaO, CaO, SrO, and ZrO_2 are also grown by this method.

(DENNIS ELWELL)

1. J. C. Brice, *The Growth of Crystals from Liquids*, North Holland, Amsterdam, 1973.

17.2.4.2. Growth from High-Melting Solutions

Solution growth techniques, which are used for materials that cannot be grown as high quality crystals from a pure melt, are preferred for one or more of the following reasons:

1. The material to be crystallized melts incongruently, and cannot be grown from a melt of the same composition.
2. The material has a high vapor pressure at its melting point, or one component has a high vapor pressure, so that it tends to be nonstoichiometric when grown from the melt.
3. The material has too high a melting point to be grown from the melt.
4. The material undergoes a phase transition that results in severe strain or even fracture on cooling; or
5. Better quality crystals can be grown from solution than from the melt.

With regard to crystal quality, solution-grown crystals may exhibit a lower dislocation density than the melt-grown material, as well as a lower concentration of point defects because of a lower growth temperature; but solvent atoms may enter the crystal as impurities, and solvent inclusions result when growth is unstable. Avoiding solvent inclusions requires a growth rate much slower than that used for crystal growth from the melt. (e.g., millimeters per day).

Solution-grown crystals are faceted (Fig. 1), although the transition from growth from an impure melt to solution growth has no clearly marked boundaries, and crystals can be grown from solution using the techniques described above for melt growth. This is especially true in crystal growth from nonstoichiometric melts, which are a special case of

Inorganic Reactions and Methods, Volume 18
Edited by J. J. Zuckerman, Jim D. Atwood

$CaSc_2O_4$, $GdMoO_4$, $LiNbO_3$, Bi superconductors, and $Y_3Al_5O_{12}$, and laser action has been demonstrated in a fine $Y_3Al_5O_{12}$ (Nd) fiber.

(DENNIS ELWELL)

1. Y. Mimura, Y. Okamura, Y. Komazawa, C. Ota, *Jpn. J. Appl. Phys., 19*, 269 (1980).
2. T. J. Bridges, J. S. Hasiak, A. R. Strnad, *Opt. Lett., 5*, 85 (1980).
3. C. A. Burrus, L. A. Coldeen, *Appl. Phys. Lett., 31*, 383 (1977).

17.2.4.1.9. Arc-Fusion Method.

In the arc fusion method, a large powder charge (typically 60 kg) is inserted into an insulated enclosure and a molten core is produced at the center by striking an arc between carbon electrodes. The melt is then solidified by slow reduction of the current between the electrodes, and the resulting mass may contain large crystals, although nucleation is uncontrolled.

This method is used commercially to grow crystals of MgO, and single crystals weighing up to 300 g are produced[1]. The crystals are of poor crystallographic quality, since they are grown rapidly and are subject to severe stresses during cooling. Crystals of other refractory oxides such as BaO, CaO, SrO, and ZrO_2 are also grown by this method.

(DENNIS ELWELL)

1. J. C. Brice, *The Growth of Crystals from Liquids*, North Holland, Amsterdam, 1973.

17.2.4.2. Growth from High-Melting Solutions

Solution growth techniques, which are used for materials that cannot be grown as high quality crystals from a pure melt, are preferred for one or more of the following reasons:

1. The material to be crystallized melts incongruently, and cannot be grown from a melt of the same composition.
2. The material has a high vapor pressure at its melting point, or one component has a high vapor pressure, so that it tends to be nonstoichiometric when grown from the melt.
3. The material has too high a melting point to be grown from the melt.
4. The material undergoes a phase transition that results in severe strain or even fracture on cooling; or
5. Better quality crystals can be grown from solution than from the melt.

With regard to crystal quality, solution-grown crystals may exhibit a lower dislocation density than the melt-grown material, as well as a lower concentration of point defects because of a lower growth temperature; but solvent atoms may enter the crystal as impurities, and solvent inclusions result when growth is unstable. Avoiding solvent inclusions requires a growth rate much slower than that used for crystal growth from the melt. (e.g., millimeters per day).

Solution-grown crystals are faceted (Fig. 1), although the transition from growth from an impure melt to solution growth has no clearly marked boundaries, and crystals can be grown from solution using the techniques described above for melt growth. This is especially true in crystal growth from nonstoichiometric melts, which are a special case of

Inorganic Reactions and Methods, Volume 18
Edited by J. J. Zuckerman, Jim D. Atwood

$CaSc_2O_4$, $GdMoO_4$, $LiNbO_3$, Bi superconductors, and $Y_3Al_5O_{12}$, and laser action has been demonstrated in a fine $Y_3Al_5O_{12}$ (Nd) fiber.

(DENNIS ELWELL)

1. Y. Mimura, Y. Okamura, Y. Komazawa, C. Ota, *Jpn. J. Appl. Phys., 19*, 269 (1980).
2. T. J. Bridges, J. S. Hasiak, A. R. Strnad, *Opt. Lett., 5*, 85 (1980).
3. C. A. Burrus, L. A. Coldeen, *Appl. Phys. Lett., 31*, 383 (1977).

17.2.4.1.9. Arc-Fusion Method.

In the arc fusion method, a large powder charge (typically 60 kg) is inserted into an insulated enclosure and a molten core is produced at the center by striking an arc between carbon electrodes. The melt is then solidified by slow reduction of the current between the electrodes, and the resulting mass may contain large crystals, although nucleation is uncontrolled.

This method is used commercially to grow crystals of MgO, and single crystals weighing up to 300 g are produced[1]. The crystals are of poor crystallographic quality, since they are grown rapidly and are subject to severe stresses during cooling. Crystals of other refractory oxides such as BaO, CaO, SrO, and ZrO_2 are also grown by this method.

(DENNIS ELWELL)

1. J. C. Brice, *The Growth of Crystals from Liquids*, North Holland, Amsterdam, 1973.

17.2.4.2. Growth from High-Melting Solutions

Solution growth techniques, which are used for materials that cannot be grown as high quality crystals from a pure melt, are preferred for one or more of the following reasons:

1. The material to be crystallized melts incongruently, and cannot be grown from a melt of the same composition.
2. The material has a high vapor pressure at its melting point, or one component has a high vapor pressure, so that it tends to be nonstoichiometric when grown from the melt.
3. The material has too high a melting point to be grown from the melt.
4. The material undergoes a phase transition that results in severe strain or even fracture on cooling; or
5. Better quality crystals can be grown from solution than from the melt.

With regard to crystal quality, solution-grown crystals may exhibit a lower dislocation density than the melt-grown material, as well as a lower concentration of point defects because of a lower growth temperature; but solvent atoms may enter the crystal as impurities, and solvent inclusions result when growth is unstable. Avoiding solvent inclusions requires a growth rate much slower than that used for crystal growth from the melt. (e.g., millimeters per day).

Solution-grown crystals are faceted (Fig. 1), although the transition from growth from an impure melt to solution growth has no clearly marked boundaries, and crystals can be grown from solution using the techniques described above for melt growth. This is especially true in crystal growth from nonstoichiometric melts, which are a special case of

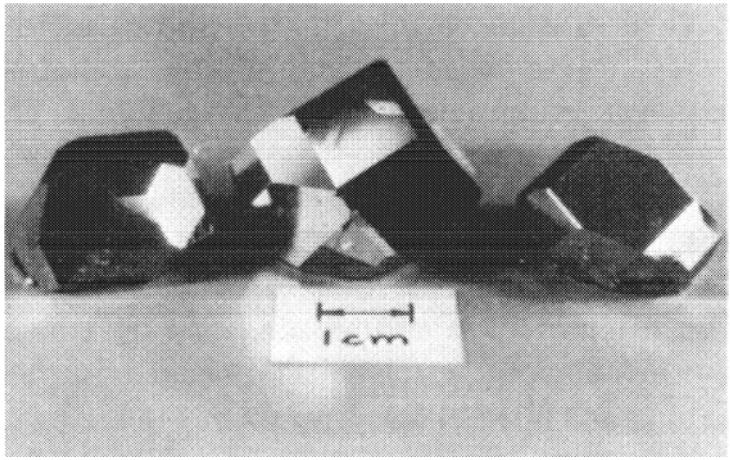

Figure 1. Crystals of Al-coated $Y_3Al_5O_{12}$ grown from high temperature solution. (From Ref. 1.)

TABLE 1. PROPERTIES OF AN IDEAL SOLVENT

1. High solubility for the crystal constituents.
2. The crystal phase required should be the only stable solid phase.
3. Appreciable change of solubility with temperature.
4. Viscosity in the range of 1 to 10 cP.
5. Low melting point.
6. Low volatility at the highest applied temperature (except when the solvent evaporation technique is used).
7. Low reactivity with the container material.
8. Absence of elements that are incorporated into the crystal.
9. Ready availability in high purity at low cost.
10. Density appropriate for the mode of growth.
11. Ease of separation from the grown crystal by chemical or physical means.
12. Low tendency of the solvent to "creep" out of the crucible.
13. Low toxicity.

Source: Ref. 2.

solution growth in which no additional component is introduced (e.g., $BaTiO_3$ crystal growth from melts containing excess TiO_2); nonfaceted crystals may occur in this case.

The terms "high melting" and "solution" are not exactly defined in this context. The experiments described normally range from 300 to 1800°C, and the solute concentration is 1–30 mol% or wt%. It is difficult to specify the best solvent in terms of fundamental properties like the strength of chemical bonding between solute and solvent, but the physical properties of an ideal solvent are listed in Table 1.

For solubility, a solvent should be similar to the solute, but that condition favors mutual solid solubility and, therefore, contamination of the crystal with solute atoms. The optimum solvent is, therefore, one that is similar in chemical bond type to the solute,

TABLE 2. EXAMPLES OF SOLVENT–SOLUTE PAIRS WITH CRYSTAL CHEMICAL DIFFERENCES

Difference of cationic and anionic radii
CeO_2, ThO_2 from Li_2WO_4
CoO, TiO_2 from NaCl
Difference of cationic radii
MgO, $MgAl_2O_4$ from PbF_2, $Be_3Al_2Si_3O_{18}$ from Li_2MoO_4, Na_2MoO_4, etc.
$Y_3Fe_5O_{12}$ from $BaO \cdot 0.6B_2O_3$
Al_2O_3 from LaF_3
Difference of anionic radii
$BaTiO_3$ from $BaCl_2$
$PbZrO_3$ from $PbCl_2$
$BaWO_4$ from $BaCl_2$
CaO, CoO, CuO from NaCl
Difference of valency states of both cation and anion
$PbTiO_3$, $BaTiO_3$ from KF
Al_2O_3 from PbF_2
$Y_4Si_3O_{12}$ from KF
TiO_2 from Na_3AlF_6, NaCl
Difference of valency state of cation
VO_2 from V_2O_5
$ZrSiO_4$ from Li_2O–MoO_3, Na_2O–MoO_3
Al_2O_3 from PbO
Difference of valency state of anion
Al_2O_3 from LaF_3, PbF_2
$MgAl_2O_4$, MgO, TiO_2, MnO from PbF_2
$BaTiO_3$ from $BaCl_2$

Source: Ref. 2.

but crystal chemical differences between solvent and solute exist to prevent solid solubility. Some examples are listed in Table 2; they illustrate the tendency for fluorides or oxide-containing solvents to be used for crystal growth of refractory oxides (the term "flux" is applied to a molten salt solvent). Lead compounds such as PbO and PbF_2, and borates such as BaB_4O_7, are the most widely used fluxes. Sulfides and halides are used as solvents for more covalent solutes, and metallic solvents for more highly conducting refractory materials. Examples of refractory materials and successful solvents are listed in Table 3.

Many systems used for high temperature solution growth are extremely complex, and their compositions are chosen by empirical procedures. Phase diagrams are often not available.

One approach toward predicting the compositions of complex melts treats the ternary oxides such as $ThGeO_4$, which are crystallized from a melt containing a refractory oxide (ThO_2) and a basic oxide (K_2O or PbO)[3]. An excess of the acidic oxide is required, above the stoichiometric ratio, depending on the difference in melting point of the refractory and acidic oxide. Larger crystals can be grown by replacing the basic oxide with the corresponding fluoride, and the addition of a small quantity of B_2O_3 or MoO_3 often forms complexes and reduces the number of crystals nucleated.

TABLE 3. EXAMPLES OF HIGH TEMPERATURE SOLVENTS FOR CRYSTAL GROWTH OF CERAMIC MATERIALS

Material	Solvent
Al_2O_3	PbF_2
BN	Li_3N
$BaTiO_3$	TiO_2, KF
C (graphite or diamond)	Fe, Ni
$CaCO_3$	Li_2CO_3
$CaY_2Mg_2Ge_3O_{12}$	$CaO/GeO_2/B_2O_3$
CeO_2	Li_2O/MoO_3
$K(Ta, Nb)O_3$	K_2O/K_2CO_3
SiC	Si
SmB_6	Al
TaC	Fe
ThO_2	PbF_2/Bi_2O_3
$Y_3Fe_5O_{12}$	$PbO/PbF_2/B_2O_3$

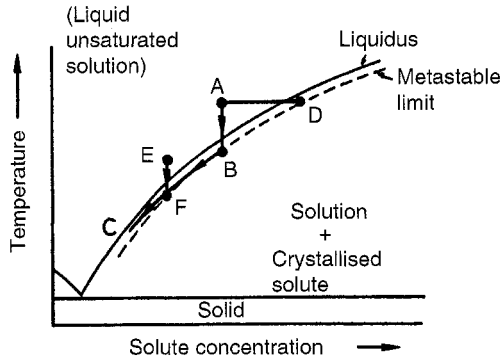

Figure 2. Methods of achieving supersaturation in high temperature solutions: *ABC*, slow cooling; *AD*, evaporation; *EF*, thermal gradient transport. (From Ref. 2.).

Reviews of crystal growth from high temperature solution are available[2,4]. The crystal growth of magnetic garnets is reviewed, and apparatus for the growth of large crystals from high temperature solution is described[5–7]. Crystals weighing several hundred grams can be routinely grown from high temperature solutions.

Crystals are grown from high temperature solutions by slow cooling, solvent evaporation, and solute transport in a temperature gradient. These routes to crystal growth are illustrated in Figure 2, which also shows the metastable range of supersaturated solution in which nucleation will not occur, although growth will take place on seed crystals. These processes are treated individually in the subsections that follow, together with other techniques that are important in crystal growth from high-melting solutions.

(DENNIS ELWELL)

1. A. W. Morris, D. Elwell, *J. Mater. Sci., 14*, 2139 (1979).
2. D. Elwell, H. J. Scheel, *Crystal Growth from High-Temperature Solutions*, Academic Press, London, 1975.
3. B. M. Wanklyn, *J. Cryst. Growth., 37*, 334 (1977).
4. D. Elwell, in *Crystal Growth*, 2nd ed. B. R. Pamplin, ed., Pergamon Press, Oxford, 1980, p. 463.
5. W. Tolksdorf, F. Welz, *Cryst., 1*, 1 (1980).
6. V. A. Timofeeva, A. B. Bykov, *Prog. Cryst. Growth Charact., 2*, 377 (1979).
7. R. Hergt, P. Gornert, *Phys. Status Solidi A, 21*, 77 (1974).

17.2.4.2.1. Slow Cooling.

The linear growth rate, v of a crystal is related to the cooling rate dT/dt:

$$v = \frac{V}{A\rho}\frac{dn_e}{dT}\frac{dT}{dt} \tag{a}$$

where V is the solution volume, A the area being deposited, ρ the density of the crystal, and n_e the solute solubility at temperature T. Constant linear growth, therefore, requires an increased cooling rate as the crystals grow and their area increases. However, the maximum stable growth rate, v_{max}, decreases as the crystal grows larger[1]. Optimum cooling programs are calculated based on the assumption that $v_{max} \propto L^{-1/2}$ for a crystal of side L; the programs are approximately linear when the crystal reaches millimeter size, but slower cooling rates are necessary ($\Delta T \sim t^3$ approximately) during the early stages when the crystal is small (see Fig. 1). The maximum linear rate of stable growth is of the order of 10^{-5} mm/s^{-1}, and a typical cooling rate is 1°C/h. Close control of the furnace temperature is important, and control to better than 0.1°C at temperatures exceeding 1000°C is possible[2,3].

Seeding can both eliminate the requirement for slow cooling during the early stages of growth and reduce the risk of multiple nucleation. A seed left in contact with the growth medium tends to dissolve, and introduction of a seed into the melt after homogenization can lead to thermal shock. The crystal is introduced by a 120° rotation into a spherical crucible, and the region around the crystal is cooled locally by a flow of gas in a closed tube with its end located close to the seed.[3] This method relies on the ease of fabrication of platinum crucibles, but it is complex, especially the requirement to vent

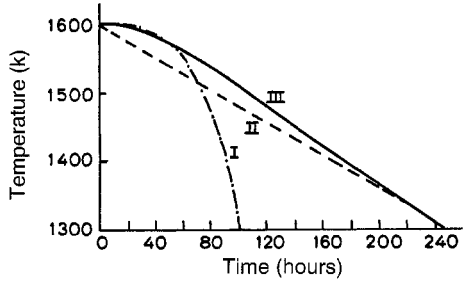

Figure 1. Cooling programs for crystal growth by slow cooling: I, constant linear growth rate; II, constant cooling rate; III, optimum allowing for decrease in maximum stable growth rate as crystal becomes larger. (From Ref. 1.)

Inorganic Reactions and Methods, Volume 18
Edited by J. J. Zuckerman, Jim D. Atwood

1. A. W. Morris, D. Elwell, *J. Mater. Sci., 14*, 2139 (1979).
2. D. Elwell, H. J. Scheel, *Crystal Growth from High-Temperature Solutions*, Academic Press, London, 1975.
3. B. M. Wanklyn, *J. Cryst. Growth., 37*, 334 (1977).
4. D. Elwell, in *Crystal Growth*, 2nd ed. B. R. Pamplin, ed., Pergamon Press, Oxford, 1980, p. 463.
5. W. Tolksdorf, F. Welz, *Cryst., 1*, 1 (1980).
6. V. A. Timofeeva, A. B. Bykov, *Prog. Cryst. Growth Charact., 2*, 377 (1979).
7. R. Hergt, P. Gornert, *Phys. Status Solidi A, 21*, 77 (1974).

17.2.4.2.1. Slow Cooling.

The linear growth rate, v of a crystal is related to the cooling rate dT/dt:

$$v = \frac{V}{A\rho}\frac{dn_e}{dT}\frac{dT}{dt} \tag{a}$$

where V is the solution volume, A the area being deposited, ρ the density of the crystal, and n_e the solute solubility at temperature T. Constant linear growth, therefore, requires an increased cooling rate as the crystals grow and their area increases. However, the maximum stable growth rate, v_{max}, decreases as the crystal grows larger[1]. Optimum cooling programs are calculated based on the assumption that $v_{max} \propto L^{-1/2}$ for a crystal of side L; the programs are approximately linear when the crystal reaches millimeter size, but slower cooling rates are necessary ($\Delta T \sim t^3$ approximately) during the early stages when the crystal is small (see Fig. 1). The maximum linear rate of stable growth is of the order of 10^{-5} mm/s^{-1}, and a typical cooling rate is 1°C/h. Close control of the furnace temperature is important, and control to better than 0.1°C at temperatures exceeding 1000°C is possible[2,3].

Seeding can both eliminate the requirement for slow cooling during the early stages of growth and reduce the risk of multiple nucleation. A seed left in contact with the growth medium tends to dissolve, and introduction of a seed into the melt after homogenization can lead to thermal shock. The crystal is introduced by a 120° rotation into a spherical crucible, and the region around the crystal is cooled locally by a flow of gas in a closed tube with its end located close to the seed.[3] This method relies on the ease of fabrication of platinum crucibles, but it is complex, especially the requirement to vent

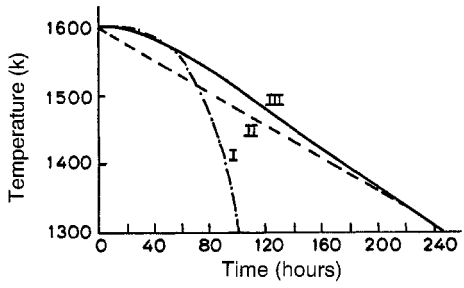

Figure 1. Cooling programs for crystal growth by slow cooling: I, constant linear growth rate; II, constant cooling rate; III, optimum allowing for decrease in maximum stable growth rate as crystal becomes larger. (From Ref. 1.)

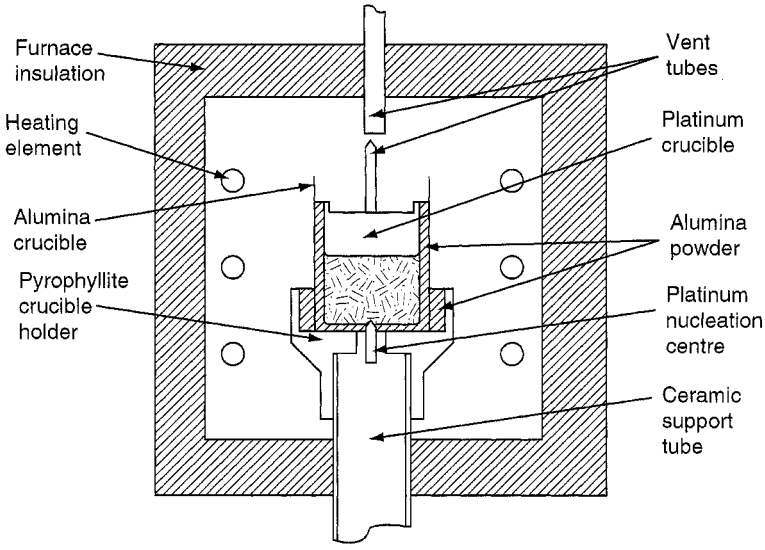

Figure 2. Diagram of furnace used for unseeded crystal growth by slow cooling of high temperature solutions. (From Ref. 5.)

the crucible during the initial heating stage but minimize solvent evaporation during growth. $Y_3Al_5O_{12}$ crystals are shown in Figure 2.

Stirring the melt during crystal growth is important, both as a means of homogenizing the bulk solution and to decrease differences in local supersaturation between the corners and faces of a growing crystal. The most effective means of stirring a closed crucible is the accelerated crucible rotation technique[4], which can be applied to various geometries, although optimization studies on the rotation program are rare. One disadvantage of changing the rotation rate in periodic fashion is there exists corresponding temperature fluctuation at the crystal–solution interface; therefore, a periodic variation in the growth rate, and the optimum stirring program may lead to unacceptable changes in the local temperature[3]. In addition, excessive changes in rotation rate may cause crystals formed by spontaneous nucleation on a cold finger to be dislodged[5].

Thus, when a suitable cooling program is adopted, close temperature control and stirring by means of smooth changes in crucible rotation rate can give large crystals.

Systematic approaches to large crystal growth from high-melting solutions are applied to only a small number of materials; instead, slow cooling using unstirred crucibles 25–100 mL in volume (compared >500 mL for growth of large crystals) is employed for producing the first crystals of novel materials, particularly ternary and quaternary compositions. This approach is valuable when expensive rare earth compounds are used, and the information on crystallization may be employed in the growth of larger crystals, if required.

(DENNIS ELWELL)

1. H. J. Scheel, D. Elwell, *J. Cryst. Growth, 12*, 153 (1972).
2. D. Elwell, H. J. Scheel, *Crystal Growth from High-Temperature Solutions*, Academic Press, London, 1975.
3. W. Tolksdorf, F. Welz, *Crystal, 1*, 1 (1980).
4. H. J. Scheel, E. O. Schulz-Dubois, *J. Cryst. Growth, 8*, 304 (1971).
5. A. W. Morris, D. Elwell, *J. Mater. Sci., 14*, 2139 (1979).

17.2.4.2.2. Solvent Evaporation.

If the volume, V, of a solution changes at a rate dV/dt because of solvent evaporation, the linear growth rate of a crystal of area A is:

$$v = \frac{n_e}{\rho A}\frac{dV}{dt} \qquad \text{(a)}$$

with other symbols corresponding to those of equation (a) in 17.2.4.2.1. Solvent evaporation is used for materials that react with the solvent at lower temperatures. For example, HfO_2 reacts with PbO to form $PbHfO_3$ below 1200°C, but HfO_2 crystals can be grown by PbO evaporation, provided the temperature is kept above 1200°C. Crystals of other materials such as ThO_2 are prepared by this method (see list in Ref. 1), but the rate of evaporation (hence the linear growth rate) is difficult to control unless the temperature is varied, which removes the advantage due to isothermal growth. Although crucible weighing could be used to vary the growth rate by adjusting the size of the aperture through which evaporation occurs, in practice slow cooling is preferred.

(DENNIS ELWELL)

1. D. Elwell, H. J. Scheel, *Crystal Growth from High-Temperature Solutions*, Academic Press, London, 1975.

17.2.4.2.3. Solute Transport in a Temperature Gradient.

To transport solute in a temperature gradient, undissolved nutrient is maintained at some temperature (E in Fig. 2 of 17.2.4.2), and a flow of solution occurs to a lower temperature (F in the same figure), where a seed is located and growth occurs because the solution is supersaturated. The growth rate depends primarily on the temperature difference $\Delta T = (E - F)$[1], and can be controlled by adjustment to this parameter.

Transport may be done in a sealed enclosure for volatile solvents, but usually the nutrient is located at the base of the crucible in the top seeding geometry. Refractory oxides are grown from viscous solvents of low volatility, such as the BaO/B_2O_3 eutectic. The solution is stirred by rotating the seed and by thermal convection, but nonmixing regions may occur within the melt. Few large crystals of good quality are grown by the gradient transport/top-seeding arrangement, some exceptions being $NiFe_2O_4$, $Y_3Fe_5O_{12}$, and $KNbO_3$ (see Fig. 1).

An arrangement for using thermal transport with a stirred solution is available[2]. The advantage of thermal gradient transport is that, since the crystal grows under steady state

Inorganic Reactions and Methods, Volume 18
Edited by J. J. Zuckerman, Jim D. Atwood

1. H. J. Scheel, D. Elwell, *J. Cryst. Growth, 12*, 153 (1972).
2. D. Elwell, H. J. Scheel, *Crystal Growth from High-Temperature Solutions*, Academic Press, London, 1975.
3. W. Tolksdorf, F. Welz, *Crystal, 1*, 1 (1980).
4. H. J. Scheel, E. O. Schulz-Dubois, *J. Cryst. Growth, 8*, 304 (1971).
5. A. W. Morris, D. Elwell, *J. Mater. Sci., 14*, 2139 (1979).

17.2.4.2.2. Solvent Evaporation.

If the volume, V, of a solution changes at a rate dV/dt because of solvent evaporation, the linear growth rate of a crystal of area A is:

$$v = \frac{n_e}{\rho A}\frac{dV}{dt} \qquad \text{(a)}$$

with other symbols corresponding to those of equation (a) in 17.2.4.2.1. Solvent evaporation is used for materials that react with the solvent at lower temperatures. For example, HfO_2 reacts with PbO to form $PbHfO_3$ below 1200°C, but HfO_2 crystals can be grown by PbO evaporation, provided the temperature is kept above 1200°C. Crystals of other materials such as ThO_2 are prepared by this method (see list in Ref. 1), but the rate of evaporation (hence the linear growth rate) is difficult to control unless the temperature is varied, which removes the advantage due to isothermal growth. Although crucible weighing could be used to vary the growth rate by adjusting the size of the aperture through which evaporation occurs, in practice slow cooling is preferred.

(DENNIS ELWELL)

1. D. Elwell, H. J. Scheel, *Crystal Growth from High-Temperature Solutions*, Academic Press, London, 1975.

17.2.4.2.3. Solute Transport in a Temperature Gradient.

To transport solute in a temperature gradient, undissolved nutrient is maintained at some temperature (E in Fig. 2 of 17.2.4.2), and a flow of solution occurs to a lower temperature (F in the same figure), where a seed is located and growth occurs because the solution is supersaturated. The growth rate depends primarily on the temperature difference $\Delta T = (E - F)$[1], and can be controlled by adjustment to this parameter.

Transport may be done in a sealed enclosure for volatile solvents, but usually the nutrient is located at the base of the crucible in the top seeding geometry. Refractory oxides are grown from viscous solvents of low volatility, such as the BaO/B_2O_3 eutectic. The solution is stirred by rotating the seed and by thermal convection, but nonmixing regions may occur within the melt. Few large crystals of good quality are grown by the gradient transport/top-seeding arrangement, some exceptions being $NiFe_2O_4$, $Y_3Fe_5O_{12}$, and $KNbO_3$ (see Fig. 1).

An arrangement for using thermal transport with a stirred solution is available[2]. The advantage of thermal gradient transport is that, since the crystal grows under steady state

Inorganic Reactions and Methods, Volume 18
Edited by J. J. Zuckerman, Jim D. Atwood

1. H. J. Scheel, D. Elwell, *J. Cryst. Growth, 12*, 153 (1972).
2. D. Elwell, H. J. Scheel, *Crystal Growth from High-Temperature Solutions*, Academic Press, London, 1975.
3. W. Tolksdorf, F. Welz, *Crystal, 1*, 1 (1980).
4. H. J. Scheel, E. O. Schulz-Dubois, *J. Cryst. Growth, 8*, 304 (1971).
5. A. W. Morris, D. Elwell, *J. Mater. Sci., 14*, 2139 (1979).

17.2.4.2.2. Solvent Evaporation.

If the volume, V, of a solution changes at a rate dV/dt because of solvent evaporation, the linear growth rate of a crystal of area A is:

$$v = \frac{n_e}{\rho A}\frac{dV}{dt} \qquad \text{(a)}$$

with other symbols corresponding to those of equation (a) in 17.2.4.2.1. Solvent evaporation is used for materials that react with the solvent at lower temperatures. For example, HfO_2 reacts with PbO to form $PbHfO_3$ below 1200°C, but HfO_2 crystals can be grown by PbO evaporation, provided the temperature is kept above 1200°C. Crystals of other materials such as ThO_2 are prepared by this method (see list in Ref. 1), but the rate of evaporation (hence the linear growth rate) is difficult to control unless the temperature is varied, which removes the advantage due to isothermal growth. Although crucible weighing could be used to vary the growth rate by adjusting the size of the aperture through which evaporation occurs, in practice slow cooling is preferred.

(DENNIS ELWELL)

1. D. Elwell, H. J. Scheel, *Crystal Growth from High-Temperature Solutions*, Academic Press, London, 1975.

17.2.4.2.3. Solute Transport in a Temperature Gradient.

To transport solute in a temperature gradient, undissolved nutrient is maintained at some temperature (E in Fig. 2 of 17.2.4.2), and a flow of solution occurs to a lower temperature (F in the same figure), where a seed is located and growth occurs because the solution is supersaturated. The growth rate depends primarily on the temperature difference $\Delta T = (E - F)$[1], and can be controlled by adjustment to this parameter.

Transport may be done in a sealed enclosure for volatile solvents, but usually the nutrient is located at the base of the crucible in the top seeding geometry. Refractory oxides are grown from viscous solvents of low volatility, such as the BaO/B_2O_3 eutectic. The solution is stirred by rotating the seed and by thermal convection, but nonmixing regions may occur within the melt. Few large crystals of good quality are grown by the gradient transport/top-seeding arrangement, some exceptions being $NiFe_2O_4$, $Y_3Fe_5O_{12}$, and $KNbO_3$ (see Fig. 1).

An arrangement for using thermal transport with a stirred solution is available[2]. The advantage of thermal gradient transport is that, since the crystal grows under steady state

Figure 1. As-grown crystal of potassium niobate with two optical elements cut from similar top-seeded crystals. (Courtesy of P. Bordui, Crystal Technology.)

conditions, solid solutions are more uniform in composition than those grown by methods that rely on programmed cooling.

(DENNIS ELWELL)

1. R. D. Dawson, D. Elwell, J. C. Brice, *J. Cryst. Growth, 23*, 65 (1974).
2. W. Tolksdorf, F. Welz, *J. Crsyt. Growth, 20*, 47 (1973).

17.2.4.2.4. Traveling Solvent Zone Methods.

A second temperature gradient method uses a thin zone of solvent, which is made to migrate through a polycrystalline source so that the source material crystallizes onto a seed. The sample may be fixed, but usually the sample is moved through the gradient, in which case the molten zone tends to remain intact. The most successful form of the traveling solvent zone method is that used to grow crystals of $CaCO_3$[1]. The apparatus utilizes a platinum strip heater as the means of localizing the hot zone. This technique is used to grow $BaTiO_3$ crystals at temperatures as high as 1500°C, with the strip heater located inside a furnace to provide background heating[2].

(DENNIS ELWELL)

1. J. J. Brissot, C. Belin, *J. Cryst. Growth, 8*, 213 (1971).
2. C. E. Turner, N. H. Mason, A. W. Morris, *J. Cryst. Growth, 56*, 137 (1982).

Inorganic Reactions and Methods, Volume 18
Edited by J. J. Zuckerman, Jim D. Atwood

Figure 1. As-grown crystal of potassium niobate with two optical elements cut from similar top-seeded crystals. (Courtesy of P. Bordui, Crystal Technology.)

conditions, solid solutions are more uniform in composition than those grown by methods that rely on programmed cooling.

(DENNIS ELWELL)

1. R. D. Dawson, D. Elwell, J. C. Brice, *J. Cryst. Growth, 23*, 65 (1974).
2. W. Tolksdorf, F. Welz, *J. Crsyt. Growth, 20*, 47 (1973).

17.2.4.2.4. Traveling Solvent Zone Methods.

A second temperature gradient method uses a thin zone of solvent, which is made to migrate through a polycrystalline source so that the source material crystallizes onto a seed. The sample may be fixed, but usually the sample is moved through the gradient, in which case the molten zone tends to remain intact. The most successful form of the traveling solvent zone method is that used to grow crystals of $CaCO_3$[1]. The apparatus utilizes a platinum strip heater as the means of localizing the hot zone. This technique is used to grow $BaTiO_3$ crystals at temperatures as high as 1500°C, with the strip heater located inside a furnace to provide background heating[2].

(DENNIS ELWELL)

1. J. J. Brissot, C. Belin, *J. Cryst. Growth, 8*, 213 (1971).
2. C. E. Turner, N. H. Mason, A. W. Morris, *J. Cryst. Growth, 56*, 137 (1982).

Inorganic Reactions and Methods, Volume 18
Edited by J. J. Zuckerman, Jim D. Atwood

17.2.4.2.5. Flux Reaction Techniques[1].

Crystals can be grown by reaction between two interdiffusing species to produce a supersaturated solution (e.g., the I.G. Farben process for crystal growth of emerald). Emerald, $Be_3Al_2Si_6O_{18}$ (doped with Cr) is made by dissolving BeO and Al_2O_3 in a molten salt solvent and holding solid SiO_2 in contact with the solution so that the rate of crystallization is determined by the dissolution of the SiO_2. Reactants are also supplied via the vapor phase, as in the growth of GaN by passing ammonia over molten gallium at about 950°C.

(DENNIS ELWELL)

1. D. Elwell, in *Crystal Growth and Materials*, E. Kaldis, H. J. Scheel, eds., North Holland, Amsterdam, 1977, p. 606.

17.2.4.2.6. Electrocrystallization.

Conducting ceramic materials (borides, oxides, sulfides, silicides, carbides, etc.) are synthesized by electrolysis of molten salt solutions[1]. Crystals several millimeters or more in size, usually cannot be grown, but large crystals of LaB_6 were grown from La_2O_3, B_2O_3, Li_2O, and LiF; the stable growth of large crystals requires a current density below 20 mA/cm^2.

Electrodeposition is one of a few techniques used to crystallize high-melting materials at convenient temperatures [e.g., tantalum carbide, TaC (mp 3900°C) and niobium carbide, NbC (mp 3500°C) are crystallized at 750°C][2]. The preparation involves electrolysis of melts containing Ta_2O_5 (or Nb_2O_5), $Na_2B_4O_7$, Na_2CO_3, NaF, and KF.

(DENNIS ELWELL)

1. D. Elwell in "Crystal Growth and Materials," Ed. E. Kaldis & H. J. Scheel, N. Holland, Amsterdam, 1977, p. 606.
2. A. J. Hockman, R. S. Feigelson, *Abstracts, Fall Meeting of the Electrochemical Society*, Denver, CO, 1981.

17.2.4.2.7. Liquid Phase Epitaxy (LPE).

In LPE, crystalline materials are prepared as thin films on single crystal substrates. The substrate must match the film material closely in structure, lattice constant, and expansion coefficient if good quality, unstrained films are to be prepared, but it is possible to tailor the substrate composition to meet the requirements for a particular film material. Crystal growth occurs when a vertical substrate wafer is inserted into a melt previously supersaturated by cooling below its liquidus temperature. For garnet growth, the solvent is PbO/B_2O_3 and layer growth occurs at 900–1000°C[1,2].

Although most materials grown by LPE have the garnet structure, spinel ferrites can be grown similarly[3], and films of hexagonal ferrites are also prepared[4]. Only small quantities are required, and the crystallographic quality of the film can be high, but a suitable substrate is required and the measurement or device must be made on a thin layer rather than a bulk crystal.

(DENNIS ELWELL)

1. J. M. Robertson, *J. Cryst. Growth, 45*, 233 (1978).
2. P. Gornert, *J. Cryst. Growth, 52*, 88 (1981).

Inorganic Reactions and Methods, Volume 18
Edited by J. J. Zuckerman, Jim D. Atwood

17.2.4.2.5. Flux Reaction Techniques[1].

Crystals can be grown by reaction between two interdiffusing species to produce a supersaturated solution (e.g., the I.G. Farben process for crystal growth of emerald). Emerald, $Be_3Al_2Si_6O_{18}$ (doped with Cr) is made by dissolving BeO and Al_2O_3 in a molten salt solvent and holding solid SiO_2 in contact with the solution so that the rate of crystallization is determined by the dissolution of the SiO_2. Reactants are also supplied via the vapor phase, as in the growth of GaN by passing ammonia over molten gallium at about 950°C.

(DENNIS ELWELL)

1. D. Elwell, in *Crystal Growth and Materials*, E. Kaldis, H. J. Scheel, eds., North Holland, Amsterdam, 1977, p. 606.

17.2.4.2.6. Electrocrystallization.

Conducting ceramic materials (borides, oxides, sulfides, silicides, carbides, etc.) are synthesized by electrolysis of molten salt solutions[1]. Crystals several millimeters or more in size, usually cannot be grown, but large crystals of LaB_6 were grown from La_2O_3, B_2O_3, Li_2O, and LiF; the stable growth of large crystals requires a current density below 20 mA/cm^2.

Electrodeposition is one of a few techniques used to crystallize high-melting materials at convenient temperatures [e.g., tantalum carbide, TaC (mp 3900°C) and niobium carbide, NbC (mp 3500°C) are crystallized at 750°C][2]. The preparation involves electrolysis of melts containing Ta_2O_5 (or Nb_2O_5), $Na_2B_4O_7$, Na_2CO_3, NaF, and KF.

(DENNIS ELWELL)

1. D. Elwell in "Crystal Growth and Materials," Ed. E. Kaldis & H. J. Scheel, N. Holland, Amsterdam, 1977, p. 606.
2. A. J. Hockman, R. S. Feigelson, *Abstracts, Fall Meeting of the Electrochemical Society*, Denver, CO, 1981.

17.2.4.2.7. Liquid Phase Epitaxy (LPE).

In LPE, crystalline materials are prepared as thin films on single crystal substrates. The substrate must match the film material closely in structure, lattice constant, and expansion coefficient if good quality, unstrained films are to be prepared, but it is possible to tailor the substrate composition to meet the requirements for a particular film material. Crystal growth occurs when a vertical substrate wafer is inserted into a melt previously supersaturated by cooling below its liquidus temperature. For garnet growth, the solvent is PbO/B_2O_3 and layer growth occurs at 900–1000°C[1,2].

Although most materials grown by LPE have the garnet structure, spinel ferrites can be grown similarly[3], and films of hexagonal ferrites are also prepared[4]. Only small quantities are required, and the crystallographic quality of the film can be high, but a suitable substrate is required and the measurement or device must be made on a thin layer rather than a bulk crystal.

(DENNIS ELWELL)

1. J. M. Robertson, *J. Cryst. Growth, 45*, 233 (1978).
2. P. Gornert, *J. Cryst. Growth, 52*, 88 (1981).

Inorganic Reactions and Methods, Volume 18
Edited by J. J. Zuckerman, Jim D. Atwood

17.2.4.2.5. Flux Reaction Techniques[1].

Crystals can be grown by reaction between two interdiffusing species to produce a supersaturated solution (e.g., the I.G. Farben process for crystal growth of emerald). Emerald, $Be_3Al_2Si_6O_{18}$ (doped with Cr) is made by dissolving BeO and Al_2O_3 in a molten salt solvent and holding solid SiO_2 in contact with the solution so that the rate of crystallization is determined by the dissolution of the SiO_2. Reactants are also supplied via the vapor phase, as in the growth of GaN by passing ammonia over molten gallium at about 950°C.

(DENNIS ELWELL)

1. D. Elwell, in *Crystal Growth and Materials*, E. Kaldis, H. J. Scheel, eds., North Holland, Amsterdam, 1977, p. 606.

17.2.4.2.6. Electrocrystallization.

Conducting ceramic materials (borides, oxides, sulfides, silicides, carbides, etc.) are synthesized by electrolysis of molten salt solutions[1]. Crystals several millimeters or more in size, usually cannot be grown, but large crystals of LaB_6 were grown from La_2O_3, B_2O_3, Li_2O, and LiF; the stable growth of large crystals requires a current density below 20 mA/cm^2.

Electrodeposition is one of a few techniques used to crystallize high-melting materials at convenient temperatures [e.g., tantalum carbide, TaC (mp 3900°C) and niobium carbide, NbC (mp 3500°C) are crystallized at 750°C][2]. The preparation involves electrolysis of melts containing Ta_2O_5 (or Nb_2O_5), $Na_2B_4O_7$, Na_2CO_3, NaF, and KF.

(DENNIS ELWELL)

1. D. Elwell in "Crystal Growth and Materials," Ed. E. Kaldis & H. J. Scheel, N. Holland, Amsterdam, 1977, p. 606.
2. A. J. Hockman, R. S. Feigelson, *Abstracts, Fall Meeting of the Electrochemical Society*, Denver, CO, 1981.

17.2.4.2.7. Liquid Phase Epitaxy (LPE).

In LPE, crystalline materials are prepared as thin films on single crystal substrates. The substrate must match the film material closely in structure, lattice constant, and expansion coefficient if good quality, unstrained films are to be prepared, but it is possible to tailor the substrate composition to meet the requirements for a particular film material. Crystal growth occurs when a vertical substrate wafer is inserted into a melt previously supersaturated by cooling below its liquidus temperature. For garnet growth, the solvent is PbO/B_2O_3 and layer growth occurs at 900–1000°C[1,2].

Although most materials grown by LPE have the garnet structure, spinel ferrites can be grown similarly[3], and films of hexagonal ferrites are also prepared[4]. Only small quantities are required, and the crystallographic quality of the film can be high, but a suitable substrate is required and the measurement or device must be made on a thin layer rather than a bulk crystal.

(DENNIS ELWELL)

1. J. M. Robertson, *J. Cryst. Growth, 45*, 233 (1978).
2. P. Gornert, *J. Cryst. Growth, 52*, 88 (1981).

3. J. M. Robertson, M. Jansen, B. Hoekstra, P. F. Bongers, *J. Cryst. Growth, 41*, 29 (1977).
4. F. S. Stearns, H. L. Glass, *Mater. Res. Bull., 11*, 1319 (1976).

17.2.4.3. Hydrothermal Synthesis of Ceramics

Crystals can be grown from aqueous solutions under pressure. The solubility of ceramic materials in water below its boiling point is low, but it may become significant at, say, 300°C in autoclaves, where the vapor pressure exceeds 1000 atm (Fig. 1). The

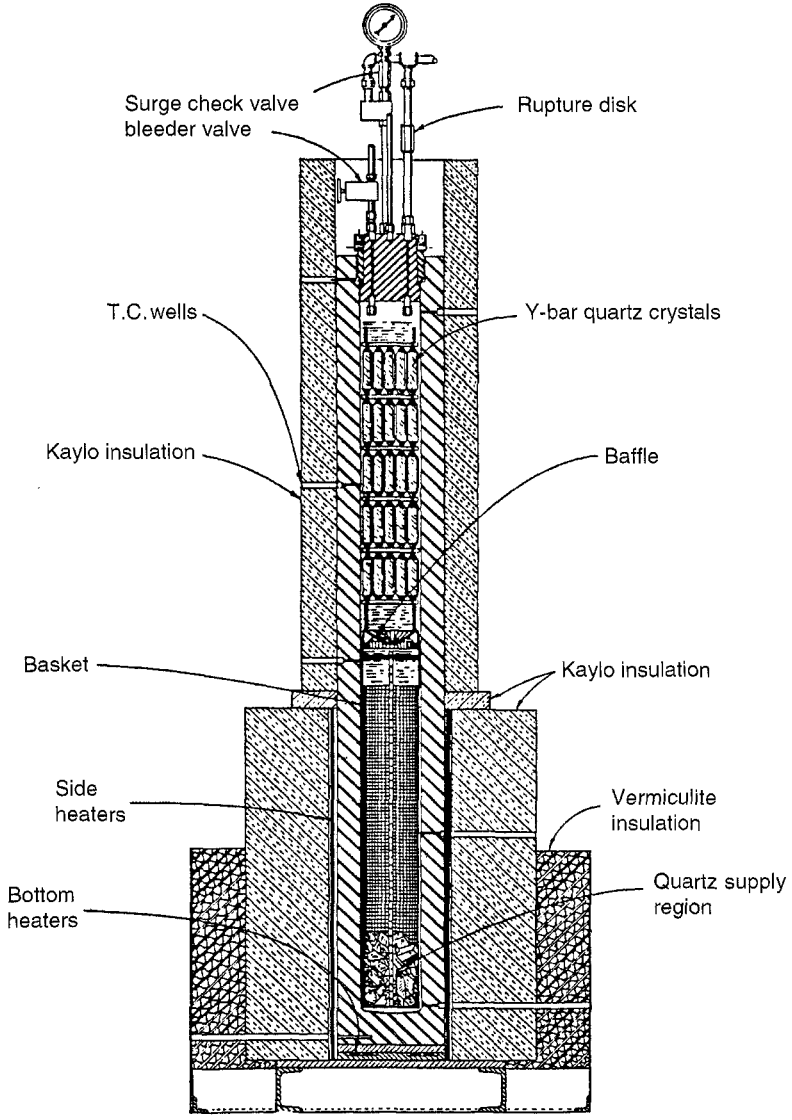

Figure 1. Autoclave used for hydrothermal growth of quartz. (Courtesy of D. R. Kinloch.)

Inorganic Reactions and Methods, Volume 18
Edited by J. J. Zuckerman, Jim D. Atwood

3. J. M. Robertson, M. Jansen, B. Hoekstra, P. F. Bongers, *J. Cryst. Growth*, *41*, 29 (1977).
4. F. S. Stearns, H. L. Glass, *Mater. Res. Bull.*, *11*, 1319 (1976).

17.2.4.3. Hydrothermal Synthesis of Ceramics

Crystals can be grown from aqueous solutions under pressure. The solubility of ceramic materials in water below its boiling point is low, but it may become significant at, say, 300°C in autoclaves, where the vapor pressure exceeds 1000 atm (Fig. 1). The

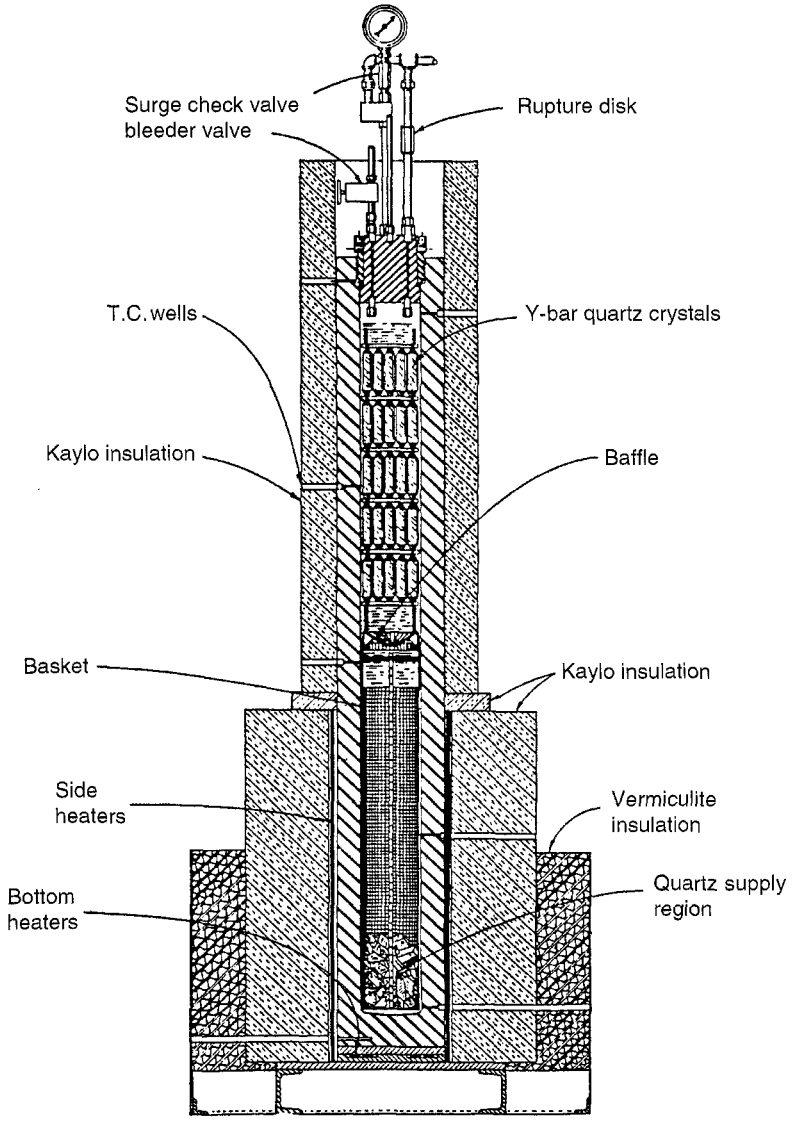

Figure 1. Autoclave used for hydrothermal growth of quartz. (Courtesy of D. R. Kinloch.)

TABLE 1. EXAMPLES OF CERAMIC MATERIALS CRYSTALLIZED FROM HIGH TEMPERATURE SOLUTION

Al_2O_3	Fe_2SiO_4	$Zn_2Cr_2O_4$
$BaWO_4$	$Mg(OH)_2$	ZnO
$CaCO_3$	$Mn_8Be_6Si_6O_{24}S_2$	ZnS
Cr_2O_3	$SrMoO_4$	$ZrSiO_4$
Fe_3O_4	$Na_8Cl_2Al_6Si_6O_{24}$	$Zr(Y)O_2$

pressure to be contained at a chosen temperature may be varied by changing the percentage of the original volume filled with water at room temperature.

Hydrothermal growth is successful for quartz, (SiO_2) and simulates the method by which quartz grows in nature. Nearly 10^6 kg of quartz are now made annually by this method[1]. The solubility of quartz in water is too low for good crystal growth even at 500°C, but dissolution is achieved by addition of a salt called a mineralizer (e.g., Na_2CO_3 or NaOH). Growth involves transport of the SiO_2 in a temperature gradient between small pieces of nutrient in the lower, hotter region and a number of seed plates supported on a frame in the upper, cooler region. The temperature difference between the nutrient and growth regions is typically 40°C. The rate of growth is about 1 mm/day, and the crystal quality is high.

Materials in addition to quartz that can be crystallized hydrothermally include carbonates, germanates, and silicates (see Table 1)[2].

Hydrothermal growth is used for the growth of materials such as silicates, which form glasses and are, therefore, difficult to crystallize by alternative methods. As for quartz, silicates grow hydrothermally in nature, which makes the synthesis of such materials as fayalite (Fe_2SiO_4)[3] of interest. Materials such as tourmaline and malachite are crystallized only hydrothermally.

With the exceptions of quartz and emerald, the typical crystals grown hydrothermally are small. There is no inherent reason for this. Hydrothermal synthesis of fine powders of barium titanate and similar dielectric materials is of importance in capacitor manufacture.

(DENNIS ELWELL)

1. G. Bartels, D. Mateika, J. M. Robertson, *J. Cryst. Growth*, *47*, 414 (1979).
2. R. A. Laudise, *The Growth of Single Crystals*, Prentice-Hall, Englewood Cliffs, NJ, 1970, p. 275.
3. A. N. Lobachev, ed., *Hydrothermal Growth of Crystals*, Consultants Bureau, New York, 1971.

17.2.4.4. Growth from Other Solutions

The arbitrary assignment of 300°C as the lowest melting point for a "high-melting" solvent leaves only a small selection of solvents for crystal growth of ceramic materials. Solubility in water (see 17.2.4.3) is low unless high temperatures and pressures are applied, and this also applies to other solvents such as liquid ammonia and organic molecules such as alcohol, acetone, and benzene. Ceramic materials, especially oxides, are synthesized by decomposition of organic materials containing the metallic elements in the correct ratio, but this method yields fine powders rather than crystals. Layers of silicon are prepared by, (for example, electrolysis of solutions of $SiCl_4$ in propylene carbonate), and refractory silicides might be prepared by a modification of this method.

Inorganic Reactions and Methods, Volume 18
Edited by J. J. Zuckerman, Jim D. Atwood

TABLE 1. EXAMPLES OF CERAMIC MATERIALS CRYSTALLIZED FROM HIGH TEMPERATURE SOLUTION

Al_2O_3	Fe_2SiO_4	$Zn_2Cr_2O_4$
$BaWO_4$	$Mg(OH)_2$	ZnO
$CaCO_3$	$Mn_8Be_6Si_6O_{24}S_2$	ZnS
Cr_2O_3	$SrMoO_4$	$ZrSiO_4$
Fe_3O_4	$Na_8Cl_2Al_6Si_6O_{24}$	$Zr(Y)O_2$

pressure to be contained at a chosen temperature may be varied by changing the percentage of the original volume filled with water at room temperature.

Hydrothermal growth is successful for quartz, (SiO_2) and simulates the method by which quartz grows in nature. Nearly 10^6 kg of quartz are now made annually by this method[1]. The solubility of quartz in water is too low for good crystal growth even at 500°C, but dissolution is achieved by addition of a salt called a mineralizer (e.g., Na_2CO_3 or NaOH). Growth involves transport of the SiO_2 in a temperature gradient between small pieces of nutrient in the lower, hotter region and a number of seed plates supported on a frame in the upper, cooler region. The temperature difference between the nutrient and growth regions is typically 40°C. The rate of growth is about 1 mm/day, and the crystal quality is high.

Materials in addition to quartz that can be crystallized hydrothermally include carbonates, germanates, and silicates (see Table 1)[2].

Hydrothermal growth is used for the growth of materials such as silicates, which form glasses and are, therefore, difficult to crystallize by alternative methods. As for quartz, silicates grow hydrothermally in nature, which makes the synthesis of such materials as fayalite (Fe_2SiO_4)[3] of interest. Materials such as tourmaline and malachite are crystallized only hydrothermally.

With the exceptions of quartz and emerald, the typical crystals grown hydrothermally are small. There is no inherent reason for this. Hydrothermal synthesis of fine powders of barium titanate and similar dielectric materials is of importance in capacitor manufacture.

(DENNIS ELWELL)

1. G. Bartels, D. Mateika, J. M. Robertson, *J. Cryst. Growth*, *47*, 414 (1979).
2. R. A. Laudise, *The Growth of Single Crystals*, Prentice-Hall, Englewood Cliffs, NJ, 1970, p. 275.
3. A. N. Lobachev, ed., *Hydrothermal Growth of Crystals*, Consultants Bureau, New York, 1971.

17.2.4.4. Growth from Other Solutions

The arbitrary assignment of 300°C as the lowest melting point for a "high-melting" solvent leaves only a small selection of solvents for crystal growth of ceramic materials. Solubility in water (see 17.2.4.3) is low unless high temperatures and pressures are applied, and this also applies to other solvents such as liquid ammonia and organic molecules such as alcohol, acetone, and benzene. Ceramic materials, especially oxides, are synthesized by decomposition of organic materials containing the metallic elements in the correct ratio, but this method yields fine powders rather than crystals. Layers of silicon are prepared by, (for example, electrolysis of solutions of $SiCl_4$ in propylene carbonate), and refractory silicides might be prepared by a modification of this method.

The layers so formed are, however, thin because of the low conductivity at low temperatures.

Tin is used as a solvent to grow crystals of $CdSiP_2$ and CuP_2, and crystals of HgS are grown by slow cooling from solutions in Hg and Na_2S_4. The polysulfides offer a useful range of low-melting solvents for crystallization of refractory sulfides. Mercury is used to grow crystals of conducting refractory materials such as Mn_5Si_3, Ni_2Si, Pt_2Si, and rare earth germanides and silicides. However, the crystals grown are small, and high-melting solvents give better results[1].

(DENNIS ELWELL)

1. D. Elwell, H. J. Scheel, *Crystal Growth from High-Temperature Solutions*, Academic Press, London, 1975.

17.2.5. Chemical Vapor Deposition

Chemical vapor deposition (CVD) is a process by which reactive molecules in the gas phase are transported to a surface at which they chemically react and form a solid film. CVD has advantages over other coating techniques in that the deposition is done cleanly without the use of solvents; moreover, large areas can be coated routinely, the process is amenable to mass production, and high deposition rates can be achieved. In addition, CVD allows a great degree of control over the film purity, thickness, and uniformity. The technique can be used to deposit all classes of materials (metals, semiconductors, insulators, alloys, etc.) for a host of diverse applications such as wear-resistant coatings, corrosion/oxidation-resistant coatings, microelectronic circuits and packaging layers, and optical coatings.

In general, the goal of a CVD process is to deposit a high quality layer of a given material, where "quality" refers to a variety of characteristics including uniformity, thickness, conformality, microstructure, morphology, and certain magnetic, optical, or electric properties. A more detailed description of film morphology and quality appears later (see 17.2.5.1.3.).

There are several excellent texts on CVD and related processes[1-8]. Books completely dedicated to CVD and the materials that can be formed in such processes include the following: an effective review of the common deposition strategies for silicon nitride, silicon carbide, and boron nitride along with a limited review on the production of other materials[2]; information on the fundamental physics and chemistry involved with CVD and a comprehensive review of equipment requirements, applications, and specific chemistry for most materials[1]; superb treatments of the fundamentals of CVD including thermodynamics, transport concerns, and discussion of reaction kinetics[3,4]; discussions of microelectronics applications for CVD[5,6]; and considerations of aspects of CVD and related topics on the deposition of thin films[7]. For CVD using metal–organic molecules [i.e., metal–organic chemical vapor deposition (MOCVD) organometallic vapor phase epitaxy (OMVPE)] a thorough introduction is available[8].

The most recent research and development discoveries can be obtained from the open literature in a variety of well-known journals. Among such sources are the five volumes of symposia proceedings published by the Materials Research Society on the CVD of refectory metals and ceramics[9-11] and the MOCVD of electronic ceramics[12,13]

Inorganic Reactions and Methods, Volume 18
Edited by J. J. Zuckerman, Jim D. Atwood

The layers so formed are, however, thin because of the low conductivity at low temperatures.

Tin is used as a solvent to grow crystals of $CdSiP_2$ and CuP_2, and crystals of HgS are grown by slow cooling from solutions in Hg and Na_2S_4. The polysulfides offer a useful range of low-melting solvents for crystallization of refractory sulfides. Mercury is used to grow crystals of conducting refractory materials such as Mn_5Si_3, Ni_2Si, Pt_2Si, and rare earth germanides and silicides. However, the crystals grown are small, and high-melting solvents give better results[1].

(DENNIS ELWELL)

1. D. Elwell, H. J. Scheel, *Crystal Growth from High-Temperature Solutions*, Academic Press, London, 1975.

17.2.5. Chemical Vapor Deposition

Chemical vapor deposition (CVD) is a process by which reactive molecules in the gas phase are transported to a surface at which they chemically react and form a solid film. CVD has advantages over other coating techniques in that the deposition is done cleanly without the use of solvents; moreover, large areas can be coated routinely, the process is amenable to mass production, and high deposition rates can be achieved. In addition, CVD allows a great degree of control over the film purity, thickness, and uniformity. The technique can be used to deposit all classes of materials (metals, semiconductors, insulators, alloys, etc.) for a host of diverse applications such as wear-resistant coatings, corrosion/oxidation-resistant coatings, microelectronic circuits and packaging layers, and optical coatings.

In general, the goal of a CVD process is to deposit a high quality layer of a given material, where "quality" refers to a variety of characteristics including uniformity, thickness, conformality, microstructure, morphology, and certain magnetic, optical, or electric properties. A more detailed description of film morphology and quality appears later (see 17.2.5.1.3.).

There are several excellent texts on CVD and related processes[1-8]. Books completely dedicated to CVD and the materials that can be formed in such processes include the following: an effective review of the common deposition strategies for silicon nitride, silicon carbide, and boron nitride along with a limited review on the production of other materials[2]; information on the fundamental physics and chemistry involved with CVD and a comprehensive review of equipment requirements, applications, and specific chemistry for most materials[1]; superb treatments of the fundamentals of CVD including thermodynamics, transport concerns, and discussion of reaction kinetics[3,4]; discussions of microelectronics applications for CVD[5,6]; and considerations of aspects of CVD and related topics on the deposition of thin films[7]. For CVD using metal–organic molecules [i.e., metal–organic chemical vapor deposition (MOCVD) organometallic vapor phase epitaxy (OMVPE)] a thorough introduction is available[8].

The most recent research and development discoveries can be obtained from the open literature in a variety of well-known journals. Among such sources are the five volumes of symposia proceedings published by the Materials Research Society on the CVD of refectory metals and ceramics[9-11] and the MOCVD of electronic ceramics[12,13]

The addition to *Advanced Materials* entitled *Chemical Vapor Deposition*, which began in 1995, also provides many recent developments, along with several review articles on the CVD of a variety of ceramic systems. In addition, summaries of current research issues can be obtained from the most recent proceedings of European and international conferences on CVD[14,15].

With such a wealth of knowledge available in the scientific literature, only a brief review of the background material is presented here. Rather, this review on the CVD of refractory ceramics concentrates on the selection of CVD precursors, the chemistry of those precursors, and their reactions as related to specific ceramics of technological interest.

This review of CVD principles, reactions, and applications begins with an introduction to the fundamental processes involved in CVD processing. These include thermodynamics, kinetics, and transport issues. Then the discussion briefly touches on the desirable qualities of the deposit that is formed. Next the chemistry and precursors are introduced, to familiarize the reader with common reactions that are widely used, followed by a brief discussion of nonconventinal or enhanced CVD technologies. Finally, the CVD of several technologically significant materials is reviewed to illustrate the direction of current work in the field.

(C. L. AARDAHL, J. W. ROGERS, JR.)

1. H. O. Pierson, *Handbook of Chemical Vapor Deposition (CVD): Principles, Technology, and Applications*, Noyes, Park Ridge, NJ, 1992.
2. F. S. Galasso, *Chemical Vapor Deposited Materials*, CRC Press, Boca Raton, FL, 1991.
3. M. L. Hitchman, K. F. Jensen, eds., *Chemical Vapor Deposition: Principles and Applications*, Academic Press, London, 1993.
4. M. Ohring, *The Materials Science of Thin Films*, Academic Press, San Diego, CA, 1992.
5. A. Sherman, *Chemical Vapor Deposition for Microelectronics*, Noyes, Park Ridge, NJ, 1987.
6. D. W. Hess, K. F. Jensen, eds., *Microelectronics Processing: Chemical Engineering Aspects*, American Chemical Society, Washington, DC, 1989.
7. K. L. Schuegraf, *Handbook of Thin-Film Deposition Processes and Techniques: Principles, Methods, Equipment, and Applications*, Noyes, Park Ridge, NJ, 1998.
8. G. B. Stringfellow, *Organometallic Vapor-Phase Epitaxy: Theory and Practice*, Academic Press, San Diego, CA, 1989.
9. T. M. Besmann, B. M. Gallois, J. W. Warren, eds., *MRS Symp. Proc.*, Vol. 250: *Chemical Vapor Deposition of Refractory Metals and Ceramics II*, Metal Research Society, Pittsburgh, 1992.
10. T. M. Besmann, B. M. Gallois, eds., *MRS Symp. Proc.*, Vol. 168: *Chemical Vapor Deposition of Refractory Metals and Ceramics*, Material Research Society, Pittsburgh, 1990.
11. B. M. Gallois, W. Y. Lee, M.A. Pickering eds., *MRS Symp. Proc.*, Vol. 363: *Chemical Vapor Deposition of Refractory Metals and Ceramics III*, Metal Research Society, Pittsburgh, 1995.
12. S. B. Desu, D. B. Beach, P. C. Van Buskirk, eds., *MRS Symp. Proc.*, Vol. 415: *Metal-Organic Chemical Vapor Deposition of Electronic Ceramics II*, Metal Research Society, Pittsburgh, 1996.
13. S. B. Desu, ed., *MRS Symp. Proc.*, Vol. 335: *Metal-Organic Chemical Vapor Deposition of Electronic Ceramics*, Metal Research Society, Pittsburgh, 1994.
14. K. F. Jensen, G. W. Cullen, eds., *CVD XII: Proc. 12th Int. Symp. Chem. Vapor Deposition*, Electrochemical Society, Pennington, NJ, 1993.
15. G. A. Battiston, R. Gerbasi, M. Porchia, eds., *Proc. 10th European Conf. Chem. Vapor Deposition*, Jesolo Lido, Venice, 1995.

17.2.5.1. Fundamentals

As in other physiochemical processes, CVD can be best understood by examining the reaction/deposition in a fundamental manner. Thermodynamics, kinetics, and heat,

Inorganic Reactions and Methods, Volume 18
Edited by J. J. Zuckerman, Jim D. Atwood

The addition to *Advanced Materials* entitled *Chemical Vapor Deposition*, which began in 1995, also provides many recent developments, along with several review articles on the CVD of a variety of ceramic systems. In addition, summaries of current research issues can be obtained from the most recent proceedings of European and international conferences on CVD[14,15].

With such a wealth of knowledge available in the scientific literature, only a brief review of the background material is presented here. Rather, this review on the CVD of refractory ceramics concentrates on the selection of CVD precursors, the chemistry of those precursors, and their reactions as related to specific ceramics of technological interest.

This review of CVD principles, reactions, and applications begins with an introduction to the fundamental processes involved in CVD processing. These include thermodynamics, kinetics, and transport issues. Then the discussion briefly touches on the desirable qualities of the deposit that is formed. Next the chemistry and precursors are introduced, to familiarize the reader with common reactions that are widely used, followed by a brief discussion of nonconventinal or enhanced CVD technologies. Finally, the CVD of several technologically significant materials is reviewed to illustrate the direction of current work in the field.

(C. L. AARDAHL, J. W. ROGERS, JR.)

1. H. O. Pierson, *Handbook of Chemical Vapor Deposition (CVD): Principles, Technology, and Applications*, Noyes, Park Ridge, NJ, 1992.
2. F. S. Galasso, *Chemical Vapor Deposited Materials*, CRC Press, Boca Raton, FL, 1991.
3. M. L. Hitchman, K. F. Jensen, eds., *Chemical Vapor Deposition: Principles and Applications*, Academic Press, London, 1993.
4. M. Ohring, *The Materials Science of Thin Films*, Academic Press, San Diego, CA, 1992.
5. A. Sherman, *Chemical Vapor Deposition for Microelectronics*, Noyes, Park Ridge, NJ, 1987.
6. D. W. Hess, K. F. Jensen, eds., *Microelectronics Processing: Chemical Engineering Aspects*, American Chemical Society, Washington, DC, 1989.
7. K. L. Schuegraf, *Handbook of Thin-Film Deposition Processes and Techniques: Principles, Methods, Equipment, and Applications*, Noyes, Park Ridge, NJ, 1998.
8. G. B. Stringfellow, *Organometallic Vapor-Phase Epitaxy: Theory and Practice*, Academic Press, San Diego, CA, 1989.
9. T. M. Besmann, B. M. Gallois, J. W. Warren, eds., *MRS Symp. Proc.*, Vol. 250: *Chemical Vapor Deposition of Refractory Metals and Ceramics II*, Metal Research Society, Pittsburgh, 1992.
10. T. M. Besmann, B. M. Gallois, eds., *MRS Symp. Proc.*, Vol. 168: *Chemical Vapor Deposition of Refractory Metals and Ceramics*, Material Research Society, Pittsburgh, 1990.
11. B. M. Gallois, W. Y. Lee, M.A. Pickering eds., *MRS Symp. Proc.*, Vol. 363: *Chemical Vapor Deposition of Refractory Metals and Ceramics III*, Metal Research Society, Pittsburgh, 1995.
12. S. B. Desu, D. B. Beach, P. C. Van Buskirk, eds., *MRS Symp. Proc.*, Vol. 415: *Metal-Organic Chemical Vapor Deposition of Electronic Ceramics II*, Metal Research Society, Pittsburgh, 1996.
13. S. B. Desu, ed., *MRS Symp. Proc.*, Vol. 335: *Metal-Organic Chemical Vapor Deposition of Electronic Ceramics*, Metal Research Society, Pittsburgh, 1994.
14. K. F. Jensen, G. W. Cullen, eds., *CVD XII: Proc. 12th Int. Symp. Chem. Vapor Deposition*, Electrochemical Society, Pennington, NJ, 1993.
15. G. A. Battiston, R. Gerbasi, M. Porchia, eds., *Proc. 10th European Conf. Chem. Vapor Deposition*, Jesolo Lido, Venice, 1995.

17.2.5.1. Fundamentals

As in other physiochemical processes, CVD can be best understood by examining the reaction/deposition in a fundamental manner. Thermodynamics, kinetics, and heat,

mass, and momentum transport all play important roles in the growing of thin films by means of chemically based methods that involve gas phase delivery of reactants.

17.2.5.1.1. Thermodynamics.

The first step in determining whether a chemical reaction is feasible for a CVD process is to ascertain whether the reaction is thermodynamically possible. (i.e., is the energy of the system minimized when reactants go to products at a given temperature and pressure?). This can be determined by examining the change in Gibbs free energy of the reaction, ΔG_r. If ΔG_r is negative, then the reaction is thermodynamically driven to the products. If the thermodynamic properties of the reactants and products are known as a function of temperature and pressure, ΔG_r can be obtained by means of

$$\Delta G_r = \sum z_i \Delta G_{f_i}^\circ + RT \ln \left[\prod_i a_i^{z_i} \right] \quad (T, P \text{ constant}). \tag{a}$$

Where, for the ith species, $\Delta G_{f_i}^\circ$ is the Gibbs free energy of formation, a_i is the activity, and z_i is the stoichiometric coefficient in the balanced reaction statement (by convention, z_i is negative for reactants and positive for products). The absolute temperature is T; R is the gas constant, and P is the absolute pressure. The standard Gibbs free energy of formation, ΔG_f°, can be obtained from standard tables, from values of the standard enthalpy ΔH_f° and entropy ΔS_f° of formation for each species via

$$\Delta G_f^\circ = \Delta H_f^\circ - T\Delta S_f^\circ \tag{b}$$

or from tabulations of heat capacity as a function of temperature (see Ref. 1, Table 12-1). The activity can be estimated as $a_i = 1$ for pure solids or $a_i = y_i P$ for gases if the gases are ideal. Here, P is the total pressure in the reaction chamber and y_i is the mole fraction of the ith species in the gas phase. Ideal gas behaviour is a reasonable assumption for most CVD precursors because reactors are seldom run above atmospheric pressure, and in the low pressure limit, all gases approach ideality. If the pressure in the reactor is sufficiently high, and the reactants are highly polar molecules, an analysis based on fugacities may be necessary.

The thermodynamic feasibility of a specific reaction does not guarantee the formation of a high quality film. Transport issues and chemical kinetics play an important role in the final electronic, optical and structural properties of films that are formed.

(C. L. AARDAHL, J. W. ROGERS, JR.)

1. B. G. Kyle, *Chemical and Process Thermodynamics*, PTR Prentice Hall, Englewood Cliffs, NJ, 1992.

17.2.5.1.2. Kinetics and Transport Considerations.

Once the thermodynamics has been analyzed, the delivery of reactants to the surface and the rate of deposition must be addressed. Regardless of the thermodynamic driving force, a specific reaction may still be unattractive because the film is formed too slowly.

Forced convection is the manner in which gases are delivered to a reactor, and the flow field in a CVD reactor with many substrates is quite complicated[1]. However, all reactors have one feature in common: boundary layer flow above the deposition surface. This leads to the following order of steps to deposit a film: convective flow of reactants to

Inorganic Reactions and Methods, Volume 18
Edited by J. J. Zuckerman, Jim D. Atwood

mass, and momentum transport all play important roles in the growing of thin films by means of chemically based methods that involve gas phase delivery of reactants.

17.2.5.1.1. Thermodynamics.

The first step in determining whether a chemical reaction is feasible for a CVD process is to ascertain whether the reaction is thermodynamically possible. (i.e., is the energy of the system minimized when reactants go to products at a given temperature and pressure?). This can be determined by examining the change in Gibbs free energy of the reaction, ΔG_r. If ΔG_r is negative, then the reaction is thermodynamically driven to the products. If the thermodynamic properties of the reactants and products are known as a function of temperature and pressure, ΔG_r can be obtained by means of

$$\Delta G_r = \sum z_i \Delta G_{f_i}^\circ + RT \ln \left[\prod_i a_i^{z_i} \right] \quad (T, P \text{ constant}). \tag{a}$$

Where, for the ith species, $\Delta G_{f_i}^\circ$ is the Gibbs free energy of formation, a_i is the activity, and z_i is the stoichiometric coefficient in the balanced reaction statement (by convention, z_i is negative for reactants and positive for products). The absolute temperature is T; R is the gas constant, and P is the absolute pressure. The standard Gibbs free energy of formation, ΔG_f°, can be obtained from standard tables, from values of the standard enthalpy ΔH_f° and entropy ΔS_f° of formation for each species via

$$\Delta G_f^\circ = \Delta H_f^\circ - T\Delta S_f^\circ \tag{b}$$

or from tabulations of heat capacity as a function of temperature (see Ref. 1, Table 12-1). The activity can be estimated as $a_i = 1$ for pure solids or $a_i = y_i P$ for gases if the gases are ideal. Here, P is the total pressure in the reaction chamber and y_i is the mole fraction of the ith species in the gas phase. Ideal gas behaviour is a reasonable assumption for most CVD precursors because reactors are seldom run above atmospheric pressure, and in the low pressure limit, all gases approach ideality. If the pressure in the reactor is sufficiently high, and the reactants are highly polar molecules, an analysis based on fugacities may be necessary.

The thermodynamic feasibility of a specific reaction does not guarantee the formation of a high quality film. Transport issues and chemical kinetics play an important role in the final electronic, optical and structural properties of films that are formed.

(C. L. AARDAHL, J. W. ROGERS, JR.)

1. B. G. Kyle, *Chemical and Process Thermodynamics*, PTR Prentice Hall, Englewood Cliffs, NJ, 1992.

17.2.5.1.2. Kinetics and Transport Considerations.

Once the thermodynamics has been analyzed, the delivery of reactants to the surface and the rate of deposition must be addressed. Regardless of the thermodynamic driving force, a specific reaction may still be unattractive because the film is formed too slowly.

Forced convection is the manner in which gases are delivered to a reactor, and the flow field in a CVD reactor with many substrates is quite complicated[1]. However, all reactors have one feature in common: boundary layer flow above the deposition surface. This leads to the following order of steps to deposit a film: convective flow of reactants to

the reaction zone, diffusion of the reactants through a boundary layer, adsorption of reactants on the surface, surface chemical reactions and surface diffusion, desorption of by-products from the surface, diffusion of the by-products through a boundary layer, and convective flow of the byproducts out of the reaction zone. To grow high quality films, it is useful to know as much as possible about each of these steps. Provided the surface is held at constant temperature, the two important factors that govern the rate of deposition are the mass transport limitations and the surface kinetic limitations. If the boundary layer is very thick, the deposition may be limited by mass transfer; if the intrinsic surface reaction kinetics are too slow, the deposition may be reaction rate limited[2]. Industrial-scale CVD reactors have been optimized to account for these issues.

Another important design factor is the uniformity of the films that are deposited. Good uniformity can usually be achieved by engineering the boundary layer thickness to provide equal mass transfer across the entire substrate. Several successful designs have been reported[3]. Early designs employed a Cartesian flow geometry, but increased knowledge and modeling efforts of mass transfer effects in CVD resulted in construction of reactors with curvilinear gas flows. If the gas impinges normal to the growth surface, and the substrate is rotated in the azimuthal direction (e.g., rotating disk reactor or shower head reactor), a particularly uniform boundary layer can be obtained. Such impinging jet reactors are gaining wide acceptance in research and industrial applications because of the volume of reactant gases per unit area of film can be significantly reduced with no sacrifice in film quality.

Substrate heating is required in CVD reactors. Since the films are grown under isothermal conditions, the substrate must be held at a constant growth temperature for an extended period of time. The achievement of this requirement is facilitated in two ways, and reactors are classified into two groups depending on how the substrate is heated. In a hot-wall design, the entire reactor is placed in a tube furnace and the substrate, the region of forced gas convention, and the walls of the reactor are maintained at the same temperature. Of course the ends of the reactor are cooler than the middle because of heat loss from the ends and the introduction of cold gas at the entrance of the reactor. To remedy this imbalance, a three-zone furnace, with independent feedback control for each zone, is usually employed. Substrates are loaded only in the portion of the reactor where the temperature can be accurately maintained.

A hot-wall reactor design has several advantages and disadvantages. Such units have high capacity, the substrates can be coated on all sides, and temperature control is relatively easy. Because the entire forced convection region is heated, however, gas phase reactions and nucleation can be a problem for some precursors and precursor combinations. In addition, because of the high loading, uniform gas flow to all faces of the substrate is difficult, leading to non uniformity of the deposit. Both these difficulties can be mitigated by lowering the deposition pressure and operating in the surface kinetically limited growth regime at lower deposition rates.

The other common reactor type is a cold-wall reactor. Here only the substrate is heated, and the gas in the forced convection region as well as the reactor walls are considerably colder than the substrate. This design has limited capacity: the substrate is usually coated on one face only and although uniform gas flow to the substrate is easier to control, heating the substrate is relatively difficult. These reactors are usually operated under mass transport limited conditions. Heating is accomplished in one of four ways:

1. The substrate is mounted on a graphite susceptor (usually SiC-coated) and a radio frequency (rf) field is used to inductively heat the susceptor.
2. A high temperature coil is mounted in proximity to the substrate and radiation emitted by the coil provides heat.
3. Electrical current is passed through the substrate itself to heat it resistively.
4. A lamp (such as those used in rapid thermal processing) is used to heat the surface radiatively.

Heat is lost from the surface by conduction through the susceptor and mount, by forced convection of gas over the substrate, and by radiation to the reactor walls, provided the temperature of the substrate is sufficiently high. Endothermic chemical reactions also result in heat loss from the film. The substrate temperature is monitored with a thermocouple or an optical pyrometer and controlled using a traditional proportional-integral-derivative (PID) controller and power source.

(C. L. AARDAHL, J. W. ROGERS, JR.)

1. M. L. Hitchman, K. F. Jensen, eds., *Chemical Vapor Deposition: Principles and Applications*, Academic Press, London, 1993.
2. H. S. Fogler, *Elements of Chemical Reaction Engineering*, Prentice Hall, Englewood Cliffs, NJ, 1992.
3. K. F. Jensen, in *Chemical Vapor Deposition: Principles and Applications*, M. L. Hitchman, K. F. Jensen, eds., Academic Press, London, 1993, p. 33.

17.2.5.1.3. Film Growth and Morphology.

The microstructure and chemical composition of a CVD deposit is directly related to the conditions in the reactor at the time the film was formed. Factors having an impact include chemistry of the reaction, crystallinity and cleanliness of the substrate, and mobility of the reactants on the reaction surface. In general, high temperature growth yields crystalline deposits while low deposition temperatures result in amorphous materials unless very low growth rates are employed. Between these two extremes, a polycrystalline deposit will be formed. This is by no means a universal law; for example, silicon dioxide is usually grown as an amorphous deposit at relatively high temperature. The degree of crystallinity is determined by the mobility of the reactants and products on the growth surface at the time of reaction. A higher surface temperature results in an increased diffusivity of species on the film surface, which allows reactants to move across on the surface until they bind to the crystalline edge of a step or island of molecules. This allows the deposit to grow as a crystalline film. At lower temperature, molecules are much more likely to form islands on the surface due to the immobility of the surface molecules. These islands eventually coalesce, resulting in grain boundaries characteristic of polycrystalline films. At the lowest growth temperatures, molecules have virtually no mobility on the surface and are fixed in the configuration they assume after surface reaction. This forces the film to have no order, and the deposit is considered amorphous.

The substrate will also affect crystal growth. If the substrate is clean and single crystalline (as in a silicon wafer), and the growth temperature is high, the film may grow epitaxially. At low temperature, the film will most likely be amorphous regardless of the substrate quality. If the substrate is not molecularly smooth, the same behavior is observed, but grain effects arise in the films at higher temperatures. For example, rather

Inorganic Reactions and Methods, Volume 18
Edited by J. J. Zuckerman, Jim D. Atwood

1. The substrate is mounted on a graphite susceptor (usually SiC-coated) and a radio frequency (rf) field is used to inductively heat the susceptor.
2. A high temperature coil is mounted in proximity to the substrate and radiation emitted by the coil provides heat.
3. Electrical current is passed through the substrate itself to heat it resistively.
4. A lamp (such as those used in rapid thermal processing) is used to heat the surface radiatively.

Heat is lost from the surface by conduction through the susceptor and mount, by forced convection of gas over the substrate, and by radiation to the reactor walls, provided the temperature of the substrate is sufficiently high. Endothermic chemical reactions also result in heat loss from the film. The substrate temperature is monitored with a thermocouple or an optical pyrometer and controlled using a traditional proportional-integral-derivative (PID) controller and power source.

(C. L. AARDAHL, J. W. ROGERS, JR.)

1. M. L. Hitchman, K. F. Jensen, eds., *Chemical Vapor Deposition: Principles and Applications*, Academic Press, London, 1993.
2. H. S. Fogler, *Elements of Chemical Reaction Engineering*, Prentice Hall, Englewood Cliffs, NJ, 1992.
3. K. F. Jensen, in *Chemical Vapor Deposition: Principles and Applications*, M. L. Hitchman, K. F. Jensen, eds., Academic Press, London, 1993, p. 33.

17.2.5.1.3. Film Growth and Morphology.

The microstructure and chemical composition of a CVD deposit is directly related to the conditions in the reactor at the time the film was formed. Factors having an impact include chemistry of the reaction, crystallinity and cleanliness of the substrate, and mobility of the reactants on the reaction surface. In general, high temperature growth yields crystalline deposits while low deposition temperatures result in amorphous materials unless very low growth rates are employed. Between these two extremes, a polycrystalline deposit will be formed. This is by no means a universal law; for example, silicon dioxide is usually grown as an amorphous deposit at relatively high temperature. The degree of crystallinity is determined by the mobility of the reactants and products on the growth surface at the time of reaction. A higher surface temperature results in an increased diffusivity of species on the film surface, which allows reactants to move across on the surface until they bind to the crystalline edge of a step or island of molecules. This allows the deposit to grow as a crystalline film. At lower temperature, molecules are much more likely to form islands on the surface due to the immobility of the surface molecules. These islands eventually coalesce, resulting in grain boundaries characteristic of polycrystalline films. At the lowest growth temperatures, molecules have virtually no mobility on the surface and are fixed in the configuration they assume after surface reaction. This forces the film to have no order, and the deposit is considered amorphous.

The substrate will also affect crystal growth. If the substrate is clean and single crystalline (as in a silicon wafer), and the growth temperature is high, the film may grow epitaxially. At low temperature, the film will most likely be amorphous regardless of the substrate quality. If the substrate is not molecularly smooth, the same behavior is observed, but grain effects arise in the films at higher temperatures. For example, rather

than depositing epitaxial layers, columnar crystals will be formed at high temperatures because islands may be single crystalline, but mismatched with each other. Similar issues arise when the precursor flux is altered. A high reactant flux results in increased concentration of surface molecules that reduces the mobility of those molecules, which can result in poor film crystallinity.

The reactor conditions can be altered to some degree to induce growth of a desired phase. For instance, at moderate temperature, the process pressure can be lowered (LPCVD) which reduces the reactant flux, thereby allowing the growth to be reaction rate limited. In this mode, deposits will grow as fine-grained materials which have the best mechanical performance for wear-resistant applications.

(C. L. AARDAHL, J. W. ROGERS, JR.)

17.2.5.2. Reaction Pathways

Unlike other common techniques such as molecular beam epitaxy (MBE) and physical vapor deposition (PVD), the term "chemical vapor deposition" implies that to form the film a chemical reaction takes place. The reactants in this case are chosen to react and produce a specific coating of interest; hence they are called precursor molecules. Properties necessary for a good precursor include thermal stability at its vaporization temperature and sufficient vapor pressure [at least 1 torr (133.3 Pa)] at a reasonable temperature ($\sim$200°C maximum) for effective gas phase delivery to the growth surface. In addition, the molecules must be obtainable at high purity and must not undergo parasitic or side reactions, which would lead to film contamination/degradation. Several classes of molecules fit this description, depending on the final material that is desired. These include hydrides, halides, organometallics, carbonyls, and hydrocarbons. The types of reaction in which these molecules participate are discussed in the remainder of this section.

(C. L. AARDAHL, J. W. ROGERS, JR.)

17.2.5.2.1. Pyrolysis.

Pyrolysis reactions involve the thermal decomposition of a gas molecule into smaller fragments or atoms, which are deposited on a substrate to form a film. Thermal cracking of hydrocarbons is used to deposit carbon (e.g., graphite or diamond) films depending on the processing conditions, while metal-containing precursor gases are used for metallization. Pyrolysis or thermal CVD is usually done with a single precursor gas, although concurrent decomposition by means of multiple precursor molecules is possible.

Ceramic materials cannot be grown from a single precursor molecule by means of pyrolysis unless a suitable single-source precursor can be obtained. Most single-source precursors for the growth of ceramic materials are metal–organics that contain a covalent bond between the atoms that will comprise the film. For example, aluminum nitride can be deposited via the thermal decomposition of alkylalumnium azides or alkylaluminum amides[1]. Unfortunately, ceramic films deposited by means of pyrolysis of single-source precursors often contain unacceptable levels of carbon contamination resulting from the decomposition of organic ligands in the precursor. Carbon contamination from single-source precursors can be reduced if a carbide film is desired. An example would be the

formation of silicon carbide by methyltrichlorosilane pyrolysis[2,3]

$$Si(CH_3)Cl_3 \longrightarrow SiC + 3HCl \quad (a)$$

Here, carbon contamination is reduced because most of the carbon in the precursor molecule is used to construct the carbide deposit. Only incomplete pyrolysis products contaminate the film.

(C. L. AARDAHL, J. W. ROGERS, JR.)

1. D. C. Boyd, R. T. Haasch, D.R. Mantell, R. K. Schulze, J. F. Evans, W. L. Gladfelter, *Chem. Mater., 1*, 119 (1989).
2. R.F. Davis, in *MRS Symp. Proc.*, Vol. 168: *Chemical Vapor Deposition of Refractory Metals and Ceramics*, T.M. Besmann, B.M. Gallois, eds., Meterials Research Society, Pittsburgh, 1990, p. 145.
3. H.O. Pierson, *Handbook of Chemical Vapor Deposition (CVD): Principles, Technology, and Applications*, Noyes, Park Ridge, NJ, 1992.

17.2.5.2.2. Oxidation/Hydrolysis.

Oxidation and hydrolysis reactions are two common methods of producing oxide films. In this class of reaction, the metal precursor contains metal atoms in a reduced valence state, usually a metal hydride or metal halide. The oxidizing agent is an oxygen containing gas such as O_2, O_3, CO_2, H_2O, or N_2O. The reaction is a simple oxidation scheme. Examples of such reactions are:

$$GeH_4 + O_2 \longrightarrow GeO_2 + 2H_2 \quad (a)$$

$$SiCl_4 + 2CO_2 + 2H_2 \longrightarrow SiO_2 + 4HCl + 2CO \quad (b)$$

$$2AlCl_3 + 3H_2O \longrightarrow Al_2O_3 + 6HCl \quad (c)$$

Atomic oxygen generated in a plasma can also be used as the oxidizer, which allows a decreased deposition temperature. This is possible because the oxygen atoms have sufficient energy to partially compensate for the thermal energy required for non-plasma reactions. Plasma-enhanced processing is discussed further in 17.2.5.3.

(C. L. AARDAHL, J. W. ROGERS, JR.)

1. H.O. Pierson, Handbook of Chemical Vapor Deposition (CVD): Principles, Technology, and Applications, Noyes, Park Ridge, NJ, 1992.

17.2.5.2.3. Reduction.

Hydrogen gas is a strong reducing agent commonly used to reduce metal halides. The major advantage of using a reduction rather than a pyrolysis reaction is the reduced heating requirement for reaction. Generally, reduction with hydrogen gas can be carried out at much lower temperatures than pyrolysis reactions to yield the same products. Common examples of such reactions are[1]:

$$WF_6 + 3H_2 \longrightarrow W + 6HF \quad (a)$$

$$SiCl_4 + 2H_2 \longrightarrow Si + 4HCl \quad (b)$$

Inorganic Reactions and Methods, Volume 18
Edited by J. J. Zuckerman, Jim D. Atwood

formation of silicon carbide by methyltrichlorosilane pyrolysis[2,3]

$$Si(CH_3)Cl_3 \longrightarrow SiC + 3HCl \quad (a)$$

Here, carbon contamination is reduced because most of the carbon in the precursor molecule is used to construct the carbide deposit. Only incomplete pyrolysis products contaminate the film.

(C. L. AARDAHL, J. W. ROGERS, JR.)

1. D. C. Boyd, R. T. Haasch, D.R. Mantell, R. K. Schulze, J. F. Evans, W. L. Gladfelter, *Chem. Mater., 1*, 119 (1989).
2. R.F. Davis, in *MRS Symp. Proc.*, Vol. 168: *Chemical Vapor Deposition of Refractory Metals and Ceramics*, T.M. Besmann, B.M. Gallois, eds., Meterials Research Society, Pittsburgh, 1990, p. 145.
3. H.O. Pierson, *Handbook of Chemical Vapor Deposition (CVD): Principles, Technology, and Applications*, Noyes, Park Ridge, NJ, 1992.

17.2.5.2.2. Oxidation/Hydrolysis.

Oxidation and hydrolysis reactions are two common methods of producing oxide films. In this class of reaction, the metal precursor contains metal atoms in a reduced valence state, usually a metal hydride or metal halide. The oxidizing agent is an oxygen containing gas such as O_2, O_3, CO_2, H_2O, or N_2O. The reaction is a simple oxidation scheme. Examples of such reactions are:

$$GeH_4 + O_2 \longrightarrow GeO_2 + 2H_2 \quad (a)$$

$$SiCl_4 + 2CO_2 + 2H_2 \longrightarrow SiO_2 + 4HCl + 2CO \quad (b)$$

$$2AlCl_3 + 3H_2O \longrightarrow Al_2O_3 + 6HCl \quad (c)$$

Atomic oxygen generated in a plasma can also be used as the oxidizer, which allows a decreased deposition temperature. This is possible because the oxygen atoms have sufficient energy to partially compensate for the thermal energy required for non-plasma reactions. Plasma-enhanced processing is discussed further in 17.2.5.3.

(C. L. AARDAHL, J. W. ROGERS, JR.)

1. H.O. Pierson, Handbook of Chemical Vapor Deposition (CVD): Principles, Technology, and Applications, Noyes, Park Ridge, NJ, 1992.

17.2.5.2.3. Reduction.

Hydrogen gas is a strong reducing agent commonly used to reduce metal halides. The major advantage of using a reduction rather than a pyrolysis reaction is the reduced heating requirement for reaction. Generally, reduction with hydrogen gas can be carried out at much lower temperatures than pyrolysis reactions to yield the same products. Common examples of such reactions are[1]:

$$WF_6 + 3H_2 \longrightarrow W + 6HF \quad (a)$$

$$SiCl_4 + 2H_2 \longrightarrow Si + 4HCl \quad (b)$$

Inorganic Reactions and Methods, Volume 18
Edited by J. J. Zuckerman, Jim D. Atwood

formation of silicon carbide by methyltrichlorosilane pyrolysis[2,3]

$$Si(CH_3)Cl_3 \longrightarrow SiC + 3HCl \quad (a)$$

Here, carbon contamination is reduced because most of the carbon in the precursor molecule is used to construct the carbide deposit. Only incomplete pyrolysis products contaminate the film.

(C. L. AARDAHL, J. W. ROGERS, JR.)

1. D. C. Boyd, R. T. Haasch, D.R. Mantell, R. K. Schulze, J. F. Evans, W. L. Gladfelter, *Chem. Mater., 1*, 119 (1989).
2. R.F. Davis, in *MRS Symp. Proc.*, Vol. 168: *Chemical Vapor Deposition of Refractory Metals and Ceramics*, T.M. Besmann, B.M. Gallois, eds., Meterials Research Society, Pittsburgh, 1990, p. 145.
3. H.O. Pierson, *Handbook of Chemical Vapor Deposition (CVD): Principles, Technology, and Applications*, Noyes, Park Ridge, NJ, 1992.

17.2.5.2.2. Oxidation/Hydrolysis.

Oxidation and hydrolysis reactions are two common methods of producing oxide films. In this class of reaction, the metal precursor contains metal atoms in a reduced valence state, usually a metal hydride or metal halide. The oxidizing agent is an oxygen containing gas such as O_2, O_3, CO_2, H_2O, or N_2O. The reaction is a simple oxidation scheme. Examples of such reactions are:

$$GeH_4 + O_2 \longrightarrow GeO_2 + 2H_2 \quad (a)$$

$$SiCl_4 + 2CO_2 + 2H_2 \longrightarrow SiO_2 + 4HCl + 2CO \quad (b)$$

$$2AlCl_3 + 3H_2O \longrightarrow Al_2O_3 + 6HCl \quad (c)$$

Atomic oxygen generated in a plasma can also be used as the oxidizer, which allows a decreased deposition temperature. This is possible because the oxygen atoms have sufficient energy to partially compensate for the thermal energy required for non-plasma reactions. Plasma-enhanced processing is discussed further in 17.2.5.3.

(C. L. AARDAHL, J. W. ROGERS, JR.)

1. H.O. Pierson, Handbook of Chemical Vapor Deposition (CVD): Principles, Technology, and Applications, Noyes, Park Ridge, NJ, 1992.

17.2.5.2.3. Reduction.

Hydrogen gas is a strong reducing agent commonly used to reduce metal halides. The major advantage of using a reduction rather than a pyrolysis reaction is the reduced heating requirement for reaction. Generally, reduction with hydrogen gas can be carried out at much lower temperatures than pyrolysis reactions to yield the same products. Common examples of such reactions are[1]:

$$WF_6 + 3H_2 \longrightarrow W + 6HF \quad (a)$$

$$SiCl_4 + 2H_2 \longrightarrow Si + 4HCl \quad (b)$$

To form ceramic materials such as oxides, carbides, nitrides, borides, and silicides, a coreduction procedure is needed. An example of a coreduction reaction is that used in the production of titanium diboride[1]:

$$TiCl_4 + 2BCl_3 + 5H_2 \longrightarrow TiB_2 + 10HCl \quad (c)$$

Here, both halide species are reduced by hydrogen.

(C. L. AARDAHL, J. W. ROGERS, JR.)

1. H.O. Pierson, Handbook of Chemical Vapor Deposition (CVD): Principles, Technology, and Applications, Noyes, Park Ridge, NJ, 1992.

17.2.5.2.4. Carbidization/Nitridation.

If single-source precursors are unavailable, carbides can be produced by reacting a metal halide or metal hydride with a hydrocarbon gas. Often the hydrocarbon is methane, and the carbide formation reaction may be written as follows:

$$SiH_4 + CH_4 \longrightarrow SiC + 4H_2 \quad (a)$$

or

$$SiCl_4 + CH_4 \longrightarrow SiC + 4HCl \quad (b)$$

To perform nitridation, a metal hydride or metal halide is reacted with ammonia as in

$$3SiH_4 + 4NH_3 \longrightarrow Si_3N_4 + 12H_2 \quad (c)$$

or

$$BCl_3 + NH_3 \longrightarrow BN + 3HCl \quad (d)$$

17.2.5.2.5. Disproportionation.

Disproportionation can be used to deposit metals that are stable in multiple valence states depending on the temperature in the reactor. The precursor is typically a halide as for germanium deposition[1]:

$$2GeI_2 \longrightarrow Ge + GeI_4 \quad (a)$$

This reaction takes place at 300°C, but one must be careful to avoid the reverse reaction that occurs at 600°C. Generally, the metals and its higher valence halide are most stable at lower temperatures.

(C. L. AARDAHL, J. W. ROGERS, JR.)

1. M. Ohring, *The Materials Science of Thin Films*, Academic Press, San Diego, CA, 1952.

17.2.5.3. Plasma CVD (PCVD)

In traditional CVD, thermal energy is used to activate the reaction; in other words, a heated substrate supplies the energy necessary for the reaction to proceed at a given temperature. Sometimes the reaction temperature required for a sufficient growth rate is so high that there are side reactions, decomposition of the deposit or deleterious effects on the substrate. In such a case, to induce the reaction to occur at lower growth

Inorganic Reactions and Methods, Volume 18
Edited by J. J. Zuckerman, Jim D. Atwood

To form ceramic materials such as oxides, carbides, nitrides, borides, and silicides, a coreduction procedure is needed. An example of a coreduction reaction is that used in the production of titanium diboride[1]:

$$TiCl_4 + 2BCl_3 + 5H_2 \longrightarrow TiB_2 + 10HCl \quad (c)$$

Here, both halide species are reduced by hydrogen.

(C. L. AARDAHL, J. W. ROGERS, JR.)

1. H.O. Pierson, Handbook of Chemical Vapor Deposition (CVD): Principles, Technology, and Applications, Noyes, Park Ridge, NJ, 1992.

17.2.5.2.4. Carbidization/Nitridation.

If single-source precursors are unavailable, carbides can be produced by reacting a metal halide or metal hydride with a hydrocarbon gas. Often the hydrocarbon is methane, and the carbide formation reaction may be written as follows:

$$SiH_4 + CH_4 \longrightarrow SiC + 4H_2 \quad (a)$$

or

$$SiCl_4 + CH_4 \longrightarrow SiC + 4HCl \quad (b)$$

To perform nitridation, a metal hydride or metal halide is reacted with ammonia as in

$$3SiH_4 + 4NH_3 \longrightarrow Si_3N_4 + 12H_2 \quad (c)$$

or

$$BCl_3 + NH_3 \longrightarrow BN + 3HCl \quad (d)$$

17.2.5.2.5. Disproportionation.

Disproportionation can be used to deposit metals that are stable in multiple valence states depending on the temperature in the reactor. The precursor is typically a halide as for germanium deposition[1]:

$$2GeI_2 \longrightarrow Ge + GeI_4 \quad (a)$$

This reaction takes place at 300°C, but one must be careful to avoid the reverse reaction that occurs at 600°C. Generally, the metals and its higher valence halide are most stable at lower temperatures.

(C. L. AARDAHL, J. W. ROGERS, JR.)

1. M. Ohring, *The Materials Science of Thin Films*, Academic Press, San Diego, CA, 1952.

17.2.5.3. Plasma CVD (PCVD)

In traditional CVD, thermal energy is used to activate the reaction; in other words, a heated substrate supplies the energy necessary for the reaction to proceed at a given temperature. Sometimes the reaction temperature required for a sufficient growth rate is so high that there are side reactions, decomposition of the deposit or deleterious effects on the substrate. In such a case, to induce the reaction to occur at lower growth

Inorganic Reactions and Methods, Volume 18
Edited by J. J. Zuckerman, Jim D. Atwood

To form ceramic materials such as oxides, carbides, nitrides, borides, and silicides, a coreduction procedure is needed. An example of a coreduction reaction is that used in the production of titanium diboride[1]:

$$TiCl_4 + 2BCl_3 + 5H_2 \longrightarrow TiB_2 + 10HCl \quad (c)$$

Here, both halide species are reduced by hydrogen.

(C. L. AARDAHL, J. W. ROGERS, JR.)

1. H.O. Pierson, Handbook of Chemical Vapor Deposition (CVD): Principles, Technology, and Applications, Noyes, Park Ridge, NJ, 1992.

17.2.5.2.4. Carbidization/Nitridation.

If single-source precursors are unavailable, carbides can be produced by reacting a metal halide or metal hydride with a hydrocarbon gas. Often the hydrocarbon is methane, and the carbide formation reaction may be written as follows:

$$SiH_4 + CH_4 \longrightarrow SiC + 4H_2 \quad (a)$$

or

$$SiCl_4 + CH_4 \longrightarrow SiC + 4HCl \quad (b)$$

To perform nitridation, a metal hydride or metal halide is reacted with ammonia as in

$$3SiH_4 + 4NH_3 \longrightarrow Si_3N_4 + 12H_2 \quad (c)$$

or

$$BCl_3 + NH_3 \longrightarrow BN + 3HCl \quad (d)$$

17.2.5.2.5. Disproportionation.

Disproportionation can be used to deposit metals that are stable in multiple valence states depending on the temperature in the reactor. The precursor is typically a halide as for germanium deposition[1]:

$$2GeI_2 \longrightarrow Ge + GeI_4 \quad (a)$$

This reaction takes place at 300°C, but one must be careful to avoid the reverse reaction that occurs at 600°C. Generally, the metals and its higher valence halide are most stable at lower temperatures.

(C. L. AARDAHL, J. W. ROGERS, JR.)

1. M. Ohring, *The Materials Science of Thin Films*, Academic Press, San Diego, CA, 1952.

17.2.5.3. Plasma CVD (PCVD)

In traditional CVD, thermal energy is used to activate the reaction; in other words, a heated substrate supplies the energy necessary for the reaction to proceed at a given temperature. Sometimes the reaction temperature required for a sufficient growth rate is so high that there are side reactions, decomposition of the deposit or deleterious effects on the substrate. In such a case, to induce the reaction to occur at lower growth

temperature energy must be delivered to the reactants in a form other than heat. This requirement has led to the development of so-called *enhanced* CVD processes, in which the energy required to increase the reaction rate is delivered to the reactants as electromagnetic radiation, electricity, ions, or electrons.

Electrical energy may be passed to the reactants via a low current gas discharge or plasma. Because energy is delivered in a form other than heat, plasma CVD can be used to deposit films at a much lower temperature. Lower temperature processing can be a tremendous advantage in some applications, such as semiconductor processing, where layers deposited in a prior step are subject to degradation upon exposure to excessive temperatures. A plasma can be generated by means of a dc field at low pressure, but ac fields are more commonly used. For many years, a radio frequency (rf) of 13.56 MHz has been used to generate plasmas, but recent advances in microwave technology have produced an electron cyclotron resonance (ECR) based plasma[1–3] that is stable at 2.45 GHz. Other drive systems to facilitate the formation of plasmas are based on helicon[4] and inductively coupled devices[5]. Rf plasmas have been widely studied and are capable of producing high quality films, but the newer technologies have an advantage over rf sources because the plasma has a larger concentration of energetic charge carriers. A larger density of charge carriers in the plasma results in greater interaction of the charge carriers with precursor molecules than for rf plasmas. This in turn results in the ability to move to lower processing temperatures and pressures without sacrifice in growth rate. Plasma CVD has been widely studied and is the only enhanced process that has gained wide industrial acceptance. Several reviews[6–8] discuss PCVD in greater detail.

(C. L. AARDAHL, J. W. ROGERS, JR.)

1. P. Bulkin, N. Bertrand, B. Drevillon. *Thin Solid Films, 296*, 66 (1997).
2. J. Pelletier, T. Lagarde, *Thin Solid Films, 241*, 240 (1994).
3. F. Plais, B. Agius, F. Abel, J. Siejka, M. Puech, P. Ravel, P. Alnot, N. Proust, *J. Electrochem. Soc., 139*, 1489 (1992).
4. C. Charles, G. Girout-Matlakowski, R.W. Boswell, A. Goullet, G. Turban, C. Cardinaud, *J. Vac. Sci. Technol. A, 11*, 2954 (1993).
5. J.B. Carter, J.P. Holland, E. Peltzer, B. Richardson, E. Bogle, H. T. Nguyen, Y. Melaku, D. Gates, M. Ben-Dor, *J. Vac. Sci. Technol. A, 11*, 1301 (1993).
6. M. Konuma, *Film Deposition by Plasma Techniques*, Springer-Verlag, New York, 1992.
7. G. Lucovsky, D.E. Ibbotson, D.W. Hess, eds., *Materials Research Society Symposium Proceedings*, Vol. 165: *Characterization of Plasma-Enhanced CVD Processes*, Materials Research Society, Pittsburgh, 1990.
8. G. Bruno, P. Capezzuto, A. Madan, eds., *Plasma Deposition of Amorphous Silicon-Based Materials*, Academic Press, Boston, 1995.

17.2.5.4. Nonconventional CVD Techniques

Several newer CVD techniques have gained favor in the research community. For the most part, these methods have not been implemented in industrial processes; nevertheless, the techniques are discussed briefly to illustrate the direction of future technologies in CVD processing and relevant chemistry associated with these methods.

These specialized forms of CVD, referred to as *nontraditional* techniques for the purpose of this review, include laser (LCVD), aerosol (ACVD), hot filament (HFCVD), and ion beam (IBCVD) chemical vapor deposition. In such *enhanced* CVD technologies, a thermal CVD reaction occurs simultaneously with another driving force, which results

Inorganic Reactions and Methods, Volume 18
Edited by J. J. Zuckerman, Jim D. Atwood

temperature energy must be delivered to the reactants in a form other than heat. This requirement has led to the development of so-called *enhanced* CVD processes, in which the energy required to increase the reaction rate is delivered to the reactants as electromagnetic radiation, electricity, ions, or electrons.

Electrical energy may be passed to the reactants via a low current gas discharge or plasma. Because energy is delivered in a form other than heat, plasma CVD can be used to deposit films at a much lower temperature. Lower temperature processing can be a tremendous advantage in some applications, such as semiconductor processing, where layers deposited in a prior step are subject to degradation upon exposure to excessive temperatures. A plasma can be generated by means of a dc field at low pressure, but ac fields are more commonly used. For many years, a radio frequency (rf) of 13.56 MHz has been used to generate plasmas, but recent advances in microwave technology have produced an electron cyclotron resonance (ECR) based plasma[1–3] that is stable at 2.45 GHz. Other drive systems to facilitate the formation of plasmas are based on helicon[4] and inductively coupled devices[5]. Rf plasmas have been widely studied and are capable of producing high quality films, but the newer technologies have an advantage over rf sources because the plasma has a larger concentration of energetic charge carriers. A larger density of charge carriers in the plasma results in greater interaction of the charge carriers with precursor molecules than for rf plasmas. This in turn results in the ability to move to lower processing temperatures and pressures without sacrifice in growth rate. Plasma CVD has been widely studied and is the only enhanced process that has gained wide industrial acceptance. Several reviews[6–8] discuss PCVD in greater detail.

(C. L. AARDAHL, J. W. ROGERS, JR.)

1. P. Bulkin, N. Bertrand, B. Drevillon. *Thin Solid Films, 296*, 66 (1997).
2. J. Pelletier, T. Lagarde, *Thin Solid Films, 241*, 240 (1994).
3. F. Plais, B. Agius, F. Abel, J. Siejka, M. Puech, P. Ravel, P. Alnot, N. Proust, *J. Electrochem. Soc., 139*, 1489 (1992).
4. C. Charles, G. Girout-Matlakowski, R.W. Boswell, A. Goullet, G. Turban, C. Cardinaud, *J. Vac. Sci. Technol. A, 11*, 2954 (1993).
5. J.B. Carter, J.P. Holland, E. Peltzer, B. Richardson, E. Bogle, H. T. Nguyen, Y. Melaku, D. Gates, M. Ben-Dor, *J. Vac. Sci. Technol. A, 11*, 1301 (1993).
6. M. Konuma, *Film Deposition by Plasma Techniques*, Springer-Verlag, New York, 1992.
7. G. Lucovsky, D.E. Ibbotson, D.W. Hess, eds., *Materials Research Society Symposium Proceedings*, Vol. 165: *Characterization of Plasma-Enhanced CVD Processes*, Materials Research Society, Pittsburgh, 1990.
8. G. Bruno, P. Capezzuto, A. Madan, eds., *Plasma Deposition of Amorphous Silicon-Based Materials*, Academic Press, Boston, 1995.

17.2.5.4. Nonconventional CVD Techniques

Several newer CVD techniques have gained favor in the research community. For the most part, these methods have not been implemented in industrial processes; nevertheless, the techniques are discussed briefly to illustrate the direction of future technologies in CVD processing and relevant chemistry associated with these methods.

These specialized forms of CVD, referred to as *nontraditional* techniques for the purpose of this review, include laser (LCVD), aerosol (ACVD), hot filament (HFCVD), and ion beam (IBCVD) chemical vapor deposition. In such *enhanced* CVD technologies, a thermal CVD reaction occurs simultaneously with another driving force, which results

in a deposit with superior qualities or formation of a deposit that otherwise would not be formed. Often, such specialized methods are the only way to deposit a given material.

(C. L. AARDAHL, J. W. ROGERS, JR.)

17.2.5.4.1. Laser/Photo CVD.

In the case of LCVD, a coherent light wave or laser beam serves to inject energy into the chemical reaction, thereby facilitating a more favorable product. The light can act as a benefactor in two ways: in *thermal* LCVD, absorbed radiation heats the gas to provide thermal energy for the reaction; and in *photo* LCVD, light breaks down gas phase reactants photochemically, which results in a reduced thermal energy requirement for the reaction. In photo LCVD, a luminous source such as an arc lamp can be used, but lasers are preferred because they deliver high power over a narrow distribution of photon energy. In fact, if the laser light is spatially manipulated, as in a hologram, the deposition can take place preferentially in space. This property has led to the production of highly tailored optical components and graded coatings via CVD. Recent texts provide a more detailed review of thermal and photo LCVD[1,2].

(C. L. AARDAHL, J. W. ROGERS, JR.)

1. J.G. Eden, *Photochemical Vapor Deposition*, Wiley-Interscience, New York, 1992.
2. J. Mazumder and A. Kar, *Theory and Application of Laser Chemical Vapor Deposition*, Plenum Press, New York, 1995.

17.2.5.4.2. Hot Filament CVD.

HFCVD is performed by placing a heated filament or wire above the substrate. Precursor molecules are pyrolyzed above the wire, and reactive intermediates or products adsorb to the deposition surface. This technique is advantageous because the substrate can be kept at a lower temperature, since the heated filament provides the necessary energy for cracking the precursor molecules. As a result, high temperature reactions can still be used to deposit refractories on heat sensitive substrates. Thus far, HFCVD has been used mainly for the deposition of diamond films, but implementation of this technique for the growth of ceramics is not far in the future.

(C. L. AARDAHL, J. W. ROGERS, JR.)

17.2.5.4.3. Ion Beam CVD.

IBCVD[1–5] involves the use of energetic ions to facilitate chemical reaction of gas phase precursors. There are two modes in which the ions can play a role: the kinetic energy of the ions can supply energy to the reactants, which lowers the thermal energy requirement for reaction, and/or the ions themselves may be highly reactive and incorporated into the film. The former will occur if the ions are inert, as they are when an Ar^+ gun is used with simultaneous dosing of reactants. Reactive ions include O_2^+ and N_2^+ which can be used as the oxygen and nitrogen sources for oxides and nitrides, respectively.

(C. L. AARDAHL, J. W. ROGERS, JR.)

1. K. Baba, R. Hatada, *Surf. Coat. Technol.*, *66*, 368 (1994).
2. K. Baba, R. Hatada, S. Nagata, H. Fujiyama, G.K. Wolf, W. Ensinger, *Surf. Coat. Technol.*, *74–75*, 292 (1995).

Inorganic Reactions and Methods, Volume 18
Edited by J. J. Zuckerman, Jim D. Atwood

in a deposit with superior qualities or formation of a deposit that otherwise would not be formed. Often, such specialized methods are the only way to deposit a given material.

(C. L. AARDAHL, J. W. ROGERS, JR.)

17.2.5.4.1. Laser/Photo CVD.

In the case of LCVD, a coherent light wave or laser beam serves to inject energy into the chemical reaction, thereby facilitating a more favorable product. The light can act as a benefactor in two ways: in *thermal* LCVD, absorbed radiation heats the gas to provide thermal energy for the reaction; and in *photo* LCVD, light breaks down gas phase reactants photochemically, which results in a reduced thermal energy requirement for the reaction. In photo LCVD, a luminous source such as an arc lamp can be used, but lasers are preferred because they deliver high power over a narrow distribution of photon energy. In fact, if the laser light is spatially manipulated, as in a hologram, the deposition can take place preferentially in space. This property has led to the production of highly tailored optical components and graded coatings via CVD. Recent texts provide a more detailed review of thermal and photo LCVD[1,2].

(C. L. AARDAHL, J. W. ROGERS, JR.)

1. J.G. Eden, *Photochemical Vapor Deposition*, Wiley-Interscience, New York, 1992.
2. J. Mazumder and A. Kar, *Theory and Application of Laser Chemical Vapor Deposition*, Plenum Press, New York, 1995.

17.2.5.4.2. Hot Filament CVD.

HFCVD is performed by placing a heated filament or wire above the substrate. Precursor molecules are pyrolyzed above the wire, and reactive intermediates or products adsorb to the deposition surface. This technique is advantageous because the substrate can be kept at a lower temperature, since the heated filament provides the necessary energy for cracking the precursor molecules. As a result, high temperature reactions can still be used to deposit refractories on heat sensitive substrates. Thus far, HFCVD has been used mainly for the deposition of diamond films, but implementation of this technique for the growth of ceramics is not far in the future.

(C. L. AARDAHL, J. W. ROGERS, JR.)

17.2.5.4.3. Ion Beam CVD.

IBCVD[1–5] involves the use of energetic ions to facilitate chemical reaction of gas phase precursors. There are two modes in which the ions can play a role: the kinetic energy of the ions can supply energy to the reactants, which lowers the thermal energy requirement for reaction, and/or the ions themselves may be highly reactive and incorporated into the film. The former will occur if the ions are inert, as they are when an Ar^+ gun is used with simultaneous dosing of reactants. Reactive ions include O_2^+ and N_2^+ which can be used as the oxygen and nitrogen sources for oxides and nitrides, respectively.

(C. L. AARDAHL, J. W. ROGERS, JR.)

1. K. Baba, R. Hatada, *Surf. Coat. Technol., 66*, 368 (1994).
2. K. Baba, R. Hatada, S. Nagata, H. Fujiyama, G.K. Wolf, W. Ensinger, *Surf. Coat. Technol., 74–75*, 292 (1995).

3. K. Baba, R. Hatada, *Surf. Coat. Technol., 84*, 429 (1996).
4. A. Caballero, D. Leinen, A. Fernandez, A. R. Gonzalez-Elipe, *Surf. Coat. Technol., 80*, 23 (1996).
5. J. P. Espinos, A. Fernandez, A. Caballero, V. M. Jimenez, J. C. Sanchez-Lopez, L. Contreras, D. Leinen, A. R. Gonzalez-Elipe, *Chem. Vapor Deposition, 3*, 219 (1997).

17.2.5.4.4. Aerosol CVD.

In ACVD, also referred to as particle CVD, small particles are used to deliver reactants to the deposition surface. Here, energy is not imparted to the reactants; rather, precursors may be transported to the substrate by a means other than gas transport. This technique is used only when the desired precursors have insufficient vapor pressure to be carried to the surface as a gas. Generally, the precursor of interest is dissolved in a solvent and sprayed into the vapor phase by means of atomizer, electrospray, or nebulizer. This aerosol is convectively carried to the surface, and the precursor within the particles reacts at some point in transit.

In spray pyrolysis the precursor reacts thermally in particle form and the product species is deposited as particles on the surface. Such films must be annealed or sintered after the particles have been deposited to make a uniform coating. Alternately, the precursor may be deposited on a heated surface and react thermally upon contact. In this case, any remaining solvent is driven from the surface by evaporation to the gas phase.

(C. L. AARDAHL, J. W. ROGERS, JR.)

17.2.5.5. Technologically Significant Ceramics via CVD

Numerous ceramics are deposited via chemical vapor deposition. Oxide, carbide, nitride, and boride films can all be produced from gas phase precursors. This section gives details on the production-scale reactions for materials that are widely produced. In addition, a survey of the latest research including novel precursors and chemical reactions is provided. The discussion begins with the mature technologies of silicon dioxide, aluminum oxide, and silicon nitride CVD. Then the focus turns to the deposition of thin films having characteristics that are attractive for future applications in microelectronics, micromachinery, and hard coatings for tools and parts. These materials include aluminum nitride, boron nitride, titanium nitride, titanium dioxide, silicon carbide, and mixed-metal oxides such as those of the perovskite structure and those used as high T_c superconductors.

This is by no means an exhaustive review of all ceramic materials deposited by CVD. The materials discussed were chosen to illustrate the chemistry of CVD, and articles and reviews that indicate the current direction of research are presented.

(C. L. AARDAHL, J. W. ROGERS, JR.)

17.2.5.5.1. Silicon Dioxide.

Silicon dioxide is the most widely used ceramic material in the semiconductor industry, and the majority of SiO_2 deposits in microelectronic circuits are formed by CVD. Silica layers are used as diffusion sources, intermetallic dielectrics, and dopant and etch barriers in the microelectronics industry. CVD of SiO_2 is also commonly used in manufacturing energy-efficient glass windows, surface coatings for fiber optics, and micromechanical applications[1,2].

Inorganic Reactions and Methods, Volume 18
Edited by J. J. Zuckerman, Jim D. Atwood

3. K. Baba, R. Hatada, *Surf. Coat. Technol., 84*, 429 (1996).
4. A. Caballero, D. Leinen, A. Fernandez, A. R. Gonzalez-Elipe, *Surf. Coat. Technol., 80*, 23 (1996).
5. J. P. Espinos, A. Fernandez, A. Caballero, V. M. Jimenez, J. C. Sanchez-Lopez, L. Contreras, D. Leinen, A. R. Gonzalez-Elipe, *Chem. Vapor Deposition, 3*, 219 (1997).

17.2.5.4.4. Aerosol CVD.

In ACVD, also referred to as particle CVD, small particles are used to deliver reactants to the deposition surface. Here, energy is not imparted to the reactants; rather, precursors may be transported to the substrate by a means other than gas transport. This technique is used only when the desired precursors have insufficient vapor pressure to be carried to the surface as a gas. Generally, the precursor of interest is dissolved in a solvent and sprayed into the vapor phase by means of atomizer, electrospray, or nebulizer. This aerosol is convectively carried to the surface, and the precursor within the particles reacts at some point in transit.

In spray pyrolysis the precursor reacts thermally in particle form and the product species is deposited as particles on the surface. Such films must be annealed or sintered after the particles have been deposited to make a uniform coating. Alternately, the precursor may be deposited on a heated surface and react thermally upon contact. In this case, any remaining solvent is driven from the surface by evaporation to the gas phase.

(C. L. AARDAHL, J. W. ROGERS, JR.)

17.2.5.5. Technologically Significant Ceramics via CVD

Numerous ceramics are deposited via chemical vapor deposition. Oxide, carbide, nitride, and boride films can all be produced from gas phase precursors. This section gives details on the production-scale reactions for materials that are widely produced. In addition, a survey of the latest research including novel precursors and chemical reactions is provided. The discussion begins with the mature technologies of silicon dioxide, aluminum oxide, and silicon nitride CVD. Then the focus turns to the deposition of thin films having characteristics that are attractive for future applications in microelectronics, micromachinery, and hard coatings for tools and parts. These materials include aluminum nitride, boron nitride, titanium nitride, titanium dioxide, silicon carbide, and mixed-metal oxides such as those of the perovskite structure and those used as high T_c superconductors.

This is by no means an exhaustive review of all ceramic materials deposited by CVD. The materials discussed were chosen to illustrate the chemistry of CVD, and articles and reviews that indicate the current direction of research are presented.

(C. L. AARDAHL, J. W. ROGERS, JR.)

17.2.5.5.1. Silicon Dioxide.

Silicon dioxide is the most widely used ceramic material in the semiconductor industry, and the majority of SiO_2 deposits in microelectronic circuits are formed by CVD. Silica layers are used as diffusion sources, intermetallic dielectrics, and dopant and etch barriers in the microelectronics industry. CVD of SiO_2 is also commonly used in manufacturing energy-efficient glass windows, surface coatings for fiber optics, and micromechanical applications[1,2].

A number of reactions and precursors have been used to deposit SiO_2 from the gas phase. The most common silicon precursors are silane and chlorosilanes, which readily react with a variety of oxidizers above 400°C[3,4]. There are two reactions that take place between silane and oxygen gas:

$$SiH_4 + O_2 \longrightarrow SiO_2 + 2H_2 \quad (a)$$

$$SiH_4 + 2O_2 \longrightarrow SiO_2 + 2H_2O \quad (b)$$

At 450°C, the reactions take place simultaneously, but reaction (b) is favored in a limited oxygen supply. Reaction (a) can be used exclusively in a plasma at 200–300°C and 0.15–0.3 torr with a gas phase composition of 10 parts silane in 1 part oxygen with a carrier gas of argon or helium. Carbon dioxide can also be used as the oxygen source, where the reaction is[5]

$$SiH_4 + 2CO_2 + 2H_2 \longrightarrow SiO_2 + 4H_2 + 2CO \quad (c)$$

in a plasma at 200–600°C and a pressure just below 1 torr. Nitrous oxide is another oxidizer that will react with silane in a plasma at 200–350°C by the following reaction[2]:

$$SiH_4 + 2N_2O \longrightarrow SiO_2 + 2H_2 + 2N_2 \quad (d)$$

Nitrous oxide can also be used at atmospheric pressure with dichlorosilane at a temperature of 850°C[2]:

$$SiCl_2H_2 + 2N_2O \longrightarrow SiO_2 + 2HCl + 2N_2 \quad (e)$$

It is becoming more common to use metal–organic precursors for the production of SiO_2 because higher purity can be obtained. Commonly, silicon alkoxides are used as single-source precursors. The most common alkoxide precursor is tetraethyl orthosilicate or tetraethoxysilane (TEOS), which will react 700°C and $\sim$1 torr[4,6,7]:

$$Si(OC_2H_5)_4 \longrightarrow SiO_2 + 2C_2H_5OH + 2C_2H_4 \quad (f)$$

(The actual product distribution depends on the deposition temperature for this reaction[8,9]). As the length of the alkoxide ligands is increased, the deposition temperature can be reduced because the O—C bond weakens with increasing hydrocarbon size. Nevertheless, there is a limit to the size of ligands because bulky alkoxide groups will result in a solid precursor with insufficient volatility.

The state of the art in the CVD of SiO_2 and related materials was recently reviewed[10]. Current research is focused on development of precursors for MOCVD, various enhanced deposition methods, and scale-up of existing technologies to larger substrate sizes. Particular interest has been shown in plasma-enhanced processes using rf and ECR sources and standard precursors such as TEOS and silane. The chemistry does not change, but the plasma reduces the thermodynamic limitations, resulting in lower growth temperatures. For TEOS[11] and silane[12], when plasma deposition is used the temperature can be reduced to as low as 50°C and room temperature, respectively. Silane has also been used in combination with a combined ECR plasma/IBCVD technique to deposit SiO_2 that shows superior corrosion resistance[13]. Another precursor that has been employed in thermal CVD is diacetoxy di-*t*-butoxysilane, which decomposes at 450°C[14].

(C. L. AARDAHL, J. W. ROGERS, JR.)

1. A. Stoffel, A. Kovacs, W. Kronast, B. Muller, *J. Micromech. Microeng., 6*, 1 (1996).
2. H. O. Pierson, *Handbook of Chemical Vapor Deposition (CVD): Principles, Technology, and Applications*, Noyes, Park Ridge, NJ, 1992.
3. W. Kern, V. S. Ban, in *Thin Film Processes*, J. Vossen,W. Kern, eds., Academic Press, New York, 1978, p. 290.
4. K. L. Schuegraf, *Handbook of Thin-Film Deposition Processes and Techniques: Principles, Methods, Equipment, and Applications*, Noyes, Park Ridge, NJ. 1988.
5. D. Stinton, T. Besmann, R. Lowden, *Ceram. Bull., 67*, 350 (1988).
6. C. Powell, J. Oxley, J. M. J. Blocher, *Vapor Deposition*, Wiley, New York, 1966.
7. D. Doppalapudi, R. Mulpuri, S. N. Basu, V. K. Sarin, in *MRS Symp. Proc.*, Vol. 363: *Chemical Vapor Deposition of Refractory Metal and Ceramics III*, B.M. Gallois, W.Y. Lee and M.A. Pickering, eds., Materials Research Society, Pittsburgh, 1995, p. 95.
8. L. Gamble, M. Hugenschmidt, C. T. Campbell, T. A. Jurgens, J. W. Rogers Jr., *J. Am. Chem. Soc., 115*, 12096 (1993).
9. T. A. Jurgens, J. W. Rogers Jr., *J. Phys. Chem., 99*, 731 (1995).
10. A. R. Barron, *Adv. Mater. Opt. Electron., 6*, 101 (1996).
11. T. Nakamura, A. Shida, K. Matsui, *Jpn. J. Appl. Phys. Pt. 1, 34*, 6214 (1995).
12. P. Bulkin, N. Bertrand, B. Drevillon, *Thin Solid Films, 296*, 66 (1997).
13. K. Baba, R. Hatada, S. Nagata, H. Fujiyama, G. K. Wolf, W. Ensinger, *Surf. Coat. Technol., 74*, 292 (1995).
14. S. B. Desu, in *MRS Symp. Proc.*, Vol. 168: *Chemical Vapor Deposition of Refractory Metals and Ceramics*, T. M. Besmann and B. M. Gallois, eds, Materials Research Society, Pittsburgh, 1990, p. 221.

17.2.5.5.2. Aluminum Oxide.

Alumina films are used for surface coatings on carbide tools, as dielectric layers in transistor fabrication, as matched substrates (sapphire) for the growth of optically active materials such as gallium nitride, and as coatings for optical components.

Comapred to the numerous options for silica, there are relatively few precursors available for the deposition of high quality alumina. The most common precursor is aluminum trichloride ($AlCl_3$), which undergoes hydrolysis above 1050°C by the reaction[1,2]:

$$2AlCl_3 + 3H_2 + 3CO_2 \longrightarrow Al_2O_3 + 3CO + 6HCl \qquad \text{(a)}$$

Here, hydrogen and carbon dioxide react to form water vapor (and carbon monoxide via water–gas shift), which hydrolyzes the aluminum trichloride. If the deposition surface is temperature sensitive, a metal–organic precursor is preferred. Again, an alkoxide is generally used[3]:

$$2Al(OC_3H_7)_3 \longrightarrow Al_2O_3 + 3(C_3H_7)OH + 3C_3H_6 \qquad \text{(b)}$$

Aluminum alkyls such as trimethylaluminum can be used at low temperature (250°C) in an oxidizing ambient[4], but these films suffer large carbon contamination compared with films produced using reactions (a) and (b). A combined ECR plasma/accelerated ion beam process has recently been used to deposit alumina at 700°C with the precursor $Al[OCH(CH_3)_2]_3$[5]. The use of an oxygen ion beam with trimethylaluminum as the precursor has resulted in alumina films, but the films must be annealed at 730°C to obtain crystalline material[6].

(C. L. AARDAHL, J. W. ROGERS, JR.)

1. H. O. Pierson, *Handbook of Chemical Vapor Deposition (CVD): Principles, Technology, and Applications*, Noyes, Park Ridge, NJ, 1992.

Inorganic Reactions and Methods, Volume 18
Edited by J. J. Zuckerman, Jim D. Atwood

1. A. Stoffel, A. Kovacs, W. Kronast, B. Muller, *J. Micromech. Microeng., 6*, 1 (1996).
2. H. O. Pierson, *Handbook of Chemical Vapor Deposition (CVD): Principles, Technology, and Applications*, Noyes, Park Ridge, NJ, 1992.
3. W. Kern, V. S. Ban, in *Thin Film Processes*, J. Vossen,W. Kern, eds., Academic Press, New York, 1978, p. 290.
4. K. L. Schuegraf, *Handbook of Thin-Film Deposition Processes and Techniques: Principles, Methods, Equipment, and Applications*, Noyes, Park Ridge, NJ. 1988.
5. D. Stinton, T. Besmann, R. Lowden, *Ceram. Bull., 67*, 350 (1988).
6. C. Powell, J. Oxley, J. M. J. Blocher, *Vapor Deposition*, Wiley, New York, 1966.
7. D. Doppalapudi, R. Mulpuri, S. N. Basu, V. K. Sarin, in *MRS Symp. Proc.*, Vol. 363: *Chemical Vapor Deposition of Refractory Metal and Ceramics III*, B.M. Gallois, W.Y. Lee and M.A. Pickering, eds., Materials Research Society, Pittsburgh, 1995, p. 95.
8. L. Gamble, M. Hugenschmidt, C. T. Campbell, T. A. Jurgens, J. W. Rogers Jr., *J. Am. Chem. Soc., 115*, 12096 (1993).
9. T. A. Jurgens, J. W. Rogers Jr., *J. Phys. Chem., 99*, 731 (1995).
10. A. R. Barron, *Adv. Mater. Opt. Electron., 6*, 101 (1996).
11. T. Nakamura, A. Shida, K. Matsui, *Jpn. J. Appl. Phys. Pt. 1, 34*, 6214 (1995).
12. P. Bulkin, N. Bertrand, B. Drevillon, *Thin Solid Films, 296*, 66 (1997).
13. K. Baba, R. Hatada, S. Nagata, H. Fujiyama, G. K. Wolf, W. Ensinger, *Surf. Coat. Technol., 74*, 292 (1995).
14. S. B. Desu, in *MRS Symp. Proc.*, Vol. 168: *Chemical Vapor Deposition of Refractory Metals and Ceramics*, T. M. Besmann and B. M. Gallois, eds, Materials Research Society, Pittsburgh, 1990, p. 221.

17.2.5.5.2. Aluminum Oxide.

Alumina films are used for surface coatings on carbide tools, as dielectric layers in transistor fabrication, as matched substrates (sapphire) for the growth of optically active materials such as gallium nitride, and as coatings for optical components.

Comapred to the numerous options for silica, there are relatively few precursors available for the deposition of high quality alumina. The most common precursor is aluminum trichloride ($AlCl_3$), which undergoes hydrolysis above 1050°C by the reaction[1,2]:

$$2AlCl_3 + 3H_2 + 3CO_2 \longrightarrow Al_2O_3 + 3CO + 6HCl \qquad \text{(a)}$$

Here, hydrogen and carbon dioxide react to form water vapor (and carbon monoxide via water–gas shift), which hydrolyzes the aluminum trichloride. If the deposition surface is temperature sensitive, a metal–organic precursor is preferred. Again, an alkoxide is generally used[3]:

$$2Al(OC_3H_7)_3 \longrightarrow Al_2O_3 + 3(C_3H_7)OH + 3C_3H_6 \qquad \text{(b)}$$

Aluminum alkyls such as trimethylaluminum can be used at low temperature (250°C) in an oxidizing ambient[4], but these films suffer large carbon contamination compared with films produced using reactions (a) and (b). A combined ECR plasma/accelerated ion beam process has recently been used to deposit alumina at 700°C with the precursor $Al[OCH(CH_3)_2]_3$[5]. The use of an oxygen ion beam with trimethylaluminum as the precursor has resulted in alumina films, but the films must be annealed at 730°C to obtain crystalline material[6].

(C. L. AARDAHL, J. W. ROGERS, JR.)

1. H. O. Pierson, *Handbook of Chemical Vapor Deposition (CVD): Principles, Technology, and Applications*, Noyes, Park Ridge, NJ, 1992.

2. C. Powell, J. Oxley, J. M. J. Blocher, *Vapor Deposition*, Wiley, New York, 1966.
3. G. Prauer, H. Altena, B. Lux, *Int. J. Refract. Hard Met. 5*, 165 (1986).
4. W. Kern, V.S. Ban, in *Thin Film processes*, J. Vossen, W. Kern, eds., Academic Press, New York, 1978, p. 291.
5. H. Nakai, H. Kuwahara, J. Shinohara, T. Kawaratani, T. Sassa, Y. Ikegami, *Nucl. Instrum. Methods Phys. Res. B, 112*, 280 (1996).
6. A. Caballero, D. Leinen, A. Fernandez, A.R. Gonzalez-Elipe, *Surf. Coat. Technol., 80*, 23 (1996).

17.2.5.5.3. Silicon Nitride.

Used extensively in industrial applications, silicon nitride (Si_3N_4) has very good structural integrity. Therefore, parts that must endure high stress and high temperature, such as turbine blades, cutting tools, bearings, and other engine parts, are made of this material. Silicon nitride also plays a crucial role in high power electronics, in microelectronic circuits, and in micromechanics[1,2].

CVD is used extensively to deposit Si_3N_4 in all these applications. As in the production of SiO_2, the most common precursors for silicon are the chlorosilanes or silane, with the oxidant replaced by a nitrogen source such as ammonia:

$$3SiCl_4 + 4NH_3 \longrightarrow Si_3N_4 + 12HCl \quad \text{(a)}$$

$$3SiH_2Cl_2 + 4NH_3 \longrightarrow Si_3N_4 + 6HCl + 6H_2 \quad \text{(b)}$$

$$3SiH_4 + 4NH_3 \longrightarrow Si_3N_4 + 12H_2 \quad \text{(c)}$$

The deposition temperature for reaction (c) is 700–1150°C, and the chlorosilanes react at 755–850°C[3,4]. Plasma processing can be used to reduce the deposition temperature to 250–400°C[5,6]. LCVD has also been used to reduce the deposition temperature to this range[7].

The use of ammonia can result in large amounts of hydrogen incorporation in the films. Hydrogen inclusion can be reduced by using nitrogen gas with a rf or ECR plasma source along with silane[3,8,9]. A plasma must be used to crack N_2 because the energy of the N–N bond is much higher than that of the N–H bond in ammonia. Hydrazine is another nitrogen source that has been used to reduce the deposition temperature[10].

A combined aerosol-assisted/laser-assisted technique has been used to deposit Si_3N_4 from a single-source precursor[11]. The precursor was silazane monomer having cyclic structure of $(CH_3SiHNH)_x$, where $x = 3$ or 4. The chemistry of deposition is a straight pyrolysis process following the unbalanced equation:

$$(CH_3SiHNH)_x + NH_3 + \text{laser heat} \longrightarrow Si_3N_4 + CH_4 \quad \text{(d)}$$

(C. L. AARDAHL, J. W. ROGERS, JR.)

1. A. Stoffel, A. Kovacs, W. Kronast, B. Muller, *J. Micromech. Microeng., 6*, 1 (1996).
2. J. G. E. Gardeniers, H. A. C. Tilmans, C. C. G. Visser, *J. Vac. Sci. Technol. A, 14*, 2879 (1996).
3. H. O. Pierson, *Handbook of Chemical Vapor Deposition (CVD): Principles, Technology, and Applications*, Noyes, Park Ridge, NJ, 1992.
4. W. Kern, V. S. Ban, in *Thin Film Processes*, J. Vossen, W. Kern, eds., Academic Press, New York, 1978, p. 298.
5. D. L. Smith, A. S. Alimonda, C. C. Chen, S. E. Ready, B. Wacker, *J. Electrochem. Soc., 137*, 614 (1990).

Inorganic Reactions and Methods, Volume 18
Edited by J. J. Zuckerman, Jim D. Atwood

2. C. Powell, J. Oxley, J. M. J. Blocher, *Vapor Deposition*, Wiley, New York, 1966.
3. G. Prauer, H. Altena, B. Lux, *Int. J. Refract. Hard Met. 5*, 165 (1986).
4. W. Kern, V.S. Ban, in *Thin Film processes*, J. Vossen, W. Kern, eds., Academic Press, New York, 1978, p. 291.
5. H. Nakai, H. Kuwahara, J. Shinohara, T. Kawaratani, T. Sassa, Y. Ikegami, *Nucl. Instrum. Methods Phys. Res. B, 112*, 280 (1996).
6. A. Caballero, D. Leinen, A. Fernandez, A.R. Gonzalez-Elipe, *Surf. Coat. Technol., 80*, 23 (1996).

17.2.5.5.3. Silicon Nitride.

Used extensively in industrial applications, silicon nitride (Si_3N_4) has very good structural integrity. Therefore, parts that must endure high stress and high temperature, such as turbine blades, cutting tools, bearings, and other engine parts, are made of this material. Silicon nitride also plays a crucial role in high power electronics, in microelectronic circuits, and in micromechanics[1,2].

CVD is used extensively to deposit Si_3N_4 in all these applications. As in the production of SiO_2, the most common precursors for silicon are the chlorosilanes or silane, with the oxidant replaced by a nitrogen source such as ammonia:

$$3SiCl_4 + 4NH_3 \longrightarrow Si_3N_4 + 12HCl \quad \text{(a)}$$

$$3SiH_2Cl_2 + 4NH_3 \longrightarrow Si_3N_4 + 6HCl + 6H_2 \quad \text{(b)}$$

$$3SiH_4 + 4NH_3 \longrightarrow Si_3N_4 + 12H_2 \quad \text{(c)}$$

The deposition temperature for reaction (c) is 700–1150°C, and the chlorosilanes react at 755–850°C[3,4]. Plasma processing can be used to reduce the deposition temperature to 250–400°C[5,6]. LCVD has also been used to reduce the deposition temperature to this range[7].

The use of ammonia can result in large amounts of hydrogen incorporation in the films. Hydrogen inclusion can be reduced by using nitrogen gas with a rf or ECR plasma source along with silane[3,8,9]. A plasma must be used to crack N_2 because the energy of the N–N bond is much higher than that of the N–H bond in ammonia. Hydrazine is another nitrogen source that has been used to reduce the deposition temperature[10].

A combined aerosol-assisted/laser-assisted technique has been used to deposit Si_3N_4 from a single-source precursor[11]. The precursor was silazane monomer having cyclic structure of $(CH_3SiHNH)_x$, where $x = 3$ or 4. The chemistry of deposition is a straight pyrolysis process following the unbalanced equation:

$$(CH_3SiHNH)_x + NH_3 + \text{laser heat} \longrightarrow Si_3N_4 + CH_4 \quad \text{(d)}$$

(C. L. AARDAHL, J. W. ROGERS, JR.)

1. A. Stoffel, A. Kovacs, W. Kronast, B. Muller, *J. Micromech. Microeng., 6*, 1 (1996).
2. J. G. E. Gardeniers, H. A. C. Tilmans, C. C. G. Visser, *J. Vac. Sci. Technol. A, 14*, 2879 (1996).
3. H. O. Pierson, *Handbook of Chemical Vapor Deposition (CVD): Principles, Technology, and Applications*, Noyes, Park Ridge, NJ, 1992.
4. W. Kern, V. S. Ban, in *Thin Film Processes*, J. Vossen, W. Kern, eds., Academic Press, New York, 1978, p. 298.
5. D. L. Smith, A. S. Alimonda, C. C. Chen, S. E. Ready, B. Wacker, *J. Electrochem. Soc., 137*, 614 (1990).

6. Y. Kasama, T. Ohmi, K. Fukuda, H. Fukui, C. Iwasaki, S. Ono, in *MRS Symp. Proc.* Vol. 415: *Metal-Organic Vapor Deposition of Electronic Ceramics II*, S. B. Desu, D. B. Beach, P. C. Van Buskirk, eds., Materials Research Society, Pittsburgh, 1996, p. 57.
7. V. K. Rathi, M. Gupta, R. Thangaraj, K. S. Chari, O. P. Agnihotri, *Thin Solid Films, 266*, 219 (1995).
8. D. V. Tsu, G. Lucovsky, *J. Vac. Sci. Technol. A, 4*, 480 (1986).
9. M. Chang, J. Wong, D. Wang, *Solid State Technol.*, 193 (1988).
10. W.-C. Yeh, R. Ishihara, S. Morishita, M. Matsumura, *Jpn. J. Appl. Phys. Pt. 1, 35*, 1509 (1996).
11. T. D. Xiao, P. R. Strutt, K. E. Gonsalves, in *MRS Symp. Proc.*, Vol. 168: *Chemical Vapor Deposition of Refractory Metals and Ceramics*, T. M. Besmann, B. M. Gallois, eds., Materials Research Society, Pittsburgh, 1990, p. 299.

17.2.5.5.4. Titanium Dioxide.

Titania is a very common material that is often used as a whitening pigment, but interest in the CVD of TiO_2 is increasing in response to its newfound use as a catalyst in environmental cleanup applications and as dielectric layers in thin film capacitors. Other common uses for TiO_2 coatings include high refractive index coatings for optics, fiber optics, and optical waveguides. The oxidation of halides is a common technique for the deposition of titanium dioxide, with the most common halide being the tetrachloride:

$$TiCl_4 + O_2 + 2H_2 \longrightarrow TiO_2 + 4HCl \qquad (a)$$

This reaction occurs between 400 and 1000°C[1]. Alkoxides such as titanium isopropoxide and titanium ethoxide have also been used to obtain deposition at temperatures as low as 300°C[2–4]. Most recently, IBCVD has been applied in the room temperature deposition of TiO_2 films using titanium alkoxides and O_2^+ ions[5].

(C. L. AARDAHL, J. W. ROGERS, JR.)

1. W. Kern, V. S. Ban, in *Thin Film Processes*, J. Vossen, W. Kern, eds., Academic Press, New York, 1978, p. 293.
2. M. Balog, M. Schieber, S. Patai, M. Michman, *J. Cryst. Growth, 17*, 298 (1972).
3. H. O. Pierson, *Handbook of Chemical Vapor Deposition (CVD): Principles, Technology, and Applications*, Noyes, Park Ridge, NJ, 1992.
4. H. L. M. Chang, J. C. Parker, H. You, J. J. Xu, D. J. Lam, in *MRS Symp. Proc.*, Vol. 168: *Chemical Vapor Depostion of Refractory Metals and Ceramics*, T.M. Besmann and B.M. Gallois, eds., Materials Research Society, Pittsburgh, 1990, p. 343.
5. J. P. Espions, A. Fernandez, A. Caballero, V. M. Jimenez, J. C. Sanchez-Lopez, L. Contreras, D. Leinen, A. R. Gonzalez-Elipe, *Chem. Vapor Depositon, 3*, 219 (1997).

17.2.5.5.5. Titanium Nitride.

For many years, CVD TiN has been used for wear-and erosion-resistant applications. TiN has a low coefficient of friction and is relatively chemically inert, which makes it attractive for this purpose. In addition, the coating of stainless steel with TiN is of interest for increased biocompatibility of surgical tools and human implants[1]. The reactions used to deposit TiN are very similar to those used for the deposition of TiO_2. $TiCl_4$ is the most common titanium precursor. Nitrogen or ammonia can be used as the nitrogen source.

$$TiCl_4 + 1/2N_2 + 2H_2 \longrightarrow TiN + 4HCl \qquad (a)$$

$$TiCl_4 + NH_3 + 1/2H_2 \longrightarrow TiN + 4HCl \qquad (b)$$

Inorganic Reactions and Methods, Volume 18
Edited by J. J. Zuckerman, Jim D. Atwood

6. Y. Kasama, T. Ohmi, K. Fukuda, H. Fukui, C. Iwasaki, S. Ono, in *MRS Symp. Proc.* Vol. 415: *Metal-Organic Vapor Deposition of Electronic Ceramics II*, S. B. Desu, D. B. Beach, P. C. Van Buskirk, eds., Materials Research Society, Pittsburgh, 1996, p. 57.
7. V. K. Rathi, M. Gupta, R. Thangaraj, K. S. Chari, O. P. Agnihotri, *Thin Solid Films, 266*, 219 (1995).
8. D. V. Tsu, G. Lucovsky, *J. Vac. Sci. Technol. A, 4*, 480 (1986).
9. M. Chang, J. Wong, D. Wang, *Solid State Technol.*, 193 (1988).
10. W.-C. Yeh, R. Ishihara, S. Morishita, M. Matsumura, *Jpn. J. Appl. Phys. Pt. 1, 35*, 1509 (1996).
11. T. D. Xiao, P. R. Strutt, K. E. Gonsalves, in *MRS Symp. Proc.*, Vol. 168: *Chemical Vapor Deposition of Refractory Metals and Ceramics*, T. M. Besmann, B. M. Gallois, eds., Materials Research Society, Pittsburgh, 1990, p. 299.

17.2.5.5.4. Titanium Dioxide.

Titania is a very common material that is often used as a whitening pigment, but interest in the CVD of TiO_2 is increasing in response to its newfound use as a catalyst in environmental cleanup applications and as dielectric layers in thin film capacitors. Other common uses for TiO_2 coatings include high refractive index coatings for optics, fiber optics, and optical waveguides. The oxidation of halides is a common technique for the deposition of titanium dioxide, with the most common halide being the tetrachloride:

$$TiCl_4 + O_2 + 2H_2 \longrightarrow TiO_2 + 4HCl \qquad \text{(a)}$$

This reaction occurs between 400 and 1000°C[1]. Alkoxides such as titanium isopropoxide and titanium ethoxide have also been used to obtain deposition at temperatures as low as 300°C[2–4]. Most recently, IBCVD has been applied in the room temperature deposition of TiO_2 films using titanium alkoxides and O_2^+ ions[5].

(C. L. AARDAHL, J. W. ROGERS, JR.)

1. W. Kern, V. S. Ban, in *Thin Film Processes*, J. Vossen, W. Kern, eds., Academic Press, New York, 1978, p. 293.
2. M. Balog, M. Schieber, S. Patai, M. Michman, *J. Cryst. Growth, 17*, 298 (1972).
3. H. O. Pierson, *Handbook of Chemical Vapor Deposition (CVD): Principles, Technology, and Applications*, Noyes, Park Ridge, NJ, 1992.
4. H. L. M. Chang, J. C. Parker, H. You, J. J. Xu, D. J. Lam, in *MRS Symp. Proc.*, Vol. 168: *Chemical Vapor Depostion of Refractory Metals and Ceramics*, T.M. Besmann and B.M. Gallois, eds., Materials Research Society, Pittsburgh, 1990, p. 343.
5. J. P. Espions, A. Fernandez, A. Caballero, V. M. Jimenez, J. C. Sanchez-Lopez, L. Contreras, D. Leinen, A. R. Gonzalez-Elipe, *Chem. Vapor Depositon, 3*, 219 (1997).

17.2.5.5.5. Titanium Nitride.

For many years, CVD TiN has been used for wear-and erosion-resistant applications. TiN has a low coefficient of friction and is relatively chemically inert, which makes it attractive for this purpose. In addition, the coating of stainless steel with TiN is of interest for increased biocompatibility of surgical tools and human implants[1]. The reactions used to deposit TiN are very similar to those used for the deposition of TiO_2. $TiCl_4$ is the most common titanium precursor. Nitrogen or ammonia can be used as the nitrogen source.

$$TiCl_4 + 1/2N_2 + 2H_2 \longrightarrow TiN + 4HCl \qquad \text{(a)}$$

$$TiCl_4 + NH_3 + 1/2H_2 \longrightarrow TiN + 4HCl \qquad \text{(b)}$$

Inorganic Reactions and Methods, Volume 18
Edited by J. J. Zuckerman, Jim D. Atwood

6. Y. Kasama, T. Ohmi, K. Fukuda, H. Fukui, C. Iwasaki, S. Ono, in *MRS Symp. Proc.* Vol. 415: *Metal-Organic Vapor Deposition of Electronic Ceramics II*, S. B. Desu, D. B. Beach, P. C. Van Buskirk, eds., Materials Research Society, Pittsburgh, 1996, p. 57.
7. V. K. Rathi, M. Gupta, R. Thangaraj, K. S. Chari, O. P. Agnihotri, *Thin Solid Films, 266*, 219 (1995).
8. D. V. Tsu, G. Lucovsky, *J. Vac. Sci. Technol. A, 4*, 480 (1986).
9. M. Chang, J. Wong, D. Wang, *Solid State Technol.*, 193 (1988).
10. W.-C. Yeh, R. Ishihara, S. Morishita, M. Matsumura, *Jpn. J. Appl. Phys. Pt. 1, 35*, 1509 (1996).
11. T. D. Xiao, P. R. Strutt, K. E. Gonsalves, in *MRS Symp. Proc.*, Vol. 168: *Chemical Vapor Deposition of Refractory Metals and Ceramics*, T. M. Besmann, B. M. Gallois, eds., Materials Research Society, Pittsburgh, 1990, p. 299.

17.2.5.5.4. Titanium Dioxide.

Titania is a very common material that is often used as a whitening pigment, but interest in the CVD of TiO_2 is increasing in response to its newfound use as a catalyst in environmental cleanup applications and as dielectric layers in thin film capacitors. Other common uses for TiO_2 coatings include high refractive index coatings for optics, fiber optics, and optical waveguides. The oxidation of halides is a common technique for the deposition of titanium dioxide, with the most common halide being the tetrachloride:

$$TiCl_4 + O_2 + 2H_2 \longrightarrow TiO_2 + 4HCl \qquad \text{(a)}$$

This reaction occurs between 400 and 1000°C[1]. Alkoxides such as titanium isopropoxide and titanium ethoxide have also been used to obtain deposition at temperatures as low as 300°C[2–4]. Most recently, IBCVD has been applied in the room temperature deposition of TiO_2 films using titanium alkoxides and O_2^+ ions[5].

(C. L. AARDAHL, J. W. ROGERS, JR.)

1. W. Kern, V. S. Ban, in *Thin Film Processes*, J. Vossen, W. Kern, eds., Academic Press, New York, 1978, p. 293.
2. M. Balog, M. Schieber, S. Patai, M. Michman, *J. Cryst. Growth, 17*, 298 (1972).
3. H. O. Pierson, *Handbook of Chemical Vapor Deposition (CVD): Principles, Technology, and Applications*, Noyes, Park Ridge, NJ, 1992.
4. H. L. M. Chang, J. C. Parker, H. You, J. J. Xu, D. J. Lam, in *MRS Symp. Proc.*, Vol. 168: *Chemical Vapor Depostion of Refractory Metals and Ceramics*, T.M. Besmann and B.M. Gallois, eds., Materials Research Society, Pittsburgh, 1990, p. 343.
5. J. P. Espions, A. Fernandez, A. Caballero, V. M. Jimenez, J. C. Sanchez-Lopez, L. Contreras, D. Leinen, A. R. Gonzalez-Elipe, *Chem. Vapor Depositon, 3*, 219 (1997).

17.2.5.5.5. Titanium Nitride.

For many years, CVD TiN has been used for wear-and erosion-resistant applications. TiN has a low coefficient of friction and is relatively chemically inert, which makes it attractive for this purpose. In addition, the coating of stainless steel with TiN is of interest for increased biocompatibility of surgical tools and human implants[1]. The reactions used to deposit TiN are very similar to those used for the deposition of TiO_2. $TiCl_4$ is the most common titanium precursor. Nitrogen or ammonia can be used as the nitrogen source.

$$TiCl_4 + 1/2N_2 + 2H_2 \longrightarrow TiN + 4HCl \qquad \text{(a)}$$

$$TiCl_4 + NH_3 + 1/2H_2 \longrightarrow TiN + 4HCl \qquad \text{(b)}$$

If nitrogen is used, the ideal deposition temperature is 1000°C. The deposition temperature is lower for the ammonia reaction (575–700°C)[2]. Plasma processing can be used to reduce the processing temperature to 500°C[3,4]. Thermal laser CVD has also been used to deposit TiN at reduced temperature[5,6]. In an alternate approach, titanium tetraiodide is the precursor (with no plasma) at a deposition temperature under 450°C[7].

Recognition of TiN as a supreb barrier to diffusional and electrical activity has resulted in extensive research on the CVD of TiN for microelectronic layers. Significant advances have been made in the area of plasma-assisted CVD where dc glow[8], ECR[9], and helicon[10] plasmas have all been used. Implementation of such plasmas can reduce the processing temperature of reaction (b) to 400°C. For plasma deposition of TiN using titanium isopropoxide, the deposition temperature can be as low as 100°C, where the chemistry is outlined as follows[9]:

$$Ti[OCH(CH_3)_2]_4 + 1/2N_2 + \text{ECR plasma} \longrightarrow TiN + 4CH_3COCH_3 + 2H_2 \quad \text{(c)}$$

For TiN deposition, by far the most active area of research has been precursor design. As with all nitride deposition, ammonia limits the lowest depositon temperature because of its high thermal stability. This has led investigators to design single-source precursors based on a variety of geometries. A number of these molecules have been synthesized based on the dialkylamido geometry of $Ti(NR_2)_4$[11–13] and titanium amide–amine complexes[14].

(C. L. AARDAHL, J. W. ROGERS, JR.)

1. M. H. Staia, B. Lewis, J. Cawley, T. Hudson, *Surf. Coat Technol., 76–77*, 231 (1995).
2. H. O. Pierson, *Handbook of Chemical Vapor Deposition (CVD): Principles, Technology, and Applications*, Noyes, Park Ridge, NJ, 1992.
3. P. Mayr, H. R. Stock, *J. Vac. Sci. Technol. A, 4*, 2726 (1986).
4. N. J. Ianno, A. U. Ahmed, D. E. Englebert, *J. Electrochem. Soc., 136*, 1 (1989).
5. B. Chen, N. Biunno, R.K. Singh, J. Narayan, in *MRS Symp. Proc.*, Vol. 168: *Chemical Vapor Deposition of Refractory Metals and Ceramics*, T. M. Besmann and B. M. Gallois, eds., Materials Research Society, Pittsburgh, 1990, p. 287.
6. G. Reisse and R. Ebert, *Appl. Surf. Sci., 106*, 268 (1996).
7. C. Faltermeier, C. Goldberg, M. Jones, A. Upham, D. Manager, G. Peterson, J. Lau, A.E. Kaloyeros, B. Arkles, A. Paranjpe, *J. Electrochem. Soc., 144*, 1002 (1997).
8. J. Patscheider, L. Shizhi, S. Veprek, *Plasma Chem. Plasma Process., 16*, 341 (1996).
9. A. Weber, R. Poeckelmann, C.-P. Klages, *Microelectron. Eng., 33*, 277, (1997).
10. R. Tobe, A. Sekiguchi, M. Sasaki, O. Okada, N. Hosokawa, *Thin Solid Films, 281–282*, 155 (1996).
11. R. M. Fix, R. G. Gordon, D. M. Hoffman, in *MRS Symp. Proc.*, Vol. 168: Chemical Vapor Deposition of Refractory Metals and Ceramics, T. M. Besmann, B. M. Gallois, eds., Materials Research Society, Pittsburgh, 1990, p. 357.
12. J. N. Musher, R. G. Gordon, *J. Electrochem. Soc., 143*, 736 (1996).
13. H.-K. Shin, H. J. Shin, J. -G. Lee, S. W. Kang, B. T. Ahn, *Chem. Mater., 9*, 76 (1997).
14. C. H. Winter, P. H. Sheridan, T. S. Lewkebandara, M. J. Heeg, J. W. Proscia, *J. Am. Chem. Soc., 114*, 1095 (1992).

17.2.5.5.6. Boron Nitride.

Boron nitride is an extremely refractory material and is chemically inert. In its cubic configuration, which can be formed at high pressure, it rivals diamond in hardness; therefore, there is considerable interst in the CVD of this material for ultrahard coatings

Inorganic Reactions and Methods, Volume 18
Edited by J. J. Zuckerman, Jim D. Atwood

If nitrogen is used, the ideal deposition temperature is 1000°C. The deposition temperature is lower for the ammonia reaction (575–700°C)[2]. Plasma processing can be used to reduce the processing temperature to 500°C[3,4]. Thermal laser CVD has also been used to deposit TiN at reduced temperature[5,6]. In an alternate approach, titanium tetraiodide is the precursor (with no plasma) at a deposition temperature under 450°C[7].

Recognition of TiN as a supreb barrier to diffusional and electrical activity has resulted in extensive research on the CVD of TiN for microelectronic layers. Significant advances have been made in the area of plasma-assisted CVD where dc glow[8], ECR[9], and helicon[10] plasmas have all been used. Implementation of such plasmas can reduce the processing temperature of reaction (b) to 400°C. For plasma deposition of TiN using titanium isopropoxide, the deposition temperature can be as low as 100°C, where the chemistry is outlined as follows[9]:

$$Ti[OCH(CH_3)_2]_4 + 1/2N_2 + \text{ECR plasma} \longrightarrow TiN + 4CH_3COCH_3 + 2H_2 \quad (c)$$

For TiN deposition, by far the most active area of research has been precursor design. As with all nitride deposition, ammonia limits the lowest depositon temperature because of its high thermal stability. This has led investigators to design single-source precursors based on a variety of geometries. A number of these molecules have been synthesized based on the dialkylamido geometry of $Ti(NR_2)_4$[11–13] and titanium amide–amine complexes[14].

(C. L. AARDAHL, J. W. ROGERS, JR.)

1. M. H. Staia, B. Lewis, J. Cawley, T. Hudson, *Surf. Coat Technol., 76–77*, 231 (1995).
2. H. O. Pierson, *Handbook of Chemical Vapor Deposition (CVD): Principles, Technology, and Applications*, Noyes, Park Ridge, NJ, 1992.
3. P. Mayr, H. R. Stock, *J. Vac. Sci. Technol. A, 4*, 2726 (1986).
4. N. J. Ianno, A. U. Ahmed, D. E. Englebert, *J. Electrochem. Soc., 136*, 1 (1989).
5. B. Chen, N. Biunno, R.K. Singh, J. Narayan, in *MRS Symp. Proc.*, Vol. 168: *Chemical Vapor Deposition of Refractory Metals and Ceramics*, T. M. Besmann and B. M. Gallois, eds., Materials Research Society, Pittsburgh, 1990, p. 287.
6. G. Reisse and R. Ebert, *Appl. Surf. Sci., 106*, 268 (1996).
7. C. Faltermeier, C. Goldberg, M. Jones, A. Upham, D. Manager, G. Peterson, J. Lau, A.E. Kaloyeros, B. Arkles, A. Paranjpe, *J. Electrochem. Soc., 144*, 1002 (1997).
8. J. Patscheider, L. Shizhi, S. Veprek, *Plasma Chem. Plasma Process., 16*, 341 (1996).
9. A. Weber, R. Poeckelmann, C.-P. Klages, *Microelectron. Eng., 33*, 277, (1997).
10. R. Tobe, A. Sekiguchi, M. Sasaki, O. Okada, N. Hosokawa, *Thin Solid Films, 281–282*, 155 (1996).
11. R. M. Fix, R. G. Gordon, D. M. Hoffman, in *MRS Symp. Proc.*, Vol. 168: Chemical Vapor Deposition of Refractory Metals and Ceramics, T. M. Besmann, B. M. Gallois, eds., Materials Research Society, Pittsburgh, 1990, p. 357.
12. J. N. Musher, R. G. Gordon, *J. Electrochem. Soc., 143*, 736 (1996).
13. H.-K. Shin, H. J. Shin, J. -G. Lee, S. W. Kang, B. T. Ahn, *Chem. Mater., 9*, 76 (1997).
14. C. H. Winter, P. H. Sheridan, T. S. Lewkebandara, M. J. Heeg, J. W. Proscia, *J. Am. Chem. Soc., 114*, 1095 (1992).

17.2.5.5.6. Boron Nitride.

Boron nitride is an extremely refractory material and is chemically inert. In its cubic configuration, which can be formed at high pressure, it rivals diamond in hardness; therefore, there is considerable interst in the CVD of this material for ultrahard coatings

on cutting tools and for high temperature vessels such as those needed in metal purification processes. BN is also attractive in microelectronics applications because of its high dielectric properites.

The reactions used to form boron nitride have been studied extensively, and several are used in practice. Metal halides are the most common boron precursors, and ammonia typically serves as the nitrogen source[1]:

$$BX_3 + NH_3 \longrightarrow BN + 3HX \quad (X = Cl, F) \tag{a}$$

For the chloride reaction, a deposition temperature of 1300–1600°C is used with higher temperatures resulting in a higher density deposit. Using the fluoride precursor results in slight reduction in processing temperature (1100–1200°C).

An alternative boron source is diborane, which can be used for processing at reduced pressure (~1 torr) and a much lower temperature (300–400°C)[1]:

$$B_2H_6 + 2NH_3 \longrightarrow 2BN + 6H_2 \tag{b}$$

At a slightly higher temperature of 700°C, the single-source precursor borazine can be decomposed on a surface to form boron nitride[1]:

$$B_3H_3N_3 \longrightarrow 3BN + 3/2H_2 \tag{c}$$

BN can also be deposited using metal–organic precursors such as triethyl boron and ammonia[1].

$$B(C_2H_5)_3 + NH_3 \longrightarrow BN + 3C_2H_6 \tag{d}$$

Recent research on the preparation of BN thin films has concentrated on the use of plasmas to reduce the deposition temperature[2]. Other research has focused on the use of an alternate nitrogen source, such as NF_3, with BX_3 (X = F or Cl) and B_2H_6 precursor gases to further reduce the deposition temperature. Microwave plasmas have also been used to deposit BN with borane–dimethyl amine and nitrogen gas[3].

(C. L. AARDAHL, J. W. ROGERS, JR.)

1. H. O. Pierson, *Handbook of Chemical Vapor Deposition (CVD): Principles, Technology, and Applications*, Noyes, Park Ridge, NJ, 1992.
2. S. Matsumoto, N. Nishida, K. Akashi, K. Sugai, *J. Mater. Sci., 31*, 713 (1996).
3. O. Baehr, P. Thevenin, A. Bath, A. Koukab, E. Losson, B. Lepley, *Mater. Sci. Eng. B, 46*, 101 (1997).

17.2.5.5.7. Aluminum Nitride.

Aluminum nitride has received attention as an alternative to SiO_2 dielectric layers in microelectronic circuits because of its high dielectric strength. Being a refractory ceramic with high thermal conductivity, AlN is useful for electronics packaging. There are also uses for AlN as a piezoelectric material because of its high surface acoustic wave velocity.

CVD of AlN is typically performed using aluminum halide (X = Cl or Br) precursors with ammonia. The reaction

$$AlX_3 + NH_3 \longrightarrow AlN + 3HX \tag{a}$$

readily takes place between and 900 and 1100°C, with the bromide precursor reacting at slightly lower temperature than the chloride analogue[1]. Trimethylaluminum has also

Inorganic Reactions and Methods, Volume 18
Edited by J. J. Zuckerman, Jim D. Atwood

on cutting tools and for high temperature vessels such as those needed in metal purification processes. BN is also attractive in microelectronics applications because of its high dielectric properites.

The reactions used to form boron nitride have been studied extensively, and several are used in practice. Metal halides are the most common boron precursors, and ammonia typically serves as the nitrogen source[1]:

$$BX_3 + NH_3 \longrightarrow BN + 3HX \quad (X = Cl, F) \tag{a}$$

For the chloride reaction, a deposition temperature of 1300–1600°C is used with higher temperatures resulting in a higher density deposit. Using the fluoride precursor results in slight reduction in processing temperature (1100–1200°C).

An alternative boron source is diborane, which can be used for processing at reduced pressure ($\sim$1 torr) and a much lower temperature (300–400°C)[1]:

$$B_2H_6 + 2NH_3 \longrightarrow 2BN + 6H_2 \tag{b}$$

At a slightly higher temperature of 700°C, the single-source precursor borazine can be decomposed on a surface to form boron nitride[1]:

$$B_3H_3N_3 \longrightarrow 3BN + 3/2H_2 \tag{c}$$

BN can also be deposited using metal–organic precursors such as triethyl boron and ammonia[1].

$$B(C_2H_5)_3 + NH_3 \longrightarrow BN + 3C_2H_6 \tag{d}$$

Recent research on the preparation of BN thin films has concentrated on the use of plasmas to reduce the deposition temperature[2]. Other research has focused on the use of an alternate nitrogen source, such as NF_3, with BX_3 (X = F or Cl) and B_2H_6 precursor gases to further reduce the deposition temperature. Microwave plasmas have also been used to deposit BN with borane–dimethyl amine and nitrogen gas[3].

(C. L. AARDAHL, J. W. ROGERS, JR.)

1. H. O. Pierson, *Handbook of Chemical Vapor Deposition (CVD): Principles, Technology, and Applications*, Noyes, Park Ridge, NJ, 1992.
2. S. Matsumoto, N. Nishida, K. Akashi, K. Sugai, *J. Mater. Sci., 31*, 713 (1996).
3. O. Baehr, P. Thevenin, A. Bath, A. Koukab, E. Losson, B. Lepley, *Mater. Sci. Eng. B, 46*, 101 (1997).

17.2.5.5.7. Aluminum Nitride.

Aluminum nitride has received attention as an alternative to SiO_2 dielectric layers in microelectronic circuits because of its high dielectric strength. Being a refractory ceramic with high thermal conductivity, AlN is useful for electronics packaging. There are also uses for AIN as a piezoelectric material because of its high surface acoustic wave velocity.

CVD of AlN is typically performed using aluminum halide (X = Cl or Br) precursors with ammonia. The reaction

$$AlX_3 + NH_3 \longrightarrow AlN + 3HX \tag{a}$$

readily takes place between and 900 and 1100°C, with the bromide precursor reacting at slightly lower temperature than the chloride analogue[1]. Trimethylaluminum has also

been used to deposit AlN between 900 and 1400°C[2,3]:

$$(CH_3)_3Al + NH_3 \longrightarrow AlN + 3CH_4 \qquad (b)$$

Such high processing temperatures have limited the use of CVD AlN in microelectronics because certain layers cannot tolerate excessive thermal conditions. The problem is further complicated by carbon contamination that results from incomplete pyrolysis of trimethylaluminum, and in the case of halide deposition, the large substrate temperature produces a substantial number of N vacanies, which result in a high n-type background dopant level.

These two issues have contributed to extensive research on metal–organic precursors for the deposition of nitrides of metals in groups III–V. There has been considerable interest, as well as progress, in CVD of GaN and AlN because these materials have been in the technological spotlight recently, and their depositions involve similar chemistry. The synthesis of new precursors continues to proceed at a high rate. The precursor strategies that have resulted are summarized in several recent review articles[4–7].

Trimethylaluminum is still studied widely as an AlN precursor, and the mechanism of AlN formation has been proven to progress via an adduct [$Al(CH_3)_3$:NH_3], which decomposes in stepwise fashion through amides and imides until AlN is formed[8–11]. Lengthening the alkyl ligands that are coordinated to the aluminum atom is beneficial because the molecule will more readily undergo β-hydrogen elimination. As a result, triethylaluminum and triisobutylaluminum pyrolyze more cleanly to Al, which results in less residual carbon. Unfortunately, long alkyl ligands result in a decreased vapor pressure of the precursor molecule, impeding gas phase transport.

Further research into adduct compounds involved the investigation of coordinatively saturated precursors like the amine alane adducts. Such precursors can be used at a relatively low temperature, which reduces the number of nitrogen vacancies in the AlN film[12–14]. In addition, carbon contamination is virtually nonexistent because the entire amine group leaves intact during pyrolysis. One drawback to the amine–alanes is the readiness with which they react with ammonia gas in the vapor phase. This complication requires the use of sequential dosing or atomic layer growth[15] strategies during CVD.

(C. L. AARDAHL, J. W. ROGERS, JR.)

1. H. O. Pierson, *Handbook of Chemical Vapor Deposition (CVD): Principles, Technology, and Applications*, Noyes, Park Ridge, NJ, 1992.
2. L. Baixia, L. Yinkui, L. Yi, *J. Mater. Chem.*, *3*, 117 (1993).
3. S. Strite, H. Morkoc, *J. Vac. Sci, Technol. B*, *10*, 1237 (1992).
4. D. A. Neumayer, J. G. Ekerdt, *Chem. Mater.*, *8*, 9 (1996).
5. A. C. Jones, C. R. Whitehouse, J. S. Roberts, *Chem. Vapor Deposition*, *1*, 65 (1995).
6. D. M. Hoffman, S. P. Rangarajan, S. D. Athavale, D. J. Economou, J.-R. Liu, Z. Zheng, W.-K. Chu, *J. Vac. Sci. Technol. A*, *14*, 306 (1996).
7. F. Maury, *Chem. Vapor Deposition*, *2*, 113 (1996).
8. F. C. Sauls, L. V. Interrante, Z. Jiang, *Inorg. Chem.*, *29*, 2989 (1990).
9. C. C. Amato, J. B. Hudson, L. V. Interrante, *Appl. Surf. Sci.*, *54*, 18 (1992).
10. B. S. Ault, *J. Phys. Chem.*, *96*, 7908 (1992).
11. F. C. Sauls, L. V. Interrante, *Coord. Chem. Rev.*, *128*, 193 (1993).
12. A. Molassioti, M. Moser, A. Stapor, F. Scholz, M. Hostalek, L. Pohl, *Appl. Phys. Lett.*, *54*, 857 (1988).
13. C. R. Abernathy, *J. Vac. Sci. Technol. A*, *11*, 869 (1993).
14. J. N. J. Kidder, J. S. Kuo, A. Ludviksson, T. P. Pearsall, J. W. Rogers, Jr., J. M. Grant, L. R. Allen, S. T. Hsu, *J. Vac. Sci. Technol. A*, *13*, 711 (1995).
15. T. Suntola and M. Simpson, eds., *Atomic Layer Epitaxy*, Blackie and Sons, London, 1990.

Inorganic Reactions and Methods, Volume 18
Edited by J. J. Zuckerman, Jim D. Atwood

17.2.5.5.8. Silicion Carbide.

Silicon carbide is a durable and very hard material. It is used in a wide range of applications including coating layers for nuclear reactors, graphite susceptors, nuclear waste containers, and heat-exchanger tubes. Silicon carbide has also been used in radiation sensors and radiation shielding deposits. The CVD of SiC has been common for several years, but epitaxially grown SiC has received even more attention recently because it is a good substrate for the deposition of gallium nitride. The CVD of SiC has been reviewed in detail[1–3].

In industrial-scale CVD of SiC, the deposit can be formed with a single-source precursor or with two precursors. Single-source precursors must contain a Si—C bond as in methyltricholorosilane or methylsilane[4]:

$$CH_3SiCl_3 \longrightarrow SiC + 3HCl \quad (a)$$

$$CH_3SiH_3 \longrightarrow SiC + 3H_2 \quad (b)$$

As the number of chlorine atoms in the precursor is increased, the deposition temperature rises. The ideal reaction temperature for reaction (a) is 1100°C versus 900°C for reaction (b). The principal advantage to these precursors is the comparatively low carbon contamination in the films as nearly all of the carbon atoms in the precursor are incorporated into the SiC.

This is not the case for dual-precursor schemes because hydrocarbons undergo incomplete pyrloysis, which leaves nonbonded carbon in the films. Common reactions used to deposit SiC in this case are[2,4]:

$$SiH_4 + CH_4 \longrightarrow SiC + 4H_2 \quad (c)$$

$$3SiH_4 + C_3H_8 \longrightarrow 3SiC + 10H_2 \quad (d)$$

$$6SiH_4 + C_6H_6 \longrightarrow 6SiC + 15H_2 \quad (e)$$

The advantage of using two precursor gases is a reduced deposition temperature, except in the case of methane. Reactions (d) and (e) yield SiC at 800°C, but plasma processing can lower the temperature to 200°C[5]. If disilane and acetylene are used with excimer LCVD, the deposition temperature for SiC can be reduced to this level[6].

(C. L. AARDAHL, J. W. ROGERS, JR.)

1. F. T. J. Smith, E. Carnall, L.S. Ladd, *Int. J. High Technol. Ceram. 3*, 263 (1987).
2. R. F. Davis, in *MRS Symp. Proc.*, Vol. 168: *Chemical Vapor Deposition of Refractory Metals and Ceramics*, T. M. Besmann, B. M. Gallois, eds., Materials Research Society, Pittsburgh, 1990, p. 145.
3. W. J. Choyke, H. Matsunami, G. Pensl, eds., *Silicon Carbide: A Review of Fundamental Questions and Applications*, Wiley, New York, 1997.
4. H. O. Pierson, *Handbook of Chemical Vapour Deposition (CVD): Principles, Technology, and Applications*, Noyes, Park Ridge, NJ, 1992.
5. D. Stinton, T. Bessman, R. Lowden, *Ceram. Bull., 67*, 350 (1988).
6. T. Noda, H. Suzuki, H. Araki, F. Abe, M. Okada, *J. Mater, Sci. Lett., 11*, 477 (1992).

17.2.5.5.9. Metal Oxides and High T_c Superconductors.

Metal oxides such as high T_c superconductors (HTS) and the high dielectric perovskites have come to the forefront of electronics research over the last few years. The

Inorganic Reactions and Methods, Volume 18
Edited by J. J. Zuckerman, Jim D. Atwood

17.2.5.5.8. Silicion Carbide.

Silicon carbide is a durable and very hard material. It is used in a wide range of applications including coating layers for nuclear reactors, graphite susceptors, nuclear waste containers, and heat-exchanger tubes. Silicon carbide has also been used in radiation sensors and radiation shielding deposits. The CVD of SiC has been common for several years, but epitaxially grown SiC has received even more attention recently because it is a good substrate for the deposition of gallium nitride. The CVD of SiC has been reviewed in detail[1–3].

In industrial-scale CVD of SiC, the deposit can be formed with a single-source precursor or with two precursors. Single-source precursors must contain a Si—C bond as in methyltricholorosilane or methylsilane[4]:

$$CH_3SiCl_3 \longrightarrow SiC + 3HCl \quad (a)$$

$$CH_3SiH_3 \longrightarrow SiC + 3H_2 \quad (b)$$

As the number of chlorine atoms in the precursor is increased, the deposition temperature rises. The ideal reaction temperature for reaction (a) is 1100°C versus 900°C for reaction (b). The principal advantage to these precursors is the comparatively low carbon contamination in the films as nearly all of the carbon atoms in the precursor are incorporated into the SiC.

This is not the case for dual-precursor schemes because hydrocarbons undergo incomplete pyrloysis, which leaves nonbonded carbon in the films. Common reactions used to deposit SiC in this case are[2,4]:

$$SiH_4 + CH_4 \longrightarrow SiC + 4H_2 \quad (c)$$

$$3SiH_4 + C_3H_8 \longrightarrow 3SiC + 10H_2 \quad (d)$$

$$6SiH_4 + C_6H_6 \longrightarrow 6SiC + 15H_2 \quad (e)$$

The advantage of using two precursor gases is a reduced deposition temperature, except in the case of methane. Reactions (d) and (e) yield SiC at 800°C, but plasma processing can lower the temperature to 200°C[5]. If disilane and acetylene are used with excimer LCVD, the deposition temperature for SiC can be reduced to this level[6].

(C. L. AARDAHL, J. W. ROGERS, JR.)

1. F. T. J. Smith, E. Carnall, L.S. Ladd, *Int. J. High Technol. Ceram. 3*, 263 (1987).
2. R. F. Davis, in *MRS Symp. Proc.*, Vol. 168: *Chemical Vapor Deposition of Refractory Metals and Ceramics*, T. M. Besmann, B. M. Gallois, eds., Materials Research Society, Pittsburgh, 1990, p. 145.
3. W. J. Choyke, H. Matsunami, G. Pensl, eds., *Silicon Carbide: A Review of Fundamental Questions and Applications*, Wiley, New York, 1997.
4. H. O. Pierson, *Handbook of Chemical Vapour Deposition (CVD): Principles, Technology, and Applications*, Noyes, Park Ridge, NJ, 1992.
5. D. Stinton, T. Bessman, R. Lowden, *Ceram. Bull., 67*, 350 (1988).
6. T. Noda, H. Suzuki, H. Araki, F. Abe, M. Okada, *J. Mater, Sci. Lett., 11*, 477 (1992).

17.2.5.5.9. Metal Oxides and High T_c Superconductors.

Metal oxides such as high T_c superconductors (HTS) and the high dielectric perovskites have come to the forefront of electronics research over the last few years. The

development of new superconductors has finally led to materials that superconduct above that of liquid nitrogen temperature, and some of the perovskites are being examined closely as a replacement for SiO_2 dielectric layers in microelectronic circuits. As these technologies develop, the deposition processes that can be used to grow such films have also undergone a great deal of refinement. CVD can compete with sol–gel and physical vapor deposition (e.g., sputtering, coevaporation, and laser ablation) techniques. In addition, CVD allows control of critical parameters such as oxygen activity and stoichiometric ratio of the metal atoms. Further advantages include increased areas of deposition, deposition on substrates of complex geometry, and deposition of high quality films without postannealing.

Two types of precursor can be used in CVD of superconducting mixed oxides: metal halides[1–3] and metal–organics[4–10]. The use of metal–organic molecules results in some carbon in the films, which can hinder performance, so metal halides gained popularity in early work. Halide precursors call for a much higher deposition temperature. In the case of metal halide reactions, the chemistry follows that presented earlier (see 17.2.5.2.2) but with multiple reactions occurring simultaneously. The gas phase composition and temperature are controlled to obtain the desired stoichiometry. An example of such a reaction would be that used to make $Bi_2Sr_2CaCu_2O_{8+x}$(or Bi-2212)[3] at 760–820°C:

$$2BiI_3 + 2CuI + CaI_2 + 2SrI_2 + (8 + x)/2O_2 \longrightarrow Bi_2Sr_2CaCu_2O_{8+x} + 7I_2 \qquad \text{(a)}$$

The use of metal–organic precursors is more complicated. In fact, most of the current research in this area involves design of precursors that facilitate lower levels of carbon contamination in the HTS film. A further requirement is that the precursor be volatile enough to partition into the gas phase. Thus far, mononuclear metal complexes are the only metal precursors to show adequate volatility[9,11]. The most versatile ligands for these complexes are the β-diketonates, which are formed when β-diketones of the form $RCOCH_2COR'$ undergo deprotonation. Sufficient volatility is obtained when R and R′ are methyl, trifluoromethyl, *t*-butyl, or $—CF_2CF_2CF_3$ groups.

One of the promising superconducting materials, $YBa_2Cu_3O_{7-\delta}$ (YBCO or Y-123), requires barium in the correct stoichiometric ratio. However, polymerization results in the β-diketonate precursors when barium is the metal coordination site. This reaction can be avoided by coordinating a third neutral ligand such as tetrahydrofuran, trimethylamine, or suitable polyethers to the barium atom[9]. Tetraglyme, a methoxy-terminated polyether, and alkoxide ligands have also been used to increase the stability of β-diketonates[12,13].

Formation of Y-123 is similar to that of Bi-2212 in that reactants of appropriate gas phase composition are flowed over a heated substrate (> 600°C) and the deposit is formed. Oxygen is the most common oxidizer, although more aggressive oxidizers such as nitrous oxide, ozone, and oxygen radicals have been used to lower the deposition temperature. Alternate oxygen sources are advantageous in work with plasma or photo MOCVD[9]. The development of liquid delivery MOCVD (LDMOCVD) for deposition of Y-123 has also been a topic of recent interest. Here precursors are dissolved in an organic solvent and then fed into the reaction chamber as a homogeneous mixture[14]. This procedure requires further exposure to oxygen gas after the initial deposition to complete oxidation of the film.

All the aforementioned precursors are pivotal to the development of nonsuperconducting metal oxide films such as the barium titanates, barium tantalates, and tantalum

oxide. The perovskites contain a permanent dipole in the crystal lattice, which results in a very high dielectric constant for these materials. Hypothetically, thicker layers of these materials could be used to replace relatively thin layers of SiO_2 in microelectronic circuits without loss of dielectric intergrity. This possibility suggests that reduction of feature size in future generation computer chips could rely heavily on technological advances in these perovskite systems. The growth, of nonsuperconducting mixed oxides is a much younger field than that of HTS growth, but deposition is done in the same fashion as for HTS films. The precursors would differ only in replacement of the metal atom in the coordinated complex. For some of the metals, such as titanium and tantalum, alkoxides may be used in lieu of the β-diketonate forms.

(C. L. AARDAHL, J. W. ROGERS, JR.)

1. M. Ihara, T. Kimura, H. Yamawaki, K. Ikeda, *IEEE Trans. Magn., MAG-25*, 2470 (1989).
2. A. Harsta, in *Advances in Science and Technology*, Vol. 8, *Superconductivity and Superconducting Materials Technologies*, P. Vincenzini, eds., Techna, Florence, 1995. p. 549.
3. A.Harsta, S. Lundquist, *Chem. Vapor Deposition, 2*, 109 (1996).
4. M. Leskela, H. Molsa, L. Niinisto, *Supercond. Sci. Technol., 6*, 627 (1993).
5. K.-H. Dahmen, T. Gerfin, *Prog. Cryst. Growth Charact., 27*, 117 (1993).
6. T. Sugimoto, in *Materials Science Forum*, Vol. 137–139: *Advances in High-T_c Superconductivity*, J. J. Pouch, S. A. Alterovitz, R. R. Romanofsky, A. F. Hepp, eds., Trans Tech, Aedersmannsdorf, Switzerland, 1993, p. 395.
7. C. N. R. Rao, A. K. Ganguli, *Chem. Soc. Rev., 24*, 1 (1995).
8. D. L. Schulz, T. J. Marks, in *CVD of Nonmetals*, W.S. Rees, ed., VCH, Weinheim, Germany, 1996.
9. I. M. Watson, *Chem. Vapour Deposition, 3*, 9 (1997).
10. C. Gomez-Aleixandre, O. Sanchez, J. M. Albella, J. Santiso, A. Figueras, *Adv. Mater., 7*, 111 (1995).
11. W. S. Rees, H. A. Luten, V. L. Goedken, in *MRS Symp. Proc.*, Vol. 363: *Chemical Vapour Deposition of Refractory Metals and Ceramics III*, B. M. Gallois, W. Y. Lee, M. A. Pickering, eds., Materials Research Society, Pittsburgh, 1995, p. 195.
12. H. A. I. Luten, D. J. Otway, W. S. J. Rees, in *MRS Symp. Proc.*, Vol. 415: *Metal-Organic Chemical Vapour Deposition of Electronic Ceramics II*, S.B. Desu, D. B. Beach, P.C. Van Buskirk, eds., Materials Research Society, Pittsburgh, 1996, p. 99.
13. D. J. Otway, H. A. Luten, K. M. Abdul Malik, M. B. Hursthouse, W. S. J. Rees, in *MRS Symp. Proc.*, Vol. 415: *Metal-Organic Chemical Vapour Deposition of Electronic Ceramics II*, S.B. Desu, D. B. Beach, P. C. Van Buskirk, eds., Materials Research Society, Pittsburgh, 1996, p. 105.
14. D. B. Studebaker, G. Doubinina, J. Zhang, Y. Y. Wang, V. P. Dravid, T. J. Marks, in *MRS Symp. Proc.*, Vol. 415: *Metal-Organic Chemical Vapour Deposition of Electronic Ceramics II*, S. B. Desu, D. B. Beach, P. C. Van Buskirk, eds., Materials Research Society, Pittsburgh, 1996, p. 255.

17.2.6. Doping

The choice of impurity source and experimental setup for doping a semiconductor depends on the impurity and on factors such as vapor pressure and purity of the impurity source, solid solubility in the semiconductor, and alloying or compound formation on the semiconductor surface.

The form of the doping source whether it be solid, liquid or gaseous, is important in deciding whether to use a closed-tube diffusion system or an open one. In the former case, the semiconductor and the source of diffusing impurity are placed in a cleaned quartz tube, which is evacuated, sealed, and then heated to the desired temperature. Although

Inorganic Reactions and Methods, Volume 18
Edited by J. J. Zuckerman, Jim D. Atwood

oxide. The perovskites contain a permanent dipole in the crystal lattice, which results in a very high dielectric constant for these materials. Hypothetically, thicker layers of these materials could be used to replace relatively thin layers of SiO_2 in microelectronic circuits without loss of dielectric intergrity. This possibility suggests that reduction of feature size in future generation computer chips could rely heavily on technological advances in these perovskite systems. The growth, of nonsuperconducting mixed oxides is a much younger field than that of HTS growth, but deposition is done in the same fashion as for HTS films. The precursors would differ only in replacement of the metal atom in the coordinated complex. For some of the metals, such as titanium and tantalum, alkoxides may be used in lieu of the β-diketonate forms.

(C. L. AARDAHL, J. W. ROGERS, JR.)

1. M. Ihara, T. Kimura, H. Yamawaki, K. Ikeda, *IEEE Trans. Magn., MAG-25*, 2470 (1989).
2. A. Harsta, in *Advances in Science and Technology*, Vol. 8, *Superconductivity and Superconducting Materials Technologies*, P. Vincenzini, eds., Techna, Florence, 1995. p. 549.
3. A.Harsta, S. Lundquist, *Chem. Vapor Deposition, 2*, 109 (1996).
4. M. Leskela, H. Molsa, L. Niinisto, *Supercond. Sci. Technol., 6*, 627 (1993).
5. K.-H. Dahmen, T. Gerfin, *Prog. Cryst. Growth Charact., 27*, 117 (1993).
6. T. Sugimoto, in *Materials Science Forum*, Vol. 137–139: *Advances in High-T_c Superconductivity*, J. J. Pouch, S. A. Alterovitz, R. R. Romanofsky, A. F. Hepp, eds., Trans Tech, Aedersmannsdorf, Switzerland, 1993, p. 395.
7. C. N. R. Rao, A. K. Ganguli, *Chem. Soc. Rev., 24*, 1 (1995).
8. D. L. Schulz, T. J. Marks, in *CVD of Nonmetals*, W.S. Rees, ed., VCH, Weinheim, Germany, 1996.
9. I. M. Watson, *Chem. Vapour Deposition, 3*, 9 (1997).
10. C. Gomez-Aleixandre, O. Sanchez, J. M. Albella, J. Santiso, A. Figueras, *Adv. Mater., 7*, 111 (1995).
11. W. S. Rees, H. A. Luten, V. L. Goedken, in *MRS Symp. Proc.*, Vol. 363: *Chemical Vapour Deposition of Refractory Metals and Ceramics III*, B. M. Gallois, W. Y. Lee, M. A. Pickering, eds., Materials Research Society, Pittsburgh, 1995, p. 195.
12. H. A. I. Luten, D. J. Otway, W. S. J. Rees, in *MRS Symp. Proc.*, Vol. 415: *Metal-Organic Chemical Vapour Deposition of Electronic Ceramics II*, S.B. Desu, D. B. Beach, P.C. Van Buskirk, eds., Materials Research Society, Pittsburgh, 1996, p. 99.
13. D. J. Otway, H. A. Luten, K. M. Abdul Malik, M. B. Hursthouse, W. S. J. Rees, in *MRS Symp. Proc.*, Vol. 415: *Metal-Organic Chemical Vapour Deposition of Electronic Ceramics II*, S.B. Desu, D. B. Beach, P. C. Van Buskirk, eds., Materials Research Society, Pittsburgh, 1996, p. 105.
14. D. B. Studebaker, G. Doubinina, J. Zhang, Y. Y. Wang, V. P. Dravid, T. J. Marks, in *MRS Symp. Proc.*, Vol. 415: *Metal-Organic Chemical Vapour Deposition of Electronic Ceramics II*, S. B. Desu, D. B. Beach, P. C. Van Buskirk, eds., Materials Research Society, Pittsburgh, 1996, p. 255.

17.2.6. Doping

The choice of impurity source and experimental setup for doping a semiconductor depends on the impurity and on factors such as vapor pressure and purity of the impurity source, solid solubility in the semiconductor, and alloying or compound formation on the semiconductor surface.

The form of the doping source whether it be solid, liquid or gaseous, is important in deciding whether to use a closed-tube diffusion system or an open one. In the former case, the semiconductor and the source of diffusing impurity are placed in a cleaned quartz tube, which is evacuated, sealed, and then heated to the desired temperature. Although

solid elements, alloys, or compounds are usually used, liquids and gases can also be used as impurity sources for closed-tube diffusion.

The apparatus for open-tube diffusion consists of a silica furnace tube with a continuously flowing gas. The exit end may be at atmospheric pressure or at reduced pressure. The impurity source may be a vaporizing solid whose vapors are carried to the semiconductor by a carrier gas. The carrier gas may be bubbled through a liquid impurity source. The carrier gas takes up source molecules, which then decompose at elevated temperatures. Liquid sources are maintained at or near room temperature. This arrangement has an advantage over the use of solid sources in terms of easier control of source temperature and, thus, impurity concentrations in the carrier gas.

Direct gas sources provide an easy way of introducing impurities into a diffusion furnace, and they can be diluted by a carrier gas, (e.g., dopant trihalides or hydrides can be diluted with nitrogen mixed with oxygen). The vapor phase reactions produce on the semiconductor surfaces dopant oxides from which diffusion can occur.

The most controllable method of introducing dopants into semiconductors is ion implantation. Ions are created by means of a confined electric discharge, which is sustained by the vapor of the impurity source material. The ion beam is extracted from the source, accelerated, mass-analyzed, and then deflected across the semiconductor surface to provide a uniform dose by a raster scan. The ions penetrate the surface and are then diffused in a separate diffusion furnace.

Neutron transmutation doping is specific to silicon. In this process, phosphorus-doped silicon can be obtained by using a stream of thermal neutrons to transmute silicon atoms to phosphorus. The nuclear reaction provides an even doping distribution throughout the silicon.

(RICHARD B. FAIR)

17.2.6.1. Doping from Solids

This section describes how solid doping sources are obtained by means of periodic grouping.

17.2.6.1.1. Group I Dopants.

Metallic Li deposited on Si and Ge surfaces is heated in a closed tube in a He atmosphere at 450–1000°C[1]. The Li-diffused layer is n-type. The doping layer consists of Li_2Si + Si, especially above the eutectic temperature of 650°C. The dimorphic silicide, Li_4Si, may also be formed, depending on the composition of the Li–Si compound[2].

The doping of Ge with Li is also carried out by spreading solutions of $LiAlH_4$[3] and LiOH[4] spread on the Ge surface.

Group IB metals have low solubilities in semiconducting materials. These elements must be absent from semiconductors in which pn junctions with low leakage are formed, but diffusion from deposited films of Cu, Ag, and Au occurs in Ge, Si, CdS, InSb, GaAs, AlSb, CdTe, ZnSe, PbSe, and InAs[5].

(RICHARD B. FAIR)

1. C. S. Fuller, J. A. Ditzenberger, *Phys. Rev., 91*, 193 (1953).
2. F. A. Shunk, *Constitution of Binary Alloys*, 2nd suppl., McGraw-Hill, New York, 1969.
3. B. Pratt, F. Friedman, *J. Appl. Phys., 37*, 1893 (1966).

4. J. O . Kesslee, B. E. Tompkins, J. Blanc, *Solid-State Electron., 6*, 297 (1963).
5. B. L. Sharma, *Diffusion in Semiconductors*, Trans Tech Publications, 1970.

17.2.6.1.2. Group II Dopants.

Group IIA and IIB elements such as Be, Mg, and Zn are used to dope semiconductors of groups III–V such as GaAs, InAs, InP, GaSb, and GaP. The diffusion source should approach an equilibrium composition as defined by the components in the ternary phase diagram for a given temperature; for example, in the Zn–GaAs system, the starting source material for Zn diffusion in sealed ampules is either elemental Zn, dilute solutions of Zn in Ga, or various combinations of Zn and As[1–3]. The partial pressures of the Ga and As dopants control the impurity surface concentrations in the semiconductors from groups III–V. The diffusion mechanism for impurities that reside substitutionally in the lattice depends on the vacancy concentration, hence on the solid source composition. For Zn diffusion into GaAs, Zn enters GaAs either interstitially or as a substitutional acceptor[4]:

$$Zn_I^+ + V_{Ga} \rightleftharpoons Zn_{Ga}^- + 2e^+ \qquad \text{(a)}$$

where V_{Ga} is a gallium vacancy. The reaction for the formation of Ga vacancies is:

$$Ga \rightleftharpoons Ga(l) + V_{Ga} \qquad \text{(b)}$$

where Ga(l) is the liquid Ga species from the decomposition reaction of solid GaAs:

$$GaAs(s) \rightleftharpoons Ga(l) + \tfrac{1}{2}As_2(g) \qquad \text{(c)}$$

From these reactions, the concentration of V_{Ga} is[4]:

$$[V_{Ga}] = K(T)p_{As_2}^{1/2} \qquad \text{(d)}$$

where $K(T)$ is a temperature-dependent constant and $p_{As_2}^{1/2}$ is the partial pressure of As_2 over the GaAs. In addition, $[V_{As}] \propto p_{As_2}^{-1/2}$. Thus, the source composition influences the diffusion mechanism inside the GaAs.

(RICHARD B. FAIR)

1. H. C. Casey Jr., M. B. Panish, *Trans. Metall. Soc. AIME, 242*, 406 (1968).
2. A. R. Calawa, *Solid-State Research Report No. 4*, Lincoln Laboratory, MIT, Lexington, MA, 1963.
3. M. H. Pilkuhn, H. Rupprecht, *Trans. Metall. Soc. AIME, 230*, 296 (1964).
4. H. C. Casey Jr., in *Atomic Diffusion in Semiconductors*, D. Shaw, ed., p. 351.

17.2.6.1.3. Group III Dopants.

Group III elements are used as acceptor dopants in Ge and Si. The most common solid sources for diffusing B are BN, B_2O_3, B-doped SiO_2, and H_3BO_3. High purity H_3BO_3 is readily available, and since it dehydrates at high temperatures to form B_2O_3:

$$2H_3BO_3 \xrightarrow[185°C]{\Delta} B_2O_3 + 3H_2O \qquad \text{(a)}$$

it is used interchangeably with B_2O_3[1]. When solid sources of boron are used, boron oxide is formed on the semiconductor surface. It is reduced to elemental B by Si:

$$B_2O_3 + \tfrac{3}{2}Si \rightleftharpoons 2B + \tfrac{3}{2}SiO_2 \qquad \text{(b)}$$

and the reduced B diffuses into the silicon.

Inorganic Reactions and Methods, Volume 18
Edited by J. J. Zuckerman, Jim D. Atwood

4. J. O . Kesslee, B. E. Tompkins, J. Blanc, *Solid-State Electron., 6*, 297 (1963).
5. B. L. Sharma, *Diffusion in Semiconductors*, Trans Tech Publications, 1970.

17.2.6.1.2. Group II Dopants.

Group IIA and IIB elements such as Be, Mg, and Zn are used to dope semiconductors of groups III–V such as GaAs, InAs, InP, GaSb, and GaP. The diffusion source should approach an equilibrium composition as defined by the components in the ternary phase diagram for a given temperature; for example, in the Zn–GaAs system, the starting source material for Zn diffusion in sealed ampules is either elemental Zn, dilute solutions of Zn in Ga, or various combinations of Zn and As[1–3]. The partial pressures of the Ga and As dopants control the impurity surface concentrations in the semiconductors from groups III–V. The diffusion mechanism for impurities that reside substitutionally in the lattice depends on the vacancy concentration, hence on the solid source composition. For Zn diffusion into GaAs, Zn enters GaAs either interstitially or as a substitutional acceptor[4]:

$$Zn_I^+ + V_{Ga} \rightleftharpoons Zn_{Ga}^- + 2e^+ \qquad \text{(a)}$$

where V_{Ga} is a gallium vacancy. The reaction for the formation of Ga vacancies is:

$$Ga \rightleftharpoons Ga(l) + V_{Ga} \qquad \text{(b)}$$

where Ga(l) is the liquid Ga species from the decomposition reaction of solid GaAs:

$$GaAs(s) \rightleftharpoons Ga(l) + \tfrac{1}{2}As_2(g) \qquad \text{(c)}$$

From these reactions, the concentration of V_{Ga} is[4]:

$$[V_{Ga}] = K(T)p_{As_2}^{1/2} \qquad \text{(d)}$$

where $K(T)$ is a temperature-dependent constant and $p_{As_2}^{1/2}$ is the partial pressure of As_2 over the GaAs. In addition, $[V_{As}] \propto p_{As_2}^{-1/2}$. Thus, the source composition influences the diffusion mechanism inside the GaAs.

(RICHARD B. FAIR)

1. H. C. Casey Jr., M. B. Panish, *Trans. Metall. Soc. AIME, 242*, 406 (1968).
2. A. R. Calawa, *Solid-State Research Report No. 4*, Lincoln Laboratory, MIT, Lexington, MA, 1963.
3. M. H. Pilkuhn, H. Rupprecht, *Trans. Metall. Soc. AIME, 230*, 296 (1964).
4. H. C. Casey Jr., in *Atomic Diffusion in Semiconductors*, D. Shaw, ed., p. 351.

17.2.6.1.3. Group III Dopants.

Group III elements are used as acceptor dopants in Ge and Si. The most common solid sources for diffusing B are BN, B_2O_3, B-doped SiO_2, and H_3BO_3. High purity H_3BO_3 is readily available, and since it dehydrates at high temperatures to form B_2O_3:

$$2H_3BO_3 \xrightarrow[185°C]{\Delta} B_2O_3 + 3H_2O \qquad \text{(a)}$$

it is used interchangeably with B_2O_3[1]. When solid sources of boron are used, boron oxide is formed on the semiconductor surface. It is reduced to elemental B by Si:

$$B_2O_3 + \tfrac{3}{2}Si \rightleftharpoons 2B + \tfrac{3}{2}SiO_2 \qquad \text{(b)}$$

and the reduced B diffuses into the silicon.

Inorganic Reactions and Methods, Volume 18
Edited by J. J. Zuckerman, Jim D. Atwood

4. J. O . Kesslee, B. E. Tompkins, J. Blanc, *Solid-State Electron., 6*, 297 (1963).
5. B. L. Sharma, *Diffusion in Semiconductors*, Trans Tech Publications, 1970.

17.2.6.1.2. Group II Dopants.

Group IIA and IIB elements such as Be, Mg, and Zn are used to dope semiconductors of groups III–V such as GaAs, InAs, InP, GaSb, and GaP. The diffusion source should approach an equilibrium composition as defined by the components in the ternary phase diagram for a given temperature; for example, in the Zn–GaAs system, the starting source material for Zn diffusion in sealed ampules is either elemental Zn, dilute solutions of Zn in Ga, or various combinations of Zn and As[1–3]. The partial pressures of the Ga and As dopants control the impurity surface concentrations in the semiconductors from groups III–V. The diffusion mechanism for impurities that reside substitutionally in the lattice depends on the vacancy concentration, hence on the solid source composition. For Zn diffusion into GaAs, Zn enters GaAs either interstitially or as a substitutional acceptor[4]:

$$Zn_I^+ + V_{Ga} \rightleftharpoons Zn_{Ga}^- + 2e^+ \qquad \text{(a)}$$

where V_{Ga} is a gallium vacancy. The reaction for the formation of Ga vacancies is:

$$Ga \rightleftharpoons Ga(l) + V_{Ga} \qquad \text{(b)}$$

where Ga(l) is the liquid Ga species from the decomposition reaction of solid GaAs:

$$GaAs(s) \rightleftharpoons Ga(l) + \tfrac{1}{2}As_2(g) \qquad \text{(c)}$$

From these reactions, the concentration of V_{Ga} is[4]:

$$[V_{Ga}] = K(T)p_{As_2}^{1/2} \qquad \text{(d)}$$

where $K(T)$ is a temperature-dependent constant and $p_{As_2}^{1/2}$ is the partial pressure of As_2 over the GaAs. In addition, $[V_{As}] \propto p_{As_2}^{-1/2}$. Thus, the source composition influences the diffusion mechanism inside the GaAs.

(RICHARD B. FAIR)

1. H. C. Casey Jr., M. B. Panish, *Trans. Metall. Soc. AIME, 242*, 406 (1968).
2. A. R. Calawa, *Solid-State Research Report No. 4*, Lincoln Laboratory, MIT, Lexington, MA, 1963.
3. M. H. Pilkuhn, H. Rupprecht, *Trans. Metall. Soc. AIME, 230*, 296 (1964).
4. H. C. Casey Jr., in *Atomic Diffusion in Semiconductors*, D. Shaw, ed., p. 351.

17.2.6.1.3. Group III Dopants.

Group III elements are used as acceptor dopants in Ge and Si. The most common solid sources for diffusing B are BN, B_2O_3, B-doped SiO_2, and H_3BO_3. High purity H_3BO_3 is readily available, and since it dehydrates at high temperatures to form B_2O_3:

$$2H_3BO_3 \xrightarrow[185°C]{\Delta} B_2O_3 + 3H_2O \qquad \text{(a)}$$

it is used interchangeably with B_2O_3[1]. When solid sources of boron are used, boron oxide is formed on the semiconductor surface. It is reduced to elemental B by Si:

$$B_2O_3 + \tfrac{3}{2}Si \rightleftharpoons 2B + \tfrac{3}{2}SiO_2 \qquad \text{(b)}$$

and the reduced B diffuses into the silicon.

Depending on the O_2 concentration in the diffusion furnace, Si–B compound may form at the glass–Si interface[2]:

$$x\text{Si} + y\text{B} \rightleftharpoons \text{Si–B compound} \tag{c}$$

Those diffraction patterns closely resemble SiB_4 or SiB_6[2,3].

On oxidation:

$$\text{Si–B compound} + O_2 \rightleftharpoons SiO_2 + B_2O_3. \tag{d}$$

Small amounts of H_2O in the furnace also affect the vapor transport in B_2O_3. For a BN source[4]:

Oxidation:

$$2BN_2 + 3O_2 \longrightarrow 2B_2O_3 + 2N_2 \tag{e}$$

$$B_2O_3 + H_2O \longrightarrow 2HBO_2 \tag{f}$$

Deposition:

$$2HBO_2 + 2Si \longrightarrow 2SiO_2 + 2B + H_2 \tag{g}$$

The vapor pressure of HBO_2 is orders of magnitude greater than that of B_2O_3 at 900°C[5]. Chemical vapor deposition of BN directly on Si is also used as a solid diffusion source[6]. When the deposition temperature is below 1000°C, the BN film is amorphous. Reaction between BN and Si is unknown. However, BN decomposes when heated in N_2.

In sealed-tube diffusion of Al from an Al metal source, reaction occurs with the quartz walls of the tube, with O_2 and with moisture (residual after evacuating the ampule). Possible reactions at the diffusion temperature are[7]:

$$2Al(g) + \tfrac{3}{2}O_2(g) \longrightarrow Al_2O_3(s) \tag{h}$$

$$4Al(g) + 3SiO_2(s) \longrightarrow 2Al_2O_3(s) + 3Si(s) \tag{i}$$

Thus, in the presence of O_2 and quartz, the liquid Al source will be oxidized to form a stable Al_2O_3 skin to seal or consume the Al source. This limits the concentration of Al that can be diffused into the Si wafer.

In the parts per billion water vapor range, the primary transporting gaseous species are Al and AlH. However, in the parts per million water vapor range, the partial pressures of the volatile species diminishes, and an oxide skin forms[7].

Gallium can be diffused from its oxide when a reducing carrier gas such as H_2 or CO is used in an open-tube system. Reducing reactions at the source may include[8]:

$$Ga_2O_3 + 2H_2 \longrightarrow Ga_2O + 2H_2O \tag{j}$$

$$Ga_2O_3 + 2CO \longrightarrow Ga_2O + 2CO_2 \tag{k}$$

before any Ga will be transported to the semiconductor. The Ga_2O is volatile and is carried to the semiconductor in this form. For silicon:

$$2Ga_2O + Si \rightleftharpoons 4Ga. \tag{l}$$

(RICHARD B. FAIR)

1. W. R. Foster, *Research on Phase Equilibria Between Boron Oxides and Refractory Oxides, Including Silicon and Aluminum Oxides*, AD230526, Ohio State University, Columbus, 1959.
2. E. Arai, H. Nakamura, Y. Terunuma, *J. Electrochem. Soc., 120*, 980 (1973).

3. A. Armigliato, D. Nobili, P. Ostoja, M. Servidori, S. Solmi, in *Semiconductor Silicon 1977*, H. R. Huff, E. Sirtl, eds., *Electrochemical Society*, Princeton, NJ, 1977, p. 638.
4. D. Rupprecht, J. Stack, *J. Electrochem. Soc., 120*, 1266 (1973).
5. S. P. Randall, J. L. Margrave, *J. Inorg. Nucl. Chem., 16*, 29 (1960).
6. M. Hirayama, K. Shohno, *J. Electrochem. Soc., 122*, 1671 (1975).
7. P. Rai-Choudhury, F. A. Selim, W. J. Takei, *J. Electrochem. Soc., 124*, 762 (1977).
8. C. J. Frosch, L. Derick, *J. Electrochem. Soc., 105*, 695 (1958).

17.2.6.1.4. Group V Dopants.

Solid sources used for P doping of Si or Ge include anhydrous P_2O_5, red P, $NH_4H_2PO_4$, $(NH_4)_2HPO_4$, P-doped SiO_2 deposited directly on the semiconductor, and PN[1]. These sources cause formation of P_2O_5 on the semiconductor surface. It is reduced to elemental P reacting with Si:

$$P_2O_5 + \tfrac{5}{2}Si \rightleftharpoons \tfrac{5}{2}SiO_2 + 2P \qquad (a)$$

and the reduced P diffuses into the Si.

Open-tube As diffusion involves a solid As_2O_3 source. With an O_2 carrier gas, As_2O_3 deposits on the Si[2,3]:

$$As_2O_3 + \tfrac{3}{2}Si \rightleftharpoons \tfrac{3}{2}SiO_2 + 2As \qquad (b)$$

Other solid As sources that have been tried are $AsBr_3$, AsI_3[4], and As[5]. No detectable doping occurs with AsI_3 because of its low vapor pressure[4].

Closed-tube diffusions occur with As-doped Si powders[6], elemental As[7], and SiAs[8]. Elemental As produces badly attacked surfaces. The dominant vapor species are As_4 and As_2[9]. Molecular dissociation must occur first:

$$As_4(g) \rightleftharpoons 4As(g) \qquad (c)$$

$$As_2(g) \rightleftharpoons 2As(g) \qquad (d)$$

If the monomer in the gas phase is in equilibrium with the monomer in the solid phase, As(s), then:

$$As(g) \rightleftharpoons As(s) \rightleftharpoons As^+ + e^- \qquad (e)$$

The open-tube system is suitable for Sb diffusion using Sb_2O_4[2], $SbCl_3$, $SbBr_3$[4], and Sb_3Cl_5[10]. The film deposited on the Si usually is Sb_2O_5. Diffusion is also performed from mixed SiO_2–Sb_2O_5 layers[11]. The Sb incorporation reaction is:

$$Sb_2O_5 + \tfrac{5}{2}Si \rightleftharpoons \tfrac{5}{2}SiO_2 + 2Sb \qquad (f)$$

(RICHARD B. FAIR)

1. A. M. Smith, in *Fundamentals of Silicon Integrated Device Technology*, Vol. 1, R. M. Burger, R. P. Donovan, eds., Prentice-Hall, Englewood Cliffs, NJ, 1967, p. 183.
2. D. J. Frosch, L. Derick, *J. Electrochem. Soc., 104*, 547 (1962).
3. R. B. Fair, *J. Electrochem. Soc., 119*, 1389 (1972).
4. W. van Gelder, J. F. Roberts, unpublished results, 1971.
5. E. S. Raub, unpublished results, 1969.
6. M. L. Joshi, Fall Meeting of the Electrochemical Society, Atlantic City, NJ, Abstract 238, 1970.
7. Y. Nakajima, S. Ohkawa, Y. Fukukawa, Spring Meeting of the Electrochemical Society, Washington, DC, Abstract 77, 1971.

Inorganic Reactions and Methods, Volume 18
Edited by J. J. Zuckerman, Jim D. Atwood

3. A. Armigliato, D. Nobili, P. Ostoja, M. Servidori, S. Solmi, in *Semiconductor Silicon 1977*, H. R. Huff, E. Sirtl, eds., *Electrochemical Society*, Princeton, NJ, 1977, p. 638.
4. D. Rupprecht, J. Stack, *J. Electrochem. Soc., 120*, 1266 (1973).
5. S. P. Randall, J. L. Margrave, *J. Inorg. Nucl. Chem., 16*, 29 (1960).
6. M. Hirayama, K. Shohno, *J. Electrochem. Soc., 122*, 1671 (1975).
7. P. Rai-Choudhury, F. A. Selim, W. J. Takei, *J. Electrochem. Soc., 124*, 762 (1977).
8. C. J. Frosch, L. Derick, *J. Electrochem. Soc., 105*, 695 (1958).

17.2.6.1.4. Group V Dopants.

Solid sources used for P doping of Si or Ge include anhydrous P_2O_5, red P, $NH_4H_2PO_4$, $(NH_4)_2HPO_4$, P-doped SiO_2 deposited directly on the semiconductor, and PN[1]. These sources cause formation of P_2O_5 on the semiconductor surface. It is reduced to elemental P reacting with Si:

$$P_2O_5 + \tfrac{5}{2}Si \rightleftharpoons \tfrac{5}{2}SiO_2 + 2P \qquad (a)$$

and the reduced P diffuses into the Si.

Open-tube As diffusion involves a solid As_2O_3 source. With an O_2 carrier gas, As_2O_3 deposits on the Si[2,3]:

$$As_2O_3 + \tfrac{3}{2}Si \rightleftharpoons \tfrac{3}{2}SiO_2 + 2As \qquad (b)$$

Other solid As sources that have been tried are $AsBr_3$, AsI_3[4], and As[5]. No detectable doping occurs with AsI_3 because of its low vapor pressure[4].

Closed-tube diffusions occur with As-doped Si powders[6], elemental As[7], and SiAs[8]. Elemental As produces badly attacked surfaces. The dominant vapor species are As_4 and As_2[9]. Molecular dissociation must occur first:

$$As_4(g) \rightleftharpoons 4As(g) \qquad (c)$$

$$As_2(g) \rightleftharpoons 2As(g) \qquad (d)$$

If the monomer in the gas phase is in equilibrium with the monomer in the solid phase, As(s), then:

$$As(g) \rightleftharpoons As(s) \rightleftharpoons As^+ + e^- \qquad (e)$$

The open-tube system is suitable for Sb diffusion using Sb_2O_4[2], $SbCl_3$, $SbBr_3$[4], and Sb_3Cl_5[10]. The film deposited on the Si usually is Sb_2O_5. Diffusion is also performed from mixed SiO_2–Sb_2O_5 layers[11]. The Sb incorporation reaction is:

$$Sb_2O_5 + \tfrac{5}{2}Si \rightleftharpoons \tfrac{5}{2}SiO_2 + 2Sb \qquad (f)$$

(RICHARD B. FAIR)

1. A. M. Smith, in *Fundamentals of Silicon Integrated Device Technology*, Vol. 1, R. M. Burger, R. P. Donovan, eds., Prentice-Hall, Englewood Cliffs, NJ, 1967, p. 183.
2. D. J. Frosch, L. Derick, *J. Electrochem. Soc., 104*, 547 (1962).
3. R. B. Fair, *J. Electrochem. Soc., 119*, 1389 (1972).
4. W. van Gelder, J. F. Roberts, unpublished results, 1971.
5. E. S. Raub, unpublished results, 1969.
6. M. L. Joshi, Fall Meeting of the Electrochemical Society, Atlantic City, NJ, Abstract 238, 1970.
7. Y. Nakajima, S. Ohkawa, Y. Fukukawa, Spring Meeting of the Electrochemical Society, Washington, DC, Abstract 77, 1971.

8. E. I. Povilonis, C. F. Gibbon, unpublished results, 1972.
9. T. L. Chu, R. W. Kelm, S. S. Chu, *J. Appl. Phys., 42*, 1169 (1971).
10. W. R. Runyan, *Silicon Semiconductor Technology*, McGraw-Hill, New York, 1965, p. 149.
11. F. L. Gittler, R. A. Porter, *J. Electrochem. Soc., 117*, 1551 (1970).

17.2.6.1.5. Group VI Dopants.

Donors such as elemental S, Se, Te, or Sn diffuse into GaAs[1–4]. With S, alloying and formation of sulfides occurs during diffusion, producing surface erosion of Si wafers[5]. Similar problems occur with GaAs, since both donor elements and As are reactive and volatile. In the presence of S, the transport of As and Ga from the surface of GaAs wafers is enhanced by formation of volatile compounds[6].

The use of Al_2S_3 as a doping source in a sealed-tube system[7] reduces the vapor pressure of S, thus limiting surface erosion. Junctions are also obtained in GaAs using Al_2Se_3, Al_2Te_3, As_2S_2, Ga_2S_3, GeS, GeS_2, MoS_3, $MoSe_2$, SnS, and As_2Se_5[7].

(RICHARD B. FAIR)

1. B. Goldstein, *Phys. Rev., 121*, 1305 (1961).
2. L. J. Viehard, *J. Phys. Chem. Solids, 21*, 318 (1961).
3. L. R. Weisberg, *Trans. Metall. Soc. AIME, 230*, 291 (1964).
4. R. W. Fane, A. J. Goss, *Solid-State Electron., 6*, 383 (1963).
5. R. O. Carlson, R. N. Hall, E. M. Pell, *J. Phys. Chem. Solids, 8*, 81 (1959).
6. L. R. Weisberg, Ed., Scientific Rep. No. 7, *High Temperature Semiconductor Research* (RCA), April–June 1961, p. 34.
7. R. G. Frieser, *J. Electrochem. Soc., 112*, 697 (1965).

17.2.6.2. Doping from Liquids

Liquid doping sources are usually of two forms: (1) a solution of dopant material is directly applied to the semiconductor surface and dried prior to diffusion; or (2) a carrier gas is bubbled through the liquid source and the source molecules are carried into an open-tube furnace. Doping may then occur from the gas phase or from a deposited solid phase on the semiconductor. Also, in some cases solid sources deposited on semiconductors become liquid at diffusion temperatures (e.g., borosilicate glasses containing ca. 30 mol% B_2O_3 become liquid at $\sim$1000°C)[1].

(RICHARD B. FAIR)

17.2.6.2.1. Directly Applied Liquid Sources.

Liquid sources can be painted on, spun on, or applied by electrolysis. Electroplating of Sn^{-113} on InSb is accomplished by using $SnCl_2$ in HCl + 50 mL H_2O + concentrated aqueous 0.1 mL $NaHC_4H_4O_6$[2]. Also, Cd^{-115m} is deposited on the surface of InSb by electrolysis of an aqueous solution of $^{115m}CdCl_2$[3]. A doping source for Si consists of CH_3OH saturated with B_2O_3 and painted on the Si surface[4]. Commercially available liquid doping sources for Si are spun on the wafer surface and then dried at 250°C to form a doped oxide. The basic contents of these solutions are ethoxysilane or methoxysilane for SiO_2 formation, H_3BO_3 or As_2O_3 dissolved in methanol for the dopant, and acetone and ethyl acetate for controlling viscosity and film adherence[5].

(RICHARD B. FAIR)

Inorganic Reactions and Methods, Volume 18
Edited by J. J. Zuckerman, Jim D. Atwood

8. E. I. Povilonis, C. F. Gibbon, unpublished results, 1972.
9. T. L. Chu, R. W. Kelm, S. S. Chu, *J. Appl. Phys.*, *42*, 1169 (1971).
10. W. R. Runyan, *Silicon Semiconductor Technology*, McGraw-Hill, New York, 1965, p. 149.
11. F. L. Gittler, R. A. Porter, *J. Electrochem. Soc.*, *117*, 1551 (1970).

17.2.6.1.5. Group VI Dopants.

Donors such as elemental S, Se, Te, or Sn diffuse into GaAs[1–4]. With S, alloying and formation of sulfides occurs during diffusion, producing surface erosion of Si wafers[5]. Similar problems occur with GaAs, since both donor elements and As are reactive and volatile. In the presence of S, the transport of As and Ga from the surface of GaAs wafers is enhanced by formation of volatile compounds[6].

The use of Al_2S_3 as a doping source in a sealed-tube system[7] reduces the vapor pressure of S, thus limiting surface erosion. Junctions are also obtained in GaAs using Al_2Se_3, Al_2Te_3, As_2S_2, Ga_2S_3, GeS, GeS_2, MoS_3, $MoSe_2$, SnS, and As_2Se_5[7].

(RICHARD B. FAIR)

1. B. Goldstein, *Phys. Rev.*, *121*, 1305 (1961).
2. L. J. Viehard, *J. Phys. Chem. Solids*, *21*, 318 (1961).
3. L. R. Weisberg, *Trans. Metall. Soc. AIME*, *230*, 291 (1964).
4. R. W. Fane, A. J. Goss, *Solid-State Electron.*, *6*, 383 (1963).
5. R. O. Carlson, R. N. Hall, E. M. Pell, *J. Phys. Chem. Solids*, *8*, 81 (1959).
6. L. R. Weisberg, Ed., Scientific Rep. No. 7, *High Temperature Semiconductor Research* (RCA), April–June 1961, p. 34.
7. R. G. Frieser, *J. Electrochem. Soc.*, *112*, 697 (1965).

17.2.6.2. Doping from Liquids

Liquid doping sources are usually of two forms: (1) a solution of dopant material is directly applied to the semiconductor surface and dried prior to diffusion; or (2) a carrier gas is bubbled through the liquid source and the source molecules are carried into an open-tube furnace. Doping may then occur from the gas phase or from a deposited solid phase on the semiconductor. Also, in some cases solid sources deposited on semiconductors become liquid at diffusion temperatures (e.g., borosilicate glasses containing ca. 30 mol% B_2O_3 become liquid at $\sim$1000°C)[1].

(RICHARD B. FAIR)

17.2.6.2.1. Directly Applied Liquid Sources.

Liquid sources can be painted on, spun on, or applied by electrolysis. Electroplating of Sn^{-113} on InSb is accomplished by using $SnCl_2$ in HCl + 50 mL H_2O + concentrated aqueous 0.1 mL $NaHC_4H_4O_6$[2]. Also, Cd^{-115m} is deposited on the surface of InSb by electrolysis of an aqueous solution of $^{115m}CdCl_2$[3]. A doping source for Si consists of CH_3OH saturated with B_2O_3 and painted on the Si surface[4]. Commercially available liquid doping sources for Si are spun on the wafer surface and then dried at 250°C to form a doped oxide. The basic contents of these solutions are ethoxysilane or methoxysilane for SiO_2 formation, H_3BO_3 or As_2O_3 dissolved in methanol for the dopant, and acetone and ethyl acetate for controlling viscosity and film adherence[5].

(RICHARD B. FAIR)

Inorganic Reactions and Methods, Volume 18
Edited by J. J. Zuckerman, Jim D. Atwood

8. E. I. Povilonis, C. F. Gibbon, unpublished results, 1972.
9. T. L. Chu, R. W. Kelm, S. S. Chu, *J. Appl. Phys.*, *42*, 1169 (1971).
10. W. R. Runyan, *Silicon Semiconductor Technology*, McGraw-Hill, New York, 1965, p. 149.
11. F. L. Gittler, R. A. Porter, *J. Electrochem. Soc.*, *117*, 1551 (1970).

17.2.6.1.5. Group VI Dopants.

Donors such as elemental S, Se, Te, or Sn diffuse into GaAs[1–4]. With S, alloying and formation of sulfides occurs during diffusion, producing surface erosion of Si wafers[5]. Similar problems occur with GaAs, since both donor elements and As are reactive and volatile. In the presence of S, the transport of As and Ga from the surface of GaAs wafers is enhanced by formation of volatile compounds[6].

The use of Al_2S_3 as a doping source in a sealed-tube system[7] reduces the vapor pressure of S, thus limiting surface erosion. Junctions are also obtained in GaAs using Al_2Se_3, Al_2Te_3, As_2S_2, Ga_2S_3, GeS, GeS_2, MoS_3, $MoSe_2$, SnS, and As_2Se_5[7].

(RICHARD B. FAIR)

1. B. Goldstein, *Phys. Rev.*, *121*, 1305 (1961).
2. L. J. Viehard, *J. Phys. Chem. Solids*, *21*, 318 (1961).
3. L. R. Weisberg, *Trans. Metall. Soc. AIME*, *230*, 291 (1964).
4. R. W. Fane, A. J. Goss, *Solid-State Electron.*, *6*, 383 (1963).
5. R. O. Carlson, R. N. Hall, E. M. Pell, *J. Phys. Chem. Solids*, *8*, 81 (1959).
6. L. R. Weisberg, Ed., Scientific Rep. No. 7, *High Temperature Semiconductor Research* (RCA), April–June 1961, p. 34.
7. R. G. Frieser, *J. Electrochem. Soc.*, *112*, 697 (1965).

17.2.6.2. Doping from Liquids

Liquid doping sources are usually of two forms: (1) a solution of dopant material is directly applied to the semiconductor surface and dried prior to diffusion; or (2) a carrier gas is bubbled through the liquid source and the source molecules are carried into an open-tube furnace. Doping may then occur from the gas phase or from a deposited solid phase on the semiconductor. Also, in some cases solid sources deposited on semiconductors become liquid at diffusion temperatures (e.g., borosilicate glasses containing ca. 30 mol% B_2O_3 become liquid at $\sim$1000°C)[1].

(RICHARD B. FAIR)

17.2.6.2.1. Directly Applied Liquid Sources.

Liquid sources can be painted on, spun on, or applied by electrolysis. Electroplating of Sn^{-113} on InSb is accomplished by using $SnCl_2$ in HCl + 50 mL H_2O + concentrated aqueous 0.1 mL $NaHC_4H_4O_6$[2]. Also, Cd^{-115m} is deposited on the surface of InSb by electrolysis of an aqueous solution of $^{115m}CdCl_2$[3]. A doping source for Si consists of CH_3OH saturated with B_2O_3 and painted on the Si surface[4]. Commercially available liquid doping sources for Si are spun on the wafer surface and then dried at 250°C to form a doped oxide. The basic contents of these solutions are ethoxysilane or methoxysilane for SiO_2 formation, H_3BO_3 or As_2O_3 dissolved in methanol for the dopant, and acetone and ethyl acetate for controlling viscosity and film adherence[5].

(RICHARD B. FAIR)

1. D. M. Brown, P. R. Kennicott, *J. Electrochem. Soc., 118*, 293 (1971).
2. S. M. Sze, L. Y. Wei, *Phys. Rev., 124*, 84 (1961).
3. B. I. Boltaks, V. I. Sokolov, *Sov. Phys.-Solid State, 5*, 785 (1963).
4. E. L. Williams, *J. Electrochem. Soc., 108*, 795 (1961).
5. P. M. Prasad, M. V. Rao, V. P. S. Singh, *Int. J. Electron. 47*, 503 (1979).

17.2.6.2.2. Liquid Sources for Open-Tube Diffusion.

The liquid source is usually maintained near room temperature, and an inert gas is bubbled through the source. A commonly used source for doping Si is BBr_3, which needs a small percentage of O_2 in the carrier gas to form B_2O_3 on the Si surface. Diffusion without O_2 blackens the Si[1]. In the high temperature deposition furnace:

$$2BBr_3(g) + \tfrac{3}{2}O_2(g) = B_2O_3(g) + 3Br_2(g) \qquad (a)$$

Since the vapor pressure of B_2O_3 is low (10^{-2} N/m^2 at 1000°C), liquid B_2O_3 is deposited on the Si surface. If the initial partial pressure of BBr_3 is kept low enough[2], formation of a boron skin (SiB_4 or SiB_6) on the Si wafers is avoided, and B-rich borosilicate glass is deposited instead.

When $H_2O(g)$ is used as the oxidant, then[3]:

$$BBr_3(g) + 2H_2O(g) \rightleftharpoons HBO_2(g) + 3HBr(g) \qquad (b)$$

The HBO_2 may be regarded as a buffering agent for B_2O_3 vapor. If the H_2O partial pressure is maintained at 10^3 N/m^2 then a partial pressure of B_2O_3 of 10^{-3} N/m^2 results in a HBO_2 partial pressure of 10 N/m^2 through:

$$2HBO_2(g) \rightleftharpoons H_2O(g) + B_2O_3(g) \qquad (c)$$

Thus, as a result of the lower B_2O_3 partial pressures, the BBr_3–H_2O system allows control of much lower concentration B diffusions in Si than the BBr_3–O_2 system.

For n-type doping, $POCl_3$[1] and PBr_3[4] are commonly used. A low flow of O_2 is required to facilitate decomposition of $POCl_3$ to P_2O_5 and to protect the Si surface. With PBr_3, no O_2 is needed in the carrier gas. For As doping, $AsBr_3$ was tried[5], but only low concentration As diffusions in Si were obtained.

Planar diffusion into GaAs is performed from Sn-doped SiO_2 prepared by pyrolysis of a mixture of ethyl orthosilicate and either tetramethyltin or tetraethyltin[6,7]. However, the inequality in vapor pressure of the two liquids in the bubbler causes large changes in composition with use. A more stable source uses Ar bubbled through tetramethyltin with SiH_4 and O_2 flowing in the tube[8].

(RICHARD B. FAIR)

1. A. M. Smith, in *Fundamentals of Silicon Integrated Device Technology*, R. M. Burger, R. P. Donovan eds., Prentice-Hall, Englewood Cliffs, NJ, 1967, p. 263.
2. P. C. Parekh, D. R. Goldstein, *Proc. IEEE, 57*, 1507 (1969).
3. R. F. Lever, H. M. Demsky, *IBM J. Res. Dev., 18*, 40 (1974).
4. T. C. Madden, W. M. Gibson, *Rev. Sci. Instrum., 34*, 50 (1963).
5. R. O. Druckenmiller, unpublished results, 1970.
6. W. von Muench, *IBM J. Res. Dev., 10*, 438 (1966).
7. C. F. Gibbon, D. R. Ketchow, *J. Electrochem. Soc., 118*, 975 (1971).
8. B. J. Baliga, S. K. Ghandhi, *J. Electrochem. Soc., 126*, 135 (1979).

Inorganic Reactions and Methods, Volume 18
Edited by J. J. Zuckerman, Jim D. Atwood

1. D. M. Brown, P. R. Kennicott, *J. Electrochem. Soc., 118*, 293 (1971).
2. S. M. Sze, L. Y. Wei, *Phys. Rev., 124*, 84 (1961).
3. B. I. Boltaks, V. I. Sokolov, *Sov. Phys.-Solid State, 5*, 785 (1963).
4. E. L. Williams, *J. Electrochem. Soc., 108*, 795 (1961).
5. P. M. Prasad, M. V. Rao, V. P. S. Singh, *Int. J. Electron. 47*, 503 (1979).

17.2.6.2.2. Liquid Sources for Open-Tube Diffusion.

The liquid source is usually maintained near room temperature, and an inert gas is bubbled through the source. A commonly used source for doping Si is BBr_3, which needs a small percentage of O_2 in the carrier gas to form B_2O_3 on the Si surface. Diffusion without O_2 blackens the Si[1]. In the high temperature deposition furnace:

$$2BBr_3(g) + \tfrac{3}{2}O_2(g) = B_2O_3(g) + 3Br_2(g) \qquad (a)$$

Since the vapor pressure of B_2O_3 is low (10^{-2} N/m^2 at 1000°C), liquid B_2O_3 is deposited on the Si surface. If the initial partial pressure of BBr_3 is kept low enough[2], formation of a boron skin (SiB_4 or SiB_6) on the Si wafers is avoided, and B-rich borosilicate glass is deposited instead.

When $H_2O(g)$ is used as the oxidant, then[3]:

$$BBr_3(g) + 2H_2O(g) \rightleftharpoons HBO_2(g) + 3HBr(g) \qquad (b)$$

The HBO_2 may be regarded as a buffering agent for B_2O_3 vapor. If the H_2O partial pressure is maintained at 10^3 N/m^2 then a partial pressure of B_2O_3 of 10^{-3} N/m^2 results in a HBO_2 partial pressure of 10 N/m^2 through:

$$2HBO_2(g) \rightleftharpoons H_2O(g) + B_2O_3(g) \qquad (c)$$

Thus, as a result of the lower B_2O_3 partial pressures, the BBr_3–H_2O system allows control of much lower concentration B diffusions in Si than the BBr_3–O_2 system.

For n-type doping, $POCl_3$[1] and PBr_3[4] are commonly used. A low flow of O_2 is required to facilitate decomposition of $POCl_3$ to P_2O_5 and to protect the Si surface. With PBr_3, no O_2 is needed in the carrier gas. For As doping, $AsBr_3$ was tried[5], but only low concentration As diffusions in Si were obtained.

Planar diffusion into GaAs is performed from Sn-doped SiO_2 prepared by pyrolysis of a mixture of ethyl orthosilicate and either tetramethyltin or tetraethyltin[6,7]. However, the inequality in vapor pressure of the two liquids in the bubbler causes large changes in composition with use. A more stable source uses Ar bubbled through tetramethyltin with SiH_4 and O_2 flowing in the tube[8].

(RICHARD B. FAIR)

1. A. M. Smith, in *Fundamentals of Silicon Integrated Device Technology*, R. M. Burger, R. P. Donovan eds., Prentice-Hall, Englewood Cliffs, NJ, 1967, p. 263.
2. P. C. Parekh, D. R. Goldstein, *Proc. IEEE, 57*, 1507 (1969).
3. R. F. Lever, H. M. Demsky, *IBM J. Res. Dev., 18*, 40 (1974).
4. T. C. Madden, W. M. Gibson, *Rev. Sci. Instrum., 34*, 50 (1963).
5. R. O. Druckenmiller, unpublished results, 1970.
6. W. von Muench, *IBM J. Res. Dev., 10*, 438 (1966).
7. C. F. Gibbon, D. R. Ketchow, *J. Electrochem. Soc., 118*, 975 (1971).
8. B. J. Baliga, S. K. Ghandhi, *J. Electrochem. Soc., 126*, 135 (1979).

Inorganic Reactions and Methods, Volume 18
Edited by J. J. Zuckerman, Jim D. Atwood

17.2.6.3. Doping from the Vapor

The two most common gaseous doping sources are dopant trihalides and dopant hydrides. Since BCl_3 is a gas at room temperature and pressure, it can be liquefied under pressure to yield a large supply in a small container. The chemistry of the dopant transfer process is less complex than the standard B_2O_3 process, since the reactants, BCl_3 and H_2 (carrier gas), and the product, HCl, are volatile and do not remain on the Si wafer. Diffusion takes place in a reducing ambient, and the Si surface is subject to damage. At large BCl_3 concentrations, the Si becomes covered with a tough black deposit[1].

The path for B_2H_6 doping of Si is[2]:

$$B_2H_6(g) \longrightarrow BH_3(g) \longrightarrow B(g) \longrightarrow B(Si) \longrightarrow B^-(Si) + p^+ \quad \text{(a)}$$

where B(Si) is the B dissolved in solid Si and $B^-(Si)$ is the ionized B acceptor atom. It is also possible to form B_2O_3–SiO_2 film diffusion sources by the oxidation of SiH_4 and B_2H_6 by O_2 or NO[3]:

$$B_2H_6 + 3NO \rightleftharpoons B_2O_3 + 3H_2 + \tfrac{3}{2}N_2 \quad \text{(b)}$$

$$2B_2H_6 + 3O_2 \rightleftharpoons 2B_2O_3 + 6H_2 \quad \text{(c)}$$

$$SiH_4 + 2NO \rightleftharpoons SiO_2 + N_2 + 2H_2 \quad \text{(d)}$$

$$SiH_4 + O_2 \rightleftharpoons SiO_2 + 2H_2 \quad \text{(e)}$$

The details of these latter thermally activated, surface-catalyzed, heterogeneous branching chain reactions are complex[4]. Premature reactions in the gas stream before gases reach the heated wafers must be avoided. The reduction of B_2O_3 by Si at the glass interface releases free B from the glass for doping.

Thermal cracking of PH_3 in a monoxidizing atmosphere can be described by:

$$2PH_3 \xrightarrow[440°C]{\triangle} 3H_2 + 2P \quad \text{(f)}$$

Diffusion at 1000–1100°C gives erratic results while causing damage to the Si surface[5]. Random pitting results, suggesting enhanced reactions at surface defect sites. In the presence of low concentrations of O_2, additional vapor phase reactions occur[1,5]:

$$4P + 5O_2 \rightleftharpoons 2P_2O_5 \quad \text{(g)}$$

$$2PH_3 + 3O_2 \rightleftharpoons P_2O_5 + 3H_2O \quad \text{(h)}$$

Thus, the PH_3 source requires an oxidizing atmosphere to create P_2O_5, which is transported to the Si surface and reduced:

$$2P_2O_5 + 5Si \rightleftharpoons 5SiO_2 + 4P \quad \text{(i)}$$

The kinetics of the oxidation of AsH_3 can be described by a first-order reaction[6]. The rate of oxidation depends on $[O_2]^{3/2}$. When SiH_4 is added to the gas stream for depositing As-doped SiO_2 doping films, the O_2 concentration can be used to control As doping[7]. At the Si surface, As_2O_3 is reduced:

$$\tfrac{3}{2}Si + As_2O_3 \rightleftharpoons \tfrac{3}{2}SiO_2 + 2As \quad \text{(j)}$$

Layers of Sb-doped SiO_2 can be deposited by means of $(CH_3)_3Sb$ vapor diluted in N_2 with SiH_4 and O_2:

$$SiH_4 + 2(CH_3)_3Sb + 15O_2 \rightleftharpoons SiO_2 + Sb_2O_5 + 6CO_2 + 11H_2O \qquad (k)$$

The addition of $(CH_3)_3Sb$ to SiH_4 decreases the SiH_4 oxidation rate. The trimethylstibine may act as a chain breaker in the oxidation of SiH_4, or the Si surface may catalyze the formation of Sb_2O_5, but not the SiO_2 formation. A similar effect is observed with the AsH_3–SiH_4 system, where the As becomes strongly bound to surface sites that are active in the pyrolysis of SiH_4[9].

(RICHARD B. FAIR)

1. A. M. Smith, in *Fundamentals of Silicon Integrated Device Technology*, R. M. Burger, R. P. Donovan, eds., Prentice Hall, Englewood Cliffs, NJ. 1967, p. 263.
2. J. Bloem, *J. Electrochem. Soc.*, *118*, 1837 (1971).
3. D. M. Brown, P. R. Kennicott, *J. Electrochem. Soc.*, *118*, 293 (1971).
4. H. J. Emeléus, K. Stewart, *J. Chem. Soc.*, 1182 (1935).
5. J. S. Kesperis, *J. Electrochem. Soc.*, *117*, 554 (1970).
6. G. R. Weber, unpublished results, 1970.
7. R. B. Fair, *J. Electrochem. Soc.*, *119*, 1389 (1972).
8. F. L. Gittler, R. A. Porter, *J. Electrochem. Soc.*, *117*, 1551 (1970).
9. R. F. C. Farrow, J. D. Filby, *J. Electrochem. Soc.*, *118*, 149 (1971).

17.2.6.4. Ion Implantation

The most useful application of ion beams is the doping of semiconductor crystals and devices by energetic ions. The type of source selected to generate singly or doubly ionized, positive or negative ions depends on performance parameters, including elements or compounds most easily ionized, total ion current, emittance, ion energy spread, brightness, size, and cost[1]. The most versatile and most commonly used sources are based on electron impact ionization. These sources can be categorized according to the method of introduction of the material to be ionized, as discussed in the subsections that follow.

(RICHARD B. FAIR)

17.2.6.4.1. Gas Flow or Liquid Vapor.

The most common doping compound gases are BF_3, BCl_3, PCl_3, PH_3, PF_5, AsH_3, AsF_3, $AsCl_3$, SbH_3, SbF_3, CS_2, SO_2, H_2Se, H_2Te_3, and $SnCl_4$. The compound BCl_3 is convenient, but it can deactivate the electron filament if present in excess. Also, since boron halides hydrolyze readily, a clean, dry apparatus must be used. Dilute stabilized mixtures of B_2H_6 with inert gases are available, but the B-beam fraction obtained is low[2]. **The As and Sb compounds are highly toxic**, and so GaAs and elemental Sb may be preferred (see below). Sources of S or Sn are suitable. Filament deactivation may occur with PCl_3 if excess vapor is present. Since halides of P hydrolyze readily, a clean, dry apparatus must be used. Toxic PH_3 can also be used, but a large [PH] fraction is produced[2].

(RICHARD B. FAIR)

Inorganic Reactions and Methods, Volume 18
Edited by J. J. Zuckerman, Jim D. Atwood

Layers of Sb-doped SiO_2 can be deposited by means of $(CH_3)_3Sb$ vapor diluted in N_2 with SiH_4 and O_2:

$$SiH_4 + 2(CH_3)_3Sb + 15O_2 \rightleftharpoons SiO_2 + Sb_2O_5 + 6CO_2 + 11H_2O \qquad (k)$$

The addition of $(CH_3)_3Sb$ to SiH_4 decreases the SiH_4 oxidation rate. The trimethylstibine may act as a chain breaker in the oxidation of SiH_4, or the Si surface may catalyze the formation of Sb_2O_5, but not the SiO_2 formation. A similar effect is observed with the AsH_3–SiH_4 system, where the As becomes strongly bound to surface sites that are active in the pyrolysis of SiH_4[9].

(RICHARD B. FAIR)

1. A. M. Smith, in *Fundamentals of Silicon Integrated Device Technology*, R. M. Burger, R. P. Donovan, eds., Prentice Hall, Englewood Cliffs, NJ. 1967, p. 263.
2. J. Bloem, *J. Electrochem. Soc.*, *118*, 1837 (1971).
3. D. M. Brown, P. R. Kennicott, *J. Electrochem. Soc.*, *118*, 293 (1971).
4. H. J. Emeléus, K. Stewart, *J. Chem. Soc.*, 1182 (1935).
5. J. S. Kesperis, *J. Electrochem. Soc.*, *117*, 554 (1970).
6. G. R. Weber, unpublished results, 1970.
7. R. B. Fair, *J. Electrochem. Soc.*, *119*, 1389 (1972).
8. F. L. Gittler, R. A. Porter, *J. Electrochem. Soc.*, *117*, 1551 (1970).
9. R. F. C. Farrow, J. D. Filby, *J. Electrochem. Soc.*, *118*, 149 (1971).

17.2.6.4. Ion Implantation

The most useful application of ion beams is the doping of semiconductor crystals and devices by energetic ions. The type of source selected to generate singly or doubly ionized, positive or negative ions depends on performance parameters, including elements or compounds most easily ionized, total ion current, emittance, ion energy spread, brightness, size, and cost[1]. The most versatile and most commonly used sources are based on electron impact ionization. These sources can be categorized according to the method of introduction of the material to be ionized, as discussed in the subsections that follow.

(RICHARD B. FAIR)

17.2.6.4.1. Gas Flow or Liquid Vapor.

The most common doping compound gases are BF_3, BCl_3, PCl_3, PH_3, PF_5, AsH_3, AsF_3, $AsCl_3$, SbH_3, SbF_3, CS_2, SO_2, H_2Se, H_2Te_3, and $SnCl_4$. The compound BCl_3 is convenient, but it can deactivate the electron filament if present in excess. Also, since boron halides hydrolyze readily, a clean, dry apparatus must be used. Dilute stabilized mixtures of B_2H_6 with inert gases are available, but the B-beam fraction obtained is low[2]. **The As and Sb compounds are highly toxic**, and so GaAs and elemental Sb may be preferred (see below). Sources of S or Sn are suitable. Filament deactivation may occur with PCl_3 if excess vapor is present. Since halides of P hydrolyze readily, a clean, dry apparatus must be used. Toxic PH_3 can also be used, but a large [PH] fraction is produced[2].

(RICHARD B. FAIR)

1. R. G. Wilson, G. R. Brewer, *Ion Beams with Applications to Ion Implantation*, Wiley, New York, 1973.
2. G. Dearnaley, J. H. Freeman, R. S. Nelson, J. Stephen, *Ion Implantation*, North Holland, Amsterdam, 1973.

17.2.6.4.2. External Thermal Oven.

The most common source materials used in external thermal ovens are elemental solids and metal chlorides such as $AlCl_3$, $BeCl_2$, $SnCl_2$ and $MnCl_2$. Other compounds include GaAs, CdS, GaN, CdSe, ZnSe, and CdTe[1]. With elemental Al, Zn, In, Mn, etc., care must be taken to avoid metallization of insulators in the source. **Care must also be taken with $BeCl_2$ because of the formation of toxic BeO**[2].

(RICHARD B. FAIR)

1. R. C. Wilson, G. R. Brewer, *Ion Beams with Applications to Ion Implantation*, Wiley, New York, 1973.
2. G. Dearnaley, J. H. Freeman, R. S. Nelson, J. Stephen, *Ion Implantation*, North Holland, Amsterdam, 1973.

17.2.6.4.3. Sputtering, Electron Bombardment, Oxide–Chloride Conversion.

Any solid element that is not an insulator can be sputtered to produce a vapor for ionization. Elements with high sputtering coefficients and high melting temperatures, namely, In, Sn, Sb, Zn, and Cd, are best. The more refractory elements such as C and Mo should be vaporized by electron bombardment[1].

Some doping element sources exist as oxides, such as Ga_2O_3 and Cr_2O_3[2]. These metals are difficult to separate from O, but this can be done in the presence of heat and Cl[1]. When such oxides are used with CCl_4 for internal chlorination, precise temperature control is not required.

(RICHARD B. FAIR)

1. R. G. Wilson, G. R. Brewer, *Ion Beams with Applications to Ion Implantation*, Wiley, New York, 1973.
2. G. Dearnaley, J. H. Freeman, R. S. Nelson, J. Stephen, *Ion Implantation*, North Holland, Amsterdam, 1973.

17.2.6.5. Neutron Transmutation Doping

Neutron transmutation doping is the nuclear conversion of Si atoms into P dopant atoms by exposing undoped Si crystals to a suitable flux of neutrons. The mixture of Si isotopes is: $^{28}Si^- = 92.21$, $^{29}Si^- = 4.7$, and $^{30}Si^- = 3.09$. These isotopes are homogeneously distributed. During irradiation with thermal neutrons[1]:

$$^{30}Si(n, \gamma) \longrightarrow {}^{31}Si \xrightarrow{2.6\,h} {}^{31}P + \beta^- \qquad \text{(a)}$$

The formation of Si^{-31} and its decay into stable P^{31}, causes dopant atoms to be created uniformly throughout the thickness of a Si wafer. The isotopes Si^{-28} and Si^{-29} will also capture neutrons and will be transmuted into Si^{-29} and Si^{-30}, respectively. However, these reactions do not contribute to the doping process.

In neutron transmutation–doped Si, radiation damage is caused by primary γ-rays, by fast neutron bombardment, and by recoils from reaction and decay processes.

Inorganic Reactions and Methods, Volume 18
Edited by J. J. Zuckerman, Jim D. Atwood

1. R. G. Wilson, G. R. Brewer, *Ion Beams with Applications to Ion Implantation*, Wiley, New York, 1973.
2. G. Dearnaley, J. H. Freeman, R. S. Nelson, J. Stephen, *Ion Implantation*, North Holland, Amsterdam, 1973.

17.2.6.4.2. External Thermal Oven.

The most common source materials used in external thermal ovens are elemental solids and metal chlorides such as $AlCl_3$, $BeCl_2$, $SnCl_2$ and $MnCl_2$. Other compounds include GaAs, CdS, GaN, CdSe, ZnSe, and CdTe[1]. With elemental Al, Zn, In, Mn, etc., care must be taken to avoid metallization of insulators in the source. **Care must also be taken with $BeCl_2$ because of the formation of toxic BeO**[2].

(RICHARD B. FAIR)

1. R. C. Wilson, G. R. Brewer, *Ion Beams with Applications to Ion Implantation*, Wiley, New York, 1973.
2. G. Dearnaley, J. H. Freeman, R. S. Nelson, J. Stephen, *Ion Implantation*, North Holland, Amsterdam, 1973.

17.2.6.4.3. Sputtering, Electron Bombardment, Oxide–Chloride Conversion.

Any solid element that is not an insulator can be sputtered to produce a vapor for ionization. Elements with high sputtering coefficients and high melting temperatures, namely, In, Sn, Sb, Zn, and Cd, are best. The more refractory elements such as C and Mo should be vaporized by electron bombardment[1].

Some doping element sources exist as oxides, such as Ga_2O_3 and Cr_2O_3[2]. These metals are difficult to separate from O, but this can be done in the presence of heat and Cl[1]. When such oxides are used with CCl_4 for internal chlorination, precise temperature control is not required.

(RICHARD B. FAIR)

1. R. G. Wilson, G. R. Brewer, *Ion Beams with Applications to Ion Implantation*, Wiley, New York, 1973.
2. G. Dearnaley, J. H. Freeman, R. S. Nelson, J. Stephen, *Ion Implantation*, North Holland, Amsterdam, 1973.

17.2.6.5. Neutron Transmutation Doping

Neutron transmutation doping is the nuclear conversion of Si atoms into P dopant atoms by exposing undoped Si crystals to a suitable flux of neutrons. The mixture of Si isotopes is: $^{28}Si^- = 92.21$, $^{29}Si^- = 4.7$, and $^{30}Si^- = 3.09$. These isotopes are homogeneously distributed. During irradiation with thermal neutrons[1]:

$$^{30}Si(n, \gamma) \longrightarrow {}^{31}Si \xrightarrow{2.6\ h} {}^{31}P + \beta^- \qquad \text{(a)}$$

The formation of Si^{-31} and its decay into stable P^{31}, causes dopant atoms to be created uniformly throughout the thickness of a Si wafer. The isotopes Si^{-28} and Si^{-29} will also capture neutrons and will be transmuted into Si^{-29} and Si^{-30}, respectively. However, these reactions do not contribute to the doping process.

In neutron transmutation–doped Si, radiation damage is caused by primary γ-rays, by fast neutron bombardment, and by recoils from reaction and decay processes.

Inorganic Reactions and Methods, Volume 18
Edited by J. J. Zuckerman, Jim D. Atwood

1. R. G. Wilson, G. R. Brewer, *Ion Beams with Applications to Ion Implantation*, Wiley, New York, 1973.
2. G. Dearnaley, J. H. Freeman, R. S. Nelson, J. Stephen, *Ion Implantation*, North Holland, Amsterdam, 1973.

17.2.6.4.2. External Thermal Oven.

The most common source materials used in external thermal ovens are elemental solids and metal chlorides such as $AlCl_3$, $BeCl_2$, $SnCl_2$ and $MnCl_2$. Other compounds include GaAs, CdS, GaN, CdSe, ZnSe, and CdTe[1]. With elemental Al, Zn, In, Mn, etc., care must be taken to avoid metallization of insulators in the source. **Care must also be taken with $BeCl_2$ because of the formation of toxic BeO**[2].

(RICHARD B. FAIR)

1. R. C. Wilson, G. R. Brewer, *Ion Beams with Applications to Ion Implantation*, Wiley, New York, 1973.
2. G. Dearnaley, J. H. Freeman, R. S. Nelson, J. Stephen, *Ion Implantation*, North Holland, Amsterdam, 1973.

17.2.6.4.3. Sputtering, Electron Bombardment, Oxide–Chloride Conversion.

Any solid element that is not an insulator can be sputtered to produce a vapor for ionization. Elements with high sputtering coefficients and high melting temperatures, namely, In, Sn, Sb, Zn, and Cd, are best. The more refractory elements such as C and Mo should be vaporized by electron bombardment[1].

Some doping element sources exist as oxides, such as Ga_2O_3 and Cr_2O_3[2]. These metals are difficult to separate from O, but this can be done in the presence of heat and Cl[1]. When such oxides are used with CCl_4 for internal chlorination, precise temperature control is not required.

(RICHARD B. FAIR)

1. R. G. Wilson, G. R. Brewer, *Ion Beams with Applications to Ion Implantation*, Wiley, New York, 1973.
2. G. Dearnaley, J. H. Freeman, R. S. Nelson, J. Stephen, *Ion Implantation*, North Holland, Amsterdam, 1973.

17.2.6.5. Neutron Transmutation Doping

Neutron transmutation doping is the nuclear conversion of Si atoms into P dopant atoms by exposing undoped Si crystals to a suitable flux of neutrons. The mixture of Si isotopes is: $^{28}Si^- = 92.21$, $^{29}Si^- = 4.7$, and $^{30}Si^- = 3.09$. These isotopes are homogeneously distributed. During irradiation with thermal neutrons[1]:

$$^{30}Si(n, \gamma) \longrightarrow {}^{31}Si \xrightarrow{2.6\ h} {}^{31}P + \beta^- \qquad \text{(a)}$$

The formation of Si^{-31} and its decay into stable P^{31}, causes dopant atoms to be created uniformly throughout the thickness of a Si wafer. The isotopes Si^{-28} and Si^{-29} will also capture neutrons and will be transmuted into Si^{-29} and Si^{-30}, respectively. However, these reactions do not contribute to the doping process.

In neutron transmutation–doped Si, radiation damage is caused by primary γ-rays, by fast neutron bombardment, and by recoils from reaction and decay processes.

Inorganic Reactions and Methods, Volume 18
Edited by J. J. Zuckerman, Jim D. Atwood

1. R. G. Wilson, G. R. Brewer, *Ion Beams with Applications to Ion Implantation*, Wiley, New York, 1973.
2. G. Dearnaley, J. H. Freeman, R. S. Nelson, J. Stephen, *Ion Implantation*, North Holland, Amsterdam, 1973.

17.2.6.4.2. External Thermal Oven.

The most common source materials used in external thermal ovens are elemental solids and metal chlorides such as $AlCl_3$, $BeCl_2$, $SnCl_2$ and $MnCl_2$. Other compounds include GaAs, CdS, GaN, CdSe, ZnSe, and CdTe[1]. With elemental Al, Zn, In, Mn, etc., care must be taken to avoid metallization of insulators in the source. **Care must also be taken with $BeCl_2$ because of the formation of toxic BeO**[2].

(RICHARD B. FAIR)

1. R. C. Wilson, G. R. Brewer, *Ion Beams with Applications to Ion Implantation*, Wiley, New York, 1973.
2. G. Dearnaley, J. H. Freeman, R. S. Nelson, J. Stephen, *Ion Implantation*, North Holland, Amsterdam, 1973.

17.2.6.4.3. Sputtering, Electron Bombardment, Oxide–Chloride Conversion.

Any solid element that is not an insulator can be sputtered to produce a vapor for ionization. Elements with high sputtering coefficients and high melting temperatures, namely, In, Sn, Sb, Zn, and Cd, are best. The more refractory elements such as C and Mo should be vaporized by electron bombardment[1].

Some doping element sources exist as oxides, such as Ga_2O_3 and Cr_2O_3[2]. These metals are difficult to separate from O, but this can be done in the presence of heat and Cl[1]. When such oxides are used with CCl_4 for internal chlorination, precise temperature control is not required.

(RICHARD B. FAIR)

1. R. G. Wilson, G. R. Brewer, *Ion Beams with Applications to Ion Implantation*, Wiley, New York, 1973.
2. G. Dearnaley, J. H. Freeman, R. S. Nelson, J. Stephen, *Ion Implantation*, North Holland, Amsterdam, 1973.

17.2.6.5. Neutron Transmutation Doping

Neutron transmutation doping is the nuclear conversion of Si atoms into P dopant atoms by exposing undoped Si crystals to a suitable flux of neutrons. The mixture of Si isotopes is: $^{28}Si^- = 92.21$, $^{29}Si^- = 4.7$, and $^{30}Si^- = 3.09$. These isotopes are homogeneously distributed. During irradiation with thermal neutrons[1]:

$$^{30}Si(n, \gamma) \longrightarrow {}^{31}Si \xrightarrow{2.6\,h} {}^{31}P + \beta^- \qquad \text{(a)}$$

The formation of Si^{-31} and its decay into stable P^{31}, causes dopant atoms to be created uniformly throughout the thickness of a Si wafer. The isotopes Si^{-28} and Si^{-29} will also capture neutrons and will be transmuted into Si^{-29} and Si^{-30}, respectively. However, these reactions do not contribute to the doping process.

In neutron transmutation–doped Si, radiation damage is caused by primary γ-rays, by fast neutron bombardment, and by recoils from reaction and decay processes.

Annealing is necessary to eliminate this damage and to reestablish lattice order. Oxygen donor defect complexes are created after neutron irradiation of Si crystals[2]. These complexes affect the radial distribution of resistivity across a Si wafer, but annealing at 1200°C eliminates them.

(RICHARD B. FAIR)

1. H. Herzer, in *Semiconductor Silicon 1977*, H. R. Huff, E. Sirtl, eds., Electrochemical Society, Princeton, NJ, 1977, p. 106.
2. H. M. Liaw, C. J. Varker, in *Semiconductor Silicon 1977*, H. R. Huff, E. Sirtl, eds., Electrochemical Society, Princeton, NJ, 1977, p. 116.

Inorganic Reactions and Methods, Volume 18
Edited by J. J. Zuckerman, Jim D. Atwood

17.3. The Synthesis and Fabrication of Ceramics for Special Application

17.3.1. Introduction

Ceramics have many applications depending on the components. The following sections describe preparation of ceramic materials ranging from graphite (sporting equipment) to superconductors and control rods for nuclear reactors.

(JIM D. ATWOOD)

17.3.2. Preparation of Glasses for Special Applications

17.3.2.1. Bonding, Kinetic, and Other Factors That Favor Glass Formation

17.3.2.1.1. Glass Formation.

The formation of glasses is not restricted to silicate materials, nor to inorganic oxides. Organic and inorganic materials may form structures that are noncrystalline (i.e., lacking long-range order). Included are oxide materials, polymers, salts, organics, chalcogenides, and metals. Rapid cooling can prevent crystallization of any substance if the final temperature is low enough to prevent structural rearrangement. A glass is "an inorganic substance in a condition which is continuous with, and analogous to, the liquid state of that substance, but which, as the result of a reversible change in viscosity during cooling, has attained so high a degree of viscosity as to be for all practical purposes rigid"[1].

The distinction between a glass and a supercooled liquid can be illustrated by a volume–temperature diagram (Fig. 1). When a liquid that does not form a glass is cooled, it will crystallize at or slightly below the melting point (path A). If there are insufficient crystal nuclei or if the viscosity is too high to allow sufficient crystallization rates, undercooling of the liquid can occur. However, the viscosity of the liquid rapidly increases with decreasing temperatures, and atomic rearrangement slows down more than would be typical for a supercooled liquid. This results in a deviation from the metastable equilibrium curve, as shown by paths B and C in Figure 1[2].

This change in slope with temperature is characteristic of a glass. Structural rearrangement is too slow to be detected experimentally, and additional volume changes are linear with continued cooling, the same as for other solids. The cooling rate determines when the deviations begin. Thus, for example, slower cooling (path B in Fig. 1) results in deviation from the extrapolated liquid curve at lower temperature. Figure 1 shows that the point of intersection of the two slopes defines a transformation point, the glass transition temperature T_g, for a given cooling rate. Practical limitations on cooling rate limit the transformation range $T_g \rightarrow T_g'$, in which the cooling rate affects structure-sensitive properties such as density, refractive index, and volume resistivity[3]. The structure, which is frozen in during the glass transformation, persists at lower

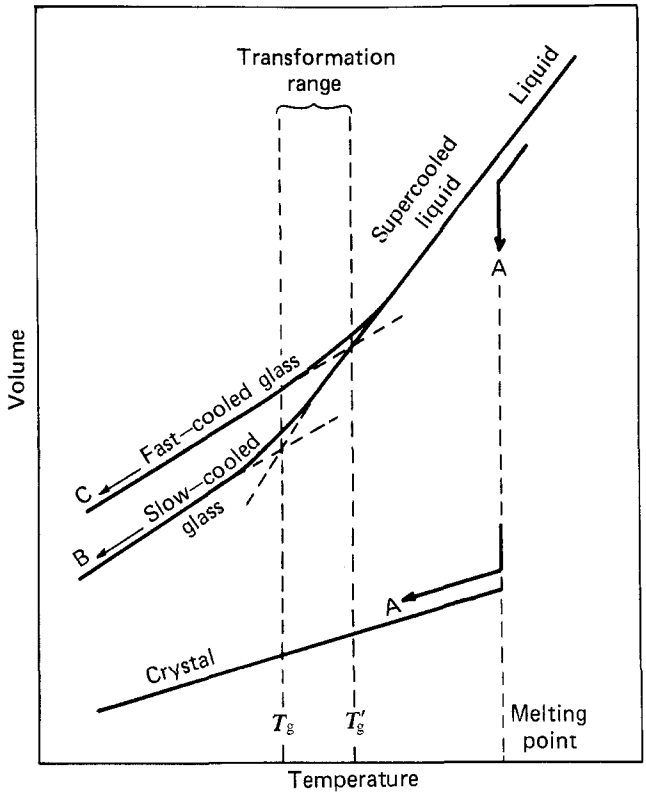

Figure 1. Volume–temperature relationships for glasses, liquids, supercooled liquids, and crystals. (From Ref. 2.)

temperatures. The fictive temperature is the temperature at which the glass structure would have been the equilibrium structure[4].

Kinetic treatments[5] suggest several factors that determine whether materials will form glasses: a high viscosity at the melting point, a large rate of increase of viscosity with falling temperature below the melting point, absence of nucleating heterogeneities, a large barrier to crystal nucleation, and a requirement that for significant redistribution of solute for crystallization.

Glasses can also be prepared by methods other than cooling from a liquid state, including solution evaporation, reactive sputtering, vapor deposition, neutron bombardment, and shock wave vitrification[6,7]. These techniques suggest that the purely kinetic explanation of the glassy state is subject to question, and that the previous definitions need to be modified. One proposal would define glasses based on isotropy and relaxation time measurements[8].

(DAVID A. THOMPSON)

1. G. W. Morey, *The Properties of Glass*, 2nd ed., Reinhold, New York, 1954, p. 28.
2. D. C. Boyd, D. A. Thompson, in *Kirk-Othmer Encyclopedia of Chemical Technology*, Vol. II, 3rd ed., Wiley, New York, 1980.

3. H. N. Ritland, *J. Am. Ceram. Soc., 37*, 370 (1954).
4. A. Q. Tool, *J. Res. Natl. Bur. Stand., 37*, 73 (1946).
5. D. R. Uhlman, *J. Non-cryst. Solids*, 0000.
6. N. J. Kreidl, *Glass Ind., 58*, 26 (1977).
7. D. R. Secrist, J.D. Mackenzie, *Glass Ind., 45*, 408, 451 (1964).
8. A. R. Cooper, P. K. Gupta, *J. Am. Ceram. Soc., 58*, 350 (1975).

17.3.2.1.2. Glass Structure.

The basic structural unit of silicate glasses is the tetrahedron, with a central silicon atom with four oxygens coordinated about it. Oxygens shared between two tetrahedra are bridging oxygens. In pure vitreous silica all the oxygens are bridging. Those that are not shared are nonbridging. The relationship between these tetrahedra causes controversy among theorists and has yet to be resolved. The crystallite theory is modified by proponents of the random network theory. However, results from modern structural methods support a description that lies between these two theories.

The index of refraction of SiO_2 near α–β transition of quartz is discontinuous[1] and X-ray investigations of vitreous silica show that crystallites are present in vitreous silica[2]. The crystal size required by the data would be less than 0.8 nm, and thus the term "crystal" loses meaning for these dimensions[3].

In the random network theory of glass[4], the atoms form a three-dimensional connected structure without periodic order and with energy content comparable to that of the corresponding crystalline material. The coordination number of an atom determines its role in a glass structure, and the fulfillment of four rules determines whether an oxide is to be a glass former:

1. Each oxygen atom must be linked to no more than two cations.
2. The number of oxygen atoms around any one cation must be small (i.e., three or four).
3. The oxygen polyhedra must share corners, not edges or faces, to form a three-dimensional network.
4. At least three corners must be shared. For one-component glasses, each polyhedron shares corners with at least three other polyhedra, such that the network is continuous in three dimensions. In multicomponent glasses additional cations are distributed throughout holes in the network.

On the basis of these rules[4,5], P_2O_3, As_2O_3, Sb_2O_3, V_2O_5, Sb_2O_5, Nb_2O_5, and Ta_2O_5, and each indeed forms glasses. The only fluoride that fulfills the rules is BeF_2, which readily forms a glass.

A relationship between bond strength and glass formation is also suggested[5]. Glass formers have cation–oxygen bond strengths greater than 335 kJ/mol. In multiple-component systems, oxides that have lower bond strengths do not become part of the network and are modifiers. Oxides that have energies near 335 kJ/mol may not become part of the network and are intermediates. The coordination number of the cation is taken into account in the calculation of the dissociation energies used to predict glass formation. In multiple-component glasses the terms *formers*, *modifiers*, and *intermediates* define the respective roles of individual oxides. However, an oxide like PbO may be either a modifier or intermediate, depending on its coordination and the glass system considered.

Other correlations of glass formation and properties include the following[6]: cation valence of 3 or greater, glass formation increases with decreasing cation size and electronegativity between 1.5 and 2.1. These criteria describe four types of oxide: (1) the

Inorganic Reactions and Methods, Volume 18
Edited by J. J. Zuckerman, Jim D. Atwood

3. H. N. Ritland, *J. Am. Ceram. Soc., 37*, 370 (1954).
4. A. Q. Tool, *J. Res. Natl. Bur. Stand., 37*, 73 (1946).
5. D. R. Uhlman, *J. Non-cryst. Solids*, 0000.
6. N. J. Kreidl, *Glass Ind., 58*, 26 (1977).
7. D. R. Secrist, J.D. Mackenzie, *Glass Ind., 45*, 408, 451 (1964).
8. A. R. Cooper, P. K. Gupta, *J. Am. Ceram. Soc., 58*, 350 (1975).

17.3.2.1.2. Glass Structure.

The basic structural unit of silicate glasses is the tetrahedron, with a central silicon atom with four oxygens coordinated about it. Oxygens shared between two tetrahedra are bridging oxygens. In pure vitreous silica all the oxygens are bridging. Those that are not shared are nonbridging. The relationship between these tetrahedra causes controversy among theorists and has yet to be resolved. The crystallite theory is modified by proponents of the random network theory. However, results from modern structural methods support a description that lies between these two theories.

The index of refraction of SiO_2 near α–β transition of quartz is discontinuous[1] and X-ray investigations of vitreous silica show that crystallites are present in vitreous silica[2]. The crystal size required by the data would be less than 0.8 nm, and thus the term "crystal" loses meaning for these dimensions[3].

In the random network theory of glass[4], the atoms form a three-dimensional connected structure without periodic order and with energy content comparable to that of the corresponding crystalline material. The coordination number of an atom determines its role in a glass structure, and the fulfillment of four rules determines whether an oxide is to be a glass former:

1. Each oxygen atom must be linked to no more than two cations.
2. The number of oxygen atoms around any one cation must be small (i.e., three or four).
3. The oxygen polyhedra must share corners, not edges or faces, to form a three-dimensional network.
4. At least three corners must be shared. For one-component glasses, each polyhedron shares corners with at least three other polyhedra, such that the network is continuous in three dimensions. In multicomponent glasses additional cations are distributed throughout holes in the network.

On the basis of these rules[4,5], P_2O_3, As_2O_3, Sb_2O_3, V_2O_5, Sb_2O_5, Nb_2O_5, and Ta_2O_5, and each indeed forms glasses. The only fluoride that fulfills the rules is BeF_2, which readily forms a glass.

A relationship between bond strength and glass formation is also suggested[5]. Glass formers have cation–oxygen bond strengths greater than 335 kJ/mol. In multiple-component systems, oxides that have lower bond strengths do not become part of the network and are modifiers. Oxides that have energies near 335 kJ/mol may not become part of the network and are intermediates. The coordination number of the cation is taken into account in the calculation of the dissociation energies used to predict glass formation. In multiple-component glasses the terms *formers*, *modifiers*, and *intermediates* define the respective roles of individual oxides. However, an oxide like PbO may be either a modifier or intermediate, depending on its coordination and the glass system considered.

Other correlations of glass formation and properties include the following[6]: cation valence of 3 or greater, glass formation increases with decreasing cation size and electronegativity between 1.5 and 2.1. These criteria describe four types of oxide: (1) the

strong glass formers (e.g., Si, B, Ge, As, P), (2) the intermediate formers that require rapid cooling (e.g., Sb, V, W, Mo, Te), (3) oxides that form glasses in binary mixtures with non-glass formers (e.g., Al, Ga, Ti, Ta, Nb, Bi), and (4) other oxides that do not form glasses.

(DAVID A. THOMPSON)

1. A. A. Lebedev, *Arb. Staatl. Opt. Inst., Leningrad, 2*, (1921).
2. J. T. Randall, H. P. Rooksby, B. S. Cooper, *J. Soc. Glass Technol., 14*, 219 (1930); N. Valenkov, E. Pori-Koshitz, Z. Kristallogr., *45*, 195 (1936).
3. B. E. Warren, I. Biscoe, *J. Am. Ceram. Soc., 21*, 49 (1938).
4. W. H. Zachariasen, *J. Am. Chem. Soc., 54*, 3841 (1932).
5. K.H. Sun, *J. Am. Ceram. Soc., 30*, 277 (1947).
6. J. E. Stanworth, *J. Am. Ceram. Soc., 54*, 61 (1971).

17.3.2.1.3. Composition of Glasses.

The majority of glasses are silicates that contain modifiers and intermediates. Addition of a modifier such as NaO_2 to the silica network will alter the structure by cleaving the Si—O—Si bonds to form Si—O—Na linkages at temperatures below the melting points of pure metals[1]:

$$Na_2CO_3 + SiO_2 \xrightarrow{50°C} Na_2SiO_3 + CO_2 \quad \text{(a)}$$

$$Na_2SiO_3 + SiO_2 \xrightarrow{700°C} Na_2Si_2O_5 \quad \text{(b)}$$

Continued heating to 780°C yields a eutectic of $3Na_2O \cdot 7SiO_2$ composition.

Separating the silica tetrahedra makes the glass more fluid and, therefore, more amenable to conventional melting and forming methods. Modifiers also cause decreases in resistivity, increases in thermal expansion and, lower chemical durability. Glasses with a SiO_2:Na_2O molecular ratio less than one have so many nonbridging oxygens that they lack a continuous, three-dimensional structure (see criterion 4 in 17.3.3.1.2).

The effectiveness of an alkali oxide (Li_2O, Cs_2O) as flux to decrease viscosity increases with its' size of the cation and, therefore, with the polarizability. Large ions such as Cs^+ are easily polarized and thus more likely to give up their oxygen to break the Si—O—Si bonds (see above). Lithium, on the other hand, is more likely to keep its oxygen, so its fluxing power is less. This behavior is consistent with the case of glass formation as the size-to-charge ratio of the modifier is increased. Phase separation can occur when less polarizable oxides are present[2]. Alkaline earth silicates are similar to alkali silicates, but the alkaline earths have less fluxing power than the alkalies. Divalent ions are less mobile than monovalent; hence resistivities of alkaline earth glasses are higher. Divalent oxides increase the resistivity of alkali-containing glasses.

Alumina occurs frequently in silicate glasses, adopting a four-coordinated structure with alkalies to give an $NaAlO_2$ tetrahedral unit that substitutes into the SiO_2 network. The extra negative charge associated with four bridging oxygens surrounding Al^{3+} is offset by the Na^+ ion. A maximum in viscosity occurs at unit ratio of Al_2O_3:Na_2O.

Boron oxide can behave as a flux (i.e., soften glass for easier melting); unlike alkalies, however, boron oxide increases expansion only slightly. This is the basis of the class of low in expansion commercial borosilicates that melt relatively.

(DAVID A. THOMPSON)

Inorganic Reactions and Methods, Volume 18
Edited by J. J. Zuckerman, Jim D. Atwood

strong glass formers (e.g., Si, B, Ge, As, P), (2) the intermediate formers that require rapid cooling (e.g., Sb, V, W, Mo, Te), (3) oxides that form glasses in binary mixtures with non–glass formers (e.g., Al, Ga, Ti, Ta, Nb, Bi), and (4) other oxides that do not form glasses.

(DAVID A. THOMPSON)

1. A. A. Lebedev, *Arb. Staatl. Opt. Inst., Leningrad, 2*, (1921).
2. J. T. Randall, H. P. Rooksby, B. S. Cooper, *J. Soc. Glass Technol., 14*, 219 (1930); N. Valenkov, E. Pori-Koshitz, Z. Kristallogr., *45*, 195 (1936).
3. B. E. Warren, I. Biscoe, *J. Am. Ceram. Soc., 21*, 49 (1938).
4. W. H. Zachariasen, *J. Am. Chem. Soc., 54*, 3841 (1932).
5. K.H. Sun, *J. Am. Ceram. Soc., 30*, 277 (1947).
6. J. E. Stanworth, *J. Am. Ceram. Soc., 54*, 61 (1971).

17.3.2.1.3. Composition of Glasses.

The majority of glasses are silicates that contain modifiers and intermediates. Addition of a modifier such as NaO_2 to the silica network will alter the structure by cleaving the Si—O—Si bonds to form Si—O—Na linkages at temperatures below the melting points of pure metals[1]:

$$Na_2CO_3 + SiO_2 \xrightarrow{50°C} Na_2SiO_3 + CO_2 \quad \text{(a)}$$

$$Na_2SiO_3 + SiO_2 \xrightarrow{700°C} Na_2Si_2O_5 \quad \text{(b)}$$

Continued heating to 780°C yields a eutectic of $3Na_2O \cdot 7SiO_2$ composition.

Separating the silica tetrahedra makes the glass more fluid and, therefore, more amenable to conventional melting and forming methods. Modifiers also cause decreases in resistivity, increases in thermal expansion and, lower chemical durability. Glasses with a SiO_2:Na_2O molecular ratio less than one have so many nonbridging oxygens that they lack a continuous, three-dimensional structure (see criterion 4 in 17.3.3.1.2).

The effectiveness of an alkali oxide (Li_2O, Cs_2O) as flux to decrease viscosity increases with its' size of the cation and, therefore, with the polarizability. Large ions such as Cs^+ are easily polarized and thus more likely to give up their oxygen to break the Si—O—Si bonds (see above). Lithium, on the other hand, is more likely to keep its oxygen, so its fluxing power is less. This behavior is consistent with the case of glass formation as the size-to-charge ratio of the modifier is increased. Phase separation can occur when less polarizable oxides are present[2]. Alkaline earth silicates are similar to alkali silicates, but the alkaline earths have less fluxing power than the alkalies. Divalent ions are less mobile than monovalent; hence resistivities of alkaline earth glasses are higher. Divalent oxides increase the resistivity of alkali-containing glasses.

Alumina occurs frequently in silicate glasses, adopting a four-coordinated structure with alkalies to give an $NaAlO_2$ tetrahedral unit that substitutes into the SiO_2 network. The extra negative charge associated with four bridging oxygens surrounding Al^{3+} is offset by the Na^+ ion. A maximum in viscosity occurs at unit ratio of Al_2O_3:Na_2O.

Boron oxide can behave as a flux (i.e., soften glass for easier melting); unlike alkalies, however, boron oxide increases expansion only slightly. This is the basis of the class of low in expansion commercial borosilicates that melt relatively.

(DAVID A. THOMPSON)

1. C. V. Thomasson, F. W. Wilburn, *Phys. Chem. Glasses, 1*, 52 (1960).
2. V. I. Aver'yanov, E. A. Porai-Koshits, *The Structure of Glass*, Vol. 6, Part 1, Consultants Bureau, New York, 1966, p. 98.

17.3.2.2. Glasses for Light Transmission; Fiber Optics

17.3.2.2.1. Optical Fiber Characteristics.

Transmission of light in glass fibers is used in medical devices[1,2] called fiberscopes, in cathode ray tube faceplaces, and to provide flexible or remote light sources for automobile instrument panels and similar applications. Now glass technology[3,4] makes long-range telecommunication systems possible. Optical waveguide glass fiber made from vapor phase deposited raw materials are sufficiently impurity-free to be able to transmit light over many kilometers with attenuation of less than 1 db/km. Light is contained within the waveguide by controlling reflection losses between core and cladding glasses. Typically, a GeO_2–SiO_2 core glass and a SiO_2 cladding glass of lower refractive index transmit light falling within a specific angle.

There are single and multimode fibers. A fiber is called multimode if its core diameter, the difference of refractive index between core and cladding, and the

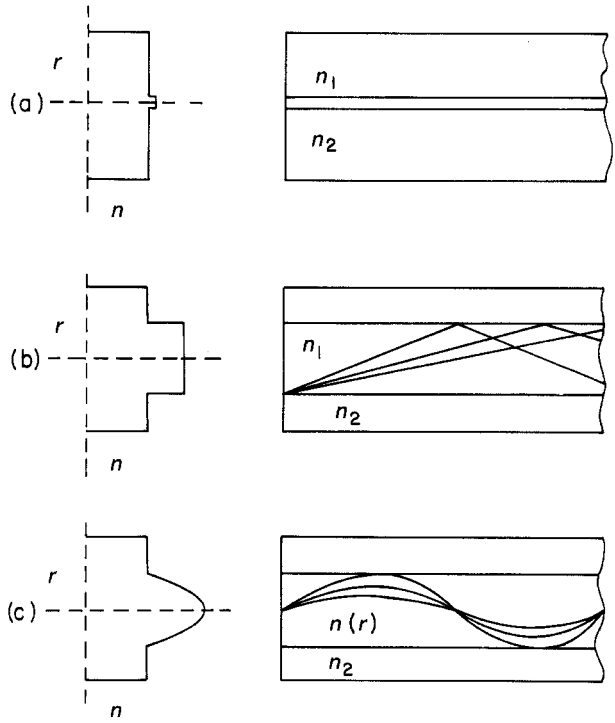

Figure 1. Optical waveguide types: (a) Single mode, (b) multimode step index, and (c) multimode graded index.

Inorganic Reactions and Methods, Volume 18
Edited by J. J. Zuckerman, Jim D. Atwood

1. C. V. Thomasson, F. W. Wilburn, *Phys. Chem. Glasses, 1*, 52 (1960).
2. V. I. Aver'yanov, E. A. Porai-Koshits, *The Structure of Glass*, Vol. 6, Part 1, Consultants Bureau, New York, 1966, p. 98.

17.3.2.2. Glasses for Light Transmission; Fiber Optics

17.3.2.2.1. Optical Fiber Characteristics.

Transmission of light in glass fibers is used in medical devices[1,2] called fiberscopes, in cathode ray tube faceplaces, and to provide flexible or remote light sources for automobile instrument panels and similar applications. Now glass technology[3,4] makes long-range telecommunication systems possible. Optical waveguide glass fiber made from vapor phase deposited raw materials are sufficiently impurity-free to be able to transmit light over many kilometers with attenuation of less than 1 db/km. Light is contained within the waveguide by controlling reflection losses between core and cladding glasses. Typically, a GeO_2–SiO_2 core glass and a SiO_2 cladding glass of lower refractive index transmit light falling within a specific angle.

There are single and multimode fibers. A fiber is called multimode if its core diameter, the difference of refractive index between core and cladding, and the

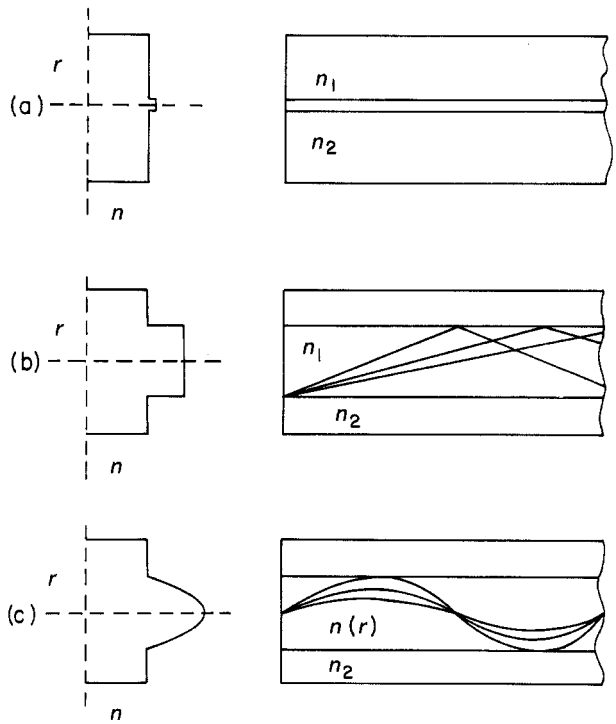

Figure 1. Optical waveguide types: (a) Single mode, (b) multimode step index, and (c) multimode graded index.

wavelength of light being used allow propagation of light traveling at various angles within the fiber (see Fig. 1). Two light rays launched simultaneously, one along the fiber axis and the other at an off-axis angle, will have different path lengths and will arrive separately at the end of the fiber. This effect, called pulse dispersion, limits the rate at which distinguishable pulses can be transmitted. A graded index multimode fiber decreases differences in the light paths by providing a high index at the center (lowest velocity) and a radially decreasing index. Reductions of pulse width of more than 100 fold are achieved by refractive index grading in this manner. Single-mode fibers have lower dispersion than a simple step index multimode fiber and therefore are able to transmit at significantly higher data rates. Small core size makes alignment for coupling more difficult than for multiple-mode fiber.

(DAVID A. THOMPSON)

1. J. W. Hicks Jr.; U.S. Patent 3,004,368 (1961, Optical Company).
2. R. R. Strock, R.A. Phaneuf; U.S. Patent 3,624,816 (1971).
3. P. C. Schultz, in *Fiber Optics: Advances in Research and Development*, B. Bendow, S. S. Mitra eds., lenum Press, New York, 1979.
4. P. C. Schultz, *Appl. Opt., 18*, 3684 (1979); *Chem. Abstr.*, 91219463.

17.3.2.2.2. Vapor Phase Oxidation Techniqes.

Fibers are drawn from a blank or preform that is prepared by vapor deposition. Reactions of $SiCl_4$, $GeCl_4$, BCl_3, and $POCl_3$ are used to produce glasses of $SiO_2 \cdot GeO_2$, $SiO_2 \cdot B_2O_3 \cdot GeO_2$ or $SiO_2 \cdot B_2O_3$ and P_2O_5–GeO_2–SiO_2 glass-forming systems. Volatile halides are held at a constant temperature to produce a vapor pressure sufficient to deliver required amounts of materials (Fig. 1) Temperatures are below 50°C to minimize concentrations of less volatile impurities such as $FeCl_3$, VCl_4 and $CuCl_2$ which absorb light strongly in the visible and near-infrased regions. The first and second hydroxyl ($\sim$ 1400 and 930 nm, respectively) also absorb, but may be minimized by gaseous chlorine treatment of the preform[1]. The reaction kinetics[2] of metal-halide oxidation within a methane–oxygen gas flame suggest that the oxidation is 99% complete in 0.58 s at 1300°C, 0.09 s at 1400°C and an estimated 0.004 s at 1600°C:

$$SiCl_4 + O_2 \longrightarrow SiO_2 + 2Cl_2 \qquad \text{(a)}$$

Rate are comparable for $GeCl_4$ and BCl_3, but $POCl_3$ is slower.

Volatile organometallic or non halide raw materials such as SiH_4, $(CH_3)_3B$, $Si(CH_3)_4$, $(C_2H_5)_2Zn$, and $(CH_3)_3P$, offer viable alternatives[3]. Reactants necessary to achieve each glass composition must be selected to minimize effects of ligand exchange, adduct formation and thermal instability.

Figure 2 depicts the outside vapor phase depostion (OVD) process. Metal halide vapors are transported by oxygen carrier gas via a bubbler system through mass flow controllers to be mixed, delivered to a burner, and reacted in a gas–oxygen flame to form particles called soot. Soot is collected on a removable porous rod (bait rod) during repeated traverses of the burner along a rotating rod. The burner produces soot having a particle diameter of less than 0.1 μm and a surface area of 20 m^2/g at about 2 g/min (Fig. 2). The composition of the soot may be varied by flow adjustments to obtain profiles of compostion that control refractive index layer-by-layer deposition. Preforms are sintered at 1200–1500°C in a controlled atmosphere (e.g., He[4]) to a bubble-free glass blank from which fiber is drawn. The central hole (from the porous bait rod) closes during sintering or during fiber draw at 1800–2200°C.

Inorganic Reactions and Methods, Volume 18
Edited by J. J. Zuckerman, Jim D. Atwood

wavelength of light being used allow propagation of light traveling at various angles within the fiber (see Fig. 1). Two light rays launched simultaneously, one along the fiber axis and the other at an off-axis angle, will have different path lengths and will arrive separately at the end of the fiber. This effect, called pulse dispersion, limits the rate at which distinguishable pulses can be transmitted. A graded index multimode fiber decreases differences in the light paths by providing a high index at the center (lowest velocity) and a radially decreasing index. Reductions of pulse width of more than 100 fold are achieved by refractive index grading in this manner. Single-mode fibers have lower dispersion than a simple step index multimode fiber and therefore are able to transmit at significantly higher data rates. Small core size makes alignment for coupling more difficult than for multiple-mode fiber.

(DAVID A. THOMPSON)

1. J. W. Hicks Jr.; U.S. Patent 3,004,368 (1961, Optical Company).
2. R. R. Strock, R.A. Phaneuf; U.S. Patent 3,624,816 (1971).
3. P. C. Schultz, in *Fiber Optics: Advances in Research and Development*, B. Bendow, S. S. Mitra eds., lenum Press, New York, 1979.
4. P. C. Schultz, *Appl. Opt., 18*, 3684 (1979); *Chem. Abstr.*, 91219463.

17.3.2.2.2. Vapor Phase Oxidation Techniqes.

Fibers are drawn from a blank or preform that is prepared by vapor deposition. Reactions of $SiCl_4$, $GeCl_4$, BCl_3, and $POCl_3$ are used to produce glasses of $SiO_2 \cdot GeO_2$, $SiO_2 \cdot B_2O_3 \cdot GeO_2$ or $SiO_2 \cdot B_2O_3$ and P_2O_5–GeO_2–SiO_2 glass-forming systems. Volatile halides are held at a constant temperature to produce a vapor pressure sufficient to deliver required amounts of materials (Fig. 1) Temperatures are below 50°C to minimize concentrations of less volatile impurities such as $FeCl_3$, VCl_4 and $CuCl_2$ which absorb light strongly in the visible and near-infrased regions. The first and second hydroxyl ($\sim$ 1400 and 930 nm, respectively) also absorb, but may be minimized by gaseous chlorine treatment of the preform[1]. The reaction kinetics[2] of metal-halide oxidation within a methane–oxygen gas flame suggest that the oxidation is 99% complete in 0.58 s at 1300°C, 0.09 s at 1400°C and an estimated 0.004 s at 1600°C:

$$SiCl_4 + O_2 \longrightarrow SiO_2 + 2Cl_2 \qquad \text{(a)}$$

Rate are comparable for $GeCl_4$ and BCl_3, but $POCl_3$ is slower.

Volatile organometallic or non halide raw materials such as SiH_4, $(CH_3)_3B$, $Si(CH_3)_4$, $(C_2H_5)_2Zn$, and $(CH_3)_3P$, offer viable alternatives[3]. Reactants necessary to achieve each glass composition must be selected to minimize effects of ligand exchange, adduct formation and thermal instability.

Figure 2 depicts the outside vapor phase depostion (OVD) process. Metal halide vapors are transported by oxygen carrier gas via a bubbler system through mass flow controllers to be mixed, delivered to a burner, and reacted in a gas–oxygen flame to form particles called soot. Soot is collected on a removable porous rod (bait rod) during repeated traverses of the burner along a rotating rod. The burner produces soot having a particle diameter of less than 0.1 μm and a surface area of 20 m^2/g at about 2 g/min (Fig. 2). The composition of the soot may be varied by flow adjustments to obtain profiles of compostion that control refractive index layer-by-layer deposition. Preforms are sintered at 1200–1500°C in a controlled atmosphere (e.g., He[4]) to a bubble-free glass blank from which fiber is drawn. The central hole (from the porous bait rod) closes during sintering or during fiber draw at 1800–2200°C.

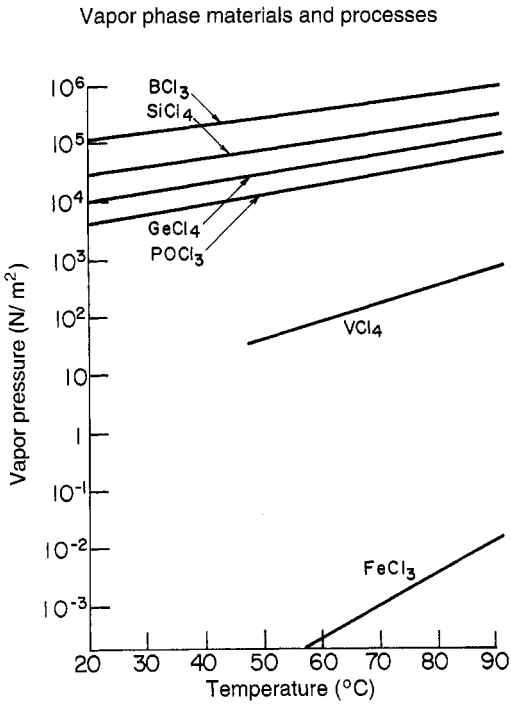

Figure 1. Relation of vapor pressures for metal halide additives and some potential impurities.

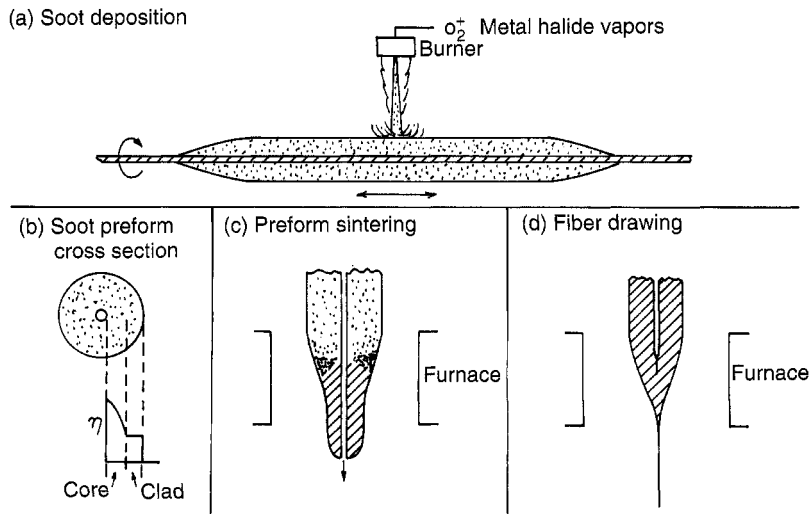

Figure 2. Schematic representation of the lateral deposition version of the OVD process.

In the inside vapor phase deposition process (IVD) a silica glass tube (25 mm o.d. × 1.5 mm wall × 1 m long) is used to contain volatile halide fumes, which are carried by oxygen gas. An oxygen–hydrogen burner traverses the outside of the rotating tube, causing metal halide oxidation to produce a core glass ~0.5 mm thick on the inside of the tube. The burner temperature is increased to collapse the tube, which becomes the cladding of the fiber. Alternatives to burners include microwave and plasma processing[5] by the IVD process, which deposite a layer of glass from the vapor phase.

Blanks of vapor phase deposited glass can also be prepared by axially depositing both core and cladding glasses onto the end of a target rod[5]. The porous soot rod is then drawn slowly through a furnace, where it is consolidated prior to drawing fiber [Vapor phase axial deposition (VAD) process]. It is easy to envision a continuous process of deposition, consolidation, and drawing of fiber by the VAD method.

An approach comparable to that for directly melted glasses is collection of the soot from high purity, vapor phase deposition and melting in containers designed to draw a composite fiber[6]. Low melting (~1400°C) glasses in the Ga_2O_3–GeO_2–P_2O_5 system produce step index fibers of 0.2–0.3 numerical aperture and attenuation of less than 10 dB/km at 820 nm. Gradient index fibers are prepared by melting Na_2O–B_2O_3–SiO_2 glasses containing BaO or CaO to achieve an index difference by diffusion during fiber draw[7].

(DAVID A. THOMPSON)

1. R. D. DeLuca, U.S. Patent *3*, 933,454 (1976).
2. D. R. Powers, *J. Am, Ceram, Sec., 61*, 295 (1978), Chem. Abstr., 89095628.
3. Stephen B. Miller, *Abstr. Am. Chem. Soc. Meeting*, 1980.
4. D. B. Keck, P.C. Schultz, F. Zimar, U.S. Patent Re 28, 029 (1974).
5. P. C. Schultz, *Appl. Opt.*, 18, 3684 (1979).
6. K. Inoue, J. Goto, T. Arima, O.Nakamura, T. Akamatsu, *Abstr, Int. Conf. Integrated Optics and Optical Fiber Communications*, Tokyo, July 1977, p. 387.
7. K. J. Beales, C.R. Day, W. J. Duncan, A. C. Dunn, P. L. Dunn, G. R. Newns, S. Partington, *Am. Ceram. Soc. Ann. Meeting*, Cincinnati, OH, May, 1979, p. 378.

17.3.2.3. High Index of Refractive Glasses

Typical refractive indices of oxide glass range from 1.4 for borosilicate to 1.51 for soda–lime silica types. Ranges of refractive index for optical glasses are indicated in Figure 1. The measure of variation of refractive index with wavelength, called dispersion, is V_d, where $V_d = (n_d - 1)/(n_F - n_C)$, and d, F, and C refer to heluim d, and hydrogen F, and hydrogen C lines at 587.6, 486.1, and 656.3 nm, respectively. A review of the physical and optical properties of common optical glasses appears in Figure 1[1].

The interaction between a glass and light is related to the susceptibility of displacement of electrical charge, which in turn is related to the polarizability. Ionic polarizability increases with the size of ions involved; however, structural considerations are also important. Refractive index (see Table 1), dielectric constant, polarizability, and molar volume are related in the molar refractivity, R_m:

$$R_m = \frac{V_m(n^2 - 1)}{(n^2 + 1)} \qquad \text{(a)}$$

Inorganic Reactions and Methods, Volume 18
Edited by J. J. Zuckerman, Jim D. Atwood

In the inside vapor phase deposition process (IVD) a silica glass tube (25 mm o.d. × 1.5 mm wall × 1 m long) is used to contain volatile halide fumes, which are carried by oxygen gas. An oxygen–hydrogen burner traverses the outside of the rotating tube, causing metal halide oxidation to produce a core glass ~0.5 mm thick on the inside of the tube. The burner temperature is increased to collapse the tube, which becomes the cladding of the fiber. Alternatives to burners include microwave and plasma processing[5] by the IVD process, which deposite a layer of glass from the vapor phase.

Blanks of vapor phase deposited glass can also be prepared by axially depositing both core and cladding glasses onto the end of a target rod[5]. The porous soot rod is then drawn slowly through a furnace, where it is consolidated prior to drawing fiber [Vapor phase axial deposition (VAD) process]. It is easy to envision a continuous process of deposition, consolidation, and drawing of fiber by the VAD method.

An approach comparable to that for directly melted glasses is collection of the soot from high purity, vapor phase deposition and melting in containers designed to draw a composite fiber[6]. Low melting (~1400°C) glasses in the Ga_2O_3–GeO_2–P_2O_5 system produce step index fibers of 0.2–0.3 numerical aperture and attenuation of less than 10 dB/km at 820 nm. Gradient index fibers are prepared by melting Na_2O–B_2O_3–SiO_2 glasses containing BaO or CaO to achieve an index difference by diffusion during fiber draw[7].

(DAVID A. THOMPSON)

1. R. D. DeLuca, U.S. Patent *3*, 933,454 (1976).
2. D. R. Powers, *J. Am, Ceram, Sec., 61*, 295 (1978), Chem. Abstr., 89095628.
3. Stephen B. Miller, *Abstr. Am. Chem. Soc. Meeting*, 1980.
4. D. B. Keck, P.C. Schultz, F. Zimar, U.S. Patent Re 28, 029 (1974).
5. P. C. Schultz, *Appl. Opt.*, 18, 3684 (1979).
6. K. Inoue, J. Goto, T. Arima, O.Nakamura, T. Akamatsu, *Abstr, Int. Conf. Integrated Optics and Optical Fiber Communications*, Tokyo, July 1977, p. 387.
7. K. J. Beales, C.R. Day, W. J. Duncan, A. C. Dunn, P. L. Dunn, G. R. Newns, S. Partington, *Am. Ceram. Soc. Ann. Meeting*, Cincinnati, OH, May, 1979, p. 378.

17.3.2.3. High Index of Refractive Glasses

Typical refractive indices of oxide glass range from 1.4 for borosilicate to 1.51 for soda–lime silica types. Ranges of refractive index for optical glasses are indicated in Figure 1. The measure of variation of refractive index with wavelength, called dispersion, is V_d, where $V_d = (n_d - 1)/(n_F - n_C)$, and d, F, and C refer to heluim d, and hydrogen F, and hydrogen C lines at 587.6, 486.1, and 656.3 nm, respectively. A review of the physical and optical properties of common optical glasses appears in Figure 1[1].

The interaction between a glass and light is related to the susceptibility of displacement of electrical charge, which in turn is related to the polarizability. Ionic polarizability increases with the size of ions involved; however, structural considerations are also important. Refractive index (see Table 1), dielectric constant, polarizability, and molar volume are related in the molar refractivity, R_m:

$$R_m = \frac{V_m(n^2 - 1)}{(n^2 + 1)} \qquad \text{(a)}$$

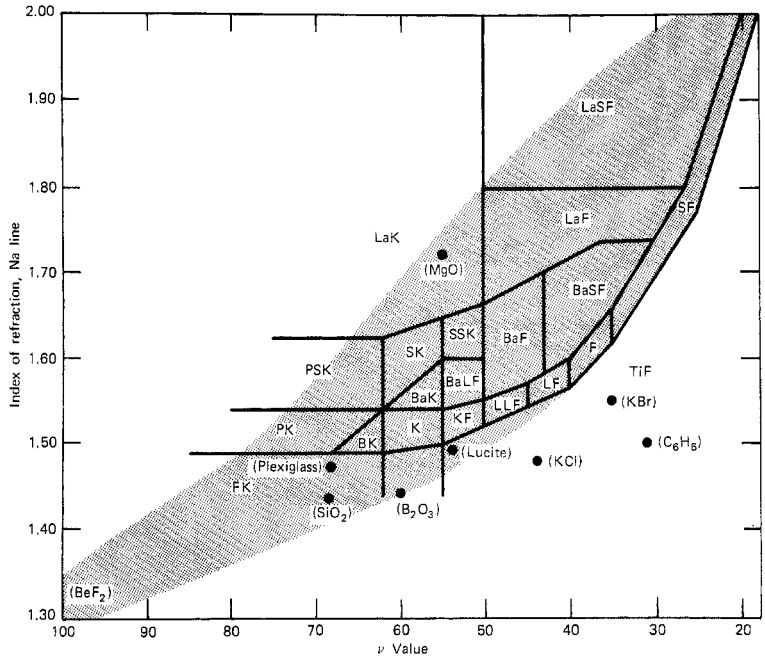

Figure 1. Index of refraction versus dispersion and optical classification of glasses; shaded area indicates region of glass formation M. Plexiglas is a methyl methacrylate; Lucite is an acrylic resin. BaF, barium flint; BaK, Barium crown; Balf, light barium flint; BaSF, heavy barium flint; BK, borosilicate crown; F, flint; FK, fluorcrown; K, crown; KF, crown flint; LaF, lanthanum flint; LaSF, heavy lanthanum flint; LaK, lanthanum crown; LF, light flint; LLF, very light flint; PK, phosphate crown; PSK, heavy phosphate crown; SF, heavy flint; SK, heavy crown, SSK, very heavy crown, TiF, titanium flint.

Table 1. Refractive Indices of Several Inorganic Compounds n_d

Glasses		Compounds	
BeF_2	1.275	SiO_2	
B_2O_3	1.485	α-Quartz	1.544–1.553
SiO_2	1.458	Tridymite	1.469–1.473
GeO_2	1.607	Cristobalite	1.484–1.487
		LiF	1.392
		NaF	1.325
		KF	1.361
		CaF	1.478
		NaCl	1.550
		NaBr	1.641

where, V_m = molar volume and n = refractive index. For a compound (X_aY_b) the molar refractivity is related to contributions of X and Y ($R_m = aR_x + bR_y$) for ionic compounds. Oxygen anions contribute the most to R_m for oxide glasses. However, the molar refractivity of oxygen depends on effects of adjacent modifiers and on whether the oxygen

anion is bridging. Glasses of high refractive index have low molar volume, which frequently means the glass has high density.

(DAVID A. THOMPSON)

1. G. W. Movy, The Prospectus of Glass, 2nd Ed., Reinfold Publishing Corp., New York, 1954, p. 28.

17.3.2.3.1. Glass Composition.

Reviews of glass compositions of importance for optical applications[1], including a quantum mechanical treatment[2], are numerous. Tabulations of properties of optical glasses and simple glass -forming systems are a useful starting point, as are descriptions of properties of commercial optical glasses[3]. The oxides that occur frequently in optical glasses are shown in Table 1. Correlations between dispersion, density, and refractive index in a class of glasses (eg., lead silicates) may be changed dramatically by a different glass composition. Barium-containing glasses have lower dispersion than lead glasses, but the refractive indices of these glasses are comparable. This is related to absorption characteristics of Pbo-containing glasses[4]. Lanthanum also increases n_d with less increase in dispersion than other oxides[5,6]. Germania additions for silica increase both index dispersion.

High indices may be achieved with the $PbO \cdot Bi_2O_3$ glasses[7] (~ 2.5) or chalcogenide glasses, As_2S_3 ($n_d = 2.65$), or the As–Ge–Se system. Chalcogenide melts are made in sealed and evacuated thick-walled silica glass tubes, which are heated to $\sim 1000°C$. A rocking motion of the tube assures homogeneity[8,9]. Chalcogenide glasses and crystalline Ge ($n_d \sim 4.1$) are most important for their infrared transmitting properties.

TABLE 1. OXIDES FREQUENTLY USED IN OPTICAL GLASSES TO ACHIEVE A HIGH REFRACTIVE INDEX

Oxide	Density of Oxide (g/cm^3)	Glass Formation range of Binary Silicate System (mol % SiO_2)
ThO_2	9.86	
Tl_2O	9.52	100–60
PbO	9.5	100–33
Bi_2O_3	8.76	100–53.5
Ta_2O_5	8.2	
CdO	8.15	100–44
Gd_2O_3	7.64	
La_2O_3	6.48	
GeO_2	6.24	100–0
TeO_2	5.76	
BaO	5.72	100–60
ZnO	5.61	100–51.3
ZrO_2	5.6	
B_2O_3	4.84	
Nb_2O_5	4.47	
TiO_3	4.27	100–92.7
SiO_2 (Tridymite)	2.26	

Inorganic Reactions and Methods, Volume 18
Edited by J. J. Zuckerman, Jim D. Atwood

anion is bridging. Glasses of high refractive index have low molar volume, which frequently means the glass has high density.

(DAVID A. THOMPSON)

1. G. W. Movy, The Prospectus of Glass, 2nd Ed., Reinfold Publishing Corp., New York, 1954, p. 28.

17.3.2.3.1. Glass Composition.

Reviews of glass compositions of importance for optical applications[1], including a quantum mechanical treatment[2], are numerous. Tabulations of properties of optical glasses and simple glass -forming systems are a useful starting point, as are descriptions of properties of commercial optical glasses[3]. The oxides that occur frequently in optical glasses are shown in Table 1. Correlations between dispersion, density, and refractive index in a class of glasses (eg., lead silicates) may be changed dramatically by a different glass composition. Barium-containing glasses have lower dispersion than lead glasses, but the refractive indices of these glasses are comparable. This is related to absorption characteristics of Pbo-containing glasses[4]. Lanthanum also increases n_d with less increase in dispersion than other oxides[5,6]. Germania additions for silica increase both index dispersion.

High indices may be achieved with the $PbO \cdot Bi_2O_3$ glasses[7] ($\sim$2.5) or chalcogenide glasses, As_2S_3 ($n_d = 2.65$), or the As–Ge–Se system. Chalcogenide melts are made in sealed and evacuated thick-walled silica glass tubes, which are heated to $\sim$1000°C. A rocking motion of the tube assures homogeneity[8,9]. Chalcogenide glasses and crystalline Ge ($n_d \sim 4.1$) are most important for their infrared transmitting properties.

TABLE 1. OXIDES FREQUENTLY USED IN OPTICAL GLASSES TO ACHIEVE A HIGH REFRACTIVE INDEX

Oxide	Density of Oxide (g/cm^3)	Glass Formation range of Binary Silicate System (mol % SiO_2)
ThO_2	9.86	
Tl_2O	9.52	100–60
PbO	9.5	100–33
Bi_2O_3	8.76	100–53.5
Ta_2O_5	8.2	
CdO	8.15	100–44
Gd_2O_3	7.64	
La_2O_3	6.48	
GeO_2	6.24	100–0
TeO_2	5.76	
BaO	5.72	100–60
ZnO	5.61	100–51.3
ZrO_2	5.6	
B_2O_3	4.84	
Nb_2O_5	4.47	
TiO_3	4.27	100–92.7
SiO_2 (Tridymite)	2.26	

The refractive indices of alkali silicate glasses ($Na_2O \cdot SiO_2$) vary linearly with modifier concentration. Where change of coordination occurs such as with B_2O_3, Al_2O_3, or Geo_2[10], maxima and minima of refractive index vs. composition are observed.

Glasses frequently require composition control to ensure compliance with standards of chemical corrosion resistance, glass quality, resistance to crystallization, and density, color, and grinding or polishing characteristics in addition to optical properties.

(DAVID A. THOMPSON)

1. M. A. Matveev, G. M. Matveev, B. N. Frenkel, *Calculation and Control of Electrical, Optical and Thermal Properties of Glass*, Ordentlich, Holon, Israel, 1975.
2. S. T. Pantelides, W. A. Harrison, *Phys, Rev., 13*, 2667 (1976); *Chem. Abstr.*, 85010530.
3. C. J. Parker, *Optical Materials—Refractive, Applied Optics and Optical Engineering*, Vol, VII, Academic Press, Newyork, 1979, p. 47.
4. B. Kim, M. Yamane, *Yogyo Kyokaikshi, 88*, 191 (1980); *Chem, Abstr.*, 93100303.
5. E. H. Hamilton, O. H. Graver, Z. Zabawsky, C. H. Hahner, *J. Res. Natl. Bur. Stand., 40*, 361 (1948).
6. B. Kim, M. Yamane, Yogyo Kyokaikshi, *J. Am. Ceram. Soc., 31*, 132 (1948); *Chem. Abstr.*, 42005183.
7. W. H. Dumbaugh, *Phys. Chem. Glasses, 19*, 121 (1978).
8. A. E. Owen, *Contemp. Phys., 11*, 227 (1970).
9. K. Weiser, *Prog. Solid-State Chem., 11*, 403 (1976).
10. H. Rawson, D. Warner, *J. Non-Cryst. Solids, 29*, 231 (1978).

17.3.2.3.2. Applications.

Some oxide glasses have refractive indices of about 2.0 or above. The glass microspheres (50–100 μm diameter) used to reflect light in paints for signs, auto license plates etc[1] contain greater than 50 (mol %) PBO, Bi_2O_3, TiO_2, or TEO_2 for high refractive index, in addition to silica and other glass modifiers. Beads of glass may also contain colorants which selectively absorb visible light but transmit in the infrared[2]. Although beads are made by melting, crushing and grinding, and passing the material particles through a flame to form spheres, the gel route is also used to prepare TiO_2-containing spheres[3].

Optical glass compositions are designed to facilitate the melting and forming of high quality glass pieces. Refractive index control is achieved by composition control; however, a post forming annealing treatment can be used to adjust the refractive index by altering density. Optical glasses can have either anomalously high or low dispersions[4] based on the chart given earlier (Fig. 1 in 17.3.2.3).Thoria, although useful for achieving high refractive index, is used infrequently owing to its radioactivity. Glasses containing PbO ($n_d > 1.7$) are hydrated in steam at $\sim 300°C$[5] to lower T_g enough to permit optical quality lenses to be molded at low temperature[6].

High index fibers from conventional melts contain oxides such as Nb_2O_5 and Ta_2O_5 and others listed on Table 1 in 17.3.2.3.1. Glasses containing Tl_2O ($n_d \sim 1.8$) exchange K^+ for Tl^+ in a bath of molten KNO_3 at $\sim 500°C$. The resulting composition profile produces a parabolic index profile, with high index ($n_d \sim 1.6$) at the center of a fiber or rod, enabling it to transmit light[7]. Rapid diffusion of monovalent ions is required for this process. Silver for alkali ion diffusion to achieve gradient index is also used, but coloration owing to silver reduction may occur.

(DAVID A. THOMPSON)

Inorganic Reactions and Methods, Volume 18
Edited by J. J. Zuckerman, Jim D. Atwood

The refractive indices of alkali silicate glasses ($Na_2O \cdot SiO_2$) vary linearly with modifier concentration. Where change of coordination occurs such as with B_2O_3, Al_2O_3, or Geo_2[10], maxima and minima of refractive index vs. composition are observed.

Glasses frequently require composition control to ensure compliance with standards of chemical corrosion resistance, glass quality, resistance to crystallization, and density, color, and grinding or polishing characteristics in addition to optical properties.

(DAVID A. THOMPSON)

1. M. A. Matveev, G. M. Matveev, B. N. Frenkel, *Calculation and Control of Electrical, Optical and Thermal Properties of Glass*, Ordentlich, Holon, Israel, 1975.
2. S. T. Pantelides, W. A. Harrison, *Phys, Rev., 13*, 2667 (1976); *Chem. Abstr.*, 85010530.
3. C. J. Parker, *Optical Materials—Refractive, Applied Optics and Optical Engineering*, Vol, VII, Academic Press, Newyork, 1979, p. 47.
4. B. Kim, M. Yamane, *Yogyo Kyokaikshi, 88*, 191 (1980); *Chem, Abstr.*, 93100303.
5. E. H. Hamilton, O. H. Graver, Z. Zabawsky, C. H. Hahner, *J. Res. Natl. Bur. Stand., 40*, 361 (1948).
6. B. Kim, M. Yamane, Yogyo Kyokaikshi, *J. Am. Ceram. Soc., 31*, 132 (1948); *Chem. Abstr.*, 42005183.
7. W. H. Dumbaugh, *Phys. Chem. Glasses, 19*, 121 (1978).
8. A. E. Owen, *Contemp. Phys., 11*, 227 (1970).
9. K. Weiser, *Prog. Solid-State Chem., 11*, 403 (1976).
10. H. Rawson, D. Warner, *J. Non-Cryst. Solids, 29*, 231 (1978).

17.3.2.3.2. Applications.

Some oxide glasses have refractive indices of about 2.0 or above. The glass microspheres (50–100 μm diameter) used to reflect light in paints for signs, auto license plates etc[1] contain greater than 50 (mol %) PBO, Bi_2O_3, TiO_2, or TEO_2 for high refractive index, in addition to silica and other glass modifiers. Beads of glass may also contain colorants which selectively absorb visible light but transmit in the infrared[2]. Although beads are made by melting, crushing and grinding, and passing the material particles through a flame to form spheres, the gel route is also used to prepare TiO_2-containing spheres[3].

Optical glass compositions are designed to facilitate the melting and forming of high quality glass pieces. Refractive index control is achieved by composition control; however, a post forming annealing treatment can be used to adjust the refractive index by altering density. Optical glasses can have either anomalously high or low dispersions[4] based on the chart given earlier (Fig. 1 in 17.3.2.3).Thoria, although useful for achieving high refractive index, is used infrequently owing to its radioactivity. Glasses containing PbO ($n_d > 1.7$) are hydrated in steam at $\sim 300°C$[5] to lower T_g enough to permit optical quality lenses to be molded at low temperature[6].

High index fibers from conventional melts contain oxides such as Nb_2O_5 and Ta_2O_5 and others listed on Table 1 in 17.3.2.3.1. Glasses containing Tl_2O ($n_d \sim 1.8$) exchange K^+ for Tl^+ in a bath of molten KNO_3 at $\sim 500°C$. The resulting composition profile produces a parabolic index profile, with high index ($n_d \sim 1.6$) at the center of a fiber or rod, enabling it to transmit light[7]. Rapid diffusion of monovalent ions is required for this process. Silver for alkali ion diffusion to achieve gradient index is also used, but coloration owing to silver reduction may occur.

(DAVID A. THOMPSON)

1. F. V. Tooley, ed., *The Handbook of Glass Manufacture*, Books for Industry, New York, 1974.
2. C. F. Tung, U.S. Patent 3,563,771 (1971); *Chem, Abstr.*, 74090660.
3. V. Urbanek, J. Dolezal, M. Tympl, F. Smetak, *Nukleon*, 9 (1978).
4. H. Broemer, W. Huber, Meinert, J. Spincic, German patent 2,216,566 (1973); *Chem. Abstr.*, 80030103.
5. R. F. Bartholomew, in *Glass*, Vol. III, M. Tomazowa, R, Doremus, eds., Academic Press, New York.
6. R. F. Bartholomew, U.S. Patent 4,026,692 (1977); *Chem. Abstr.*, 87057369.
7. I. Kitano, K. Koizumi, Y. Ikeda, H. Matsumura, U.S. Patent 3,830.640, (1974).

17.3.2.4. Strong and Shatter-Resistant Glasses

Glass is limited to nonstructural applications because of its brittle nature. The observed strength of glass is but a fraction of its intrinsic strength of ~ 35 GPa (5×10^6 psi) based on Si–O bond energies[1]. The existence of surface imperfections is used to explain[2] the relatively low strengths of glass summarized in Figure 1. To increase the

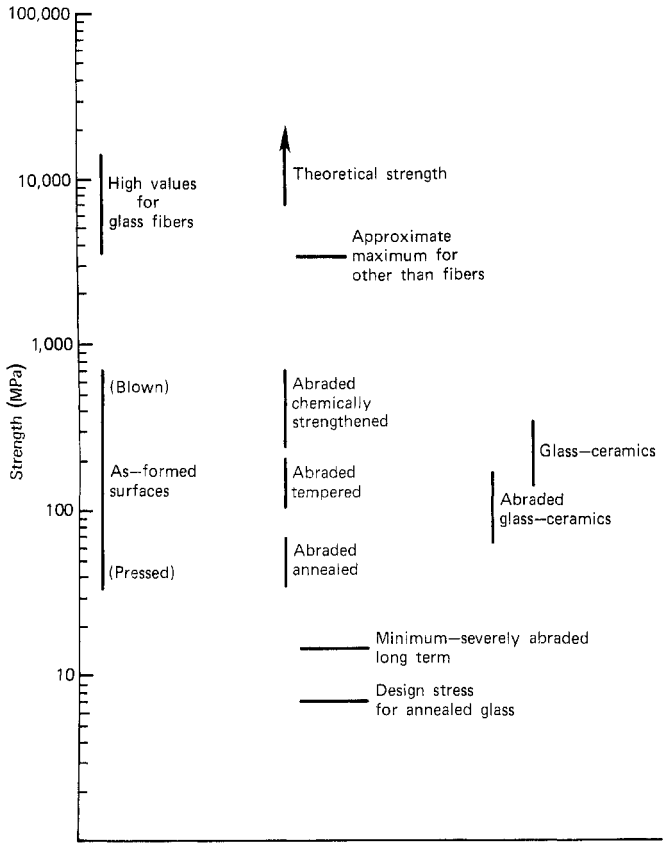

Figure 1. Strength scale for glass and glass ceramics. (To convert mega pascals to pounds per square inch, multiply by 145.)

Inorganic Reactions and Methods, Volume 18
Edited by J. J. Zuckerman, Jim D. Atwood

1. F. V. Tooley, ed., *The Handbook of Glass Manufacture*, Books for Industry, New York, 1974.
2. C. F. Tung, U.S. Patent 3,563,771 (1971); *Chem, Abstr.*, 74090660.
3. V. Urbanek, J. Dolezal, M. Tympl, F. Smetak, *Nukleon*, 9 (1978).
4. H. Broemer, W. Huber, Meinert, J. Spincic, German patent 2,216,566 (1973); *Chem. Abstr.*, 80030103.
5. R. F. Bartholomew, in *Glass*, Vol. III, M. Tomazowa, R, Doremus, eds., Academic Press, New York.
6. R. F. Bartholomew, U.S. Patent 4,026,692 (1977); *Chem. Abstr.*, 87057369.
7. I. Kitano, K. Koizumi, Y. Ikeda, H. Matsumura, U.S. Patent 3,830,640, (1974).

17.3.2.4. Strong and Shatter-Resistant Glasses

Glass is limited to nonstructural applications because of its brittle nature. The observed strength of glass is but a fraction of its intrinsic strength of ~ 35 GPa (5×10^6 psi) based on Si–O bond energies[1]. The existence of surface imperfections is used to explain[2] the relatively low strengths of glass summarized in Figure 1. To increase the

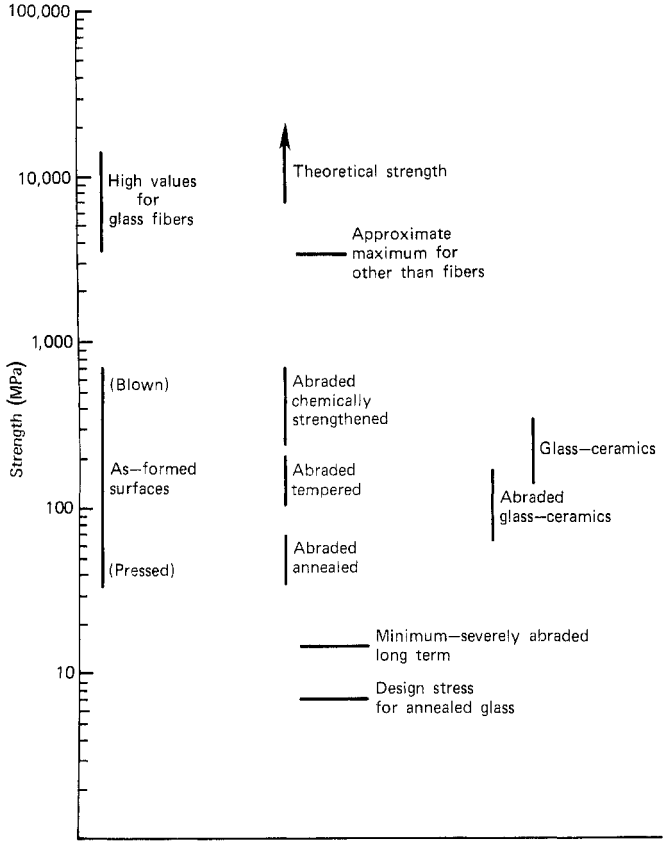

Figure 1. Strength scale for glass and glass ceramics. (To convert mega pascals to pounds per square inch, multiply by 145.)

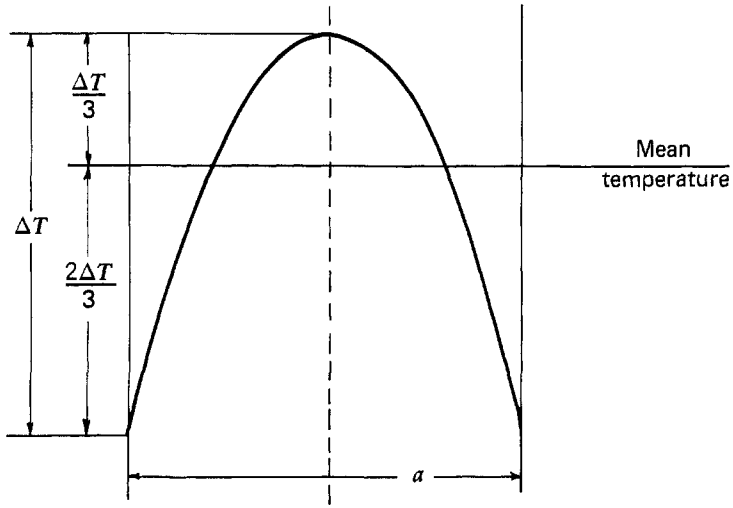

Figure 2. Temperature distribution through a section of glass of thickness *a*, which has been cooled at a constant rate.

strength of glass, defect-free surfaces must be formed, or measures must be taken to ensure that the flaws that exist will not act as sources of fracture. If compressive surface layers are formed on glass by either physical or chemical processes, crack propagation is slowed. The tensile stress needed to break glass is the sum of the compressive stress in the surface plus the strength of the untreated glass. Glass pieces heated and rapidly quenched in water are early examples of thermal tempering to achieve a compressive layer[3]. Chemical tempering alters glass composition, either by ion exchange or lamination that imparts compressive surface forces. Automobile and airplane cockpit windows, ophthalmic lenses, laboratory pipets, architectural panels, and consumer ware are examples of glass items strengthened by one of these methods[4].

(DAVID A. THOMPSON)

1. R. J. Charles, *Prog. Ceram. Sci., 1*, 1 (1961).
2. A. A. Griffith, *Philos. Trans. R. Soc. London, Ser. A, 221*, 163 (1973).
3. D. G. Holloway, *The Physical Properties of Glass*, Wykeham Publications, London, 1973, p. 189.
4. A. G. Pincus, T. R. Holmes, *Annealing and Strengthening in the Glass Industry*, Books for Industry, New York, 1977.

17.3.2.4.1. *Thermal Tempering.*

Attempts to thermally temper glass date from the 1870s[1] however, both theory and practice were documented in 1942[2]. Thermal tempering is the opposite of annealing. Annealing requires slow cooling from temperatures above the glass transition temperature, T_g to minimize potential temperature gradients from the surface to the interior of the glass. Tempering requires that a temperature gradient be formed on cooling below the softening point (Table 1). Above T_g, structural relaxation occurs. If a parabolic temperature profile (see Fig. 2 in 17.3.2.4) is maintained during cooling through the glass

Inorganic Reactions and Methods, Volume 18
Edited by J. J. Zuckerman, Jim D. Atwood

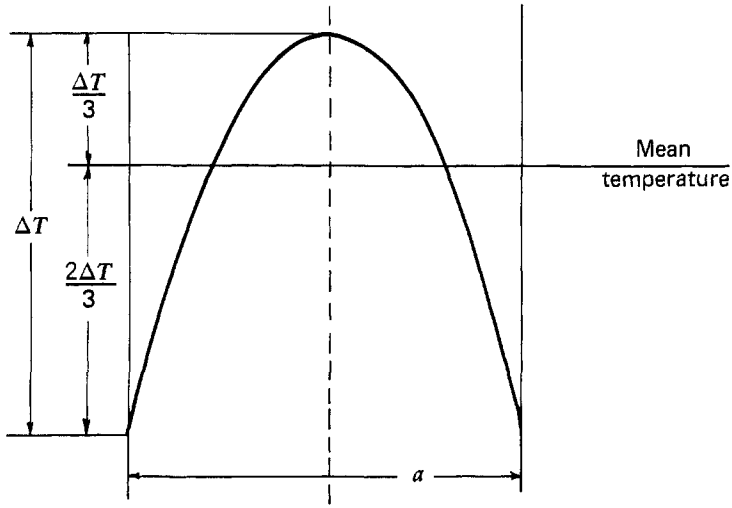

Figure 2. Temperature distribution through a section of glass of thickness a, which has been cooled at a constant rate.

strength of glass, defect-free surfaces must be formed, or measures must be taken to ensure that the flaws that exist will not act as sources of fracture. If compressive surface layers are formed on glass by either physical or chemical processes, crack propagation is slowed. The tensile stress needed to break glass is the sum of the compressive stress in the surface plus the strength of the untreated glass. Glass pieces heated and rapidly quenched in water are early examples of thermal tempering to achieve a compressive layer[3]. Chemical tempering alters glass composition, either by ion exchange or lamination that imparts compressive surface forces. Automobile and airplane cockpit windows, ophthalmic lenses, laboratory pipets, architectural panels, and consumer ware are examples of glass items strengthened by one of these methods[4].

(DAVID A. THOMPSON)

1. R. J. Charles, *Prog. Ceram. Sci., 1*, 1 (1961).
2. A. A. Griffith, *Philos. Trans. R. Soc. London, Ser. A, 221*, 163 (1973).
3. D. G. Holloway, *The Physical Properties of Glass*, Wykeham Publications, London, 1973, p. 189.
4. A. G. Pincus, T. R. Holmes, *Annealing and Strengthening in the Glass Industry*, Books for Industry, New York, 1977.

17.3.2.4.1. *Thermal Tempering.*

Attempts to thermally temper glass date from the 1870s[1] however, both theory and practice were documented in 1942[2]. Thermal tempering is the opposite of annealing. Annealing requires slow cooling from temperatures above the glass transition temperature, T_g to minimize potential temperature gradients from the surface to the interior of the glass. Tempering requires that a temperature gradient be formed on cooling below the softening point (Table 1). Above T_g, structural relaxation occurs. If a parabolic temperature profile (see Fig. 2 in 17.3.2.4) is maintained during cooling through the glass

TABLE 1. COMPOSITIONS (wt%) AND PROPERTIES OF GLASSES FOR STRENGTHENED APPLICATIONS

	K^+ Ion Exchange 16 h at −400°C		Laminate	
Composition (wt%)	Na_2O–CaO–SiO_2	Na_2O–Al_2O_3–SiO_2	Core (opal)	Cladding (clear)
SiO_2	73	54.5	64	50
Al_2O_3	1	19	6	15
B_2O_3		2	5	6
Na_2O	16.5	16	3	
K_2O		2	3	
MgO	3.5		1	6
CaO	5	2	15	15
BaO				
TiO_2		4.5		
F^-			3	
K^+ exchanged (mg/cm^2)	0.5	0.5		
		Properties[a]		
Softening point, °C	696			890
Annealing point, °C	514		610	710
Strain point, °C	473		563	670
Expansion coefficient (0°–300°C), $\times 10^7$/°C	93.5		71	48
Density, g/cm^3	2.47		2.47	2.57
Liquidus, °C				1089
Young's modulus, Gpa	70		78	87
Poisson's ratio	0.22		0.22	0.25
Modulus of rupture, kg/mm^2				
No abrasion	49 ± 20	61 ± 1		
150 Grit	12 ± 4	48 ± 4		
Stress in cladding, kg/mm^2			21.1 (30,000 psi)	
Stress in cladding from tempering, kg/mm^2			24.6 (35,000 psi)	

[a]Strength data refer to the ion-exchanged or laminated sample. Remaining data describe glasses before treatment.

transition point, tensile stress occurs in the interior with a compressive stress layer on the surface that is deeper than most severe flaws. Compressed air is a cooling medium that causes no surface damage. Air flotation processes have largely replaced tongs for handling large sheets of glass.

Stresses induced by tempering are related to the temperature gradient, expansion coefficient ratio of applied stress to strain (E modulus) and transverse to longitudinal strain ratio (Poisson's ratio) of the glass. The glasses most readily tempered have high softening points (to facilitate development of a temperature gradient) and thermal expansion coefficients.

(DAVID A. THOMPSON)

1. D. La Bastie, *Bull. Soc, Encouragement, 2*, 132 (1875).
2. J. T. Littleton, H. R. Lillie, W. W. Shaver, U.S. Patent 2,285,595 (1942); *Chem. Abstr.*, 36006767: U.S. Patent 2,285,596 (1942); *Chem. Abstr.*, 2285596.

Inorganic Reactions and Methods, Volume 18
Edited by J. J. Zuckerman, Jim D. Atwood

17.3.2.4.2. Chemical Strengthening.

When immersed in fused KNO_3-containing salts, glasses containing sodium exchange larger K^+ ions for Na^+; the K^+ ions occupy sodium sites within the silica network. This tendency to expand the surface is resisted by the unexchanged silicate network in the interior, which induces compression of the surface layer[1]. As shown in Figure 1, stress profiles for chemically strengthened glasses differ from those achieved by thermal tempering. Higher strengths (500 MN/m^2) and thinner glass articles (<2 mm thick) are possible by chemical strengthening. Cutting or finishing is performed prior to strengthening to avoid damage to the compressive layer.

To be suitable for ion exchange, glass compositions must exhibit high mobility of an alkali that can be replaced by a larger alkali (e.g., Na^+ for Li^+; K^+ for Na^+, Cs^+ for K^+). It is advantageous to have a high T, which allows for higher salt bath temperatures without stress relaxation. Soda–alumina–silica and soda–zirconia–silica are such glass-forming systems[2]. Commonly used Na_2O-CaO-SiO_2 glasses are not easily strengthened owing to slow diffusion, which generates a shallow compressive profile and stress relaxation during exchange (low strain point[3] (see Table 1 in 17.3.2.4.1).

Molten salts contained in 309 stainless steel or Vycor brand glass containers are used as baths[4]. Sodium nitrate (mp 310°C) can be used up to ~450°C, $NaNO_3$ and Na_2SO_4 up to 525°C and KNO_3 up to 525°C. Addition of sulfate allows higher temperatures, as do combinations of other salt mixtures. The time and temperature of treatment depend on the ion to be exchanged, the glass composition, and the fracture properties desired. For example, most prescription ophthalmic lenses are configuration and given a 16 h treatment at ~400°C in KNO_3, ground and polished to the desired. Pastes applied to the surface of glass also cause exchange during heat treatment, but the process is not used as a commercial alternative to salt bath strengthening[4].

Other methods of chemically strengthening glass include Li^+ ions diffused into a sodium-containing glass to create a composition profile in which the resulting surface has a lower expansion than the core region, and thus develops a compressive layer on

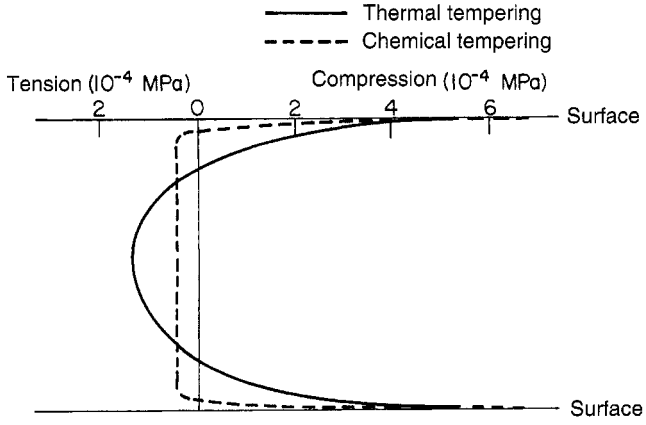

Figure 1. Schematic representation of the stress distribution in physically tempered and ion-exchanged glasses. (From Ref. 2.)

cooling below T_g[5]. High temperatures cause deformation, which limits the usefulness of this method. Two glasses that differ in composition and in thermal expansion characteristics can be laminated to produce a composite glass, which is shaped into strong, lightweight dinnerware[6]. Heat treatments are also used that result in dealkalization of the glass surface to achieve compressive layers. Treatments in SO_2 atmospheres form alkali or alkaline earth sulfates on the surface (bloom) and incorporate water into the glass[7]. Depths of exchange of 50 μm are noted for Na_2O-Al_2O_3-SiO_2 glasses. Copper(I) halide vapors strengthen glass (500 MPa vs. 150 MPa untreated).

Major disadvantages of chemical strengthening by ion exchange include costs, (in time and materials). In addition, not all compositions may be strengthened to useful depth profiles; and the temperature used permits stress release by continued diffusion of alkali or structural relaxation of the network.

(DAVID A. THOMPSON)

1. S. S. Kistler, *J. Am. Ceram. Soc., 45*, 59 (1962).
2. M. E. Nordberg, E. L. Mochel, H. M. Garfinkel, J. S. Olcott, *J. Am. Ceram. Soc., 47*, 215 (1964).
3. J. B. Ward, B. Sugarman, C. Symmers, *Glass Technol. 6*, 90 (1965).
4. R. F. Bartholomew, H. M. Garfinkel, in *Glass: Science and Technology*, Vol. 5, Academic Press, New York, 1980, p. 217.
5. J. S. Olcott, S. D. Stookey, U. S. Patent 2, 998, 675 (1961); *Chem. Abstr.*, 56003138.
6. W. H. Dumbaugh, J. E. Flannery, J. E. Megles, *J. Non-Cryst. Solids, 39*, 469 (1980).
7. E. L. Mochel, M. E. Nordberg, T. H. Elmer, *J. Am. Ceram. Soc., 49*, 585 (1966).

17.3.2.5. Radiation–Resistant Glasses

Glasses that are resistant to potentially damaging effects of radiation are important for many items, including transparent windows[1] bulbs, or tubes, optical waveguide fibers[2], electronic components[3], lasers, nuclear waste storage receptacles, solar cells[4], and X-ray grating elements[5]. Damage may be caused by radiation high intensity visible and infrared, ultraviolet, γ-ray, and X-ray and by particles or ions[6,7].

(DAVID A. THOMPSON)

1. D. C. Boyd, D. A. Thompson, in *Kirk-Othmer Encyclopedia of Chemical Technology*, Vol. II, 3rd ed., Wiley, New York, 1980.
2. G. H. Sigel, *Proc. IEEE, 68*, 1236 (1980).
3. F. A. Frankovsky, M. Shatzkes, Study of Effect of High-Intensity Pulsed Nuclear Radiation on Electronic Parts and Materials, Report No. IBM-65-521-14, Contract No. DA28-043-AMC-00212(E), 1965.
4. W. Luft, *Energy Convers., 16*, 159 (1977).
5. A. Franks, M. Stedman, *Nucl. Instrum. Methods, 172*, 249 (1980).
6. N. J. Kreidl, in *Ceramics in Severe Environments*, Vol. III, W. W. Kriegl, N. Palmour, eds., Plenum Press, New York, 1971, p. 521.
7. E. J. Friebele, D. L. Griscom, in *Treatise on Materials Science and Technology*, Vol. II: *Glass*, Academic Press, New York, p. 257.

17.3.2.5.1. Particle Radiation.

Radiation damage depends on radiation type, dosage, temperature, and glass composition. Particle bombardment induces structural changes while ionizing radiation causes electronic changes. Neutron radiation causes collisions, charge interaction, or transmutation changes depending on the glass composition. Collisional damage includes

Inorganic Reactions and Methods, Volume 18
Edited by J. J. Zuckerman, Jim D. Atwood

cooling below T_g[5]. High temperatures cause deformation, which limits the usefulness of this method. Two glasses that differ in composition and in thermal expansion characteristics can be laminated to produce a composite glass, which is shaped into strong, lightweight dinnerware[6]. Heat treatments are also used that result in dealkalization of the glass surface to achieve compressive layers. Treatments in SO_2 atmospheres form alkali or alkaline earth sulfates on the surface (bloom) and incorporate water into the glass[7]. Depths of exchange of 50 μm are noted for Na_2O-Al_2O_3-SiO_2 glasses. Copper(I) halide vapors strengthen glass (500 MPa vs. 150 MPa untreated).

Major disadvantages of chemical strengthening by ion exchange include costs, (in time and materials). In addition, not all compositions may be strengthened to useful depth profiles; and the temperature used permits stress release by continued diffusion of alkali or structural relaxation of the network.

(DAVID A. THOMPSON)

1. S. S. Kistler, *J. Am. Ceram. Soc., 45*, 59 (1962).
2. M. E. Nordberg, E. L. Mochel, H. M. Garfinkel, J. S. Olcott, *J. Am. Ceram. Soc., 47*, 215 (1964).
3. J. B. Ward, B. Sugarman, C. Symmers, *Glass Technol. 6*, 90 (1965).
4. R. F. Bartholomew, H. M. Garfinkel, in *Glass: Science and Technology*, Vol. 5, Academic Press, New York, 1980, p. 217.
5. J. S. Olcott, S. D. Stookey, U. S. Patent 2, 998, 675 (1961); *Chem. Abstr.*, 56003138.
6. W. H. Dumbaugh, J. E. Flannery, J. E. Megles, *J. Non-Cryst. Solids, 39*, 469 (1980).
7. E. L. Mochel, M. E. Nordberg, T. H. Elmer, *J. Am. Ceram. Soc., 49*, 585 (1966).

17.3.2.5. Radiation–Resistant Glasses

Glasses that are resistant to potentially damaging effects of radiation are important for many items, including transparent windows[1] bulbs, or tubes, optical waveguide fibers[2], electronic components[3], lasers, nuclear waste storage receptacles, solar cells[4], and X-ray grating elements[5]. Damage may be caused by radiation high intensity visible and infrared, ultraviolet, γ-ray, and X-ray and by particles or ions[6,7].

(DAVID A. THOMPSON)

1. D. C. Boyd, D. A. Thompson, in *Kirk-Othmer Encyclopedia of Chemical Technology*, Vol. II, 3rd ed., Wiley, New York, 1980.
2. G. H. Sigel, *Proc. IEEE, 68*, 1236 (1980).
3. F. A. Frankovsky, M. Shatzkes, Study of Effect of High-Intensity Pulsed Nuclear Radiation on Electronic Parts and Materials, Report No. IBM-65-521-14, Contract No. DA28-043-AMC-00212(E), 1965.
4. W. Luft, *Energy Convers., 16*, 159 (1977).
5. A. Franks, M. Stedman, *Nucl. Instrum. Methods, 172*, 249 (1980).
6. N. J. Kreidl, in *Ceramics in Severe Environments*, Vol. III, W. W. Kriegl, N. Palmour, eds., Plenum Press, New York, 1971, p. 521.
7. E. J. Friebele, D. L. Griscom, in *Treatise on Materials Science and Technology*, Vol. II: *Glass*, Academic Press, New York, p. 257.

17.3.2.5.1. Particle Radiation.

Radiation damage depends on radiation type, dosage, temperature, and glass composition. Particle bombardment induces structural changes while ionizing radiation causes electronic changes. Neutron radiation causes collisions, charge interaction, or transmutation changes depending on the glass composition. Collisional damage includes

Inorganic Reactions and Methods, Volume 18
Edited by J. J. Zuckerman, Jim D. Atwood

cooling below T_g[5]. High temperatures cause deformation, which limits the usefulness of this method. Two glasses that differ in composition and in thermal expansion characteristics can be laminated to produce a composite glass, which is shaped into strong, lightweight dinnerware[6]. Heat treatments are also used that result in dealkalization of the glass surface to achieve compressive layers. Treatments in SO_2 atmospheres form alkali or alkaline earth sulfates on the surface (bloom) and incorporate water into the glass[7]. Depths of exchange of 50 μm are noted for Na_2O-Al_2O_3-SiO_2 glasses. Copper(I) halide vapors strengthen glass (500 MPa vs. 150 MPa untreated).

Major disadvantages of chemical strengthening by ion exchange include costs, (in time and materials). In addition, not all compositions may be strengthened to useful depth profiles; and the temperature used permits stress release by continued diffusion of alkali or structural relaxation of the network.

(DAVID A. THOMPSON)

1. S. S. Kistler, *J. Am. Ceram. Soc., 45*, 59 (1962).
2. M. E. Nordberg, E. L. Mochel, H. M. Garfinkel, J. S. Olcott, *J. Am. Ceram. Soc., 47*, 215 (1964).
3. J. B. Ward, B. Sugarman, C. Symmers, *Glass Technol. 6*, 90 (1965).
4. R. F. Bartholomew, H. M. Garfinkel, in *Glass: Science and Technology*, Vol. 5, Academic Press, New York, 1980, p. 217.
5. J. S. Olcott, S. D. Stookey, U. S. Patent 2, 998, 675 (1961); *Chem. Abstr.*, 56003138.
6. W. H. Dumbaugh, J. E. Flannery, J. E. Megles, *J. Non-Cryst. Solids, 39*, 469 (1980).
7. E. L. Mochel, M. E. Nordberg, T. H. Elmer, *J. Am. Ceram. Soc., 49*, 585 (1966).

17.3.2.5. Radiation–Resistant Glasses

Glasses that are resistant to potentially damaging effects of radiation are important for many items, including transparent windows[1] bulbs, or tubes, optical waveguide fibers[2], electronic components[3], lasers, nuclear waste storage receptacles, solar cells[4], and X-ray grating elements[5]. Damage may be caused by radiation high intensity visible and infrared, ultraviolet, γ-ray, and X-ray and by particles or ions[6,7].

(DAVID A. THOMPSON)

1. D. C. Boyd, D. A. Thompson, in *Kirk-Othmer Encyclopedia of Chemical Technology*, Vol. II, 3rd ed., Wiley, New York, 1980.
2. G. H. Sigel, *Proc. IEEE, 68*, 1236 (1980).
3. F. A. Frankovsky, M. Shatzkes, Study of Effect of High-Intensity Pulsed Nuclear Radiation on Electronic Parts and Materials, Report No. IBM-65-521-14, Contract No. DA28-043-AMC-00212(E), 1965.
4. W. Luft, *Energy Convers., 16*, 159 (1977).
5. A. Franks, M. Stedman, *Nucl. Instrum. Methods, 172*, 249 (1980).
6. N. J. Kreidl, in *Ceramics in Severe Environments*, Vol. III, W. W. Kriegl, N. Palmour, eds., Plenum Press, New York, 1971, p. 521.
7. E. J. Friebele, D. L. Griscom, in *Treatise on Materials Science and Technology*, Vol. II: *Glass*, Academic Press, New York, p. 257.

17.3.2.5.1. Particle Radiation.

Radiation damage depends on radiation type, dosage, temperature, and glass composition. Particle bombardment induces structural changes while ionizing radiation causes electronic changes. Neutron radiation causes collisions, charge interaction, or transmutation changes depending on the glass composition. Collisional damage includes

disorder and phase changes that produce changes of refractive index, density, heat capacity, and thermal conductivity. Radiation-resistant fused silica and quartz are damaged by high intensities of ($>10^{19}$ neutrons/cm^2) neutrons (>100 eV) yielding a disordered metamict silica with a density between that of fused silica and quartz[1]. Bombardment by krypton, hydrogen, deuterium, and helium produces surface changes, such as low refractive index. The capture of neutrons by borosilicate glasses produces lithium from boron by transmutation; hence boron-containing glasses must not be used in neutron environments[2]. Glasses containing K^+, Ca^{2+}, Zn^{2+}, As^{3+}, Ce^{3+} and Co^{3+} should also be avoided because of decomposition to other radioactive species[3].

(DAVID A. THOMPSON)

1. E. J. Freibele, D. L. Griscom, in *Treatise on Materials Science and Technology*, Vol. II: *Glass*, Academic Press, New York, 1979, p. 257.
2. N. J. Kreidl, J. Rood, in *Optical Materials, Applied Optics and Optical Engineering*, R. Kinglake, ed., Academic Press, New York, 1965.
3. W. A. Hanning, *Abstr. Annual Meeting, Soc. Photo-Optical Instrumentation Eng.*, St. Louis MO, 1966.

17.3.2.5.2. Ionizing Radiation.

Radiation sources including X-rays, γ-rays, and ultraviolet produce preferential light absorption at color centers in glass by formation of free electrons and holes. These are trapped at a defect such a vacancy, an interstitial atom, a multivalent impurity, or a nonbridging oxygen[1]. The types of color center induced in silica, soda-lime-silica, borate, and phosphate glasses are elucidated by optical and electron spin resonance studies of irradiated samples. Table 1 summarizes composition variables and reaction types that induce damage.

Most effects of ionizing radiation are related to impurities in the glass, including germanium and aluminum ions, iron, titanium, and manganese, which act as electron and hole traps. Defects consist of E′ centers (unpaired electron in a network-forming atom (e.g., Si, Ge, B, P, Al) and nonbridging anion hole, HC, centers (h oles trapped in a nonbonding p-π orbital of the anion[2]. Extremely high ($\sim 10^9$ r) doses of radiation cause intrinsic oxygen vacancy defects in pure silica that absorb $\sim$215 and 230 nm. Absorption bands associated with nonbridging oxygens usually occur near 620 nm (intensity-dependent on alkali, 415–490 nm (Li < Na < K < Cs), and 300 nm (alkali concentration dependent 10). Multicomponent glasses that are resistant to γ or X-ray damage (protected optical glasses) contain multivalent oxides, such as CeO_2, which compete with hole trap centers for charge[3]. Ceria may dissipate energy in borosilicate glasses by luminescence[4]. Concentrations of 0.1–0.2 wt% CeO_2 inhibit radiation damage of lead glass shielding windows, solar cell cover glasses, cathode ray tube faceplates[5], and pharmaceutical glasses.

Color changes in commercial flat and container glasses from ultraviolet-visible radiation are possible[6]. In soda–lime–silica glasses, this effect is evaluated as a function of glass composition by additions of impurities, decolorizers, and fining agents including nitrates, Fe_2O_3, As_2O_3, CeO_2, MnO_2, and Sb_2O_3[7]. Evaluations of glasses for solar mirrors consider absorptions arising from simulated solar exposure of several glasses. Optical crown glasses (see Fig. 1 in 17.3.2.3) and fused quartz are used for fiber light guides for focused solar concentrators.

Inorganic Reactions and Methods, Volume 18
Edited by J. J. Zuckerman, Jim D. Atwood

disorder and phase changes that produce changes of refractive index, density, heat capacity, and thermal conductivity. Radiation-resistant fused silica and quartz are damaged by high intensities of ($>10^{19}$ neutrons/cm^2) neutrons (>100 eV) yielding a disordered metamict silica with a density between that of fused silica and quartz[1]. Bombardment by krypton, hydrogen, deuterium, and helium produces surface changes, such as low refractive index. The capture of neutrons by borosilicate glasses produces lithium from boron by transmutation; hence boron-containing glasses must not be used in neutron environments[2]. Glasses containing K^+, Ca^{2+}, Zn^{2+}, As^{3+}, Ce^{3+} and Co^{3+} should also be avoided because of decomposition to other radioactive species[3].

(DAVID A. THOMPSON)

1. E. J. Freibele, D. L. Griscom, in *Treatise on Materials Science and Technology*, Vol. II: *Glass*, Academic Press, New York, 1979, p. 257.
2. N. J. Kreidl, J. Rood, in *Optical Materials, Applied Optics and Optical Engineering*, R. Kinglake, ed., Academic Press, New York, 1965.
3. W. A. Hanning, *Abstr. Annual Meeting, Soc. Photo-Optical Instrumentation Eng.*, St. Louis MO, 1966.

17.3.2.5.2. Ionizing Radiation.

Radiation sources including X-rays, γ-rays, and ultraviolet produce preferential light absorption at color centers in glass by formation of free electrons and holes. These are trapped at a defect such a vacancy, an interstitial atom, a multivalent impurity, or a nonbridging oxygen[1]. The types of color center induced in silica, soda-lime-silica, borate, and phosphate glasses are elucidated by optical and electron spin resonance studies of irradiated samples. Table 1 summarizes composition variables and reaction types that induce damage.

Most effects of ionizing radiation are related to impurities in the glass, including germanium and aluminum ions, iron, titanium, and manganese, which act as electron and hole traps. Defects consist of E′ centers (unpaired electron in a network-forming atom (e.g., Si, Ge, B, P, Al) and nonbridging anion hole, HC, centers (h oles trapped in a nonbonding p-π orbital of the anion[2]. Extremely high ($\sim 10^9$ r) doses of radiation cause intrinsic oxygen vacancy defects in pure silica that absorb $\sim$215 and 230 nm. Absorption bands associated with nonbridging oxygens usually occur near 620 nm (intensity-dependent on alkali, 415–490 nm (Li < Na < K < Cs), and 300 nm (alkali concentration dependent 10). Multicomponent glasses that are resistant to γ or X-ray damage (protected optical glasses) contain multivalent oxides, such as CeO_2, which compete with hole trap centers for charge[3]. Ceria may dissipate energy in borosilicate glasses by luminescence[4]. Concentrations of 0.1–0.2 wt% CeO_2 inhibit radiation damage of lead glass shielding windows, solar cell cover glasses, cathode ray tube faceplates[5], and pharmaceutical glasses.

Color changes in commercial flat and container glasses from ultraviolet-visible radiation are possible[6]. In soda–lime–silica glasses, this effect is evaluated as a function of glass composition by additions of impurities, decolorizers, and fining agents including nitrates, Fe_2O_3, As_2O_3, CeO_2, MnO_2, and Sb_2O_3[7]. Evaluations of glasses for solar mirrors consider absorptions arising from simulated solar exposure of several glasses. Optical crown glasses (see Fig. 1 in 17.3.2.3) and fused quartz are used for fiber light guides for focused solar concentrators.

TABLE 1. FACTORS AFFECTING INDUCED OPTICAL ABSORPTION

Glass structure
Polarizing power of network modifier (z/r^2)
Concentration of nonbridging oxygens
Coordination number of certain cations
Type of structural groupings in glass
Melting conditions
Photochemical reactions
Multivalent additives
Impurities

Source: Ref.

High intensity visible and infrared radiation from laser sources damage glass by surface reactions, heating of platinum inclusions (< 1 μm), or by a self-focusing process. The latter causes rapid heating and plasma formation within a glass as a result of increases in refractive index of glass with increasing radiation intensity (10^{10}W/cm^2). This effect is minimized by a low nonlinear refractive index coefficient n_2 in materials having a low refractive index and dispersion[7]. [11]Fluoride-based glasses, including fluorophosphate, fluorosilicate, and fluoroberyllate types, have the lowest index and dispersion (e.g., BeF_2, with $n_d \sim 1.27$, $V_d \sim 106$), giving nonlinear refractive indices of $\sim 0.25 \times 0.5 \times 10^{-13}$ esu vs. $1\text{–}5 \times 10^{13}$ esu for silicate and phosphate glasses[12].

Glasses containing BeF_2 melt in graphite crucibles under nitrogen at ~ 1000°C using NH_4BF_4. Additional fluorides are added to control optical properties and inhibit devitrification. This includes 10–30 mol % AlF_3, NaF, KF, RbF, and CaF_2[13].

(DAVID A. THOMPSON)

1. Bishay, *J. Non-cryst. Solids, 3*, 54 (1970).
2. E. J. Friebele, D. L. Griscom, in *Treatise on Materials Science and Technology*, Vol. II: *Glass*, Academic Press, New York, p. 257.
3. N. J. Kreidl, in *Ceramics in Severe Environments*, Vol. III, W. W. Kriegl, N. Palmour, eds., Plenum Press, New York, 1971, p. 521.
4. St. Gebala, E. Rysiakiewicz, *Szklo Ceram., 30*, 65 (1979); Chem. Abstr., 91131408.
5. J. S. Stroud, *J. Chem. Phys., 37*, 836 (1962).
6. G. E. Rindone, *Trans. Int. Conf. Glass*, Paris, 1956, p. 373.
7. J. F. White, W. B. Silverman, *J. Am. Ceram. Soc., 33*, 252 (1950).
8. J. Vitko Jr., J. E. Shelby, *Abstr. Solar Reflective Materials Workshop*, 1980 (Sand 79-8754).
9. V. S. Dvernyakov, V. V. Pasichnyi, I. E. Kasich-Pilipeniko, T. V. Eremina, D. K. Sattarov, M. I. Moraveva, I. E. Galant, *Appl. Solar Energy, 15*, 32 (1979).
10. D. L. Cunningham, K. C. Clark, *J. Chem. Phys., 61*, 1118 (1974); *Chem. Abstr.*, 81113264.
11. C. D. Cooper, G. C. Cobb, D. L. Tolnas, *J. Mol. Spectrosc., 7*, 223 (1961).
12. A. Glass, K. L. Cummings, *Laser Program Annual Report*—1975 (to 1979), Lawrence Livermore Laboratory, Contract No. W-7405-Eng-48.
13. W. H. Dumbaugh, D. W. Morgan, *J. Non-Cryst. Solids, 38*, 211 (1980).

17.3.2.6. Glass–Metals Seals

The use of glass in glass–metal seals is justified by its transparency, its relatively low permeability to gases, its desirable electrical properties, and the relative ease with which it can be fused to metal to make vacuum-tight seals. Glass, unlike many crystalline materials, can be altered to control expansion coefficient, viscosity, electrical resistivity,

Inorganic Reactions and Methods, Volume 18
Edited by J. J. Zuckerman, Jim D. Atwood

TABLE 1. FACTORS AFFECTING INDUCED OPTICAL ABSORPTION

Glass structure
Polarizing power of network modifier (z/r^2)
Concentration of nonbridging oxygens
Coordination number of certain cations
Type of structural groupings in glass
Melting conditions
Photochemical reactions
Multivalent additives
Impurities

Source: Ref.

High intensity visible and infrared radiation from laser sources damage glass by surface reactions, heating of platinum inclusions (< 1 μm), or by a self-focusing process. The latter causes rapid heating and plasma formation within a glass as a result of increases in refractive index of glass with increasing radiation intensity (10^{10}W/cm^2). This effect is minimized by a low nonlinear refractive index coefficient n_2 in materials having a low refractive index and dispersion[7]. [11]Fluoride-based glasses, including fluorophosphate, fluorosilicate, and fluoroberyllate types, have the lowest index and dispersion (e.g., BeF_2, with $n_d \sim 1.27$, $V_d \sim 106$), giving nonlinear refractive indices of $\sim 0.25 \times 0.5 \times 10^{-13}$ esu vs. $1\text{–}5 \times 10^{13}$ esu for silicate and phosphate glasses[12].

Glasses containing BeF_2 melt in graphite crucibles under nitrogen at $\sim 1000°C$ using NH_4BF_4. Additional fluorides are added to control optical properties and inhibit devitrification. This includes 10–30 mol % AlF_3, NaF, KF, RbF, and CaF_2[13].

(DAVID A. THOMPSON)

1. Bishay, *J. Non-cryst. Solids, 3*, 54 (1970).
2. E. J. Friebele, D. L. Griscom, in *Treatise on Materials Science and Technology*, Vol. II: *Glass*, Academic Press, New York, p. 257.
3. N. J. Kreidl, in *Ceramics in Severe Environments*, Vol. III, W. W. Kriegl, N. Palmour, eds., Plenum Press, New York, 1971, p. 521.
4. St. Gebala, E. Rysiakiewicz, *Szklo Ceram., 30*, 65 (1979); Chem. Abstr., 91131408.
5. J. S. Stroud, *J. Chem. Phys., 37*, 836 (1962).
6. G. E. Rindone, *Trans. Int. Conf. Glass*, Paris, 1956, p. 373.
7. J. F. White, W. B. Silverman, *J. Am. Ceram. Soc., 33*, 252 (1950).
8. J. Vitko Jr., J. E. Shelby, *Abstr. Solar Reflective Materials Workshop*, 1980 (Sand 79-8754).
9. V. S. Dvernyakov, V. V. Pasichnyi, I. E. Kasich-Pilipeniko, T. V. Eremina, D. K. Sattarov, M. I. Moraveva, I. E. Galant, *Appl. Solar Energy, 15*, 32 (1979).
10. D. L. Cunningham, K. C. Clark, *J. Chem. Phys., 61*, 1118 (1974); *Chem. Abstr.*, 81113264.
11. C. D. Cooper, G. C. Cobb, D. L. Tolnas, *J. Mol. Spectrosc., 7*, 223 (1961).
12. A. Glass, K. L. Cummings, *Laser Program Annual Report*—1975 (to 1979), Lawrence Livermore Laboratory, Contract No. W-7405-Eng-48.
13. W. H. Dumbaugh, D. W. Morgan, *J. Non-Cryst. Solids, 38*, 211 (1980).

17.3.2.6. Glass–Metals Seals

The use of glass in glass–metal seals is justified by its transparency, its relatively low permeability to gases, its desirable electrical properties, and the relative ease with which it can be fused to metal to make vacuum-tight seals. Glass, unlike many crystalline materials, can be altered to control expansion coefficient, viscosity, electrical resistivity,

chemical resistance, and thermal sensitivity over relatively wide ranges. Glass-to-metal seals are of two types[1]: *Matched seals* keep stresses within safe limits by using a glass and metal with compatible coefficients of expansion, and *unmatched seals* have large differences of thermal expansion between glass and metal. Fracture in unmatched seals is avoided by using small diameter metal or ductile metal, or by selecting a graded seal consisting of glasses of intermediate expansion with a final glass of matched expansion. Thermal expansion coefficients of glasses and metals cover similar ranges (Table 1) and additions of glass modifiers and intermediates (see 17.3.2.1.2) control viscosity, electrical, and expansion characteristics[2]. Tungsten and molybdenum are sealed to borosilicate compositions (Tables 2 and 3) except for high pressure discharge lamps, where an alkaline earth aluminosilicate glass is necessary because of the high softening temperature and absence of alkali (to avoid alkali halide reactions). Barium and lead oxides, in combination with Al_2O_3, substitute for boron oxide in both tungsten and molybdenum sealing glasses. Dumet and nickel–iron alloys are sealed with glasses containing lead oxide to raise expansion and soften the glass. Electrical applications require substitution of K_2O for Na_2O to increase resistivity. These glasses are used for sealing copper-coated nickel–iron leads in incandescent lamps. Iron-sealing glasses require high thermal expansion, which is obtained by large amounts of PbO (Corning Code 1990 glass). Kovar sealing glasses illustrate that the transformation temperature of the alloy can be matched with that of the glass by use of alkali and boron oxide addition (Corning Code 7052 glass)[3].

The stress resulting in a glass–metal seal is related to both the thermal expansion difference and the temperature at which the viscosity of the glass is such that stresses start to form during cooling (setting temperature). Both depend on the cooling rate. Therefore,

Table 1. Coefficients of Thermal Expansion (CTE) of Single Oxide Glasses and Metals for Room Temperature

Metal	($\times 10^{-7}$/°C)	Glass	($\times 10^{-7}$/°C)
Al	230		
Cu	167	SiO_2	5–6
Ni	128	GeO_2	77
Fe	129		
Pt	89	B_2O_3	150
W	45		

Table 2. Approximate Compositions of Commercial Glasses

Corning Glass Code	Use	Composition (wt %)								
		SiO_2	Al_2O_3	B_2O_3	Li_2O	Na_2O	K_2O	BaO	PbO	Others
7070	Low loss electrical	72	1	25	0.5	0.5	1			
7740	General	81	2	13		4				
7720	Tungsten sealing	74	1	15		4			6	
7052	Kovar sealing	64	8	19	1	2	3	3		
7570	Solder sealing	3	11	12					74	
0080	General	73	1			17				(MgO, CaO)
1990	Iron sealing	41			2	5	12		40	

Source: Ref. 2.

TABLE 3. THERMAL EXPANSION MISMATCHES BETWEEN GLASSES AND METALS (PPM)[a]

Product code	W	Mo	Kovar	Al_2O_3	Pt	1010 Steel
7070 Borosilicate, electrical	$\overline{290}$	$\overline{690}$	$\overline{770}$	—		
7740 Borosilicate, lab ware	$\overline{550}$	—	—	—		
7720 Borosilicate, tungsten sealing	$\overline{12}$	—				
7052 Borosilicate, Kovar sealing	$\overline{320}$	$\overline{50}$	$\overline{20}$	$\overline{800}$	—	
7550 Lead borate (solder sealing)	+	+	+	$\overline{720}$	$\overline{60}$	—
0080 Soda–lime–silica (general)				+	370	—
1990 Alkali–lead–silicate (iron sealing)				+	+	30

[a]Bar over number indicates that glass CTE is lower than that of metal.

careful control of composition and cooling schedule are usually required. The set point of the glass is close to the strain point. Prediction of stresses in seals is complicated by stress relaxation effects and the temperature dependence of the thermal expansion coefficient of the glass[4]. Therefore, a sandwich seal (i.e., a plate of metal between two plates of glass is usually used to measure stresses[5]. Photoelastic methods are used to measure stress as the composite cools below the glass set point. An upper limit of 10 MN/m^2 calculated stress is used as a guide for glass-matched seals.

(DAVID A. THOMPSON)

1. J. H. Patridge, *Glass-to-Metal Seals*, Society of Glass Technology, Sheffield, England, 1949.
2. D. C. Boyd, D. A. Thompson, in *Kirk-Othmer. Encyclopedia of Chemical Technology*, Vol. II, 3rd ed., Wiley, New York, 1980.
3. H. E. Hagy, *Electron Packag. Prod., 18*, 182 (1978).
4. A. K. Varshneya, *J. Am. Ceram. Soc., 63*, 311 (1980).
5. H. E. Hagy, A. F. Smith, *J. Can. Ceram. Soc., 38*, 63 (1969).

17.3.2.7. Glasses for other Applications

17.3.2.7.1. Glass Frits.

Protective and decorative enamels, solder glasses for glass-to-glass or glass-to-metal seals, and a variety of sintered glass products are made from finely crushed ground glass

Inorganic Reactions and Methods, Volume 18
Edited by J. J. Zuckerman, Jim D. Atwood

TABLE 3. THERMAL EXPANSION MISMATCHES BETWEEN GLASSES AND METALS (PPM)[a]

Product code	W	Mo	Kovar	Al_2O_3	Pt	1010 Steel
7070 Borosilicate, electrical	$\overline{290}$	$\overline{690}$	$\overline{770}$	—		
7740 Borosilicate, lab ware	$\overline{550}$	—	—	—		
7720 Borosilicate, tungsten sealing	$\overline{12}$	—				
7052 Borosilicate, Kovar sealing	$\overline{320}$	$\overline{50}$	$\overline{20}$	$\overline{800}$	—	
7550 Lead borate (solder sealing)	+	+	+	$\overline{720}$	$\overline{60}$	—
0080 Soda–lime–silica (general)				+	370	—
1990 Alkali–lead–silicate (iron sealing)				+	+	30

[a]Bar over number indicates that glass CTE is lower than that of metal.

careful control of composition and cooling schedule are usually required. The set point of the glass is close to the strain point. Prediction of stresses in seals is complicated by stress relaxation effects and the temperature dependence of the thermal expansion coefficient of the glass[4]. Therefore, a sandwich seal (i.e., a plate of metal between two plates of glass is usually used to measure stresses[5]. Photoelastic methods are used to measure stress as the composite cools below the glass set point. An upper limit of 10 MN/m^2 calculated stress is used as a guide for glass-matched seals.

(DAVID A. THOMPSON)

1. J. H. Patridge, *Glass-to-Metal Seals*, Society of Glass Technology, Sheffield, England, 1949.
2. D. C. Boyd, D. A. Thompson, in *Kirk-Othmer. Encyclopedia of Chemical Technology*, Vol. II, 3rd ed., Wiley, New York, 1980.
3. H. E. Hagy, *Electron Packag. Prod., 18*, 182 (1978).
4. A. K. Varshneya, *J. Am. Ceram. Soc., 63*, 311 (1980).
5. H. E. Hagy, A. F. Smith, *J. Can. Ceram. Soc., 38*, 63 (1969).

17.3.2.7. Glasses for other Applications

17.3.2.7.1. Glass Frits.

Protective and decorative enamels, solder glasses for glass-to-glass or glass-to-metal seals, and a variety of sintered glass products are made from finely crushed ground glass

frit. Enamels and solder glasses are designed to be fluid (viscosity ~ 300 pa·s) at their processing temperatures, while the substrates to which they are joined remain relatively rigid (viscosity = 10^8–10^{13} pa·s). Protective coatings such as porcelain enamels and glazes for both metal and glass, are ball-milled with a variety of clays, electrolytes, and fluids to achieve the correct particle shape and size distribution (< 74 μm to < 44 μm) before dipping, spraying, or dusting on the ware for final firing (glazing).

Compositions of frit glasses vary with application, but for porcelain enamel coatings[1,2] SiO_2, Al_2O_3, B_2O_3, Na_2O, and K_2O form the glass, and additions of CoO, NiO, and MnO_2 control glass-to-meal reactions for better adhesion[3]. Addition of TiO_2 to the glass gives a titania enamel that is used as a second coating. Examples of other frit glass compositions include borosilicates, zirconium silicates, and alkali–lead silicates. Glass frits that crystallize during firing are devitrifying frits (e.g., PbO-B_2O_3-ZnO). Rapid quenching from the molten state involves high thermal stresses that shock and break into small pieces suitable for charging into a ball mill. More commonly, glass is either quenched in water (dry gaged) or quenched between water-cooled metal rollers to make thin, friable ribbon. The thin-rolled ribbon provides more uniform mill feed, (dry gaging sometimes form clinkerlike tempered pieces, which are difficult to mill.

Small, complex glass articles such as thread guides for the textile industry and television gun mounts are made by a multiform process. Dry-milled powder is mixed with an organic binder and a fluid vehicle, then atomized by a spray dryer into small, dried agglomerates of glass powder and binder with good flow characteristics. The articles are subsequently pressed to the desired shape and fired.

(DAVID A. THOMPSON)

1. A. I. Andrews, *Porcelain Enamels*, Garrard Press, Champaign, *I*, 1961.
2. C. W. Parmelee, *Ceramic Glazes*, 3rd ed., Cahners Publishing, Boston, 1973.
3. J. A. Pask, in *Modern Aspects of the Vitreous State*, Vol. 3, J.C. Mackenzie, ed., Butterworth, Washington, DC, 1964, p. 1.

17.3.2.7.2. Porous Glass.

A glass having an initial composition of 67% SiO_2, 26% B_2O_3, and 7% Na_2O[1] separates upon heat treatment into an alkali–borate phase and a phase containing 96% SiO_2, 3% B_2O_3, 0.4% Al_2O_3, and traces of Na_2O and As_2O_3. The alkali–borate phase is leached with hot HNO_3 or HCL. Commercially available porous glass (Corning Code 7930 glass) has a density of 1.5 g/cm^3, pore diameter of 4 nm, and internal surface area of ~ 200 m^2/g. Porous glass absorbs both water and organic materials from air, which are removed by 30% H_2O_2 treatment and heating in air at 400–500°C.

Porous glass is used as substrates for immobilization of enzymes[2], for porous disks for electrodes, and as a precursor for Vycor (96% SiO_2) brand glass. The latter is a result of consolidation of the porous glass at ~ 1000°C.

(DAVID A. THOMPSON)

1. H. P. Hood, M. E. Nordberg, U.S. Patent 2, 106, 744 (1938); Chem. Abstr. 32002703.
2. H. H. Weetall, in Immobilized Enzymes for Industrial Reactors, Academic Press, New York, 1975, p. 21.

17.3.2.7.3. Unconventional Melting and Glass Films.

Unconventional melting of glasses includes[1] splat cooling, which is used extensively to produce amorphous metals; laser spin melting, which can produce 100–800 μm

Inorganic Reactions and Methods, Volume 18
Edited by J. J. Zuckerman, Jim D. Atwood

frit. Enamels and solder glasses are designed to be fluid (viscosity ~ 300 pa·s) at their processing temperatures, while the substrates to which they are joined remain relatively rigid (viscosity = 10^8–10^{13} pa·s). Protective coatings such as porcelain enamels and glazes for both metal and glass, are ball-milled with a variety of clays, electrolytes, and fluids to achieve the correct particle shape and size distribution (< 74 μm to < 44 μm) before dipping, spraying, or dusting on the ware for final firing (glazing).

Compositions of frit glasses vary with application, but for porcelain enamel coatings[1,2] SiO_2, Al_2O_3, B_2O_3, Na_2O, and K_2O form the glass, and additions of CoO, NiO, and MnO_2 control glass-to-meal reactions for better adhesion[3]. Addition of TiO_2 to the glass gives a titania enamel that is used as a second coating. Examples of other frit glass compositions include borosilicates, zirconium silicates, and alkali–lead silicates. Glass frits that crystallize during firing are devitrifying frits (e.g., PbO-B_2O_3-ZnO). Rapid quenching from the molten state involves high thermal stresses that shock and break into small pieces suitable for charging into a ball mill. More commonly, glass is either quenched in water (dry gaged) or quenched between water-cooled metal rollers to make thin, friable ribbon. The thin-rolled ribbon provides more uniform mill feed, (dry gaging sometimes form clinkerlike tempered pieces, which are difficult to mill.

Small, complex glass articles such as thread guides for the textile industry and television gun mounts are made by a multiform process. Dry-milled powder is mixed with an organic binder and a fluid vehicle, then atomized by a spray dryer into small, dried agglomerates of glass powder and binder with good flow characteristics. The articles are subsequently pressed to the desired shape and fired.

(DAVID A. THOMPSON)

1. A. I. Andrews, *Porcelain Enamels*, Garrard Press, Champaign, *I*, 1961.
2. C. W. Parmelee, *Ceramic Glazes*, 3rd ed., Cahners Publishing, Boston, 1973.
3. J. A. Pask, in *Modern Aspects of the Vitreous State*, Vol. 3, J.C. Mackenzie, ed., Butterworth, Washington, DC, 1964, p. 1.

17.3.2.7.2. Porous Glass.

A glass having an initial composition of 67% SiO_2, 26% B_2O_3, and 7% Na_2O[1] separates upon heat treatment into an alkali–borate phase and a phase containing 96% SiO_2, 3% B_2O_3, 0.4% Al_2O_3, and traces of Na_2O and As_2O_3. The alkali–borate phase is leached with hot HNO_3 or HCL. Commercially available porous glass (Corning Code 7930 glass) has a density of 1.5 g/cm^3, pore diameter of 4 nm, and internal surface area of ~ 200 m^2/g. Porous glass absorbs both water and organic materials from air, which are removed by 30% H_2O_2 treatment and heating in air at 400–500°C.

Porous glass is used as substrates for immobilization of enzymes[2], for porous disks for electrodes, and as a precursor for Vycor (96% SiO_2) brand glass. The latter is a result of consolidation of the porous glass at ~ 1000°C.

(DAVID A. THOMPSON)

1. H. P. Hood, M. E. Nordberg, U.S. Patent 2, 106, 744 (1938); Chem. Abstr. 32002703.
2. H. H. Weetall, in Immobilized Enzymes for Industrial Reactors, Academic Press, New York, 1975, p. 21.

17.3.2.7.3. Unconventional Melting and Glass Films.

Unconventional melting of glasses includes[1] splat cooling, which is used extensively to produce amorphous metals; laser spin melting, which can produce 100–800 μm

Inorganic Reactions and Methods, Volume 18
Edited by J. J. Zuckerman, Jim D. Atwood

frit. Enamels and solder glasses are designed to be fluid (viscosity ~ 300 pa·s) at their processing temperatures, while the substrates to which they are joined remain relatively rigid (viscosity = 10^8–10^{13} pa·s). Protective coatings such as porcelain enamels and glazes for both metal and glass, are ball-milled with a variety of clays, electrolytes, and fluids to achieve the correct particle shape and size distribution (< 74 μm to < 44 μm) before dipping, spraying, or dusting on the ware for final firing (glazing).

Compositions of frit glasses vary with application, but for porcelain enamel coatings[1,2] SiO_2, Al_2O_3, B_2O_3, Na_2O, and K_2O form the glass, and additions of CoO, NiO, and MnO_2 control glass-to-meal reactions for better adhesion[3]. Addition of TiO_2 to the glass gives a titania enamel that is used as a second coating. Examples of other frit glass compositions include borosilicates, zirconium silicates, and alkali–lead silicates. Glass frits that crystallize during firing are devitrifying frits (e.g., PbO-B_2O_3-ZnO). Rapid quenching from the molten state involves high thermal stresses that shock and break into small pieces suitable for charging into a ball mill. More commonly, glass is either quenched in water (dry gaged) or quenched between water-cooled metal rollers to make thin, friable ribbon. The thin-rolled ribbon provides more uniform mill feed, (dry gaging sometimes form clinkerlike tempered pieces, which are difficult to mill.

Small, complex glass articles such as thread guides for the textile industry and television gun mounts are made by a multiform process. Dry-milled powder is mixed with an organic binder and a fluid vehicle, then atomized by a spray dryer into small, dried agglomerates of glass powder and binder with good flow characteristics. The articles are subsequently pressed to the desired shape and fired.

(DAVID A. THOMPSON)

1. A. I. Andrews, *Porcelain Enamels*, Garrard Press, Champaign, *I*, 1961.
2. C. W. Parmelee, *Ceramic Glazes*, 3rd ed., Cahners Publishing, Boston, 1973.
3. J. A. Pask, in *Modern Aspects of the Vitreous State*, Vol. 3, J.C. Mackenzie, ed., Butterworth, Washington, DC, 1964, p. 1.

17.3.2.7.2. Porous Glass.

A glass having an initial composition of 67% SiO_2, 26% B_2O_3, and 7% Na_2O[1] separates upon heat treatment into an alkali–borate phase and a phase containing 96% SiO_2, 3% B_2O_3, 0.4% Al_2O_3, and traces of Na_2O and As_2O_3. The alkali–borate phase is leached with hot HNO_3 or HCL. Commercially available porous glass (Corning Code 7930 glass) has a density of 1.5 g/cm^3, pore diameter of 4 nm, and internal surface area of ~ 200 m^2/g. Porous glass absorbs both water and organic materials from air, which are removed by 30% H_2O_2 treatment and heating in air at 400–500°C.

Porous glass is used as substrates for immobilization of enzymes[2], for porous disks for electrodes, and as a precursor for Vycor (96% SiO_2) brand glass. The latter is a result of consolidation of the porous glass at ~ 1000°C.

(DAVID A. THOMPSON)

1. H. P. Hood, M. E. Nordberg, U.S. Patent 2, 106, 744 (1938); Chem. Abstr. 32002703.
2. H. H. Weetall, in Immobilized Enzymes for Industrial Reactors, Academic Press, New York, 1975, p. 21.

17.3.2.7.3. Unconventional Melting and Glass Films.

Unconventional melting of glasses includes[1] splat cooling, which is used extensively to produce amorphous metals; laser spin melting, which can produce 100–800 μm

spheres of refractory oxide glasses; and melting under high pressure, to permit the incorporation of enormous quantities of volatile components into the glass structure[1]. Solid state transformations (e.g., shock and irradiation) produce amorphous materials from bulk crystalline phases by destroying the lattice structure at low temperatures.

Glass films are used in the semiconductor industry because of their dielectric properties, and are used for encapsulating integrated circuits and other electronic devices because they provide a hermetic seal. Glass films are formed by both reactive and non reactive deposition methods, (e.g., evaporation, sputtering, and ion implantation or ion platting for the latter).

In Reactive sputtering, highly active metal atoms are reacted with a gas prior to either deposition on a cold substrate. For example, the presence of oxygen or nitrogen combined with a high-purity silicon metal cathode in a sputtering chamber leads to the deposition of high purity amorphous silicon dioxide or silicon nitride. The high quench rate and the absence of impurities make possible the production of $PbTeO_3$, GeO_2, SiO_2, and Al_2O_3–SiO_2, glasses.

Thermal oxidation is an old and common method of forming a primary passivating film of SiO_2 on silicon. The metal is heated in dry oxygen, in wet oxygen, or in steam. A silica layer grows inwardly from the surface by a thermal oxidation mechanism. The silicon wafer is heated to 600–1200°C to achieve 1 μm thick films in about an hour.

(DAVID A. THOMPSON)

1. G. W. Scherer and P. C. Schultz in *Glass: Science and Technology*, Vol. III, N. J. Kreidl, D. R. Uhlmann, eds., Academic Press, New York, 1979.

17.3.3. Preparation of Glass Ceramics

17.3.3.1. Glass Ceramic Systems

Glass ceramics are polycrystalline ceramics consisting of from 50 to more than 90 vol% crystalline phases dispersed in a glass matrix. They are prepared by crystallizing a glass precursor, hence the term "glass ceramic". Several advantages are inherent in this technique of preparing ceramics: properties of the ceramic such as thermal expansion, electrical conductivity, and dielectric properties can be adjusted over a large range by varying the composition of the parent glass; fabrication processes may be automated and inexpensive (similar to glass fabrication); and unique ceramics may be produced (e.g., machinable glass ceramics and zero thermal expansion ceramics).

Conversion of glass to a polycrystalline ceramic is accompanied by increased strength (two to four times), increased fracture toughness (two to four times), increased electrical resistivity (10^4 times), increased deformation temperature (200–400°C), increased abrasion resistance, and increased thermal shock resistance. All these factors contribute to many applications for glass ceramics: dinnerware, cooking utensils, stove tops, radomes, hermetic seals to metals, building materials, and so on.

This work was supported by the United States Department of Energy under Contract DE-AC04-94AL85000. Sandia is a multiprogram laboratory operated by Sandia Corporation, a Lockheed Martin Company, for the United States Department of Energy.

Inorganic Reactions and Methods, Volume 18
Edited by J. J. Zuckerman, Jim D. Atwood

spheres of refractory oxide glasses; and melting under high pressure, to permit the incorporation of enormous quantities of volatile components into the glass structure[1]. Solid state transformations (e.g., shock and irradiation) produce amorphous materials from bulk crystalline phases by destroying the lattice structure at low temperatures.

Glass films are used in the semiconductor industry because of their dielectric properties, and are used for encapsulating integrated circuits and other electronic devices because they provide a hermetic seal. Glass films are formed by both reactive and non reactive deposition methods, (e.g., evaporation, sputtering, and ion implantation or ion platting for the latter).

In Reactive sputtering, highly active metal atoms are reacted with a gas prior to either deposition on a cold substrate. For example, the presence of oxygen or nitrogen combined with a high-purity silicon metal cathode in a sputtering chamber leads to the deposition of high purity amorphous silicon dioxide or silicon nitride. The high quench rate and the absence of impurities make possible the production of $PbTeO_3$, GeO_2, SiO_2, and Al_2O_3–SiO_2, glasses.

Thermal oxidation is an old and common method of forming a primary passivating film of SiO_2 on silicon. The metal is heated in dry oxygen, in wet oxygen, or in steam. A silica layer grows inwardly from the surface by a thermal oxidation mechanism. The silicon wafer is heated to 600–1200°C to achieve 1 μm thick films in about an hour.

(DAVID A. THOMPSON)

1. G. W. Scherer and P. C. Schultz in *Glass: Science and Technology*, Vol. III, N. J. Kreidl, D. R. Uhlmann, eds., Academic Press, New York, 1979.

17.3.3. Preparation of Glass Ceramics

17.3.3.1. Glass Ceramic Systems

Glass ceramics are polycrystalline ceramics consisting of from 50 to more than 90 vol% crystalline phases dispersed in a glass matrix. They are prepared by crystallizing a glass precursor, hence the term "glass ceramic". Several advantages are inherent in this technique of preparing ceramics: properties of the ceramic such as thermal expansion, electrical conductivity, and dielectric properties can be adjusted over a large range by varying the composition of the parent glass; fabrication processes may be automated and inexpensive (similar to glass fabrication); and unique ceramics may be produced (e.g., machinable glass ceramics and zero thermal expansion ceramics).

Conversion of glass to a polycrystalline ceramic is accompanied by increased strength (two to four times), increased fracture toughness (two to four times), increased electrical resistivity (10^4 times), increased deformation temperature (200–400°C), increased abrasion resistance, and increased thermal shock resistance. All these factors contribute to many applications for glass ceramics: dinnerware, cooking utensils, stove tops, radomes, hermetic seals to metals, building materials, and so on.

This work was supported by the United States Department of Energy under Contract DE-AC04-94AL85000. Sandia is a multiprogram laboratory operated by Sandia Corporation, a Lockheed Martin Company, for the United States Department of Energy.

Glass ceramics result from the propensity for glass, which is metastable, to transform to the more stable crystalline form. Commercial glasses are carefully formulated to reduce their tendency to crystallize during forming and annealing. Nevertheless, with relatively small changes in chemical composition and appropriate heating, these glasses can also be crystallized, although generally their properties will not be very useful. However, glass ceramics are specially formulated to develop a controlled assemblage of crystalline phases to produce desired properties. The phase assemblage is determined both by the composition of the glass and the processes of nucleation and crystallization brought about by the particular heating cycle used.

Glass ceramics offer a broad range of properties and combinations of properties that are not attainable in conventionally, formed ceramics or glasses. Increasing knowledge of nucleation and crystallization processes is enhancing our ability to develop specific crystalline phases and microstructures. This capability, along with a worldwide emphasis on effectively using abundant mineral resources and waste products such as slags and fly ash, should stimulate continued growth in glass ceramic technology and science.

(ROBERT J. EAGAN, RONALD E. LOEHMAN)

17.3.3.1.1. Nucleation.

The high performance of glass ceramics results from their very small crystallite size. Large thermal expansion differences between the crystal and residual glass phase or large anisotropy in expansion of the crystal, which would result in catastrophic stresses around large crystals in a glass, are easily accommodated with small grains, often of submicrometer size. Moreover, the mechanical strength of a ceramic body is generally much higher with small grains than with large ones. Thus, the key to producing glass ceramics with small crystallite sizes is the ability to nucleate crystallization from many sites within the bulk of the glass.

Many commercial glass ceramics employ heterogeneous nucleation, in which a minor phase initially precipitates out of a cooling glass melt and provides sites for the subsequent crystallization of the major phase. Colloidal metal particles, such as gold and copper, that form when photosensitive glasses are exposed to ultraviolet light are effective nucleating agents[1,2]. Prolonged heat treatment at higher temperatures than normally used to develop the photographic image can convert photosensitive glass to a polycrystalline ceramic. Other nucleating agents include oxides with high field strength cations such as TiO_2, ZrO_2, and P_2O_5, and dispersions of the platinum group metals.

Though nucleation mechanisms in glass ceramics are not completely understood, the temperature dependence of the process is qualitatively explained by a model derived for simple monatomic systems[3]. The model defines a nucleus as a collection of atoms with periodicity characteristic of a crystal that does not spontaneously revert to the disordered liquid state. When a nucleus forms, there is a change ΔG in the Gibbs energy of the system. This change consists of a free energy reduction per unit volume associated with changing to a more stable crystalline phase, Δgv, and an increase in free energy per unit surface area associated with forming a new surface, Δgs, between the crystalline and liquid phase:

$$\Delta G = -\tfrac{4}{3}\pi r^3 \Delta gv + 4\pi r^2 \Delta gs \qquad \text{(a)}$$

At small r, the interfacial energy term is dominant, but as r increases, the two terms become equal. At this radius, r^*, the nucleus is stable; that is, it will tend to grow because

that reduces the free energy of the system. The change in free energy at the critical size of the nucleus is ΔG^*:

$$\Delta G^* = \frac{16\pi(\Delta gs)^3}{3(\Delta gv)^2} \tag{b}$$

For simple systems, the nucleation rate, I, can be expressed as the probability of forming stable nuclei[4]:

$$I \approx A \exp\left(\frac{-\Delta G^*}{kT}\right) \tag{c}$$

The preexponential, A, is related to the movement of atoms or molecules to and from the nucleus. This expression does not account for diffusion effects in transporting atoms across the nucleus–liquid interface. To explain the observed temperature dependence of nucleation rate (Fig. 1), we include an energy barrier for diffusion, Q:

$$I = A \exp\left(\frac{-\Delta G^*}{kT}\right) \exp\left(\frac{-Q}{kT}\right) \tag{d}$$

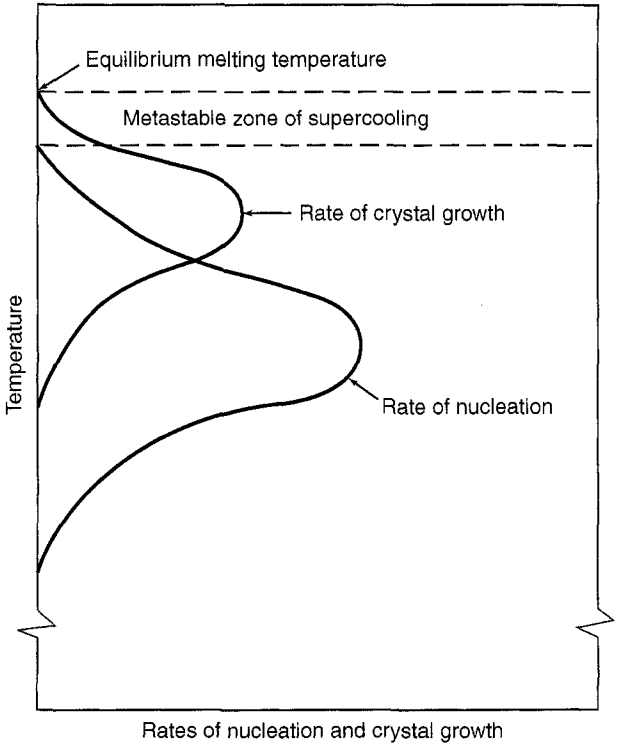

Figure 1. Nucleation rate and growth rate initially increase with supercooling, then decrease as atomic mobility is reduced by the increasing viscosity of the glass. Typical linear growth rates of crystals are 1–20 μm/min.

As a melt is cooled below its liquidus (the equilibrium melting temperature of the crystalline phases), the nucleation rate is initially small because $\Delta G^*/T$ is large. Further cooling reduces $\Delta G^*/T$ until it approximately equals Q/T. At this temperature, the maximum nucleation rate occurs. Further cooling increases Q/T relative to $\Delta G^*/T$; that is, diffusion becomes the limiting factor, and nucleation eventually stops. Because the maximum nucleation rate often occurs at a lower temperature than the temperature at which the crystal growth rate is maximum, numerous nuclei can form.

The ability of noble metal particles to serve as nuclei for growth of crystalline phases is attributed to the ability of the particle to act as a site for epitaxial growth. This proposal requires that the particle be wet by the glass (low contact angle), that it be sufficiently large (>80 Å) to allow a stable crystal nucleus to form, and that the crystallographic lattice dimensions of the particle be similar to those of the crystalline phase growing on it. This model and the experimental evidence to support it in glass systems are well developed.

The nucleating effects of oxides of high field strength cations (e.g., TiO_2) are most often attributed to their tendency to cause phase separation in glasses[5]. Experimental evidence for the effect is much less clear than for metallic nucleating agents, in part because phase separation itself is difficult to observe. It is hypothesized that the high field strength ions cause local ordering in the glass structure, which leads to a more unstable phase (i.e., a phase relatively rich in alkali ions that starts to crystallize before the bulk glass, or a phase boundary formed between two glasses that acts as a site for crystallization). Oxide nucleating agents are widely used because they are effective for many glass ceramics and are relatively inexpensive compared to noble metal dispersions.

(ROBERT J. EAGAN, RONALD E. LOEHMAN)

1. S.D. Stookey, *Ind. Eng. Chem.*, *51*, 805 (1959).
2. U.S. Patent, 2,920,971 (1960).
3. G. Tamman, *The States of Aggregation*, Van Nostrand, New York, 1925.
4. J. Frenkel, *Kinetic Theory of Liquids*, Clarendon Press, Oxford, 1946.
5. R. Becker, *Am. Phys.*, *32*, 128 (1938).

17.3.3.1.2. Heat Treatment.

In addition to requiring nucleating agents to promote crystallization, glass ceramics usually must be heat-treated at the critical nucleating, crystallization, and annealing temperatures to restructure the glass (Fig. 1). These temperatures can be conveniently determined, to a first approximation, by differential thermal analysis (DTA)[1] (Fig. 2).

Glass ceramics are melted from raw materials such as silica (SiO_2), feldspar (K_2O–Al_2O_3–$6SiO_2$), limestone ($CaCO_3$), and rutile (TiO_2) by the same processes used to prepare glass. However, slightly higher temperatures or more corrosion-resistant refractories may be required. Forming processes are also similar to those for glasses, though modifications may be required because the precursor glasses are "short" (i.e., change viscosity more rapidly with temperature, and, therefore, must be formed either more quickly or at higher temperatures.

The precursor glass article may be annealed and cooled to room temperature for inspection (it is usually transparent), or it may be cooled to the nucleation temperature

Inorganic Reactions and Methods, Volume 18
Edited by J. J. Zuckerman, Jim D. Atwood

As a melt is cooled below its liquidus (the equilibrium melting temperature of the crystalline phases), the nucleation rate is initially small because $\Delta G^*/T$ is large. Further cooling reduces $\Delta G^*/T$ until it approximately equals Q/T. At this temperature, the maximum nucleation rate occurs. Further cooling increases Q/T relative to $\Delta G^*/T$; that is, diffusion becomes the limiting factor, and nucleation eventually stops. Because the maximum nucleation rate often occurs at a lower temperature than the temperature at which the crystal growth rate is maximum, numerous nuclei can form.

The ability of noble metal particles to serve as nuclei for growth of crystalline phases is attributed to the ability of the particle to act as a site for epitaxial growth. This proposal requires that the particle be wet by the glass (low contact angle), that it be sufficiently large (>80 Å) to allow a stable crystal nucleus to form, and that the crystallographic lattice dimensions of the particle be similar to those of the crystalline phase growing on it. This model and the experimental evidence to support it in glass systems are well developed.

The nucleating effects of oxides of high field strength cations (e.g., TiO_2) are most often attributed to their tendency to cause phase separation in glasses[5]. Experimental evidence for the effect is much less clear than for metallic nucleating agents, in part because phase separation itself is difficult to observe. It is hypothesized that the high field strength ions cause local ordering in the glass structure, which leads to a more unstable phase (i.e., a phase relatively rich in alkali ions that starts to crystallize before the bulk glass, or a phase boundary formed between two glasses that acts as a site for crystallization). Oxide nucleating agents are widely used because they are effective for many glass ceramics and are relatively inexpensive compared to noble metal dispersions.

(ROBERT J. EAGAN, RONALD E. LOEHMAN)

1. S.D. Stookey, *Ind. Eng. Chem.*, *51*, 805 (1959).
2. U.S. Patent, 2,920,971 (1960).
3. G. Tamman, *The States of Aggregation*, Van Nostrand, New York, 1925.
4. J. Frenkel, *Kinetic Theory of Liquids*, Clarendon Press, Oxford, 1946.
5. R. Becker, *Am. Phys.*, *32*, 128 (1938).

17.3.3.1.2. Heat Treatment.

In addition to requiring nucleating agents to promote crystallization, glass ceramics usually must be heat-treated at the critical nucleating, crystallization, and annealing temperatures to restructure the glass (Fig. 1). These temperatures can be conveniently determined, to a first approximation, by differential thermal analysis (DTA)[1] (Fig. 2).

Glass ceramics are melted from raw materials such as silica (SiO_2), feldspar (K_2O–Al_2O_3–$6SiO_2$), limestone ($CaCO_3$), and rutile (TiO_2) by the same processes used to prepare glass. However, slightly higher temperatures or more corrosion-resistant refractories may be required. Forming processes are also similar to those for glasses, though modifications may be required because the precursor glasses are "short" (i.e., change viscosity more rapidly with temperature, and, therefore, must be formed either more quickly or at higher temperatures.

The precursor glass article may be annealed and cooled to room temperature for inspection (it is usually transparent), or it may be cooled to the nucleation temperature

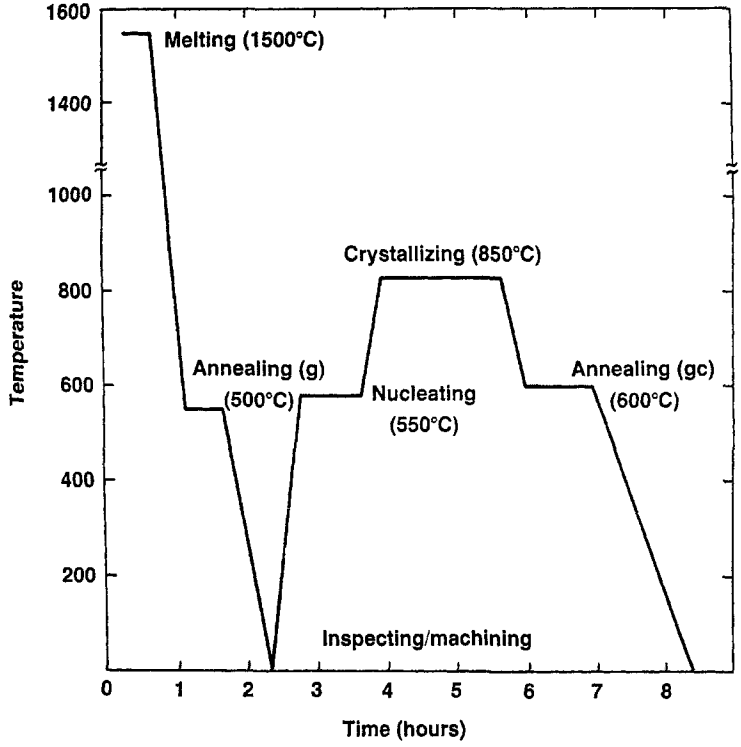

Figure 1. Idealized heat treatment schedule for melting a glass ceramic and converting it to a polycrystalline ceramic. Hold temperatures for annealing the glass (g) and nucleating and crystallizing correspond to data derived from the differential thermal analysis shown in Figure 2. The melting behavior depends on the fluidity of the glass. The annealing temperature of the glass ceramic (gc) depends on the composition of the residual glass, which can be established by analyzing the crystallized glass ceramic.

and held for a period of time, typically 30–120 minutes. The nucleation temperature is approximately at the glass transition temperature and corresponds to a viscosity of $= 10^{11}$ poise. The temperature dependence of the nucleation rate must be experimentally determined for each glass ceramic composition.

The nucleated glass is converted to a polycrystalline ceramic by heating it to a temperature at which crystal growth occurs and holding it for a period of time, typically 30–300 minutes. The rate at which the glass ceramic is heated to this temperature is critical. It must be slow enough to allow some crystallization to occur to stiffen the glass ceramic sufficiently to prevent slumping due to the rapid decrease in the viscosity of the glass with increasing temperature[2].

(ROBERT J. EAGAN, RONALD E. LOEHMAN)

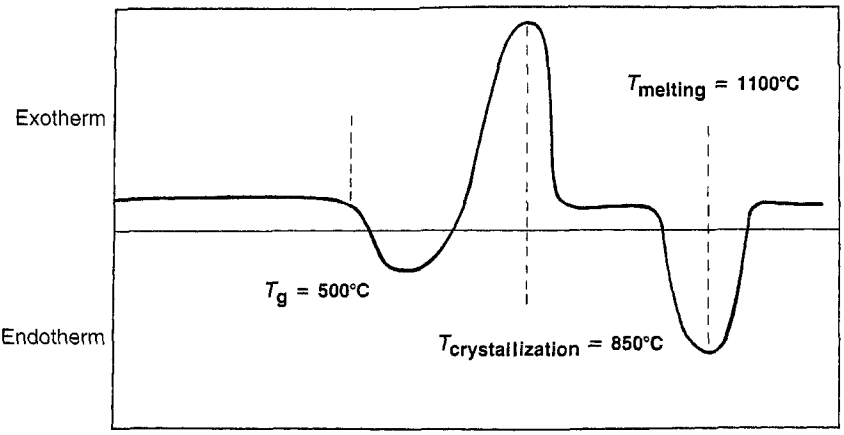

Figure 2. Thermal analysis of a simple glass ceramic shows an annealing temperature of ≈500°C, a peak crystallization temperature of 850°C, and a melting temperature of that crystalline phase of ≈1100°C. These temperatures are approximate temperatures for nucleating (500°C) and crystallizing (850°C) this glass ceramic.

1. T. Ramsey, *Am. Ceramic Soc. Bull., 50*, 671 (1971).
2. P. W. McMillan, *Glass Ceramics*, 2nd ed., Academic Press, London 1979. (An excellent review.)

17.3.3.1.3. Crystal Growth.

A crystal growth model[1] derived to explain the rate of crystal growth from monatomic melts applies to glass ceramics, but values of the parameters used in the equations are not well defined. The model proposes that crystallization rate is a function of the difference between the rate at which atoms jump from the melt to the crystal and the rate at which they jump from the crystal back to the melt. The energy that the atoms must acquire to jump from the melt to the crystal ΔGa, is less than the energy required for the reverse jump, $\Delta Ga + \Delta G$, where ΔG is the difference in free energy between the glass and the crystal. The rates at which atoms leave the liquid, Q_{LS}, and solid, Q_{SL}, depend on the energy required for the jump:

$$Q_{LS} = \nu_0 \exp\left(\frac{-\Delta Ga}{RT}\right) \tag{a}$$

$$Q_{SL} = \nu_0 \exp\left[-\left(\frac{\Delta Ga}{RT} + \frac{\Delta G}{RT}\right)\right] \tag{b}$$

where ν_0 is the fundamental vibration frequency of atoms, R is the molar gas constant, and T is temperature.

The net rate of transfer from the liquid to the crystal is the difference between frequency of jumps in each direction:

$$Q = Q_{LS} - Q_{SL} = \nu_0\left[1 - \exp\left(\frac{-\Delta G}{RT}\right)\right]\exp\left(\frac{-\Delta Ga}{RT}\right) \tag{c}$$

Inorganic Reactions and Methods, Volume 18
Edited by J. J. Zuckerman, Jim D. Atwood

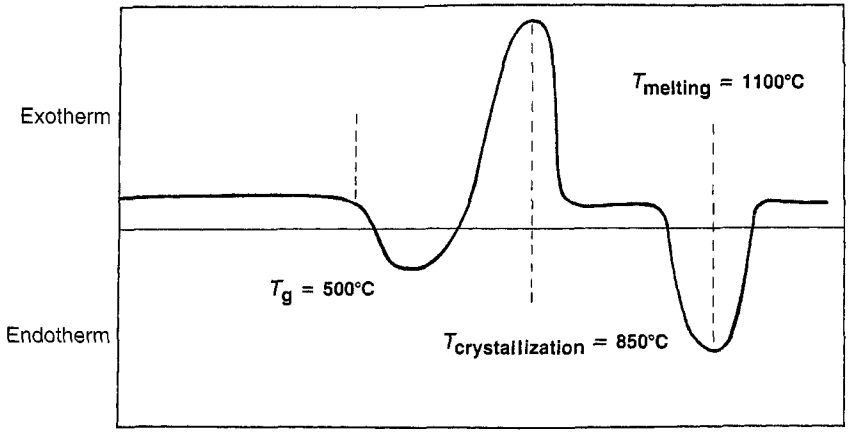

Figure 2. Thermal analysis of a simple glass ceramic shows an annealing temperature of ≈500°C, a peak crystallization temperature of 850°C, and a melting temperature of that crystalline phase of ≈1100°C. These temperatures are approximate temperatures for nucleating (500°C) and crystallizing (850°C) this glass ceramic.

1. T. Ramsey, *Am. Ceramic Soc. Bull., 50,* 671 (1971).
2. P. W. McMillan, *Glass Ceramics,* 2nd ed., Academic Press, London 1979. (An excellent review.)

17.3.3.1.3. Crystal Growth.

A crystal growth model[1] derived to explain the rate of crystal growth from monatomic melts applies to glass ceramics, but values of the parameters used in the equations are not well defined. The model proposes that crystallization rate is a function of the difference between the rate at which atoms jump from the melt to the crystal and the rate at which they jump from the crystal back to the melt. The energy that the atoms must acquire to jump from the melt to the crystal ΔGa, is less than the energy required for the reverse jump, $\Delta Ga + \Delta G$, where ΔG is the difference in free energy between the glass and the crystal. The rates at which atoms leave the liquid, Q_{LS}, and solid, Q_{SL}, depend on the energy required for the jump:

$$Q_{LS} = \nu_0 \exp\left(\frac{-\Delta Ga}{RT}\right) \tag{a}$$

$$Q_{SL} = \nu_0 \exp\left[-\left(\frac{\Delta Ga}{RT} + \frac{\Delta G}{RT}\right)\right] \tag{b}$$

where ν_0 is the fundamental vibration frequency of atoms, R is the molar gas constant, and T is temperature.

The net rate of transfer from the liquid to the crystal is the difference between frequency of jumps in each direction:

$$Q = Q_{LS} - Q_{SL} = \nu_0\left[1 - \exp\left(\frac{-\Delta G}{RT}\right)\right]\exp\left(\frac{-\Delta Ga}{RT}\right) \tag{c}$$

The increase in length due to the addition of one layer of atoms, Λ, multiplied by the number of atoms transferred per unit time per unit area, is the growth rate, U:

$$U = \Lambda v_0 \exp\left(\frac{-\Delta Ga}{RT}\right)\left[1 - \exp\left(\frac{-\Delta G}{RT}\right)\right] \quad \text{(d)}$$

The growth rate can be related to melt viscosity, η, by defining a rate constant D'':

$$D'' = D_0 \exp\left(\frac{-\Delta Ga}{RT}\right) \quad \text{(e)}$$

where $D_0 = \lambda^2 v_0$ and using the Stokes–Einstein relation:

$$D'' = \frac{kT}{3\pi\eta\lambda} \quad \text{(f)}$$

where v is the coefficient of shear viscosity and k is the Boltzmann constant.

As indicated earlier (17.3.3.1.2, Fig. 1), crystal growth rates initially increase as a melt is cooled below the liquidus, then decrease as the viscosity of the melt increases to the point at which ionic mobility is very small:

$$U = \frac{kT}{3\pi\lambda^2\eta}\left[1 - \exp\left(\frac{-\Delta G}{RT}\right)\right] \quad \text{(g)}$$

After crystallization, a glass ceramic is 50–95 vol% crystalline. If the glass ceramic contains substantial glass, it must be annealed to relieve stress in the glass phase. Large articles or high thermal expansion pieces must cool slowly to minimize stresses generated by thermal gradients.

The microstructure (i.e., the shape and size of the crystalline phase) depends to some extent on the nucleation process, the crystal growth mechanism, and the rate of growth. Growth from many nucleation sites limits the crystallite size because the crystals soon impinge on one another and stop growing. Conversely, growth from only a few sites leads to a few large crystals. The crystal growth process also influences the microstructure. Prolonged heat treatment at high temperatures causes large crystals to grow through Ostwald ripening.

Spherulitic crystals also are often found in glass ceramics. Spherulitic growth, or branching growth from a central point, is common in viscous systems where ionic mobility is the rate-limiting step. Models developed for polymer systems apply to glass ceramics and qualitatively explain the tendency to form spherulites[2].

(ROBERT J. EAGAN, RONALD E. LOEHMAN)

1. W. Hillig, D. Turnbull, *J. Chem. Phys.*, *24*, 914 (1956).
2. H. Keith, F. Padden, *J. Appl. Phys.*, *35*, 1270 (1964).

17.3.3.1.4. Chemical Composition.

The Li_2O–Al_2O_3–SiO_2 system is the basis of some commercially important low thermal expansion glass ceramics, photosensitive glass ceramics, and higher thermal expansion glass ceramics that form seals with metals[2]. The crystalline phases developed

Inorganic Reactions and Methods, Volume 18
Edited by J. J. Zuckerman, Jim D. Atwood

The increase in length due to the addition of one layer of atoms, Λ, multiplied by the number of atoms transferred per unit time per unit area, is the growth rate, U:

$$U = \Lambda v_0 \exp\left(\frac{-\Delta Ga}{RT}\right)\left[1 - \exp\left(\frac{-\Delta G}{RT}\right)\right] \quad \text{(d)}$$

The growth rate can be related to melt viscosity, η, by defining a rate constant D'':

$$D'' = D_0 \exp\left(\frac{-\Delta Ga}{RT}\right) \quad \text{(e)}$$

where $D_0 = \lambda^2 v_0$ and using the Stokes–Einstein relation:

$$D'' = \frac{kT}{3\pi\eta\lambda} \quad \text{(f)}$$

where v is the coefficient of shear viscosity and k is the Boltzmann constant.

As indicated earlier (17.3.3.1.2, Fig. 1), crystal growth rates initially increase as a melt is cooled below the liquidus, then decrease as the viscosity of the melt increases to the point at which ionic mobility is very small:

$$U = \frac{kT}{3\pi\lambda^2\eta}\left[1 - \exp\left(\frac{-\Delta G}{RT}\right)\right] \quad \text{(g)}$$

After crystallization, a glass ceramic is 50–95 vol% crystalline. If the glass ceramic contains substantial glass, it must be annealed to relieve stress in the glass phase. Large articles or high thermal expansion pieces must cool slowly to minimize stresses generated by thermal gradients.

The microstructure (i.e., the shape and size of the crystalline phase) depends to some extent on the nucleation process, the crystal growth mechanism, and the rate of growth. Growth from many nucleation sites limits the crystallite size because the crystals soon impinge on one another and stop growing. Conversely, growth from only a few sites leads to a few large crystals. The crystal growth process also influences the microstructure. Prolonged heat treatment at high temperatures causes large crystals to grow through Ostwald ripening.

Spherulitic crystals also are often found in glass ceramics. Spherulitic growth, or branching growth from a central point, is common in viscous systems where ionic mobility is the rate-limiting step. Models developed for polymer systems apply to glass ceramics and qualitatively explain the tendency to form spherulites[2].

(ROBERT J. EAGAN, RONALD E. LOEHMAN)

1. W. Hillig, D. Turnbull, *J. Chem. Phys.*, *24*, 914 (1956).
2. H. Keith, F. Padden, *J. Appl. Phys.*, *35*, 1270 (1964).

17.3.3.1.4. Chemical Composition.

The Li_2O–Al_2O_3–SiO_2 system is the basis of some commercially important low thermal expansion glass ceramics, photosensitive glass ceramics, and higher thermal expansion glass ceramics that form seals with metals[2]. The crystalline phases developed

in each formulation depend on the relative amounts of Li_2O, Al_2O_3, SiO_2, and small amounts of other oxide additions, the nucleating agent, and the crystallization heat treatment (Table 1).

Many aluminosilicate glass ceramics are based on framework structures of AlO_4 tetrahedra, which, when crystallized, posseses low thermal expansions. This gives the glass ceramics based on them near zero expansions and thus excellent dimensional stability, thermal shock resistance, and mechanical strength. Aluminosilicate glass ceramics are used commercially as telescope mirrors, thermally stable structures for satellites and space probes, gyroscope components, heat-resistant windows, stove tops, and cookware.

Crystalline phases that form in this system include lithium disilicate (Li_2O–$2SiO_2$, thermal expansion, $\alpha = 110 \times 10^{-7}°C^{-1}$, 20–600°C), lithium metasilicate (Li_2O–SiO_2, $\alpha \sim 130 \times 10^{-7}°C^{-1}$), β-eucryptite (Li_2O–Al_2O_3–SiO_2, $\alpha = -86 \times 10^{-7}°C^{-1}$ (parallel to the c-axis), 20–700°C), β-spodumene (Li_2O–Al_2O_3–$4SiO_2$, $\alpha = 9 \times 10^{-7}°C^{-1}$, 20–1000°C), quartz ($SiO_2$, $\alpha = 237 \times 10^{-7}°C^{-1}$, 20–600°C), and cristobalite (SiO_2, $\alpha = 271 \times 10^{-7}°C^{-1}$, 20–600°C). Note that the thermal expansion coefficient of beta eucryptite is negative along the crystallographic c-axis. The expansion perpendicular to the c-axis is positive and the net expansion of glass ceramics based on randomly oriented beta eucryptite crystallites is near zero.

In many cases, more than one crystalline phase forms. Often, phases that form initially transform into another phase as heat treatment progresses. For example, crystalline phases of β-quartz solid solutions (e.g., β-eucryptite), which are not stable at high temperatures, convert to more stable phases (e.g., β-spodumene, cristobalite, sapphirine, or lithium disilicate). The stable high temperature phase may have different properties—in this case, higher thermal expansion. Therefore, glass ceramics with the same chemical composition may have very different properties, depending on the heat treatment.

The MgO–Al_2O_3–SiO_2 family is the basis of glass ceramics with low thermal expansion, high strength, and low dielectric loss that are used for cookware and radomes. The principal crystalline phase developed in these glass ceramics is cordierite ($2MgO$-$2Al_2O_3$-$5SiO_2$, $\alpha = 26 \times 10^{-7}°C^{-1}$, 25–700°C) (Table 1). As with the Li_2O–Al_2O_3–SiO_2 system, crystal phase development is critically dependent on heat treatment. Changing the nucleating agent and heat treatment permits the formation of glass ceramics having high coefficients of thermal expansion.

Glass ceramics based on the PbO–ZnO–B_2O_3–SiO_2 system are used as solder glasses: that is, they fuse at low temperatures ($\sim$ 450°C) and can bond other glasses and

TABLE 1. COMPOSITION AND PROPERTIES OF Li_2O–Al_2O_3–SiO_2 AND MgO–Al_2O_3–SiO_2 GLASS CERAMICS

Glass	Oxide Content (wt %)						Crystal Phases	$\alpha \times 10^{-7}°C^{-1}$[a]
	SiO_2	Al_2O_3	Li_2O	MgO	TiO_2	P_2O_5		
1	68	21.4	3.8	0	5.7	0	β-Eucryptite	−10
2	65	21	9	0	4.5	0	β-Spodumene, rutile	15
3	45.5	30.5	0	12.5	11.5	0	Cordierite, rutile	14
4	56	20	0	15	9	0	Cordierite, rutile, cristobalite	56
5	82.3	0	11.0	3.7	0	3	Quartz, lithium disilicate	145

[a] α = Coefficient of thermal expansion.

ceramics together without degrading them. Typical applications include bonding parts of television picture tubes and sealing electronic components. These glasses crystallize slowly to permit the glass to flow and wet the seal area. The principal crystalline phases are lead and zinc borates. Often a solder glass ceramic crystallizes only partly, but that can be sufficient to increase its use temperature to approximately that of the sealing temperature.

Glass ceramics that contain fluorophlogopite mica ($KMg_3AlSi_3O_{11}F_2$) as the principal crystalline phase (~60 vol%) are machinable by conventional metalworking techniques[3,4]. They are made by crystallizing glasses containing 30–50 wt % SiO_2, 3–20 wt % B_2O_3, 10–20 wt % Al_2O_3, 4–12 wt % K_2O, 15–25 wt % MgO, and 4–10 wt % F. The microstructure of small, randomly oriented mica plates fractures easily during machining but resists extensive crack propagation. These glass ceramics are stable to ~1000°C.

Refractory glass ceramics stable in the 1300–1700°C temperature range are made from the Al_2O_3–SiO_2, BaO–Al_2O_3–SiO_2 and BaO–Al_2O_3–SiO_2–TiO_2 systems[5]. These glass ceramics are difficult to melt, requiring melting temperatures of 1800, 1700, and 1650°C, respectively, but they are completely dense and strong, and can be formed into complex shapes by usual glass forming techniques.

Glass ceramics prepared from steel blast furnace slags are chemically complex because the slag compositions are variable and contain minor amounts of many oxides. However, the principles of glass ceramic formation are the same as previously noted[6]. The glass ceramics typically contain 50–60 wt % SiO_2, 8–25 wt % CaO, 8–15 wt % Al_2O_3, 2–15 wt % MgO, 6–10 wt % (K_2O + Na_2O), and 0.5–3 wt % FeO, plus small concentrations of numerous other oxides. The slags are used as raw materials in a typical glass melting operation together with modifying additions of sand and clay. The main crystalline phases in the glass ceramics are wollastonite ($CaSiO_3$) and diopside ($CaMgSi_2O_6$) in a matrix that is about 30% residual glass. Metal sulfide particles nucleate the crystallization. The use of slags for preparing glass ceramics is most highly developed in Russia and eastern Europe, where the annual production of slagsitall, as it is called, is a million tons, the largest volume use of any glass ceramic. Slagsitalls are low cost materials that are primarily used for floor and wall coverings, parts for industrial machinery, chimney liners, and components of chemical process equipment, as well as for other uses calling for high hardness, abrasion resistance, and corrosion resistance.

Glass ceramics derived from phosphate glasses in the Na_2O–BaO–P_2O_5 system have thermal expansion coefficients exceeding $200 \times 10^{-7}°C^{-1}$[7]. Because they crystallize at temperatures less than 500°C, they are potentially useful for making seals to aluminum. The composition of such glass ceramics is about 40 mol % Na_2O, 10 mol % BaO, 1 mol % Al_2O_3, and 49 mol % P_2O_5 with 0.01 wt % Pt as a nucleating agent.

(ROBERT J. EAGAN, RONALD E. LOEHMAN)

1. L. R. Pinckney, Phase-separated glasses and glass ceramics, in *Engineered Materials Handbook*, Vol. 4, ASM International, Metals Park, OH, 1991, p. 431.
2. R. E. Loehman, T. J. Headley, Design of high thermal expansion glass-ceramics through microstructural control, in *Ceramic Microstructures '86: Role of Interfaces*, J. A. Pask and A. G. Evans, eds., Plenum Press, New York, 1987.
3. C. Chyung, G. Beall, D. Grossman, *Proceedings of the Tenth International Congress on Glass, 14*, 33 (1974).
4. G. Beall, U.S. Patent 3, 689, 293 (1972).
5. J. Macdowell, G. Beall, *J. Am. Ceram. Soc., 52*, 17 (1969).

6. S. Scholes, *Glass Ind.*, *5* (1974).
7. J. Wilder, *Glass Ceramics for Sealing to High Thermal Expansion Metals*, Sandia Laboratories Report SAND802192, 1980, Available through NTIS.

17.3.3.2. Optimizing Mechanical Strength

Glass ceramics are usually two to three times stronger than glass when measured under similar conditions. They are stronger because they contain high volume fractions of crystalline phases that are inherently stronger than glasses of similar composition; also, because those crystals are very small, crack propagation is more difficult. Crystals are inherently stronger than glasses because their structural periodicity allows shorter bond lengths, which leads to higher ultimate strengths. In normal use conditions, the strengths of glasses and ceramics are determined by the number and size of the surface flaws at which brittle fracture originates under load. In glasses, cracks propagate unimpeded once the critical stress level has been exceeded for the particular surface flaw population. For flaws of similar size, glass ceramics require higher stress levels to propagate cracks because the crystal grains tend to impede crack growth.

(ROBERT J. EAGAN, RONALD E. LOEHMAN)

17.3.3.2.1. Strength and Fracture Toughness.

The strength or modulus of rupture quoted for glass ceramics is determined by loading test bars in flexure. This value can vary by a factor of ten or more for a given material, depending on the surface finish of the test specimens. Fracture strength, σ_f, depends[1] on the size of surface flaws c, the elastic modulus E, and the work of fracture γ_f:

$$\sigma_f = A\left(\frac{2E\gamma_f}{\pi c}\right)^{1/2} \tag{a}$$

Most studies of the strength of glass ceramics have determined modulus of rupture as a function of crystal size (strength increases as crystal size decreases), volume fraction of crystalline phase (strength increases with the volume fraction of crystalline phase), and internal stresses generated either by the difference in thermal expansion between the crystalline phases and residual glass or by anisotropic thermal expansion of the crystalline phase (strength decreases as the difference or anisotropy increases).

Although modulus of rupture is a useful comparative measure if surface conditions are specified, fracture toughness is a more useful property, especially for the development of glass ceramic compositions and crystallization heat treatments.

Fracture toughness, K_{IC}, is a measure of the difficulty of propagating an existing crack through a material. For cracks that are large relative to the microstructure (usually true in glass ceramics), fracture toughness can be considered to be a bulk material property rather than a function of the flaw population as is the case for strength:

$$K_{IC} = [2E\gamma_f]^{1/2} \tag{b}$$

$$K_{IC} = Y\sigma_f c^{1/2} \tag{c}$$

In equation (c), Y is a geometric constant related to the shape of a flaw.

Inorganic Reactions and Methods, Volume 18
Edited by J. J. Zuckerman, Jim D. Atwood

6. S. Scholes, *Glass Ind.*, *5* (1974).
7. J. Wilder, *Glass Ceramics for Sealing to High Thermal Expansion Metals*, Sandia Laboratories Report SAND802192, 1980, Available through NTIS.

17.3.3.2. Optimizing Mechanical Strength

Glass ceramics are usually two to three times stronger than glass when measured under similar conditions. They are stronger because they contain high volume fractions of crystalline phases that are inherently stronger than glasses of similar composition; also, because those crystals are very small, crack propagation is more difficult. Crystals are inherently stronger than glasses because their structural periodicity allows shorter bond lengths, which leads to higher ultimate strengths. In normal use conditions, the strengths of glasses and ceramics are determined by the number and size of the surface flaws at which brittle fracture originates under load. In glasses, cracks propagate unimpeded once the critical stress level has been exceeded for the particular surface flaw population. For flaws of similar size, glass ceramics require higher stress levels to propagate cracks because the crystal grains tend to impede crack growth.

(ROBERT J. EAGAN, RONALD E. LOEHMAN)

17.3.3.2.1. Strength and Fracture Toughness.

The strength or modulus of rupture quoted for glass ceramics is determined by loading test bars in flexure. This value can vary by a factor of ten or more for a given material, depending on the surface finish of the test specimens. Fracture strength, σ_f, depends[1] on the size of surface flaws c, the elastic modulus E, and the work of fracture γ_f:

$$\sigma_f = A\left(\frac{2E\gamma_f}{\pi c}\right)^{1/2} \tag{a}$$

Most studies of the strength of glass ceramics have determined modulus of rupture as a function of crystal size (strength increases as crystal size decreases), volume fraction of crystalline phase (strength increases with the volume fraction of crystalline phase), and internal stresses generated either by the difference in thermal expansion between the crystalline phases and residual glass or by anisotropic thermal expansion of the crystalline phase (strength decreases as the difference or anisotropy increases).

Although modulus of rupture is a useful comparative measure if surface conditions are specified, fracture toughness is a more useful property, especially for the development of glass ceramic compositions and crystallization heat treatments.

Fracture toughness, K_{IC}, is a measure of the difficulty of propagating an existing crack through a material. For cracks that are large relative to the microstructure (usually true in glass ceramics), fracture toughness can be considered to be a bulk material property rather than a function of the flaw population as is the case for strength:

$$K_{IC} = [2E\gamma_f]^{1/2} \tag{b}$$

$$K_{IC} = Y\sigma_f c^{1/2} \tag{c}$$

In equation (c), Y is a geometric constant related to the shape of a flaw.

Fracture toughness is usually measured by inducing a large flaw with a diamond indenter or sawed notch, then loading the specimen to failure. Upon measuring the flaw size and load, one can use equation (c) to calculate K_{IC}.

Applying fracture mechanics techniques to characterize brittle materials has become an important subfield of materials science, and a reasonable understanding of the relation between toughness, composition, and microstructure is available. Silicate glasses have toughness values of 0.7–1.0 $MPam^{1/2}$, alumina ceramics values of 4–5 $MPam^{1/2}$, and glass ceramics values of 1–4 $MPam^{1/2}$, (the fracture toughness of metals is often > 50 $MPam^{1/2}$).

To accurately establish the factors that control strength and toughness of glass ceramics, it would be desirable to have a uniformly dispersed crystalline phase of simple geometry in a glass matrix whose mechanical behavior is well known. For that reason, model glass ceramics (hot-pressed borosilicate glasses containing dispersed Al_2O_3 spheres) have been studied[2]. The fracture toughness, K_{IC}, of such materials increases linearly with volume fraction of inclusions from 1 $MPam^{1/2}$ for the base glass to 3 $MPam^{1/2}$ at 40 vol % alumina, and in direct proportion with composite elastic modulus. Fractographic analysis reveals substantial differences in the interaction of the crack front with inclusions, depending on the sign of the thermal expansion mismatch, $\Delta\alpha$, between the crystal and the glass. Nevertheless, the effect of $\Delta\alpha$ on K_{IC} is small. If $\Delta\alpha$ were large enough to cause microcracking, the toughness probably would increase, an actual decrease in the strength not withstanding. Similar, but less well-quantified trends have been observed for several glass ceramics.

Based on these observations, attaining optimum strength in a glass ceramic requires a dispersion of small, high modulus crystals, with minimum glass phase and little stress in the grain boundaries. Strong glass ceramics with these attributes have modulus of rupture values of 350 MPa (50,000 psi) and toughness values of 2–4 $MPam^{1/2}$. Much greater increases in strength may be achieved by creating a compressive layer on the surfaces of the glass ceramic or by reinforcing the glass ceramic with fibers or whiskers.

(ROBERT J. EAGAN, RONALD E. LOEHMAN)

1. A. Jaytilaka, *Fracture of Engineering Brittle Materials*, Applied Science Publications, London, 1979. (A good review of ceramic fracture.)
2. J. Swearengen, E. Beauchamp, R. Eagan, *Proceedings of the Conference on Fracture of Ceramics*, Pennsylvania State University, July 27–29, 1977.

17.3.3.2.2. Surface Treatments to Increase Strength.

Compressive layers may be formed on glass ceramics by controlling the crystallization sequence so that the surface crystallizes and becomes rigid before the interior. As the interior subsequently crystallizes, it shrinks, thereby placing the surface in compression. Preferential surface crystallization may occur if the article is heated in a wet atmosphere[1] or if the surface is abraded to provide nucleation sites.

Surface compressive layers also may be formed by ion exchange, in a process similar to the commercial practice for making chemically strengthened glass. In one process, large ions stuffed into sites formerly occupied by smaller ions create compressive stress. In another process, ion exchange modifies the crystalline phases to produce a low thermal expansion phase on the surface.[2] As the article with the low expansion surface layer cools from the ion exchange bath temperature, very high surface compressive

Inorganic Reactions and Methods, Volume 18
Edited by J. J. Zuckerman, Jim D. Atwood

Fracture toughness is usually measured by inducing a large flaw with a diamond indenter or sawed notch, then loading the specimen to failure. Upon measuring the flaw size and load, one can use equation (c) to calculate K_{IC}.

Applying fracture mechanics techniques to characterize brittle materials has become an important subfield of materials science, and a reasonable understanding of the relation between toughness, composition, and microstructure is available. Silicate glasses have toughness values of 0.7–1.0 $MPam^{1/2}$, alumina ceramics values of 4–5 $MPam^{1/2}$, and glass ceramics values of 1–4 $MPam^{1/2}$, (the fracture toughness of metals is often > 50 $MPam^{1/2}$).

To accurately establish the factors that control strength and toughness of glass ceramics, it would be desirable to have a uniformly dispersed crystalline phase of simple geometry in a glass matrix whose mechanical behavior is well known. For that reason, model glass ceramics (hot-pressed borosilicate glasses containing dispersed Al_2O_3 spheres) have been studied[2]. The fracture toughness, K_{IC}, of such materials increases linearly with volume fraction of inclusions from 1 $MPam^{1/2}$ for the base glass to 3 $MPam^{1/2}$ at 40 vol % alumina, and in direct proportion with composite elastic modulus. Fractographic analysis reveals substantial differences in the interaction of the crack front with inclusions, depending on the sign of the thermal expansion mismatch, $\Delta\alpha$, between the crystal and the glass. Nevertheless, the effect of $\Delta\alpha$ on K_{IC} is small. If $\Delta\alpha$ were large enough to cause microcracking, the toughness probably would increase, an actual decrease in the strength not withstanding. Similar, but less well-quantified trends have been observed for several glass ceramics.

Based on these observations, attaining optimum strength in a glass ceramic requires a dispersion of small, high modulus crystals, with minimum glass phase and little stress in the grain boundaries. Strong glass ceramics with these attributes have modulus of rupture values of 350 MPa (50,000 psi) and toughness values of 2–4 $MPam^{1/2}$. Much greater increases in strength may be achieved by creating a compressive layer on the surfaces of the glass ceramic or by reinforcing the glass ceramic with fibers or whiskers.

(ROBERT J. EAGAN, RONALD E. LOEHMAN)

1. A. Jaytilaka, *Fracture of Engineering Brittle Materials*, Applied Science Publications, London, 1979. (A good review of ceramic fracture.)
2. J. Swearengen, E. Beauchamp, R. Eagan, *Proceedings of the Conference on Fracture of Ceramics*, Pennsylvania State University, July 27–29, 1977.

17.3.3.2.2. Surface Treatments to Increase Strength.

Compressive layers may be formed on glass ceramics by controlling the crystallization sequence so that the surface crystallizes and becomes rigid before the interior. As the interior subsequently crystallizes, it shrinks, thereby placing the surface in compression. Preferential surface crystallization may occur if the article is heated in a wet atmosphere[1] or if the surface is abraded to provide nucleation sites.

Surface compressive layers also may be formed by ion exchange, in a process similar to the commercial practice for making chemically strengthened glass. In one process, large ions stuffed into sites formerly occupied by smaller ions create compressive stress. In another process, ion exchange modifies the crystalline phases to produce a low thermal expansion phase on the surface.[2] As the article with the low expansion surface layer cools from the ion exchange bath temperature, very high surface compressive

stresses are produced. Glass ceramics treated this way can achieve modulus of rupture values of 2450 MPa (350,000 psi).

Compressive layers can also be formed by coating a high thermal expansion glass ceramic (e.g., nepheline type) with a low thermal expansion glass, a process similar to glazing clay-based ceramics. The compressive stresses are less than those produced by ion exchange, but modulus of rupture values are increased two to three times over that of the base glass ceramic.

(ROBERT J. EAGAN, RONALD E. LOEHMAN)

1. F. Ernsberger, U.S. Patent 3,756,798 (1973).
2. G.H. Beall, D.A. Duke, Glass ceramic technology, in *Glass: Science and Technology*, Vol. 1, Uhlmann, Kreidl, eds., Academic Press, New York, 1983.

17.3.3.2.3. Glass Ceramic Composites.

Incorporating high elastic modulus fibers in glass ceramics produces composites with improved mechanical properties. Glass ceramics are outstanding candidates for such composites because they are generally tougher and more refractory than glasses and because their coefficients of thermal expansion can be tailored to be near that of the reinforcing fiber. Glass ceramic matrices in the lithium aluminosilicate family are used with SiC fibers to give fracture toughness values of 30 $MPam^{1/2}$ and modulus of rupture values of 1050 MPa (150,000 psi)[1]. The potential applications of high performance glass ceramic composites include aerospace components such as turbine blades, heat exchangers, and other parts that must operate at high temperatures and stresses.

(ROBERT J. EAGAN, RONALD E. LOEHMAN)

1. K. M. Prewo, J. J. Brennon, G. K. Layden, *Am. Ceram. Soc. Bull.*, *65*, 305 (1986).

17.3.3.3. Optimizing Thermal Shock Resistance

Rapid heating or cooling of a glass ceramic generates transient compressive or tensile stresses, respectively, in the surface layers. The magnitude of the stress depends on the specimen size, the heating or cooling rate, and the material properties of elastic modulus, thermal expansion, thermal diffusivity, and Poisson's ratio. The ability to survive the stress increases in proportion to the fracture toughness of the glass ceramic. Glasses are generally less resistant to thermal shock than glass ceramics of the same thermal diffusivity characteristics because they have higher thermal expansion and Poisson's ratio, and high thermal diffusivity. Because, as noted earlier, toughness is proportional to $E^{1/2}$ a compromise in modulus is required to achieve the optimum.

Glass ceramics, especially those in the Li_2O–Al_2O_3–SiO_2 system that crystallize to form β-spodumene, have very good thermal shock resistance, primarily because they have low thermal expansion coefficients. Of the properties that affect thermal shock resistance, the major effect is exerted by thermal expansion coefficient (Fig. 1)[1]. Other properties that could influence thermal shock resistance, such as the thermal diffusivity and elastic modulus, do not vary greatly with composition or processing conditions in silicate glass ceramics. Glasses are generally less resistant to thermal shock than glass

Inorganic Reactions and Methods, Volume 18
Edited by J. J. Zuckerman, Jim D. Atwood

stresses are produced. Glass ceramics treated this way can achieve modulus of rupture values of 2450 MPa (350,000 psi).

Compressive layers can also be formed by coating a high thermal expansion glass ceramic (e.g., nepheline type) with a low thermal expansion glass, a process similar to glazing clay-based ceramics. The compressive stresses are less than those produced by ion exchange, but modulus of rupture values are increased two to three times over that of the base glass ceramic.

(ROBERT J. EAGAN, RONALD E. LOEHMAN)

1. F. Ernsberger, U.S. Patent 3,756,798 (1973).
2. G.H. Beall, D.A. Duke, Glass ceramic technology, in *Glass: Science and Technology*, Vol. 1, Uhlmann, Kreidl, eds., Academic Press, New York, 1983.

17.3.3.2.3. Glass Ceramic Composites.

Incorporating high elastic modulus fibers in glass ceramics produces composites with improved mechanical properties. Glass ceramics are outstanding candidates for such composites because they are generally tougher and more refractory than glasses and because their coefficients of thermal expansion can be tailored to be near that of the reinforcing fiber. Glass ceramic matrices in the lithium aluminosilicate family are used with SiC fibers to give fracture toughness values of 30 $MPam^{1/2}$ and modulus of rupture values of 1050 MPa (150,000 psi)[1]. The potential applications of high performance glass ceramic composites include aerospace components such as turbine blades, heat exchangers, and other parts that must operate at high temperatures and stresses.

(ROBERT J. EAGAN, RONALD E. LOEHMAN)

1. K. M. Prewo, J. J. Brennon, G. K. Layden, *Am. Ceram. Soc. Bull., 65*, 305 (1986).

17.3.3.3. Optimizing Thermal Shock Resistance

Rapid heating or cooling of a glass ceramic generates transient compressive or tensile stresses, respectively, in the surface layers. The magnitude of the stress depends on the specimen size, the heating or cooling rate, and the material properties of elastic modulus, thermal expansion, thermal diffusivity, and Poisson's ratio. The ability to survive the stress increases in proportion to the fracture toughness of the glass ceramic. Glasses are generally less resistant to thermal shock than glass ceramics of the same thermal diffusivity characteristics because they have higher thermal expansion and Poisson's ratio, and high thermal diffusivity. Because, as noted earlier, toughness is proportional to $E^{1/2}$ a compromise in modulus is required to achieve the optimum.

Glass ceramics, especially those in the Li_2O–Al_2O_3–SiO_2 system that crystallize to form β-spodumene, have very good thermal shock resistance, primarily because they have low thermal expansion coefficients. Of the properties that affect thermal shock resistance, the major effect is exerted by thermal expansion coefficient (Fig. 1)[1]. Other properties that could influence thermal shock resistance, such as the thermal diffusivity and elastic modulus, do not vary greatly with composition or processing conditions in silicate glass ceramics. Glasses are generally less resistant to thermal shock than glass

Inorganic Reactions and Methods, Volume 18
Edited by J. J. Zuckerman, Jim D. Atwood

stresses are produced. Glass ceramics treated this way can achieve modulus of rupture values of 2450 MPa (350,000 psi).

Compressive layers can also be formed by coating a high thermal expansion glass ceramic (e.g., nepheline type) with a low thermal expansion glass, a process similar to glazing clay-based ceramics. The compressive stresses are less than those produced by ion exchange, but modulus of rupture values are increased two to three times over that of the base glass ceramic.

(ROBERT J. EAGAN, RONALD E. LOEHMAN)

1. F. Ernsberger, U.S. Patent 3,756,798 (1973).
2. G.H. Beall, D.A. Duke, Glass ceramic technology, in *Glass: Science and Technology*, Vol. 1, Uhlmann, Kreidl, eds., Academic Press, New York, 1983.

17.3.3.2.3. Glass Ceramic Composites.

Incorporating high elastic modulus fibers in glass ceramics produces composites with improved mechanical properties. Glass ceramics are outstanding candidates for such composites because they are generally tougher and more refractory than glasses and because their coefficients of thermal expansion can be tailored to be near that of the reinforcing fiber. Glass ceramic matrices in the lithium aluminosilicate family are used with SiC fibers to give fracture toughness values of 30 $MPam^{1/2}$ and modulus of rupture values of 1050 MPa (150,000 psi)[1]. The potential applications of high performance glass ceramic composites include aerospace components such as turbine blades, heat exchangers, and other parts that must operate at high temperatures and stresses.

(ROBERT J. EAGAN, RONALD E. LOEHMAN)

1. K. M. Prewo, J. J. Brennon, G. K. Layden, *Am. Ceram. Soc. Bull.*, *65*, 305 (1986).

17.3.3.3. Optimizing Thermal Shock Resistance

Rapid heating or cooling of a glass ceramic generates transient compressive or tensile stresses, respectively, in the surface layers. The magnitude of the stress depends on the specimen size, the heating or cooling rate, and the material properties of elastic modulus, thermal expansion, thermal diffusivity, and Poisson's ratio. The ability to survive the stress increases in proportion to the fracture toughness of the glass ceramic. Glasses are generally less resistant to thermal shock than glass ceramics of the same thermal diffusivity characteristics because they have higher thermal expansion and Poisson's ratio, and high thermal diffusivity. Because, as noted earlier, toughness is proportional to $E^{1/2}$ a compromise in modulus is required to achieve the optimum.

Glass ceramics, especially those in the Li_2O–Al_2O_3–SiO_2 system that crystallize to form β-spodumene, have very good thermal shock resistance, primarily because they have low thermal expansion coefficients. Of the properties that affect thermal shock resistance, the major effect is exerted by thermal expansion coefficient (Fig. 1)[1]. Other properties that could influence thermal shock resistance, such as the thermal diffusivity and elastic modulus, do not vary greatly with composition or processing conditions in silicate glass ceramics. Glasses are generally less resistant to thermal shock than glass

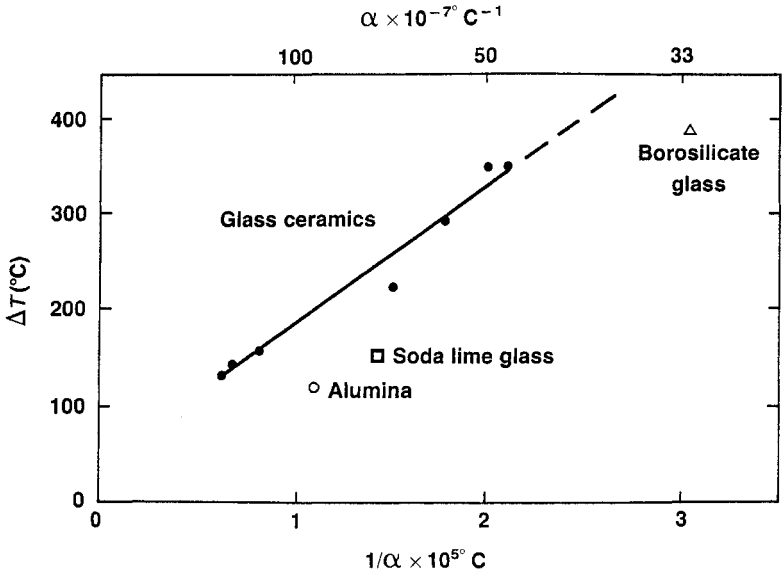

Figure 1. For several glass ceramics, the temperature interval causing thermal shock failure, ΔT, is approximately inversely proportional to the linear coefficient of thermal expansion of these materials. Glasses and alumina ceramics have less thermal shock resistance than glass ceramics of comparable thermal expansion.[1]

ceramics of the same thermal expansion characteristics because they have higher thermal expansion and, even if the expansion coefficients were the same, glasses are not as tough as glass ceramics. Alumina ceramics are also less resistant to thermal shock than many glass ceramics. The difference arises from the higher elastic modulus of alumina (four times that of β-spodumene glass ceramics) and the lower thermal expansion coefficient of crystalline β-spodumene.

Thermal shock resistance can also be improved by the surface treatments used to increase mechanical strength (see 17.3.3.2). The stresses induced by thermal shock must exceed the compressive surface stresses to cause a crack to propagate, resulting in failure during quenching.

(ROBERT J. EAGAN, RONALD E. LOEHMAN)

1. P. W. McMillan, *Glass Ceramics*, 2nd ed., Academic Press, London 1979. (An excellent review.)

17.3.3.4. Controlling Electrical Properties

Electrical properties of glass ceramics are determined by the properties of both the crystalline phases and the residual glass. Electrical conductivity and dielectric loss (at low frequencies) are dominated by the concentration and mobility of alkali ions in the glass phase. The dielectric constant is dominated by the crystalline phase, especially when that phase consists of high dielectric constant materials such as ferroelectric crystals. The

Inorganic Reactions and Methods, Volume 18
Edited by J. J. Zuckerman, Jim D. Atwood

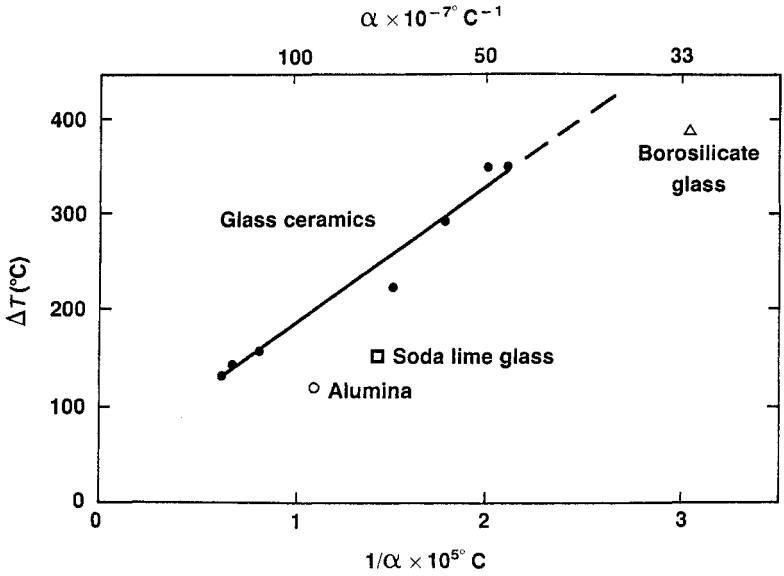

Figure 1. For several glass ceramics, the temperature interval causing thermal shock failure, ΔT, is approximately inversely proportional to the linear coefficient of thermal expansion of these materials. Glasses and alumina ceramics have less thermal shock resistance than glass ceramics of comparable thermal expansion.[1]

ceramics of the same thermal expansion characteristics because they have higher thermal expansion and, even if the expansion coefficients were the same, glasses are not as tough as glass ceramics. Alumina ceramics are also less resistant to thermal shock than many glass ceramics. The difference arises from the higher elastic modulus of alumina (four times that of β-spodumene glass ceramics) and the lower thermal expansion coefficient of crystalline β-spodumene.

Thermal shock resistance can also be improved by the surface treatments used to increase mechanical strength (see 17.3.3.2). The stresses induced by thermal shock must exceed the compressive surface stresses to cause a crack to propagate, resulting in failure during quenching.

(ROBERT J. EAGAN, RONALD E. LOEHMAN)

1. P. W. McMillan, *Glass Ceramics*, 2nd ed., Academic Press, London 1979. (An excellent review.)

17.3.3.4. Controlling Electrical Properties

Electrical properties of glass ceramics are determined by the properties of both the crystalline phases and the residual glass. Electrical conductivity and dielectric loss (at low frequencies) are dominated by the concentration and mobility of alkali ions in the glass phase. The dielectric constant is dominated by the crystalline phase, especially when that phase consists of high dielectric constant materials such as ferroelectric crystals. The

dielectric strength of pore-free glass ceramics is comparable to that of conventional ceramics with similar alkali content.

(ROBERT J. EAGAN, RONALD E. LOEHMAN)

17.3.3.4.1. Electrical Conductivity and Dielectric Loss.

Except for a few glass ceramics that contain semiconducting phases, electrical conduction occurs by the migration of relatively mobile alkali ions in the glass phase under the influence of an electric field. The conductivity of glass ceramics relative to the glass from which they are formed can be lowered by up to four orders of magnitude if the alkali ions are immobilized in the crystalline phase. For example, the conductivity of a Li_2O–SiO_2–Al_2O_3 glass is reduced when it is crystallized to Li_2O–$2SiO_2$ in a matrix of essentially an Al_2O_3–SiO_2 glass. This change is particularly advantageous when high thermal expansion glass ceramics are used as insulators in electrical connectors because the high thermal expansion characteristics can be derived from the alkali-containing crystalline phase dispersed in a low alkaali, low conductivity glass. Glass ceramics that contain few or no alkali ions (e.g., cordierite glass ceramics) have low dielectric loss. Since they can be made into complex shapes, and are strong and homogeneous, they are used as insulators in high frequency applications such as radomes. By contrast, many high thermal expansion glasses that would make matched-expansion seals to metals, have high concentrations of alkali ions or lead oxide and, therefore, are not refractory, chemically durable, or particularly good as electrical insulators.

(ROBERT J. EAGAN, RONALD E. LOEHMAN)

17.3.3.4.2. Ferroelectric Glass Ceramics.

Ferroelectric glass ceramics can be made by crystallizing ferroelectric Pb, Cd, or Ba niobate in a silicate glass matrix[1]. These glass ceramics have dielectric constants greater than 500 and loss tangents ($\tan \delta$) of $\sim 2\%$. They can be made economically into ribbons for capacitor dielectrics, and they have excellent dielectric strength. However, the dielectric constants are less than those obtained by conventional ceramic processes because the ferroelectric phase is diluted by the glass matrix.

Crystalline dispersions of several niobate crystals or barium titanate (up to 70 vol %) in a silicate glass phase form transparent ferroelectric glass ceramics[2]. The small size of the crystals (~ 500 Å) accounts for transparency.

(ROBERT J. EAGAN, RONALD E. LOEHMAN)

1. A. Herczog, *J. Am. Ceram. Soc.*, *47*, 107 (1964).
2. M. Layton, A. Herczog, *Glass Technol.*, *10*, 50 (1969).

17.3.3.5. Control of Transparency and Color

Most glass ceramics are opaque because light is scattered at interfaces characterized by a change in refractive index (e.g., at crystal–crystal, glass–crystal). Transparent glass ceramics are prepared by limiting the size of the crystallites and matching the refractive indices of the glass and crystalline phases. In addition to the transparent ferroelectric glass ceramics noted in 17.3.3.4, transparent, low thermal expansion glass ceramics can be

Inorganic Reactions and Methods, Volume 18
Edited by J. J. Zuckerman, Jim D. Atwood

dielectric strength of pore-free glass ceramics is comparable to that of conventional ceramics with similar alkali content.

(ROBERT J. EAGAN, RONALD E. LOEHMAN)

17.3.3.4.1. Electrical Conductivity and Dielectric Loss.

Except for a few glass ceramics that contain semiconducting phases, electrical conduction occurs by the migration of relatively mobile alkali ions in the glass phase under the influence of an electric field. The conductivity of glass ceramics relative to the glass from which they are formed can be lowered by up to four orders of magnitude if the alkali ions are immobilized in the crystalline phase. For example, the conductivity of a Li_2O–SiO_2–Al_2O_3 glass is reduced when it is crystallized to Li_2O–$2SiO_2$ in a matrix of essentially an Al_2O_3–SiO_2 glass. This change is particularly advantageous when high thermal expansion glass ceramics are used as insulators in electrical connectors because the high thermal expansion characteristics can be derived from the alkali-containing crystalline phase dispersed in a low alkaali, low conductivity glass. Glass ceramics that contain few or no alkali ions (e.g., cordierite glass ceramics) have low dielectric loss. Since they can be made into complex shapes, and are strong and homogeneous, they are used as insulators in high frequency applications such as radomes. By contrast, many high thermal expansion glasses that would make matched-expansion seals to metals, have high concentrations of alkali ions or lead oxide and, therefore, are not refractory, chemically durable, or particularly good as electrical insulators.

(ROBERT J. EAGAN, RONALD E. LOEHMAN)

17.3.3.4.2. Ferroelectric Glass Ceramics.

Ferroelectric glass ceramics can be made by crystallizing ferroelectric Pb, Cd, or Ba niobate in a silicate glass matrix[1]. These glass ceramics have dielectric constants greater than 500 and loss tangents ($\tan \delta$) of $\sim 2\%$. They can be made economically into ribbons for capacitor dielectrics, and they have excellent dielectric strength. However, the dielectric constants are less than those obtained by conventional ceramic processes because the ferroelectric phase is diluted by the glass matrix.

Crystalline dispersions of several niobate crystals or barium titanate (up to 70 vol %) in a silicate glass phase form transparent ferroelectric glass ceramics[2]. The small size of the crystals (~ 500 Å) accounts for transparency.

(ROBERT J. EAGAN, RONALD E. LOEHMAN)

1. A. Herczog, *J. Am. Ceram. Soc.*, *47*, 107 (1964).
2. M. Layton, A. Herczog, *Glass Technol.*, *10*, 50 (1969).

17.3.3.5. Control of Transparency and Color

Most glass ceramics are opaque because light is scattered at interfaces characterized by a change in refractive index (e.g., at crystal–crystal, glass–crystal). Transparent glass ceramics are prepared by limiting the size of the crystallites and matching the refractive indices of the glass and crystalline phases. In addition to the transparent ferroelectric glass ceramics noted in 17.3.3.4, transparent, low thermal expansion glass ceramics can be

made from Li_2O–Al_2O_3–SiO_2 glasses[1]. The crystal size is controlled by crystallizing the glasses at lower than normal temperatures (i.e., $<900°C$).

Glass ceramics generally are colored by additions of transition metal oxides. Rather than being in the glass phase, these oxides may form colored crystalline precipitates such as titanates or aluminates. The color is dependent on the particular coordination of the transition metal ion in the glass matrix. The coordination may change as crystallization occurs through change in the composition of the residual glass or by incorporation of the ion into a crystal phase.

(ROBERT J. EAGAN, RONALD E. LOEHMAN)

1. G. Beall, in *High Temperature Oxides*, Part IV, A. Alper. ed., Academic Press, New York, 1971.

17.3.3.6. Photochromic Glass and Glass Ceramics

Full-color photosensitive glasses are made by producing a dispersion of silver crystals of specific geometry on silver halide nuclei[1]. The theories of nucleation and growth (see 17.3.3.1) that apply to glass ceramics also apply to forming theses crystalline dispersions in glass, although they are not usually considered glass ceramics.

Colors develop because of selective absorption by anisotropic silver crystals less than 500 Å long. The anisotropic crystals are produced by precipitating a cubic alkali halide crystal, NaF, on silver metal particles (the normal photochromic process) and growing a second halide crystal (e.g., NaBr) on the NaF crystal. Growth occurs preferentially from the (100) face of the NaF crystal in the form of a pyramid consisting of very small dendrites.

To develop color absorption, silver metal must be precipitated at the top of the halide pyramid. A second exposure to ultraviolet light, followed by a heat treatment, crystallizes the rest of the silver on nuclei formed earlier by a dendritic growth process. Since the growth is primarily along one axis of the dendrite, the length of these dendrites varies inversely as the number of nuclei. Color is a function of the aspect ratio of the silver particles. Thus, short exposures give long aspect ratios and colors at the low end of the spectrum, while long exposures give more equiaxed crystallites and red-yellow hues.

(ROBERT J. EAGAN, RONALD E. LOEHMAN)

1. S. Stookey, G. H. Beall, J. E. Pierson, *J. Appl. Phys.*, *49*, 5114 (1978).

17.3.4. Preparation of Carbons and Graphites

It is estimated that a little under 0.2% of the earth's crust is carbon, most of it existing as coal. In addition, there are a variety of organic materials: naturally occurring graphite deposits and metallic carbonates. The major sources of raw materials for the preparation of commercial carbons and graphites fall in this latter group, coal itself being of minor importance. All carbonaceous materials are prepared by pyrolysis, or thermal degradation. The heating of the raw material decomposes it, releasing the other major elements (H, O, S, N etc.) in various gaseous forms, thus leaving a residue that is mainly carbon. Other impurities, which are mainly metals, may be simply boiled off at very high temperatures, removed by treatment with chlorine or fluorine (e.g., as SbF_5) at somewhat

Inorganic Reactions and Methods, Volume 18
Edited by J. J. Zuckerman, Jim D. Atwood

made from Li_2O–Al_2O_3–SiO_2 glasses[1]. The crystal size is controlled by crystallizing the glasses at lower than normal temperatures (i.e., $<900°C$).

Glass ceramics generally are colored by additions of transition metal oxides. Rather than being in the glass phase, these oxides may form colored crystalline precipitates such as titanates or aluminates. The color is dependent on the particular coordination of the transition metal ion in the glass matrix. The coordination may change as crystallization occurs through change in the composition of the residual glass or by incorporation of the ion into a crystal phase.

(ROBERT J. EAGAN, RONALD E. LOEHMAN)

1. G. Beall, in *High Temperature Oxides*, Part IV, A. Alper. ed., Academic Press, New York, 1971.

17.3.3.6. Photochromic Glass and Glass Ceramics

Full-color photosensitive glasses are made by producing a dispersion of silver crystals of specific geometry on silver halide nuclei[1]. The theories of nucleation and growth (see 17.3.3.1) that apply to glass ceramics also apply to forming theses crystalline dispersions in glass, although they are not usually considered glass ceramics.

Colors develop because of selective absorption by anisotropic silver crystals less than 500 Å long. The anisotropic crystals are produced by precipitating a cubic alkali halide crystal, NaF, on silver metal particles (the normal photochromic process) and growing a second halide crystal (e.g., NaBr) on the NaF crystal. Growth occurs preferentially from the (100) face of the NaF crystal in the form of a pyramid consisting of very small dendrites.

To develop color absorption, silver metal must be precipitated at the top of the halide pyramid. A second exposure to ultraviolet light, followed by a heat treatment, crystallizes the rest of the silver on nuclei formed earlier by a dendritic growth process. Since the growth is primarily along one axis of the dendrite, the length of these dendrites varies inversely as the number of nuclei. Color is a function of the aspect ratio of the silver particles. Thus, short exposures give long aspect ratios and colors at the low end of the spectrum, while long exposures give more equiaxed crystallites and red-yellow hues.

(ROBERT J. EAGAN, RONALD E. LOEHMAN)

1. S. Stookey, G. H. Beall, J. E. Pierson, *J. Appl. Phys.*, *49*, 5114 (1978).

17.3.4. Preparation of Carbons and Graphites

It is estimated that a little under 0.2% of the earth's crust is carbon, most of it existing as coal. In addition, there are a variety of organic materials: naturally occurring graphite deposits and metallic carbonates. The major sources of raw materials for the preparation of commercial carbons and graphites fall in this latter group, coal itself being of minor importance. All carbonaceous materials are prepared by pyrolysis, or thermal degradation. The heating of the raw material decomposes it, releasing the other major elements (H, O, S, N etc.) in various gaseous forms, thus leaving a residue that is mainly carbon. Other impurities, which are mainly metals, may be simply boiled off at very high temperatures, removed by treatment with chlorine or fluorine (e.g., as SbF_5) at somewhat

Inorganic Reactions and Methods, Volume 18
Edited by J. J. Zuckerman, Jim D. Atwood

made from Li_2O–Al_2O_3–SiO_2 glasses[1]. The crystal size is controlled by crystallizing the glasses at lower than normal temperatures (i.e., $<900°C$).

Glass ceramics generally are colored by additions of transition metal oxides. Rather than being in the glass phase, these oxides may form colored crystalline precipitates such as titanates or aluminates. The color is dependent on the particular coordination of the transition metal ion in the glass matrix. The coordination may change as crystallization occurs through change in the composition of the residual glass or by incorporation of the ion into a crystal phase.

(ROBERT J. EAGAN, RONALD E. LOEHMAN)

1. G. Beall, in *High Temperature Oxides*, Part IV, A. Alper. ed., Academic Press, New York, 1971.

17.3.3.6. Photochromic Glass and Glass Ceramics

Full-color photosensitive glasses are made by producing a dispersion of silver crystals of specific geometry on silver halide nuclei[1]. The theories of nucleation and growth (see 17.3.3.1) that apply to glass ceramics also apply to forming theses crystalline dispersions in glass, although they are not usually considered glass ceramics.

Colors develop because of selective absorption by anisotropic silver crystals less than 500 Å long. The anisotropic crystals are produced by precipitating a cubic alkali halide crystal, NaF, on silver metal particles (the normal photochromic process) and growing a second halide crystal (e.g., NaBr) on the NaF crystal. Growth occurs preferentially from the (100) face of the NaF crystal in the form of a pyramid consisting of very small dendrites.

To develop color absorption, silver metal must be precipitated at the top of the halide pyramid. A second exposure to ultraviolet light, followed by a heat treatment, crystallizes the rest of the silver on nuclei formed earlier by a dendritic growth process. Since the growth is primarily along one axis of the dendrite, the length of these dendrites varies inversely as the number of nuclei. Color is a function of the aspect ratio of the silver particles. Thus, short exposures give long aspect ratios and colors at the low end of the spectrum, while long exposures give more equiaxed crystallites and red-yellow hues.

(ROBERT J. EAGAN, RONALD E. LOEHMAN)

1. S. Stookey, G. H. Beall, J. E. Pierson, *J. Appl. Phys.*, *49*, 5114 (1978).

17.3.4. Preparation of Carbons and Graphites

It is estimated that a little under 0.2% of the earth's crust is carbon, most of it existing as coal. In addition, there are a variety of organic materials: naturally occurring graphite deposits and metallic carbonates. The major sources of raw materials for the preparation of commercial carbons and graphites fall in this latter group, coal itself being of minor importance. All carbonaceous materials are prepared by pyrolysis, or thermal degradation. The heating of the raw material decomposes it, releasing the other major elements (H, O, S, N etc.) in various gaseous forms, thus leaving a residue that is mainly carbon. Other impurities, which are mainly metals, may be simply boiled off at very high temperatures, removed by treatment with chlorine or fluorine (e.g., as SbF_5) at somewhat

lower temperatures, or simply leached out with a strong aqueous solution of an acid (HCl, HNO_3, or H_2SO_4) followed by an aqueous leach.

Because of the inherent simplicity of the carbonization process and the multitude of carbonaceous materials available, both naturally occurring and synthetically produced, there is an endless variety of forms of carbon and graphite. Indeed, there are more forms of carbon than of any other element. The sections that follow discuss different materials, making reference to many different precursors, or starting materials. The final product is not only a function of starting material(s), but also of heat treatment temperature, heating rate to that temperature, heating time, and surrounding atmosphere.

In discussing carbons and graphites it would be helpful to have a clear disinction between the two terms. Unfortunately none exists. "Carbon" is the terminology used for the chemical element and also for the more disordered forms of the material. These are not necessarily totally amorphous forms, and in some respects may be quite crystalline.

The term "graphite" refers to the true, well-ordered single crystal as first described by Bernal in 1924[1] with the structure shown in Figure 1, but is also used for polycrystalline materials and of some materials with quite a high proportion of very disordered regions. The use of the term "amorphous graphite" for some natural graphite deposits in Mexico, Korea, and other parts of the world may seem scientifically absurd, yet is quite common.

Preparing a carbon or graphite involves heating a precursor to a temperature high enough to drive off the volatiles and leave a mainly carbonaceous framework, sometimes called a char. In this char the carbon atoms are mainly retained in their original arrangement, thus retaining some of the past history of the material. For example, charcoal retains the pore structure of the original wood. Further heating of the char may, or may not, result in the formation of a graphite. Carbons that graphitize are called "soft" carbons, while those that resist graphitization, even when heated to temperatures around

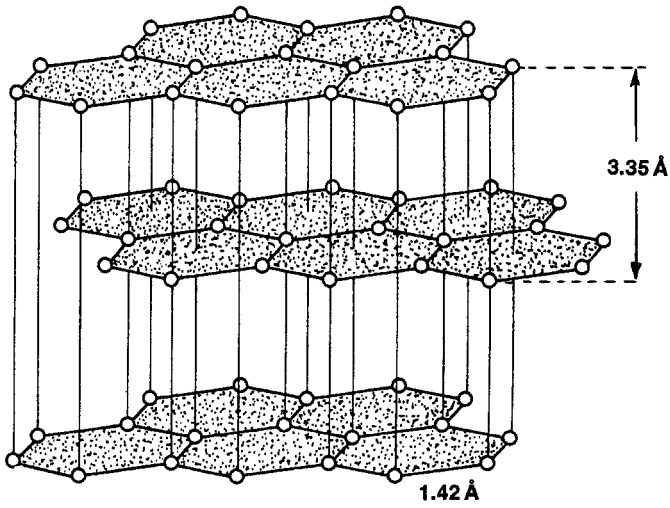

Figure 1. The crystal structure of graphite.

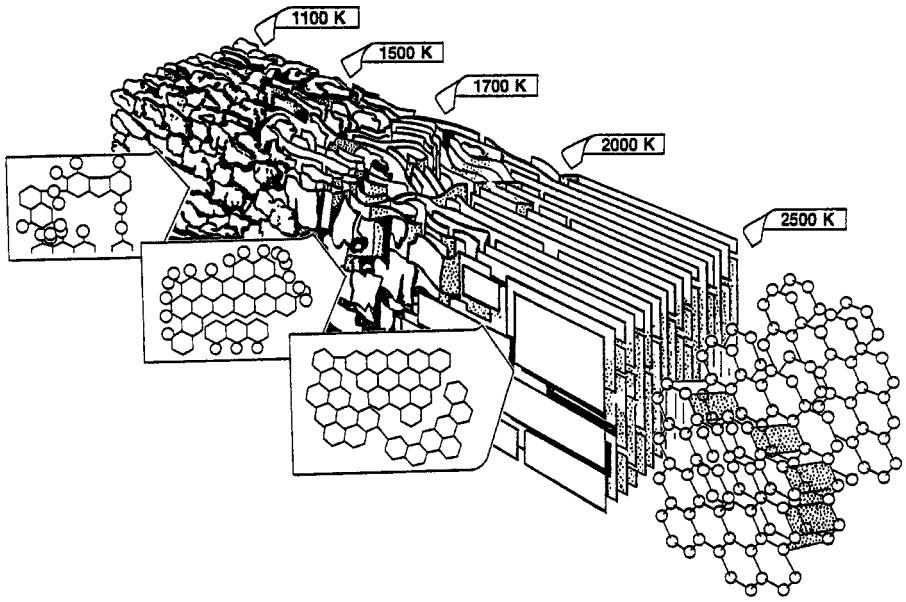

Figure 2. Model of changes from mesophase to graphite during heat treatment. (Courtesy of Prof. H. Marsh.)

3000°C, are called "hard" carbons. This change from precursor to a random carbon, after carbonization, to a highly ordered carbon after graphitization, is illustrated in Figure 2.

Chars retain the structure of the precursor because of the low mobility of carbon atoms at all temperatures below 1000°C. To destroy this randomized, or amorphous structure, there must be free mobility of the carbon atoms so that they can be rearranged into the graphite structure of Figure 1, and in fact such mobility does not usually occur below a temperature of 2200°C. The graphite lattice, however, imparts limitations to the mobility of the atoms. In this structure the carbon atoms are bonded to three other coplanar carbon atoms, 1.42 Å apart, the bonds oriented at 120° to each other. The carbon "layer plane," known as a graphene layer, thus consists of an arrangement of close-packed open hexagons, often referred to as a "chicken-wire" arrangement. In the normal hexagonal graphite structure, layer planes are arranged 3.35 Å apart in an —ABABA— stacking sequence, with half the atoms in one plane lying directly over atoms of the adjacent plane, while the other half lie over the centers of the hexagons.

A graphite single crystal consists of over a million layer planes, up to several millimeters across, arranged in this ABABA stacking sequence. A char, on the other hand, may contain only very small volumes with such order, perhaps connected by very disordered regions. Within such a structure, carbon atoms may become mobile at high enough temperatures, but motion is normally confined to directions parallel to the layer planes and is not easy because of the high binding energy (10.5 eV) of the atoms within

the layer planes. The forces that hold adjacent layer planes together are of the van der Waals type, and there is no great driving force for these layers to orient themselves perfectly. Graphite manufacture also is subject to limitations because, unlike metals, carbon cannot be melted, cast, and recrystallized. All transformations must therefore occur in the solid state.

Graphitization consists of the motion of carbon atoms to produce (1) layer plane growth, (2) rotation of aligned adjacent graphene layers so that they can join to form one larger layer plane, and (3) the reorientation of adjacent layer planes to form a crystal. Several studies of the graphitization process have been made, and definitive reviews[2,3] give different interpretations of the data. It is well established that graphitization is a kinetic process governed by an activation energy of 10^6 J/mol. As such, temperatures usually in excess of 2300°C, are required.

The subsections that follow very briefly summarize some of the many methods employed in making carbon and graphite materials. The wide variety of materials produced by the industry and the possibilities for adjusting processing variables to produce special properties have resulted in the application of the nickname "black art" to graphite manufacture. Many of the specifics of the processes are proprietary and are based on empirical knowledge rather than scientific understanding. More often, manufacturing techniques are influenced by the particular equipment available at a given plant rather than recent advances in processing.

(PETER A. THROWER)

1. J. D. Bernal. *Proc. R. Soc. London A, 106,* 749 (1924).
2. D. B. Fischbach, in *Chemistry and Physics of Carbon.*, Vol. 7, P. L. Walker Jr., ed., Dekker, New York, 1971, p. 1.
3. A. Pacault, in *Chemistry and Physics of Carbon*, Vol. 7, P. L. Walker Jr., ed., Dekker, New York, 1971, p. 107.

17.3.4.1. Graphite

The production of bulk graphite is a major industry. Artifacts up to 76 cm in diameter and 3 met long are produced as electrodes for the electric arc steelmaking furnace, but many artifacts are much smaller. On a weight basis, the former accounts for the bulk of the market; on a piece basis, the latter accounts for the bulk of the market.

The vast majority of manufactured graphite, called "synthetic" or "Acheson" graphite, is made from at least two starting materials, a filler such as coke, and a binder to hold the coke particles together. The coke filler is carefully sized to a controlled particle size distribution that depends on the end use of the final artifact. Sometimes additives facilitate the processing as extrusion aids, or iron (III) oxide is added as a puffing inhibitor. In some specialized applications natural grapfhite or carbon black may be added to produce lubricative or abrasive qualities in the final product, and other adjuvants may sometimes be needed, such as MoS_2 to enhance lubrication in an inert atmosphere or vacuum.

The normal scheme of manufacture is shown in Figures 1 and 2. The various stages are described in the subsections that follow.

(PETER A. THROWER)

Inorganic Reactions and Methods, Volume 18
Edited by J. J. Zuckerman, Jim D. Atwood

the layer planes. The forces that hold adjacent layer planes together are of the van der Waals type, and there is no great driving force for these layers to orient themselves perfectly. Graphite manufacture also is subject to limitations because, unlike metals, carbon cannot be melted, cast, and recrystallized. All transformations must therefore occur in the solid state.

Graphitization consists of the motion of carbon atoms to produce (1) layer plane growth, (2) rotation of aligned adjacent graphene layers so that they can join to form one larger layer plane, and (3) the reorientation of adjacent layer planes to form a crystal. Several studies of the graphitization process have been made, and definitive reviews[2,3] give different interpretations of the data. It is well established that graphitization is a kinetic process governed by an activation energy of 10^6 J/mol. As such, temperatures usually in excess of 2300°C, are required.

The subsections that follow very briefly summarize some of the many methods employed in making carbon and graphite materials. The wide variety of materials produced by the industry and the possibilities for adjusting processing variables to produce special properties have resulted in the application of the nickname "black art" to graphite manufacture. Many of the specifics of the processes are proprietary and are based on empirical knowledge rather than scientific understanding. More often, manufacturing techniques are influenced by the particular equipment available at a given plant rather than recent advances in processing.

(PETER A. THROWER)

1. J. D. Bernal. *Proc. R. Soc. London A, 106*, 749 (1924).
2. D. B. Fischbach, in *Chemistry and Physics of Carbon.*, Vol. 7, P. L. Walker Jr., ed., Dekker, New York, 1971, p. 1.
3. A. Pacault, in *Chemistry and Physics of Carbon*, Vol. 7, P. L. Walker Jr., ed., Dekker, New York, 1971, p. 107.

17.3.4.1. Graphite

The production of bulk graphite is a major industry. Artifacts up to 76 cm in diameter and 3 met long are produced as electrodes for the electric arc steelmaking furnace, but many artifacts are much smaller. On a weight basis, the former accounts for the bulk of the market; on a piece basis, the latter accounts for the bulk of the market.

The vast majority of manufactured graphite, called "synthetic" or "Acheson" graphite, is made from at least two starting materials, a filler such as coke, and a binder to hold the coke particles together. The coke filler is carefully sized to a controlled particle size distribution that depends on the end use of the final artifact. Sometimes additives facilitate the processing as extrusion aids, or iron (III) oxide is added as a puffing inhibitor. In some specialized applications natural grapfhite or carbon black may be added to produce lubricative or abrasive qualities in the final product, and other adjuvants may sometimes be needed, such as MoS_2 to enhance lubrication in an inert atmosphere or vacuum.

The normal scheme of manufacture is shown in Figures 1 and 2. The various stages are described in the subsections that follow.

(PETER A. THROWER)

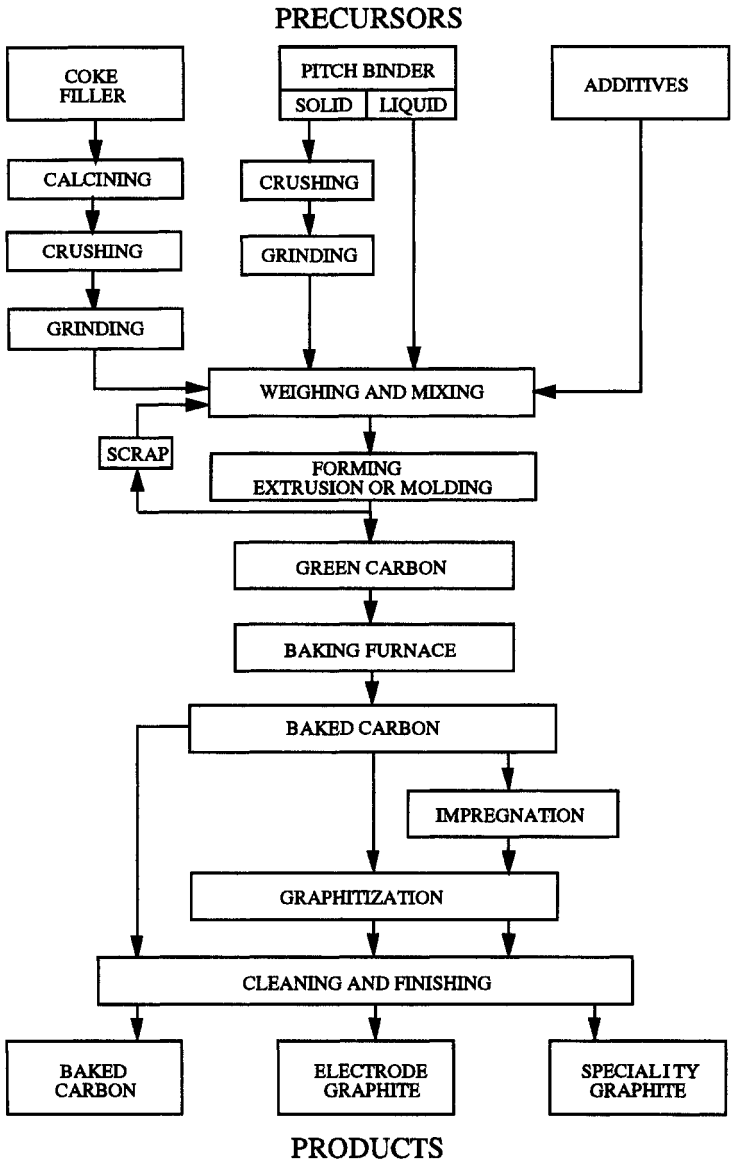

Figure 1. Flowchart of processes involved in graphite manufacture.

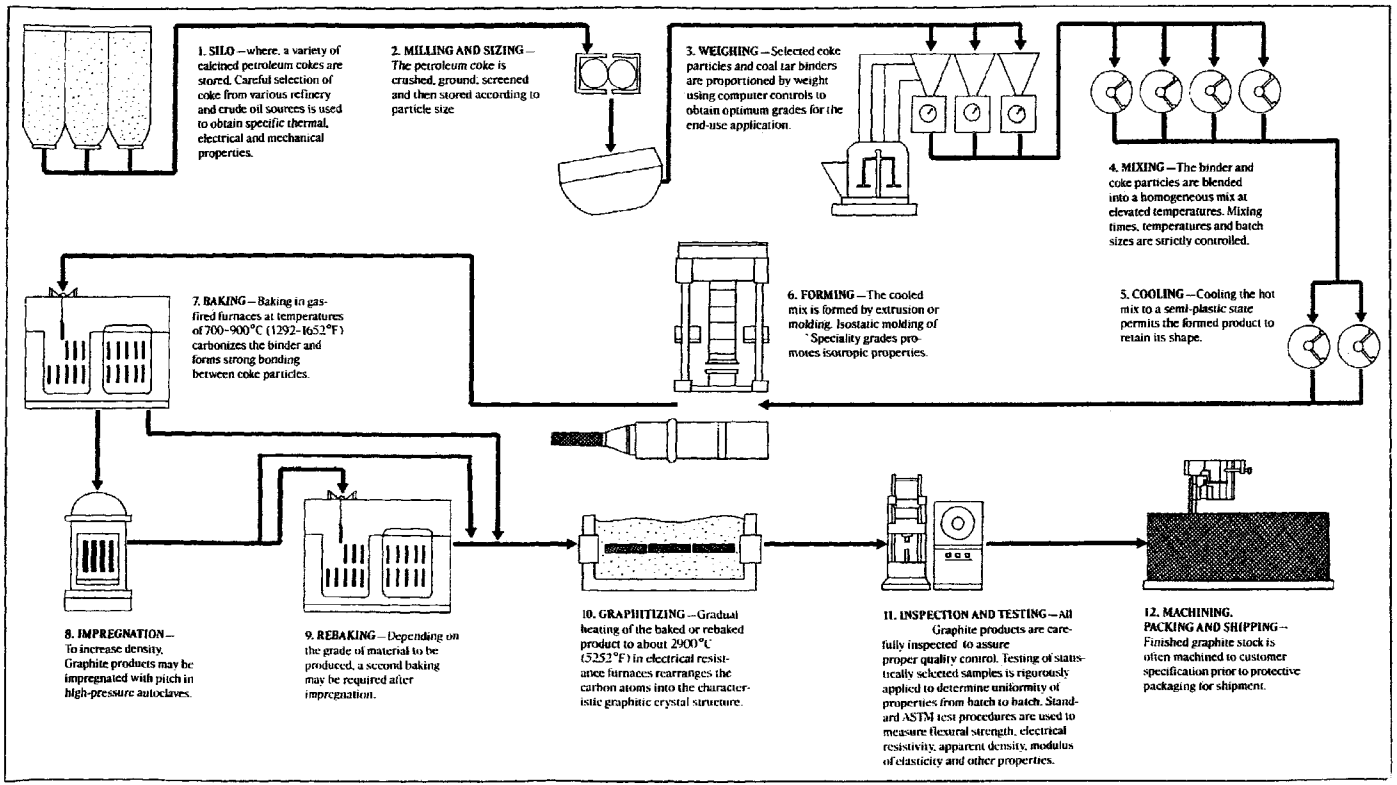

Figure 2. The manufacture of graphite. (Courtesy of Sigri-Great Lakes Carbon.)

17.3.4.1.1. Raw Materials and Their Preparation.

The starting materials are mainly derived from either petroleum or coal, usually petroleum coke as the filler and coal tar pitch as the binder. Petroleum pitch is used as the impregnant. For all its shortcomings, coal tar pitch has been shown to be the superior binder because it has some 12–15 wt % quinoline insolubles (QI). The latter are thought to enhance the strength of the final artifact, especially electrodes in the electric arc steel furnace. The QIs have been found to increase the strength of the bond formed between filler particles formed during the baking process[1,2] and the manner in which the coal tar pitch wets the filler during the mixing cycle[3]. Coal tar pitch is the preferred binder because of its high carbon yield (usually in the range of 50–65 wt %), its fluidity at mixing and forming temperatures[4] (normally 145 and 120–125°C, respectively), and its ability to wet the filler particles to produce a rigid carbon bond between filler particles during the baking process. The high carbon yield of coal tar pitch is essential prior to the production process, there has been no carbonization of the binder (and the impregnant).

Coal tar pitch is a by-product of the production of metallurgical coke and is produced by distillation of tar from bituminous coal. Petroleum pitch, produced by the cracking of petroleum, is used in relatively small quantities compared to coal tar pitch. Although having a higher softening point (typically 120°C vs. 110°C), it has a lower viscosity up to 200°C and, importantly, contains no QI. This latter property makes it ideal as an impregnant but not as a binder. The lack of QI in petroleum pitch yields a final graphite product with unacceptably low strength[5]. Such low strength materials are not acceptable in today's ultrahigh performance electric arc steel furnaces. The QI-free nature of petroleum pitch allows a free flow through a porous, baked carbon, since there are no particles to plug up the system, and thus impregnation is uniform.

Impregnation increases the density of both the baked and graphitized products and, more importantly, lowers the longitudinal resistivity of the graphite artifact. Being brittle at room temperature, solid coal tar pitch can be crushed before it is mixed with the filler. Modern production facilities add the binder as a liquid to attain a more uniform green mix and, thus, a more uniform, consistent product. Liquid pitch must be below 160°C or maintained rigorously air-free for mixing and storage. Above 160°C coal tar pitch reacts with oxygen to form a cross-linked structure between graphitoid layers[6]. Such irreversible cross-link formation is a source of glasslike carbons which, upon subsequent processing to higher temperatures, yield brittle products high in resistivity and coefficient of thermal expansion. Such materials are unacceptable for use as electrothermic electrodes in the electric arc steel furnace. However, such cross-linking is useful in the production of carbon brushes, where high electrical resistance is desirable. When used for this purpose, the technique is called "air blowing."

The primary filler used in graphites is petroleum coke, a by-product of the cracking of petroleum to make gasoline. The heavy residues produced by cracking are rich in polyaromatic compounds and may be coked in several ways, the most common of which is the delayed coking process[1]. The production of coke from pitch proceeds through a liquid crystal state known as the mesophase, which has been the subject of extensive research with good understanding of the process[8,9]. The structure of the coke depends to a large extent on the precursor or feedstock. Of special interest are needle cokes, which are produced from aromatic feedstocks. The greater the aromaticity of the pitch, the more ordered the molecules in the mesophase, thus producing an ordered primordial layer structure in the coke, which is most susceptible to subssequent graphitization. The

small ordered layer plane domains in needle coke are easily visible in an optical microscope and are especially visible and distinguishable from each other using scanning electron microscope (SEM) techniques[10].

Coke produced in a fluid bed by spraying residuum onto a hot coke particle is known as fluid coke. Because the coking process is almost immediate, there is very little order to the crystallites formed, and the final product has an onionskin structure. This characteristic limits layer plane growth during graphitization and imposes constraints on the coke particles (diameter ~ 500 μm) which, in turn, restricts densification during later heat treatment. An advantage of fluid coke in designing the final graphite is its inherent isotropy, due to its onionskin layer plane arrangement. A similar microstructure exists in Gilsocoke, a material produced from a naturally occurring deposit called nintaite, where the coke particles show multicoalescence of spherical particles (diameter ~ 500 μm). The onionskin structure of this coke has higher layer plane order than that of fluid coke, and in high quality isotropic graphites used in the nuclear industry have been produced from this material.

Raw or green coke usually has to be calcined before use in graphite production. Calcining consists of heating it to 1200–1400°C to remove volatiles, mostly methane and hydrogen, and to produce densification. The densities of delayed cokes can be as high as 2.1 g/cm^3 after calcination, whereas fluid cokes have densities in the range 1.9–2.0 g/cm^3.

The calcined coke is crushed, screened, and milled to prepare it for mixing with the pitch binder. The size required depends on the final product desired. A high strength graphite, or one on which a fine surface finish is required, must be fine-grained, usually less than 200 mesh, Tyler series. Such materials may be used in the nuclear and aerospace industries and for electrical discharge machining applications. On the other hand, electrodes like those used in the electric arc steel furnaces are usually much coarser, with needle coke particles over 2 cm in diameter and 3 cm long. The formulation, (i.e., the mix of coke particle sizes) may range from greater than 2 cm to a flour fraction with particles less than 200 mesh. It is not uncommon for a given formulation to have three definite particle size fractions of coarse particles, called tailings, in addition to the flour fraction. The particular formulation depends on the end use of the product. The particle size fractions are chosen to maximize the packing efficiency during forming.

The art of mixing various size fractions is empirical, aimed at minimizing the amount of binder required to produce an adequate density. As a rule, binder requirements increase with decreasing size of filler particle.

Another factor is the shape of the particles. Spherical particles such as Gilsocoke pack quite differently from the acicular needle coke. It is here that past experience is paramount. The blending of the coke fractions with the binder is a crucial step in the manufacture of any graphite.

(PETER A. THROWER)

1. *The Effect of the Nature of Quinoline Insolubles on Electrode Pitch Binder Properties*, Report 33, British Carbonization Research Association, Wingerworth, Derbyshire, November 1976.
2. L. F. King, W. D. Robertson, *Fuel, 47*, 197 (1968).
3. E. A. Heintz, *Carbon, 24*, 131 (1986).
4. R. W. Wallouch, H. N. Murty, E. A. Heintz, *Ind. Eng. Chem. Prod. Res. Dev., 16*, 325 (1977).
5. R. Menéndez, E. M. Cray, H. Marsh, R. W. Pysz, E. A. Heintz, *Carbon, 29*, 107 (1991).
6. J. B. Barr, I. C. Lewis, *Carbon, 16*, 459 (1978).
7. K. E. Rose, *Hydrocarbon Process, 50*, 85 (1971).

8. H. Marsh, C. Cornford, in *Petroleum Derived Carbons*, M. L. Deviney, T. M. O'Grady, eds., American Chemical Society, Washington, DC, 1976, p. 266.
9. J. L. White, in *Petroleum-Derived Carbons*, M. L. Deviney, T. M. O'Grady, eds., American Chemical Society, Washington, DC, 1976, p. 282.
10. R. W. Pysz, S. L. Hoff, E. A. Heintz, *Carbon*, *27*, 935 (1989).

17.3.4.1.2. Mixing and Forming.

The various filler particles are placed in a heated mixer for blending, followed by addition of crushed or liquid binder. Binder levels are usually in the region of 25 wt % of the total mix, but levels are expressed as parts binder per hundred pounds of filler (pph). To ensure that the binder uniformly coats the filler particles, the mixer must be maintained at a temperature permitting the binder to be relatively free-flowing. This temperature has been found to be some 35–40°C above the softening point of the binder[1]. For a binder with a softening point of about 110°C, this temperature would be 145°C. When high softening point binders are employed, the system must be maintained air-free if mixing temperatures will exceed 160°C (see above). To accomplish this, steam jackets are used to control the mixing temperature. It is essential that the binder be distributed evenly throughout the mix; otherwise, the structural integrity of the final product will be unsatisfactory.

After the mix has cooled to about 125°C, a temperature slightly above the softening point of the coal tar pitch, it is ready to be formed into the final shape. This process shapes the material and forces the filler particles into closer packing, thus increasing the bulk density. There are two important forming methods: extrusion and molding.

The extrusion technique is used to form the majority of carbon and graphite products in the form of cylindrical or rectangular logs. The extrusion press consists of a heated chamber, known as a mud chamber, which is filled with the binder–filler mix. On one side of the chamber, a hydraulic ram forces the mix through a die of desired shape. It is during this processing step that the anisotropy usually present in graphite materials is introduced. The elongated, acicular particles pass through the die with their long axes parallel to the extrusion direction. This produces a grain in the structure, with the primordial layer planes parallel to the extrusion direction. In the final graphitized product this orientation causes in-plane properties, such as high thermal and electrical conductivity, to predominate, while the cross-plane properties, such as low thermal and electrical conductivity, have a greater influence on properties perpendicular to the extrusion direction.

Molding is used to form nearly all small carbon and graphite products such as seals and brushes, as well as larger crucibles, and so on. The hot binder–filler mix is simply compressed by means of a plunger or ram into a mold of the required shape. Pressures vary widely depending on the mix, application, and so on, but are usually in the range of 15–210 MPa. During this process the coke particles are preferentially aligned with their primordial layer planes perpendicular to the pressing direction. High electrical and thermal conductivity in the final product is thus obtained perpendicular to the pressing or molding direction. This gives a graphite crucible the advantage of attaining uniform temperature relatively rapidly. Molded formulations usually have a finer grain size filler and higher binder levels than extruded formulations. The differences in particle alignment for the molding and extrusion processes are illustrated in Figure 1.

In some specialized applications requiring an isotropic product, an isostatic, or hydrostatic, molding technique may be used. The application of pressure in all directions

Inorganic Reactions and Methods, Volume 18
Edited by J. J. Zuckerman, Jim D. Atwood

8. H. Marsh, C. Cornford, in *Petroleum Derived Carbons*, M. L. Deviney, T. M. O'Grady, eds., American Chemical Society, Washington, DC, 1976, p. 266.
9. J. L. White, in *Petroleum-Derived Carbons*, M. L. Deviney, T. M. O'Grady, eds., American Chemical Society, Washington, DC, 1976, p. 282.
10. R. W. Pysz, S. L. Hoff, E. A. Heintz, *Carbon, 27*, 935 (1989).

17.3.4.1.2. Mixing and Forming.

The various filler particles are placed in a heated mixer for blending, followed by addition of crushed or liquid binder. Binder levels are usually in the region of 25 wt % of the total mix, but levels are expressed as parts binder per hundred pounds of filler (pph). To ensure that the binder uniformly coats the filler particles, the mixer must be maintained at a temperature permitting the binder to be relatively free-flowing. This temperature has been found to be some 35–40°C above the softening point of the binder[1]. For a binder with a softening point of about 110°C, this temperature would be 145°C. When high softening point binders are employed, the system must be maintained air-free if mixing temperatures will exceed 160°C (see above). To accomplish this, steam jackets are used to control the mixing temperature. It is essential that the binder be distributed evenly throughout the mix; otherwise, the structural integrity of the final product will be unsatisfactory.

After the mix has cooled to about 125°C, a temperature slightly above the softening point of the coal tar pitch, it is ready to be formed into the final shape. This process shapes the material and forces the filler particles into closer packing, thus increasing the bulk density. There are two important forming methods: extrusion and molding.

The extrusion technique is used to form the majority of carbon and graphite products in the form of cylindrical or rectangular logs. The extrusion press consists of a heated chamber, known as a mud chamber, which is filled with the binder–filler mix. On one side of the chamber, a hydraulic ram forces the mix through a die of desired shape. It is during this processing step that the anisotropy usually present in graphite materials is introduced. The elongated, acicular particles pass through the die with their long axes parallel to the extrusion direction. This produces a grain in the structure, with the primordial layer planes parallel to the extrusion direction. In the final graphitized product this orientation causes in-plane properties, such as high thermal and electrical conductivity, to predominate, while the cross-plane properties, such as low thermal and electrical conductivity, have a greater influence on properties perpendicular to the extrusion direction.

Molding is used to form nearly all small carbon and graphite products such as seals and brushes, as well as larger crucibles, and so on. The hot binder–filler mix is simply compressed by means of a plunger or ram into a mold of the required shape. Pressures vary widely depending on the mix, application, and so on, but are usually in the range of 15–210 MPa. During this process the coke particles are preferentially aligned with their primordial layer planes perpendicular to the pressing direction. High electrical and thermal conductivity in the final product is thus obtained perpendicular to the pressing or molding direction. This gives a graphite crucible the advantage of attaining uniform temperature relatively rapidly. Molded formulations usually have a finer grain size filler and higher binder levels than extruded formulations. The differences in particle alignment for the molding and extrusion processes are illustrated in Figure 1.

In some specialized applications requiring an isotropic product, an isostatic, or hydrostatic, molding technique may be used. The application of pressure in all directions

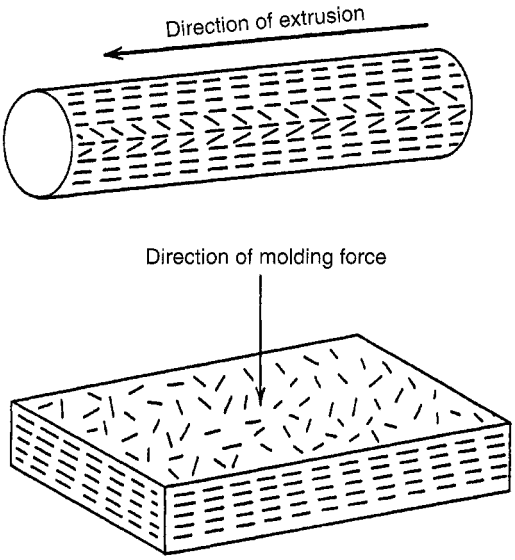

Figure 1. Crystallite orientations in extruded and molded graphites. (Courtesy of Dr. E. Heintz.)

tends to retain the filler particles in a random distribution of orientations; however, the technique is usually practical only for smaller blocks, not for finished shape products.

After the extruded or molded part is cooled, it becomes hard and rigid as the temperature falls below the softening point of the binder. It may then be moved to the baking furnace.

(PETER A. THROWER)

1. R. W. Walloch, H. N. Murty, E. A. Heintz, *Ind. Eng. Chem. Prod. Res. Dev.*, *16*, 325 (1977).

17.3.4.1.3. Baking.

In the baking cycle, the binder is converted to solid carbonaceous material, which forms bonds between the filler particles producing a strong product. During this process the binder passes through its thermoplastic state and eventually decomposes, causing considerable gas evolution. These processes impose two constraints on the baking operation. First, the green carbon must be supported, to prevent slumping as the binder passes through its softening point. Second, heating rates must be slow enough to allow the evolved gases to escape without blowing up the structure. It is estimated that over 150 m^3 of gaseous products is released for every cubic meter of green carbon.

The green carbon is loaded into a baking furnace and packed with ground coke and/or sand for support. Large electrodes are usually baked in large, upright stainless steel saggers with a mixture of coke and sand mixture for added support. The packing material also separates the individual pieces and prevents sticking when they become plastic during the initial stages of the baking cycle. The pack is porous enough to allow the evolved gases to escape. The temperature is then raised to 800–1000°C, very slowly at

Inorganic Reactions and Methods, Volume 18
Edited by J. J. Zuckerman, Jim D. Atwood

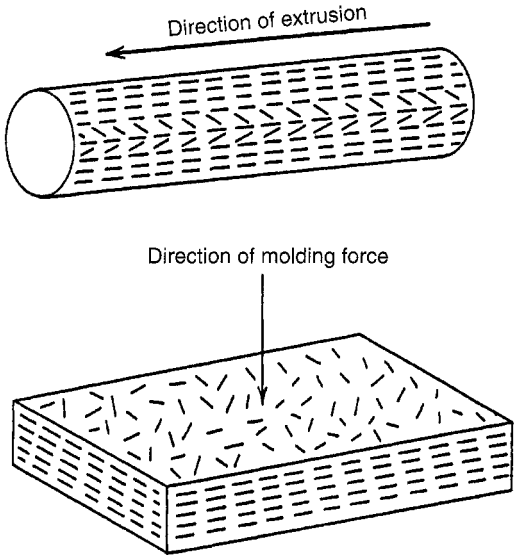

Figure 1. Crystallite orientations in extruded and molded graphites. (Courtesy of Dr. E. Heintz.)

tends to retain the filler particles in a random distribution of orientations; however, the technique is usually practical only for smaller blocks, not for finished shape products.

After the extruded or molded part is cooled, it becomes hard and rigid as the temperature falls below the softening point of the binder. It may then be moved to the baking furnace.

(PETER A. THROWER)

1. R. W. Walloch, H. N. Murty, E. A. Heintz, *Ind. Eng. Chem. Prod. Res. Dev.*, *16*, 325 (1977).

17.3.4.1.3. Baking.

In the baking cycle, the binder is converted to solid carbonaceous material, which forms bonds between the filler particles producing a strong product. During this process the binder passes through its thermoplastic state and eventually decomposes, causing considerable gas evolution. These processes impose two constraints on the baking operation. First, the green carbon must be supported, to prevent slumping as the binder passes through its softening point. Second, heating rates must be slow enough to allow the evolved gases to escape without blowing up the structure. It is estimated that over 150 m^3 of gaseous products is released for every cubic meter of green carbon.

The green carbon is loaded into a baking furnace and packed with ground coke and/or sand for support. Large electrodes are usually baked in large, upright stainless steel saggers with a mixture of coke and sand mixture for added support. The packing material also separates the individual pieces and prevents sticking when they become plastic during the initial stages of the baking cycle. The pack is porous enough to allow the evolved gases to escape. The temperature is then raised to 800–1000°C, very slowly at

first, then more rapidly, until the maximum temperature has been attained and it is time for a soak. The baking process usually requires 10–14 days for coarse-grained formulations such as electrodes. Fine-grained formulations, even of a small physical size, may require up to 35 days for the baking cycle to give the escaping gases time to leave and to ensure that the artifact does not fracture during the baking. It can take another 10–14 days to cool the baked pieces to 400°C, at which point the material will not burn or be thermally shocked to fracture on exposure to air. Sagger baking usually takes place in a car-bottom kiln. The loaded, hot saggers are taken out of the kiln at the highest temperature and are allowed to cool out of the furnace for faster unloading of the baked rods. After unpacking, the baked carbon is scraped to remove packing material and inspected for flaws before further processing.

(PETER A. THROWER)

17.3.4.1.4. Impregnation.

There may be significant cost advantages to omitting the impregnation step; for many high performance applications, however, the final density of the finished graphitized product would be too low if impregnation were not performed between the baking and graphitization stages. Impregnation also lowers the longitudinal resistivity of electrothermic electrodes, making them more efficient in electric arc steel furnaces. The surface of the baked carbon is carefully cleaned to allow the impregnant access to the interior. It is then placed in an autoclave, where it is heated to around 250°C, dried, and evacuated. Heated petroleum pitch or QI-free coal tar pitch is then introduced, and pressure is applied to hasten penetration of the binder to the inner pores of the structure. After removal and cleaning, the artifact will have an increased weight of around 15%. At this stage a second baking cycle of 7–8 days is necessary before the material is either impregnated for a second time or taken to the graphitizing furnace. For nuclear and aerospace applications, the graphite may be impregnated several times. However, each impregnation shows diminishing returns in the improvement of properties and adds greatly to the cost. Each impregnation–baking cycle takes several days.

Impregnation may use QI-free coal tar pitch, petroleum pitch, furfuryl alcohol, or other organic materials. Linseed oil has also been used for chloralkali anodes to enhance performance. Petroleum pitch has the advantage of containing no quinoline insolubles, which reduce the penetration of the impregnant by blocking the pores near the outer surface of the artifact. A density increase of around 5% (1.6–1.7 g/cm^3) in the final graphite is typical for a single impregnation, but the increase in strength and modulus are much larger, often in the 60–80% range. Electrical and thermal conductivities show slight improvements in performance.

(PETER A. THROWER)

17.3.4.1.5. Graphitization.

The final major step in the manufacture of graphite is heat treatment at around 3000°C, which causes carbon atom migration, allowing an ordering, or crystallization, to occur. This migration begins to be significant at around 2200°C, and the term "graphite" is often loosely applied to materials heated above this temperature, even though little real graphite crystal development has occurred. As mentioned earlier, some carbons do not graphitize; but in those that do, crystal development follows the line of the primordial layer planes in the coke. The size and orientation of the crystallites can be varied by

changing the starting materials, the forming process, and the time and temperature of graphitization.

Most large graphite blocks are graphitized using either Acheson furnaces, which were introduced in 1895, or by the more efficient longitudinal graphitization furnaces. The former furnaces can be enormous (15 m long × 3 m × 3 m), having a capacity of 80 electrodes that are 60 cm in diameter by 235 cm. long. The baked carbon is stacked inside the furnace between electrodes at the ends, and is packed and covered with coarsely ground metallurgical coke, with a final top layer (~ 50 cm) of a blend of coke, silicon carbide, and sand. This layer acts as a thermal and electrical insulator and also serves to protect the product from oxidation. Heating occurs by passing large currents (> 50,000 A) through the furnace resistive load. The thermal capacity of such a large structure causes long heating and cooling times—around 5 and 10 days, respectively.

After cooling, the graphitized blocks are removed from the furnace, cleaned, and inspected to determine whether property specifications have been met. Typical load-to-load cycles of an Acheson furnace are 30 days, making the process both time and capital intensive. After machining and finishing, the blocks are ready for delivery to the customer. For some materials the total manufacturing time may be as much as 5 months.

Longitudinal graphitization is more efficient, with graphitizer load-to-load times of 4–6 days and a capacity of 16–20 rods (60 cm diameter × 235 cm long) laid side by side in a double row. This produces electrodes with superior uniformity (i.e., acceptable densities, lower longitudinal electrical resistivity, lower longitudinal coefficients of thermal expansion, and higher flexural strength than the Acheson process). Whereas the Acheson process forces current through the coke resistor pack placed between adjacent transverse rows and through the rods across the diameter (the transverse direction), where the resistance is highest, the longitudinal process passes the current through the rods in the longitudinal direction. Heating in the Acheson process is more by energy transfer from radiating resistor coke than by direct heating of the baked carbon rods. In both cases, the furnaces are covered and completely surrounded with a metallurgical coke insulation referred to as "graphitizer pack."

In the graphitizing process, the crystallites present in the baked carbon align and grow, approaching, but never attaining, the perfect graphite structure shown earlier (see 17.3.4, Fig. 1). The industrial graphitization process at the micro level also illustrated earlier (see Section 17.3.4, Fig. 2) indicates that the random structures of the precursors and baked carbon gradually approach the long-range order typical of graphite, but always some residual defects remain.

After graphitization, the electrodes are machined to a desired, final configuration. In the electric arc furnace, elecrodes are joined by threaded graphite connecting pins, called nipples, screwed into threaded sockets that have been machined in the electrode end faces. Such a configuration forms a continuous column in the electric arc furnace.

Other techniques involving resistive tube furnaces, induction furnaces, and even direct resistive heating of the components are available for graphitizing smaller pieces of material. These batch processes require much shorter graphitization cycle times.

(PETER A. THROWER)

17.3.4.1.6. Other Techniques.

Among the hundreds of grades of graphite offered for sale by manufacturers, there are a number of speciality materials that undergo special proprietary processing.

Binderless graphites[1] having up to 95% theoretical density have been produced by heating finely ground, partially calcined coke in an autoclave under an isostatic pressure. The methane and other organics released from the coke during heating are pyrolyzed and probably form a thin pyrocarbon bond between the filler particles. The final product can be both highly isotropic and very strong. It is suspected that variations of this technique are used in production of some of the commercial fine-grained, high strength, isotropic graphites available today.

(PETER A. THROWER)

1. W. Chard, M. Conway, D. Niesz, in *Petroleum Derived Carbons*, M. L. Deviney, T. M. O'Grady, eds., American Chemical Society, Washington, DC, 1976, p. 155.

17.3.4.2. Pyrolytic Carbons

The term "pyrolytic carbon" can be applied to carbon filaments, carbon blacks, and carbon films, as well as to the more massive deposits which are the subject of this section. Pyrocarbon materials, made by chemical vapor deposition (CVD), vary in density, properties, and structure as much as the bulk materials discussed in 17.3.4.1. A heated hydrocarbon gas decomposes into an entire series of molecular species with a wide spectrum of carbon contents and molecular weights[1]. Within this pyrolyzing atmosphere, "droplets" form that pyrolyze and condense on a nearby surface, or large carbonaceous complexes may condense directly on the surface of the chamber. The former condition produces a fluffy, sooty, soft carbon, not far removed from carbon black, while the latter produces a hard solid carbon. The second of these materials is of primary interest here. The structure of the carbon produced by the CVD process has been shown[2] to depend on the type of hydrocabon and its concentration, the pyrolysis temperature, the contact time, and the geometry of the pyrolyzing chamber. Of these, the pyrolysis temperature is perhaps the most important, but it is the nature of the chamber that conveniently divides the carbons produced into two distinct types.

(PETER A. THROWER)

1. H. B. Palmer, C. F. Cullis, in *Chemistry and Physics of Carbon*, Vol. 2, P. L. Walker Jr., ed., Dekker, New York, 1966, p. 265.
2. J. C. Bokros, in *Chemistry and Physics of Carbon*, Vol. 5, P.L. Walker Jr., ed., Dekker, New York, 1969, p. 1.

17.3.4.2.1. Stationary Mandrels.

A furnace containing a graphite mandrel on which deposition is to occur is used to produce massive pieces of pyrocarbon for rocket nozzles and nose cones. Hydrocarbon gas such as methane, natural gas, or propylene is diluted with an inert gas and introduced into the furnace containing the heated mandrel, whereupon pyrocarbon is deposited on its surface. In this case difficulties arise because there is no mixing of the gas and there are large gradients in the temperature and composition of the gas. For example, as the gas progresses down the tube the concentration of hydrocarbon is depleted because of the carbon deposition; therefore the amount and the structure of the deposit vary with position.

The density of the pyrocarbon depends on the deposition temperature, showing a minimum at around 1700°C for both methane and propane precursors[1]. This minimum

Inorganic Reactions and Methods, Volume 18
Edited by J. J. Zuckerman, Jim D. Atwood

Binderless graphites[1] having up to 95% theoretical density have been produced by heating finely ground, partially calcined coke in an autoclave under an isostatic pressure. The methane and other organics released from the coke during heating are pyrolyzed and probably form a thin pyrocarbon bond between the filler particles. The final product can be both highly isotropic and very strong. It is suspected that variations of this technique are used in production of some of the commercial fine-grained, high strength, isotropic graphites available today.

(PETER A. THROWER)

1. W. Chard, M. Conway, D. Niesz, in *Petroleum Derived Carbons*, M. L. Deviney, T. M. O'Grady, eds., American Chemical Society, Washington, DC, 1976, p. 155.

17.3.4.2. Pyrolytic Carbons

The term "pyrolytic carbon" can be applied to carbon filaments, carbon blacks, and carbon films, as well as to the more massive deposits which are the subject of this section. Pyrocarbon materials, made by chemical vapor deposition (CVD), vary in density, properties, and structure as much as the bulk materials discussed in 17.3.4.1. A heated hydrocarbon gas decomposes into an entire series of molecular species with a wide spectrum of carbon contents and molecular weights[1]. Within this pyrolyzing atmosphere, "droplets" form that pyrolyze and condense on a nearby surface, or large carbonaceous complexes may condense directly on the surface of the chamber. The former condition produces a fluffy, sooty, soft carbon, not far removed from carbon black, while the latter produces a hard solid carbon. The second of these materials is of primary interest here. The structure of the carbon produced by the CVD process has been shown[2] to depend on the type of hydrocabon and its concentration, the pyrolysis temperature, the contact time, and the geometry of the pyrolyzing chamber. Of these, the pyrolysis temperature is perhaps the most important, but it is the nature of the chamber that conveniently divides the carbons produced into two distinct types.

(PETER A. THROWER)

1. H. B. Palmer, C. F. Cullis, in *Chemistry and Physics of Carbon*, Vol. 2, P. L. Walker Jr., ed., Dekker, New York, 1966, p. 265.
2. J. C. Bokros, in *Chemistry and Physics of Carbon*, Vol. 5, P.L. Walker Jr., ed., Dekker, New York, 1969, p. 1.

17.3.4.2.1. Stationary Mandrels.

A furnace containing a graphite mandrel on which deposition is to occur is used to produce massive pieces of pyrocarbon for rocket nozzles and nose cones. Hydrocarbon gas such as methane, natural gas, or propylene is diluted with an inert gas and introduced into the furnace containing the heated mandrel, whereupon pyrocarbon is deposited on its surface. In this case difficulties arise because there is no mixing of the gas and there are large gradients in the temperature and composition of the gas. For example, as the gas progresses down the tube the concentration of hydrocarbon is depleted because of the carbon deposition; therefore the amount and the structure of the deposit vary with position.

The density of the pyrocarbon depends on the deposition temperature, showing a minimum at around 1700°C for both methane and propane precursors[1]. This minimum

Inorganic Reactions and Methods, Volume 18
Edited by J. J. Zuckerman, Jim D. Atwood

Binderless graphites[1] having up to 95% theoretical density have been produced by heating finely ground, partially calcined coke in an autoclave under an isostatic pressure. The methane and other organics released from the coke during heating are pyrolyzed and probably form a thin pyrocarbon bond between the filler particles. The final product can be both highly isotropic and very strong. It is suspected that variations of this technique are used in production of some of the commercial fine-grained, high strength, isotropic graphites available today.

(PETER A. THROWER)

1. W. Chard, M. Conway, D. Niesz, in *Petroleum Derived Carbons*, M. L. Deviney, T. M. O'Grady, eds., American Chemical Society, Washington, DC, 1976, p. 155.

17.3.4.2. Pyrolytic Carbons

The term "pyrolytic carbon" can be applied to carbon filaments, carbon blacks, and carbon films, as well as to the more massive deposits which are the subject of this section. Pyrocarbon materials, made by chemical vapor deposition (CVD), vary in density, properties, and structure as much as the bulk materials discussed in 17.3.4.1. A heated hydrocarbon gas decomposes into an entire series of molecular species with a wide spectrum of carbon contents and molecular weights[1]. Within this pyrolyzing atmosphere, "droplets" form that pyrolyze and condense on a nearby surface, or large carbonaceous complexes may condense directly on the surface of the chamber. The former condition produces a fluffy, sooty, soft carbon, not far removed from carbon black, while the latter produces a hard solid carbon. The second of these materials is of primary interest here. The structure of the carbon produced by the CVD process has been shown[2] to depend on the type of hydrocabon and its concentration, the pyrolysis temperature, the contact time, and the geometry of the pyrolyzing chamber. Of these, the pyrolysis temperature is perhaps the most important, but it is the nature of the chamber that conveniently divides the carbons produced into two distinct types.

(PETER A. THROWER)

1. H. B. Palmer, C. F. Cullis, in *Chemistry and Physics of Carbon*, Vol. 2, P. L. Walker Jr., ed., Dekker, New York, 1966, p. 265.
2. J. C. Bokros, in *Chemistry and Physics of Carbon*, Vol. 5, P.L. Walker Jr., ed., Dekker, New York, 1969, p. 1.

17.3.4.2.1. Stationary Mandrels.

A furnace containing a graphite mandrel on which deposition is to occur is used to produce massive pieces of pyrocarbon for rocket nozzles and nose cones. Hydrocarbon gas such as methane, natural gas, or propylene is diluted with an inert gas and introduced into the furnace containing the heated mandrel, whereupon pyrocarbon is deposited on its surface. In this case difficulties arise because there is no mixing of the gas and there are large gradients in the temperature and composition of the gas. For example, as the gas progresses down the tube the concentration of hydrocarbon is depleted because of the carbon deposition; therefore the amount and the structure of the deposit vary with position.

The density of the pyrocarbon depends on the deposition temperature, showing a minimum at around 1700°C for both methane and propane precursors[1]. This minimum

may be eliminated by reducing the partial pressure of the hydrocarbon, thus lowering saturation levels in the pyrolyzing gas and preventing the formation of soot. The incorporation of this undesirable form of carbon into the deposit causes the decrease in density.

Pyrolytic carbons deposited on stationary formers normally show well-defined growth structures, which are nucleated by surface imperfections or by droplets nucleated on the surface, (Fig. 1). These growth cones contain imperfect graphite basal planes lying preferentially parallel to the substrate. If the surface is very smooth, very few growth features are produced and the layer planes form a laminar structure. Materials such as these are known as substrate-nucleated pyrocarbons. If hydrocarbon levels are increased to cause nuclei to form in the gas phase, these will be incorporated into the deposit, each nucleus acting as the origin of another growth cone. When growth cones are developed throughout the structure, the material is referred to as continuously, or regeneratively, nucleated. The preferred orientation of the defective, small-layer-plane units parallel to the substrate gives the pyrocarbon anisotropic properties even though the structure is no-where near that of a perfect graphite crystal. Thermal conductivity perpendicular to the deposit is therefore very poor, which usually sets up a high temperature gradient across the deposit. This limits the thickness of the deposit that can be obtained, either because the surface exposed to the gas becomes too cool for deposition, or because differential strains in the material produce lamellar cracking on cooling.

Not only are the layer planes small and defective, they are also stacked with twists and tilts between them. This twisting of the layers with respect to each other gives rise to the term "turbostratic" carbon for these materials. The turbostratic, well-oriented, substrate-nucleated pyrocarbons are ideal candidates for graphitization, and the highly oriented pyrolytic graphite (HOPG) used for X-ray and neutron monochromators is produced from these precursors[2].

While simple thermal annealing at temperatures around 3000°C produces graphitization of these materials, and annealing at 3600°C gives materials whose basal plane properties approach those of the single crystal, there always remains an angular spread of 2–3° in the *c*-axes of the constituent crystallites. This mosaic spread is reduced to as low as 0.2° by a process involving annealing to 3200–3600°C while, at the same time, applying a compressive stress perpendicular to the deposition plane. Pressures of up to 105 Pa

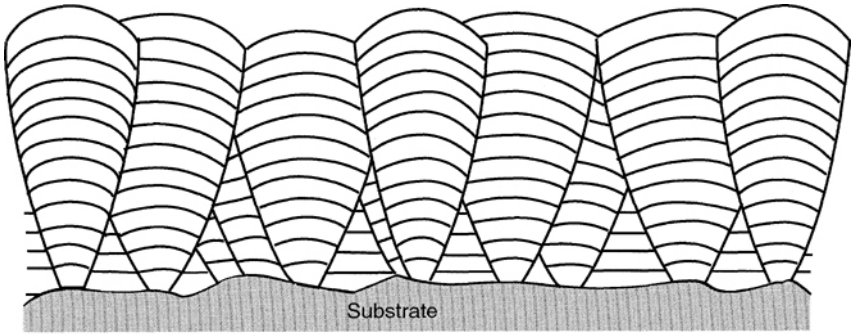

Figure 1. Typical layer arrangement in a substrated-nucleated pyrolytic graphite.

have been reported, but actual pressures at temperature are unknown because the material is plastic under those conditions. Not only can flat plates be produced, but also singly and doubly curved plates, if suitably shaped compression rams are used. Such materials are of importance for producing focused, monochromated X-ray beams, and, on a unit weight basis, are the most expensive forms of graphite commercially available.

(PETER A. THROWER)

1. R. J. Diefendorf, *J. Chim. Phys. (Paris)*, 7, 85 (1960).
2. A. W. Moore, in *Chemistry and Physics of Carbon*, Vol. 11, P. L. Walker Jr., P. A. Thrower, eds., Dekker, New York, 1973, p. 69.

17.3.4.2.2. Fluidized Beds.

When a bed of the particles to be coated is held in a furnace while a mixture of hydrocarbon and inert gases is passed through it, there is fluidization of the bed. The hydrocarbon gas pyrolyzes in the bed, and carbon is deposited on the particles. The advantage of this method is the continuous mixing, which produces a fairly uniform temperature and gas concentration throughout the bed. This results in a more controlled, uniform deposit. The incentive to develop was the need to coat nuclear fuel particles with a material that could retain the products of the fission reaction in a nuclear reactor. Depending on the reaction conditions, many types of structure may be formed within the deposit. These are classified as laminar, isotropic, and granular. The first two are similar to the substrate and continuously nucleated materials already discussed. The granular carbons are produced at high bed temperatures (1700–2000°C) and low hydrocarbon gas concentrations (– 5%), where the values in parentheses are for methane. One advantage of the fluidized-bed technique is the ability to change the temperature and the type and composition of the gas. In this way layers of different structures may be laid on top of each other. A porous, low density deposit followed by an impervious, strong, high density deposit is of great utility in retaining the fission gases in nuclear fuel particles. Another advantage is the ability to introduce other elements into the fluidizing gas for codeposition with the carbon, an important example being the codeposition of silicon to produce a fine dispersion of silicon carbide in the carbon. This material has been used in bioengineering for the coating of heart valves, and other specialized components[1].

(PETER A. THROWER)

1. J. C. Bokros, in *Chemistry and Physics of Carbon*, Vol. 5, P. L. Walker Jr., ed., Dekker, New York, 1969, p. 1.

17.3.4.3. Glassy Carbon

When certain polymers are thermally degraded, a material resembling a black glass is produced. Its shiny surface and its brittle character have earned it the name vitreous or glassy carbon. Commercial production is very limited and has declined in recent years. Few of the uses proposed when this substance was introduced in 1967 have come to fruition[1]. Details of manufacture are proprietary, but the general principles seem to be well defined. Precursors for glassy carbon are polymers with a degree of cross-linking.

Inorganic Reactions and Methods, Volume 18
Edited by J. J. Zuckerman, Jim D. Atwood

have been reported, but actual pressures at temperature are unknown because the material is plastic under those conditions. Not only can flat plates be produced, but also singly and doubly curved plates, if suitably shaped compression rams are used. Such materials are of importance for producing focused, monochromated X-ray beams, and, on a unit weight basis, are the most expensive forms of graphite commercially available.

(PETER A. THROWER)

1. R. J. Diefendorf, *J. Chim. Phys. (Paris)*, 7, 85 (1960).
2. A. W. Moore, in *Chemistry and Physics of Carbon*, Vol. 11, P. L. Walker Jr., P. A. Thrower, eds., Dekker, New York, 1973, p. 69.

17.3.4.2.2. Fluidized Beds.

When a bed of the particles to be coated is held in a furnace while a mixture of hydrocarbon and inert gases is passed through it, there is fluidization of the bed. The hydrocarbon gas pyrolyzes in the bed, and carbon is deposited on the particles. The advantage of this method is the continuous mixing, which produces a fairly uniform temperature and gas concentration throughout the bed. This results in a more controlled, uniform deposit. The incentive to develop was the need to coat nuclear fuel particles with a material that could retain the products of the fission reaction in a nuclear reactor. Depending on the reaction conditions, many types of structure may be formed within the deposit. These are classified as laminar, isotropic, and granular. The first two are similar to the substrate and continuously nucleated materials already discussed. The granular carbons are produced at high bed temperatures (1700–2000°C) and low hydrocarbon gas concentrations (– 5%), where the values in parentheses are for methane. One advantage of the fluidized-bed technique is the ability to change the temperature and the type and composition of the gas. In this way layers of different structures may be laid on top of each other. A porous, low density deposit followed by an impervious, strong, high density deposit is of great utility in retaining the fission gases in nuclear fuel particles. Another advantage is the ability to introduce other elements into the fluidizing gas for codeposition with the carbon, an important example being the codeposition of silicon to produce a fine dispersion of silicon carbide in the carbon. This material has been used in bioengineering for the coating of heart valves, and other specialized components[1].

(PETER A. THROWER)

1. J. C. Bokros, in *Chemistry and Physics of Carbon*, Vol. 5, P. L. Walker Jr., ed., Dekker, New York, 1969, p. 1.

17.3.4.3. Glassy Carbon

When certain polymers are thermally degraded, a material resembling a black glass is produced. Its shiny surface and its brittle character have earned it the name vitreous or glassy carbon. Commercial production is very limited and has declined in recent years. Few of the uses proposed when this substance was introduced in 1967 have come to fruition[1]. Details of manufacture are proprietary, but the general principles seem to be well defined. Precursors for glassy carbon are polymers with a degree of cross-linking.

Inorganic Reactions and Methods, Volume 18
Edited by J. J. Zuckerman, Jim D. Atwood

have been reported, but actual pressures at temperature are unknown because the material is plastic under those conditions. Not only can flat plates be produced, but also singly and doubly curved plates, if suitably shaped compression rams are used. Such materials are of importance for producing focused, monochromated X-ray beams, and, on a unit weight basis, are the most expensive forms of graphite commercially available.

(PETER A. THROWER)

1. R. J. Diefendorf, *J. Chim. Phys. (Paris)*, *7*, 85 (1960).
2. A. W. Moore, in *Chemistry and Physics of Carbon*, Vol. 11, P. L. Walker Jr., P. A. Thrower, eds., Dekker, New York, 1973, p. 69.

17.3.4.2.2. Fluidized Beds.

When a bed of the particles to be coated is held in a furnace while a mixture of hydrocarbon and inert gases is passed through it, there is fluidization of the bed. The hydrocarbon gas pyrolyzes in the bed, and carbon is deposited on the particles. The advantage of this method is the continuous mixing, which produces a fairly uniform temperature and gas concentration throughout the bed. This results in a more controlled, uniform deposit. The incentive to develop was the need to coat nuclear fuel particles with a material that could retain the products of the fission reaction in a nuclear reactor. Depending on the reaction conditions, many types of structure may be formed within the deposit. These are classified as laminar, isotropic, and granular. The first two are similar to the substrate and continuously nucleated materials already discussed. The granular carbons are produced at high bed temperatures (1700–2000°C) and low hydrocarbon gas concentrations (− 5%), where the values in parentheses are for methane. One advantage of the fluidized-bed technique is the ability to change the temperature and the type and composition of the gas. In this way layers of different structures may be laid on top of each other. A porous, low density deposit followed by an impervious, strong, high density deposit is of great utility in retaining the fission gases in nuclear fuel particles. Another advantage is the ability to introduce other elements into the fluidizing gas for codeposition with the carbon, an important example being the codeposition of silicon to produce a fine dispersion of silicon carbide in the carbon. This material has been used in bioengineering for the coating of heart valves, and other specialized components[1].

(PETER A. THROWER)

1. J. C. Bokros, in *Chemistry and Physics of Carbon*, Vol. 5, P. L. Walker Jr., ed., Dekker, New York, 1969, p. 1.

17.3.4.3. Glassy Carbon

When certain polymers are thermally degraded, a material resembling a black glass is produced. Its shiny surface and its brittle character have earned it the name vitreous or glassy carbon. Commercial production is very limited and has declined in recent years. Few of the uses proposed when this substance was introduced in 1967 have come to fruition[1]. Details of manufacture are proprietary, but the general principles seem to be well defined. Precursors for glassy carbon are polymers with a degree of cross-linking.

These cross-linkages remain in the carbonized material, allowing only limited layer plane growth and orientation during subsequent heat treating. Indeed, after heating to 2700°C the crystallite size in these materials is only around 5 nm parallel to the layer planes and 3 nm perpendicular. The interlayer spacing is then 0.35 nm, much greater than the 0.335 nm for a perfect graphite crystal. The difficulty in graphitizing the material is demonstrated by transmission electron microscope studies that show the structure as stacks of ribbons of approximately 10 graphite layer planes, which are tangled and knotted together. Little opportunity for layer plane development occurs without a complete breakdown of the structure. Since carbon does not liquefy at normal pressures, the disorder is locked in, and the material is an excellent example of a hard carbon. Some of the precursors that have been used are cellulose, phenolic resins, and polyfurfuryl alcohol.

Cellulose carbon is made by dispersing cellulose powder in water and then centrifuging to obtain the shape of the part to be manufactured. When dried, the part can be machined so that it produces the surface finish and thickness required. It is then heated to cause degradation; because of the large volumes of gaseous products evolved during the early stages of decomposition, however, the heating rate must be extremely slow. Heating rates of 1–5°C/h are often mentioned. The buildup of gas pressure in the decomposing cellulose is balanced by an external gas pressure (14 MPa), which can be reduced as porosity is developed in the structure. When the temperature has reached around 500°C, there is enough porosity for the material to be further heat-treated in a conventional furnace under ambient pressure. The final heat treatment temperature may be in the range of 1000–3000°C.

Furfuryl alcohol, a thermosetting resin, is used to produce unusual shapes of glassy carbon artifacts by repeatedly painting the resin on a die of the required shape and size. After adequate thickness has been obtained, the whole article may be slowly heated to produce carbonization. A manufacturing technique using 12:1 phenol hexamine has been developed[2] in which resin preheated to 300–330°C is crushed and compacted into disks under a pressure of 350 MPa. Sintering under a small load (105 Pa) produces a disk that maintains its shape during carbonization. Heating rates similar to those already mentioned are used during the carbonization stage.

Although the density of glassy carbon is only around 1.5 g/cm^3, its permeability is about 10 orders of magnitude less than that of a bulk binder–filler graphite. The porosity that develops during the initial heating stages (to ~800°C) heals itself as the temperature is further increased. The mechanism for this is not understood. The shrinkage of the carbon from the precursor dimensions is greater than 25%, but experience allows manufacturers to machine the precursor to dimensions such that the finished product will be of the desired shape and size. This is particularly important because the resulting glassy carbon is very hard and almost impossible to machine. The large amounts of gas evolved during the processing limit final thicknesses to around 5 mm; a cellular type of glassy carbon has been developed that is available in thicknesses up to 10 mm, however. The cell size can be varied to produce materials ranging from a fine foam to a very open three-dimensional net. These materials are known as reticulated vitreous carbons.

(PETER A. THROWER)

1. F. C. Cowlard, I. C. Lewis, *J. Mater. Sci.*, *2*, 507 (1967).
2. G. M. Jenkins, K. Kawamura, *Polymeric Carbons*, Cambridge University Press, Cambridge, 1976.

Inorganic Reactions and Methods, Volume 18
Edited by J. J. Zuckerman, Jim D. Atwood

17.3.4.4. Carbon Fibers

Although carbon filaments can be made by means of the techniques described for glassy carbon and pyrocarbon, the fibers of most interest are those that have a more graphitic structure. This is because these fibers are designed to take advantage of the extreme strength and stiffness of the graphite layer planes. A graphite crystal has a very high Young's modulus (1060 GPa) parallel to the layer planes. However a force applied a few degrees away from this direction causes shear of the layers over each other with a drastic lowering of the modulus ($\sim$ 500 GPa at 10°), as indicated in Figure 1. To obtain a high modulus fiber it is therefore necessary to have primary graphite layer planes (graphene layers) aligned very close to the fiber axis. The method used to introduce this orientation depends on the precursor[1,2]. In addition, however, some departure from perfect large graphene layers aligned parallel to the fiber axis is necessary because the fibers would otherwise fail in compression as a result of the low shear strength between the layers. The presence of disclinations and turbostratic disorder within the fibers is therefore an advantage in this regard. In general, the presence of large graphene layers oriented parallel to the fiber axis makes for a high tensile modulus and high thermal conduction, which are advantageous for thermal management applications, but tensile and compressive strengths are lower.

(PETER A. THROWER)

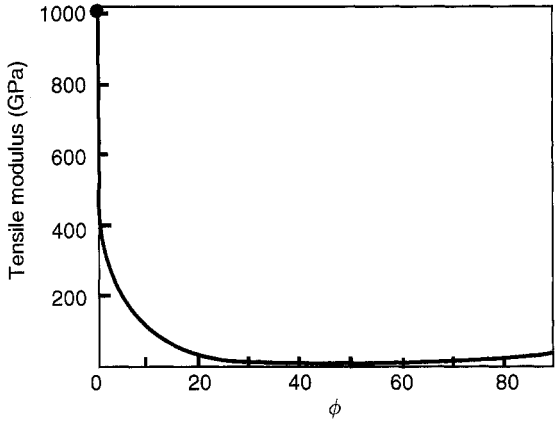

Figure 1. Tensile modulus of graphite crystal as a functions of the angle (ϕ) of the applied stress to the layer planes.

1. P. J. Goodhew, A. J. Clarke, J. E. Bailey, *Mater. Sci. Eng., 17*, 3 (1975).
2. R. J. Diefendorf, in *Petroleum Derived Carbons*, M. L. Deviney and T. M. O'Grady, eds., American Chemical Society, Washington, DC, 1976, p. 315.

17.3.4.4.1. Cellulose (Rayon)-Based Fibers.

For cellulose, or rayon-based fibers[1] production involves three distinct steps: heat treatment to $\sim$350°C to form a thermally stable char, carbonization at 1000–2000°C,

Inorganic Reactions and Methods, Volume 18
Edited by J. J. Zuckerman, Jim D. Atwood

17.3.4.4. Carbon Fibers

Although carbon filaments can be made by means of the techniques described for glassy carbon and pyrocarbon, the fibers of most interest are those that have a more graphitic structure. This is because these fibers are designed to take advantage of the extreme strength and stiffness of the graphite layer planes. A graphite crystal has a very high Young's modulus (1060 GPa) parallel to the layer planes. However a force applied a few degrees away from this direction causes shear of the layers over each other with a drastic lowering of the modulus ($\sim$ 500 GPa at 10°), as indicated in Figure 1. To obtain a high modulus fiber it is therefore necessary to have primary graphite layer planes (graphene layers) aligned very close to the fiber axis. The method used to introduce this orientation depends on the precursor[1,2]. In addition, however, some departure from perfect large graphene layers aligned parallel to the fiber axis is necessary because the fibers would otherwise fail in compression as a result of the low shear strength between the layers. The presence of disclinations and turbostratic disorder within the fibers is therefore an advantage in this regard. In general, the presence of large graphene layers oriented parallel to the fiber axis makes for a high tensile modulus and high thermal conduction, which are advantageous for thermal management applications, but tensile and compressive strengths are lower.

(PETER A. THROWER)

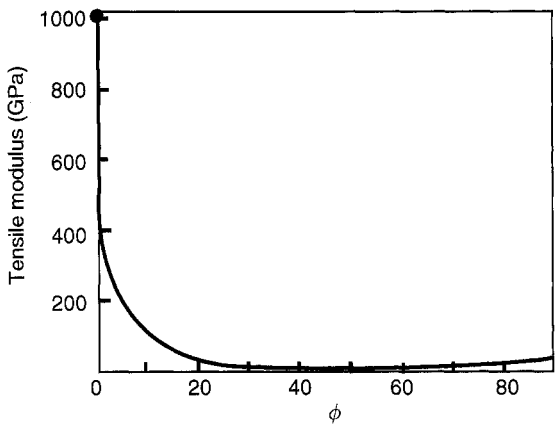

Figure 1. Tensile modulus of graphite crystal as a functions of the angle (ϕ) of the applied stress to the layer planes.

1. P. J. Goodhew, A. J. Clarke, J. E. Bailey, *Mater. Sci. Eng., 17*, 3 (1975).
2. R. J. Diefendorf, in *Petroleum Derived Carbons*, M. L. Deviney and T. M. O'Grady, eds., American Chemical Society, Washington, DC, 1976, p. 315.

17.3.4.4.1. Cellulose (Rayon)-Based Fibers.

For cellulose, or rayon-based fibers[1] production involves three distinct steps: heat treatment to $\sim$350°C to form a thermally stable char, carbonization at 1000–2000°C,

and graphitization at temperatures up to 3000°C. The heat treatment is usually performed in reactive atmospheres (O_2, Cl_2, or HCl) to prevent evolved tars from redepositing on the fiber, and also to improve process rates and weight yields. Carbonization to temperatures above 1000°C is very rapid (<1 min) and is usually done in an inert atmosphere. At this stage there is no real order to the material, and heating to graphitization temperatures does not help. High strength, high modulus fibers may be produced by straining the carbonized yarn at temperatures in the range of 2800–3000°C, where layer plane alignment is produced. Increased stretching is accompanied by an increase in Young's modulus, with almost perfect alignment of the layer planes parallel to the fiber axis achieved with a strain of 180%. Strength also increases with increased strain, and values of 2.8 GPa tensile strength and 800 GPa Young's modulus have been reported. Introducing alignment by stretching during the high temperature graphitization step is difficult to control and makes high modulus rayon-based fibers very expensive. In addition, they exhibit some inferior properties when incorporated into composites. As a consequence the process has been abandoned for commercial purposes in favor of processes using polyacrylonitrile (PAN) or pitch as precursors.

(PETER A. THROWER)

1. R. Bacon, in *Chemistry and Physics of Carbon*, Vol. 9, P. L. Walker Jr., P. A. Thrower, eds., Dekker, New York, 1973, p. 1.

17.3.4.4.2. PAN-Based Fibers.

Polyacrylonitrile (acrylic) fibers (—$[CH_2CH(CN)]_n$—) are made in large quantities for textile use (Courtelle, Orlon, etc), and they provide an inexpensive and readily available source of raw material. Here again there are three distinct manufacturing steps: preoxidation or stabilization, carbonization, and graphitization. A continuous "tow" of between 3000 and 10,000 fibers moves slowly through these three stages without interruption. During the stabilizing[1] heat treatment at around 220°C for several hours in air, the thermoplastic PAN is converted into a nonplastic cyclic compound that does not melt at the higher carbonization temperature. By applying tension to prevent the ~25% length shrinkage that would otherwise occur, the polymer chains are straightened and a high degree of alignment is introduced. The oxidizing atmosphere cyclizes the polymer chains to form a ladder polymer with the release of large amounts of heat. Heat release must be controlled to prevent loss of molecular orientation and even fiber melting. After stabilization, the required orientation for a high modulus fiber is present, and tension is not required during the later processing stages.

The stabilized fibers are now heated in an inert atmosphere, usually ultrapure nitrogen, between 1000 and 1500°C, passing through a series of ovens with increasing pyrolyzing temperatures and enough tension to keep them moving. Any remaining nitrogen, hydrogen, and oxygen are released, and a carbonaceous fiber is produced. During this stage, the cyclic molecular chains link to form structures resembling the layer planes of graphite. A final, brief heat treatment at temperatures up to 3000°C increases crystallite size and improves orientation, thus increasing Young's modulus, but, as mentioned earlier, decreasing tensile strength.

The properties of PAN fibers (~10 μm diameter) are very dependent on the final heat treatment temperature (HTT). Tensile strength reaches a maximum (3.5 GPa) at a HTT of around 1500°C, and then decreases, while Young's modulus continues to

Inorganic Reactions and Methods, Volume 18
Edited by J. J. Zuckerman, Jim D. Atwood

and graphitization at temperatures up to 3000°C. The heat treatment is usually performed in reactive atmospheres (O_2, Cl_2, or HCl) to prevent evolved tars from redepositing on the fiber, and also to improve process rates and weight yields. Carbonization to temperatures above 1000°C is very rapid (<1 min) and is usually done in an inert atmosphere. At this stage there is no real order to the material, and heating to graphitization temperatures does not help. High strength, high modulus fibers may be produced by straining the carbonized yarn at temperatures in the range of 2800–3000°C, where layer plane alignment is produced. Increased stretching is accompanied by an increase in Young's modulus, with almost perfect alignment of the layer planes parallel to the fiber axis achieved with a strain of 180%. Strength also increases with increased strain, and values of 2.8 GPa tensile strength and 800 GPa Young's modulus have been reported. Introducing alignment by stretching during the high temperature graphitization step is difficult to control and makes high modulus rayon-based fibers very expensive. In addition, they exhibit some inferior properties when incorporated into composites. As a consequence the process has been abandoned for commercial purposes in favor of processes using polyacrylonitrile (PAN) or pitch as precursors.

(PETER A. THROWER)

1. R. Bacon, in *Chemistry and Physics of Carbon*, Vol. 9, P. L. Walker Jr., P. A. Thrower, eds., Dekker, New York, 1973, p. 1.

17.3.4.4.2. PAN-Based Fibers.

Polyacrylonitrile (acrylic) fibers (—$[CH_2CH(CN)]_n$—) are made in large quantities for textile use (Courtelle, Orlon, etc), and they provide an inexpensive and readily available source of raw material. Here again there are three distinct manufacturing steps: preoxidation or stabilization, carbonization, and graphitization. A continuous "tow" of between 3000 and 10,000 fibers moves slowly through these three stages without interruption. During the stabilizing[1] heat treatment at around 220°C for several hours in air, the thermoplastic PAN is converted into a nonplastic cyclic compound that does not melt at the higher carbonization temperature. By applying tension to prevent the ~25% length shrinkage that would otherwise occur, the polymer chains are straightened and a high degree of alignment is introduced. The oxidizing atmosphere cyclizes the polymer chains to form a ladder polymer with the release of large amounts of heat. Heat release must be controlled to prevent loss of molecular orientation and even fiber melting. After stabilization, the required orientation for a high modulus fiber is present, and tension is not required during the later processing stages.

The stabilized fibers are now heated in an inert atmosphere, usually ultrapure nitrogen, between 1000 and 1500°C, passing through a series of ovens with increasing pyrolyzing temperatures and enough tension to keep them moving. Any remaining nitrogen, hydrogen, and oxygen are released, and a carbonaceous fiber is produced. During this stage, the cyclic molecular chains link to form structures resembling the layer planes of graphite. A final, brief heat treatment at temperatures up to 3000°C increases crystallite size and improves orientation, thus increasing Young's modulus, but, as mentioned earlier, decreasing tensile strength.

The properties of PAN fibers (~10 μm diameter) are very dependent on the final heat treatment temperature (HTT). Tensile strength reaches a maximum (3.5 GPa) at a HTT of around 1500°C, and then decreases, while Young's modulus continues to

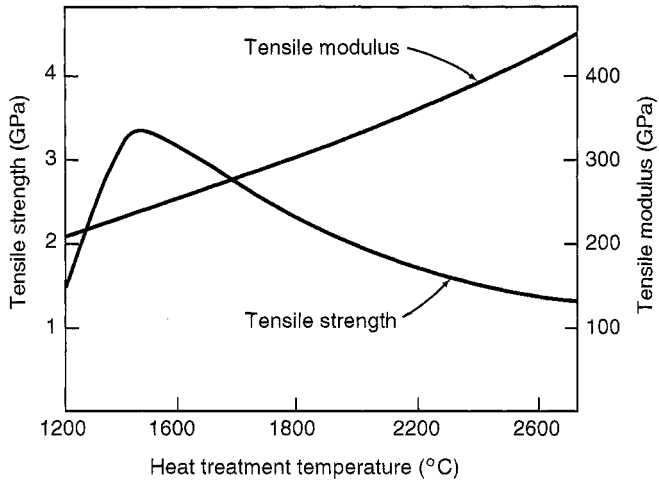

Figure 1. Effect of carbonization temperature on properties of PAN-based fibers.

increase with increasing HTT with values over 480 GPa achieved (Fig. 1)[2]. The carbonization temperature that produces maximum tensile strength has been shown to depend on the precursor used[3]. Three types of PAN fiber are recognized: type I fibers have been subjected to an HTT of at least 2800°C, and thus have a high modulus; type II fibers are high strength fibers with a final HTT of around 1500°C; and type III fibers are of inferior quality with neither the high modulus of type I nor the higher tensile strength of type II. They are cheaper than either type I or type II PAN fibers or rayon-based fibers and have been used extensively in sporting goods.

(PETER A. THROWER)

1. W. Watt, W. Johnson, *Appl. Polym. Symp.*, *9*, 215 (1969); *Nature*, *257*, 210 (1975).
2. R. Moreton, W. Watt, W. Johnson, *Nature*, *213*, 690 (1967).
3. E. Fitzer, W. Frohs, M. Heine, *Carbon*, *24*, 387 (1986).

17.3.4.4.3. Pitch-Based Fibers.

Two categories of pitch-based fiber exist: isotropic carbon fiber produced from an isotropic pitch precursor, and an oriented, anisotropic fiber produced from a mesophase pitch precursor. Isotropic fibers were developed from low melting point isotropic pitches[1]. The precursor was melt-spun into fibers, which were oxidized to render them infusible, and then carbonized. Their low strengths and moduli make these fibers unsuitable for use in advanced composites. Orientation was accomplished by a hot-stretching process (>2200°C), but it is accompanied by the same processing difficulties encountered in the rayon precursor process. A different approach was suggested by the discovery of carbonaceous mesophase[2].

While rayon and PAN are well-defined chemical compounds, pitch produced either from distillation of coal tar or as petroleum residuum is a complex mixture of hydrocarbon and heterocyclic molecules with molecular weights ranging from 200 to over 1000. Heating such a mixture above ~400°C produces condensation and polymerization

Inorganic Reactions and Methods, Volume 18
Edited by J. J. Zuckerman, Jim D. Atwood

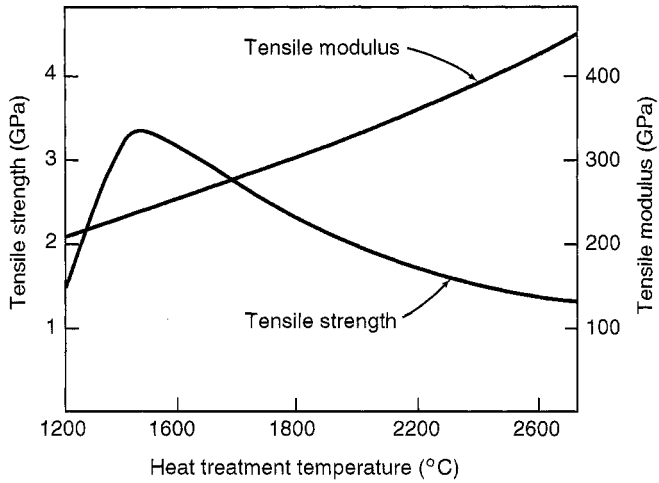

Figure 1. Effect of carbonization temperature on properties of PAN-based fibers.

increase with increasing HTT with values over 480 GPa achieved (Fig. 1)[2]. The carbonization temperature that produces maximum tensile strength has been shown to depend on the precursor used[3]. Three types of PAN fiber are recognized: type I fibers have been subjected to an HTT of at least 2800°C, and thus have a high modulus; type II fibers are high strength fibers with a final HTT of around 1500°C; and type III fibers are of inferior quality with neither the high modulus of type I nor the higher tensile strength of type II. They are cheaper than either type I or type II PAN fibers or rayon-based fibers and have been used extensively in sporting goods.

(PETER A. THROWER)

1. W. Watt, W. Johnson, *Appl. Polym. Symp., 9*, 215 (1969); *Nature, 257*, 210 (1975).
2. R. Moreton, W. Watt, W. Johnson, *Nature, 213*, 690 (1967).
3. E. Fitzer, W. Frohs, M. Heine, *Carbon, 24*, 387 (1986).

17.3.4.4.3. Pitch-Based Fibers.

Two categories of pitch-based fiber exist: isotropic carbon fiber produced from an isotropic pitch precursor, and an oriented, anisotropic fiber produced from a mesophase pitch precursor. Isotropic fibers were developed from low melting point isotropic pitches[1]. The precursor was melt-spun into fibers, which were oxidized to render them infusible, and then carbonized. Their low strengths and moduli make these fibers unsuitable for use in advanced composites. Orientation was accomplished by a hot-stretching process (>2200°C), but it is accompanied by the same processing difficulties encountered in the rayon precursor process. A different approach was suggested by the discovery of carbonaceous mesophase[2].

While rayon and PAN are well-defined chemical compounds, pitch produced either from distillation of coal tar or as petroleum residuum is a complex mixture of hydrocarbon and heterocyclic molecules with molecular weights ranging from 200 to over 1000. Heating such a mixture above ~400°C produces condensation and polymerization

reactions resulting in the formation of large flat aromatic molecules that orient into an anisotropic liquid crystal phase, or mesophase. This phase first appears as small spheres which, as heating continues, collide and coalesce to form larger spheres, the mesophase spheres. This mesophase is thermodynamically stable and does not convert to an isotropic liquid until heated above the mesophase–liquid transition temperature. However, before this happens carbonization occurs. The anisotropy of the mesophase is therefore retained in a carbonized product, where it manifests itself as a preferred orientation of the primordial graphite layer planes. This is the same process that occurs upon coking.

In fiber manufacture the liquid mesophase is oriented by shear during a melt-spinning process. The forces involved result in a highly oriented structure, with the mesophase spheres elongated into cylinders parallel to the fiber axis (circumferential fibers), although radial and isotropic microstructures can be produced, depending on spinning conditions and geometry. These different configurations give different surface properties. The spun fiber is then stabilized (thermoset) in an oxidizing atmosphere, carbonized, and graphitized as for the PAN fibers[3]. A 800 GPa modulus, 2.2 GPa tensile strength fiber has been produced, but fibers with lower strengths and moduli can be produced quite cheaply and have found extensive use in sporting goods.

As already mentioned, fibers of many different microstructures can be produced depending on the geometry of the spinneret through which the mesophase pitch is squeezed. In some the graphite layers are arranged as concentric cylinders with a structure similar to that of a leek of scallion. In others the layers radiate from the center like spokes in a wheel. In recent years there has been considerable interest in fibers of cross-sectional geometries other than circular. C-shaped, trilobal, and ribbon fibers can be produced by adjusting the shape of the spinneret[4]. While the former two seem to offer enhanced mechanical properties when used in composites, the ribbon fibers were developed to provide excellent thermal conduction[5]. As explained earlier, this comes with a loss in strength.

Another interesting development in carbon fiber processing has been special synthetic pitches for fiber spinning. Foremost among these is the naphthalene pitch developed by Mochida et al. in Japan[6,7], using a HF/BF_3 catalyst for pitch production. Fibers produced from this precursor exhibit easier processing characteristics and promise properties at least equal to those produced from other sources. The obvious difference is the narrow spectrum of molecular weights in the precursor compared with traditional pitches. Tensile strengths and moduli have been achieved with values as high as 4.0 and 880 GPa, respectively. The latter is over 80% of the value for a graphene layer, indicating a very high degree of layer orientation in the fiber. The pitch is commercially available from Mitsubishi Gas Chemical.

Another development is the formation of synthetic mesophase pitch containing up to 7 mol% boron using 9-chloroborafluorene precursor[8]. The presence of substitutional boron has long been acknowledged as an oxidation inhibitor for graphite, and is also recognized as a graphitization catalyst[9]; hence the incorporation of boron in the mesophase has the potential for producing fibers with a higher modulus for lower graphitization temperatures, and with a greater oxidation resistance.

(PETER A. THROWER)

1. S. Otani, *Carbon, 3,* 31 (1965).
2. J. D. Brooks, G. H. Taylor, *Carbon, 3,* 185 (1965).

3. B. Rand, in *Handbook of Composites*, Vol. 1, *Strong Fibers*, W. Watt, B. V. Perov, eds., Elsevier, Amsterdam, 1985, p. 495.
4. D. D. Edie, N. R. Fox, B. C. Barnett, C. C. Fain, *Carbon, 24*, 447 (1986).
5. D. D. Edie, C. C. Fain, K. E. Robinson, A. M. Harper, D. K. Rogers, *Carbon, 31*, 941 (1993).
6. S.-H. Yoon, Y. Korai, I. Mochida, I. Kato, *Carbon, 32*, 273 (1994).
7. F. Fortin, S.-H. Yoon, Y. Korai, I. Mochida, *Carbon, 32*, 1119 (1991).
8. R. Hu, T. C. Chung, *Carbon, 34*, 1181 (1994).
9. L. E. Jones, P. A. Thrower, *Carbon, 29*, 251 (1991).

17.3.4.4.4. Vapor-Grown Fibers.

The production of carbon fibers or filaments by decomposing a hydrocarbon gas over a transition metal catalyst has been the subject of extensive research[1]. The product consists of filaments with diameters in the range of 1–100 μm and lengths up to 100 mm. In microstructure, it is different from traditional carbon fibers, resulting in a "sword and sheath" fracture mode[2] without catastrophic failure. Since, in addition, these fibers are produced in a single step with no really expensive processing, they are attractive candidates for reinforcing composites.

(PETER A. THROWER)

1. R. T. K. Baker, P. S. Harris, in *Chemistry and Physics of Carbon*, Vol. 14, P. L. Walker Jr., P. A. Thrower, eds., Dekker, New York, 1978, p. 83.
2. G. G. Tibbetts, C. P. Beetz, Jr., *J. Phys. D, 20*, 292 (1987).

17.3.4.5. Carbon–Carbon Composites

Carbon fibers are used almost exclusively in composite materials. Carbon fiber reinforced plastics (CFRPs) are used extensively in many sporting goods, and carbon fiber reinforced cement is used in architecture[1]. The most complex and expensive use is in the carbon–carbon composites. Because the fibers only have strength along their length, composites are made using 3D-woven fibers, or laminates of 2D-woven fibers, which either are impregnated and processed in the same manner as bulk graphites, or are infiltrated with pyrocarbon[2]. In the latter case (chemical vapor infiltration, or CVI) the pyrocarbon is deposited directly in the pores of the structure, producing a rigid 3D body. Difficulties arise because the pyrocarbon deposits preferentially at the entrances to the pores through which the pyrolyzing gases enter the structure. This is often solved (unsatisfactorily) by periodically machining away the outer surfaces, or by establishing thermal gradients in the preform so that deposition rates are higher for lower (depleted) gas concentrations.

A recent modification to the CVI process has been development of a "forced flow–thermal gradient chemical vapor infiltration" technique (FCVI), which has been examined for propylene, propane, and methane gas precursors[3].

The more usual manufacturing technique is to infiltrate the fiber mat with pitch, which then is pyrolyzed to produce carbon. Unfortunately the low carbon yields from the pitch, together with the effects of gas evolution during pyrolysis, mean that the process has to be repeated several times to produce a satisfactory material for some aerospace applications. With each impregnation, forcing the impregnating pitch into the pore structure becomes more difficult, and the amount of pore filling decreases. These problems can be solved to some extent by using less viscous impregnants for the later impregnations. Shrinkage of the pitch during pyrolysis also produces some loss of

Inorganic Reactions and Methods, Volume 18
Edited by J. J. Zuckerman, Jim D. Atwood

3. B. Rand, in *Handbook of Composites*, Vol. 1, *Strong Fibers*, W. Watt, B. V. Perov, eds., Elsevier, Amsterdam, 1985, p. 495.
4. D. D. Edie, N. R. Fox, B. C. Barnett, C. C. Fain, *Carbon, 24*, 447 (1986).
5. D. D. Edie, C. C. Fain, K. E. Robinson, A. M. Harper, D. K. Rogers, *Carbon, 31*, 941 (1993).
6. S.-H. Yoon, Y. Korai, I. Mochida, I. Kato, *Carbon, 32*, 273 (1994).
7. F. Fortin, S.-H. Yoon, Y. Korai, I. Mochida, *Carbon, 32*, 1119 (1991).
8. R. Hu, T. C. Chung, *Carbon, 34*, 1181 (1994).
9. L. E. Jones, P. A. Thrower, *Carbon, 29*, 251 (1991).

17.3.4.4.4. Vapor-Grown Fibers.

The production of carbon fibers or filaments by decomposing a hydrocarbon gas over a transition metal catalyst has been the subject of extensive research[1]. The product consists of filaments with diameters in the range of 1–100 μm and lengths up to 100 mm. In microstructure, it is different from traditional carbon fibers, resulting in a "sword and sheath" fracture mode[2] without catastrophic failure. Since, in addition, these fibers are produced in a single step with no really expensive processing, they are attractive candidates for reinforcing composites.

(PETER A. THROWER)

1. R. T. K. Baker, P. S. Harris, in *Chemistry and Physics of Carbon*, Vol. 14, P. L. Walker Jr., P. A. Thrower, eds., Dekker, New York, 1978, p. 83.
2. G. G. Tibbetts, C. P. Beetz, Jr., *J. Phys. D, 20*, 292 (1987).

17.3.4.5. Carbon–Carbon Composites

Carbon fibers are used almost exclusively in composite materials. Carbon fiber reinforced plastics (CFRPs) are used extensively in many sporting goods, and carbon fiber reinforced cement is used in architecture[1]. The most complex and expensive use is in the carbon–carbon composites. Because the fibers only have strength along their length, composites are made using 3D-woven fibers, or laminates of 2D-woven fibers, which either are impregnated and processed in the same manner as bulk graphites, or are infiltrated with pyrocarbon[2]. In the latter case (chemical vapor infiltration, or CVI) the pyrocarbon is deposited directly in the pores of the structure, producing a rigid 3D body. Difficulties arise because the pyrocarbon deposits preferentially at the entrances to the pores through which the pyrolyzing gases enter the structure. This is often solved (unsatisfactorily) by periodically machining away the outer surfaces, or by establishing thermal gradients in the preform so that deposition rates are higher for lower (depleted) gas concentrations.

A recent modification to the CVI process has been development of a "forced flow–thermal gradient chemical vapor infiltration" technique (FCVI), which has been examined for propylene, propane, and methane gas precursors[3].

The more usual manufacturing technique is to infiltrate the fiber mat with pitch, which then is pyrolyzed to produce carbon. Unfortunately the low carbon yields from the pitch, together with the effects of gas evolution during pyrolysis, mean that the process has to be repeated several times to produce a satisfactory material for some aerospace applications. With each impregnation, forcing the impregnating pitch into the pore structure becomes more difficult, and the amount of pore filling decreases. These problems can be solved to some extent by using less viscous impregnants for the later impregnations. Shrinkage of the pitch during pyrolysis also produces some loss of

Inorganic Reactions and Methods, Volume 18
Edited by J. J. Zuckerman, Jim D. Atwood

3. B. Rand, in *Handbook of Composites*, Vol. 1, *Strong Fibers*, W. Watt, B. V. Perov, eds., Elsevier, Amsterdam, 1985, p. 495.
4. D. D. Edie, N. R. Fox, B. C. Barnett, C. C. Fain, *Carbon, 24*, 447 (1986).
5. D. D. Edie, C. C. Fain, K. E. Robinson, A. M. Harper, D. K. Rogers, *Carbon, 31*, 941 (1993).
6. S.-H. Yoon, Y. Korai, I. Mochida, I. Kato, *Carbon, 32*, 273 (1994).
7. F. Fortin, S.-H. Yoon, Y. Korai, I. Mochida, *Carbon, 32*, 1119 (1991).
8. R. Hu, T. C. Chung, *Carbon, 34*, 1181 (1994).
9. L. E. Jones, P. A. Thrower, *Carbon, 29*, 251 (1991).

17.3.4.4.4. Vapor-Grown Fibers.

The production of carbon fibers or filaments by decomposing a hydrocarbon gas over a transition metal catalyst has been the subject of extensive research[1]. The product consists of filaments with diameters in the range of 1–100 μm and lengths up to 100 mm. In microstructure, it is different from traditional carbon fibers, resulting in a "sword and sheath" fracture mode[2] without catastrophic failure. Since, in addition, these fibers are produced in a single step with no really expensive processing, they are attractive candidates for reinforcing composites.

(PETER A. THROWER)

1. R. T. K. Baker, P. S. Harris, in *Chemistry and Physics of Carbon*, Vol. 14, P. L. Walker Jr., P. A. Thrower, eds., Dekker, New York, 1978, p. 83.
2. G. G. Tibbetts, C. P. Beetz, Jr., *J. Phys. D, 20*, 292 (1987).

17.3.4.5. Carbon–Carbon Composites

Carbon fibers are used almost exclusively in composite materials. Carbon fiber reinforced plastics (CFRPs) are used extensively in many sporting goods, and carbon fiber reinforced cement is used in architecture[1]. The most complex and expensive use is in the carbon–carbon composites. Because the fibers only have strength along their length, composites are made using 3D-woven fibers, or laminates of 2D-woven fibers, which either are impregnated and processed in the same manner as bulk graphites, or are infiltrated with pyrocarbon[2]. In the latter case (chemical vapor infiltration, or CVI) the pyrocarbon is deposited directly in the pores of the structure, producing a rigid 3D body. Difficulties arise because the pyrocarbon deposits preferentially at the entrances to the pores through which the pyrolyzing gases enter the structure. This is often solved (unsatisfactorily) by periodically machining away the outer surfaces, or by establishing thermal gradients in the preform so that deposition rates are higher for lower (depleted) gas concentrations.

A recent modification to the CVI process has been development of a "forced flow–thermal gradient chemical vapor infiltration" technique (FCVI), which has been examined for propylene, propane, and methane gas precursors[3].

The more usual manufacturing technique is to infiltrate the fiber mat with pitch, which then is pyrolyzed to produce carbon. Unfortunately the low carbon yields from the pitch, together with the effects of gas evolution during pyrolysis, mean that the process has to be repeated several times to produce a satisfactory material for some aerospace applications. With each impregnation, forcing the impregnating pitch into the pore structure becomes more difficult, and the amount of pore filling decreases. These problems can be solved to some extent by using less viscous impregnants for the later impregnations. Shrinkage of the pitch during pyrolysis also produces some loss of

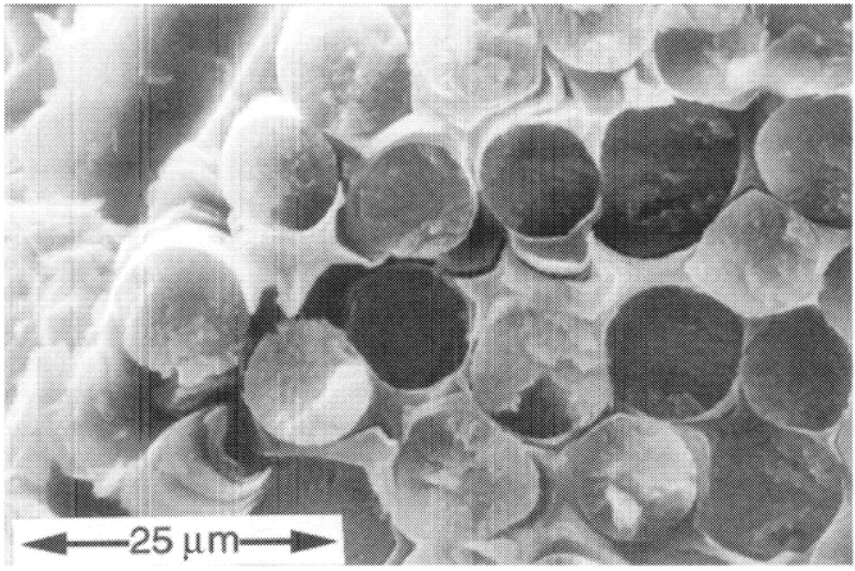

Figure 1. Carbon–carbon composite showing lack of fiber–matrix adhesion.

adhesion between fiber and matrix, which sometimes results in a pore that is impossible to fill despite many repeated infiltrations. Such separations are evident in Figure 1.

As many as seven to ten successive impregnations may be necessary, each followed by a slow pyrolysis stage and a high temperature graphitization. Pyrolysis cannot be allowed to proceed at a rapid rate because otherwise the evolving gases would blow the piece apart. As a result, materials can take several months to produce and, because of the large times and amounts of energy used in their production,they are among the most expensive materials produced.

Primary applications of carbon–carbon composite materials are in the aerospace industry, where in spite of their high cost, they can still be very cost effective. The use of carbon–carbon composites for the brakes of the Concorde supersonic aircraft is reported to have produced a weight saving of over 1000 lb, which translates into significant economies in operation.

(PETER A. THROWER)

1. M. Inagaki, *Carbon*, *29*, 287 (1991).
2. W. V. Kotlensky, in *Chemistry and Physics of Carbon*, Vol. 9, P. L. Walker Jr., P. A. Thrower, eds., Dekker, New York, 1973, p. 173.
3. S. Vaidyraman, W. J. Lackey, P. G. Agrawal, G. B. Freeman, *Carbon*, *33*, 1211 (1995).

17.3.4.6. Activated Carbons

The graphene layer of graphite adsorbs various molecular species on its edges. The total area of such edges in a carbonaceous material is known as the active surface area, and carbons with such areas of several hundreds (500–3000) of square meters per gram of

Inorganic Reactions and Methods, Volume 18
Edited by J. J. Zuckerman, Jim D. Atwood

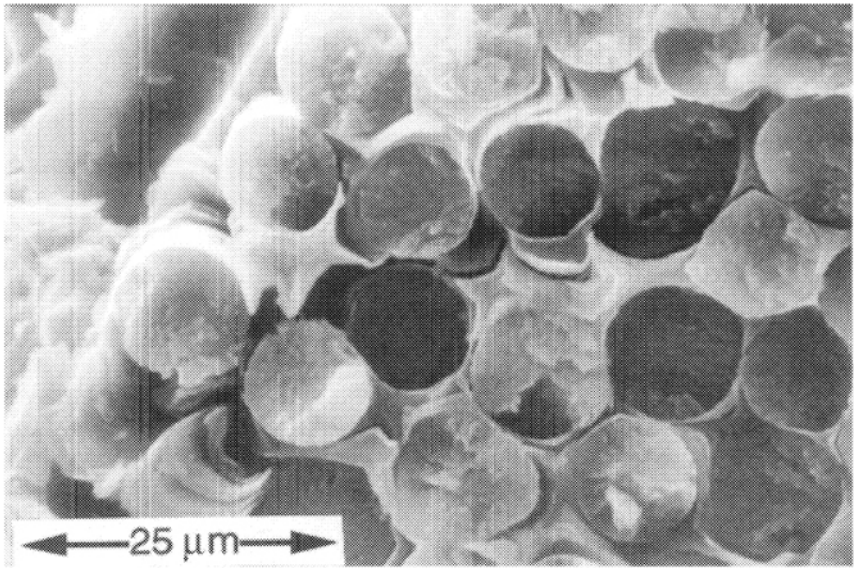

Figure 1. Carbon–carbon composite showing lack of fiber–matrix adhesion.

adhesion between fiber and matrix, which sometimes results in a pore that is impossible to fill despite many repeated infiltrations. Such separations are evident in Figure 1.

As many as seven to ten successive impregnations may be necessary, each followed by a slow pyrolysis stage and a high temperature graphitization. Pyrolysis cannot be allowed to proceed at a rapid rate because otherwise the evolving gases would blow the piece apart. As a result, materials can take several months to produce and, because of the large times and amounts of energy used in their production,they are among the most expensive materials produced.

Primary applications of carbon–carbon composite materials are in the aerospace industry, where in spite of their high cost, they can still be very cost effective. The use of carbon–carbon composites for the brakes of the Concorde supersonic aircraft is reported to have produced a weight saving of over 1000 lb, which translates into significant economies in operation.

(PETER A. THROWER)

1. M. Inagaki, *Carbon*, *29*, 287 (1991).
2. W. V. Kotlensky, in *Chemistry and Physics of Carbon*, Vol. 9, P. L. Walker Jr., P. A. Thrower, eds., Dekker, New York, 1973, p. 173.
3. S. Vaidyraman, W. J. Lackey, P. G. Agrawal, G. B. Freeman, *Carbon*, *33*, 1211 (1995).

17.3.4.6. Activated Carbons

The graphene layer of graphite adsorbs various molecular species on its edges. The total area of such edges in a carbonaceous material is known as the active surface area, and carbons with such areas of several hundreds (500–3000) of square meters per gram of

carbon are readily available. These materials are so diverse that they merit a separate volume (see, e.g., Patrick[1]). Almost any organic material can be used as the precursor for activated carbons. Peat, coal, lignite, wood, and coconut shell have been used on a commercial scale, but there have been also reports of various nuts and kernels (e.g., peach pits and olive stones) being used for this purpose[2]. Even spent coffee grounds have been investigated.

The activation process (development of large surface areas) may be achieved using both chemical and physical approaches. The former involve carbonizing the precursor, usually wood, after impregnation with various acids or metallic salts. However the technique does not give good control over porosity development, and the physical approach is usually preferred. In this approach the porosity is developed by gasification with an oxidizing gas at 700–1100°C.

Each activated carbon has a unique pore structure and spectrum of pore sizes and, as such, serves a different purpose. A molecule is adsorbed only if it can penetrate the pores, with the result that different materials adsorb different molecules. It is this feature that allows these materials to be used as molecular sieves for the separation of various molecular species, including isomers.

Adsorption by activated carbons is used extensively in large-scale industrial processes to remove various pollutants. The material has also been used in cigarette filters and in faucet-mounted household water purification devices. There is also interest in the use of these materials for the storage and transport of natural gas.

(PETER A. THROWER)

1. J. W. Patrick, ed., *Porosity in Carbons*, Halstead Press, New York, 1995.
2. J. Rivera-Utrilla, M. A. Ferro-Garcia, A. Mata-Arjona, C. Gonzalez-Gomez, *J. Chem. Tech. Biotechnol.*, *34A*, 243 (1984).

17.3.4.7. Carbon Blacks

The group of carbonaceous solids consisting almost exclusively of elemental carbon in the form of near-spherical particles of colloidal size is designated "carbon balcks." These particles agglomerate into different forms, one of which is almost linear and gives rise to the name Black Pearls® because of its resemblance to a string of pearls when viewed under an electron microscope. The generic "carbon blacks" are produced by incomplete combustion or thermal decomposition of hydrocarbons using a variety of techniques. Of these two approaches the former is more important. About 90% of carbon black produced is used in the tire industry, with significant use also in copying machine toners and printing ink.

Of processes using incomplete combustion, the most important is the so-called oil furnace black process, in which aromatic residuum petroleum oils are preheated and then injected (atomized) into a furnace at around 1400°C. Combustion is halted by the injection of a water spray, and the carbon black is formed. The degree of aggregation of the carbon black spheres increases with increasing aromaticity of the feedstock; properties and yield can be changed by varying processing variables. Other carbon blacks prepared by incomplete combustion are lampblack and channel black.

The thermal black and acetylene black processes are based on thermal decomposition in the absence of oxygen in a closed system. In the former two refractory-lined reactors operate in parallel at around 1300°C. One is heated by burning a mixture of fuel

Inorganic Reactions and Methods, Volume 18
Edited by J. J. Zuckerman, Jim D. Atwood

carbon are readily available. These materials are so diverse that they merit a separate volume (see, e.g., Patrick[1]). Almost any organic material can be used as the precursor for activated carbons. Peat, coal, lignite, wood, and coconut shell have been used on a commercial scale, but there have been also reports of various nuts and kernels (e.g., peach pits and olive stones) being used for this purpose[2]. Even spent coffee grounds have been investigated.

The activation process (development of large surface areas) may be achieved using both chemical and physical approaches. The former involve carbonizing the precursor, usually wood, after impregnation with various acids or metallic salts. However the technique does not give good control over porosity development, and the physical approach is usually preferred. In this approach the porosity is developed by gasification with an oxidizing gas at 700–1100°C.

Each activated carbon has a unique pore structure and spectrum of pore sizes and, as such, serves a different purpose. A molecule is adsorbed only if it can penetrate the pores, with the result that different materials adsorb different molecules. It is this feature that allows these materials to be used as molecular sieves for the separation of various molecular species, including isomers.

Adsorption by activated carbons is used extensively in large-scale industrial processes to remove various pollutants. The material has also been used in cigarette filters and in faucet-mounted household water purification devices. There is also interest in the use of these materials for the storage and transport of natural gas.

(PETER A. THROWER)

1. J. W. Patrick, ed., *Porosity in Carbons*, Halstead Press, New York, 1995.
2. J. Rivera-Utrilla, M. A. Ferro-Garcia, A. Mata-Arjona, C. Gonzalez-Gomez, *J. Chem. Tech. Biotechnol.*, *34A*, 243 (1984).

17.3.4.7. Carbon Blacks

The group of carbonaceous solids consisting almost exclusively of elemental carbon in the form of near-spherical particles of colloidal size is designated "carbon balcks." These particles agglomerate into different forms, one of which is almost linear and gives rise to the name Black Pearls® because of its resemblance to a string of pearls when viewed under an electron microscope. The generic "carbon blacks" are produced by incomplete combustion or thermal decomposition of hydrocarbons using a variety of techniques. Of these two approaches the former is more important. About 90% of carbon black produced is used in the tire industry, with significant use also in copying machine toners and printing ink.

Of processes using incomplete combustion, the most important is the so-called oil furnace black process, in which aromatic residuum petroleum oils are preheated and then injected (atomized) into a furnace at around 1400°C. Combustion is halted by the injection of a water spray, and the carbon black is formed. The degree of aggregation of the carbon black spheres increases with increasing aromaticity of the feedstock; properties and yield can be changed by varying processing variables. Other carbon blacks prepared by incomplete combustion are lampblack and channel black.

The thermal black and acetylene black processes are based on thermal decomposition in the absence of oxygen in a closed system. In the former two refractory-lined reactors operate in parallel at around 1300°C. One is heated by burning a mixture of fuel

and air to reach the required temperature, at which point this mixture is switched to the other reactor and the feedstock is introduced. The feedstock then decomposes to carbon black and hydrogen while the other reactor is being heated. To ensure continuous production, the gas flows are switched about every 5 minutes. The decomposition of acetylene, however, is exothermic and therefore, after start-up, heat has to be removed from the reactor. For this reason there is no need for the second reactor. Acetylene blacks are mostly lamellar rather than spherical and are more graphitic than other carbon blacks.

For more details on the production and properties of carbon black the reader is advised to consult one of the many reviews of the subject. A good starting point would be the books of Donnet et al[1]. and Kinoshita[2].

(PETER A. THROWER)

1. J.-B. Donnet, R. C. Bansal, M.-J. Wang, eds., *Carbon Black*, Dekker, New York, 1993.
2. K. Kinoshita, *Carbon—Electrochemical and Physicochemical Properties*, Wiley-Interscience, New York, 1988.

17.3.5. Preparation of Boron Nitride

Boron nitride (BN) is a versatile ceramic that is found and used in various crystallographic and geometrical forms. Although there are chemical similarities, the conditions for the synthesis and fabrication of each form (hexagonal, cubic, polymorphs of BN, fibers, two-dimensional forms and composites) have different requirements and are discussed separately.

17.3.5.1. Hexagonal BN

17.3.5.1.1. Preparation of Hexagonal BN.

The common product of reactions forming BN at low pressures and moderate temperatures is a white, low density (2.25 g/cm^3), hexagonal crystal ($a_0 = 251$ pm, $c_0 = 669$ pm). It is easily scratched and is as soft as the mineral gypsum. Chemically, it may be regarded as a heteroaromatic analogue of graphite, where all the carbon atoms have been replaced by B^- and N^+ pairs. Borazine ($B_3N_3H_6$), formerly called borazole, is a similar analogue of benzene. Hexagonal BN, also called α-BN or graphitic BN, was first prepared prior to 1842[1] and remained a laboratory curiosity for over 100 years.

There are many methods of preparing hexagonal BN, and Table 1 summarizes the major reaction schemes, principally involving low pressures[$< 10^5$ Pa (1 bar)]. Reactions between boric oxide and ammonia, usually on a support phase such as calcium phosphate or preformed BN, are generally preferred as commercial methods because they use the cheapest raw materials. However, there are problems with the leaching stages required to remove the calcium phosphate or other support phase[2]. The rate of chemical vapor deposition (CVD) at 1400°C of BCl_3 in NH_3–H_2 mixtures strongly affects the moisture stability of the final BN material, since ammonium borate hydrates easily form[3]. Crystal growth using a $Ca_3B_2N_4$–LiF mixture as flux precursor is described in[4]. Heating boric acid with a nitrogenous organic material such as urea, biuret, triuret, cyanuric acid, ammelide, melamine, thiorea, guanidine, cyanamide, dicyandiamide, or

Inorganic Reactions and Methods, Volume 18
Edited by J. J. Zuckerman, Jim D. Atwood

and air to reach the required temperature, at which point this mixture is switched to the other reactor and the feedstock is introduced. The feedstock then decomposes to carbon black and hydrogen while the other reactor is being heated. To ensure continuous production, the gas flows are switched about every 5 minutes. The decomposition of acetylene, however, is exothermic and therefore, after start-up, heat has to be removed from the reactor. For this reason there is no need for the second reactor. Acetylene blacks are mostly lamellar rather than spherical and are more graphitic than other carbon blacks.

For more details on the production and properties of carbon black the reader is advised to consult one of the many reviews of the subject. A good starting point would be the books of Donnet et al[1]. and Kinoshita[2].

(PETER A. THROWER)

1. J.-B. Donnet, R. C. Bansal, M.-J. Wang, eds., *Carbon Black*, Dekker, New York, 1993.
2. K. Kinoshita, *Carbon—Electrochemical and Physicochemical Properties*, Wiley-Interscience, New York, 1988.

17.3.5. Preparation of Boron Nitride

Boron nitride (BN) is a versatile ceramic that is found and used in various crystallographic and geometrical forms. Although there are chemical similarities, the conditions for the synthesis and fabrication of each form (hexagonal, cubic, polymorphs of BN, fibers, two-dimensional forms and composites) have different requirements and are discussed separately.

17.3.5.1. Hexagonal BN

17.3.5.1.1. Preparation of Hexagonal BN.

The common product of reactions forming BN at low pressures and moderate temperatures is a white, low density (2.25 g/cm^3), hexagonal crystal ($a_0 = 251$ pm, $c_0 = 669$ pm). It is easily scratched and is as soft as the mineral gypsum. Chemically, it may be regarded as a heteroaromatic analogue of graphite, where all the carbon atoms have been replaced by B^- and N^+ pairs. Borazine ($B_3N_3H_6$), formerly called borazole, is a similar analogue of benzene. Hexagonal BN, also called α-BN or graphitic BN, was first prepared prior to 1842[1] and remained a laboratory curiosity for over 100 years.

There are many methods of preparing hexagonal BN, and Table 1 summarizes the major reaction schemes, principally involving low pressures[$< 10^5$ Pa (1 bar)]. Reactions between boric oxide and ammonia, usually on a support phase such as calcium phosphate or preformed BN, are generally preferred as commercial methods because they use the cheapest raw materials. However, there are problems with the leaching stages required to remove the calcium phosphate or other support phase[2]. The rate of chemical vapor deposition (CVD) at 1400°C of BCl_3 in NH_3–H_2 mixtures strongly affects the moisture stability of the final BN material, since ammonium borate hydrates easily form[3]. Crystal growth using a $Ca_3B_2N_4$–LiF mixture as flux precursor is described in[4]. Heating boric acid with a nitrogenous organic material such as urea, biuret, triuret, cyanuric acid, ammelide, melamine, thiorea, guanidine, cyanamide, dicyandiamide, or

TABLE 1. REACTANTS FOR FORMATION OF HEXAGONAL BN

B Source	N Source	Temperature Range	Comments	Ref.
H_3BO_3	Melamine	950°C	Melamine diborate intermediate	5
H_3BO_3	Urea + NH_3	500–950°C	BNO intermediate	6
H_3BO_3	Urea + NH_3	700–1000°C	Turbostratic product	7
H_3BO_3	N plasma	1700–2300°C	With carbon reactant	12
H_3BO_3	NH_4SCN			22
$(RO)_3B_{25}O_{36}\cdot(NH_3)_8$	NH_3	400–800°C	Turbostratic BN	9
B_2O_3	NH_3	900°C	With Ca orthophospate	23
B_2O_3, H_3BO_3	NH_3	500–900°C	Continuous process	13
B_2O_3, H_3BO_3	Melamine	1600–2100°C	BN reactor vessel	14
Borates	N_2	200–1200°C	Leaching of alkali metal salts	15
Borax	NH_4Cl	850–2000°C	$+H_2O$ to remova NaCl	16
CaB_6	N_2		B_2O_3 additive	17
BP	NH_3	1100°C	BN from B produced	18
BCl_3	NH_3	>600°C	Amorphous B compound <40°C	24
B (dissolved)	NH_3	600–950°C	Metal halide melts	19
B (dissolved)	N_2	1400–1600°C	Fe, Fe–C, Fe–Si melt	20
BN (cubic)	BN (cubic)	1200–2000°C	< 4.2 GPa with ammonium borate	21
	N_2, NH_3		Effect of Li Carbothermal synthesis	25
B_2O_3	NH_3 (s)	623–753 K	Supercritical NH_3 + CaO	26
B_2O_3	N_2–NH_3	1373–1773 K	Kinetics	27
$LiBF_4$	Li_3N	1770–2100 K	Self-propagating reaction	28
B	N–H plasma	—	Interemediate hydride	29
B_2O_3	NH_3	350–900°C	BN yield 66%	30
BCl_3	NH_3	700–1400°C	Vapor phase to powders	31
$(NH_3)_3B_{10}H_{14}$	NH_3	300–800°C,	Crystal hexagonal BN at 1500°C	32, 33
B_2H_6	NH_3	78 K	Synchrotron radiation	35
			Flame reaction	34
BCl_3	NH_3–N_2	1920 K	CO_2 laser synthesis	36

semicarbazide promotes a turbostratic structure, rather than a well-defined one[5–9]. Turbostratic describes an intermediate form of carbon where the graphite (hexagonal) structure is stacked roughly parallel and equidistant, but shows random rotation and translation about the layer normal[9, 10]. There is lack of orientation from layer to layer[11]. A typical reaction scheme is:

$$H_3BO_3 + 2 \text{ urea} \xrightarrow{60°C} H_2O + \text{liquid} \xrightarrow{N_2,\ 160°C} \text{BNO residue} \quad \text{(a)}$$

$$\text{BNO} + NH_3 \xrightarrow{500–950°C} \text{BN} + H_2O \quad \text{(b)}$$

Turbostratic BN is also produced by the reaction of an alkyl polyborate–ammonium complex with ammonia[9]:

$$(RO)_3B_{25}O_{34}\cdot(NH_3)_8 + NH_3 \xrightarrow{400–800°C} \text{BN (turbostratic)} \quad \text{(c)}$$

The alkyl polyborate–ammonium complex can be obtained by disproportionation of trialkoxyboroxine with ammonia. The lower reaction temperatures afforded by use of organic complexes promote the turbostratic phase structure. There are differences in the ease of conversion to graphitic (hexagonal) BN; seed crystallography is one variable. Dehydrated H_3BO_3 is also converted to BN by mixing it with carbon black and heating to ~2050°C in a N plasma. A high degree of ordering is found in single crystal hexagonal BN powders[12]. The nitridation of oxygen-containing boron compounds such as B_2O_3, H_3BO_3, alkali (e.g., Na, K), and alkaline earth (e.g., Ca, Mg) borates represents a favored scheme for a continuous production processes[13–16]. Borides such as CaB_6[17] and BP[18] are also used as starting reactants. Oxides give high yields, e.g.:

$$3CaB_6 + B_2O_3 + 10N_2 = 20BN + 3CaO \quad \text{(d)}$$

The reaction of BP with N_2 or NH_3 follows different mechanisms. The latter begins at 800°C, during which NH_3 dissociates to H and N, which substitute the P in BP, and cubic BP transforms to hexagonal BN. The reaction of BP with N begins at 1100°C with the decomposition of BP to $B_{13}P_2$, P, and elemental B. The latter in turn adsorbs molecular nitrogen and forms BN[18], which can also be precipitated from melts, such as alkali or alkaline earth halides[19] or iron-containing C or Si[20]. Cubic BN can be converted to hexagonal BN at various temperatures and pressures depending on the presence of catalysts[21].

(E. G. WOLFF)

1. W. H. Balmain, *J. Prakt. Chem., 27*, 422 (1842).
2. R. Thompson, in '*Progress in Boron Chemistry*' Vol. 2, R. J. Brotherton, H. Steinberg, Pergamon Press, Oxford, 1970.
3. T. Matsuda, *J. Mater. Sci., 24*, 2353 (1989).
4. *Phys. Abstr.*, 91–127742.
5. W. S. Lenihan, R. W. Reidl, U S. Patent 3,241,918 (1966); *Ceram. Abstr.*, June 1966, p. 155b.
6. T. E. O'Connor, *J. Am. Chem. Soc., 84*, 1753 (1962); *Cer. Abstr.*, October 1965, p. 295i.
7. T. E. O'Connor, U. S. Patent, 3,241,919 (1966); *Ceram. Abstr.*, June 1996, p. 155i.
8. E. P. Sadkovskii, E. V. Yurchenko, I. G. Kuznetsova, D. N. Poluboyarinov, *Tr. Mosk. Khim. Tekhnol. Inst., 68*, 130 (1971); *Ceram. Abstr.*, September 1973, p. 209g.
9. J. Thomas, N. E. Weston, T. E. O'Connor, *J. Am. Chem. Soc., 84*, 4619 (1962).
10. J. Biscoe, B. E. Warren, *J. Appl. Phys., 13*, 364 (1942).
11. J. Economy, R. V. Anderson, *J. Polym. Sci., A., Polym. Chem., 19*, 283 (1967).
12. V. D. Parkhomenko, Yu, I. Krasnokutski, V. M., Zadorozhniii, N. A. Zhigulina Izv. *Akad. Nauk USSR, Neorg. Mater., 15*, 602 (1979); *Chem. Abstr.*, 091-02-008665 (1979).
13. A. Lipp, U. S. Patent 3,208,824 (1965), also German Patent 1,165,557 (1964).
14. A. Babl, H. J. Geng, U. S. Patent 3,473,894 (1969); *Ceram. Abstr.*, April 1969, p. 107a.
15. H. Knorre, G. Kuhner, U. S. Patent 3,411,882 (1968); *Ceram. Abstr.*, April 1969, p. 107d.
16. A. Muta, U. S. Patent 3,169,828 (1965); *Ceram. Abstr.*, May 1965, p. 156j.
17. K. A. Schwartz, *Ber. Dtsch, Keram. Ges., 56*, 5 (1979).
18. T. S. Bartnitskaya, S. V. Muchnik, K. A. Lynchak, L. A. Ivanchenko, I. I. Timofeeva, V. B. Chernogorenko, *Izv. Akad. Nauk SSSR, Neorg. Mater., 14*, 197 (1978); *Chem. Abstr.*, 088-22-163115 (1978).
19. D. L. Ball, *Trans. AIME., 239*, 31, (1967).
20. Union Carbide Corp. British Patent 874, 166 (1961).
21. T. Kobayashi, *J. Chem. Phys., 70*, 5898 (1979).
22. H. Saito, M. Ushio, *Yogyo Kyokai Shi, 77*, 151 (1969).
23. T. A. Ingles, P. P. Popper, in *Special Ceramics*, P. P. Popper, ed., Academic Press, New York, 1960, p. 144.
24. H. Tagawa, E. Ishii, *Kogyo Kagaku Zasshi. 70*, 617, (1967); *Ceram. Abstr.* March 1969, p. 177i.
25. T. S. Bartnitskaya, V. I. Lyashenko, A. V. Kurdyumov, N. F. Ostrovskaya, I. G. Rogovaya, *Porshk. Metallurg., 33* (7–8), 1 (1994).

26. K. Yokoi, K. Ito, M. Tokuda, *Mater. Trans. Jpn. Inst. Met.*, *36*(5), 645 (1995).
27. Su Jong Yoon, A. Jha, *J. Mater. Sci.*, *31*(9), 2265 (1996).
28. V. L. Solozhenko, V. Z. Yurkevich, G. Will, *J. Am. Ceram. Soc.*, *79*, 2798 (1996).
29. V. P. Gorbatenko, I. V. Evgenov, V. S. Pegov, *Fiz. Khim. Obrab. Mater.*, *24*, 38 (1990).
30. A. K. Basu, M. Mukerji, *Bull. Mater. Sci.*, *13*, 165 (1990).
31. Soo-Sik Kim, Un-Ho Ko, *J. Korean Inst. Met.*, *28*, 336 (1990).
32. T. Yogo, S. Matsuo, S. Naka, *Yogyo-Kyokai-Shi*, *95*, 94 (1987).
33. T. Yogo, S. Naka, *J. Mater. Sci.*, *25*, 374 (1990).
34. W. G. Berl and W. E. Wilson, *Nature*, *191*, 380 (1961).
35. D. R. Strongin, J. K. Molem, M. W. Ruckman, M. Strongin, *Appl. Phys. Lett.*, *60*, 2561 (1992).
36. M. I. Baraton, L. Boulanger, M. Cauchetier, V. Lorenzelli, M. Luce, T. Merle, P. Quintard, Y. H. Zhou, *J. Eur. Ceram. Soc.*, *13*, 371 (1994).

17.3.5.1.2. Purification of Hexagonal BN.

Oxides are the most frequent residual impurities in hexagonal BN (hBN). They may be removed by reaction with ammonia at above 960°C or by heating in a nitrogen stream to 1650°C, where the oxides volatilize[1,2]. The boron oxide impurities promote transformation of the turbostratic structures to a more ordered layer lattice. Purification can also be effected by a $HCl–HNO_3$ mixture[2]. Treatment with a mixture of boron oxide (1–10%) and lead fluoride (90–99%) at 600–700°C removes B_4C and crystalline B[3]. High purity powders obtained by arc vaporization[4,5] can be hot-pressed to solid shapes without the use of additives. The purest single crystals give the smallest electron paramagnetic resonance (EPR) intensity, and removal of C impurities is traceable by this method[6].

A ternary B–N–O diagram was suggested to guide synthesis of hBN[7]. Both appearance and structural ordering of reference amorphous boron in the production of hBN are highly dependent on the partial pressure of nitrogen[8].

(E. G. WOLFF)

1. T. E. O'Connor, *J. Am. Ceram. Soc.*, *84*, 1753 (1962).
2. V. B. Shipilo, *Vestsi Akad. Nauk B, SSR Ser Fiz.-Tekh. Navk*, *3*, 55 (1980); *Chem. Abstr.*, 094-14-108086 (1981).
3. T. V. Bavina, O. N. Breusov, USSR Patent 575, 856 (1978); *Chem. Abstr.*, 089-10-77119 (1978).
4. Research Group, Tsinghua University, *Ching Hua Ta Tsueh Hsueh Pao*, *78*, 15 (1978); *Chem. Abstr.* 091-08-059545 (1979).
5. W. E. Kuhn, *Electrochem. Tech. 4*, 166 (1966); *Ceram. Abstr.* March 1967, p. 71d.
6. D. Geist, in *Boron and Refractory Borides*, V. I. Matkovich, ed., Springer-Verlag, Berlin, 1977, p. 65.
7. M. Hubacek, M. Ueki, *J. Solid State Chem.*, *123*(2), 215 (1996).
8. Yu. G. Andreev, T. Lundstrom, *J. Alloys Comp.*, *216*, L5 (1994).

17.3.5.1.3. Consolidation of Hexagonal BN.

Pure BN is difficult to consolidate to solid shapes unless the particles are fine (see 17.3.5.1.2), high pressures [$> 3.5 \times 10^6$ N/m^2 (35 bar)] and temperatures (>3000°C) are used, or long heating and cooling times in inert atmospheres are employed during firing of isostatic cold-pressed articles at 1100–1400°C[1]. For either cold pressing and sintering or hot pressing, as much as 20% impurities are added (e.g., CaO, MgO, and $BaCO_3$ reduce both the temperatures and time for optimum sintering (to 900°C and 1–2 h[1]). Another approach is to cold-press 60–90% fine BN powder with 10–40% of a low-melting compound containing B and N (e.g., boric acid and urea). Final firing is accomplished at 1000–1400°C in ammonia[2]. The amount of B_2O_3 liquid phase in the

Inorganic Reactions and Methods, Volume 18
Edited by J. J. Zuckerman, Jim D. Atwood

26. K. Yokoi, K. Ito, M. Tokuda, *Mater. Trans. Jpn. Inst. Met.*, *36*(5), 645 (1995).
27. Su Jong Yoon, A. Jha, *J. Mater. Sci.*, *31*(9), 2265 (1996).
28. V. L. Solozhenko, V. Z. Yurkevich, G. Will, *J. Am. Ceram. Soc.*, *79*, 2798 (1996).
29. V. P. Gorbatenko, I. V. Evgenov, V. S. Pegov, *Fiz. Khim. Obrab. Mater.*, *24*, 38 (1990).
30. A. K. Basu, M. Mukerji, *Bull. Mater. Sci.*, *13*, 165 (1990).
31. Soo-Sik Kim, Un-Ho Ko, *J. Korean Inst. Met.*, *28*, 336 (1990).
32. T. Yogo, S. Matsuo, S. Naka, *Yogyo-Kyokai-Shi*, *95*, 94 (1987).
33. T. Yogo, S. Naka, *J. Mater. Sci.*, *25*, 374 (1990).
34. W. G. Berl and W. E. Wilson, *Nature*, *191*, 380 (1961).
35. D. R. Strongin, J. K. Molem, M. W. Ruckman, M. Strongin, *Appl. Phys. Lett.*, *60*, 2561 (1992).
36. M. I. Baraton, L. Boulanger, M. Cauchetier, V. Lorenzelli, M. Luce, T. Merle, P. Quintard, Y. H. Zhou, *J. Eur. Ceram. Soc.*, *13*, 371 (1994).

17.3.5.1.2. Purification of Hexagonal BN.

Oxides are the most frequent residual impurities in hexagonal BN (hBN). They may be removed by reaction with ammonia at above 960°C or by heating in a nitrogen stream to 1650°C, where the oxides volatilize[1,2]. The boron oxide impurities promote transformation of the turbostratic structures to a more ordered layer lattice. Purification can also be effected by a $HCl–HNO_3$ mixture[2]. Treatment with a mixture of boron oxide (1–10%) and lead fluoride (90–99%) at 600–700°C removes B_4C and crystalline B[3]. High purity powders obtained by arc vaporization[4,5] can be hot-pressed to solid shapes without the use of additives. The purest single crystals give the smallest electron paramagnetic resonance (EPR) intensity, and removal of C impurities is traceable by this method[6].

A ternary B–N–O diagram was suggested to guide synthesis of hBN[7]. Both appearance and structural ordering of reference amorphous boron in the production of hBN are highly dependent on the partial pressure of nitrogen[8].

(E. G. WOLFF)

1. T. E. O'Connor, *J. Am. Ceram. Soc.*, *84*, 1753 (1962).
2. V. B. Shipilo, *Vestsi Akad. Nauk B, SSR Ser Fiz.-Tekh. Navk*, *3*, 55 (1980); *Chem. Abstr.*, 094-14-108086 (1981).
3. T. V. Bavina, O. N. Breusov, USSR Patent 575, 856 (1978); *Chem. Abstr.*, 089-10-77119 (1978).
4. Research Group, Tsinghua University, *Ching Hua Ta Tsueh Hsueh Pao*, *78*, 15 (1978); *Chem. Abstr.* 091-08-059545 (1979).
5. W. E. Kuhn, *Electrochem. Tech. 4*, 166 (1966); *Ceram. Abstr.* March 1967, p. 71d.
6. D. Geist, in *Boron and Refractory Borides*, V. I. Matkovich, ed., Springer-Verlag, Berlin, 1977, p. 65.
7. M. Hubacek, M. Ueki, *J. Solid State Chem.*, *123*(2), 215 (1996).
8. Yu. G. Andreev, T. Lundstrom, *J. Alloys Comp.*, *216*, L5 (1994).

17.3.5.1.3. Consolidation of Hexagonal BN.

Pure BN is difficult to consolidate to solid shapes unless the particles are fine (see 17.3.5.1.2), high pressures [$> 3.5 \times 10^6$ N/m^2 (35 bar)] and temperatures (>3000°C) are used, or long heating and cooling times in inert atmospheres are employed during firing of isostatic cold-pressed articles at 1100–1400°C[1]. For either cold pressing and sintering or hot pressing, as much as 20% impurities are added (e.g., CaO, MgO, and $BaCO_3$ reduce both the temperatures and time for optimum sintering (to 900°C and 1–2 h[1]). Another approach is to cold-press 60–90% fine BN powder with 10–40% of a low-melting compound containing B and N (e.g., boric acid and urea). Final firing is accomplished at 1000–1400°C in ammonia[2]. The amount of B_2O_3 liquid phase in the

Inorganic Reactions and Methods, Volume 18
Edited by J. J. Zuckerman, Jim D. Atwood

26. K. Yokoi, K. Ito, M. Tokuda, *Mater. Trans. Jpn. Inst. Met.*, *36*(5), 645 (1995).
27. Su Jong Yoon, A. Jha, *J. Mater. Sci.*, *31*(9), 2265 (1996).
28. V. L. Solozhenko, V. Z. Yurkevich, G. Will, *J. Am. Ceram. Soc.*, *79*, 2798 (1996).
29. V. P. Gorbatenko, I. V. Evgenov, V. S. Pegov, *Fiz. Khim. Obrab. Mater.*, *24*, 38 (1990).
30. A. K. Basu, M. Mukerji, *Bull. Mater. Sci.*, *13*, 165 (1990).
31. Soo-Sik Kim, Un-Ho Ko, *J. Korean Inst. Met.*, *28*, 336 (1990).
32. T. Yogo, S. Matsuo, S. Naka, *Yogyo-Kyokai-Shi*, *95*, 94 (1987).
33. T. Yogo, S. Naka, *J. Mater. Sci.*, *25*, 374 (1990).
34. W. G. Berl and W. E. Wilson, *Nature*, *191*, 380 (1961).
35. D. R. Strongin, J. K. Molem, M. W. Ruckman, M. Strongin, *Appl. Phys. Lett.*, *60*, 2561 (1992).
36. M. I. Baraton, L. Boulanger, M. Cauchetier, V. Lorenzelli, M. Luce, T. Merle, P. Quintard, Y. H. Zhou, *J. Eur. Ceram. Soc.*, *13*, 371 (1994).

17.3.5.1.2. Purification of Hexagonal BN.

Oxides are the most frequent residual impurities in hexagonal BN (hBN). They may be removed by reaction with ammonia at above 960°C or by heating in a nitrogen stream to 1650°C, where the oxides volatilize[1,2]. The boron oxide impurities promote transformation of the turbostratic structures to a more ordered layer lattice. Purification can also be effected by a $HCl–HNO_3$ mixture[2]. Treatment with a mixture of boron oxide (1–10%) and lead fluoride (90–99%) at 600–700°C removes B_4C and crystalline B[3]. High purity powders obtained by arc vaporization[4,5] can be hot-pressed to solid shapes without the use of additives. The purest single crystals give the smallest electron paramagnetic resonance (EPR) intensity, and removal of C impurities is traceable by this method[6].

A ternary B–N–O diagram was suggested to guide synthesis of hBN[7]. Both appearance and structural ordering of reference amorphous boron in the production of hBN are highly dependent on the partial pressure of nitrogen[8].

(E. G. WOLFF)

1. T. E. O'Connor, *J. Am. Ceram. Soc.*, *84*, 1753 (1962).
2. V. B. Shipilo, *Vestsi Akad. Nauk B, SSR Ser Fiz.-Tekh. Navk*, *3*, 55 (1980); *Chem. Abstr.*, 094-14-108086 (1981).
3. T. V. Bavina, O. N. Breusov, USSR Patent 575, 856 (1978); *Chem. Abstr.*, 089-10-77119 (1978).
4. Research Group, Tsinghua University, *Ching Hua Ta Tsueh Hsueh Pao*, *78*, 15 (1978); *Chem. Abstr.* 091-08-059545 (1979).
5. W. E. Kuhn, *Electrochem. Tech. 4*, 166 (1966); *Ceram. Abstr.* March 1967, p. 71d.
6. D. Geist, in *Boron and Refractory Borides*, V. I. Matkovich, ed., Springer-Verlag, Berlin, 1977, p. 65.
7. M. Hubacek, M. Ueki, *J. Solid State Chem.*, *123*(2), 215 (1996).
8. Yu. G. Andreev, T. Lundstrom, *J. Alloys Comp.*, *216*, L5 (1994).

17.3.5.1.3. Consolidation of Hexagonal BN.

Pure BN is difficult to consolidate to solid shapes unless the particles are fine (see 17.3.5.1.2), high pressures [$> 3.5 \times 10^6$ N/m^2 (35 bar)] and temperatures (>3000°C) are used, or long heating and cooling times in inert atmospheres are employed during firing of isostatic cold-pressed articles at 1100–1400°C[1]. For either cold pressing and sintering or hot pressing, as much as 20% impurities are added (e.g., CaO, MgO, and $BaCO_3$ reduce both the temperatures and time for optimum sintering (to 900°C and 1–2 h[1]). Another approach is to cold-press 60–90% fine BN powder with 10–40% of a low-melting compound containing B and N (e.g., boric acid and urea). Final firing is accomplished at 1000–1400°C in ammonia[2]. The amount of B_2O_3 liquid phase in the

sinter affects the fabrication conditions[3]. A variation is to mix 0.5–40% boric acid with 60–99.5 wt% B_2O_3 fibers. This is heated in N_2, NH_3, or dry inert gases above the acid melting point but below the decomposition temperature of the B_2O_3 fiber until the acid has melted on the fiber surface. Then it is heated in NH_3 for 2–24 h at 200–900°C to be converted to BN. Partially nitrided B_2O_3 fibers can also be used[4]. Work on BN consolidation covers hot pressing[5,6], continuous production[7–9], and general manufacturing[10,11]. Inexpensive reactants (such as B_2O_3, H_3BO_3, and borates) under conditions where rapid reaction with N-containing compounds can occur are used. Solid diluents must be inert to the chemicals involved in the nitriding steps and must melt above ~1300°C; candidates include (Ca or Ba)$_3(PO_4)_2$, (Mg, Ca or Ba)F_2, and $Mg_2P_2O_7$. For continuous operation it is desirable to use a countercurrent or crossflow of ammonia to the boron-containing particles to prevent high concentrations of the H_2O by-product from reacting with the BN[9].

Pure hexagonal or turbostratic BN has poor sinterability, and so it is difficult to fabricate a bulky hBN compact by normal pressure sintering and even by hot pressing unless additives are used. Chemical vapor deposition allows simultaneous synthesis and consolidation of pure and dense films or shapes. CVD in the BCl_3–NH_3–H_2–Ar reactant system was investigated in the low temperature regime 500–1300°C as well as by pulse chemical vapor infiltration in the B_2H_6–NH_3–N_2–Ar reactant system[12].

(E. G. WOLFF)

1. T. A. Ingles, P. P. Popper, in *Special Ceramics*, P. P. Popper, ed., Academic Press, New York, 1960, p. 144.
2. R. Ya. Popil'skii, E. P. Sadkovskii, I. G. Kuznetsova, D. N. Poluboyarinov, *French Patent* 2,367, 019 (1978); *Chem. Abstr.*, 090-20-155978 (1979).
3. E. P. Sadkovskii, E. N. Yurchenko, I. G. Kuznetsova, D. N. Poluboyarinov, *Tr. Mosk, Khim. Tekhnol. Inst.*, *68*, 130 (1971); *Ceram. Abstr.*, September 1973, p. 209g.
4. R. S. Hamilton, *German Patent* 2,748,853 (1978); *Chem. Abstr.*, 090-14-108738 (1979).
5. K. D. Modylevskaya, M. D. Lyutaya, J. N. Nazarchuk, *Zavod. Lab.*, *27*, 1345 (1961).
6. V. M. Steptsov, G. V. Samsonov, *Vapr. Poroshk. Metall. Prochn. Mater.*, *6*, 65 (1958).
7. H. A. Beale, *Ind. Res. Dev.*, *21*, 143 (1979).
8. Electroschmelzwerk Kempten GmbH, British Patent 990, 652 (1965).
9. A. Lipp, U. S. Patent 3,208, 824 (1965).
10. A. A. R. Wood, E. C. Shears, U. S. Patent 3, 182, 412 (1965).
11. Electroschmelzwerk Kempten GmbH, British Patent 1, 516,689 (1978).
12. K. Sugiyama, H. Itoh in *Materials Science Forum*, Trans Tech, Aedermannsdorf, Switzerland, Vols. 54 and 55, J. J. Pouch, S. A. Alterovitz, eds., Trans Tech 1990, p. 141.

17.3.5.2. Cubic BN

17.3.5.2.1. Preparation of Cubic BN.

Cubic boron nitride (cBN) is also called c-BN, Borazon (a trade name), zinc-blende BN (zBN), or sphaleritic BN. It is analogous to the diamond form of carbon and has a relatively high density (3.45 g/cm^3), a microhardness as high as 10,000 kg/mm^2, and a high thermal conductivity. Whereas hBN has B–N distances as low as 145 pm, the cubic form, with $a_0 = 360$ pm, has a B–N separation of 157 pm. Cubic BN is the high pressure form of BN and was originally thought to be obtainable only by conversion of hBN at high temperatures (1600°C) and very high pressures (>11 GPa), a reaction assisted by groups I–V metals and their nitrides as catalysts[1]. Cubic BN was first synthesized in 1957[1] by converting hBN at 11 GPa, or 5–6 GPa when catalysts were

Inorganic Reactions and Methods, Volume 18
Edited by J. J. Zuckerman, Jim D. Atwood

sinter affects the fabrication conditions[3]. A variation is to mix 0.5–40% boric acid with 60–99.5 wt% B_2O_3 fibers. This is heated in N_2, NH_3, or dry inert gases above the acid melting point but below the decomposition temperature of the B_2O_3 fiber until the acid has melted on the fiber surface. Then it is heated in NH_3 for 2–24 h at 200–900°C to be converted to BN. Partially nitrided B_2O_3 fibers can also be used[4]. Work on BN consolidation covers hot pressing[5,6], continuous production[7–9], and general manufacturing[10,11]. Inexpensive reactants (such as B_2O_3, H_3BO_3, and borates) under conditions where rapid reaction with N-containing compounds can occur are used. Solid diluents must be inert to the chemicals involved in the nitriding steps and must melt above ~1300°C; candidates include (Ca or Ba)$_3$(PO$_4$)$_2$, (Mg, Ca or Ba)F_2, and $Mg_2P_2O_7$. For continuous operation it is desirable to use a countercurrent or crossflow of ammonia to the boron-containing particles to prevent high concentrations of the H_2O by-product from reacting with the BN[9].

Pure hexagonal or turbostratic BN has poor sinterability, and so it is difficult to fabricate a bulky hBN compact by normal pressure sintering and even by hot pressing unless additives are used. Chemical vapor deposition allows simultaneous synthesis and consolidation of pure and dense films or shapes. CVD in the BCl_3–NH_3–H_2–Ar reactant system was investigated in the low temperature regime 500–1300°C as well as by pulse chemical vapor infiltration in the B_2H_6–NH_3–N_2–Ar reactant system[12].

(E. G. WOLFF)

1. T. A. Ingles, P. P. Popper, in *Special Ceramics*, P. P. Popper, ed., Academic Press, New York, 1960, p. 144.
2. R. Ya. Popil'skii, E. P. Sadkovskii, I. G. Kuznetsova, D. N. Poluboyarinov, *French Patent* 2,367, 019 (1978); *Chem. Abstr.*, 090-20-155978 (1979).
3. E. P. Sadkovskii, E. N. Yurchenko, I. G. Kuznetsova, D. N. Poluboyarinov, *Tr. Mosk, Khim. Tekhnol. Inst.*, *68*, 130 (1971); *Ceram. Abstr.*, September 1973, p. 209g.
4. R. S. Hamilton, *German Patent* 2,748,853 (1978); *Chem. Abstr.*, 090-14-108738 (1979).
5. K. D. Modylevskaya, M. D. Lyutaya, J. N. Nazarchuk, *Zavod. Lab.*, *27*, 1345 (1961).
6. V. M. Steptsov, G. V. Samsonov, *Vapr. Poroshk. Metall. Prochn. Mater.*, *6*, 65 (1958).
7. H. A. Beale, *Ind. Res. Dev.*, *21*, 143 (1979).
8. Electroschmelzwerk Kempten GmbH, British Patent 990, 652 (1965).
9. A. Lipp, U. S. Patent 3,208, 824 (1965).
10. A. A. R. Wood, E. C. Shears, U. S. Patent 3, 182, 412 (1965).
11. Electroschmelzwerk Kempten GmbH, British Patent 1, 516,689 (1978).
12. K. Sugiyama, H. Itoh in *Materials Science Forum*, Trans Tech, Aedermannsdorf, Switzerland, Vols. 54 and 55, J. J. Pouch, S. A. Alterovitz, eds., Trans Tech 1990, p. 141.

17.3.5.2. Cubic BN

17.3.5.2.1. Preparation of Cubic BN.

Cubic boron nitride (cBN) is also called c-BN, Borazon (a trade name), zinc-blende BN (zBN), or sphaleritic BN. It is analogous to the diamond form of carbon and has a relatively high density (3.45 g/cm^3), a microhardness as high as 10,000 kg/mm^2, and a high thermal conductivity. Whereas hBN has B–N distances as low as 145 pm, the cubic form, with a_0 = 360 pm, has a B–N separation of 157 pm. Cubic BN is the high pressure form of BN and was originally thought to be obtainable only by conversion of hBN at high temperatures (1600°C) and very high pressures (>11 GPa), a reaction assisted by groups I–V metals and their nitrides as catalysts[1]. Cubic BN was first synthesized in 1957[1] by converting hBN at 11 GPa, or 5–6 GPa when catalysts were

used. Solvent methods include growth in a $LiBN_2$ solvent[3] and the Mg_3N_2–hBN system[4]. Kinetics of spontaneous crystallization of cBN were studied at $P = 4.8$ GPa and $T = 2000$ K. MgB_2 served as a solvent catalyst[5]. A further review of solvent catalyst methods involving alkali and alkaline earth boron nitrogen compounds is available[6,7].

Table 1 summarizes the range of catalysts, as well as conditions for the conversion of hexagonal to cubic BN. Catalysts that react with hexagonal BN to form ammonium borate, such as H_2O, urea, ammonium nitrate, ammonium sulfate, and boric acid are potentialy effective[8] in tests with up to 40 wt % of catalyst[9]. Pyrophyllite is used as a solid pressure medium, and known phase transitions of Bi, Tl, and Ba serve to calibrate the pressure.

The P–T synthesis region varies with each catalyst used, but does not fall below ~ 4.5 GN/m^2, and the minimum pressure point falls at ~ 1600–1800°C. When $P \geq 6$ GN/m^2, the effect of certain catalysts is more pronounced, e.g., H_2O, urea, or boric acid permits synthesis of cubic BN at 800–1000°C, ~ 500–700°C lower than with Li or Mg catalyst. Water in the hexagonal BN starting material reduces the transition pressure and temperature[10]. Ammonium borate made by reaction of H_2O with hexagonal BN at high pressure and temperature works as a flux, dissolving hexagonal BN to crystallize as cubic BN. Better catalysts for cubic BN synthesis are those which react with hexagonal BN under high pressure to make ammonium borate, e.g., H_2O, urea, ammonium nitrate

TABLE 1. PREPARATION OF CUBIC BN

Catalyst	Temperature (°C)	Pressure GN/m^2	Pressure kbar	Comments	Ref.
Li, Mg	1700–2000	5.5–6.5	55–65	Thermodynamics	22
H_2O, urea, fluorides	>800	4–6	40–60	0.2–1 μm product	8
H_2O, urea, H_3BO_3	1400	4.6–5.6	46–56	Pyrophyllite solvent	9
	>2000	6.5	65	Density of 3.43 g/cm^3	11
ZnO, $Zn(OH)_2$	1600	6.5	65	also Zn nitride, amide	12
BBr_3–H_2–N_2	1200–2000	5.1–7	51–70	—	13
Li, Mg nitride				Borazon®	23
Fe_3Al	1550	4.5	45	80 μm crystals	24
Ag–Cd	1000	3.2	32	150 μm crystals	24
NH_4(F, Cl, Br, or I)	1400	4.5	45	0.1–0.5 μm	25
Mg, MgB_2	1300–2000	6	60	$B_{1.0-1.13}N$	26
(Li, Na)H	1000–2500	3–7	30–70	300–700 μm	27
$(NH_4)_2SiF_6$	1200	3.5	35	0.8–2.5 μm	28
S, Se, Te	2600–2700	7–7.5	70–75	Electrical properties	14
Si, AlN	1700	5.5	55	>25% at >150 μm	29
B (excess)	1500–2000	5–9.5	50–9.5	To 80 atom % B	30
Urea	900–1000	4.3	43	Crystal size dependence	31
$C_2B_{10}H_{12}CN_5H_3$	100–1500°C	0.2–0.8		cBN, diamond	32
Mg–B–N	2100 K	2.5		Amorphous to cBN	20
Mg_3BN_3		>4 GPa		H_2O catalyst	33
hBN–Mg				wBN also found	34, 35
(Li, Ca, Mg)N–hBN				cBN from liquid phase	35
(Al, B, Si, Ti)N–hBN				Solid state reactions	35
hBN, Mg_2NF				Mg, Li, Mn, Zr flux precursors	36
NH_3 BH_3		High		Shock compression	37
NH_3 BH_3	1300°C	6.5 GPa		Reaction with NH_3	38

or sulfate, and H_3BO_3. The amount of oxygen in cubic BN (e.g., with an H_2O catalyst) shifts the P–T stability region of BN[9]. In vacuum, oxygen and B_2O_3 are removed, but the BN may decompose to give free B, especially at higher temperatures[11]. Certain catalysts (e.g., Zn compounds) work in small amounts.

Cubic BN can be prepared by a number of static and dynamic compression methods, depending on the relative amounts of hBN and rhombohedral BN (rBN) in the initial sample and on the temperature–pressure conditions. References to cBN resulting when an oversaturated solution of BN is cooled in AlN, or a B–phosphide mixture is treated with ammonia, were reported[1]. Conversion from hBN may be achieved by pretreatment in BBr_3–N_3–N_2 mixtures at 3 GPa and 1100°C[13], or with small additions of Al (e.g., 0.46 wt %)[14]. Flux-assisted conversions of hBN to cBN using the high pressure–high temperature route (HP-HT) are based on nitrofluoride additives to modify yield, crystallite size, and grain growth[15]. A direct phase transformation of pyrolytic BN to sphaleritic BN has been described[16].

Low pressure polycrystalline diamond deposition processes have recently improved the wear resistance of specialty tools. Because of oxidation, however, diamond cannot be used under high temperature conditions, nor can it be used with iron, cobalt, or nickel alloys. Cubic BN is chemically more stable, and recently cBN layers were deposited on (1110)-oriented silicon and high speed steel substrates in a hollow cathode arc evaporation device[17]. The films had a maximum cBN content of 95% and on high speed steel hBN and cBN grow simultaneously. A method involving a mixed vapor of B and N atoms that is bombarded with a beam of energetic ions has been proposed[18]. Cubic boron nitride was shown to be thermodynamically stable up to temperatures of 1600 K, and the threshold pressure for cBN crystallization can be reduced from 4 GPa to 2 GPa with supercritical fluids, suggesting further possibilities for low pressure synthesis of cBN[19,20]. Continuous growth of cBN[21] and further development of films are covered in 17.3.5.5.

(E. G. WOLFF)

1. R. Thompson, in *Progress in Boron Chemistry*, Vol. 2, R. J. Brotherton, H. Steinberg, eds., Pergamon Press, Oxford, 1970.
2. R. H. Wentorf, *J. Chem. Phys.*, *26*, 956 (1957).
3. *Phys. Abstr.*, 89-56779.
4. *Phys. Abstr.*, 95-113133.
5. V. B. Shipilo, V. V. Sergeev, *Poroshk. Metallurg.*, *24*, 48 (1985).
6. *Phys. Abstr.*, 94-155841.
7. S. Nakano, H. Fujioka, O. Fukunaga, *AIP Conf. Proc.*, *309*, 1275 (1994).
8. T. Kobayashi, *Mater. Res. Bull.*, *14*, 1541 (1979).
9. T. Kobayashi, *J. Chem. Phys.*, *70*, 5898 (1979).
10. K. Susa, T. Kobayashi, S. Taniguchi, *Mater. Res. Bull.*, *9*, 1443 (1974).
11. F. R. Corigan, Belgan Patent 883, 730 (1980); *Chem. Abstr.*, 0094-16-126330 (1981).
12. V. I. Farafontov, M. I. Sokhor, N. G. Kushkova, V. V. Digonskii, V. S. Lysanov, *German Patent* 2,829,383 (1979); *Chem. Abstr.*, 090-26-208930 (1979).
13. E. Wolf, H. Oppermann, H. Hennig, East German Patent 140,984 (1980); *Chem. Abstr.*, 094-14-105747 (1981).
14. V. B. Shipilo, *Vesti Akad. Nauk, B. SSR. Ser. Fiz-Tekh. Nauk*, *3*, 55 (1980); *Chem. Abstr.*, 094-14-108086 (1981).
15. G. Demarzeau, V. Gonnet, *High Pressure Res.*, *12*, 301, (1994).
16. V. B. Shipilo, E. M. Shishonok, A. M. Zaitsev, A. A. Mel'nikov, A. I. Olekhnovich, *J. Appl. Spectrosc. 49*, 947 (1988).
17. K. L. Barth, W. Sigle, D. Stockle, J. Ulmer, A. Lunk, *Thin Solid Films*, *301*, 65 (1997).
18. D. T. Quinto, NIST-ATP-RFP (97-02) Program Announcement (1997).

19. V. L. Solozhenko, *High Pressure Res., 13*(4), 199 (1995).
20. N. V. Novikov, V. L. Solozhenko, *J. Chem. Vapor. Deposit., 4*, 240 (1996).
21. *Chem. Abstr.*, 92-04-027787 (1980).
22. K. Kuroda, H. Konno, T. Matoba, *Kogyo Kagaku Zasshi, 69*, 365 (1996); *Ceram. Abstr.*, July 1968, p. 217d.
23. R. H. Wentorf, *J. Chem. Phys., 34*, 809 (1961).
24. H. Saito, M. Ushio, S. Nagao, *Yogyo Kyokai Shi, 78*, 1 (1970); *Ceram. Abstr.*, February 1972, p. 36i.
25. T. Kobayashi, K. Susa, Japanese Patent 78-45, 700 (1978); *Chem. Abstr.*, 089-08-61949, (1978).
26. N. E. Filonenko, L. I. Fel'dgun, M. V. Kharitonova, *Adgez. Rusplavov Paika Mater., 1*, (1976); *Chem. Abstr.*, 088-12-75975 (1978).
27. L. F. Vereshchagin, I. S. Gladkaya, G. A. Dubitskii, V. N. Slesarev, *Izv. Akad. Nauk SSSR, Neorg. Mater., 15*, 256 (1979); *Chem. Abstr.*, 090-18-145113 (1979).
28. T. Kobayashi, Japanese Patent 79, 148, 199 (1979); *Chem. Abstr.* 092-14-115- 292 (1980).
29. T. Kabayama, T. Ikezawa, T. Kajiura, M. Ogata Japanese Patent 79-77, 299 (1979); *Chem. Abstr.* 091-22-177435 (1979).
30. N. N. Sirota, M. M. Zhuk, Russian Patent 729, 122 (1980); *Chem. Abstr.*, 093-14-136557 (1980).
31. T. Kobayashi, M. Ishibashi, K. Susa, *Yogyo Kyokai Shi, 86*, 202 (1978); *Ceram. Abstr., 58* (1–2), 49c (1979).
32. O. A. Voronov, L. S. Kashevarova, *Proc. 4th Intl. Symp. on Diamond Mater. Electrochem. Soc., 731*, 318 (1995).
33. S. Nakano, H. Ikawa, O. Fukunaga, *J. Am. Ceram. Soc., 75*, 240 (1992).
34. M. M. Bindal, S. K. Singhal, B. P. Singh, R. K. Nayar, R. Chopra, A. Dhar, *J. Cryst. Growth, 112*, 386, (1991).
35. G. Bacquillon, C. Loriers-Susse, J. Loriers, *J. Mater. Sci., 28*, 3547 (1993).
36. G. Demazeau, G. Biardeau, L. Vel, *Mater. Lett., 10*, 139 (1990).
37. R. Liepins, K. P. Staudhammer, K. A. Johnson, M. Thomson, *Mater. Lett., 7*, 44, (1988).
38. T. Yogo, S. Naka, H. Iwahara, *J. Mater. Sci., 26*, 3758 (1991).

17.3.5.2.2. Consolidation of Cubic BN.

Briquetted hexagonal BN, heated in vacuum, cooled in NH_3 to ambient and below with solid CO_2, may be pressed at 1500°C and 5.5 GN/m^2 (55 bar) to yield nearly 100% pure crystalline cubic BN[1]. Most high-hardness, solid shapes, sinters, or cermets containing cubic BN require binders and additional fabrication steps, e.g., 40–97% powdered cubic BN, Al_2O_3, and a 75 : 25 $Al(H_2PO_4)_3$–Al_2O_3 mixture with Fe, Ti, Al, or Si heated to 500°C after compaction to remove volatile matter and then pressed at 4–6 GN/m^2, heated to 1200–1700°C for more than 100 min to form $AlPO_4$, and cooled to promote cross-links between granular cubic BN and the $AlPO_4$ and Al_2O_3[2]. Cubic BN, TiN, TiO_2, and Ti alloys can be hot-pressed together at temperatures exceeding >1400°C and high pressures (e.g., 5.5 GN/m^2) to give a hard isotropic cermet for tool applications[3]. A recent description of the reactive ultrahigh pressure sintering of cBN is available[4].

cBN can be synthesized from amorphous BN with $P > 6$ GPa and $T > 800$°C[5]. A cBN CVD process similar to that of diamond is considered possible, but atomic attachment kinetics during crystal growth could cause problems[6,7]. cBN was synthesized from BN powder formed by pressure pyrolysis of borazine below 700°C and 100 MPa. The conversion of BN powder to cBN was strongly influenced by residual hydrogen[8]. A carbothermic method for converting hBN to cBN was analyzed[9]. Binders of TiN/TiC were used to make cBN compacts[10]. Reaction sintering of hBN with a catalyst such as Mg nitride leads to dense cBN compacts[11]. When HCl is added during the hBN-to-cBN transformation, at 6.5 GPa and 1900°C, a translucent cBN results[12,13]; transition pressure and temperature are reduced by the presence of water. Indeed, 40 wt % water reduces these conditions by about 50 kb and 600°C[10].

Inorganic Reactions and Methods, Volume 18
Edited by J. J. Zuckerman, Jim D. Atwood

19. V. L. Solozhenko, *High Pressure Res., 13*(4), 199 (1995).
20. N. V. Novikov, V. L. Solozhenko, *J. Chem. Vapor. Deposit., 4*, 240 (1996).
21. *Chem. Abstr.*, 92-04-027787 (1980).
22. K. Kuroda, H. Konno, T. Matoba, *Kogyo Kagaku Zasshi, 69*, 365 (1996); *Ceram. Abstr.*, July 1968, p. 217d.
23. R. H. Wentorf, *J. Chem. Phys., 34*, 809 (1961).
24. H. Saito, M. Ushio, S. Nagao, *Yogyo Kyokai Shi, 78*, 1 (1970); *Ceram. Abstr.*, February 1972, p. 36i.
25. T. Kobayashi, K. Susa, Japanese Patent 78-45, 700 (1978); *Chem. Abstr.*, 089-08-61949, (1978).
26. N. E. Filonenko, L. I. Fel'dgun, M. V. Kharitonova, *Adgez. Rusplavov Paika Mater., 1*, (1976); *Chem. Abstr.*, 088-12-75975 (1978).
27. L. F. Vereshchagin, I. S. Gladkaya, G. A. Dubitskii, V. N. Slesarev, *Izv. Akad. Nauk SSSR, Neorg. Mater., 15*, 256 (1979); *Chem. Abstr.*, 090-18-145113 (1979).
28. T. Kobayashi, Japanese Patent 79, 148, 199 (1979); *Chem. Abstr.* 092-14-115- 292 (1980).
29. T. Kabayama, T. Ikezawa, T. Kajiura, M. Ogata Japanese Patent 79-77, 299 (1979); *Chem. Abstr.* 091-22-177435 (1979).
30. N. N. Sirota, M. M. Zhuk, Russian Patent 729, 122 (1980); *Chem. Abstr.*, 093-14-136557 (1980).
31. T. Kobayashi, M. Ishibashi, K. Susa, *Yogyo Kyokai Shi, 86*, 202 (1978); *Ceram. Abstr., 58* (1–2), 49c (1979).
32. O. A. Voronov, L. S. Kashevarova, *Proc. 4th Intl. Symp. on Diamond Mater. Electrochem. Soc., 731*, 318 (1995).
33. S. Nakano, H. Ikawa, O. Fukunaga, *J. Am. Ceram. Soc., 75*, 240 (1992).
34. M. M. Bindal, S. K. Singhal, B. P. Singh, R. K. Nayar, R. Chopra, A. Dhar, *J. Cryst. Growth, 112*, 386, (1991).
35. G. Bacquillon, C. Loriers-Susse, J. Loriers, *J. Mater. Sci., 28*, 3547 (1993).
36. G. Demazeau, G. Biardeau, L. Vel, *Mater. Lett., 10*, 139 (1990).
37. R. Liepins, K. P. Staudhammer, K. A. Johnson, M. Thomson, *Mater. Lett., 7*, 44, (1988).
38. T. Yogo, S. Naka, H. Iwahara, *J. Mater. Sci., 26*, 3758 (1991).

17.3.5.2.2. Consolidation of Cubic BN.

Briquetted hexagonal BN, heated in vacuum, cooled in NH_3 to ambient and below with solid CO_2, may be pressed at 1500°C and 5.5 GN/m^2 (55 bar) to yield nearly 100% pure crystalline cubic BN[1]. Most high-hardness, solid shapes, sinters, or cermets containing cubic BN require binders and additional fabrication steps, e.g., 40–97% powdered cubic BN, Al_2O_3, and a 75 : 25 $Al(H_2PO_4)_3$–Al_2O_3 mixture with Fe, Ti, Al, or Si heated to 500°C after compaction to remove volatile matter and then pressed at 4–6 GN/m^2, heated to 1200–1700°C for more than 100 min to form $AlPO_4$, and cooled to promote cross-links between granular cubic BN and the $AlPO_4$ and Al_2O_3[2]. Cubic BN, TiN, TiO_2, and Ti alloys can be hot-pressed together at temperatures exceeding >1400°C and high pressures (e.g., 5.5 GN/m^2) to give a hard isotropic cermet for tool applications[3]. A recent description of the reactive ultrahigh pressure sintering of cBN is available[4].

cBN can be synthesized from amorphous BN with $P > 6$ GPa and $T > 800$°C[5]. A cBN CVD process similar to that of diamond is considered possible, but atomic attachment kinetics during crystal growth could cause problems[6,7]. cBN was synthesized from BN powder formed by pressure pyrolysis of borazine below 700°C and 100 MPa. The conversion of BN powder to cBN was strongly influenced by residual hydrogen[8]. A carbothermic method for converting hBN to cBN was analyzed[9]. Binders of TiN/TiC were used to make cBN compacts[10]. Reaction sintering of hBN with a catalyst such as Mg nitride leads to dense cBN compacts[11]. When HCl is added during the hBN-to-cBN transformation, at 6.5 GPa and 1900°C, a translucent cBN results[12,13]; transition pressure and temperature are reduced by the presence of water. Indeed, 40 wt % water reduces these conditions by about 50 kb and 600°C[10].

Descriptions of shock compression and very high pressure sintering[14], detonation methods[15], and shock wave sintering of powders of sphaleritic BN[16, 17] are available.

(E. G. WOLFF)

1. K. Susa, T. Kobayashi, Japanese patent 78-102, 900 (1978); *Chem. Abstr.*, 090-08-57366 (1979).
2. T. Kuratomi, Japanese patent 80-109, 278 (1980); *Chem. Abstr.*, 094-14-108161 (1981).
3. T. Kuratomi, Japanese patent 80-100-272 (1980); *Chem. Abstr.*, 094 16-126335 (1981).
4. Sheng Yin, *Int. J. Self-Propagating High Temp. Synt.*, *4*(2), 209 (1995).
5. H. Sumiya, T. Iseki, A. Onodera, *Mater. Res. Bull.*, *18*, 1203 (1983).
6. S. Bohr, R. Haubner, B. Lux, *Diamonds Relat. Mater.*, *4*(5–6), 714 (1995).
7. G. Demazeau, *Diamonds Relat. Mater.*, *4*(4), 284 (1995).
8. S.-I. Hirano, A. Fujii, T. Yogo, S. Naka, *J. Am. Ceram. Soc.*, *73*, 2238 (1990).
9. S. N. Pikalov, A. M. Germanskii, *Poroshk. Metallurg.*, *26*, 82 (1987).
10. B.H. Agarwala, B. P. Singh, S. K. Singhal, *J. Mater. Sci.*, *21*, 1765 (1986).
11. O. Fukunaga, *J. Phys. Colloq.*, *45*, 315 (1984),
12. H. Sei, M. Akaishi, S. Yamaoka, *Diamonds Relat. Mater.*, *2*, 1160 (1993).
13. M. Akaishi, T. Satoh, M. Ishii, T. Taniguchi, S. Yamaoka, *J. Mater. Sci. Lett.*, *12*, 1883 (1993).
14. *Phys. Abstr.*, 84-30669.
15. R. Trebinski, E. Wlodarczyk, S. Cudzilo, J. Paszula, W. Trzcininski, *AIP Conf. Proc.*, *309*, 1283 (1994).
16. V. F. Britun, V. I. Kovtun, V. I. Trefilov, *Poroshkv. Metallurg.*, *33*(7), 38 (1994).
17. L. F. Vereshchagin, F. I. Dubovitskii, A. N. Dremin, V. N. Slesarev, Y. A. Shifrin, E. N. Yakovlev, Russian Patent 63, 618 (1978); *Chem. Abstr.*, 092-04-027387 (1980).

17.3.5.3. Other Polymorphs of BN

17.3.5.3.1. Wurtzite BN.

Wurtzite-type BN (wBN or γBN) is close to cubic BN in density and will transform to cubic BN above 55 GN/m^2 and 1450°C. It will also convert to hexagonal BN below about 60 GN/m^2 and above 1000°C[1]. wBN is a metastable form at pressures and temperatures where cBN is fabricated. The powder can be synthesized from graphitic or hexagonal BN by shock compression and an alkaline fusion technique. The effect of TiB_2 and boron additives on the transformation of wBN to cBN has been studied. TiB_2 shifts the formation region of cBN to higher temperatures while B shifts it to lower temperatures[1]. wBN can be synthesized by static compression at pressures exceeding 5.5 GN/m^2 and low temperatures[2] or by shock compression[1,3].

Wurtzite (wBN) can be prepared by various static and dynamic compression methods[9], depending on the relative amounts of hBN and rBN in the initial sample, and the *T-P* conditions of the consolidation. Phase stability data for wBN is available[5]. hBN can be converted to cBN and wBN at pressures from 12 to 40 GPa and temperatures between 300 and 1200 K[6], also with the use of Mg as a catalyst[7]. A mixture of hBN, H_2O, and an alkaline solution (e.g., NaOH) may be subjected to a shock wave at or above 10 GPa to prepare high quality wBN[8]. wBN is transformed to zBN by shock compression at pressure above 100 GPa[9], while static high pressure transforms zBN to wBN[10]. However, the reverse transformations are also possible[11]. Additional references on wBN are given in physics abstracts[12–21].

(E G. WOLFF)

1. T. Akashi, A. Sawaoka, S. Saito, *J. Am. Ceram. Soc.*, *61*, 245 (1978).
2. F. P. Bundy, R. H. Wentorf, *J. Chem. Phys.*, *38*, 1144 (1963).
3. A. N. Dremin, *Gorenie Uzryv*, *77*, 88 (1977); *Chem. Abstr.*, 089-02-010814 (1978).

Inorganic Reactions and Methods, Volume 18
Edited by J. J. Zuckerman, Jim D. Atwood

Descriptions of shock compression and very high pressure sintering[14], detonation methods[15], and shock wave sintering of powders of sphaleritic BN[16,17] are available.

(E. G. WOLFF)

1. K. Susa, T. Kobayashi, Japanese patent 78-102, 900 (1978); *Chem. Abstr.*, 090-08-57366 (1979).
2. T. Kuratomi, Japanese patent 80-109, 278 (1980); *Chem. Abstr.*, 094-14-108161 (1981).
3. T. Kuratomi, Japanese patent 80-100-272 (1980); *Chem. Abstr.*, 094 16-126335 (1981).
4. Sheng Yin, *Int. J. Self-Propagating High Temp. Synt.*, *4*(2), 209 (1995).
5. H. Sumiya, T. Iseki, A. Onodera, *Mater. Res. Bull.*, *18*, 1203 (1983).
6. S. Bohr, R. Haubner, B. Lux, *Diamonds Relat. Mater.*, *4*(5–6), 714 (1995).
7. G. Demazeau, *Diamonds Relat. Mater.*, *4*(4), 284 (1995).
8. S.-I. Hirano, A. Fujii, T. Yogo, S. Naka, *J. Am. Ceram. Soc.*, *73*, 2238 (1990).
9. S. N. Pikalov, A. M. Germanskii, *Poroshk. Metallurg.*, *26*, 82 (1987).
10. B.H. Agarwala, B. P. Singh, S. K. Singhal, *J. Mater. Sci.*, *21*, 1765 (1986).
11. O. Fukunaga, *J. Phys. Colloq.*, *45*, 315 (1984),
12. H. Sei, M. Akaishi, S. Yamaoka, *Diamonds Relat. Mater.*, *2*, 1160 (1993).
13. M. Akaishi, T. Satoh, M. Ishii, T. Taniguchi, S. Yamaoka, *J. Mater. Sci. Lett.*, *12*, 1883 (1993).
14. *Phys. Abstr.*, 84-30669.
15. R. Trebinski, E. Wlodarczyk, S. Cudzilo, J. Paszula, W. Trzcininski, *AIP Conf. Proc.*, *309*, 1283 (1994).
16. V. F. Britun, V. I. Kovtun, V. I. Trefilov, *Poroshkv. Metallurg.*, *33*(7), 38 (1994).
17. L. F. Vereshchagin, F. I. Dubovitskii, A. N. Dremin, V. N. Slesarev, Y. A. Shifrin, E. N. Yakovlev, Russian Patent 63, 618 (1978); *Chem. Abstr.*, 092-04-027387 (1980).

17.3.5.3. Other Polymorphs of BN

17.3.5.3.1. Wurtzite BN.

Wurtzite-type BN (wBN or γBN) is close to cubic BN in density and will transform to cubic BN above 55 GN/m^2 and 1450°C. It will also convert to hexagonal BN below about 60 GN/m^2 and above 1000°C[1]. wBN is a metastable form at pressures and temperatures where cBN is fabricated. The powder can be synthesized from graphitic or hexagonal BN by shock compression and an alkaline fusion technique. The effect of TiB_2 and boron additives on the transformation of wBN to cBN has been studied. TiB_2 shifts the formation region of cBN to higher temperatures while B shifts it to lower temperatures[1]. wBN can be synthesized by static compression at pressures exceeding 5.5 GN/m^2 and low temperatures[2] or by shock compression[1,3].

Wurtzite (wBN) can be prepared by various static and dynamic compression methods[9], depending on the relative amounts of hBN and rBN in the initial sample, and the *T-P* conditions of the consolidation. Phase stability data for wBN is available[5]. hBN can be converted to cBN and wBN at pressures from 12 to 40 GPa and temperatures between 300 and 1200 K[6], also with the use of Mg as a catalyst[7]. A mixture of hBN, H_2O, and an alkaline solution (e.g., NaOH) may be subjected to a shock wave at or above 10 GPa to prepare high quality wBN[8]. wBN is transformed to zBN by shock compression at pressure above 100 GPa[9], while static high pressure transforms zBN to wBN[10]. However, the reverse transformations are also possible[11]. Additional references on wBN are given in physics abstracts[12–21].

(E G. WOLFF)

1. T. Akashi, A. Sawaoka, S. Saito, *J. Am. Ceram. Soc.*, *61*, 245 (1978).
2. F. P. Bundy, R. H. Wentorf, *J. Chem. Phys.*, *38*, 1144 (1963).
3. A. N. Dremin, *Gorenie Uzryv*, *77*, 88 (1977); *Chem. Abstr.*, 089-02-010814 (1978).

4. P. K. Lam, R. M. Wentzcovitch, M. L. Cohen, in *Materials Science Forum*, Vols. 54 and 55, J. J. Pouch, S. A. Alterovitz, eds., Trans Tech, Aedermannsdorf, 1990, p. 165.
5. A. Onodera, H. Sumiya, K. Higashi, N. Takahashi, R. Oshima, H. Saka, K. Nobugai, F. Kanamaru, *High Temp. High Pressures, 24*, 45 (1992).
6. T. Sekine, *Proc. APS Topical Conf. Shock Compression, 1023*, 511 (1989).
7. M. M. Bindal, S. K. Singhal, B. P. Singh, R. K. Nayar, R. Chopra, A. Dhar, *J. Cryst. Growth, 112*, 386 (1991).
8. Japanese Patent 28-28, 880, to Institute of New Chemical Problems, Academy of Sciences USSR (1978); *Chem. Abstr.*, 089-24-202891 (1978).
9. T. Akashi, Han-Ryong Pak, A. B. Sawaoka, *J. Mater. Sci., 21*, 4060 (1986).
10. A. Onodera, H. Miyazaki, N. Fujimoto, *J. Chem. Phys., 74*, 5814 (1981).
11. S. Saito, A. Sawaoka, *Proc. 7th Intl. AIRAPT Conf.* 590, 541 (1980).
12. *Phys. Abstr.*, 95-28021.
13. *Phys. Abstr.*, 95-28021.
14. *Phys. Abstr.*, 93-133989.
15. *Phys. Abstr.*, 94-64120.
16. *Phys. Abstr.*, 91-97957.
17. *Phys. Abstr.*, 90-69810.
18. *Phys. Abstr.*, 91-97957.
19. *Phys. Abstr.*, 86-112597.
20. *Phys. Abstr.*, 85-67299.
21. *Phys. Abstr.*, 83-63220.

17.3.5.3.2. Rhombohedral BN.

Rhombohedral BN (rBN) forms in the fusion product of KCN and $Na_2B_4O_7$[1] and by deposition at 1500°C from hexagonal BN vapor originally formed at 2100°C in a graphite resistance tube furnace. Products collect on a pitted carbon film[2].

Carbothermal reduction and simultaneous nitridation of amorphous B_2O_3 at 1000–1450°C leads to fine-grained rBN and hBN[3]. rBN is often obtained in CVD of hBN or turbostratic BN[4]. Transformations (e.g., shock induced) of rBN to zBN are described[5,6]. β-rhombohedral crystallites are found in CVD films by means of hot tungsten filaments and BCl_3 and NH_3–H_2 gas mixtures[7]. rBN is also found in cBN films grown by ion-assisted deposition[8]. rBN allows for a diffusionless pathway for cBN synthesis under high pressure (unlike the high activation energy route required for hBN conversion to cBN). rBN synthesis is also reported in *Physics Abstracts*[9–13].

(E. G. WOLFF)

1. A. Herold, B. Marzluf P. Perio. *Hebd. Seances Acad. Sci., 246*, 1866 (1958).
2. Y. Matsui, Y. Sekikawa, T. Sato, T. Ishii, S. Isakosawa, K. Shii, *J. Mater. Sci., 16*, 1115 (1981).
3. T. S. Bartnitskaya, T. Ya. Kosolapova, A. V. Kurdyumov, G. S. Oleinik, A. N. Pilyankevich, *J. Less-Common Met., 117*, 253 (1986).
4. T. Matsuda, N. Uno, H. Nakae, T. Hirai, *J. Mater. Sci., 21*, 649 (1986).
5. A. Onodera, K. Inoue, H. Yoshihara, H. Nakae, T. Matsuda, T. Harai, *J. Mater. Sci., 25*, 4279 (1990).
6. T. Sekine, T. Sato, *J. Appl. Phys., 74*, 2440 (1993).
7. H. Satoh, K. Yoshida, W. A. Yarbrough, *J. Mater. Res., 8*, 8 (1993).
8. D. L. Medlin, T. A. Friedman, P. B. Mirkarimi, M. J. Mills, K. F. McCarty, *Phys. Rev. B, 50*, 7884 (1994).
9. *Phys. Abstr.*, 94-160932.
10. *Phys. Abstr.*, 94-69318.
11. *Phys. Abstr.*, 93-134252.
12. *Phys. Abstr.*, 92-97149.
13. *Phys. Abstr.*, 81-64860.

Inorganic Reactions and Methods, Volume 18
Edited by J. J. Zuckerman, Jim D. Atwood

4. P. K. Lam, R. M. Wentzcovitch, M. L. Cohen, in *Materials Science Forum*, Vols. 54 and 55, J. J. Pouch, S. A. Alterovitz, eds., Trans Tech, Aedermannsdorf, 1990, p. 165.
5. A. Onodera, H. Sumiya, K. Higashi, N. Takahashi, R. Oshima, H. Saka, K. Nobugai, F. Kanamaru, *High Temp. High Pressures, 24*, 45 (1992).
6. T. Sekine, *Proc. APS Topical Conf. Shock Compression, 1023*, 511 (1989).
7. M. M. Bindal, S. K. Singhal, B. P. Singh, R. K. Nayar, R. Chopra, A. Dhar, *J. Cryst. Growth, 112*, 386 (1991).
8. Japanese Patent 28-28, 880, to Institute of New Chemical Problems, Academy of Sciences USSR (1978); *Chem. Abstr.*, 089-24-202891 (1978).
9. T. Akashi, Han-Ryong Pak, A. B. Sawaoka, *J. Mater. Sci., 21*, 4060 (1986).
10. A. Onodera, H. Miyazaki, N. Fujimoto, *J. Chem. Phys., 74*, 5814 (1981).
11. S. Saito, A. Sawaoka, *Proc. 7th Intl. AIRAPT Conf.* 590, 541 (1980).
12. *Phys. Abstr.*, 95-28021.
13. *Phys. Abstr.*, 95-28021.
14. *Phys. Abstr.*, 93-133989.
15. *Phys. Abstr.*, 94-64120.
16. *Phys. Abstr.*, 91-97957.
17. *Phys. Abstr.*, 90-69810.
18. *Phys. Abstr.*, 91-97957.
19. *Phys. Abstr.*, 86-112597.
20. *Phys. Abstr.*, 85-67299.
21. *Phys. Abstr.*, 83-63220.

17.3.5.3.2. Rhombohedral BN.

Rhombohedral BN (rBN) forms in the fusion product of KCN and $Na_2B_4O_7$[1] and by deposition at 1500°C from hexagonal BN vapor originally formed at 2100°C in a graphite resistance tube furnace. Products collect on a pitted carbon film[2].

Carbothermal reduction and simultaneous nitridation of amorphous B_2O_3 at 1000–1450°C leads to fine-grained rBN and hBN[3]. rBN is often obtained in CVD of hBN or turbostratic BN[4]. Transformations (e.g., shock induced) of rBN to zBN are described[5,6]. β-rhombohedral crystallites are found in CVD films by means of hot tungsten filaments and BCl_3 and NH_3–H_2 gas mixtures[7]. rBN is also found in cBN films grown by ion-assisted deposition[8]. rBN allows for a diffusionless pathway for cBN synthesis under high pressure (unlike the high activation energy route required for hBN conversion to cBN). rBN synthesis is also reported in *Physics Abstracts*[9–13].

(E. G. WOLFF)

1. A. Herold, B. Marzluf P. Perio. *Hebd. Seances Acad. Sci., 246*, 1866 (1958).
2. Y. Matsui, Y. Sekikawa, T. Sato, T. Ishii, S. Isakosawa, K. Shii, *J. Mater. Sci., 16*, 1115 (1981).
3. T. S. Bartnitskaya, T. Ya. Kosolapova, A. V. Kurdyumov, G. S. Oleinik, A. N. Pilyankevich, *J. Less-Common Met., 117*, 253 (1986).
4. T. Matsuda, N. Uno, H. Nakae, T. Hirai, *J. Mater. Sci., 21*, 649 (1986).
5. A. Onodera, K. Inoue, H. Yoshihara, H. Nakae, T. Matsuda, T. Harai, *J. Mater. Sci., 25*, 4279 (1990).
6. T. Sekine, T. Sato, *J. Appl. Phys., 74*, 2440 (1993).
7. H. Satoh, K. Yoshida, W. A. Yarbrough, *J. Mater. Res., 8*, 8 (1993).
8. D. L. Medlin, T. A. Friedman, P. B. Mirkarimi, M. J. Mills, K. F. McCarty, *Phys. Rev. B, 50*, 7884 (1994).
9. *Phys. Abstr.*, 94-160932.
10. *Phys. Abstr.*, 94-69318.
11. *Phys. Abstr.*, 93-134252.
12. *Phys. Abstr.*, 92-97149.
13. *Phys. Abstr.*, 81-64860.

Inorganic Reactions and Methods, Volume 18
Edited by J. J. Zuckerman, Jim D. Atwood

17.3.5.3.3. Tetragonal BN.

A tetragonal form of BN can be prepared by vapor deposition on BN-coated Ta or graphite substrates at 1200–1600°C. The composition is close to $B_{50}N_{1.8}$; the density is 2.46 g/cm^3, and the lattice constants are $a = 864.6$ pm and $c = 512.7$ pm[1]. Shock loading of diamond/BN mixtures produced several phases, including a tetragonal phase with the composition $B_{25}N$[2].

(E. G. WOLFF)

1. H. J. Becher, R. Mattes, in *Boron and Refractory Borides*, V. I. Matkovich, ed., Springer–Verlag, Berlin, 1977, p. 113.
2. M. J. Paislet, Y. Horie, R. F. Davis, K. Dan, H. Tamura, A. B. Sawaoka, *J. Mater. Sci. Let., 12*, 1768 (1993).

17.3.5.3.4. Other Structural Modifications.

Further ultrahigh pressure structural modifications of zinc-blende BN are considered possible, with a rock salt structure preferred over a β-Sn structure[1]. A metastable E-BN phase is obtained during electron-beam-assisted crystallization of BN[2]. Other metastable phases of BN are reported in the condensation products upon sudden cooling in conditions of a pulsed plasma discharge[3,4]. Disordered structures are reported when mixed plasma/chemical processes are used[5]. Some compounds of type B_nN_m are listed in Table 1[6–28].

(E. G. WOLFF)

TABLE 1. LITERATURE REFERENCES TO COMPOUNDS OF TYPE B_nN_m

Compound	Ref.
B_nN	17
BN_n	9, 18, 21, 22
B_nN_m	6, 12, 14, 26
BN_2	8
BN_3	7, 19, 20, 27
BN_4	10
B_2N	25
B_3N	7, 11, 16
B_2N_2	25
B_2N_3	10
B_3N_2	10
B_3N_3	5, 28
B_4N_4	5, 13
$B_{12}N_{12}$	15
$B_{30}N_{30}$	23
$B_{50}N_2$	24

1. P. K. Lam, R. M. Wentzcovitch, M. L. Cohen, in *Materials Science Forum*, Vols. 2, 54, 55, J. J. Pouch, S. A. Alterovitz, eds., Trans Tech, 1990, p. 165.
2. P. Vincenzini, *Forum on New materials, 8th CIMTEC-World Ceramics Congress* June 1994, TECHNA, Italy, 1995, p. 201.

Inorganic Reactions and Methods, Volume 18
Edited by J. J. Zuckerman, Jim D. Atwood

17.3.5.3.3. Tetragonal BN.

A tetragonal form of BN can be prepared by vapor deposition on BN-coated Ta or graphite substrates at 1200–1600°C. The composition is close to $B_{50}N_{1.8}$; the density is 2.46 g/cm^3, and the lattice constants are $a = 864.6$ pm and $c = 512.7$ pm[1]. Shock loading of diamond/BN mixtures produced several phases, including a tetragonal phase with the composition $B_{25}N$[2].

(E. G. WOLFF)

1. H. J. Becher, R. Mattes, in *Boron and Refractory Borides*, V. I. Matkovich, ed., Springer–Verlag, Berlin, 1977, p. 113.
2. M. J. Paislet, Y. Horie, R. F. Davis, K. Dan, H. Tamura, A. B. Sawaoka, *J. Mater. Sci. Let., 12*, 1768 (1993).

17.3.5.3.4. Other Structural Modifications.

Further ultrahigh pressure structural modifications of zinc-blende BN are considered possible, with a rock salt structure preferred over a β-Sn structure[1]. A metastable E-BN phase is obtained during electron-beam-assisted crystallization of BN[2]. Other metastable phases of BN are reported in the condensation products upon sudden cooling in conditions of a pulsed plasma discharge[3,4]. Disordered structures are reported when mixed plasma/chemical processes are used[5]. Some compounds of type B_nN_m are listed in Table 1[6–28].

(E. G. WOLFF)

TABLE 1. LITERATURE REFERENCES TO COMPOUNDS OF TYPE B_nN_m

Compound	Ref.
B_nN	17
BN_n	9, 18, 21, 22
B_nN_m	6, 12, 14, 26
BN_2	8
BN_3	7, 19, 20, 27
BN_4	10
B_2N	25
B_3N	7, 11, 16
B_2N_2	25
B_2N_3	10
B_3N_2	10
B_3N_3	5, 28
B_4N_4	5, 13
$B_{12}N_{12}$	15
$B_{30}N_{30}$	23
$B_{50}N_2$	24

1. P. K. Lam, R. M. Wentzcovitch, M. L. Cohen, in *Materials Science Forum*, Vols. 2, 54, 55, J. J. Pouch, S. A. Alterovitz, eds., Trans Tech, 1990, p. 165.
2. P. Vincenzini, *Forum on New materials, 8th CIMTEC-World Ceramics Congress* June 1994, TECHNA, Italy, 1995, p. 201.

3. V. P. Elyutin, I. V. Blinkov, I. I. Goryunova, A. V. Ivanov, Yu. N. Parkhomenko, Izv. *Akad. Nauk Neorg. Mater. 26*, 978 (1990).
4. *Phys. Abstr.*, 94-30049.
5. *Phys. Abstr.*, 92-3803.
5. *Phys. Abstr.*, 95-26617.
6. *Phys. Abstr.*, 95-46548.
7. *Phys. Abstr.*, 94-105740.
8. *Phys. Abstr.*, 94-105732.
9. *Phys. Abstr.*, 94-159475.
10. *Phys. Abstr.*, 95-123589.
11. *Phys. Abstr.*, 94-33533.
12. *Phys. Abstr.*, 94-26648.
13. *Phys. Abstr.*, 93-114699.
14. *Phys. Abstr.*, 93-141260.
15. *Phys. Abstr.*, 93-33638.
16. *Phys. Abstr.*, 93-33418.
17. *Phys. Abstr.*, 93-54231.
18. *Phys. Abstr.*, 93-33181.
19. *Phys. Abstr.*, 91-86910.
20. *Phys. Abstr.*, 91-107038.
21. *Phys. Abstr.*, 89-143182.
22. *Phys. Abstr.*, 91-10427.
23. *Phys. Abstr.*, 92-140875.
24. *Phys. Abstr.*, 92-103202.
25. *Phys. Abstr.*, 92-95348.
26. *Phys. Abstr.*, 87-42816.
27. *Phys. Abstr.*, 87-106860.
28. *Phys. Abstr.*, 84-1034.

17.3.5.3.5. Miscellaneous.

Polymeric precursors have been developed which are stable at room temperature and when polymerized convert to ceramics in high yield. Such precursors may be synthesized by reaction of a vinylsilane, vinylmethylsilane, acetylene silane, or acetylene alkyl silane with a borane or a borane:amine derivative[1]. The reactants are mixed in an inert atmosphere, either neat or in an aprotic solvent like acetonitrile, tetrahydrofuran, or a hydrocarbon, or in a mixture of such solvents. The reaction mixture is heated for 0.1 to 120 h at 90–170°C. The solvent, if any, is then removed. The polymer is pyrolyzed in argon or N_2 at 500–1500°C for 1 h. BN and other ceramics such as B_4C, or $Si_pB_qC_rN_s$ compounds can be made, where p, q, r, and s have various numerical values. To date, no measurements of the crystallographic form of the resultant BN compound have been made. Other precursors convertible to BN include poly (2-vinylpentaborane) oligomers[2].

High purity submicrometer (100–150 Å) powders of BN have been synthesized in the range -75 to $+750$°C, by means of reactions of borax and carbamide (urea) in ammonia[3]. Metal borohydrides and boron halides in NH_3 and ammonium salts with benzene solutions of BCl_3 were also studied. BN ceramic aerogels were also described[4].

(E. G. WOLFF)

1. S. Riccitiello, M. T. Hsu, T. S. Chen, U.S. Patent 5, 130, 278 (July 14, 1992); also from NASA Tech Briefs, May 1996.
2. M. G. L. Mirabelli, L. G. Sneddon *Inorg. Chem. 27*, 3271 (1988).
3. R. S. Kalyoncu, Bureau of Mines Report, USA #9012 (1986).
4. *Phys. Abstr.*, 90-84108.

Inorganic Reactions and Methods, Volume 18
Edited by J. J. Zuckerman, Jim D. Atwood

3. V. P. Elyutin, I. V. Blinkov, I. I. Goryunova, A. V. Ivanov, Yu. N. Parkhomenko, Izv. *Akad. Nauk Neorg. Mater. 26*, 978 (1990).
4. *Phys. Abstr.*, 94-30049.
5. *Phys. Abstr.*, 92-3803.
5. *Phys. Abstr.*, 95-26617.
6. *Phys. Abstr.*, 95-46548.
7. *Phys. Abstr.*, 94-105740.
8. *Phys. Abstr.*, 94-105732.
9. *Phys. Abstr.*, 94-159475.
10. *Phys. Abstr.*, 95-123589.
11. *Phys. Abstr.*, 94-33533.
12. *Phys. Abstr.*, 94-26648.
13. *Phys. Abstr.*, 93-114699.
14. *Phys. Abstr.*, 93-141260.
15. *Phys. Abstr.*, 93-33638.
16. *Phys. Abstr.*, 93-33418.
17. *Phys. Abstr.*, 93-54231.
18. *Phys. Abstr.*, 93-33181.
19. *Phys. Abstr.*, 91-86910.
20. *Phys. Abstr.*, 91-107038.
21. *Phys. Abstr.*, 89-143182.
22. *Phys. Abstr.*, 91-10427.
23. *Phys. Abstr.*, 92-140875.
24. *Phys. Abstr.*, 92-103202.
25. *Phys. Abstr.*, 92-95348.
26. *Phys. Abstr.*, 87-42816.
27. *Phys. Abstr.*, 87-106860.
28. *Phys. Abstr.*, 84-1034.

17.3.5.3.5. Miscellaneous.

Polymeric precursors have been developed which are stable at room temperature and when polymerized convert to ceramics in high yield. Such precursors may be synthesized by reaction of a vinylsilane, vinylmethylsilane, acetylene silane, or acetylene alkyl silane with a borane or a borane:amine derivative[1]. The reactants are mixed in an inert atmosphere, either neat or in an aprotic solvent like acetonitrile, tetrahydrofuran, or a hydrocarbon, or in a mixture of such solvents. The reaction mixture is heated for 0.1 to 120 h at 90–170°C. The solvent, if any, is then removed. The polymer is pyrolyzed in argon or N_2 at 500–1500°C for 1 h. BN and other ceramics such as B_4C, or $Si_pB_qC_rN_s$ compounds can be made, where p, q, r, and s have various numerical values. To date, no measurements of the crystallographic form of the resultant BN compound have been made. Other precursors convertible to BN include poly (2-vinylpentaborane) oligomers[2].

High purity submicrometer (100–150 Å) powders of BN have been synthesized in the range -75 to $+750$°C, by means of reactions of borax and carbamide (urea) in ammonia[3]. Metal borohydrides and boron halides in NH_3 and ammonium salts with benzene solutions of BCl_3 were also studied. BN ceramic aerogels were also described[4].

(E. G. WOLFF)

1. S. Riccitiello, M. T. Hsu, T. S. Chen, U.S. Patent 5, 130, 278 (July 14, 1992); also from NASA Tech Briefs, May 1996.
2. M. G. L. Mirabelli, L. G. Sneddon *Inorg. Chem. 27*, 3271 (1988).
3. R. S. Kalyoncu, Bureau of Mines Report, USA #9012 (1986).
4. *Phys. Abstr.*, 90-84108.

Inorganic Reactions and Methods, Volume 18
Edited by J. J. Zuckerman, Jim D. Atwood

17.3.5.4. One-Dimensional Form (Fibers)

Boron nitride fibers offer an interesting crystallographic analogue and commercial complement to the more common graphite fibers[1–3]. Unlike graphite, BN fibers have low electrical conductivity and are transparent to microwaves, but similar mechanical properties such as thermal expansion anisotropy may be expected. Better corrosion resistance is also found. The fibers are economical to synthesize[4–6]. The production process is based on three steps: fiberization of a B_2O_3 melt to make a precursor fiber, nitriding of the B_2O_3 precursor, and stabilization of BN (analogous to graphitization). The original B_2O_3 filament can be made by drawing a B_2O_3 melt through steel bushings, using a dodecane sizing to prevent H_2O attack[7]. Slow heating in NH_3 is required to allow the by-product H_2O to escape. The heterogeneous reaction is a diffusion-controlled process. The precursor for stretching has 48–52% N content, and only ~5 s at 2000°C is needed to orient the crystallites. The reaction mechanism proposed is[3,6–8]:

Formation of addition compound:

$$n\mathrm{B_2O_3}\ (\text{fiber}) \xrightarrow[200^\circ\mathrm{C}]{\mathrm{NH_3}} (\mathrm{B_2O_3})_n \cdot \mathrm{NH_3} \qquad \text{(a)}$$

Formation of nitrided cyclic structure:

$$(\mathrm{B_2O_3})_n \cdot \mathrm{NH_3} \xrightarrow[350-800^\circ\mathrm{C}]{\mathrm{NH_3}} (\mathrm{BN})_x \cdot (\mathrm{B_2O_3})_y \cdot (\mathrm{NH_3})_z + \mathrm{H_2O} \qquad \text{(b)}$$

Final stabilization:

$$(\mathrm{BN})_x \cdot (\mathrm{B_2O_3})_y \cdot (\mathrm{NH_3})_z \xrightarrow[>1500^\circ\mathrm{C}]{\mathrm{N_2}} \mathrm{BN}\ (\text{fiber}) + \mathrm{B_2O_3} + \mathrm{NH_3} \qquad \text{(c)}$$

The first two reactions (nitriding) are the rate-determining steps. The final stabilization is completed in seconds. The conversion of B_2O_3 to BN approaches 70% yield. The fiber properties depend on additional variables such as degree of nitridation of the precursor[7]. Substitution reaction (b) leads to mixtures of cyclic BN and boroxine rings. Further nitriding leads to coalescence of the cyclic rings into a highly disordered, three-dimensional, layer-type BN structure that resembles a turbostratic (hexagonal) BN, although there is more stability on heating and in H_2O. The fibers do not revert to hexagonal or rhombohedral BN even after heating to 2500°C[9]. The elastic modulus is subsequently increased by a stretch process at 2300°C or higher. Fibers of BN are also used as a precursor for carbonitride filaments[10]:

$$\mathrm{BN} + \mathrm{NbCl_5} + \mathrm{H_2} \xrightarrow[\text{at } 1500^\circ\mathrm{C}]{\mathrm{CH_4 \text{ or } C_4H_{10}}} \mathrm{NbC_xN_{1-x}} \text{ or } \mathrm{NbN} \qquad \text{(c)}$$

Hollow BN fibers are made by depositing a coating of BN on carbon fibers, heating in an oxidizing atmosphere to form CO or CO_2, and leaving a BN coating. The reaction between BF_3 and NH_3 at 1200–1400°C may be used[11]. Yarn and BN/BN composites can be made with similar techniques (see 17.3.5.6).

A review of the development of high performance BN fibers has appeared[8]. BN fibers have also been prepared by nitriding boron filaments[12]. The boron fibers

themselves are made by vapor deposition of boron on a heated tungsten filament. The boron with the tungsten core is first oxidized by heating at 560°C. It is then heated to 1000–1400°C in an ammonia atmosphere for 6 h to form a BN fiber. Boron nitride fiber mats have been made for use as electric cell separators in a lithium sulfide battery[13]. BN fibers from poly(borazine) preceramics were reported[14]. Arc discharge synthesis was used to form pure BN nanotubes using HfB_2 electrodes[15].

(E. G. WOLFF)

1. R. S. Hamilton, AFML-TR-74-115, Pt. IV (1978).
2. J. Economy, R. Anderson, *Inorg. Chem., 5*, 989 (1966).
3. J. Economy, R. Lin, in *Boron and Refractory Borides*, V. I. Matkovich, ed., Springer-Verlag, Berlin, 1977, p. 552.
4. J. Economy, R. E. Highsmith, J. H. Mason, U.S. Patent 3, 837, 997 (1974); *Chem. Abstr.*, 082-04-021015 (1975).
5. J. Economy, private communication, 1965.
6. J. Economy, R. V. Anderson, U.S. Patents 3, 429, 722 and 3, 668, 059 (1969).
7. R. Y. Lin, J. Economy, H. H. Murty, R. Ohnsorg, *J. Appl. Polym. Sci. Appl. Polym. Symp.*, No. 29, 175 (1975).
8. R. S. Hamilton in *Advanced Composites Technology*, T/C Press, Los Angeles, 1978.
9. J. Economy, R. V. Anderson, *J. Polym. Sci., Phys. Chem., 19*, 283 (1967).
10. J. Economy, R. Y. Lin, W. D. Smith, C. K. Jun, AFML-TR-72-189 (1972).
11. L. Boyne J. Hill, British Patent Appl. 2, 014, 972 (1979), *Chem. Abstr.*, 092-10-077995 (1980).
12. W. C. Miller, in M. Grayson, ed., *Encyclopedia of Textiles, Fibers, and Nonwoven Fabrics*, Wiley, New York, (1984), pp. 443–450.
13. P. Brocke, H. Schurmans, J. Verhoest, *Inorganic Fibers and Composite Materials: A Survey of Recent Developments*, Pergamon Press, Oxford, 1984.
14. *Phys. Abstr.*, 94-71371.
15. A. Loiseau, F. Willaime, N. Demoncy, G. Hug, H. Pescard, *Phys. Rev. Lett., 76*, 4737 (1996).

17.3.5.5. Two-Dimensional Forms of BN

17.3.5.5.1. Thin Films of BN.

Thin films of BN made from any of the three major types of BN are thermal and electrical insulators. Hexagonal BN is the common form, and vapor deposition is the usual mode of fabrication[1–7]. For example transparent, vitreous BN films can be deposited to a thickness of 12–50 μm on Mo and Ta substrates heated to 770–1300°C by pyrolysis of 2, 4.6-trichloroborazine vapor at low pressure; orientation with (001) planes parallel to the substrate. Grain size decreases with substrate temperature and boride interlayers are also formed[1]. Pyrolysis of Me_3NBF_3, Pr_2NBBr_2, β, β^1, β^{11}-trichloroborazine with and without NH_3, BBr_3–NH_3, and BBr_3–NH_3-cycloheptatriene mixtures also give BN films—both hexagonal and cubic forms. The amount of cubic BN in the film increases as the temperature for film deposition is reduced[2]. Room temperature stresses tend to be tensile for B_2N and compressive for BN films, with a tendency toward tensile in all films on heating[3]. A Si-doped BN film is preferable to either B_2N or BN for use as an X-ray mask, since it is not optically transparent and does not wrinkle. An alloy, principally of boron, is evaporated in the presence of NH_3 and deposited on a stainless steel substrate to give 20% cBN, 25% hBN, and the rest iron boride (Fe_2B). No X-ray peaks are found for the alloying elements in the film[4], but their presence is noted through their effect on residual stresses, and angular shifting of diffraction peaks. The composition of the deposited material is BN_x, where x is just less than 1. The current–voltage (I–V)

Inorganic Reactions and Methods, Volume 18
Edited by J. J. Zuckerman, Jim D. Atwood

themselves are made by vapor deposition of boron on a heated tungsten filament. The boron with the tungsten core is first oxidized by heating at 560°C. It is then heated to 1000–1400°C in an ammonia atmosphere for 6 h to form a BN fiber. Boron nitride fiber mats have been made for use as electric cell separators in a lithium sulfide battery[13]. BN fibers from poly(borazine) preceramics were reported[14]. Arc discharge synthesis was used to form pure BN nanotubes using HfB_2 electrodes[15].

(E. G. WOLFF)

1. R. S. Hamilton, AFML-TR-74-115, Pt. IV (1978).
2. J. Economy, R. Anderson, *Inorg. Chem., 5*, 989 (1966).
3. J. Economy, R. Lin, in *Boron and Refractory Borides*, V. I. Matkovich, ed., Springer-Verlag, Berlin, 1977, p. 552.
4. J. Economy, R. E. Highsmith, J. H. Mason, U.S. Patent 3, 837, 997 (1974); *Chem. Abstr.*, 082-04-021015 (1975).
5. J. Economy, private communication, 1965.
6. J. Economy, R. V. Anderson, U.S. Patents 3, 429, 722 and 3, 668, 059 (1969).
7. R. Y. Lin, J. Economy, H. H. Murty, R. Ohnsorg, *J. Appl. Polym. Sci. Appl. Polym. Symp.*, No. 29, 175 (1975).
8. R. S. Hamilton in *Advanced Composites Technology*, T/C Press, Los Angeles, 1978.
9. J. Economy, R. V. Anderson, *J. Polym. Sci., Phys. Chem., 19*, 283 (1967).
10. J. Economy, R. Y. Lin, W. D. Smith, C. K. Jun, AFML-TR-72-189 (1972).
11. L. Boyne J. Hill, British Patent Appl. 2, 014, 972 (1979), *Chem. Abstr.*, 092-10-077995 (1980).
12. W. C. Miller, in M. Grayson, ed., *Encyclopedia of Textiles, Fibers, and Nonwoven Fabrics*, Wiley, New York, (1984), pp. 443–450.
13. P. Brocke, H. Schurmans, J. Verhoest, *Inorganic Fibers and Composite Materials: A Survey of Recent Developments*, Pergamon Press, Oxford, 1984.
14. *Phys. Abstr.*, 94-71371.
15. A. Loiseau, F. Willaime, N. Demoncy, G. Hug, H. Pescard, *Phys. Rev. Lett., 76*, 4737 (1996).

17.3.5.5. Two-Dimensional Forms of BN

17.3.5.5.1. Thin Films of BN.

Thin films of BN made from any of the three major types of BN are thermal and electrical insulators. Hexagonal BN is the common form, and vapor deposition is the usual mode of fabrication[1–7]. For example transparent, vitreous BN films can be deposited to a thickness of 12–50 μm on Mo and Ta substrates heated to 770–1300°C by pyrolysis of 2, 4.6-trichloroborazine vapor at low pressure; orientation with (001) planes parallel to the substrate. Grain size decreases with substrate temperature and boride interlayers are also formed[1]. Pyrolysis of Me_3NBF_3, Pr_2NBBr_2, β, β^1, β^{11}-trichloroborazine with and without NH_3, BBr_3–NH_3, and BBr_3–NH_3-cycloheptatriene mixtures also give BN films—both hexagonal and cubic forms. The amount of cubic BN in the film increases as the temperature for film deposition is reduced[2]. Room temperature stresses tend to be tensile for B_2N and compressive for BN films, with a tendency toward tensile in all films on heating[3]. A Si-doped BN film is preferable to either B_2N or BN for use as an X-ray mask, since it is not optically transparent and does not wrinkle. An alloy, principally of boron, is evaporated in the presence of NH_3 and deposited on a stainless steel substrate to give 20% cBN, 25% hBN, and the rest iron boride (Fe_2B). No X-ray peaks are found for the alloying elements in the film[4], but their presence is noted through their effect on residual stresses, and angular shifting of diffraction peaks. The composition of the deposited material is BN_x, where x is just less than 1. The current–voltage (I–V)

characteristics for the unformed devices agreed with the theoretical value for Schottky emission, while the formed devices exhibited voltage-controlled negative resistance. This behavior fitted the relation $I = \alpha V + \beta V^2$ below about 10^{-5} torr. BN films are also formed by glow discharges using Si, Nb, or Au-Al cathodes.

Isotropic hBN films are commonly deposited by CVD methods for semiconductor applications[9,10]. Ammonia (NH_3) and hydrazine (N_2H_4) produce ultrathin layers of BN on Ru and B/Ru surfaces[11]. Hydrazine reacts with B to produce B–N adlayers with stoichiometries close to 1:1 and decomposition temperatures above 1100 K. Ionized species derived from a borazine ($B_3N_3H_6$) plasma can be used for direct ion beam deposition. Metal organic chemical vapor deposition (MOCVD) employing triethylboron and trimethoxyborane can be used. A low pressure CVD process is based on ammonia, diborane, hydrogen, and inert gases such as nitrogen or helium[12]. Similar processes result in B–N–H films[13]. Borazine is also a convenient B source for plasma–chemical synthesis of BN layers (e.g., on InSb layers)[14]. Microwave discharges can help to form transparent thin films[15].

As indicated in 15.3.5.2.1, cubic films of BN are still hard to grow, but much progress has been made on the synthesis of BN films in general[16,17]. Immediate applications include thin membranes for X-ray masks, electronic applications for high temperature active devices and insulators, and friction-reducing coatings. Limitations include the need for toxic starting materials and high substrate temperatures. The literature describes work on sputter deposition, radio frequency (rf) magnetron sputtering from a BN target, chemical vapor deposition, plasma CVD, and pulsed laser evaporation[16].

Novel methods described[16] include bombardment of a substrate by an ion beam of one element (e.g., N ions with energies of 200–40 keV) and simultaneous physical vapor deposition (PVD) of another one, e.g., boron from electron beam evaporation[18]. Activated reactive evaporation processes yield cBN films on Si plates[19]. Nitrogen ion implantation[20] and ion-beam assisted deposition of boron[21] are other methods employed. Synthesis of cBN films is described for a variety of techniques, including plasma-assisted growth[22–29], pulsed laser deposition[30–33], ion assisted pulsed laser deposition[34–36], UV-irradiation-assisted growth[37], ion beam deposition[37,38], ion-assisted growth[39–41], activated reactive evaporation[28,42], rf heating (13.56 MHz)[26–28], and molecular beam epitaxy[44]. Dissociation of BH_3NH_3, H_3BO_3, B_2H_6, and $NaBH_4$ compounds with reactive gases (H_2 and NH_3)[26–28] is also used to make thin films of cBN.

(E. G. WOLFF)

1. S. Koide, K. Nakamura, K. Yoshimura, *Kenkyu Kiyo_Nihon Daigaku Bunrigakubu, 79*, 9 (1979); *Chem. Abstr.*, 094-04-019465 (1981).
2. E. A. Balabanova, A. I. Vargunin, E. M. Orlova, I. Koli, E. B. Sukolov, L. S. Sukhanova, *Zh. Neorg. Khim., 80*, 1973 (1980); *Chem. Abstr.*, 093-14-142189 (1980).
3. T. F. Retajczyk, A. K. Sinha, *Appl. Phys. Lett., 36*, 161 (1980).
4. H. A. Beale, *Ind. Res. Dev., 21* 143 (1979).
5. L. E. Branovich, W. B. P. Fitzpatrick, L. M. Long, U.S. Patent 3, 692, 566 (1972).
6. L. E. Branovich, W. B. P. Fitzpatrick, L. M. Long, U.S. Patent 3, 825, 440 (1974).
7. K. Tanaka, Y. Uemura, M. Iwata, *Oyo Butsuri, 46*, 120 (1977); *Chem. Abstr.* 087-14-110399 (1977).
8. M. Iwata, Y. Uemura, K. Tanaka, *Chikkabutsukei Yudentai Maku ni Kansuru Sogo Kenkyu, 79*, 27 (1979); *Chem. Abstr.*, 094-10-75268 (1981).
9. J. L. Hurd, D. L. Perry, B. T. Lee, K. M. Yu, E. D. Bourret, E. E. Haller, *J. Mater. Res., 4*, 350 (1989).
10. H. Saiton, T. Ishiguro, Y. Ichinose, *J. Vac. Soc. Jpn., 31*, 628 (1988).

11. J. A. Rodrigez, C. M. Truong, D. W. Goodman, *J. Vac. Sci. Technol., A, 10*, 955 (1992).
12. S. S. Dana, in *Synthesis and Properties of Boron Nitride, Materials Science Forum* Vol. 54, 55, J. J. Pouch, S. A. Alterovitz, eds., Trans Tech, Aedermannsdort, 1990, p. 229.
13. M. Karnezos, in *Synthesis and Properties of Boron Nitride, Materials Science Forum* Vols. 54, 55, J. J. Pouch, S. A. Alterovitz, Trans Tech, Aedermannsdort, 1990, p. 261.
14. V. I. Belyi, T. P. Smirnova, A. P Solov'ev, I. L. Yashkin, *Mikroelektronika, 15*, 146 (1986).
15. *Phys. Abstr.*, 89-31855.
16. Synthesis and properties of boron nitride, in *Materials Science Forum*, Vols. 54 and 55, J. J. Pouch, S. A. Alterovitz, Trans Tech, Aedermannsdort, 1990.
17. M. Z. Karim, D. C. Cameron, M. S. J. Hashmi, *Mater. Design, 13*, 207 (1992).
18. S. Nishiyama, N. Kuratani, A. Ebe, K. Ogata, *Phys. Res. B (Netherlands), B80*, 1485 (1993).
19. M. Murakawa, S. Watanabe, *Surf. Coat. Technol., 43*, 128 (1990).
20. T. Baazi, E. J. Knystautas, *Thin Solid Films, 232*, 185 (1993).
21. G.Sene, D. Bouchier, S. Ilias, M. A. Djouadi, J. Pescallon, V. Stambouli, P. Moller, G. Hug, *Diamonds Relat. Mater., 5*(3–5), 530 (1996).
22. D. H. Berns, M. A. Cappelli, *Appl. Phys. Lett., 68*(19), 2711 (1996).
23. Yan Pengxun, Yang Size, *Phys. Status Solidi, 151*, 191 (1995); *145*, 29 (1994).
24. T. Ishiguro, H. Saitoh, Y. Ichinose, *J. Jpn. Soc. Precis. Eng., 53*, 1527 (1987).
25. C. Deshpandey, R. F. Bunshah, *Thin Solid Films, 163*, 131 (1988).
26. H. Saitoh, T. Hirose, H. Matsui, Y. Hirotsu, Y. Ichinose, *Surf. Coat. Technol., 39*, 265 (1989).
27. H. Saitoh, Y. Hirotsu, Y. Ichinose, *J. Jpn. Inst. Met., 54*, 186 (1990).
28. Wanlu Wang, Rongbin Ji, Jingyiun Gao, Kejun Liao, Xiaolan Zhang, *Phys. Status Solidi A, 136*, K89 (1993).
29. Kejun Liao, Wanlu Wang, *Phys. Status Solidi A, 144*, K73 (1994).
30. Y. Suda, T. Nakazono, K. Ebihara, K. Baba, *Thin Solid Films, 281*, 324 (1996).
31. H. Chen, Y. He, R. H. Prince, *Diamonds Relat. Mater., 5*, 552 (1996).
32. G. L. Doll, J. A. Sell, C. A. Taylor, R. Clarke, *Phys. Rev. B, 43*, 6816 (1991).
33. S. B. Ogale, A. P. Malshe, S. M. Kanetkar, *Mater. Manuf. Process., 8*, 19 (1993).
34. T. A. Friedman, L. J. Berbardez, K. F. McCarty, E. J. Klaus, D. K. Otteson, H. A. Johnson, W. M. Clift, *Appl. Phys. Lett.*, 63, 1342 (1993).
35. D. L. Medlin, T. A. Friedman, P. B. Mirkarimi, P. Rez, M. J. Mills, K. F. McCarty, *J. Appl. Phys. 76*, 295, (1994).
36. T. A. Friedman, P. B. Mirkarimi, D. L. Medlin, K. F. McCarty, E. J. Klaus, D. R. Boehme, H. A. Johnson, M. J. Mills, *J. Appl. Phys., 76*, 3088 (1944).
37. B. Rauschenbach, *Diamond Relat. Mater., 5*, 883 (1996).
38. Z. Xia, G. L. Zhang, W. L. Lin, *MRS Symp. Low Energy Beam*, Anaheim, *315* (1991).
39. N. Savvides, *Thin Solid Films, 163*, 13 (1988).
40. T. Ikeda, *Appl. Phys. Lett., 61*, 786 (1992).
41. P. B. Mirkarimi, K. F. McCarty, D. L. Medlin, W. G. Wolfer, T. A. Friedman, E. J. Klaus, G. F. Cardinale, D. G. Howitt, *J. Mater. Res., 9*, 2925 (1994).
42. K. L. Chopra, V. Agarwal, V. D. Vankar, C. V. Deshpandey, R. F. Bunshah, *Thin Solid Films, 126*, 307 (1985).
43. K. Inagawa, *J. Vac. Soc. Jpn., 31*, 621 (1988).
44. R. F. Davis, M. J. Paisley, Z. Sitar, D. J. Kester, K. S. Ailey, C. Wang, *Microelectron. J., 25*, 661 (1994).

17.3.5.5.2. Pyrolytic BN.

Pyrolytic BN (pBN) is analogous to pyrolytic graphite, the *a*-direction layer planes of the hexagonal structure deposit parallel to the substrate surface[1–4]. Attention to the substrate crystallography and its temperature is required during deposition. Thicknesses exceeding 25 μm are feasible. Thermal conductivity and infrared transmission are of interest[4].

Pyrolytic BN was deposited on Nicalon NL202 silicon carbide yarns at 1000–1200°C to improve aerodynamic resistance and oxidation behavior of silicon carbide[5]. Yarns were fed into a CVD furnace at a rate of 0.01 m/s. The pBN was made by

Inorganic Reactions and Methods, Volume 18
Edited by J. J. Zuckerman, Jim D. Atwood

11. J. A. Rodrigez, C. M. Truong, D. W. Goodman, *J. Vac. Sci. Technol., A, 10*, 955 (1992).
12. S. S. Dana, in *Synthesis and Properties of Boron Nitride, Materials Science Forum* Vol. 54, 55, J. J. Pouch, S. A. Alterovitz, eds., Trans Tech, Aedermannsdort, 1990, p. 229.
13. M. Karnezos, in *Synthesis and Properties of Boron Nitride, Materials Science Forum* Vols. 54, 55, J. J. Pouch, S. A. Alterovitz, Trans Tech, Aedermannsdort, 1990, p. 261.
14. V. I. Belyi, T. P. Smirnova, A. P Solov'ev, I. L. Yashkin, *Mikroelektronika, 15*, 146 (1986).
15. *Phys. Abstr.*, 89-31855.
16. Synthesis and properties of boron nitride, in *Materials Science Forum*, Vols. 54 and 55, J. J. Pouch, S. A. Alterovitz, Trans Tech, Aedermannsdort, 1990.
17. M. Z. Karim, D. C. Cameron, M. S. J. Hashmi, *Mater. Design, 13*, 207 (1992).
18. S. Nishiyama, N. Kuratani, A. Ebe, K. Ogata, *Phys. Res. B (Netherlands), B80*, 1485 (1993).
19. M. Murakawa, S. Watanabe, *Surf. Coat. Technol., 43*, 128 (1990).
20. T. Baazi, E. J. Knystautas, *Thin Solid Films, 232*, 185 (1993).
21. G.Sene, D. Bouchier, S. Ilias, M. A. Djouadi, J. Pescallon, V. Stambouli, P. Moller, G. Hug, *Diamonds Relat. Mater., 5*(3–5), 530 (1996).
22. D. H. Berns, M. A. Cappelli, *Appl. Phys. Lett., 68*(19), 2711 (1996).
23. Yan Pengxun, Yang Size, *Phys. Status Solidi, 151*, 191 (1995); *145*, 29 (1994).
24. T. Ishiguro, H. Saitoh, Y. Ichinose, *J. Jpn. Soc. Precis. Eng., 53*, 1527 (1987).
25. C. Deshpandey, R. F. Bunshah, *Thin Solid Films, 163*, 131 (1988).
26. H. Saitoh, T. Hirose, H. Matsui, Y. Hirotsu, Y. Ichinose, *Surf. Coat. Technol., 39*, 265 (1989).
27. H. Saitoh, Y. Hirotsu, Y. Ichinose, *J. Jpn. Inst. Met., 54*, 186 (1990).
28. Wanlu Wang, Rongbin Ji, Jingyiun Gao, Kejun Liao, Xiaolan Zhang, *Phys. Status Solidi A, 136*, K89 (1993).
29. Kejun Liao, Wanlu Wang, *Phys. Status Solidi A, 144*, K73 (1994).
30. Y. Suda, T. Nakazono, K. Ebihara, K. Baba, *Thin Solid Films, 281*, 324 (1996).
31. H. Chen, Y. He, R. H. Prince, *Diamonds Relat. Mater., 5*, 552 (1996).
32. G. L. Doll, J. A. Sell, C. A. Taylor, R. Clarke, *Phys. Rev. B, 43*, 6816 (1991).
33. S. B. Ogale, A. P. Malshe, S. M. Kanetkar, *Mater. Manuf. Process., 8*, 19 (1993).
34. T. A. Friedman, L. J. Berbardez, K. F. McCarty, E. J. Klaus, D. K. Otteson, H. A. Johnson, W. M. Clift, *Appl. Phys. Lett.*, 63, 1342 (1993).
35. D. L. Medlin, T. A. Friedman, P. B. Mirkarimi, P. Rez, M. J. Mills, K. F. McCarty, *J. Appl. Phys. 76*, 295, (1994).
36. T. A. Friedman, P. B. Mirkarimi, D. L. Medlin, K. F. McCarty, E. J. Klaus, D. R. Boehme, H. A. Johnson, M. J. Mills, *J. Appl. Phys., 76*, 3088 (1944).
37. B. Rauschenbach, *Diamond Relat. Mater., 5*, 883 (1996).
38. Z. Xia, G. L. Zhang, W. L. Lin, *MRS Symp. Low Energy Beam*, Anaheim, *315* (1991).
39. N. Savvides, *Thin Solid Films, 163*, 13 (1988).
40. T. Ikeda, *Appl. Phys. Lett., 61*, 786 (1992).
41. P. B. Mirkarimi, K. F. McCarty, D. L. Medlin, W. G. Wolfer, T. A. Friedman, E. J. Klaus, G. F. Cardinale, D. G. Howitt, *J. Mater. Res., 9*, 2925 (1994).
42. K. L. Chopra, V. Agarwal, V. D. Vankar, C. V. Deshpandey, R. F. Bunshah, *Thin Solid Films, 126*, 307 (1985).
43. K. Inagawa, *J. Vac. Soc. Jpn., 31*, 621 (1988).
44. R. F. Davis, M. J. Paisley, Z. Sitar, D. J. Kester, K. S. Ailey, C. Wang, *Microelectron. J., 25*, 661 (1994).

17.3.5.5.2. Pyrolytic BN.

Pyrolytic BN (pBN) is analogous to pyrolytic graphite, the *a*-direction layer planes of the hexagonal structure deposit parallel to the substrate surface[1–4]. Attention to the substrate crystallography and its temperature is required during deposition. Thicknesses exceeding 25 μm are feasible. Thermal conductivity and infrared transmission are of interest[4].

Pyrolytic BN was deposited on Nicalon NL202 silicon carbide yarns at 1000–1200°C to improve aerodynamic resistance and oxidation behavior of silicon carbide[5]. Yarns were fed into a CVD furnace at a rate of 0.01 m/s. The pBN was made by

reactions of BCl_3 and NH_3 at pressures below 0.1 Torr. Coatings of 0.1–0.7 μm were obtained and gave moderate oxidation protection of SiC in air at 1000°C. Some loss of protection was attributed to initial moisture pickup, since the free energy for the reaction

$$pBN + 3H_2O \longrightarrow H_3BO_3 + NH_3$$

is −18 kcal/mol at room temperature and negative to 190°C. CVD of BCl_3–N_2–NH_3 mixtures at 1300–2100°C and 1–20 torr pressures produces various BN structure modifications, including hexagonal and tetragonal BN, amorphous in the pyrolytic layers[6]. Pyrolytic BN has also been prepared by formation and subsequent pyrolysis of a B–N complex such as $(CH_3O)_3B \cdot NH_3$, $F_3B \cdot NH_3$, or B-trichloroborazole[7].

Additional literature references to pyrolytic BN[8–21] include mentions of commercial products such as Boralloy pBN, which exhibits exceptional dielectric strength, chemical inertness, and anisotropic thermal and electrical properties. Applications include crucibles, high temperature insulators, and heating elements[21].

(E. G. WOLFF)

1. D. Belforti, B. Bovarnick *Nature*, *4779*, 901 (1961).
2. M. Basche, D. Schiff, *Mater. Design Eng.*, *59*, 78 (1964).
3. N. J. Archer, *Spec. Publ., - Chem. Soc., 30 (High Temp. Chem. Inorg. Ceram. Mater. Proc. Conf.), 167* (1977); *Chem. Abstr.* 088-10-65011 (1978).
4. P.-C. Li, M. P. Lepie, *J. Am. Ceram. Soc.*, *48*, 277 (1965).
5. A. W. Moore NASA-CR-189817, Jan. 28, 1992.
6. A. S. Rozenberg, Yu. A. Sinenko, N. V. Chukanov, *J. Mater. Sci.*, *28*, 5675 (1993).
7. R. Thompson, in *Progress in Boron Chemisry*, Vol. 2, R. J. Brotherton, Steinberg, eds., Pergamon Press, Oxford, 1970.
8. *Phys. Abstr.*, 94-108473.
9. *Phys. Abstr.*, 91-3203.
10. *Phys. Abstr.*, 91-4780.
11. *Phys. Abstr.*, 89-3389.
12. *Phys. Abstr.*, 90-9934.
13. *Phys. Abstr.*, 89-9129.
14. *Phys. Abstr.*, 92-124463.
15. *Phys. Abstr.*, 92-135865.
16. *Phys. Abstr.*, 91-92116.
17. *Phys. Abstr.*, 87-106023.
18. *Phys. Abstr.*, 87-44523.
19. *Phys. Abstr.*, 88-123797.
20. Union Carbide Coatings Service Corporation, *Boralloy*, Publication CP-4779 (1997).
21. Union Carbide, *Boralloy*, Advanced Ceramics Corporation brochure (1997).

17.3.5.6. BN Composites

Multidimensional BN fiber infiltrated (matrix) composites are analogous to carbon–carbon composites and overcome the brittleness and low to moderate thermal shock resistance of hot-pressed BN. With the availability of BN fibers (see 17.3.5.4), a weave of three or more dimensions is possible. Chemical vapor deposition may produce a turbostatic BN matrix that is sensitive to H_2O, while liquid impregnation requires multiple reimpregnation cycles[1]. One scheme is to impregnate a BN woven fiber preform with H_3BO_3, dry, sinter in NH_3, and hot-press.

In another approach, 3–6 mm lengths of BN fiber are blended with a hot aqueous solution saturated with H_3BO_3 and urea. This mixture is spread over a fine screen to

Inorganic Reactions and Methods, Volume 18
Edited by J. J. Zuckerman, Jim D. Atwood

reactions of BCl_3 and NH_3 at pressures below 0.1 Torr. Coatings of 0.1–0.7 μm were obtained and gave moderate oxidation protection of SiC in air at 1000°C. Some loss of protection was attributed to initial moisture pickup, since the free energy for the reaction

$$pBN + 3H_2O \longrightarrow H_3BO_3 + NH_3$$

is −18 kcal/mol at room temperature and negative to 190°C. CVD of BCl_3–N_2–NH_3 mixtures at 1300–2100°C and 1–20 torr pressures produces various BN structure modifications, including hexagonal and tetragonal BN, amorphous in the pyrolytic layers[6]. Pyrolytic BN has also been prepared by formation and subsequent pyrolysis of a B–N complex such as $(CH_3O)_3B \cdot NH_3$, $F_3B \cdot NH_3$, or B-trichloroborazole[7].

Additional literature references to pyrolytic BN[8–21] include mentions of commercial products such as Boralloy pBN, which exhibits exceptional dielectric strength, chemical inertness, and anisotropic thermal and electrical properties. Applications include crucibles, high temperature insulators, and heating elements[21].

(E. G. WOLFF)

1. D. Belforti, B. Bovarnick *Nature*, *4779*, 901 (1961).
2. M. Basche, D. Schiff, *Mater. Design Eng.*, *59*, 78 (1964).
3. N. J. Archer, *Spec. Publ.*, - *Chem. Soc.*, *30* (*High Temp. Chem. Inorg. Ceram. Mater. Proc. Conf.*), *167* (1977); *Chem. Abstr.* 088-10-65011 (1978).
4. P.-C. Li, M. P. Lepie, *J. Am. Ceram. Soc.*, *48*, 277 (1965).
5. A. W. Moore NASA-CR-189817, Jan. 28, 1992.
6. A. S. Rozenberg, Yu. A. Sinenko, N. V. Chukanov, *J. Mater. Sci.*, *28*, 5675 (1993).
7. R. Thompson, in *Progress in Boron Chemisry*, Vol. 2, R. J. Brotherton, Steinberg, eds., Pergamon Press, Oxford, 1970.
8. *Phys. Abstr.*, 94-108473.
9. *Phys. Abstr.*, 91-3203.
10. *Phys. Abstr.*, 91-4780.
11. *Phys. Abstr.*, 89-3389.
12. *Phys. Abstr.*, 90-9934.
13. *Phys. Abstr.*, 89-9129.
14. *Phys. Abstr.*, 92-124463.
15. *Phys. Abstr.*, 92-135865.
16. *Phys. Abstr.*, 91-92116.
17. *Phys. Abstr.*, 87-106023.
18. *Phys. Abstr.*, 87-44523.
19. *Phys. Abstr.*, 88-123797.
20. Union Carbide Coatings Service Corporation, *Boralloy*, Publication CP-4779 (1997).
21. Union Carbide, *Boralloy*, Advanced Ceramics Corporation brochure (1997).

17.3.5.6. BN Composites

Multidimensional BN fiber infiltrated (matrix) composites are analogous to carbon–carbon composites and overcome the brittleness and low to moderate thermal shock resistance of hot-pressed BN. With the availability of BN fibers (see 17.3.5.4), a weave of three or more dimensions is possible. Chemical vapor deposition may produce a turbostatic BN matrix that is sensitive to H_2O, while liquid impregnation requires multiple reimpregnation cycles[1]. One scheme is to impregnate a BN woven fiber preform with H_3BO_3, dry, sinter in NH_3, and hot-press.

In another approach, 3–6 mm lengths of BN fiber are blended with a hot aqueous solution saturated with H_3BO_3 and urea. This mixture is spread over a fine screen to

form a sheet and oven-dried under a pressure of 0.1 MN/m^2. The paper like board is heated in NH_3 to convert the H_3BO_3 to a matrix of BN.

Decomposition of urea supplies additional NH_3 for the nitriding reaction. A low density product results[1]. In a variation leading to higher densities (1.85 g/cm^3)[2], BN fibers are blended with a partially nitrided precursor boron oxide fiber followed by a hot press and thermal cycling (to 2000°C, 30 MN/m^2). Retention of BN fiber integrity is a major objective, since boric oxide promotes the phase transformation of BN from a turbostratic into a more hexagonal form above 1400°C. Rapid removal of B_2O_3 or thermal quenching to impede the transformation is required[2]. Use of hollow BN fibers from a C felt or fabric impregnation with BN to form a BN/BN composite is also feasible[3].

BN fibers have been used to reinforce composites made with a boron nitride matrix for use in electrical and electronic applications requiring both electrical insulation and high thermal conductivity[4]. Composites analogous to carbon–carbon three-dimensional systems have been woven, impregnated, and hot-pressed to utilize special properties such as radar transparency, low dielectric attenuation, and unique thermochemical behavior for applications such as antenna windows and heat shields. In work with BN matrices[5] carbonfibers, for example, have been impregnated with a borazine oligomer. Specimens, typically 50 vol % unidirectional carbon or carbon-coated Nicalon (SiC + 28% SiO_2 + 10% C) fibers, are hot-pressed at 20 MPa up to 400°C and subsequently heat-treated in nitrogen at 1200°C for 3 h[6]. The oligomeric phase used has been shown to exhibit liquid crystalline character[7,8], which is considered to account for the high degree of orientation of the BN, especially at an interface.

BN fibers are used in aluminum matrices because they are one of the few materials easily wet by molten aluminum[9]. hBN–AlN composites are described[10–13]. Gel methods resulted in an hAlN–turbostratic hBN composite[12]. zBN–based composites, e.g., with Al, Si, Ti nitride matrices, were reported[14]. A nanostructure composite was made by low temperature conversion of an aqueous solution of simple Al, B, and N-containing compounds to intermediate precursor (gel) materials[13]. BN–AlN composite fabrication is also described[15–20].

Cylindrically converging shock waves on powders were used to make mixtures of diamonds and hBN[21]. BN fiber reinforced ZrO_2 was described[22,23]. A nanostructured composite of magnetic particles of Fe_xN in a nonmagnetic matrix of BN is made via an inorganic gel[24]. Fabrication of BN–B_4 composites was reported[25,26]. Consolidation of novel sintered composites formed from high pressure crystallization of amorphous ceramics was also described[27]. The literature discusses other ceramics reinforced with BN fibers, as well[28,29].

(E. G. WOLFF)

1. J. Economy, R. E. Highsmith, J. H. Mason, U. S. Patent 3, 837, 997 (1974).
2. R. Y. Lin, J. Economy, H. D. Batha, *Bull. Am. Ceram. Soc.*, *55*, 781 (1976).
3. L. Boyne, J. Hill, British Patent Appl. 2, 014, 972 (1979); *Chem. Abstr.*, 092-10-077995 (1980).
4. T. F. Cooke, in *International Encyclopedia of Composites*, Vol. 2, S. M. Lee, ed., VCH Publishers, New York, (1990), p. 152.
5. C. G. Cofer, J. Economy, Y. Xu, A. Zangvil, E. Lara-Curzio, M. K. Ferber and K. L. More, *Comp. Sci. Technol.*, *56*, 967 (1996).
6. D. P. Kim, J. Economy, *Chem. Mater.*, *5*, 1216 (1993).
7. D. P. Kim, J. Economy, *Chem. Mater.*, 6, 395 (1994).
8. C. G. Cofer, D. P. Kim, J. Economy, *Ceram. Trans.*, *46*, 189 (1995).

9. W. C. Miller, in M. Grayson, ed., *Encyclopedia of Textiles, Fibers, and Nonwoven Fabrics*, Wiley, New York, 1984, pp. 443–450.
10. K. Tanemoto, T. Kania, *Key Eng. Mater., 108*, 85 (1995).
11. T. Kanai, A. Ando, K. Tanemoto, *Jpn. J. Appl. Phys., 31*, 1426 (1992).
12. T. D. Xiao, K. E. Gonsalves, P. R. Strutt, *J. Am. Ceram. Soc., 76*, 987 (1993).
13. P. R. Strutt, T. D. Xiao, K. E. Gonsalves, R. Boland, *Nanostructured Mater., 2*, 347 (1993).
14. A. Onodera, N. Takahashi, H. Yoshihara, H. Matsunami, T. Haria, *J. Mater. Sci., 25*, 4157 (1990).
15. *Phys. Abstr.*, 91-122026.
16. *Phys. Abstr.*, 90-119788.
17. *Phys. Abstr.*, 92-61426.
18. *Phys. Abstr.*, 90-119659.
19. *Phys. Abstr.*, 92-25868.
20. *Phys. Abstr.*, 92-13023.
21. M. J. Paisley, Y. Horie, R. F. Davis, K. Dan, H. Tamura, A. B. Sawaoka, *J. Mater. Sci. Lett., 12*, 1768 (1993).
22. *Phys. Abstr.*, 92-43890.
23. *Phys. Abstr.*, 92-49805.
24. K. E. Gonsalves, G.-M. Chow, Y. Zhang, J. I. Budnick, T. D. Xiao, *Adv. Mater., 6*, 291, (1994).
25. *Phys. Abstr.*, 93-135712.
26. *Phys. Abstr.*, 93-9228.
27. *Phys. Abstr.*, 91-4924.
28. *Phys. Abstr.*, 88-141395.
29. *Phys. Abstr.*, 87-119341.

17.3.6. Preparation of Ceramics of Controlled Thermal Conductivity

The use of ceramics for their high thermal conductivity is limited. Indeed, ceramics are materials with rather low thermal conductivities, since their bonding generally falls into the category of ionic–covalent. The ionic–covalent bonding implies that electrons are localized in their bond system, hence cannot transport thermal energy through the material by moving freely about. Two categories of ceramics are thought of as having high thermal conductivities. The first group consists of atoms of low atomic mass in a well-organized, simple crystal structure with strong bonds. These are the conditions for which thermal conductivity by phonons or lattice waves is optimum. The most common commercial material in this category is beryllium oxide (BeO). Semiconducting materials form the second category of high thermal conductivity ceramic materials. In this case, although the bonding is covalent, increasing temperature causes an increase in number of free electrons, with the result that the ceramic materials retain a relatively high thermal conductivity at high temperatures. Silicon carbide (SiC) is a well-known example of this type of material.

As energy becomes a larger fraction of the cost of manufacturing items that require heat treatment, there has been an increasing interest in conservation of energy by use of insulation. This has been particularly noticeable when high temperatures are involved. High temperature thermal insulating requirements are best satisfied by ceramic materials, which withstand much higher temperatures than polymers before decomposition. Moreover, since free electrons in ceramics are very limited, most ceramics have lower thermal conductivities than metals.

(ORVILLE HUNTER, JR.)

Inorganic Reactions and Methods, Volume 18
Edited by J. J. Zuckerman, Jim D. Atwood

9. W. C. Miller, in M. Grayson, ed., *Encyclopedia of Textiles, Fibers, and Nonwoven Fabrics*, Wiley, New York, 1984, pp. 443–450.
10. K. Tanemoto, T. Kania, *Key Eng. Mater.*, *108*, 85 (1995).
11. T. Kanai, A. Ando, K. Tanemoto, *Jpn. J. Appl. Phys.*, *31*, 1426 (1992).
12. T. D. Xiao, K. E. Gonsalves, P. R. Strutt, *J. Am. Ceram. Soc.*, *76*, 987 (1993).
13. P. R. Strutt, T. D. Xiao, K. E. Gonsalves, R. Boland, *Nanostructured Mater.*, *2*, 347 (1993).
14. A. Onodera, N. Takahashi, H. Yoshihara, H. Matsunami, T. Haria, *J. Mater. Sci.*, *25*, 4157 (1990).
15. *Phys. Abstr.*, 91-122026.
16. *Phys. Abstr.*, 90-119788.
17. *Phys. Abstr.*, 92-61426.
18. *Phys. Abstr.*, 90-119659.
19. *Phys. Abstr.*, 92-25868.
20. *Phys. Abstr.*, 92-13023.
21. M. J. Paisley, Y. Horie, R. F. Davis, K. Dan, H. Tamura, A. B. Sawaoka, *J. Mater. Sci. Lett.*, *12*, 1768 (1993).
22. *Phys. Abstr.*, 92-43890.
23. *Phys. Abstr.*, 92-49805.
24. K. E. Gonsalves, G.-M. Chow, Y. Zhang, J. I. Budnick, T. D. Xiao, *Adv. Mater.*, *6*, 291, (1994).
25. *Phys. Abstr.*, 93-135712.
26. *Phys. Abstr.*, 93-9228.
27. *Phys. Abstr.*, 91-4924.
28. *Phys. Abstr.*, 88-141395.
29. *Phys. Abstr.*, 87-119341.

17.3.6. Preparation of Ceramics of Controlled Thermal Conductivity

The use of ceramics for their high thermal conductivity is limited. Indeed, ceramics are materials with rather low thermal conductivities, since their bonding generally falls into the category of ionic–covalent. The ionic–covalent bonding implies that electrons are localized in their bond system, hence cannot transport thermal energy through the material by moving freely about. Two categories of ceramics are thought of as having high thermal conductivities. The first group consists of atoms of low atomic mass in a well-organized, simple crystal structure with strong bonds. These are the conditions for which thermal conductivity by phonons or lattice waves is optimum. The most common commercial material in this category is beryllium oxide (BeO). Semiconducting materials form the second category of high thermal conductivity ceramic materials. In this case, although the bonding is covalent, increasing temperature causes an increase in number of free electrons, with the result that the ceramic materials retain a relatively high thermal conductivity at high temperatures. Silicon carbide (SiC) is a well-known example of this type of material.

As energy becomes a larger fraction of the cost of manufacturing items that require heat treatment, there has been an increasing interest in conservation of energy by use of insulation. This has been particularly noticeable when high temperatures are involved. High temperature thermal insulating requirements are best satisfied by ceramic materials, which withstand much higher temperatures than polymers before decomposition. Moreover, since free electrons in ceramics are very limited, most ceramics have lower thermal conductivities than metals.

(ORVILLE HUNTER, JR.)

17.3.6.1. Preparation of Oxides of High Thermal Conductivity

Beryllium oxide (BeO) is the only oxide ceramic having a thermal conductivity large enough to justify describing it as a high thermal conductivity material. The chemical bonding in ceramic oxides is by forces of the covalent–ionic type, so there are no free electrons to act as heat carriers. Instead, the mechanism of heat conduction entails lattice waves or phonons. Beryllium oxide has a particularly high phonon thermal conductivity because the masses of the beryllium and oxygen ions are small and the bond strength between the ions is large, as indicated by a melting point of 2570°C. However, the lack of free electrons causes electrical conductivity to be very low. A major concern in the handling of BeO powder and heat treating during manufacturing of BeO ceramic pieces is the toxicity of this material. *Inhalation of fine BeO powder or vapor fumes containing Be is at best extremely dangerous and can be fatal.* In the final sintered solid piece, the danger is greatly reduced but grinding or sawing can create enough dust to constitute a danger.

The production of BeO ceramics is generally by classical ceramic processing methods described in 17.2. Pores hinder thermal conductivity, however, and to maximize this property, porosity must be reduced.

A typical process for forming a BeO ceramic product would start by ball-milling a fine BeO powder with an organic binder and water. This slip is then spray-dried to form a free-flowing powder made up of nearly spherical, uniformly distributed agglomerates of BeO powder. The spray-dried material is then dry pressed or isostatically pressed into the desired shape or into a blank that is near the desired shape. Grinding is often carried out on the green (unfired) piece to improve size and shape tolerances, since the final fired shape is harder and more difficult to grind. The firing temperature is in the 1500–1600°C range. At these temperatures, moisture in the air will react with the BeO, causing it to volatilize. This is a concern not only because material is lost but also because toxic vapor is created. To avoid this volatilization problem, firing is done in an electric kiln flushed with dried air.

The high thermal conductivity of BeO combined with other properties make it a unique material. The mode of heat transfer is by lattice waves, since the electrons are tightly bonded to the ions. The lack of free electrons causes the electrical conductivity and dielectric loss to be low. This combination of high thermal conductivity and low electrical conductivity is unique among commercially available materials that are economically feasible for most applications.

(ORVILLE HUNTER, JR.)

17.3.6.2. Preparation of Other Ceramics of High Thermal Conductivity

The ceramic nonoxide materials that have high thermal conductivities are the carbides, nitrides, and perhaps borides. In particular, silicon carbide and silicon nitride have received the bulk of the attention among these materials because they are refractory, resist oxidation at high temperatures, and retain a significant amount of their strength at high temperatures. Their thermal conductivity is high enough to render them extremely resistant to thermal shock. The preparation of these specific materials is described in detail in 17.3.9.

(ORVILLE HUNTER, JR.)

17.3.6.3. Preparation of Oxides of Low Thermal Conductivity

Fibrous materials and bricks are the most common forms of low thermal conductivity ceramic materials. In a system that is cycled up and down in temperature during a manufacturing process, heat loss can be reduced by lowering the heat capacity of the material until less heat is needed to raise the temperature a given amount. Both in cyclic heating and under steady state conditions, energy savings can be accomplished by reducing the thermal conductivity so that less heat will pass through the material. Both these reductions can be accomplished by reducing, up to a point, the proportion of solid material in the body (i.e., by increasing the porosity).

The quantity of pores as well as the shape and size distribution influence thermal conductivity. There are two distinct textures of pores: cellular and granular. Cellular texture has pores enclosed by the walls of the solid matrix, while in the granular texture a film of air surrounds the particles except at points where the particles are bonded together. Granular texture is likely to lead to open channels between the pores, resulting in gas permeability through the insulating material. Hot gas diffusing through the open channels can be a significant mode of heat transfer, thereby increasing thermal conductivity. This type of heat transfer will be particularly important if there is a difference in gas pressure across the insulating material. It is desirable to have low permeability to reduce thermal conductivity.

The effect of pore size is important in determining thermal conductivity. Heat can be transferred across pores by conduction, radiation, and convection. Convection becomes significant only when the pore size is large; most insulating materials are manufactured with pores small enough to ensure that this mode of heat transfer is negligible. Obviously, as porosity increases it eventually reaches a point where convention becomes a dominant transfer mode. At room temperature and slightly above, the actual conductivity of the air in the pores is the principal mode of heat transfer. Since the thermal conductivity of air is small, the resulting conductivity of the porous insulating material is considerably less than it would be for the same material in a pore-free form.

The idea of inducing porosity mechanically represents one of the most economical methods of creating porous materials. In one such approach, a mixture of solid materials, water, and a foaming agent, is mechanically beaten. A second method, which seems to have gained more attention, is to prepare the slip of water, deflocculating agent, and solid material plus binder separately from the foam, whereupon the two parts are mixed together to form a slurry. Bubble formation can be enhanced by blowing in air during the final mixing step. Forming is accomplished by casting the slurry into molds, where it is allowed to dry before firing. This method is an attractive way to produce a porosity-containing aggregate by crushing the fired product. It is difficult to use this method for introducing the porosity into the final shape because drying and firing shrinkage is large and variable.

A porous structure with small pores uniformly distributed can be achieved chemically by evolution of gas with the mixed slurry followed by stabilization of the bubble structure. The gas must be formed by reaction between two evenly and finely dispersed substances. Also, the rate of reaction must be slow, particularly immediately after mixing, so that the gas-producing substances can be incorporated properly before a significant amount of gas has evolved. Otherwise, much of the gas is lost during the mixing step. Mixtures of carbonates with acids such as dolomite and sulfuric acid have been used. Stabilization of the mixture to prevent bubbles from rising to the surface can be

accomplished by means of an additive that sets up in a short time, such as plaster of Paris. Alternatively, foaming agents can be added: the raw materials including the carbonates are first mixed together; then the dry material is mixed with dilute acid, which causes the effervescence. Shaping is accomplished by casting the resulting slip into molds, where it is left to dry.

The most common method of directly forming insulating bricks is by mixing a combustible or fugitive material in the mix before the heat treatment step. The combustible, such as sawdust, burns during firing, leaving open pores in the brick. Bricks can be shaped by classical procedures such as extrusion and semidry pressing. Since the combustible materials ignite and burn over a rather narrow temperature range, extreme care must be taken during firing. To reduce thermal conductivity, it is desirable to not have open channels between pores. To avoid sealing the combustible materials in the brick, which would cause bloating the firing schedule must be arranged to ensure that the combustibles are removed before the pores start sintering shut.

Thermal insulating oxide materials generally are of one of the following types:

1. A solid, continuous matrix containing porosity in either continuous or discontinuous form. This structure is usually rigid, in the form of brick or blocks. It can also be a castable (concrete) material, which is made rigid by adding water and casting the product in place.
2. A blanket or mat of fibers loosely placed together in several forms such as blown, spun, or woven fibers. In this case the material is flexible because the fibers are not bonded to each other.
3. A structure of fibers infiltrated with a material to bond the fibers together. Such materials can vary from flexible to reasonably rigid.

(ORVILLE HUNTER, JR.)

17.3.6.3.1. Castable and Brick Insulation.

Since thermal insulating capacity is created by having voids or pores in a product, a major part of the technology is associated with producing the pores. Pores can be introduced either by using an aggregate that is porous as an ingredient in a product or by introducing the pores directly into the final product. The most familiar of the aggregates are expanded vermiculite and perlite—naturally occurring minerals that exfoliate on rapid heating to form porous aggregate. Other aggregates are formed by various methods, some of which are proprietary. In one method dried clay pellets, with or without additives, are dropped through a vertical furnace, where the clay vitrifies and expands, forming an aggregate with a porous structure. Other methods for forming porosity include mechanical foaming of a wet slurry causing air bubbles to be trapped in the foam, and a chemical method whereby a gas, such as carbon dioxide, is released during the forming process to produce the necessary pores. These mechanically and chemically foamed materials can be used directly as insulating products after heat treatment, or they may be heat-treated and then crushed to form an aggregate for use in products such as castables.

(ORVILLE HUNTER, JR.)

17.3.6.3.2. Ceramic/Glass Fiber Blank Insulation.

There are two distinct types of ceramic/glass fiber. The first is commonly referred to as fiberglass. Other similar products (e.g., rock wool, glass wool, mineral wool) differ

mainly in the source and purity of the raw materials used for their production. All these products are designed for use at or near room temperature and typically serve as insulation for buildings. The second category of fibers consists of refractory ceramic fibers. These products are produced from high purity materials and are used for insulation at temperatures commonly as high as 1400°C and sometimes above 1600°C.

The most common methods of production of fiberglass and refractory ceramic fiber are spinning and blowing. In both methods the raw material is heated to a molten state at a temperature sufficiently high to ensure a flow. In the blowing method, a stream of molten material flows through an orifice in the bottom of the furnace. The stream is blasted with high pressure steam, which causes the stream of material to break up into small, fiber-shaped pieces. The fibers, which freeze immediately into a glass, retaining their shape, accumulate as a blanket of fiber on a moving belt. The steam-blowing step can be replaced in the process with spinning cylinders onto which the stream of molten material falls. The centrifugal force of the spinners causes the stream to break up into the fibers.

Commercially available fiberglass and refractory ceramic fibers produced by spinning and blowing are based on their ability to form glass, which is a function of their silica content. Fiberglass-type products generally contain various amounts of silica, alumina, alkaline earths, alkalies, and iron oxide. The refractory ceramic fibers are generally high purity silica–alumina or silica–alumina–zirconia compositions. As the amount of alumina increases, the use of temperature increases, but is limited by the difficulty of forming fibers as the silica content decreases.

A method for forming fibers that overcomes the difficulty described above is by sol–gel processing, which allows formation of fibers of nearly pure alumina and pure mullite. It also allows the formation of different fibers, such as stabilized zirconia fibers. In this process solutions, sols, gels, or suspensions of the desired fiber comosition are suspended in a suitable fugitive solvent with organic binders that burn out during treatment. The suspension is forced through orifices, forming fiber shapes at room temperature. The evaporation of the solvent leaves a fiber held together by the organic binder. This fiber is then heat-treated to remove the binder and, in some cases, to crystallize the fibers.

(ORVILLE HUNTER, JR.)

17.3.6.3.3. Bonded Fibers.

To gain the advantages of low density fibers and at the same time to have rigid or semirigid material, fibers can be bonded together by another material. The most common method of forming these shapes is by vacuum casting. The fibers, along with colloidal silica and an organic binder such as starch, are first mixed in a slurry. The starch causes the colloidal silica to become unstable and to precipitate. A vacuum is then drawn on one side of a screen, causing the water to be removed and the solid material to deposit onto the screen. The shape of the screen determines the shape of the piece. Drying causes the starch to give the piece enough strength for handling at room temperature; when the temperature increases, the silica creates bridges between the fibers, imparting significant strength to the pieces.

(ORVILLE HUNTER, JR.)

Further Reading

J. B. Dillion, *Thermal Insulation Recent Developments*, Noyes, Park Ridge, NJ, 1978.
J. I. Duffy, ed., *Refractory Materials Developments Since 1977*, Noyes *Data Corporation*, Park Ridge, NJ, 1980.
G. B. Rothenberg, *Refractory Materials*, Noyes, Park Ridge, NJ, 1976.
E. Ryshkewitch, 'Features of BeO ceramics,' *Powder Metall. Int.*, *1*(2), 1969.
F. Singer, S. Singer, *Industrial Ceramics*, Chemical Publishing, New York, 1963.

17.3.7. Preparation of Solid State Electrolytes

Electrochemical devices and systems based on solid state polycrystalline ceramic electrolytes find numerous applications including oxygen sensors, advanced secondary energy storage batteries, power-generating fuel cells, thermoelectric power generation devices, electrowinning and/or purification of sodium, and separation of oxygen from air. For example, sodium ion conducting β''-alumina electrolytes are being developed for energy storage beta-batteries based on the Na/S and Na/Ni/$NiCl_2$ anode–cathode couples[1,2]. These batteries have potential applications as rechargeable traction and energy storage batteries in electric vehicles and electric utility load-leveling systems, respectively. This electrolyte is also the key electrolyte element in the alkali metal thermoelectric converter (AMTEC) or sodium heat engine (SHE), which converts waste heat directly into electrical energy at high efficiency[3]. Oxygen ion conductors such as stabilized zirconia are used as the electrolyte in oxygen sensors for the control of combustion processes in automotive engines and heating systems and in the control of oxygen concentration in the processing and purification of metals and alloys during melting and solidification. This electrolyte is the key element in the development of the high temperature solid oxide fuel cell (SOFC), which directly converts chemical energy in a gaseous fuel such as H_2, CO, CH_4, or CH_3OH into electrical power (i.e., electrochemical oxidation of the fuel gas into CO_2 and/or H_2O)[1,4]. Solid state electrolytes, which are conductive to specific ions such as sodium and oxygen, also have potential applications in industrial electrochemical processing such as the electrowinning and/or purification of sodium and the separation of oxygen from air in "oxygen-pumping" devices[5].

The field of solid state electrolytes is enormous and has great potential for commercial exploitation. Solid electrolytes can be prepared which are conductive with respect to a host of ionic species including but not limited to Na^+, O^{2-}, Li^+, protonic species, K^+, Ag^+, and other monovalent, divalent, and trivalent cations as well as anions in the halogen family. To cover the preparation of all these materials would be a task far beyond the scope of this review. Consequently, considerable attention is given to the preparation of two solid electrolytes: Na β''-alumina, a sodium ion conductor, and stabilized zirconia, an oxygen ion conductor. Both these solid electrolytes are projected to have, or currently have, widespread use in sensors, storage batteries, fuel cells, other power generation devices, as well as in industrial processing. Some attention is given to other possibly competing sodium and oxygen ion conductors such as NASICON ($Na_3Zr_2PSi_2O_{12}$), bismuth oxide, and cerium oxide. A few comments are made about ceramic proton and lithium ion conductors which, over time, may emerge as viable solid electrolytes for energy storage and power generation devices. Finally, because of their relative ease of fabrication, ionic conducting glasses have received some attention. Accordingly, sodium ion conducting glasses such as sodium borosilicate and NASIGLAS ($Na_{0.84}Al_{0.16}Zr_{0.05}Si_{0.45}O_{1.66}$) are discussed briefly.

Inorganic Reactions and Methods, Volume 18
Edited by J. J. Zuckerman, Jim D. Atwood

Further Reading

J. B. Dillion, *Thermal Insulation Recent Developments*, Noyes, Park Ridge, NJ, 1978.
J. I. Duffy, ed., *Refractory Materials Developments Since 1977*, Noyes *Data Corporation*, Park Ridge, NJ, 1980.
G. B. Rothenberg, *Refractory Materials*, Noyes, Park Ridge, NJ, 1976.
E. Ryshkewitch, 'Features of BeO ceramics,' *Powder Metall. Int.*, *1*(2), 1969.
F. Singer, S. Singer, *Industrial Ceramics*, Chemical Publishing, New York, 1963.

17.3.7. Preparation of Solid State Electrolytes

Electrochemical devices and systems based on solid state polycrystalline ceramic electrolytes find numerous applications including oxygen sensors, advanced secondary energy storage batteries, power-generating fuel cells, thermoelectric power generation devices, electrowinning and/or purification of sodium, and separation of oxygen from air. For example, sodium ion conducting β''-alumina electrolytes are being developed for energy storage beta-batteries based on the Na/S and Na/Ni/$NiCl_2$ anode–cathode couples[1,2]. These batteries have potential applications as rechargeable traction and energy storage batteries in electric vehicles and electric utility load-leveling systems, respectively. This electrolyte is also the key electrolyte element in the alkali metal thermoelectric converter (AMTEC) or sodium heat engine (SHE), which converts waste heat directly into electrical energy at high efficiency[3]. Oxygen ion conductors such as stabilized zirconia are used as the electrolyte in oxygen sensors for the control of combustion processes in automotive engines and heating systems and in the control of oxygen concentration in the processing and purification of metals and alloys during melting and solidification. This electrolyte is the key element in the development of the high temperature solid oxide fuel cell (SOFC), which directly converts chemical energy in a gaseous fuel such as H_2, CO, CH_4, or CH_3OH into electrical power (i.e., electrochemical oxidation of the fuel gas into CO_2 and/or H_2O)[1,4]. Solid state electrolytes, which are conductive to specific ions such as sodium and oxygen, also have potential applications in industrial electrochemical processing such as the electrowinning and/or purification of sodium and the separation of oxygen from air in "oxygen-pumping" devices[5].

The field of solid state electrolytes is enormous and has great potential for commercial exploitation. Solid electrolytes can be prepared which are conductive with respect to a host of ionic species including but not limited to Na^+, O^{2-}, Li^+, protonic species, K^+, Ag^+, and other monovalent, divalent, and trivalent cations as well as anions in the halogen family. To cover the preparation of all these materials would be a task far beyond the scope of this review. Consequently, considerable attention is given to the preparation of two solid electrolytes: Na β''-alumina, a sodium ion conductor, and stabilized zirconia, an oxygen ion conductor. Both these solid electrolytes are projected to have, or currently have, widespread use in sensors, storage batteries, fuel cells, other power generation devices, as well as in industrial processing. Some attention is given to other possibly competing sodium and oxygen ion conductors such as NASICON ($Na_3Zr_2PSi_2O_{12}$), bismuth oxide, and cerium oxide. A few comments are made about ceramic proton and lithium ion conductors which, over time, may emerge as viable solid electrolytes for energy storage and power generation devices. Finally, because of their relative ease of fabrication, ionic conducting glasses have received some attention. Accordingly, sodium ion conducting glasses such as sodium borosilicate and NASIGLAS ($Na_{0.84}Al_{0.16}Zr_{0.05}Si_{0.45}O_{1.66}$) are discussed briefly.

To place into perspective the solid state electrolytes, Table 1 compares the ionic resistivities of a broad range of ionic conducting solids[1,2,6–29]. The data in this table are separated into five categories: aqueous electrolytes, single crystal sodium ion conductors (β-alumina and β''-alumina), polycrystalline and glassy sodium ion conductors, polycrystalline oxygen ion conductors, and polycrystalline hydrogen ion (proton) conductors. The sodium ion conductors cover the β/β''-aluminas, NASICON, and conducting glasses. The oxygen ion conductors in Table 1 cover a broad class of compounds with the face-centered-cubic, cubic fluorite, perovskite, and pyrochlore crystal structures. The most important of these with the lowest ionic resistivities are those based on ZrO_2, CeO_2, and Bi_2O_3.

For an ionic conducting solid electrolyte to be seriously considered for use in a practical electrochemical device, which operates at a given temperature T, the maximum value for the area-specific resistance R_{as} should be about $0.5\ \Omega \cdot cm^2$. R_{as} is the product of the electrolyte resistivity ρ at T in ohm-centimeters and the membrane thickness t (cm) in the direction of current flow. Table 2 lists maximum limits on electrolyte resistivity for various electrolyte membrane thicknesses.

We can conclude from the calculations summarized in Table 2 that electrochemical devices, which use solid electrolytes in bulk form with relatively thick walls (1–2 mm), require ionic resistivities on the order of $3–5\ \Omega \cdot cm$ at operating temperature (a very stringent requirement, which excludes many of the materials in Table 1). Devices that involve thin membranes ($\sim 500\ \mu m$) or thin films ($\leq 100\ \mu m$) can tolerate higher electrolyte resistivities (i.e., $10–250\ \Omega \cdot cm$, depending on the membrane or film thickness) and thus permit a wider selection of the materials given in Table 1.

With the conductivity of an aqueous electrolyte (e.g., 1N KCl) serving as a reference, comparable conductivities can be achieved in solid electrolytes under certain conditions. Some of the best solid ionic conductors, commonly referred to as "superionic conductors", have resistivities comparable to those of aqueous electrolytes at room temperature (e.g., $RbAg_4I_5$ and single crystal MgO-stabilized β''-alumina). However, they are either in the form of single crystals, which is impractical for most applications, or composed of very expensive and relatively unstable materials. Resistivities comparable to those of aqueous electrolytes can be achieved in solid electrolytes at higher temperatures in both superionic conductors like β''-alumina (i.e., 300°C) and normal ionic conductors such as stabilized zirconia (800–1000°C), stabilized cerium oxide (≥ 800°C), and stabilized bismuth oxide (≥ 600°C). Sodium ion conducting glasses are much less conductive than polycrystalline β''-alumina.

The data in Table 1 also illustrate several additional facets of solid state ionic conduction. First the fast (or super) ion conductors are characterized by very low activation energies for conduction (12–36 kJ/mol) compared to the "normal" ionic conductors (> 60 kJ/mol). The low activation energy for superionic conduction is a major contributing factor to the high ionic conductivity at relatively low temperatures.

Omitted from consideration in this section are solid electrolytes that are based on the dispersion of a normal ionic conductor (e.g., LiI, LiCl) in an insulating phase (e.g., Al_2O_3, SiO_2)[30]. Resistivities in these dispersed systems are very attractive ($< 10\ \Omega \cdot cm$ at 300°C) for applications principally in primary energy batteries (i.e., single discharge), which operate at very low discharge current densities ($< \sim 5\ mA/cm^2$). The β-alumina and zirconia electrolytes operate in devices (e.g., secondary rechargeable batteries, power generation devices) having current densities in excess of $100\ mA/cm^2$ and, for short periods of time, up to $1000\ mA/cm^2$.

TABLE 1. IONIC RESISTIVITIES OF SOLID ELECTROLYTES

Material	Resistivity ($\Omega \cdot$ cm)	Activation Energy (kJ/mol)	Ref.
KCl (aqueous)	~ 10 (at 25°C)	—	6
$RbAg_4I_5$ (Polycrystal) (Ag^+ ion conductor)	~ 4 (at 25°C)	12	7, 8
Single Crystal β-Alumina and β''-Alumina (at 25°C)			
β''-Alumina			
$Na_{1.67}Mg_{0.67}Al_{10.33}O_{17}$ (Na^+ ion conductor)	21 (20°C)	Variable	9, 10
β-Alumina			
$Na_{1.16}Al_{11}O_{17.08}$ (Na^+ ion conductor)	72	~ 15	9–11
$AgAl_{11}O_{17}$ (Ag^+ ion conductor)	150	~ 16	9
$KAl_{11}O_{17}$ (K^+ ion conductor)	1.5×10^4	28	12
$LiAl_{11}O_{17}$ (Li^+ ion conductor)	10^5	35	12
Polycrystalline and Glassy Na^- Ion Conductors (at 300°C)			
β''-Alumina			
$Na_{1.76}Li_{0.38}Al_{10.62}O_{17}$	670 (22°C)	~ 30	10
$Na_{1.76}Li_{0.38}Al_{10.62}O_{17}$	4–5	~ 22	10
$Na_{1.67}Li_{0.67}Al_{10.33}O_{17}$	6–7	—	1
Mixed Li_2O–MgO stabilization	6–7	~ 24	10
β-Alumina			
$Na_{1.6}Al_{11}O_{17.3}$	$> 10^3$ (22°C)	~ 30	10
$Na_{1.6}Al_{11}O_{17.3}$	17	~ 15	10
Other Na^- ion conductors			
$Na_3Zr_2PSi_2O_{12}$ (NASICON)	4–5	~ 23	13–16
$Na_5YSi_4O_{12}$	7	~ 14	13
Sodium borosilicate glass	20,000	—	2, 17
NASIGLAS	140	49	1
Polycrystalline Oxygen Ion Conductors (1000°C)			
Bi_2O_3 + 25 mol % Y_2O_3	0.9	64	18
Cubic fluorite			
CeO_2 + 20 mol % Sm_2O_3	3.6	12	19
CeO_2 + 20 mol % Gd_2O_3	5.6	44	19
CeO_2 + 20 mol % Y_2O_3	12	26	19
ZrO_2 + 10 mol % Sc_2O_3	4	63	20
ZrO_2 + 4 mol % Y_2O_3 + 4 mol % Yb_2O_3	7	79	21
ZrO_2 + 8 mol % Y_2O_3	10	96	20
ZrO_2 + 10 mol % Y_2O_3	15	77	21
ZrO_2 + 15 mol % CaO	58	117	20
HfO_2 + 8 mol % Y_2O_3	34	108	20
HfO_2 + 12 mol % CaO	250	138	20
ThO_2 + 7.5 mol % Y_2O_3	135	115	22
ThO_2 + 15 mol % CaO	1086	107	20
Pervoskite			
$BaCeO_3$ + 10 mol % Gd_2O_3	200	—	23, 24
Pyrochlore			
$Gd_2Zr_2O_7$	100	—	25
$Sm_2Zr_2O_7$	200	—	26
Polycrystalline Hydrogen Ion (Proton) Conductors (1000°C)			
$BaCe_{0.9}Nd_{0.1}O_{3-\delta}$	25	—	27
$SrCe_{0.9}Y_{0.1}O_{3-\delta}$	100	—	28
$BaThO_3 + Nd_2O_3$	< 10	—	29

TABLE 2. MAXIMUM ELECTROLYTE RESISTIVITY, $R_{as} \leq 0.5\ \Omega \cdot cm^2$

t (μm)	t (mm)	Maximum Resistivity ($\Omega \cdot cm$)
2000	2	2.5
1000	1	5
500	0.5	10
100	0.1	50
50	0.05	100
20	0.02	250

Lithium ion conductors are very much desired in commercial applications because of the relatively high open circuit voltages (up to 4 V) that can be achieved in electrochemical devices employing lithium-based anodes with high chemical activities (or chemical potentials). Many of the polycrystalline lithium-based solid electrolytes, that have been studied to date have ionic resistivities at 300°C in the range between 20 and 200 $\Omega \cdot cm$[1-3]. While thin-film applications for these materials are possible, the biggest drawback associated with lithium ion conductors is their chemical and electrochemical instability over time at temperatures of interest in environments very high in lithium chemical activity.

Many polycrystalline ceramic electrolytes are prepared in bulk form (with wall thicknesses >500–1500 μm) by processes that involve the following basic steps: (1) powder synthesis and treatment (calcining, milling, etc.); (2) green forming of the powder into the desired shape by isostatic pressing, slip casting, extrusion, electrophoretic deposition, and tape casting; and (3) firing (sintering) and subsequent heat treatment[2]. Sometimes solid electrolytes are prepared in the form of thin membranes (300–500 μm) or as thin films (10–100 μm) by chemical vapor deposition (CVD), electrochemical vapor deposition (EVD), slurry coating, and other related techniques[4]. All these processes are described in some detail for polycrystalline sodium β''-alumina and stabilized zirconia. They also are described briefly for some of the alternative sodium and oxygen ion ceramic electrolytes. The section concludes with a brief discussion on polycrystalline ceramic proton conductors.

(R. S. GORDON)

1. R. S. Gordon, W. Fischer, A. V. Virkar, in *Ceramic Transactions*: Vol. 65, *Role of Ceramics in Advanced Electrochemical Systems*, P. N. Kumpta, G. S. Roher, U. Balachadran, eds., American Ceramic Society, Westerville, OH, 1996, pp. 203–237. Current review on the application of ceramics in the sodium sulfur battery and the solid oxide fuel cell.
2. J. L. Sudworth, A. R. Tilley, eds., *The Sodium Sulfur Battery*, Chapman & Hall, New York, 1985. Excellent overview of sodium–sulfur battery including its design and important components.
3. N. Weber, *Energy Convers., 14*, 1 (1974).
4. N. Q. Minh, *J. Am. Ceram. Soc., 76*, 563 (1993). Excellent review of the solid oxide fuel cell including a thorough treatment of the ceramic components (electrolyte, anode, cathode, and interconnect).
5. A. C. Khandkar, A. V. Joshi, *Electrochem. Soc. Interface, 2*, 26 (1993).
6. J. Mackowiak, *Physical Chemistry for Metallurgists*, American Elsevier, New York, 1965.
7. J. N. Bradley, P. D. Green, *Trans. Faraday Soc., 63*, 424 (1967).
8. B. B. Owens, G. R. Argue, *Science, 157*, 308 (1967).

9. J. T. Kummer, *Prog. Solid State Chem., 7*, 141 (1972). Excellent exposition on the β-alumina and β″-alumina electrolytes.
10. G. R. Miller, D. G. Paquette, *National Bureau of Standards Bulletin*, NSRDS-NBS 61, Part III (1979). Thorough compilation on the properties of the β/β″-aluminas.
11. M. S. Whittingham, R. A. Huggins, *J. Chem. Phys., 54*, 414 (1971).
12. G. C. Farrington, in *Membrane Transport Processes*, Vol. I, C. Stevens, R. Ister, eds. Raven Press, New York, 1979, pp. 43–71.
13. R. S. Gordon, G. R. Miller, T. D. Hadnagy, B. J. McEntire, J. R. Rasmussen, in *Energy and Ceramics*, P. Vincenzini, ed., Elsevier Scientific Publishing, New York, 1980, pp. 925–949. Thorough review on the application of ceramics in in high performance batteries.
14. G. R. Miller, B. J. McEntire, T. D. Hadnagy, J. R. Rasmussen, R. S. Gordon, A. V. Virkar, in *Fast Ion Transport in Solids*, P. Vashishta, J. N. Mundy, G. D. Shenoy, eds. Elsevier North Holland, New York, 1979, pp. 83–86.
15. R. S. Gordon, G. R. Miller, B. J. McEntire, E. D. Beck, J. R. Rasmussen, *Solid State Ionics, 3–4*, 243 (1981).
16. B. J. McEntire, R. A. Bartlett, G. R. Miller, R. S. Gordon, *J. Am. Ceram. Soc., 66*, 738 (1983).
17. I. Bloom, G. H. Kucera, S. Bradley, P. A. Nelson, M. F. Roche, in *Symposium Proceedings*, Vol. 87-5: *Sodium-Sulfur Batteries*, A. R. Langrebe, R. D. Weaver, R. K. Sen, eds., Electrochemical Society, Pennington, NJ, 1987, pp. 125–141.
18. T. Takahashi, H. Iwahara, T. Arao, *J. Appl. Electrochem., 5*, 187 (1975).
19. H. Yahiro, E. Eguchi, H. Arai, *Solid State Ionics, 36*, 71 (1989).
20. T. H. Etsell, S. N. Flengas, *Chem. Rev., 70*, 339 (1970). Thorough review of oxide electrolytes.
21. F. J. Rohr, in *Solid Electrolytes*, P. Hagenmuller, W. van Gool, eds., Academic Press, New York, 1978, pp. 431–449. Excellent overview of solid oxide fuel cell.
22. J. W. Patterson, E. C. Bogren, R. A. Rapp, *J. Electrochem. Soc., 114*, 752 (1967).
23. N. Bonanos, B. Ellis, K. S. Knight, M. N. Mahmood, Solid State Ionics, *35*, 179 (1989).
24. N. Bonanos, B. Ellis, M. N. Mahmood, *Solid State Ionics, 44*, 305 (1991).
25. H. L. Tuller, P.K. Moon, *Mater. Sci. Eng. B, 1*, 171 (1988).
26. J. A. Kilner, R.J. Brook, *Solid State Ionics, 6*, 237 (1982).
27. H. Iwahara, H. Uchida, K. Ono, K. Ogaki, J. *Electrochem. Soc., 135*, 529 (1988).
28. H. Iwahara, T. Esaka, H. Uchida, N. Maeda, *Solid State Ionics, 3–4*, 359 (1981).
29. T. Tsui, T. Suzuki, H. Iwahara, *Solid State Ionics, 70–71*, 291 (1994).
30. C. C. Liang, A. V. Joshi, N. E. Hamilton, *J. Appl. Electrochem., 8*, 445 (1978).

17.3.7.1. β-Alumina Ceramic Electrolytes

The term, "β-alumina" refers to either of two closely related compounds with spinel-type layer structures[1–3]. These are β-alumina and β″-alumina, found in the binary system Na_2O–Al_2O_3 and within boundaries of certain ternary systems involving Al_2O_3, Na_2O, Li_2O, or MgO. Ternary oxides of special interest are spinel formers with Al_2O_3, the primary ones of interest being Li_2O and MgO. Small amounts of these oxides stabilize the β″ phase at high temperatures ($\leq$1600°C), where rapid densification (sintering) is possible. The terms β and β″ are misnomers. These compounds are not polymorphs of Al_2O_3. Early X-ray and chemical investigations of these materials failed to detect the presence of Na_2O which is present in amounts up to 9–13 mol %.

Compounds in the β/β″ family permit not only fast Na ion diffusion but also rapid transport of other monovalent ions[3,4] (e.g., K^+, Ag^+, Cu^+, Cs^+, Rb^+), hydronium ions (H_3O^+), divalent ions (e.g., Ca^{2+}, Ba^{2+}) and trivalent cations[5,6]. As it turns out, the Na ion has the highest mobility in these two structures. The sodium β-alumina and β″-alumina compounds are nonstoichiometric aluminates that are derivatives of the yet unknown stoichiometric sodium aluminate, $NaAl_{11}O_{17}$ ($Na_2O \cdot 11Al_2O_3$), with an excess of Na_2O.

These two basic compounds consist of "cubic" Al–O spinel blocks, similar to the $MgAl_2O_4$ structure, wherein trivalent aluminum ions are located in the octahedrally and

Inorganic Reactions and Methods, Volume 18
Edited by J. J. Zuckerman, Jim D. Atwood

9. J. T. Kummer, *Prog. Solid State Chem., 7*, 141 (1972). Excellent exposition on the β-alumina and β″-alumina electrolytes.
10. G. R. Miller, D. G. Paquette, *National Bureau of Standards Bulletin*, NSRDS-NBS 61, Part III (1979). Thorough compilation on the properties of the β/β″-aluminas.
11. M. S. Whittingham, R. A. Huggins, *J. Chem. Phys., 54*, 414 (1971).
12. G. C. Farrington, in *Membrane Transport Processes*, Vol. I, C. Stevens, R. Ister, eds. Raven Press, New York, 1979, pp. 43–71.
13. R. S. Gordon, G. R. Miller, T. D. Hadnagy, B. J. McEntire, J. R. Rasmussen, in *Energy and Ceramics*, P. Vincenzini, ed., Elsevier Scientific Publishing, New York, 1980, pp. 925–949. Thorough review on the application of ceramics in in high performance batteries.
14. G. R. Miller, B. J. McEntire, T. D. Hadnagy, J. R. Rasmussen, R. S. Gordon, A. V. Virkar, in *Fast Ion Transport in Solids*, P. Vashishta, J. N. Mundy, G. D. Shenoy, eds. Elsevier North Holland, New York, 1979, pp. 83–86.
15. R. S. Gordon, G. R. Miller, B. J. McEntire, E. D. Beck, J. R. Rasmussen, *Solid State Ionics, 3–4*, 243 (1981).
16. B. J. McEntire, R. A. Bartlett, G. R. Miller, R. S. Gordon, *J. Am. Ceram. Soc., 66*, 738 (1983).
17. I. Bloom, G. H. Kucera, S. Bradley, P. A. Nelson, M. F. Roche, in *Symposium Proceedings*, Vol. 87-5: *Sodium-Sulfur Batteries*, A. R. Langrebe, R. D. Weaver, R. K. Sen, eds., Electrochemical Society, Pennington, NJ, 1987, pp. 125–141.
18. T. Takahashi, H. Iwahara, T. Arao, *J. Appl. Electrochem., 5*, 187 (1975).
19. H. Yahiro, E. Eguchi, H. Arai, *Solid State Ionics, 36*, 71 (1989).
20. T. H. Etsell, S. N. Flengas, *Chem. Rev., 70*, 339 (1970). Thorough review of oxide electrolytes.
21. F. J. Rohr, in *Solid Electrolytes*, P. Hagenmuller, W. van Gool, eds., Academic Press, New York, 1978, pp. 431–449. Excellent overview of solid oxide fuel cell.
22. J. W. Patterson, E. C. Bogren, R. A. Rapp, *J. Electrochem. Soc., 114*, 752 (1967).
23. N. Bonanos, B. Ellis, K. S. Knight, M. N. Mahmood, Solid State Ionics, *35*, 179 (1989).
24. N. Bonanos, B. Ellis, M. N. Mahmood, *Solid State Ionics, 44*, 305 (1991).
25. H. L. Tuller, P.K. Moon, *Mater. Sci. Eng. B, 1*, 171 (1988).
26. J. A. Kilner, R.J. Brook, *Solid State Ionics, 6*, 237 (1982).
27. H. Iwahara, H. Uchida, K. Ono, K. Ogaki, J. *Electrochem. Soc., 135*, 529 (1988).
28. H. Iwahara, T. Esaka, H. Uchida, N. Maeda, *Solid State Ionics, 3–4*, 359 (1981).
29. T. Tsui, T. Suzuki, H. Iwahara, *Solid State Ionics, 70–71*, 291 (1994).
30. C. C. Liang, A. V. Joshi, N. E. Hamilton, *J. Appl. Electrochem., 8*, 445 (1978).

17.3.7.1. β-Alumina Ceramic Electrolytes

The term, "β-alumina" refers to either of two closely related compounds with spinel-type layer structures[1–3]. These are β-alumina and β″-alumina, found in the binary system Na_2O–Al_2O_3 and within boundaries of certain ternary systems involving Al_2O_3, Na_2O, Li_2O, or MgO. Ternary oxides of special interest are spinel formers with Al_2O_3, the primary ones of interest being Li_2O and MgO. Small amounts of these oxides stabilize the β″ phase at high temperatures ($\leq$1600°C), where rapid densification (sintering) is possible. The terms β and β″ are misnomers. These compounds are not polymorphs of Al_2O_3. Early X-ray and chemical investigations of these materials failed to detect the presence of Na_2O which is present in amounts up to 9–13 mol %.

Compounds in the β/β″ family permit not only fast Na ion diffusion but also rapid transport of other monovalent ions[3,4] (e.g., K^+, Ag^+, Cu^+, Cs^+, Rb^+), hydronium ions (H_3O^+), divalent ions (e.g., Ca^{2+}, Ba^{2+}) and trivalent cations[5,6]. As it turns out, the Na ion has the highest mobility in these two structures. The sodium β-alumina and β″-alumina compounds are nonstoichiometric aluminates that are derivatives of the yet unknown stoichiometric sodium aluminate, $NaAl_{11}O_{17}$ ($Na_2O \cdot 11Al_2O_3$), with an excess of Na_2O.

These two basic compounds consist of "cubic" Al–O spinel blocks, similar to the $MgAl_2O_4$ structure, wherein trivalent aluminum ions are located in the octahedrally and

tetrahedrally coordinated interstices defined by the close packing of oxygen ions. The unit cell of β-alumina consists of two of these spinel blocks while the unit cell of the β″-alumina structure has three spinel blocks. The main difference between the β and β″ structures is that β-alumina contains two spinel-like structures related by a twofold screw axis in a hexagonal unit cell, whereas β″-alumina has three spinel-like structures related by a threefold screw axis of rhombohedral symmetry. The spinel blocks in these structures are connected along the "c" axes by bridging oxygen ions, situated at widely spaced intervals in the conduction planes.

The conducting ions, such as Na^+, populate the planes between the spinel blocks. For optimum two-dimensional ion conduction in these planes, it is preferable that not all the available sites be occupied by the mobile cations. As the temperatures increases, the mobile ions in these conducting planes become disordered and occupy positions at random. The ionic mobility of the Na^+ in these planes is higher in the β structure than it is in the β″ structure because of the particular configuration of the bridging oxygen ions that act as obstacles to ionic motion within the plane. Na ion conduction is anisotropic and two-dimensional within these conduction planes for both the β and β″ structures. No ionic conduction exists in a direction perpendicular to the conduction plane.

In the β″-alumina structure, the phase is stabilized at high temperatures by small amounts of monovalent (e.g., Li_2O) or divalent (e.g., MgO, ZnO, NiO) oxides[7,8]. In these stabilized structures, the cation dopant substitutes directly for trivalent aluminum ions in the spinel block (i.e., Li''_{Al}, Mg'_{Al}) and is electrically compensated by additional sodium ions ($Na_i^{\bullet}$) in the conduction plane.

Monovalent ion stabilized β″-alumina is represented by the general composition $Na_{1+2z}Li_zAl_{11-z}O_{17}$, in which Li_2O is incorporated into the β-alumina structure by the following defect reaction, using Kroger–Vink notation:

$$Li_2O + 2Na_2O = 2Li''_{Al} + 3O_O + 4Na_i^{\bullet} \qquad \text{(a)}$$

The optimum sodium ion conductivity in lithia-stabilized β″-alumina occurs at $z \sim 0.33$, which corresponds to $Na_2O \cdot 0.2\,Li_2O \cdot 6.43Al_2O_3$ with approximately 13.1 mol % Na_2O and 2.6 mol % Li_2O.

Divalent ion-stabilized β″-alumina is represented by the general composition $Na_{1+y}M_yAl_{11-y}O_{17}$, where M can be Mg, Ni, or Zn. When $y = 1$, all the sodium ion sites in the conduction plane are filled. For optimum sodium ion conductivity, $y \approx 0.67$, which corresponds to $Na_2O \cdot 0.8\,MgO \cdot 6.19Al_2O_3$ with approximately 12.5 mol % Na_2O and 10 mol% MgO. MgO is incorporated into the β″-alumina crystal structure by the following defect reaction

$$2MgO + Na_2O = 2Mg'_{Al} + 3O_O + 2Na_i^{\bullet} \qquad \text{(b)}$$

Because of charge compensation effects, Li_2O stabilization leads to twice the number of additional sodium ions in the conduction planes (per mole of cation dopant) than is the case for MgO (or ZnO or NiO) stabilization. Li_2O and MgO can be intermixed in appropriate combinations to form a β″-alumina composition with mixed stabilization.

The β-alumina (two-block structure) can be represented by the general composition, $Na_{1+x}Al_{11}O_{17+x/2}$. A typical composition of β-alumina is $Na_{1.2}Al_{11}O_{17.1}$ ($Na_2O \cdot 9.165Al_2O_3$) with $x = 0.2$. The excess Na^+ ions in the conduction plane ($Na_i^{\bullet}$) are charge-compensated by oxygen ions in interstitial sites (i.e. O_i'' according to the following

defect incorporation reaction:

$$Na_2O = 2Na_i^{\cdot} + O_i'' \qquad (c)$$

The conductivity data in Table 1 of 17.3.7, show (1) that the Na^+ ion conductivity is higher in the monocrystalline form for each structural type and (2) that the Na^+ ion conductivity in the β'' phase is significantly higher than that in the β phase . The Na^+ ion conductivity in polycrystalline β''-alumina is comparable to that in monocrystal β-alumina. The higher ionic conductivity in the β'' structure compared to the β phase is due to the higher concentration and mobility of sodium ions in the conduction planes.

Grain boundaries offer some impedance to sodium ion conduction (i.e., approximately a factor of five increase for polycrystalline β''-alumina at 300°C)[9-12]. They also increase the activation energy for conduction by approximate factors of 1.6–2 depending on the temperature and grain size. Sodium ion grain boundary conduction is dominant in polycrystalline β''-alumina when the grain size is very small ($\leq$ 1–2 μm) and when the temperature is below ~100°C.

The activation energy for sodium ion conduction in monocrystalline β-alumina is approximately 15 KJ/mol. It is variable in monocrystalline β''-alumina and increases as the temperature is lowered[1]. In polycrystalline material, the activation energies are variable in both the β and β'' structures and decrease with temperature[1]. In general, they increase as the temperature and/or the grain size decreases, probably as a result of the increasing contributions of grain boundary conduction[10]. The activation energy for sodium ion grain boundary conduction in polycrystalline lithia-stabilized β''-alumina is approximately 32 KJ/mol[10].

The electrolyte material with the greatest technological interest is polycrystalline β''-alumina, stabilized with either Li_2O or MgO. Typical Na^+ ion resistivities of commercial materials at 300°C are in the range of 3.5–6.3 Ω·cm, depending on the exact composition, the stabilizer selected, grain size, crystallographic texture, storage conditions, and processing history[9]. Commercially viable β''-alumina electrolytes are ploycrystalline for several reasons:

1. Sodium ion conduction is anisotropic in single crystals, and large shapes with the proper orientation are very difficult and expensive to fabricate.
2. Single crystals are mechanically weak and cleave along the basal planes.
3. Ionic conductivity (although somewhat lower) is reasonably isotropic in polycrystalline "ceramic" materials, which can be fabricated economically with excellent mechanical properties.

The sodium ions in the β-type aluminas can be replaced by a host of monovalent and divalent ionic species (Ag^+, Cu^+, Li^+, K^+, Rb^+, Ba^{2+}, Sr^{2+}, Cd^{2+})[3-6]. In all cases the conductivity is decreased. These cation-substituted β-type aluminas may have some specific applications as selective ion sensors; however, very little is known about the preparation of these materials in the form of polycrystalline ceramics, other than by the ion exchange of sodium β and β'' single crystals (sometimes polycrystals) in various molten salts. These homologues, while interesting, have not been developed in polycrystalline form and are not discussed further.

(R. S. GORDON)

1. J. T. Kummer, *Prog. Solid State Chem.*, 7, 141 (1972).
2. N. Weber, in *Superionic Conductors*, G. D. Mahan, W. L. Roth, eds., Plenum Press, New York, 1976, pp. 37–46.

3. D. F. Shriver, G. C. Farrington, *Chem. News, 63*, 42 (1985).
4. G. C. Farrington, in *Membrane Transport Processes*, Vol. I. C Stevens, R. Ister, eds., Raven Press, New York, 1979, pp. 43–71.
5. B. Dunn, G. C. Farrington, *Mater. Res. Bull., 15*, 1773 (1980).
6. B. Dunn, R. M. Ostrom, R. Seevers, G. C. Farrington, *Solid State Ionics, 5*, 203 (1981).
7. G. M. Brown, D. A. Schwinn, J. B. Bates, W. E. Brundage, *Solid State Ionics, 5*, 147 (1981).
8. R. Collongues, J. Thery, J. P. Boilot, in *Solid Electrolytes*, P. Hagenmuller, W. VanGool, eds. Academic Press, New York, 1978, p. 273.
9. R. S. Gordon, W. Fischer, A.V. Virkar, in *Ceramics Transactions*, Vol. 65: *Role of Ceramics in Advanced Electrochemical Systems*, P. N. Kupta, G. S. Roher, Balachandran, eds., American Ceramic Society, Westerville, OH, 1996, pp. 203–237.
10. A. V. Virkar, G.R. Miller, R.S. Gordon, *J. Am. Ceram. Soc., 61*, 250 (1978).
11. G. E. Youngblood, R.S. Gordon, *Ceramurgia Int., 4*, 93 (1978).
12. G. E. Youngblood, G.R. Miller, R.S. Gordon, *J. Am. Ceram. Soc., 61*, 86 (1978).

17.3.7.1.1. Powder Synthesis and Treatment.

The most common technique used to prepare the β-type (i.e., β or β″) alumina is to mechanically blend the component oxides or precursor compounds in powder form prior to a calcination or prereaction step at temperatures between 1000° and 1260°C[1]. Commercially available aluminum oxide powders (0.3–0.5 μm average crystallite size) in the alpha (corundum) polymorph are typically used[1]. They are derived from three common sources: decomposition of gibbsite [$Al(OH)_3$], which is precipitated from soda liquors in the Bayer process; preparation and decomposition of alum salts; and preparation from aluminum chloride precursors[1]. Na_2CO_3 is usually the source of Na_2O. Sources of Li_2O have included Li_2CO_3, $LiNO_3$, and $Li_2C_2O_4$. MgO is usually added as the commercially available oxide.

Calcination at 1000°C results in the decomposition of salts with volatile constituents (e.g., carbonates, oxalates) with essentially negligible conversion of α-alumina to the β-type structures[2]. Higher temperature calcination ($\leq$1260°C) normally results in the conversion of α-alumina into a multiphase mixture of β-alumina and β″-alumina with smaller amounts of $NaAlO_2$, $LiAlO_2$, and unreacted α-alumina[2]. Because crystallite coarsening occurs during calcination, the powders must be milled (ball or vibratory milling) prior to forming, bisquing, sintering, and annealing to achieve a reactive (or sinterable) powder with an average particle size below 1 μm.

In the case of lithia-stabilized β″-alumina, a two-powder process (so-called zeta-process) is frequently employed to more uniformly distribute the minority stabilizing constituent (Li_2O). Lithium aluminate ($Li_2O \cdot 5Al_2O_3$) is prepared by blending and calcining 1260°C a blended mixture of Na_2CO_3 and α-alumina to form a soda-rich component with an alumina-to-soda mol ratio of approximately 5.24. The zeta and soda component powders are then milled together in the appropriate proportions to yield the desired composition, $Na_2O \cdot 0.2Li_2O \cdot 6.0Al_2O_3$, prior to firing with a slight soda excess (viz, 13.9 mol %). The improved distribution of lithium oxide in the precursor powders facilitates conversion to the β″ phase and control of exaggerated grain growth during the firing operation[2].

Zeta-process and conventionally calcined powders can be made flowable for rapid mold filling in automated isostatic pressing of thin-walled cylindrical tubes by the technique of slurry spray drying (S^2D). Here the calcined and milled precursor powder is dispersed in an aqueous slurry (i.e., a stable, high solids content, low viscosity suspension) prior to spray-drying[1,3] into spherical agglomerates.

Inorganic Reactions and Methods, Volume 18
Edited by J. J. Zuckerman, Jim D. Atwood

3. D. F. Shriver, G. C. Farrington, *Chem. News*, *63*, 42 (1985).
4. G. C. Farrington, in *Membrane Transport Processes*, Vol. I. C Stevens, R. Ister, eds., Raven Press, New York, 1979, pp. 43–71.
5. B. Dunn, G. C. Farrington, *Mater. Res. Bull.*, *15*, 1773 (1980).
6. B. Dunn, R. M. Ostrom, R. Seevers, G. C. Farrington, *Solid State Ionics*, *5*, 203 (1981).
7. G. M. Brown, D. A. Schwinn, J. B. Bates, W. E. Brundage, *Solid State Ionics*, *5*, 147 (1981).
8. R. Collongues, J. Thery, J. P. Boilot, in *Solid Electrolytes*, P. Hagenmuller, W. VanGool, eds. Academic Press, New York, 1978, p. 273.
9. R. S. Gordon, W. Fischer, A.V. Virkar, in *Ceramics Transactions*, Vol. 65: *Role of Ceramics in Advanced Electrochemical Systems*, P. N. Kupta, G. S. Roher, Balachandran, eds., American Ceramic Society, Westerville, OH, 1996, pp. 203–237.
10. A. V. Virkar, G.R. Miller, R.S. Gordon, *J. Am. Ceram. Soc.*, *61*, 250 (1978).
11. G. E. Youngblood, R.S. Gordon, *Ceramurgia Int.*, *4*, 93 (1978).
12. G. E. Youngblood, G.R. Miller, R.S. Gordon, *J. Am. Ceram. Soc.*, *61*, 86 (1978).

17.3.7.1.1. Powder Synthesis and Treatment.

The most common technique used to prepare the β-type (i.e., β or β″) alumina is to mechanically blend the component oxides or precursor compounds in powder form prior to a calcination or prereaction step at temperatures between 1000° and 1260°C[1]. Commercially available aluminum oxide powders (0.3–0.5 μm average crystallite size) in the alpha (corundum) polymorph are typically used[1]. They are derived from three common sources: decomposition of gibbsite [$Al(OH)_3$], which is precipitated from soda liquors in the Bayer process; preparation and decomposition of alum salts; and preparation from aluminum chloride precursors[1]. Na_2CO_3 is usually the source of Na_2O. Sources of Li_2O have included Li_2CO_3, $LiNO_3$, and $Li_2C_2O_4$. MgO is usually added as the commercially available oxide.

Calcination at 1000°C results in the decomposition of salts with volatile constituents (e.g., carbonates, oxalates) with essentially negligible conversion of α-alumina to the β-type structures[2]. Higher temperature calcination ($\leq$1260°C) normally results in the conversion of α-alumina into a multiphase mixture of β-alumina and β″-alumina with smaller amounts of $NaAlO_2$, $LiAlO_2$, and unreacted α-alumina[2]. Because crystallite coarsening occurs during calcination, the powders must be milled (ball or vibratory milling) prior to forming, bisquing, sintering, and annealing to achieve a reactive (or sinterable) powder with an average particle size below 1 μm.

In the case of lithia-stabilized β″-alumina, a two-powder process (so-called zeta-process) is frequently employed to more uniformly distribute the minority stabilizing constituent (Li_2O). Lithium aluminate ($Li_2O \cdot 5Al_2O_3$) is prepared by blending and calcining 1260°C a blended mixture of Na_2CO_3 and α-alumina to form a soda-rich component with an alumina-to-soda mol ratio of approximately 5.24. The zeta and soda component powders are then milled together in the appropriate proportions to yield the desired composition, $Na_2O \cdot 0.2Li_2O \cdot 6.0Al_2O_3$, prior to firing with a slight soda excess (viz, 13.9 mol %). The improved distribution of lithium oxide in the precursor powders facilitates conversion to the β″ phase and control of exaggerated grain growth during the firing operation[2].

Zeta-process and conventionally calcined powders can be made flowable for rapid mold filling in automated isostatic pressing of thin-walled cylindrical tubes by the technique of slurry spray drying (S^2D). Here the calcined and milled precursor powder is dispersed in an aqueous slurry (i.e., a stable, high solids content, low viscosity suspension) prior to spray-drying[1,3] into spherical agglomerates.

To eliminate the labor- and energy- intensive steps of calcination and milling, the technique of slurry–solution spray-drying (S^3D) has been developed to prepare β-alumina precursor powders with suitable rheological properties for automatic isostatic pressing[4–8]. In this technique soluble alkali salts (normally NaOH and LiOH) are dissolved in a stable, high solids content, low viscosity aqueous suspension of α-alumina powder. (In MgO stabilized material, MgO powder can be added directly to the slurry.) The slurry–solution is then spray-dried directly into powder form (spherical agglomerates), which is suitable for rapid mold filling and subsequent isostatic pressing. The removal of volatiles, reaction of the precursor phases to the β″ form, and densification of the formed ceramic article can then, in principle, be combined into a single continuous firing operation with the precalcination and milling operations removed from the fabrication scheme. Seeding additives and/or zirconia (undoped or partially stabilized) second phase additions, discussed later, can be easily incorporated into the S^3D processing route[3].

While the dry powder, S^2D, and S^3D processing routes have been developed at the pilot scale, there has been interest over the years in developing a process for the preparation of reactive (submicrometer) or sinterable single-phase β″ powders that are chemically homogeneous on an atomic or microscopic scale. The development of such a powder could, in principle, offer side benefits in electrolyte fabrication such as the elimination of postsintering annealing, a processing step currently required to complete phase conversion to single-phase β″-alumina with the requisite high sodium ion conductivity. Furthermore, a higher degree of chemical homogeneity might also permit the development of more uniform, fine-grained microstructures in the fired ceramic. With these goals in mind, several techniques have been investigated to synthesize chemically homogenous and submicrometer β″-alumina powders: oxalate coprecipitation, gel processing, solution spray-drying and freezing, and organometallic synthesis[9–11].

(i) Oxalate Coprecipitation. A insoluble coordination precursor compound (a trioxolatoaluminate anion complex) for lithia-stabilized β″-alumina that has the proper concentrations of Na and Li cations can, in principle, be prepared by the following precipitation reaction from an aqueous solution:

$$2Al(OH)_3 + 3M_2C_2O_4 + 3H_2C_2O_4 \longrightarrow 2M_3(Al(C_2O_4)_3) + 6H_2O \qquad (a)$$

in which $M = Li^+$, Na^+, and NH_4^+. A precipitate, which upon calcination gives the correct final stoichiometry (e.g. 8.9 wt % Na_2O, 0.8 wt % Li_2O) is obtained in a very low yield (~2%) based on Al_2O_3 input[9]. This technique is impractical for large-scale production because of the low yield, plus the sensitivity of precipitate stoichiometry to pH, dilution, and concentrations of Na and Li.

When compounds of this type are heated, the first crystalline phase to appear in the 700–1000°C temperature range is the so-called λ-$Na_2O \cdot xAl_2O_3$ phase (x varies from 3 to 12) with the mullite crystal structure[12]. This phase is the low temperature precursor to the β and β″ intergrowth phases, which begin to form at 1100°C[13]. At 1200°C all the λ phase converts to a mixture of the β and β″ phases.

(ii) Gel Processing. In this approach[9,14], an ethylene glycol–water solution of Na, Li, and Al citrates plus excess citric acid is heated to evaporate the excess solvent and form a rigid, transparent polyester gel according to the following reaction sequence:

$$(Al^{3+}, Na^+, Li^+)\text{ citrates} + \text{(excess) } HOCH_2CH_2OH$$

$$\xrightarrow{200°C} \text{polyester gel} \xrightarrow{600°C–1250°C} \beta\text{–}\beta'' \text{ precursor} \qquad (b)$$

Calcination of the gel above 600°C produces an amorphous white powder that also transforms to the λ phase on heating at 900–1000°C. At 1200°C the λ phase converts to a mixture of β and β″.

(iii) Solution Spray-Drying. In this technique[9,10], soluble salts (e.g., nitrates) of aluminium, sodium, and lithium are dissolved in water and then spray-dried into a dry powder. When the spray-dried powder is heated, the λ phase forms first and then transforms on further heating to the β phase (not β″) at 850–870°C. The amount of the β″ phase does not become appreciable until temperature exceeding 1200°C have been reached. The β″ phase is always observed in conjunction with the β phase, probably in the form of intergrowth structures[13].

(iv) Organometallic Synthesis. Here metal alkoxides are formed from reactant metals and appropriate alcohols[11,15] (e.g., the compounds $Mg(Al(OC_3H_7)_4)_2$ or $Al(OC_3H_7)_3$, $NaOC_3H_7$, and $LiOC_2H_5$). These alkoxides are then partially hydrolyzed (0.95 mol water/mol alkoxide). After hydrolysis, the alkali alkoxide solutions are added to the aluminium (with or without magnesium addition) alkoxide solution, resulting in reactions of the following type:

$$NaOH + Al(OR)_3 \longrightarrow Na\text{–}O\text{–}Al(OR)_2 + ROH \qquad (c)$$

Once the alkali alkoxide solutions have been added and the dispersed precipitate has been homogenized, the remaining alkoxides are precipitated by addition of methanol to form insoluble methoxides. Care must be taken to avoid segregation during precipitation due to differing solubilities and reactivities between the various metal alkoxides. When the desired precipitate is heated, the λ phase is again the first crystalline phase to form at temperatures below 600°C. The lambda-to-beta transition occurs at 700°C. No β″ phase formation occurs below 1200°C.

The foregoing powder synthesis techniques, along with others such as polymerization and decomposition of complex double alkoxides and the melt and spray decomposition of mixed nitrates, produce precursor powders with a high degree of chemical homogeneity. However upon subsequent calcination of the products of these reactions, the crystallization path invariably passes through the following sequence of reactions:

$$\text{homogeneous noncrystalline} \xrightarrow{< 600\text{–}1000^\circ C} \lambda \text{ phase}$$

$$\xrightarrow{700\text{–}1100^\circ C} \beta \text{ phase} \xrightarrow{> 1100\text{–}1200^\circ C} \beta\text{–}\beta'' \text{ intergrowth phases} \qquad (d)$$

While it may be possible to form homogeneous monophase β-alumina powders at temperatures below 1100°C, the feasibility of forming the desired β″-alumina phase at low temperatures in any from of stabilization is remote, at best. Furthermore, most of these techniques involve expensive reactants, employ elaborate processing schemes, and have, in some cases, very low reaction yields, features that detract further from their viability in the large-scale fabrication of ceramic electrolytes.

While attempts to synthesize single-phase β″-alumina at low temperatures have not been successful to date, these studies have given some insight on what precursor phases are stable or metastable in the low temperature region[11,13]. Finally, as will become apparent from the discussion on sintering and densification in the text section, a high degree of chemical homogeneity prior to densification, while desirable in the processing

of some ceramics such as stabilized zirconia, may not be the preferred starting point for β″-alumina processing[16].

(R. S. GORDON)

1. B. J. McEntire, G. R. Miller, R. S. Gordon, in *Processing of Metal and Ceramic Powders* (R. M. German, K. W. Lay, eds.,) *Conference Proceedings*, Metallurgical Society of AIME, Louisville, KY, Oct. 12–14, 1981, pp. 215–239.
2. G. E. Youngblood, A. V. Virkar, W. R. Cannon, R. S. Gordon, *Am. Ceram. Soc. Bull., 56*, 206 (1977).
3. M. L. Miller, B. J. McEntire, G. R. Miller, R. S. Gordon, *Am. Ceram. Soc. Bull., 58*, 522 (1979).
4. B. J. McEntire, R. H. Snow, A. V. Virkar, in *Symposium Proceedings*, Vol. 87-5: *Sodium–Sulfur Batteries*, A. R. Langrebe, R. D. Weaver, R. K. Sen, eds., Electrochemical Society, Pennington, N. J, 1987, pp. 95–107.
5. G. J. May, *J. Power Sources, 3*, 1 (1978).
6. S. R. Tan, G. J. May, *Sci. Ceram., 9*, 103 (1977)
7. D. W. Johnson Jr., S. M. Granstaff Jr., W. W. Rhodes, *Am. Ceram. Soc. Bull., 58*, 849 (1979).
8. E. M. Vogel, D. W. Johnson Jr., M. F. Yan, *Am. Ceram. Soc. Bull., 60*, 494 (1981).
9. M. L. Miller, R. S. Gordon, University of Utah, (unpublished work).
10. L. Stewart, *Phase Transformations of the $NaAlO_2$–Al_2O_3 System*, Honors B. S. thesis, University of Utah, Salt Lake City, 1976.
11. J. D. Hodge, *Bull. Am. Ceram. Soc., 62*, 244 (1983).
12. A. G. Elliot, R. A. Huggins, *J. Am. Ceram. Soc., 58*, 497 (1975).
13. P. E. D. Morgan, *Mater. Res. Bull., 11*, 233 (1976).
14. M. P. Pechini, U. S. Patent 3,330,697 (1967).
15. B. E. Yoldas, D. P. Partlow, *Bull Am. Ceram. Soc., 59*, 640 (1980).
16. A. D. Jatkar, I. B. Cutler, A. V. Virkar, R. S. Gordon, in *Processing of Crystalline Ceramics*, H. Palmour III, R. F. Davis, T. M. Hare, eds. Plenum Press, New York, 1978, pp. 421–431.

17.3.7.1.2. Forming (Green) of Tubular and Planar Shapes.

In the energy storage batteries and power generation devices under development, the most common geometric shape for the β″-alumina electrolyte is a thin-walled (1–2.5 mm) tube [15 mm < outer diameter (o.d.) < 50 mm, and lengths between 200 and 500 mm] closed at one end[1]. Three basic procedures have been employed for forming thin-walled electrolyte tubing closed at one end[2]: (1) isostatic pressing of powders prepared by (a) dry powder blending, calcining, and milling, (b) slurry spray-drying (S^2D) of powders prepared by (a), and (c) slurry–solution spray-drying (S^3D) of unconverted powders, (2) electrophoretic deposition (EPD) of prereacted and milled powders, and (3) extrusion.

Preliminary development work has been conducted on the tape casting of thin ($\leq$ 500 μm) plates of β″-alumina. For higher power outputs per unit volume, future designs for the electrolytes in these electrochemical energy storage and conversion systems will likely incorporate ceramics fabricated as thin ($\leq$ 0.5 mm), flat plates having linear dimensions up to 100 mm[1].

(i) Isostatic Pressing. Isostatic pressing is the technique most commonly used to fabricate thin-walled electrolyte tubing closed at one end[2–6]. It is typically accomplished with either prereacted (and milled) powders in the S^2D process or with unconverted powders in the S^3D process. Both these techniques were described in 17.3.7.1.1. Spray-drying is performed to improve the rheological properties of the powder for rapid, efficient, and uniform packing of isostatic pressing molds. Mold filling is very difficult and time-consuming with dry-blended, calcined, and milled powders that have not been made flowable by a technique such as spray-drying.

Inorganic Reactions and Methods, Volume 18
Edited by J. J. Zuckerman, Jim D. Atwood

of some ceramics such as stabilized zirconia, may not be the preferred starting point for β″-alumina processing[16].

(R. S. GORDON)

1. B. J. McEntire, G. R. Miller, R. S. Gordon, in *Processing of Metal and Ceramic Powders* (R. M. German, K. W. Lay, eds.,) *Conference Proceedings*, Metallurgical Society of AIME, Louisville, KY, Oct. 12–14, 1981, pp. 215–239.
2. G. E. Youngblood, A. V. Virkar, W. R. Cannon, R. S. Gordon, *Am. Ceram. Soc. Bull., 56*, 206 (1977).
3. M. L. Miller, B. J. McEntire, G. R. Miller, R. S. Gordon, *Am. Ceram. Soc. Bull., 58*, 522 (1979).
4. B. J. McEntire, R. H. Snow, A. V. Virkar, in *Symposium Proceedings*, Vol. 87-5: *Sodium–Sulfur Batteries*, A. R. Langrebe, R. D. Weaver, R. K. Sen, eds., Electrochemical Society, Pennington, N. J, 1987, pp. 95–107.
5. G. J. May, *J. Power Sources, 3*, 1 (1978).
6. S. R. Tan, G. J. May, *Sci. Ceram., 9*, 103 (1977)
7. D. W. Johnson Jr., S. M. Granstaff Jr., W. W. Rhodes, *Am. Ceram. Soc. Bull., 58*, 849 (1979).
8. E. M. Vogel, D. W. Johnson Jr., M. F. Yan, *Am. Ceram. Soc. Bull., 60*, 494 (1981).
9. M. L. Miller, R. S. Gordon, University of Utah, (unpublished work).
10. L. Stewart, *Phase Transformations of the $NaAlO_2$–Al_2O_3 System*, Honors B. S. thesis, University of Utah, Salt Lake City, 1976.
11. J. D. Hodge, *Bull. Am. Ceram. Soc., 62*, 244 (1983).
12. A. G. Elliot, R. A. Huggins, *J. Am. Ceram. Soc., 58*, 497 (1975).
13. P. E. D. Morgan, *Mater. Res. Bull., 11*, 233 (1976).
14. M. P. Pechini, U. S. Patent 3,330,697 (1967).
15. B. E. Yoldas, D. P. Partlow, *Bull Am. Ceram. Soc., 59*, 640 (1980).
16. A. D. Jatkar, I. B. Cutler, A. V. Virkar, R. S. Gordon, in *Processing of Crystalline Ceramics*, H. Palmour III, R. F. Davis, T. M. Hare, eds. Plenum Press, New York, 1978, pp. 421–431.

17.3.7.1.2. Forming (Green) of Tubular and Planar Shapes.

In the energy storage batteries and power generation devices under development, the most common geometric shape for the β″-alumina electrolyte is a thin-walled (1–2.5 mm) tube [15 mm < outer diameter (o.d.) < 50 mm, and lengths between 200 and 500 mm] closed at one end[1]. Three basic procedures have been employed for forming thin-walled electrolyte tubing closed at one end[2]: (1) isostatic pressing of powders prepared by (a) dry powder blending, calcining, and milling, (b) slurry spray-drying (S^2D) of powders prepared by (a), and (c) slurry–solution spray-drying (S^3D) of unconverted powders, (2) electrophoretic deposition (EPD) of prereacted and milled powders, and (3) extrusion.

Preliminary development work has been conducted on the tape casting of thin ($\leq$ 500 μm) plates of β″-alumina. For higher power outputs per unit volume, future designs for the electrolytes in these electrochemical energy storage and conversion systems will likely incorporate ceramics fabricated as thin ($\leq$ 0.5 mm), flat plates having linear dimensions up to 100 mm[1].

(i) Isostatic Pressing. Isostatic pressing is the technique most commonly used to fabricate thin-walled electrolyte tubing closed at one end[2–6]. It is typically accomplished with either prereacted (and milled) powders in the S^2D process or with unconverted powders in the S^3D process. Both these techniques were described in 17.3.7.1.1. Spray-drying is performed to improve the rheological properties of the powder for rapid, efficient, and uniform packing of isostatic pressing molds. Mold filling is very difficult and time-consuming with dry-blended, calcined, and milled powders that have not been made flowable by a technique such as spray-drying.

(ii) Electrophoretic Deposition (EPD). In the EPD process, calcined and vibratory-milled powders are dispersed in a dielectric organic liquid (e.g., amyl alcohol) in a stainless steel chamber and electrophoretically deposited on stainless steel mandrels into tabular shapes[4,7,8] closed at one end. Upon application of an electric field (~700 V/cm), negatively charged particles are deposited uniformly around the mandrel in a few minutes. After deposition, the tube is dried on the mandrel and released. The deposition step is rapid, while the drying step is rate limiting and dictates the number of mandrels for the required production output. The process is flexible and can be used to fabricate β″-alumina tubes with a range of dimensions: o.d., 5–40 mm; lengths, 9600 mm; wall thickness, 0.2–4.0 mm. A semiautomatic EPD process includes continuous powder calcining and an alcohol recovery process.

(iii) Extrusion. Extrusion[4,9,10] has been investigated as a possible forming process. Because of the problem of water-soluble components (Na_2O) in the β″-alumina precursor compounds, nonaqueous or polymeric binder systems are required. Lithia-stabilized β″-alumina tubing up to 10 mm o.d. and 300 mm long with wall thickness between 0.3 and 1.3 mm has been fabricated by extrusion starting with precalcined and milled powders. These tubes can be fired to acceptable properties. Unfortunately, extruded tubing is open at both ends and not compatible with current cell designs in various electrochemical devices. An ultrasonic technique for the bonding of β″ end caps to open-ended tubes prior to sintering has been developed[10].

(iv) Tape Casting. Tape casting of calcined and milled precursor powders has been used to prepare 300–500 μm thick plates of lithia-stabilized β″-alumina up to approximately 50 mm in diameter[1,11]. An organic-based solvent-binder/plasticizer-dispersant system has been developed for tape casting on polyester film substrates. The critical processing step is removal of the organics in the bisquing operation (40 h at 1200°C) prior to sintering. The resulting plates, after sintering at 1590° C followed by a postsintering anneal at lower temperatures, have Na^+ ion resistivities perpendicular to the plate of ~8.4 Ω cm (300°C). These are substantially higher than those in standard electrolyte tubing of the same composition (i.e., 4–5 Ω cm), indicating the possible presence of an unfavorably oriented crystallographic texture in the plates[12]. These plates can be fragile, and substantial work remains in the development of tape cast components with resistivities close to 5 Ω cm and strengths over 200 MPa, which are thin (<500 μm, preferably around 300 μm), flat, and of reasonable size (i.e., ≥100 mm).

(R. S. GORDON)

1. R. S. Gordon, W. Fischer, A. V. Virkar, in *Ceramic Transactions Role of Ceramics in Advanced Electrochemical Systems*, P. N. Kumpta, G. S. Roher, Balachandran, eds., American Ceramic Society, Westerville, OH, 1996, pp. 203–237.
2. J. L. Sudworth, A. R. Tilley, in *The Sodium Sulfur Battery*, J. L. Sudworth, A. R. Tilley, eds., Chapman & Hall, New York, 1985, pp. 90–102.
3. M. L. Miller, B. J. McEntire, G. R. Miller, R. S. Gordon, *Am. Ceram. Soc. Bull., 58*, 522 (1979).
4. R. S. Gordon, G. R. Miller, T. D. Hadnagy, B. J. McEntire, J. R. Rasmussen, in *Energy and Ceramics*, P. Vincenzeni, eds., Elsevier Scientific Publishing, New York, 1980, pp. 925–949.
5. B. J. McEntire, G. R. Miller, R. S. Gordon, in *Processing of Metal and Ceramic Powders*, R. M. German, K. W. Lay, eds., *Conference Proceedings*, Metallurgical Society of AIME, Louisville, KY, Oct. 12–14, 1981.
6. B. J. McEntire, R. H. Snow, A. V. Virkar, in *Symposium Proceedings*, Vol. 87-5; *Sodium–Sulfur Batteries*, A. R. Langrebe, R. D. Weaver, R. K. Sen, eds., Electrochemical Society, Pennington, NJ, 1987, pp. 95–107.

7. R. W. Powers, in *The Sodium Sulfur Battery*, J. L. Sudworth, A. R. Tilley, eds., Chapman & Hall, New York, 1985, pp. 95–102.
8. S. N. Heavens, *Br. Ceram. Proc.*, *36*, 119 (1986).
9. J. L. Sudworth, A. R. Tilley, in *The Sodium Sulfur Battery*, J. L. Sudworth, A. R. Tilley, eds., Chapman & Hall, New York, 1985, pp. 90–92.
10. G. Tennenhouse, Ford Motor Company, private communication.
11. D. Prouse, R. S. Gordon, Ceramatec, Inc., unpublished work.
12. G. E. Youngblood, R. S. Gordon, *Ceramurgia Int.*, *4*, 93 (1978).

17.3.7.1.3. Sintering (Densification) and Annealing.

Prior to the sintering and annealing operations in the fabrication of electrolyte tubing, the green-formed shapes are bisque-fired ($\leq 1200°C$) to remove binders and lubricants[1]. During reactive liquid phase sintering of β″-alumina at 1575–1585° C, four processes normally occur in parallel[2–4]:

1. Phase conversion from high density (3.98 g/cm^3) α-alumina to the lower density (3.27 g/cm^3) β″-alumina phase (*Note*: In precalcined and milled powders, all the α-alumina is typically converted to a β/β″ mixture prior to sintering.)
2. Densification (removal of porosity) assisted by the presence of transient liquid phases.
3. Grain growth.
4. Volatilization of the Na_2O component.

The desired results after sintering and annealing are 100% conversion to the β″ phase for maximum sodium ion conductivity; maximum mass density to eliminate porosity, particularly large pores, in the microstructure; uniform, fine grain size below 10 μm, to maximize strength and minimize sources or singularities for fracture; and no loss of Na_2O to control composition and eventually the sodium ion conductivity.

In contrast to stabilized zirconia ceramics, a controlled amount of compositional inhomogeneity is desired in the fabrication of β″-alumina to promote the formation of transient liquid phases, which enhance rapid densification. On the soda-rich side of the β-alumina–Na_2O binary phase diagram, liquid forms at temperatures around 1585°C[5]. In ternary systems such as Li_2O–Na_2O–Al_2O_3 and MgO–Na_2O–Al_2O_3, it is reasonable to expect liquid formation at even lower temperatures (perhaps around 1450–1480°C)[6]. The reactive liquid phase sintering of β″-alumina ceramics is sensitive to the rate of heating, suggesting that transient or fugitive liquids, which form at temperatures over 1450°C because of chemical inhomogeneities, are responsible for the rapid densification kinetics[2]. Attempts to form precursor powders that are chemically homogeneous (as described in 17.3.7.1.1) have produced very slow densification kinetics and unacceptably low sintered densities at temperatures below 1600°C. For the stabilized zirconias, which densify by a solid state diffusion process, a sub-micrometer powder that is compositionally homogeneous is the desired starting point prior to densification at the lowest possible temperature.

The densification of β″-alumina is very rapid, probably owing to the presence of transient, reactive liquid phases, which promote not only pore removal but also phase conversion to the desired β″ phase. Because densification is so rapid (i.e., several minutes at a firing temperature of $\sim$1575–1585°C), a post sintering anneal is usually required ($\sim$1 h at 1450–1475°C) to complete phase conversion to the β″-alumina phase, resulting in a ceramic electrolyte with the lowest possible Na^+ ion resistivity at 300°C (i.e., 8–25 Ω cm after sintering and < 5 Ω cm after annealing)[1,2]. Depending on the composition and firing schedules, a presintering heat treatment at 1475°C is sometimes incorporated

Inorganic Reactions and Methods, Volume 18
Edited by J. J. Zuckerman, Jim D. Atwood

7. R. W. Powers, in *The Sodium Sulfur Battery*, J. L. Sudworth, A. R. Tilley, eds., Chapman & Hall, New York, 1985, pp. 95–102.
8. S. N. Heavens, *Br. Ceram. Proc.*, *36*, 119 (1986).
9. J. L. Sudworth, A. R. Tilley, in *The Sodium Sulfur Battery*, J. L. Sudworth, A. R. Tilley, eds., Chapman & Hall, New York, 1985, pp. 90–92.
10. G. Tennenhouse, Ford Motor Company, private communication.
11. D. Prouse, R. S. Gordon, Ceramatec, Inc., unpublished work.
12. G. E. Youngblood, R. S. Gordon, *Ceramurgia Int.*, *4*, 93 (1978).

17.3.7.1.3. Sintering (Densification) and Annealing.

Prior to the sintering and annealing operations in the fabrication of electrolyte tubing, the green-formed shapes are bisque-fired ($\leq$1200°C) to remove binders and lubricants[1]. During reactive liquid phase sintering of β″-alumina at 1575–1585° C, four processes normally occur in parallel[2–4]:

1. Phase conversion from high density (3.98 g/cm^3) α-alumina to the lower density (3.27 g/cm^3) β″-alumina phase (*Note*: In precalcined and milled powders, all the α-alumina is typically converted to a β/β″ mixture prior to sintering.)
2. Densification (removal of porosity) assisted by the presence of transient liquid phases.
3. Grain growth.
4. Volatilization of the Na_2O component.

The desired results after sintering and annealing are 100% conversion to the β″ phase for maximum sodium ion conductivity; maximum mass density to eliminate porosity, particularly large pores, in the microstructure; uniform, fine grain size below 10 μm, to maximize strength and minimize sources or singularities for fracture; and no loss of Na_2O to control composition and eventually the sodium ion conductivity.

In contrast to stabilized zirconia ceramics, a controlled amount of compositional inhomogeneity is desired in the fabrication of β″-alumina to promote the formation of transient liquid phases, which enhance rapid densification. On the soda-rich side of the β-alumina–Na_2O binary phase diagram, liquid forms at temperatures around 1585°C[5]. In ternary systems such as Li_2O–Na_2O–Al_2O_3 and MgO–Na_2O–Al_2O_3, it is reasonable to expect liquid formation at even lower temperatures (perhaps around 1450–1480°C)[6]. The reactive liquid phase sintering of β″-alumina ceramics is sensitive to the rate of heating, suggesting that transient or fugitive liquids, which form at temperatures over 1450°C because of chemical inhomogeneities, are responsible for the rapid densification kinetics[2]. Attempts to form precursor powders that are chemically homogeneous (as described in 17.3.7.1.1) have produced very slow densification kinetics and unacceptably low sintered densities at temperatures below 1600°C. For the stabilized zirconias, which densify by a solid state diffusion process, a sub-micrometer powder that is compositionally homogeneous is the desired starting point prior to densification at the lowest possible temperature.

The densification of β″-alumina is very rapid, probably owing to the presence of transient, reactive liquid phases, which promote not only pore removal but also phase conversion to the desired β″ phase. Because densification is so rapid (i.e., several minutes at a firing temperature of $\sim$1575–1585°C), a post sintering anneal is usually required ($\sim$1 h at 1450–1475°C) to complete phase conversion to the β″-alumina phase, resulting in a ceramic electrolyte with the lowest possible Na^+ ion resistivity at 300°C (i.e., 8–25 Ω cm after sintering and <5 Ω cm after annealing)[1,2]. Depending on the composition and firing schedules, a presintering heat treatment at 1475°C is sometimes incorporated

into the firing schedule before the peak sintering temperature for densification is reached. This procedure is used to partially chemically homogenize the powder prior to sintering to avoid exaggerated grain growth. A two-peak firing schedule is sometimes utilized to achieve this result[8]. Thus by carefully designed sintering and annealing schedules, strong (~200 MPa), conductive (~4 Ω cm at 300° C), and dense (~3.23 g/cm^3: i.e., >99% of theoritical density) β″-alumina electrolytes can be fabricated with moderate grain size (large grains <50–100 μm).

While the presence of reactive liquid phases promotes rapid densification, the same feature can also lead to the formation of an undesirable duplex grain structure, which is common in the β″-aluminas. This type of microstructure consists of a fine-grained matrix (several micrometers) in which large straight-sided grains, some as large as several hundred micrometers, are present[2]. Exaggerated grain growth can be mitigated to some degree by minimizing the time at the peak sintering temperature or employing the presintering heat treatment discussed earlier.

Seeding catalysis[4,9] has been used to enhance the kinetics of phase conversion during sintering and to promote competitive grain growth. In this technique, very fine seeds (<5 μm) of the pure β″-alumina phase are incorporated into the starting powders or spray-drying slurries in amounts ranging between 2 and 5 wt %. The seeds act as sites for the nucleation and growth of β″-alumina grains during sintering. The number of these nucleation sites determines the average grain size of the fired ceramic. A relatively uniform microstructure with a moderate grain size (15–20 μm) can be obtained after firing with the largest grains in the distribution under 50–100 μm. Seeding eliminates the need for any pre-sintering firing schedules and, when optimized, may reduce or eliminate altogether the requirement for a post sintering anneal to complete phase conversion. Seeding can be incorporated into both dry and liquid (e.g., EPD, S^{2}D, and S^{3}D) techniques for media processing.

Zirconia additions (unstabilized or partially stabilized with Y_2O_3) up to 15 wt % have been incorporated as chemically begin second-phase particles into both dry powder (e.g., zeta process) and spray-drying (S^{3}D, S^{4}D) processes to achieve higher fracture strengths and fracture toughness values while maintaining the Na^+ ion resistivity below 6 Ω cm (at 300°C)[10–12]. A side benefit to the zirconia additions is control of exaggerated grain growth. The resulting microstructures are fine grained (<5 μm) and uniform. Unstabilized zirconia additions, upto 6 wt %, can be used to control grain growth and enhance the mechanical strength. Care must be exercised to monitor and control water-sensitivity effects, particularly with the use of unstabilized zirconia as a second-phase strengthening additive to β″-alumina[12].

β″-alumina ceramics, which are fabricated from spray-dried slurries (S^{3}D process) containing unconverted α-alumina powders, can be fired with precise dimensional tolerances, since the linear shrinkage on firing is 9–11% compared to dry powder, S^{2}D, or EPD processes involving the firing of prereacted (β/β″) powders with linear shrinkage values between 15 and 20%. The lower shrinkage values in the S^{3}D process are due to phase conversion during densification from the high density α-alumina precursor reactant to the lower density β″-alumina phase.

Sintering of β″-alumina tubing or flat plates is accomplished by encapsulation (usually chemically inert magnesia-based refractories) to prevent the loss of the volatite soda component[10,13,14]. Vertical batch sintering of electrolyte tubes is employed to control the ovality of the fired ceramic within acceptable limits. Ultimately, a continuous sintering process of horizontally saggered ware will likely be adopted for large-scale

production[15]. Control of ovality, particularly in large o.d. (>25 mm) tubing with thin walls (~1 mm), is more difficult in the horizontal mode of firing than it is when ware is placed vertically in the sintering furnace.

(R. S. GORDON)

1. M. L. Miller, B. J. McEntire, G. R. Miller, R. S. Gordon, *Am. Ceram. Soc. Bull., 58*, 522 (1979).
2. G. E. Youngblood, A. V. Virkar, W. R. Cannon, R. S. Gordon, *Am. Ceram. Soc. Bull., 56*, 206 (1977).
3. B. J. McEntire, G. R. Miller, R. S. Gordon, in *Processing of Metal and Ceramic Powders*, R. M. German, K. W. Lay, eds., *Conference Proceedings*, Metallurgical Society of AIME, Louisville, KY, Oct. 12–14, 1981, pp.215–239.
4. B. J. McEntire, R. H. Snow, A. V. Virkar, in *Symposium Proceedings*, Vol. 87-5: *Sodium–Sulfur Batteries*, A. R. Langrebe, R. D. Weaver, R. K. Sen, eds., Electrochemical Society, Pennington, NJ, 1987, pp. 95–107.
5. J. T. Kummer, *Prog. Solid State Chem., 7*, 141 (1972).
6. N. Weber, in *Superionic Conductors*, G. D. Mahan, W. L. Roth, eds., Plenum Press, New York, 1976, pp. 37–46.
7. A. D. Jatkar, I. B. Cutler, A. V. Virkar, R. S. Gordon, in *Processing of Crystalline Ceramics*, H. Palmour, R. F. Davis, T. M. Hare, eds., Plenum Press, New York, 1978, pp. 421–432.
8. J. H. Duncan, in *Sodium Sulfur Battery*, J. L. Sudworth, A. R. Tilley, eds., Chapman & Hall, New York, 1985, pp.110–114.
9. A. D. Jatkar, I. B. Cutler, R. S. Gordon, in *Processings of Sixth International Materials Symposium–Ceramic Microstructures' 76*, R. M. Fulrath, J. A. Pask, eds., Westview Press, Boulder, CO, 1977, pp. 414–422.
10. R. S. Gordon, W. Fischer, A. V. Virkar, in *Ceramic Transactions*, Vol. 65: *Role of Ceramics in Advanced Electrochemical Systems*, P. N. Kumpta, G. S. Roher, Balachandran, eds., American Ceramic Society, Westerville, OH, 1996, pp. 203–237.
11. J. R. Rasmussen, L. Viswanathan, G. R. Miller, A. V. Virkar, *SAE Technical Paper Series*, No. 830225; reprinted from SP-541 Batteries for Electric Vehicles–Research, Development, Testing and Evaluation, Society of Automotive Engineers, Warrendale, PA, 1983.
12. B. J. McEntire, K. Klemm, R. H. Snow, A. V. Virkar, in *Symposium Proceedings* Vol. 87-5: *Sodium-Sulfur Batteries*, A. R. Langrebe, R. D. Weaver, R. K. Sen, eds., Electrochemical Society, Pennington, NJ, 1987, pp. 142–162.
13. J. H. Duncan, in *Sodium Sulfur Battery*. J. L. Sudworth, A. R. Tilley, eds., Chapman & Hall, New York, 1985, pp. 106–110.
14. B. J. McEntire, G. R. Miller, R. S. Gordon, *Am. Ceram. Soc. Bull., 63*, 792 (1984).
15. R. S. Gordon, in *Sodium Sulfur Battery*, J. L. Sudworth, A. R. Tilley, eds., Chapman & Hall, New York, 1985, pp. 117–125.

17.3.7.2. Alternative Sodium Ion Conductors

Sodium ion conduction in β''-alumina is anisotropic and ceramic electrolytes produced from this material not only can be sensitive to exposure to moisture but also are somewhat difficult to densify (e.g., because of problems related to Na_2O evaporation, conversion to single-phase β''-alumina, and control of exaggerated grain growth). For these reasons. Serious attempts have been made to find alternative materials that have Na^+ ion conductivities comparable to or higher than β''-alumina but are easier and/or potentially more economical to fabricate[1,2]. Here we review attempts to develop alternatives. They fall into two classes of materials: the crystalline NASICON family of compounds and conducting glasses.

Table 1 lists sodium ion resistivities at 300°C for polycrystalline ceramic conductors (e.g., β''-alumina, and NASICON) and sodium ion conducting glasses (e.g., NASIGLAS and a sodium borosilicate glass). (The terms NASICON and NASIGLAS were defined

Inorganic Reactions and Methods, Volume 18
Edited by J. J. Zuckerman, Jim D. Atwood

production[15]. Control of ovality, particularly in large o.d. (>25 mm) tubing with thin walls (~1 mm), is more difficult in the horizontal mode of firing than it is when ware is placed vertically in the sintering furnace.

(R. S. GORDON)

1. M. L. Miller, B. J. McEntire, G. R. Miller, R. S. Gordon, *Am. Ceram. Soc. Bull., 58*, 522 (1979).
2. G. E. Youngblood, A. V. Virkar, W. R. Cannon, R. S. Gordon, *Am. Ceram. Soc. Bull., 56*, 206 (1977).
3. B. J. McEntire, G. R. Miller, R. S. Gordon, in *Processing of Metal and Ceramic Powders*, R. M. German, K. W. Lay, eds., *Conference Proceedings*, Metallurgical Society of AIME, Louisville, KY, Oct. 12–14, 1981, pp.215–239.
4. B. J. McEntire, R. H. Snow, A. V. Virkar, in *Symposium Proceedings*, Vol. 87-5: *Sodium–Sulfur Batteries*, A. R. Langrebe, R. D. Weaver, R. K. Sen, eds., Electrochemical Society, Pennington, NJ, 1987, pp. 95–107.
5. J. T. Kummer, *Prog. Solid State Chem., 7*, 141 (1972).
6. N. Weber, in *Superionic Conductors*, G. D. Mahan, W. L. Roth, eds., Plenum Press, New York, 1976, pp. 37–46.
7. A. D. Jatkar, I. B. Cutler, A. V. Virkar, R. S. Gordon, in *Processing of Crystalline Ceramics*, H. Palmour, R. F. Davis, T. M. Hare, eds., Plenum Press, New York, 1978, pp. 421–432.
8. J. H. Duncan, in *Sodium Sulfur Battery*, J. L. Sudworth, A. R. Tilley, eds., Chapman & Hall, New York, 1985, pp.110–114.
9. A. D. Jatkar, I. B. Cutler, R. S. Gordon, in *Processings of Sixth International Materials Symposium–Ceramic Microstructures'* 76, R. M. Fulrath, J. A. Pask, eds., Westview Press, Boulder, CO, 1977, pp. 414–422.
10. R. S. Gordon, W. Fischer, A. V. Virkar, in *Ceramic Transactions*, Vol. 65: *Role of Ceramics in Advanced Electrochemical Systems*, P. N. Kumpta, G. S. Roher, Balachandran, eds., American Ceramic Society, Westerville, OH, 1996, pp. 203–237.
11. J. R. Rasmussen, L. Viswanathan, G. R. Miller, A. V. Virkar, *SAE Technical Paper Series*, No. 830225; reprinted from SP-541 Batteries for Electric Vehicles–Research, Development, Testing and Evaluation, Society of Automotive Engineers, Warrendale, PA, 1983.
12. B. J. McEntire, K. Klemm, R. H. Snow, A. V. Virkar, in *Symposium Proceedings* Vol. 87-5: *Sodium-Sulfur Batteries*, A. R. Langrebe, R. D. Weaver, R. K. Sen, eds., Electrochemical Society, Pennington, NJ, 1987, pp. 142–162.
13. J. H. Duncan, in *Sodium Sulfur Battery*. J. L. Sudworth, A. R. Tilley, eds., Chapman & Hall, New York, 1985, pp. 106–110.
14. B. J. McEntire, G. R. Miller, R. S. Gordon, *Am. Ceram. Soc. Bull., 63*, 792 (1984).
15. R. S. Gordon, in *Sodium Sulfur Battery*, J. L. Sudworth, A. R. Tilley, eds., Chapman & Hall, New York, 1985, pp. 117–125.

17.3.7.2. Alternative Sodium Ion Conductors

Sodium ion conduction in β''-alumina is anisotropic and ceramic electrolytes produced from this material not only can be sensitive to exposure to moisture but also are somewhat difficult to densify (e.g., because of problems related to Na_2O evaporation, conversion to single-phase β''-alumina, and control of exaggerated grain growth). For these reasons. Serious attempts have been made to find alternative materials that have Na^+ ion conductivities comparable to or higher than β''-alumina but are easier and/or potentially more economical to fabricate[1,2]. Here we review attempts to develop alternatives. They fall into two classes of materials: the crystalline NASICON family of compounds and conducting glasses.

Table 1 lists sodium ion resistivities at 300°C for polycrystalline ceramic conductors (e.g., β''-alumina, and NASICON) and sodium ion conducting glasses (e.g., NASIGLAS and a sodium borosilicate glass). (The terms NASICON and NASIGLAS were defined

TABLE 1. ALTERNATIVE SODIUM ION CONDUCTORS/SODIUM ION RESISTIVITY: MAXIMUM THICKNESS FOR AREA-SPECIFIC RESISTANCE $< 0.5\ \Omega\text{-cm}^2$ (300°C)

Electrolyte	Ionic Resistivity (Ω-cm)	Maximum Membrance Thickness (mm)
β''-Alumina	4	1.25
β-Alumina	17	0.30
NASICON	4	1.25
NASIGLAS	140	0.036
Na borosilicate glass	2×10^4	2.5×10^{-4}

in 17.3.7.) The maximum membrane thickness is also listed for each material, such that the area-specific resistance of electrolyte in an electrochemical device is $\leq 0.5\ \Omega \cdot \text{cm}^2$.

The data presented in Table 1 permit several conclusion to be drawn on the potential use of these materials as electrolytes in electrochemical devices with practical values for the area-specific resistance. Only the β''-alumina and NASICON electrolytes possess sufficient conductivities for use as membranes with thicknesses of 1 mm or greater. The sodium ion conductivities of polycrystalline NASICON and β''-alumina are comparable. The glassy electrolytes must be used in the form of thin films (≤ 50 μm and possibly under 10–15 μm) or as capillary tubes with very thin walls (10–50 μm).

(R. S. GORDON)

1. G. R. Miller, B. J. McEntire, T. D. Hadnagy, J. R. Rasmussen, R. S. Gordon, A. V. Virkar, in *Fast Ion Transport in Solids*, P. Vashishta, J. N. Mundy, G. D. Shenoy, eds., Elsevier North Holland, New York, 1979, pp. 83–86.
2. R. S. Gordon, G. R. Miller, B. J. McEntire, E. D. Beck, J. R. Rasmussen, *Solid State Ionics, 3–4*, 243 (1981).

17.3.7.2.1. NASICON.

NASICON, a rough acronym for "sodium superionic conductor", is a term that represents a family of crystalline sodium ion conducting ceramics of the general composition $Na_{1+x}Zr_2Si_xP_{3-x}O_{12}$ (with $0.4 < x < 2.8$)[1,2]. The sodium ion conductivity of this material at 300°C is a maximum in the range $x = 2.0$–2.3 and is approximately equivalent to the highest reported for polycrystalline β''-alumina. The resistivity of NASICON ($x = 2$) was compared earlier with β- and β''-alumina (see 17.3.7, Table 1). Other sodium ion conducting ceramics have been synthesized including $Na_5YSi_4O_{12}$[3], a family of NASICON materials possessing isostructural characteristics—$Na_{1+x}Zr_{2-x}M_xP_3O_{12}$ ($0 < x < 2$, M = Y, Yb, and In[4], and $Na_2Sc_2P_3O_{12}$[5]. The ionic conductivities of these materials are excellent and comparable to those of the sodium β''-aluminas.

Unlike β''-alumina, which is a two-dimensional ionic conductor, NASICON possesses a crystal structure that allows sodium ion migration in three dimensions. The basic structure consists of a three-dimensional network of PO_4 an SiO_4 tetrahedra corner-shared with ZrO_6 octahedra, with sodium ions in interstitial positions.

When the discovery of NASICON was first announced, its preparation was claimed to be free of the difficulties attributed to the processing of β''-alumina electrolytes[6–9]. Since that time, considerable effort has been devoted to powder synthesis, forming, and

Inorganic Reactions and Methods, Volume 18
Edited by J. J. Zuckerman, Jim D. Atwood

TABLE 1. ALTERNATIVE SODIUM ION CONDUCTORS/SODIUM ION RESISTIVITY: MAXIMUM THICKNESS FOR AREA-SPECIFIC RESISTANCE $< 0.5\ \Omega\text{-cm}^2$ (300°C)

Electrolyte	Ionic Resistivity (Ω-cm)	Maximum Membrance Thickness (mm)
β''-Alumina	4	1.25
β-Alumina	17	0.30
NASICON	4	1.25
NASIGLAS	140	0.036
Na borosilicate glass	2×10^4	2.5×10^{-4}

in 17.3.7.) The maximum membrane thickness is also listed for each material, such that the area-specific resistance of electrolyte in an electrochemical device is $\leq 0.5\ \Omega \cdot \text{cm}^2$.

The data presented in Table 1 permit several conclusion to be drawn on the potential use of these materials as electrolytes in electrochemical devices with practical values for the area-specific resistance. Only the β''-alumina and NASICON electrolytes possess sufficient conductivities for use as membranes with thicknesses of 1 mm or greater. The sodium ion conductivities of polycrystalline NASICON and β''-alumina are comparable. The glassy electrolytes must be used in the form of thin films (≤ 50 μm and possibly under 10–15 μm) or as capillary tubes with very thin walls (10–50 μm).

(R. S. GORDON)

1. G. R. Miller, B. J. McEntire, T. D. Hadnagy, J. R. Rasmussen, R. S. Gordon, A. V. Virkar, in *Fast Ion Transport in Solids*, P. Vashishta, J. N. Mundy, G. D. Shenoy, eds., Elsevier North Holland, New York, 1979, pp. 83–86.
2. R. S. Gordon, G. R. Miller, B. J. McEntire, E. D. Beck, J. R. Rasmussen, *Solid State Ionics, 3–4*, 243 (1981).

17.3.7.2.1. NASICON.

NASICON, a rough acronym for "sodium superionic conductor", is a term that represents a family of crystalline sodium ion conducting ceramics of the general composition $Na_{1+x}Zr_2Si_xP_{3-x}O_{12}$ (with $0.4 < x < 2.8$)[1,2]. The sodium ion conductivity of this material at 300°C is a maximum in the range $x = 2.0$–2.3 and is approximately equivalent to the highest reported for polycrystalline β''-alumina. The resistivity of NASICON ($x = 2$) was compared earlier with β- and β''-alumina (see 17.3.7, Table 1). Other sodium ion conducting ceramics have been synthesized including $Na_5YSi_4O_{12}$[3], a family of NASICON materials possessing isostructural characteristics—$Na_{1+x}Zr_{2-x}M_xP_3O_{12}$ ($0 < x < 2$, M = Y, Yb, and In[4], and $Na_2Sc_2P_3O_{12}$[5]. The ionic conductivities of these materials are excellent and comparable to those of the sodium β''-aluminas.

Unlike β''-alumina, which is a two-dimensional ionic conductor, NASICON possesses a crystal structure that allows sodium ion migration in three dimensions. The basic structure consists of a three-dimensional network of PO_4 an SiO_4 tetrahedra corner-shared with ZrO_6 octahedra, with sodium ions in interstitial positions.

When the discovery of NASICON was first announced, its preparation was claimed to be free of the difficulties attributed to the processing of β''-alumina electrolytes[6–9]. Since that time, considerable effort has been devoted to powder synthesis, forming, and

sintering, as well as electrolyte characterization and static and electrochemical corrosion testing in liquid sodium.

Two different approaches have been used in the preparation of polycrystalline NASICON ceramics[6,7,10-12]: (1) mechanical blending, calcination, and milling of component oxides or oxide precursors, and (2) gel processing. Raw materials used in the first set of processes include Na_2CO_3, $Na_3PO_4 \cdot 12H_2O$ or Na_3PO_4, $NH_4H_2PO_4$, ZrO_2, SiO_2, and even $ZrSiO_4$ for the $x = 2$ NASICON composition. In gel processing, soluble (in water) or dispersible (silica) metal oxide precursors are mixed in solution and dried to form an amorphous glassy matrix that is chemically homogeneous. The material is then calcined and milled to form a sinterable powder. The raw materials in this method include $NaNO_3$, $NH_4H_2PO_4$, citric acid, liquid ammonium–zirconium–carbonate, and colloidal silica. The function of the citric acid is to aid in formation of glassy matrix.

These two methods of synthesis have led to the discovery that at compositions around $x = 2$, a monophase, polycrystalline NASION is very difficult to produce, even though it can be sintered to reasonable mass density (>3.20 g/cm^3) at relatively low temperatures (1100–1375°C). Unfortunately these materials contain a ZrO_2 second phase, possess poor mechanical strength with a low fracture toughness, have an anomalous thermal expansion behaviour, and are subject to chemical and phase instability during densification[7,10].

Finally, static and electrochemical (two-way Na–Na cell tests at current densities under 50 mA/cm^2) testing at 300°C revealed a basic instability of the material in liquid sodium[7]. In view of the basic incompatibility of the material with liquid sodium and the difficulty encountered in producing single-phase material with adequate mechanical properties, NASICON has been dropped, at least for the time being, as a viable alternative to β''-alumina.

(R. S. GORDON)

1. H. Y. -P. Hong, *Mater. Res. Bull., 11*, 173 (1976).
2. J. B. Goodenough, H. Y.-P. Hong, J. A. Kafalas, *Mater. Res. Bull., 11*, 203 (1976).
3. H. Y.- P. Hong, *Mater. Res. Bull., 13*, 757 (1978).
4. T. Shun-bao, Lin Zu-Yiang, Shanghai Institute of Ceramics, Shanghai, China, private communication.
5. H. Y.- P. Hong, in *Fast Ion Transport in Solids*, P. Vashishta, J. N. Mundy, G. D. Shenoy, eds., Elsevier North Holland, New York, 1979, pp. 431–434.
6. G. R. Miller, B. J. McEntire, T. D. Hadnagy, J. R. Rasmussen, R. S. Gordon, A.V. Virkar, in *Fast Ion Transport in Solids*, P. Vashista, J. N. Mundy, G. D. Shenoy, eds., Elsevier North Holland, New York, 1979, pp. 83–86.
7. R. S. Gordon, G. R. Miller, B. J. McEntire, E. D. Beck, J. R. Rasmussen, *Solid State Ionics, 3–4*, 243 (1981).
8. J. P. Boilot, J. P. Salanie, G. Desplanches, D. le Potier, *Mater. Res. Bull., 14*, 1469 (1979).
9. G. Desplanches, D. Gourier, A. Wicker, *Am. Ceram. Soc. Bull., 59*, 377 (1980).
10. B. J. McEntire, R. A. Bartlett, G. R. Miller, R. S. Gordon, *J. Am. Ceram. Soc., 66*, 738 (1983).
11. W. C. Marcilly, P. Courty, B. Delmon, *J. Am. Ceram. Soc., 53*, 56 (1970).
12 .J. A. Pompa, A. M. Van Diepen, *Mater. Res. Bull., 9*, 1119 (1974).

17.3.7.2.2. Sodium Ion Conducting Glasses.

Glassy electrolytes are potentially attractive because of the commercial availability of manufacturing technology for producing glass components in different shapes at high production rates (e.g., mass production of lightbulbs). All the challenges encountered in powder preparation, milling, calcining, and sintering are circumvented in glass making, which consists primarily of a melting/refining operation followed directly by forming into

Inorganic Reactions and Methods, Volume 18
Edited by J. J. Zuckerman, Jim D. Atwood

sintering, as well as electrolyte characterization and static and electrochemical corrosion testing in liquid sodium.

Two different approaches have been used in the preparation of polycrystalline NASICON ceramics[6,7,10-12]: (1) mechanical blending, calcination, and milling of component oxides or oxide precursors, and (2) gel processing. Raw materials used in the first set of processes include Na_2CO_3, $Na_3PO_4 \cdot 12H_2O$ or Na_3PO_4, $NH_4H_2PO_4$, ZrO_2, SiO_2, and even $ZrSiO_4$ for the $x = 2$ NASICON composition. In gel processing, soluble (in water) or dispersible (silica) metal oxide precursors are mixed in solution and dried to form an amorphous glassy matrix that is chemically homogeneous. The material is then calcined and milled to form a sinterable powder. The raw materials in this method include $NaNO_3$, $NH_4H_2PO_4$, citric acid, liquid ammonium–zirconium–carbonate, and colloidal silica. The function of the citric acid is to aid in formation of glassy matrix.

These two methods of synthesis have led to the discovery that at compositions around $x = 2$, a monophase, polycrystalline NASION is very difficult to produce, even though it can be sintered to reasonable mass density (>3.20 g/cm^3) at relatively low temperatures (1100–1375°C). Unfortunately these materials contain a ZrO_2 second phase, possess poor mechanical strength with a low fracture toughness, have an anomalous thermal expansion behaviour, and are subject to chemical and phase instability during densification[7,10].

Finally, static and electrochemical (two-way Na–Na cell tests at current densities under 50 mA/cm^2) testing at 300°C revealed a basic instability of the material in liquid sodium[7]. In view of the basic incompatibility of the material with liquid sodium and the difficulty encountered in producing single-phase material with adequate mechanical properties, NASICON has been dropped, at least for the time being, as a viable alternative to β''-alumina.

(R. S. GORDON)

1. H. Y. -P. Hong, *Mater. Res. Bull., 11*, 173 (1976).
2. J. B. Goodenough, H. Y.-P. Hong, J. A. Kafalas, *Mater. Res. Bull., 11*, 203 (1976).
3. H. Y.- P. Hong, *Mater. Res. Bull., 13*, 757 (1978).
4. T. Shun-bao, Lin Zu-Yiang, Shanghai Institute of Ceramics, Shanghai, China, private communication.
5. H. Y.- P. Hong, in *Fast Ion Transport in Solids*, P. Vashishta, J. N. Mundy, G. D. Shenoy, eds., Elsevier North Holland, New York, 1979, pp. 431–434.
6. G. R. Miller, B. J. McEntire, T. D. Hadnagy, J. R. Rasmussen, R. S. Gordon, A.V. Virkar, in *Fast Ion Transport in Solids*, P. Vashista, J. N. Mundy, G. D. Shenoy, eds., Elsevier North Holland, New York, 1979, pp. 83–86.
7. R. S. Gordon, G. R. Miller, B. J. McEntire, E. D. Beck, J. R. Rasmussen, *Solid State Ionics, 3–4*, 243 (1981).
8. J. P. Boilot, J. P. Salanie, G. Desplanches, D. le Potier, *Mater. Res. Bull., 14*, 1469 (1979).
9. G. Desplanches, D. Gourier, A. Wicker, *Am. Ceram. Soc. Bull., 59*, 377 (1980).
10. B. J. McEntire, R. A. Bartlett, G. R. Miller, R. S. Gordon, *J. Am. Ceram. Soc., 66*, 738 (1983).
11. W. C. Marcilly, P. Courty, B. Delmon, *J. Am. Ceram. Soc., 53*, 56 (1970).
12 .J. A. Pompa, A. M. Van Diepen, *Mater. Res. Bull., 9*, 1119 (1974).

17.3.7.2.2. Sodium Ion Conducting Glasses.

Glassy electrolytes are potentially attractive because of the commercial availability of manufacturing technology for producing glass components in different shapes at high production rates (e.g., mass production of lightbulbs). All the challenges encountered in powder preparation, milling, calcining, and sintering are circumvented in glass making, which consists primarily of a melting/refining operation followed directly by forming into

the final part by automated techniques for glass blowing or forming. The random network structure of soda-based glasses, however, tends to limit the mobility of Na^+ ions to rates considerably lower than those found in crystalline materials, where channels in the structure allow for rapid ion transport.

The pioneering work in developing sodium ion conducting glass electrolytes was conducted on a modified sodium borate glass (i.e., $Na_2O \cdot 2B_2O_3 \cdot 0.2SiO_2 \cdot 0.16$ NaCl) with a sodium ion resistivity of 20,000 $\Omega \cdot$ cm at 300°C. Because of this high resistivity, Na/S cells require many thousands of very small hollow glass fibers or capillaries, each with an o.d. of 80–90 μm, a length of about 100 mm, and a wall thickness between 10 and 15 μm. These glass capillaries are sealed at one end, and at the open end, the fibers are held together by a glass sheet or header. Further development of this glass electrolyte was suspended primarily because the material experienced long-term chemical stability problems in liquid sodium and liquid sulfur–sodium polysulfide at 300°C. Problems also exist related to the sensitivity of the glass electrolyte to calcium, potassium, and sodium oxide impurities in liquid sodium[1,2].

Since glass forming is economical relative to conventional ceramic manufacturing from powdered raw materials, an alternative glass (NASIGLAS) has been developed with a higher conductivity (refer to Table 1 in 17.3.7.2)[2]. This glass has a relatively high soda content in the $Na_2O \cdot Al_2O_3 \cdot ZrO_2 \cdot SiO_2$ system. For example, the lowest Na^+ ion resistivity (viz., $\sim$ 130 $\Omega \cdot$ cm at 300°C) is reported for the following composition (mol%): 41 Na_2O, 6.4 Al_2O_3, 4.0 ZrO_2, and 44.6 SiO_2. With the lower resistivity, the number of glass tubes required in a device like the sodium–sulfur battery for an electric vehicle would be reduced from thousands to hundreds. The composition with the best resistance to corrosion in liquid sodium and liquid sulfur or sodium polysulfide is (in mol %) 42 Na_2O, $8Al_2O_3$, $5ZrO_2$, and 45 SiO_2. Glass at this composition has a Na^+ ion resistivity at 300°C of 141 $\Omega \cdot$ cm. The viability of this electrolyte alternative has not been demonstrated, however, so further development is required.

(R. S. GORDON)

1. J. L. Sudworth, A. R. Tilley, in *The Sodium Sulfur Battery*, J. L. Sudworth, A. R. Tilley, eds., Chapman & Hall, New York, NY, 1985, pp. 130–131.
2. I. Bloom, G. H. Kucera, S. Bradley, P. A. Nelson, M. F. Roche, in *Symposium Proceedings*, Vol. 87-5: *Sodium-Sulfur Batteries*, A. R. Landgrebe, R. D. Weaver, R. K. Sen, eds., Electrochemical Society, Pennington, NJ, 1987, pp. 125–141.

17.3.7.3. Zircronia-Based Ceramic Electrolytes.

The crystalline form of interest in Zr-based ceramic compounds is the cubic fluorite structure based on the mineral CaF_2. In this structure, consisting of interpenetrating face-centered-cubic and simple cublic arrays of cations (Zr^{4+}) and anions (O^{2-}), respectively, oxygen ion conductivity is enhanced by replacing zirconium (Zr^{4+}) ions on the cation lattice with soluble dopant cations having a valence less than 4, typically divalent (Mg^{2+}, Ca^{2+}) and trivalent (Y^{3+}, Yb^{3+}, Sc^{3+}) cations. These dopants, which are in solid solution, are incorporated into the zirconia structure by the following types of defect reaction:

$$Y_2O_3 = 2Y'_{Zr} + V^{\cdot\cdot}_O + 3O_O \quad \text{(a)}$$

$$CaO = Ca''_{Zr} + V^{\cdot\cdot}_O + O_O \quad \text{(b)}$$

Inorganic Reactions and Methods, Volume 18
Edited by J. J. Zuckerman, Jim D. Atwood

the final part by automated techniques for glass blowing or forming. The random network structure of soda-based glasses, however, tends to limit the mobility of Na^+ ions to rates considerably lower than those found in crystalline materials, where channels in the structure allow for rapid ion transport.

The pioneering work in developing sodium ion conducting glass electrolytes was conducted on a modified sodium borate glass (i.e., $Na_2O \cdot 2B_2O_3 \cdot 0.2SiO_2 \cdot 0.16$ NaCl) with a sodium ion resistivity of 20,000 $\Omega \cdot$ cm at 300°C. Because of this high resistivity, Na/S cells require many thousands of very small hollow glass fibers or capillaries, each with an o.d. of 80–90 μm, a length of about 100 mm, and a wall thickness between 10 and 15 μm. These glass capillaries are sealed at one end, and at the open end, the fibers are held together by a glass sheet or header. Further development of this glass electrolyte was suspended primarily because the material experienced long-term chemical stability problems in liquid sodium and liquid sulfur–sodium polysulfide at 300°C. Problems also exist related to the sensitivity of the glass electrolyte to calcium, potassium, and sodium oxide impurities in liquid sodium[1,2].

Since glass forming is economical relative to conventional ceramic manufacturing from powdered raw materials, an alternative glass (NASIGLAS) has been developed with a higher conductivity (refer to Table 1 in 17.3.7.2)[2]. This glass has a relatively high soda content in the $Na_2O \cdot Al_2O_3 \cdot ZrO_2 \cdot SiO_2$ system. For example, the lowest Na^+ ion resistivity (viz., $\sim$ 130 $\Omega \cdot$ cm at 300°C) is reported for the following composition (mol%): 41 Na_2O, 6.4 Al_2O_3, 4.0 ZrO_2, and 44.6 SiO_2. With the lower resistivity, the number of glass tubes required in a device like the sodium–sulfur battery for an electric vehicle would be reduced from thousands to hundreds. The composition with the best resistance to corrosion in liquid sodium and liquid sulfur or sodium polysulfide is (in mol %) 42 Na_2O, $8Al_2O_3$, $5ZrO_2$, and 45 SiO_2. Glass at this composition has a Na^+ ion resistivity at 300°C of 141 $\Omega \cdot$ cm. The viability of this electrolyte alternative has not been demonstrated, however, so further development is required.

(R. S. GORDON)

1. J. L. Sudworth, A. R. Tilley, in *The Sodium Sulfur Battery*, J. L. Sudworth, A. R. Tilley, eds., Chapman & Hall, New York, NY, 1985, pp. 130–131.
2. I. Bloom, G. H. Kucera, S. Bradley, P. A. Nelson, M. F. Roche, in *Symposium Proceedings*, Vol. 87-5: *Sodium-Sulfur Batteries*, A. R. Landgrebe, R. D. Weaver, R. K. Sen, eds., Electrochemical Society, Pennington, NJ, 1987, pp. 125–141.

17.3.7.3. Zircronia-Based Ceramic Electrolytes.

The crystalline form of interest in Zr-based ceramic compounds is the cubic fluorite structure based on the mineral CaF_2. In this structure, consisting of interpenetrating face-centered-cubic and simple cublic arrays of cations (Zr^{4+}) and anions (O^{2-}), respectively, oxygen ion conductivity is enhanced by replacing zirconium (Zr^{4+}) ions on the cation lattice with soluble dopant cations having a valence less than 4, typically divalent (Mg^{2+}, Ca^{2+}) and trivalent (Y^{3+}, Yb^{3+}, Sc^{3+}) cations. These dopants, which are in solid solution, are incorporated into the zirconia structure by the following types of defect reaction:

$$Y_2O_3 = 2Y'_{Zr} + V^{\cdot\cdot}_O + 3O_O \qquad \text{(a)}$$

$$CaO = Ca''_{Zr} + V^{\cdot\cdot}_O + O_O \qquad \text{(b)}$$

The substitutional cation dopant (i.e., Y'_{Zr}, Ca''_{Zr}) is compensated in the crystal lattice by an appropriate concentration of oxygen ion vacancies (i.e., $V_O^{\cdot\cdot}$). Typical dopant concentrations for optimum conductivity are ~13–15 mol % CaO and ~8–10 mol% Y_2O_3[1]. These dopants also stabilize the crystal structure in the cubic fluorite phase at the sintering (~1450°C) and in-service operating temperatures (600–1100°). The mechanism of ionic conduction involves migration of O^{2-} ions in the anion sublattice by exchange with oxygen ion vacancies. The O^{2-} ion conductivity of yttria-stabilized ziroconia at 1100°C is comparable that of Na^+ ion conductivity in β''-alumina at 300° C.

For proper operation of an electrochemical device (e.g., fuel cell, sensor, oxygen pump), the ceramic electrolyte must be a chemically stable oxygen ion conductor, with essentially no electronic conductivity, at the range of temperatures and oxygen partial pressures over which the device is operated[2,3]. To achieve the desired electrical performance from such devices, the magnitude of oxygen ion conductivity must be as high as possible. The class of oxygen ion conductors that currently best meets these requirements is polycrystalline zirconia stabilized with appropriate concentrations of Y_2O_3, Yb_2O_3, or Sc_2O_3 (refer to Table 1 in 17.3.7). Other compounds in this class are those based on solid solutions (alloys) in which ThO_2 and HfO_2 are the host oxides. The O^{2-} ion resistivities (refer to Table 1 in 17.3.7) are too high for most applications, even though ThO_2-based materials are thermodynamically more stable than the zirconia-based electrolytes.

Polycrystalline zirconia ceramics in the fully stabilized cubic structure (e.g., $\geq$ 7–8 mol% Y_2O_3) have somewhat inferior mechanical properties and poor thermal shock resistance, which can limit their application in bulk or monolithic ceramic shapes [e.g., thick-walled (1–2 mm) tubular oxygen sensors in automotive exhaust manifolds]. This is a less serious issue if the zirconia electrolyte is used in the form of a thin plate, coating, or film ($<$500 μm). The mechanical properties of these ceramics can be improved significantly by adjusting the stabilizing dopant composition to lower values (e.g., 5–6 mol% Y_2O_3) within the region of partial stabilization[4].

Partially stabilized zirconia (PSZ) ceramics, in addition to the stabilized cubic phase, usually contain various amounts of zirconia in the tetragonal and monoclinic crystal forms. By appropriate heat treatments, these ceramics can be toughened by tetragonal-to-monoclinic phase transformation. Transformation-toughened PSZ electrolytes, partially stabilized with yttrium oxide, possess fracture strengths and thermal shock resistance values two to three times higher than those in fully stabilized material. The ionic conductivity in PSZ ceramics is lowered slightly by the presence of isolated nonconducting second phases in the microstructure. (*Note*: Higher values of the area-specific resistance R_{as} are acceptable in voltage devices like sensors compared to current devices such as the solid oxide fuel cell.) However, in the Y_2O_3-stabilized material, this effect is minimal; these ceramics also exhibit minimum degradation in their mechanical properties when exposed over time to environments containing water vapor[5].

(R. S. GORDON)

1. T. H. Etsell, S. N. Flengas, *Chem. Rev.*, *70*, 339 (1970).
2. R. S. Gordon, W. Fischer, A. V. Virkar, in *Ceramic Transactions* Vol. 65: *Role of Ceramics in Advanced Electrochemical Systems*, P. N. Kumpta, G. S. Roher, U. Balachandran, eds., American Ceramic Society, Westerville, OH, 1996, pp. 203–237.
3. N. Q. Minh, *J. Am. Ceram. Soc.*, *76*, 563 (1993).
4. A. H. Heur, L. W. Hobbs, in *Advanes in Ceramics*, Vol. 3: *Science And Technology of Zirconia*, A. H. Heur, L. W. Hobbs, eds., American Ceramic Society, Columbus, OH, 1981. pp. 98–115.
5. K. Kobayashi, H. Kawajima, T. Masaki, *Solid State Ionics*, *3–4*, 489 (1981).

Inorganic Reactions and Methods, Volume 18
Edited by J. J. Zuckerman, Jim D. Atwood

17.3.7.3.1. Powder Synthesis and Treatment.

Historically, stabilized (and partially stabilized) zirconia ceramics were prepared from powders in which the component oxides are mechanically blended prior to forming and sintering. Because solid state diffusion is sluggish, firing temperatures in excess of 1800°C are normally required. Furthermore, the dopant was nonuniformly distributed, leading to inferior electrical properties. Trace impurities in the raw materials can also lead to enhancement of electronic conductivity in certain temperature ranges, which is also undesirable. To overcome these problems, several procedures have been developed to prepare reactive (small particle size) and chemically pure and homogeneous precursor powders for both fully stabilized and partially stabilized material. Two of these are alkoxide synthesis and hydroxide coprecipitation.

(i) Alkoxide Synthesis. Using yttria-stabilized zirconia (YSZ) as an example, the alkoxide precursors for zirconium and yttrium are prepared by the following reactions[1,2]:

$$ZrCl_4 + 4C_3H_2OH + 4NH_3 \xrightarrow[C_6H_6]{5^\circ C} Zr(OC_3H_7)_4 + NH_4Cl \qquad (a)$$

$$Y + HgCl_2 + 3C_3H_7OH \xrightarrow[C_6H_6]{82^\circ C} Y(OC_3H_7)_3 + Hg + HCl + \tfrac{1}{2}H_2 \qquad (b)$$

Reactions (a) and (b) are completed, followed by filtration, distillation of C_6H_6, and recrystallization of the alkoxide compounds. The two alkoxide solutions (in benzene or *n*-hexane) are mixed and intimately mixed oxides are then coprecipitated as a result of the following hydrolysis reactions:

$$Zr(OC_3H_7)_4 + 2H_2O \longrightarrow ZrO_2 + 4C_3H_7OH \qquad (c)$$

$$2Y(OC_3H_7)_3 + 2H_2O \longrightarrow Y_2O_3 + 3C_3H_7OH \qquad (d)$$

After precipitation, the resultant powder is dried (100–110°C) and then milled to reduce the size of the agglomerates. Depending on the dopant concentration, calcination at 850°C yields a fully (cubic) or partially stabilized (cubic, tetragonal, etc.) powder with an average crystallite size of 40 nm (0.04 μm). After compaction, these powders can be sintered to near-theoretical density at 1450°C, a temperature 400°C lower than that possible with powders prepared from mechanically blended component oxides.

(ii) Hydroxide Coprecipitation. In this process[3,4], hydroxide gels are coprecipitated from chlorides in aqueous solutions as follows:

$$ZrCl_4 + aYCl_3 + (4 + 3a)NH_4OH \rightarrow Zr(OH)_4 + Y(OH)_3 + (4 + 3a)NH_4Cl \qquad (e)$$

The mixed solid hydroxides are washed with water to remove residual chloride ions, washed in alcohol (ethanol or propanol), and dried at 120°C. The hydroxide gel is decomposed at 500–1000°C, leading to a loosely agglomerated powder. The alcohol washing[5] is important in forming a precursor powder with weak and small ($\sim$1 μm) agglomerates. Very fine crystallites (20–50 nm) can be formed depending on the calcination temperature. Powders prepared and treated in the foregoing manner can be sintered to high densities in fully or partially stabilized form at temperatures as low as 1300°C.

In summary, alkoxide synthesis and hydroxide coprecipitation can be used to prepare chemically homogeneous particulates (< 100 nm) of partially and fully stabilized zirconia precursors. These powders, which are chemically homogeneous with respect to the stabilizer and chemically pure with respect to impurities, can be densified to very high sintered densities at relatively low temperatures (i.e., well below half the melting temperature of pure ZrO_2). These powders are suitable precursor powders for a number of forming operations including dry or isostatic pressing, electrophoretic deposition, extrusion, tape casting, and/or calendaring and film casting by numerous techniques[6]. In contrast to the β-aluminas, in which the precursor powders have water-soluble alkali constituents that require organic-based vehicles for many of these fabrication techniques, water-based solvents, binders, lubricants, etc. can be employed in operations (tape casting, extrusion, etc.) on stabilized and partially stabilized zirconia powder systems.

(R. S. GORDON)

1. K. S. Mazdiyasni, C. T. Lynch, J. S. Smith, *J. Am. Ceram. Soc., 48*, 372 (1965).
2. K. S. Mazdiyasni, C. T. Lynch, J. S. Smith, *J. Am. Ceram. Soc., 50*, 532 (1967).
3. K. Haberko, A. Ciesla, A. Pron, *Ceramurgia Int., 3*, 111 (1975).
4. K. Haberko, *Ceramurgia Int., 5*, 148 (1979).
5. C. S. Scott, J. S. Reed, *Am. Ceram. Soc. Bull. 58*, 587 (1979).
6. N. Q. Minh, *J. Am. Ceram. Soc., 76*, 563 (1993).

17.3.7.3.2. Densification Characteristics.

In contrast to the β''-aluminas, fine and chemically homogeneous powders are desired for the precursors prior to forming and sintering. This is probably because the densification mechanism differs in these materials (solid state diffusion vs. transient liquid phase sintering). The most important factor in solid state sintering at low temperatures (i.e., typically $\sim$1450°C) is a very fine crystallite size (< 100 nm), either as primary particulates or in weakly bonded small agglomerates (0.5–1 μm). Agglomerate-free particulates of fully stabilized zirconia prepared by alkoxide synthesis and subsequent centrifugal casting can be sintered to full density at temperatures down to 1100°C[1]. This very low temperature may be of interest in thin films or slurry coatings (< 50–100 μm) on another substrate material, where a low densification temperature would be very desirable. While fine, unagglomerated crystallites ensure a high sintered density at the lowest possible firing temperature, chemical homogeneity (and high purity) permits the attainment of optimum O^{2-} ion conductivity and minimum impurity-induced electronic conduction in the ceramic electrolyte.

Liquid-forming additives[2] can be used to reduce the densification temperature (1500–1600°C) of zirconia ceramics prepared from mechanically blended oxides. In contrast to β''-alumina, these additives form extrinsic (impurity-controlled) liquids that leave crystalline or glassy second phases at grain boundaries after firing. These phases, unless they are conductive, can degrade the ionic conductivity by more than an order of magnitude. In the case of β''-alumina, the liquid phases are intrinsic to the material. As the system approaches chemical homogeneity and equilibrium during firing, the liquids disappear, leaving no trace in the microstructure after densification (other than the presence of some exaggerated grain growth, which must be kept under control). Typical extrinsic liquid-forming additives (several mole or weight percent) in zirconia include SiO_2, CaO, Al_2O_3, TiO_2, Bi_2O_3, or kaolin [$Al_2(Si_2O_5)(OH)_2$]. Bi_2O_3, in combination with CaO or Y_2O_3, forms a reasonably conductive grain boundary phase (Bi_2O_3

Inorganic Reactions and Methods, Volume 18
Edited by J. J. Zuckerman, Jim D. Atwood

In summary, alkoxide synthesis and hydroxide coprecipitation can be used to prepare chemically homogeneous particulates (< 100 nm) of partially and fully stabilized zirconia precursors. These powders, which are chemically homogeneous with respect to the stabilizer and chemically pure with respect to impurities, can be densified to very high sintered densities at relatively low temperatures (i.e., well below half the melting temperature of pure ZrO_2). These powders are suitable precursor powders for a number of forming operations including dry or isostatic pressing, electrophoretic deposition, extrusion, tape casting, and/or calendaring and film casting by numerous techniques[6]. In contrast to the β-aluminas, in which the precursor powders have water-soluble alkali constituents that require organic-based vehicles for many of these fabrication techniques, water-based solvents, binders, lubricants, etc. can be employed in operations (tape casting, extrusion, etc.) on stabilized and partially stabilized zirconia powder systems.

(R. S. GORDON)

1. K. S. Mazdiyasni, C. T. Lynch, J. S. Smith, *J. Am. Ceram. Soc., 48*, 372 (1965).
2. K. S. Mazdiyasni, C. T. Lynch, J. S. Smith, *J. Am. Ceram. Soc., 50*, 532 (1967).
3. K. Haberko, A. Ciesla, A. Pron, *Ceramurgia Int., 3*, 111 (1975).
4. K. Haberko, *Ceramurgia Int., 5*, 148 (1979).
5. C. S. Scott, J. S. Reed, *Am. Ceram. Soc. Bull. 58*, 587 (1979).
6. N. Q. Minh, *J. Am. Ceram. Soc., 76*, 563 (1993).

17.3.7.3.2. Densification Characteristics.

In contrast to the β''-aluminas, fine and chemically homogeneous powders are desired for the precursors prior to forming and sintering. This is probably because the densification mechanism differs in these materials (solid state diffusion vs. transient liquid phase sintering). The most important factor in solid state sintering at low temperatures (i.e., typically $\sim$1450°C) is a very fine crystallite size (< 100 nm), either as primary particulates or in weakly bonded small agglomerates (0.5–1μm). Agglomerate-free particulates of fully stabilized zirconia prepared by alkoxide synthesis and subsequent centrifugal casting can be sintered to full density at temperatures down to 1100°C[1]. This very low temperature may be of interest in thin films or slurry coatings (< 50–100 μm) on another substrate material, where a low densification temperature would be very desirable. While fine, unagglomerated crystallites ensure a high sintered density at the lowest possible firing temperature, chemical homogeneity (and high purity) permits the attainment of optimum O^{2-} ion conductivity and minimum impurity-induced electronic conduction in the ceramic electrolyte.

Liquid-forming additives[2] can be used to reduce the densification temperature (1500–1600°C) of zirconia ceramics prepared from mechanically blended oxides. In contrast to β''-alumina, these additives form extrinsic (impurity-controlled) liquids that leave crystalline or glassy second phases at grain boundaries after firing. These phases, unless they are conductive, can degrade the ionic conductivity by more than an order of magnitude. In the case of β''-alumina, the liquid phases are intrinsic to the material. As the system approaches chemical homogeneity and equilibrium during firing, the liquids disappear, leaving no trace in the microstructure after densification (other than the presence of some exaggerated grain growth, which must be kept under control). Typical extrinsic liquid-forming additives (several mole or weight percent) in zirconia include SiO_2, CaO, Al_2O_3, TiO_2, Bi_2O_3, or kaolin [$Al_2(Si_2O_5)(OH)_2$]. Bi_2O_3, in combination with CaO or Y_2O_3, forms a reasonably conductive grain boundary phase (Bi_2O_3

stabilized with Y_2O_3 is a good oxygen ion conductor) and leads to sintering temperatures as low as 1080°C. The ionic conductivity of this material is degraded by only a factor of 3. To be effective, the liquids must wet the zirconia grains, and the matrix zirconia material must have limited solubility in the liquid.

While relatively impure commercial sources of the component oxides [e.g., commercial zirconia is derived from the mineral zircon, ($ZrSiO_4$)] can be used in mechanically mixed powder blends as the starting raw materials for fabrication of stabilized and partially stabilized zirconia ceramics, significant sacrifice in the resulting properties (i.e., O^{2-} ion conductivity) can be expected. This is a result of the use of liquid-forming additives to achieve reasonable temperatures of densification. While this practice may be acceptable for ceramics produced in bulk form for relatively low performance applications, it is probably not acceptable in high performance materials required for advanced electrochemical devices. This is particularly the case when the ceramic electrolytes are used in the form of highly conducting thin films, coatings, or thin plates. Under such circumstances, chemically homogeneous and high purity precursor powders that can be densified at the lowest possible temperature (i.e., $\leq$ 1450°C) are preferred. These materials have the highest possible O^{2-} ion conductivities and the lowest impurity-induced electronic conductivity.

(R. S. GORDON)

1. W. H. Rhodes, *J. Am. Ceram. Soc.*, *64*, 19 (1981).
2. R. J. Brook, Advances in Ceramics, Vol 3: in *Science and Technology of Zirconia*, A. H. Heur, L. W. Hobbs, eds., American Ceramic Society, Columbus, OH, 1981, pp. 272–285.

17.3.7.3.3. Thin Films and Coatings.

Thin films and coatings can be fabricated by vapor deposition [i.e., chemical vapor deposition (CVD) and electrochemical vapor deposition (EVD)], sputtering, sol–gel processing, and electrophoretic deposition[1,2]. Electrochemical vapor deposition, a thin-film technique, is used to form thin ($\sim$40 μm) layers of dense yttria-stabilized zirconia in the seal-less tubular solid oxide fuel cell[3,4]. Thin layers of stabilized zirconia are required in this application to keep the internal resistance and the operating temperature of the electrochemical device as low as possible.

In EVD, a modified form of chemical vapor deposition (CVD), an electrochemical potential gradient is used to grow a thin, dense layer of the ionic conducting oxide (e.g., yttria-stabilized zirconia) on a porous substrate. EVD is either a single-step or a two-step process depending on the nature of the substrate. For a porous substrate, the first step involves pore closure by CVD (i.e., deposition from the vapor of an oxide layer by reaction of a chloride gas precursor compound with water vapor or oxygen):

$$MCl_x + (x/2)H_2O \longrightarrow MO_{x/2} + xHCl \qquad \text{(a)}$$

Once the pores in the substrate have closed, the reactant vapors are no longer in direct contact with each other. Film growth then proceeds under the driving force of an electrochemical potential gradient over the deposited film. In this step, oxygen ions formed on the water vapor side of the substrate diffuse through the thin metal oxide layer to the metal chloride (vapor) side. Here oxygen ions react with the metal chloride vapors to form the metal oxide product. The two electrochemical reactions that control the rate of oxide film growth are as follows:

Inorganic Reactions and Methods, Volume 18
Edited by J. J. Zuckerman, Jim D. Atwood

stabilized with Y_2O_3 is a good oxygen ion conductor) and leads to sintering temperatures as low as 1080°C. The ionic conductivity of this material is degraded by only a factor of 3. To be effective, the liquids must wet the zirconia grains, and the matrix zirconia material must have limited solubility in the liquid.

While relatively impure commercial sources of the component oxides [e.g., commercial zirconia is derived from the mineral zircon, $(ZrSiO_4)$] can be used in mechanically mixed powder blends as the starting raw materials for fabrication of stabilized and partially stabilized zirconia ceramics, significant sacrifice in the resulting properties (i.e., O^{2-} ion conductivity) can be expected. This is a result of the use of liquid-forming additives to achieve reasonable temperatures of densification. While this practice may be acceptable for ceramics produced in bulk form for relatively low performance applications, it is probably not acceptable in high performance materials required for advanced electrochemical devices. This is particularly the case when the ceramic electrolytes are used in the form of highly conducting thin films, coatings, or thin plates. Under such circumstances, chemically homogeneous and high purity precursor powders that can be densified at the lowest possible temperature (i.e., $\leq$ 1450°C) are preferred. These materials have the highest possible O^{2-} ion conductivities and the lowest impurity-induced electronic conductivity.

(R. S. GORDON)

1. W. H. Rhodes, *J. Am. Ceram. Soc., 64*, 19 (1981).
2. R. J. Brook, Advances in Ceramics, Vol 3: in *Science and Technology of Zirconia*, A. H. Heur, L. W. Hobbs, eds., American Ceramic Society, Columbus, OH, 1981, pp. 272–285.

17.3.7.3.3. Thin Films and Coatings.

Thin films and coatings can be fabricated by vapor deposition [i.e., chemical vapor deposition (CVD) and electrochemical vapor deposition (EVD)], sputtering, sol–gel processing, and electrophoretic deposition[1,2]. Electrochemical vapor deposition, a thin-film technique, is used to form thin ($\sim$40 μm) layers of dense yttria-stabilized zirconia in the seal-less tubular solid oxide fuel cell[3,4]. Thin layers of stabilized zirconia are required in this application to keep the internal resistance and the operating temperature of the electrochemical device as low as possible.

In EVD, a modified form of chemical vapor deposition (CVD), an electrochemical potential gradient is used to grow a thin, dense layer of the ionic conducting oxide (e.g., yttria-stabilized zirconia) on a porous substrate. EVD is either a single-step or a two-step process depending on the nature of the substrate. For a porous substrate, the first step involves pore closure by CVD (i.e., deposition from the vapor of an oxide layer by reaction of a chloride gas precursor compound with water vapor or oxygen):

$$MCl_x + (x/2)H_2O \longrightarrow MO_{x/2} + xHCl \qquad \text{(a)}$$

Once the pores in the substrate have closed, the reactant vapors are no longer in direct contact with each other. Film growth then proceeds under the driving force of an electrochemical potential gradient over the deposited film. In this step, oxygen ions formed on the water vapor side of the substrate diffuse through the thin metal oxide layer to the metal chloride (vapor) side. Here oxygen ions react with the metal chloride vapors to form the metal oxide product. The two electrochemical reactions that control the rate of oxide film growth are as follows:

Water vapor side of the substrate

$$(x/2)H_2O + xe' = (x/2)H_2 + (x/2)O^{2-} \quad (b)$$

Metal chloride vapor side of growing oxide

$$MeCl_x + (x/2)O^{2-} \longrightarrow MeO_{x/2} + (x/2)Cl_2 + xe' \quad (c)$$

Since oxygen ions are the fastest ion-diffusing species in the film, the oxide thin film grows in the direction of the chloride gas phase. The oxygen ion flux during growth of the oxide is balanced by the electron flux and the scale growth is self-leveling, resulting in a uniform film thickness. The growth rate of the film can be controlled by varying the reactant concentration, temperature, and pressure. The disadvantages of the process are the high reaction temperature, the presence of corrosive gases, and the relatively low deposition rates. The technique is generally applicable to any oxide ionic conductor.

(R. S. GORDON)

1. N. Q. Minh, *J. Am. Ceram. Soc.*, *76*, 563 (1993).
2. F. J. Rohr, in *Solid Electrolytes*, P. Hagenmuller, W. van Gool, eds., Academic Press, New York, 1978, pp. 431–449.
3. A. O. Isenberg, in *Electrode Materials and Processes for Energy Conversion and Storage*, PV 77-6, J. D. E. McIntyre, S. Srinivasan, F. G. Will, eds., Electrochemical Society Softbound Proceedings Series, Princeton, NJ, 1977, p. 572.
4. J. F. Jue, J. Jusko, A. V. Virkar, *J. Electrochem. Soc.*, *139*, 2458 (1992).

17.3.7.4. Alternate Oxygen Ion Conducting Electrolytes

Other oxygen ion conductors that have potential use as solid electrolytes in electrochemical devices are stabilized bismuth and cerium oxides and oxide compounds with the perovskite and pyrochlore crystal structures. The ionic conductivity and related properties of these compounds in comparison with those of the standard yttria–stabilized zirconia (YSZ) electrolyte are briefly described in this section. Many of the powder preparation and ceramic fabrication techniques described above for zirconia-based electrolytes can be adapted to these alternative conductors and are not discussed further.

(R. S. GORDON)

17.3.7.4.1. Bismuth Oxide.

The oxygen ion conductivity of yttria-stabilized bismuth oxide (25 mol% Y_2O_3) is approximately 45 times higher than that of YSZ at 600°C[1]. In fact, the pure form of the cubic phase has an even higher conductivity [$\sim 1\ (\Omega \cdot cm)^{-1}$] near its melting temperature of 825°C. Among the oxygen ion conductors, pure and stabilized forms of bismuth oxide have the highest O^{2-} ion conductivities. The high conductivity in pure bismuth oxide is due to an intrinsic oxygen vacancy concentration of $\sim$ 25%. The cubic phase of bismuth oxide undergoes a phase transition to the monoclinic polymorph below 730°C. The cubic phase can be stabilized to lower temperatures by addition of various rare earth oxides: Y_2O_3, Nb_2O_3, Ta_2O_5, or WO_3.

The O^{2-} ion conductivity of bismuth oxide is decreased with increasing concentration of Y_2O_3 dopant. Dopant concentrations of at least 25 mol% Y_2O_3 are necessary to stabilize the cubic structure at temperatures below 730°C. The higher conductivity of stabilized bismuth oxide compared to yttria-stabilized zirconia offers the possibility of its use as a solid electrolyte in the solid oxide fuel cell at reduced temperatures. However, the

Inorganic Reactions and Methods, Volume 18
Edited by J. J. Zuckerman, Jim D. Atwood

Water vapor side of the substrate

$$(x/2)H_2O + xe' = (x/2)H_2 + (x/2)O^{2-} \quad (b)$$

Metal chloride vapor side of growing oxide

$$MeCl_x + (x/2)O^{2-} \longrightarrow MeO_{x/2} + (x/2)Cl_2 + xe' \quad (c)$$

Since oxygen ions are the fastest ion-diffusing species in the film, the oxide thin film grows in the direction of the chloride gas phase. The oxygen ion flux during growth of the oxide is balanced by the electron flux and the scale growth is self-leveling, resulting in a uniform film thickness. The growth rate of the film can be controlled by varying the reactant concentration, temperature, and pressure. The disadvantages of the process are the high reaction temperature, the presence of corrosive gases, and the relatively low deposition rates. The technique is generally applicable to any oxide ionic conductor.

(R. S. GORDON)

1. N. Q. Minh, *J. Am. Ceram. Soc.*, *76*, 563 (1993).
2. F. J. Rohr, in *Solid Electrolytes*, P. Hagenmuller, W. van Gool, eds., Academic Press, New York, 1978, pp. 431–449.
3. A. O. Isenberg, in *Electrode Materials and Processes for Energy Conversion and Storage*, PV 77-6, J. D. E. McIntyre, S. Srinivasan, F. G. Will, eds., Electrochemical Society Softbound Proceedings Series, Princeton, NJ, 1977, p. 572.
4. J. F. Jue, J. Jusko, A. V. Virkar, *J. Electrochem. Soc.*, *139*, 2458 (1992).

17.3.7.4. Alternate Oxygen Ion Conducting Electrolytes

Other oxygen ion conductors that have potential use as solid electrolytes in electrochemical devices are stabilized bismuth and cerium oxides and oxide compounds with the perovskite and pyrochlore crystal structures. The ionic conductivity and related properties of these compounds in comparison with those of the standard yttria–stabilized zirconia (YSZ) electrolyte are briefly described in this section. Many of the powder preparation and ceramic fabrication techniques described above for zirconia-based electrolytes can be adapted to these alternative conductors and are not discussed further.

(R. S. GORDON)

17.3.7.4.1. Bismuth Oxide.

The oxygen ion conductivity of yttria-stabilized bismuth oxide (25 mol% Y_2O_3) is approximately 45 times higher than that of YSZ at 600°C[1]. In fact, the pure form of the cubic phase has an even higher conductivity [$\sim 1\ (\Omega \cdot cm)^{-1}$] near its melting temperature of 825°C. Among the oxygen ion conductors, pure and stabilized forms of bismuth oxide have the highest O^{2-} ion conductivities. The high conductivity in pure bismuth oxide is due to an intrinsic oxygen vacancy concentration of $\sim$ 25%. The cubic phase of bismuth oxide undergoes a phase transition to the monoclinic polymorph below 730°C. The cubic phase can be stabilized to lower temperatures by addition of various rare earth oxides: Y_2O_3, Nb_2O_3, Ta_2O_5, or WO_3.

The O^{2-} ion conductivity of bismuth oxide is decreased with increasing concentration of Y_2O_3 dopant. Dopant concentrations of at least 25 mol% Y_2O_3 are necessary to stabilize the cubic structure at temperatures below 730°C. The higher conductivity of stabilized bismuth oxide compared to yttria-stabilized zirconia offers the possibility of its use as a solid electrolyte in the solid oxide fuel cell at reduced temperatures. However, the

principal disadvantages of this material are the limited range of oxygen partial pressures over which the material remains an ionic conductor, its tendency to phase-transform into the low conductivity monoclinic phase at temperatures below 730°C, and its tendency to be reduced into bismuth metal at oxygen partial pressures lower than about 10^{-13} atm at 600°C. While tetravalent dopants (e.g., 1–10 mol% ZrO_2) in substitutional solid solution, are effective in inhibiting the kinetics of transformation into the monoclinic phase[2], the material is still unstable in atmospheres with oxygen partial pressures comparable to the fuel gas in the solid oxide fuel cell. Therefore, practical use of this material as the electrolyte in some electrochemical devices may require protection from direct exposure to reducing gas environments.

(R. S. GORDON)

1. T. Takahashi, H. Iwahara, T. Arao, *J. Appl. Electrochem., 5*, 187 (1975).
2. K. Z. Fung, A. V. Virkar, *J. Am. Ceram. Soc., 74*, 1970 (1991).

17.3.7.4.2. Cerium Oxide

Yttria-doped (~20 mol% Y_2O_3) cerium oxide also has a higher O^{2-} ion conductivity than yttria-stabilized zirconia (~factors of 11–18 at 600°C), which would make it an attractive choice for an electrolyte at lower temperatures ($\leq$ 800°C)[1]. However, doped cerium oxides tend to undergo reduction, with formation of trivalent cerium ions and oxygen ion vacancies, $V_O^{\cdot\cdot}$ leading to the onset of electronic conductivity according to:

$$O_O \longrightarrow \tfrac{1}{2} O_2 + V_O^{\cdot\cdot} + 2e' \qquad \text{(a)}$$

This tendency for reduction restricts the range of oxygen partial pressures over which the ionic transference number remains close to unity. For example, at 800°C, the oxygen partial pressure in the lower limit is restricted to partial pressures over 10^{-12} atm. This lower limit has been extended with no loss in conductivity to 10^{-21} atm at 700°C in ceria doped with 20 mol% Gd_2O_3 by replacing ~3% of the gadolinium with praseodymium.

Another approach to developing an electrolyte with a higher O^{2-} ion conductivity, which is compatible with highly reducing atmospheres, is to deposit a thin layer (5–10 μm) of YSZ or yttria-stabilized ThO_2 on the low oxygen partial pressure side of a thicker (125–150 μm) high conductivity electrolyte such as stabilized ceria or bismuth oxide[2,3]. The composite electrolyte has the advantage of stability at low oxygen partial pressures, while the ohmic internal resistance of the electrolyte composite is considerably lower than an electrolyte composed entirely of yttria-stabilized zirconia. These thin electrolyte layers can be deposited by the EVD process described earlier or by dip-coating and sintering.

(R. S. GORDON)

1. N. Q. Minh, *J. Am. Cerm. Soc., 76*, 563 (1993).
2. A. V. Virkar, *J. Electrochem. Soc., 138*, 1481 (1991).
3. J. F. Jue, J. Jusko, A. V. Virkar, *J. Electrochem. Soc., 139*, 2458 (1992).

17.3.7.4.3. Perovskite and Pyrochlore Oxides.

Perovskite (ABO_3 in which A is divalent and B is tetravalent) and pyrochlore ($A_2B_2O_7$ in which A is trivalent and B is tetravalent) oxide compounds have been proposed as oxygen ion conducting electrolytes for electrochemical devices[1–3]. Some of the perovskite structures (e.g., $BaCeO_3$ and $SrCeO_3$) are generating interest because of

Inorganic Reactions and Methods, Volume 18
Edited by J. J. Zuckerman, Jim D. Atwood

principal disadvantages of this material are the limited range of oxygen partial pressures over which the material remains an ionic conductor, its tendency to phase-transform into the low conductivity monoclinic phase at temperatures below 730°C, and its tendency to be reduced into bismuth metal at oxygen partial pressures lower than about 10^{-13} atm at 600°C. While tetravalent dopants (e.g., 1–10 mol% ZrO_2) in substitutional solid solution, are effective in inhibiting the kinetics of transformation into the monoclinic phase[2], the material is still unstable in atmospheres with oxygen partial pressures comparable to the fuel gas in the solid oxide fuel cell. Therefore, practical use of this material as the electrolyte in some electrochemical devices may require protection from direct exposure to reducing gas environments.

(R. S. GORDON)

1. T. Takahashi, H. Iwahara, T. Arao, *J. Appl. Electrochem., 5*, 187 (1975).
2. K. Z. Fung, A. V. Virkar, *J. Am. Ceram. Soc., 74*, 1970 (1991).

17.3.7.4.2. Cerium Oxide

Yttria-doped (~20 mol% Y_2O_3) cerium oxide also has a higher O^{2-} ion conductivity than yttria-stabilized zirconia (~factors of 11–18 at 600°C), which would make it an attractive choice for an electrolyte at lower temperatures ($\leq$ 800°C)[1]. However, doped cerium oxides tend to undergo reduction, with formation of trivalent cerium ions and oxygen ion vacancies, $V_O^{\cdot\cdot}$ leading to the onset of electronic conductivity according to:

$$O_O \longrightarrow \tfrac{1}{2}\, O_2 + V_O^{\cdot\cdot} + 2e' \qquad \text{(a)}$$

This tendency for reduction restricts the range of oxygen partial pressures over which the ionic transference number remains close to unity. For example, at 800°C, the oxygen partial pressure in the lower limit is restricted to partial pressures over 10^{-12} atm. This lower limit has been extended with no loss in conductivity to 10^{-21} atm at 700°C in ceria doped with 20 mol% Gd_2O_3 by replacing ~3% of the gadolinium with praseodymium.

Another approach to developing an electrolyte with a higher O^{2-} ion conductivity, which is compatible with highly reducing atmospheres, is to deposit a thin layer (5–10 μm) of YSZ or yttria-stabilized ThO_2 on the low oxygen partial pressure side of a thicker (125–150 μm) high conductivity electrolyte such as stabilized ceria or bismuth oxide[2,3]. The composite electrolyte has the advantage of stability at low oxygen partial pressures, while the ohmic internal resistance of the electrolyte composite is considerably lower than an electrolyte composed entirely of yttria-stabilized zirconia. These thin electrolyte layers can be deposited by the EVD process described earlier or by dip-coating and sintering.

(R. S. GORDON)

1. N. Q. Minh, *J. Am. Cerm. Soc., 76*, 563 (1993).
2. A. V. Virkar, *J. Electrochem. Soc., 138*, 1481 (1991).
3. J. F. Jue, J. Jusko, A. V. Virkar, *J. Electrochem. Soc., 139*, 2458 (1992).

17.3.7.4.3. Perovskite and Pyrochlore Oxides.

Perovskite (ABO_3 in which A is divalent and B is tetravalent) and pyrochlore ($A_2B_2O_7$ in which A is trivalent and B is tetravalent) oxide compounds have been proposed as oxygen ion conducting electrolytes for electrochemical devices[1–3]. Some of the perovskite structures (e.g., $BaCeO_3$ and $SrCeO_3$) are generating interest because of

Inorganic Reactions and Methods, Volume 18
Edited by J. J. Zuckerman, Jim D. Atwood

principal disadvantages of this material are the limited range of oxygen partial pressures over which the material remains an ionic conductor, its tendency to phase-transform into the low conductivity monoclinic phase at temperatures below 730°C, and its tendency to be reduced into bismuth metal at oxygen partial pressures lower than about 10^{-13} atm at 600°C. While tetravalent dopants (e.g., 1–10 mol% ZrO_2) in substitutional solid solution, are effective in inhibiting the kinetics of transformation into the monoclinic phase[2], the material is still unstable in atmospheres with oxygen partial pressures comparable to the fuel gas in the solid oxide fuel cell. Therefore, practical use of this material as the electrolyte in some electrochemical devices may require protection from direct exposure to reducing gas environments.

(R. S. GORDON)

1. T. Takahashi, H. Iwahara, T. Arao, *J. Appl. Electrochem., 5*, 187 (1975).
2. K. Z. Fung, A. V. Virkar, *J. Am. Ceram. Soc., 74*, 1970 (1991).

17.3.7.4.2. Cerium Oxide

Yttria-doped (~20 mol% Y_2O_3) cerium oxide also has a higher O^{2-} ion conductivity than yttria-stabilized zirconia (~factors of 11–18 at 600°C), which would make it an attractive choice for an electrolyte at lower temperatures ($\leq$ 800°C)[1]. However, doped cerium oxides tend to undergo reduction, with formation of trivalent cerium ions and oxygen ion vacancies, $V_O^{\cdot\cdot}$ leading to the onset of electronic conductivity according to:

$$O_O \longrightarrow \tfrac{1}{2}\, O_2 + V_O^{\cdot\cdot} + 2e' \qquad \text{(a)}$$

This tendency for reduction restricts the range of oxygen partial pressures over which the ionic transference number remains close to unity. For example, at 800°C, the oxygen partial pressure in the lower limit is restricted to partial pressures over 10^{-12} atm. This lower limit has been extended with no loss in conductivity to 10^{-21} atm at 700°C in ceria doped with 20 mol% Gd_2O_3 by replacing ~3% of the gadolinium with praseodymium.

Another approach to developing an electrolyte with a higher O^{2-} ion conductivity, which is compatible with highly reducing atmospheres, is to deposit a thin layer (5–10 μm) of YSZ or yttria-stabilized ThO_2 on the low oxygen partial pressure side of a thicker (125–150 μm) high conductivity electrolyte such as stabilized ceria or bismuth oxide[2,3]. The composite electrolyte has the advantage of stability at low oxygen partial pressures, while the ohmic internal resistance of the electrolyte composite is considerably lower than an electrolyte composed entirely of yttria-stabilized zirconia. These thin electrolyte layers can be deposited by the EVD process described earlier or by dip-coating and sintering.

(R. S. GORDON)

1. N. Q. Minh, *J. Am. Cerm. Soc., 76*, 563 (1993).
2. A. V. Virkar, *J. Electrochem. Soc., 138*, 1481 (1991).
3. J. F. Jue, J. Jusko, A. V. Virkar, *J. Electrochem. Soc., 139*, 2458 (1992).

17.3.7.4.3. Perovskite and Pyrochlore Oxides.

Perovskite (ABO_3 in which A is divalent and B is tetravalent) and pyrochlore ($A_2B_2O_7$ in which A is trivalent and B is tetravalent) oxide compounds have been proposed as oxygen ion conducting electrolytes for electrochemical devices[1–3]. Some of the perovskite structures (e.g., $BaCeO_3$ and $SrCeO_3$) are generating interest because of

their proton-conducting characteristics. To date, none of these compounds have exhibited O^{2-} conductivities higher than the baseline YSZ electrolyte (refer to Table 1 in 17.3.7). The pyrochlore compounds do have two attractive features: (1) high intrinsic O^{2-} ion conductivity (hence no doping is required) and (2) with the equilibrium pyrochlore phase, no long-term aging effects are expected. Because the oxygen ion resistivities are higher (100–200 Ω cm), these materials may eventually find applications in the form of thin-film (20–50 μm) electrolytes.

(R. S. GORDON)

1. N. Q. Minh, *J. Am. Ceram. Soc.*, *76*, 563 (1993).
2. H. L. Tuller, P. K. Moon, *Mater. Sci. Eng.*, *B1*, 171 (1988).
3. J. A. Kilner, R. J. Brook, *Solid State Ionics*, *6*, 237 (1982).

17.3.7.5. Proton-Conducting Solid Electrolytes

Proton conductors with attractive conductivities are in the class of doped perovskite materials with the following compositions: $BaCe_{0.9}Nd_{0.1}O_{3-\delta}$ and $SrCe_{0.9}Y_{0.1}O_{3-\delta}$ and solid solutions of $BaThO_3$ and Nd_2O_3[1–3].

Protons can be incorporated into the perovskite structure by incorporation of water from the atmosphere:

$$H_2O + V_O^{\cdot\cdot} = O_O + 2H_i^{\cdot} \qquad (a)$$

If the resulting protons ($H_i^{\cdot}$) are associated with OH^- ions substituting in the lattice for O^{2-} ions, then reaction (b) is more accurate.

$$H_2O + O_O + V_O^{\cdot\cdot} = 2OH_O^{\cdot} \qquad (b)$$

Protons can migrate through the lattice either as interstitials or by hopping from one oxygen ion to another. Another possibility is the migration of OH^- ions via exchange with oxygen ion vacancies. Currently the experimental evidence supports the hopping conduction mechanism.

The low ionic resistivities of these materials (reported to be under 10 Ω cm at 1000°C in some compositions) make them very attractive candidates for use in electrochemical devices such as the solid oxide fuel cell. Their proton conductivity is highly dependent on the partial pressure of water in the atmosphere. Whether these materials exhibit long-term stability in highly oxidizing and/or highly reducing atmospheres remains to be seen[4]. Many of the preparation techniques discussed for the oxygen ion conductors should be applicable to this relatively new class of ionic conductors.

(R. S. GORDON)

1. H. Iwahara, H. Uchida, K. Ono, K. Ogaki, *J. Electrochem. Soc.*, *135*, 529 (1988).
2. H. Iwahara, T. Esaka, H. Uchida, N. Maeda, *Solid State Ionics*, *3–4*, 359 (1981).
3. T. Tsui, T. Suzuki, H. Iwahara, *Solid State Ionics*, *70–71*, 291 (1994).
4. A. V. Virkar, University of Utah, Salt Lake City, private communication.

17.3.8. Preparation of Semiconductors

17.3.8.1. Elemental Semiconductors

The large number of applications of the elemental semiconductors silicon and germanium is reflected in the wide range of purity and crystalline perfection over which

Inorganic Reactions and Methods, Volume 18
Edited by J. J. Zuckerman, Jim D. Atwood

their proton-conducting characteristics. To date, none of these compounds have exhibited O^{2-} conductivities higher than the baseline YSZ electrolyte (refer to Table 1 in 17.3.7). The pyrochlore compounds do have two attractive features: (1) high intrinsic O^{2-} ion conductivity (hence no doping is required) and (2) with the equilibrium pyrochlore phase, no long-term aging effects are expected. Because the oxygen ion resistivities are higher (100–200 Ω cm), these materials may eventually find applications in the form of thin-film (20–50 μm) electrolytes.

(R. S. GORDON)

1. N. Q. Minh, *J. Am. Ceram. Soc., 76*, 563 (1993).
2. H. L. Tuller, P. K. Moon, *Mater. Sci. Eng., B1*, 171 (1988).
3. J. A. Kilner, R. J. Brook, *Solid State Ionics, 6*, 237 (1982).

17.3.7.5. Proton-Conducting Solid Electrolytes

Proton conductors with attractive conductivities are in the class of doped perovskite materials with the following compositions: $BaCe_{0.9}Nd_{0.1}O_{3-\delta}$ and $SrCe_{0.9}Y_{0.1}O_{3-\delta}$ and solid solutions of $BaThO_3$ and Nd_2O_3[1–3].

Protons can be incorporated into the perovskite structure by incorporation of water from the atmosphere:

$$H_2O + V_O^{\cdot\cdot} = O_O + 2H_i^{\cdot} \qquad (a)$$

If the resulting protons ($H_i^{\cdot}$) are associated with OH^- ions substituting in the lattice for O^{2-} ions, then reaction (b) is more accurate.

$$H_2O + O_O + V_O^{\cdot\cdot} = 2OH_O^{\cdot} \qquad (b)$$

Protons can migrate through the lattice either as interstitials or by hopping from one oxygen ion to another. Another possibility is the migration of OH^- ions via exchange with oxygen ion vacancies. Currently the experimental evidence supports the hopping conduction mechanism.

The low ionic resistivities of these materials (reported to be under 10 Ω cm at 1000°C in some compositions) make them very attractive candidates for use in electrochemical devices such as the solid oxide fuel cell. Their proton conductivity is highly dependent on the partial pressure of water in the atmosphere. Whether these materials exhibit long-term stability in highly oxidizing and/or highly reducing atmospheres remains to be seen[4]. Many of the preparation techniques discussed for the oxygen ion conductors should be applicable to this relatively new class of ionic conductors.

(R. S. GORDON)

1. H. Iwahara, H. Uchida, K. Ono, K. Ogaki, *J. Electrochem. Soc., 135*, 529 (1988).
2. H. Iwahara, T. Esaka, H. Uchida, N. Maeda, *Solid State Ionics, 3–4*, 359 (1981).
3. T. Tsui, T. Suzuki, H. Iwahara, *Solid State Ionics, 70–71*, 291 (1994).
4. A. V. Virkar, University of Utah, Salt Lake City, private communication.

17.3.8. Preparation of Semiconductors

17.3.8.1. Elemental Semiconductors

The large number of applications of the elemental semiconductors silicon and germanium is reflected in the wide range of purity and crystalline perfection over which

Inorganic Reactions and Methods, Volume 18
Edited by J. J. Zuckerman, Jim D. Atwood

their proton-conducting characteristics. To date, none of these compounds have exhibited O^{2-} conductivities higher than the baseline YSZ electrolyte (refer to Table 1 in 17.3.7). The pyrochlore compounds do have two attractive features: (1) high intrinsic O^{2-} ion conductivity (hence no doping is required) and (2) with the equilibrium pyrochlore phase, no long-term aging effects are expected. Because the oxygen ion resistivities are higher (100–200 Ω cm), these materials may eventually find applications in the form of thin-film (20–50 μm) electrolytes.

(R. S. GORDON)

1. N. Q. Minh, *J. Am. Ceram. Soc., 76*, 563 (1993).
2. H. L. Tuller, P. K. Moon, *Mater. Sci. Eng., B1*, 171 (1988).
3. J. A. Kilner, R. J. Brook, *Solid State Ionics, 6*, 237 (1982).

17.3.7.5. Proton-Conducting Solid Electrolytes

Proton conductors with attractive conductivities are in the class of doped perovskite materials with the following compositions: $BaCe_{0.9}Nd_{0.1}O_{3-\delta}$ and $SrCe_{0.9}Y_{0.1}O_{3-\delta}$ and solid solutions of $BaThO_3$ and Nd_2O_3[1–3].

Protons can be incorporated into the perovskite structure by incorporation of water from the atmosphere:

$$H_2O + V_O^{\cdot\cdot} = O_O + 2H_i^{\cdot} \qquad (a)$$

If the resulting protons ($H_i^{\cdot}$) are associated with OH^- ions substituting in the lattice for O^{2-} ions, then reaction (b) is more accurate.

$$H_2O + O_O + V_O^{\cdot\cdot} = 2OH_O^{\cdot} \qquad (b)$$

Protons can migrate through the lattice either as interstitials or by hopping from one oxygen ion to another. Another possibility is the migration of OH^- ions via exchange with oxygen ion vacancies. Currently the experimental evidence supports the hopping conduction mechanism.

The low ionic resistivities of these materials (reported to be under 10 Ω cm at 1000°C in some compositions) make them very attractive candidates for use in electrochemical devices such as the solid oxide fuel cell. Their proton conductivity is highly dependent on the partial pressure of water in the atmosphere. Whether these materials exhibit long-term stability in highly oxidizing and/or highly reducing atmospheres remains to be seen[4]. Many of the preparation techniques discussed for the oxygen ion conductors should be applicable to this relatively new class of ionic conductors.

(R. S. GORDON)

1. H. Iwahara, H. Uchida, K. Ono, K. Ogaki, *J. Electrochem. Soc., 135*, 529 (1988).
2. H. Iwahara, T. Esaka, H. Uchida, N. Maeda, *Solid State Ionics, 3–4*, 359 (1981).
3. T. Tsui, T. Suzuki, H. Iwahara, *Solid State Ionics, 70–71*, 291 (1994).
4. A. V. Virkar, University of Utah, Salt Lake City, private communication.

17.3.8. Preparation of Semiconductors

17.3.8.1. Elemental Semiconductors

The large number of applications of the elemental semiconductors silicon and germanium is reflected in the wide range of purity and crystalline perfection over which

these semiconductors are currently produced. Low cost infrared lenses, for example, can be manufactured from low purity polycrystalline material, while at the other extreme, nuclear radiation detectors require nearly ideal single crystals of several centimeters in diameter and length with impurity concentrations as low as 0.001 ppb (1 in 10^{12}). These widely varying requirements have led to a number of manufacturing methods/processes.

Metallurgical silicon—obtained from the reduction of various forms of quartz with carbon—is the starting material for semiconductor-grade silicon. Metallurgical silicon is converted to silicon tetrachloride ($SiCl_4$) and trichlorosilane ($SiHCl_3$), which are purified by fractional distillation. Pure polycrystalline silicon is obtained by chemical vapor deposition of the silicon compounds on an electrically heated silicon rod[1]. These rods are left to grow up to ~ 15 cm diameter. The purity of such polysilicon is typically better than 1 ppb of electrically active impurities (i.e., mainly group IIIB and VB elements). For many applications, the impurity of the polysilicon at this stage is sufficient, and conversion into a single crystal is obtained with either the Czochralski[2] or the floating-zone process[3].

The Czochralski method uses a melt in a rotating silica crucible inside a resistance-heated graphite susceptor. The ambient is typically 1 atm of argon. A counterrotating single crystal seed (usually oriented along $\langle 111 \rangle$ or $\langle 100 \rangle$) is dipped into the melt. Heat is lost through the seed, setting up a temperature gradient leading to crystal growth. Single crystals of almost cylindrical shape, typically 15 or 20 cm in diameter and over 100 cm long, are routinely grown for semiconductor device applications. Crystals of 30 and 40 cm diameter are now being developed. All crystals are free of extended defects such as dislocations or stacking faults.

Reduction of the silica crucible by the melted silicon yields free oxygen, which in turn reacts with the graphite heater elements. A large number of simultaneously occurring reactions[4] lead to an oxygen concentration of $\cong 10^{18}$ cm^{-3} and a carbon concentration of $\cong 5 \times 10^{17-18}$ cm^{-3} in the final crystal. Although both impurities are neutral when atomically dispersed in the silicon crystal lattice, they readily form electrically active impurity complexes. It is one of the more important aspects of electronic device development that the presence of this high oxygen concentration has turned out to be beneficial and is specified and controlled by the crystal grower. Slices of the single crystal (wafers) are given heat treatments that alternately dissolve and reprecipitate the excess oxygen to the interior, which leads to a near-surface region depleted of defects and a center with SiO_2 precipitates that getter heavy metal impurities while strengthening the wafer by precipitation hardening. This process has been named "defect engineering" and is crucial to all integrated circuit devices[5].

Depending on the specific application, the silicon crystal is doped with donors or acceptors. Because of impurity segregation between the melt and the solid, one cannot obtain a constant impurity concentration profile along the growth axis of a single crystal. Reintroduction of doping pellets (small silicon pieces with a very high impurity concentration) and counterdoping during the growth process lead to more constant impurity profiles.

The floating-zone purification and crystal growing technique[3] avoids the crucible. A melted zone up to a few centimeters long is supported by the silicon surface tension and by radiofrequency eddy currents between two vertical silicon cylinders. The radiofrequency field is also the heating source. The liquid zone is typically kept at a fixed position. The upper silicon rod is fed downward to the zone, while the lower rod is withdrawn toward the bottom of the floating zone apparatus. The geometry can be used

for zone purification (see 17.2.7.1), in which case both solid silicon cylinders are polycrystalline. After sufficient purification has been achieved, a final pass starting with a single crystal seed at the bottom yields a single crystal.

Extreme mechanical stability is required for single crystal growth in a floating-zone puller. It is possible to grow crystals with diameters exceeding 12.5 cm and lengths over 100 cm. The temperature distribution and heat flow pattern are very unfavorable for large crystal diameters in a floating-zone machine. Rapid multiplication of any dislocations present turns a single crystal polycrystalline. This is why dislocation-free crystals must be grown. The point defects (mainly silicon interstitials and vacancies), unavoidably present at the melting point, condense in dislocation-free crystals into a variety of defects, distributed in spiral patterns along the crystal growth axis. Crystal growth velocity and the temperature distribution strongly affect the type and distribution of these swirl defect patterns[6]. The most prominent defects—the A-type swirls—are due to condensation of interstitials into platelets surrounded by dislocation loops. Floating-zone silicon, because of its high purity, is used mainly for high voltage devices (rectifier diodes, silicon-controlled rectifiers, transistors), while Czochralski silicon is used for near-surface, low voltage devices such as integrated circuits.

Germanium is, for all practical purposes, no longer used in electronic amplifying and logic devices. It is, on the other hand, a very important semiconductor for IR optics, IR photoconductors, milli Kelvin thermistors and nuclear radiation detectors. Germanium is found in lead, copper, zinc, and silver ores. After a number of extraction and purification steps, $GeCl_4$ is obtained. Fractional distillation is followed by a hydrolysis step that gives $Ge(OH)_4$. Calcination leads to GeO_2, which is reduced to elemental germanium at 650°C in a graphite boat in a pure hydrogen atmosphere. Zone purification (see 17.2.7.1) is used to obtain intrinsic polycrystalline germanium (i.e., germanium with electrically active impurities $< 3.5 \times 10^{13}$ cm^{-3}, the intrinsic carrier concentration at room temperature).

Single crystal growth has been performed in a graphite boat in a process known as "zone leveling". The small surface tension and the high density of liquid germanium do not permit vertical floating-zone growth. The most commonly used technique for germanium single crystal growth is the Czochralski method. A modification of the graphite crucible—the floating crucible assembly—allows the growth of crystals with nearly constant impurity profiles. Germanium single crystals used in nuclear radiation detector fabrication are ultrapure, with net impurity concentrations below 10^{10} cm^{-3} (one impurity in 4×10^{12} germanium atoms). Such crystals are grown from a melt contained in a synthetic quartz crucible and a pure hydrogen atmosphere[7]. Infrared spectroscopy of such pure crystals revealed a large number of hydrogen-related impurity complexes[8]. In recent years germanium has found renewed interest for fabrication of sensitive photoconductors operating at liquid helium temperatures for detection of far-infrared radiation from sources in outer space or in the laboratory[9] and of neutron transmutation doped thermistors for the detection of extremely small quantities of energy (e.g., millimeter waves collected by radiotelescopes)[10].

(EUGENE E. HALLER)

*This work prepared for the U.S. Department of Energy under Contract No. DE-AC03-76SF00098.

1. L. D. Crossman, J. A. Baker, in *Semiconductor Silicon 1977*, H. R. Huff, E. Sirtl, eds., Electrochemical Society, Princeton, NJ, 1977, pp. 8–31; see also *Semiconductor Silicon* 1998, H. R. Huff, U. Gösele, H. Tsuya, eds., Electrochemical Society, Pennington, NJ, 1998.

2. G. K. Teal, E. Bühler, *Phys. Rev. 87*, 140 (1952); J. R. Carruthers, A. F. Witt, R. E. Reusser, in *Semiconductor Silicon 1977*, H. R. Huff, E. Sirtl, eds., Electrochemical Society, Princeton, NJ, 1977, pp. 61–82.
3. W. Keller, A. Mühlbauer, Floating-zone silicon, in *Preparation and Properties of Solid State Materials*, Vol. 5, Dekker, New York/Basel, 1981.
4. F. Schmid, C. P. Khattak, T. G. Digges Jr., L. Kaufman, *J. Electrochem Soc., 126*, 935 (1979).
5. See articles in *MRS Symp. Proc.*, Vol. 378: *Defect and Impurity Engineered Semiconductors and Devices*, S. Ashok, J. Chevallier, I. Akasaki, N. M. Johnson, B. L. Sopori, eds., Materials Research Society, Pittsburgh, 1995.
6. A. J. R. deKock, in *Handbook of Semiconductors*, Vol. 4, C. Hilsum, ed., North-Holland Publishing, Amsterdam, 1980, p. 247.
7. W. L. Hansen, *Nucl. Instrum. Methods, 94*, 377 (1971); R. N. Hall, T. J. Soltys, *IEEE Trans. Nucl. Sci. NS-18*, 160 (1971).
8. E. E. Haller, W. L. Hansen, F. S. Goulding, *Adv. Phys. 30*, 93 (1981); see also E. E. Haller, Semiconductor physics in ultra-pure germanium, *Festkörperprobleme/Advances in Solid State Physics XXVI*, P. Grosse, ed., Vieweg, Braunschweig, 1986, pp. 203–229.
9. E. E. Haller, Advanced infrared detectors, *Infrared Phys. Technol., 35* (2/3), 127 (1994).
10. E. E. Haller, K. M. Itoh, J. W. Beeman, W. L. Hansen, V. I. Ozhogin, Neutron transmutation doped natural and isotopically engineered germanium thermistors, *SPIE Proc., 2198*, 630 (1994).

17.3.8.2. Preparation of the Nitrides of Al and Ga[1]

The nitrides of aluminum (AlN) and gallium (GaN) are wide, direct band gap materials (6.2 and 3.5 eV, respectively). Solid solutions of these two materials span the entire UV range[2]. In solid solutions with InN (1.9 eV), materials with a continuum of band gaps in the 1.9–6.2 eV range may be obtained [having the thermodynamically preferred wurtzite (hexagonal) form]. A more limited range is theoretically accessible for zinc-blende polytypes. The materials have useful physical properties such as high temperature stability, high thermal conductivity, and high elastic stiffness. Thus, there is a broad range of potential uses[3] (e.g., light-emitting diodes[4], high temperature electronic equipment[5], field effect transistors, photodetectors[6]).

The applications generally involve the nitrides as a thin film. However, nanoparticulate materials are emerging as an important form of the material. In some cases (described in the appropriate subsection), a thin film or nanoparticulate material may be obtained from the same precursor molecule simply by changing the deposition conditions. This section on Al and Ga nitrides discusses both separate-source precursor combinations and single-source precursor approaches. The chemistry of these processes rather than the engineering aspects is described. However, the equipment and techniques employed are often the deciding factors in crystalline film growth.

(DAVID A. ATWOOD)

1. An excellent review of Al and Ga nitride formation is provided by : D. A. Neumayer, J. G. Ekerdt, *Chem. Matter., 8*, 9 (1996). For AlN alone see: N. Kuramoto, H. Taniguchi, I. Aso, *Ceram. Bull. 68*, 883 (1989) For GaN alone see: S. Strite, H. Morkoc, *J. Vac. Sci. Technol., B, 10*, 1237 (1992); H. Morkoc, S. Strite, G. B. Gao, M. E. Lin, B. Sverdlov, M.Burns, *J.Appl. Phys., 76*, 1363 (1994). For an overview of the properties of group IIIB nitrides see: *Properties of Group III Nitrides*, J. H. Edgar, (ed.), INSPEC, London, 1994.
2. M. Matloubian, M. Gershenzon, *J. Electron. Mater., 14*, 663 (1985).
3. M. J. Mroz, Jr., *Ceram Bull., 70*, 849 (1991); H. Morkoc, S. Strite, G. B. Gao, M. E. Lin, B. Sverdlov, M. Burns, *J. Appl. Phys., 76*, 1363 (1994).
4. T. Matsuoka, A. Ohki, T. Ohno, Y. Kawaguchi, *J. Cryst. Growth, 138*, 727 (1994); S. Nakamura, M. Senoh, N. Iwasa, S. Nagahama, *Jpn. J. Appl. Phys., 34*, 797 (1995); H. Morkoc, S. N. Mohammad, *Science, 51*, 267 (1995).

Inorganic Reactions and Methods, Volume 18
Edited by J. J. Zuckerman, Jim D. Atwood

2. G. K. Teal, E. Bühler, *Phys. Rev. 87*, 140 (1952); J. R. Carruthers, A. F. Witt, R. E. Reusser, in *Semiconductor Silicon 1977*, H. R. Huff, E. Sirtl, eds., Electrochemical Society, Princeton, NJ, 1977, pp. 61–82.
3. W. Keller, A. Mühlbauer, Floating-zone silicon, in *Preparation and Properties of Solid State Materials*, Vol. 5, Dekker, New York/Basel, 1981.
4. F. Schmid, C. P. Khattak, T. G. Digges Jr., L. Kaufman, *J. Electrochem Soc., 126*, 935 (1979).
5. See articles in *MRS Symp. Proc.*, Vol. 378: *Defect and Impurity Engineered Semiconductors and Devices*, S. Ashok, J. Chevallier, I. Akasaki, N. M. Johnson, B. L. Sopori, eds., Materials Research Society, Pittsburgh, 1995.
6. A. J. R. deKock, in *Handbook of Semiconductors*, Vol. 4, C. Hilsum, ed., North-Holland Publishing, Amsterdam, 1980, p. 247.
7. W. L. Hansen, *Nucl. Instrum. Methods, 94*, 377 (1971); R. N. Hall, T. J. Soltys, *IEEE Trans. Nucl. Sci. NS-18*, 160 (1971).
8. E. E. Haller, W. L. Hansen, F. S. Goulding, *Adv. Phys. 30*, 93 (1981); see also E. E. Haller, Semiconductor physics in ultra-pure germanium, *Festkörperprobleme/Advances in Solid State Physics XXVI*, P. Grosse, ed., Vieweg, Braunschweig, 1986, pp. 203–229.
9. E. E. Haller, Advanced infrared detectors, *Infrared Phys. Technol., 35* (2/3), 127 (1994).
10. E. E. Haller, K. M. Itoh, J. W. Beeman, W. L. Hansen, V. I. Ozhogin, Neutron transmutation doped natural and isotopically engineered germanium thermistors, *SPIE Proc., 2198*, 630 (1994).

17.3.8.2. Preparation of the Nitrides of Al and Ga[1]

The nitrides of aluminum (AlN) and gallium (GaN) are wide, direct band gap materials (6.2 and 3.5 eV, respectively). Solid solutions of these two materials span the entire UV range[2]. In solid solutions with InN (1.9 eV), materials with a continuum of band gaps in the 1.9–6.2 eV range may be obtained [having the thermodynamically preferred wurtzite (hexagonal) form]. A more limited range is theoretically accessible for zinc-blende polytypes. The materials have useful physical properties such as high temperature stability, high thermal conductivity, and high elastic stiffness. Thus, there is a broad range of potential uses[3] (e.g., light-emitting diodes[4], high temperature electronic equipment[5], field effect transistors, photodetectors[6]).

The applications generally involve the nitrides as a thin film. However, nanoparticulate materials are emerging as an important form of the material. In some cases (described in the appropriate subsection), a thin film or nanoparticulate material may be obtained from the same precursor molecule simply by changing the deposition conditions. This section on Al and Ga nitrides discusses both separate-source precursor combinations and single-source precursor approaches. The chemistry of these processes rather than the engineering aspects is described. However, the equipment and techniques employed are often the deciding factors in crystalline film growth.

(DAVID A. ATWOOD)

1. An excellent review of Al and Ga nitride formation is provided by : D. A. Neumayer, J. G. Ekerdt, *Chem. Matter., 8*, 9 (1996). For AlN alone see: N. Kuramoto, H. Taniguchi, I. Aso, *Ceram. Bull. 68*, 883 (1989) For GaN alone see: S. Strite, H. Morkoc, *J. Vac. Sci. Technol., B, 10*, 1237 (1992); H. Morkoc, S. Strite, G. B. Gao, M. E. Lin, B. Sverdlov, M.Burns, *J.Appl. Phys., 76*, 1363 (1994). For an overview of the properties of group IIIB nitrides see: *Properties of Group III Nitrides*, J. H. Edgar, (ed.), INSPEC, London, 1994.
2. M. Matloubian, M. Gershenzon, *J. Electron. Mater., 14*, 663 (1985).
3. M. J. Mroz, Jr., *Ceram Bull., 70*, 849 (1991); H. Morkoc, S. Strite, G. B. Gao, M. E. Lin, B. Sverdlov, M. Burns, *J. Appl. Phys., 76*, 1363 (1994).
4. T. Matsuoka, A. Ohki, T. Ohno, Y. Kawaguchi, *J. Cryst. Growth, 138*, 727 (1994); S. Nakamura, M. Senoh, N. Iwasa, S. Nagahama, *Jpn. J. Appl. Phys., 34*, 797 (1995); H. Morkoc, S. N. Mohammad, *Science, 51*, 267 (1995).

5. R. F. Davis, Z. Sitar, B. E. Williams, H. S. Kong, H. J. Kim, J. W. Palmour, J. A. Edmond, J. Ryu, J. T. Glass, C. H. Carter, Jr., *Mater. Sci. Eng. B*, *1*, 77 (1988).
6. A. C. Jones, C. R. Whitehouse, J. S. Roberts, *Chem. Vapour Deposition*, *1*, 365 (1995).

17.3.8.2.1. Separate Source Syntheses[1] in the Gas Phase.

Separate-source syntheses in the gas phase generally employ simple reagents. These are commonly of the form, R_3M [where R = H, Me[2], other allkyls[3] (and combinations thereof) Cl[4] and Br[5]] for the group IIIB element, and either NH_3 or N_2 for the nitride source. Since NH_3 has a poor cracking efficiency at low temperatures, other nitride sources, such as hydrazine[6] and hydrazoic acid[7] have been explored. The primary difficulty is delivering the group VB reagent to the site of the deposition in a pure form[8]. Nevertheless, these reagents are easily obtained and relatively well understood by comparison to alternative sources. This has led to great diversity in the engineering techniques used to combine them and form the solid state material.

Spectroscopic studies indicate that AlN forms from combination of Me_3Al and NH_3 at temperatures exceeding 300°C[9]. The epitaxial material is formed utilizing temperatures in excess of 1000°C. When $x > 0.4$ the resulting films are insulating.

$$Me_3Al + NH_3 \xrightarrow{1200°C} AlN \quad \text{(a)}$$

$$Me_3Ga + NH_3 \xrightarrow{800-975°C} GaN \quad \text{(b)}$$

$$Et_3Ga + NH_3 \xrightarrow{1000°C} GaN \quad \text{(c)}$$

$$Me_3Al/Me_3Ga + NH_3 \xrightarrow{775-1050°C} Al_xGa_{1-x}N \quad \text{(d)}$$

Until recently, fabrication of devices from these materials was limited by the high growth temperatures. However, this limitation is being addressed by means of activated forms of nitrogen[14]. For instance, epitaxial GaN with molecular beam epitaxy (MBE)[15] or MOCVD[16] can be prepared below 700°C with plasma-activated nitrogen. Both nitride have also been prepared by means of photochemical decomposition technique[17]. Problems associated with substrate mismatch have been tempered somewhat by the use of buffer layers[1,18]. Substantially lowered temperatures have also been obtained using ALE with or without buffered layers. For example, with NH_3 as the nitrogen source, crystalline films were obtained for GaN (550°C with $GaMe_3$)[19], and InGaN (600°C with $EtMe_2In$ and Me_3Ga)[20].

(DAVID A. ATWOOD)

1. For a good overview of this area see : D. A. Neumayer, J. G. Ekerdt, *Chem. Mater.*, *8*, 9 (1996); from homoleptic amides, see: D. M. Hoffman, *Polyhedron*, *13*, 1169 (1994).
2. T. R. Gow, R. Lin, L. A. Cadwell, F. Lee, A. L. Backman, R. I. Masel, *Chem. Mater.*, *1*, 406 (1989).
3. For $^tBu^3Ga$ and $^tBu^3Ga$, see: A. S. Grady, R. E. Linney, R. D. Markwell, G. P. Mills, D. K. Russell, P. J. Williams, A. C. Jones, *J. Mater. Chem.*, *2*, 539 (1992).
4. H. P. Maruska, J. J. Tietjen, *J. Solid State Commun.*, *15*, 327 (1969).
5. W. Zhang, R. Vargas, T. Goto, Y. Someno, T. Hirai, *Appl. Phys. Lett.*, *64*, 1359 (1994).
6. D. K. Gaskill, N. Bottka, M. C. Lin, *J. Cryst. Growth*, *77*, 418 (1986); D. K. Gaskill, N. Bottka, M. C. Lin, *Appl. Phys. Lett.*, *48*, 1449 (1986).
7. Y. Bu, M. C. Lin, L. P. Fu, D. G. Chtchekine, G. D. Gilliland, Y. Chen, S. E. Ralph, S. R. Stock, *Appl. Phys. Lett.*, *66*, 2433 (1995).

Inorganic Reactions and Methods, Volume 18
Edited by J. J. Zuckerman, Jim D. Atwood

5. R. F. Davis, Z. Sitar, B. E. Williams, H. S. Kong, H. J. Kim, J. W. Palmour, J. A. Edmond, J. Ryu, J. T. Glass, C. H. Carter, Jr., *Mater. Sci. Eng. B, 1*, 77 (1988).
6. A. C. Jones, C. R. Whitehouse, J. S. Roberts, *Chem. Vapour Deposition, 1*, 365 (1995).

17.3.8.2.1. Separate Source Syntheses[1] in the Gas Phase.

Separate-source syntheses in the gas phase generally employ simple reagents. These are commonly of the form, R_3M [where R = H, Me[2], other allkyls[3] (and combinations thereof) Cl[4] and Br[5]] for the group IIIB element, and either NH_3 or N_2 for the nitride source. Since NH_3 has a poor cracking efficiency at low temperatures, other nitride sources, such as hydrazine[6] and hydrazoic acid[7] have been explored. The primary difficulty is delivering the group VB reagent to the site of the deposition in a pure form[8]. Nevertheless, these reagents are easily obtained and relatively well understood by comparison to alternative sources. This has led to great diversity in the engineering techniques used to combine them and form the solid state material.

Spectroscopic studies indicate that AlN forms from combination of Me_3Al and NH_3 at temperatures exceeding 300°C[9]. The epitaxial material is formed utilizing temperatures in excess of 1000°C. When $x > 0.4$ the resulting films are insulating.

$$Me_3Al + NH_3 \xrightarrow{1200°C} AlN \quad \text{(a)}$$

$$Me_3Ga + NH_3 \xrightarrow{800-975°C} GaN \quad \text{(b)}$$

$$Et_3Ga + NH_3 \xrightarrow{1000°C} GaN \quad \text{(c)}$$

$$Me_3Al/Me_3Ga + NH_3 \xrightarrow{775-1050°C} Al_xGa_{1-x}N \quad \text{(d)}$$

Until recently, fabrication of devices from these materials was limited by the high growth temperatures. However, this limitation is being addressed by means of activated forms of nitrogen[14]. For instance, epitaxial GaN with molecular beam epitaxy (MBE)[15] or MOCVD[16] can be prepared below 700°C with plasma-activated nitrogen. Both nitride have also been prepared by means of photochemical decomposition technique[17]. Problems associated with substrate mismatch have been tempered somewhat by the use of buffer layers[1,18]. Substantially lowered temperatures have also been obtained using ALE with or without buffered layers. For example, with NH_3 as the nitrogen source, crystalline films were obtained for GaN (550°C with $GaMe_3$)[19], and InGaN (600°C with $EtMe_2In$ and Me_3Ga)[20].

(DAVID A. ATWOOD)

1. For a good overview of this area see : D. A. Neumayer, J. G. Ekerdt, *Chem. Mater., 8*, 9 (1996); from homoleptic amides, see: D. M. Hoffman, *Polyhedron, 13*, 1169 (1994).
2. T. R. Gow, R. Lin, L. A. Cadwell, F. Lee, A. L. Backman, R. I. Masel, *Chem. Mater., 1*, 406 (1989).
3. For $^{i}Bu^{3}Ga$ and $^{t}Bu^{3}Ga$, see: A. S. Grady, R. E. Linney, R. D. Markwell, G. P. Mills, D. K. Russell, P. J. Williams, A. C. Jones, *J. Mater. Chem., 2*, 539 (1992).
4. H. P. Maruska, J. J. Tietjen, *J. Solid State Commun., 15*, 327 (1969).
5. W. Zhang, R. Vargas, T. Goto, Y. Someno, T. Hirai, *Appl. Phys. Lett., 64*, 1359 (1994).
6. D. K. Gaskill, N. Bottka, M. C. Lin, *J. Cryst. Growth, 77*, 418 (1986); D. K. Gaskill, N. Bottka, M. C. Lin, *Appl. Phys. Lett., 48*, 1449 (1986).
7. Y. Bu, M. C. Lin, L. P. Fu, D. G. Chtchekine, G. D. Gilliland, Y. Chen, S. E. Ralph, S. R. Stock, *Appl. Phys. Lett., 66*, 2433 (1995).

8. D. F. Foster, S. A. Rushworth, D. J. Cole-Hamilton, A. C. Jones, J. P. Stagg, *Chemtronics, 3*, 38 (1988).
9. C. Soto, V. Boiadjiev, W. T. Tysoe, *Chem. Mater., 8*, 2359 (1996).
10. H. M. Manasevit, F. M. Erdmann, W. I. Simpson, *J. Electrochem. Soc., 118*, 1864 (1971).
11. M. Matloubian, M. Gershenzon, *J. Electron. Mater., 14*, 663 (1985).
12. T. Detchprohm, K. Hiramatsu, N. Sawaki, I. Akasaki, *J. Cryst. Growth, 137*, 170 (1994).
13. M. A. Khan, J. N. Kuznia, J.M. Van Hove, D. T. Olson, S. Krishnankutty, R. M. Kolbas, *Appl. Phys. Lett., 58*, 526 (1991).
14. S. T. Zembutsu, *J. Cryst. Growth, 77*, 250 (1986); J. L. Dupuie, E. Gulari, *Appl. Phys. Lett., 59*, 549 (1991); J. Sumakeris, Z. Sitar, T. K. S. Ailery, K. L. More, R. F. Davis, *Thin Solid Films*, 244 (1993).
15. M. J. Paisley, R F. Davis, *J. Cryst. Growth, 127*, 136 (1993).
16. S. W. Choi, K. J. Bachmann, G. Lucovsky, *J. Mater. Res., 8*,847 (1993); W. Zhang, R. Vargas, T. Goto, Y. Someno, T. Hirai, *Appl. Phys. Lett., 64*, 1359 (1994).
17. P. C. John, J. J. Alwan, J. G. Eden, *Thin Solid Films, 218*, 75 (1992).
18. N. Kuznia, M. A. Khan, D. T. Olson, R. Kaplan, J. Freitas, *J. Appl. Phys., 73*, 4700 (1993); N. H. Karam, T. Parodos, P. Colter, D. McNulty, W. Rowland, J. Schetzina, N. El-Masry, S. M. Bedair, *Appl. Phys. Lett., 67*, 94 (1995).
19. N. H. Karam, T. Parodos, P. Colter, D. McNulty, W. Rowland, J. Schetzina, N. El-Masry, S. M. Bedair, *Appl. Phys. Lett., 67*, 94 (1995).
20. K. S. Boutros, F. G. McIntosh, J. C. Robert, S. M. Bedair, E. L. Piner, N. A. El-Masry, *Appl. Phys. Lett., 67*, 1857 (1995).

17.3.8.2.2. Separate Source Syntheses in the Solid State.

Because of the high melting points and high dissociation pressure of N_2 during their formation[1], Czochralski or Bridgman growth techniques are not applicable to group IIIB nitrides[2]. However, freed from the restrictions of having to use volatile precursors, solid state techniques have a wider variety of precursor molecules from which to choose. Thus, many routes are available to pure, single-phase (wurtzite) AlN and GaN. For instance, elemental Ga can be combined with nitrogen sources such as NaN_3 or NH_3. The NaN_3 route, called the "Na flux" method[3], involves the combination of high purity Ga(0) and NaN_3 in a sealed stainless steel tube followed by a period of heating:

$$Ga^0 + 8NaN_3 \xrightarrow[24-96h]{600-800^\circ C} GaN + Na^0 + N_2 \qquad (a)$$

When lower ratios of the Ga:NaN_3 reagents are used, Na_xGa_y intermetallics form. Heating Ga(0):

$$Ga^0 + 8NaN_3 \xrightarrow{975^\circ C} GaN \qquad (b)$$

or Ga_2O_3:

$$Ga0 + 8NaN_3 \xrightarrow{1050^\circ C} GaN + 3H_2O \qquad (c)$$

in the presence of flowing NH_3 leads to formation of GaN[4]. The reaction is conducted over the course of 1–4 h in a hot-wall reactor with the reagents contained in a quartz boat.

Inorganic Reactions and Methods, Volume 18
Edited by J. J. Zuckerman, Jim D. Atwood

8. D. F. Foster, S. A. Rushworth, D. J. Cole-Hamilton, A. C. Jones, J. P. Stagg, *Chemtronics, 3*, 38 (1988).
9. C. Soto, V. Boiadjiev, W. T. Tysoe, *Chem. Mater., 8*, 2359 (1996).
10. H. M. Manasevit, F. M. Erdmann, W. I. Simpson, *J. Electrochem. Soc., 118*, 1864 (1971).
11. M. Matloubian, M. Gershenzon, *J. Electron. Mater., 14*, 663 (1985).
12. T. Detchprohm, K. Hiramatsu, N. Sawaki, I. Akasaki, *J. Cryst. Growth, 137*, 170 (1994).
13. M. A. Khan, J. N. Kuznia, J.M. Van Hove, D. T. Olson, S. Krishnankutty, R. M. Kolbas, *Appl. Phys. Lett., 58*, 526 (1991).
14. S. T. Zembutsu, *J. Cryst. Growth, 77*, 250 (1986); J. L. Dupuie, E. Gulari, *Appl. Phys. Lett., 59*, 549 (1991); J. Sumakeris, Z. Sitar, T. K. S. Ailery, K. L. More, R. F. Davis, *Thin Solid Films*, 244 (1993).
15. M. J. Paisley, R F. Davis, *J. Cryst. Growth, 127*, 136 (1993).
16. S. W. Choi, K. J. Bachmann, G. Lucovsky, *J. Mater. Res., 8*,847 (1993); W. Zhang, R. Vargas, T. Goto, Y. Someno, T. Hirai, *Appl. Phys. Lett., 64*, 1359 (1994).
17. P. C. John, J. J. Alwan, J. G. Eden, *Thin Solid Films, 218*, 75 (1992).
18. N. Kuznia, M. A. Khan, D. T. Olson, R. Kaplan, J. Freitas, *J. Appl. Phys., 73*, 4700 (1993); N. H. Karam, T. Parodos, P. Colter, D. McNulty, W. Rowland, J. Schetzina, N. El-Masry, S. M. Bedair, *Appl. Phys. Lett., 67*, 94 (1995).
19. N. H. Karam, T. Parodos, P. Colter, D. McNulty, W. Rowland, J. Schetzina, N. El-Masry, S. M. Bedair, *Appl. Phys. Lett., 67*, 94 (1995).
20. K. S. Boutros, F. G. McIntosh, J. C. Robert, S. M. Bedair, E. L. Piner, N. A. El-Masry, *Appl. Phys. Lett., 67*, 1857 (1995).

17.3.8.2.2. Separate Source Syntheses in the Solid State.

Because of the high melting points and high dissociation pressure of N_2 during their formation[1], Czochralski or Bridgman growth techniques are not applicable to group IIIB nitrides[2]. However, freed from the restrictions of having to use volatile precursors, solid state techniques have a wider variety of precursor molecules from which to choose. Thus, many routes are available to pure, single-phase (wurtzite) AlN and GaN. For instance, elemental Ga can be combined with nitrogen sources such as NaN_3 or NH_3. The NaN_3 route, called the "Na flux" method[3], involves the combination of high purity Ga(0) and NaN_3 in a sealed stainless steel tube followed by a period of heating:

$$Ga^0 + 8NaN_3 \xrightarrow[24-96h]{600-800^\circ C} GaN + Na^0 + N_2 \qquad (a)$$

When lower ratios of the Ga:NaN_3 reagents are used, Na_xGa_y intermetallics form. Heating Ga(0):

$$Ga^0 + 8NaN_3 \xrightarrow{975^\circ C} GaN \qquad (b)$$

or Ga_2O_3:

$$Ga0 + 8NaN_3 \xrightarrow{1050^\circ C} GaN + 3H_2O \qquad (c)$$

in the presence of flowing NH_3 leads to formation of GaN[4]. The reaction is conducted over the course of 1–4 h in a hot-wall reactor with the reagents contained in a quartz boat.

Carbothermal syntheses involve combination of the oxide (Al_2O_3 or Ga_2O_3) with a source of carbon followed by heating in the presence of either N_2 or NH_3. Typical reactions are conducted in a closed glass reactor or in a silica crucible. Shorter reaction times can be used in a microwave-assisted carbothermal nitridation[5]. In this reaction high purity Ga_2O_3 (99.9999%) is combined with carbon black in a 2:1 ratio and then sealed under an N_2 or NH_3 atmosphere. The reaction vessel is then microwaved for 32 min to afford highly crystalline hexagonal GaN.

(DAVID A. ATWOOD)

17.3.8.3. Single-Source Precursors to AlN and GaN[1]

By comparison to separate-source techniques, the single-source precursor approach offers advantage such as reduced toxicity and flammability of reagents, better control of stoichiometry, a simplified reactor design, and dramatically reduced deposition temperatures (but still in the range necessary for the formation of crystalline films and particles). Moreover, such a method might become "atom efficient" in both the group IIIB and group VB elements. This approach is normally designed to be conducted with inert carrier gases at low pressures. However, use of NH_3 as the carrier gas often alleviates problem associated with preferential nitrogen loss during the deposition process.

The single-source precursor approach uses adducts of R_3M (R = H or alkyl) compounds with NH_3, either directly or by displacement of coordinated NMe_3[1]. The adduct[2] then undergoes successive alkane eliminations to form the MN material. Thus, it is logical that an intermediate in this process, if sufficiently volatile, might serve as a good MOCVD precursor in its own right. This can be considered the case for the molecules of formula $[R_2MNH_2]_3$ (M = Al; R = Me[3,4], Et$_3$, ^{i}Bu[3], ^{t}Bu[4], SiMe$_3$[5], (SiMe$_3$)$_2$N[6], and H[7]; M = Ga; R = Me, Et, and H[8]) but not $[RMNH]_n$, which are oligomeric and volatile[9].

The trimers can be used to prepare AlN and GaN at much lower temperatures than are necessary when separate-source techniques are used. The use of $[Me_2AlNH_2]_3$ is representative of this process[3,4]:

$$[Me_2AlNH_2]_3 \xrightarrow{600°C} 3AlN + 6CH_4 \qquad (a)$$

Decomposition of $[H_2GaNH_2]_3$ leads to isolation of nanoparticles of the rare metastable cubic phase of the material[7,10]:

$$[H_2GaNH_2]_3 \xrightarrow{600°C} 3GaN + 6H_2 \qquad (b)$$

No carbon or hydrogen impurities are detected. Isolation of the cubic, rather than the common wurtzite phase was attributed to a topochemical reaction based on the structure of the precursor.

Likewise, amido derivatives, $[Al(NR_2)_3]_2$ and $[HAl(NR_2)_2]_2$ (R = Me, Et) can be used to prepare these materials, albeit in low quality[11]. Others, such as, alkylaluminum derivatives of ethylenediamine[12]

$$[RAl\{NH(CH_2)_2NH\}]_x \xrightarrow[NH_3]{1000°C} AlN + C_2H_6 + NH_2(CH_2)_2NH_2 \qquad (c)$$

and the hydrazido derivative $[Me_2GaNHNMe_2]$[13,14]

$$[Me_2GaNHNMe_2]_2 \xrightarrow{500°C} GaN + NH_2NMe_2 + \text{by-products} \quad \text{(d)}$$

have been used, but with disadvantages such as high temperatures and rupture of the Ga–N bond during decomposition, respectively. The use of amides, such as $[Ga(NMe_2)_3]_2$, in transamination reactions lowered the decomposition temperatures and improved the quality of the solid state material[15]:

$$[Ga(NMe_2)_3]_2 \xrightarrow[NH_3]{200°C} 2GaN + 6HNMe_2 \quad \text{(e)}$$

The materials isolated from these reactions were predominantly wurtzite (hexagonal) phase, although in rare instances, depending on the nature of the precursor and the level of heating during and after decomposition, the zinc-blende (cubic) structure was obtained[16]. The majority of these precursors lead to films that are excessively contaminated with C (5%) and O (4%) and low in the necessary N. A comparison of precursors containing N—C bonds (e.g., $[Me_2Al(NMe_2)]_2$, $[Me_2Al(aziridine)]_3$, and $[Et_2Al\{NH(^tBu)\}]_2$) and those without such bonds (utilizing the azide, N_3^-, group as the nitrogen source) clearly established that the first type of precursor led to poor films with a great deal of carbon and oxygen contamination[17]. Taken as a whole, however, these experiments demonstrated two principles that guide the search for future nitride precursors: (1) N—C bonds should not be present, since they lead to carbon incorporation, and (2) a source of additional nitrogen may be necessary, since N_2 is eliminated from the material.

The compound $Al(NH_2)_3$ is ideal in this regard, since it contains no carbon and an excess of nitrogen. However, it is unstable and decomposes to an amide–imide, $[(Al(NH)(NH_2)]_n$[18], which can be converted, at elevated temperatures, to amorphous AlN[19]:

$$\text{“}Al(NH_2)_3\text{”} \xrightarrow[-NH_3]{} [Al(NH)(NH_2)]_n \xrightarrow[-NH_3]{600°C} AlN \quad \text{(f)}$$

Crystalline AlN with low carbon incorporation (0.3%) can also be made from the imide–amide oligomer starting with $H_3Al\text{-}NMe_3$ as the aluminum source and an overpressure of NH_3[20]. In a similar manner, pyrolysis of a solid having the composition $[Ga(NH)_{3/2}]_n$ is useful in preparation of GaN having low carbon incorporation ($<0.22\%$)[21]:

$$[Ga(NH)_{3/2}]_n \xrightarrow{450\text{–}500°C} GaN + CH_4 + HNMe_2 + NH_3 \quad \text{(g)}$$

Characterization of the material shows that it is a mixture of cubic and hexagonal phases. Decomposition of the precursor in tetramethylhexanediamine leads to formation of particles smaller than 1 nm.

The use of the azide group (N_3^-) also fulfills the two requirements of a “good” precursor molecule. In their most simple manifestation they are of the form: $[R_2MN_3]_3$

(M = Al; R = Me and Et[12,22]; M = Ga; R = Me[12b,23], Et[24]) and can be decomposed to AlN:

$$[R_2AlN_3]_3 \xrightarrow[(R = Me, Et)]{400\text{–}600^\circ C} AlN + N_2 + \text{by-products} \qquad (h)$$

and GaN:

$$[R_2GaN_3]_3 \xrightarrow[(R = Me, Et)]{350\text{–}450^\circ C} GaN + N_2 + \text{by-products} \qquad (i)$$

at relatively low temperatures through organometallic CVD (OMCVD). While the mechanism of decomposition is still under examination, azide precursors containing the ethyl substituent decompose to some extent through a β-hydride elimination mechanism. For instance, the effluent gases from $[Et_2AlN_3]_3$ are C_2H_4 (70%) and C_2H_6 (30%). In contrast, the percentages were 25/75, respectively, when $[Et_2AlNH_2]_3$ was used[3].

The precursor system $\{Bn_2MN_3\}_n$ (M = Al, Ga) decomposes through homolytic elimination of the Bn groups, but it is uncertain how pure the resulting MN materials are[29].

Epitaxial films of GaN can be prepared with $(Me_2N)_2GaN_3]_2$, a molecule in which the Ga—C bonds have also been excluded[25]:

$$[(Me_2N)_2GaN_3]_2 \xrightarrow{580^\circ C} GaN + N_2 + \text{by-products} \qquad (j)$$

The films contained extremely low carbon (5×10^{20} atoms/cm^3) and oxygen (2×10^{21} atoms/cm^3) contamination. A more nitrogen-rich precursor $[(CH_2)_3NMe_2Ga(N_3)_2]$ is a monomeric liquid and possesses a high vapour pressure ($\sim$10 torr at 25°C)[26]. The exceptional stability of this compound is attributed to the intramolecular coordination of the NMe_2 group and to absence of bridging—N_3 groups. It can be used to prepare crystalline films of GaN with minor amounts of contaminants :

$$[\{(CH_2)_3NMe_2\}Ga(Na(N_3)_2] \xrightarrow[-N_2,H_2]{350\text{–}500^\circ C} GaN + Me_2NCH_2CH{=}CH_2 \qquad (k)$$

The tri-azide $[Ga(N_3)_3]_\infty$ is an ideal carbon-free (no N—C or Ga—C bonds) precursor to GaN[27]. In its native form it can explode under the appropriate conditions. However, it is remarkably stable when complexed to Lewis bases. Although these compounds do not sublime, they can be used to form GaN in condensed phases:

$$[(base)_3Ga(N_3)_3] \xrightarrow{400^\circ C} GaN + N_2 + base \qquad (l)$$

For instance, a dip-coating technique can be used to prepare GaN films from either $[Ga(N_3)_3]_\infty$ or the base-stabilized species[18]. A unique azide that contains no carbon or hydrogen is $[Cl_2GaN_3]_3$. It can be used to form GaN under ultra high vacuum CVD conditions[28]. A related derivative, monomeric Cl_2GaN_3–NMe_3, has a higher vapor pressure and can be used to form pure GaN (1–2 atom % carbon and chlorine) more effectively[24]:

$$3Cl_2Ga(N_3)\text{–}NMe_3 \xrightarrow{650\text{–}700^\circ C} GaN + 2GaCl_3 + 3NMe_3 + 4N_2 \qquad (m)$$

(DAVID A. ATWOOD)

1. For an excellent coverage of Al and Ga nitrides see : D. A. Neumayer, J. G. Ekerdt, *Chem. Mater.*, *8*, 9 (1996). For AlN alone see: L. Baixia, L. Yinkui, L. Yi, *J. Mater. Chem.*, *3*, 117 (1993). For GaN alone see: S. Strite, H. Morkoc, *J. Vac. Sci. Technol.*, *B*, *10*, 1237 (1992); H. Morkoc, S. Strite, G. B. Gao, M. E. Lin, B. Sverdlov, M. Burns, *J. Appl. Phys.*, *76*, 1363 (1994); H. Morkoc, S. N. Mohammad, *Science*, *51*, 267 (1995).
2. H. M. Manasevit, F.M. Erdman, W. I. Simpson, *J. Electrochem. Soc.*, *118*, 1864 (1971); W. Seifert, R. Franzheld, F. Bonisch, E. Butter, *Cryst. Res. Technol*, 21, 9, (1986); H. Liu, D. C. Bertolet, J. W. Rogers Jr., *Sur. Sci.*, *320*, 145 (1994).
3. L. V. Interrante, L. Carpenter, Jr., C. Whitmarsh, W. Lee, M. Garbaukas, G. A. Slack, *Mater. Res. Soc. Symp. Proc.*, *73*, 359 (1986).
4. L. V. Interrante, W. Lee, M. McConnell, N. Lewis, E. Hall, *J.Electrochem. Soc.*, *136*, 472 (1989); L.V. Interrante, G. A. Sigel, M. Garbauskas, C. Hejna, Slack, G. A. *Inorg. Chem.*, *28*, 252 (1989).
5. J. F. Janik, E. N. Duesler, R. T. Paine, *Inorg. Chem.*, *26*, 4341 (1987).
6. K. J. L. Paciorek, J. H. Nakahara, L. A. Hoferkamp, C. George, J. L. Flippen-Anderson, R. Gilardi, W. R. Schmidt, *Chem. Mater.*, *3*, 82 (1991).
7. D. C. Bertolet, H. Liu, J. W. Rogers Jr., *Appl. Phys.*, *75*, 5385 (1994).
8. J. -W. Hwang, S. A. Hanson, D. B. Britton, J. F. Evans, K. F. Jensen, W. L. Gladfelter, *Chem, Mater.*, *2*, 342 (1990); J. -W. Hwang, J. P. Campbell, J. Kozubowski, S. A. Hanson, J. F. Evans, W. L. Gladfelter, *Chem. Mater.*, *7*, 517 (1995).
9. A. Storr, *J. Chem. Soc. A*, 2605 (1968).
10. Cubic GaN has also been grown with MBE: M. J. Paisley, Z. Sitar, J. B. Posthill, R. F. Davis, *J. Vac. Sci. Technol. A*, 7, *3*, 701 (1989); for a study of hexagonal vs. cubic GaN, see: M. Giehler, M. Ramsteiner, O. Brandt, H. Yang, K. H. Ploog, *Appl. Phys. Lett.*, *67*, 733 (1995).
11. Y. Takahashi, K. Yamashita, S. Motojima, K. Sugiyama, *Sur. Sci.*, *86*, 238 (1979).
12. Z. Jiang, L. V. Interrante, *Chem. Mater.*, *2*, 439 (1990).
13. For early work on Me_3Ga and hydrazine, see: D. K. Gaskill, N. Bottka, M. C. Lin, *J. Cryst. Growth*, *77*, 418 (1986).
14. (a) D. A. Neumayer, A. H. Cowley, A. Decken, R. A. Jones, V. Lakhotia, J. G. Ekerdt, *Inorg. Chem. 34*, 4698 (1995). (b) V. Lakhotia, D. A. Neumayer, A. H. Cowley, R. A. Jones, J. K. Ekerdt, *Chem., Mater.*, *7*, 546 (1995).
15. R. G. Gordon, D. M. Hoffman, U. Riaz, *Mater. Res. Soc. Symp. Proc.*, *204*, 95 (1991); R. G. Gordon, D. M. Hoffman, U. Riaz, *Mater. Res. Soc. Symp. Proc.*, *242*, 445 (1992); D. M. Hoffman, *Polyhedron*, 8, 1169 (1994); R. G. Gordon, *Mater. Res. Soc. Symp. Proc.*, *335*, 9 (1994).
16. J. -W. Hwang, J. P. Campbell, J. Kozubowski, S. A. Hanson, J. F. Evans, W. L. Gladfelter, *Chem. Mater.*, *7*, 517 (1995).
17. W. L. Gladfelter, D. C. Boyd, J. -W. Hwang, R. T. Haasch, J. F. Evans, K. -L. Ho, K. V. Jensen, *Mater. Res. Soc. Symp. Proc.*, *131*, 447 (1989).
18. T. Wade, J. Park, E. G. Garza, C. B. Ross, D. M. Smith, R. M. Crooks, *J. Am. Chem. Soc.*, *114*, 9457 (1992).
19. L. Maya, Adv. *Ceram. Mater.*, *1*, 150 (1986).
20. W. Rockensuss, H. W. Roesky, *Adv. Mater.*, *5*, 443 (1993).
21. J. F. Janik, R. L. Wells, *Chem. Mater.*, *8*, 2708 (1996).
22. R. K. Schulze, D. R. Mantell, W. L. Gladfelter, J. J. Evans, *J. Vac. Sci. Technol. A*, *6*, 2162 (1988); D. C. Boyd, R. T. Haasch, D. R. Mantell, R. K. Schulze, J. F. Evans, W. L. Gladfelter, *Chem. Mater.*, *1*, 119 (1989).
23. D. A. Atwood, R. A. Jones, A. H. Cowley, J. L. Atwood, S. G. Bott, *J. Organomet. Chem.*, *394*, C6 (1990).
24. J. Kouvetakis, D. B. Beach, *Chem. Mater.*, *1*, 476 (1989).
25. D. A. Neumayer, A. . Cowley, A. Decken, R. A. Jones, V. Lakhotia, J. G. Ekerdt, *J. Am. Chem. Soc.*, *117*, 5893 (1995).
26. A. Miehr, O. Ambacher, W. Rieger, T. Metzger, E. Born, R. A. Fischer, *Chem. Vap. Deposition*, *2*, 51 (1996).
27. R. A. Fischer, A. Miehr, E. Herdtweck, M. R. Mattner, O. Ambacher, T. Metzger, E. Born, S. Weinkauf, C. R. Pulham, S. Parsons, *Chem. Eur. J.*, *2*, 1353 (1996).
28. J. Kouvetakis, J. McMurran, P. Matsunaga, M. O'Keeffe, J. L. Hubbard, *Inorg. Chem.*, *36*, 1792 (1997).
29. M.-A. Muñoz-Hernández, D. Rutherford, T. Tiainen, D. A. Atwood, *J. Organomet. Chem.* (1998) in press.

Inorganic Reactions and Methods, Volume 18
Edited by J. J. Zuckerman, Jim D. Atwood

17.3.8.4. Indium Nitride

Indium nitride is important material for its ability to form solid solutions with aluminum and gallium nitride, allowing the engineering of materials with precise band gaps spanning the gamut of group IIIB nitride materials. With a direct band gap and low carrier effective mass, it may also find utility in high speed photonic devices[1]. However, InN is difficult to prepare because of its inherent thermal instability. Low temperature decomposition routes are, thus, necessary information of this material.

The carbon-free precursor $[In(NH_3)_3]n$ is useful in this regard. In a two-step procedure it is quantitatively decomposed to InN[2]:

$$[In(NH_2)_3]_n \xrightarrow[-NH_3]{207^\circ C} \xrightarrow{415^\circ C, N_2} InN \qquad (a)$$

A volatile, air-stable precursor, $[\{(CH_2)_3NMe_2\}_2In(N_3)]$, is also available for formation of Polycrystalline material[3]:

$$[\{(CH_2)_3NMe_2\}_2In(N_3)] \xrightarrow{350-500^\circ C} InN + N_2 + H_2 + Me_2NCH_2CH{=}CH_2 \qquad (b)$$

Carbon and oxygen impurities are below 1 atom %. Based on the gases that are eliminated from this precursor, it is clear that the nitrogen source in the deposition is the azide group. It is found that the best films are formed under vacuum without additional sources of nitrogen (such as N_2 and NH_3). Homoleptic indium amides can be used when volatilized in the presence of NH_3[4].

(DAVID A. ATWOOD)

1. W. A. Bryden and T. J. Kistenmacher, in : *Properties of Group III Nitrides*, J. H. Edgar, ed., INSPEC, London, 1994, p. 117.
2. A. P. Purdy, *Inorg. Chem.*, *33*, 282 (1994).
3. R. A. Fischer, A. Miehr, T. Metzger, E. Born, O. Ambacher, H. Angerer, R. Dimitrov, *Chem. Mater.*, *8*, 1356 (1996).
4. J. Kim, S. G. Bott, D. M. Hoffman, *Inorg. Chem*, *37*, 3835 (1998).

17.3.8.5. Semiconductors of Groups IIB–VIB

17.3.8.5.1. Preparation of the Compounds in Polycrystalline Form.

The compounds of groups IIB–IVB are often prepared in polycrystalline form as phosphors, catalysts (15.2.2.2) and infrared transmitting materials. Their use as semiconductors is almost exclusively for optoelectronic purposes (i.e., light emission and detection). Thus the phosphor preparation technology has relevance to preparation of these semiconductors in powder form. The most common reactions employed are

$$ZnSO_4 + (NH_4)_2S \longrightarrow ZnS\downarrow + (NH_4)_2SO_4 \qquad (a)$$

or

$$ZnCl_2 + H_2S \longrightarrow ZnS\downarrow + 2HCl \qquad (b)$$

Inorganic Reactions and Methods, Volume 18
Edited by J. J. Zuckerman, Jim D. Atwood

17.3.8.4. Indium Nitride

Indium nitride is important material for its ability to form solid solutions with aluminum and gallium nitride, allowing the engineering of materials with precise band gaps spanning the gamut of group IIIB nitride materials. With a direct band gap and low carrier effective mass, it may also find utility in high speed photonic devices[1]. However, InN is difficult to prepare because of its inherent thermal instability. Low temperature decomposition routes are, thus, necessary information of this material.

The carbon-free precursor $[In(NH_3)_3]n$ is useful in this regard. In a two-step procedure it is quantitatively decomposed to InN[2]:

$$[In(NH_2)_3]_n \xrightarrow[-NH_3]{207^\circ C} \xrightarrow{415^\circ C, N_2} InN \qquad (a)$$

A volatile, air-stable precursor, $[\{(CH_2)_3NMe_2\}_2In(N_3)]$, is also available for formation of Polycrystalline material[3]:

$$[\{(CH_2)_3NMe_2\}_2In(N_3)] \xrightarrow{350-500^\circ C} InN + N_2 + H_2 + Me_2NCH_2CH{=}CH_2 \qquad (b)$$

Carbon and oxygen impurities are below 1 atom %. Based on the gases that are eliminated from this precursor, it is clear that the nitrogen source in the deposition is the azide group. It is found that the best films are formed under vacuum without additional sources of nitrogen (such as N_2 and NH_3). Homoleptic indium amides can be used when volatilized in the presence of NH_3[4].

(DAVID A. ATWOOD)

1. W. A. Bryden and T. J. Kistenmacher, in : *Properties of Group III Nitrides*, J. H. Edgar, ed., INSPEC, London, 1994, p. 117.
2. A. P. Purdy, *Inorg. Chem., 33*, 282 (1994).
3. R. A. Fischer, A. Miehr, T. Metzger, E. Born, O. Ambacher, H. Angerer, R. Dimitrov, *Chem. Mater., 8*, 1356 (1996).
4. J. Kim, S. G. Bott, D. M. Hoffman, *Inorg. Chem, 37*, 3835 (1998).

17.3.8.5. Semiconductors of Groups IIB–VIB

17.3.8.5.1. Preparation of the Compounds in Polycrystalline Form.

The compounds of groups IIB–IVB are often prepared in polycrystalline form as phosphors, catalysts (15.2.2.2) and infrared transmitting materials. Their use as semiconductors is almost exclusively for optoelectronic purposes (i.e., light emission and detection). Thus the phosphor preparation technology has relevance to preparation of these semiconductors in powder form. The most common reactions employed are

$$ZnSO_4 + (NH_4)_2S \longrightarrow ZnS\downarrow + (NH_4)_2SO_4 \qquad (a)$$

or

$$ZnCl_2 + H_2S \longrightarrow ZnS\downarrow + 2HCl \qquad (b)$$

and variants of these, including reduction with carbon or hydrocarbons[1]. Hydrazine reduction is favored for selenides and tellurides[2,3].

These reactions were used to prepare source material for crystal growth. However, the aqueous reactions inevitably yield material that has hydroxyl contamination, despite the very low level of metallic impurities. Thus, "dry" techniques were developed, taking advantage of the high purity of the group II metals, and the high purity of the chalcogenide hydrides.

Direct synthesis from the elements is inhibited by the tendency of the chalcogenides to passivate the metal, which is usually in shot or bar form. This passivation is severe in the case of high heat of formation compounds, but mercury compounds and even their alloys with cadmium compounds are usually prepared by direct reaction. Reacting the elements at a temperature above the melting point could alleviate the passivation problem; however, the vapor pressures of the elements are extreme at the melting point [e.g., $>2 \times 10^7$ Pa (Pascals) for ZnSe]. In addition, the exothermicity results in an explosion hazard. This is true regardless of whether sealed tubes are used. This disadvantage has been overcome by means of systems with an operating pressure of up to 2×10^8 Pa[4], but at considerable expense.

Finely divided powders have been used in some cases (e.g., for CdSe[5]), but the large surface area increases the adsorption of contaminants. In addition, the explosion hazard may not be reduced very much: the passivation reactions still take place down to submicrometer sizes, self-diffusion through passivation layers is slow, and the heat of reaction (136 kJ/mol for CdSe) is high.

Direct reaction of the elements can also be achieved in a sealed quartz ampule, with a hand torch to control the reaction[6]. Besides the obvious hazard, it is difficult to assure completion, and silicon contamination from the quartz can be expected. A better approach is the reaction of a vapor stream of the metal with a chalcogenide hydride.

$$Zn + H_2Se \longrightarrow ZnSe + H_2 \qquad (c)$$

This yields material of very high metallic purity[7] and vastly reduces the problems of oxygen (e.g., from sulfate) and other light element contamination.

In the specific case of the HgTe–CdTe alloy system[8], direct synthesis has been achieved in heavy-walled sealed quartz ampules using the same melt stoichiometry as that desired for the final alloy composition. Temperatures used depend on the liquidus of the composition, of course, but typically are about 800°C and 8×10^6 Pa. Rapid quenching avoids segregation into CdTe-rich (first-to-freeze) and HgTe-rich (last-to-freeze)portions. Microscopic inhomogeneities (1–10 μm) remain, but these can be removed by annealing at a few degrees below the liquidus.

(BRIAN J. FITZPATRICK)

1. W. Espe, *Materials of High Vacuum Technology*, Vol. 3, Pergamon Press, Oxford, 1968. Ch. 15.
2. W. C. Benzing, J. B. Conn, J. V. Magee, E. J. Sheehan, *J. Am. Chem. Soc., 80*, 2657 (1958).
3. S. M. Kulifay, *J. Am. Chem. Soc., 83*, 4916 (1961).
4. K. K. Dubenskiy, V. A. Sokolov, G. A. Ananin, *Sov. J. Op. Technol., 36*, 118 (1969).
5. A. Reisman, M. Berkenblit, *J. Phys. Chem., 67*, 22 (1963).
6. A. Libicky, in *Proceedings of the International Conference on II–VI Compounds*, W. A. Benjamin, New York, 1967, p. 389.
7. W. C. Holton, R. K. Watts, R. D. Stinedurf, *J. Cryst. Growth, 6*, 97 (1969).
8. T. C. Harman, *J. Electron. Mater, 1*, 230 (1972).

Inorganic Reactions and Methods, Volume 18
Edited by J. J. Zuckerman, Jim D. Atwood

17.3.8.5.2. Preparation of Compounds in Single Crystalline Form.

A greater variety of reactions is used for single crystal growth than for powder synthesis. In addition, some processes that appear to be primarily physical (such as evaporation) involve dissociation–recombination reactions that are sometimes driven by foreign elements.

The earliest example of synthetic crystal growth involved the growth of CdS, using the reaction[1,2]:

$$Cd + H_2S \longrightarrow CdS + H_2 \qquad (a)$$

Only small needles, platelets, and ribbons can be grown by this technique, but both purity and perfection are high. Sublimation in a flowing inert carrier gas, however, avoids hydrogen, an amphoteric impurity that passivates both donors and acceptors. Normally, this is thought to be a dissociative process, for example:

$$2CdS(s) \longrightarrow 2Cd(v) + S_2(v) \qquad (b)$$

However, this idea has been questioned, and molecular species have been observed in the vapor[3]. Dissociative and nondissociative mechanisms may be operative, depending on conditions; many processes are very far from equilibrium. The deposition yield is very high, and so, if extensive dissociation is occuring, recombination is very efficient.

Sublimation can also be used to grow bulk boules that are more suited for electrical studies. Open[4], closed[5], and semi-closed[6] systems have been used. Cadmium sulfide and selenide were early examples of this method[7], but zinc compounds have also been grown[8,9]. To increase the rate of growth of these compounds, hydrogen has been added to the growth ampule[8] or very high temperatures ($>1100°C$)[9] have been used. These methods result in side reactions with the quartz. Halogen transport, taking place between 800 and 900°C[10], may provide a solution to this problem. Incorporation of the halide may even be beneficial, since halides are good donors in compounds of groups II–VI. This is a reversible reaction carried out very close to equilibrium:

$$ZnSe(s) + I_2(v) \longrightarrow ZnI_2(v) + 1/2Se_2(v) \qquad (c)$$

This reaction is reversed at the "cold" end of a sealed ampule, and thus solid material is deposited. For good crystal growth, very low gradients ($\sim 5°C/cm$) must be used[10]. This results in low growth rates; in addition, there seems to be a "ripening" phenomenon, in which the reaction slows with time, leaving facets so perfect that nucleation is inhibited at these low supersaturations.

Melt growth of the less refractory compounds (HgSe, HgTe, CdTe, ZnTe) is usually done in sealed ampules by the Bridgman–Stockbarger technique, that is, moving the ampule through a gradient[11]. The higher melting compounds usually require a pressurized chamber. The sealed quartz ampules could be supported, but are usually abandoned in favor of a large overpressure of inert gas[12]. These pressures are necessary not merely to contain the equilibrium vapor of the compounds, in no case greater than 5×10^5 Pa, but to suppress the decomposition into the elements, which have vastly greater vapor pressures. Mechanical operation at these pressures is difficult, and thus temperature lowering (gradient freeze) techniques are usually used instead of Bridgeman growth[13]. However, sealed ampule growth of ZnSe by a Bridgman method has been achieved[14]. Sealing of the melt might be achieved by means of a liquid encapsulant, such as boric

oxide, used successfully in the case of gallium arsenide and other compounds of groups III–V; however, B_2O_3 emulsifies with ZnSe[15] (although not with CdSe or CdTe[16]) and no interesting crystal growth results have been reported.

Zone melting resembles Bridgman growth but differs in that only a small fraction of the charge is melted. Thus overall evaporation can be reduced, contact of the melt with the walls is reduced, and ternary alloys can be grown with uniform composition. There is a self-sealing and self-releasing technique in which condensed vapor from the melt seals the exit of the crucible at the start. This seal may be later volatilized by movement of the hot zone, releasing the charge[17].

Solution growth avoids many of the container reaction problems of the vapor and melt methods, since the solvent can hold contaminants in solution. Finding good solvents is a problem, however. The compounds of groups III–V benefit from the use of gallium and indium, low melting, high surface tension metals. Unfortunately, they are strongly incorporated, and usually undesirable, in compounds of groups II–VI. Good small platelets that are suitable for structural and spectroscopic studies can be grown. The seeded variant of this, liquid phase epitaxy, uses solvents such as tin and bismuth to produce material of very high purity[18]. Incorporation of the vital dopant nitrogen as an acceptor was first proven by this technique; however, the concentration range is very limited. Metal solvents with melting points up to that of Sb have been used, as well as fused salts, usually chlorides. Electrolysis of a fused salt mixture has also been used, but contamination with the oxide is a problem.

Vapor phase epitaxy (VPE) can be accomplished by transport or pyrolysis reactions, or reactive evaporation. The simplest method is sealed ampule halogen transport of the compound, reaction (c); this can also be done in an open-flow system. The halogen is incorporated as an n-type dopant and depending on the application, this may be a problem. The vapor pressures of the elements are high enough to make transport by an inert gas an apparently feasible option. For many reasons, hydrogen is inevitably used for this process: H_2 is easily purified and it aids in the reduction of oxides on the source materials. Moreover, H_2 suppresses the tendency of Se to form eight membered rings and other relatively unreactive species, as well as direct reaction (homogeneous nucleation) of Zn and Se. Reduction of the quartzware may be minimized by low temperature growth[19]. However, hydrogen may also passivate both donors and acceptors.

A method that overcomes some of these limitations is metal–organic chemical vapor deposition (MOCVD), sometimes called organometallic vapor phase epitaxy (OMVPE)[20]. An organometallic compound such as a group IIB alkyl reacts with a chalcogenide hydride on a substrate that is at the highest temperature in the chamber:

$$(C_2H_5)Zn(v) + H_2Se(g) \longrightarrow ZnSe(s) + 2C_2H_6(g) \qquad (d)$$

This is an irreversible system, and the reaction does not depend on transport from a hotter to a colder zone. Gas phase nucleation is reduced, and the reaction temperature is low (300–500°C). The hydrogen passivation occurs, but still this effect may be partially alleviated by substitution of an alkyl chalcogenide to avoid the hydrogen selenide. Alkylselenium compounds originally were used to avoid the very toxic H_2Se. The criteria (e.g., toxicity, decomposition into stable products) for selection of these alternative precursors have been reviewed[20].

Molecular beam epitaxy (MBE) is really evaporation followed by condensation and reaction on a substrate, done under very clean, ultrahigh vacuum conditions at

temperatures of, 200–400°C. Usually elemental sources are used, but hybrids of this technique with OMVPE have been tried[21].

The formation reactions on the surface in MBE would appear to be straightforward. However, usually substrates of group III–V compounds, such as GaAs, are used, leading to a difficult situation at the interface. Without careful control of the stoichiometry, stacking defects can be generated, in part because of the tendency to form Ga_2Se_3. Thus, zinc-rich conditions are needed at the start. The stoichiometry of the GaAs also has to be adjusted to an arsenic-rich condition to take advantage of Zn–As bonding[22,23]. This does provide both an incentive and an opportunity to study bonding on an atomic scale.

The most common analysis method, electron diffraction, gives excellent information about surface structure, but only indirect information about surface reactions. More direct information can be obtained from scanning tunneling microscopy[24]. Dimerization of selenium on the GaAs surface is deleterious to smooth layer-by-layer growth; "zinc irradiation", or saturation of the surface with zinc, allows the reaction of selenium to proceed smoothly. The mechanism of depolymerization of the source selenium is not well established, but it is believed that selenium atoms migrate on the surface to bond with zinc. This is called "migration-enhanced epitaxy"[25]. This area of research may change as "native" substrates, bulk group II–VI compound crystals, are introduced.

(BRIAN J. FITZPATRICK)

1. R. Lorenz, *Chem. Ber.*, *24*, 1509 (1891).
2. R. Frerichs, *Phys. Rev.*, *72*, 594 (1947).
3. R. J. Caveney, *J. Cryst. Growth*, *2*, 85 (1968).
4. L. C. Greene, D. C. Reynolds, S. J. Czyzak, W. M. Baker, *J. Chem. Phys.*, *29*, 1375 (1958).
5. W. W. Piper, S. J. Polich, *J. Appl. Phys.*, *32*, 1278 (1961).
6. P. Vohl, *Mater. Res. Bull.*, *4*, 689 (1969).
7. G. H. Dierssen, T. Gabor, *J. Cryst. Growth*, *43*, 572 (1978).
8. Yu. V. Korostelin, V. I. Koslofsky, A. S. Nasibov, Ya. K. Skasyrsky, P. V. Shapkin, *Proc. P. N. Lebedev Phys. Inst.*, *202*, 201 (1991).
9. G. Cantwell, W. C. Harsch, H. L. Cotal, B. G. Markey, S. W. S. McKeever, J. E. Thomas, *J. Appl. Phys.*, *71*, 2931 (1992).
10. E. Kaldis, in *Crystal Growth: Theory and Techniques*, vol. 1, Plenum Press, Landau, 1974, V. 1, p. 49.
11. K. Zanio, *Semiconductors and Semimetals*, Vol. 13, Academic Press, New York, 1978, p. 11.
12. L. C. Greene, D. C. Reynolds, S. J. Czyzak, W. M. Baker, *J. Chem. Phys.*, *29*, 1375 (1958).
13. M. Demianuk and J. Zmija, *Acta Phys. Polon.*, *A51*, 673 (1977).
14. G. H. Dierssen, T. Gabor, *J. Cryst. Growth*, *43*, 572 (1978).
15. A. G. Fischer, in *Crystal Growth*, 2nd ed., B. M. Pamplin, ed., Pergamon Press, Oxford, 1980, p. 380.
16. A. L. Marbahk, P. M. Shurygin, G. S. Dubovikov, *Inorg. Mater.*, *10*, 353 (1974).
17. B. J. Fitzpatrick, T. F. McGee III, P. M. Harnack, *J. Cryst. Growth*, *78*, 242 (1986).
18. B. J. Fitzpatrick, C. J. Werkhoven, T. F. McGee III, P. M. Harnack, S. P. Herko, R. N. Bhargava, P. J. Dean, *IEEE Trans. Electro. Devices*, *ED-28*, 440 (1981).
19. T. Kyotani, M. Isshiki, K. Masumoto, *J. Electrochem. Soc.*, *136*, 2376 (1989).
20. Volume 170 of the *Journal of Crystal Growth* (1977) is devoted to MOCVD, with many papers compounds of groups II–VI. A discussion of the chemistry of precursors is P. O'Brien, M. A. Malik, M. Chunggaze, T. Trindade, J. R. Walsh (p. 23). An illustration of the power of the technique to grow the quaternary alloy ZnMgSSe is the paper by M. Heuken, J. Sollner, W. Taudt, S. Lampe, H. Hamadeh (p. 30).
21. M. Imaizumi, H. Kuroki, Y. Endoh, M. Suita, K. Ohtsuka, T. Isu, M. Nunoshita, *J. Cryst. Growth*, *159*, 1167 (1996).
22. M. Tamargo, J. L. de Miguel, D. M. Hwang, H. H. Farrell, *J. Vac. Sci. Technol.*, *B6*, 784 (1988).
23. C. C. Chu, T. B. Ng, J. Han, G. C. Hua, R. L. Gunshor, E. Ho, E. L. Warlick, L. A. Kolodziejski, A. V. Nurmikko, *Appl. Phys. Lett.*, *69*, 602 (1996).

24. M. Pashley, D. Li, *Mater. Sci. Eng. B, 30*, 73 (1995).
25. J. M. Gaines, J. Petruzzello, B. Greenberg, *J. Appl. Phys., 73*, 2835 (1993).

17.3.8.5.3. Film Formation.

The simplest method of film formation is evaporation, which is a less elegant and expensive form of MBE in which a non-single crystalline substrate such as glass or metal is used. Evaporation from a compound source is most common, because it is easy and efficient. It is assumed that dissociation follows evaporation into the vapor state and that recombination after condensation re-forms the compound. However, there is evidence for association in the vapor state[1] and this may explain the small amount of free element found. The high heat of formation (159 kJ/mol in the CdS case) explains both phenomena (association in the vapor state or efficient recombination). Distinction between them may eventually come from MBE studies, where ZnS is grown from a compound source.

For large area film formation at low cost, the spray pyrolysis process[2] is used. A solution of a metal chloride or acetylacetonate with a source such as thiourea in a polar solvent is pyrolysed on a hot (300–500°C) substrate. A typical reaction is

$$CdCl_2 + (NH_2)_2CS + H_2O \longrightarrow CdS + (NH_2)_2CO + 2HCl \qquad (a)$$

Aqueous deposition follows the same reactions as (a), More likely, however, a complexing agent, such as NH_3, is used to reduce the reaction rate to improve film structure[3]. This process can also be done electrolytically (with, e.g., $CdSO_4$ and TeO_2 as reactants); with underpotential deposition, the growth of one atomic layer at a time may be achieved[4].

(BRIAN J. FITZPATRICK)

1. R. J. Caveney, *J. Cryst. Growth, 2*, 85 (1968).
2. J. Ebothe, P. Chartier, H. Nguyen Cong, *Thin Solid Films, 138*, 1 (1986).
3. D. Lincot, R. O. Borges, *J. Electrochem. Soc., 139*, 1880 (1992).
4. B. M. Huang, L. P. Colletti, B. W. Gregory, J. L. Anderson, J. L. Stickney, *J. Electrochem. Soc., 142*, 3007 (1995).

17.3.8.6. Other Crystalline Semiconductors

Crystalline semiconductors have a wide variety of properties: very high conductivity may be seen, but bipolar (p and n type) conductivity is rare in high band gap compounds; many of these are difficult to prepare in pure form, and single crystal growth is very difficult. Compounds that have a band gap but are normally considered insulators (e.g., NaCl, SiO_2) are omitted from this consideration.

(BRIAN J. FITZPATRICK)

17.3.8.6.1. Group IA–VB and Group IA–VIB Compounds.

The very high reactivity of the alkali metals, even in compound form, requires that these compounds be prepared in high vacuum. Since these are used as photoemissive materials, inside photomultiplier tubes, this is not a problem in use, but detailed studies of properties and even composition are difficult[1]. Usually, such materials are made by allowing alkali vapor to come in contact with a thin film of the group V or VI element. For crystallographic studies, however, powders have been used. Temperatures from 130 to 240°C have been used; the alkali vapor has been released from a compound such as the

Inorganic Reactions and Methods, Volume 18
Edited by J. J. Zuckerman, Jim D. Atwood

24. M. Pashley, D. Li, *Mater. Sci. Eng. B, 30*, 73 (1995).
25. J. M. Gaines, J. Petruzzello, B. Greenberg, *J. Appl. Phys., 73*, 2835 (1993).

17.3.8.5.3. Film Formation.

The simplest method of film formation is evaporation, which is a less elegant and expensive form of MBE in which a non-single crystalline substrate such as glass or metal is used. Evaporation from a compound source is most common, because it is easy and efficient. It is assumed that dissociation follows evaporation into the vapor state and that recombination after condensation re-forms the compound. However, there is evidence for association in the vapor state[1] and this may explain the small amount of free element found. The high heat of formation (159 kJ/mol in the CdS case) explains both phenomena (association in the vapor state or efficient recombination). Distinction between them may eventually come from MBE studies, where ZnS is grown from a compound source.

For large area film formation at low cost, the spray pyrolysis process[2] is used. A solution of a metal chloride or acetylacetonate with a source such as thiourea in a polar solvent is pyrolysed on a hot (300–500°C) substrate. A typical reaction is

$$CdCl_2 + (NH_2)_2CS + H_2O \longrightarrow CdS + (NH_2)_2CO + 2HCl \qquad (a)$$

Aqueous deposition follows the same reactions as (a), More likely, however, a complexing agent, such as NH_3, is used to reduce the reaction rate to improve film structure[3]. This process can also be done electrolytically (with, e.g., $CdSO_4$ and TeO_2 as reactants); with underpotential deposition, the growth of one atomic layer at a time may be achieved[4].

(BRIAN J. FITZPATRICK)

1. R. J. Caveney, *J. Cryst. Growth, 2*, 85 (1968).
2. J. Ebothe, P. Chartier, H. Nguyen Cong, *Thin Solid Films, 138*, 1 (1986).
3. D. Lincot, R. O. Borges, *J. Electrochem. Soc., 139*, 1880 (1992).
4. B. M. Huang, L. P. Colletti, B. W. Gregory, J. L. Anderson, J. L. Stickney, *J. Electrochem. Soc., 142*, 3007 (1995).

17.3.8.6. Other Crystalline Semiconductors

Crystalline semiconductors have a wide variety of properties: very high conductivity may be seen, but bipolar (p and n type) conductivity is rare in high band gap compounds; many of these are difficult to prepare in pure form, and single crystal growth is very difficult. Compounds that have a band gap but are normally considered insulators (e.g., NaCl, SiO_2) are omitted from this consideration.

(BRIAN J. FITZPATRICK)

17.3.8.6.1. Group IA–VB and Group IA–VIB Compounds.

The very high reactivity of the alkali metals, even in compound form, requires that these compounds be prepared in high vacuum. Since these are used as photoemissive materials, inside photomultiplier tubes, this is not a problem in use, but detailed studies of properties and even composition are difficult[1]. Usually, such materials are made by allowing alkali vapor to come in contact with a thin film of the group V or VI element. For crystallographic studies, however, powders have been used. Temperatures from 130 to 240°C have been used; the alkali vapor has been released from a compound such as the

Inorganic Reactions and Methods, Volume 18
Edited by J. J. Zuckerman, Jim D. Atwood

24. M. Pashley, D. Li, *Mater. Sci. Eng. B, 30*, 73 (1995).
25. J. M. Gaines, J. Petruzzello, B. Greenberg, *J. Appl. Phys., 73*, 2835 (1993).

17.3.8.5.3. Film Formation.

The simplest method of film formation is evaporation, which is a less elegant and expensive form of MBE in which a non-single crystalline substrate such as glass or metal is used. Evaporation from a compound source is most common, because it is easy and efficient. It is assumed that dissociation follows evaporation into the vapor state and that recombination after condensation re-forms the compound. However, there is evidence for association in the vapor state[1] and this may explain the small amount of free element found. The high heat of formation (159 kJ/mol in the CdS case) explains both phenomena (association in the vapor state or efficient recombination). Distinction between them may eventually come from MBE studies, where ZnS is grown from a compound source.

For large area film formation at low cost, the spray pyrolysis process[2] is used. A solution of a metal chloride or acetylacetonate with a source such as thiourea in a polar solvent is pyrolysed on a hot (300–500°C) substrate. A typical reaction is

$$CdCl_2 + (NH_2)_2CS + H_2O \longrightarrow CdS + (NH_2)_2CO + 2HCl \qquad (a)$$

Aqueous deposition follows the same reactions as (a), More likely, however, a complexing agent, such as NH_3, is used to reduce the reaction rate to improve film structure[3]. This process can also be done electrolytically (with, e.g., $CdSO_4$ and TeO_2 as reactants); with underpotential deposition, the growth of one atomic layer at a time may be achieved[4].

(BRIAN J. FITZPATRICK)

1. R. J. Caveney, *J. Cryst. Growth, 2*, 85 (1968).
2. J. Ebothe, P. Chartier, H. Nguyen Cong, *Thin Solid Films, 138*, 1 (1986).
3. D. Lincot, R. O. Borges, *J. Electrochem. Soc., 139*, 1880 (1992).
4. B. M. Huang, L. P. Colletti, B. W. Gregory, J. L. Anderson, J. L. Stickney, *J. Electrochem. Soc., 142*, 3007 (1995).

17.3.8.6. Other Crystalline Semiconductors

Crystalline semiconductors have a wide variety of properties: very high conductivity may be seen, but bipolar (p and n type) conductivity is rare in high band gap compounds; many of these are difficult to prepare in pure form, and single crystal growth is very difficult. Compounds that have a band gap but are normally considered insulators (e.g., NaCl, SiO_2) are omitted from this consideration.

(BRIAN J. FITZPATRICK)

17.3.8.6.1. Group IA–VB and Group IA–VIB Compounds.

The very high reactivity of the alkali metals, even in compound form, requires that these compounds be prepared in high vacuum. Since these are used as photoemissive materials, inside photomultiplier tubes, this is not a problem in use, but detailed studies of properties and even composition are difficult[1]. Usually, such materials are made by allowing alkali vapor to come in contact with a thin film of the group V or VI element. For crystallographic studies, however, powders have been used. Temperatures from 130 to 240°C have been used; the alkali vapor has been released from a compound such as the

chromate by reduction with ferrotitanium. More recently, Cs–K–Te has been made by a similar process[2]. A related compound made by similar techniques is Cs_2O, a semiconductor that is rarely made in thicknesses greater than a few atomic layers[3]. This is used as a coating to lower the work function for electron emission of semiconductors such as GaP. The small amount of oxygen required is supplied by diffusion through silver.

(BRIAN J. FITZPATRICK)

1. A. H. Sommer, *Photoemissive Materials*, Wiley, New York, 1968.
2. D. Bisero, B. M. van Oerle, G. J. Ernst, J. W. J. Verschuur, W. J. Witteman, *Appl. Phys. Lett.*, *70*, 1491 (1997).
3. C. W. Bates, N. Alexander, *J. Opt. Soc. Am. A*, *2*, 1848 (1985).

17.3.8.6.2. Group IIA–VIB Compounds.

The oxides of the heavier elements (Ca, Sr, Ba), made by decomposition of their carbonates at temperatures of about 900°C[1], have appreciable semiconductivity, and strong electron emission at high temperatures. Single crystals are generally grown by vapor[2] or solution[3] techniques, because of the high melting points and reactivity of the compounds (e.g., BaO melts at 2196°C).

The chalcogenides are generally prepared in bulk polycrystalline form by direct reaction of the elements[4–6], although occasionally hydrides are used. Alumina or graphite crucibles are usually used, because the alkaline earths easily reduce quartz. "Graphitized" silica (with the inside surface coated with some form of carbon derived from the pyrolysis of acetone, methane, a light aromatic, or another organic compound) is hard to make pinhole free and may fail because of the carbon–metal reaction. Work with this material can entail a major explosion hazard. Even without the complication of a sealed ampule, these compounds are hazardous because of their high heat of formation (e.g., 347 J/mol in the case of MgS). These conditions yield material that is good for many property measurements, but reactivity of the elements causes problems. Surprisingly, reduction of oxyradical compounds like the selenates works, but a subsequent step, such as evaporation, results in far better material; it is likely that the very strongly bonded alkaline earth oxides are refined out by such a procedure.

Normally, these compounds in bulk polycrystalline form have the rock salt structure; however, evaporation has been used to deposit thin films that have the tetrahedrally bonded hexagonal (wurtzite) structure[7].

Recently, Mg and Be compounds have been used in alloys with ZnSe to make blue and green semiconductor lasers. Bulk growth by zone melting[8] and molecular beam epitaxy (MBE)[9,10] has been used. In these cases, good semiconductor material has been obtained; dilution with group IIB compounds may be responsible. However, growth of pure MgS in very thin films on ZnSe has been achieved[11]; the epitaxial orientation effect of the substrate results in a tetrahedral cubic (sphalerite or zinc-blende) structure. It is likely that improvements in these materials will take place at a rapid rate, driven in part by applications and in part by newer, cleaner synthetic methods.

(BRIAN J. FITZPATRICK)

1. F. Rosebury, *Handbook of Electron Tube and Vacuum Techniques*, Addison-Wesley, Reading, MA, 1965.
2. R. L. Sproull, W. C. Dash, W. W. Tyler, A. R. Moore, *Rev. Sci. Instrum.*, *22*, 410 (1951).
3. E. M. Pell, *Phys. Rev.*, *87*, 457 (1952).
4. E. Miller, K. Komarek, I. Cadoff, *Trans. Met. Soc. AIME*, *218*, 978 (1960).

Inorganic Reactions and Methods, Volume 18
Edited by J. J. Zuckerman, Jim D. Atwood

chromate by reduction with ferrotitanium. More recently, Cs–K–Te has been made by a similar process[2]. A related compound made by similar techniques is Cs_2O, a semiconductor that is rarely made in thicknesses greater than a few atomic layers[3]. This is used as a coating to lower the work function for electron emission of semiconductors such as GaP. The small amount of oxygen required is supplied by diffusion through silver.

(BRIAN J. FITZPATRICK)

1. A. H. Sommer, *Photoemissive Materials*, Wiley, New York, 1968.
2. D. Bisero, B. M. van Oerle, G. J. Ernst, J. W. J. Verschuur, W. J. Witteman, *Appl. Phys. Lett.*, *70*, 1491 (1997).
3. C. W. Bates, N. Alexander, *J. Opt. Soc. Am. A*, *2*, 1848 (1985).

17.3.8.6.2. Group IIA–VIB Compounds.

The oxides of the heavier elements (Ca, Sr, Ba), made by decomposition of their carbonates at temperatures of about 900°C[1], have appreciable semiconductivity, and strong electron emission at high temperatures. Single crystals are generally grown by vapor[2] or solution[3] techniques, because of the high melting points and reactivity of the compounds (e.g., BaO melts at 2196°C).

The chalcogenides are generally prepared in bulk polycrystalline form by direct reaction of the elements[4–6], although occasionally hydrides are used. Alumina or graphite crucibles are usually used, because the alkaline earths easily reduce quartz. "Graphitized" silica (with the inside surface coated with some form of carbon derived from the pyrolysis of acetone, methane, a light aromatic, or another organic compound) is hard to make pinhole free and may fail because of the carbon–metal reaction. Work with this material can entail a major explosion hazard. Even without the complication of a sealed ampule, these compounds are hazardous because of their high heat of formation (e.g., 347 J/mol in the case of MgS). These conditions yield material that is good for many property measurements, but reactivity of the elements causes problems. Surprisingly, reduction of oxyradical compounds like the selenates works, but a subsequent step, such as evaporation, results in far better material; it is likely that the very strongly bonded alkaline earth oxides are refined out by such a procedure.

Normally, these compounds in bulk polycrystalline form have the rock salt structure; however, evaporation has been used to deposit thin films that have the tetrahedrally bonded hexagonal (wurtzite) structure[7].

Recently, Mg and Be compounds have been used in alloys with ZnSe to make blue and green semiconductor lasers. Bulk growth by zone melting[8] and molecular beam epitaxy (MBE)[9,10] has been used. In these cases, good semiconductor material has been obtained; dilution with group IIB compounds may be responsible. However, growth of pure MgS in very thin films on ZnSe has been achieved[11]; the epitaxial orientation effect of the substrate results in a tetrahedral cubic (sphalerite or zinc-blende) structure. It is likely that improvements in these materials will take place at a rapid rate, driven in part by applications and in part by newer, cleaner synthetic methods.

(BRIAN J. FITZPATRICK)

1. F. Rosebury, *Handbook of Electron Tube and Vacuum Techniques*, Addison-Wesley, Reading, MA, 1965.
2. R. L. Sproull, W. C. Dash, W. W. Tyler, A. R. Moore, *Rev. Sci. Instrum.*, *22*, 410 (1951).
3. E. M. Pell, *Phys. Rev.*, *87*, 457 (1952).
4. E. Miller, K. Komarek, I. Cadoff, *Trans. Met. Soc. AIME*, *218*, 978 (1960).

5. W. M. Yim, J. P. Dismukes, E. J. Stofko, R. J. Paff, *J. Phys. Chem. Solids, 33*, 501 (1972).
6. J. Marine, T. Ternisien, B. Schaub, A. Laugier, D. Barbier, J. C. Guillaume, J. F. Rommeluere, J. Chevallier, *J. Electron. Mater., 7*, 17 (1978).
7. H. Mittendorf, *Z. Phys., 183*, 113 (1965).
8. B. J. Fitzpatrick, U. S. Patent 5, 521, 934, (May 28, 1996).
9. H. Okuyama, K. Nakano, T. Miyajima, K. Akimoto, *Jpn. J. Appl. Phys., 30*, L1620 (1991).
10. A. Waag, F. Fischer, H. J. Lugauer, T. Litz, J. Laubender, U. Lunz, U. Zehnder, W. Ossau, T. Gebhardt, M. Moller, G. Landwehr, *J. Appl. Phys., 80*, 792, (1996).
11. I. Suemune, T. Obinata, K. Uesugi, H. Suzuki, H. Kumano, H. Nashiki, J. Nakahara, *J. Cryst. Growth, 170*, 480 (1997).

17.3.8.6.3. Group IIA–IVB Compounds.

Compounds in groups IIA–IVB may be prepared in bulk form by direct reaction and grown by gradient freeze[1] or Bridgman[2] techniques. Thin-film direct reaction is capable of making Mg_2Si in epitaxial form on silicon[3].

(BRIAN J. FITZPATRICK)

1. R. G. Morris, R. D. Redin, G. C. Danielson, *Phys. Rev., 109*, 1909 (1958).
2. B. D. Lichter, *J. Electrochem. Soc., 109*, 819 (1962).
3. G. S. Tompa, Y. B. Li, D. Agassi, S. I. Kim, S. K. Hong, *J. Electron. Mater., 25*, 925 (1996).

17.3.8.6.4. Transition Metal Oxides.

The semiconducting forms of the transition metal oxides are almost never fully oxidized but often have nearly Daltonide stoichiometry. Oxidation of the metal powder, decomposition of the carbonates, and oxidation of a volatile precursor are all employed. Metal carbonyls, such as $Ni(CO)_4$ and $Fe(CO)_5$, are very useful, since distillation is a facile method of purification for these volatile liquids. Caution: $Ni(CO)_4$ is very toxic, and generates CO upon decomposition.

It is difficult to distinguish generation of defects such as oxygen vacancies and the creation of a new compound with a different oxidation state. For example, Fe_2O_3 (hematite) is only weakly semiconducting, but it can be reduced to Fe_3O_4 (magnetite), which has very high conductivity because of charge transfer between the Fe^{2+} and Fe^{3+} ions. This reduction can be done with CO–CO_2 mixtures at temperatures around 400°C, but can be controlled with more precision by implantation of hydrogen[1]. In this case, the orientation of the cubic magnetite is determined by the orientation of the hexagonal hematite. Further reduction leads to FeO (wustite), a metallic conductor.

Reactive evaporation and sputtering are techniques for synthesis that are popular because the stoichiometry may be controlled by varying the oxygen concentration in the vapor phase. The level of control is limited in evaporation by formation in the vapor phase of oxide particles that disturb the growth of the film. Nevertheless, material with a good range of semiconductor properties can be obtained. Classical intuition leads to the expectation that such material would always be oxygen-deficient, and, since oxygen vacancies are usually thought to be donors, n-type. However, p-type NiO has been made[2], so it is likely that precisely oxidized material can be made in favourable cases.

Cu_2O, uncontaminated by CuO, has been made by exposing Cu films 200–850 nm thick to multiply-scanned Ar^+ laser irradiation[3].

The sol–gel method, a nanoparticle synthesis technique, has been shown to be very flexible in film deposition. Smooth amorphous films can be deposited, and crystallized

Inorganic Reactions and Methods, Volume 18
Edited by J. J. Zuckerman, Jim D. Atwood

5. W. M. Yim, J. P. Dismukes, E. J. Stofko, R. J. Paff, *J. Phys. Chem. Solids, 33*, 501 (1972).
6. J. Marine, T. Ternisien, B. Schaub, A. Laugier, D. Barbier, J. C. Guillaume, J. F. Rommeluere, J. Chevallier, *J. Electron. Mater., 7*, 17 (1978).
7. H. Mittendorf, *Z. Phys., 183*, 113 (1965).
8. B. J. Fitzpatrick, U. S. Patent 5, 521, 934, (May 28, 1996).
9. H. Okuyama, K. Nakano, T. Miyajima, K. Akimoto, *Jpn. J. Appl. Phys., 30*, L1620 (1991).
10. A. Waag, F. Fischer, H. J. Lugauer, T. Litz, J. Laubender, U. Lunz, U. Zehnder, W. Ossau, T. Gebhardt, M. Moller, G. Landwehr, *J. Appl. Phys., 80*, 792, (1996).
11. I. Suemune, T. Obinata, K. Uesugi, H. Suzuki, H. Kumano, H. Nashiki, J. Nakahara, *J. Cryst. Growth, 170*, 480 (1997).

17.3.8.6.3. Group IIA–IVB Compounds.

Compounds in groups IIA–IVB may be prepared in bulk form by direct reaction and grown by gradient freeze[1] or Bridgman[2] techniques. Thin-film direct reaction is capable of making Mg_2Si in epitaxial form on silicon[3].

(BRIAN J. FITZPATRICK)

1. R. G. Morris, R. D. Redin, G. C. Danielson, *Phys. Rev., 109*, 1909 (1958).
2. B. D. Lichter, *J. Electrochem. Soc., 109*, 819 (1962).
3. G. S. Tompa, Y. B. Li, D. Agassi, S. I. Kim, S. K. Hong, *J. Electron. Mater., 25*, 925 (1996).

17.3.8.6.4. Transition Metal Oxides.

The semiconducting forms of the transition metal oxides are almost never fully oxidized but often have nearly Daltonide stoichiometry. Oxidation of the metal powder, decomposition of the carbonates, and oxidation of a volatile precursor are all employed. Metal carbonyls, such as $Ni(CO)_4$ and $Fe(CO)_5$, are very useful, since distillation is a facile method of purification for these volatile liquids. Caution: $Ni(CO)_4$ is very toxic, and generates CO upon decomposition.

It is difficult to distinguish generation of defects such as oxygen vacancies and the creation of a new compound with a different oxidation state. For example, Fe_2O_3 (hematite) is only weakly semiconducting, but it can be reduced to Fe_3O_4 (magnetite), which has very high conductivity because of charge transfer between the Fe^{2+} and Fe^{3+} ions. This reduction can be done with CO–CO_2 mixtures at temperatures around 400°C, but can be controlled with more precision by implantation of hydrogen[1]. In this case, the orientation of the cubic magnetite is determined by the orientation of the hexagonal hematite. Further reduction leads to FeO (wustite), a metallic conductor.

Reactive evaporation and sputtering are techniques for synthesis that are popular because the stoichiometry may be controlled by varying the oxygen concentration in the vapor phase. The level of control is limited in evaporation by formation in the vapor phase of oxide particles that disturb the growth of the film. Nevertheless, material with a good range of semiconductor properties can be obtained. Classical intuition leads to the expectation that such material would always be oxygen-deficient, and, since oxygen vacancies are usually thought to be donors, n-type. However, p-type NiO has been made[2], so it is likely that precisely oxidized material can be made in favourable cases.

Cu_2O, uncontaminated by CuO, has been made by exposing Cu films 200–850 nm thick to multiply-scanned Ar^+ laser irradiation[3].

The sol–gel method, a nanoparticle synthesis technique, has been shown to be very flexible in film deposition. Smooth amorphous films can be deposited, and crystallized

Inorganic Reactions and Methods, Volume 18
Edited by J. J. Zuckerman, Jim D. Atwood

5. W. M. Yim, J. P. Dismukes, E. J. Stofko, R. J. Paff, *J. Phys. Chem. Solids, 33*, 501 (1972).
6. J. Marine, T. Ternisien, B. Schaub, A. Laugier, D. Barbier, J. C. Guillaume, J. F. Rommeluere, J. Chevallier, *J. Electron. Mater., 7*, 17 (1978).
7. H. Mittendorf, *Z. Phys., 183*, 113 (1965).
8. B. J. Fitzpatrick, U. S. Patent 5, 521, 934, (May 28, 1996).
9. H. Okuyama, K. Nakano, T. Miyajima, K. Akimoto, *Jpn. J. Appl. Phys., 30*, L1620 (1991).
10. A. Waag, F. Fischer, H. J. Lugauer, T. Litz, J. Laubender, U. Lunz, U. Zehnder, W. Ossau, T. Gebhardt, M. Moller, G. Landwehr, *J. Appl. Phys., 80*, 792, (1996).
11. I. Suemune, T. Obinata, K. Uesugi, H. Suzuki, H. Kumano, H. Nashiki, J. Nakahara, *J. Cryst. Growth, 170*, 480 (1997).

17.3.8.6.3. Group IIA–IVB Compounds.

Compounds in groups IIA–IVB may be prepared in bulk form by direct reaction and grown by gradient freeze[1] or Bridgman[2] techniques. Thin-film direct reaction is capable of making Mg_2Si in epitaxial form on silicon[3].

(BRIAN J. FITZPATRICK)

1. R. G. Morris, R. D. Redin, G. C. Danielson, *Phys. Rev., 109*, 1909 (1958).
2. B. D. Lichter, *J. Electrochem. Soc., 109*, 819 (1962).
3. G. S. Tompa, Y. B. Li, D. Agassi, S. I. Kim, S. K. Hong, *J. Electron. Mater., 25*, 925 (1996).

17.3.8.6.4. Transition Metal Oxides.

The semiconducting forms of the transition metal oxides are almost never fully oxidized but often have nearly Daltonide stoichiometry. Oxidation of the metal powder, decomposition of the carbonates, and oxidation of a volatile precursor are all employed. Metal carbonyls, such as $Ni(CO)_4$ and $Fe(CO)_5$, are very useful, since distillation is a facile method of purification for these volatile liquids. Caution: $Ni(CO)_4$ is very toxic, and generates CO upon decomposition.

It is difficult to distinguish generation of defects such as oxygen vacancies and the creation of a new compound with a different oxidation state. For example, Fe_2O_3 (hematite) is only weakly semiconducting, but it can be reduced to Fe_3O_4 (magnetite), which has very high conductivity because of charge transfer between the Fe^{2+} and Fe^{3+} ions. This reduction can be done with CO–CO_2 mixtures at temperatures around 400°C, but can be controlled with more precision by implantation of hydrogen[1]. In this case, the orientation of the cubic magnetite is determined by the orientation of the hexagonal hematite. Further reduction leads to FeO (wustite), a metallic conductor.

Reactive evaporation and sputtering are techniques for synthesis that are popular because the stoichiometry may be controlled by varying the oxygen concentration in the vapor phase. The level of control is limited in evaporation by formation in the vapor phase of oxide particles that disturb the growth of the film. Nevertheless, material with a good range of semiconductor properties can be obtained. Classical intuition leads to the expectation that such material would always be oxygen-deficient, and, since oxygen vacancies are usually thought to be donors, n-type. However, p-type NiO has been made[2], so it is likely that precisely oxidized material can be made in favourable cases.

Cu_2O, uncontaminated by CuO, has been made by exposing Cu films 200–850 nm thick to multiply-scanned Ar^+ laser irradiation[3].

The sol–gel method, a nanoparticle synthesis technique, has been shown to be very flexible in film deposition. Smooth amorphous films can be deposited, and crystallized

controllably. A good example[3] is the reaction:

$$Nb(OC_2H_5)_5 + H_2O \xrightarrow{(HCl)} NbO_x \text{ (sol–gel)}$$

Molybdenum and tungsten oxides are generally similarly prepared, but even though the lower oxidation state compounds should be interesting, the trioxides receive most of the attention. Electrodeposition[4] from a hydrogen peroxide solution yields films that are crystalline as deposited; higher temperature preparation techniques often result in amorphous films. The peroxide would be expected to result in fully oxidized material as deposited, but subsequent heat treatment is needed to achieve this state.

Rare earth oxides, such as EuO, can be prepared by reactive evaporation, with the same capability to control the oxidation state as above[5].

Metal acetoacetonates have often been used in spray pyrolysis, as explained in 17.3.8.5.3, but advances in sol–gel processing have tended to reduce the importance of this method.

(BRIAN J. FITZPATRICK)

1. Y. Watanabe, S. Takemura, Y. Kashiwaya, K. Ishii, *J. Phys. D*, *29*, 8 (1996).
2. S. Passerini, B. Scrosati, *J. Electrochem. Soc.*, *141*, 889 (1994).
3. B. Ohtani, K. Iwai, S. Nishimoto, T. Inui, *J. Electrochem. Soc.*, *141*, 2439 (1994).
4. A. Guerfi, R. W. Paynter, L. H. Dao, *J. Electrochem. Soc.*, *142*, 3457 (1995).
5. M. Lubeeka, A. Wegrzyn, *Vacuum*, *37*, 111 (1987).

17.3.8.6.5. Transition Metal Chalcogenides.

Although the transition metal chalcogenides usually are quite refractory, direct reaction is feasible in many cases. In some cases (e.g., W and Mo), the oxide is volatile, making the surface at least accessible to reaction. In addition, the metals often have high rates of diffusion in the compounds, thus reducing the surface passivation effect of compound formation. This is probably because diffusion "jumps" are more probable in the presence of elements that can change their charge states. This property can be helpful in conversion of an oxide to a sulfide via H_2S or CS_2.

The general tendency toward synthesis of thinner films, driven both by applications and by the more microscopic analytical techniques, is well illustrated in this group of compounds. The interdiffused multilayer process deposits alternate layers of metal and chalcogenide, which are heated to promote direct reaction. An example is the growth of Nb_5Se_4 from films of tens of nanometers[1]. This procedure is also successful for $MoSe_2$. Because of the volatility of selenium, the last layer is metal, used as a cap[2].

Synthesis and crystal growth can be achieved with halogen transport in a sealed ampule. WS_2 and WSe_2 have been grown and doped quite readily on the metal sublattice, using niobium for p-type and rhenium for n-type. On the chalcogen sublattice, chlorine, as expected, is successful as an n-type dopant, but iodine is found to be a p-type dopant. This illustrates the low predictability, and the difficulty of data interpretation, of doping in compound semiconductors, even in the case of a near-equilibrium synthesis technique. Alloy formation, however, can be very good, as illustrated for $RuS_{2-x}Se_x$[3].

Ternary compounds (not alloys) such as $CdCr_2Se_4$ can be grown from a $PbCl_2$–$CdCl_2$ flux[4]. These are magnetic semiconductors, but they have been eclipsed by the manganese- and iron-based alloys with zinc and cadmium chalcogenides, such as $Cd_{1-x}Mn_xTe$. The pure compounds, usually made by direct reaction, are often used as

Inorganic Reactions and Methods, Volume 18
Edited by J. J. Zuckerman, Jim D. Atwood

controllably. A good example[3] is the reaction:

$$Nb(OC_2H_5)_5 + H_2O \xrightarrow{(HCl)} NbO_x \text{ (sol–gel)}$$

Molybdenum and tungsten oxides are generally similarly prepared, but even though the lower oxidation state compounds should be interesting, the trioxides receive most of the attention. Electrodeposition[4] from a hydrogen peroxide solution yields films that are crystalline as deposited; higher temperature preparation techniques often result in amorphous films. The peroxide would be expected to result in fully oxidized material as deposited, but subsequent heat treatment is needed to achieve this state.

Rare earth oxides, such as EuO, can be prepared by reactive evaporation, with the same capability to control the oxidation state as above[5].

Metal acetoacetonates have often been used in spray pyrolysis, as explained in 17.3.8.5.3, but advances in sol–gel processing have tended to reduce the importance of this method.

(BRIAN J. FITZPATRICK)

1. Y. Watanabe, S. Takemura, Y. Kashiwaya, K. Ishii, *J. Phys. D, 29*, 8 (1996).
2. S. Passerini, B. Scrosati, *J. Electrochem. Soc., 141*, 889 (1994).
3. B. Ohtani, K. Iwai, S. Nishimoto, T. Inui, *J. Electrochem. Soc., 141*, 2439 (1994).
4. A. Guerfi, R. W. Paynter, L. H. Dao, *J. Electrochem. Soc., 142*, 3457 (1995).
5. M. Lubeeka, A. Wegrzyn, *Vacuum, 37*, 111 (1987).

17.3.8.6.5. Transition Metal Chalcogenides.

Although the transition metal chalcogenides usually are quite refractory, direct reaction is feasible in many cases. In some cases (e.g., W and Mo), the oxide is volatile, making the surface at least accessible to reaction. In addition, the metals often have high rates of diffusion in the compounds, thus reducing the surface passivation effect of compound formation. This is probably because diffusion "jumps" are more probable in the presence of elements that can change their charge states. This property can be helpful in conversion of an oxide to a sulfide via H_2S or CS_2.

The general tendency toward synthesis of thinner films, driven both by applications and by the more microscopic analytical techniques, is well illustrated in this group of compounds. The interdiffused multilayer process deposits alternate layers of metal and chalcogenide, which are heated to promote direct reaction. An example is the growth of Nb_5Se_4 from films of tens of nanometers[1]. This procedure is also successful for $MoSe_2$. Because of the volatility of selenium, the last layer is metal, used as a cap[2].

Synthesis and crystal growth can be achieved with halogen transport in a sealed ampule. WS_2 and WSe_2 have been grown and doped quite readily on the metal sublattice, using niobium for p-type and rhenium for n-type. On the chalcogen sublattice, chlorine, as expected, is successful as an n-type dopant, but iodine is found to be a p-type dopant. This illustrates the low predictability, and the difficulty of data interpretation, of doping in compound semiconductors, even in the case of a near-equilibrium synthesis technique. Alloy formation, however, can be very good, as illustrated for $RuS_{2-x}Se_x$[3].

Ternary compounds (not alloys) such as $CdCr_2Se_4$ can be grown from a $PbCl_2$–$CdCl_2$ flux[4]. These are magnetic semiconductors, but they have been eclipsed by the manganese- and iron-based alloys with zinc and cadmium chalcogenides, such as $Cd_{1-x}Mn_xTe$. The pure compounds, usually made by direct reaction, are often used as

source material for alloy synthesis, by the same techniques used for compounds of groups II–VI (see 17.3.8.5).

(BRIAN J. FITZPATRICK)

1. M. Fukuta, M. D. Hornbostel, D. C. Johnson, *J. Am. Chem. Soc., 116,* 9136 (1994).
2. J. Pouzet, J. C. Bernede, *Rev. Phys. Appl., 25,* 807 (1990).
3. J.-K. Huang, Y.-S. Huang, T.-R. Yang, *J. Appl. Phys., 78,* 2691 (1995).
4. D. Kuse, *IBM J. of Res. and Dev., 14,* 315 (1970).

17.3.8.6.6. Transition Metal Pnictides and Compounds with Group IV Elements.

Direct reaction is the method of choice for synthesis of transition metal pnictides and compounds of group IV elements in general, despite the wide range of reactivities represented. Sealed silica ampules, often coated with carbon (see above), are used to contain the reactants. Fortunately, however, the volatility of antimony and most of the other elements is low enough to permit the use of open or semi-sealed graphite, vitreous carbon, alumina, or boron nitride crucibles. $CoSb_3$, "filled" (doped in an interstitial site) with rare earth atoms to reduce the thermal conductivity, is of interest[1]. Transition metal silicides and germanides are usually prepared by direct reactions[2]; low volatility is helpful, but the reactivity is severe, especially for the silicides. Even pyrolytic boron nitride crucibles are eroded; these compounds would seem to be good candidates for container-free (e.g., float-zone) preparation and growth methods.

(BRIAN J. FITZPATRICK)

1. B. C. Sales, D. Mandrus, R. K. Williams, *Science, 272,* 1325 (1996).
2. A. Borshchevsky, J.-P. Fleurial, *J. Crys. Growth, 137,* 283 (1994).3.

17.3.8.6.7. Group IA Halides.

Copper and silver halides are usually prepared for semiconductor purposes by melt techniques[1]. More recently, "endosemiconductors", in which silver halides are synthesized in sodalite cages by ion exchange from fused salts, have attracted great interest[2], because a "one molecule" semiconductor can be made, and also because the Ag–X distance can be varied.

(BRIAN J. FITZPATRICK)

1. C. B. Childs, *J. Cryst. Growth, 38,* 262 (1977).
2. G. Ozin, in *Materials Chemistry, an Emerging Discipline,* ACS Advances in Chemistry Series, American Chemical Society, Washington, D.C., 1995, p. 335.

17.3.8.6.8. Chalcopyrites.

These chalcopyrites have near-stoichiometric amounts of cations of two types, with a general formula of II–IV–V_2 or I–III–VI_2. They can be considered to be analogues of the corresponding III–V and II–VI compounds, and have a tetrahedral zinc-blende structure with a small tetragonal distortion. Direct reaction is aided, especially, in the I–III–V_2 case, by the presence of two different types of cation, that mitigate the effect of passivation layers on the anion. For example, if a layer of zinc phosphide forms, it is attacked by germanium, allowing the reaction to continue. $CuInSe_2$ has been synthesized by direct reaction in a microwave oven[1]. Film deposition can use either a presynthesized or multiple-element source; the latter (preferred) allows for slight variations in the Cu/In

Inorganic Reactions and Methods, Volume 18
Edited by J. J. Zuckerman, Jim D. Atwood

source material for alloy synthesis, by the same techniques used for compounds of groups II–VI (see 17.3.8.5).

(BRIAN J. FITZPATRICK)

1. M. Fukuta, M. D. Hornbostel, D. C. Johnson, *J. Am. Chem. Soc., 116*, 9136 (1994).
2. J. Pouzet, J. C. Bernede, *Rev. Phys. Appl., 25*, 807 (1990).
3. J.-K. Huang, Y.-S. Huang, T.-R. Yang, *J. Appl. Phys., 78*, 2691 (1995).
4. D. Kuse, *IBM J. of Res. and Dev., 14*, 315 (1970).

17.3.8.6.6. Transition Metal Pnictides and Compounds with Group IV Elements.

Direct reaction is the method of choice for synthesis of transition metal pnictides and compounds of group IV elements in general, despite the wide range of reactivities represented. Sealed silica ampules, often coated with carbon (see above), are used to contain the reactants. Fortunately, however, the volatility of antimony and most of the other elements is low enough to permit the use of open or semi-sealed graphite, vitreous carbon, alumina, or boron nitride crucibles. $CoSb_3$, "filled" (doped in an interstitial site) with rare earth atoms to reduce the thermal conductivity, is of interest[1]. Transition metal silicides and germanides are usually prepared by direct reactions[2]; low volatility is helpful, but the reactivity is severe, especially for the silicides. Even pyrolytic boron nitride crucibles are eroded; these compounds would seem to be good candidates for container-free (e.g., float-zone) preparation and growth methods.

(BRIAN J. FITZPATRICK)

1. B. C. Sales, D. Mandrus, R. K. Williams, *Science, 272,* 1325 (1996).
2. A. Borshchevsky, J.-P. Fleurial, *J. Crys. Growth, 137,* 283 (1994).3.

17.3.8.6.7. Group IA Halides.

Copper and silver halides are usually prepared for semiconductor purposes by melt techniques[1]. More recently, "endosemiconductors", in which silver halides are synthesized in sodalite cages by ion exchange from fused salts, have attracted great interest[2], because a "one molecule" semiconductor can be made, and also because the Ag–X distance can be varied.

(BRIAN J. FITZPATRICK)

1. C. B. Childs, *J. Cryst. Growth, 38*, 262 (1977).
2. G. Ozin, in *Materials Chemistry, an Emerging Discipline*, ACS Advances in Chemistry Series, American Chemical Society, Washington, D.C., 1995, p. 335.

17.3.8.6.8. Chalcopyrites.

These chalcopyrites have near-stoichiometric amounts of cations of two types, with a general formula of II–IV–V_2 or I–III–VI_2. They can be considered to be analogues of the corresponding III–V and II–VI compounds, and have a tetrahedral zinc-blende structure with a small tetragonal distortion. Direct reaction is aided, especially, in the I–III–V_2 case, by the presence of two different types of cation, that mitigate the effect of passivation layers on the anion. For example, if a layer of zinc phosphide forms, it is attacked by germanium, allowing the reaction to continue. $CuInSe_2$ has been synthesized by direct reaction in a microwave oven[1]. Film deposition can use either a presynthesized or multiple-element source; the latter (preferred) allows for slight variations in the Cu/In

Inorganic Reactions and Methods, Volume 18
Edited by J. J. Zuckerman, Jim D. Atwood

source material for alloy synthesis, by the same techniques used for compounds of groups II–VI (see 17.3.8.5).

(BRIAN J. FITZPATRICK)

1. M. Fukuta, M. D. Hornbostel, D. C. Johnson, *J. Am. Chem. Soc., 116*, 9136 (1994).
2. J. Pouzet, J. C. Bernede, *Rev. Phys. Appl., 25*, 807 (1990).
3. J.-K. Huang, Y.-S. Huang, T.-R. Yang, *J. Appl. Phys., 78*, 2691 (1995).
4. D. Kuse, *IBM J. of Res. and Dev., 14*, 315 (1970).

17.3.8.6.6. Transition Metal Pnictides and Compounds with Group IV Elements.

Direct reaction is the method of choice for synthesis of transition metal pnictides and compounds of group IV elements in general, despite the wide range of reactivities represented. Sealed silica ampules, often coated with carbon (see above), are used to contain the reactants. Fortunately, however, the volatility of antimony and most of the other elements is low enough to permit the use of open or semi-sealed graphite, vitreous carbon, alumina, or boron nitride crucibles. $CoSb_3$, "filled" (doped in an interstitial site) with rare earth atoms to reduce the thermal conductivity, is of interest[1]. Transition metal silicides and germanides are usually prepared by direct reactions[2]; low volatility is helpful, but the reactivity is severe, especially for the silicides. Even pyrolytic boron nitride crucibles are eroded; these compounds would seem to be good candidates for container-free (e.g., float-zone) preparation and growth methods.

(BRIAN J. FITZPATRICK)

1. B. C. Sales, D. Mandrus, R. K. Williams, *Science, 272,* 1325 (1996).
2. A. Borshchevsky, J.-P. Fleurial, *J. Crys. Growth, 137,* 283 (1994).3.

17.3.8.6.7. Group IA Halides.

Copper and silver halides are usually prepared for semiconductor purposes by melt techniques[1]. More recently, "endosemiconductors", in which silver halides are synthesized in sodalite cages by ion exchange from fused salts, have attracted great interest[2], because a "one molecule" semiconductor can be made, and also because the Ag–X distance can be varied.

(BRIAN J. FITZPATRICK)

1. C. B. Childs, *J. Cryst. Growth, 38*, 262 (1977).
2. G. Ozin, in *Materials Chemistry, an Emerging Discipline*, ACS Advances in Chemistry Series, American Chemical Society, Washington, D.C., 1995, p. 335.

17.3.8.6.8. Chalcopyrites.

These chalcopyrites have near-stoichiometric amounts of cations of two types, with a general formula of II–IV–V_2 or I–III–VI_2. They can be considered to be analogues of the corresponding III–V and II–VI compounds, and have a tetrahedral zinc-blende structure with a small tetragonal distortion. Direct reaction is aided, especially, in the I–III–V_2 case, by the presence of two different types of cation, that mitigate the effect of passivation layers on the anion. For example, if a layer of zinc phosphide forms, it is attacked by germanium, allowing the reaction to continue. $CuInSe_2$ has been synthesized by direct reaction in a microwave oven[1]. Film deposition can use either a presynthesized or multiple-element source; the latter (preferred) allows for slight variations in the Cu/In

Inorganic Reactions and Methods, Volume 18
Edited by J. J. Zuckerman, Jim D. Atwood

source material for alloy synthesis, by the same techniques used for compounds of groups II–VI (see 17.3.8.5).

(BRIAN J. FITZPATRICK)

1. M. Fukuta, M. D. Hornbostel, D. C. Johnson, *J. Am. Chem. Soc., 116*, 9136 (1994).
2. J. Pouzet, J. C. Bernede, *Rev. Phys. Appl., 25*, 807 (1990).
3. J.-K. Huang, Y.-S. Huang, T.-R. Yang, *J. Appl. Phys., 78*, 2691 (1995).
4. D. Kuse, *IBM J. of Res. and Dev., 14*, 315 (1970).

17.3.8.6.6. Transition Metal Pnictides and Compounds with Group IV Elements.

Direct reaction is the method of choice for synthesis of transition metal pnictides and compounds of group IV elements in general, despite the wide range of reactivities represented. Sealed silica ampules, often coated with carbon (see above), are used to contain the reactants. Fortunately, however, the volatility of antimony and most of the other elements is low enough to permit the use of open or semi-sealed graphite, vitreous carbon, alumina, or boron nitride crucibles. $CoSb_3$, "filled" (doped in an interstitial site) with rare earth atoms to reduce the thermal conductivity, is of interest[1]. Transition metal silicides and germanides are usually prepared by direct reactions[2]; low volatility is helpful, but the reactivity is severe, especially for the silicides. Even pyrolytic boron nitride crucibles are eroded; these compounds would seem to be good candidates for container-free (e.g., float-zone) preparation and growth methods.

(BRIAN J. FITZPATRICK)

1. B. C. Sales, D. Mandrus, R. K. Williams, *Science, 272,* 1325 (1996).
2. A. Borshchevsky, J.-P. Fleurial, *J. Crys. Growth, 137,* 283 (1994).3.

17.3.8.6.7. Group IA Halides.

Copper and silver halides are usually prepared for semiconductor purposes by melt techniques[1]. More recently, "endosemiconductors", in which silver halides are synthesized in sodalite cages by ion exchange from fused salts, have attracted great interest[2], because a "one molecule" semiconductor can be made, and also because the Ag–X distance can be varied.

(BRIAN J. FITZPATRICK)

1. C. B. Childs, *J. Cryst. Growth, 38*, 262 (1977).
2. G. Ozin, in *Materials Chemistry, an Emerging Discipline*, ACS Advances in Chemistry Series, American Chemical Society, Washington, D.C., 1995, p. 335.

17.3.8.6.8. Chalcopyrites.

These chalcopyrites have near-stoichiometric amounts of cations of two types, with a general formula of II–IV–V_2 or I–III–VI_2. They can be considered to be analogues of the corresponding III–V and II–VI compounds, and have a tetrahedral zinc-blende structure with a small tetragonal distortion. Direct reaction is aided, especially, in the I–III–V_2 case, by the presence of two different types of cation, that mitigate the effect of passivation layers on the anion. For example, if a layer of zinc phosphide forms, it is attacked by germanium, allowing the reaction to continue. $CuInSe_2$ has been synthesized by direct reaction in a microwave oven[1]. Film deposition can use either a presynthesized or multiple-element source; the latter (preferred) allows for slight variations in the Cu/In

ratio, a refinement of importance in determining the conductivity. This is in contrast with the statement above about stoichiometry, but a distinction should be made between gross and fine stoichiometry: "fine" referring here to changes in the ~100 ppm range, which control the electrical conductivity, and "gross" referring to changes of several percent or more. "Gross" stoichiometry prevails in virtually all synthesis techniques, direct reaction (above), iodine transport[2], and electrodeposition[3], and is maintained in melt growth. "Fine" stoichiometry can be adjusted by vapor annealing.

$CdGa_2Se_4$ and its homologues (defect chalcopyrites) are similar enough to the other chalcopyrites to permit the same techniques to be used for them.

These compounds have relatively low melting points, in the 700–1100°C range, but they have high heats of formation, comparable to the corresponding II-VI and III-V compounds; thus, elemental reactions must be handled with care. In particular, any use of elemental phosphorus always requires caution[4].

(BRIAN J. FITZPATRICK)

1. C. C. Landry, A. R. Barron, *Science, 260*, 1653 (1990).
2. K. Balakrishnan, B. Vengatesan, P. Ramaswamy, *J. Mater. Sci., 29*, 1879 (1994).
3. L. Thouin, J. Vedel, *J. Electrochem. Soc., 142*, 2996 (1995).
4. D. Bliss, M. Harris, J. Horrigan, W. M. Higgins, A. F. Armington, J. A.Adamski, *J. Cryst. Growth, 137*, 145 (1994).

17.3.8.6.9. IIB–VA Compounds.

IIB–VA compounds are often prepared by epitaxial growth on a substrate of bulk III–V compound, using transport agents such as halides, or organometallic precursors such as group II alkyls and group V hydrides or alkyls. Vapor growth from the elements yields small crystals and allows preparation of either of the two gross stoichiometries ($II–V_2$ or $II_3–V_2$). A good example of careful phosphorus reaction is the synthesis of Zn_3P_2–Cd_3P_2 alloys; here, the elements are heated at 10°C/h from 400°C to 850°C[1].

(BRIAN J. FITZPATRICK)

1. D. R. Rao, A. Nayak, *J. Mater. Sci., 27*, 4389 (1992).

17.3.8.6.10. IIB–VIIA Compounds.

HgI_2 has the highest bandgap-density product among semiconductors; it is usually grown by evaporation[1].

(BRIAN J. FITZPATRICK)

1. Z. Li, W. Li, J. Liu, B. Zhao, S. Zhu, H. Xu, H. Yuan, *J. Cryst. Growth, 156*, 86 (1995).

17.3.8.6.11. IIIA–VIA Compounds.

Direct reaction, which is preferred for the IIIA–VIA compounds, is facilitated by the fluidity and generally benign nature of indium and gallium[1]. Even though reactivity problems are low, control of the gross stoichiometry can be difficult, particularly if a "sub-stoichiometric" compound such as GaSe is sought. The 1:1 compounds are layer compounds with very weak bonding between the layers; inclusions of the defect-zinc-blende-structured Ga_2Se_3 must be avoided.

(BRIAN J. FITZPATRICK)

1. C. Ferrer, A. Segura, M. Andres, V. Munoz, J. Pellicer, *J. Appl. Phys., 79*, 3200 (1996).

Inorganic Reactions and Methods, Volume 18
Edited by J. J. Zuckerman, Jim D. Atwood

ratio, a refinement of importance in determining the conductivity. This is in contrast with the statement above about stoichiometry, but a distinction should be made between gross and fine stoichiometry: "fine" referring here to changes in the ~100 ppm range, which control the electrical conductivity, and "gross" referring to changes of several percent or more. "Gross" stoichiometry prevails in virtually all synthesis techniques, direct reaction (above), iodine transport[2], and electrodeposition[3], and is maintained in melt growth. "Fine" stoichiometry can be adjusted by vapor annealing.

$CdGa_2Se_4$ and its homologues (defect chalcopyrites) are similar enough to the other chalcopyrites to permit the same techniques to be used for them.

These compounds have relatively low melting points, in the 700–1100°C range, but they have high heats of formation, comparable to the corresponding II-VI and III-V compounds; thus, elemental reactions must be handled with care. In particular, any use of elemental phosphorus always requires caution[4].

(BRIAN J. FITZPATRICK)

1. C. C. Landry, A. R. Barron, *Science, 260*, 1653 (1990).
2. K. Balakrishnan, B. Vengatesan, P. Ramaswamy, *J. Mater. Sci., 29*, 1879 (1994).
3. L. Thouin, J. Vedel, *J. Electrochem. Soc., 142*, 2996 (1995).
4. D. Bliss, M. Harris, J. Horrigan, W. M. Higgins, A. F. Armington, J. A.Adamski, *J. Cryst. Growth, 137*, 145 (1994).

17.3.8.6.9. IIB–VA Compounds.

IIB–VA compounds are often prepared by epitaxial growth on a substrate of bulk III–V compound, using transport agents such as halides, or organometallic precursors such as group II alkyls and group V hydrides or alkyls. Vapor growth from the elements yields small crystals and allows preparation of either of the two gross stoichiometries ($II–V_2$ or $II_3–V_2$). A good example of careful phosphorus reaction is the synthesis of Zn_3P_2–Cd_3P_2 alloys; here, the elements are heated at 10°C/h from 400°C to 850°C[1].

(BRIAN J. FITZPATRICK)

1. D. R. Rao, A. Nayak, *J. Mater. Sci., 27*, 4389 (1992).

17.3.8.6.10. IIB–VIA Compounds.

HgI_2 has the highest bandgap-density product among semiconductors; it is usually grown by evaporation[1].

(BRIAN J. FITZPATRICK)

1. Z. Li, W. Li, J. Liu, B. Zhao, S. Zhu, H. Xu, H. Yuan, *J. Cryst. Growth, 156*, 86 (1995).

17.3.8.6.11. IIIA–VIA Compounds.

Direct reaction, which is preferred for the IIIA–VIA compounds, is facilitated by the fluidity and generally benign nature of indium and gallium[1]. Even though reactivity problems are low, control of the gross stoichiometry can be difficult, particularly if a "sub-stoichiometric" compound such as GaSe is sought. The 1:1 compounds are layer compounds with very weak bonding between the layers; inclusions of the defect-zinc-blende-structured Ga_2Se_3 must be avoided.

(BRIAN J. FITZPATRICK)

1. C. Ferrer, A. Segura, M. Andres, V. Munoz, J. Pellicer, *J. Appl. Phys., 79*, 3200 (1996).

Inorganic Reactions and Methods, Volume 18
Edited by J. J. Zuckerman, Jim D. Atwood

ratio, a refinement of importance in determining the conductivity. This is in contrast with the statement above about stoichiometry, but a distinction should be made between gross and fine stoichiometry: "fine" referring here to changes in the ~100 ppm range, which control the electrical conductivity, and "gross" referring to changes of several percent or more. "Gross" stoichiometry prevails in virtually all synthesis techniques, direct reaction (above), iodine transport[2], and electrodeposition[3], and is maintained in melt growth. "Fine" stoichiometry can be adjusted by vapor annealing.

$CdGa_2Se_4$ and its homologues (defect chalcopyrites) are similar enough to the other chalcopyrites to permit the same techniques to be used for them.

These compounds have relatively low melting points, in the 700–1100°C range, but they have high heats of formation, comparable to the corresponding II-VI and III-V compounds; thus, elemental reactions must be handled with care. In particular, any use of elemental phosphorus always requires caution[4].

(BRIAN J. FITZPATRICK)

1. C. C. Landry, A. R. Barron, *Science, 260*, 1653 (1990).
2. K. Balakrishnan, B. Vengatesan, P. Ramaswamy, *J. Mater. Sci., 29*, 1879 (1994).
3. L. Thouin, J. Vedel, *J. Electrochem. Soc., 142*, 2996 (1995).
4. D. Bliss, M. Harris, J. Horrigan, W. M. Higgins, A. F. Armington, J. A.Adamski, *J. Cryst. Growth, 137*, 145 (1994).

17.3.8.6.9. IIB–VA Compounds.

IIB–VA compounds are often prepared by epitaxial growth on a substrate of bulk III–V compound, using transport agents such as halides, or organometallic precursors such as group II alkyls and group V hydrides or alkyls. Vapor growth from the elements yields small crystals and allows preparation of either of the two gross stoichiometries ($II–V_2$ or $II_3–V_2$). A good example of careful phosphorus reaction is the synthesis of Zn_3P_2–Cd_3P_2 alloys; here, the elements are heated at 10°C/h from 400°C to 850°C[1].

(BRIAN J. FITZPATRICK)

1. D. R. Rao, A. Nayak, *J. Mater. Sci., 27*, 4389 (1992).

17.3.8.6.10. IIB–VIA Compounds.

HgI_2 has the highest bandgap-density product among semiconductors; it is usually grown by evaporation[1].

(BRIAN J. FITZPATRICK)

1. Z. Li, W. Li, J. Liu, B. Zhao, S. Zhu, H. Xu, H. Yuan, *J. Cryst. Growth, 156*, 86 (1995).

17.3.8.6.11. IIIA–VIA Compounds.

Direct reaction, which is preferred for the IIIA–VIA compounds, is facilitated by the fluidity and generally benign nature of indium and gallium[1]. Even though reactivity problems are low, control of the gross stoichiometry can be difficult, particularly if a "sub-stoichiometric" compound such as GaSe is sought. The 1:1 compounds are layer compounds with very weak bonding between the layers; inclusions of the defect-zinc-blende-structured Ga_2Se_3 must be avoided.

(BRIAN J. FITZPATRICK)

1. C. Ferrer, A. Segura, M. Andres, V. Munoz, J. Pellicer, *J. Appl. Phys., 79*, 3200 (1996).

Inorganic Reactions and Methods, Volume 18
Edited by J. J. Zuckerman, Jim D. Atwood

ratio, a refinement of importance in determining the conductivity. This is in contrast with the statement above about stoichiometry, but a distinction should be made between gross and fine stoichiometry: "fine" referring here to changes in the ~100 ppm range, which control the electrical conductivity, and "gross" referring to changes of several percent or more. "Gross" stoichiometry prevails in virtually all synthesis techniques, direct reaction (above), iodine transport[2], and electrodeposition[3], and is maintained in melt growth. "Fine" stoichiometry can be adjusted by vapor annealing.

$CdGa_2Se_4$ and its homologues (defect chalcopyrites) are similar enough to the other chalcopyrites to permit the same techniques to be used for them.

These compounds have relatively low melting points, in the 700–1100°C range, but they have high heats of formation, comparable to the corresponding II-VI and III-V compounds; thus, elemental reactions must be handled with care. In particular, any use of elemental phosphorus always requires caution[4].

(BRIAN J. FITZPATRICK)

1. C. C. Landry, A. R. Barron, *Science, 260*, 1653 (1990).
2. K. Balakrishnan, B. Vengatesan, P. Ramaswamy, *J. Mater. Sci., 29*, 1879 (1994).
3. L. Thouin, J. Vedel, *J. Electrochem. Soc., 142*, 2996 (1995).
4. D. Bliss, M. Harris, J. Horrigan, W. M. Higgins, A. F. Armington, J. A.Adamski, *J. Cryst. Growth, 137*, 145 (1994).

17.3.8.6.9. IIB–VA Compounds.

IIB–VA compounds are often prepared by epitaxial growth on a substrate of bulk III–V compound, using transport agents such as halides, or organometallic precursors such as group II alkyls and group V hydrides or alkyls. Vapor growth from the elements yields small crystals and allows preparation of either of the two gross stoichiometries ($II–V_2$ or $II_3–V_2$). A good example of careful phosphorus reaction is the synthesis of Zn_3P_2–Cd_3P_2 alloys; here, the elements are heated at 10°C/h from 400°C to 850°C[1].

(BRIAN J. FITZPATRICK)

1. D. R. Rao, A. Nayak, *J. Mater. Sci., 27*, 4389 (1992).

17.3.8.6.10. IIB–VIA Compounds.

HgI_2 has the highest bandgap-density product among semiconductors; it is usually grown by evaporation[1].

(BRIAN J. FITZPATRICK)

1. Z. Li, W. Li, J. Liu, B. Zhao, S. Zhu, H. Xu, H. Yuan, *J. Cryst. Growth, 156*, 86 (1995).

17.3.8.6.11. IIIA–VIA Compounds.

Direct reaction, which is preferred for the IIIA–VIA compounds, is facilitated by the fluidity and generally benign nature of indium and gallium[1]. Even though reactivity problems are low, control of the gross stoichiometry can be difficult, particularly if a "sub-stoichiometric" compound such as GaSe is sought. The 1:1 compounds are layer compounds with very weak bonding between the layers; inclusions of the defect-zinc-blende-structured Ga_2Se_3 must be avoided.

(BRIAN J. FITZPATRICK)

1. C. Ferrer, A. Segura, M. Andres, V. Munoz, J. Pellicer, *J. Appl. Phys., 79*, 3200 (1996).

Inorganic Reactions and Methods, Volume 18
Edited by J. J. Zuckerman, Jim D. Atwood

17.3.8.6.12. IVA–VA Compounds.

Direct reaction is feasible for the IVA–VA compounds. This is surprising, since a low vapor pressure element, such as silicon, would be expected to passivate on exposure to phosphorus or arsenic. The "valve metal" analogy to electrochemical reactions may be invoked here: fresh silicon probably diffuses rapidly through the compound, providing a continuous supply of reactant. A cold zone with a temperature of less than 500°C supplies phosphorus to the silicon, kept slightly near the 1:1 SiP melting point of 1166°C[1].

(BRIAN J. FITZPATRICK)

1. Y. A. Ugai, L. I. Sokolov, E. G. Goncharov, A. N. Lukin, *Inorganic Materials* (English translation from the Russian), *17*, 851 (1981).

17.3.8.6.13. IVA–VIA Compounds.

Films of IVA–VIA compounds have been prepared by the aqueous reactions of group IV nitrates with thio- or selenourea, in basic solution. More recently, bulk crystals, especially of the alloys, have been made by direct reaction. Control of stoichiometry is always difficult. At present, molecular beam epitaxy (precise evaporation of the elements) has become preeminent, because alloys of PbTe with both SnTe and EuTe can be made[1]. It is surprising that a rare earth atom can be substituted into such a lattice, and even more surprising that its electronic behavior appears to be that of a substituent with a valence of +2. SnO_2, while differing widely from the "lead salts", is also a IV–VI compound that can be prepared as films by spray pyrolysis of the chloride, or by reactive evaporation or sputtering.

(BRIAN J. FITZPATRICK)

1. T. C. Harman, D. L. Spears, M. J. Manfra, *J. Electron. Mater.*, *25*, 1121 (1996).

17.3.8.6.14. VA–VIA Compounds.

Direct reaction is used for VA–VIA compounds, the major problem being the tendency for glass formation (this is desired for some applications). Epitaxial growth of Sb_2Te_3 on Bi_2Te_3 has been achieved, despite the large lattice mismatch[1].

(BRIAN J. FITZPATRICK)

1. B. Gardes, J. Ameziane, G. Brun, J. C. Tedenac, J. Boyer, *J. Mater. Sci.*, *29*, 2751 (1994).

17.3.8.6.15. More Complex Compounds.

Numerous compounds do not conveniently fit into the foregoing classifications but have quite interesting semiconducting properties. Indium tin oxide (ITO) and cadmium stannate are transparent conductors, usually deposited as films by evaporation or sputtering with a controlled partial pressure or oxygen[1]. $LaCrO_3$ powders are prepared by a glycine–nitrate process, followed by calcination at 1000°C, and sintering at 1500–1700°C[2]. There are other complex compounds of the "main group" elements, and of these elements with alkali metals; their preparations usually follow the methods above.

(BRIAN J. FITZPATRICK)

Inorganic Reactions and Methods, Volume 18
Edited by J. J. Zuckerman, Jim D. Atwood

17.3.8.6.12. IVA–VA Compounds.

Direct reaction is feasible for the IVA–VA compounds. This is surprising, since a low vapor pressure element, such as silicon, would be expected to passivate on exposure to phosphorus or arsenic. The "valve metal" analogy to electrochemical reactions may be invoked here: fresh silicon probably diffuses rapidly through the compound, providing a continuous supply of reactant. A cold zone with a temperature of less than 500°C supplies phosphorus to the silicon, kept slightly near the 1:1 SiP melting point of 1166°C[1].

(BRIAN J. FITZPATRICK)

1. Y. A. Ugai, L. I. Sokolov, E. G. Goncharov, A. N. Lukin, *Inorganic Materials* (English translation from the Russian), *17*, 851 (1981).

17.3.8.6.13. IVA–VIA Compounds.

Films of IVA–VIA compounds have been prepared by the aqueous reactions of group IV nitrates with thio- or selenourea, in basic solution. More recently, bulk crystals, especially of the alloys, have been made by direct reaction. Control of stoichiometry is always difficult. At present, molecular beam epitaxy (precise evaporation of the elements) has become preeminent, because alloys of PbTe with both SnTe and EuTe can be made[1]. It is surprising that a rare earth atom can be substituted into such a lattice, and even more surprising that its electronic behavior appears to be that of a substituent with a valence of +2. SnO_2, while differing widely from the "lead salts", is also a IV–VI compound that can be prepared as films by spray pyrolysis of the chloride, or by reactive evaporation or sputtering.

(BRIAN J. FITZPATRICK)

1. T. C. Harman, D. L. Spears, M. J. Manfra, *J. Electron. Mater., 25*, 1121 (1996).

17.3.8.6.14. VA–VIA Compounds.

Direct reaction is used for VA–VIA compounds, the major problem being the tendency for glass formation (this is desired for some applications). Epitaxial growth of Sb_2Te_3 on Bi_2Te_3 has been achieved, despite the large lattice mismatch[1].

(BRIAN J. FITZPATRICK)

1. B. Gardes, J. Ameziane, G. Brun, J. C. Tedenac, J. Boyer, *J. Mater. Sci., 29*, 2751 (1994).

17.3.8.6.15. More Complex Compounds.

Numerous compounds do not conveniently fit into the foregoing classifications but have quite interesting semiconducting properties. Indium tin oxide (ITO) and cadmium stannate are transparent conductors, usually deposited as films by evaporation or sputtering with a controlled partial pressure or oxygen[1]. $LaCrO_3$ powders are prepared by a glycine–nitrate process, followed by calcination at 1000°C, and sintering at 1500–1700°C[2]. There are other complex compounds of the "main group" elements, and of these elements with alkali metals; their preparations usually follow the methods above.

(BRIAN J. FITZPATRICK)

Inorganic Reactions and Methods, Volume 18
Edited by J. J. Zuckerman, Jim D. Atwood

17.3.8.6.12. IVA–VA Compounds.

Direct reaction is feasible for the IVA–VA compounds. This is surprising, since a low vapor pressure element, such as silicon, would be expected to passivate on exposure to phosphorus or arsenic. The "valve metal" analogy to electrochemical reactions may be invoked here: fresh silicon probably diffuses rapidly through the compound, providing a continuous supply of reactant. A cold zone with a temperature of less than 500°C supplies phosphorus to the silicon, kept slightly near the 1:1 SiP melting point of 1166°C[1].

(BRIAN J. FITZPATRICK)

1. Y. A. Ugai, L. I. Sokolov, E. G. Goncharov, A. N. Lukin, *Inorganic Materials* (English translation from the Russian), *17*, 851 (1981).

17.3.8.6.13. IVA–VIA Compounds.

Films of IVA–VIA compounds have been prepared by the aqueous reactions of group IV nitrates with thio- or selenourea, in basic solution. More recently, bulk crystals, especially of the alloys, have been made by direct reaction. Control of stoichiometry is always difficult. At present, molecular beam epitaxy (precise evaporation of the elements) has become preeminent, because alloys of PbTe with both SnTe and EuTe can be made[1]. It is surprising that a rare earth atom can be substituted into such a lattice, and even more surprising that its electronic behavior appears to be that of a substituent with a valence of +2. SnO_2, while differing widely from the "lead salts", is also a IV–VI compound that can be prepared as films by spray pyrolysis of the chloride, or by reactive evaporation or sputtering.

(BRIAN J. FITZPATRICK)

1. T. C. Harman, D. L. Spears, M. J. Manfra, *J. Electron. Mater.*, *25*, 1121 (1996).

17.3.8.6.14. VA–VIA Compounds.

Direct reaction is used for VA–VIA compounds, the major problem being the tendency for glass formation (this is desired for some applications). Epitaxial growth of Sb_2Te_3 on Bi_2Te_3 has been achieved, despite the large lattice mismatch[1].

(BRIAN J. FITZPATRICK)

1. B. Gardes, J. Ameziane, G. Brun, J. C. Tedenac, J. Boyer, *J. Mater. Sci.*, *29*, 2751 (1994).

17.3.8.6.15. More Complex Compounds.

Numerous compounds do not conveniently fit into the foregoing classifications but have quite interesting semiconducting properties. Indium tin oxide (ITO) and cadmium stannate are transparent conductors, usually deposited as films by evaporation or sputtering with a controlled partial pressure or oxygen[1]. $LaCrO_3$ powders are prepared by a glycine–nitrate process, followed by calcination at 1000°C, and sintering at 1500–1700°C[2]. There are other complex compounds of the "main group" elements, and of these elements with alkali metals; their preparations usually follow the methods above.

(BRIAN J. FITZPATRICK)

Inorganic Reactions and Methods, Volume 18
Edited by J. J. Zuckerman, Jim D. Atwood

17.3.8.6.12. IVA–VA Compounds.

Direct reaction is feasible for the IVA–VA compounds. This is surprising, since a low vapor pressure element, such as silicon, would be expected to passivate on exposure to phosphorus or arsenic. The "valve metal" analogy to electrochemical reactions may be invoked here: fresh silicon probably diffuses rapidly through the compound, providing a continuous supply of reactant. A cold zone with a temperature of less than 500°C supplies phosphorus to the silicon, kept slightly near the 1:1 SiP melting point of 1166°C[1].

(BRIAN J. FITZPATRICK)

1. Y. A. Ugai, L. I. Sokolov, E. G. Goncharov, A. N. Lukin, *Inorganic Materials* (English translation from the Russian), *17*, 851 (1981).

17.3.8.6.13. IVA–VIA Compounds.

Films of IVA–VIA compounds have been prepared by the aqueous reactions of group IV nitrates with thio- or selenourea, in basic solution. More recently, bulk crystals, especially of the alloys, have been made by direct reaction. Control of stoichiometry is always difficult. At present, molecular beam epitaxy (precise evaporation of the elements) has become preeminent, because alloys of PbTe with both SnTe and EuTe can be made[1]. It is surprising that a rare earth atom can be substituted into such a lattice, and even more surprising that its electronic behavior appears to be that of a substituent with a valence of +2. SnO_2, while differing widely from the "lead salts", is also a IV–VI compound that can be prepared as films by spray pyrolysis of the chloride, or by reactive evaporation or sputtering.

(BRIAN J. FITZPATRICK)

1. T. C. Harman, D. L. Spears, M. J. Manfra, *J. Electron. Mater.*, *25*, 1121 (1996).

17.3.8.6.14. VA–VIA Compounds.

Direct reaction is used for VA–VIA compounds, the major problem being the tendency for glass formation (this is desired for some applications). Epitaxial growth of Sb_2Te_3 on Bi_2Te_3 has been achieved, despite the large lattice mismatch[1].

(BRIAN J. FITZPATRICK)

1. B. Gardes, J. Ameziane, G. Brun, J. C. Tedenac, J. Boyer, *J. Mater. Sci.*, *29*, 2751 (1994).

17.3.8.6.15. More Complex Compounds.

Numerous compounds do not conveniently fit into the foregoing classifications but have quite interesting semiconducting properties. Indium tin oxide (ITO) and cadmium stannate are transparent conductors, usually deposited as films by evaporation or sputtering with a controlled partial pressure or oxygen[1]. $LaCrO_3$ powders are prepared by a glycine–nitrate process, followed by calcination at 1000°C, and sintering at 1500–1700°C[2]. There are other complex compounds of the "main group" elements, and of these elements with alkali metals; their preparations usually follow the methods above.

(BRIAN J. FITZPATRICK)

1. T. J. Coutts, X. Wu, W. P. Mulligan, J. M. Webb, *J. Electron. Mater., 25*, 935 (1996). The stoichiometry as listed is wrong, probably due to a typographical error; there are two cadmium atoms per formula unit.
2. T. R. Armstrong, J. W. Stevenson, L. R. Pederson, P. E. Rainey, *J. Electrochem. Soc., 143*, 2919 (1996).

17.3.8.7. Amorphous Semiconductors

Inexpensive solar cells can be made from hydrogenated, amorphous silicon, a-Si:H.[1] Amorphous semiconductors are made under non-equilibrium conditions, i.e., at low temperatures. In approaching equilibrium conditions, the material tends to become micro- or polycrystalline.

Sputtering is used to transport atoms from a target to a substrate. However, the sputtering gas tends to be incorporated in the amorphous layer. For Ge produced by sputtering with Ar, the amorphous layer contains a large concentration of Ar that evolves when the sample is shocked mechanically or thermally[2]. To produce a-Ge:H or a-Si:H by sputtering, H_2 is added to the Ar[3]. The a–Si:H can be doped to produce n- or p-type by adding PH_3 or B_2H_6, respectively, to the sputtering gas[4], but impurities at high concentration may catalyze the microcrystallization of the layer[5].

The most common deposition technique is the glow-discharge decomposition (gdd) of volatile inorganic compounds – e.g., SiH_4 to make a-Si:H. Several variants are available where the ionized plasma is driven by: a dc electric field (with the substrate on either the anode or the cathode), an ac field (60 Hz), an rf inductive, or rf capacitive (sometimes with a superposed dc bias). These techniques can be used in the presence of a magnetic field. The pressure of SiH_4 is in the range 1 to 700 Pascal with the substrate at 200–300°C. Above 350°C, H_2 evolves from the a-Si:H layer[6,7].

In the glow-discharge, the plasma consists of electron and mostly neutral radicals[8]. These reactions occur concurrently[8–10]:

$$e^- + SiH_4 \longrightarrow SiH_3 + H + e^- \qquad \Delta H = 4.1\ eV \qquad (a)$$

$$e^- + SiH_4 \longrightarrow SiH_2 + H_2 + e^- \qquad \Delta H = 2.2\ eV \qquad (b)$$

$$e^- + SiH_4 \longrightarrow SiH + H_2 + H + e^- \qquad (c)$$

$$e^- + SiH_4 \longrightarrow Si + 2H_2 + e^- \qquad (d)$$

$$e^- + SiH_3 \longrightarrow SiH_2 + H + e^- \qquad \Delta H = 2.6\ eV \qquad (e)$$

$$SiH_2 \longrightarrow Si + H_2 \qquad (f)$$

$$SiH_3 \longrightarrow SiH + H_2 \qquad (g)$$

$$H + SiH_4 \longrightarrow SiH_3 + H_2 \qquad \Delta H = -0.39\ eV \qquad (h)$$

$$[SiH_2]^+ + SiH_4 \longrightarrow [SiH_3]^+ + SiH_3 \qquad \Delta H = -0.04\ eV \qquad (i)$$

Furthermore, disilane forms exothermically[8]:

$$SiH_3 + SiH_3 \longrightarrow Si_2H_6 \qquad \Delta H = -3.17\ eV \qquad (j)$$

$$SiH_2 + SiH_4 \longrightarrow Si_2H_6 \qquad \Delta H = -2.15\ eV \qquad (k)$$

These reactions imply the existence of the intermediate radicals SiH_3 and SiH_2.

Inorganic Reactions and Methods, Volume 18
Edited by J. J. Zuckerman, Jim D. Atwood

1. T. J. Coutts, X. Wu, W. P. Mulligan, J. M. Webb, *J. Electron. Mater.*, *25*, 935 (1996). The stoichiometry as listed is wrong, probably due to a typographical error; there are two cadmium atoms per formula unit.
2. T. R. Armstrong, J. W. Stevenson, L. R. Pederson, P. E. Rainey, *J. Electrochem. Soc.*, *143*, 2919 (1996).

17.3.8.7. Amorphous Semiconductors

Inexpensive solar cells can be made from hydrogenated, amorphous silicon, a-Si:H.[1] Amorphous semiconductors are made under non-equilibrium conditions, i.e., at low temperatures. In approaching equilibrium conditions, the material tends to become micro- or polycrystalline.

Sputtering is used to transport atoms from a target to a substrate. However, the sputtering gas tends to be incorporated in the amorphous layer. For Ge produced by sputtering with Ar, the amorphous layer contains a large concentration of Ar that evolves when the sample is shocked mechanically or thermally[2]. To produce a-Ge:H or a-Si:H by sputtering, H_2 is added to the Ar[3]. The a–Si:H can be doped to produce n- or p-type by adding PH_3 or B_2H_6, respectively, to the sputtering gas[4], but impurities at high concentration may catalyze the microcrystallization of the layer[5].

The most common deposition technique is the glow-discharge decomposition (gdd) of volatile inorganic compounds – e.g., SiH_4 to make a-Si:H. Several variants are available where the ionized plasma is driven by: a dc electric field (with the substrate on either the anode or the cathode), an ac field (60 Hz), an rf inductive, or rf capacitive (sometimes with a superposed dc bias). These techniques can be used in the presence of a magnetic field. The pressure of SiH_4 is in the range 1 to 700 Pascal with the substrate at 200–300°C. Above 350°C, H_2 evolves from the a-Si:H layer[6,7].

In the glow-discharge, the plasma consists of electron and mostly neutral radicals[8]. These reactions occur concurrently[8–10]:

$$e^- + SiH_4 \longrightarrow SiH_3 + H + e^- \qquad \Delta H = 4.1\ eV \qquad (a)$$

$$e^- + SiH_4 \longrightarrow SiH_2 + H_2 + e^- \qquad \Delta H = 2.2\ eV \qquad (b)$$

$$e^- + SiH_4 \longrightarrow SiH + H_2 + H + e^- \qquad (c)$$

$$e^- + SiH_4 \longrightarrow Si + 2H_2 + e^- \qquad (d)$$

$$e^- + SiH_3 \longrightarrow SiH_2 + H + e^- \qquad \Delta H = 2.6\ eV \qquad (e)$$

$$SiH_2 \longrightarrow Si + H_2 \qquad (f)$$

$$SiH_3 \longrightarrow SiH + H_2 \qquad (g)$$

$$H + SiH_4 \longrightarrow SiH_3 + H_2 \qquad \Delta H = -0.39\ eV \qquad (h)$$

$$[SiH_2]^+ + SiH_4 \longrightarrow [SiH_3]^+ + SiH_3 \qquad \Delta H = -0.04\ eV \qquad (i)$$

Furthermore, disilane forms exothermically[8]:

$$SiH_3 + SiH_3 \longrightarrow Si_2H_6 \qquad \Delta H = -3.17\ eV \qquad (j)$$

$$SiH_2 + SiH_4 \longrightarrow Si_2H_6 \qquad \Delta H = -2.15\ eV \qquad (k)$$

These reactions imply the existence of the intermediate radicals SiH_3 and SiH_2.

Note that H can etch a-Si:H, releasing SiH_4, so that adding H to the plasma (i.e., diluting SiH_4 with H_2) can slow the deposition process and affect the morphology of the layer. On the other hand, the amount of hydrogen incorporated in the a-Si:H increases when the substrate temperature, T_s, is decreased – until a yellow polymer of $(SiH_x)_n$ is formed. By starting from higher silanes, e.g., Si_2H_6 or Si_3H_8, an a-Si:H deposit is obtained at lower temperature[11,12].

Doped a-Si:H is obtained by adding PH_3 or B_2H_6 to the SiH_4. The donor concentration, N_D, in the solid scales with the proportion of PH_3:

$$N_D/N_{Si} = K[N(PH_3)/N(SiH_4)] \tag{l}$$

where $K \sim 0.2$ over at least three orders of magnitude[13].

The a-Si:H can also be produced by chemical vapor deposition or pyrolysis of SiH_4 at $\sim 600°C$ with the substrate at $T_s < 400°C$. The reaction proceeds via the steps[14,15]:

$$SiH_4(g) \longrightarrow SiH_2(g) + H_2(g) \qquad 5.39 \text{ kcal/mole} \tag{m}$$

$$SiH_2(g) \longrightarrow 2SiH^*(g) \tag{n}$$

$$2SiH^*(g) \longrightarrow 2Si(s) + H_2(g) \tag{o}$$

Photodissociation of SiH_4 is induced with a CO_2 laser operating at 10.59 μm, which couples to a strong absorption mode of the molecule[16].

Other amorphous semiconductors include: a-Ge:H by sputtering[4], by gdd[17]; a-Si_xGe_{1-x} by gdd of $SiH_4 + GeH_4$[17]; a-C:H by gdd of C_2H_2[18] and with doping[19]; a-Si_xC_{1-x}:H by gdd of $SiH_4 + C_2H_4$[20] or of $Si(CH_3)_4$[21] or by sputtering[22]; a-Si_xB_{1-x}:H by gdd of $SiH_4 + B_2H_6$[23]; a-SiO_x by gdd of $SiH_4 + N_2O$[24]; a-Si_xAs_{1-x}:H by gdd of $SiH_4 + AsH_3$[25]; a-GaP:H by sputtering[26] or by gdd of $Ga(CH_3)_3 + PH_3$[27] a-GaN by sputtering with N_2[27] or by gdd of $Ga(CH_3)_3 + NH_3$[27].

(J. I. PANKOVE)

1. D. E. Carlson, C. R. Wronski, *Appl. Phys. Lett., 28*, 671 (1976).
2. A. Matsuda, A. Mineo, T. Kurosu, K. J. Callanan, M. Kikuchi, *Solid State Commun., 13*, 1685 (1973).
3. G. A. N. Connell, J. R.Pawlick, *Phys. Rev., Sect. B, 13*, 787 (1976).
4. W. Paul, A. Lewis, G. A. N. Connell, T. Moustakas, *Solid State Commun., 20*, 969 (1976).
5. S. Veprek, Z. Iqbal, H. R. Oswald, F. A. Sarott, J. Wagner, *Proc. 9th Int. Conf. Amorphous, Liquid Semiconductors*, 1981, *J. Phys., 42*, C4–251.
6. J. I. Pankove, D. E. Carlson, *Appl. Phys. Lett., 31*, 450 (1977).
7. H. Fritzsche, M. Tanielian, C. C. Tsai, P. J. Gaczi, *J. Appl. Phys., 50*, 3366 (1979).
8. G. Turban, Y. Catherine, B. Grolleau, *Thin Solid Films, 77*, 287 (1981).
9. R. W. Griffith, *Solar Materials Science*, L. E. Murr, ed. Academic Press, New York, NY, 1980, p. 665.
10. T-Y. Yu, T. M. H. Cheng, V. Kempter, F. W. Lampe, *J. Phys. Chem., 76*, 3321 (1972).
11. I. Shimizu, S. Oda, K. Saito, H. Tomita, E. Inoue, *Proc. 9th Int. Conf. Amorphous, Liquid Semiconductors*, 1981, *J. Phys., 42*, C4–1123.
12. B. A. Scott, M. H. Brodsky, D. C. Green, P. B. Kirby, R. M. Plecenik, E. E. Simonyi, *Appl. Phys. Lett., 37*, 725 (1980).
13. W. E. Spear, P. G. LeComber, *Solid State Commun., 17*, 1193 (1975).
14. M. Hirose, *Proc. 9th Int. Conf., Amorphous, Liquid Semiconductors*, 1981, *J. Phys., 42*, C4-705.
15. B. A. Scott, R. M. Plecenik, E. E. Simonyi, *Appl. Phys. Lett., 39*, 73 (1981).
16. M. Hanabusa, A. Namiki, Y. Yoshihara, *Appl. Phys. Lett., 35*, 626 (1979).

17. J. Chevalier, H. Wieder, A. Onton, C. R. Guarnieri, *Solid State Commun., 24*, 867 (1977).
18. D. A. Anderson, *Phil. Mag., 35*, 17 (1977).
19. B. Meyerson, F. W. Smith, *Solid State Commun., 34*, 531 (1980).
20. D. A. Anderson, W. E. Spear, *Phil. Mag., 35*, 1 (1977).
21. H. Munekata, S. Murasato, H. Kukimoto, *Appl. Phys. Lett., 37*, 536 (1980).
22. H. Matsunami, H. Masashiro, T. Tanaka, *J. Electronic Mater., 8*, 249 (1979).
23. C. C. Tsai, *Phys. Rev. Sect. B, 19*, 2041 (1979).
24. R. Carius, R. Fischer, E. Holtzenkampfer, J. Stuke, *Proc. 9th Int. Conf. Amorphous, Liquid Semiconductors*, 1981, *J. Phys., 42* C4–1025
25. J. C. Knights, *Phil. Mag., 34*, 663 (1976).
26. N. Matsumoto, K. Kumabe, *Jpn J. Appl. Phys., 18*, 1011 (1979).
27. J. C. Knights, R. A. Lujan, *J. Appl. Phys., 49*, 1291 (1978).
28. T. Hariu, T. Usuba, H. Adachi, Y. Shibata, *Appl. Phys. Lett., 32*, 252 (1978).

17.3.9. Preparation of Metallic Ceramics

Metallic carbides, nitrides, and oxides are used industrially in many applications; their physical properties are also of intrinsic interest. This section pinpoints various preparative techniques and reviews methods of crystal growth for this group of compounds. More detailed discussion is found in the reviews cited and in the references therein. The discussion is confined to binary compounds, M_aX_b (M is a cation; X = C, N, or O; a and b are simple integers) that display metallic properties; the very numerous ternaries $M_aM'_cX_b$ (M, M′ being different cations) cannot be described in this brief presentation.

The representative binary carbide[1], nitride[2], and oxide systems displaying metallic properties are summarized in Figure 1, where they are arranged in conformity with the

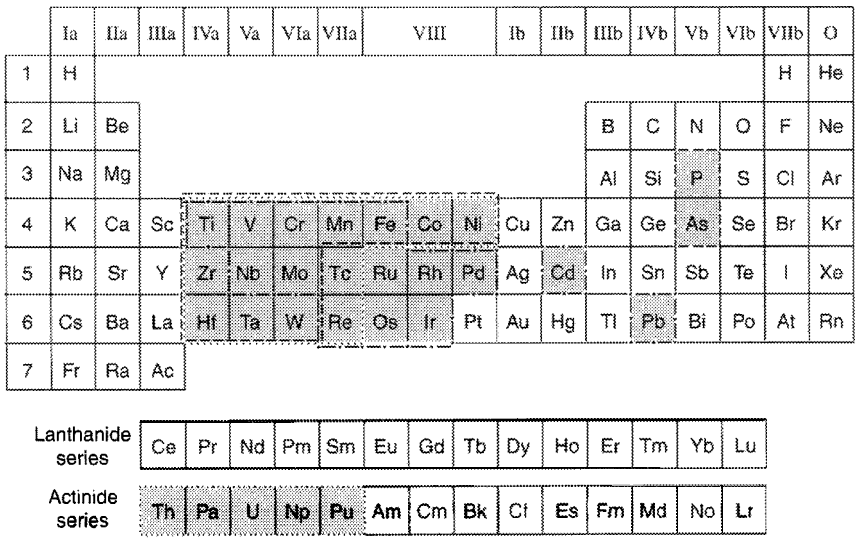

Figure 1. Binary metallic oxides (chain dotted lines), nitrides (dotted lines), and carbides (dashed lines) indicated on the periodic table.

Inorganic Reactions and Methods, Volume 18
Edited by J. J. Zuckerman, Jim D. Atwood

17. J. Chevalier, H. Wieder, A. Onton, C. R. Guarnieri, *Solid State Commun., 24*, 867 (1977).
18. D. A. Anderson, *Phil. Mag., 35*, 17 (1977).
19. B. Meyerson, F. W. Smith, *Solid State Commun., 34*, 531 (1980).
20. D. A. Anderson, W. E. Spear, *Phil. Mag., 35*, 1 (1977).
21. H. Munekata, S. Murasato, H. Kukimoto, *Appl. Phys. Lett., 37*, 536 (1980).
22. H. Matsunami, H. Masashiro, T. Tanaka, *J. Electronic Mater., 8*, 249 (1979).
23. C. C. Tsai, *Phys. Rev. Sect. B, 19*, 2041 (1979).
24. R. Carius, R. Fischer, E. Holtzenkampfer, J. Stuke, *Proc. 9th Int. Conf. Amorphous, Liquid Semiconductors*, 1981, *J. Phys., 42* C4–1025
25. J. C. Knights, *Phil. Mag., 34*, 663 (1976).
26. N. Matsumoto, K. Kumabe, *Jpn J. Appl. Phys., 18*, 1011 (1979).
27. J. C. Knights, R. A. Lujan, *J. Appl. Phys., 49*, 1291 (1978).
28. T. Hariu, T. Usuba, H. Adachi, Y. Shibata, *Appl. Phys. Lett., 32*, 252 (1978).

17.3.9. Preparation of Metallic Ceramics

Metallic carbides, nitrides, and oxides are used industrially in many applications; their physical properties are also of intrinsic interest. This section pinpoints various preparative techniques and reviews methods of crystal growth for this group of compounds. More detailed discussion is found in the reviews cited and in the references therein. The discussion is confined to binary compounds, M_aX_b (M is a cation; X = C, N, or O; a and b are simple integers) that display metallic properties; the very numerous ternaries $M_aM'_cX_b$ (M, M′ being different cations) cannot be described in this brief presentation.

The representative binary carbide[1], nitride[2], and oxide systems displaying metallic properties are summarized in Figure 1, where they are arranged in conformity with the

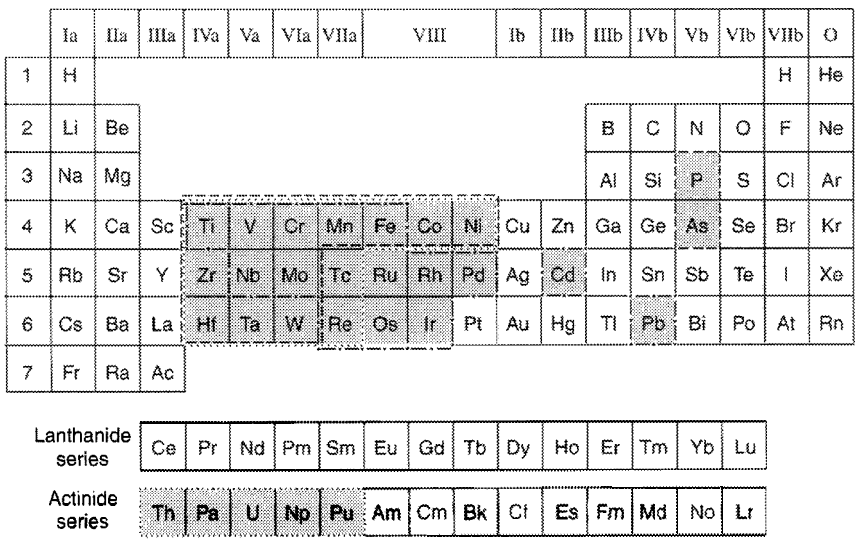

Figure 1. Binary metallic oxides (chain dotted lines), nitrides (dotted lines), and carbides (dashed lines) indicated on the periodic table.

TABLE 1. BINARY OXIDE, NITRIDE, AND CARBIDE SYSTEMS DISPLAYING METALLIC PROPERTIES

Oxides	Nitrides	Carbides
		P_2C_6
TiO, Ti_2O_3, Ti_nO_{2n-1}	Ti_2N, TiN	TiC
VO, V_2O_3, VO_2, V_nO_{2n-1}	V_2N, VN	V_2C, V_4C_3, V_6C_5, V_8C_7, VC
CrO_2	Cr_2N, CrN	$C_{23}C_6$, Cr_7C_3, Cr_3C_2
MnO_2, Mo_nO_{3n-1}	Mn_4N, Mn_2N, Mn_3N_2	$Mn_{23}C_6$, $Mn_{15}C_4$, Mn_3C, Mn_5C_2, Mn_7C_3
Fe_3O_4	Fe_4N, Fe_2N	Fe_3C, Fe_5C_3, Fe_2C
	Co_3N, Co_2N, Co_3N_2	Co_3C
	Ni_3N, Ni_3N_2	$Ni_3 \cdot C$
		As_2C_6
	ZrN	ZrC_{1-x}
	Nb_2N, Nb_4N_3, NbN_{1+x}	Nb_2C, Nb_3C_2, NbC, Nb_4C_3
	Mo_2N, MoN	Mo_2C, Mo_3C_2, MoC
	TcN	
RuO_2		
RhO_2		
PdO		
CdO		
	Hf_2N, HfN	HfC_{1-x}
	Ta_2N, TaN, Ta_3N_5	Ta_2C, Ta_3C_2, TaC, Ta_4C_3
	W_2N, WN	W_2C, WC_{1-x}
ReO_2, ReO_3	Re_2N	
IrO_2		
PbO_2		
	ThN, Th_2N_3	
	PaN_2	
	UN, U_2N_3, UN_2	
	NpN	
	PuN	

periodic table, and listed completely in Table 1. These binaries are largely clustered about the 3d-, 4d-, and 5d-transition series. No sharp dividing line between metallic and nonmetallic compounds can be drawn, there being many borderline cases. Many carbides and nitrides display metallic characteristics, and oxides once regarded only as insulators, also contain many members whose properties rival those of conventional metals.

Each subsection describes representative synthetic techniques, followed by techniques for single crystal growth.

(J. M. HONIG, H. R. HARRISON*)

1. R. Kieffer, F. Benesovsky, in *Kirk-Othmer Encyclopedia of Chemical Technology*, Vol. 4, 3rd ed., Wiley, New York, 1978, pp. 476–505.
2. F. Benesovsky, R. Kieffer, in *Kirk-Othmer Encyclopedia of Chemical Technology*, Vol. 13, 2nd ed., Wiley, New York, 1967, pp. 814–825.

* Deceased.

Inorganic Reactions and Methods, Volume 18
Edited by J. J. Zuckerman, Jim D. Atwood

17.3.9.1. Metallic Oxides

17.3.9.1.1. Introductory Comments.

Oxides may be subdivided into the following categories: refractory, insulating, and semiconducting materials; metallic oxides; materials undergoing metal–insulator transitions; and gaseous oxides.

The distribution of metallic oxides among the elements of the periodic table was shown in 17.3.9 (Fig. 1); this group is less numerous and not as greatly distributed among the transition elements as are the corresponding carbides and nitrides. Furthermore, the metallic oxides of the 3d-transition elements are characterized by relatively high reistivities in comparison with normal metals or with the compounds cited in later sections. Finally, Ti_2O_3, V_2O_3, VO_2, NbO_2, and many members of the Magnéli series (Ti_nO_{2n-1}, V_nO_{2n-1}, Mo_nO_{3n-1}) undergo one or more metal–insulator or magnetic ordering transitions when the temperature is altered. Reviews of the properties and methods of synthesis of oxides are available[1–10].

As with the carbides and nitrides, metallic oxides depart from strict stoichiometry; the oxygen/metal ratios can be altered and controlled by annealing under specified temperatures and oxygen pressures, P_{O_2}. Where the required P_{O_2} is large, as in RuO_2, direct control of the oxygen over pressure is readily achieved; where P_{O_2} is below 10^2 N/m^2 (10^{-3} bar), as in V_2O_3 or Fe_3O_4, buffering mixtures such as CO/CO_2 or H_2O/H_2 may be employed. This technique is reviewed in more detail elsewhere[11–16].

(J. M. HONIG, H. R. HARRISON*)

1. A. Magnéli, in *The Chemistry of Extended Defects in Nonmetallic Solids*, L. Eyring, M. O'Keefe, eds., North Holland, Amsterdam, 1970, pp. 148–163.
2. J. B. Goodenough, in *Progress in Solid State Chemistry*, Vol. 5, H. Reiss, ed., Pergamon Press, Oxford, 1971, pp. 145–399.
3. A. M. Anthony, R. Collongues, in *Preparative Methods in Solid State Chemistry*, P. Hagenmuller, ed., Academic Press, New York, 1972, pp. 147–249.
4. J. B. Goodenough, J. A. Kafalas, J. M. Longo, in *Preparative Methods in Solid State Chemistry*, P. Hagenmuller, ed., Academic Press, New York, 1972, pp. 2–69.
5. P. Kofstad, *Nonstoichiometry, Diffusion, and Electrical Conductivity in Binary Metal Oxides*, Wiley, New York, 1972.
6. J. D. M. McConnell, in *MTP International Review of Science, Transition Metals, Part I, Inorganic Chemistry*, Series One, Vol. 5, H. J. Emeléus, D. W. A. Sharp, eds., Butterworths, London, 1972, pp. 33–63.
7. H. Schäfer, in *Preparative Methods in Solid State Chemistry*, P. Hagenmuller, ed., Academic Press, New York, 1972, pp. 252–277.
8. A. Wold, D. Bellevance in *Preparative Methods in Solid State Chemistry*, P. Hagenmuller, ed., Academic Press, New York, 1972, pp. 279–308.
9. E. A. V. Ebsworth, J. A. Conner, J. J. Turner, in *Comprehensive Inorganic Chemistry*, Vol. 2, J. C. Bailor, H. J. Emeléus, R. Nyholm, A. F. Trotman-Dickenson, eds., Pergamon Press, Oxford, 1973, pp. 279–741.
10. A. Navrotsky, in *MTP International Review of Science, Inorganic Chemistry, Series Two*, Vol. 5, H. J. Emeléus, D. W. Sharp, eds., Butterworths, London, 1974, pp. 29–70.
11. J. Smiltens, *J. Chem. Phys.*, *20*, 990 (1952).
12. Y. Syono, *Jpn. J. Geophys.*, *4*, 71 (1965).
13. J. S. Huebner, in *Research Techniques for High Pressure and High Temperature*, G.C. Ulmer, ed., Springer-Verlag, New York, 1971, pp. 123–177.

* Deceased.

14. P. Deines, R. H. Nafziger, G. C. Ulmer, E. Woerman, *Temperature–Oxygen Fugacity Tables for Selected Gas Mixtures in the System C–H–O at One Atmosphere Total Pressure*, Bulletin of the Earth and Mineral Sciences Experiment Station, No. 88, Pennsylvania State University, 1974.
15. H. R. Harrison, R. Aragón, *Mater. Res. Bull., 13*, 1097 (1978).
16. S. A. Shivashankar, R. Aragón, H. R. Harrison, C. J. Sandberg, J. M. Honig, *J. Electrochem. Soc., 128*, 2472 (1981).

17.3.9.1.2. Synthetic Methods.

Several techniques are extensively used for preparation of metallic oxides:

1. Oxidation of metallic elements under controlled oxygen atmospheres as described above (e.g., $Ru + O_2 = RuO_2$). At the elevated temperatures required for these processes, steam also serves as an excellent oxidizing agent.
2. Reaction of a metal and high valence oxide to form an oxide of intermediate valence (e.g., in $3Nb + Nb_2O_5 \rightarrow 5NbO$), which must be carried out under carefully controlled oxygen partial pressures; product formation is assisted by heating all constituents above their melting points (e.g., in an arc melter).
3. Extractive metallurgical processes of minerals containing the desired oxide. Here it is important to keep track of contaminants.
4. Hydrothermal techniques, such as used for the preparation of CrO_2, which may be prepared from an aqueous solution [$5–30 \times 10^7$ N/m^2 (500–300 bar) at 400–525°C][1], by reduction of CrO_3 by means $CaCl_2 \cdot 2H_2O$ under pressure [4.5×10^6 N/m^2 (45 bar) at 360°C for 24 h][2]. A similar technique involves oxidizing Cr_2O_3, particularly by means of NH_4ClO_4 under pressure [2×10^8 N/m^2 (2 kbar) at 400°C for up to 2 h]; CrO_2 is produced with no extraneous phases[3].

   The techniques listed below have been used primarily for synthesis of nonmetallic oxides, but in principle they should also be applicable to metallic oxides.
5. Precipitation of hydroxides (or other oxygen-containing solids) from solution, followed by dehydration of the product.
6. Decomposition of carbonates, sulfates, or nitrates at elevated temperatures, accompanied, respectively, by the generation of CO_2, SO_3, or NO_2; usually such reactions require high temperatures to be driven to completion.
7. Metathetical reactions in fused salts (e.g., $FePO_4 + Fe_2O_3 + POCl_3$) in molten NaCl.
8. Partial reduction of higher valence oxides (e.g., $V_2O_5 + H_2 \rightarrow V_2O_3 + H_2O$). This procedure is complementary to the process described above[3]. Careful adjustment of temperature and H_2 pressure is required to achieve the desired intermediate stoichiometry.
9. Reaction of volatile halides with water vapor or steam, (e.g., $TiCl_4 + 2H_2O \rightarrow TiO_2 + 4HCl$ or $2AlCl_3 + 3H_2O \rightarrow Al_2O_3 + 6HCl$).
10. Electrochemical techniques as described in Ref. 4. In most cases these are used to prepare ternary oxides such as vanadates or molybdates, e.g., $Co_{1+x}V_{2-x}O_4$ ($0.11 < x < 0.56$) is synthesized by passing current through a mixture of Co_3O_4, V_2O_5, and WO_3–Na_2WO_4 at 800–960° using Pt electrodes[5]; molybdenum bronzes may be similarly prepared at 550°C, using MoO_3 and K_2MoO_4 in various proportions.

(J. M. HONIG, H. R. HARRISON*)

* Deceased.

Inorganic Reactions and Methods, Volume 18
Edited by J. J. Zuckerman, Jim D. Atwood

14. P. Deines, R. H. Nafziger, G. C. Ulmer, E. Woerman, *Temperature–Oxygen Fugacity Tables for Selected Gas Mixtures in the System C–H–O at One Atmosphere Total Pressure*, Bulletin of the Earth and Mineral Sciences Experiment Station, No. 88, Pennsylvania State University, 1974.
15. H. R. Harrison, R. Aragón, *Mater. Res. Bull., 13*, 1097 (1978).
16. S. A. Shivashankar, R. Aragón, H. R. Harrison, C. J. Sandberg, J. M. Honig, *J. Electrochem. Soc., 128*, 2472 (1981).

17.3.9.1.2. Synthetic Methods.

Several techniques are extensively used for preparation of metallic oxides:

1. Oxidation of metallic elements under controlled oxygen atmospheres as described above (e.g., $Ru + O_2 = RuO_2$). At the elevated temperatures required for these processes, steam also serves as an excellent oxidizing agent.
2. Reaction of a metal and high valence oxide to form an oxide of intermediate valence (e.g., in $3Nb + Nb_2O_5 \rightarrow 5NbO$), which must be carried out under carefully controlled oxygen partial pressures; product formation is assisted by heating all constituents above their melting points (e.g., in an arc melter).
3. Extractive metallurgical processes of minerals containing the desired oxide. Here it is important to keep track of contaminants.
4. Hydrothermal techniques, such as used for the preparation of CrO_2, which may be prepared from an aqueous solution [$5–30 \times 10^7$ N/m^2 (500–300 bar) at 400–525°C][1], by reduction of CrO_3 by means $CaCl_2 \cdot 2H_2O$ under pressure [4.5×10^6 N/m^2 (45 bar) at 360°C for 24 h][2]. A similar technique involves oxidizing Cr_2O_3, particularly by means of NH_4ClO_4 under pressure [2×10^8 N/m^2 (2 kbar) at 400°C for up to 2 h]; CrO_2 is produced with no extraneous phases[3].

   The techniques listed below have been used primarily for synthesis of nonmetallic oxides, but in principle they should also be applicable to metallic oxides.
5. Precipitation of hydroxides (or other oxygen-containing solids) from solution, followed by dehydration of the product.
6. Decomposition of carbonates, sulfates, or nitrates at elevated temperatures, accompanied, respectively, by the generation of CO_2, SO_3, or NO_2; usually such reactions require high temperatures to be driven to completion.
7. Metathetical reactions in fused salts (e.g., $FePO_4 + Fe_2O_3 + POCl_3$) in molten NaCl.
8. Partial reduction of higher valence oxides (e.g., $V_2O_5 + H_2 \rightarrow V_2O_3 + H_2O$). This procedure is complementary to the process described above[3]. Careful adjustment of temperature and H_2 pressure is required to achieve the desired intermediate stoichiometry.
9. Reaction of volatile halides with water vapor or steam, (e.g., $TiCl_4 + 2H_2O \rightarrow TiO_2 + 4HCl$ or $2AlCl_3 + 3H_2O \rightarrow Al_2O_3 + 6HCl$).
10. Electrochemical techniques as described in Ref. 4. In most cases these are used to prepare ternary oxides such as vanadates or molybdates, e.g., $Co_{1+x}V_{2-x}O_4$ ($0.11 < x < 0.56$) is synthesized by passing current through a mixture of Co_3O_4, V_2O_5, and WO_3–Na_2WO_4 at 800–960° using Pt electrodes[5]; molybdenum bronzes may be similarly prepared at 550°C, using MoO_3 and K_2MoO_4 in various proportions.

(J. M. HONIG, H. R. HARRISON*)

* Deceased.

1. T. J. Swoboda, P. Arthur, N. L. Cox, J. N. Ingraham, A. L. Oppegard, M. S. Sadler, *J. Appl. Phys., 32*, 374S (1961).
2. D. K. Agrawal, A. K. Biswas, C. N. R. Rao, E. C. Subbarao, *Mater. Res. Bull., 13*, 1135 (1978).
3. G. Demazeau, P. Maestro, T. Plante, M. Pouchard, P. Hagenmuller, *Mater. Res. Bull., 14*, 121 (1979).
4. H. Schäfer, in *Preparative Methods in Solid State Chemistry*, P. Hagenmuller, ed., Academic Press, New York, 1972, pp. 252–277.
5. D. B. Rogers, A. Ferretti, W. Kunnmann, *J. Phys. Chem. Solids, 27*, 1445 (1966).

17.3.9.1.3. Crystal Growth.

The techniques for growth of oxide single crystals of appropriate size and perfection advanced rapidly in the decades following World War II. The principles and techniques are covered in a number of monographs on crystal growth[1–6] and are only briefly described below:

(i) The Bridgman–Stockbarger Technique. The material, placed in a long narrow crucible with a conic tip, is heated past its melting point. The ampule is then gradually removed from the hot zone; a seed crystal solidifies in the conical tip, and this propagates as a single crystal as the freezing interface moves upward. Crystals of Fe_3O_4 (1 cm in all dimensions) are grown by this technique in Pt crucibles[7,8].

(ii) The Czochralski–Kyropoulos Technique. The oxide powder is placed in a crucible (usually a refractory metal) and heated past its melting point. A water-cooled rotating seed rod is lowered into the melt and rapidly withdrawn to form a thin neck that produces a single seed crystal. Withdrawal then proceeds more slowly, and permits the growth of a crystal of reasonable diameter. Large (≥ 1 cm all dimensions) Ti_2O_3 crystals have been obtained by this technique utilizing Mo crucibles[9,10].

(iii) The Tri-Arc Technique. The oxide charge is melted by an arc plasma maintained between a set of three peripherally mounted electrodes and a water-cooled copper base. The charge is placed on a concave graphite hearth, situated in the middle of the base. No crucible is required because the molten charge is protected from the hearth by a skin of unmolten material. A seed rod is lowered through the relatively cool central zone, and a crystal is pulled by the Czochralski technique, as described above. Only rather slender crystals (≤ 3–4 mm diameter) can be pulled because of the limited area of the cool zone between the arcs. To avoid oxidizing the tungsten electrodes, the operation must be conducted at low oxygen partial pressures; this restricts the method to oxides that require a low overpressure of oxygen. Single crystals of V_2O_3 are grown by this technique[11]; a crucibleless technique is absolutely essential, since molten V_2O_3 dissolves everything. Crystals of NbO have also been grown by this technique[10,12], as well as crystals of TiO, VO, and Ti_2O_3[10].

(iv) The Arc Transfer Technique. Electrodes are formed of the metal whose oxide is to be grown. A dc arc is struck in air or oxygen; the material is oxidized in transit and grows as a single crystal on the positive electrode. This method works best with oxides in their highest oxidation state. This is also a crucibleless technique; relatively large crystals can be grown (up to 5 mm diameter $\times$ 3 cm long). Crystals of VO_2 (in Ar)[13] and Fe_3O_4 (with Fe_2O_3 inclusions)[13,14] have been produced, as well as a variety of nonmetallic oxides.

Inorganic Reactions and Methods, Volume 18
Edited by J. J. Zuckerman, Jim D. Atwood

1. T. J. Swoboda, P. Arthur, N. L. Cox, J. N. Ingraham, A. L. Oppegard, M. S. Sadler, *J. Appl. Phys., 32*, 374S (1961).
2. D. K. Agrawal, A. K. Biswas, C. N. R. Rao, E. C. Subbarao, *Mater. Res. Bull., 13*, 1135 (1978).
3. G. Demazeau, P. Maestro, T. Plante, M. Pouchard, P. Hagenmuller, *Mater. Res. Bull., 14*, 121 (1979).
4. H. Schäfer, in *Preparative Methods in Solid State Chemistry*, P. Hagenmuller, ed., Academic Press, New York, 1972, pp. 252–277.
5. D. B. Rogers, A. Ferretti, W. Kunnmann, *J. Phys. Chem. Solids, 27*, 1445 (1966).

17.3.9.1.3. Crystal Growth.

The techniques for growth of oxide single crystals of appropriate size and perfection advanced rapidly in the decades following World War II. The principles and techniques are covered in a number of monographs on crystal growth[1–6] and are only briefly described below:

(i) The Bridgman–Stockbarger Technique. The material, placed in a long narrow crucible with a conic tip, is heated past its melting point. The ampule is then gradually removed from the hot zone; a seed crystal solidifies in the conical tip, and this propagates as a single crystal as the freezing interface moves upward. Crystals of Fe_3O_4 (1 cm in all dimensions) are grown by this technique in Pt crucibles[7,8].

(ii) The Czochralski–Kyropoulos Technique. The oxide powder is placed in a crucible (usually a refractory metal) and heated past its melting point. A water-cooled rotating seed rod is lowered into the melt and rapidly withdrawn to form a thin neck that produces a single seed crystal. Withdrawal then proceeds more slowly, and permits the growth of a crystal of reasonable diameter. Large (≥ 1 cm all dimensions) Ti_2O_3 crystals have been obtained by this technique utilizing Mo crucibles[9,10].

(iii) The Tri-Arc Technique. The oxide charge is melted by an arc plasma maintained between a set of three peripherally mounted electrodes and a water-cooled copper base. The charge is placed on a concave graphite hearth, situated in the middle of the base. No crucible is required because the molten charge is protected from the hearth by a skin of unmolten material. A seed rod is lowered through the relatively cool central zone, and a crystal is pulled by the Czochralski technique, as described above. Only rather slender crystals (≤ 3–4 mm diameter) can be pulled because of the limited area of the cool zone between the arcs. To avoid oxidizing the tungsten electrodes, the operation must be conducted at low oxygen partial pressures; this restricts the method to oxides that require a low overpressure of oxygen. Single crystals of V_2O_3 are grown by this technique[11]; a crucibleless technique is absolutely essential, since molten V_2O_3 dissolves everything. Crystals of NbO have also been grown by this technique[10,12], as well as crystals of TiO, VO, and Ti_2O_3[10].

(iv) The Arc Transfer Technique. Electrodes are formed of the metal whose oxide is to be grown. A dc arc is struck in air or oxygen; the material is oxidized in transit and grows as a single crystal on the positive electrode. This method works best with oxides in their highest oxidation state. This is also a crucibleless technique; relatively large crystals can be grown (up to 5 mm diameter $\times$ 3 cm long). Crystals of VO_2 (in Ar)[13] and Fe_3O_4 (with Fe_2O_3 inclusions)[13,14] have been produced, as well as a variety of nonmetallic oxides.

(v) The Verneuil or Flame-Fusion Technique. Powder is allowed to fall at a continuous slow rate from a hopper through an oxyhydrogen flame onto a base. Again, no crucible is involved; very large single crystals can be grown by this method. However, because of the limited range of H_2/O_2 partial pressures that can be maintained in oxyhydrogen flames, the technique is mostly limited to certain nonmetallic oxides. Single crystals of Fe_3O_4 are grown by this procedure[15].

(vi) Solution Growth, Flux Growth, and Hydrothermal Techniques. A solvent in which the material to be grown is dissolved (at temperatures that are relatively low for solution growth, and relatively high for flux and hydrothermal growth); dissolution to saturation, and under pressure in hydrothermal growth, is followed by slow cooling, to initiate precipitation of the solute into single crystals. The technique is useful for incongruently melting materials (i.e., materials that dissociate before melting or for those with very high melting points, which can effectively be lowered by dissolving the material in a solute), but a serious drawback is that it is difficult to avoid inclusions of the flux in the grown crystals. Small CdO ($\sim$1 mm maximum) are grown in Ag crucibles in molten KOH[16]. The hydrothermal technique is also utilized to grow blocks of Fe_3O_4 (free of Fe_2O_3 inclusions) up to 3 mm in size[17], needles of MnO_2 up to 1 mm long[18], CdO crystals of octahedral habit 1–2 mm in size[19], and small crystals of CrO_2[20]. Slab like (up to $7 \times 3 \times 2$ mm)[3] crystals of MoO_2 have been grown by an electrolytic variant[21].

(vii) Chemical Vapor Transport Technique. The charge and an appropriate transport agent (typically I_2, $TeCl_4$, or Cl_2) are sealed in an ampule, which is placed in the hot zone of a gradient furnace. The material is transported to the cooler zone where single crystals grow. It is difficult to control the size of the resulting crystals and to avoid incorporation of the transport gas in the crystals. The method has the advantage of requiring only simple apparatus (perhaps for this reason the number of investigations utilizing this technique is large) and more importantly, it is possible to grow crystals that exhibit only a narrow stability range, such as the Magnéli phases of V, Ti, and Mo (V_nO_{2n-1}, Ti_nO_{2n-1}, and Mo_nO_{3n-1}). Crystals of MoO_2 may be grown to a few millimeters using I_2[22,23] or $TeCl_4$[24]; the Mo_nO_{3n-1} Magnéli series[24]; the Ti_2O_{2n-1} Magnéli series[25,26], VO_2[27], and the V_nO_{2n-1} Magnéli series[28–33] have been reported on extensively. Crystals of CdO of size 60–150 mm^3 are grown by sublimation[34], and also by the Piper–Polich method (as large as $7 \times 7 \times 20$ mm^3), a modification of the customary vapor transport technique, which involves slowly pulling the ampule through a gradient furnace[35]. Small crystals of NbO are also grown[36], as well as block crystals of Fe_3O_4, 3–4 mm in size[37]. Crystals of RuO_2 may be grown to the size of a few millimeters by transport with O_2[38].

(viii) Skull Melting[39–46]. This process relies on coupling between the material to be melted and radiofrequency electromagnetic radiation (200 kHz–4 MHz and 20–50 kW) supplied by a commercial generator. The molten change is confined in container made of *individually separated, water-cooled copper fingers; the space between fingers allows* penetration of the applied electromagnetic field. The process is crucibleless (the molten charge is contained in a sintered shell of its own material), the ambient may be reducing or oxidizing, and there is no intrinsic temperature limitation: even ThO_2 single crystals have been grown at their melting point of 3400°C[47,48]. Thus, all three desirable criteria are realized by this technique. With slow cooling, large crystals of high perfection are

found in the central region of the frozen boule. Large (≥ 1 cm, all dimensions) crystals of Fe_3O_4[44] and V_2O_3[49] are grown by this very versatile technique.

(J. M. HONIG, H. R. HARRISON*)

1. R. A. Laudise, *The Growth of Single Crystals*, Prentice-Hall, Englewood Cliffs, NJ, 1970.
2. P. Hartman, *Crystal Growth: An Introduction*, North Holland, Amsterdam, 1973.
3. B. R. Pamplin, *Crystal Growth*, Pergamon Press, Oxford, 1975.
4. W. Bardsley, D. T. J. Hurle, J. B. Mullin, *Crystal Growth: A Tutorial Approach*, North Holland, Amsterdam, 1979.
5. C. H. L. Goodman, *Crystal Growth: Theory and Technique*, Vols. 1 and 2, Plenum Press, London, 1974, 1978.
6. F. A. Kröger, *The Chemistry of Imperfect Crystals*, Vol. 1: *Preparation, Purification, Crystal Growth, and Phase Theory*, 2nd ed., North Holland, Amsterdam, 1973.
7. J. Smiltens, *J. Chem. Phys.*, *20*, 990 (1952).
8. Y. Syono, *Jpn. J. Geophys.*, *4*, 71 (1965).
9. T. B. Reed, R. E. Fahey, J. M. Honig, *Mater. Res. Bull.*, *2*, 561 (1967).
10. T. B. Reed, in *Ferrites: Proceedings of an International Conference*, Y. Hoshino, S. Iida, M. Sugimoto, eds., University Park Press, Baltimore, MD, 1970, pp. 289–295.
11. J. C. C. Fan, T. B. Reed, *Mater. Res. Bull.*, *7*, 1403 (1972).
12. J. M. Honig, G. Yuochunas, T. B. Reed, E. R. Pollard, *J. Cryst. Growth*, *30*, 42 (1975).
13. J. R. Drabble, *J. Cryst. Growth*, *3/4*, 804 (1968).
14. B. A. Smith, I. G. Austin, *J. Cryst. Growth*, *1*, 79 (1967).
15. E. J. Scott, *J. Chem. Phys.*, *23*, 2459 (1955).
16. K. Kumar, *J. Electrochem. Soc.*, *122*, 1142 (1975).
17. S. Hirano, S. Somiya, *J. Cryst. Growth*, *35*, 273 (1976).
18. N. Yamamoto, T. Endo, M. Shimada, T. Takada, *Jpn. J. Appl. Phys.*, *13*, 723 (1974).
19. L. N. Dem'yanets, N. V. Suvorova, *Sov. Phys.-Crystallogr. (Engl. Transl.)*, *18*, 133 (1974).
20. P. Porta, M. Marezio, J. P. Remeika, P. D. Dernier, *Mater. Res. Bull.*, *7*, 157 (1972).
21. D. S. Perloff, A. Wold, in *Crystal Growth*, H. S. Peiser, ed., Pergamon Press, Oxford, 1967, pp. 361–363.
22. L. Ben-Dor, Y. Shimony, *Mater. Res. Bull.*, *9*, 837 (1974).
23. O. Bertrand, L. C. Dufour, *J. Cryst. Growth*, *35*, 325 (1976).
24. Y. Bando, Y. Kato, T. Takada, *Bull. Inst. Chem. Res.*, *54*, 330 (1976).
25. R. Roy, W. B. White, *J. Cryst. Growth*, *13/14*, 78 (1972).
26. J. Mercier, S. Lakkis, *J. Cryst. Growth*, *20*, 195 (1973).
27. Y. Bando, M. Kyoto, T. Takada, S. Muranaka, *J. Cryst. Growth*, *45*, 20 (1978).
28. Y. Bando, K. Nagasawa, Y. Kato, T. Takada, *Jpn. J. Appl. Phys.*, *8*, 633 (1969).
29. S. Kachi, K. Kosuge, H. Okinaka, *J. Solid State Chem.*, *6*, 258 (1973).
30. N. N. Khoi, T. R. Simon, H. K. Eastwood, *Mater. Res. Bull.*, *11*, 873 (1976).
31. Y. Hirotsu, S. P. Faile, H. Sato, *Mater. Res. Bull.*, *13*, 895 (1978).
32. E. Wolf, H. Oppermann, G. Krabbes, W. Reichelt, in *Current Topics in Materials Science*, Vol. 1, E. Kaldis, ed., North Holland, Amsterdam, 1978, pp. 697–742.
33. H. Kuwamoto, N. Otsuka, H. Sato, *J. Solid State Chem.*, *36* (1981).
34. K. J. Fischer, K. E. Spear, *J. Cryst. Growth*, *16*, 142 (1972).
35. P. Höschl, C. Konak, V. Prosser, *Mater. Res. Bull.*, *4*, 87 (1969).
36. H. Kodama, H. Komatsu, *J. Cryst. Growth*, *36*, 121 (1976).
37. P. Peshev, A. Toshev, *Mater. Res. Bull.*, *10*, 1335 (1975).
38. H. Schäfer, in *Preparative Methods in Solid State Chemistry*, P. Hagenmuller, ed., Academic Press, New York, 1972, pp. 252–277.
39. D. Michel, *Rev. Int. Hautes Temp. Refract.*, *9*, 225 (1972).
40. V. I. Aleksandrov, V. V. Osiko, A. M. Prokhorov, V. M. Tatarintsev, *Vestn. Akad. Nauk SSR*, No. 12, 29 (1973).
41. J. F. Wenkus, M. L. Cohen, A. G. Emslie, W. P. Menashi, P. F. Strong, Final Technical Report AFCRL-TR-75-0213, February 1975.

* Deceased.

42. D. Michel, M. Perez y Jorba, R. Collongues, *J. Cryst. Growth, 43*, 546 (1978).
43. V. I. Aleksandrov, V. V. Osiko, A. M. Prokhorov, V. M. Tatarintsev, in *Current Topics in Materials Science*, Vol. 1, E. Kaldis, ed., North Holland, Amsterdam, 1978, pp. 421–480.
44. H. R. Harrison, R. Aragón, *Mater. Res. Bull., 13*, 1097 (1978).
45. H. R. Harrison, R. Aragón, C. J. Sandberg, *Mater. Res. Bull., 15*, 571 (1980).
46. R. F. Sekerka, R. A. Hartzell, B. J. Farr, *J. Cryst. Growth, 50*, 783 (1980).
47. J. E. Keem, H. R. Harrison, S. P. Faile, H. Sato, J. M. Honig, *Am. Ceram. Soc. Bull., 56*, 1022 (1977).
48. C. C. Herrick, R. G. Behrens, *J. Cryst. Growth, 51*, 183 (1981).
49. S. A. Shivashankar, R. Aragón, H. R. Harrison, C. J. Sandberg, J. M. Honig, *J. Electrochem. Soc., 128*, 2472 (1981).

17.3.9.2. Metallic Carbides

17.3.9.2.1. General Comments.

The binary carbide compounds are divided into four categories:

1. Saltlike carbides and acetylides, principally combinations of C with elements of groups IA, IIA, IB, and IIB.
2. Metallic or interstitial carbides, involving elements of groups IVB, VB, VIB and Mn, Fe, Co, Ni, P, As, U and Pu.
3. Diamond-like carbides; these include compounds of C with B and Si.
4. Volatile, nonmetallic carbides, involving principally elements in groups VIA and VIIA.

A listing of the principal metallic carbides was provided in 17.3.9 (Fig. 1), along with the most common stoichiometric compositions (Table 1). Metallic carbides are stable over wide composition ranges, which do not necessarily encompass the ideal stoichiometry. For example, TiC_x is encountered in the range $0.28 \leq x \leq 1$; VC is stable in the range VC_x, $0.75 \leq x \leq 0.96$, which does not include the stoichiometric composition; Nb_2C is stable as NbC_x with $0.35 \leq x \leq 0.5$; TaC also exists only off-stoichiometry. Such wide compositional variations arise from the small size of the C atom, which can readily fit into interstices between metal atoms in the lattice; these sites may be filled to widely different degrees.

Preparative techniques and physical as well as structural characteristics are reviewed in articles and books[1–9].

(J. M. HONIG, H. R. HARRISON*)

1. P. Schwarzkopf, R. Kieffer, *Refractory Hard Metals*, Macmillan, New York: 1953.
2. R. Kieffer, F. Benesovsky, *Hartstoffe*, Springer-Verlag, Vienna, 1963.
3. H. J. Goldschmidt, *Interstitial Alloys*, Butterworths, London, 1967, Chapter 4.
4. E. K. Storms, *The Refractory Carbides*, Academic Press, New York, 1967.
5. L. E. Toth, *Transition Metal Carbides and Nitrides*, Academic Press, New York, 1971.
6. E. K. Storms, in *MTP International Review of Science, Solid State Chemistry, Inorganic Chemistry*, Series One, Vol. 10, H. J. Emeléus, L. E. J. Roberts, eds., Butterworths, London, 1972, pp. 37–78.
7. S. Windisch, H. Nowotny, in *Preparative Methods in Solid State Chemistry*, P. Hagenmuller, ed., Academic Press, New York, 1972, pp. 553–562.

* Deceased.

Inorganic Reactions and Methods, Volume 18
Edited by J. J. Zuckerman, Jim D. Atwood

42. D. Michel, M. Perez y Jorba, R. Collongues, *J. Cryst. Growth, 43*, 546 (1978).
43. V. I. Aleksandrov, V. V. Osiko, A. M. Prokhorov, V. M. Tatarintsev, in *Current Topics in Materials Science*, Vol. 1, E. Kaldis, ed., North Holland, Amsterdam, 1978, pp. 421–480.
44. H. R. Harrison, R. Aragón, *Mater. Res. Bull., 13*, 1097 (1978).
45. H. R. Harrison, R. Aragón, C. J. Sandberg, *Mater. Res. Bull., 15*, 571 (1980).
46. R. F. Sekerka, R. A. Hartzell, B. J. Farr, *J. Cryst. Growth, 50*, 783 (1980).
47. J. E. Keem, H. R. Harrison, S. P. Faile, H. Sato, J. M. Honig, *Am. Ceram. Soc. Bull., 56*, 1022 (1977).
48. C. C. Herrick, R. G. Behrens, *J. Cryst. Growth, 51*, 183 (1981).
49. S. A. Shivashankar, R. Aragón, H. R. Harrison, C. J. Sandberg, J. M. Honig, *J. Electrochem. Soc., 128*, 2472 (1981).

17.3.9.2. Metallic Carbides

17.3.9.2.1. General Comments.

The binary carbide compounds are divided into four categories:

1. Saltlike carbides and acetylides, principally combinations of C with elements of groups IA, IIA, IB, and IIB.
2. Metallic or interstitial carbides, involving elements of groups IVB, VB, VIB and Mn, Fe, Co, Ni, P, As, U and Pu.
3. Diamond-like carbides; these include compounds of C with B and Si.
4. Volatile, nonmetallic carbides, involving principally elements in groups VIA and VIIA.

A listing of the principal metallic carbides was provided in 17.3.9 (Fig. 1), along with the most common stoichiometric compositions (Table 1). Metallic carbides are stable over wide composition ranges, which do not necessarily encompass the ideal stoichiometry. For example, TiC_x is encountered in the range $0.28 \leq x \leq 1$; VC is stable in the range VC_x, $0.75 \leq x \leq 0.96$, which does not include the stoichiometric composition; Nb_2C is stable as NbC_x with $0.35 \leq x \leq 0.5$; TaC also exists only off-stoichiometry. Such wide compositional variations arise from the small size of the C atom, which can readily fit into interstices between metal atoms in the lattice; these sites may be filled to widely different degrees.

Preparative techniques and physical as well as structural characteristics are reviewed in articles and books[1–9].

(J. M. HONIG, H. R. HARRISON*)

1. P. Schwarzkopf, R. Kieffer, *Refractory Hard Metals*, Macmillan, New York: 1953.
2. R. Kieffer, F. Benesovsky, *Hartstoffe*, Springer-Verlag, Vienna, 1963.
3. H. J. Goldschmidt, *Interstitial Alloys*, Butterworths, London, 1967, Chapter 4.
4. E. K. Storms, *The Refractory Carbides*, Academic Press, New York, 1967.
5. L. E. Toth, *Transition Metal Carbides and Nitrides*, Academic Press, New York, 1971.
6. E. K. Storms, in *MTP International Review of Science, Solid State Chemistry, Inorganic Chemistry*, Series One, Vol. 10, H. J. Emeléus, L. E. J. Roberts, eds., Butterworths, London, 1972, pp. 37–78.
7. S. Windisch, H. Nowotny, in *Preparative Methods in Solid State Chemistry*, P. Hagenmuller, ed., Academic Press, New York, 1972, pp. 553–562.

* Deceased.

8. A. K. Holliday, G. Hughes, S. M. Walker, in *Comprehensive Inorganic Chemistry*, Vol. 1, J. C. Bailar, H. J. Emeléus, R. Nyholm, A. F. Trotman-Dickenson, eds., Pergamon Press, Oxford, 1973, pp. 1203–1215.
9. R. Kieffer, F. Benesovski, in *Kirk-Othmer Encyclopedia of Chemical Technology*, Vol. 4, 3rd ed., Wiley, New York, 1978, pp. 476–505.

17.3.9.2.2. Preparative Methods.

The following techniques for preparation of carbides are in general use

(i) Direct Combination of Elements. For example, reactions of the type

$$Nb + C \longrightarrow NbC \tag{a}$$

are carried out in the range of 1200–2300°C; too high a temperature range may initiate decomposition. A finely ground mixture of the metal and C is melted or sintered; in some cases the starting materials are first compressed in the presence of organic binders or other liquids that are then removed by pumping at 200–400°C prior to the final sintering process. Where the melting point of the metal is sufficiently low, the reaction may be carried out in the liquid phase by keeping the final mixture above its melting point. Arc melting may unite the elements; however, such processes may lead to complications because of the high temperature gradients that result in nonuniformities of composition.

(ii) Reaction of Metal Hydrides with C. Conditions for reactions of the type e.g.:

$$2TiH + 2C \longrightarrow 2TiC + H_2 \tag{b}$$

are the same as discussed above. This method has the advantage of facilitating the final reaction step because the hydriding process tends to produce finely subdivided particles.

(iii) Reactions of Metal Oxides with C. Examples include

$$2C + MO \longrightarrow MC + CO \tag{c}$$

$$C + MO + M' \longrightarrow MC + M'O \tag{d}$$

as in $Nb_2O_5 + 7C \rightarrow 2NbC + 5CO$ in reaction (c). In reaction (d) M′ represents a metal that has a greater affinity for O than does M. The advantage of this procedure resides in the lower operational temperatures; the disadvantage is that it is difficult to obtain pure carbides by this route: at least some oxide contamination is encountered in the end product.

(iv) Reactions Involving CO or CO_2. Examples include

$$2CO + M \longrightarrow MC + CO_2 \tag{e}$$

$$CO + MO \longrightarrow MC + CO_2 \tag{f}$$

$$CO_2 + M \longrightarrow MC + O_2 \tag{g}$$

These pressures can be used only if the metal, M, has a greater affinity for C than for O. Again, it is difficult to avoid oxgen contamination.

(v) Use of Hydrocarbons. Such processes include

$$C_m H_n + H_2\,(/N_2) + M \longrightarrow MC + H_2\,(/N_2) + C_m, H_n, \tag{h}$$

Inorganic Reactions and Methods, Volume 18
Edited by J. J. Zuckerman, Jim D. Atwood

8. A. K. Holliday, G. Hughes, S. M. Walker, in *Comprehensive Inorganic Chemistry*, Vol. 1, J. C. Bailar, H. J. Emeléus, R. Nyholm, A. F. Trotman-Dickenson, eds., Pergamon Press, Oxford, 1973, pp. 1203–1215.
9. R. Kieffer, F. Benesovski, in *Kirk-Othmer Encyclopedia of Chemical Technology*, Vol. 4, 3rd ed., Wiley, New York, 1978, pp. 476–505.

17.3.9.2.2. Preparative Methods.

The following techniques for preparation of carbides are in general use

(i) Direct Combination of Elements. For example, reactions of the type

$$Nb + C \longrightarrow NbC \tag{a}$$

are carried out in the range of 1200–2300°C; too high a temperature range may initiate decomposition. A finely ground mixture of the metal and C is melted or sintered; in some cases the starting materials are first compressed in the presence of organic binders or other liquids that are then removed by pumping at 200–400°C prior to the final sintering process. Where the melting point of the metal is sufficiently low, the reaction may be carried out in the liquid phase by keeping the final mixture above its melting point. Arc melting may unite the elements; however, such processes may lead to complications because of the high temperature gradients that result in nonuniformities of composition.

(ii) Reaction of Metal Hydrides with C. Conditions for reactions of the type e.g.:

$$2TiH + 2C \longrightarrow 2TiC + H_2 \tag{b}$$

are the same as discussed above. This method has the advantage of facilitating the final reaction step because the hydriding process tends to produce finely subdivided particles.

(iii) Reactions of Metal Oxides with C. Examples include

$$2C + MO \longrightarrow MC + CO \tag{c}$$

$$C + MO + M' \longrightarrow MC + M'O \tag{d}$$

as in $Nb_2O_5 + 7C \rightarrow 2NbC + 5CO$ in reaction (c). In reaction (d) M′ represents a metal that has a greater affinity for O than does M. The advantage of this procedure resides in the lower operational temperatures; the disadvantage is that it is difficult to obtain pure carbides by this route: at least some oxide contamination is encountered in the end product.

(iv) Reactions Involving CO or CO_2. Examples include

$$2CO + M \longrightarrow MC + CO_2 \tag{e}$$

$$CO + MO \longrightarrow MC + CO_2 \tag{f}$$

$$CO_2 + M \longrightarrow MC + O_2 \tag{g}$$

These pressures can be used only if the metal, M, has a greater affinity for C than for O. Again, it is difficult to avoid oxgen contamination.

(v) Use of Hydrocarbons. Such processes include

$$C_m H_n + H_2\,(/N_2) + M \longrightarrow MC + H_2\,(/N_2) + C_m, H_n, \tag{h}$$

Occasionally, CO is also added to the gaseous mixture. For example, Nb heated in the presence of C, CH_4, CO, H_2 at 1300–1500°C produces NbC and by-products such as CO_2 and H_2.

(vi) Use of Hydrocarbons and Volatile Metal Halides MX_l. An example of the reduction represented by

$$C_mH_n + H_2 + MH_l \longrightarrow MC + C_{m'}H_{n'} + lHX \quad (i)$$

is the reaction $HfCl_4 + CH_4 \rightarrow HfC + 4HCl$. Because of the volatility of the components, a continuous flow process may be used, in which the reagents are passed over an incandescent tungsten filament at 2400–2800°C in the presence of H_2 gas. Another process is illustrated by the reaction of $TaCl_4$ and C_2H_2 to yield TaC and HCl, which requires the use of a heated surfaces such as graphite at 1300–1500°C. Formation of crystals is favored by operating at lower pressures.

(vii) Menstruum Techniques. These processes involve use of low-melting alloys, such as a 70% Fe–30 wt% Ni solution, acts as a bath that is nearly saturated with the desired metal and with graphite powder. The material is typically heated to 2000°C for 30 min in a static atmosphere of an inert gas and then gradually cooled. The reacted carbide is retrieved by dissolving the flux with hot HCl.

(viii) Special Techniques. Examples involve CaC_2 according to $CaC_2 + 2MO \rightarrow 2MC + CaO$, metal carbonyls such as $Mo(CO)_6$ in hydrogen to obtain Mo_2C and hydrocarbons (can be run at temperatures as low as 500°C), and organometallic compounds that are heated to produce the carbide and CO_2 and hydrocarbons.

(J. M. HONIG, H. R. HARRISON*)

17.3.9.2.3. Single Crystal Growth.

The methods for growth of single crystals of metallic carbides are like those for crystalline metallic nitrides; however, carbide crystals significantly larger than nitride crystals can be grown. The following techniques are in common use.

(i) Chemical Vapor Transport. This technique [see 17.3.9.1.3, (vii)] has been used to grow crystals of TiC and ZrC on a variety of substrates by different transport agents; however, the crystals produced are very small (~ 100 μm)[1–3].

(ii) Modified Hot Wire. A metal filament is heated in a gas mixture containing various hydrocarbons and H_2 or Ar. Crystals produced by this technique are small (~ 100 μm), but square-pyramidal ZrC up to 2 mm on an edge has been grown in propane at 2100°C[4], and square-pyramidal TiC with edge lengths up to 7 mm has been grown in propane at 1600–2000°C[5].

(iii) Flux (Menstruum Method). This technique, [see 17.3.10.2.2, is advantageous because the high temperatures required to melt the metallic carbides directly are circumvented by means of a flux that dissolves the carbide. For example, WC is melted in Co at 1600°C in an alumina crucible under Ar, then lowered to 1500°C at the rate of 1–3°C/min, then cooled to room temperature, at which point the Co flux is dissolved

* Deceased.

away in boiling HCl. Platelets as large as 5 mm on an edge have been grown[6]. Similarly, TaC and HfC crystals have been obtained from molten Fe[7]; ZrC, from molten NaCl[8]; and TiC (2 mm, maximum) and TaC (1 mm, maximum), from molten Al[9].

(iv) Modified (Flux) Czochralski. This method, similar to the above technique, grows larger and better quality WC crystals by lowering a seed crystal into a WC–Co solution, and then slowly withdrawing it in the classic Czochralski seed-pulling method. Crystals ~1 cm have been grown, with few Co inclusions[6, 10].

(v) Verneuil Technique. Single crystals of Mo_2C, TiC, ZrC, and NbC have been grown by means of this technique, in which powder is allowed to fall through a heating zone (in this case, an electric arc which replaces the classic oxygen–hydrogen flame) onto a single crystal pedestal. However, only millimeter-size crystals, which often develop cracks upon cooling, are produced[6,11].

(vi) Strain Anneal (Zone Annealing), Floating Zone, and Zone Leveling. These related methods all rely on the very high electrical conductivity of metallic carbides. A high intensity rf (typically 450 kHz) electromagnetic filed is applied: the high temperatures required to melt the material (or almost to melt it, in the case of strain anneal). are produced by induction heating. The crystals are grown under high He pressures [typically $1–3 \times 10^6$ N/m^2 (10–30 bar)] to suppress evaporation. Nonstoichiometric ZrC and VC have been obtained by a variation of the usual strain anneal process by heating an assembly consisting of a Zr or V rod in a tightly fitting graphite cylinder tightly plugged at the end by graphite. When heating above the melting point of Zr and V is applied, carbide begins to form, under considerable strain. Prolonged heating at higher temperatures results in grain growth by strain annealing of ZrC or VC, producing crystals sometimes as large as the initial metal rod[6]. In a variation of this technique, fully dense carbide rods are subjected to a critical axial compression strain at a high temperature (~2500°C for HfC); recrystallization then occurs at even higher annealing temperatures (~2900°C for HfC). Not only ZrC but also TaC, HfC, and Ta_2C (which could not be obtained by the method described above) are grown up to 6 mm dia × 25 mm long[6]. Crystals of VC_{1-x} and TiC_{1-x} up to 1 cm in diameter and 8 cm long are grown by a conventional floating zone technique[6,12]. This crucibleless technique involves passing a molten zone along a vertical rod (held only at the ends) previously prepared by hot pressing or sintering. A narrow zone is required to ensure that surface tension will be able to keep the molten zone in place.

This technique has been applied to VC[13], Mo_2C[14], and TiC[15], with increasing attention paid to the variations in stoichiometry of these carbides. The zone leveling technique has been utilized to avoid the normal variation in composition along the length of a crystal produced by the usual floating zone technique because a melt in equilibrium with a solid is not of the same composition. In this technique two starting rods of slightly different composition are butted against each other to compensate for this effect. Crystals of TiC_x[16], ZrC_x[17] and HfC_x of very uniform composition have been produced.

(J. M. HONIG, H. R. HARRISON*)

1. K. Naito, N. Kamegashia, N. Fuijiwara, *J. Cryst. Growth*, *45*, 506 (1978).
2. N. Tamrari, A. Kato, *J. Cryst. Growth*, *46*, 221 (1979).

* Deceased.

3. A. Kato, N. Tamari, *J. Cryst. Growth, 49*, 199 (1980).
4. K. Sugiyama, H. Mizuno, S. Motojima, Y. Takahashi, *J. Cryst. Growth, 44*, 617 (1978).
5. K. Sugiya, H. Mizuno, S. Motojima, Y. Takahashi, *J. Cryst. Growth, 46*, 788 (1979).
6. L. E. Toth, *Transition Metal Carbides and Nitrides*, Academic Press, New York, 1971.
7. D. J. Rowcliffe, G. E. Hollox, *J. Mater. Sci., 6*, 1261 (1971).
8. Yu.G. Zainurin, *Dokl. Akad. Nauk SSSR, 207*, 105 (1972).
9. I. Higashi, Y. Takahashi, T. Atoda, *J. Cryst. Growth, 33*, 207 (1976).
10. A. P. Gerk, J. J. Gilman, *J. Appl. Phys., 39*, 4497 (1968).
11. A. D. Kiffer, WADD TR6-0-52, Defense Document Center No. AD–238–061 (1960).
12. W. Precht, G. E. Hollox, *J. Cryst. Growth, 3/4*, 818 (1968).
13. J. Billingham, P. S. Bell, M. H. Lewis, *J. Cryst. Growth, 13/14*, 693 (1972).
14. A. N. Christensen, *J. Cryst. Growth, 33*, 58 (1976).
15. A. N. Christensen, *J. Cryst. Growth, 33*, 99 (1976).
16. F. Yajima, T. Tanaka, E. Bannai, S. Kawai, *J. Cryst. Growth, 47*, 493 (1979).
17. S. Otani, T. Tanaka, A. Hara, *J. Cryst. Growth, 51*, 164 (1981)
18. S. Otani, T. Tanaka, A. Hara, *J. Cryst. Growth, 51*, 381 (1981).

17.3.9.3. Metallic Nitrides

17.3.9.3.1. General Comments.

Nitrides are grouped into four distinct categories:

1. Salt-like or ionic nitrides, in which N forms primarily ionic bonds to alkali metals, rare earth metals, and members of group IIIA. Although actinide nitrides are also included in this grouping, they may equally well be classified as metallic. Compounds in this group are readily hydrolyzed and must thus be protected from moisture.
2. Metallic nitrides, sometimes termed interstitial compounds, are formed from combinations of N with transition metals of groups IVA, VA, and VIA. As the name implies, they exhibit electrical conductivity and most of the general characteristics associated with standard metals. They are also refractory and hard, and usually depart from the ideal stoichiometry ratios displayed above (see 17.3.9, Table 1). They readily form solid solutions with carbides and oxides, which gives rise to problems when it is necessary to obtain nitrides in pure form. Included in this category are numerous ternary nitrides of a transition metal with a group B metal.
3. Diamond-like nitrides in which N bonds covalently to elements of groups IIIB and IVB; they are chemically stable, refractory, and nonconducting.
4. Gaseous nitrides, in which N links to members of group VIB or VIIB, many of which either are gaseous of form volatile liquids or solids at room temperature. Compounds in this group tend to be unstable or explosive.

A listing of metallic nitrides, together with the most commonly encountered stoichiometries provided above (see 17.3.9, Table 1), this tabulation is incomplete because of contradictory claims. For example, GaN has been considered to be nonmetallic; however, in more recent work it is claimed that the material is a good conductor. Methods of preparation and properties of metallic nitrides have been reviewed[1–13].

(J. M. HONIG, H. R. HARRISON*)

1. B. R. Brown, in *Mellor's Comprehensive Treatise on Inorganic and Theoretical Chemistry*, Vol. VIII, Suppl. I, Wiley, New York, 1964, pp. 150–239.

* Deceased.

Inorganic Reactions and Methods, Volume 18
Edited by J. J. Zuckerman, Jim D. Atwood

3. A. Kato, N. Tamari, *J. Cryst. Growth, 49*, 199 (1980).
4. K. Sugiyama, H. Mizuno, S. Motojima, Y. Takahashi, *J. Cryst. Growth, 44*, 617 (1978).
5. K. Sugiya, H. Mizuno, S. Motojima, Y. Takahashi, *J. Cryst. Growth, 46*, 788 (1979).
6. L. E. Toth, *Transition Metal Carbides and Nitrides*, Academic Press, New York, 1971.
7. D. J. Rowcliffe, G. E. Hollox, *J. Mater. Sci., 6*, 1261 (1971).
8. Yu.G. Zainurin, *Dokl. Akad. Nauk SSSR, 207*, 105 (1972).
9. I. Higashi, Y. Takahashi, T. Atoda, *J. Cryst. Growth, 33*, 207 (1976).
10. A. P. Gerk, J. J. Gilman, *J. Appl. Phys., 39*, 4497 (1968).
11. A. D. Kiffer, WADD TR6-0-52, Defense Document Center No. AD–238–061 (1960).
12. W. Precht, G. E. Hollox, *J. Cryst. Growth, 3/4*, 818 (1968).
13. J. Billingham, P. S. Bell, M. H. Lewis, *J. Cryst. Growth, 13/14*, 693 (1972).
14. A. N. Christensen, *J. Cryst. Growth, 33*, 58 (1976).
15. A. N. Christensen, *J. Cryst. Growth, 33*, 99 (1976).
16. F. Yajima, T. Tanaka, E. Bannai, S. Kawai, *J. Cryst. Growth, 47*, 493 (1979).
17. S. Otani, T. Tanaka, A. Hara, *J. Cryst. Growth, 51*, 164 (1981)
18. S. Otani, T. Tanaka, A. Hara, *J. Cryst. Growth, 51*, 381 (1981).

17.3.9.3. Metallic Nitrides

17.3.9.3.1. General Comments.

Nitrides are grouped into four distinct categories:

1. Salt-like or ionic nitrides, in which N forms primarily ionic bonds to alkali metals, rare earth metals, and members of group IIIA. Although actinide nitrides are also included in this grouping, they may equally well be classified as metallic. Compounds in this group are readily hydrolyzed and must thus be protected from moisture.
2. Metallic nitrides, sometimes termed interstitial compounds, are formed from combinations of N with transition metals of groups IVA, VA, and VIA. As the name implies, they exhibit electrical conductivity and most of the general characteristics associated with standard metals. They are also refractory and hard, and usually depart from the ideal stoichiometry ratios displayed above (see 17.3.9, Table 1). They readily form solid solutions with carbides and oxides, which gives rise to problems when it is necessary to obtain nitrides in pure form. Included in this category are numerous ternary nitrides of a transition metal with a group B metal.
3. Diamond-like nitrides in which N bonds covalently to elements of groups IIIB and IVB; they are chemically stable, refractory, and nonconducting.
4. Gaseous nitrides, in which N links to members of group VIB or VIIB, many of which either are gaseous of form volatile liquids or solids at room temperature. Compounds in this group tend to be unstable or explosive.

A listing of metallic nitrides, together with the most commonly encountered stoichiometries provided above (see 17.3.9, Table 1), this tabulation is incomplete because of contradictory claims. For example, GaN has been considered to be nonmetallic; however, in more recent work it is claimed that the material is a good conductor. Methods of preparation and properties of metallic nitrides have been reviewed[1–13].

(J. M. HONIG, H. R. HARRISON*)

1. B. R. Brown, in *Mellor's Comprehensive Treatise on Inorganic and Theoretical Chemistry*, Vol. VIII, Suppl. I, Wiley, New York, 1964, pp. 150–239.

* Deceased.

2. H. Schäfer, *Chemical Transport Reactions*, Academic Press, New York, 1964.
3. R. Juza, in *Advances in Inorganic and Radiochemistry*, Vol. 9, H. J. Emeléus, A. G. Sharpe, eds., Academic Press, New York, 1966, pp. 81–131.
4. F. Benesovsky, R. Kieffer, in *Kirk-Othmer Encyclopedia of Chemical Technology*, Vol. 13, 2nd ed., Wiley, New York, 1967, pp. 814–825.
5. H. J. Goldschmidt, *Interstitial Alloys*, Plenum Press, New York, 1967, Chapter 5.
6. R. Nitsche, *Fortschr. Miner.*, *44*, 231 (1967).
7. D. R. Glasson, S. A. A. Jayaweera, *J. Appl. Chem.*, *18*, 65, 77 (1968).
8. K. E. Spear, *J. Chem. Educ.*, *49*, 81 (1972).
9. E. K. Storms, in *MTP International Review of Science, Solid State Chemistry, Inorganic Chemistry*, Series One, Vol. 10, H. J. Emeléus, L. E. J. Roberts, eds.), Butterworths, London, 1972, pp. 37–78.
10. K. Jones, in *Comprehensive Inorganic Chemistry*, Vol. 4, J. C. Bailar, H. J. Emeléus, R. Nyholm, A. F. Trotman-Dickenson, eds., Pergamon Press, Oxford, 1973, pp. 228–239.
11. W. Jeitschko, in *MTP International Review of Science, Transition Metals Part I, Inorganic Chemistry*, Series Two, Vol. 5, H. J. Emeléus, D. W. A. Sharp, eds., Butterworths, London, 1974, pp. 220–281.
12. H. A. Johansen, in *Survey of Progress in Chemistry*, Vol. 8, A. F. Scott, ed, Academic Press, New York, 1977, pp. 57–81.
13. J. Lang, Y. Laurent, M. Maunaye, R. Marchant, *Prog. Cryst. Growth Charact.*, *2*, 207 (1979).

17.3.9.3.2. Preparative Techniques.

Metallic nitrides have been prepared by the following methods.

(i) Combination of Elements. Representative examples include

$$Cr + \tfrac{1}{2} N_2 \longrightarrow CrN, \quad Ti + \tfrac{1}{2} N_2 \longrightarrow TiN \tag{a}$$

Generally, N_2 is introduced at $1 \times 10^5 N/m^2$ (1 bar) temperatures in the range of 400–1600°C have been employed, although most reactions are carried out between 800 and 1400°C. The reaction is aided by use of finely divided powder (frequently prepared by prereacting the metal in H_2) and by increasing the overpressure of N_2.

(ii) Reaction of NH_3 with Elements of Their Nitrides. Examples include

$$2V + 2NH_3 \longrightarrow 2VN + 3H_2 \tag{b}$$

The method lends itself to control of the partial pressure of N_2 gas through utilization of NH_3/H_2 buffering gas mixtures[1]. The equilibration reaction proceeds via $2NH_3 \rightarrow N_2 + 3H_2$. Adjustment of the N_2 partial pressure controls the stoichiometric composition of the sample. This procedure is particularly useful in the formation of lower nitrides such as Fe_4N, Fe_2N, Co_3N, Co_2N, Co_3N_2, Ni_3N, and Ni_3N_2. Many such phases exhibit wide regions of stability as manifested in considerable deviations from ideal stoichiometry. Reactions are usually carried out in the low temperature range of 400–600°C.

(iii) Reaction of Metal Oxide and NH_3/H_2 Mixtures. Examples include

$$2TiO_2 + 2NH_3 + H_2 \longrightarrow 2TiN + 4H_2O \tag{c}$$

This reaction is carried out in the range of 500–900°C, depending on the chemical affinity of the reagents. One difficulty is the incomplete removal of oxygen; oxynitrides are

Inorganic Reactions and Methods, Volume 18
Edited by J. J. Zuckerman, Jim D. Atwood

2. H. Schäfer, *Chemical Transport Reactions*, Academic Press, New York, 1964.
3. R. Juza, in *Advances in Inorganic and Radiochemistry*, Vol. 9, H. J. Emeléus, A. G. Sharpe, eds., Academic Press, New York, 1966, pp. 81–131.
4. F. Benesovsky, R. Kieffer, in *Kirk-Othmer Encyclopedia of Chemical Technology*, Vol. 13, 2nd ed., Wiley, New York, 1967, pp. 814–825.
5. H. J. Goldschmidt, *Interstitial Alloys*, Plenum Press, New York, 1967, Chapter 5.
6. R. Nitsche, *Fortschr. Miner.*, *44*, 231 (1967).
7. D. R. Glasson, S. A. A. Jayaweera, *J. Appl. Chem.*, *18*, 65, 77 (1968).
8. K. E. Spear, *J. Chem. Educ.*, *49*, 81 (1972).
9. E. K. Storms, in *MTP International Review of Science, Solid State Chemistry, Inorganic Chemistry*, Series One, Vol. 10, H. J. Emeléus, L. E. J. Roberts, eds.), Butterworths, London, 1972, pp. 37–78.
10. K. Jones, in *Comprehensive Inorganic Chemistry*, Vol. 4, J. C. Bailar, H. J. Emeléus, R. Nyholm, A. F. Trotman-Dickenson, eds., Pergamon Press, Oxford, 1973, pp. 228–239.
11. W. Jeitschko, in *MTP International Review of Science, Transition Metals Part I, Inorganic Chemistry*, Series Two, Vol. 5, H. J. Emeléus, D. W. A. Sharp, eds., Butterworths, London, 1974, pp. 220–281.
12. H. A. Johansen, in *Survey of Progress in Chemistry*, Vol. 8, A. F. Scott, ed, Academic Press, New York, 1977, pp. 57–81.
13. J. Lang, Y. Laurent, M. Maunaye, R. Marchant, *Prog. Cryst. Growth Charact.*, *2*, 207 (1979).

17.3.9.3.2. Preparative Techniques.

Metallic nitrides have been prepared by the following methods.

(i) Combination of Elements. Representative examples include

$$Cr + \tfrac{1}{2} N_2 \longrightarrow CrN, \quad Ti + \tfrac{1}{2} N_2 \longrightarrow TiN \tag{a}$$

Generally, N_2 is introduced at $1 \times 10^5 N/m^2$ (1 bar) temperatures in the range of 400–1600°C have been employed, although most reactions are carried out between 800 and 1400°C. The reaction is aided by use of finely divided powder (frequently prepared by prereacting the metal in H_2) and by increasing the overpressure of N_2.

(ii) Reaction of NH_3 with Elements of Their Nitrides. Examples include

$$2V + 2NH_3 \longrightarrow 2VN + 3H_2 \tag{b}$$

The method lends itself to control of the partial pressure of N_2 gas through utilization of NH_3/H_2 buffering gas mixtures[1]. The equilibration reaction proceeds via $2NH_3 \rightarrow N_2 + 3H_2$. Adjustment of the N_2 partial pressure controls the stoichiometric composition of the sample. This procedure is particularly useful in the formation of lower nitrides such as Fe_4N, Fe_2N, Co_3N, Co_2N, Co_3N_2, Ni_3N, and Ni_3N_2. Many such phases exhibit wide regions of stability as manifested in considerable deviations from ideal stoichiometry. Reactions are usually carried out in the low temperature range of 400–600°C.

(iii) Reaction of Metal Oxide and NH_3/H_2 Mixtures. Examples include

$$2TiO_2 + 2NH_3 + H_2 \longrightarrow 2TiN + 4H_2O \tag{c}$$

This reaction is carried out in the range of 500–900°C, depending on the chemical affinity of the reagents. One difficulty is the incomplete removal of oxygen; oxynitrides are

obtained as the end product, the O/N and metal/N ratios being determined by reaction conditions. Nitriding by ammonia may be carried out at lower temperatures.

(iv) Reaction of Metal Oxides with N_2 and C or Carbides. Examples include

$$2TiO_2 + 4C + N_2 \longrightarrow 2TiN + 4\,CO \quad (d)$$

$$2TiO_2 + 4TiC + 3N_2 \longrightarrow 6TiN + 4CO \quad (e)$$

$$UO_2 + 2C + \tfrac{1}{2}\,N_2 \longrightarrow UN + 2CO \quad (f)$$

Reactions (d)–(f) represent idealized cases: this type of reaction is incomplete and produces nitrides containing appreciable amounts of C and O; the reaction is driven toward completion at high N_2 overpressures. These processess can be carried out on a commerical scale because of the ready availability of many metal oxides, as long as high purity is not an important criterion. Reaction temperatures are in the range of 1200–1400°C.

(v) Reaction of Volatile Halides with NH_3/N_2 or N_2/H_2 Mixtures. Examples include

$$2TiCl_4 + 10NH_3 + H_2 \longrightarrow 2TiN + 8NH_4Cl \quad (g)$$

$$2TiCl_4 + 5N_2 + 16H_2 \longrightarrow 2TiN + 8NH_4Cl \quad (h)$$

$$2ZrCl_4 + N_2 + 4H_2 \longrightarrow 2ZrN + 8\,HCl \quad (i)$$

This procedure can be used for continuous flow: the gas mixture is brought into contact with a hot tungsten filament; the halide is decomposed, and the resulting nitride deposited on the wire. Reaction temperatures in the range of 1500–2000°C are achieved by an incandescent filament over which the reaction mixture is being introduced. Only thermally stable nitrides can be prepared in this manner. Alternatively, the halide can be reached in N_2/H_2 on a hot surface or in a hot plasma generated electrically. The final compositions are dictated by the partial N_2 pressures.

(vi) Generation of Lower Nitrides. A metal is added to the nitride in appropriate amounts to form the desired compound, e.g.:

$$VN + V \longrightarrow V_2N \quad (j)$$

$$TaN + Ta \longrightarrow Ta_2N \quad (k)$$

The reaction may be achieved by heating in vacuo.

(vii) Special Processes. In some instances the following special techniques are available:

1. Decompositon of metal amides or imides; usually, this procedure is employed for synthesis of nonmetallic nitrides.
2. Reaction of organometallic compounds with NH_3; again, this procedure is used primarily for generation of nonmetallic nitrides.
3. Formation of UN or of ThN via higher nitrides. Here $3Th + 2N_2 \rightarrow 2Th_3N_4$ or $2U + (3 + x)\,N_2 \rightarrow 2U_2N_{3+x}$ are the relevant reactions at 400–700°C that lead to intermediates, which are then heated at 1100–1500°C in vacuo to produce the mononitride.

4. For VN, a special route involves heating NH_4VO_3 in NH_3 at 1100°C.
5. For iron–nitrogen compounds, rf sputtering in N_2 (with or without H_2) can be used, in particular to produce single phase Fe_3N[2].

(J. M. HONIG, H. R. HARRISON*)

1. R. Arnott, A. Wold, *J. Phys. Chem. Solids, 15* 152 (1960).
2. C. Lo, V. Krishnaswamy, K. R. P. M. Rao, R. Messier, L. N. Mulay, *Mater. Res. Bull., 15*, 1267 (1980).

17.3.9.3.3. Growth of Single Crystals.

Little work has been done on the growth of single crystals of nitrides in general, and metallic nitrides in particularly[1-3]. The usual methods for growing single crystals, which have yielded impressive results for oxides or carbides, are not as successful for nitrides because of different problems associated with nitride chemistry and because efforts in this area have been concentrated on only a few compounds. The largest crystals grown do not exceed 25 mm, and most are only a millimeter in size[1].

(i) Zone Annealing and Zone Melting. The most successful techniques for growth of metallic nitrides are the same as for metallic carbides: namely zone annealing and zone melting (floating zone) [see, 17.3.9.2.3, (vi)][4-10] However, nitride crystals so grown are usually significantly smaller than the corresponding carbide crystals. Zone melting often cannot be used because of cracking, dissociation, evaporation of materials, and great variation in sample stoichiometry. In such cases, zone annealing may succeed. In each case, isostatically pressed powder is first heated in a N_2 atmosphere to promote nitride formation. Crystals of the following compounds have been grown, under high N_2 pressure [from $1–2 \times 10^6$ N/m^2 (10–20 bar)], at temperatures between 1750 and 2500°C (produced by rf induction heating): TiN and ZrN[4,5], δ-VN[6], δ-NbN[7,11], γ-NbN[5,8,9], and Ta_2N[10].

(ii) Chemical Vapor Transport. This technique [see 17.3.9.1.3, (viii)] has been utilized to produce small (~ 10 μm) crystals of NbN using mixtures of $NbCl_5$, Ar, H_2, C_3H_8, and N_2[12,13]; TiN has been grown by HCl transport[14].

(iii) Modified Hot Wire. This technique, mentioned in 17.3.9.2.3, (ii), has been utilized to produce crystals of TiN several millimeters in size from a mixture of $TiCl_4$, N_2, and H_2 reacted at the tip of a Mo wire twisted around a W filament[15,16]. This method is also useful for growing single crystals of ZrN[17,18].

(J. M. HONIG, H. R. HARRISON*)

1. J. Lang, Y. Laurent, M. Maunye, R. Marchend, *Prog. Cryst. Growth Charact., 2*, 207 (1979).
2. L. E. Toth, *Transition Metal Carbides and Nitrides*, Academic Press, New York, 1971.
3. H. A. Johansen, in *Survey of Progress in Chemistry*, Vol. 8, A. F. Scott, ed., Academic Press, New York, 1977, pp. 57–81.
4. A. N. Christensen, *J. Cryst. Growth, 33*, 99 (1976).
5. A. N. Christensen, S. Fregerslev, *Acta Chem. Scand., A31*, 861 (1977).
6. A. N. Christensen, P. P. Roehammer, *J. Cryst. Growth, 38*, 281 (1977).
7. A. N. Christensen, *Acta Chem. Scand., A31*, 77 (1977).
8. A. N. Christensen, *Acta Chem. Scand., A30*, 219 (1976).

* Deceased.

Inorganic Reactions and Methods, Volume 18
Edited by J. J. Zuckerman, Jim D. Atwood

4. For VN, a special route involves heating NH_4VO_3 in NH_3 at 1100°C.
5. For iron–nitrogen compounds, rf sputtering in N_2 (with or without H_2) can be used, in particular to produce single phase Fe_3N[2].

(J. M. HONIG, H. R. HARRISON*)

1. R. Arnott, A. Wold, *J. Phys. Chem. Solids, 15* 152 (1960).
2. C. Lo, V. Krishnaswamy, K. R. P. M. Rao, R. Messier, L. N. Mulay, *Mater. Res. Bull., 15*, 1267 (1980).

17.3.9.3.3. Growth of Single Crystals.

Little work has been done on the growth of single crystals of nitrides in general, and metallic nitrides in particularly[1–3]. The usual methods for growing single crystals, which have yielded impressive results for oxides or carbides, are not as successful for nitrides because of different problems associated with nitride chemistry and because efforts in this area have been concentrated on only a few compounds. The largest crystals grown do not exceed 25 mm, and most are only a millimeter in size[1].

(i) Zone Annealing and Zone Melting. The most successful techniques for growth of metallic nitrides are the same as for metallic carbides: namely zone annealing and zone melting (floating zone) [see, 17.3.9.2.3, (vi)][4–10] However, nitride crystals so grown are usually significantly smaller than the corresponding carbide crystals. Zone melting often cannot be used because of cracking, dissociation, evaporation of materials, and great variation in sample stoichiometry. In such cases, zone annealing may succeed. In each case, isostatically pressed powder is first heated in a N_2 atmosphere to promote nitride formation. Crystals of the following compounds have been grown, under high N_2 pressure [from $1–2 \times 10^6$ N/m^2 (10–20 bar)], at temperatures between 1750 and 2500°C (produced by rf induction heating): TiN and ZrN[4,5], δ-VN[6], δ-NbN[7,11], γ-NbN[5,8,9], and Ta_2N[10].

(ii) Chemical Vapor Transport. This technique [see 17.3.9.1.3, (viii)] has been utilized to produce small ($\sim$10 μm) crystals of NbN using mixtures of $NbCl_5$, Ar, H_2, C_3H_8, and N_2[12,13]; TiN has been grown by HCl transport[14].

(iii) Modified Hot Wire. This technique, mentioned in 17.3.9.2.3, (ii), has been utilized to produce crystals of TiN several millimeters in size from a mixture of $TiCl_4$, N_2, and H_2 reacted at the tip of a Mo wire twisted around a W filament[15,16]. This method is also useful for growing single crystals of ZrN[17,18].

(J. M. HONIG, H. R. HARRISON*)

1. J. Lang, Y. Laurent, M. Maunye, R. Marchend, *Prog. Cryst. Growth Charact., 2*, 207 (1979).
2. L. E. Toth, *Transition Metal Carbides and Nitrides*, Academic Press, New York, 1971.
3. H. A. Johansen, in *Survey of Progress in Chemistry*, Vol. 8, A. F. Scott, ed., Academic Press, New York, 1977, pp. 57–81.
4. A. N. Christensen, *J. Cryst. Growth, 33*, 99 (1976).
5. A. N. Christensen, S. Fregerslev, *Acta Chem. Scand., A31*, 861 (1977).
6. A. N. Christensen, P. P. Roehammer, *J. Cryst. Growth, 38*, 281 (1977).
7. A. N. Christensen, *Acta Chem. Scand., A31*, 77 (1977).
8. A. N. Christensen, *Acta Chem. Scand., A30*, 219 (1976).

* Deceased.

9. A. N. Christensen, C. Rische, *J. Cryst. Growth, 44*, 383 (1978).
10. L. E. Conroy, A. N. Christensen, *J. Solid State Chem. 20*, 205 (1977).
11. B. Scheerer, *J. Cryst. Growth, 49*, 61 (1980).
12. T. Takahashi, K. Sugiyama, Y. Suzuki, *J. Soc. Chem. Ind. Jpn., 74*, 2029 (1971).
13. T. Takahashi, H. Itoh, T. Yamaguchi, *J. Cryst. Growth, 46*, 69 (1979).
14. H. Schäfer, W. Fuhr, *Z. Anorg. Allg. Chem., 319*, 52 (1962).
15. S. Motojima, K. Baba, K. Kitatani, Y. Takahashi, K. Sugiyama, *J. Cryst. Growth, 32*, 141 (1976).
16. A. N. Pilyankevich, V. S. Sinelnikova, L. V. Strashinskaya, T. I. Shaposhinikova, S. Ya. Golub, *Poroshkv Metall., 35*, (1977).
17. K. Sugiyama, K. Watanabe, S. Motojima, Y. Takahashi, *Bull. Chem. Soc. Jpn., 52*, 420 (1970).
18. M. Miyochi, N. Tamari, A. Kato, *Nippon Kagaku Kaichi, 822* (1978).

17.3.10. Preparation of Superconductive Ceramics

Superconductivity is a phenomenon characterized by sudden and complete disappearance of electrical resistance in a substance when it is cooled below a certain tempe$rature, called the critical transition temperature, T_c. Superconductivity was discovered[1] in 1911 by measuring the resistance of solid mercury (Hg) on cooling with a sharp discontinuity in resistance at about 4.2 K (see Fig. 1). In addition to the total loss

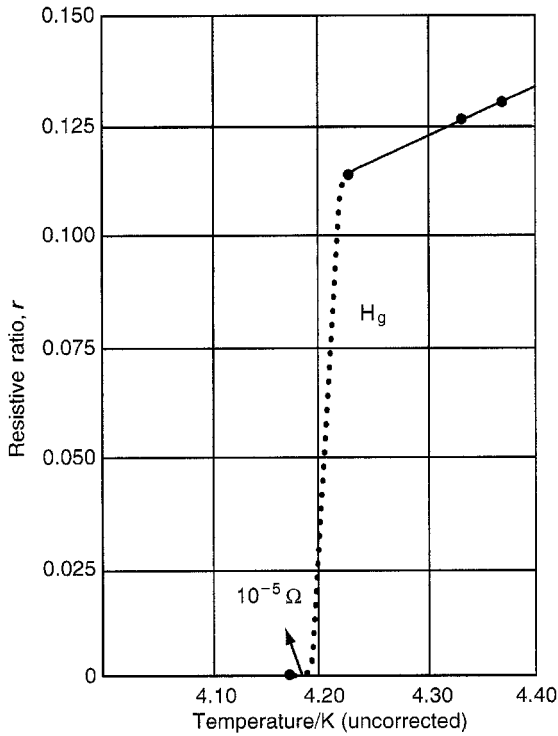

Figure 1. The resistive ratio of solid mercury vs. absolute temperature (uncorrected scale) as actually reported in 1911[1]. This observation marked the discovery of superconductivity.

Inorganic Reactions and Methods, Volume 18
Edited by J. J. Zuckerman, Jim D. Atwood

9. A. N. Christensen, C. Rische, *J. Cryst. Growth, 44*, 383 (1978).
10. L. E. Conroy, A. N. Christensen, *J. Solid State Chem. 20*, 205 (1977).
11. B. Scheerer, *J. Cryst. Growth, 49*, 61 (1980).
12. T. Takahashi, K. Sugiyama, Y. Suzuki, *J. Soc. Chem. Ind. Jpn., 74*, 2029 (1971).
13. T. Takahashi, H. Itoh, T. Yamaguchi, *J. Cryst. Growth, 46*, 69 (1979).
14. H. Schäfer, W. Fuhr, *Z. Anorg. Allg. Chem., 319*, 52 (1962).
15. S. Motojima, K. Baba, K. Kitatani, Y. Takahashi, K. Sugiyama, *J. Cryst. Growth, 32*, 141 (1976).
16. A. N. Pilyankevich, V. S. Sinelnikova, L. V. Strashinskaya, T. I. Shaposhinikova, S. Ya. Golub, *Poroshkv Metall., 35*, (1977).
17. K. Sugiyama, K. Watanabe, S. Motojima, Y. Takahashi, *Bull. Chem. Soc. Jpn., 52*, 420 (1970).
18. M. Miyochi, N. Tamari, A. Kato, *Nippon Kagaku Kaichi, 822* (1978).

17.3.10. Preparation of Superconductive Ceramics

Superconductivity is a phenomenon characterized by sudden and complete disappearance of electrical resistance in a substance when it is cooled below a certain tempe$rature, called the critical transition temperature, T_c. Superconductivity was discovered[1] in 1911 by measuring the resistance of solid mercury (Hg) on cooling with a sharp discontinuity in resistance at about 4.2 K (see Fig. 1). In addition to the total loss

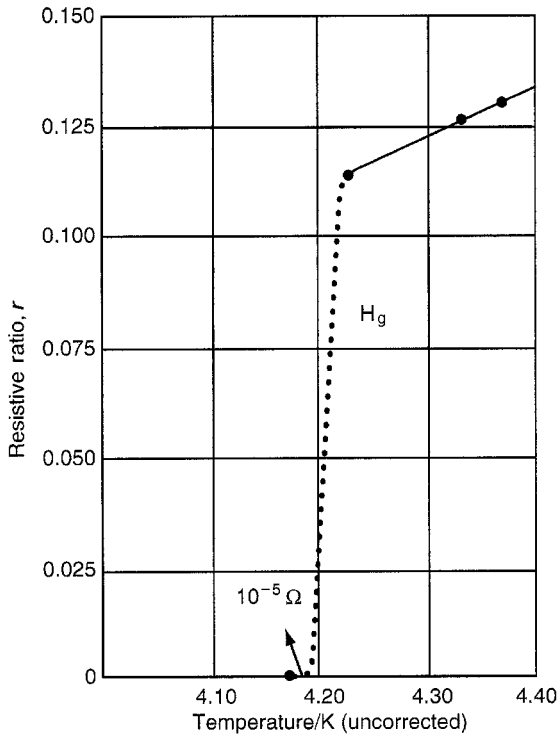

Figure 1. The resistive ratio of solid mercury vs. absolute temperature (uncorrected scale) as actually reported in 1911[1]. This observation marked the discovery of superconductivity.

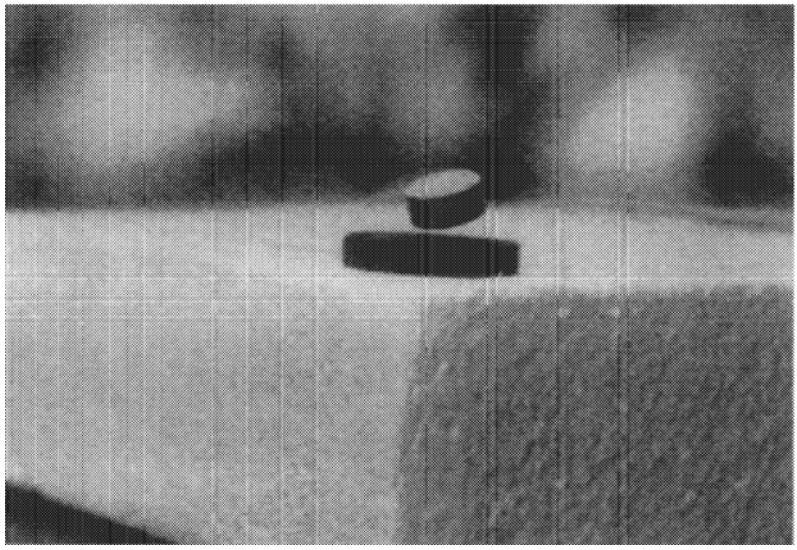

Figure 2. The Meissner effect, or the levitation of a strong magnet by the internal diamagnetic field of a high T_c superconductor.

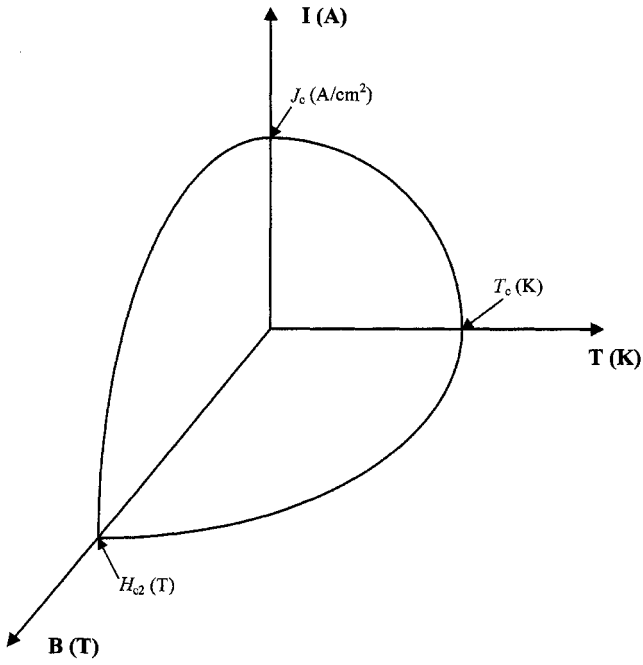

Figure 3. Relationship among T_c, J_c, and H_{c2}.

of electrical resistance, there occurs another unusual magnetic behavior: the expulsion of magnetic field from the interior of the material below T_c results in formation of a perfect diamagnetic material. This perfect diamagnetic behavior is called the *Meissner effect*, after the physicist who first observed it in superconductors[2]. The *Meissner effect* generates the levitation forces (see Fig. 2), which can be used to levitate trains for mass transportation, fly wheels for energy storage, and bearings for energy saving.

The most distinguishing features of superconductive materials are the sudden and complete disappearance of electrical resistance below T_c; the high critical current density (J_c), which allows superconductors to conduct with no power loss; and the high critical magnetic fields (H_{c2}) in which superconductivity can exist. The relationship among these features is shown in Figure 3.

Following the discovery of superconductivity in Hg in 1911, physicists, chemists, material scientists, metallurgists, electrical engineers, and others have found superconductivity in thousands of materials with T_c values from a few millikelvin to 164 K [current record T_c, obtained in $HgBa_2Ca_2Cu_3O_9$ (Hg-1223) under high pressure; see 17.3.10.2.5]. These materials include elements, alloys, carbides, nitrides, borides, sulfides, organics, and oxides.

Since 1911, superconductivity research has gone through two stages: slow and steady progress (prior 1986) and explosive progress (after 1986). Accordingly, the superconductors are simply classified into *low temperature superconductors* ($T_c < 30$ K), which

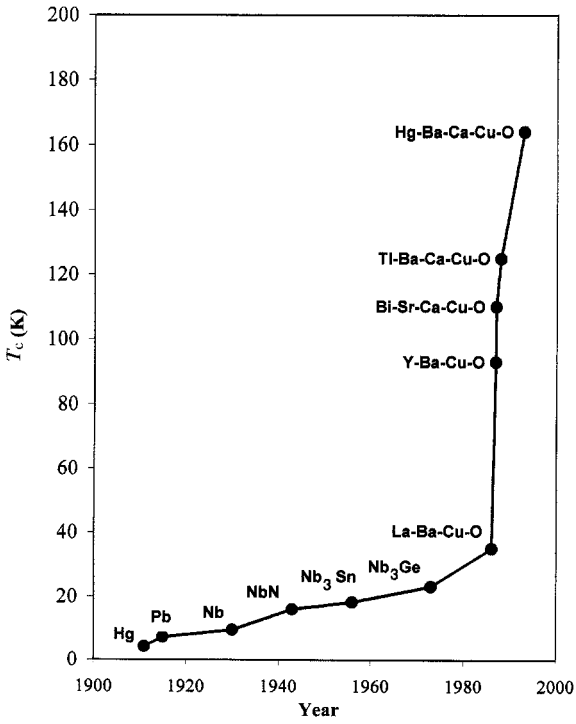

Figure 4. The increase in T_c as a function of year.

include all the elements, alloys, carbides, nitrides, borides, sulfides, organics, and part of the oxides, and *high temperature superconductors* ($T_c > 30$ K) exclusively for copper oxides discovered after 1986. A chronological progress of T_c is shown in Figure 4.

Owing to the large volume of information on low temperature superconductivity already available in the books and excellent reviews, and the high cost of refrigeration required for using the low temperature superconductors, we describe briefly the preparation of a few low temperature superconductors and then focus on the preparation of high temperature superconducting copper oxides.

(Z. REN, J. WANG)

1. H. K. Onnes, A. van Wetenschappen, *Proc. Sect. Sci. (Amsterdam)*, *14*, 113, 818 (1911).
2. W. Meissner, R. Ochsenfeld, *Naturwissenschaften*, *21*, 787 (1933).

17.3.10.1. Low Temperature Superconductors

Following the discovery of superconductivity in Hg in 1911, extensive research had been conducted to locate other superconducting elements in the periodical table. Twenty-six metallic elements have been found to be superconducting at ambient pressure, and four additional under high pressure conditions. Some of the nonmetallic elements such as silicon and sulfur were also found to be superconducting at about 7 and 6 K under pressures of 130 and 200 bar, respectively. All the ferromagnetic metallic elements (Fe, Co, Ni, etc.) and the best metallic conducting elements (e.g., Cu, Ag, Pt, Au) were found not to be superconducting to the lowest temperatures measured[1]. Table 1 lists T_c values

TABLE 1. SUPERCONDUCTING TRANSITION TEMPERATURES (T_c) OF SELECTED ELEMENTS

Element:	T_c	Nb	Pb	Ta	Hg	Sn	In	Tl	Al	Ga	Ti
T_c (K):	11.2	9.46	7.18	4.48	4.15	3.72	3.41	1.37	1.19	1.09	0.4

Source: Ref. 1.

TABLE 2. SELECTED SUPERCONDUCTING ALLOYS AND CERAMICS WITH THEIR T_c VALUES

Compound	T_c (K)
Nb_3Ge	23.2
Nb_3Ga	20.7
Nb_3Al	18.8
Nb_3Sn	18.3
Nb_3Si	18.0
V_3Si	17.1
V_3Ga	15.9
NbN	16.0
MoC	14.3
NbB	8.25
$PbMo_6S_8$	15.0
$Ba(Pb_{1-x}Bi_x)O_3$	13.2

Inorganic Reactions and Methods, Volume 18
Edited by J. J. Zuckerman, Jim D. Atwood

include all the elements, alloys, carbides, nitrides, borides, sulfides, organics, and part of the oxides, and *high temperature superconductors* ($T_c > 30$ K) exclusively for copper oxides discovered after 1986. A chronological progress of T_c is shown in Figure 4.

Owing to the large volume of information on low temperature superconductivity already available in the books and excellent reviews, and the high cost of refrigeration required for using the low temperature superconductors, we describe briefly the preparation of a few low temperature superconductors and then focus on the preparation of high temperature superconducting copper oxides.

(Z. REN, J. WANG)

1. H. K. Onnes, A. van Wetenschappen, *Proc. Sect. Sci. (Amsterdam), 14*, 113, 818 (1911).
2. W. Meissner, R. Ochsenfeld, *Naturwissenschaften, 21*, 787 (1933).

17.3.10.1. Low Temperature Superconductors

Following the discovery of superconductivity in Hg in 1911, extensive research had been conducted to locate other superconducting elements in the periodical table. Twenty-six metallic elements have been found to be superconducting at ambient pressure, and four additional under high pressure conditions. Some of the nonmetallic elements such as silicon and sulfur were also found to be superconducting at about 7 and 6 K under pressures of 130 and 200 bar, respectively. All the ferromagnetic metallic elements (Fe, Co, Ni, etc.) and the best metallic conducting elements (e.g., Cu, Ag, Pt, Au) were found not to be superconducting to the lowest temperatures measured[1]. Table 1 lists T_c values

TABLE 1. SUPERCONDUCTING TRANSITION TEMPERATURES (T_c) OF SELECTED ELEMENTS

Element:	T_c	Nb	Pb	Ta	Hg	Sn	In	Tl	Al	Ga	Ti
T_c (K):	11.2	9.46	7.18	4.48	4.15	3.72	3.41	1.37	1.19	1.09	0.4

Source: Ref. 1.

TABLE 2. SELECTED SUPERCONDUCTING ALLOYS AND CERAMICS WITH THEIR T_c VALUES

Compound	T_c (K)
Nb_3Ge	23.2
Nb_3Ga	20.7
Nb_3Al	18.8
Nb_3Sn	18.3
Nb_3Si	18.0
V_3Si	17.1
V_3Ga	15.9
NbN	16.0
MoC	14.3
NbB	8.25
$PbMo_6S_8$	15.0
$Ba(Pb_{1-x}Bi_x)O_3$	13.2

for a few of the elemental superconductors. With the knowledge obtained in the elemental superconductors, the search for other superconductors shifted to the metallic conducting alloys, carbides, nitrides, borides, sulfides, oxides, etc. During the period 1940–1985 many such alloys and ceramics were found to be superconductors, but the highest T_c was only 23.2 K, found in Nb_3Ge film made by sputtering. Table 2 lists some of these alloys and ceramics with their T_c values. Among all the alloy and ceramic superconductors, A15 phases (see 17.3.10.1.1), Chevrel phases (see 17.3.10.1.2), and some oxides (low T_c oxides) are very important.

(Z. REN, J. WANG)

1. B. L. Chamberland, *Chemistry of Superconductor Materials*, T. A. Vanderah, ed., Noyes, Park Ridge, NJ, 1992.

17.3.10.1.1. The A15 Superconductors.

There are over 70 alloys with an A15 structure and about 50 of these are superconducting. Some of the superconducting A15 alloys with their T_c values were listed in 17.3.10.1 (Table 2).

(i) Composition and Structure of A15 Alloys. The idealized composition for the A15 phase is $A_{0.75}B_{0.25}$ (A_3B), with the A atoms occurring in pairs in a line across the center of each face of the cubic cell and forming three orthogonal lines or chains of atoms as illustrated in Figure 1. The B atoms are arranged in a body-centered-cubic configuration. The A atoms occur more closely together in the chains are than in the pure crystalline A metal, and the superior superconducting properties of the A15 structure are associated with these chains. Almost all the A15 superconductors can be prepared by either direct fusion in an arc furnace, sputtering, or Chemical Vapor Deposition (CVD). In the following, we briefly describe the preparation of the A15 Nb_3Sn, which can carry large critical current density (J_c) in the presence of high magnetic fields (10^5 A/cm^2 at 8.8 T) and is the prime candidate for commercial use in high field superconducting magnets and low loss power transmission.

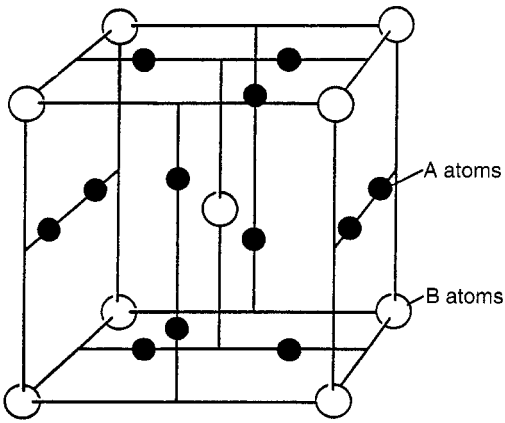

Figure 1. Cubic A15 crystal structure.

Inorganic Reactions and Methods, Volume 18
Edited by J. J. Zuckerman, Jim D. Atwood

for a few of the elemental superconductors. With the knowledge obtained in the elemental superconductors, the search for other superconductors shifted to the metallic conducting alloys, carbides, nitrides, borides, sulfides, oxides, etc. During the period 1940–1985 many such alloys and ceramics were found to be superconductors, but the highest T_c was only 23.2 K, found in Nb_3Ge film made by sputtering. Table 2 lists some of these alloys and ceramics with their T_c values. Among all the alloy and ceramic superconductors, A15 phases (see 17.3.10.1.1), Chevrel phases (see 17.3.10.1.2), and some oxides (low T_c oxides) are very important.

(Z. REN, J. WANG)

1. B. L. Chamberland, *Chemistry of Superconductor Materials*, T. A. Vanderah, ed., Noyes, Park Ridge, NJ, 1992.

17.3.10.1.1. The A15 Superconductors.

There are over 70 alloys with an A15 structure and about 50 of these are superconducting. Some of the superconducting A15 alloys with their T_c values were listed in 17.3.10.1 (Table 2).

(i) Composition and Structure of A15 Alloys. The idealized composition for the A15 phase is $A_{0.75}B_{0.25}$ (A_3B), with the A atoms occurring in pairs in a line across the center of each face of the cubic cell and forming three orthogonal lines or chains of atoms as illustrated in Figure 1. The B atoms are arranged in a body-centered-cubic configuration. The A atoms occur more closely together in the chains are than in the pure crystalline A metal, and the superior superconducting properties of the A15 structure are associated with these chains. Almost all the A15 superconductors can be prepared by either direct fusion in an arc furnace, sputtering, or Chemical Vapor Deposition (CVD). In the following, we briefly describe the preparation of the A15 Nb_3Sn, which can carry large critical current density (J_c) in the presence of high magnetic fields (10^5 A/cm^2 at 8.8 T) and is the prime candidate for commercial use in high field superconducting magnets and low loss power transmission.

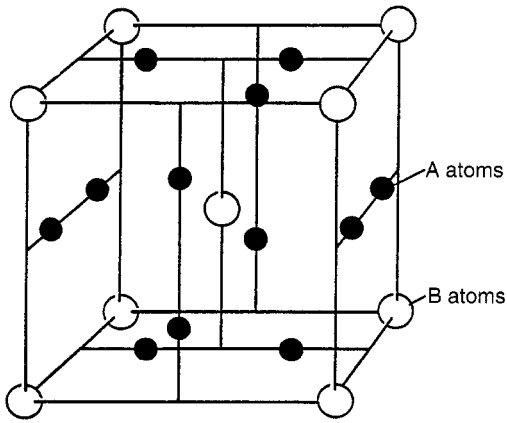

Figure 1. Cubic A15 crystal structure.

(ii) Preparation of Nb_3Sn. The A15 Nb_3Sn is formed by a peritectic reaction (at 2130°C) and exists over a composition range of 17–27 atom % Sn (see Fig. 2). The T_c varies linearly with Sn content, increasing from 6 K for the composition $Nb_{0.81}Sn_{0.19}$ to 18.3 K for the stoichiometric $Nb_{0.75}Sn_{0.25}$. The stoichiometric composition is stable over a wide temperature range (room temperature to 1650°C).

Bulk quantities of A15 Nb_3Sn are prepared by the direct union of the metals via either a sintering operation in an electric furnace or rapid induction melting under pressure. Preparation of Nb_3Sn by arc melting is not possible owing to the high melting point of the Sn with respect to Nb (the mp of Nb is ≈ 400°C higher than the bp of Sn).

For the sintered preparation, proper weights of high purity Nb and Sn powders are thoroughly mixed and compressed into a cylindrical pellet under ~ 7000 kg/cm^2. The pressed powder compact is sealed under vacuum in a quartz ampule and heated to 1200°C for ~ 2 h. After sintering the ampule is removed from the furnace and cooled in air. The porous and readily crumbled compact prepared by this method will contain over 4000 ppm oxygen owing to the oxygen content of the fine-powdered Nb and Sn.

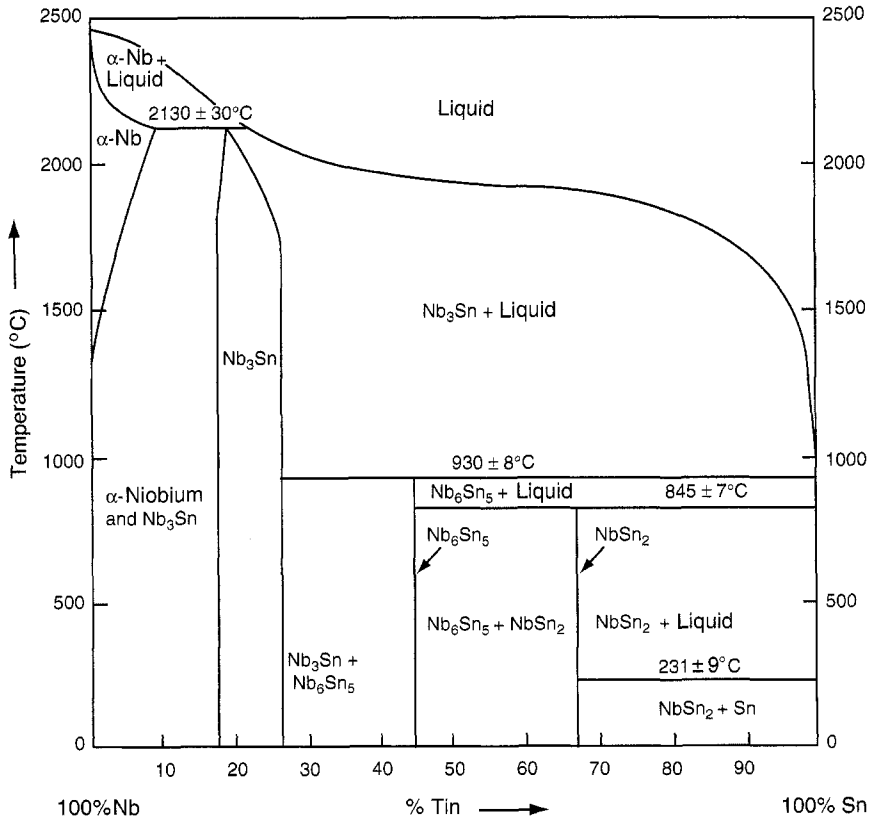

Figure 2. The niobium–tin equilibrium phase diagram showing the formation of unwanted compounds at temperatures below 930°C.

A purer, more homogeneous compound is formed by rapid induction melting under an inert atmosphere. Proper weights of high purity Nb and Sn metal lumps are placed in a beryllia or zirconia crucible and rapidly melted by induction heating under an Ar or He pressure (>1 atm). Lower frequency (5 kHz) induction heating will induce more thorough mixing of the molten metals and will produce more uniform alloys than induction heating at a higher frequency (450 kHz).

(iii) Synthesis of Nb_3Sn Film. A simple technique for forming thin films of Nb_3Sn on a Nb substrate (wire or foil) involves the reaction between $SnCl_2$ gas and Nb metal at elevated temperature:

$$17Nb + 5SnCl_2 \longrightarrow 5Nb_3Sn + 2NbCl_5 \qquad (a)$$

In a typical experiment a Nb foil $25 \times 5 \times 0.0025$ cm^3 is held at 950°C for 1 h in a stream of $SnCl_2$ vapor diluted with He gas. A strongly bonded uniform film of A15 Nb_3Sn (0.25 μm thick) forms on the surface through diffusion.

Long tape of Nb_3Sn can be produced by means of CVD with simultaneous reduction of gaseous Nb and Sn halides on heated substrates; this is the most versatile method for the preparation of adherent uniform high purity films on both metallic and ceramic substrates. The chemistry of the CVD process is known. The A15 Nb_3Sn can be formed at 675–1600°C, with 900–1200°C being the more favorable range. The overall reaction for the vapor deposition is:

$$3NbCl_4 + SnCl_2 + 7H_2 \leftrightarrow Nb_3Sn + 14HCl \qquad (b)$$

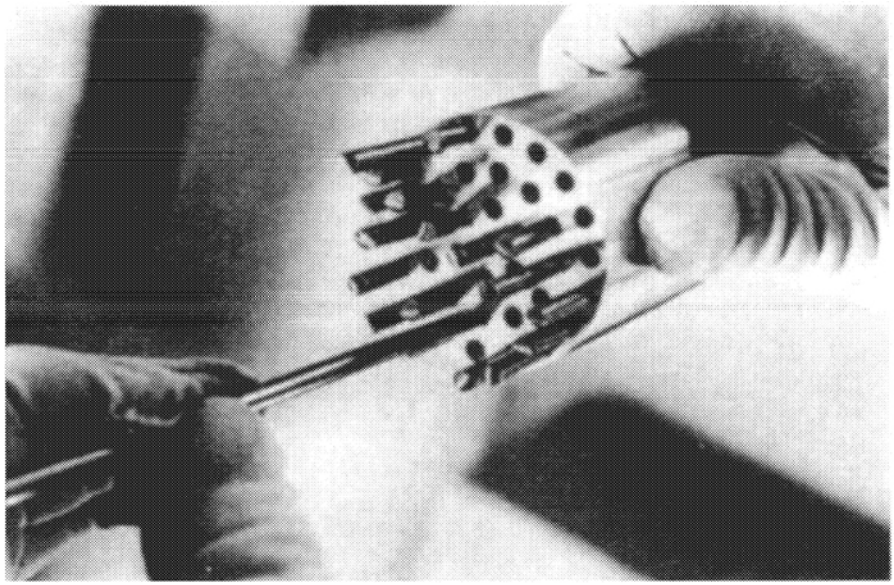

Figure 3. Stacking pure niobium rods into a drilled billet of bronze prior to drawing down to wire.

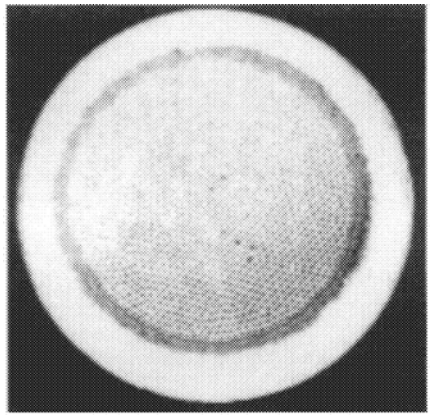

Figure 4. Filamentary Nb Sn–bronze composite with copper jacket and tantalum diffusion barrier.

By controlling the ratio of the halide vapors and the H_2 concentration, the deposited Nb_3Sn phase can be varied over a controlled composition range of $Nb_{0.82}Sn_{0.18}$ to $Nb_{0.75}Sn_{0.25}$. Two general methods are used for the introduction of the metal halides in the CVD process. The Nb and Sn halide vapors may first be prepared by the separate chlorination of the metals, with the Cl_2 gas flow controlling the ratio of the two halides, and thus the stoichiometry of the deposit. The second method uses commercially prepared $NbCl_5$ and $SnCl_2$ powders premixed in the proper ratio and introduced into a vaporizer at a controlled rate, by means of a vibrator. The mixed vapors are transported into the coating chamber, where they are mixed with H_2 gas and reduced on the hot substrate. Depending on the reaction conditions, Nb_3Sn may be deposited in a variety of forms ranging from large crystals to smooth fine-grained films. Clearly the latter are to be preferred for high current density magnet conductors.

(iv) Fabrication of Filamentary Nb_3Sn by the Bronze Process. Filamentary composites of Nb_3Sn first became possible with the invention of the bronze process for producing Nb_3Sn via a solid state reaction. Filaments of pure niobium are drawn down in a matrix of copper–tin bronze[1]. Figure 3 shows the multiple-stacking procedure in which rods of niobium are put into holes drilled in a bronze cylinder, which may then be extruded and drawn or simply drawn directly. After reaching its final size, the wire is given a prolonged heat treatment, typically for 1–10 days at 700°C. During this heat treatment, tin diffuses through the bronze and reacts with the niobium to form the desired Nb_3Sn (see Fig. 4).

(Z. REN, J. WANG)

1. M. N. Wilson, *Superconducting Magnets*, Oxford Science Publications, Oxford 1983.

17.3.10.1.2. Carbide, Nitride, Boride, and Sulfide (Chevrel) Superconductors.

Searching for higher transition superconductors was not limited to the A15 alloys. Many carbides, nitrides, borides, sulfides, etc. were also found to be superconducting.

Inorganic Reactions and Methods, Volume 18
Edited by J. J. Zuckerman, Jim D. Atwood

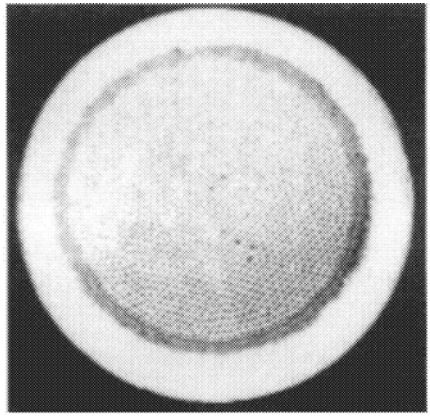

Figure 4. Filamentary Nb Sn–bronze composite with copper jacket and tantalum diffusion barrier.

By controlling the ratio of the halide vapors and the H_2 concentration, the deposited Nb_3Sn phase can be varied over a controlled composition range of $Nb_{0.82}Sn_{0.18}$ to $Nb_{0.75}Sn_{0.25}$. Two general methods are used for the introduction of the metal halides in the CVD process. The Nb and Sn halide vapors may first be prepared by the separate chlorination of the metals, with the Cl_2 gas flow controlling the ratio of the two halides, and thus the stoichiometry of the deposit. The second method uses commercially prepared $NbCl_5$ and $SnCl_2$ powders premixed in the proper ratio and introduced into a vaporizer at a controlled rate, by means of a vibrator. The mixed vapors are transported into the coating chamber, where they are mixed with H_2 gas and reduced on the hot substrate. Depending on the reaction conditions, Nb_3Sn may be deposited in a variety of forms ranging from large crystals to smooth fine-grained films. Clearly the latter are to be preferred for high current density magnet conductors.

(iv) Fabrication of Filamentary Nb_3Sn by the Bronze Process. Filamentary composites of Nb_3Sn first became possible with the invention of the bronze process for producing Nb_3Sn via a solid state reaction. Filaments of pure niobium are drawn down in a matrix of copper–tin bronze[1]. Figure 3 shows the multiple-stacking procedure in which rods of niobium are put into holes drilled in a bronze cylinder, which may then be extruded and drawn or simply drawn directly. After reaching its final size, the wire is given a prolonged heat treatment, typically for 1–10 days at 700°C. During this heat treatment, tin diffuses through the bronze and reacts with the niobium to form the desired Nb_3Sn (see Fig. 4).

(Z. REN, J. WANG)

1. M. N. Wilson, *Superconducting Magnets*, Oxford Science Publications, Oxford 1983.

17.3.10.1.2. Carbide, Nitride, Boride, and Sulfide (Chevrel) Superconductors.

Searching for higher transition superconductors was not limited to the A15 alloys. Many carbides, nitrides, borides, sulfides, etc. were also found to be superconducting.

Some selected superconducting carbides, nitrides, borides, and sulfides are presented in Table 1 with their T_c values. Among these superconducting ceramics, the most influential factor was the crystal structure. Many of the important superconductors were based on the NaCl-type structure (also referred to as the B1 structure by metallurgists) and the

Table 1. Selected Superconducting Carbides, Nitrides, Borides, and Sulfides with Their T_c Values

Carbide	T_c (K)	Nitride	T_c (K)	Boride	T_c (K)	Sulfide	T_c (K)
MoC	14.3	MoN	12.0	Mo_2B	5.85	NbPS	12.5
NbC	11.1	NbN	16.0	NbB	8.25	$PbMo_6S_8$	15.0
La_2C_3	11.0	VN	8.5	TaB	4.0	$SnMo_6S_8$	14.0
Nb_2C	9.1	Nb_2N	8.6	$NbB_{2.5}$	6.4	$CuMo_6S_8$	10.8
TaC	10.35	ZrN	10.7	ZrB_{12}	6.02	$LaMo_6S_8$	11.4
$ThC_{1.45}$	8.2	ThN	3.3	HfB	3.1	$Sr_{0.2}MoS_2$	5.6
$YC_{1.45}$	11.5	TiN	5.49	Re_2B	4.6	$CuRh_2S_4$	4.8

Source: Ref. 1.

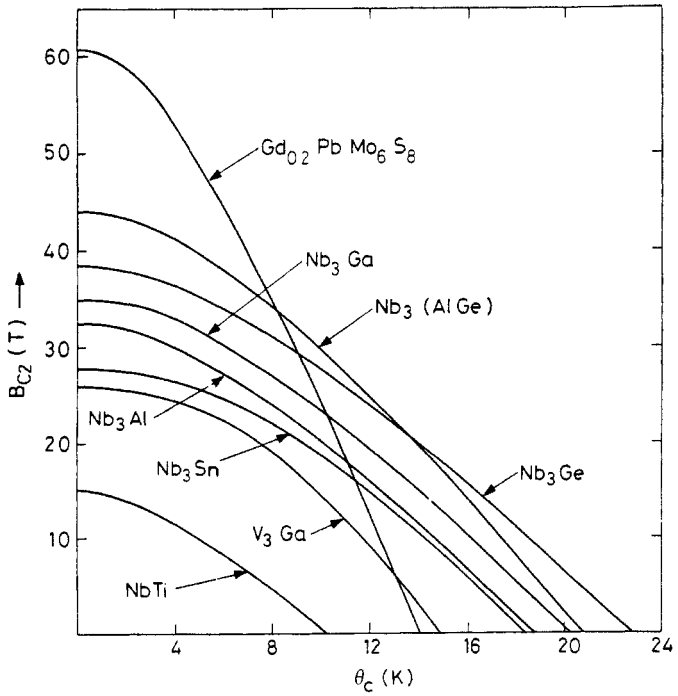

Figure 1. Relationship between critical field and temperature of the best high field superconductors.

Chevrel structure. The Chevrel compounds have the general formula $A_nMo_6B_8$, where A is a metal or mixture of metals, B is either sulfur, selenium, or tellurium, and $n < 4$. The structure is complicated, with clusters of Mo_6B_8 in which the Mo atoms are situated at the corners of an octahedron, and channels between these clusters containing the A atoms. About 100 compounds of this type are known, and roughly half of them are superconducting. The most important feature of the Chevrel phases is their extremely high critical field (H_{c2}). The ternary compounds $PbMo_6S_8$ and $LaMo_6S_8$ have H_{c2} at zero K of 53 and 44 T, respectively. The quaternary compound $PbGd_{0.2}Mo_6S_8$ has the highest measured H_{c2} of 54 T at 4.2 K, which may be extrapolated to over 60 T at zero K[2]. Figure 1 shows the temperature dependence of H_{c2} of a few low T_c superconductors[2]. Research samples of these materials are usually made by heating powder compacts for many hours at temperatures above 1000°C.

(Z. REN, J. WANG)

1. B. L. Chamberland, *Chemistry of Superconductor Materials*, T. A. Vanderah, Noyes Park Ridge, NJ, 1992.
2. M. N. Wilson, *Superconducting Magnets*, Oxford Science Publications, Oxford, 1983.

17.3.10.1.3. Oxide Superconductors.

Since all the current high T_c superconductors are oxides, low T_c oxides are important. NbO was first found to be superconducting in 1933[1]. Since then much effort has been devoted to investigating superconductivity in oxides, but not many oxides display this property. Table 1 presents a chronological listing of the different oxide superconductors reported prior to 1975[2]. Of particular interest is the compound $Ba(Pb_{1-x}Bi_x)O_3$ with T_c of 13 K[3], and $Ba_{0.6}K_{0.4}BiO_{3-x}$ with a T_c of 28 K[4].

(i) Composition and Structure. These oxide materials adopt the perovskite-type structure. Before the discovery of $Ba(Pb_{1-x}Bi_x)O_3$, it was known that $BaPbO_3$, a distorted perovskite with pseudo-orthorhombic symmetry, exhibited metallic conducting

TABLE 1. A CHRONOLOGICAL LIST OF SUPERCONDUCTING OXIDES DISCOVERED PRIOR TO 1975

Compound	T_c (K)	Year Discovered
NbO	~ 1.5	1933
$SrTiO_3$	~ 0.3	1964
A_xWO_3[a]	0.01–7.7	1964–1975
TiO	~ 1.0	1965
A_xMoO_3[b]	1.3–4.2	1966
$Ag_7O_8^+NO_3^-$	1.04	1966
A_xReO_3[c]	1.3–3.6	1969
$Li_{1+x}Ti_{2-x}O_4$	13.7	1973
$Ba(Pb_{1-x}Bi_x)O_3$	13.2	1975

[a]A can be Li, Na, K, Rb, Cs, Ca, Sr, Ba, Cu, In, Tl, Sn, etc.
[b]A can be Na or K.
[c]A can be Na or K.
Source: Ref. 2.

Inorganic Reactions and Methods, Volume 18
Edited by J. J. Zuckerman, Jim D. Atwood

Chevrel structure. The Chevrel compounds have the general formula $A_nMo_6B_8$, where A is a metal or mixture of metals, B is either sulfur, selenium, or tellurium, and $n < 4$. The structure is complicated, with clusters of Mo_6B_8 in which the Mo atoms are situated at the corners of an octahedron, and channels between these clusters containing the A atoms. About 100 compounds of this type are known, and roughly half of them are superconducting. The most important feature of the Chevrel phases is their extremely high critical field (H_{c2}). The ternary compounds $PbMo_6S_8$ and $LaMo_6S_8$ have H_{c2} at zero K of 53 and 44 T, respectively. The quaternary compound $PbGd_{0.2}Mo_6S_8$ has the highest measured H_{c2} of 54 T at 4.2 K, which may be extrapolated to over 60 T at zero K[2]. Figure 1 shows the temperature dependence of H_{c2} of a few low T_c superconductors[2]. Research samples of these materials are usually made by heating powder compacts for many hours at temperatures above 1000°C.

(Z. REN, J. WANG)

1. B. L. Chamberland, *Chemistry of Superconductor Materials*, T. A. Vanderah, Noyes Park Ridge, NJ, 1992.
2. M. N. Wilson, *Superconducting Magnets*, Oxford Science Publications, Oxford, 1983.

17.3.10.1.3. Oxide Superconductors.

Since all the current high T_c superconductors are oxides, low T_c oxides are important. NbO was first found to be superconducting in 1933[1]. Since then much effort has been devoted to investigating superconductivity in oxides, but not many oxides display this property. Table 1 presents a chronological listing of the different oxide superconductors reported prior to 1975[2]. Of particular interest is the compound $Ba(Pb_{1-x}Bi_x)O_3$ with T_c of 13 K[3], and $Ba_{0.6}K_{0.4}BiO_{3-x}$ with a T_c of 28 K[4].

(i) Composition and Structure. These oxide materials adopt the perovskite-type structure. Before the discovery of $Ba(Pb_{1-x}Bi_x)O_3$, it was known that $BaPbO_3$, a distorted perovskite with pseudo-orthorhombic symmetry, exhibited metallic conducting

TABLE 1. A CHRONOLOGICAL LIST OF SUPERCONDUCTING OXIDES DISCOVERED PRIOR TO 1975

Compound	T_c (K)	Year Discovered
NbO	~ 1.5	1933
$SrTiO_3$	~ 0.3	1964
A_xWO_3[a]	0.01–7.7	1964–1975
TiO	~ 1.0	1965
A_xMoO_3[b]	1.3–4.2	1966
$Ag_7O_8^+NO_3^-$	1.04	1966
A_xReO_3[c]	1.3–3.6	1969
$Li_{1+x}Ti_{2-x}O_4$	13.7	1973
$Ba(Pb_{1-x}Bi_x)O_3$	13.2	1975

[a]A can be Li, Na, K, Rb, Cs, Ca, Sr, Ba, Cu, In, Tl, Sn, etc.
[b]A can be Na or K.
[c]A can be Na or K.
Source: Ref. 2.

properties to very low temperatures but was not a superconductor down to 4.2 K. $BaBiO_3$ was also studied and exhibited insulating properties. Surprisingly, the solid solution $Ba(Pb_{1-x}Bi_x)O_3$ between the components $BaPbO_3$ and $BaBiO_3$ is superconducting. The compositional range for superconductivity in $Ba(Pb_{1-x}Bi_x)O_3$ is $0.05 < x < 0.3$ with T_c varying between 9 and 13 K. The optimal composition is $x = 0.3$ with $T_c = 13$ K. A typical R–T curve of $Ba(Bi_{0.2}Pb_{0.8})O_3$ is shown in Figure 1. A optimal T_c of 30.5 K, higher than the legendary 23.2 K, is obtained with the composition of $Ba_{0.6}K_{0.4}BiO_{3-x}^{5}$ (see Fig. 2).

(ii) Synthesis of $BaPb_{0.7}Bi_{0.3}O_3$ and $Ba_{0.6}K_{0.4}BiO_{3-x}$. The synthesis of $BaPb_{0.7}Bi_{0.3}O_3$ was carried out by mixing stoichiometric quantities of $BaCO_3$, PbO_2, and Bi_2O_3, firing for 24 h at 800°C, remixing and refiring for 24 h at 850°C, followed by pressing into pellets and air annealing for 24 h at 930°C[6]. The synthesis of

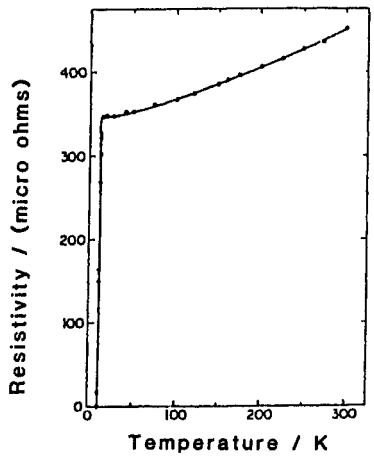

Figure 1. Electrical resistance vs. absolute temperature for $Ba(Bi_{0.20}Pb_{0.80})O_3$ ($T_c = 11$ K).

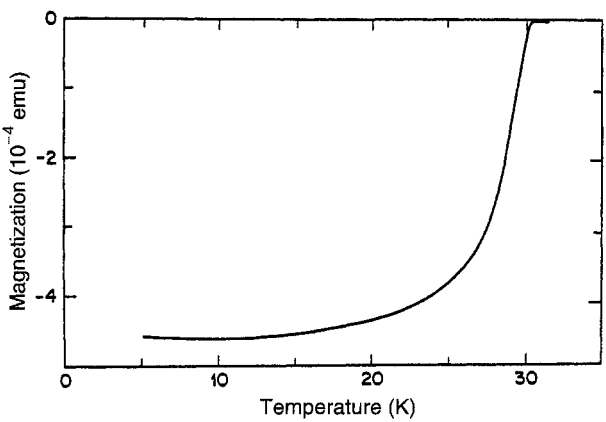

Figure 2. Magnetization vs. absolute temperature for crystals of $Ba_{0.60}K_{0.40}BiO_3$ ($T_c = 30.5$ K).

$Ba_{0.6}K_{0.4}BiO_{3-x}$ was achieved by mixing stoichiometric quantities of BaO, KO_2, and dried Bi_2O_3, and firing in dry nitrogen gas at 700°C for 1 h. This material is then annealed in oxygen for 4 h at 450°C, followed by slowly cooling to room temperature[7].

(iii) Growth of $BaPb_{0.7}Bi_{0.3}O_3$ and $Ba_{0.6}K_{0.4}BiO_{3-x}$ Single Crystals. There are three ways to grow single crystals of $Ba(Pb_{1-x}Bi_x)O_3$: hydrothermal technique, high temperature (~900°C) halide flux technique, and self-flux technique (excess PbO_2 and Bi_2O_3)[8]. The most suitable method to grow $Ba_{1-x}K_xBiO_3$ single crystals is high temperature flux, with KOH the flux of choice[9].

(iv) Growth of $BaPb_{0.7}Bi_{0.3}O_3$ and $Ba_{0.6}K_{0.4}BiO_{3-x}$ Thin Films. Thin film preparation of $Ba(Pb_{1-x}Bi_x)O_3$ was carried out by either sputtering or laser ablation. A nonstoichiometric target was required for sputtering[10], whereas a stoichiometric target will be adequate for laser ablation[11]. The fabrication of $Ba_{1-x}K_xBiO_3$ thin films requires low temperature deposition techniques because of the thermal instability of $Ba_{1-x}K_xBiO_3$[12].

(Z. REN, J. WANG)

1. W. Meissner, H. Franz, H. Westerhoff, *Ann. Phys.*, *17*, 593 (1933).
2. B. L. Chamberland, *Chemistry of Superconductor Materials*, T. A. Vanderah, ed., Noyes Park Ridge, NJ, 1992.
3. A. W. Sleight, J. L. Gillson, P. E. Bierstedt, *Solid State Commun.*, *17*, 27 (1975).
4. R. J. Cava, B. Batlogg, G. P. Espinosa, A. P. Ramirez, J. J. Krajewski, W. F. Peck Jr., L. W. Rupp Jr., A. S. Cooper, *Nature*, *339*, 291 (1988).
5. L. F. Schneemeyer, J. K. Thomas, T. Siegrist, B. Batlogg, L. W. Rupp, R. L. Opila, R. J. Cava, D. W. Murphy, *Nature*, *335*, 421 (1988).
6. Y. Khan, K. Nahm, M. Rosenberg, and H. Willner, *Phys. Status Solidi. (A)*, *39*, 79 (1977).
7. D. G. Hinks, D. R. Richards, B. Dabrowski, A. W. Mitchell, J. D. Jorgensen, D. T. Marx, *Physica C*, *156*, 477 (1988).
8. A. Katsui, Y. Hidaka, H. Takagi, *J. Cryst. Growth*, *66*, 228 (1984).
9. J. P. Wignacourt, J. S. Swinnea, H. Steienfink, J. B. Goodenough, *Appl. Phys. Lett.*, *53*, 1753 (1988).
10. M. Suzuki, T. Murakami, *Jpn. J. Appl. Phys.*, *22*, 1794 (1983).
11. S. V. Zaltsev, A. N. Martynyuk, E. A. Protasov, *Sov. Phys. Solid State*, *25*, 100 (1983).
12. Y. Enomoto, T. Murakami, K. Moriwaki, *Jpn. J. Appl. Phys.*, *28*, L1355 (1988).

17.3.10.2. High Temperature Superconductors

Since the discovery of high temperature superconductivity ($T_c > 30$ K) in the La–Ba–Cu–O system[1], hundreds of high temperature superconducting oxides have been found, with the record T_c of 164 K in Hg-1223 under high pressure[2]. According to their major chemical difference, these superconductors can be classified into six major categories: K_2NiF_4-type cuprates, rare-earth-based cuprates, bismuth-based cuprates, thallium-based cuprates, mercury-based cuprates, and other cuprates. Details of every superconductor are not presented, but at least one typical composition of each major type will be discussed in detail. Interested readers can read the relevant literature to get specific information on other systems.

(Z. REN, J. WANG)

1. J. G. Bednorz, K. A. Muller, *Z. Phys. B. Condens. Matter.*, *64*, 189 (1986).
2. L. Gao, Y. Y. Xue, F. Chen, Q. Xiong, R. L. Meng, D. Ramirez, C. W. Chu, J. H. Eggert, and H. K. Mao, *Phys. Rev. B*, *50*, 4260 (1994).

Inorganic Reactions and Methods, Volume 18
Edited by J. J. Zuckerman, Jim D. Atwood

$Ba_{0.6}K_{0.4}BiO_{3-x}$ was achieved by mixing stoichiometric quantities of BaO, KO_2, and dried Bi_2O_3, and firing in dry nitrogen gas at 700°C for 1 h. This material is then annealed in oxygen for 4 h at 450°C, followed by slowly cooling to room temperature[7].

(iii) Growth of $BaPb_{0.7}Bi_{0.3}O_3$ and $Ba_{0.6}K_{0.4}BiO_{3-x}$ Single Crystals. There are three ways to grow single crystals of $Ba(Pb_{1-x}Bi_x)O_3$: hydrothermal technique, high temperature (~900°C) halide flux technique, and self-flux technique (excess PbO_2 and Bi_2O_3)[8]. The most suitable method to grow $Ba_{1-x}K_xBiO_3$ single crystals is high temperature flux, with KOH the flux of choice[9].

(iv) Growth of $BaPb_{0.7}Bi_{0.3}O_3$ and $Ba_{0.6}K_{0.4}BiO_{3-x}$ Thin Films. Thin film preparation of $Ba(Pb_{1-x}Bi_x)O_3$ was carried out by either sputtering or laser ablation. A nonstoichiometric target was required for sputtering[10], whereas a stoichiometric target will be adequate for laser ablation[11]. The fabrication of $Ba_{1-x}K_xBiO_3$ thin films requires low temperature deposition techniques because of the thermal instability of $Ba_{1-x}K_xBiO_3$[12].

(Z. REN, J. WANG)

1. W. Meissner, H. Franz, H. Westerhoff, *Ann. Phys., 17*, 593 (1933).
2. B. L. Chamberland, *Chemistry of Superconductor Materials*, T. A. Vanderah, ed., Noyes Park Ridge, NJ, 1992.
3. A. W. Sleight, J. L. Gillson, P. E. Bierstedt, *Solid State Commun., 17*, 27 (1975).
4. R. J. Cava, B. Batlogg, G. P. Espinosa, A. P. Ramirez, J. J. Krajewski, W. F. Peck Jr., L. W. Rupp Jr., A. S. Cooper, *Nature, 339*, 291 (1988).
5. L. F. Schneemeyer, J. K. Thomas, T. Siegrist, B. Batlogg, L. W. Rupp, R. L. Opila, R. J. Cava, D. W. Murphy, *Nature, 335*, 421 (1988).
6. Y. Khan, K. Nahm, M. Rosenberg, and H. Willner, *Phys. Status Solidi. (A), 39*, 79 (1977).
7. D. G. Hinks, D. R. Richards, B. Dabrowski, A. W. Mitchell, J. D. Jorgensen, D. T. Marx, *Physica C, 156*, 477 (1988).
8. A. Katsui, Y. Hidaka, H. Takagi, *J. Cryst. Growth, 66*, 228 (1984).
9. J. P. Wignacourt, J. S. Swinnea, H. Steienfink, J. B. Goodenough, *Appl. Phys. Lett., 53*, 1753 (1988).
10. M. Suzuki, T. Murakami, *Jpn. J. Appl. Phys., 22*, 1794 (1983).
11. S. V. Zaltsev, A. N. Martynyuk, E. A. Protasov, *Sov. Phys. Solid State, 25*, 100 (1983).
12. Y. Enomoto, T. Murakami, K. Moriwaki, *Jpn. J. Appl. Phys., 28*, L1355 (1988).

17.3.10.2. High Temperature Superconductors

Since the discovery of high temperature superconductivity ($T_c > 30$ K) in the La–Ba–Cu–O system[1], hundreds of high temperature superconducting oxides have been found, with the record T_c of 164 K in Hg-1223 under high pressure[2]. According to their major chemical difference, these superconductors can be classified into six major categories: K_2NiF_4-type cuprates, rare-earth-based cuprates, bismuth-based cuprates, thallium-based cuprates, mercury-based cuprates, and other cuprates. Details of every superconductor are not presented, but at least one typical composition of each major type will be discussed in detail. Interested readers can read the relevant literature to get specific information on other systems.

(Z. REN, J. WANG)

1. J. G. Bednorz, K. A. Muller, *Z. Phys. B. Condens. Matter., 64*, 189 (1986).
2. L. Gao, Y. Y. Xue, F. Chen, Q. Xiong, R. L. Meng, D. Ramirez, C. W. Chu, J. H. Eggert, and H. K. Mao, *Phys. Rev. B, 50*, 4260 (1994).

Inorganic Reactions and Methods, Volume 18
Edited by J. J. Zuckerman, Jim D. Atwood

17.3.10.2.1. K_2NiF_4-Type Cuprates.

There are two major types of superconductor with the structure of K_2NiF_4: hole-doped $La_{2-x}A_xCuO_4$ (A = Ba or Sr) and electron-doped $Nd_{2-x}B_xCuO_4$ (B = Ce or other elements). The importance of $La_{2-x}A_xCuO_4$ is obvious because all the high T_c superconductors were discovered after the discovery of high T_c superconductivity in La–Ba–Cu–O system. $Nd_{2-x}B_xCuO_4$ is also important for theoretical reasons, though its T_c is lower than that of $La_{2-x}A_xCuO_4$.

(i) Composition and Structure of $La_{2-x}A_xCuO_4$. The highest T_c values of 40 and 35 K in $La_{2-x}A_xCuO_4$ were obtained at $x = 0.15$ for A = Sr and Ba, respectively. The higher T_c of $La_{1.85}Sr_{0.15}CuO_4$ is attributed to the smaller size of Sr. The 35 K superconductivity as shown in Figure 1[1] was due to the presence of K_2NiF_4-type of $La_{1.85}Ba_{0.15}CuO_4$ phase (namely 214 phase). This compound has a body-centered-tetragonal structure that contains sheets of corner-sharing CuO_6 octahedra that are oriented in the *ab* plane (see Fig. 2). The octahedra are axially elongated (along the *c* axis) to give four intralayer Cu–O bond lengths of ~ 1.9 Å, and two longer bonds, ~ 2.5 Å, perpendicular to the sheets. La and Sr cations are nine coordinate sites directly above and below the CuO_2 sheets. The $LaO/CuO_2/LaO$ slab is the "perovskite" part of the

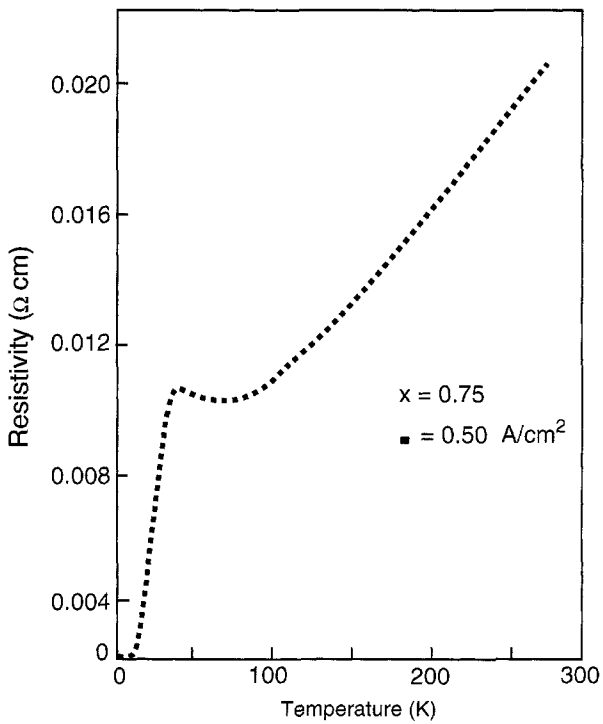

Figure 1. Resistivity of $Ba_{0.75}La_{4.25}Cu_5O_{15-5y}$ vs. absolute temperature as published by Bednorz and Muller. (Ref 1.)

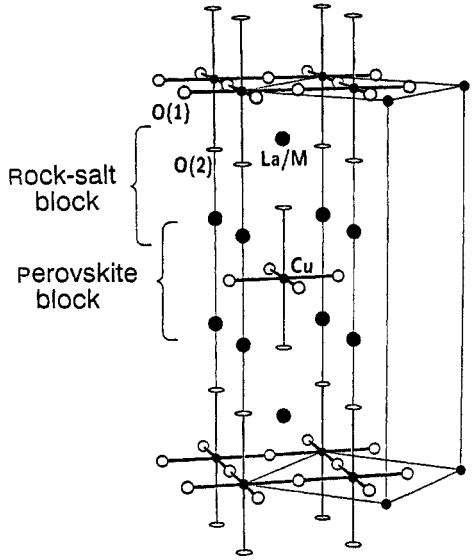

Figure 2. Tetragonal and orthorhombic unit cells of $La_{2-x}M_xCuO_4$ (e.g., M = Sr or Na) and La_2CuO_4, respectively. Metal atoms are solid, and Cu–O bonds are shown. The structure may be viewed as an intergrowth of perovskite and rock salt blocks.

structure. The LaO layers occur in pairs to form La_2O_2 slabs separating the CuO_2 sheets. The La_2O_2 slabs can be viewed as the intergrown "rock salt" portion of the structure (see Fig. 2)[2].

(ii) Synthesis of $La_{2-x}Sr_xCuO_4$. The compounds $La_{2-x}Sr_xCuO_4$ ($x = 0.05$–1.1) were prepared from the oxides La_2O_3, $SrCO_3$, and CuO_3. Appropriate amounts of the oxides were mixed and pressed into 1.27 cm diameter pellets. The pellets were heated in a platinum boat in a furnace under flowing oxygen. The temperature was increased to 1120°C in 2 h, held for 36 h, and cooled to 500°C in 1 h, after which the sample was removed. Part of the pellet was ground, and the powder was examined by x-ray diffraction (XRD). The samples were single phase for $0.05 < x < 0.3$. For $x \geq 0.4$, however, a trace of a second phase was seen. The single-phase samples were ground, pressed, and reannealed at 1200°C for another 24 h. The highest T_c and the narrowest transition width were obtained near $x = 0.15$, as shown in Figure 3, which clearly demonstrates that T_c is very sensitive to Sr concentration.

(iii) Growth of $La_{2-x}A_xCuO_4$ Single Crystals. Single crystals of $La_{1.85}Sr_{0.15}CuO_4$ were prepared by melt growth[4] or top seeding[5–7] or flux growth methods. Because of the precise dependence of T_c on the stoichiometry, T_c values of the grown crystals were considerably lower than those obtained in the bulk form.

(iv) Growth of $La_{2-x}Sr_xCuO_4$ Thin Films. The films of $La_{2-x}Sr_xCuO_4$ were deposited on a number of substrates such as $SrTiO_3$ and $LaSrAlO_4$ by laser ablation[8],

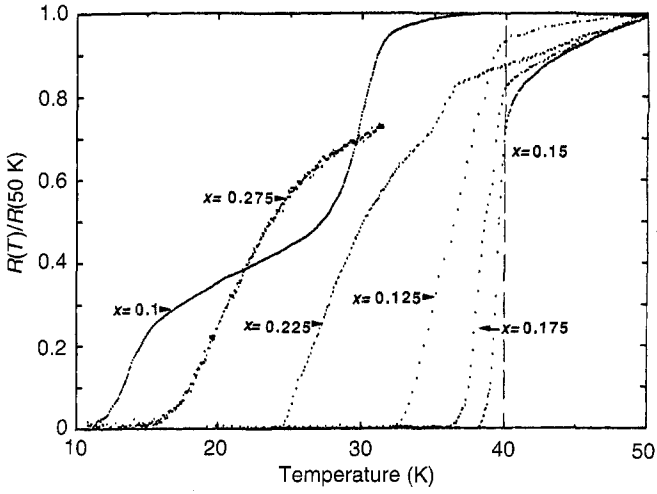

Figure 3. Resistance vs. temperature, normalized to 50 K, showing the superconducting transition for six values of strontium concentration, x. As x deviates from the optimum value of 0.15, the transition decreases and broadens. Vertical line is drawn at 40 K.

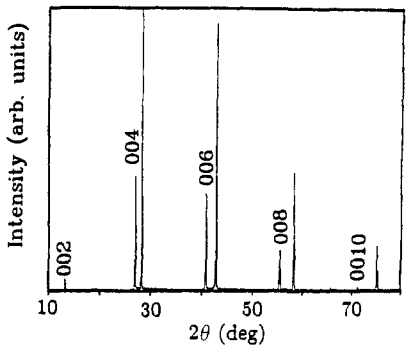

Figure 4. X-ray diffraction, Θ–2Θ scan for a $La_{1.85}Sr_{0.15}CuO_4$ film on a $LaSrAlO_4$ substrate.

molecular beam epitaxy (MBE)[9], etc. For laser ablation, the target is mounted on a rotatable holder 6 cm from the substrates. During deposition the substrate is held at 760°C in 130 mtorr O_2. After deposition the oxygen pressure is increased to 750 mtorr and the sample slowly cooled, first at a rate 180°C/h to 450°C and then at 480°C/h to room temperature. This procedure results in high-quality c-axis-oriented epitaxial films, as confirmed by XRD spectra of a film with $x = 0.15$ shown in Figure 4. The presence of only (00l) peaks indicates the phase purity and c-axis alignment. Figure 5 shows a rocking curve measured for the (006) reflection. The small value of 0.107° full width at half-maximum (FWHM) indicates excellent c-axis alignment. The ϕ-scan measurement

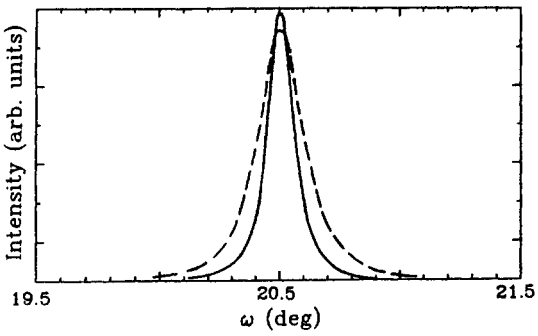

Figure 5. X-ray rocking curves for the (006) reflection: solid line, before high pressure annealing; dashed line, after high pressure annealing.

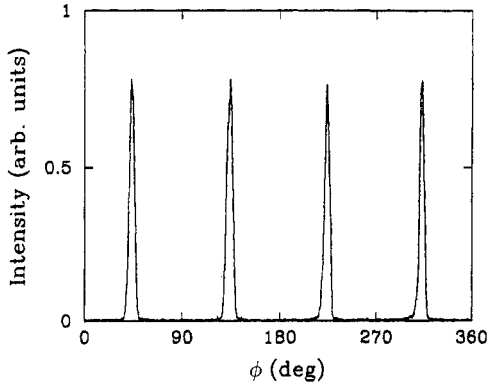

Figure 6. A ϕ scan of a $La_{1.85}Sr_{0.15}CuO_4$ film on a $LaSrAlO_4$ substrate. The peaks located at integral multiples of $\pi/2$ indicate fourfold in-plane symmetry.

shown in Figure 6 indicates an excellent in-plane alignment also. The as-grown films always have lower T_c values than the postannealed films in high pressure oxygen. Figure 7 shows the temperature dependence of the resistivity of $La_{1.85}Sr_{0.15}CuO_4$ films, both as-grown (triangles) and postannealed in high pressure oxygen (circles). The highest T_c obtained is 38 K, which is very close to that of the bulk samples. As in the case of bulk samples, T_c values of both thin (50 nm) and thick (200 nm) films are very sensitive to the oxygen content (see Fig. 8[9]).

(v) Synthesis of $Nd_{2-x}Ce_xCuO_4$. Following the original report of superconductivity in $Nd_{2-x}Ce_xCuO_4$[10], extensive research has been done on this system[11–14]. The synthesis of bulk $Nd_{2-x}Ce_xCuO_4$ involves the initial reaction and a follow-up reduction annealing. The initial reaction of the stoichiometric mixture of Nd_2O_3, CeO, and CuO must be carried out at close to 1150°C for hours in air, followed by quenching to room temperature. The quenched samples are single-phase tetragonal $Nd_{2-x}Ce_xCuO_4$, but not

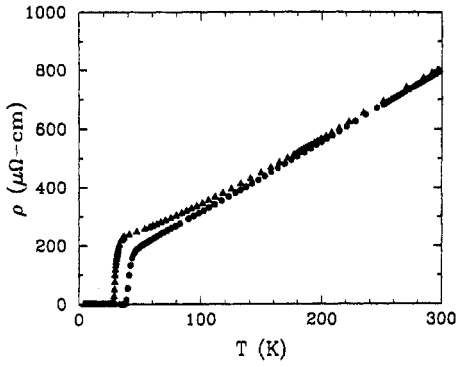

Figure 7. Temperature dependence of the resistivity of two $La_{1.85}Sr_{0.15}CuO_4$ films: triangles, before high pressure annealing; circles, after high pressure annealing.

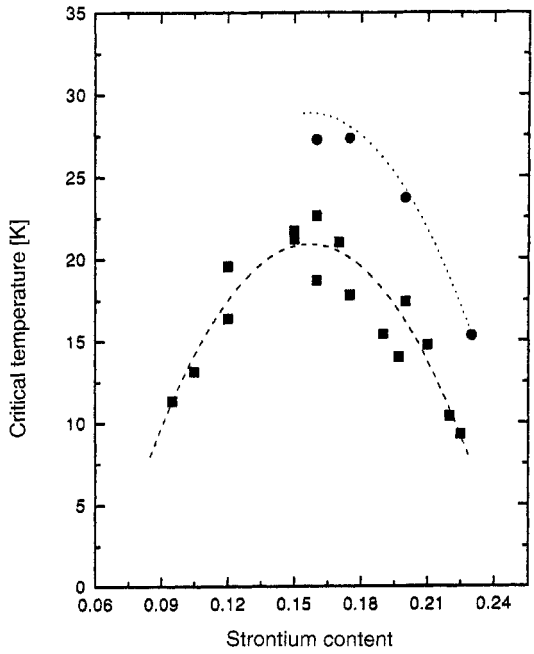

Figure 8. Critical temperature as a function of Sr concentration for thin (squares) and thick (circles) films.

superconducting because of the overoxidation of copper. To convert the sample into superconducting states, a reduction annealing step is carried out at 900°C in flowing Ar[12] He[13], or CO_2[14]. After reduction, all samples show superconductivity in the range of 20–27 K.

(vi) Growth of Single Crystal $Nd_{2-x}Ce_xCuO_4$. Single crystals of $Nd_{2-x}Ce_xCuO_4$ were first successfully made by growth in air from a CuO flux containing excess cerium at high temperature (1300°C) in an alumina crucible[15,16]. The charge was held at 1300°C for 2–4 h, then cooled to 1000°C at 2–6°C/h, followed by rapid cooling to room temperature. To induce superconductivity, the crystals had to be annealed at 900°C in flowing Ar.

(vii) Growth of Thin Film $Nd_{2-x}Ce_xCuO_4$ Thin films of $Nd_{2-x}Ce_xCuO_4$ have been prepared by laser ablation from sintered $Nd_{2-x}Ce_xCuO_4$ targets on heated substrates[17]. Typical conditions are 500°C at an ambient oxygen pressure of 10^{-4} atm, following by annealing at 900°C.

(Z. REN, J. WANG)

1. J. G. Bednorz, K. A. Muller, *Z. Phys. B, Condens. Matter, 64*, 189 (1986).
2. C. C. Torardi, *Chemistry of Superconductor Materials*, T. A. Vanderah, ed., Noyes, Park Ridge, NJ, 1992.
3. J. M. Tarascon, L. H. Greene, W. R. McKinnon, G. W. Hull, T. H. Geballe, *Science, 235*, 1373 (1987).
4. Y. Hidaka, Y. Enomoto, M. Suzuki, M. Oda, T. Murakami, *J. Cryst. Growth, 85*, 581 (1987).
5. P. J. Picone, H. P. Jenssen, D. R. Gabbe, *J. Cryst. Growth, 85*, 576 (1987).
6. P. J. Picone, H. P. Jenssen, D. R. Gabbe, *J. Cryst. Growth, 91*, 463 (1988).
7. C. Chen, B. E. Watts, B. M. Wanklyn, P. A. Thomas, P. W. Haycock, *J. Cryst. Growth, 91*, 282 (1988).
8. I. E. Trofimov, L. A. Johnson, K. V. Ramanujachary, S. Guha, M. G. Harrison, M. Greenblatt, M. Z. Cieplak, P. Lindenfeld, *Appl. Phys. Lett., 65*, 2481 (1994).
9. J.-P. Locquet, Y. Jaccard, A. Cretton, E. J. Williams, F. Arrouy, E. Machler, T. Schneider, Ø. Fisher, P. Martinoli, *Phys. Rev. B, 54*, 7481 (1996).
10. T. Tokura, H. Takagi, S. Uchida, *Nature, 337*, 345 (1989).
11. H. Takagi, S. Uchida, T. Tokura, *Phys. Rev. Lett., 62*, 1197 (1989).
12. T. C. Huang, E. Moran, A. I. Nazzal, J. B. Torrance, *Physica C, 158*, 148 (1989).
13. J. T. Markert, E. A. Early, T. Bjornholm, S. Ghamaty, B. W. Lee, J. J. Neumeier, R. D. Price, C. L. Seaman, M. B. Maple, *Physica C, 160*, 320 (1989).
14. E. Takayama-Muromachi, F. Izumi, Y. Uchida, K. Kato, H. Asano, *Physica C, 159*, 634 (1989).
15. Y. Hidaka, M. Suzuki, *Nature, 338*, 635 (1989).
16. J.-M. Tarascon, E. Wang, L. H. Greene, B. G. Bagley, G. W. Hull, S. M. D'Egidio, P. F. Miceli, Z. Z. Wang, T. W. Jing, J. Clayhold, D. Brawner, N. P. Ong, *Phys. Rev. B, 40*, 4494 (1989).
17. H. Adachi, S. Hayashi, K. Setsune, S. Hatta, T. Mitsuyu, K. Wasa, *Appl. Phys. Lett., 54*, 2713 (1989).

17.3.10.2.2. Rare-Earth-Based Cuprates.

Applying pressure to a La–Ba–Cu–O sample caused an 8 K increase of T_c at a pressure of 14 kbar[1]. This immediately led to the amazing discovery of 94 K superconductivity in the Y–Ba–Cu–O system[2] by chemical substitution of the smaller Y ion into the La site of $La_{1.85}Ba_{0.15}CuO_4$ (214). The starting composition was $Y_{1.2}Ba_{0.8}CuO_{4-y}$, which followed the 214 formula of the K_2NiF_4 structure. Soon after the discovery, a number of laboratories were able to synthesize the 94 K superconductors and found that the composition of the superconducting phase was not $Y_{1.2}Ba_{0.8}CuO_{4-y}$ (214), but $YBa_2Cu_3O_{7-x}$ (123)[3–7]. Further studies on replacement of Y by rare earth elements (Nd, Gd, Sm, etc.) led to a series of 90–96 K superconductors[8,9]. Later, two new phases with the compositions $YBa_2Cu_4O_8$[10,11] and $Y_2Ba_4Cu_7O_{15}$[12,13] were also found to be superconducting at 80 and 90 K, respectively.

(i) Composition and Structure of $YBa_2Cu_3O_{7-x}$. The stoichiometric number of oxygen in $YBa_2Cu_3O_{7-x}$ can be changed from 7 ($x = 0$) to 6 ($x = 1.0$) by heat treatment.

Inorganic Reactions and Methods, Volume 18
Edited by J. J. Zuckerman, Jim D. Atwood

(vi) Growth of Single Crystal $Nd_{2-x}Ce_xCuO_4$. Single crystals of $Nd_{2-x}Ce_xCuO_4$ were first successfully made by growth in air from a CuO flux containing excess cerium at high temperature (1300°C) in an alumina crucible[15,16]. The charge was held at 1300°C for 2–4 h, then cooled to 1000°C at 2–6°C/h, followed by rapid cooling to room temperature. To induce superconductivity, the crystals had to be annealed at 900°C in flowing Ar.

(vii) Growth of Thin Film $Nd_{2-x}Ce_xCuO_4$ Thin films of $Nd_{2-x}Ce_xCuO_4$ have been prepared by laser ablation from sintered $Nd_{2-x}Ce_xCuO_4$ targets on heated substrates[17]. Typical conditions are 500°C at an ambient oxygen pressure of 10^{-4} atm, following by annealing at 900°C.

(Z. REN, J. WANG)

1. J. G. Bednorz, K. A. Muller, *Z. Phys. B, Condens. Matter*, *64*, 189 (1986).
2. C. C. Torardi, *Chemistry of Superconductor Materials*, T. A. Vanderah, ed., Noyes, Park Ridge, NJ, 1992.
3. J. M. Tarascon, L. H. Greene, W. R. McKinnon, G. W. Hull, T. H. Geballe, *Science*, *235*, 1373 (1987).
4. Y. Hidaka, Y. Enomoto, M. Suzuki, M. Oda, T. Murakami, *J. Cryst. Growth*, *85*, 581 (1987).
5. P. J. Picone, H. P. Jenssen, D. R. Gabbe, *J. Cryst. Growth*, *85*, 576 (1987).
6. P. J. Picone, H. P. Jenssen, D. R. Gabbe, *J. Cryst. Growth*, *91*, 463 (1988).
7. C. Chen, B. E. Watts, B. M. Wanklyn, P. A. Thomas, P. W. Haycock, *J. Cryst. Growth*, *91*, 282 (1988).
8. I. E. Trofimov, L. A. Johnson, K. V. Ramanujachary, S. Guha, M. G. Harrison, M. Greenblatt, M. Z. Cieplak, P. Lindenfeld, *Appl. Phys. Lett.*, *65*, 2481 (1994).
9. J.-P. Locquet, Y. Jaccard, A. Cretton, E. J. Williams, F. Arrouy, E. Machler, T. Schneider, Ø. Fisher, P. Martinoli, *Phys. Rev. B*, *54*, 7481 (1996).
10. T. Tokura, H. Takagi, S. Uchida, *Nature*, *337*, 345 (1989).
11. H. Takagi, S. Uchida, T. Tokura, *Phys. Rev. Lett.*, *62*, 1197 (1989).
12. T. C. Huang, E. Moran, A. I. Nazzal, J. B. Torrance, *Physica C*, *158*, 148 (1989).
13. J. T. Markert, E. A. Early, T. Bjornholm, S. Ghamaty, B. W. Lee, J. J. Neumeier, R. D. Price, C. L. Seaman, M. B. Maple, *Physica C*, *160*, 320 (1989).
14. E. Takayama-Muromachi, F. Izumi, Y. Uchida, K. Kato, H. Asano, *Physica C*, *159*, 634 (1989).
15. Y. Hidaka, M. Suzuki, *Nature*, *338*, 635 (1989).
16. J.-M. Tarascon, E. Wang, L. H. Greene, B. G. Bagley, G. W. Hull, S. M. D'Egidio, P. F. Miceli, Z. Z. Wang, T. W. Jing, J. Clayhold, D. Brawner, N. P. Ong, *Phys. Rev. B*, *40*, 4494 (1989).
17. H. Adachi, S. Hayashi, K. Setsune, S. Hatta, T. Mitsuyu, K. Wasa, *Appl. Phys. Lett.*, *54*, 2713 (1989).

17.3.10.2.2. Rare-Earth-Based Cuprates.

Applying pressure to a La–Ba–Cu–O sample caused an 8 K increase of T_c at a pressure of 14 kbar[1]. This immediately led to the amazing discovery of 94 K superconductivity in the Y–Ba–Cu–O system[2] by chemical substitution of the smaller Y ion into the La site of $La_{1.85}Ba_{0.15}CuO_4$ (214). The starting composition was $Y_{1.2}Ba_{0.8}CuO_{4-y}$, which followed the 214 formula of the K_2NiF_4 structure. Soon after the discovery, a number of laboratories were able to synthesize the 94 K superconductors and found that the composition of the superconducting phase was not $Y_{1.2}Ba_{0.8}CuO_{4-y}$ (214), but $YBa_2Cu_3O_{7-x}$ (123)[3–7]. Further studies on replacement of Y by rare earth elements (Nd, Gd, Sm, etc.) led to a series of 90–96 K superconductors[8,9]. Later, two new phases with the compositions $YBa_2Cu_4O_8$[10,11] and $Y_2Ba_4Cu_7O_{15}$[12,13] were also found to be superconducting at 80 and 90 K, respectively.

(i) Composition and Structure of $YBa_2Cu_3O_{7-x}$. The stoichiometric number of oxygen in $YBa_2Cu_3O_{7-x}$ can be changed from 7 ($x = 0$) to 6 ($x = 1.0$) by heat treatment.

It was found that the change of x from 0 to 1.0 resulted in a structural change from orthorhombic to tetragonal. The transition occurs at $x = 0.5$. The orthorhombic phase ($0 < x < 0.5$) is superconducting at T_c values ranging from 94 to 0 K depending on the exact oxygen content[14], whereas the tetragonal phase ($0.5 < x < 1.0$) is semiconducting[15,16].

XRD data showed that the structure of $YBa_2Cu_3O_{7-x}$ is an oxygen-deficient perovskite with tripling of the c axis caused by ordering of the Ba and Y atoms as shown in Figure 1 and belongs to the space group $Pmmm$[17]. Compared to the ideal perovskite, $YBa_2Cu_3O_{7-x}$ has two oxygen-deficient layers: in the first, the CuO layer (at $z = 0$), two oxygen atoms are missing at the midpoints of opposite edges, and in the other, the yttrium layer (at $z = 1/2$), all the oxygen atoms are missing. The copper atoms are located at two positions labeled Cu(1) and Cu(2). Cu(1) has fourfold planar coordination with two O(1) neighboring atoms along the c axis at a distance of ~ 1.85 Å and two O(4) atoms along the b axis at a distance of ~ 1.94 Å. Cu(2) has fivefold pyramidal

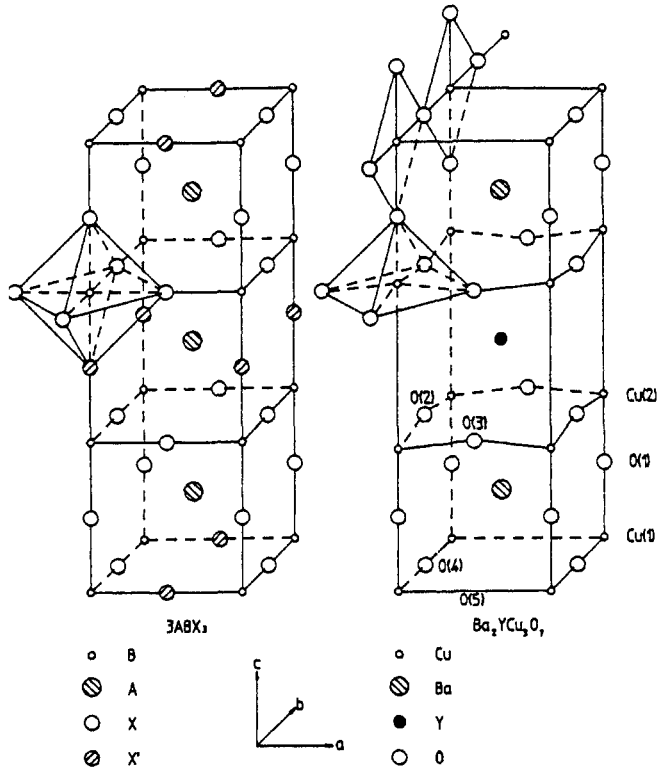

Figure 1. Structure of $Ba_2YCu_3O_{7.0}$ (right) and its relationship to the structure of perovskite (left). The atoms X′ are the oxygen atoms of perovskite that do not exist in the structure of $Ba_2YCu_3O_{7.0}$. As a consequence of this elimination, the typical chains are formed on the basel plane of the superconductor, and the atoms Cu(2) assume fivefold, pyramidal coordination.

coordination and is strongly bonded to two O(2) and two O(3) atoms with distances of ~1.93 Å (along the *b* axis) and ~1.96 Å (along the *a* axis), respectively. The fifth oxygen atom O(1) is weakly bonded to Cu(2) with a distance of ~2.3 Å (along the *c* axis). This weak Cu(2)–O(1) interaction confers a highly two-dimensional character to the CuO layers. The oxygen atoms O(2) and O(3) are almost exactly coplanar and are vertically displaced ~0.27 Å from the plane of the copper atoms Cu(2), producing the characteristic buckling of the CuO layers.

(ii) Synthesis of $YBa_2Cu_3O_{7-x}$. Single-phase $YBa_2Cu_3O_{7-x}$ can be prepared by mixing Y_2O_3, $BaCO_3$, and CuO, followed by grinding and heating at 950°C in air for several hours; pellets are formed at pressure, sintered at 950°C in flowing O_2 for several hours, and cooled to 200°C in O_2 before removal from the furnace. Additional treatment in O_2 at 700°C for several hours improves the transport superconducting properties further[18].

(iii) Growth of $YBa_2Cu_3O_{7-x}$ Single Crystals. Self-flux melt growth and top seeding techniques are commonly used to grow single crystal $YBa_2Cu_3O_{7-x}$[19–22]. For the self-flux melt growth, grams of Y_2O_3, $BaCO_3$, and CuO in a ratio of 0.5:4:8.5 were put in a ZrO_2 crucible, then heated at 880°C for tens of hours and furnace-cooled. After pulverizing, the material was heated in the same crucible at 1020°C for 15 min and cooled at a rate of 6°C/h to 960°C. The material was kept at this temperature for 24 h, then furnace-cooled to room temperature. Many blocklike single crystals were visible in the flux, and the flux had crept up on the crucible wall. To separate the crystals from the flux, the material was heated again for two days at 960°C and cooled at a rate of 10°C/h to 340°C. The maximum size of the crystals was close to 1 mm in both the *a* and *b* dimensions, but only 0.1 mm in the *c* direction[19].

(iv) Growth of $YBa_2Cu_3O_{7-x}$ Thin Films. Thin films of $YBa_2Cu_3O_{7-x}$ have been synthesized by several methods from different sources on different substrates ex situ or in situ. Excellent reviews on thin film growth of $YBa_2Cu_3O_{7-x}$ have been published[20–22]. The methods used include physical deposition such as sputtering, laser ablation, molecular beam epitaxy (MBE), and electron beam epitaxy (EBE), and chemical deposition such as regular chemical vapor deposition (CVD), metal–organic chemical vapor deposition (MOCVD), plasma-enhanced CVD and MOCVD, spray pyrolysis, and spin coating. Single or multiple sources of either metallic elements or oxide are possible. The substrates used are mainly $LaAlO_3$, $SrTiO_3$, MgO, yttrium-stabilized zirconia (YSZ), Al_2O_3, etc. Early work produced epitaxial films ex situ. Now, higher quality films are generated in situ. Among all these methods, sputtering and laser ablation were found to be the best techniques. For the in situ deposition, the substrates are normally mounted on a heater that is heated to about 700°C during deposition. Oxygen with a pressure of about 200 mtorr is maintained in the chamber during deposition. After deposition, the film is cooled to room temperature at an even higher oxygen pressure to fully oxygenate the film; the goal is to obtain a oxygen content in the range of 6.8–7.0 so that the films can reach T_c values higher than 90 K and J_c values higher than 10^6 A/cm^2, as well as showing good performance in magnetic field.

(v) Fabrication of Biaxially Textured $YBa_2Cu_3O_{7-x}$ on Metallic Substrates. Values of J_c over 10^6 A/cm^2 at 77 K and zero field can be reproducibly obtained on epitaxial thin films of $YBa_2Cu_3O_{7-x}$ made by different techniques on different substrates, whereas J_c values on randomly oriented polycrystalline samples are normally at least 100

times lower than those obtained on thin films. To achieve high J_c values close to 10^6 A/cm^2 on long length polycrystalline metallic substrates, the crystallographic orientation of the high T_c superconducting wire or tape must have a high degree of grain alignment, both out of plane and in plane, over the entire length of the conductor. Currently, two techniques can produce biaxially textured substrates and superconducting layer on top of them: ion-beam-assisted deposition (IBAD)[26–30] and rolling assisted biaxially textured substrates (RABiTS)[31,32]. Both techniques have produced biaxially textured $YBa_2Cu_3O_{7-x}$ tapes on Ni substrates having ceramic buffer layers, as well as J_c values of about 10^6 A/cm^2 at 77 K and zero field.

In the IBAD method, textured YSZ buffer layers were deposited on top of Ni-based alloys at room temperature by means of ion beam sputtering along with ion beam

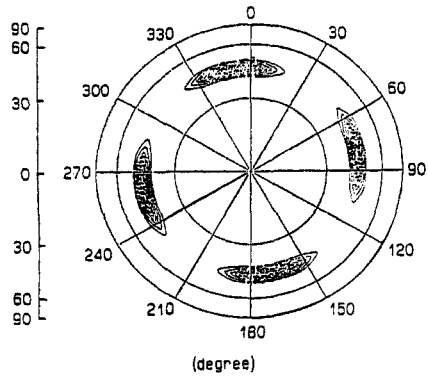

Figure 2. The X ray pole figure of $YBa_2Cu_3O_{7-x}$ (103) peak for the film grown on biaxially aligned YSZ layer deposited by IBAD.

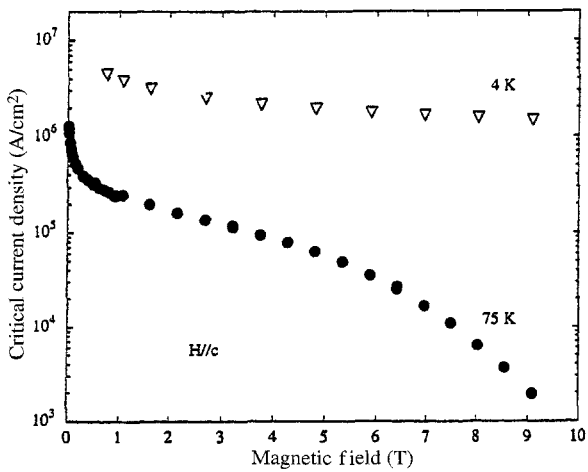

Figure 3. Critical current density as a function of magneic field for two samples (bottom: 1.3 μm thick and top: 1.1 μm thick) on mechanically polished metallic substrates for $H \| c$ and $H \perp I$. Both samples had a zero field J_c of $\sim 1 \times 10^6$ A/cm^2 at 75 K.

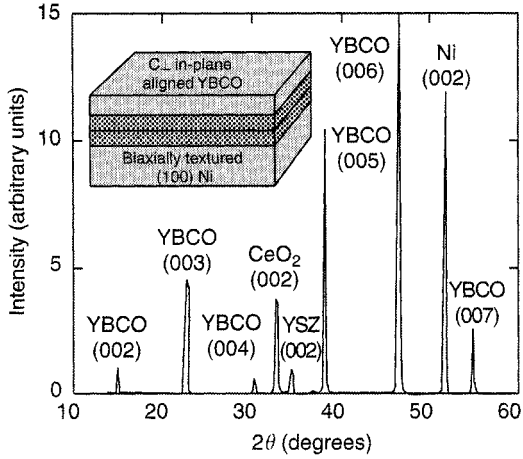

Figure 4. An XRD θ–2θ scan, along with a schematic representation, of a YBCO–YSZ–CeO_2–Ni multilayered structure. The XRD scan shows the out-of-plane (001) orientations of the YBCO and oxide buffer layers.

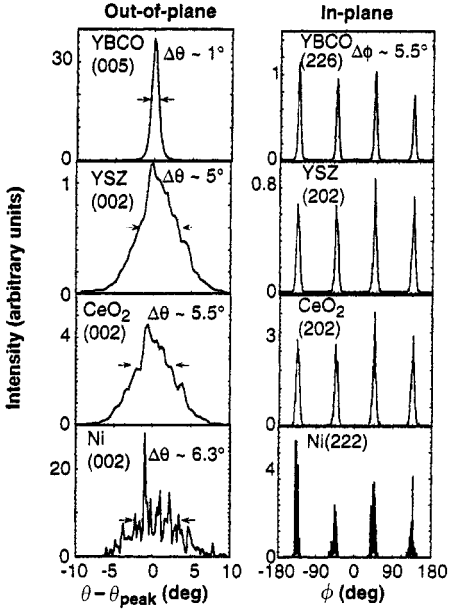

Figure 5. XRD rocking curves and ϕ scans showing the out-of-plane and in-plane texture of a YBCO–YSZ–CeO_2 multilayered structure on a rolled-textured Ni substrate.

assisting. After YSZ deposition, the samples were transferred to another vacuum chamber for pulsed laser ablation deposition of $YBa_2Cu_3O_{7-x}$ (YBCO) thick films. A thin ($\sim$200 Å) CeO_2 buffer layer was always deposited on top of YSZ for a better lattice match for the subsequent YBCO growth. The films were cooled to room

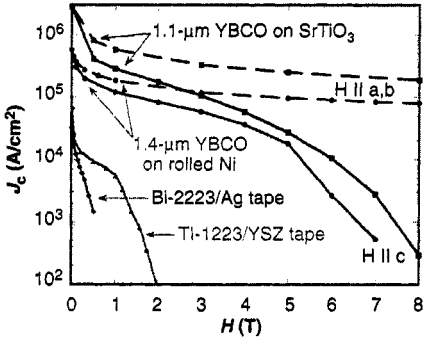

Figure 6. Magnetic field dependence of J_c, measured at 77 K, for a YBCO–YSZ–CeO_2–rolled-textured Ni (001) OSC, TI-1223 on polycrystalline YSZ, and Bi-2223/Ag tape.

temperature from the deposition temperature (700–900°C) in 300 torr of oxygen. The YBCO films were always *c* axis-aligned. The in-plane alignment was demonstrated by the X-ray pole figure of the YBCO (103) peak shown in Figure 2. The J_c dependence of the magnetic field was measured on two samples as shown in Figure 3.

By means of the RABiTS technique, in-plane textured Ni was obtained by cold rolling to 90% deformation followed by recrystallization at 1000°C for 4 h. A layer of CeO_2 was then deposited on top of the textured Ni by laser ablation. After the CeO_2 film was deposited, a layer of YSZ was deposited to alleviate cracking of CeO_2. Finally, a thick (>0.5 μm) YBCO film was deposited at 780°C in an O_2 pressure of 185 mtorr and cooled at 600°C/h to 400°C with O_2 pressure increasing to 700 torr. Figure 4 shows a θ–2θ XRD spectrum. The *c*-axis alignment is clearly seen. Out-of-plane and in-plane alignments were also demonstrated by XRD θ- and ϕ scans shown in Figure 5. The J_c dependence of magnetic field at 77 K for the film is shown in Figure 6, together with some other films for comparison[32].

(Z. REN, J. WANG)

1. C. W. Chu, P. H. Hor, R. L. Meng, L. Gao, Z. J. Huang, Y. Q. Wang, *Phys. Rev. Lett.*, *58*, 405 (1987).
2. M. K. Wu. J. R. Ashurn, C. J. Torng, P. H. Hor, R. L. Meng, L. Gao, Z. J. Huang, Y. Q. Wang, C. W. Chu, *Phys. Rev. Lett.*, *58*, 908 (1987).
3. R. J. Cava, B. Batlogg, R. B. van Dover, D. W. Murphy, S. Sunshine, T. Siegrist, J. P. Remeika, E. A. Rietman, S. Zahurak, G. P. Espinosa, *Phys. Rev. Lett.*, *58*, 1676 (1987).
4. P. M. Grant, R. B. Beyers, E. M. Engler, G. Lim, S. S. Parkin, M. L. Ramirez, V. Y. Lee, A. Nazzal, J. E. Vazquez, R. J. Savoy, *Phys. Rev. B*, *35*, 7242 (1987).
5. W. J. Gallagher, R. L. Sandstrom, T. R. Dinger, T. M. Shaw, D. A. Chance, *Solid State Commun.*, *63*, 147 (1987).
6. D. G. Hinks, L. Soderholm, D. W. Capone II, J. D. Jorgensen, I. K. Schuller, C. U. Segre, K. Zhang, J. D. Grace, *Appl. Phys. Lett.*, *50*, 1688 (1987).
7. R. Beyers, G. Lim, E. M. Engler, R. J. Savoy, T. M. Shaw, T. R. Dinger, W. J. Gallagher, R. L. Sanderstrom, *Appl. Phys. Lett.*, *50*, 1918 (1987).
8. J. M. Tarascon, W. R. McKinnon, L. H. Greene, G. W. Hull, E. M. Vogel, *Phys. Rev. B*, *36*, 226 (1987).
9. J. T. Markert, Y. Dalichaouch, M. B. Maple, *Physical Properties of High Temperature Superconductors* I, D. M. Ginsberg, ed., World Scientific, Teanek, NJ, 1989.

10. P. Marsh, R. M. Fleming, M. L. Mandich, A. M. DeSantolo, J. Kwo, M. Hong, L. J. Martinez-Miranda, *Nature, 334*, 141 (1988).
11. R. M. Hazen, L. W. Finger, D. E. Morris, *Appl. Phys. Lett., 54*, 1057 (1989).
12. P. Bordet, C. Chaillout, J. Chenavas, J. L. Hodeau, M. Marezio, J. Karpinski, E. Kaldis, *Nature, 334*, 596 (1988).
13. D. M. Pooke, R. G. Buckley, M. R. Presland, J. L. Tallon, *Phys. Rev. B, 41*, 6616 (1990).
14. R. J. Cava, B. Batlogg, C. H. Chen, E. A. Rietman, S. M. Zahurak, D. Werder, *Phys. Rev. B, 36*, 5719 (1987).
15. P. K. Gallagher, H. M. O'Bryan, S. A. Sunshine, D. W. Murphy, *Mater. Res. Bull., 22*, 995 (1987).
16. J. D. Jorgensen, B. W. Veal, W. K. Kwok, G. W. Crabtree, A. Umezawa, L. J. Nowicki, A. P. Paulikas, *Phys. Rev. B, 36*, 5731 (1987).
17. A. Santoro, *Chemistry of Superconductor Materials*, Edited by T. A. Vanderah, ed., Noyes Park Ridge, NJ, 1992.
18. R. J. Cava, Synthesis and crystal chemistry of high-T_c oxide superconductors, in *Processing and Properties of High-T_c Superconductors*, S. Jin, ed., World Scientific, River Edge, NJ, 1993.
19. M. J. V. Menken, K. Kadowaki, A. A. Menovsky, *J. Cryst. Growth, 96*, 1002 (1989).
20. T. Wolf, W. Goldacker, B. Obst, G. Roth, R. Flukiger, *J. Cryst. Growth, 96*, 1010 (1989).
21. S. M. Rao, B. H. Loo, N. P. Wang, R. J. Kelley, *J. Cryst. Growth, 110*, 989 (1991).
22. Z. F. Ren, Y. F. Chen, Y. D. Jiang, W. Y. Guan, *J. Mater. Sci. Lett., 9*, 738 (1990).
23. R. G. Humphreys, J. S. Satchell, N. G. Chew, J. A. Edwards, S. W. Goodyear, S. E. Blenkinsop, O. D. Dosser, A. G. Cullis, *Supercond. Sci. Technol., 3*, 38 (1990).
24. M. Schieber, *J. Cryst. Growth, 109*, 401 (1991).
25. T. R. Lemberger, *Physical Properties of High Temperature Superconductors*, Vol. III, D. M. Ginsberg, ed., World Scientific, River Edge, NJ, 1992.
26. Y. Iijima, N. Tanabe, O. Kohno, Y. Ikeno, *Appl. Phys. Lett., 60*, 769 (1992).
27. R. P. Reade, P. Berdahl, R. E. Russo, S. M. Garrison, *Appl. Phys. Lett., 61*, 2231 (1992).
28. X. D. Wu, S. R. Foltyn, P. N. Arendt, W. R. Blumenthal, I. H. Campbell, J. D. Cotton, J. Y. Coulter, W. L. Hults, M. P. Maley, H. F. Safar, J. L. Smith, *Appl. Phys. Lett., 67*, 2397 (1995).
29. M. Fukutomi, S. Aoki, K. Komori, R. Chatterjee, H. Maeda, *Physica C, 219*, 333 (1994).
30. F. Yang, E. Narumi, S. Patel, D. T. Shaw, *Physica C, 244*, 299 (1995).
31. A. Goyal, D. P. Norton, J. D. Budai, M. Paranthaman, E. D. Specht, D. M. Kroeger, D. K. Christen, Q. He, B. Saffian, F. A. List, D. F. Lee, P. M. Martin, C. E. Klabunde, E. Hartfield, V. K. Sikka, *Appl. Phys. Lett., 69*, 1795 (1996).
32. D. P. Norton, A. Goyal, J. D. Budai, D. K. Christen, D. M. Kroeger, E. D. Specht, Q. He, B. Saffian, M. Paranthaman, C. E. Klabunde, D. F. Lee, B. C. Sales, F. A. List, *Science, 274*, 755 (1996).

17.3.10.2.3. Bismuth-Based Cuprates.

Superconductivity at about 10 K was first observed in the Bi–Sr–Cu–O system[1]. Right after that report, double superconducting transition temperatures at 85 and 110 K were observed after Ca was added to the Bi–Sr–Cu–O system[2]. These discoveries led to worldwide attempts to prepare single-phase samples of the phases responsible for transitions at 85 and 110 K, respectively. These efforts led to the conclusion that all the superconducting phases can be described by the general formula $Bi_2Sr_2Ca_{n-1}Cu_nO_{2n+4}$, with $n = 1$, 2, and 3 corresponding to $Bi_2Sr_2CuO_6$ (Bi-2201), $Bi_2Sr_2CaCu_2O_8$ (Bi-2212), and $Bi_2Sr_2Ca_2Cu_3O_{10}$ (Bi-2223) phases, respectively.

(i) Structure of Bi-2212 and Bi-2223. The structures of Bi-2201, Bi-2212, and Bi-2223 are shown in Figure 1. Bi-2212 contains double sheets of corner-sharing CuO_4 units oriented in the (001) plane, and each copper atom has one additional oxygen atom positioned above or below the CuO_2 sheet to form square pyramids. Ca atoms reside between CuO_2 sheets in eightfold coordination with oxygen. Sr atoms reside just above and below the double CuO_2 sheets. These Sr–Cu–Ca–O perovskite slabs are interconnected by a rock salt-related double bismuth–oxygen layer. The structure of Bi-2223 is

Inorganic Reactions and Methods, Volume 18
Edited by J. J. Zuckerman, Jim D. Atwood

10. P. Marsh, R. M. Fleming, M. L. Mandich, A. M. DeSantolo, J. Kwo, M. Hong, L. J. Martinez-Miranda, *Nature*, *334*, 141 (1988).
11. R. M. Hazen, L. W. Finger, D. E. Morris, *Appl. Phys. Lett.*, *54*, 1057 (1989).
12. P. Bordet, C. Chaillout, J. Chenavas, J. L. Hodeau, M. Marezio, J. Karpinski, E. Kaldis, *Nature*, *334*, 596 (1988).
13. D. M. Pooke, R. G. Buckley, M. R. Presland, J. L. Tallon, *Phys. Rev. B*, *41*, 6616 (1990).
14. R. J. Cava, B. Batlogg, C. H. Chen, E. A. Rietman, S. M. Zahurak, D. Werder, *Phys. Rev. B*, *36*, 5719 (1987).
15. P. K. Gallagher, H. M. O'Bryan, S. A. Sunshine, D. W. Murphy, *Mater. Res. Bull.*, *22*, 995 (1987).
16. J. D. Jorgensen, B. W. Veal, W. K. Kwok, G. W. Crabtree, A. Umezawa, L. J. Nowicki, A. P. Paulikas, *Phys. Rev. B*, *36*, 5731 (1987).
17. A. Santoro, *Chemistry of Superconductor Materials*, Edited by T. A. Vanderah, ed., Noyes Park Ridge, NJ, 1992.
18. R. J. Cava, Synthesis and crystal chemistry of high-T_c oxide superconductors, in *Processing and Properties of High-T_c Superconductors*, S. Jin, ed., World Scientific, River Edge, NJ, 1993.
19. M. J. V. Menken, K. Kadowaki, A. A. Menovsky, *J. Cryst. Growth*, *96*, 1002 (1989).
20. T. Wolf, W. Goldacker, B. Obst, G. Roth, R. Flukiger, *J. Cryst. Growth*, *96*, 1010 (1989).
21. S. M. Rao, B. H. Loo, N. P. Wang, R. J. Kelley, *J. Cryst. Growth*, *110*, 989 (1991).
22. Z. F. Ren, Y. F. Chen, Y. D. Jiang, W. Y. Guan, *J. Mater. Sci. Lett.*, *9*, 738 (1990).
23. R. G. Humphreys, J. S. Satchell, N. G. Chew, J. A. Edwards, S. W. Goodyear, S. E. Blenkinsop, O. D. Dosser, A. G. Cullis, *Supercond. Sci. Technol.*, *3*, 38 (1990).
24. M. Schieber, *J. Cryst. Growth*, *109*, 401 (1991).
25. T. R. Lemberger, *Physical Properties of High Temperature Superconductors*, Vol. III, D. M. Ginsberg, ed., World Scientific, River Edge, NJ, 1992.
26. Y. Iijima, N. Tanabe, O. Kohno, Y. Ikeno, *Appl. Phys. Lett.*, *60*, 769 (1992).
27. R. P. Reade, P. Berdahl, R. E. Russo, S. M. Garrison, *Appl. Phys. Lett.*, *61*, 2231 (1992).
28. X. D. Wu, S. R. Foltyn, P. N. Arendt, W. R. Blumenthal, I. H. Campbell, J. D. Cotton, J. Y. Coulter, W. L. Hults, M. P. Maley, H. F. Safar, J. L. Smith, *Appl. Phys. Lett.*, *67*, 2397 (1995).
29. M. Fukutomi, S. Aoki, K. Komori, R. Chatterjee, H. Maeda, *Physica C*, *219*, 333 (1994).
30. F. Yang, E. Narumi, S. Patel, D. T. Shaw, *Physica C*, *244*, 299 (1995).
31. A. Goyal, D. P. Norton, J. D. Budai, M. Paranthaman, E. D. Specht, D. M. Kroeger, D. K. Christen, Q. He, B. Saffian, F. A. List, D. F. Lee, P. M. Martin, C. E. Klabunde, E. Hartfield, V. K. Sikka, *Appl. Phys. Lett.*, *69*, 1795 (1996).
32. D. P. Norton, A. Goyal, J. D. Budai, D. K. Christen, D. M. Kroeger, E. D. Specht, Q. He, B. Saffian, M. Paranthaman, C. E. Klabunde, D. F. Lee, B. C. Sales, F. A. List, *Science*, *274*, 755 (1996).

17.3.10.2.3. Bismuth-Based Cuprates.

Superconductivity at about 10 K was first observed in the Bi–Sr–Cu–O system[1]. Right after that report, double superconducting transition temperatures at 85 and 110 K were observed after Ca was added to the Bi–Sr–Cu–O system[2]. These discoveries led to worldwide attempts to prepare single-phase samples of the phases responsible for transitions at 85 and 110 K, respectively. These efforts led to the conclusion that all the superconducting phases can be described by the general formula $Bi_2Sr_2Ca_{n-1}Cu_nO_{2n+4}$, with $n = 1$, 2, and 3 corresponding to $Bi_2Sr_2CuO_6$ (Bi-2201), $Bi_2Sr_2CaCu_2O_8$ (Bi-2212), and $Bi_2Sr_2Ca_2Cu_3O_{10}$ (Bi-2223) phases, respectively.

(i) Structure of Bi-2212 and Bi-2223. The structures of Bi-2201, Bi-2212, and Bi-2223 are shown in Figure 1. Bi-2212 contains double sheets of corner-sharing CuO_4 units oriented in the (001) plane, and each copper atom has one additional oxygen atom positioned above or below the CuO_2 sheet to form square pyramids. Ca atoms reside between CuO_2 sheets in eightfold coordination with oxygen. Sr atoms reside just above and below the double CuO_2 sheets. These Sr–Cu–Ca–O perovskite slabs are interconnected by a rock salt-related double bismuth–oxygen layer. The structure of Bi-2223 is

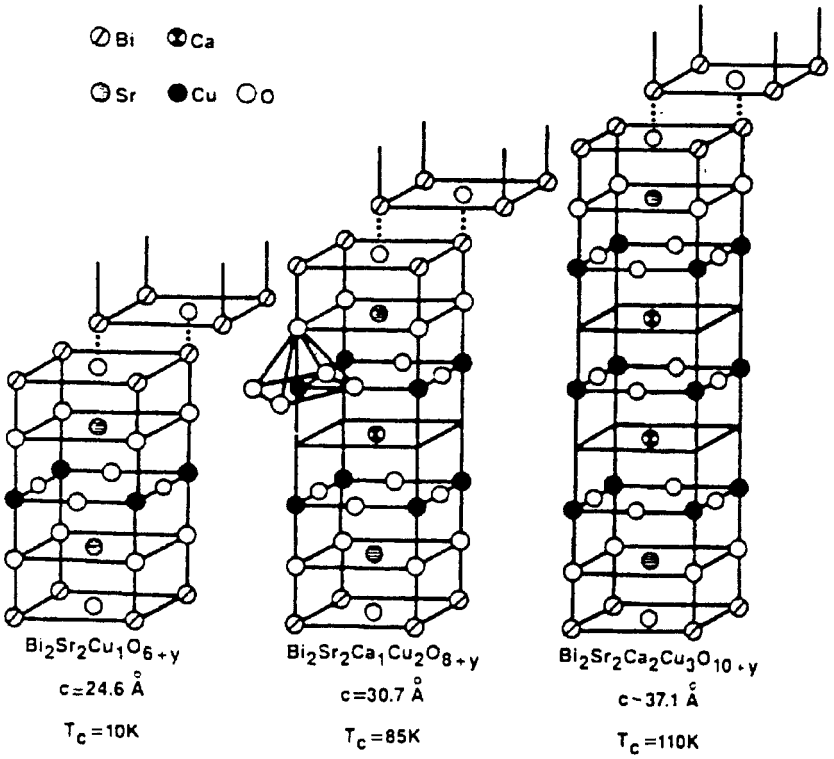

Figure 1. The crystal structures of $Bi_2Sr_2Ca_{(n-1)}Cu_nO_{(2n+4)}$ ($n = 1, 2, 3$).

similar to that of Bi-2212. The only difference between Bi-2223 and Bi-2212 is that there is one more CuO_2 layer and one more Ca layer in each unit cell of Bi-2223.

(ii) Synthesis of Bi-2212 and Bi-2223. In the synthesis of Bi-2212 and Bi-2223, Bi_2O_3, $SrCO_3$, $CaCO_3$, and CuO are often used as starting materials. These powders are mixed in stoichiometric ratios, ground in an agate mortar, and heated in an Al_2O_3 crucible at 810–820°C (Bi-2212) for 3–5 h. It is important that this initial heat treatment be carried out below the melting point of Bi_2O_3 ($\approx$825°C) to allow for reaction of the Bi_2O_3 before melting. The samples are cooled to room temperature, ground, pressed into pellets, and heated at 830°C for 3–5 h. Then the temperature is raised 10–15°C and the process is repeated until no further change is observed in the XRD pattern. Typically, heating up to 900°C four to six times is required to reach equilibrium.

Synthesis of Bi-2223 is much more difficult due because of the intergrowth of Bi-2212 phase. The successful synthesis of phase-pure Bi-2223 was not achieved until the discovery that a small amount of Pb was needed to enhance the formation of the 110 K phase[3]. This led to significant efforts to synthesize Pb-stabilized 110 K phase[4,5]. Powders of Bi_2O_3, PbO, $SrCO_3$, $CaCO_3$, and CuO in the appropriate ratios were mixed and heated at 795°C for 15 h, reground, and pressed into pellets. The pellets were sintered in air at 858°C for 90 h and reground. New pellets were pressed, sintered a second time in air

at 858°C for 65 h, then cooled at 60–150°C/h to room temperature. Phase-pure Bi-2223 samples were prepared in a wide range of compositions with the addition of 0.2–0.4 formula weight Pb. These samples show a T_c (zero resistance) above 105 K and a substantial Meissner fraction.

(iii) Growth of Bi-2212 Single Crystals. Single crystals have been grown from self-flux melts[6–10] and alkali chloride melts[11]. For the self-flux melt growth, a well-mixed charge of Bi_2O_3, $SrCO_3$, $CaCO_3$, and CuO in an appropriate stoichiometric ratio was put in a gold or ceramic vessel, heated to 1200°C, held at that temperature for 2 h, then slowly cooled to 950°C, followed by cooling at a rate of 3–4°C/h to 800°C, and finally by cooling to room temperature at a rate of 10°C/h. The crystals can be extracted from the solidified content by crashing the crucible. Normally the crystals are very thin plates, since coupling between the double bismuth layers is weak. As-made crystals have T_c values in the range of 80–90 K depending on factors such as starting composition and cooling rate.

(iv) Growth of Bi-2212 and Bi-2223 Thin Films. Thin film growth of Bi-2212 has been attempted by laser ablation[12,13], dc sputtering[14–16], MBE[17], MOCVD[18], etc. For dc sputtering, a stoichiometric Bi-2212 target is made first, then sputtered with an oxygen pressure about 2–5 mbar, at a substrate temperature of 750–860°C. A wide variety of substrates have been successfully used. As-grown Bi-2212 film shows the *c* axis aligned normal to the substrate plane. The T_c values are very sensitive to the oxygen content, as shown in Figure 2.

Bi-2223 films have been grown by laser ablation[19,20], sputtering[21–23], MOCVD[24], etc. Phase-pure Bi-2223 film is much more difficult to grow than comparable Bi-2212 film

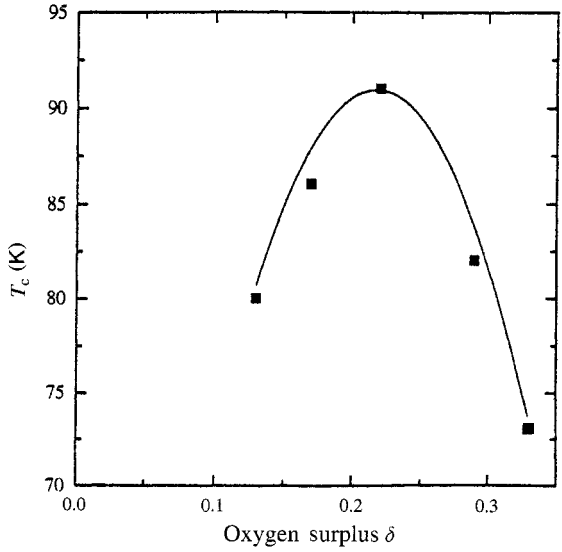

Figure 2. Parabolic dependence of T_c of BSCCO films on oxygen surplus δ; points indicate measured data, solid line, fit using quadratic equation.

owing to the intergrowth nature of 2223 with 2212 and 2201. Figure 3 shows a typical XRD spectrum of the Bi-2223 film with 2212 and 2201 as the minor phases. The as-grown films typically have T_c values substantially lower than 110 K obtained in the bulk samples. The highest T_c obtained on Bi-2223 film is about 102.5 K as shown in Figure 4[22].

(v) Fabrication of Bi-2212 and Bi-2223 Tapes. For bulk high T_c materials to be commercially useful in high field magnets, energy storage devices, motors/generators, or power transmission cables, they have to be shaped into long length composite multifilamentary wires or ribbons containing both the superconductors and normal metal. The

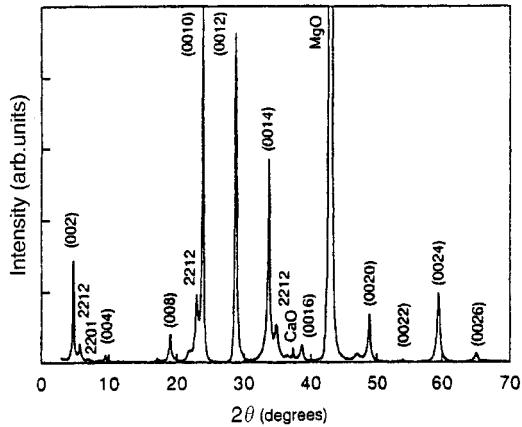

Figure 3. X-ray diffraction pattern of an as-grown $Bi_{2.0}Sr_{2.0}Ca_{2.0}Cu_{3.0}O_x$ film showing the critical temperature of 102.5 K. The diffraction lines of the pattern are indexed as the (002n) lines of 2223 phase.

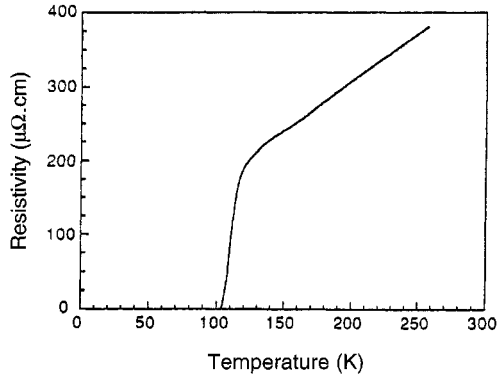

Figure 4. Temperature dependence of resistivity of an as-grown $Bi_{2.0}Sr_{2.0}Ca_{2.0}Cu_{3.0}O_x$ film with 2201 phase buffer layer showing the critical temperature of 102.5 K.

high T_c ceramic superconductors are brittle and cannot be drawn into fine wires. However, several different approaches to the fabrication of Bi-2212 and Bi-2223 wires have been reported. Up to now, the powder-in-tube (PIT) technique has played the most important role in the fabrication of long length, Bi-based superconducting wires of both Bi-2212 and Bi-2223.

Bi-2212 tapes were made by the PIT method[25]. Appropriate amounts of Bi_2O_3, $SrCO_3$, $CaCO_3$, and CuO were thoroughly mixed and calcined in three steps in the

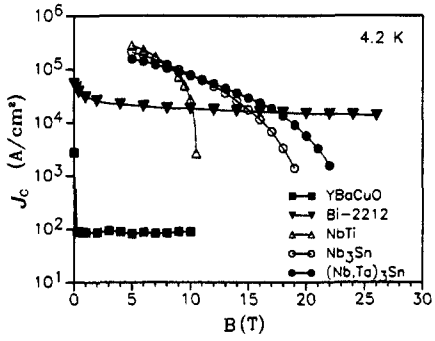

Figure 5. Critical current density of Bi-2212/Ag and $YBa_2Cu_3O_7$/Ag wires at 4.2 K in comparison with commercial NbTi, Nb_3Sn, and $(Nb,Ta)_3$ Sn multifilamentary wires (noncopper J_c)

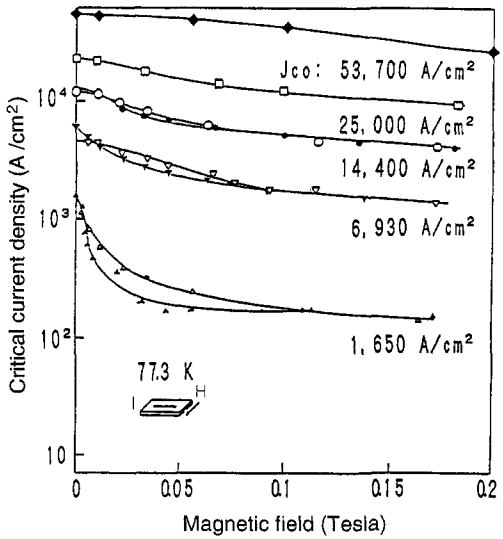

Figure 6. Magnetic field dependence of J_c of silver-sheathed Bi-2223 superconducting wire at up to 0.2 T: solid symbols, increasing magnetic field; open symbols, decreasing magnetic field.

temperature range of 800–850°C. After each calcination step, the powder was ground to improve homogeneity. The powder was then filled into a Ag tube, subsequently drawn to the final diameter required, and compressed between steel rollers. The specimens were cut off and subjected to a final annealing procedure at temperatures above 800°C to optimize superconducting properties of the Bi-2212 phase. The annealed Bi-2212 tapes show T_c (zero resistance) of about 85 K. The J_c dependence of magnetic field is shown in Figure 5. Clearly, at 4.2 K, Bi-2212 has the highest J_c value at 26 T.

For fabrication of Bi-2223 wires[26], appropriate amounts of Bi_2O_3, PbO, $SrCO_3$, $CaCO_3$, and CuO were mixed and calcined from 750°C to 860°C for 8–200 h, filled in a silver tube, drawn to a round wire, rolled or pressed into a flat tape, and then sintered.

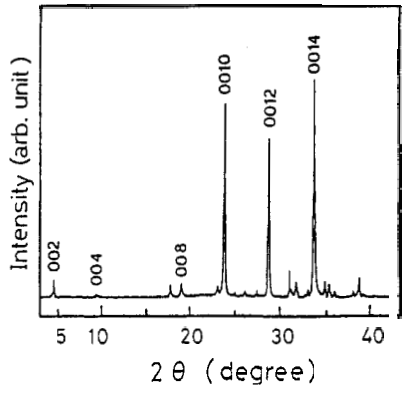

Figure 7. X-ray diffraction pattern for Bi-2223 superconductor inside silver sheath.

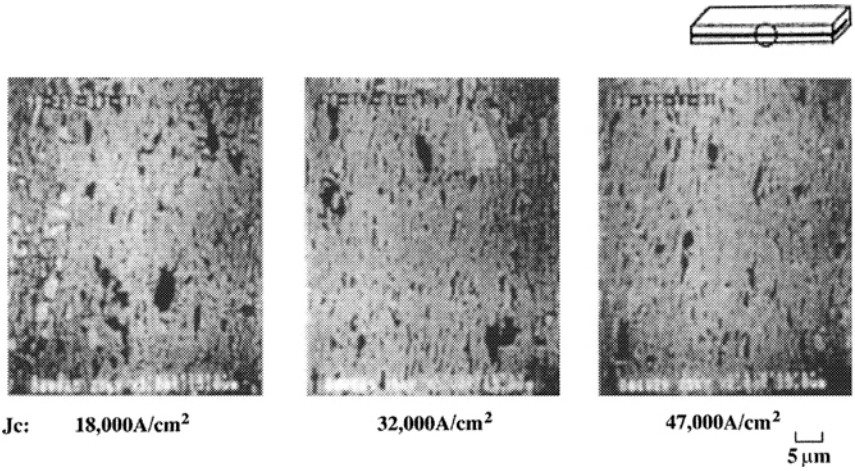

Figure 8. SEM micrographs of a longitudinal cross-sectional view of Bi-2223 superconductors inside silver sheathing.

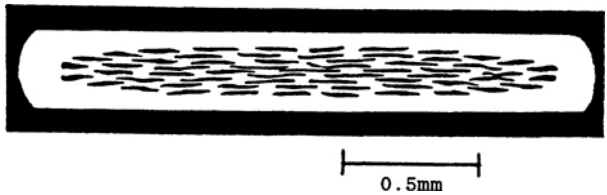

Figure 9. Cross-sectional view of a 61-filamentary wire.

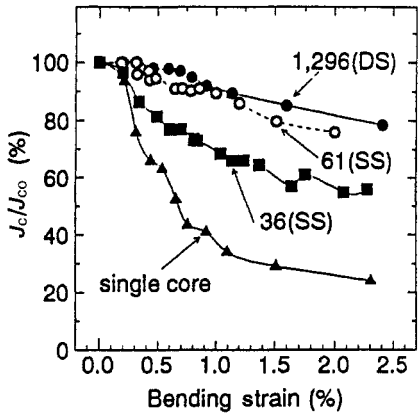

Figure 10. Bending strain characteristics of single-core and 36-, 61-, and 1296-filamentary wires.

The forming and sintering processes were repeated. The first sintering homogenized the high T_c phase (110 K), and the second sintering greatly improved the connectivity between the platelike grains. The T_c of these tapes was above 106 K. The typical size of these tape was 0.1–0.3 mm thick and 2–4 mm wide including the silver sheath. The thickness of the superconducting core was about one-third of the total thickness. A maximum J_c at 77 K and zero field reached 53,700 A/cm^2. Figure 6 shows the magnetic field dependence of J_c at up to 0.2 T and 77.3 K for tapes having different values of J_c. The microstructures of the superconducting core were investigated by XRD, scanning electron microscopy (SEM), and transmission electron microscopy (TEM). Figure 7 shows the XRD spectra indicating a strong c-axis alignment of the Bi-2223 phase with a small amount of impurity such as Ca_2PbO_4. Figure 8, a typical SEM micrograph of samples with different values of J_c, shows that higher J_c corresponds to more dense 2223 phase. To minimize the ac loss and increase the bending tolerance, multifilamentary tape is required. Figure 9 shows a cross-sectional view of a 61- filamentary tape. The J_c dependence on bending strain of the multifilamentary tape is shown in Figure 10[26].

Using these Bi-2212 and 2223 tapes, large current conductors[26], coils and magnets[26], and other products have been successfully made.

(Z. REN, J. WANG)

1. C. Michel, H. Hervieu, M. M. Borel, A. Grandin, F. Deslendes, J. Provost, B. Raveau, *Z. Phys. B*, *68*, 421 (1987).
2. H. Maeda, Y. Tanaka, M. Fukutomi, T. Assano, *Jpn. J. Appl. Phys.*, *27*, L209 (1988).
3. S. A. Sunshine, T. Siegrist, L. F. Schneemeyer, D. W. Murphy, R. J. Cava, B. Batlogg, R. B. van Dover, R. M. Fleming, S. H. Glarum, S. Nakahara, R. Farrow, J. J. Krajewski, S. M. Zahurak, J. V. Waszczak, J. H. Marshall, P. Marsh, L. W. Rupp Jr., W. F. Peck, *Phys. Rev. B*, *38*, 893 (1988).
4. H. Sasakura, S. Minamigawa, K. Nakahigashi, M. Kogachi, S. Nokanishi, N. Fukuoka, M. Yoshikawa, S. Noguchi, K. Okuda, A. Yanase, *Jpn. J. Appl. Phys.*, *28*, L1163 (1989).
5. S. Koyama, U. Endo, T. Kawai, *Jpn. J. Appl. Phys.*, *27*, L1861 (1988).
6. M. Hikita, T. Iwata, Y. Tajima, A. Katsui, *J. Cryst. Growth*, *91*, 282 (1988).
7. L. W. Lombardo, A. Kapitulnik, *J. Cryst. Growth*, *118*, 483 (1992).
8. P. D. Han, D. A. Payne, *J. Cryst. Growth*, *104*, 201 (1990).
9. Z. F. Ren, X. L. Yan, Y. D. Jiang, W. Y. Guan, *J. Cryst. Growth*, *92*, 677 (1988).
10. T. Fujii, Y. Nagano, J. Shirafuji, *J. Cryst. Growth*, *110*, 994 (1991).
11. L. F. Schneemeyer, R. B. van Dover, S. H. Glarum, S. A. Sunshine, R. M. Fleming, B. Batlogg, T. Siegrist, J. H. Marshall, J. V. Waszczak, L. W. Rupp, *Nature*, *332*, 422 (1988).
12. S. Zhu, D. H. Lowndes, B. C. Chakoumakos, J. D. Budai, D. K. Christen, X. Y. Zheng, E. Jones, B. Warmack, *Appl. Phys. Lett.*, *63*, 409 (1993).
13. P. Schmitt, L. Schultz, G. Saemann-Ischenko, *Physica C*, *168*, 475 (1990).
14. A. M. Cucolo, R. Di Leo, P. Romano, E. Bacca, M. E. Gomez, W. Lopera, P. Prieto, J. Heiras, *Appl. Phys. Lett.*, *68*, 253 (1996).
15. J. Auge, U. Rudiger, H. Frank, H. G. Roskos, G. Guntherodt, *Appl. Phys. Lett.*, *64*, 378 (1994).
16. P. Wagner, H. Adrian, C. Tome-Rosa, *Physica C*, *195*, 258 (1992).
17. J. N. Eckstein, I. Bozovic, M. Klausmeier-Brown, G. Virshup, *Thin Solid Films*, *216*, 8 (1992).
18. T. Sugimoto, M. Yashida, K. Yamaguchi, K. Sugawara, Y. Shioharu, S. Tanaka, *Appl. Phys. Lett.*, *57*, 928 (1990).
19. T. Kawai, Y. Egami, H. Tabata, S. Kawai, *Nature*, *349*, 200 (1991).
20. A. Sajjadi, I. W. Boyd, *Appl. Phys. Lett.*, *63*, 3373 (1993).
21. M. Ohkubo, J. Geerk, G. Linker, O. Meyer, *Appl. Phys. Lett.*, *67*, 2403 (1995).
22. K. Ohbayashi, T. Ohtsuki, H. Matsushita, H. Nishiwaki, Y. Takai, H. Hayakawa, *Appl. Phys. Lett.*, *64*, 369 (1994).
23. M. Ohkubo, E. Brecht, G. Linker, J. Geerk, O. Meyer, *Appl. Phys. Lett.*, *69*, 574 (1995).
24. K. Endo, H. Yamasaki, S. Misawa, S. Yoshida, K. Kajimura, *Nature*, *355*, 327 (1992).
25. K. Heine, J. Tenbrink, M. Thoner, *Appl. Phys. Lett.*, *55*, 2441 (1989).
26. K. Sato, in *Processing and Properties of High-T_c Superconductors*, S. Jin, ed., World Scientific, River Edge, NJ, 1993.

17.3.10.2.4. Thallium-Based Cuprates.

Within weeks after superconductivity was observed above 77 K in the Bi–Sr–Ca–Cu–O system, a T_c value of 120 K was reported in Tl–Ba–Ca–Cu–O system[1]. The results, which were quickly reproduced by other groups[2–8], revealed that two series of phases exist in this system with generalized chemical formula $Tl_2Ba_2Ca_{n-1}Cu_nO_{2n+4}$ and $Tl_{1-x}M_xA_2Ca_{n-1}Cu_nO_{2n+3}$ (A = Ba or Sr or a combination of both, M = Pb or Bi or a combination of both). The former is referred to as "thallium bilayers", and the latter "thallium monolayers". For the thallium bilayers, the numerical acronyms Tl-2201, Tl-2212, Tl-2223, and Tl-2234 were used with n = 1, 2, 3, and 4, respectively, and Tl-1201, Tl-1212, Tl-1223, and Tl-1234 were used for the thallium monolayers[9]. The schematic structures are shown in Figures 1 and 2[9]. The situation in thallium monolayers is much more complicated than the simple acronyms suggest because A can be either Ba or Sr or a combination of both, and Tl can be partially replaced by either Pb or Bi or a combination of both. Table 1 shows the chemical formula, the acronym, and the corresponding T_c for each composition. It is not only impractical to describe each one in detail but unnecessary, owing to the structural similarities among them. Therefore, Tl-2201 and

Inorganic Reactions and Methods, Volume 18
Edited by J. J. Zuckerman, Jim D. Atwood

1. C. Michel, H. Hervieu, M. M. Borel, A. Grandin, F. Deslendes, J. Provost, B. Raveau, *Z. Phys. B*, *68*, 421 (1987).
2. H. Maeda, Y. Tanaka, M. Fukutomi, T. Assano, *Jpn. J. Appl. Phys.*, *27*, L209 (1988).
3. S. A. Sunshine, T. Siegrist, L. F. Schneemeyer, D. W. Murphy, R. J. Cava, B. Batlogg, R. B. van Dover, R. M. Fleming, S. H. Glarum, S. Nakahara, R. Farrow, J. J. Krajewski, S. M. Zahurak, J. V. Waszczak, J. H. Marshall, P. Marsh, L. W. Rupp Jr., W. F. Peck, *Phys. Rev. B*, *38*, 893 (1988).
4. H. Sasakura, S. Minamigawa, K. Nakahigashi, M. Kogachi, S. Nokanishi, N. Fukuoka, M. Yoshikawa, S. Noguchi, K. Okuda, A. Yanase, *Jpn. J. Appl. Phys.*, *28*, L1163 (1989).
5. S. Koyama, U. Endo, T. Kawai, *Jpn. J. Appl. Phys.*, *27*, L1861 (1988).
6. M. Hikita, T. Iwata, Y. Tajima, A. Katsui, *J. Cryst. Growth*, *91*, 282 (1988).
7. L. W. Lombardo, A. Kapitulnik, *J. Cryst. Growth*, *118*, 483 (1992).
8. P. D. Han, D. A. Payne, *J. Cryst. Growth*, *104*, 201 (1990).
9. Z. F. Ren, X. L. Yan, Y. D. Jiang, W. Y. Guan, *J. Cryst. Growth*, *92*, 677 (1988).
10. T. Fujii, Y. Nagano, J. Shirafuji, *J. Cryst. Growth*, *110*, 994 (1991).
11. L. F. Schneemeyer, R. B. van Dover, S. H. Glarum, S. A. Sunshine, R. M. Fleming, B. Batlogg, T. Siegrist, J. H. Marshall, J. V. Waszczak, L. W. Rupp, *Nature*, *332*, 422 (1988).
12. S. Zhu, D. H. Lowndes, B. C. Chakoumakos, J. D. Budai, D. K. Christen, X. Y. Zheng, E. Jones, B. Warmack, *Appl. Phys. Lett.*, *63*, 409 (1993).
13. P. Schmitt, L. Schultz, G. Saemann-Ischenko, *Physica C*, *168*, 475 (1990).
14. A. M. Cucolo, R. Di Leo, P. Romano, E. Bacca, M. E. Gomez, W. Lopera, P. Prieto, J. Heiras, *Appl. Phys. Lett.*, *68*, 253 (1996).
15. J. Auge, U. Rudiger, H. Frank, H. G. Roskos, G. Guntherodt, *Appl. Phys. Lett.*, *64*, 378 (1994).
16. P. Wagner, H. Adrian, C. Tome-Rosa, *Physica C*, *195*, 258 (1992).
17. J. N. Eckstein, I. Bozovic, M. Klausmeier-Brown, G. Virshup, *Thin Solid Films*, *216*, 8 (1992).
18. T. Sugimoto, M. Yashida, K. Yamaguchi, K. Sugawara, Y. Shioharu, S. Tanaka, *Appl. Phys. Lett.*, *57*, 928 (1990).
19. T. Kawai, Y. Egami, H. Tabata, S. Kawai, *Nature*, *349*, 200 (1991).
20. A. Sajjadi, I. W. Boyd, *Appl. Phys. Lett.*, *63*, 3373 (1993).
21. M. Ohkubo, J. Geerk, G. Linker, O. Meyer, *Appl. Phys. Lett.*, *67*, 2403 (1995).
22. K. Ohbayashi, T. Ohtsuki, H. Matsushita, H. Nishiwaki, Y. Takai, H. Hayakawa, *Appl. Phys. Lett.*, *64*, 369 (1994).
23. M. Ohkubo, E. Brecht, G. Linker, J. Geerk, O. Meyer, *Appl. Phys. Lett.*, *69*, 574 (1995).
24. K. Endo, H. Yamasaki, S. Misawa, S. Yoshida, K. Kajimura, *Nature*, *355*, 327 (1992).
25. K. Heine, J. Tenbrink, M. Thoner, *Appl. Phys. Lett.*, *55*, 2441 (1989).
26. K. Sato, in *Processing and Properties of High-T_c Superconductors*, S. Jin, ed., World Scientific, River Edge, NJ, 1993.

17.3.10.2.4. Thallium-Based Cuprates.

Within weeks after superconductivity was observed above 77 K in the Bi–Sr–Ca–Cu–O system, a T_c value of 120 K was reported in Tl–Ba–Ca–Cu–O system[1]. The results, which were quickly reproduced by other groups[2–8], revealed that two series of phases exist in this system with generalized chemical formula $Tl_2Ba_2Ca_{n-1}Cu_nO_{2n+4}$ and $Tl_{1-x}M_xA_2Ca_{n-1}Cu_nO_{2n+3}$ (A = Ba or Sr or a combination of both, M = Pb or Bi or a combination of both). The former is referred to as "thallium bilayers", and the latter "thallium monolayers". For the thallium bilayers, the numerical acronyms Tl-2201, Tl-2212, Tl-2223, and Tl-2234 were used with n = 1, 2, 3, and 4, respectively, and Tl-1201, Tl-1212, Tl-1223, and Tl-1234 were used for the thallium monolayers[9]. The schematic structures are shown in Figures 1 and 2[9]. The situation in thallium monolayers is much more complicated than the simple acronyms suggest because A can be either Ba or Sr or a combination of both, and Tl can be partially replaced by either Pb or Bi or a combination of both. Table 1 shows the chemical formula, the acronym, and the corresponding T_c for each composition. It is not only impractical to describe each one in detail but unnecessary, owing to the structural similarities among them. Therefore, Tl-2201 and

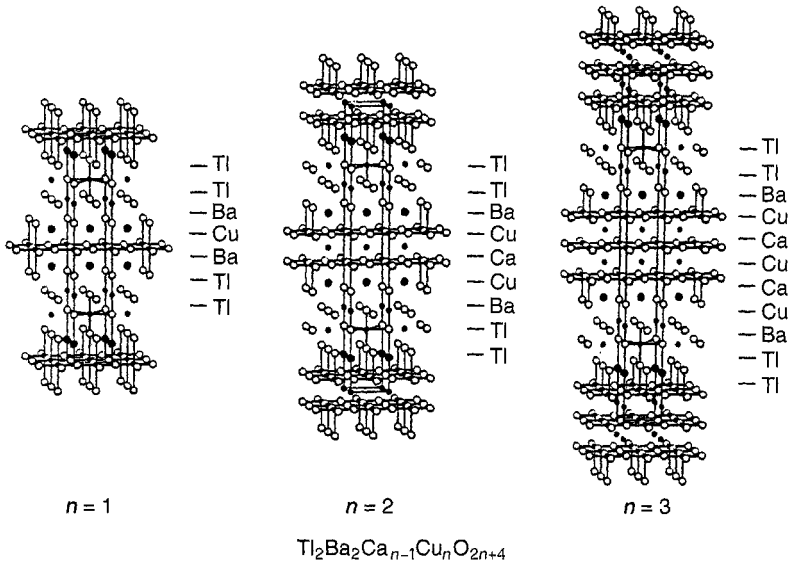

Figure 1. Structures of $Tl_2Ba_2Ca_{n-1}Cu_nO_{2n+4}$ ($n = 1, 2, 3$) Thallium atoms are shown on ideal (octahedral-type) sites for clarity. Metal atoms are solid Cu–O bonds are shown.

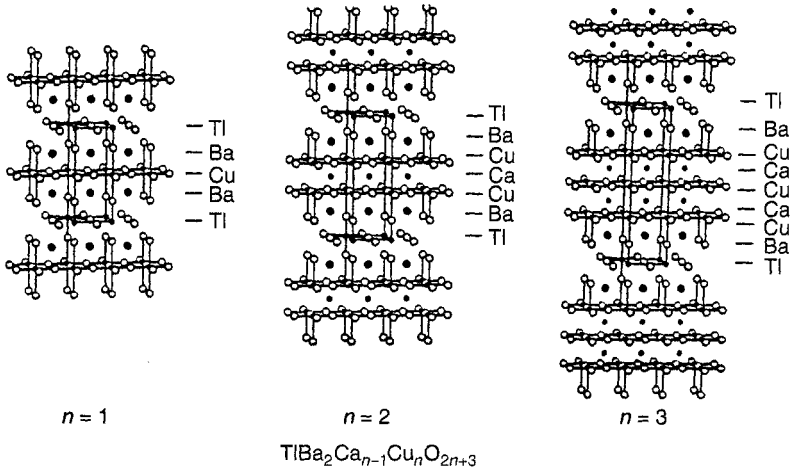

Figure 2. Structures of $TlBa_2Ca_{n-1}Cu_nO_{2n+3}$ ($n = 1, 2, 3$). Thallium atoms are shown on ideal (octahedral-type) sites for clarity. Metal atoms are solid Cu–O bonds are shown.

(Tl,Bi)-1223 or (Tl,Pb)-1223 are selected for detailed description as representatives of the thallium bilayer and monolayer compound, respectively. Tl-2201 is selected because of its structural simplicity and continuously variable T_c up to 84 K. It is the ideal candidate for fundamental studies. (Tl,Bi)-1223 and (Tl,Pb)-1223 offer a high irreversibility of field, which is very important for applications in high magnetic field.

TABLE 1. Tl-BASED SUPERCONDUCTING CUPRATES WITH THEIR ACRONYMS AND T_c VALUES

Ideal Formula	Acronym	T_c (K)
$Tl_2Ba_2CuO_6$	Tl-2201	0–90
$Tl_2Ba_2CaCu_2O_8$	Tl-2212	110
$Tl_2Ba_2Ca_2Cu_3O_{10}$	Tl-2223	125
$Tl_2Ba_2Ca_3Cu_4O_{12}$	Tl-2234	119
$TlBa_2CuO_5$	Tl-1201	0
$TlBa_2CaCu_2O_7$	Tl-1212	80
$TlBa_2Ca_2Cu_3O_9$	Tl-1223	110
$TlBa_2Ca_3Cu_4O_{11}$	Tl-1234	122
$TlBa_2Ca_4Cu_5O_{13}$	Tl-1245	110
$(Tl,Pb)Sr_2CuO_5$	(Tl,Pb)-1201	0
$(Tl,Pb)Sr_2CaCu_2O_7$	(Tl,Pb)-1212	90
$(Tl,Pb)Sr_2Ca_2Cu_3O_9$	(Tl,Pb)-1223	122
$(Tl,Bi)Sr_2CuO_5$	(Tl,Bi)-1201	0
$(Tl,Bi)Sr_2CaCu_2O_7$	(Tl,Bi)-1212	70–90
$(Tl,Bi)Sr_2Ca_2Cu_3O_9$	(Tl,Bi)-1223	110–120
$(Tl,Pb)(Sr,Ba)_2CaCu_2O_7$	(Tl,Pb)-1212	70–90
$(Tl,Pb)(Sr,Ba)_2Ca_2Cu_3O_9$	(Tl,Pb)-1223	110–120
$(Tl,Bi)(Sr,Ba)_2CaCu_2O_7$	(Tl,Bi)-1212	70–90
$(Tl,Bi)(Sr,Ba)_2Ca_2Cu_3O_9$	(Tl,Bi)-1223	110–120
$(Tl,Pb,Bi)(Sr,Ba)_2Ca_2Cu_3O_9$	(Tl,Pb,Bi)-1223	110–120

(i) Synthesis of Tl-2201. Bulk samples of Tl-2201 were prepared by solid state reaction[10]. Stoichiometric mixtures of Tl_2O_3, BaO, and CuO were pressed into pellets, wrapped in gold foil, and heated at 750–870°C for a few hours with intermittent grinding. Sintering at about 870°C for 10 h produces tetragonal symmetry, while sintering at lower temperatures (750–830°C) for 10 h produces orthorhombic symmetry. However, the tetragonal sample is never changed into an orthorhombic one by simple annealing at 800°C for 90 h, whereas an orthorhombic sample changes into a tetragonal one during additional heating at 870°C for 5 h. This indicates that the orthorhombic-to-tetragonal transition is not an ordinary thermodynamical phase transition. Moreover, the tetragonal sample can be changed to an orthorhombic one if it is annealed at 800°C with a small amount of Tl_2O_3. Figure 3 shows the XRD spectra of both the tetragonal and orthorhombic samples. The splitting of (110) into (020) and (200) due to orthorhombicity is clearly seen. Figure 4 shows the superconducting transition temperatures measured by susceptibility. Both phases show wide range T_c variation from normal metals to superconductors, with values up to 85 K.

(ii) Growth of Tl-2201 Thin Films. Even though this compound was discovered in 1987, high quality thin films were not available until 1995[11]. The films were made by rf magnetron sputtering and postdeposition annealing. The sputtering source was prepared by pressing and sintering an intimate mixture of $Tl_2O_3 + 2BaO_2 + CuO$, which had been preheated twice at 600°C for 5 h with one intermediate regrinding after the first hour

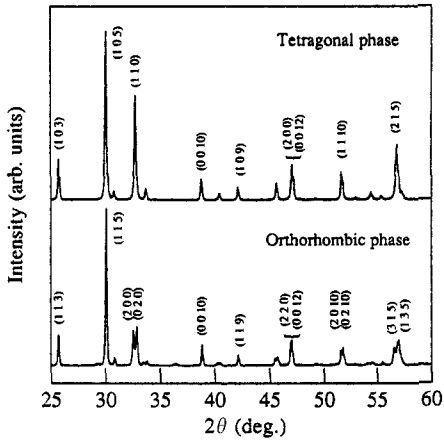

Figure 3. X-ray diffraction patterns of typical tetragonal and orthorhombic samples. All peaks are indexable, and some typical indices are shown.

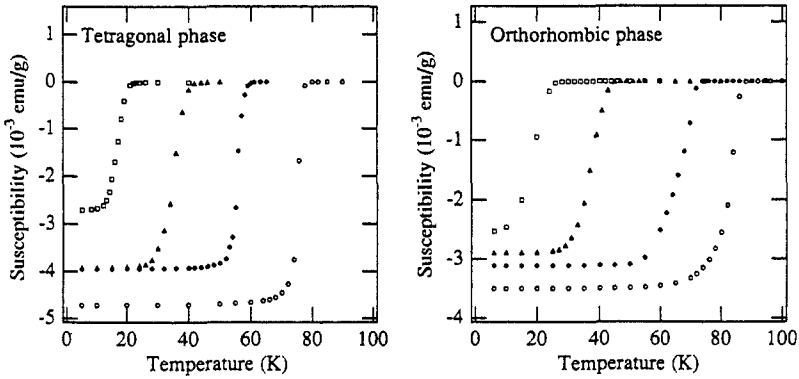

Figure 4. Meissner signals for tetragonal and orthorhombic Tl-2201 samples with various T_c values. All measurements were performed under a magnetic field of 10 Oe.

of heating. The precursor films were deposited on (100) $SrTiO_3$ or $LaAlO_3$ single crystal substrates by rf magnetron sputtering with substrates kept at room temperature during deposition. The as-deposited precursor films were amorphous and nonsuperconducting and must be heat-treated at 800–820°C for 15–30 min to form the epitaxial crystal lattice (after this initial recrystallization annealing, the films are called "as-grown"). The as-grown films are always shiny and appear to be uniform with T_c of 11–12 K. Annealing in flowing argon results in an increase in T_c up to 83 K, and by controlling the annealing temperature and time, T_c can be increased continuously from 11 K to 83 K[11,12]. Additional annealing in flowing oxygen of the 83 K film resulted in a depressed T_c down to 5 K. It seems most likely that the low T_c (11–12 K) of the as-grown films and the

depressed T_c after the additional annealing in flowing oxygen are due to excess oxygen (overdoped) and that annealing in flowing argon removes excess oxygen to approach the more optimally doped state. It was also found that the change of T_c is not due to a change in crystal lattice symmetry, but indeed due to a change in oxygen concentration in the crystal lattice.

The XRD 2θ spectra in Figure 5 show that pure Tl-2201 film can be obtained by the described procedure, with the c axis aligned along the direction normal to the substrate plane. The rocking curve (ω scan) of the (0010) reflection yielded a full width at half maximum of only 0.265° (see the inset of Figure 5), indicating good c-axis orientation. The in-plane epitaxial alignment of Tl-2201 film on $SrTiO_3$ was measured by ϕ scan of the (105) reflection of Tl-2201, and the (111) reflection of $SrTiO_3$, as shown in Figure 6. The four 90°-shifted sharp peaks indicate good in-plane alignment of Tl-2201 film with the substrate. From these patterns one can deduce that the [100] axis of Tl-2201 overlaps with that of $SrTiO_3$.

Figure 7 shows a schematic phase diagram of Tl-2201 thin films as a function of doping concentration[13]. The films used in these experiments are 1800 Å thick. The as-grown films show a T_c of 11 K, indicated by 1 in Figure 7. Its T_c increases gradually to the optimal value of 83 K indicated by 4 with the annealing condition of 360°C for under flowing argon (The temperature readings during annealing under flowing argon were given by a thermal couple embedded inside the heater. The actual temperature of the film was estimated to be 50–100°C lower than the thermal couple reading). Annealing of a similar film with the temperature set at 380°C for 7 h with flowing argon resulted in a T_c of 73 K, indicated by 5. This reduction of T_c is presumably due to the removal of

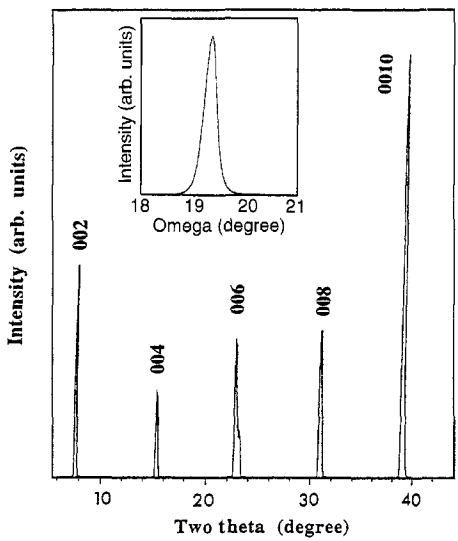

Figure 5. X-ray 2θ scan of $Tl_2Ba_2CuO_{6+\delta}$ (Tl-2201) thin film grown on single crystal $SrTiO_3$ substrate. The X-ray θ scan of the (0010) reflection of Tl-2201 film is shown in the inset.

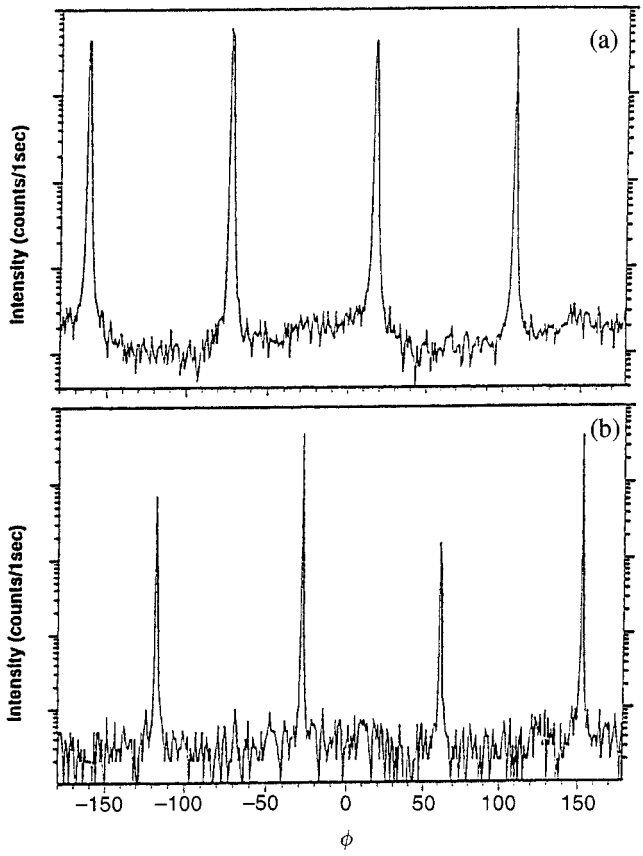

Figure 6. X-ray ϕ scans of (a) the (105) of Tl-2201 film and (b) the (111) of $SrTiO_3$ substrate.

oxygen from the crystal lattice with optimal oxygen concentration. The doping state of the crystal lattice with oxygen less than the optimal value is usually called underdoped. Continued annealing causes further decreases in T_c. Theoretically, T_c can be depressed to zero by prolonged annealing at high temperature. Experimentally, it is difficult to obtain the state of $T_c = 0$ because too high an annealing temperature will cause structural change. The lowest T_c so far obtained was 36 K on a film annealed at 440°C for 7 h with flowing argon without trying to raise the temperature further. In addition to annealing temperature and time, the film thickness is also a very important factor that affects the final T_c value under a given annealing condition. Under the annealing conditions above, the ratio of the average concentration (C_{av}) of loosely bound oxygen in the film at time t to the initial concentration (C_o) is given by $C_{av}/C_o = (8/\pi^2)\exp[-\pi^2 Dt/4l^2]$, where l is the film thickness in the c axis direction and D is the diffusion coefficient in the c-axis direction. Consequently, underdoping will be very difficult to achieve in thick films. In the study above, a thickness of 1800 Å was selected. It may be that underdoped single crystals

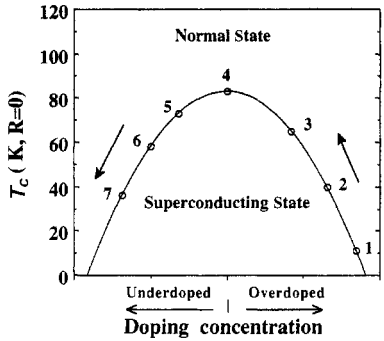

Figure 7. Schematic phase diagram of Tl-2201 thin films as a function of doping concentration; circles are experimental data points (only a few points out of the hundreds of points are shown). The line is only for a viewing guide, not the real data point. The annealing temperature and time for each point are as follows: 1, as grown; 2, 360°C for 20 min; 3, 360°C for 40 min; 4, 360°C for 1 h; 5, 380°C for 7 h; 6, 410°C for 7 h; and 7, 440°C for 7 h.

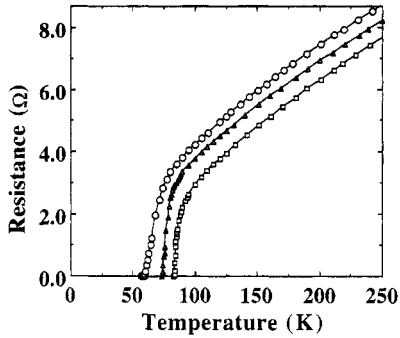

Figure 8. Typical resistance dependence of temperature of two underdoped Tl-2201 thin films (triangles and circles) to show the convex shape of the normal state resistivity and one optimally doped Tl-2201 thin film (squares) for comparison.

of Tl-2201 have not been made because the shortest dimension for oxygen to escape from the available single crystals is in the range of tens of micrometers.

Figure 8 shows typical resistance dependence of temperature for three Tl-2201 thin films that were annealed in flowing argon to become optimally doped, slightly underdoped, and deeply underdoped (4, 5, and 6 in Figure 7, respectively)[13]. The normal state resistance deviates from linear for the underdoped Tl-2201 thin films. The deviation is larger for more underdoped Tl-2201 thin films than the slightly underdoped ones, possibly indicating the existence of a pseudogap. The deviation resulted in a convex shape of the normal state resistivity. Another significant trend is seen in the transition width: the deeper the underdoping, the wider the superconducting transition. The reason for this behavior is not completely clear, but inhomogeneous oxygen diffusion during

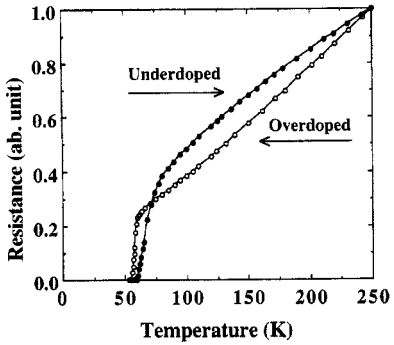

Figure 9. Typical resistance dependence of temperature of an overdoped Tl-2201 thin film to show the concave shape of the normal state resistivity (circles) and that of an underdoped Tl-2201 thin film for comparison to show the convex shape of the normal state resistivity.

annealing in flowing argon is probably to blame. For comparison, the temperature dependence of resistance of typical overdoped and underdoped Tl-2201 thin films is shown in Figure 9, which shows clearly that for overdoped Tl-2201 thin film the normal state resistance versus temperature plot is concave, whereas for underdoped Tl-2201 thin film the normal state resistance versus temperature plot is convex.

The structural simplicity of Tl-2201 is one of the major incentives for its intensive study. The microstructural crystal lattice symmetry of the Tl-2201 thin films has been studied by TEM utilizing bright-field imaging, selected-area electron diffraction (SAD), and convergent beam electron diffraction (CBED) techniques. The TEM studies were aimed at distinguishing between the tetragonal and orthorhombic crystal structures by examining at the symmetry of the crystal lattice for evidence of features associated with an orthorhombic structure such as twinning bands in bright-field imaging, spot-splitting in SAD patterns, and rotational symmetry in CBED. Plane-view samples were prepared so that the films could be viewed along the [001] axis. Figure 10a shows a bright-field image of the optimally doped Tl-2201 thin film with a T_c of 83 K in the [001] orientation. There is no evidence of twinning bands. Figure 10b is the SAD pattern from the same orientation. There is no evidence for twinning either, which would show up as spot-splitting in this pattern. Finally, the [001] CBED pattern in Figure 10c shows a 4 mm symmetry, which is consistent with a tetragonal crystal structure. Since the symmetry of this pattern for an orthorhombic crystal would be 2 mm, the possibility that the region imaged consists of single-domain, untwinned orthorhombic crystals can be excluded. The data are typical of results obtained on many spots on the sample. In view of these results and results obtained by Raman spectroscopy and X-ray diffraction[11], the structure of the optimally doped Tl-2201 films was concluded to be tetragonal, not orthorhombic, which is crucial to the pairing symmetry determination[14,15].

Similar studies have been carried out on both the heavily overdoped films with T_c of 11 K and underdoped Tl-2201 films with T_c of 58 K, and the results are shown in Figures 11 and 12, respectively. As in the case of the optimally doped Tl-2201 films, there is no evidence for twinning. Therefore we conclude that all Tl-2201 thin films made under our experimental conditions are tetragonal regardless of the doping concentration.

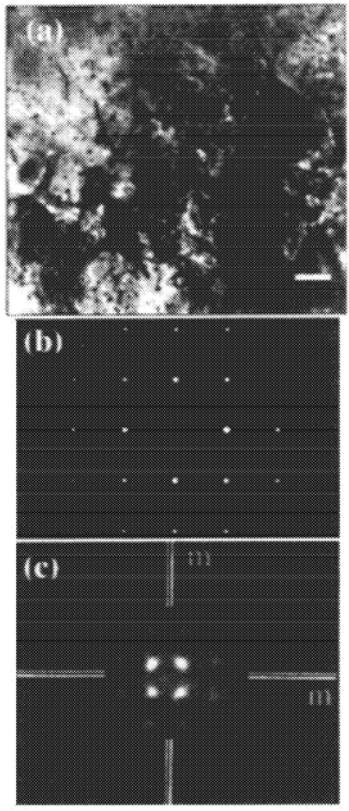

Figure 10. (a) TEM bright-field image, (b) selected area diffraction (SAD) pattern, and (c) convergent beam electron diffraction (CBED) pattern of the optimally reannealed ($T_c \sim 83$ K) Tl-2201 thin film.

(iii) Synthesis of (Tl,Pb)-1223 and (Tl,Bi)-1223. Bulk synthesis of (Tl,Bi)-1223 and (Tl,Pb)-1223 is always carried out in two steps[16]. First, preparation of a precursor powder $Sr_{1.6}Ba_{0.4}Ca_2Cu_3O_7$, and then, preparation of superconducting (Tl,Pb)-1223 or (Tl,Bi)-1223. The precursor powder is prepared by mixing BaO_2, $SrCO_3$, CaO, and CuO stoichiometrically, and heating in an Al_2O_3 crucible for 30 h at 905°C with regrinding after each 10 h of heating. The superconducting (Tl,Pb)-1223 or (Tl,Bi)-1223 was prepared by mixing one formula weight (fw) of the resulting precursor powder with 0.25 fw Tl_2O_3 and 0.5 fw PbO for (Tl,Pb)-1223 or 0.475 fw Tl_2O_3 and 0.11 fw Bi_2O_3 for (Tl,Bi)-1223, then pressing into 1.28 cm diameter pellets at 1.5×10^8 Pa. The pressed pellet was sandwiched between two gold plates, then tightly wrapped in 0.025 mm thick silver foil and heated in air for 4 h at 895°C for (Tl,Pb)-1223 or 885°C for (Tl,Bi)-1223. The resulting pellets were found to be mainly the 1223 phase according to their powder XRD spectra as shown in Figure 13. The dc magnetization data shown in the inset of Figure 13 also indicate a single superconducting transition at 114 K.

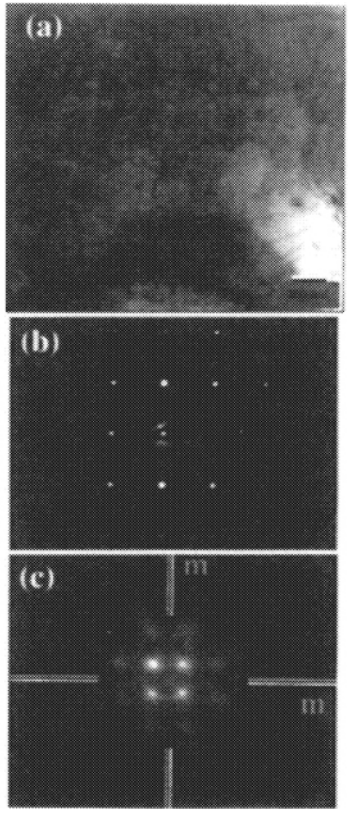

Figure 11. (a) TEM bright-field image, (b) selected area diffraction (SAD) pattern, and (c) convergent beam electron diffraction (CBED) pattern of the annealed ($T_c \sim 11$ K) Tl-2201 thin film.

(iv) Fabrication of (Tl,Pb)-1223 and (Tl,Bi)-1223 Tapes. Owing to the excellent flux pinning property and high T_c, intense research has been carried out on fabrication of (Tl,Pb)-1223 and (Tl,Bi)-1223 tapes by the powder-in-tube (PIT) method[16–20]. Early work focused on (Tl,Pb)-1223[16]. Silver-sheathed flexible tapes of (Tl,Pb)-1223 were prepared by packing a silver tube (4.35 mm i.d., 6.35 mm o.d.) with the pulverized well-reacted superconducting (Tl,Pb)-1223 powder, drawing the filled tube through a series of 13 dies with decreasing hole size, and rolling them between a pair of cylinders in successive stages of decreasing clearance. The tape was then heated at 885°C for 30 min, cooled and rolled again, and finally annealed at 845°C for 10 h. The resulting flexible and uniform short tapes exhibited transport J_c values as high as 12,000 A/cm^2, whereas J_c of 9000 A/cm^2 was achieved on long tapes (> 24 m)[16]. Figure 14 shows the J_c dependence of tape length. The flexibility was also tested by winding the tapes around Pyrex glass tubes of certain diameter. Figure 15 shows the J_c dependence on curvature or radius of the tube.

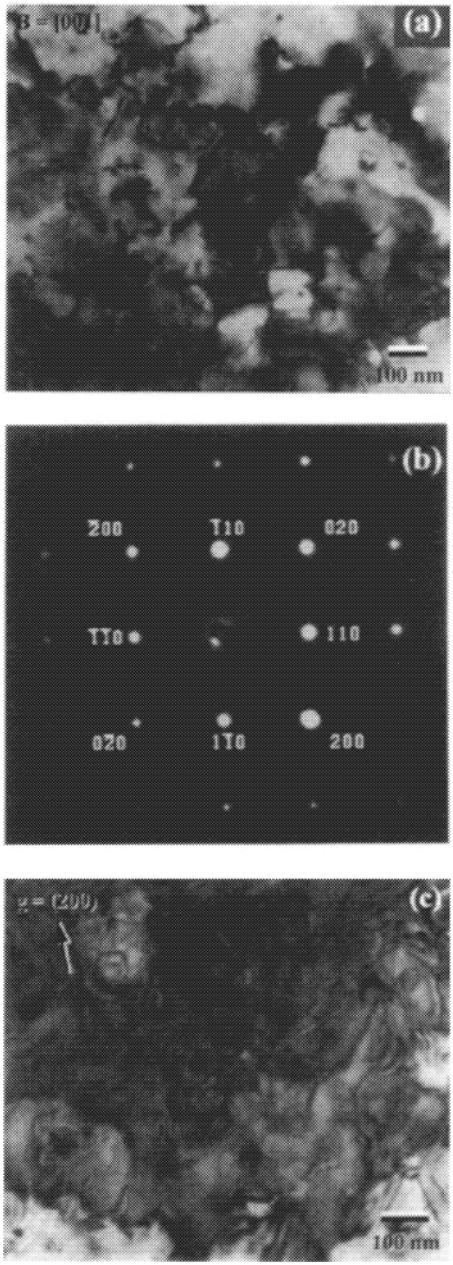

Figure 12. (a) TEM bright-field image in the [001] direction of the 58 K underdoped Tl-2201 thin film, (b) SAD pattern showing no spot splitting associated with orthorhombic structure, and (c) birght-field image with the sample tilted so that the (200) reflection is very strong to show that there are no twinning bands associated with orthorhombicity again.

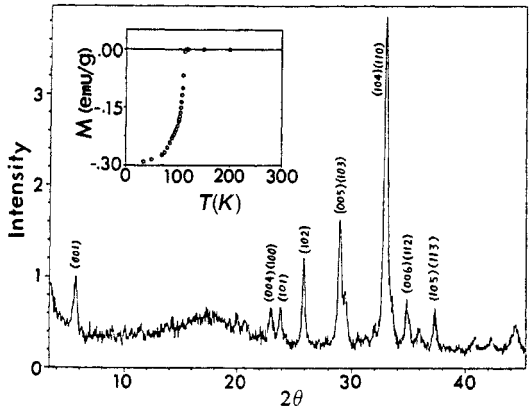

Figure 13. XRD pattern of a pulverized pellet of $Tl_{0.43}Pb_{0.5}Sr_{1.6}Ba_{0.4}Ca_2Cu_3O_{8.1}$. *Inset*: dc magnetization curve of a duplicate pellet indicates an onset T_c of 114 K.

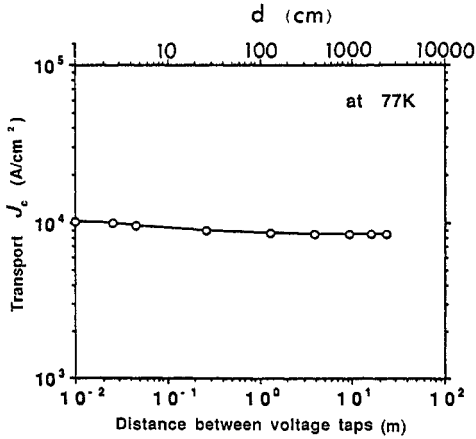

Figure 14. Transport J_c of a 24 m silver-sheathed $Tl_{0.5}Pb_{0.5}Ba_{0.4}Sr_{1.6}Ca_2Cu_3O_{8.25}$ tape. Measurements were made under liquid N_2 by the four-point method using the second and third contact points as voltage taps. The same criterion of $\Delta V = 1\ \mu V$ was used for all distances to determine the critical current, which decreased from 8.5 A to 7.0 A as the distance d between the voltage taps increased from 1 cm to 2375 cm.

Subsequently, (Tl,Bi)-1223 was found to be a better candidate for tape fabrication[17]. The fabrication of (Tl,Bi)-1223 tape is similar to that of (Tl,Pb)-1223 tape, except that an in situ reaction was used. The in situ reaction was found to be effective in producing high J_c (Tl,Pb)-1212 tapes[21] and later was used to fabricate (Tl,Bi)-1223 and (Tl,Pb)-1223 tapes. Instead of using well-reacted superconducting powder, the in situ method employs unreacted mixture of Tl_2O_3, Bi_2O_3, and $Sr_{1.6}Ba_{0.4}Ca_2Cu_3O_7$ in the required

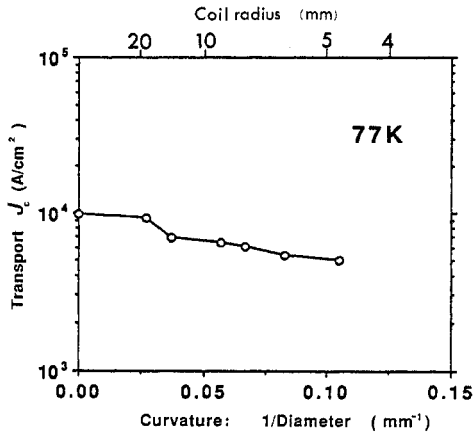

Figure 15. Transport J_c of silver sheathed $Tl_{0.5}Pb_{0.5}Ba_{0.4}Sr_{1.6}Ca_2Cu_3O_{8.25}$ coils as a function of the coil curvature or radius. The finished tapes were coiled around Pyrex tubes of different diameters without further annealing and measured under liquid N_2.

stoichiometry, as the starting material to be packed in the silver tube (4.35 mm i.d., and 6.35 mm o.d.). The packed tube was tapped on a hard surface to gain a higher packing density, drawn through 13 dies and rolled to 0.5 mm thick, then heated at 800–860°C for 10–60 min in air, taken out, cooled to room temperature, and rolled to final thickness and width of 0.087–0.232 and 1.8–2.1 mm, respectively. The rolled tapes were finally annealed at 800–860°C for 6–20 h in air to achieve high J_c. Figure 16 shows the dependence of the transport J_c and T_c on the Bi concentration in $Tl_{1-x}Bi_xSr_{1.6}Ba_{0.4}Ca_2Cu_3O_9$ [The Sr/Ba ratio was adopted from that in (Tl,Pb)-1223, and was studied again in the (Tl,Bi)-1223 system as presented next.] It is clear that J_c increases, reaches a maximum, and finally decreases with further increase in Bi concentration. The optimal J_c of 1.33×10^4 A/cm^2 was achieved with $x = 0.22$, i.e., $Tl_{0.78}Bi_{0.22}Sr_{1.6}Ba_{0.4}Ca_2Cu_3O_9$, which was simplified as (Tl,Bi)-1223. T_c also increases with the increase of Bi concentration, then levels off at 108 K after $x \geq 0.2$. With the Bi concentration fixed, the ratio of Sr/Ba was studied. Figure 17 shows that effect of Sr/Ba ratio and of the annealing temperature on the transport J_c. Clearly, the ratio 1.6/0.4 was optimal just as in (Tl,Pb)-1223. Therefore $Tl_{0.78}Bi_{0.22}Sr_{1.6}Ba_{0.4}Ca_2Cu_3O_9$ is the optimal composition for achieving high J_c[17]. Structurally, $Tl_{0.75}Bi_{0.25}Sr_{1.6}Ba_{0.4}Ca_2Cu_3O_9$, instead of $Tl_{0.78}Bi_{0.22}Sr_{1.6}Ba_{0.4}Ca_2Cu_3O_9$, might make more sense because one of the four Tl sites is replaced by Bi. Experimentally, Bi = 0.22, (slightly less than Bi = 0.25), may result in a purer (Tl,Bi)-1223 phase, hence give a slightly higher J_c. Optimal compositions [$Tl_{0.78}Bi_{0.22}Sr_{1.6}Ba_{0.4}Ca_2Cu_3O_9$ for (Tl,Bi)-1223 and $Tl_{0.5}Pb_{0.5}Sr_{1.6}Ba_{0.4}Ca_2Cu_3O_9$ for (Tl,Pb)-1223] were chosen to investigate the effect of the annealing time on the transport J_c at 77 K. Surprisingly, it was found that Bi speeded formation of superconducting 1223 phase drastically.

Figure 18 compares the results obtained by a four-probe transport measurement at 77 K for both (Tl,Bi)-1223 and (Tl,Pb)-1223, which were annealed for different lengths of time at 840°C. It shows that the transport J_c of 1.233×10^4 A/cm^2 at 77 K for (Tl,Bi)-1223

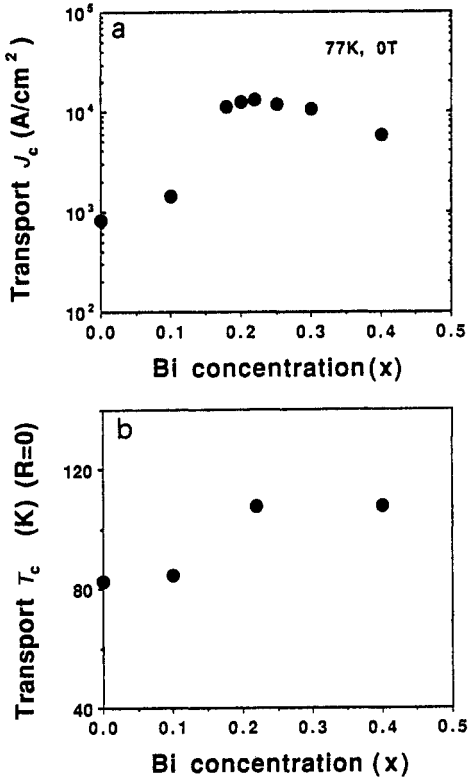

Figure 16. Dependence of the transport J_c (77 K, 0 T) and the transport T_c on the Bi concentration in the in situ synthesized siliver-sheathed superconducting tapes of $Tl_{1-x}Bi_xSr_{1.6}Ba_{0.4}Ca_2Cu_3O_{9-\delta}$.

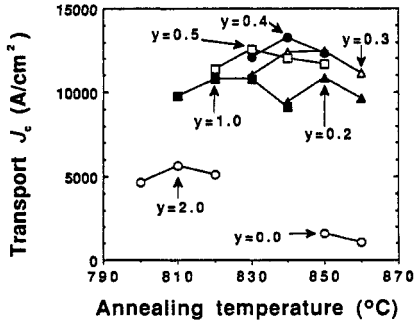

Figure 17. The effect of partial substitution of Ba for Sr and of the annealing temperature on the transport J_c (77 K, 0 T) for the in situ synthesized silver-sheathed superconducting tapes of $Tl_{1-x}Bi_xSr_{2-y}Ba_yCa_2Cu_3O_{9-\delta}$ ($x = 0.22$).

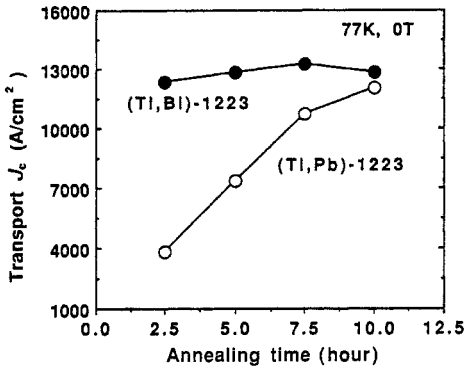

Figure 18. Comparison of the effect of the annealing time on the transport J_c (77 K, 0 T) of the in-situ synthesized superconducting tapes of $Tl_{0.78}Bi_{0.22}Sr_{1.6}Ba_{0.4}Ca_2Cu_3O_{9-\delta}$ and $Tl_{0.5}Pb_{0.5}Sr_{1.6}Ba_{0.4}Ca_2Cu_3O_{9-\delta}$.

after only 2.5 h annealing reached 93.3% of its maximal value 1.322×10^4 A/cm^2 after 7.5 h annealing. But under the same conditions, the J_c of 0.383×10^4 A/cm^2 for (Tl,Pb)-1223 reached only 31.8% of its maximal value of 1.203×10^4 A/cm^2. From the processing point of view, the short processing time is definitely an advantage. Further studies showed that J_c can be raised to over 2×10^4 A/cm^2 at 77 K and zero field by hydraulic compression before the final compression[17,20].

(v) Growth of (Tl,Bi)-1223 Thin Film. The films were made in two steps: deposition of precursor film by laser ablation and postdeposition annealing. An ablation source is required before deposition. The source was made by mixing 1 fw of the superconducting powder $Tl_{0.78}Bi_{0.22}Sr_{1.6}Ba_{0.4}Ca_2Cu_3O_9$, prepared as described above, with 0.475 fw Tl_2O_3 and 0.4 fw CaO, pressing at 10 tons in a 1.28 cm diameter die, and heating at 850°C for 0.5 h. The deposition was conducted at 80–200 mJ/pulse, and 2–8 pulses/s at substrates temperatures of 300–500°C. The substrates used were either (100) $LaAlO_3$ or YSZ. The resulting film was placed on a gold plate sitting between two similarly placed unfired pellets of $Tl_{0.95}Bi_{0.22}Sr_{1.6}Ba_{0.4}Ca_2Cu_3O_9$. The assembly was wrapped in silver foil with adequate air space for gas phase diffusion, and heated in air at 840–870°C for 25–60 min. The detailed synthesis conditions and results were reported in a series of papers[22–26]. In the following, only a brief description is given.

XRD 2θ spectra show that the films are single 1223 phase (see Figure 19a) with a full width at half-maximum (FWHM) of 0.365° measured at the (006) reflection as shown in Figure 19b. The existence in Figure 19a of (00l) peaks only indicates that the c axis is well-aligned. The four sharp peaks separated by 90° in the ϕ scan using the (103) reflection as shown in Figure 20 indicate that the films were also a- and b-axis-aligned. The as-grown films exhibited T_c values in the range of 105–111 K depending on the relative phase purity of 1223 to 1212. A typical temperature dependence of resistance is shown in Figure 21. Figure 22 shows the J_c dependence on temperature from 77 to 99 K. Within this temperature range, J_c and T exhibited a nearly linear relationship with J_c over 2.5×10^6 A/cm^2 at 77 K and zero field. Figures 23 and 24 show the J_c dependence

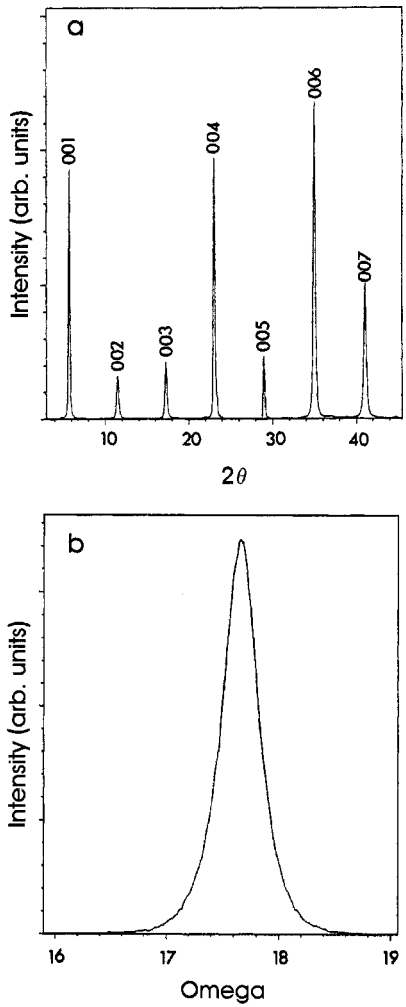

Figure 19. (a) XRD 2θ scan of a (Tl, Bi)$Sr_{1.6}Ba_{0.4}Ca_2Cu_3O_{9-\delta}$ film on (100) $LaAlO_3$ shows a single 1223 phase and near perfect c-axis alignment. (b) XRD rocking curve of the (006) reflection of (Tl, Bi)$Sr_{1.6}Ba_{0.4}Ca_2Cu_3O_{9-\delta}$ film on $LaAlO_3$. Half-width of the rocking curve = 0.365°.

on magnetic field with the field aligned perpendicular and parallel to the *c* axis, respectively[25].

(vi) Conductor Development of (Tl,Bi)-1223 on RABiTS. With the successful growth of (Tl,Bi)-1223 films on single crystal YSZ by laser ablation and postdeposition annealing in pure Ar[26] and the development of rolling assisted biaxially textured substrates (RABiTS)[27,28], the epitaxial growth of (Tl,Bi)-1223 film on RABiTS was

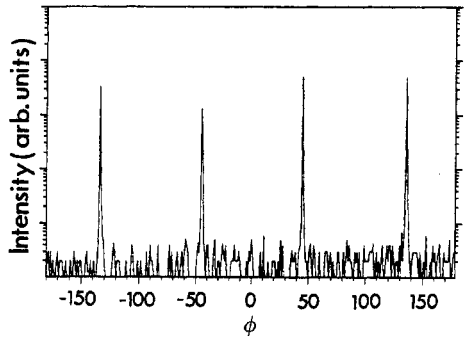

Figure 20. XRD ϕ scan of the (103) reflection for the (Tl, Bi)$Sr_{1.6}Ba_{0.4}Ca_2Cu_3O_{9-\delta}$ film on (100) $LaAlO_3$.

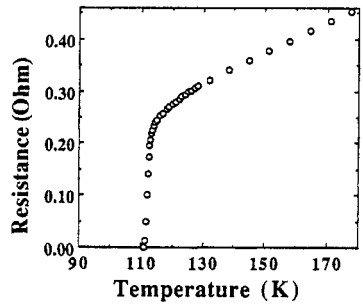

Figure 21. Temperature dependence of the resistance of a (Tl, Bi)$Sr_{1.6}Ba_{0.4}Ca_2Cu_3O_{9-\delta}$ film on $LaAlO_3$.

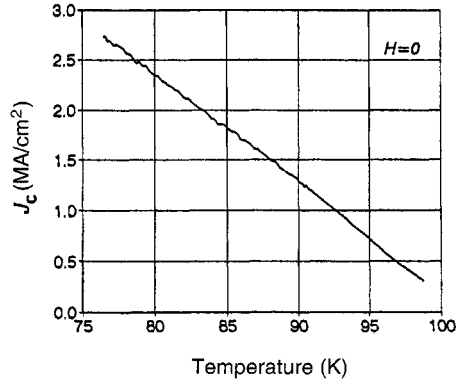

Figure 22. J_c dependence on temperature without external magnetic field applied.

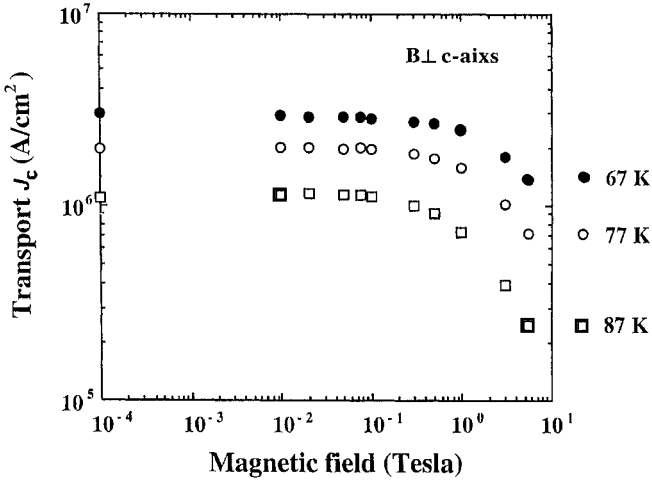

Figure 23. J_c dependence of magnetic field applied perpendicular to the c axis.

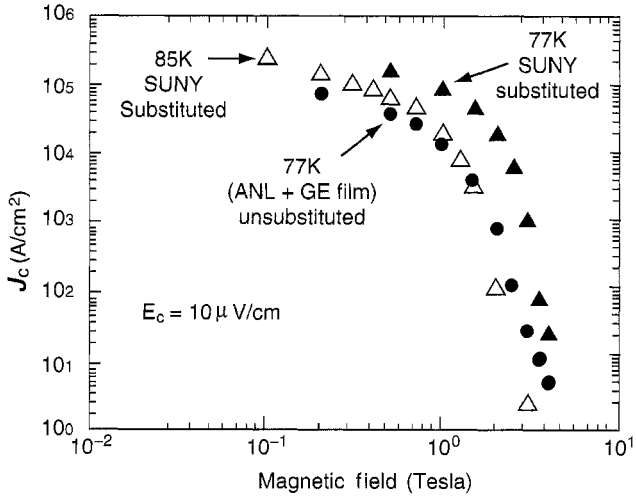

Figure 24. J_c dependence on magnetic field applied parallel to the c axis. Comparison was made on both undoped and Bi- and Sr-doped films.

successfully achieved for the first time[29]. The (Tl,Bi)-1223 superconducting films on RABiTS were prepared by pulsed laser ablation followed by postdeposition annealing in a tube furnace with flowing pure argon. The base Ni is about 125 μm thick and the top buffer layer YSZ is about 0.5 μm thick, with a 40 nm thick layer of CeO_2 in between. The details of the deposition by laser ablation and postdeposition annealing in flowing argon have been reported[26]. In brief, a laser ablation target of composition

$Tl_{1.8}Bi_{0.22}Sr_{1.6}Ba_{0.4}Ca_{2.2}Cu_{3.3}O_{10.5}$ was first prepared. Precursor films were then deposited by laser ablation conducted with deposition parameters of 80 mJ/pulse, 21 kV, and 4 pulses/s, and finally the precursor films were annealed in a tube furnace at 780–800°C for 40–60 min under flowing argon.

The XRD θ–2θ spectrum of a typical (Tl,Bi)-1223 superconducting thin film on a RABiTS is shown in Figure 25. All the major reflections are indexed as either (00*l*) peaks of (Tl,Bi)-1223 phase or (200) of the RABiTS, with weaker peaks resulting from either (00*l*) of the (Tl,Bi)-1212 phase or NiO. The thin layer of CeO_2 resulted in weaker intensity. Further optimization of the deposition and annealing parameters might eliminate (Tl,Bi)-1212 phase and improve the physical properties of the films. The presence of only (00*l*) peaks shows that the films are strongly *c* axis aligned. The degree of *c*-axis alignment has been determined by a ω scan (rocking curve) of the (Tl,Bi)-1223 (007) peak. For this peak of the (Tl,Bi)-1223 phase, the FWHM value determined from the rocking curve is about 6.8°, which is comparable with that of the RABiTS[27,28]. The out-of-plane FWHM of (005) peak of the minor (Tl,Bi)-1212 is about 11.3°, which is much larger than the 6.8° of the major (Tl,Bi)-1223 phase. Elimination of the minor (Tl,Bi)-1212 phase improves the *c* axis alignment of the major (Tl,Bi)-1223 phase. The in-plane (*a*- and *b*-axis) alignment was measured by XRD ϕ scans of the (Tl,Bi)-1223 (102) pole figure, as shown in Figure 26. The four well-developed diffraction spots with $\Delta\phi \sim 7.0°$ FWHM indicate that the *a*- and *b* axes are aligned, with no indication of 45° misoriented domains, which are frequently present in the YBCO films on YSZ as a result of the lattice mismatch[30]. Similar measurements carried out for the minor (Tl,Bi)-1212 phase showed that both *a* and *b* axes are also aligned with $\Delta\phi \sim 9.5°$ FWHM. An epitaxy for ⟨100⟩ of (Tl,Bi)-1223 film on ⟨110⟩ of YSZ substrate was derived from the ϕ scans of both the (Tl,Bi)-1223 film and the YSZ substrate.

The magnetization of the sample used for XRD θ–2θ diffraction shown in Figure 25 and pole figure shown in Figure 26 was measured in a superconducting quantum

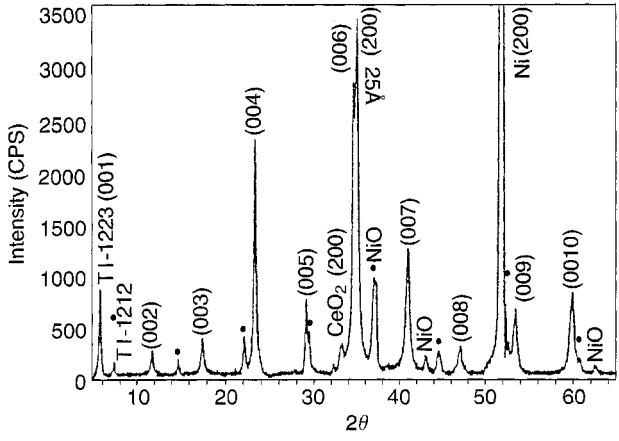

Figure 25. X-ray diffraction θ–2θ spectrum of a shorter (7 mm) (Tl, Bi)-1223 film on RABiTS, showing the presence of only (00*l*) reflections. The films are oriented with the *c* axis perpendicular to the substrate surface.

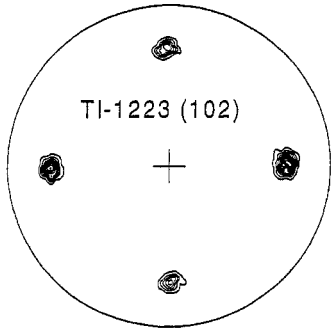

Figure 26. (102) X-ray pole figure of the (Tl, Bi)-1223 film used for the X-ray diffraction θ–2θ spectrum measurement shown in Fig. 25. The four well-developed diffraction positions indicate that a and b axes are aligned.

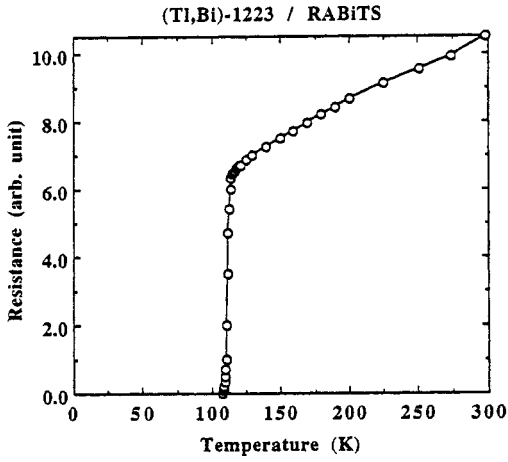

Figure 27. Temperature dependence of resistance of a particular (Ti, Bi)-1223 film made on RABiTS by laser ablation and postdeposition annealing in flowing pure Ar, showing a zero-resistance superconducting transition temperature of 107 K.

interference device (SQUID) magnetometer. The J_c calculated from Bean's model using the full width (3.5 mm) of the film as the appropriate lateral dimension was 2×10^5 A/cm^2 at 77 K and extrapolated to zero field. The value probably represents a lower bound for the transport J_c, since the effective voltage level of persistent currents measured by the magnetometer is much lower than the typical criterion 10^{-6} V/cm, used to define J_c in transport. Transport measurements on longer film processed differently showed a J_c of 1×10^5 A/cm^2 obtained at 77 K and zero field. The zero-resistance transition temperatures (T_c) of the films are in the range of 106–110 K. Figure 27 shows a typical temperature-dependent resistivity, with a zero-resistance T_c of 107 K for this particular film.

(Z. REN, J. WANG)

1. Z. Z. Sheng, A. M. Hermann, *Nature, 332*, 138 (1988).
2. R. M. Hazen, L. W. Finger, R. J. Angel, C. T. Prewitt, N. L. Ross, C. G. Hadidiacos, P. J. Heaney, D. R. Veblen, Z. Z. Sheng, A. El Ali, A. M. Hermannn, *Phys. Rev. Lett., 60*, 1657 (1988).
3. L. Gao, Z. J. Huang, R. L. Meng, P. H. Hor, J. Bechtold, Y. Y. Sun, C. W. Chu, Z. Z. Sheng, A. M. Hermann, *Nature, 332*, 623 (1988).
4. M. A. Subramanian, J. C. Calabrese, C. C. Torardi, J. Gopalakrishnan, T. R. Askew, R. B. Flippen, K. J. Morrissey, U. Chowdry, A. W. Sleight, *Nature, 332*, 420 (1988).
5. C. C. Torardi, M. A. Subramanian, J. C. Calabrese, J. Gopalakrishnan, E. M. McCarron, K. J. Morrissey, T. R. Askew, R. B. Flippen, U. Chowdry, A. W. Sleight, *Phys. Rev. B, 38*, 225 (1988).
6. S. S. P. Parkin, V. Y. Lee, A. I. Nazzal, R. Savoy, R. Beyers, S. J. La Placa, *Phys. Rev. Lett., 61*, 750 (1988).
7. C. Martin, C. Michel, A. Maignan, M. Hervieu, B. Raveau, *C. R. Acad. Sci. Paris, 307*, 27 (1988).
8. D. Bourgault, C. Martin, C. Michel, M. Hervieu, J. Provost, B. Raveau, *J. Solid State Chem., 78*, 326 (1989).
9. C. C. Torardi, in *Chemistry of Superconductor Materials*, T. A. Vanderah, Noyes, Park Ridge, NJ, 1992.
10. Y. Shimakawa, *Physica C, 204*, 247 (1993).
11. C. A. Wang, Z. F. Ren, J. H. Wang, D. K. Petrov, M. J. Naughton, W. Y. Yu, A. Petrou, *Physica C, 262*, 98 (1996).
12. Z. F. Ren, J. H. Wang, D. J. Miller, *Appl. Phys. Lett., 69*, 1798 (1996).
13. Z. F. Ren, J. H. Wang, D. J. Miller, *Appl. Phys. Lett., 71*, 1706 (1997).
14. C. C. Tsuei, J. R. Kirtley, M. Rupp. J. Z. Sun, A. Gupta, M. B. Ketchen, C. A. Wang, Z. F. Ren, J. H. Wang, M. Bhushan, *Science, 271*, 329 (1996).
15. C. C. Tsuei, J. R. Kirtley, Z. F. Ren, J. H. Wang, H. Raffy, Z. Z. Li, *Nature, 387*, 481 (1997).
16. Z. F. Ren, J. H. Wang, *Physica C, 192*, 55 (1992).
17. Z. F. Ren, J. H. Wang, *Physica C, 216*, 199 (1993).
18. Z. F. Ren, J. H. Wang, D. J. Miller, K. C. Goretta, *Physica C, 229*, 137 (1994).
19. D. J. Miller, J. G. Hu, Z. F. Ren, J. H. Wang, *J. Electron. Mater., 23*, 1151 (1994).
20. Z. F. Ren, C. A. Wang, J. H. Wang, D. J. Miller, K. C. Goretta, *Physica C, 247*, 163 (1995).
21. Z. F. Ren, J. H. Wang, *Appl. Phys. Lett., 62*, 3025 (1993).
22. Z. F. Ren, C. A. Wang, J. H. Wang, *Appl. Phys. Lett., 65*, 237 (1994).
23. C. A. Wang, Z. F. Ren, J. H. Wang, D. J. Miller, *Physica C, 245*, 171 (1995).
24. Z. F. Ren, C. A. Wang, J. H. Wang, *Handbook of Thin Film Process Technology*, D. A. Glocker, S. I. Shah, eds., Institute of Physics Publishing, Philadelphia, PA 1995.
25. Z. F. Ren, C. A. Wang, J. H. Wang, D. J. Miller, D. K. Christen, J. D. Hettinger, K. E. Gray, *Physica C, 258*, 129 (1996).
26. L. P. Guo, Z. F. Ren, J. Y. Lao, J. H. Wang, D. K. Christen, C. E. Klabunde, J. D. Budai, *Physica C, 277*, 13 (1997).
27. A. Goyal, D. P. Norton, J. D. Budai, M. Paranthaman, E. D. Specht, D. M. Kroeger, D. K. Christen, Q. He, B. Saffian, F. A. List, D. F. Lee, P. M. Martin, C. E. Klabunde, E. Hartfield, V. K. Sikka, *Appl. Phys. Lett., 69*, 1795 (1996).
28. D. P. Norton, A. Goyal, J. D. Budai, D. K. Christen, D. M. Kroeger, E. D. Specht, Q. He, B. Saffian, M. Paranthaman, C. E. Klabunde, D. F. Lee, B. C. Sales, F. A. List, *Science, 274*, 755 (1996).
29. Z. F. Ren, J. Y. Lao, L. P. Guo, J. H. Wang, J. D. Budai, D. K. Christen, A Goyal, M. Paranthaman, E. D. Specht, J. R. Thompson, *J. Superconduc., 11*, 159 (1998).
30. J. Z. Liu, Y. J. Tian, L. Li, L. P. Guo, Z. X. Zhao, *J. Appl. Phys., 77*, 1165 (1995).

17.3.10.2.5. Mercury-Based Cuprates.

Since the discovery of high T_c superconductivity in an Hg-containing system[1], a great deal of effort has been devoted to synthesizing phase-dominated or phase-pure $HgBa_2CuO_5$ (Hg-1201)[2], $HgBa_2CaCu_2O_7$ (Hg-1212)[3,4], and $HgBa_2Ca_2Cu_3O_9$ (Hg-1223)[4,5]. Hg-containing phases also have the general chemical formula $HgBa_2Ca_{n-1}Cu_nO_{2n+3}$ just like thallium monolayer phases, but the synthesis of Hg-containing phases is much more complicated and difficult because of the high volatility and toxicity of Hg and Hg-based compounds. For example, HgO decomposes at

Inorganic Reactions and Methods, Volume 18
Edited by J. J. Zuckerman, Jim D. Atwood

1. Z. Z. Sheng, A. M. Hermann, *Nature, 332*, 138 (1988).
2. R. M. Hazen, L. W. Finger, R. J. Angel, C. T. Prewitt, N. L. Ross, C. G. Hadidiacos, P. J. Heaney, D. R. Veblen, Z. Z. Sheng, A. El Ali, A. M. Hermannn, *Phys. Rev. Lett., 60*, 1657 (1988).
3. L. Gao, Z. J. Huang, R. L. Meng, P. H. Hor, J. Bechtold, Y. Y. Sun, C. W. Chu, Z. Z. Sheng, A. M. Hermann, *Nature, 332*, 623 (1988).
4. M. A. Subramanian, J. C. Calabrese, C. C. Torardi, J. Gopalakrishnan, T. R. Askew, R. B. Flippen, K. J. Morrissey, U. Chowdry, A. W. Sleight, *Nature, 332*, 420 (1988).
5. C. C. Torardi, M. A. Subramanian, J. C. Calabrese, J. Gopalakrishnan, E. M. McCarron, K. J. Morrissey, T. R. Askew, R. B. Flippen, U. Chowdry, A. W. Sleight, *Phys. Rev. B, 38*, 225 (1988).
6. S. S. P. Parkin, V. Y. Lee, A. I. Nazzal, R. Savoy, R. Beyers, S. J. La Placa, *Phys. Rev. Lett., 61*, 750 (1988).
7. C. Martin, C. Michel, A. Maignan, M. Hervieu, B. Raveau, *C. R. Acad. Sci. Paris, 307*, 27 (1988).
8. D. Bourgault, C. Martin, C. Michel, M. Hervieu, J. Provost, B. Raveau, *J. Solid State Chem., 78*, 326 (1989).
9. C. C. Torardi, in *Chemistry of Superconductor Materials*, T. A. Vanderah, Noyes, Park Ridge, NJ, 1992.
10. Y. Shimakawa, *Physica C, 204*, 247 (1993).
11. C. A. Wang, Z. F. Ren, J. H. Wang, D. K. Petrov, M. J. Naughton, W. Y. Yu, A. Petrou, *Physica C, 262*, 98 (1996).
12. Z. F. Ren, J. H. Wang, D. J. Miller, *Appl. Phys. Lett., 69*, 1798 (1996).
13. Z. F. Ren, J. H. Wang, D. J. Miller, *Appl. Phys. Lett., 71*, 1706 (1997).
14. C. C. Tsuei, J. R. Kirtley, M. Rupp. J. Z. Sun, A. Gupta, M. B. Ketchen, C. A. Wang, Z. F. Ren, J. H. Wang, M. Bhushan, *Science, 271*, 329 (1996).
15. C. C. Tsuei, J. R. Kirtley, Z. F. Ren, J. H. Wang, H. Raffy, Z. Z. Li, *Nature, 387*, 481 (1997).
16. Z. F. Ren, J. H. Wang, *Physica C, 192*, 55 (1992).
17. Z. F. Ren, J. H. Wang, *Physica C, 216*, 199 (1993).
18. Z. F. Ren, J. H. Wang, D. J. Miller, K. C. Goretta, *Physica C, 229*, 137 (1994).
19. D. J. Miller, J. G. Hu, Z. F. Ren, J. H. Wang, *J. Electron. Mater., 23*, 1151 (1994).
20. Z. F. Ren, C. A. Wang, J. H. Wang, D. J. Miller, K. C. Goretta, *Physica C, 247*, 163 (1995).
21. Z. F. Ren, J. H. Wang, *Appl. Phys. Lett., 62*, 3025 (1993).
22. Z. F. Ren, C. A. Wang, J. H. Wang, *Appl. Phys. Lett., 65*, 237 (1994).
23. C. A. Wang, Z. F. Ren, J. H. Wang, D. J. Miller, *Physica C, 245*, 171 (1995).
24. Z. F. Ren, C. A. Wang, J. H. Wang, *Handbook of Thin Film Process Technology*, D. A. Glocker, S. I. Shah, eds., Institute of Physics Publishing, Philadelphia, PA 1995.
25. Z. F. Ren, C. A. Wang, J. H. Wang, D. J. Miller, D. K. Christen, J. D. Hettinger, K. E. Gray, *Physica C, 258*, 129 (1996).
26. L. P. Guo, Z. F. Ren, J. Y. Lao, J. H. Wang, D. K. Christen, C. E. Klabunde, J. D. Budai, *Physica C, 277*, 13 (1997).
27. A. Goyal, D. P. Norton, J. D. Budai, M. Paranthaman, E. D. Specht, D. M. Kroeger, D. K. Christen, Q. He, B. Saffian, F. A. List, D. F. Lee, P. M. Martin, C. E. Klabunde, E. Hartfield, V. K. Sikka, *Appl. Phys. Lett., 69*, 1795 (1996).
28. D. P. Norton, A. Goyal, J. D. Budai, D. K. Christen, D. M. Kroeger, E. D. Specht, Q. He, B. Saffian, M. Paranthaman, C. E. Klabunde, D. F. Lee, B. C. Sales, F. A. List, *Science, 274*, 755 (1996).
29. Z. F. Ren, J. Y. Lao, L. P. Guo, J. H. Wang, J. D. Budai, D. K. Christen, A Goyal, M. Paranthaman, E. D. Specht, J. R. Thompson, *J. Superconduc., 11*, 159 (1998).
30. J. Z. Liu, Y. J. Tian, L. Li, L. P. Guo, Z. X. Zhao, *J. Appl. Phys., 77*, 1165 (1995).

17.3.10.2.5. Mercury-Based Cuprates.

Since the discovery of high T_c superconductivity in an Hg-containing system[1], a great deal of effort has been devoted to synthesizing phase-dominated or phase-pure $HgBa_2CuO_5$ (Hg-1201)[2], $HgBa_2CaCu_2O_7$ (Hg-1212)[3,4], and $HgBa_2Ca_2Cu_3O_9$ (Hg-1223)[4,5]. Hg-containing phases also have the general chemical formula $HgBa_2Ca_{n-1}Cu_nO_{2n+3}$ just like thallium monolayer phases, but the synthesis of Hg-containing phases is much more complicated and difficult because of the high volatility and toxicity of Hg and Hg-based compounds. For example, HgO decomposes at

~500°C, whereas the formation of the Hg-containing superconducting phases takes place at 800°C. Therefore, synthesis must be carried out in a tightly sealed container such as a quartz tube.

(i) Synthesis of Hg-1201, Hg-1212, and Hg-1223. Bulk synthesis of Hg-containing phases is accomplished in a two-step procedure, preparation of precursor $Ba_2Ca_{n-1}Cu_nO_x$ followed by sintering of the stoichiometric mixture of HgO and the precursor powder in a tightly sealed quartz tube. The stoichiometric precursor pellet was normally prepared from $BaCO_3$, CaO, and CuO by mixing in an agate mortar, pressing into pellets, and heating at 900°C for 24–48 h with intermediate regrinding to promote homogeneity. Since Hg-containing superconducting phases form only through a vapor (Hg)/solid (precursor) reaction, not a solid (HgO)/solid (precursor) diffusion, maintaining the Hg pressure is very important. Experimentally, Hg was supplied to the precursor pellet from a pressed pellet of a mixture of HgO and the precursor. Everything was sealed in an evacuated quartz tube and encapsulated in stainless steel tube as a precaution. The assembly was reacted in a tube furnace by slowly heating at a rate of 160°C/h to 800–860°C and mointaining this temperature for 5 h before slowly cooling to room temperature. Generally, Hg-1212 is formed between 750–820°C, and Hg-1223 above 840°C. Upon removal from the tube, the samples were annealed at 300°C in flowing oxygen for many hours to improve the T_c value. The oxygenation annealing has to be kept below 310°C to prevent Hg from evaporating. Figures 1 and 2 show the temperature dependence of resistivity of Hg-1212 and Hg-1223, respectively. Clearly, postoxygenated samples showed higher T_c values than the as-synthesized ones. With these samples available, high pressure studies were also carried out. Figure 3 shows the dependence of

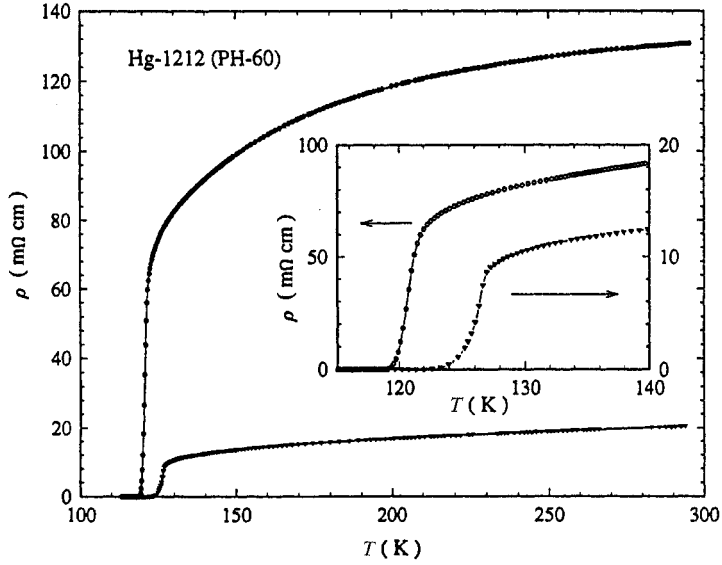

Figure 1. Resistivity ρ vs. T: circles, as-synthesized; triangules, post-oxygenated. *Inset*: Enlarged ρ vs. T curves near T_c.

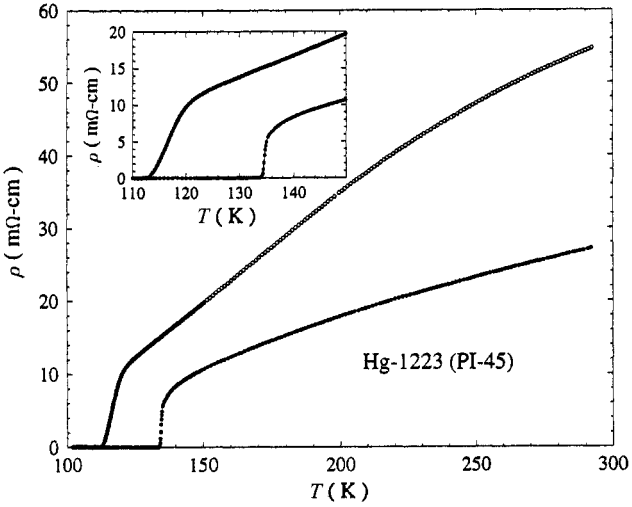

Figure 2. Resistivity ρ vs. T: open circles, as-synthesized; solid curcles, post-oxygenated. *Inset*: enlarged ρ vs. T curves near T_c.

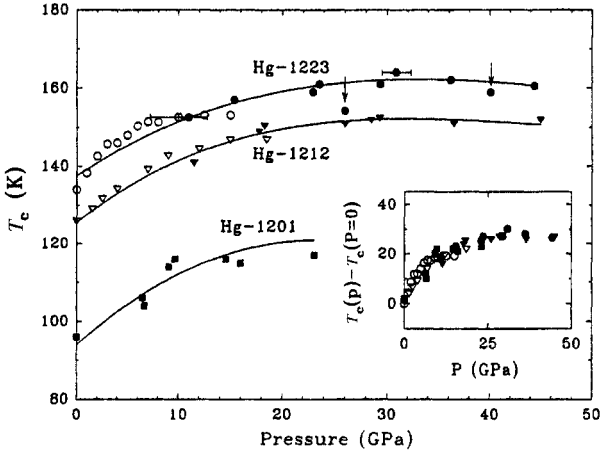

Figure 3. T_c vs. P for Hg- 1223, Hg-1212, and Hg- 1201. *Inset*: $T_c(P) - T_c(P = 0)$ for these three compounds. Arrows indicate data obtained for Hg-1223 upon pressure reduction.

T_c on pressure for all three major Hg-containing superconducting phases. It is clear that T_c increases with pressure till 30 GPa before decreasing[6]. A record T_c of 164 K was obtained on Hg-1223.

(ii) Growth of Hg-1201, Hg-1212, and Hg-1223 Thin Films. Attempts have been mode to grow epitaxial thin films of Hg-1201[7], Hg-1212[8–10], and Hg-1223[11–15]. All the

films were made by a two-step procedure: deposition of an amorphous precursor film (with or without Hg) and postdeposition annealing in a tightly sealed quartz tube with Hg supplying source. Deposition of the amorphous films was carried out by rf sputtering, pulsed laser ablation, or spray pyrolysis.

The highest quality epitaxial Hg-1212 film using atomic-scale mixing of HgO and $Ba_2CaCu_2O_5$ on (100) $SrTiO_3$ was produced by layer-by-layer pulsed laser ablation[9,10]. The films were deposited at room temperature in a vacuum ($\sim 10^{-6}$ torr). To minimize the detrimental effects of moisture and CO_2 in the air, the investigators deposited a cap layer of 500–5000 Å of HgO on top. The films were annealed in a carefully controlled Hg atmosphere at a precise temperature and O_2 partial pressure consistent with the thermodynamic requirements for stabilizing the high T_c phase. This was accomplished by enclosing the Hg-cuprate film in an evacuated quartz tube (length, 7 cm; i.d., 0.7 cm) with appropriate amounts of bulk unreacted, stoichiometric Hg-cuprate and pellets of the precursor ($Ba_2CaCu_2O_5$). The amounts of the bulk Hg-cuprate (X) and precursor (P) materials by weight needed to achieve the appropriate Hg and O_2 overpressure at the annealing temperature depend sensitively on the size of the quartz tube and other factors such as the annealing temperature and film composition. Best results were obtained with $X/P = 2$. A typical annealing schedule consists of slow heating at 150°C/h to 750–810°C, which is sustained for 1 h, followed by furnace cooling to room temperature (~ 6 h).

The X-ray diffraction pattern shown in Figure 4 indicates that nearly phase-pure Hg-1212 films can be obtained after the annealing step. The films are epitaxially aligned with the c axis normal to the substrate plane. The c-axis lattice parameter varies to some extent with the annealing treatment and has been obtained in the range of 12.48–12.6 Å, which is somewhat smaller than the value observed in the bulk (12.71 Å).

The electrical resistance as a function of temperature is characterized by a sharp transition with a zero-resistance T_c of 124 K shown in Figure 5. The ac magnetic susceptibility χ (T) (inset of Figure 5) indicates an equally sharp transition starting at 124 K. The transport J_c at 77 K and zero field[10] reached over 10^6 A/cm^2.

Based on the synthesis of Hg-1212 films, high quality epitaxial Hg-1223 films were successfully grown by rf sputtering of $Ba_2Ca_2Cu_3O_7$ and postdeposition annealing with Hg supplied from Hg-containing pellets[11–15]. The precursor $Ba_2Ca_2Cu_3O_7$ films were

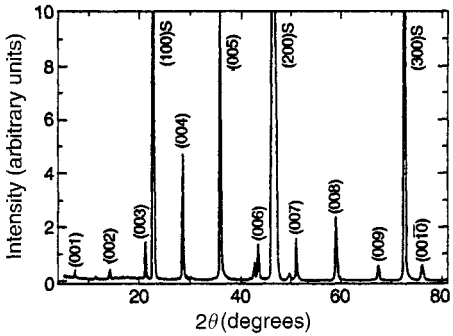

Figure 4. The XRD pattern for a Hg-1212 film (1.5 μm thick with 500 Å MgO cap layer) annealed at 800°C for 1 h with $X/P = 2$; substrate peaks in the pattern are denoted by S.

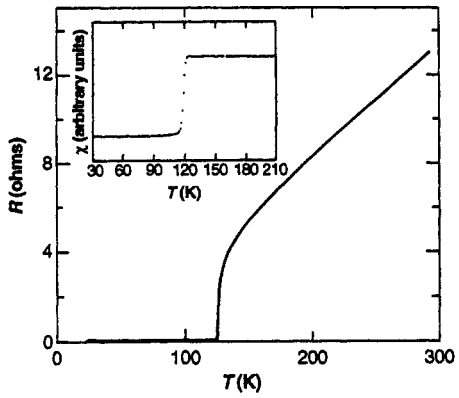

Figure 5. Electrical resistance as a function of temperature for the Hg-1212 film. *Inset*: The inductive component of the ac susceptibility for this film, which was annealed at 755°C for 1 h with $X/P = 2$.

rf-sputtered from a stoichiometric target at room temperature in 0.05 torr of pure Ar on (100) $SrTiO_3$. The target was made from $Ba(NO_3)_2$, CaO, and CuO powders in a plastic bag filled with pure Ar gas, and sintered at 900°C for 17 h in O_2 to eliminate moisture and carbonates. After regrinding, the mixed powder was pressed into a 2 in. disklike target at a pressure of 50,000 kg and baked at the same condition as in the first sintering. Before deposition was begun, the chamber was pumped to 10^{-5} torr and flushed with pure Ar gas. The target was perspired for half an hour each time before the actual deposition to remove the surface layer. The substrate is in the on-axis configuration to the source.

The as-deposited precursor films were sealed in an evacuated quartz tube with pellets of unreacted $Ba_2Ca_2Cu_3O_7$ and $HgBa_2Ca_2Cu_3O_9$ and annealed at 850°C for 30 min. To maintain the proper Hg vapor pressure needed to stabilize the Hg-1223 phase, the ratio between two bulk pellets was chosen to be 1:3. The precursor films were placed in close proximity to the $HgBa_2Ca_2Cu_3O_9$ pellet.

The X-ray diffraction analysis indicated that Hg-1223 dominates the films with small amounts of Hg-1212 phase and impurities. The films are epitaxially aligned with the *c* axis ($\sim$15.3 Å) normal to the plane of the substrate. Most films exhibit a sharp onset of diamagnetism and resistive transitions in the range of 130–133 K. Figure 6 shows the typical zero-field-cooled and field-cooled dc magnetization (M) of a Hg-1223 film in a 4 Oe magnetic field applied normal to the film plane measured in a SQUID magnetometer. The sharp resistive transition at 133 K and zero resistance at 130 K is shown in Figure 7. The estimated magnetization J_c versus temperature is shown in Figure 8. Clearly J_c exceeds 10^6 A/cm^2 at 77 K and zero field. Transport J_c at 77 K and zero field reached 3.5×10^6 A/cm^2.

(iii) Fabrication of Hg-1223 Tapes. Fabrication of Hg-1223 tape has been attempted on Ni substrate with Cr and Ag as buffer layers[16]. A precursor/buffer/Ni composite tape was reacted in a controlled Hg vapor inside a sealed quartz tube according to the vapor/solid reaction technique described above. The precursor was a thoroughly mixed powder of ReO_2, BaO, CaO, and CuO with a nominal proportion of 0.1:2:2:3 (the slight

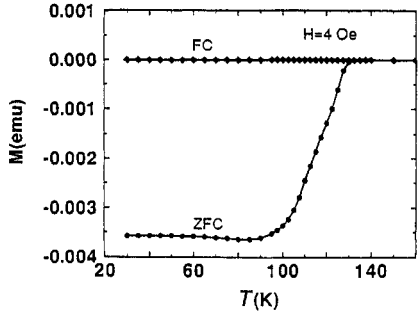

Figure 6. Typical zero-field-cooled and field-cooled dc magnetization (M) of a Hg-1223 film.

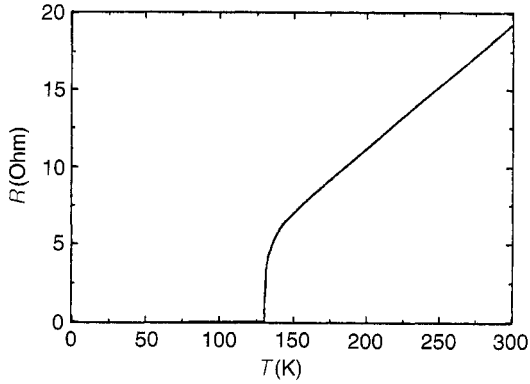

Figure 7. Temperature dependence of the resistivity of a Hg-1223 film sample.

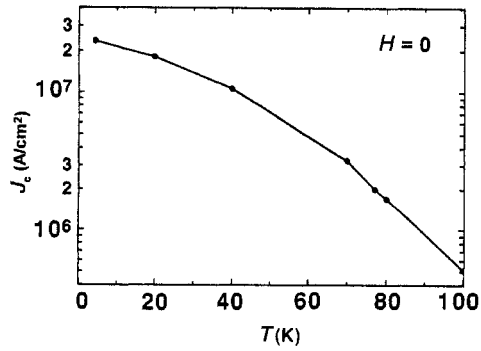

Figure 8. The temperature dependence of J_c of Hg-1223 thin films in the absence of magnetic field.

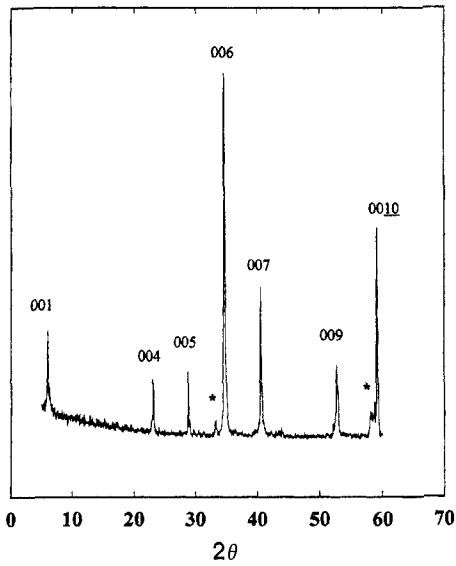

Figure 9. The X-ray diffraction pattern of the Hg-1223 tape.

addition of ReO_2 to the mixture was found to be beneficial to formation of Hg-1223 phase). The mixed powder was heated in a flowing mixture of Ar (8%) and O_2 (92%) at 840–880°C for 40–70 h, with two intermediate grindings. The posttreated precursor was then pulverized with grain sizes between 1 and 10 μm. The powder precursor was mixed with alcohol and sprayed onto the Ni tape with the buffers of Cr/Ag. The precursor/buffer/Ni tape was then compressed under a pressure of 0.27–0.55 GPa at room temperature. The thickness of the precursor layer was 10–40 μm.

To control the Hg vapor pressure, a solid Hg source of pellets of prereacted $Hg_{0.75}Re_{0.1}Ba_2Ca_2Cu_3Cl_{0.15}O_x$ was used. The pellets were obtained by compacting the well-mixed powder of HgO, $HgCl_2$, and the precursor $Re_{0.1}Ba_2Ca_2Cu_3O_x$. The presence of $HgCl_2$ was intended to reduce the formation time to 1 h from 5–55 h, and to promote the growth of Hg-1223 phase. The precursor/buffer/Ni tape and the solid Hg source were sealed inside an evacuated quartz tube and heated at 850–870°C for 1–5 h, followed by air quench to room temperature. The XRD pattern of the Hg-1223 tapes is shown in Figure 9. A preferred *c*-axis alignment was achieved. T_c and J_c on this sample were 130 K (onset) and 117 K (zero resistance) and 2.5×10^4 A/cm^2 at 77 K and zero field, respectively.

(Z. REN, J. WANG)

1. S. N. Putilin, E. V. Antipov, O. Chmaissem, M. Marezio, *Nature*, *362*, 226 (1993).
2. J. L. Wagner, P. G. Radaelli, D. G. Hinks, J. D. Jorgensen, J. F. Mitchell, B. Dabrowski, G. S. Knapp, M. A. Beno, *Physica C*, *210*, 447 (1993).
3. R. L. Meng, Y. Y. Sun, J. Kulik, Z. J. Huang, F. Chen, Y. Y. Xue, C. W. Chu, *Physica C*, *214*, 307 (1993).
4. R. L. Meng, L. Beauvais, X. N. Zhang, Z. J. Huang, Y. Y. Sun, Y. Y. Xue, C. W. Chu, *Physica C*, *216*, 21 (1993).

5. A. Schilling, M. Cantoni, J. D. Guo, H. R. Ott, *Nature, 363*, 56 (1993).
6. L. Gao, Y. Y. Xue, F. Chen, Q. Xiong, R. L. Meng, D. Ramirez, C. W. Chu, J. H. Eggert, H. K. Mao, *Phys. Rev. B, 50*, 4260 (1994).
7. H. Adachi, T. Satoh, K. Setsune, *Appl. Phys. Lett., 63*, 3628 (1993).
8. Y. Q. Wang, R. L. Meng, Y. Y. Sun, K. Ross, *Appl. Phys. Lett., 63*, 3084 (1993).
9. C. C. Tsuei, A. Gupta, G. Trafas, D. Mitzi, *Science, 263*, 1259 (1994).
10. L. Krusin-Elbaum, C. C. Tsuei, A. Gupta, *Nature, 373*, 679 (1995).
11. S. H. Yun, J. Z. Wu, B. W. Kang, A. N. Ray, A. Gapud, Y. Yang, R. Farr, G. F. Sun, S. H. Yoo, Y. Xin, W. S. He, *Appl. Phys. Lett., 67*, 2866 (1995).
12. S. H. Yun, J. Z. Wu, *Appl. Phys. Lett., 68*, 862 (1996).
13. S. H. Yun, J. Z. Wu, S. C. Tidrow, D. W. Eckart, *Appl. Phys. Lett., 68*, 2565 (1996).
14. Y. Moriwaki, T. Sugano, C. Gasser, A. Fukuoka, K. Nakanishi, S. Adachi, K. Tanabe, *Appl. Phys. Lett., 69*, 3423 (1996).
15. F. Foong, B. Bedard, Q. L. Xu, S. H. Liou, *Appl. Phys. Lett., 68*, 1153 (1996).
16. R. L. Meng, B. Hickey, Y. Q. Wang, Y. Y. Sun, L. Gao, Y. Y. Xue, C. W. Chu, *Appl. Phys. Lett., 68*, 3177 (1996).

17.3.10.2.6. Other Cuprates.

Since the first observation of high T_c superconductivity at 110 K (onset) in $(Sr_{1-x}Ca_x)_{1-y}CuO_2$[1], which was first synthesized by Siegrist et al.[2], The synthesis and superconductivity of this compound have been widely studied[3–5] because the cuprate represents the core part, known as the "infinite layer", of cuprate high T_c superconductors. The preparation of infinite layers in a single phase is difficult at ambient pressure and must be carried under high pressure up to 6 GPa.

(Z. REN, J. WANG)

1. M. Azuma, Z. Hiroi, M. Takano, Y. Bando, Y. Takeda, *Nature, 356*, 775 (1992).
2. T. Siegrist, S. M. Zahurac, D. W. Murphy, R. S. Roth, *Nature, 334*, 231 (1988).
3. X. Li, T. Kawai, *Physica C, 229*, 251 (1994).
4. S. Adachi, H. Yamauchi, S. Tanaka, N. Mori, *Physica C, 208*, 226 (1993).
5. Z. Hiroi, M. Azuma, M. Takano, Y. Takeda, *Physica C, 208*, 286 (1993).

17.3.11. Preparation of Ferroelectric Ceramics

17.3.11.1. Introduction

A ferroelectric crystal shows a spontaneous electric polarization that can be reoriented between multiple equilibrium directions by application of an electric field[1–3]. The materials known as ferroelectric ceramics have attained a high level of importance[4].

Applications of ferroelectric ceramics that directly utilize their ferroelectric properties have been reviewed[3]. However, the two major applications of ferroelectric ceramics utilize the ferroelectric properties indirectly:

1. Ceramic capacitors are prepared with their chemical compositions placing them close to a ferroelectric–paraelectric phase boundary, where the dielectric permittivity is anomalously high. These materials are commonly based on $BaTiO_3$ which is similar in structure and properties to the piezoelectric ceramics.
2. Piezoelectric ceramics, which are used as electromechanical transducers, are necessarily ferroelectric as discussed below.

Inorganic Reactions and Methods, Volume 18
Edited by J. J. Zuckerman, Jim D. Atwood

5. A. Schilling, M. Cantoni, J. D. Guo, H. R. Ott, *Nature*, *363*, 56 (1993).
6. L. Gao, Y. Y. Xue, F. Chen, Q. Xiong, R. L. Meng, D. Ramirez, C. W. Chu, J. H. Eggert, H. K. Mao, *Phys. Rev. B*, *50*, 4260 (1994).
7. H. Adachi, T. Satoh, K. Setsune, *Appl. Phys. Lett.*, *63*, 3628 (1993).
8. Y. Q. Wang, R. L. Meng, Y. Y. Sun, K. Ross, *Appl. Phys. Lett.*, *63*, 3084 (1993).
9. C. C. Tsuei, A. Gupta, G. Trafas, D. Mitzi, *Science*, *263*, 1259 (1994).
10. L. Krusin-Elbaum, C. C. Tsuei, A. Gupta, *Nature*, *373*, 679 (1995).
11. S. H. Yun, J. Z. Wu, B. W. Kang, A. N. Ray, A. Gapud, Y. Yang, R. Farr, G. F. Sun, S. H. Yoo, Y. Xin, W. S. He, *Appl. Phys. Lett.*, *67*, 2866 (1995).
12. S. H. Yun, J. Z. Wu, *Appl. Phys. Lett.*, *68*, 862 (1996).
13. S. H. Yun, J. Z. Wu, S. C. Tidrow, D. W. Eckart, *Appl. Phys. Lett.*, *68*, 2565 (1996).
14. Y. Moriwaki, T. Sugano, C. Gasser, A. Fukuoka, K. Nakanishi, S. Adachi, K. Tanabe, *Appl. Phys. Lett.*, *69*, 3423 (1996).
15. F. Foong, B. Bedard, Q. L. Xu, S. H. Liou, *Appl. Phys. Lett.*, *68*, 1153 (1996).
16. R. L. Meng, B. Hickey, Y. Q. Wang, Y. Y. Sun, L. Gao, Y. Y. Xue, C. W. Chu, *Appl. Phys. Lett.*, *68*, 3177 (1996).

17.3.10.2.6. Other Cuprates.

Since the first observation of high T_c superconductivity at 110 K (onset) in $(Sr_{1-x}Ca_x)_{1-y}CuO_2$[1], which was first synthesized by Siegrist et al.[2], The synthesis and superconductivity of this compound have been widely studied[3–5] because the cuprate represents the core part, known as the "infinite layer", of cuprate high T_c superconductors. The preparation of infinite layers in a single phase is difficult at ambient pressure and must be carried under high pressure up to 6 GPa.

(Z. REN, J. WANG)

1. M. Azuma, Z. Hiroi, M. Takano, Y. Bando, Y. Takeda, *Nature*, *356*, 775 (1992).
2. T. Siegrist, S. M. Zahurac, D. W. Murphy, R. S. Roth, *Nature*, *334*, 231 (1988).
3. X. Li, T. Kawai, *Physica C*, *229*, 251 (1994).
4. S. Adachi, H. Yamauchi, S. Tanaka, N. Mori, *Physica C*, *208*, 226 (1993).
5. Z. Hiroi, M. Azuma, M. Takano, Y. Takeda, *Physica C*, *208*, 286 (1993).

17.3.11. Preparation of Ferroelectric Ceramics

17.3.11.1. Introduction

A ferroelectric crystal shows a spontaneous electric polarization that can be reoriented between multiple equilibrium directions by application of an electric field[1–3]. The materials known as ferroelectric ceramics have attained a high level of importance[4].

Applications of ferroelectric ceramics that directly utilize their ferroelectric properties have been reviewed[3]. However, the two major applications of ferroelectric ceramics utilize the ferroelectric properties indirectly:

1. Ceramic capacitors are prepared with their chemical compositions placing them close to a ferroelectric–paraelectric phase boundary, where the dielectric permittivity is anomalously high. These materials are commonly based on $BaTiO_3$ which is similar in structure and properties to the piezoelectric ceramics.
2. Piezoelectric ceramics, which are used as electromechanical transducers, are necessarily ferroelectric as discussed below.

Inorganic Reactions and Methods, Volume 18
Edited by J. J. Zuckerman, Jim D. Atwood

5. A. Schilling, M. Cantoni, J. D. Guo, H. R. Ott, *Nature*, *363*, 56 (1993).
6. L. Gao, Y. Y. Xue, F. Chen, Q. Xiong, R. L. Meng, D. Ramirez, C. W. Chu, J. H. Eggert, H. K. Mao, *Phys. Rev. B*, *50*, 4260 (1994).
7. H. Adachi, T. Satoh, K. Setsune, *Appl. Phys. Lett.*, *63*, 3628 (1993).
8. Y. Q. Wang, R. L. Meng, Y. Y. Sun, K. Ross, *Appl. Phys. Lett.*, *63*, 3084 (1993).
9. C. C. Tsuei, A. Gupta, G. Trafas, D. Mitzi, *Science*, *263*, 1259 (1994).
10. L. Krusin-Elbaum, C. C. Tsuei, A. Gupta, *Nature*, *373*, 679 (1995).
11. S. H. Yun, J. Z. Wu, B. W. Kang, A. N. Ray, A. Gapud, Y. Yang, R. Farr, G. F. Sun, S. H. Yoo, Y. Xin, W. S. He, *Appl. Phys. Lett.*, *67*, 2866 (1995).
12. S. H. Yun, J. Z. Wu, *Appl. Phys. Lett.*, *68*, 862 (1996).
13. S. H. Yun, J. Z. Wu, S. C. Tidrow, D. W. Eckart, *Appl. Phys. Lett.*, *68*, 2565 (1996).
14. Y. Moriwaki, T. Sugano, C. Gasser, A. Fukuoka, K. Nakanishi, S. Adachi, K. Tanabe, *Appl. Phys. Lett.*, *69*, 3423 (1996).
15. F. Foong, B. Bedard, Q. L. Xu, S. H. Liou, *Appl. Phys. Lett.*, *68*, 1153 (1996).
16. R. L. Meng, B. Hickey, Y. Q. Wang, Y. Y. Sun, L. Gao, Y. Y. Xue, C. W. Chu, *Appl. Phys. Lett.*, *68*, 3177 (1996).

17.3.10.2.6. Other Cuprates.

Since the first observation of high T_c superconductivity at 110 K (onset) in $(Sr_{1-x}Ca_x)_{1-y}CuO_2$[1], which was first synthesized by Siegrist et al.[2], The synthesis and superconductivity of this compound have been widely studied[3–5] because the cuprate represents the core part, known as the "infinite layer", of cuprate high T_c superconductors. The preparation of infinite layers in a single phase is difficult at ambient pressure and must be carried under high pressure up to 6 GPa.

(Z. REN, J. WANG)

1. M. Azuma, Z. Hiroi, M. Takano, Y. Bando, Y. Takeda, *Nature*, *356*, 775 (1992).
2. T. Siegrist, S. M. Zahurac, D. W. Murphy, R. S. Roth, *Nature*, *334*, 231 (1988).
3. X. Li, T. Kawai, *Physica C*, *229*, 251 (1994).
4. S. Adachi, H. Yamauchi, S. Tanaka, N. Mori, *Physica C*, *208*, 226 (1993).
5. Z. Hiroi, M. Azuma, M. Takano, Y. Takeda, *Physica C*, *208*, 286 (1993).

17.3.11. Preparation of Ferroelectric Ceramics

17.3.11.1. Introduction

A ferroelectric crystal shows a spontaneous electric polarization that can be reoriented between multiple equilibrium directions by application of an electric field[1–3]. The materials known as ferroelectric ceramics have attained a high level of importance[4].

Applications of ferroelectric ceramics that directly utilize their ferroelectric properties have been reviewed[3]. However, the two major applications of ferroelectric ceramics utilize the ferroelectric properties indirectly:

1. Ceramic capacitors are prepared with their chemical compositions placing them close to a ferroelectric–paraelectric phase boundary, where the dielectric permittivity is anomalously high. These materials are commonly based on $BaTiO_3$ which is similar in structure and properties to the piezoelectric ceramics.
2. Piezoelectric ceramics, which are used as electromechanical transducers, are necessarily ferroelectric as discussed below.

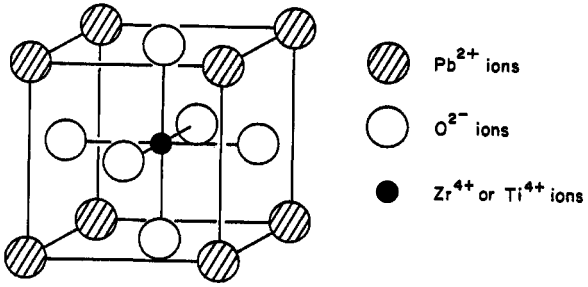

Figure 1. The cubic perovskite structure stable above the Curie temperature in the paraelectric region.

A ceramic body consists of randomly oriented crystalline grains. In ferroelectric ceramics these grains usually contain domains in which polarization is oriented along one of the allowed equilibrium directions. The ceramic body after sintering thus shows no net polarization. However, application of a large electric field in an operation known as "poling" causes reorientation of the polarization, giving a net polarization in the direction of the applied field, a portion of which remains after removal of the field. Poled ferroelectric ceramics exhibit piezoelectricity. The change of magnitude of electric polarization with stress is known as the direct piezoelectric effect[2]. The converse piezoelectric effect—a field-induced change in strain—also occurs[2].

An important group of piezoelectric ceramics are solid solutions of $PbZrO_3$ and $PbTiO_3$ represented as Pb(Zr, Ti)O_3 (and commonly referred to as PZT). At high temperature these compounds have the cubic perovskite structure (Fig. 1). In the ferroelectric phase, which is stable at room temperature, the lattice is distorted, and the asymmetry of the positive and negative ions results in a net dipole moment. Spontaneous polarization is the dipole moment per unit volume.

The following sections discuss Pb(Zr, Ti)O_3 ferroelectric ceramics. However, the preparation techniques are applicable to other materials. Ferroelectric single crystals[1,3] are not included.

(A. I. KINGON, R. E. NEWNHAM)

1. L. E. Cross, K. H. Härdtl, in *Kirk-Othmer: Encyclopedia of Chemical Technology*, Vol. 10, 3rd ed., Wiley, New York, 1980, pp. 1–30.
2. B. Jaffe, W. R. Cook, H. Jaffe, *Piezoelectric Ceramics*, Academic Press, London and New York, 1971.
3. M. E. Lines, A. M. Glass, *Principles and Applications of Ferroelectrics and Related Materials*, Clarendon Press, Oxford, 1977.
4. D. Berlincourt, *Ferroelectrics, 10*, 111 (1976).

17.3.11.2. Pb(Zr, Ti)O_3-Based Ceramics

17.3.11.2.1. The Pb (Zr, Ti)O_3 System.

The subsolidus composition–temperature phase diagram for the unmodified Pb(Zr, Ti)O_3 system is shown in Figure 1[1]. Most useful ceramic formulations are located close to

Inorganic Reactions and Methods, Volume 18
Edited by J. J. Zuckerman, Jim D. Atwood

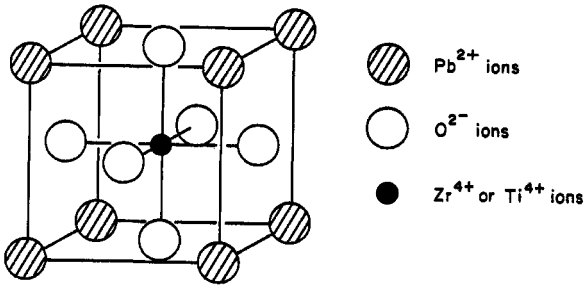

Figure 1. The cubic perovskite structure stable above the Curie temperature in the paraelectric region.

A ceramic body consists of randomly oriented crystalline grains. In ferroelectric ceramics these grains usually contain domains in which polarization is oriented along one of the allowed equilibrium directions. The ceramic body after sintering thus shows no net polarization. However, application of a large electric field in an operation known as "poling" causes reorientation of the polarization, giving a net polarization in the direction of the applied field, a portion of which remains after removal of the field. Poled ferroelectric ceramics exhibit piezoelectricity. The change of magnitude of electric polarization with stress is known as the direct piezoelectric effect[2]. The converse piezoelectric effect—a field-induced change in strain—also occurs[2].

An important group of piezoelectric ceramics are solid solutions of $PbZrO_3$ and $PbTiO_3$ represented as Pb(Zr, Ti)O_3 (and commonly referred to as PZT). At high temperature these compounds have the cubic perovskite structure (Fig. 1). In the ferroelectric phase, which is stable at room temperature, the lattice is distorted, and the asymmetry of the positive and negative ions results in a net dipole moment. Spontaneous polarization is the dipole moment per unit volume.

The following sections discuss Pb(Zr, Ti)O_3 ferroelectric ceramics. However, the preparation techniques are applicable to other materials. Ferroelectric single crystals[1,3] are not included.

(A. I. KINGON, R. E. NEWNHAM)

1. L. E. Cross, K. H. Härdtl, in *Kirk-Othmer: Encyclopedia of Chemical Technology*, Vol. 10, 3rd ed., Wiley, New York, 1980, pp. 1–30.
2. B. Jaffe, W. R. Cook, H. Jaffe, *Piezoelectric Ceramics*, Academic Press, London and New York, 1971.
3. M. E. Lines, A. M. Glass, *Principles and Applications of Ferroelectrics and Related Materials*, Clarendon Press, Oxford, 1977.
4. D. Berlincourt, *Ferroelectrics, 10*, 111 (1976).

17.3.11.2. Pb(Zr, Ti)O_3-Based Ceramics

17.3.11.2.1. The Pb (Zr, Ti)O_3 System.

The subsolidus composition–temperature phase diagram for the unmodified Pb(Zr, Ti)O_3 system is shown in Figure 1[1]. Most useful ceramic formulations are located close to

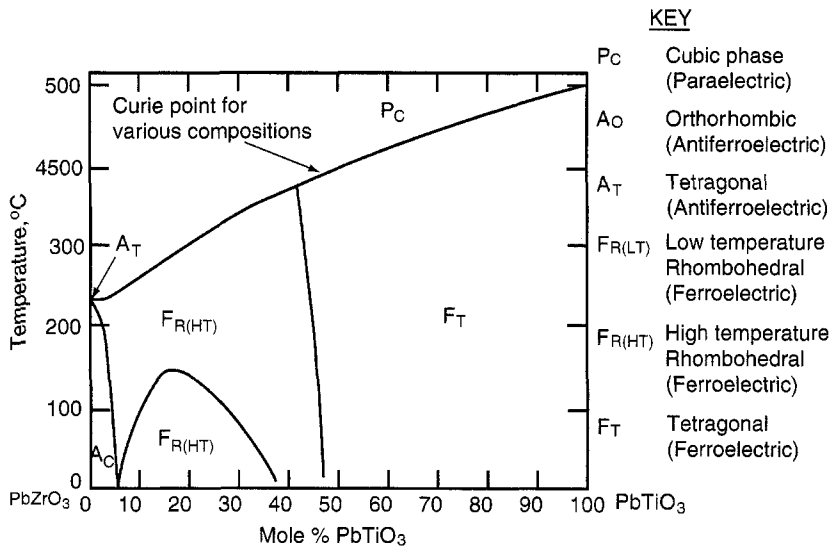

Figure 1. The subsolidus composition–temperature phase diagram for the Pb(Zr, Ti)O_3 system. Regions of phase coexistence are small in the case of all transitions. (adapted from, Ref. 1.)

the morphotrophic phase boundary at $Pb(Zr_{0.52}\,Ti_{0.48})O_3$, where the piezoelectric coefficients and dielectric permittivities show maxima[2]. ZrO_2-rich compositions near the ferroelectric–antiferroelectric phase boundary are also useful as once-off energy sources. Application of pressure to a poled ceramic of these compositions can result in a transition from the ferroelectric to the antiferroelectric state with concomitant charge release[2]. Compositions close to the boundary between low and high temperature rhombohedral ferroelectrics show large pyroelectric coefficients[3].

(A. I. KINGON, R. E. NEWNHAM)

1. B. Jaffe, W. R. Cook, H. Jaffe, *Piezoelectric Ceramics*, Academic Press, London and New York, 1971.
2. P. C. Lysne, C. M. Percival, *J. Appl. Phys.*, *48*, 1020 (1977).
3. R. Clarke, A. M. Glazer, F. W. Ainger, D. Appleby, N. J. Poole, S. G. Porter, *Ferroelectrics 11*, 359 (1976).

17.3.11.2.2. Chemical Dopants and Modifiers.

Unmodified Pb(Zr, Ti)O_3 ceramics are seldom used. The dielectric and electromechanical properties are tailored to a particular device requirement by changing the Zr/Ti ratio and by addition of dopants or modifying agents[1]. Thousands of these formulations have been documented, and some of the more important are summarized.

1. Isovalent substitutions where Sr^{2+} and Ca^{2+} substitute for Pb^{2+} in the perovskite structure. The Sr^{2+} substitution lowers the Curie temperature (ferroelectric–paraelectric transition temperature), thus raising the room temperature dielectric permittivity.

Inorganic Reactions and Methods, Volume 18
Edited by J. J. Zuckerman, Jim D. Atwood

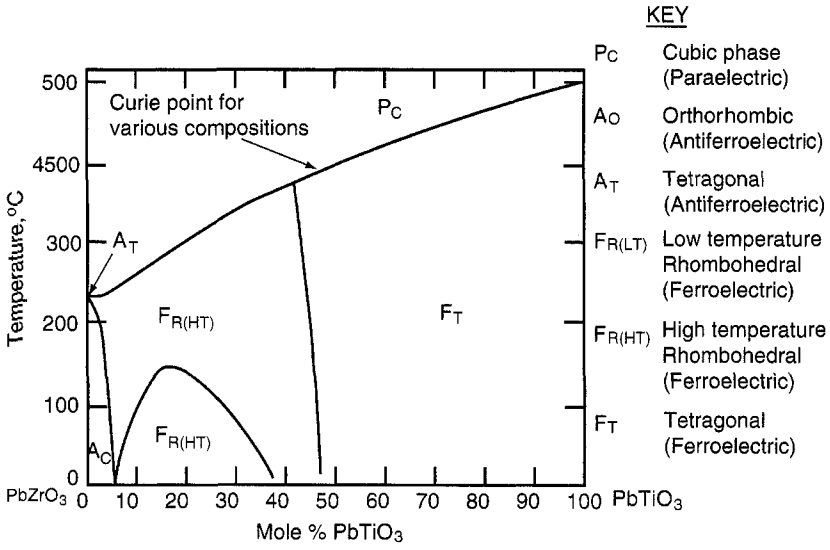

Figure 1. The subsolidus composition–temperature phase diagram for the $Pb(Zr, Ti)O_3$ system. Regions of phase coexistence are small in the case of all transitions. (adapted from, Ref. 1.)

the morphotrophic phase boundary at $Pb(Zr_{0.52}\,Ti_{0.48})O_3$, where the piezoelectric coefficients and dielectric permittivities show maxima[2]. ZrO_2-rich compositions near the ferroelectric–antiferroelectric phase boundary are also useful as once-off energy sources. Application of pressure to a poled ceramic of these compositions can result in a transition from the ferroelectric to the antiferroelectric state with concomitant charge release[2]. Compositions close to the boundary between low and high temperature rhombohedral ferroelectrics show large pyroelectric coefficients[3].

(A. I. KINGON, R. E. NEWNHAM)

1. B. Jaffe, W. R. Cook, H. Jaffe, *Piezoelectric Ceramics*, Academic Press, London and New York, 1971.
2. P. C. Lysne, C. M. Percival, *J. Appl. Phys., 48*, 1020 (1977).
3. R. Clarke, A. M. Glazer, F. W. Ainger, D. Appleby, N. J. Poole, S. G. Porter, *Ferroelectrics 11*, 359 (1976).

17.3.11.2.2. Chemical Dopants and Modifiers.

Unmodified $Pb(Zr, Ti)O_3$ ceramics are seldom used. The dielectric and electromechanical properties are tailored to a particular device requirement by changing the Zr/Ti ratio and by addition of dopants or modifying agents[1]. Thousands of these formulations have been documented, and some of the more important are summarized.

1. Isovalent substitutions where Sr^{2+} and Ca^{2+} substitute for Pb^{2+} in the perovskite structure. The Sr^{2+} substitution lowers the Curie temperature (ferroelectric–paraelectric transition temperature), thus raising the room temperature dielectric permittivity.

The piezoelectric charge coefficient is improved, and the materials is more difficult to depole. A typical composition is $Pb_{0.94}\ Sr_{0.06}(Zr_{0.53}\ Ti_{0.47})O_{3.0}$.

2. Low concentration substitutions of Pb^{2+} or (Zr^{4+}, Ti^{4+}) by ions of more positive valence results in charge stoichiometry correction by loss of PbO during sintering, i.e., in Pb site vacancies in the lattice. Typical substituents are Nb^{5+} for Ti^{4+} and La^{3+} for Pb^{2+} as in the reaction:

$$0.01La_2O_3 + 1.0\,Pb\,(Zr_{0.52}Ti_{0.48})O_{3.0}$$

$$\rightarrow 1.0\ Pb_{0.97}La_{0.02}\square_{0.01}\,(Zr_{0.52}\ Ti_{0.48})O_{3.0} + 0.03\ PbO\uparrow$$

where $\square$ indicates a vacancy in the Pb site. These additives increase the permittivity, elastic compliance, electric resistivity, and piezoelectric charge coefficient, and decrease aging effects[1]. Higher concentrations of La^{3+} dopant result in transparent ceramics used for optic and electrooptic applications[2].

3. Substitution of a more negative valence ion in the Pb or (Zr, Ti) sites results in O-position vacancies. A typical substitutent is Fe^{3+} for Ti^{4+}. Resulting properties include lower dielectric permittivity and decreased depoling effects[1].
4. Compensating valence substitutions where combination of the $PbTiO_3$–$PbZrO_3$ system with other solid solutions occurs, but charge stoichiometry must be maintained. Examples are Pb(Zr,Ti)O_3 with $Pb(Fe_{0.5}Nb_{0.5})O_3$[3] and $Pb(Mg_{0.33}Nb_{0.67})O_3$[4]. These ceramics typically have diffuse ferroelectric–paraelectric phase transitions and therefore high dielectric permittivity over a wide temperature range.

Properties of Pb (Zr, Ti)O_3 ceramic, their modifications, and other ferroelectric materials have been collated[5], and measurement techniques and definitions of term have been standardized[6,7].

(A. I. KINGON, R. E. NEWNHAM)

1. B. Jaffe, W. R. Cook, *Piezoelectric Ceramics*, Academic Press, London and New York, 1971.
2. E. T. Keve, *Ferroelectrics, 10*, 169 (1976)
3. R. W. Whatmore, A. J. Bell, *Ferroelectrics, 35*, 155 (1981).
4. J. Sato, M. Kawabuchi, A. Fukumoto, *Proceedings of the Second Meeting on Ferroelectric Materials and their Applications* (Kyoto, May 1979), Keihin, Japan, 1979, pp. 67–72
5. "Ferroelectrics and related substances," in *Landolt-Börnstein, New Series*, Vol. 16a, (K. H. Hellwege and A. M. Hellwege, eds.). Springer-Verlag, Berlin, 1981.
6. IRE Standards on Piezoelectric Crystals: Measurement of Piezoelectric Ceramics, 1961 *Proc. IRE*, 49, 1169 (1961).
7. IEEE Standard on Piezoelectricity, Std 176–1978, Institute of Eelctrical and Electronics Engineers, New York, 1978.

17.3.11.2.3. Processing Procedures.

Preparation of Pb(Zr, Ti)O_3 occurs by standard ceramic processing techniques (Fig. 1). However, the dielectric and electromechanical properties are extremely sensitive to small changes in processing conditions. Variations in raw materials (impurities, average particle size, particle size distribution, and agglomeration), homogeneity of mixing, powder packing, phase homogeneity, PbO/(Zr, Ti)O_2 stoichiometry, second-phase inclusions, incomplete reaction, sintering conditions, microstructure, and domain structure all affect the ferroelectric and piezoelectric properties of the ceramic. Many of the processing property relations have not been satisfactorily explained despite many years of research.

The piezoelectric charge coefficient is improved, and the materials is more difficult to depole. A typical composition is $Pb_{0.94}\ Sr_{0.06}(Zr_{0.53}\ Ti_{0.47})O_{3.0}$.

2. Low concentration substitutions of Pb^{2+} or (Zr^{4+}, Ti^{4+}) by ions of more positive valence results in charge stoichiometry correction by loss of PbO during sintering, i.e., in Pb site vacancies in the lattice. Typical substituents are Nb^{5+} for Ti^{4+} and La^{3+} for Pb^{2+} as in the reaction:

$$0.01La_2O_3 + 1.0\,Pb\,(Zr_{0.52}Ti_{0.48})O_{3.0}$$

$$\rightarrow 1.0\ Pb_{0.97}La_{0.02}\square_{0.01}\,(Zr_{0.52}\ Ti_{0.48})O_{3.0} + 0.03\ PbO\uparrow$$

where $\square$ indicates a vacancy in the Pb site. These additives increase the permittivity, elastic compliance, electric resistivity, and piezoelectric charge coefficient, and decrease aging effects[1]. Higher concentrations of La^{3+} dopant result in transparent ceramics used for optic and electrooptic applications[2].

3. Substitution of a more negative valence ion in the Pb or (Zr, Ti) sites results in O-position vacancies. A typical substitutent is Fe^{3+} for Ti^{4+}. Resulting properties include lower dielectric permittivity and decreased depoling effects[1].
4. Compensating valence substitutions where combination of the $PbTiO_3$–$PbZrO_3$ system with other solid solutions occurs, but charge stoichiometry must be maintained. Examples are Pb(Zr,Ti)O_3 with $Pb(Fe_{0.5}Nb_{0.5})O_3$[3] and $Pb(Mg_{0.33}Nb_{0.67})O_3$[4]. These ceramics typically have diffuse ferroelectric–paraelectric phase transitions and therefore high dielectric permittivity over a wide temperature range.

Properties of Pb (Zr, Ti)O_3 ceramic, their modifications, and other ferroelectric materials have been collated[5], and measurement techniques and definitions of term have been standardized[6,7].

(A. I. KINGON, R. E. NEWNHAM)

1. B. Jaffe, W. R. Cook, *Piezoelectric Ceramics*, Academic Press, London and New York, 1971.
2. E. T. Keve, *Ferroelectrics, 10*, 169 (1976)
3. R. W. Whatmore, A. J. Bell, *Ferroelectrics, 35*, 155 (1981).
4. J. Sato, M. Kawabuchi, A. Fukumoto, *Proceedings of the Second Meeting on Ferroelectric Materials and their Applications* (Kyoto, May 1979), Keihin, Japan, 1979, pp. 67–72
5. "Ferroelectrics and related substances," in *Landolt-Börnstein, New Series*, Vol. 16a, (K. H. Hellwege and A. M. Hellwege, eds.). Springer-Verlag, Berlin, 1981.
6. IRE Standards on Piezoelectric Crystals: Measurement of Piezoelectric Ceramics, 1961 *Proc. IRE*, 49, 1169 (1961).
7. IEEE Standard on Piezoelectricity, Std 176–1978, Institute of Eelctrical and Electronics Engineers, New York, 1978.

17.3.11.2.3. Processing Procedures.

Preparation of Pb(Zr, Ti)O_3 occurs by standard ceramic processing techniques (Fig. 1). However, the dielectric and electromechanical properties are extremely sensitive to small changes in processing conditions. Variations in raw materials (impurities, average particle size, particle size distribution, and agglomeration), homogeneity of mixing, powder packing, phase homogeneity, PbO/(Zr, Ti)O_2 stoichiometry, second-phase inclusions, incomplete reaction, sintering conditions, microstructure, and domain structure all affect the ferroelectric and piezoelectric properties of the ceramic. Many of the processing property relations have not been satisfactorily explained despite many years of research.

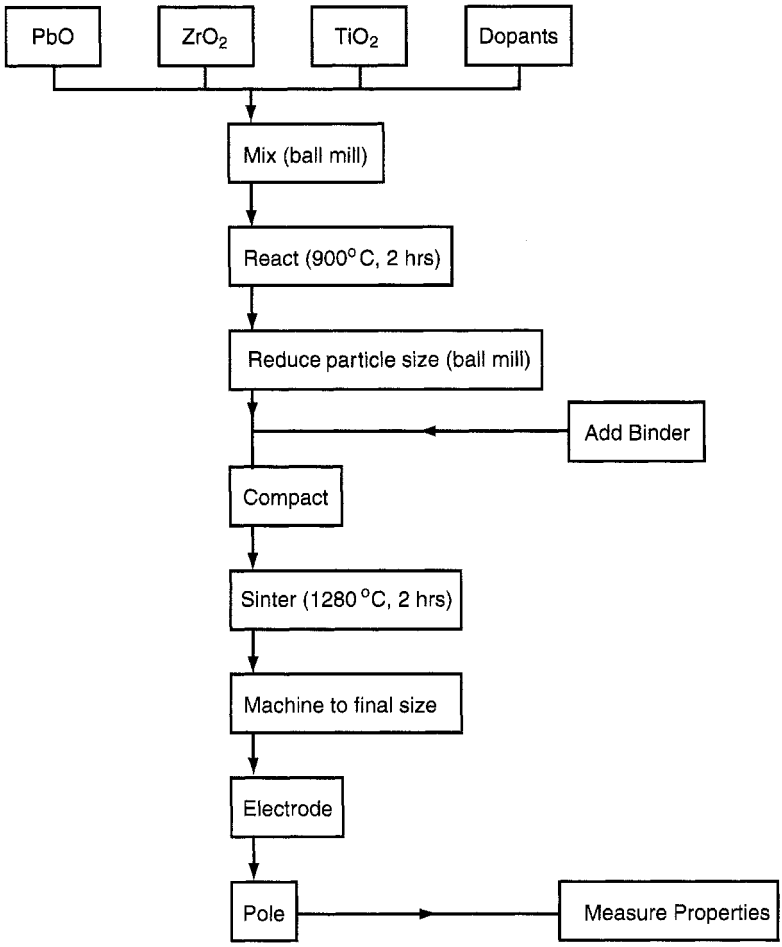

Figure 1. Typical procedure for producing Pb(Zr, Ti)O_3 ferroelectric ceramics by the mixed oxide route.

The need for precise control of properties has resulted in modifications of the mixed oxide technique. These include chemical coprecipitation from various precursors[1,2], freeze-drying[2], and molten salt synthesis[3]. The coprecipitation technique is particularly suited to large scale production.

(A. I. KINGON, R. E. NEWNHAM)

1. M. Murata, K. Wakino, K. Tanaka, Y. Hamakawa, *Mater. Res. Bull., 11*, 323 (1976).
2. J. Thomson Jr., *Am. Ceram. Soc. Bull.*, 53 (5), 421 (1974).
3. R. H. Arendt, J. H. Rosolowski, J. W. Szyrnaszek, *Mater. Res. Bull., 14*, 702 (1979).

Inorganic Reactions and Methods, Volume 18
Edited by J. J. Zuckerman, Jim D. Atwood

17.3.11.2.4. The Reaction Sequence.

Reaction conditions affect the final ceramic properties[1]. The proposed reaction sequence for solid state reaction from the mixed oxides is as follows[1,2]:

1. Reaction of PbO and TiO_2 to form $PbTiO_3$, typically at about 500°C.
2. Dissolution of some $PbTiO_3$ and ZrO_2 and PbO at about 600°C. This solid solution has been reported by a number of workers[1,2], but its exact composition has not been determined. Under certain conditions it is not observed by X-ray diffraction, and its importance in the reaction sequence and its effect on final properties is unknown[3].
3. Reaction of the PbO solid solution with the remaining $PbTiO_3$ and ZrO_2 to form $Pb(Zr, Ti)O_3$ solid solution with wide range of Zr/Ti ratios. It has been suggested that a $PbZrO_3$-rich solid solution is initially formed, along with a $PbTiO_3$-rich solid solution[2].
4. The final step is homogenization of the solid solutions to the product with a small spread in Zr/Ti ratio as observed by X-ray diffraction. This step is normally completed only during high temperature sintering[2].

In the case of coprecipitated precursors, or if the ZrO_2 is of ultrafine particle size, the reaction sequence changes. In the latter case, formation of $PbZrO_3$ is observed[4].

(A. I. KINGON, R. E. NEWNHAM)

1. D. L. Hankey, *Calcination Reaction Mechanisms and Kinetics in Lead Zirconate Titanate Powder Compacts*, Ph.D. thesis, Pennsylvania State University, 1980.
2. A. I. Kingon, *Studies in the Preparation and Characterization of Selected Ferroelectric Materials*, Ph.D. thesis, University of South Africa, 1981.
3. S. Venkataramani, *Calcining and Its Effects on Sintering and Properties of Lead Zirconate Titanate Ceramics*, Ph.D. thesis, Pennsylvania State University, 1981.
4. J. V. Biggers and S. Venkataramani, *Am. Ceram. Sci. Bull.*, *59*, 462 (1981).

17.3.11.2.5. Sintering.

The fabrication of $Pb(Zr, Ti)O_3$ ferroelectric ceramic is complicated by the high volatility of PbO at the sintering temperature of 1250–1300°C. In general, $PbO/(Zr, Ti)O_2$ stoichiometry is controlled by means of a PbO source powder either $PbZrO_3$ or $PbZrO_3 + ZrO_2$ or $Pb(Zr, Ti)O_3$ of the same composition as the ceramics being fired in the sintering enclosure. Source pellets of $PbZrO_3$ or $PbZrO_3$-rich $Pb(Zr, Ti)O_3$ may also be used. If no significant loss of PbO occurs from the enclosure during sintering, then PbO vapor phase transfer occurs between source powder and $Pb(Zr, Ti)O_3$ until equilibrium is reached at equal PbO activities. If the resultant $PbO/(Zr, Ti)O_2$ stoichiometry exceeds unity, a second phase is formed that is PbO-rich[1]. For $PbO/(Zr, Ti)O_2$ stoichiometries slightly less than unity, single-phase, PbO-deficient $PbO(Zr, Ti)O_2$ is formed[2]. Normally, however, a significant amount of PbO escapes from the sintering enclosure. Under these circumstances, it is helpful to use a source powder that has a constant PbO activity over a relatively wide range of PbO concentrations, such as $(PbZrO_3 + ZrO_2)$[3]. In this case, for $Pb(Zr, Ti)O_3$ ceramics with a Zr/Ti ratio of 52 : 48, for example, the stoichiometry that results is $Pb_{0.992}(Zr_{0.52}\ Ti_{0.48})O_{2.992}$. Properties of ceramics with this $PbO/(Zr, Ti)O_2$ stoichiometry are satisfactory[4].

Densification of $Pb(Zr, Ti)O_3$ compacts has been studied as a function of $PbO/(Zr, Ti)O_2$ stoichiometry[4,5]. When $PbO/(Zr, Ti)O_2$ stoichiometry exceeds unity, densification

Inorganic Reactions and Methods, Volume 18
Edited by J. J. Zuckerman, Jim D. Atwood

17.3.11.2.4. The Reaction Sequence.

Reaction conditions affect the final ceramic properties[1]. The proposed reaction sequence for solid state reaction from the mixed oxides is as follows[1,2]:

1. Reaction of PbO and TiO_2 to form $PbTiO_3$, typically at about 500°C.
2. Dissolution of some $PbTiO_3$ and ZrO_2 and PbO at about 600°C. This solid solution has been reported by a number of workers[1,2], but its exact composition has not been determined. Under certain conditions it is not observed by X-ray diffraction, and its importance in the reaction sequence and its effect on final properties is unknown[3].
3. Reaction of the PbO solid solution with the remaining $PbTiO_3$ and ZrO_2 to form Pb(Zr, Ti)O_3 solid solution with wide range of Zr/Ti ratios. It has been suggested that a $PbZrO_3$-rich solid solution is initially formed, along with a $PbTiO_3$-rich solid solution[2].
4. The final step is homogenization of the solid solutions to the product with a small spread in Zr/Ti ratio as observed by X-ray diffraction. This step is normally completed only during high temperature sintering[2].

In the case of coprecipitated precursors, or if the ZrO_2 is of ultrafine particle size, the reaction sequence changes. In the latter case, formation of $PbZrO_3$ is observed[4].

(A. I. KINGON, R. E. NEWNHAM)

1. D. L. Hankey, *Calcination Reaction Mechanisms and Kinetics in Lead Zirconate Titanate Powder Compacts*, Ph.D. thesis, Pennsylvania State University, 1980.
2. A. I. Kingon, *Studies in the Preparation and Characterization of Selected Ferroelectric Materials*, Ph.D. thesis, University of South Africa, 1981.
3. S. Venkataramani, *Calcining and Its Effects on Sintering and Properties of Lead Zirconate Titanate Ceramics*, Ph.D. thesis, Pennsylvania State University, 1981.
4. J. V. Biggers and S. Venkataramani, *Am. Ceram. Sci. Bull.*, *59*, 462 (1981).

17.3.11.2.5. Sintering.

The fabrication of Pb(Zr, Ti)O_3 ferroelectric ceramic is complicated by the high volatility of PbO at the sintering temperature of 1250–1300°C. In general, PbO/(Zr, Ti)O_2 stoichiometry is controlled by means of a PbO source powder either $PbZrO_3$ or $PbZrO_3 + ZrO_2$ or Pb(Zr, Ti)O_3 of the same composition as the ceramics being fired in the sintering enclosure. Source pellets of $PbZrO_3$ or $PbZrO_3$-rich Pb(Zr, Ti)O_3 may also be used. If no significant loss of PbO occurs from the enclosure during sintering, then PbO vapor phase transfer occurs between source powder and Pb(Zr, Ti)O_3 until equilibrium is reached at equal PbO activities. If the resultant PbO/(Zr, Ti)O_2 stoichiometry exceeds unity, a second phase is formed that is PbO-rich[1]. For PbO/(Zr, Ti)O_2 stoichiometries slightly less than unity, single-phase, PbO-deficient PbO(Zr, Ti)O_2 is formed[2]. Normally, however, a significant amount of PbO escapes from the sintering enclosure. Under these circumstances, it is helpful to use a source powder that has a constant PbO activity over a relatively wide range of PbO concentrations, such as ($PbZrO_3 + ZrO_2$)[3]. In this case, for Pb(Zr, Ti)O_3 ceramics with a Zr/Ti ratio of 52 : 48, for example, the stoichiometry that results is $Pb_{0.992}(Zr_{0.52}Ti_{0.48})O_{2.992}$. Properties of ceramics with this PbO/(Zr, Ti)O_2 stoichiometry are satisfactory[4].

Densification of Pb(Zr, Ti)O_3 compacts has been studied as a function of PbO/(Zr, Ti)O_2 stoichiometry[4,5]. When PbO/(Zr, Ti)O_2 stoichiometry exceeds unity, densification

is typical of a liquid-phase-assisted system. With single-phase, PbO-deficient Pb(Zr, Ti)O_3, solid state sintering occurs.

Sintering in an oxygen atmosphere increases the final density from a typical value of 96% of theoretical to 99.5% of theoretical[4].

Special sintering procedures are necessary to produce the transparent La-doped ceramics[6]. In particular, grain and pore sizes must be controlled. Hot pressing[7] and hot isostatic pressing[8] techniques are also used

Preparation techniques for other ferroelectric ceramics are similar to those described above, although none have been investigated in as much detail.

(A. I. KINGON, R. E. NEWNHAM)

1. S. Fushimi, I. Ikeda, *J. Am. Ceram. Soc., 50*, 129 (1967).
2. A. H. Webster, T. B. Weston, N. F. H. Bright, *J. Am. Ceram. Soc. Discuss. Notes*, 50, 190 (1967).
3. R. B. Atkin, R. M. Fulrath, *J. Am. Ceram. Soc., 55*, 192 (1972).
4. A. I. Kingon, *Studies in the Preparation and Characterization of Selected Ferroelectric Materials*, Ph.D. thesis, University of South Africa, 1981.
5. A. I. Kingon, J. B. Clark, *J. Am. Ceram. Soc., 66*, 256 (1983)
6. G. S. Snow, *J. Am. Ceram. Soc. Discuss Notes, 57*, 272 (1974).
7. G. H. Haertling, *J. Am. Ceram. Soc., 49*, 112 (1966).
8. L. J. Bowen, W. A. Schulze, J. V. Biggers, *Powder Met. Int., 12*, 92 (1980).

17.3.11.3. Other Ferroelectctric Ceramics

17.3.11.3.1. $PbTiO_3$-Based.

$PbTiO_3$ is ferroelectric, with useful properties[1], but production of dense, poled ceramics is difficult. Work in Japan revived interest in modified $PbTiO_3$ ceramics. In particular, compositions such as $(Pb_{0.88}\ Nd_{0.10})\ (Ti_{0.92}\ Mn_{0.02}In_{0.05})O_3$ have elastic coefficients almost independent of temperature over a wide range, making them useful in surface acoustic wave (SAW) devices[2]. The dopants also inhibit grain growth during sintering, resulting in easier poling.

(A. I. KINGON, R. E. NEWNHAM)

1. "Ferroelectrics and related substances," in Londolt-Börnstein, New Series, Vol. 16a, K. H. Hellwege and A. M. Hellwege, eds., Springer-Verlag, Berlin, 1981.
2. K. Okazaki, *Ferroelectrics, 35*, 173 (1981).

17.3.11.3.2. Perovskite Niobates and Tantalates.

Many ferroelectric perovskite phases have been reported in Na_2O–K_2O–Nb_2O_5 and Na_2O–K_2O–Ta_2O_5 systems and their modifications[1]. However, the only ceramic material to have found application is $Na_{0.5}K_{0.5}NbO_3$ for high frequency transducers[2].

$Pb(Nb_{0.67}\,Mg_{0.33})O_3$ and its $PbTiO_3$-doped modifications are useful for electrostrictive transducer applications[3]. Preparation of this material is complicated by the appearance of an unwanted pyrochlore phase.

(A. I. KINGON, R. E. NEWNHAM)

1. B. Jaffe, W. R. Cook, H. Jaffe, Piezoelectric Ceramics, Academic Press, London and New York, 1971.
2. D. Berlincourt, in *Ultrasonic Transducer Materials*, E. Mattiat, ed., Plenum Press, New York and London, 1971, pp. 63–124.
3. W. Schulze, T. R. Shrout, S. J. Jang, S. Sharp, L. E. Cross, *J. Am. Ceram. Soc., 63*, 596 (1980).

Inorganic Reactions and Methods, Volume 18
Edited by J. J. Zuckerman, Jim D. Atwood

is typical of a liquid-phase-assisted system. With single-phase, PbO-deficient Pb(Zr, Ti)O_3, solid state sintering occurs.

Sintering in an oxygen atmosphere increases the final density from a typical value of 96% of theoretical to 99.5% of theoretical[4].

Special sintering procedures are necessary to produce the transparent La-doped ceramics[6]. In particular, grain and pore sizes must be controlled. Hot pressing[7] and hot isostatic pressing[8] techniques are also used

Preparation techniques for other ferroelectric ceramics are similar to those described above, although none have been investigated in as much detail.

(A. I. KINGON, R. E. NEWNHAM)

1. S. Fushimi, I. Ikeda, *J. Am. Ceram. Soc., 50*, 129 (1967).
2. A. H. Webster, T. B. Weston, N. F. H. Bright, *J. Am. Ceram. Soc. Discuss. Notes*, 50, 190 (1967).
3. R. B. Atkin, R. M. Fulrath, *J. Am. Ceram. Soc., 55*, 192 (1972).
4. A. I. Kingon, *Studies in the Preparation and Characterization of Selected Ferroelectric Materials*, Ph.D. thesis, University of South Africa, 1981.
5. A. I. Kingon, J. B. Clark, *J. Am. Ceram. Soc., 66*, 256 (1983)
6. G. S. Snow, *J. Am. Ceram. Soc. Discuss Notes, 57*, 272 (1974).
7. G. H. Haertling, *J. Am. Ceram. Soc., 49*, 112 (1966).
8. L. J. Bowen, W. A. Schulze, J. V. Biggers, *Powder Met. Int., 12*, 92 (1980).

17.3.11.3. Other Ferroelectctric Ceramics

17.3.11.3.1. $PbTiO_3$-Based.

$PbTiO_3$ is ferroelectric, with useful properties[1], but production of dense, poled ceramics is difficult. Work in Japan revived interest in modified $PbTiO_3$ ceramics. In particular, compositions such as $(Pb_{0.88}\ Nd_{0.10})\ (Ti_{0.92}\ Mn_{0.02}In_{0.05})O_3$ have elastic coefficients almost independent of temperature over a wide range, making them useful in surface acoustic wave (SAW) devices[2]. The dopants also inhibit grain growth during sintering, resulting in easier poling.

(A. I. KINGON, R. E. NEWNHAM)

1. "Ferroelectrics and related substances," in Londolt-Börnstein, New Series, Vol. 16a, K. H. Hellwege and A. M. Hellwege, eds., Springer-Verlag, Berlin, 1981.
2. K. Okazaki, *Ferroelectrics, 35*, 173 (1981).

17.3.11.3.2. Perovskite Niobates and Tantalates.

Many ferroelectric perovskite phases have been reported in Na_2O–K_2O–Nb_2O_5 and Na_2O–K_2O–Ta_2O_5 systems and their modifications[1]. However, the only ceramic material to have found application is $Na_{0.5}K_{0.5}NbO_3$ for high frequency transducers[2].

$Pb(Nb_{0.67}Mg_{0.33})O_3$ and its $PbTiO_3$-doped modifications are useful for electrostrictive transducer applications[3]. Preparation of this material is complicated by the appearance of an unwanted pyrochlore phase.

(A. I. KINGON, R. E. NEWNHAM)

1. B. Jaffe, W. R. Cook, H. Jaffe, Piezoelectric Ceramics, Academic Press, London and New York, 1971.
2. D. Berlincourt, in *Ultrasonic Transducer Materials*, E. Mattiat, ed., Plenum Press, New York and London, 1971, pp. 63–124.
3. W. Schulze, T. R. Shrout, S. J. Jang, S. Sharp, L. E. Cross, *J. Am. Ceram. Soc., 63*, 596 (1980).

Inorganic Reactions and Methods, Volume 18
Edited by J. J. Zuckerman, Jim D. Atwood

is typical of a liquid-phase-assisted system. With single-phase, PbO-deficient Pb(Zr, Ti)O_3, solid state sintering occurs.

Sintering in an oxygen atmosphere increases the final density from a typical value of 96% of theoretical to 99.5% of theoretical[4].

Special sintering procedures are necessary to produce the transparent La-doped ceramics[6]. In particular, grain and pore sizes must be controlled. Hot pressing[7] and hot isostatic pressing[8] techniques are also used

Preparation techniques for other ferroelectric ceramics are similar to those described above, although none have been investigated in as much detail.

(A. I. KINGON, R. E. NEWNHAM)

1. S. Fushimi, I. Ikeda, *J. Am. Ceram. Soc., 50*, 129 (1967).
2. A. H. Webster, T. B. Weston, N. F. H. Bright, *J. Am. Ceram. Soc. Discuss. Notes*, 50, 190 (1967).
3. R. B. Atkin, R. M. Fulrath, *J. Am. Ceram. Soc., 55*, 192 (1972).
4. A. I. Kingon, *Studies in the Preparation and Characterization of Selected Ferroelectric Materials*, Ph.D. thesis, University of South Africa, 1981.
5. A. I. Kingon, J. B. Clark, *J. Am. Ceram. Soc., 66*, 256 (1983)
6. G. S. Snow, *J. Am. Ceram. Soc. Discuss Notes, 57*, 272 (1974).
7. G. H. Haertling, *J. Am. Ceram. Soc., 49*, 112 (1966).
8. L. J. Bowen, W. A. Schulze, J. V. Biggers, *Powder Met. Int., 12*, 92 (1980).

17.3.11.3. Other Ferroelectctric Ceramics

17.3.11.3.1. $PbTiO_3$-Based.

$PbTiO_3$ is ferroelectric, with useful properties[1], but production of dense, poled ceramics is difficult. Work in Japan revived interest in modified $PbTiO_3$ ceramics. In particular, compositions such as $(Pb_{0.88}\ Nd_{0.10})\ (Ti_{0.92}\ Mn_{0.02}In_{0.05})O_3$ have elastic coefficients almost independent of temperature over a wide range, making them useful in surface acoustic wave (SAW) devices[2]. The dopants also inhibit grain growth during sintering, resulting in easier poling.

(A. I. KINGON, R. E. NEWNHAM)

1. "Ferroelectrics and related substances," in Londolt-Börnstein, New Series, Vol. 16a, K. H. Hellwege and A. M. Hellwege, eds., Springer-Verlag, Berlin, 1981.
2. K. Okazaki, *Ferroelectrics, 35*, 173 (1981).

17.3.11.3.2. Perovskite Niobates and Tantalates.

Many ferroelectric perovskite phases have been reported in Na_2O–K_2O–Nb_2O_5 and Na_2O–K_2O–Ta_2O_5 systems and their modifications[1]. However, the only ceramic material to have found application is $Na_{0.5}K_{0.5}NbO_3$ for high frequency transducers[2].

$Pb(Nb_{0.67}Mg_{0.33})O_3$ and its $PbTiO_3$-doped modifications are useful for electrostrictive transducer applications[3]. Preparation of this material is complicated by the appearance of an unwanted pyrochlore phase.

(A. I. KINGON, R. E. NEWNHAM)

1. B. Jaffe, W. R. Cook, H. Jaffe, Piezoelectric Ceramics, Academic Press, London and New York, 1971.
2. D. Berlincourt, in *Ultrasonic Transducer Materials*, E. Mattiat, ed., Plenum Press, New York and London, 1971, pp. 63–124.
3. W. Schulze, T. R. Shrout, S. J. Jang, S. Sharp, L. E. Cross, *J. Am. Ceram. Soc., 63*, 596 (1980).

Inorganic Reactions and Methods, Volume 18
Edited by J. J. Zuckerman, Jim D. Atwood

17.3.11.3.3. Tungsten Bronzes and Other Layered Structures.

The structure of tungsten bronze materials is more complex than that of the perovskites[1], allowing a wide range of chemical substitutions. Although difficult to prepare, $PbNb_2O_6$ is the most important ferroelectric ceramic in this class, being elastically "soft" and having a large hydrostatic voltage coefficient[2].

Highly anisotropic layer structures typified by $Bi_4\ Ti_3\ O_{12}$, $PbBi_2Nb_2O_9$ and Bi_2WO_6 have been prepared[1]. These materials have high Curie temperatures, but are inherently difficult to pole. Therefore special techniques for grain orienting have been developed, including hot forging and hot pressing[3,4]. Achievement of grain orientation has also been reported by means of preparing particles with a flat morphology through molten salt synthesis followed by tape casting and conventional sintering[5].

(A. I. KINGON, R. E. NEWNHAM)

1. L. E. Cross, K. H. Härdtl, in *Kirk-Othmer: Encyclopedia of Chemical Technology*, Vol. 10, 3rd ed., Wiley, New York, 1980, pp. 1–30.
2. D. Berlincourt, in *Ultrasonic Transducer Materials*, E. Mattiat, ed., Plenum Press, New York and London, 1971, pp. 100–110.
3. Y. Nakaura, H. Igarashi, T. Taniai, K. Okazaki, *Am. Ceram. Soc. Bull., 58*, 853 (1979).
4. K. Okazaki, *Ferroelectrics, 35*, 173 (1981).
5. S. Swartz, W. A. Schulze, J. V. Biggers, *Ferroelectrics, 38*, 765 (1981).

17.3.11.4. Composite Materials

Composite piezoelectric transducers made from poled Pb–Ti–Zr (PZT) ceramics and epoxy polymers form an interesting family of materials which highlight the advantages of composite structures in improving coupled properties in soilds for transduction applications[1]. A number of different connection patterns have been fabricated with the piezoelectric ceramic in the form of spheres, fibers, layered, or three-dimensional skeletons[1]. Adding a polymer phase lowers the density, the dielectric constant, and the mechanical stiffness of the composite, thereby altering electric field and concentrating mechanical stresses on the piezoelectric ceramic phase.

For low frequency electromechanical applications in which the acoustic wavelength is much larger than the scale of component phases, some of the ceramic–polymer composites have piezoelectric voltage coefficients orders of magnitude larger than solid PZT. Such materials have obvious applications in hydrophones and other listening devices.

High frequency applications in which the wavelength is comparable to the scale of the composite macrostructure, show the full potential of composite structures. Impedance, bandwidth, and radiation pattern can be controlled in such systems in a sophisticated manner impossible in single-phase systems. By prepoling PZT fibers or ribbons[2] before the assembly of the composite, it is possible to construct polar solids of new type for use in complex transducer arrays operating in scanning and focusing modes.

Composite materials offer great versatility in coupled-property combinations, that may be exploited in future generations of piezoelectric devices.

(A. T. KINGON, R. E. NEWNHAM)

1. R. E. Newnham, L. J. Bowen, K. A. Klicker, L. E. Cross, *Mater. Eng., 11*, 93 (1980).
2. T. R. Gururaja, L. E. Cross, R. E. Newnham, *Commun. Am. Ceram. Soc., 64*, C8 (1981).

Inorganic Reactions and Methods, Volume 18
Edited by J. J. Zuckerman, Jim D. Atwood

17.3.11.3.3. Tungsten Bronzes and Other Layered Structures.

The structure of tungsten bronze materials is more complex than that of the perovskites[1], allowing a wide range of chemical substitutions. Although difficult to prepare, $PbNb_2O_6$ is the most important ferroelectric ceramic in this class, being elastically "soft" and having a large hydrostatic voltage coefficient[2].

Highly anisotropic layer structures typified by $Bi_4\ Ti_3\ O_{12}$, $PbBi_2Nb_2O_9$ and Bi_2WO_6 have been prepared[1]. These materials have high Curie temperatures, but are inherently difficult to pole. Therefore special techniques for grain orienting have been developed, including hot forging and hot pressing[3,4]. Achievement of grain orientation has also been reported by means of preparing particles with a flat morphology through molten salt synthesis followed by tape casting and conventional sintering[5].

(A. I. KINGON, R. E. NEWNHAM)

1. L. E. Cross, K. H. Härdtl, in *Kirk-Othmer: Encyclopedia of Chemical Technology*, Vol. 10, 3rd ed., Wiley, New York, 1980, pp. 1–30.
2. D. Berlincourt, in *Ultrasonic Transducer Materials*, E. Mattiat, ed., Plenum Press, New York and London, 1971, pp. 100–110.
3. Y. Nakaura, H. Igarashi, T. Taniai, K. Okazaki, *Am. Ceram. Soc. Bull., 58*, 853 (1979).
4. K. Okazaki, *Ferroelectrics, 35*, 173 (1981).
5. S. Swartz, W. A. Schulze, J. V. Biggers, *Ferroelectrics, 38*, 765 (1981).

17.3.11.4. Composite Materials

Composite piezoelectric transducers made from poled Pb–Ti–Zr (PZT) ceramics and epoxy polymers form an interesting family of materials which highlight the advantages of composite structures in improving coupled properties in soilds for transduction applications[1]. A number of different connection patterns have been fabricated with the piezoelectric ceramic in the form of spheres, fibers, layered, or three-dimensional skeletons[1]. Adding a polymer phase lowers the density, the dielectric constant, and the mechanical stiffness of the composite, thereby altering electric field and concentrating mechanical stresses on the piezoelectric ceramic phase.

For low frequency electromechanical applications in which the acoustic wavelength is much larger than the scale of component phases, some of the ceramic–polymer composites have piezoelectric voltage coefficients orders of magnitude larger than solid PZT. Such materials have obvious applications in hydrophones and other listening devices.

High frequency applications in which the wavelength is comparable to the scale of the composite macrostructure, show the full potential of composite structures. Impedance, bandwidth, and radiation pattern can be controlled in such systems in a sophisticated manner impossible in single-phase systems. By prepoling PZT fibers or ribbons[2] before the assembly of the composite, it is possible to construct polar solids of new type for use in complex transducer arrays operating in scanning and focusing modes.

Composite materials offer great versatility in coupled-property combinations, that may be exploited in future generations of piezoelectric devices.

(A. T. KINGON, R. E. NEWNHAM)

1. R. E. Newnham, L. J. Bowen, K. A. Klicker, L. E. Cross, *Mater. Eng., 11*, 93 (1980).
2. T. R. Gururaja, L. E. Cross, R. E. Newnham, *Commun. Am. Ceram. Soc., 64*, C8 (1981).

Inorganic Reactions and Methods, Volume 18
Edited by J. J. Zuckerman, Jim D. Atwood

17.3.12. Preparation of Nuclear Ceramic Materials

17.3.12.1. Fuels

The growth of nuclear energy is influenced by the development and utilization of ceramic fuels and materials for use in power reactors[1-21]. The requirements of low fuel cycle costs, coupled with high performance and reliability in the fuel elements, are factors in the competition with fossil-fueled power plants. The ceramic nuclear fuel elements and materials are subjected to unique operating conditions set by reactor core designs. In addition to accommodating the stresses and temperatures generated by reactor operation, the materials in the reactor core must withstand prolonged exposure to nuclear irradiation and to the coolant.

The choices of nuclear fuel materials and designs are dictated by the characteristics of the reactor cores, namely, the fuel enrichments, the types of coolants and moderators used, the operating temperatures and pressures, the average neutron energy (whether thermal, epithermal, or fast), the fuel burnups, and the operating time in the core. The production of a new fuel element is costly and time-consuming, requiring millions of dollars and more than a decade of effort. However,tremendous savings in power costs can

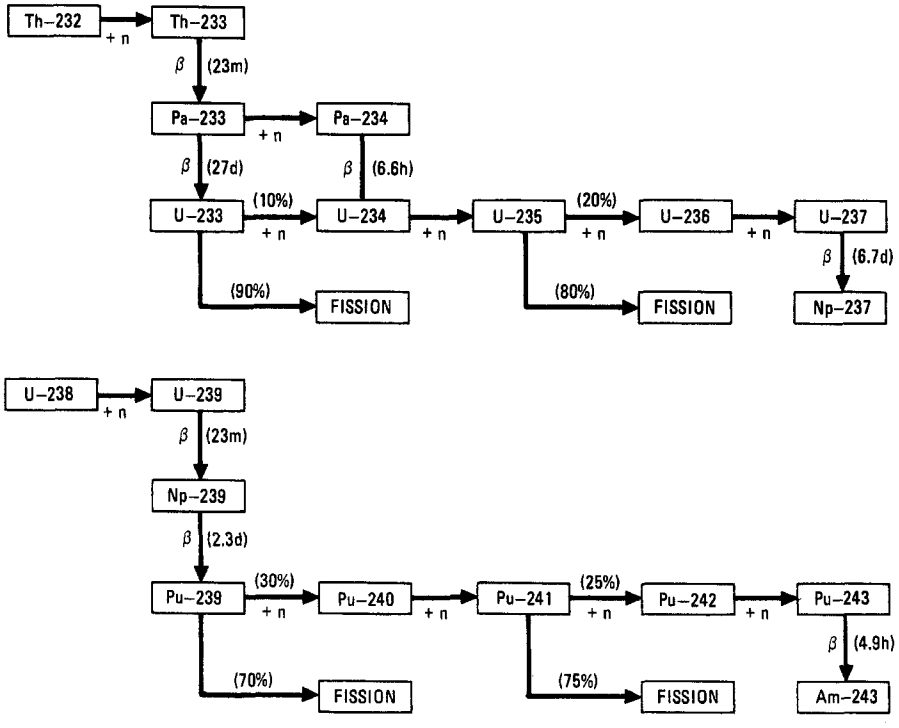

Figure 1. Nuclide chains originating with Th-232 and U-238. (After Ref. 2.)

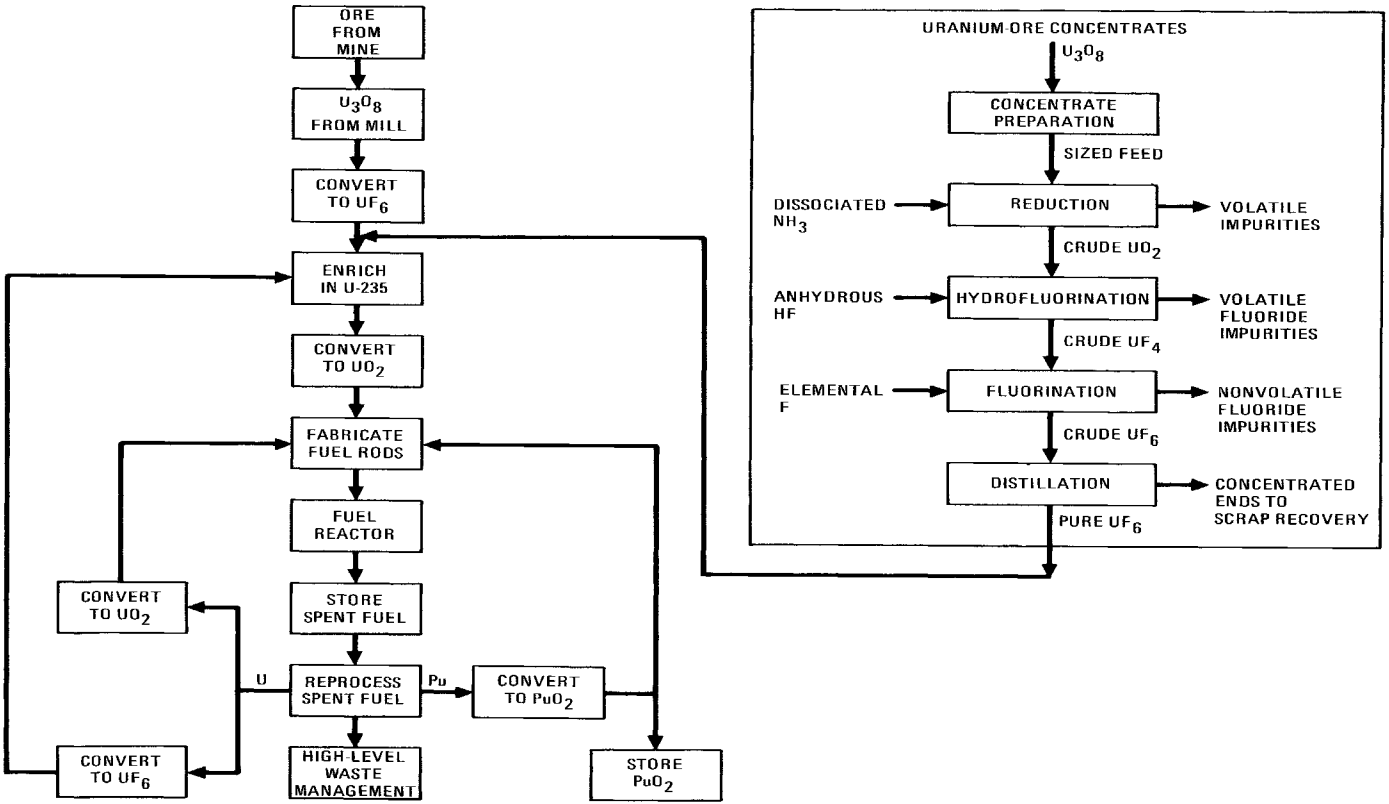

Figure 2. Overall refining process flow diagram with outline of complete uranium fuel cycle. (After Refs. 4, 7.)

result from improvements that lower the fuel cycle costs by only fractions of a mil per kilowatt-hour.

Compacted UO_2 was used in the assembly of the first nuclear exponential lattice in July 1941. The first self-sustaining controlled nuclear chain reaction was achieved in the CP-1 uranium–graphite reactor on December 2, 1942, using 32,652 kg (36 tons) of uranium oxide (both UO_2 and U_3O_8), as well as uranium metal.

The fissionable isotopes are U-233, U-235, Pu-239, and Pu-241. The fertile isotopes U-238 and Th-232 are converted to fissionable isotopes by neutron absorption (U-238 into plutonium isotopes and Th-232 into U-233). Natural uranium contains 0.71% U-235, 99.28% U-238, and 0.006% U-234. Fuel enriched in U-233 and plutonium must be produced from thorium and U-238, respectively (Fig. 1) by neutron capture; the neutrons are provided initially by fission of U-235.

The nuclear fuel cycle consists of (1) production of nuclear fuel (mining, milling, enrichment); (2) fabrication of the fuel elements; (3) reprocessing and recycling of the spent fuel to recover and reuse uranium and plutonium; and (4) storage of the radioactive waste (Fig. 2). Nuclear fuel in its natural state has a low level of radioactivity and does not present a health hazard when correct procedures and adequate ventilation are maintained, but irradiated fuel is highly radioactive and must be handled and treated in shielded facilities. Figure 3 shows the chain yields of fission products. Special precautions have to be taken to minimize dust formation and contamination in handling and fabricating ceramic fuels in powder or particle form. Enrichment of the fuel in the fissile

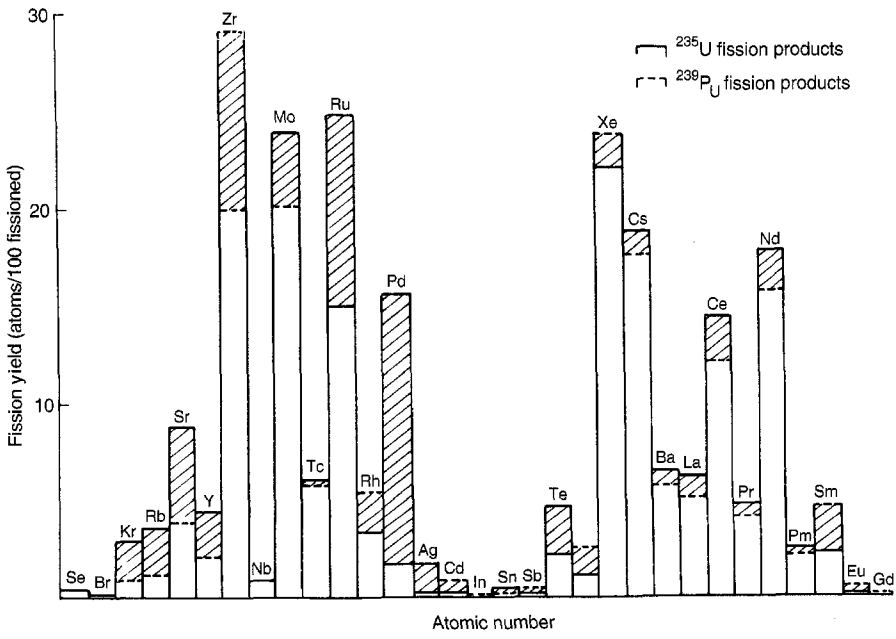

Figure 3. Yield of major fission products for fast fission of U-235 and Pu-239. (After Ref. 2.)

isotope U-235 is required for power reactors in the United States. Hence, the uranium is extracted from the oxide in the form of the hexafluoride (UF_6), which is processed through an isotope separation plant.

Ceramic fuels can be fabricated into precise shapes (usually cylindrical pellets) that are clad in tubular thin-walled metal sheathing (cladding), which is back-filled with helium and end-capped. The cladding in water-cooled reactors in Zircaloy-2 [an alloy of Zr containing 1.4%Sn, 0.13% Fe, 0.1% Cr, Cr. 0.05% Ni, 0.01% N (max)] or stainless steel. It protects the fuel from the reactor coolant, retains the volatile fission products, and provides geometrical integrity. The clad fuel pins are assembled into fuel elements.

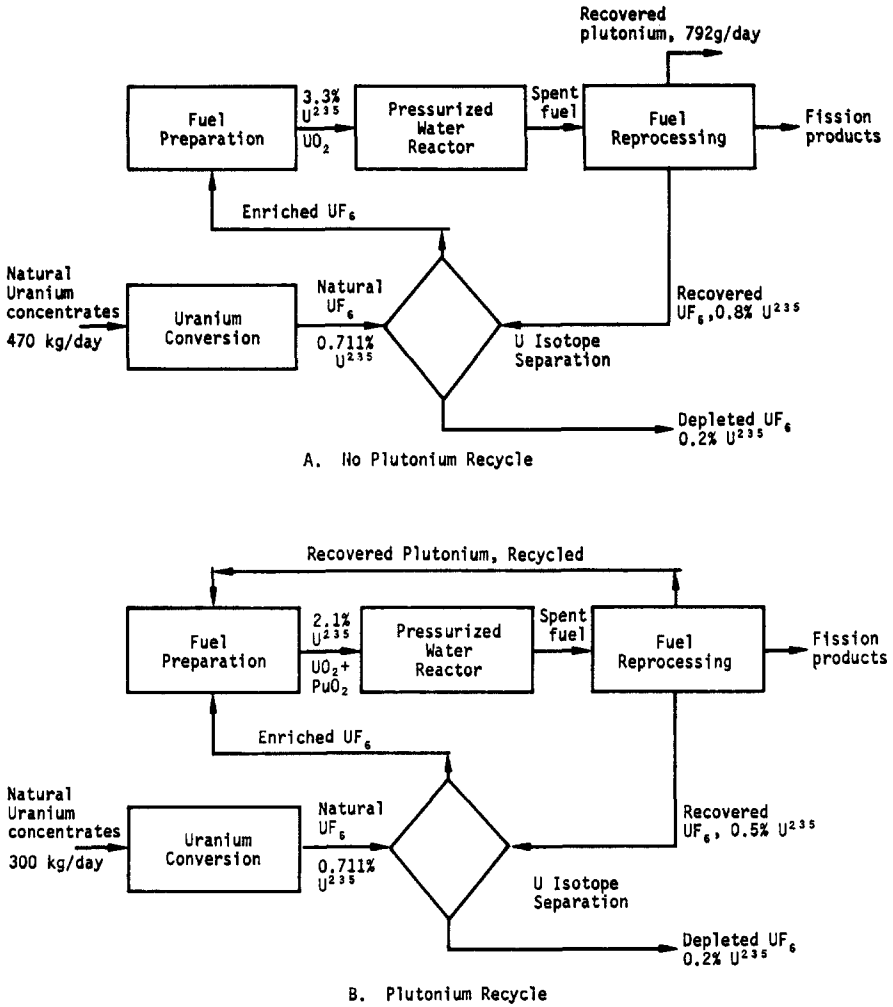

Figure 4. Fuel processing the flow sheets for 1000-MW(e) pressurized water reactor (A) without and (B) with plutonium recycle. (After Ref. 8.)

The fuel elements are held in position by grid plates in the reactor core. The fuel burnup to which a reactor may be operated is expressed as megawatt-days per kilogram (MWd/kg), where MWd is the thermal output and kg is the total uranium (sum of U-235 and U-238). In light-water power reactors the core may be operated to about 35 MWd/kg (about 3.5% burnup) before fuel elements have to be replaced. In liquid metal fast breeder reactors (LMFBRs) and high temperature helium gas-cooled reactors (HTGRs), the burnups may exceed 100 MWd/kg (~10% burnup of the heavy metal atoms).

The fuel elements in power reactor cores are distributed in zones of uranium enrichments, with the highest at the periphery to compensate for the lower neutron flux toward the periphery, and thereby achieve a flatter neutron-flux profile and higher power output. About once a year the fuel elements are discharged from the central zone of the core, and elements in the outer zones are moved inward. Fresh fuel elements are loaded

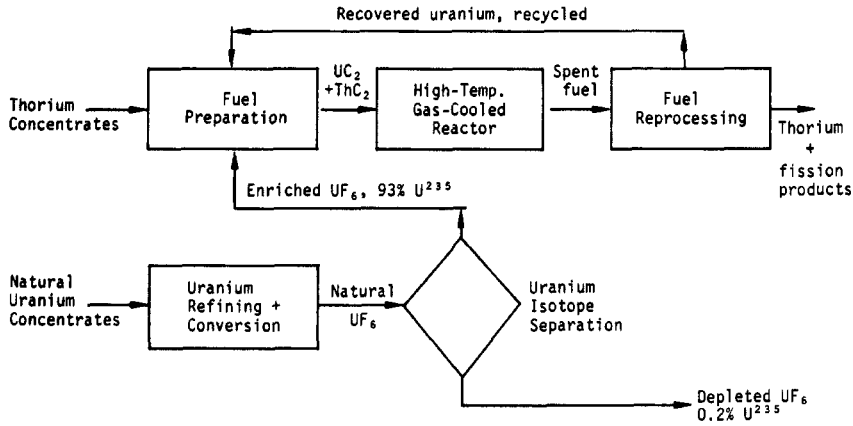

A. High-Temperature Gas-Cooled Reactor

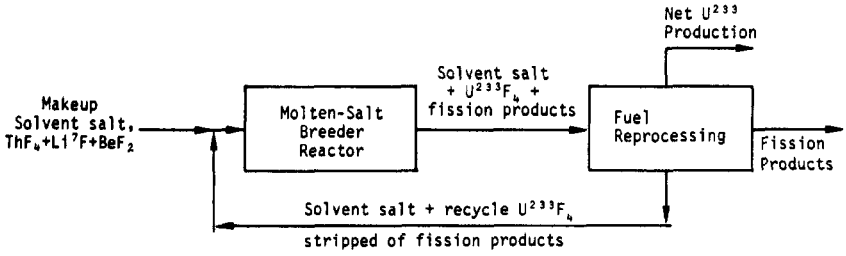

B. Molten-Salt Breeder Reactor

Figure 5. Fuel processing flow sheets for (A) HTGR and (B) Molten salt breeder reactor. (After Ref. 8.)

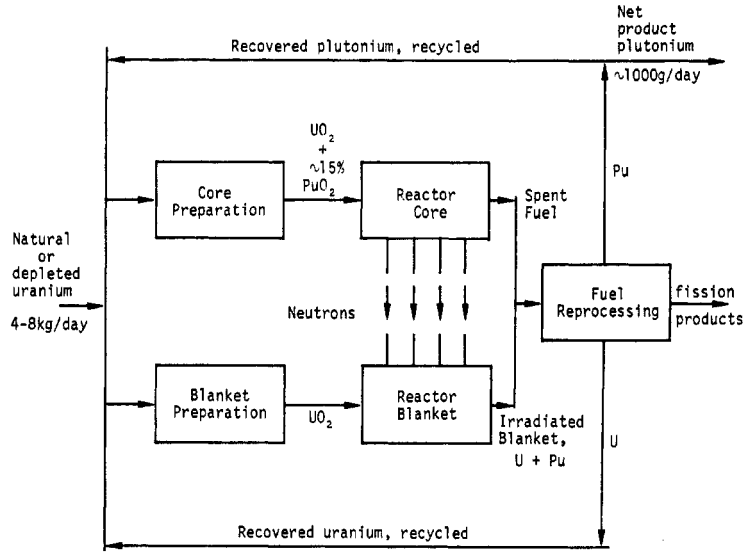

Figure 6. Fuel processing flow sheet for 1000-MW(e) fast breeder reactor. (After Ref. 8.)

TABLE 1. PROPERTIES OF FUELS

Property	Fuels			
	U	U-10% Mo	U_3Si	U-Fa[a]
Melting point, K	1405	1423	1203	1275
Density, g/cm^3	19.12	17.12	15.58	18
Heavy metal desity, g/cm^3	19.12	17.12	15.58	18
Crystal structure	[b]	[c]	bct	bcc (>1000 K)
Thermal conductivity, W/cm K	0.35 (670 K)	0.29 (870 K)	0.2 (to 1170 K)	0.33 (820 K)
Thermal expansion, 10^{-6}/K	19 (to 920 K)	12.3 (to 670 K)	16 (to 1070 K)	17 (to 820 K)
Electrical resistivity, Ω cm	35×10^{-6} (298 K)		75×10^{-6} (to 1070 K)	
Specific heat, cal/g	0.026 (to 773 K)	0.035 (to 773 K)	0.043 (to 773 K)	
Heat of fusion, cal/mol	4760			
Vapor pressure, atm	5×10^{-6} (2300 K)	5×10^{-6} (2300 K)		
Debye temperature, K	200 K			
Free energy of formation, kcal/mol				
Heat of formation, kcal/mol				
Entropy, cal/mol				
Poisson ratio	0.21	0.35		
Modulus of rupture, MPa				
Modulus of elasticity, MPa	1.7×10^5	10^5		6×10^4
Shear modulus, MPa	0.84×10^5	3×10^4		
Tensile strength, MPa	400	300	600	270
Compressive strength, MPa			2000	
Thermal neutron fission cross section, barns	4.18 (natural)	4.18 (natural)	0.159 (natural)	
Thermal neutron absorption cross section, barns	7.68 (natural)	6.68 (natural)	0.293 (natural)	
Eta (η)[d]	1.34	1.34	1.34	1.34

[a] U containing 5% fissium (0.22% Zr + 2.5% Mo + 1.5% Ru + 0.3% Rh + 0.5% Pd). U-5% fissium is bcc above 1000 K, bcc + monoclinic U_2Ru between 825 and 1000 K, and bcc + U_2Ru + tetragonal below 825 K.
[b] Orthorhombic (< 936 K), tetragonal (936–1043 K), body-centered cubic (> 1043 K).
[c] Orthorhombic plus tetragonal (< 838 K), body-centered cubic (> 838 K).
[d] Number of fission neutrons released per neutron absorbed.

TABLE 1 (*continued*)

Property	Fuels		
	UO_2	UC	UC_2
Melting point, K	3138	2780 ± 25	2773
Density, g/cm	10.96	13.61	12.86
Heavy metal desity, g/cm	9.65	12.97	11.68
Crystal structure	fcc (CaF_2)	fcc (NaCl)	fcc (CaF_2)
Thermal conductivity, W/cm K	0.03 (1270 K)	0.216 (to 1270 K)	0.35 (to 1270 K)
Thermal expansion, 10/K	10.1 (to 1270 K)	11.6 (to 1470 K)	18.1 (1970 K)
Electrical resistivity, cm	1×10^3	40.3×10^{-6} (298 K)	
Specific heat, cal/g	0.065 (700 K)	0.048 (298 K)	0.12 (298 K)
Heat of fusion, cal/mol	16,000	11,700	
Vapor pressure, atm	8.5×10^{-8} (2000 K)	1.7×10^{-10} (2300 K)	2.5×10^{-11} (2300 K)
Debye temperature, K	<600 K, 870 K		
Free energy of formation, kcal/mol	−218 (1000 K)	−23.4 (298 K)	
Heat of formation, kcal/mol	−260 (to 1500 K)	−23.63 (298 K)	−23 (298 K)
Entropy, cal/mol	18.6 (298 K)	14.15 (298 K)	16.2 (298 K)
Poisson ratio	0.3	0.284	
Modulus of rupture, MPa	80		
Modulus of elasticity, MPa	1.8×10^5	2×10^5	
Shear modulus, MPa	0.75×10^5	0.873×10^5	
Tensile strength, MPa	35		
Compressive strength, MPa	1000	350	
Thermal neutron fission cross section, barns	0.102 (natural)	0.137 (natural)	0.112 (natural)
Thermal neutron absorption cross section, barns	0.187 (natural)	0.252 (natural)	0.207 (natural)
Eta (η)[a]	1.34	1.34	1.34

[a]Number of fission neutrons released per neutron absorbed.

TABLE 1 (*continued*)

Property	Fuels			
	UN	$(U_{0.8}Pu_{0.2})O_2$	$(U_{0.8}Pu_{0.2})C$	$(U_{0.8}Pu_{0.2})N$
Melting point, K	3035 (1 atm N_2)	3023	2758 ± 25	3053
Density, g/cm^3	14.32	11.04	13.58	14.31
Heavy metal desity, g/cm^3	13.52	9.80	12.3 (2.6 Pu)	13.5 (2.7 Pu)
Crystal structure	fcc (NaCl)	Cubic (CaF_2)	fcc (NaCl)	fcc (NaCl)
Thermal conductivity, W/cm K	0.2 (1023 K)	0.027 (1270 K)	0.18 (to 1270 K)	0.19 (to 1270 K)
Thermal expansion, 10^{-6}/K	9.3 (to 1270 K)	10.3 (to 1270 K)	12.2 (to 1670 K)	9.8 (to 1270 K)
Electrical resistivity, Ω cm	1.75×10^{-4} (298 K)	2×10^4	1.82×10^{-4}	
Specific heat, cal/g	0.049 (298 K)	0.10	0.047 (298 K)	0.046 (298 K)
Heat of fusion, cal/mol	12,750		10,920	12,590
Vapor pressure, atm	4.5×10^{-7} (2000 K)		8.1×10^{-9} (2000 K)	2.1×10^{-6} (2000 K)
Debye temperature, K				
Free energy of formation, kcal/mol	−64.75 (298 K)		21.00	
Heat of formation, kcal/mol	−70.70 (298 K)		21.18	71.10
Entropy, cal/mol	15.0 (298 K)		14.80	
Poisson ratio	0.263	0.28	0.295	0.275
Modulus of rupture, MPa				
Modulus of elasticity, MPa		1.8×10^5		
Shear modulus, MPa	1.01×10^5	0.53×10^5	0.78×10^5	1.02×10^5
Tensile strength, MPa				
Compressive strength, MPa				
Thermal neutron fission cross section, barns	0.143 (natural)			
Thermal neutron absorption cross section, barns	0.327 (natural)			
Eta (η)[a]				

[a]Number of fission neutrons released per neutron absorbed.

TABLE 1 (*continued*)

Property	Fuels		
	Th	ThO_2	ThC
Melting point, K	2028	3663	2898
Density, g/cm	11.72	10.00	10.96
Heavy metal desity, g/cm	11.72	9.36	10.46
Crystal structure	fcc $<$ 1618 K $<$ bcc	Cubic (CaF_2)	Cubic (NaCl)
Thermal conductivity, W/cm K	0.45 (923 K)	0.03 (1270 K)	0.28 (to 1270 K)
Thermal expansion, 10/K	12.5 (to 923 K)	9.32 (to 1270 K)	7.8 (to 1270 K)
Electrical resistivity, cm	15.7×10^{-6}		25×10^{-6} (298 K)
Specific heat, cal/g	0.038 (970 K)	0.07 (298 K)	0.043 (298 K)
Heat of fusion, cal/mol	3300	25,000	
Vapor pressure, atm	1.3×10^{-14} (1500 K)	5×10^{-9} (2000 K)	
Debye temperature, K	163.5 K	200 K	
Free energy of formation, kcal/mol		−279(298 K)	−6.4 (298 K)
Heat of formation, kcal/mol		−293 (298 K)	−7.0 (298 K)
Entropy, cal/mol		15.59 (298 K)	12.0 (298 K)
Poisson ratio	0.27	0.17	
Modulus of rupture, MPa		80	
Modulus of elasticity, MPa	7×10^4	14×10^4	
Shear modulus, MPa	2.7×10^4	1×10^5	
Tensile strength, MPa	230	100	
Compressive strength, MPa		1500	450
Thermal neutron fission cross section, barns	—		
Thermal neutron absorption cross section, barns	7.56		
Eta (η)[a]			

[a]Number of fission neutrons released per neutron absorbed.

into the vacated outer zone. The factors that limit fuel rod performance are pellet/clad interaction, fission gas release, and rod bowing.

The economic effects of fuel design, fabrication, and quality control on nuclear power generating costs can be assessed[14]. Factors that reduce costs include decreasing fuel failure rates, increasing margin to thermal operating limits in the fuel elements, and improving fuel utilization. Fuel cycle costs are ~25% of the nuclear operating costs, and increased core output and fuel reliability will increase the plant capacity factor and reduce the total system reserve requirements and costs, particularly by decreasing the need for costly replacement power.

The performance requirements for ceramic nuclear fuel elements include the following[18]: dimensional stability to high fuel burnups, fission product retention, corrosion resistance, high thermal performance, fabricability, economic advantage, inspectability, and chemical reprocessing and recycling.

The operating characteristics of oxide fuel elements depend on the configuration and dimensions of the fuel pellets, the compositions of the cladding, fabrication methods, fuel center temperatures, and heat fluxes. There has to be a compromise between the conflicting requirements of the materials scientist, the thermal designer, and the nuclear physicist[18,22,23]. Long-term, in-pile tests under simulated reactor operating environments are used to evaluate the performance of fuel elements. Figures 1–6 illustrate fuel processing flow sheets for reactor systems of four types.

The oxides UO_2, (U, Pu)O_2, and ThO_2, which have face-centered-cubic fluorite structures and are completely miscible in solid solution, are the most extensively used

ceramic fuels. The carbide fuels UC, UC_2, (U, Pu) C, and ThC_2 are also used, and nitride fuels are prepared and irradiated in test reactors. The properties of these fuels are summarized in Table 1.

(MASSOUD T. SIMNAD)

1. M. T. Simnad, *Fuel Element Experience in Nuclear Power Reactors*, Gordon & Breach, New York, 1971.
2. M. T. Simnad, J. P. Howe, in *Material Science in Energy Technology*, G. G. Libowitz, M. S. Whittingham, eds., Academic Press, New York, 1979, p. 32.
3. M. T. Simnad, L. R. Zumwalt, eds., *Materials and Fuels for High Temperature Nuclear Energy Applications*, MIT Press, Cambridge, MA, 1964.
4. S. Glasstone, A. Sesonske, *Nuclear Reactor Engineering*, 3rd ed., Van Nostrand-Reinhold, Princeton, NJ, 1980.
5. J. R. La Marsh, *Introduction to Nuclear Engineering*, Addison-Wesley, Reading, MA, 1975.
6. M. Benedict, T. Pigford, *Nuclear Chemical Engineering*, McGraw-Hill, New York, 1976.
7. E. S. Pedersen, *Nuclear Power*, 2 vols., Ann Arbor Science Publishers, Ann. Arbor, MI, 1978.
8. D. M. Elliott, L. E. Weaver, eds., *Education and Research in the Nuclear Fuel Cycle*, University of Oklahoma Press, Norman, 1972.
9. O. Wick, ed., *Plutonium Handbook*, American Nuclear Society, La Grange Park, IL, 1980.
10. J. T. Long, *Engineering for Nuclear Fuel Reprocessing*, Gordon & Breach, New York, 1967.
11. D. R. Olander, *Fundamental Aspects of Nuclear Reactor Fuel Elements*, TID-26711-P1, National Technical Information Service, U.S. Department of Commerce, Springfield, VA, 1976.
12. R. B. Holden, *Ceramic Fuel Elements, Gordon & Breach*, New York, 1966.
13. J. E. Harris, E. C. Sykes, eds., *Physical Metallurgy of Reactor Fuel Elements*, The Metals Society, London, 1975.
14. *Nuclear Power and Its Fuel Cycle, Proc. Int. Conf.*, Salzburg, May 2–13, 1977, 8 vols.; International Atomic Energy Agency, Vienna, 1977.
15. *Nuclear Metallurgy, Proc. Biennial Conf. 1955–1977.* Vols. 1–19, American Institute of Mining Engineers, New York, 1955 to 1977.
16. R. B. Kotelnikov, S. N. Bashlykov, A. I. Kashtamon, *High Temperature Nuclear Fuels*, Atomizdat, Moscow, 1978.
17. *Conference on Reactor Materials Science, Proc. Conf.*, Alushta, USSR, May 29, 1978 (CONF-7805178-P6); Atomizdad, Moscow, 1978.
18. J. Belle, ed., *Uranium Dioxide: Properties and Nuclear Applications*, Division of Reactor Development, U.S., Atomic Energy Commission, Washington, DC, 1961.
19. M. T. Simnad, *Review of Fuel Element Developments for Water Cooled Nuclear Power Reactors*, International Atomic Energy Agency, Vienna, 1989.
20. R. G. Cochran, N. Tsoulfanidis, *The Nuclear Fuel Cycle: Analysis and Management*, American Nuclear Society La Grange Park, IL, 1990.
21. B. R. T. Frost, ed., *Nuclear Materials*, Vol. 10 in R. W. Cahn, P. Haasen, E. J. Kramer, eds., *Materials Science and Technology*, VCH, Weinheim, 1994.
22. *Fabrication of Water Reactor Fuel Elements, Proc. Symp.*, Prague, Nov. 6–10, 1978; International Atomic Energy Agency, Vienna, 1979.
23. *Light Water Reactor Fuel Performance, Proc. Topical Meeting*, Portland, Or, April 29–May 3, 1979; American Nuclear Society, La Grange, IL, 1979.

17.3.12.1.1. Uranium Dioxide Fuels.

The oxide ceramic fuels exhibit high neutron utilization, irradiation stability, corrosion resistance in conventional coolants, high melting point, compatibility with cladding, ease of manufacture, and high specific power and power per unit length of fuel pin, but low thermal conductivity, poor thermal shock resistance, and low fissionable atom density compared with metallic and carbide fuels. The high melting points of the oxide compensate for the low thermal conductivity.

Inorganic Reactions and Methods, Volume 18
Edited by J. J. Zuckerman, Jim D. Atwood

ceramic fuels. The carbide fuels UC, UC_2, (U, Pu) C, and ThC_2 are also used, and nitride fuels are prepared and irradiated in test reactors. The properties of these fuels are summarized in Table 1.

(MASSOUD T. SIMNAD)

1. M. T. Simnad, *Fuel Element Experience in Nuclear Power Reactors*, Gordon & Breach, New York, 1971.
2. M. T. Simnad, J. P. Howe, in *Material Science in Energy Technology*, G. G. Libowitz, M. S. Whittingham, eds., Academic Press, New York, 1979, p. 32.
3. M. T. Simnad, L. R. Zumwalt, eds., *Materials and Fuels for High Temperature Nuclear Energy Applications*, MIT Press, Cambridge, MA, 1964.
4. S. Glasstone, A. Sesonske, *Nuclear Reactor Engineering*, 3rd ed., Van Nostrand-Reinhold, Princeton, NJ, 1980.
5. J. R. La Marsh, *Introduction to Nuclear Engineering*, Addison-Wesley, Reading, MA, 1975.
6. M. Benedict, T. Pigford, *Nuclear Chemical Engineering*, McGraw-Hill, New York, 1976.
7. E. S. Pedersen, *Nuclear Power*, 2 vols., Ann Arbor Science Publishers, Ann. Arbor, MI, 1978.
8. D. M. Elliott, L. E. Weaver, eds., *Education and Research in the Nuclear Fuel Cycle*, University of Oklahoma Press, Norman, 1972.
9. O. Wick, ed., *Plutonium Handbook*, American Nuclear Society, La Grange Park, IL, 1980.
10. J. T. Long, *Engineering for Nuclear Fuel Reprocessing*, Gordon & Breach, New York, 1967.
11. D. R. Olander, *Fundamental Aspects of Nuclear Reactor Fuel Elements*, TID-26711-P1, National Technical Information Service, U.S. Department of Commerce, Springfield, VA, 1976.
12. R. B. Holden, *Ceramic Fuel Elements, Gordon & Breach*, New York, 1966.
13. J. E. Harris, E. C. Sykes, eds., *Physical Metallurgy of Reactor Fuel Elements*, The Metals Society, London, 1975.
14. *Nuclear Power and Its Fuel Cycle, Proc. Int. Conf.*, Salzburg, May 2–13, 1977, 8 vols.; International Atomic Energy Agency, Vienna, 1977.
15. *Nuclear Metallurgy, Proc. Biennial Conf. 1955–1977.* Vols. 1–19, American Institute of Mining Engineers, New York, 1955 to 1977.
16. R. B. Kotelnikov, S. N. Bashlykov, A. I. Kashtamon, *High Temperature Nuclear Fuels*, Atomizdat, Moscow, 1978.
17. *Conference on Reactor Materials Science, Proc. Conf.*, Alushta, USSR, May 29, 1978 (CONF-7805178-P6); Atomizdad, Moscow, 1978.
18. J. Belle, ed., *Uranium Dioxide: Properties and Nuclear Applications*, Division of Reactor Development, U.S., Atomic Energy Commission, Washington, DC, 1961.
19. M. T. Simnad, *Review of Fuel Element Developments for Water Cooled Nuclear Power Reactors*, International Atomic Energy Agency, Vienna, 1989.
20. R. G. Cochran, N. Tsoulfanidis, *The Nuclear Fuel Cycle: Analysis and Management*, American Nuclear Society La Grange Park, IL, 1990.
21. B. R. T. Frost, ed., *Nuclear Materials*, Vol. 10 in R. W. Cahn, P. Haasen, E. J. Kramer, eds., *Materials Science and Technology*, VCH, Weinheim, 1994.
22. *Fabrication of Water Reactor Fuel Elements, Proc. Symp.*, Prague, Nov. 6–10, 1978; International Atomic Energy Agency, Vienna, 1979.
23. *Light Water Reactor Fuel Performance, Proc. Topical Meeting*, Portland, Or, April 29–May 3, 1979; American Nuclear Society, La Grange, IL, 1979.

17.3.12.1.1. Uranium Dioxide Fuels.

The oxide ceramic fuels exhibit high neutron utilization, irradiation stability, corrosion resistance in conventional coolants, high melting point, compatibility with cladding, ease of manufacture, and high specific power and power per unit length of fuel pin, but low thermal conductivity, poor thermal shock resistance, and low fissionable atom density compared with metallic and carbide fuels. The high melting points of the oxide compensate for the low thermal conductivity.

Uranium dioxide can take up oxygen interstitially to form hyperstoichiometric UO_{2+x}, where x may be high as 0.25 at high temperatures. As the temperature is lowered, a phase having the composition U_4O_9 precipitates. Hypostoichiometric oxides of uranium UO_{2-x} form under conditions of low oxygen partial pressure at high temperatures and revert to stoichiometric UO_2, precipitating U on cooling. Unsintered, finely divided UO_2 powders oxidize to U_3O_8 when exposed to air at room temperature.

Nonstoichiometry diminishes the already low thermal conductivity, lowers the melting point and strength, increases creep and fission product migration and release, and alters irradiation behavior. The increase in oxygen activity with burnup can be significant in leading rods in light-water reactors (5%burnup) and in fast breeder reactor fuels (10% burnup).

The allowable values of the thermal conductivity integral and the temperatures within pellets are estimated from observation of microstructures; e.g., the melting point boundary corresponds to 2865°C, columnar grain growth to1700°C, and equiaxed growth to 1500°C. The integral conductivity values from 500°C to melting are 63–73 W/cm. The thermal conductivity of UO_2 decreases as the O/U ratio is increased.

The melting point of 2865 ± 15°C for stoichiometric UO_2 drops to 2425°C at an O/U ratio of 1.68 and to 2500°C at an O/U ratio of 2.25. Lowering of the melting point to 2620°C occurs at a burnup of 1.5×10^{21} fissions/cm^3. As the O/U exceeds 2, the rates of creep, sintering, diffusion, and other processes depending on mobile defects increase sharply.

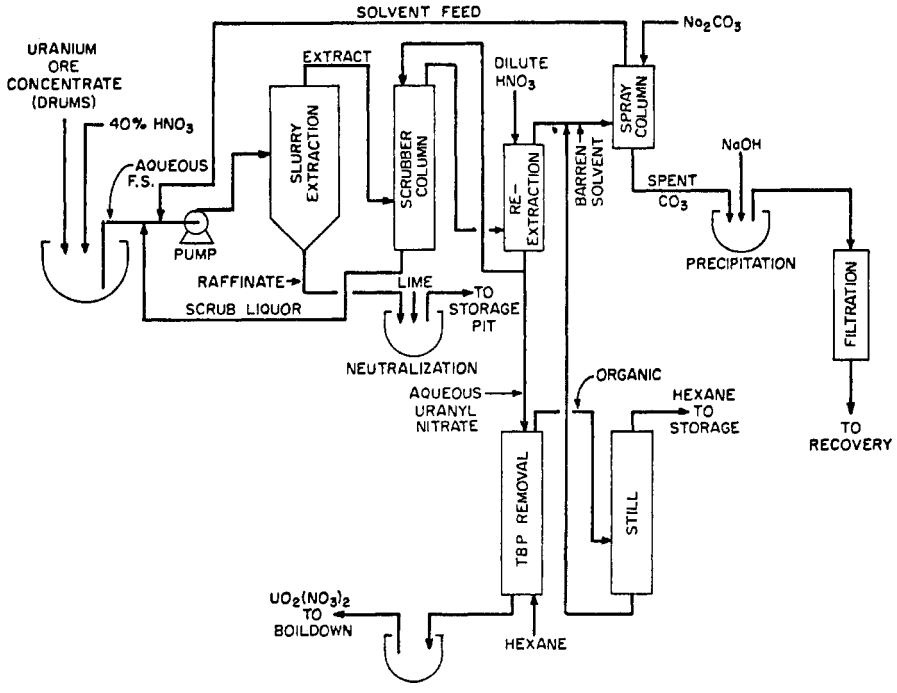

Figure 1. Purification of ore concentrate. (After Ref. 1.)

Bulk oxide fuels are fabricated by cold compaction followed by sintering at an elevated temperature. Loose particles or optimum mixtures of several sizes of spherical (sol–gel) particles are packed directly into the cladding, and such particulate fuel is subjected to vibratory compaction.

The uranium oxide (yellow cake) obtained from milling must be purified before it can be used in nuclear fuels. The characteristics of the UO_2 powder are determined by its method of preparation. Purification is accomplished by solvent extraction or by the hydrofluor process. In the solvent extraction method (Fig. 1), the uranium oxide concentrate is dissolved in nitric acid and the resulting solution is evaporated to dryness[1]. The resulting uranium nitrate is calcined at approximately 350–450°C to UO_3 (orange oxide). The UO_3 is reduced to UO_2 by hydrogen at ~ 600°C. In the hydrofluorination process, the nitrate solution may be reacted with ammonia to precipitate ammonium diuranate, which is filtered, dried, calcined, and reduced by hydrogen to UO_2. The UO_2 is converted to solid UF_4 (green salt, mp 960°C) by HF gas (Fig. 2)[1]. It is reacted with fluorine gas F_2 in enrichment plants. The reaction is exothermic and the reactor towers are cooled during operation to 450–550°C to form volatile UF_6 (sublimes 56°C) (Fig. 3)[1], which is used as the feed material in gaseous diffusion plants for the enrichment of the uranium.

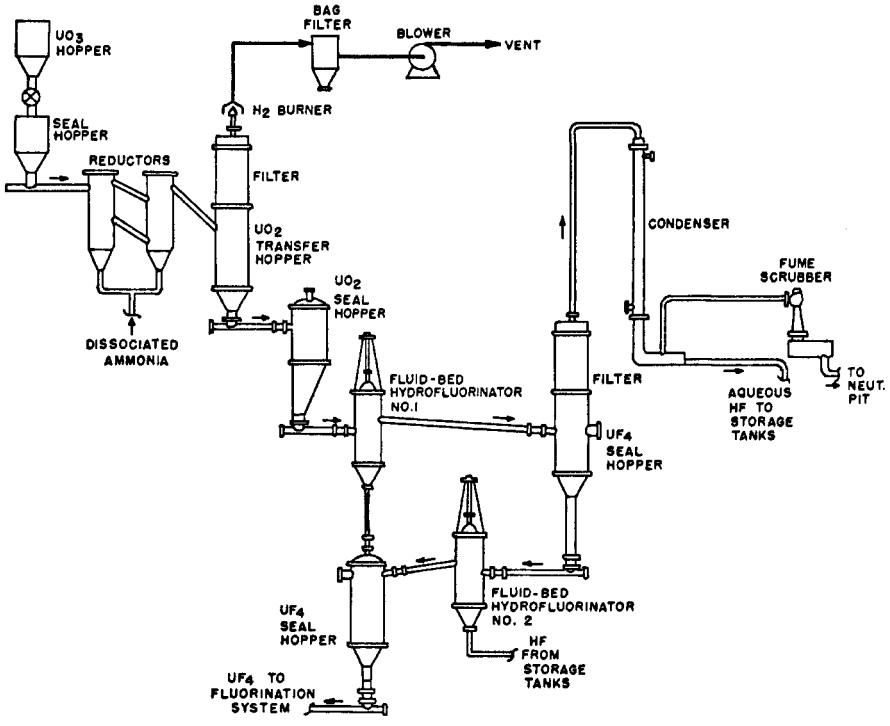

Figure 2. UO_3 to UF_4 process. (After Ref. 1.)

In the dry hydrofluor process, the U_3O_8 concentrate (yellow cake) is ground and sized into feed material for a fluidized-bed unit, where it is reduced by hydrogen to UO_2 at 540–650°C. The UO_2 particles are then reacted in two successive fluidized-bed reactors with anhydrous HF at 480–540°C and 540–650°C, respectively, to produce UF_4 (green salt). Fluorination with excess fluorine, using CaF_2 as an inert solid diluent, prevents caking and distributes the heat of reaction. Next, the UF_4 is reacted with fluorine gas at 340–480°C to produce UF_6, which is collected in cold traps (– 15°C). Further purification (> 99.97%) is accomplished by fractional distillation of the UF_6 at 0.35–0.7 MPa (50–100 psig).

Pure UO_2 is produced from UF_6 by hydrolysis and precipitation of ammonium diuranate or ammonium uranyl carbonate by addition of ammonia or ammonium carbonate, respectively. The precipitate is filtered, dried at 175°C, and calcined and reduced at 800°C in hydrogen to UO_2. The characteristics of the powder influence the processing and properties of the finished fuel pellets as well as their performance. The UO_2 is cooled under nitrogen and reduced to fine powder in wet, rubber-lined ball mills or by micronizing. Milling may be eliminated with ceramically active powder. Too much ammonia in the precipitation step will yield a gelatinous ammonium diuranate (adu), which is difficult to filter, whereas with too little the UO_2 product will be difficult to press and sinter. Sinterable UO_2 is prepared by rapid precipitation of adu. The processor is programmed to adjust excess ammonia for the solubilizing and complexing action of the fluoride concentration, which increases as UF_6 is fed into the system. Conditions of relatively low uranium solubility are desirable to maximize yields, e.g., 0.07 M (25 g/L) fluoride may require excess ammonia 0.3 to 0.9 M (5–15 g/L) to precipitate the adu in a form that will yield ceramically active UO_2 powder. The occluded fluoride impurity in the precipitated UO_2 is removed by passing steam over the adu during calcining and reduction at 800°C. Hydrogen reduction is continued after the steam treatment is stopped.

Upon exposure to air, the UO_2 powder will partially oxidize to $UO_{2.03}$ to $UO_{2.07}$, and the powder may be pyrophoric and burn to U_3O_8. The highest oxygen forms (UO_3 and U_3O_8) are formed at 500–600°C. At higher temperatures oxygen is released, and above 1100°C UO_2 is again the stable form.

The fuel for water-cooled powder reactors is enriched to contain 2–4% U-235. Higher enrichments up to 93% U-235 are used in fuels for fast breeder reactors, HTGRs, and certain research and test reactors.

The UO_2 fuel elements are produced by cold pressing and sintering cylindrical pellets of ceramic-grade UO_2, which are loaded into tubular metal cladding: Zircaloy-2 [an alloy of Zr with 1.4% Sn, 0.132Fe, 0.12Cr, 0.05%Ni, and 0.01% N(max)] or stainless steel). The cladding is sealed by welded end plugs to form a fuel rod or fuel pin, and an assembly of the fuel rods into bundles constitutes a fuel element or fuel subassembly.

The UO_2 pellets are produced by mixing the UO_2 powder with binder and lubricant materials, granulating to form free-flowing particles, compacting, heating to remove the fugitive binder and lubricant, sintering in a controlled atmosphere, and griding to final specified dimensions (Fig. 4)[2]. A large water-cooled reactor core contains several million fuel pellets.

The binders and lubricants added to the UO_2 powder prior to granulation include materials such as polyethylene glycol (Carbowax), polyvinyl alcohol (PVA), paraffin, zinc stearate, or stearic acid. The additives may be incorporated dry (in amounts up to 3 wt %), or in solution (aqueous, in alcohol, or in carbon tetrachloride). The binders

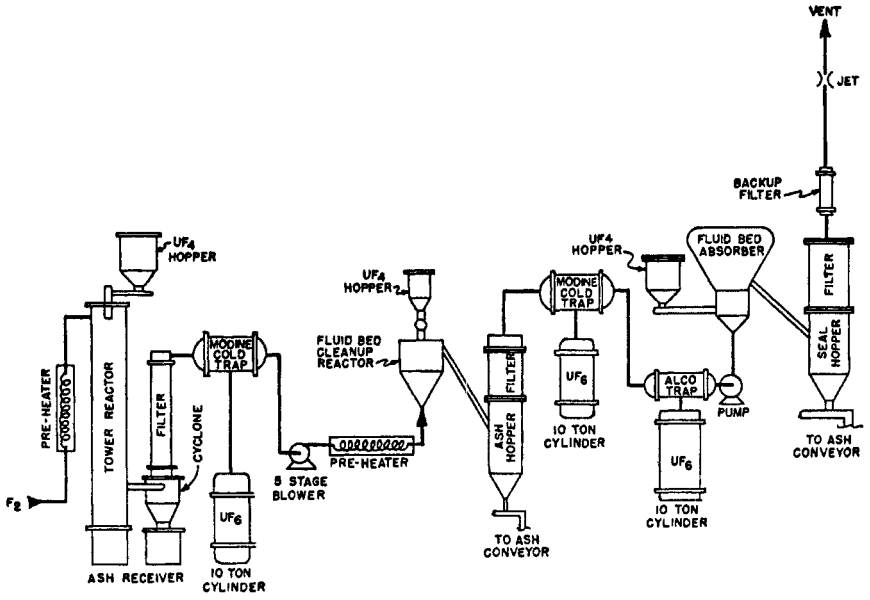

Figure 3. UF_4 to UF_6 process. (After Ref. 1.)

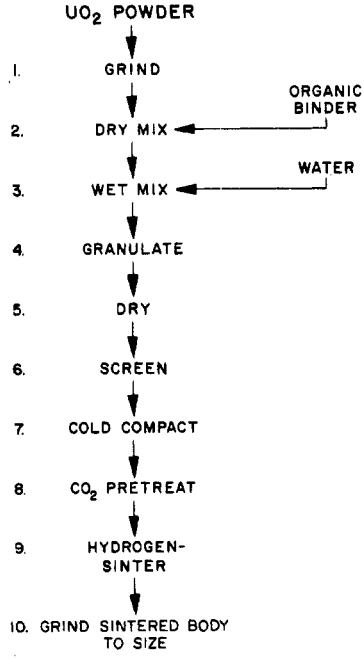

Figure 4. Process flow diagram of principal operations for fabrication of cold-pressed UO_2 fuel components. (After Ref. 2.)

strengthen the green cold-pressed compacts for ease of handling, as well as reduce the dust hazard. The lubricants provide internal lubrication during pressing and thereby improve the uniformity and yield of green pellets. Water is then added to the blend in a mixer until a stiff consistency is reached. The blended batch is pushed through a coarse mesh screen (60 mesh), dried at 70°C, and then granulated by forcing through a finer mesh screen and drying at about 80°C to produce free-flowing granules.

The granulated mixtures are compacted in double-acting, cam-operated automatic pellet presses. The ends of the green pellets are dished by means of punches with slightly convex faces. The dished configuration provides space for thermal expansion of the pellet

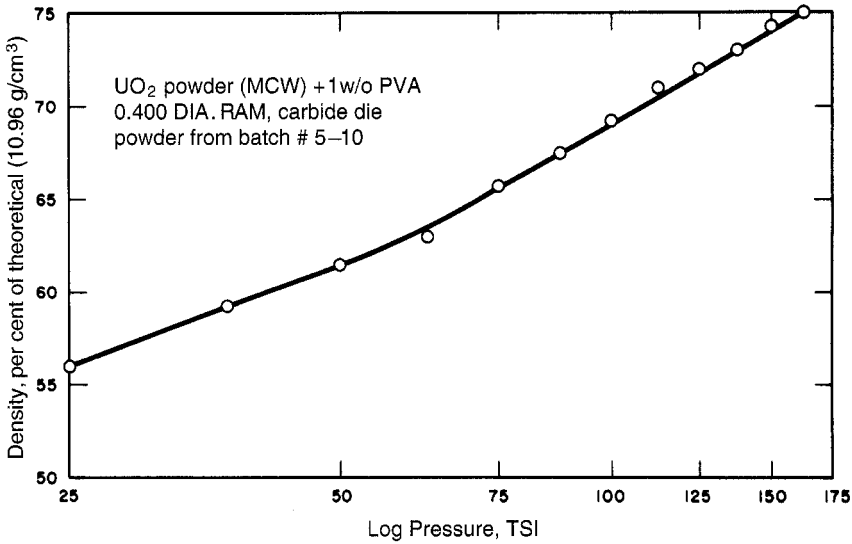

Figure 5. Compact density as a function of compacting pressure. (After Ref. 2.)

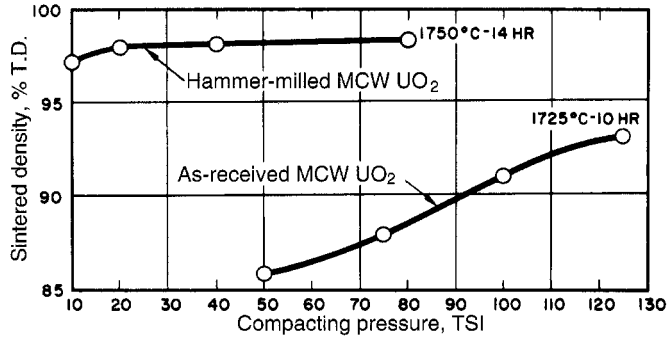

Figure 6. Relationship between compacting pressure and sintered density for mineral source (as-received MCW UO_2) and mechanically comminuted (hammer-milled MCW UO_2) powders. (After Ref. 2.)

centerline during operating conditions. Chamfering of the pellet edges also improves performance. The length-to-diameter ratio of the compacts made in double-acting presses is usually limited to a maximum of 2:1 to minimize differences in density that would result in cracking, owing to differential shrinkage during sintering.

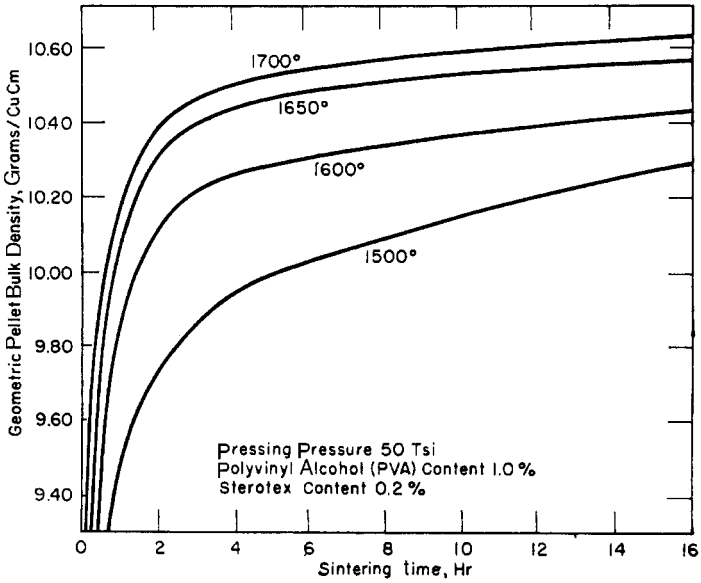

Figure 7. Effect of sintering time and temperature on fired density of pellets made from typical ceramic-grade oxide. (After Ref. 3.)

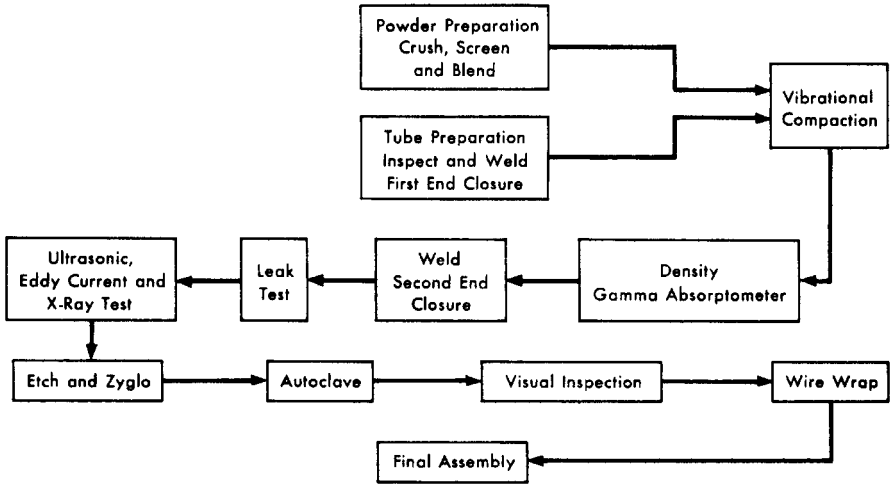

Figure 8. Steps in fuel fabrication by vibratory compaction. (After Ref. 3.)

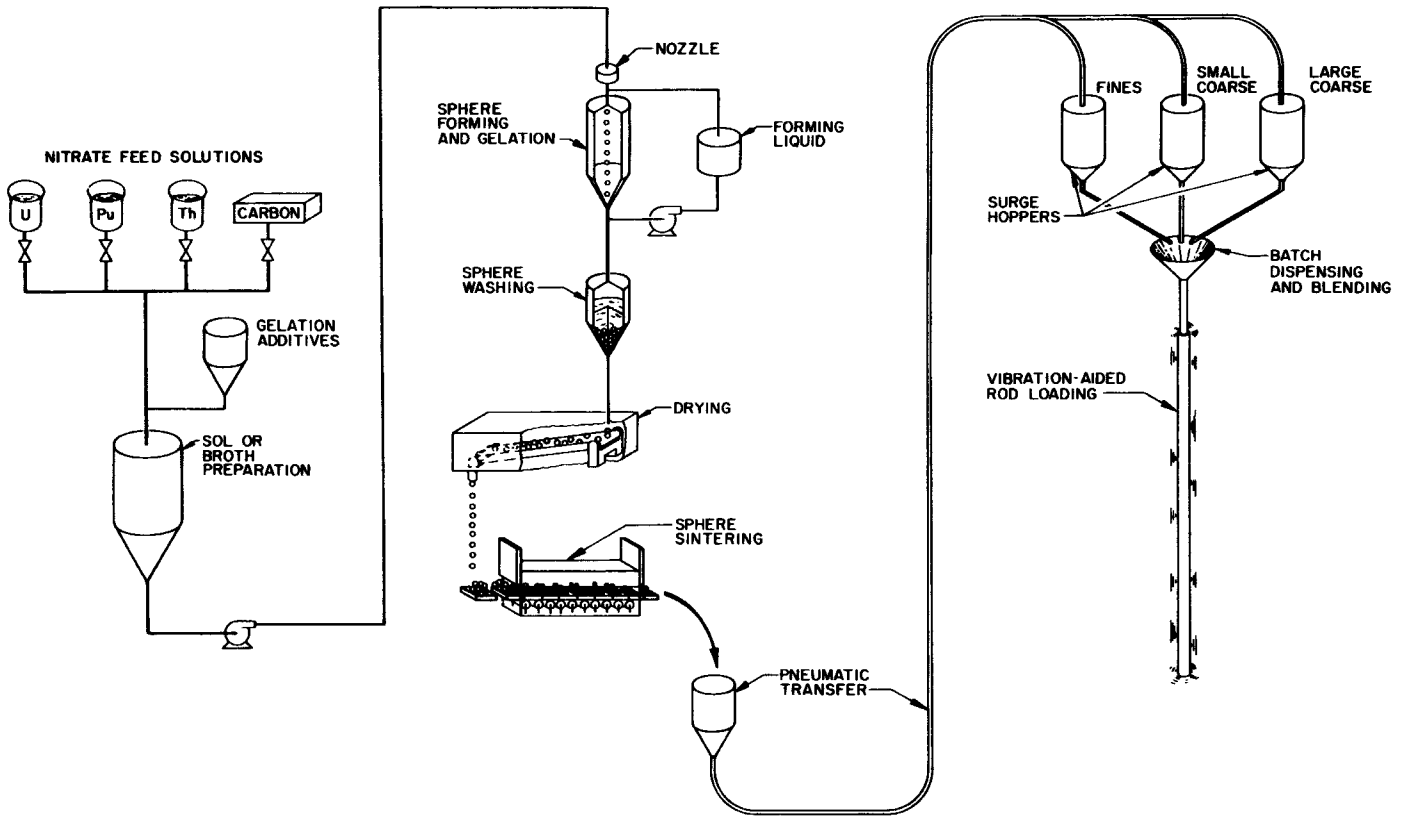

Figure 9(a). Major steps in the gel–sphere–pac process. (After Ref. 6.)

The relationships between compacting pressure and compact density and the influence of mechanical comminution are shown in Figures 5 and 6[2]. The binders and lubricants are removed from the green compacts by heating in a high flow of CO_2 for several hours at 500–800°C, which also reduces the carbon content to below 50 ppm. The pellets are then sintered in a hydrogen atmosphere at 1550–1700°C. The effect of sintering time and temperature on the pellet density is shown in Figure 7[3]. The sintered pellets may have densities ranging from 90 to 97% of theoretical density, depending on the nature of the UO_2 powder, the green compact density, and the sintering time, teglrmperature, and atmosphere. Improved UO_2 pellets are made in France by the double-cycle inverse (dci) process, where no additives are used except for 0.2% zinc stearate lubricant. In this process the UO_2 powder is produced from UF_6 by pyrohydrolysis at 250°C:

$$UF_6 + 2H_2O \longrightarrow UO_2F_2 + 4HF \qquad \text{(a)}$$

followed by hydrogen reduction at 700°C:

$$UO_2F_2 + H_2 \longrightarrow UO_2 + 2HF \qquad \text{(b)}$$

The UO_2 powder obtained by this process is readily granulated and sintered, without the addition of binders, to controlled densities. Pore size distribution can be controlled by addition of U_3O_8. The pellets have high stability (no further densification takes place during operation). The pellet density in the French (dci) process is controlled by the cold compaction pressure in forming the green compacts. The ammonium uranyl carbonate (AUC) process in Germany (KWU) produces UO_2 powder that flows freely as

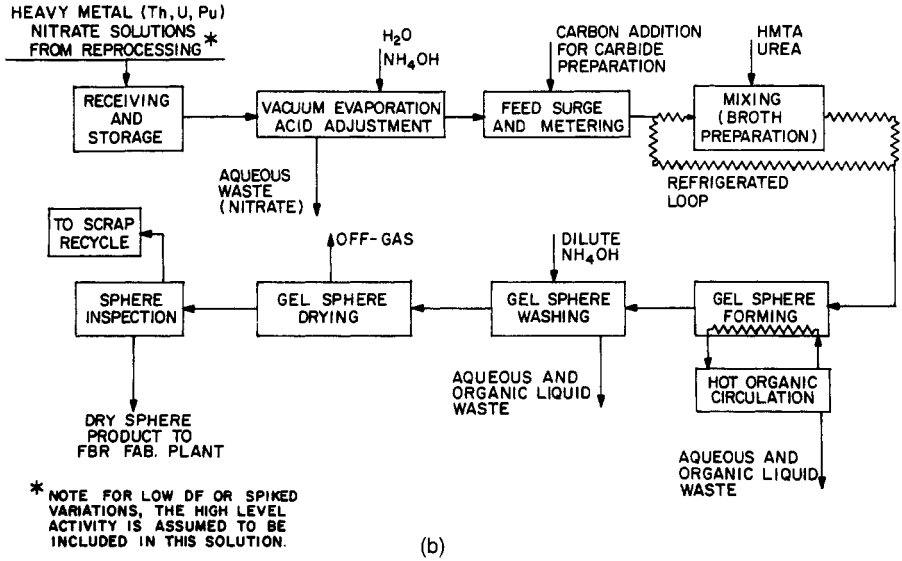

Figure 9(b). Functional flow diagram for sphere conversion. (After Ref. 5.)

calcined and does not require pretreatment such as granulation before cold compaction. The moisture and fluorine contents must be minimized (to <10 ppm each) to prevent internal corrosion failure of the cladding. The pellets are stored in a dry environment and heated in vacuum after loading into the cladding. A major fuel rod failure mechanism is mechanical interaction between the fuel pellets and the cladding in the presence of fission products (e.g., iodine, cesium, tellurium), which results in stress corrosion or intergranular cracking of the cladding.

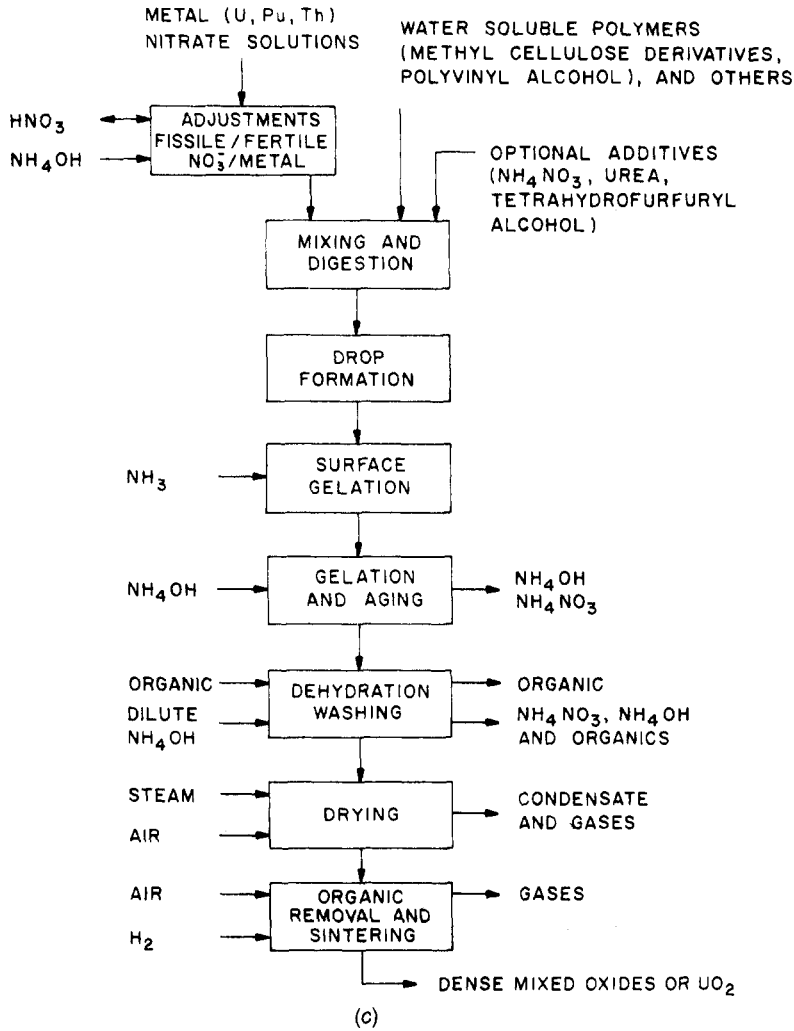

Figure 9(c). Sphere preparation by external gelation. (After Ref. 6.)

The problem of UO_2 pellet densification under irradiation causes contraction and leads to collapse of the cladding in axial gaps in sections of the fuel columns. The solution is to control the manufacturing process to ensure the production of pellets with higher density and stabilized pore structures (pore size and grain size). Prepressurizing the fuel rod with helium also avoids clad flattening.

In an alternate fuel fabrication technique, crushed or spherical fuel particles are vibratory-packed directly into the cladding tubes, thereby avoiding the problems of pellet production. The fabrication operations can be carried out automatically by remote operation at room temperature. Dust contamination is avoided, as well as radiation exposure of personnel. Irradiation tests of these fuel rods indicate improved performance over pellet fueled rods for equivalent exposures[4–9].

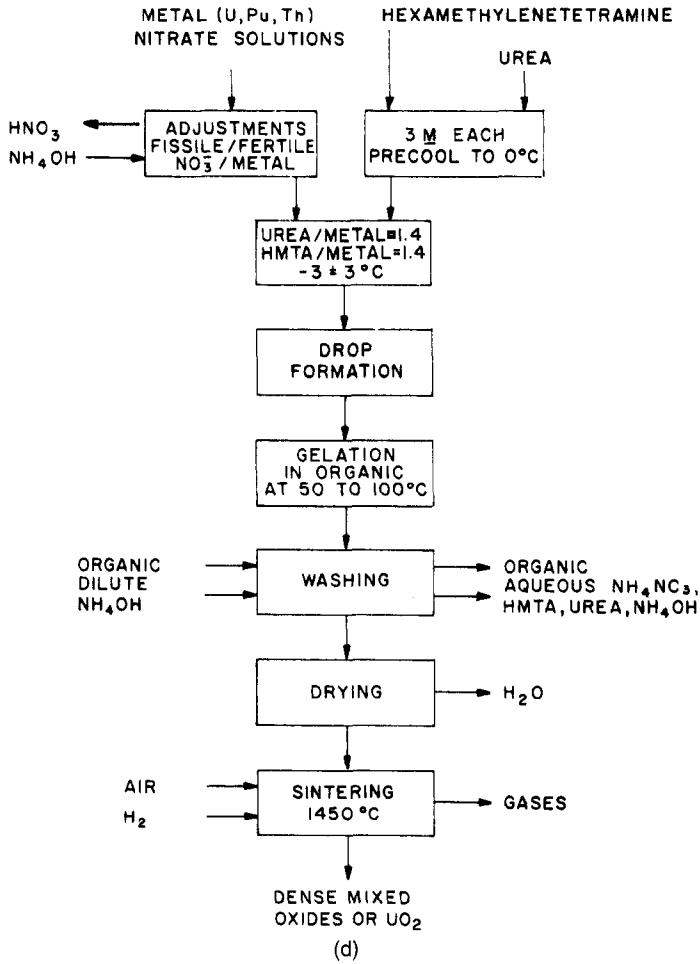

Figure 9(d). Sphere preparation by internal gelation. (After Ref. 6.)

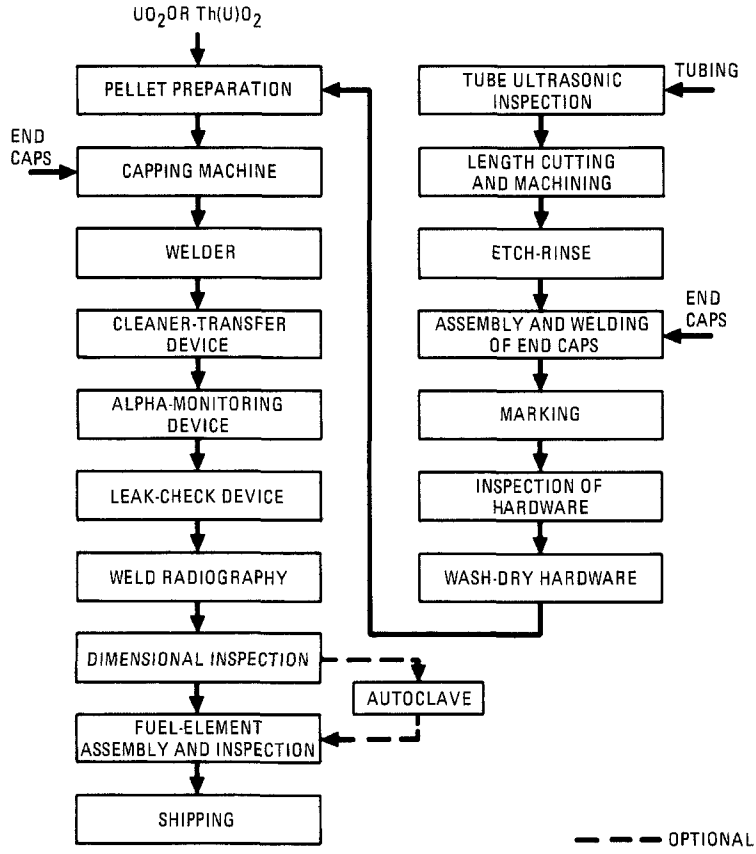

Figure 10. Fabrication flow sheet for rod bundles containing pelletized fuel. (After Ref. 10.)

In vibratory compaction, UO_2 particles derived from high density sintered or fused material are crushed and screened into particle size mixtures that can be packed directly into high density compacts in the cladding tubes (Fig. 8)[3].

Spherical fuel particles are produced by the wet chemical sol–gel process[4–9], which consists of spraying an aqueous solution or a hydrosol of salts of the fissile and/or fertile materials through nozzles into spherical droplets. Homogeneous mixed oxides are prepared by coprecipitation. The droplets are gelled by either internal precipitation or dehydration, then washed and aged, and heat treated to dry and sinter to produce high density spherical particles (Fig. 9)[5,6].

Sphere conversion is based on preparation of a special solution (broth), gelation of broth droplets to give semirigid spheres, and washing and drying to give a dry gel–sphere product. Gelation is accomplished chemically by NH_3, which is formed within the broth droplet by hexamethylenetetramine (HMTA) decomposition (internal gelation), or by

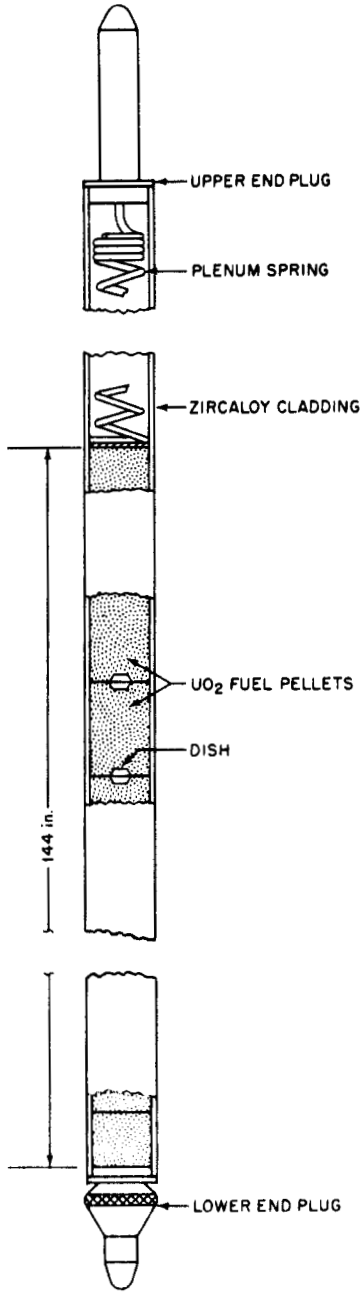

Figure 11. Fuel rod schematic for boiling water reactor. (After Ref. 11.)

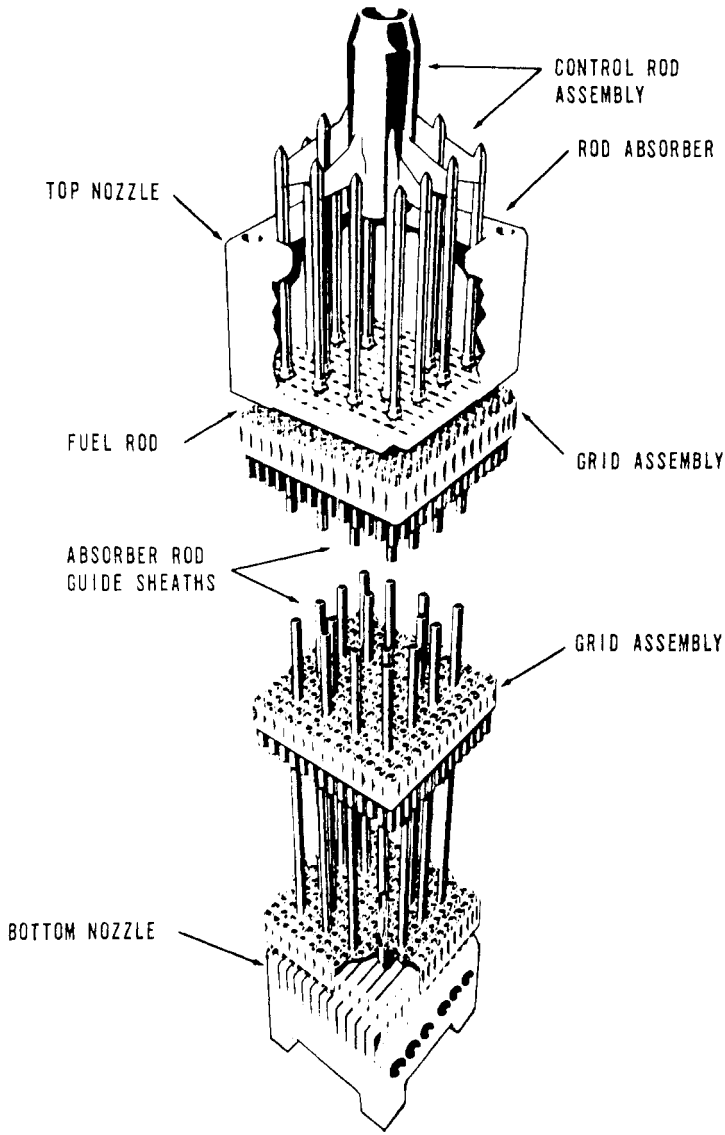

Figure 12. Pressurized water reactor rod–cluster control assembly. (After Ref. 11.)

using gaseous NH_3 and ammonium hydroxide (external gelation). The fabrication of a fuel rod proceeds as shown in Figure 10[10]. A typical fuel rod and fuel assembly are shown in Figures 11 and 12[11]. The UO_2 fuel elements are positioned in Zircaloy-2 pressure tubes, which pass through an aluminum calandria containing the heavy-water moderator (Figs. 13 and 14)[11,12]. Improved UO_2 fuels include use of duplex or

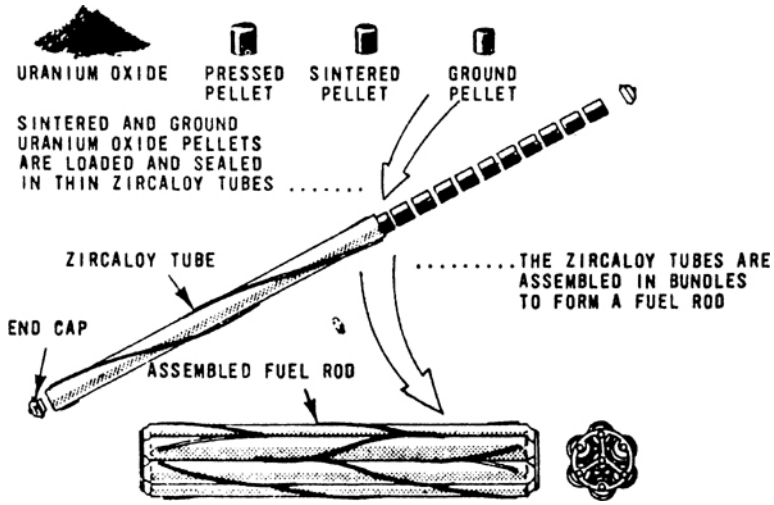

Figure 13. Each fuel rod consists of an assembly (often called a "bundle") of zirconium alloy tubes containing pellets of uranium oxide. Each rod, or bundle, is 495.3 mm (19.5 in.) long and contains about 15 kg (33 lb) of uranium oxide. (After Ref. 13.)

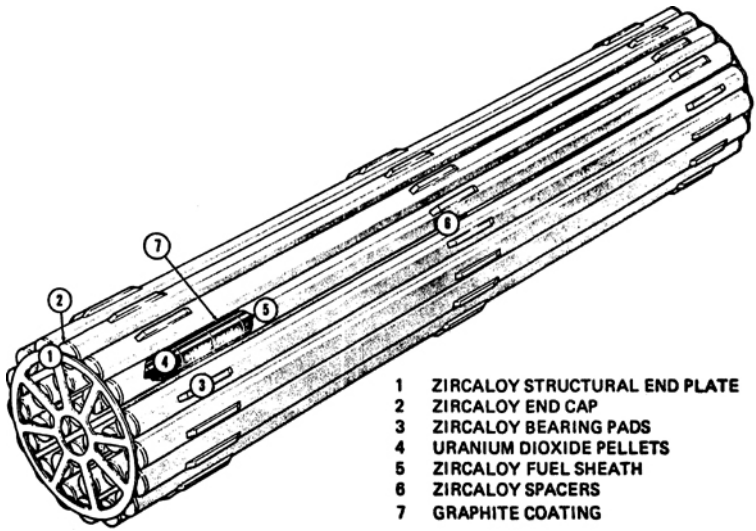

Figure 14. 28-element CANLUB fuel bundle: a 500 mm long, 100 mm diameter bundle of 28 close-packed elements. Each 15 mm diameter element contains high density UO_2 in 0.4 mm thick Zircaloy-4 sheathing, which depends on the support of the UO_2 to withstand heat transport system pressure (collapsible sheathing. A thin layer of graphite between fuel and sheathing acts as a lubricant to reduce stress concentrations and to impede stress corrosion cracking. The thin layer of graphite has been show to be effective, and such fuel has been designated CANLUB fuel. These short, simple natural uranium bundles of basically a single type for all CANDU reactors have resulted in inexpensive fuel.

dual-enrichment pellets in which an outer zone of high enrichment UO_2 surrounds an inner zone of depleted or natural UO_2, thin internal-clad liners (Zr or Cu), graphite-lubricated, fuel-clad interface, and reconstitutable subassemblies.

(MASSOUD T. SIMNAD)

1. D. M. Elliott, L. E. Weaver, eds., *Education and Research in the Nuclear Fuel Cycle*, University of Oklahoma Press, Norman, 1972.
2. J. Belle, ed., *Uranium Dioxide: Properties and Nuclear Applications*, Division of Reactor Development, U.S., Atomic Energy Commission, Washington, DC, 1961.
3. R. B. Holden, *Ceramic Fuel Elements, Gordon & Breach*, New York, 1966.
4. R. L. Beatty, R. E. Norman, K. J. Notz, *Gel-Sphere-Pac Fuel for Thermal Reactors — Assessment of Fabrication Technology and Irradiation Performance*, Report ORNL-5469, Oak Ridge National Laboratory, Oak Ridge, TN, November 1979.
5. A. R. Olsen, R. R. Judkins, *Gel-Sphere-Pac Reactor Fuel Fabrication*, Report ORNL/TM-6924, Oak Ridge National Laboratory, Oak Ridge, TN, November 1979.
6. W. J. Lackey, J. E. Selle, *Assessment of Gel-Sphere-Pac Fuel for Fast Breeder Reactors*, Report ORNL-5468, Oak Ridge National Laboratory, Oak Ridge, TN, October 1978.
7. J. Becvar, in *Fabrication of Water Reactor Fuel Elements, Symp.*, Prague, Nov. 6–10, 1978, International Atomic Energy Agency, Vienna, 1979, p. 185.
8. R. B. Matthews, M. L. Swanson, *Ceram. Bul., 58*, 223 (1979).
9. R. K. McGeary, *J. Am. Ceram Soc., 44*, 513 (1961).
10. E. S. Pedersen, *Nuclear Power*, 2 vols., Ann Arbor Science Publishers, Ann. Arbor, MI, 1978.
11. M. T. Simnad, J. P. Howe, in *Material Science in Energy Technology*, G. G. Libowitz, M. S. Whittingham, eds., Academic Press, New York, 1979, p. 32.
12. M. T. Simnad, *Fuel Element Experience in Nuclear Power Reactors*, Gordon & Breach, New York, 1971.

17.3.12.1.2. Uranium Carbide Fuels.

There are three compounds in the uranium–carbon system: UC, U_2C_3, and UC_2. The UC, with the highest uranium density, has a face-centered-cubic structure and is stoichiometric at a 4.8 wt % carbon composition. At lower carbon contents, free uranium Rmetal is present at grain boundaries and as small particles within the grains. The hyperstoichiometric UC exhibits a structure of UC_2 platelets in the UC grains. The monocarbides of Th, U, and Pu have the fcc NaCl structure and are completely miscible. ThC and UC are stable to their melting points. The tetragonal CaC_2 structure of UC_2 transforms to a fluorite-type lattice at about 1700°C.

Compared with UO_2, UC has a higher uranium density and at least five times greater thermal conductivity; it is almost as refractory.

The compatibility of UC with stainless steel depends on the stoichiometry and whether the gap between pellet and cladding is filled with gas or sodium. The cladding acts as a sink for carbon, and sodium enhances transport of carbon from the fuel to the cladding. The decarburized fuel tends to crack, and the carburized cladding loses ductility quickly, even at 600°C. With a gas gap, there is no significant interaction with stainless steel cladding below $\sim$800°C.

Mixed carbide fuels eliminate undesirable second phases or render them harmless. Alloying UC with ZrC increases the melting point and lowers the vapor pressure. Chromium and vanadium improve the compatibility of the carbide fuel with stainless steel cladding.

Uranium carbides may be prepared by reacting uranium with carbon, or uranium dioxide with carbon in vacuum at elevated temperatures, or uranium powder with a hydrocarbon such as methane.

Inorganic Reactions and Methods, Volume 18
Edited by J. J. Zuckerman, Jim D. Atwood

dual-enrichment pellets in which an outer zone of high enrichment UO_2 surrounds an inner zone of depleted or natural UO_2, thin internal-clad liners (Zr or Cu), graphite-lubricated, fuel-clad interface, and reconstitutable subassemblies.

(MASSOUD T. SIMNAD)

1. D. M. Elliott, L. E. Weaver, eds., *Education and Research in the Nuclear Fuel Cycle*, University of Oklahoma Press, Norman, 1972.
2. J. Belle, ed., *Uranium Dioxide: Properties and Nuclear Applications*, Division of Reactor Development, U.S., Atomic Energy Commission, Washington, DC, 1961.
3. R. B. Holden, *Ceramic Fuel Elements, Gordon & Breach*, New York, 1966.
4. R. L. Beatty, R. E. Norman, K. J. Notz, *Gel-Sphere-Pac Fuel for Thermal Reactors — Assessment of Fabrication Technology and Irradiation Performance*, Report ORNL-5469, Oak Ridge National Laboratory, Oak Ridge, TN, November 1979.
5. A. R. Olsen, R. R. Judkins, *Gel-Sphere-Pac Reactor Fuel Fabrication*, Report ORNL/TM-6924, Oak Ridge National Laboratory, Oak Ridge, TN, November 1979.
6. W. J. Lackey, J. E. Selle, *Assessment of Gel-Sphere-Pac Fuel for Fast Breeder Reactors*, Report ORNL-5468, Oak Ridge National Laboratory, Oak Ridge, TN, October 1978.
7. J. Becvar, in *Fabrication of Water Reactor Fuel Elements, Symp.*, Prague, Nov. 6–10, 1978, International Atomic Energy Agency, Vienna, 1979, p. 185.
8. R. B. Matthews, M. L. Swanson, *Ceram. Bul., 58*, 223 (1979).
9. R. K. McGeary, *J. Am. Ceram Soc., 44*, 513 (1961).
10. E. S. Pedersen, *Nuclear Power*, 2 vols., Ann Arbor Science Publishers, Ann. Arbor, MI, 1978.
11. M. T. Simnad, J. P. Howe, in *Material Science in Energy Technology*, G. G. Libowitz, M. S. Whittingham, eds., Academic Press, New York, 1979, p. 32.
12. M. T. Simnad, *Fuel Element Experience in Nuclear Power Reactors*, Gordon & Breach, New York, 1971.

17.3.12.1.2. Uranium Carbide Fuels.

There are three compounds in the uranium–carbon system: UC, U_2C_3, and UC_2. The UC, with the highest uranium density, has a face-centered-cubic structure and is stoichiometric at a 4.8 wt % carbon composition. At lower carbon contents, free uranium Rmetal is present at grain boundaries and as small particles within the grains. The hyperstoichiometric UC exhibits a structure of UC_2 platelets in the UC grains. The monocarbides of Th, U, and Pu have the fcc NaCl structure and are completely miscible. ThC and UC are stable to their melting points. The tetragonal CaC_2 structure of UC_2 transforms to a fluorite-type lattice at about 1700°C.

Compared with UO_2, UC has a higher uranium density and at least five times greater thermal conductivity; it is almost as refractory.

The compatibility of UC with stainless steel depends on the stoichiometry and whether the gap between pellet and cladding is filled with gas or sodium. The cladding acts as a sink for carbon, and sodium enhances transport of carbon from the fuel to the cladding. The decarburized fuel tends to crack, and the carburized cladding loses ductility quickly, even at 600°C. With a gas gap, there is no significant interaction with stainless steel cladding below $\sim$800°C.

Mixed carbide fuels eliminate undesirable second phases or render them harmless. Alloying UC with ZrC increases the melting point and lowers the vapor pressure. Chromium and vanadium improve the compatibility of the carbide fuel with stainless steel cladding.

Uranium carbides may be prepared by reacting uranium with carbon, or uranium dioxide with carbon in vacuum at elevated temperatures, or uranium powder with a hydrocarbon such as methane.

Uranium carbide is formed directly from the elements in an arc furnace by means of melting uranium with graphite. The uniformity of the product may be improved by remelting. The monocarbide also results from heating an intimate mixture of uranium and carbon particles above 1100°C. Uranium dissolved in a molten zinc–magesium alloy can be heated with graphite powder. The residual zinc–magnesium alloy is removed by vacuum distillation.

The most extensively used method is the carbothermic reaction of UO_2 with carbon under vacuum at 1600–2000°C. The pelletized mixture of UO_2 and carbon is heated in vacuum in a furnace that allows semicontinuous production (Fig. 1)[1]. The optimum reduction temperature is ~1600°C for material that is to be pressed and sintered to form pellets. The residual oxygen contents are in the range 0.35–0.63%. Higher temperatures result in a less sinterable product, while lower temperatures give unacceptably high residual oxygen contents.

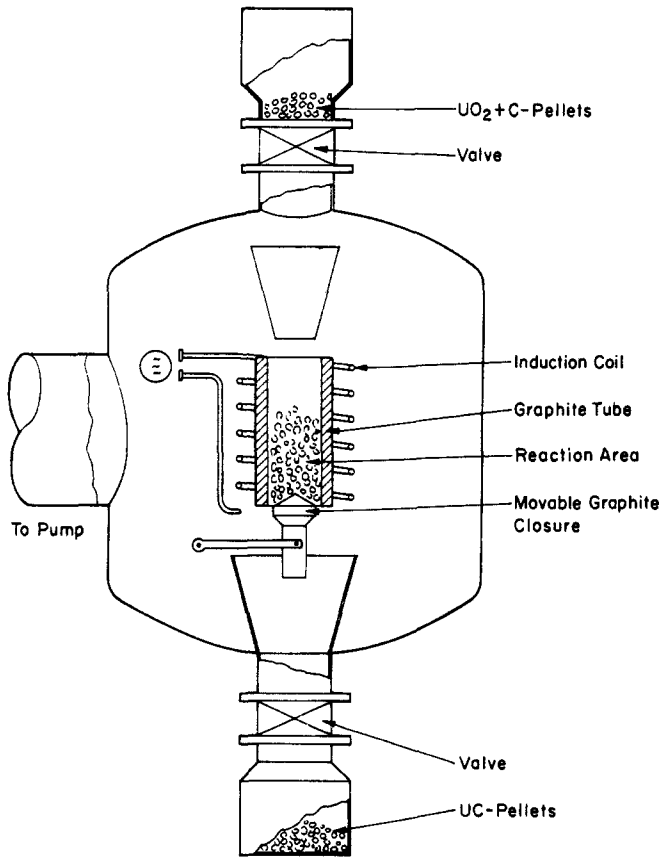

Figure 1. Schematic drawing of a semicontinuous reaction furnace for uranium carbide. (After Ref. 1.)

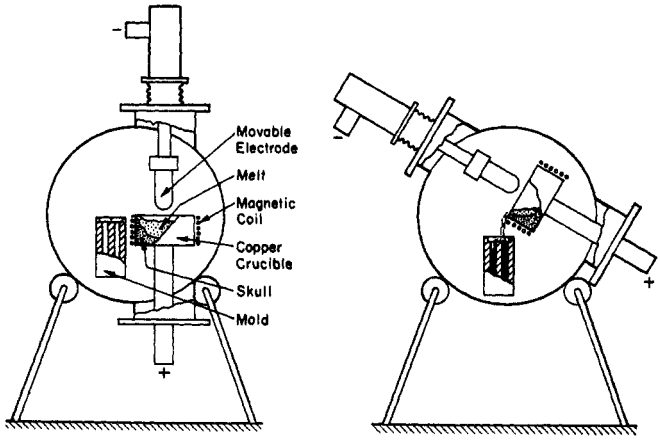

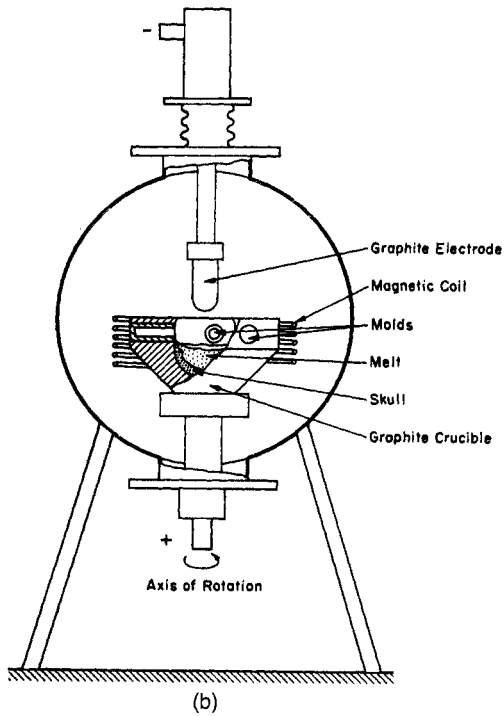

Figure 2. Skull melting furnace positioned for (a) tilt pouring (top) and (b) centrifugal casting. (After Ref. 1.)

The most sinterable uranium monocarbide powder is produced by the alkane route:

$$U_{massive} + 3/2H_2 \xrightarrow{\sim 250°C} UH_3(powder) \quad (a)$$

$$UH_3 \xrightarrow{\sim 600°C} U_{powder} + 3/2H_2 \quad (b)$$

$$U_{powder} + CH_4 \xrightarrow{\sim 600°C} UC + 2H_2 \quad (c)$$

Dehydriding UH_3 and carburization of the uranium powder formed to uranium monocarbide are carried out in a stream of methane or propane gas at 600–700°C. A purer product is produced with propane (<1000 ppm oxygen and <300 ppm nitrogen).

The finely divided, pyrophoric (<40 μm size) powder produced by the alkane route is cold-pressed and sintered under an inert atmosphere. The carbothermic material is powdered by comminution in rubber-lined jar wells, using stainless steel balls and uranium rods as grinding media.

The cold pressing is carried out in hardened steel dies. The carbide powder is first mixed with ~0.5–5% of binder lubricants, such as paraffin, camphor, Carbowax, cetyl alcohol, or beeswax dissolved in nonaqueous inert solvents such as benzene, isopropyl alcohol, or methyl alcohol. The bonded carbide powder is granulated by forcing through a screen and then loaded into the dies. The density of the cold-pressed pellets may be as high as 80% of theoretical, and the sintered pellets may be densified to ~90% of theoretical. The optimum sintering condition is 1800°C for 4 h.

Densification is promoted by metallic additives, such as nickel or iron. Densities as high as 95% are obtained by adding 0.1–0.2% Ni at sintering temperatures as low as 1525°C. The congruently evaporating composition of uranium carbide is $UC_{1.1}$, and an increase in carbon content occurs during sintering in graphite crucibles.

Spherical particles of controlled sizes can be used to fabricate high density uranium carbide fuel pins by means of vibratory packing directly into the cladding tube, as with sphere–pac oxide fuel (see 17.3.12.1.1).

Arc melting and casting of uranium carbide fuel rods is achieved in the skull-melting procedure by arc melting in a water-cooled crucible with a graphite-tipped electrode. The molten carbide is contained in the shell or skull of solid uranium carbide in the crucible and cast into suitable molds by tilt pouring (Fig. 2a) or centrifugal casting (Fig. 2b). The castings have high densities (>99%).

(MASSOUD T. SIMNAD)

1. R. B. Holden, *Ceramic Fuel Elements*, Gordon & Breach, New York, 1966.
2. L. E. Russell, B. R. T. Frost, *Carbides in Nuclear Energy*, Macmillan New York, 1964.
3. E. W. Murbach, S. Strausberg, in *Compounds of Interest in Nuclear Reactor Technology*, J. T. Waber, P. Chiotti, W. N. Miner, eds., IMD Special Report No. 13, American Institute of Mining Engineers, New York, 1964, p. 573.
4. H. Nadler, R. Chang, in *Compounds of Interest in Nuclear Reactor Technology*, J. T. Waber, P. Chiotti, W. M. Miner, eds., IMD Special Report No. 13, American Institute of Minning Engineers, New York, 1964, p. 525.

17.3.12.1.3. Uranium Nitride Fuels.

Although not used as a reactor fuel, uranium mononitride (UN) possesses desirable properties: a face-centered-cubic NaCl structure, a high melting point (2850°C for

Inorganic Reactions and Methods, Volume 18
Edited by J. J. Zuckerman, Jim D. Atwood

The most sinterable uranium monocarbide powder is produced by the alkane route:

$$U_{massive} + 3/2H_2 \xrightarrow{\sim 250^\circ C} UH_3(powder) \quad (a)$$

$$UH_3 \xrightarrow{\sim 600^\circ C} U_{powder} + 3/2H_2 \quad (b)$$

$$U_{powder} + CH_4 \xrightarrow{\sim 600^\circ C} UC + 2H_2 \quad (c)$$

Dehydriding UH_3 and carburization of the uranium powder formed to uranium monocarbide are carried out in a stream of methane or propane gas at 600–700°C. A purer product is produced with propane (<1000 ppm oxygen and <300 ppm nitrogen).

The finely divided, pyrophoric (<40 μm size) powder produced by the alkane route is cold-pressed and sintered under an inert atmosphere. The carbothermic material is powdered by comminution in rubber-lined jar wells, using stainless steel balls and uranium rods as grinding media.

The cold pressing is carried out in hardened steel dies. The carbide powder is first mixed with ~0.5–5% of binder lubricants, such as paraffin, camphor, Carbowax, cetyl alcohol, or beeswax dissolved in nonaqueous inert solvents such as benzene, isopropyl alcohol, or methyl alcohol. The bonded carbide powder is granulated by forcing through a screen and then loaded into the dies. The density of the cold-pressed pellets may be as high as 80% of theoretical, and the sintered pellets may be densified to ~90% of theoretical. The optimum sintering condition is 1800°C for 4 h.

Densification is promoted by metallic additives, such as nickel or iron. Densities as high as 95% are obtained by adding 0.1–0.2% Ni at sintering temperatures as low as 1525°C. The congruently evaporating composition of uranium carbide is $UC_{1.1}$, and an increase in carbon content occurs during sintering in graphite crucibles.

Spherical particles of controlled sizes can be used to fabricate high density uranium carbide fuel pins by means of vibratory packing directly into the cladding tube, as with sphere–pac oxide fuel (see 17.3.12.1.1).

Arc melting and casting of uranium carbide fuel rods is achieved in the skull-melting procedure by arc melting in a water-cooled crucible with a graphite-tipped electrode. The molten carbide is contained in the shell or skull of solid uranium carbide in the crucible and cast into suitable molds by tilt pouring (Fig. 2a) or centrifugal casting (Fig. 2b). The castings have high densities (>99%).

(MASSOUD T. SIMNAD)

1. R. B. Holden, *Ceramic Fuel Elements*, Gordon & Breach, New York, 1966.
2. L. E. Russell, B. R. T. Frost, *Carbides in Nuclear Energy*, Macmillan New York, 1964.
3. E. W. Murbach, S. Strausberg, in *Compounds of Interest in Nuclear Reactor Technology*, J. T. Waber, P. Chiotti, W. N. Miner, eds., IMD Special Report No. 13, American Institute of Mining Engineers, New York, 1964, p. 573.
4. H. Nadler, R. Chang, in *Compounds of Interest in Nuclear Reactor Technology*, J. T. Waber, P. Chiotti, W. M. Miner, eds., IMD Special Report No. 13, American Institute of Minning Engineers, New York, 1964, p. 525.

17.3.12.1.3. Uranium Nitride Fuels.

Although not used as a reactor fuel, uranium mononitride (UN) possesses desirable properties: a face-centered-cubic NaCl structure, a high melting point (2850°C for

congruent melting at and above 2.5×10^5 Pa nitrogen), good thermal conductivity, high uranium density (14.32 g/cm^3), compatibility with most potential cladding materials, and good irradiation stability and fission product retention. A disadvantage is the parasitic capture of neutrons in the transmutation of nitrogen atoms by the (n,α) and (n,p) reactions and the release of nitrogen during the burnup of nitride fuel. The stability of UN in air is much higher than that of uranium carbide (UC). The rate of evaporation of nitrogen at temperatures near 1700°C, under dynamic vacuum conditions or sweep-gas conditions, approaches that of uranium, so that no accumulation of liquid uranium is left on the surface of the UN[1].

Preparation is by three methods: hot isostatic pressing, cold pressing and sintering, and direct reaction of uranium with nitrogen through consumable arc melting and casting procedures[2]. The first two techniques utilize U_2N_3 powder formed by reacting uranium with nitrogen at 850°C followed by decomposition of UN at ~1300°C in a dynamic vacuum.

In the consumable-electrode method, a uranium rod is arc-melted inside a deep cavity or hearth under a nitrogen pressure of 20×10^5 Pa. Th UN castings are heat-treated (~1600°C for 8 h in vacuum) to eliminate high nitride (U_2N_3) accumulations.

(MASSOUD T. SIMNAD)

1. P. E. Lafat, R. B. Holden, in *Compounds of Interest in Nuclear Reactor Technology*, J. T. Waber, P. Chiotti, W. N. Miner, eds., IMD Special Report No. 13, American Institute of Mining Engineers, New York, 1964, p. 225.
2. R. W. Endebrock, E. L. Foster, D. L. Keller, in *Compounds of Interest in Nuclear Reactor Technology*, J. T. Waber, P. Chiotti, W. N. Miner, eds., IMD Special Report No. 13, American Institute of Mining Engineers, New York, 1964, p. 557.

17.3.12.1.4. Plutonium Ceramic Fuels.

Plutonium is obtained by neutron capture from U-238, since only an insignificant amount occurs in nature. Plutonium serves as a fissile fuel in both fast and thermal reactors[1–20]. The fissile isotopes Pu-239 and Pu-241 produced from U-238 can replace U-235 in thermal reactors, but the best use of plutonium is in fast breeder reactors, where more Pu-239 and Pu-241 are produced than are fissioned in situ. Plutonium is derived by chemical reprocessing from irradiated fuel containing U-238. The spent fuel is dissolved in nitric acid and the plutonium is precipitated as the hydroxide by adding ammonia, as the peroxide (Pu_2O_7) by addition of hydrogen peroxide, or as the oxalate with oxalic acid. The PuO_2 is obtained by heating these products in hydrogen at 500–800°C. The PuO_2 is coprecipitated or mechanically mixed with UO_2 for use in fast or thermal reactor fuels (15–20% PuO_2 in fast reactor fuel, 3–5% in thermal reactors).

Fast breeder reactor fuel rods consist of stainless-steel-clad mixed oxide $(U,Pu)O_2$ fuel; however, more stable alloys for cladding and in-core structural materials, with resistance to swelling and embrittlement under fast neutron irradiation, and more efficient fuels (carbide: see 17.3.12.1.2) or nitride (see 17.3.12.3)] are needed[21]. The mechanical, metallurgical, and chemical processes in fuel element irradiation are depicted in Figure 1. Figure 2 shows the PFR (U.K.) fast breeder fuel element, and Figures 3 and 4 illustrate the Fast Flux Test Facility (FFTF) fuel system.

Components in the process of design and fabrication of ceramic plutonium fuels at Hanford Engineering Development Laboratory (HEDL) are displayed in Figure 5. The plan for the fuel fabrication demonstration facility at HEDL is shown in Figure 6.

Inorganic Reactions and Methods, Volume 18
Edited by J. J. Zuckerman, Jim D. Atwood

congruent melting at and above 2.5×10^5 Pa nitrogen), good thermal conductivity, high uranium density (14.32 g/cm^3), compatibility with most potential cladding materials, and good irradiation stability and fission product retention. A disadvantage is the parasitic capture of neutrons in the transmutation of nitrogen atoms by the (n,α) and (n,p) reactions and the release of nitrogen during the burnup of nitride fuel. The stability of UN in air is much higher than that of uranium carbide (UC). The rate of evaporation of nitrogen at temperatures near 1700°C, under dynamic vacuum conditions or sweep-gas conditions, approaches that of uranium, so that no accumulation of liquid uranium is left on the surface of the UN[1].

Preparation is by three methods: hot isostatic pressing, cold pressing and sintering, and direct reaction of uranium with nitrogen through consumable arc melting and casting procedures[2]. The first two techniques utilize U_2N_3 powder formed by reacting uranium with nitrogen at 850°C followed by decomposition of UN at ~1300°C in a dynamic vacuum.

In the consumable-electrode method, a uranium rod is arc-melted inside a deep cavity or hearth under a nitrogen pressure of 20×10^5 Pa. Th UN castings are heat-treated (~1600°C for 8 h in vacuum) to eliminate high nitride (U_2N_3) accumulations.

(MASSOUD T. SIMNAD)

1. P. E. Lafat, R. B. Holden, in *Compounds of Interest in Nuclear Reactor Technology*, J. T. Waber, P. Chiotti, W. N. Miner, eds., IMD Special Report No. 13, American Institute of Mining Engineers, New York, 1964, p. 225.
2. R. W. Endebrock, E. L. Foster, D. L. Keller, in *Compounds of Interest in Nuclear Reactor Technology*, J. T. Waber, P. Chiotti, W. N. Miner, eds., IMD Special Report No. 13, American Institute of Mining Engineers, New York, 1964, p. 557.

17.3.12.1.4. Plutonium Ceramic Fuels.

Plutonium is obtained by neutron capture from U-238, since only an insignificant amount occurs in nature. Plutonium serves as a fissile fuel in both fast and thermal reactors[1–20]. The fissile isotopes Pu-239 and Pu-241 produced from U-238 can replace U-235 in thermal reactors, but the best use of plutonium is in fast breeder reactors, where more Pu-239 and Pu-241 are produced than are fissioned in situ. Plutonium is derived by chemical reprocessing from irradiated fuel containing U-238. The spent fuel is dissolved in nitric acid and the plutonium is precipitated as the hydroxide by adding ammonia, as the peroxide (Pu_2O_7) by addition of hydrogen peroxide, or as the oxalate with oxalic acid. The PuO_2 is obtained by heating these products in hydrogen at 500–800°C. The PuO_2 is coprecipitated or mechanically mixed with UO_2 for use in fast or thermal reactor fuels (15–20% PuO_2 in fast reactor fuel, 3–5% in thermal reactors).

Fast breeder reactor fuel rods consist of stainless-steel-clad mixed oxide $(U,Pu)O_2$ fuel; however, more stable alloys for cladding and in-core structural materials, with resistance to swelling and embrittlement under fast neutron irradiation, and more efficient fuels (carbide: see 17.3.12.1.2) or nitride (see 17.3.12.3)] are needed[21]. The mechanical, metallurgical, and chemical processes in fuel element irradiation are depicted in Figure 1. Figure 2 shows the PFR (U.K.) fast breeder fuel element, and Figures 3 and 4 illustrate the Fast Flux Test Facility (FFTF) fuel system.

Components in the process of design and fabrication of ceramic plutonium fuels at Hanford Engineering Development Laboratory (HEDL) are displayed in Figure 5. The plan for the fuel fabrication demonstration facility at HEDL is shown in Figure 6.

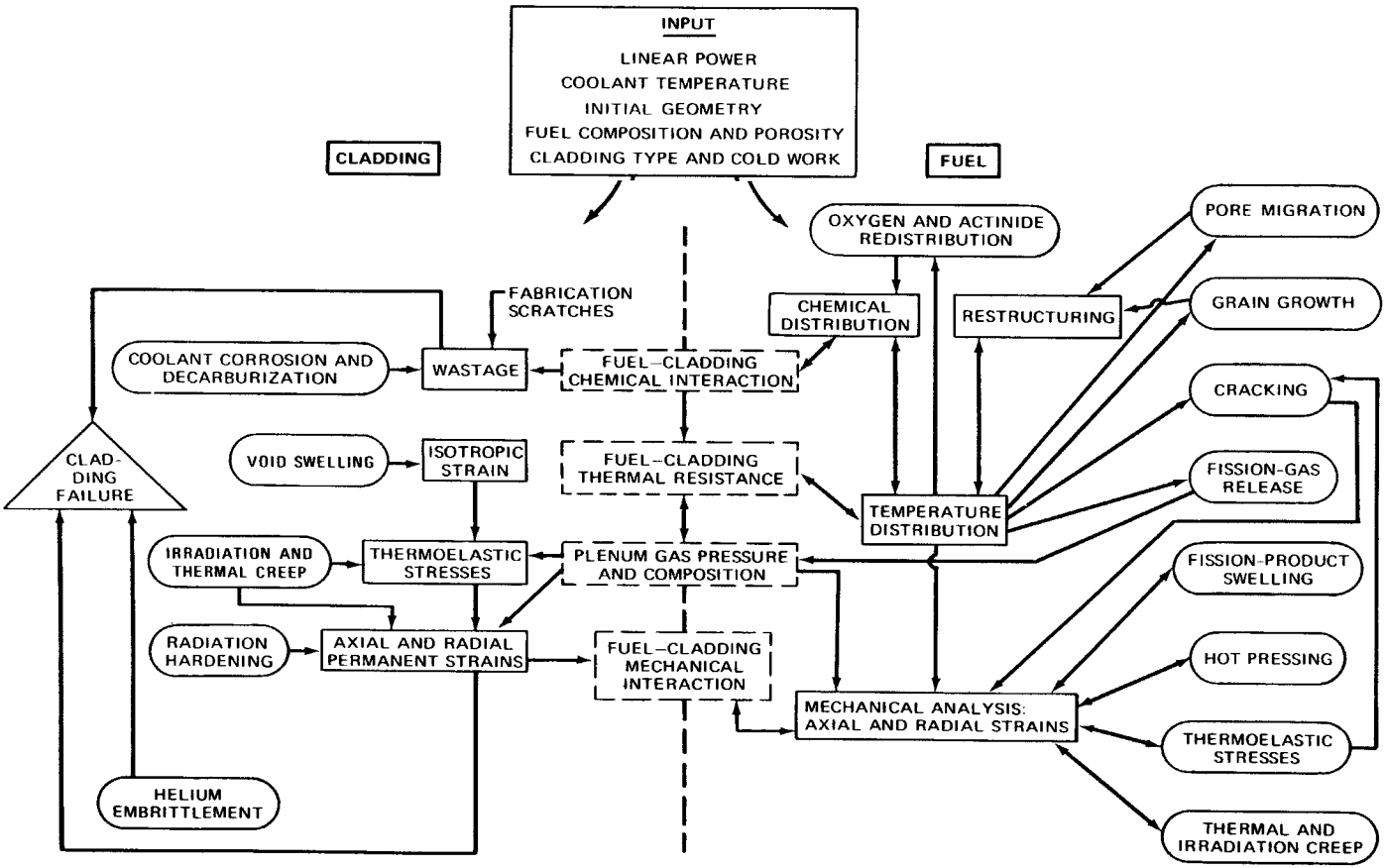

Figure 1. Interrelation of mechanical, metallurgical, and chemical processes in fuel element irradiation behavior. (After Ref. 2.)

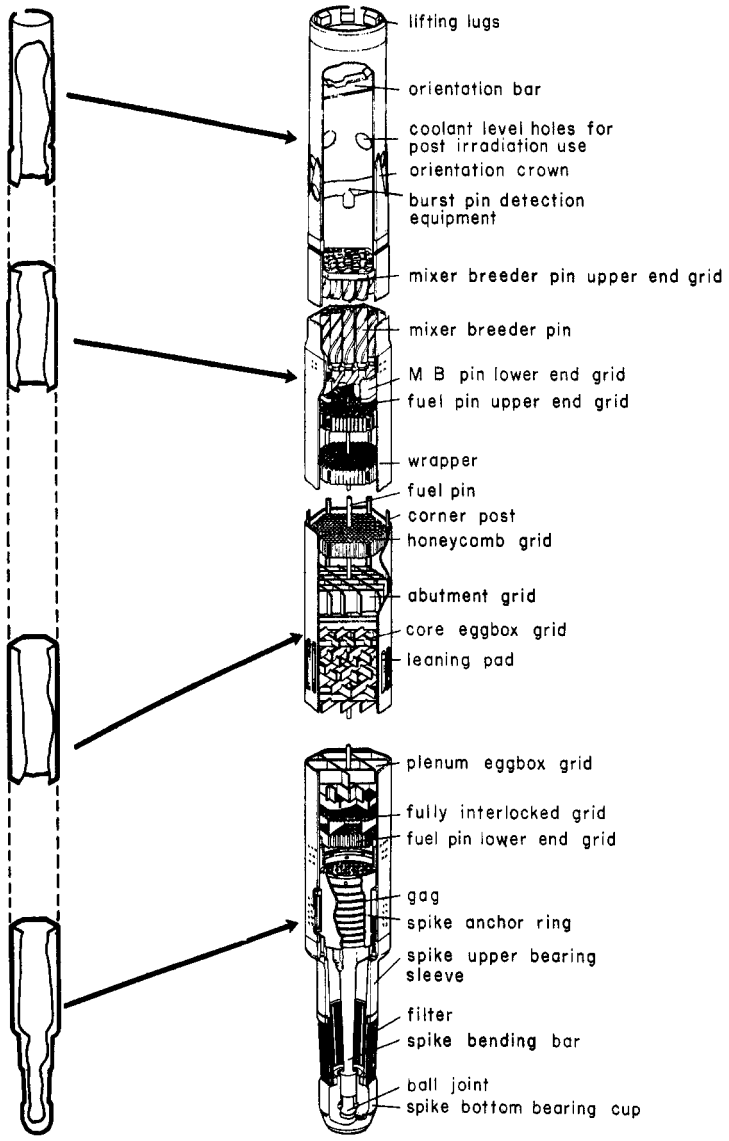

Figure 2. Arrangement of PFR fuel assembly. (After Ref. 2.)

The fuels for fast breeder reactors include alloys such as U-Pu-Zr and the ceramic materials UO_2–PuO_2, UC–PuC, and UN–PuN, but the mixed oxides, UO_2–PuO_2, are the choice for prototype fast breeder fuel elements because of their high melting temperature, compatibility with cladding and coolants, and relatively good irradiation stability and fission product retention. The disadvantages are the relatively low metal density, the

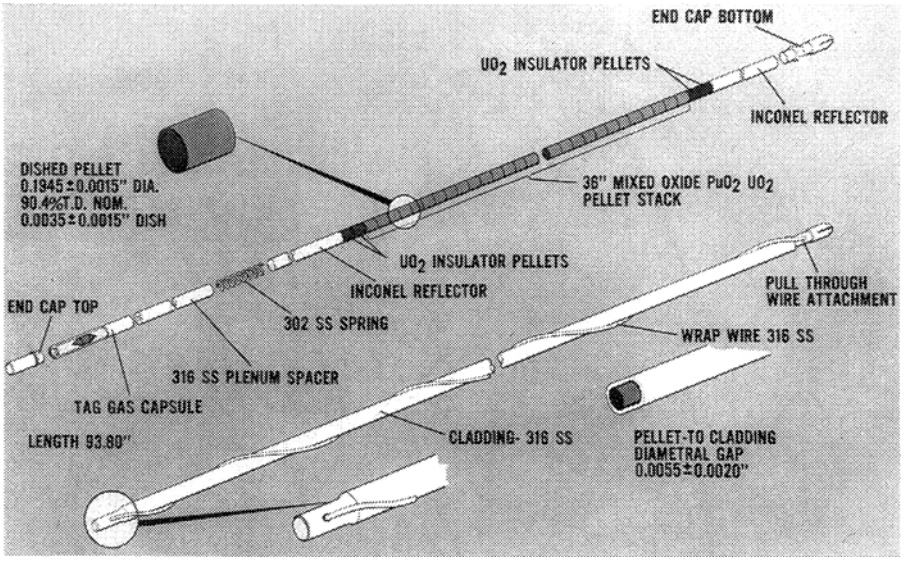

Figure 3. FFTF driver fuel pin. (After Ref. 2.)

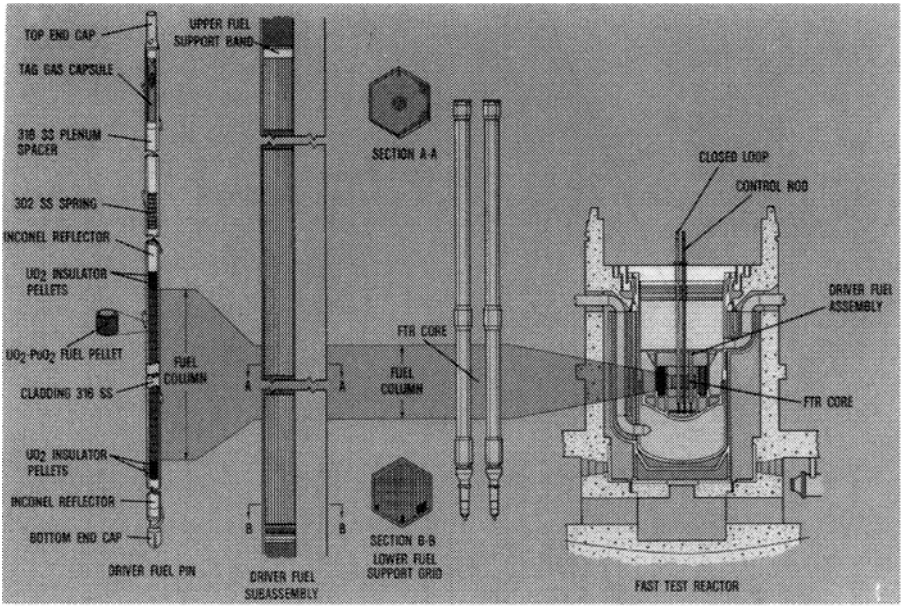

Figure 4. FFTF fuel system. (After Ref. 2.)

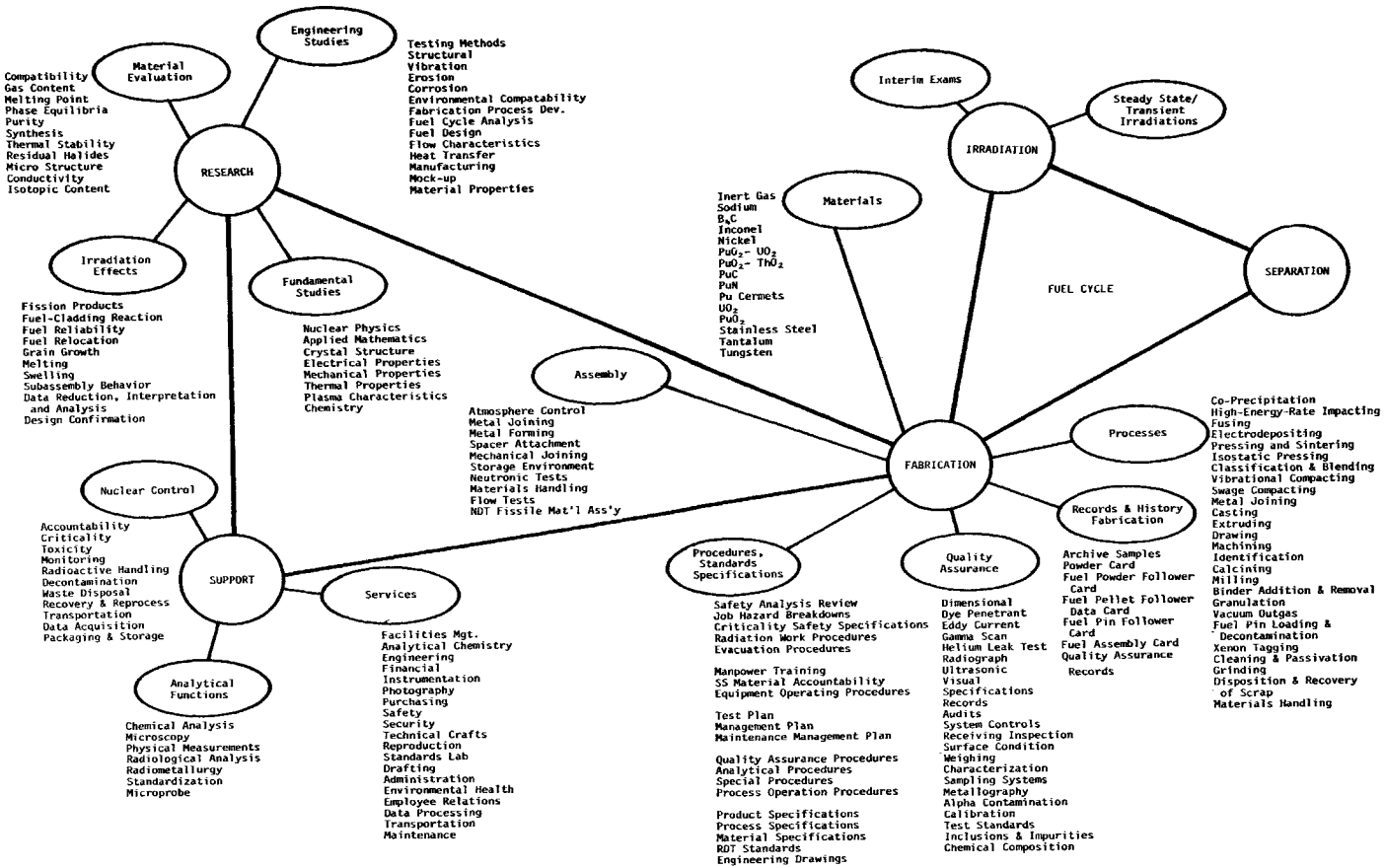

Figure 5. Typical plutonium fuel development considerations. (After Ref. 8.)

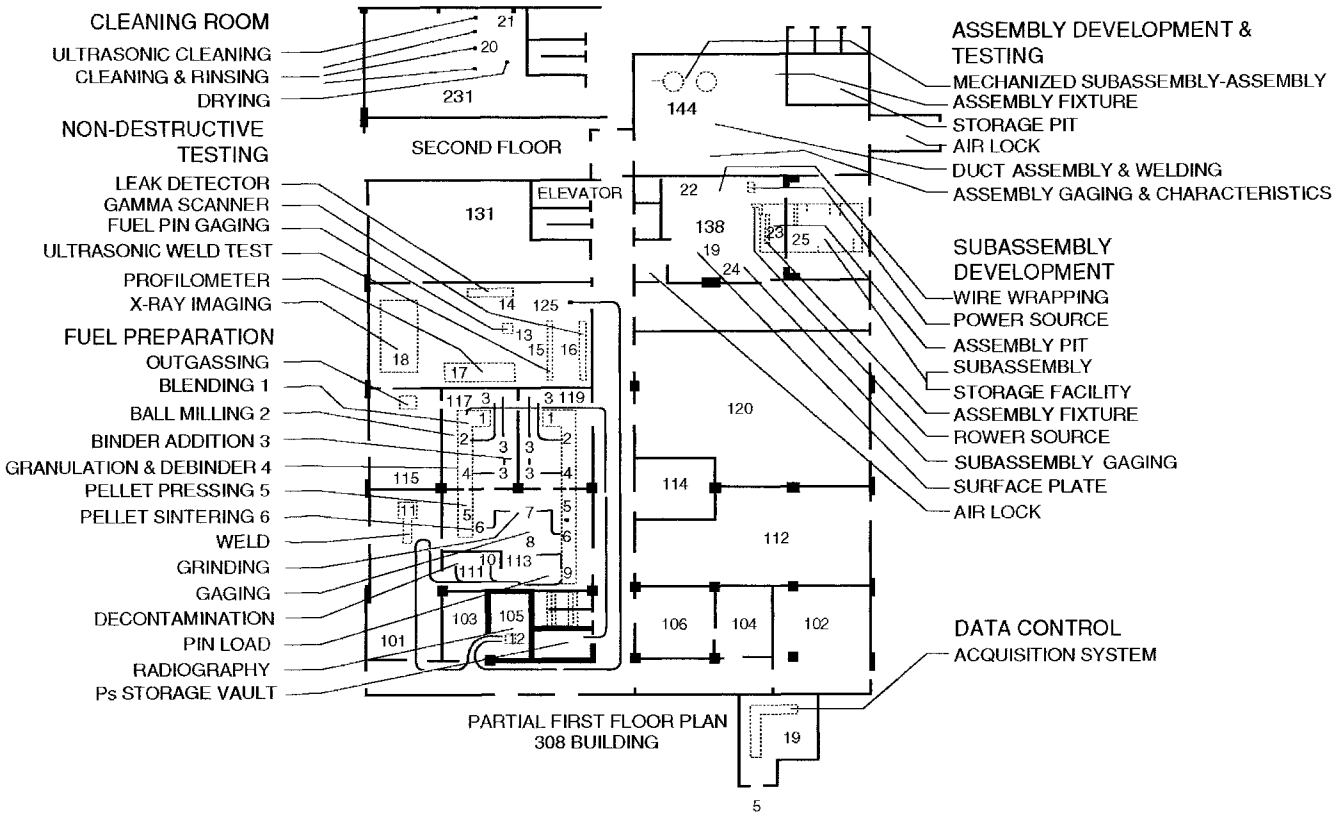

Figure 6. FFTF fuel fabrication demonstration facility. (After Ref. 8.)

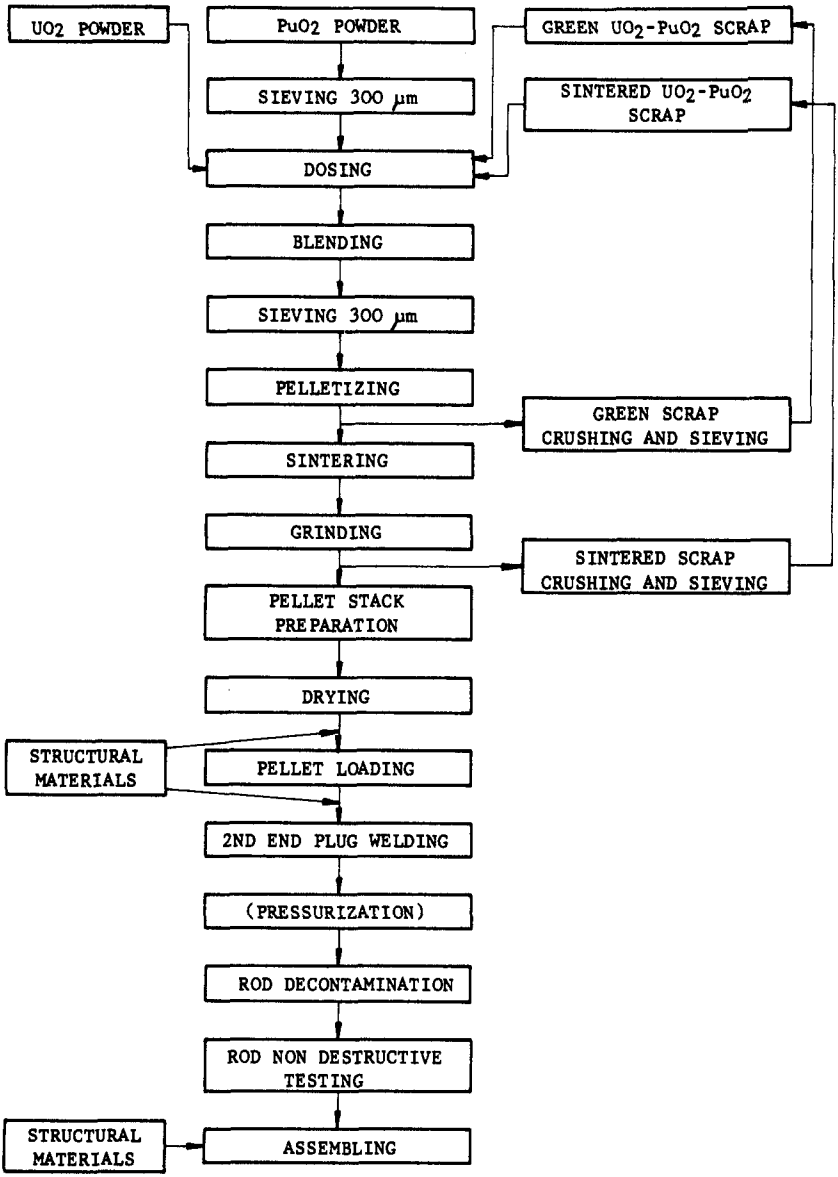

Figure 7. Mixed oxide fuel fabrication flow sheet.

moderating effect of oxygen, low thermal conductivity, excessive swelling over a critical temperature range at high burnups, and the possibility of fission product and plutonium redistribution during reactor operation.

Plutonium dioxide forms a series of solid solutions with UO_2 and has the same crystal structure (fcc, NaCl type). The good compatibility of PuO_2 with cladding materials is similar to that of UO_2. The melting point of PuO_2 (2400°C) is lower than that of UO_2 (2850°C). The mixed oxide fabrication process is shown in Figure 7 and Table 1.

TABLE 1. HIGHLIGHTS OF TYPICAL MIXED OXIDE FABRICATION PROCESS (HANFORD ENGINEERING DEVELOPMENT LABORATORY)

PuO_2	10–20 m^2/g, surface area
Calcining	675–725°C soak, 60–75 min soak time, 200°C/h rise, stainless steel crucible
Screening PuO_2	−325 mesh, 6–12 m^2/g surface area
Screening UO_2	−100 mesh, 8 m^2/g surface area
Blending	1. Hand-premix through 20-mesh screen 6-times 2. V-blend 10 min
Ball milling	Low ash, rubber-lined mills; 12 h cycle; tungsten carbide media; surface, 4–10 m^2/g
Binder addition	3 wt % Carbowax 20M in H_2O (20 wt % solution)
Drying	3–4 h at 70°C
Granulation	20 mesh
Redrying	3 h at 70°C
Prepressing	12.7 mm diameter die, 207–345 MPa
Granulation	20 mesh
Pellet pressing	138–207 MPa, 53% theoretical density green density
Binder removal	
Atmosphere	Ar–8% H_2, 6×10^{-5} m^3/s
Rate of temperature rise and cooling	120–140°C/h (200°C/h max)
Soak temperature	350–650°C
Soak time	4 h
Batch size	3 kg max
Sintering	
Atmosphere	Ar–8% H_2, dried to < 1 ppm H_2O 1 to 4.7×10^{-5} m^3/s
Soak temperature	1650°C
Soak time	4 h
Batch size	6 kg max
Cycle	23 h
(The furance is evacuated at 850°C during cooldown to reduce gas and moisture content of sintered pellets.)	
Gauging	Micrometers and dial indicators 0.025 mm accuracy
Grinding	Centerless (dry)
Pellet loading and fuel pin assembly	
Decontamination	
Closure welding	TIG weld, helium atm
Helium leak check	For cladding and weld integrity
Nondestructive testing	Gamma scan for fuel pellet placement and isotopic content
Cleaning and passivating	Caustic base cleaner and HNO_3 passivating
Surface contamination test	For removable and fixed alpha
Packaging and storage	

Source: After Ref. 2.

The mixed oxide $(U,Pu)O_2$ can be prepared by adding ammonia to a mixed nitrate solution of plutonium(IV) nitrate and uranyl nitrate. The precipitate, which consists of $Pu(OH)_4$ and $(NH_4)_2U_2O_7$, is converted to $(U,Pu)O_2$ by heating in hydrogen at 500–800°C. Typical conditions for the preparation of PuO_2 and PuO_2–UO_2 powder are listed in Table 2[22].

Pellets of UO_2–PuO_2 or $(U,Pu)O_2$ are prepared by cold pressing and sintering either a mechanical mixture of the oxides or, preferably, a chemically prepared solid solution powder, respectively. Sintering is influenced by the nature of the oxide particles (morphology and size distribution), the ratio of uranium to plutonium oxides, the sintering atmosphere, and the green (unfired) density. The presence of up to 10% PuO_2 particles reduces the sinterability of UO_2 in a mechanical mixture. Sintering in a CO–CO_2 mixture results in higher density pellets (see Figure 8). However, with solid solution oxide, $(U,Pu)O_2$, the sinterability in H_2 is enhanced with PuO_2 content and is better in H_2 than in CO_2 or Ar. The optimum temperature is 1400°C.

Cavities form in the PuO_2 particle during sintering in Ar–8% H_2 at 1675°C for 8 h owing to nucleation and growth of water bubbles at or in the PuO_2 particles during H_2 reduction. Water bubbles form because of their lower permeability in the oxide and vacancy flow (creep) from the matrix in response to excess water vapor pressure inside the bubble[14].

The mixed carbides, UC–PuC, have improved breeding and a shorter doubling time owing to their higher metal atom density and thermal conductivity, but control of composition (stoichiometry) ensure to compatibility with the cladding and the sodium coolant and to minimize swelling, is harder, and irradiation experience at high burnups and elevated temperatures is lacking[2–7,15–20]. The fabrication methods for mixed carbide fuels are similar to the techniques described for uranium carbide.

Compared with mixed oxide fuels, the mixed carbide fuels have higher heavy metal density (13 vs. 9.7 g/cm^3), better neutron economics, greater thermal conductivity (10 times greater), higher linear heat rate capability [1485 W/cm (45 kW/ft) for carbide]

TABLE 2. TYPICAL PREPARATION FOR PuO_2 AND PuO_2–UO_2 POWDER

	PuO_2	PuO_2–UO_2
Precipitation method	Continuous	Continuous
Feed solution composition	(Pu) 0.4–0.5 M (H^+) 3 M (NO_3^-) 4.6–5 M	(U + Pu) 0.4–0.5 M (H^+) 1 M (NO_3^-) 2.6–3 M
Precipitant composition	$H_2C_2O_4$ 1 M H_2O_2 0.8 M	NH_4OH 14.5 M
Precipitation temperature	35°C (95°F)	55°C (131°F)
Precipitation residence time	20 min	30 min
Intermediate compound	PlutoniumIV oxalate	Ammonium diuranate–plutonium hydroxide
Furnace temperature of intermediate compound	180°C (356°F)	180°C (356°F)
Furnace temperature for conversion to oxide	740–840°C (1364–1544°F)	740–1544°C (1364–1544°F)
Furnace atmosphere composition	Air	H_2–6% H_2

Source: Ref. 12.

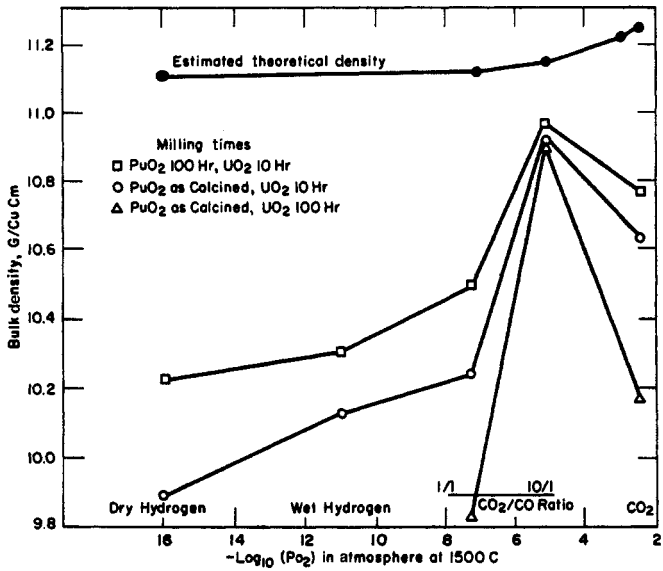

Figure 8. Density of mechanically mixed $(U_{70}Pu_{30})$-O_2 sintered in various atmospheres at 1500°C for 4 h. (After Ref. 12.)

and specific powder [up to 500 W/g(U + Pu)], improved breeding gain, and lower fuel cycle cost compared with oxide fuel at the same burnup. The mixed nitride fuels also have higher metal density (13.6 g/cm^3); greater thermal conductivity (slightly higher than the carbide); higher linear heat rate, specific power, and breeder gain; and lower fuel cycle cost compared with oxide fuels. The nitride fuel has a higher neutron penalty than the carbide fuel because of the higher neutron absorption cross section of nitrogen.

These fuels are compatible with stainless steel cladding. However, with carbide fuels prevention of carbon transport from the fuel to the cladding material or vice versa requires control of the chemical potential of carbon in the fuel (e.g., by using stoichiometric UC; by stabilizing the fuel with addition of small amounts of Cr, V, or Mo; or by Cr plating the pellets). Both carbide and nitride fuels have good compatibility with sodium but poor oxidation resistance.

The carbide and nitride elements have higher (~25%) costs of fabrication than oxide fuels. However, the total fuel element fabrication costs for a core loading may be lower because fewer elements of larger diameter are required.

(MASSOUD T. SIMNAD)

1. O. Wick, ed., *Plutonium Handbook*, American Nuclear Society, La Grange Park, IL, 1980.
2. E.C. Norman, ed., *Fast Breeder Reactor Fuel Performance, Proc. Int. Conf.*, March 5–8, 1979, Monterey, CA; American Nuclear Society, La Grange, IL, 1979.
3. *Fuel and Fuel Elements for Fast Reactors, Proc. Int. Symp.*, July 2–6, 1973, Brussels; International Atomic Energy Agency, Vienna, 1974.
4. R. Farmakes, ed., *Fast Reactor Fuel Element Technology, Proc. Int. Conf.*, April 13–15, 1971, New Orleans; American Nuclear Society, La Grange, IL, 1971.
5. J. Leary, H. Kittel, eds., *Advanced LMFBR Fuels, Proc. Int. Topical Meeting*, October 10–13, 1977, Tucson, AZ; American Nuclear Society, La Grange, IL, 1977.

6. M. J. Lineberry, H. F. McFarlante, P. I. Amerndon, R. W. Goin, D. S. Webster, in "*Fast Breeder Reactor Studies*, C. E. Till, ed., Report ANL-80-40, July 1980, Argonne National Laboratory, Argonne, IL, pp. 192–278.
7. J. F. W. Bishop, *Nucl. Energy*, *20*, 31 (1981).
8. E. A. Evans, W. F. Sheely, in *Education and Research in the Nuclear Fuel Cycle*, D. M. Elliot, L. E. Weaver, eds., University of Oklahoma Press, Norman, 1972, p. 153.
9. K. Richter, W. Bartscher, *Fabrication and Characterization of MX-Type Fuels and Fuel Pins*, Commission of European Communities Report EUR-6154, Karlsruhe, Germany, 1978.
10. *Nuclear Fuel Quality Assurance, Proc. Int. Seminar*, September 1976, Oslo, Norway; International Atomic Energy Agency, Vienna, 1976.
11. L. Mandicourt, ed., *Manufacture of the Second Core of Rapsodie-Type 2A-Fortissimo Fuel*, Report CEA-R-4881, Centre d'Etudes Nucléaires de Cadarache, France, November 1977.
12. G. Vanhellemont, in *Fabrication of Water Reactor Fuel Element, Proc. Symp.*, Prague, Nov. 6–10, 1978; International Atomic Energy Agency, Vienna, 1979, p. 225.
13. D. E. Rasmussen, E. W. Gerber, R. B. McCord, *Microstructure Characterization of Advanced Oxide Fuel*, Report HEDL-SA-1171-FP, Hanford Engineering Development Laboratories, Richland, WA, April 1977.
14. P. E. Hart, D. R. Olander, *J. Nucl. Mater.*, *78*, 315 (December 1978).
15. F. G. Reshetnikov, P. M. Verkhovyk, V. M. Makarov, *At. Energy (USSR)*, *43*, 408, 1977.
16. I. S. Golovin, A. S. Zaimovskii, N. D. Dergachev, *At. Energy (USSR)*, *43*, 1063, 1977.
17. H. Wedemeyer, E. Guenther, *Preparation of Uranium-Plutonium Carbide*, transl. of KFK-2238 (ORNL-tr-4180), 1974.
18. F. Brown, P. T. Good, R. Lapage, in *Compounds of Interest in Nuclear Reactor Technology*, J. T. Waber, P. Chiotti, W. N. Miner, eds., IMD Special Report No. 13, American Institute of Mining Engineers, New York, 1964, pp. 513–524.
19. R. W. Stratton, *Trans. Am. Nucl. Soc.*, *32*, 231, 1979.
20. S. Pickles, G. Yates, J. I. Bramman, M. B. Finlayson, *J. Nucl. Mater.*, *89*, 296 (April 1980).
21. J. P. Nichols, R. E. Brookshank, D. E. Ferguson, *Nucl. Appl.*, *1*, 176, (1965).
22. R. B. Holden, *Ceramic Fuel Elements*, Gordon & Breach, New York, 1966.

17.3.12.1.5. Thorium Ceramic Fuels.

Thorium is a fertile material in which fissionable U-233 is produced by neutron absorption (see 17.3.12.1: Fig. 1). Use of the thorium cycle in thermal reactors results in higher conversion ratios and longer fuel life and, since thorium ores are more plentiful than uranium ores, greatly expands nuclear energy resources. However, the high radioactivity of by-product U-232 present requires that the reprocessing and refabrication of the irradiated fuel be carried out remotely in shielded facilities[1]. The ThO_2 fertile material is mixed with oxides of the fissile isotopes U-235, U-233, or Pu-239 (usually $<10\%$ UO_2), or it may be used as pure ThO_2. Thorium–uranium oxide fuels are used in water-cooled power reactors, and thorium oxide- or carbide-coated particle fuels are utilized in the high temperature helium gas cooled reactors.

ThO_2 is miscible with UO_2 over the entire composition range. The low UO_2 compositions used in the fuels are stable in air at elevated temperature because ThO_2 is stable in oxygen up to its melting point (3300°C). The only stable oxide of thorium is ThO_2, and no higher oxides are formed. It has a cubic fluorite structure and low thermal conductivity. The ThO_2 fuel pellets are fabricated like UO_2 (see 17.3.12.1), and again the densities achieved are sensitive to the characteristics of the starting powder material, which can be produced by thermal decomposition of the nitrate, oxalate, hydroxide, or carbonate[2]. Higher densities at lower temperatures can be achieved with oxide powder derived from decomposition of the carbonate. The ThO_2–UO_2 mixtures are formed by coprecipitation of their salts or by mechanical mixing. Granulated mixtures of the oxides containing a binder (Carbowax) and lubricant and up to $\sim 50\%$ U_3O_8 can be

Inorganic Reactions and Methods, Volume 18
Edited by J. J. Zuckerman, Jim D. Atwood

6. M. J. Lineberry, H. F. McFarlante, P. I. Amerndon, R. W. Goin, D. S. Webster, in "*Fast Breeder Reactor Studies*, C. E. Till, ed., Report ANL-80-40, July 1980, Argonne National Laboratory, Argonne, IL, pp. 192–278.
7. J. F. W. Bishop, *Nucl. Energy*, *20*, 31 (1981).
8. E. A. Evans, W. F. Sheely, in *Education and Research in the Nuclear Fuel Cycle*, D. M. Elliot, L. E. Weaver, eds., University of Oklahoma Press, Norman, 1972, p. 153.
9. K. Richter, W. Bartscher, *Fabrication and Characterization of MX-Type Fuels and Fuel Pins*, Commission of European Communities Report EUR-6154, Karlsruhe, Germany, 1978.
10. *Nuclear Fuel Quality Assurance*, *Proc. Int. Seminar*, September 1976, Oslo, Norway; International Atomic Energy Agency, Vienna, 1976.
11. L. Mandicourt, ed., *Manufacture of the Second Core of Rapsodie-Type 2A-Fortissimo Fuel*, Report CEA-R-4881, Centre d'Etudes Nucléaires de Cadarache, France, November 1977.
12. G. Vanhellemont, in *Fabrication of Water Reactor Fuel Element*, *Proc. Symp.*, Prague, Nov. 6–10, 1978; International Atomic Energy Agency, Vienna, 1979, p. 225.
13. D. E. Rasmussen, E. W. Gerber, R. B. McCord, *Microstructure Characterization of Advanced Oxide Fuel*, Report HEDL-SA-1171-FP, Hanford Engineering Development Laboratories, Richland, WA, April 1977.
14. P. E. Hart, D. R. Olander, *J. Nucl. Mater.*, *78*, 315 (December 1978).
15. F. G. Reshetnikov, P. M. Verkhovyk, V. M. Makarov, *At. Energy (USSR)*, *43*, 408, 1977.
16. I. S. Golovin, A. S. Zaimovskii, N. D. Dergachev, *At. Energy (USSR)*, *43*, 1063, 1977.
17. H. Wedemeyer, E. Guenther, *Preparation of Uranium-Plutonium Carbide*, transl. of KFK-2238 (ORNL-tr-4180), 1974.
18. F. Brown, P. T. Good, R. Lapage, in *Compounds of Interest in Nuclear Reactor Technology*, J. T. Waber, P. Chiotti, W. N. Miner, eds., IMD Special Report No. 13, American Institute of Mining Engineers, New York, 1964, pp. 513–524.
19. R. W. Stratton, *Trans. Am. Nucl. Soc.*, *32*, 231, 1979.
20. S. Pickles, G. Yates, J. I. Bramman, M. B. Finlayson, *J. Nucl. Mater.*, *89*, 296 (April 1980).
21. J. P. Nichols, R. E. Brookshank, D. E. Ferguson, *Nucl. Appl.*, *1*, 176, (1965).
22. R. B. Holden, *Ceramic Fuel Elements*, Gordon & Breach, New York, 1966.

17.3.12.1.5. Thorium Ceramic Fuels.

Thorium is a fertile material in which fissionable U-233 is produced by neutron absorption (see 17.3.12.1: Fig. 1). Use of the thorium cycle in thermal reactors results in higher conversion ratios and longer fuel life and, since thorium ores are more plentiful than uranium ores, greatly expands nuclear energy resources. However, the high radioactivity of by-product U-232 present requires that the reprocessing and refabrication of the irradiated fuel be carried out remotely in shielded facilities[1]. The ThO_2 fertile material is mixed with oxides of the fissile isotopes U-235, U-233, or Pu-239 (usually $<10\%$ UO_2), or it may be used as pure ThO_2. Thorium–uranium oxide fuels are used in water-cooled power reactors, and thorium oxide- or carbide-coated particle fuels are utilized in the high temperature helium gas cooled reactors.

ThO_2 is miscible with UO_2 over the entire composition range. The low UO_2 compositions used in the fuels are stable in air at elevated temperature because ThO_2 is stable in oxygen up to its melting point (3300°C). The only stable oxide of thorium is ThO_2, and no higher oxides are formed. It has a cubic fluorite structure and low thermal conductivity. The ThO_2 fuel pellets are fabricated like UO_2 (see 17.3.12.1), and again the densities achieved are sensitive to the characteristics of the starting powder material, which can be produced by thermal decomposition of the nitrate, oxalate, hydroxide, or carbonate[2]. Higher densities at lower temperatures can be achieved with oxide powder derived from decomposition of the carbonate. The ThO_2–UO_2 mixtures are formed by coprecipitation of their salts or by mechanical mixing. Granulated mixtures of the oxides containing a binder (Carbowax) and lubricant and up to $\sim 50\%$ U_3O_8 can be

cold-pressed into pellets and sintered in hydrogen or in air at 1750–1850°C to form the $(Th,U)O_2$ solid solution. The U_3O_8 is prepared by heating UO_2 powder in air at 1000°C. The addition of about 1% CaO promotes sintering of ThO_2 in air (Ca has a low neutron-capture cross section). Sintered thoria exhibits good corrosion resistance in high temperature water and in sodium.

The sol–gel process is used to prepare dense, spherical particles of ThO_2 and $(Th,U)O_2$ for sphere–pac and coated-particle fuels. The thoria is dispersed in water from nitrate solutions by slow heating and steam denitration to form a stable sol from which spherical particles are produced[3,4]. The sol droplets are injected at the top of a tapered glass column containing an upward flow of 2-ethylhexarol (2-EH). The water from the sol particles is slowly extracted by suspension in the 2-EH, and the gelled spheres drop out of the column. Coalescence of the particles is prevented with surfactants in the 2-EH. The sol–gel spheres are dried in steam and Ar at 220°C and sintered in H_2 at 1300°C.

(MASSOUD T. SIMNAD)

1. W. V. Goeddel, *Annu. Rev. Nucl. Sci., 17*, 189 (1967).
2. R. B. Holden, *Ceramic Fuel Elements*, Gordon & Breach, New York, 1966.
3. R. L. Beatty, R. E. Norman, K. J. Notz, *Gel-Sphere-Pac Fuel for Thermal Reactors-Assessment of Fabrication Technology and Irradiation Performance*, Report ORNL-5469, Oak Ridge National Laboratory, Oak Ridge, TN, November 1979.
4. A. R. Olsen, R. R. Judkins, *Gel-Sphere-Pac Reactor Fuel Fabrication*, Report ORNL/TM-6924, Oak Ridge National Laboratory, Oak Ridge, TN, November 1979.

17.3.12.1.6. Coated Particle Fuels for HTGRs.

The high temperature gas reactors (HTGRs) use He gas at ~750°C and 5 MPa (685 psi) as the primary coolant, graphite as the neutron moderator and fuel element structural material, and coated Th, U carbide, or oxide fuel particles dispersed in a graphite matrix as the fuel[1–7]. Currently TRISO-UC_2 and TRISO- or BISO-ThO_2 (Fig. 1) are the candidate coated fissile and fertile fuel particles, respectively, for the large HTGRs. The TRISO coating consists of consecutive layers of porous carbon, pyrolytic carbon, silicon carbide, and pyrolytic carbon from the inner to the outer diameter. The

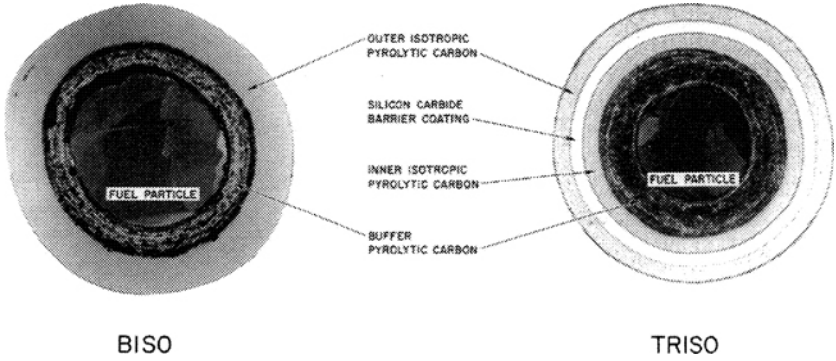

Figure 1. Typical coated fuel particles for HTGR. (After Ref. 4).

Inorganic Reactions and Methods, Volume 18
Edited by J. J. Zuckerman, Jim D. Atwood

cold-pressed into pellets and sintered in hydrogen or in air at 1750–1850°C to form the $(Th,U)O_2$ solid solution. The U_3O_8 is prepared by heating UO_2 powder in air at 1000°C. The addition of about 1% CaO promotes sintering of ThO_2 in air (Ca has a low neutron-capture cross section). Sintered thoria exhibits good corrosion resistance in high temperature water and in sodium.

The sol–gel process is used to prepare dense, spherical particles of ThO_2 and $(Th,U)O_2$ for sphere–pac and coated-particle fuels. The thoria is dispersed in water from nitrate solutions by slow heating and steam denitration to form a stable sol from which spherical particles are produced[3,4]. The sol droplets are injected at the top of a tapered glass column containing an upward flow of 2-ethylhexarol (2-EH). The water from the sol particles is slowly extracted by suspension in the 2-EH, and the gelled spheres drop out of the column. Coalescence of the particles is prevented with surfactants in the 2-EH. The sol–gel spheres are dried in steam and Ar at 220°C and sintered in H_2 at 1300°C.

(MASSOUD T. SIMNAD)

1. W. V. Goeddel, *Annu. Rev. Nucl. Sci.*, *17*, 189 (1967).
2. R. B. Holden, *Ceramic Fuel Elements*, Gordon & Breach, New York, 1966.
3. R. L. Beatty, R. E. Norman, K. J. Notz, *Gel-Sphere-Pac Fuel for Thermal Reactors-Assessment of Fabrication Technology and Irradiation Performance*, Report ORNL-5469, Oak Ridge National Laboratory, Oak Ridge, TN, November 1979.
4. A. R. Olsen, R. R. Judkins, *Gel-Sphere-Pac Reactor Fuel Fabrication*, Report ORNL/TM-6924, Oak Ridge National Laboratory, Oak Ridge, TN, November 1979.

17.3.12.1.6. Coated Particle Fuels for HTGRs.

The high temperature gas reactors (HTGRs) use He gas at ~750°C and 5 MPa (685 psi) as the primary coolant, graphite as the neutron moderator and fuel element structural material, and coated Th, U carbide, or oxide fuel particles dispersed in a graphite matrix as the fuel[1–7]. Currently TRISO-UC_2 and TRISO- or BISO-ThO_2 (Fig. 1) are the candidate coated fissile and fertile fuel particles, respectively, for the large HTGRs. The TRISO coating consists of consecutive layers of porous carbon, pyrolytic carbon, silicon carbide, and pyrolytic carbon from the inner to the outer diameter. The

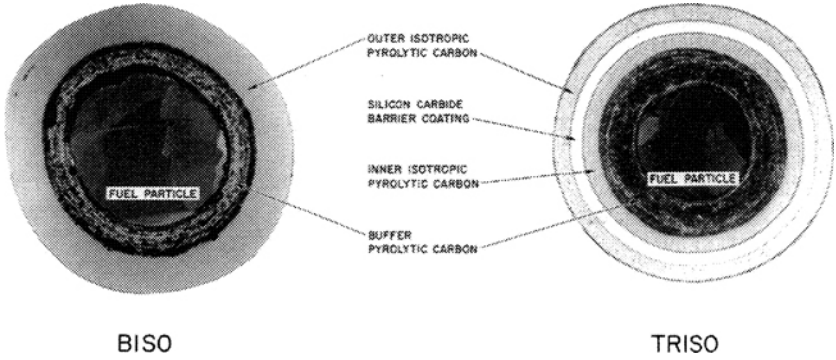

Figure 1. Typical coated fuel particles for HTGR. (After Ref. 4).

BISO coating consists of porous carbon and pyrolytic carbon from the inner to the outer diameter.

Graphite is used as a moderator and core structural material and as a diluent of the fuel. The Th, U-233 standard fuel cycle (Fig. 2), with U-235 as the initial fissionable fuel, is far superior to plutonium or U-235 in thermal systems insofar as achieves higher fuel utilization and lower power cost. A substantial portion of the power comes from fission of U-233, converted from the fertile Th-232. The carbon-to-throium ratio of 240 is optimum. The uranium requirements for the HTGR and 30–40% less than for a pressurized water reactor with plutonium recycle operation (Fig. 3). The arrangement of the fuel element is shown in Figures 4 and 5. High conductivity granulated graphite is used as shims to make the volume of all the fuel rods equal. The shim is uniformly mixed with the fissile and fertile particles before the rod is formed to produce a homogeneous mixture of particles. The particles are cemented together with a carbonaceous mix in the form of sticks before insertion into the holes in the graphite blocks.

The carbide particles are prepared from a granulated mixture consisting of UO_2, ThO_2, and carbon, which yields the required fuel carbide composition and size following conversion at high temperature (1900–2100°C) in vacuum. The particles are spheroidized by dropping them through a heat source, or by the sol–gel process.

Pyrolytic carbon and silicon carbide coatings are applied to the fuel particles by a fluidized bed, vapor phase coating technique in which the particles are levitated in a flowing gas stream within a vertical heated tube.

Pyrolytic carbon coatings are deposited from hydrocarbon gases (e.g., methane or acetylene) with argon or helium as diluents, at temperatures from 900 to 2200°C. The properties of the pyrolytic carbon coatings are controlled by varying the temperature, surface area of particles in the bed, the hydrocarbon composition, and the partial pressure (Figs. 6 and 7). Thus, it has been possible to fashion multilayered coatings. Silicon carbide coatings are deposited by pyrolysis of CH_3SiCl_3 in excess H_2 at 1400–1500°C.

The coating layer immediately surrounding the fuel particle is a porous buffer pyrocarbon, which protects the external coatings from fission-recoil damage,

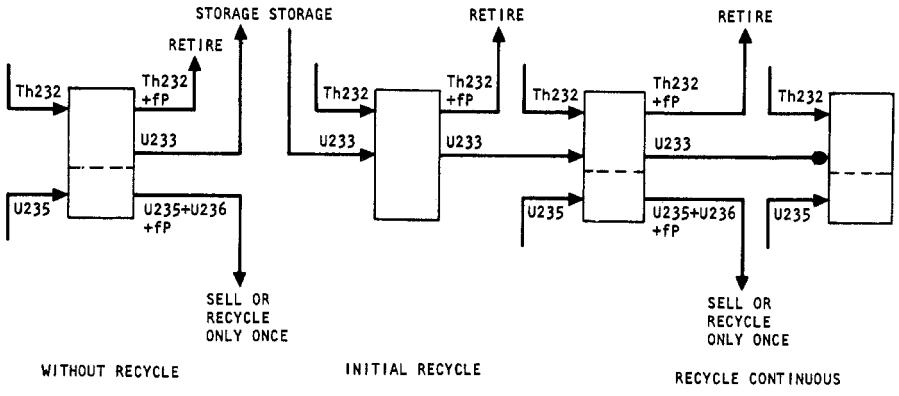

Figure 2. U-235/Th/U-233 fuel cycle modes. (After Ref. 4).

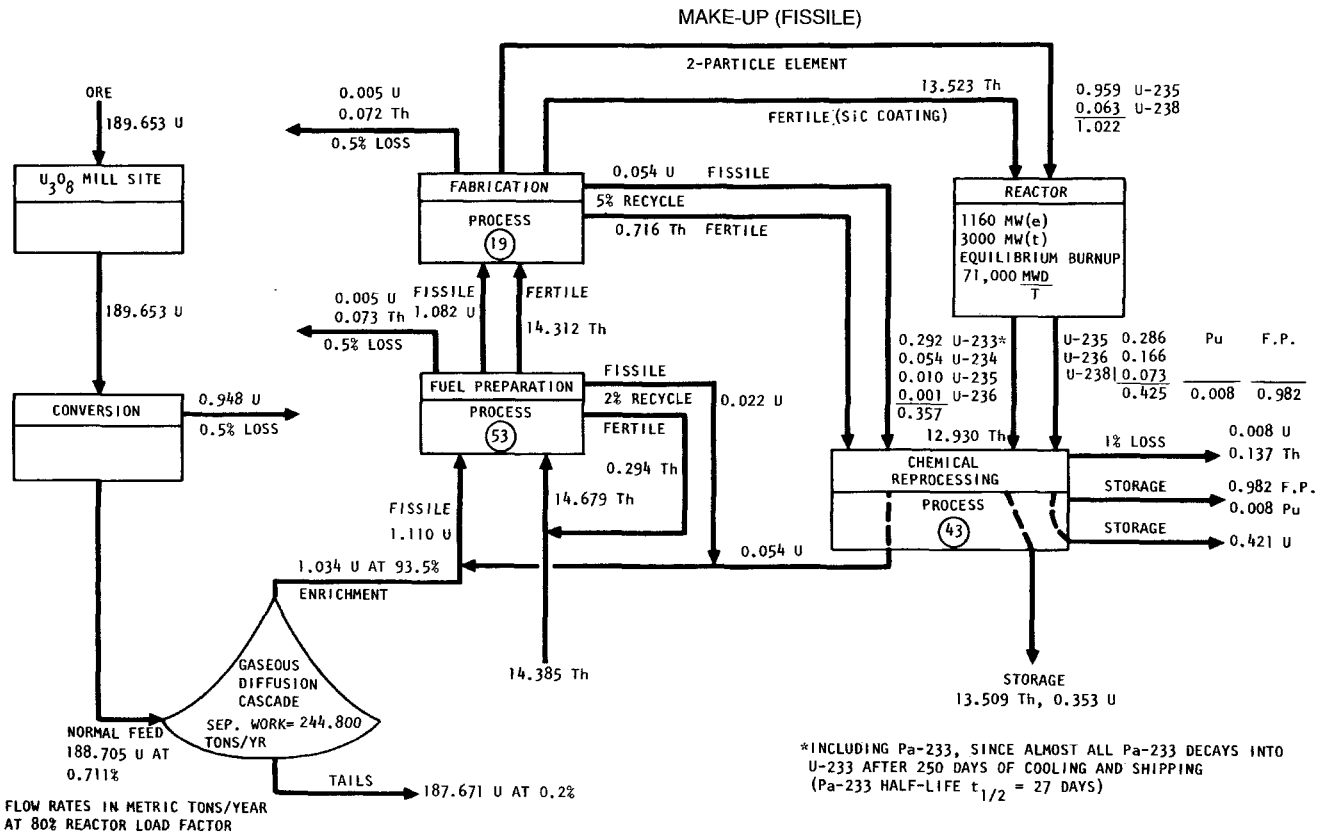

Figure 3. Equilibrium material balance flow sheet for reference HTGR at C/Th = 200 using TRISO/TRISO fuel with a 3-year cycle. (After Ref. 4.)

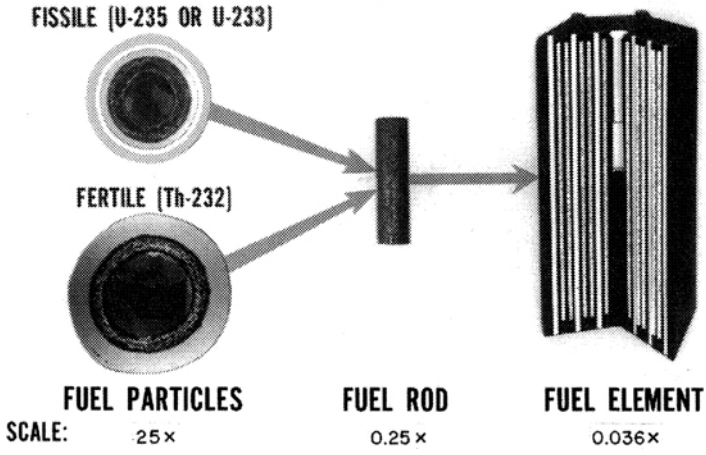

Figure 4. HTGR fuel components. (After Ref. 4).

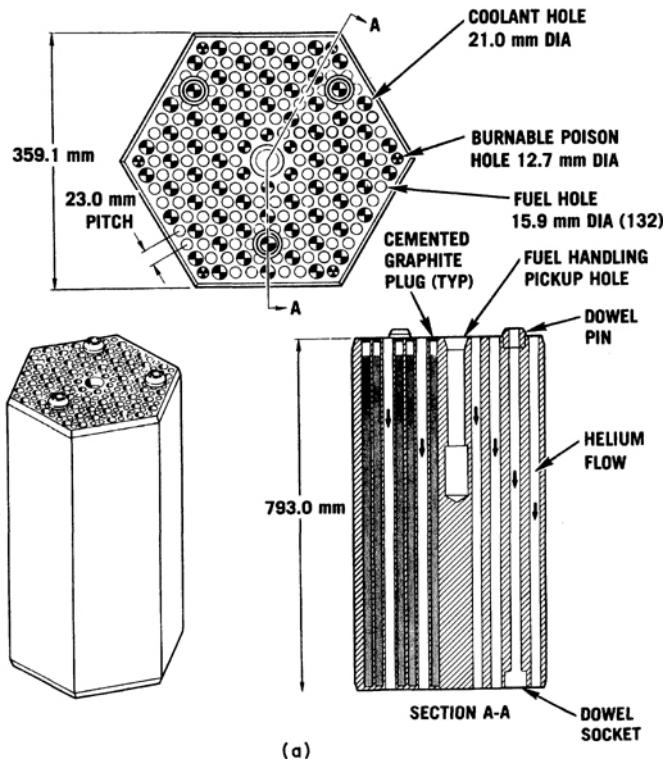

Figure 5. (a) HTGR standard fuel element and (b) HTGR control fuel element. (After Ref. 4.)

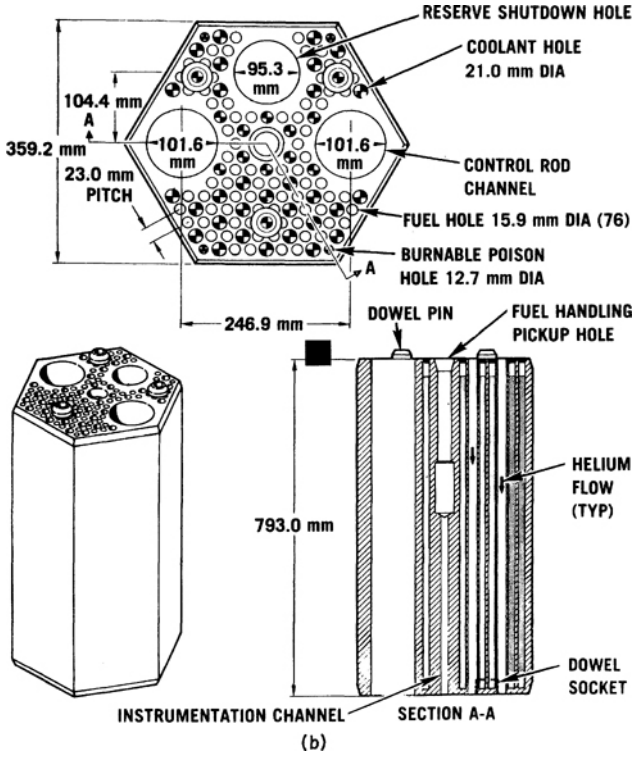

Figure 5(b).

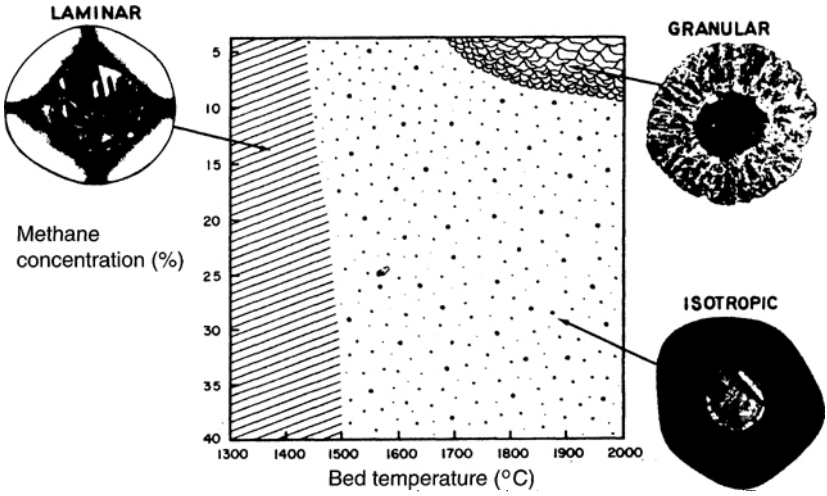

Figure 6. Illustration of the relationship between the structure of pyrolytic carbon and the deposition conditions (at constant reaction time and surface area of particles in the bed). (After Ref. 5.)

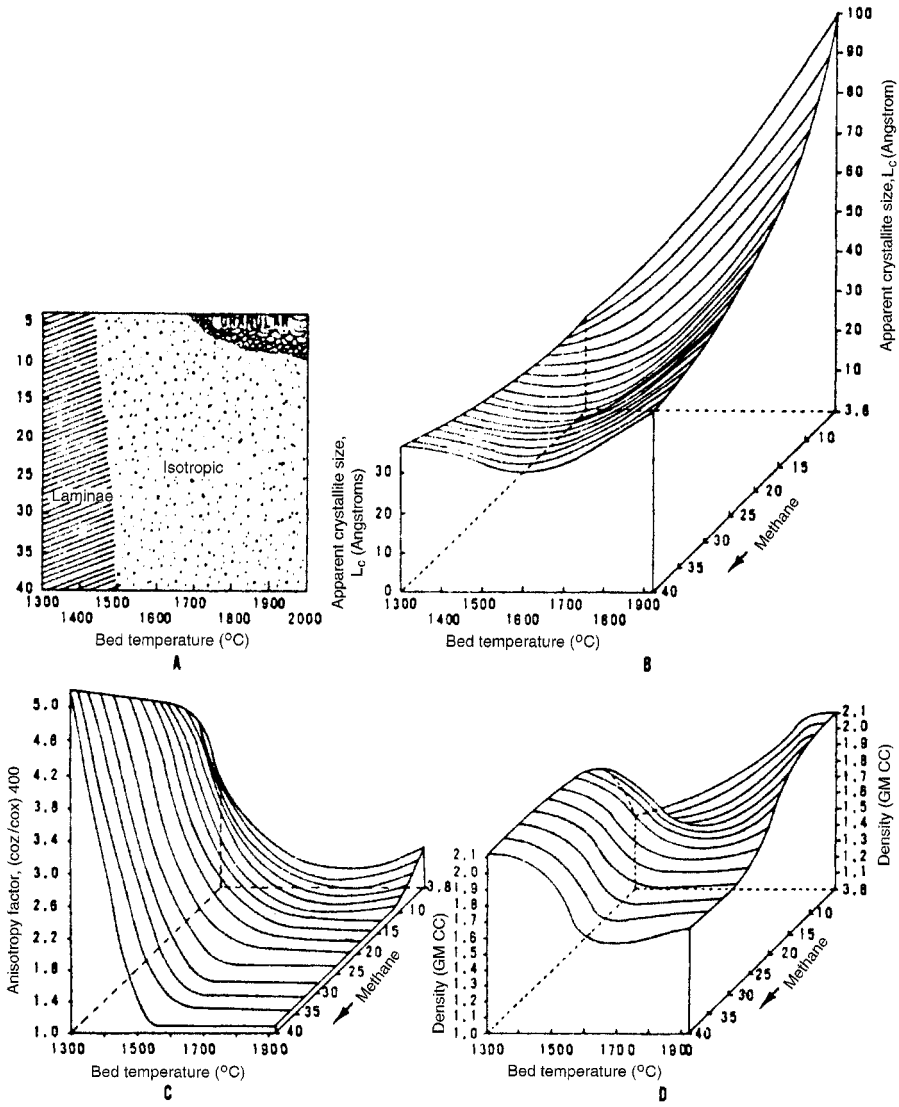

Figure 7. Diagrams showing the relationship between the structure of the carbon and its deposition conditions: (A) microstructure, (B) apparent crystallite size, (C) anisotropy factor, and (D) density. (After Ref. 5.)

accommodates fuel kernel swelling, and provides void space for the fission gases. BISO and TRISO coatings were described above. Coated $(Th,U)C_2$ particles (thorium/uranium = 5:1) in a graphite matrix (Fig. 8) are used in pebble bed reactors.

(MASSOUD T. SIMNAD)

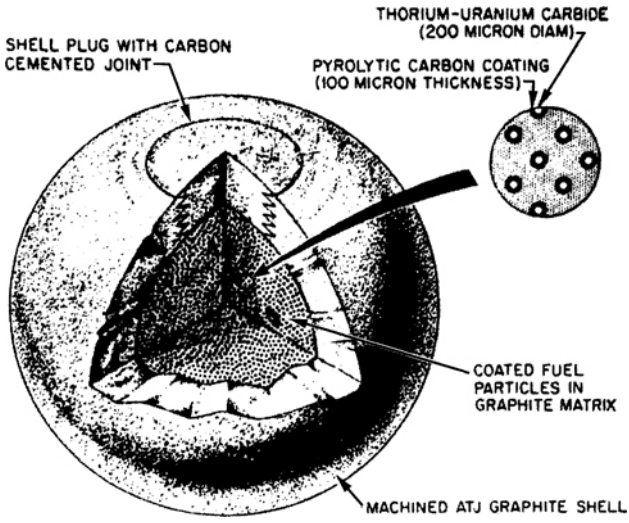

Figure 8. Spherical AVR fuel element consisting of dispersion of coated fuel particles in a carbonaceous matrix contained within a machined graphite shell. The sphere is 6 cm in diameter. (After Ref. 5.)

1. H. M. Agnew, *Sci. Am.*, *244*, 55 (1981); High temperature gas-cooled reactors, *Nucl. Eng. Design*, special issue, *26*, 230 (1974).
2. P. Fortescue, *Ann. Nucl. Energy*, *2*, 787 (1974).
3. *Gas-Cooled Reactors with Emphasis on Advanced Systems, Proc. Int. Symp.*, Oct. 13–17, 1975, Jülich, Germany; International Atomic Energy Agency, Vienna, 1976.
4. M. T. Simnad, J. P. Howe, in *Materials Science in Energy Technology*, G. G. Libowitz, M. S. Whittingham, eds., Academic Press, New York, 1979, p. 32.
5. M. T. Simnad, *Fuel Element Experience in Nuclear Power Reactors*, Gordon & Breach, New York, 1971.
6. G. Melese-d'Hospital, M. T. Simnad, *Energy-Int. J.*, *2*, 211 (1977).
7. W. V. Goeddel, *Annual Rev. Nucl. Sci.*, *17*, 189 (1967).

17.3.12.2. Moderators and Reflectors

17.3.12.2.1. Beryllium Oxide.

Beryllium oxide is used as a reflector and moderator in nuclear reactors. In addition to its low neutron-capture cross section, BeO has physical, mechanical, and chemical properties that allow its use at elevated temperatures, but its high cost and propensity to damage under irradation have limited its applications[1–5].

Reviews of BeO for nuclear reactor applications were persented at several international conferences. The literature on BiO up to 1966 has been reviewed in several papers[1–5].

The properties of BeO are governed by the nature of the starting materials and the methods of fabrication (Table 1). The important variables include composition, grain size, pore structure, and density[6].

Inorganic Reactions and Methods, Volume 18
Edited by J. J. Zuckerman, Jim D. Atwood

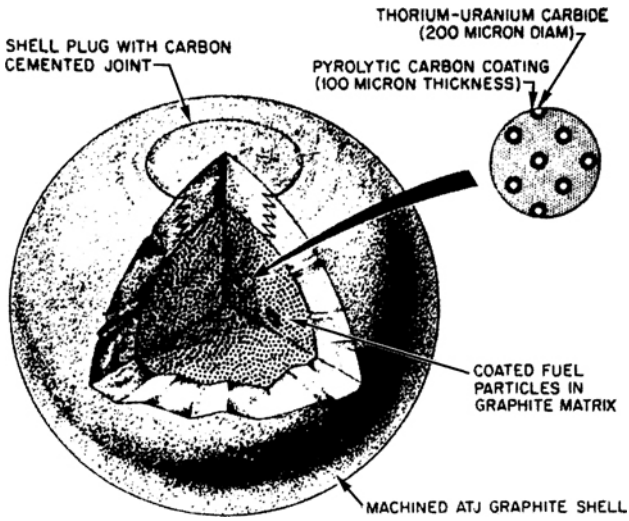

Figure 8. Spherical AVR fuel element consisting of dispersion of coated fuel particles in a carbonaceous matrix contained within a machined graphite shell. The sphere is 6 cm in diameter. (After Ref. 5.)

1. H. M. Agnew, *Sci. Am.*, *244*, 55 (1981); High temperature gas-cooled reactors, *Nucl. Eng. Design*, special issue, *26*, 230 (1974).
2. P. Fortescue, *Ann. Nucl. Energy*, *2*, 787 (1974).
3. *Gas-Cooled Reactors with Emphasis on Advanced Systems*, *Proc. Int. Symp.*, Oct. 13–17, 1975, Jülich, Germany; International Atomic Energy Agency, Vienna, 1976.
4. M. T. Simnad, J. P. Howe, in *Materials Science in Energy Technology*, G. G. Libowitz, M. S. Whittingham, eds., Academic Press, New York, 1979, p. 32.
5. M. T. Simnad, *Fuel Element Experience in Nuclear Power Reactors*, Gordon & Breach, New York, 1971.
6. G. Melese-d'Hospital, M. T. Simnad, *Energy-Int. J.*, *2*, 211 (1977).
7. W. V. Goeddel, *Annual Rev. Nucl. Sci.*, *17*, 189 (1967).

17.3.12.2. Moderators and Reflectors

17.3.12.2.1. Beryllium Oxide.

Beryllium oxide is used as a reflector and moderator in nuclear reactors. In addition to its low neutron-capture cross section, BeO has physical, mechanical, and chemical properties that allow its use at elevated temperatures, but its high cost and propensity to damage under irradation have limited its applications[1–5].

Reviews of BeO for nuclear reactor applications were persented at several international conferences. The literature on BiO up to 1966 has been reviewed in several papers[1–5].

The properties of BeO are governed by the nature of the starting materials and the methods of fabrication (Table 1). The important variables include composition, grain size, pore structure, and density[6].

TABLE 1. PHYSICAL PROPERTIES OF BeO

Density, g/cm^3	3.008
Melting point, °C	2430
Boiling point, °C	4120 ± 170
Lattice constants, pm	
a_0 at 20°C	2.69
c_0 at 20°C	4.39
a_0 at 1025°C	2.72
c_0 at 1025°C	4.43
Thermal conductivity, W/mK	
At 20°C	200
At 1000°C	22
At 1500°C	13
Average coefficient of expansion (from 25°C to temperature)	
At 20°C	—
At 1000°C	8.7×10^{-6}
At 1500°C	10.2×10^{-6}
Specific heat, J/kg K	
At 20°C	1003
At 1000°C	2050
At 1500°C	2170

Source: Ref. 3.

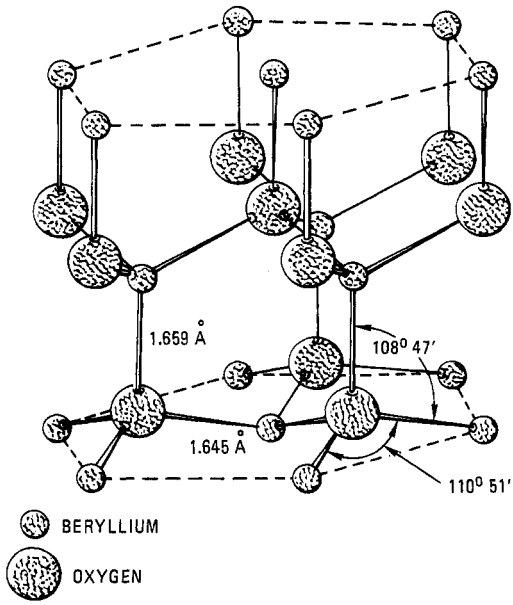

Figure 1. BeO crystal structure. (After Ref. 11.)

Modern ceramic fabrication techniques and equipment can be used on high purity, sinterable-grade BeO powder to produce beryllia shapes with improved properties at reduced cost.

Additives affect grain size, sintering temperature, and strength[7]; e.g., MgO enhances sinterability, 1% graphite reduces grain size from 14 μm to 4 μm, while 3 wt% ZrO_2 inhibits grain growth. Additing 0.5–1 wt% MgO ensures densification (> 97% theoretical), and the material retains the small grain size (5–8 μm) required for stability at high temperatures.

Isostatic or hot pressing also produces small grain size (3–8 μm) and high densities (> 99% theoretical)[8], as does addition of SiO_2, SiC, and C. Extrusion and sintering produce fine grained BeO of at least 95% theoretical density.

Synthetic BeO has the distorted, wurtzite structure[9–12] (Fig. 1), in which the oxygen z parameter is 0.379×10^{-10} m (vs 0.375×10^{-10} m for the undistorted structure. One Be–O bond distance is 1.659×10^{-10} m, while the other three to the base are 1.645×10^{-10} m.

(MASSOUD T. SIMNAD)

1. R. Smith, J. P Howe, eds., *Beryllium Oxide*, North-Holland, Amsterdam, 1964; published in *J. Nucl. Mater.*, *14* (1964).
2. B. S. Hickman, in *Studies in Radiation Effects*. Vol. 1, G. J. Dienes, ed., Gordon & Breach, New York, 1966, p. 73.
3. A. J. Rothman, in *Materials and Fuels for High-Temperature Nuclear Energy Applications*, M. T. Simnad, L. R. Zumwalt, eds., MIT Press, Cambridge, MA, 1964, p. 29.
4. R. A. Belyaev, *Beryllium Oxide: Properties and Applications*, Gasatomizdat, Moscow, 1962; AEC-TR-6157, 1962.
5. M. T. Simnad, R. A. Meyer, L. R. Zumwalt, in *Proceedings of a Conference on Nuclear Application of Nonfissionable Ceramics*, American Nuclear Society, La Grange, II, 1966, p. 169.
6. N. A. Hill, J. S. O'Neill, D. T. Livey, *Proc. Br. Ceram. Soc.*, *7*, 221 (1967).
7. R. J. Brown, N. W. Bass, *J. Nucl. Mater.*, *14*, 341 (1964).
8. S. C. Carniglia, R. E. Johnson, A. C. Hott, G. G. Bentle, *J. Nucl. Mater.*, *14*, 378 (1964).
9. J. B. Conway, R. A. Hein, *Nucleonics*, *22* (6), 71 (1964).
10. R. E. Latta, R. E. Fryxell, *The Melting Point and Phase Transformation of BeO*, U.S. AEC Report GEMP-736, General Electric, Sunnyvale, CA, April 1970.
11. D. K. Smith, H. W. Newkirk, J. S. Kahn, *J. Electrochem. Soc.*, *111*, 78 (1964); also U.S. AEC Report UCRL-7022, 1962.
12. P. J. Baldock, W. E. Spindler, T. W. Baker, *J. Nucl. Mater.*, *10*, 160 (1966); also U.K. AEA Report AERE-R-4471, 1965.

17.3.12.2.2. Metal Hydrides.

The atomic density of hydrogen in many metal hydrides is greater than that in liquid H_2 or in H_2O[1,2]. Metal hydrides are efficient moderators (Fig. 1) and neutron shielding materials, and help to minimize the core shield volume[2]. Metal-clad yttrium hydride moderators capable of operation at 1000°C in air, uranium–zirconium hydride rods as a combination fuel–moderator element are examples,[3–5] and metal-clad zirconium hydride units as moderator elements for operation up to 600°C[6–10]. The hydrogen atom density in hydrides, N_H, the number of hydrogen atoms per cubic centimeter of hydride $\times 10^{-22}$, is calculated from the hydrogen-to-metal atom ratio, H/M, the density of the hydride ρ, and the molecular weight W by:

$$N_H = (H/M)(\rho)(60.23)/W \qquad (a)$$

Inorganic Reactions and Methods, Volume 18
Edited by J. J. Zuckerman, Jim D. Atwood

Modern ceramic fabrication techniques and equipment can be used on high purity, sinterable-grade BeO powder to produce beryllia shapes with improved properties at reduced cost.

Additives affect grain size, sintering temperature, and strength[7]; e.g., MgO enhances sinterability, 1% graphite reduces grain size from 14 μm to 4 μm, while 3 wt% ZrO_2 inhibits grain growth. Additing 0.5–1 wt% MgO ensures densification (> 97% theoretical), and the material retains the small grain size (5–8 μm) required for stability at high temperatures.

Isostatic or hot pressing also produces small grain size (3–8 μm) and high densities (> 99% theoretical)[8], as does addition of SiO_2, SiC, and C. Extrusion and sintering produce fine grained BeO of at least 95% theoretical density.

Synthetic BeO has the distorted, wurtzite structure[9–12] (Fig. 1), in which the oxygen z parameter is 0.379×10^{-10} m (vs 0.375×10^{-10} m for the undistorted structure. One Be–O bond distance is 1.659×10^{-10} m, while the other three to the base are 1.645×10^{-10} m.

(MASSOUD T. SIMNAD)

1. R. Smith, J. P Howe, eds., *Beryllium Oxide*, North-Holland, Amsterdam, 1964; published in *J. Nucl. Mater., 14* (1964).
2. B. S. Hickman, in *Studies in Radiation Effects*. Vol. 1, G. J. Dienes, ed., Gordon & Breach, New York, 1966, p. 73.
3. A. J. Rothman, in *Materials and Fuels for High-Temperature Nuclear Energy Applications*, M. T. Simnad, L. R. Zumwalt, eds., MIT Press, Cambridge, MA, 1964, p. 29.
4. R. A. Belyaev, *Beryllium Oxide: Properties and Applications*, Gasatomizdat, Moscow, 1962; AEC-TR-6157, 1962.
5. M. T. Simnad, R. A. Meyer, L. R. Zumwalt, in *Proceedings of a Conference on Nuclear Application of Nonfissionable Ceramics*, American Nuclear Society, La Grange, II, 1966, p. 169.
6. N. A. Hill, J. S. O'Neill, D. T. Livey, *Proc. Br. Ceram. Soc., 7*, 221 (1967).
7. R. J. Brown, N. W. Bass, *J. Nucl. Mater., 14*, 341 (1964).
8. S. C. Carniglia, R. E. Johnson, A. C. Hott, G. G. Bentle, *J. Nucl. Mater., 14*, 378 (1964).
9. J. B. Conway, R. A. Hein, *Nucleonics, 22* (6), 71 (1964).
10. R. E. Latta, R. E. Fryxell, *The Melting Point and Phase Transformation of BeO*, U.S. AEC Report GEMP-736, General Electric, Sunnyvale, CA, April 1970.
11. D. K. Smith, H. W. Newkirk, J. S. Kahn, *J. Electrochem. Soc., 111*, 78 (1964); also U.S. AEC Report UCRL-7022, 1962.
12. P. J. Baldock, W. E. Spindler, T. W. Baker, *J. Nucl. Mater., 10*, 160 (1966); also U.K. AEA Report AERE-R-4471, 1965.

17.3.12.2.2. Metal Hydrides.

The atomic density of hydrogen in many metal hydrides is greater than that in liquid H_2 or in H_2O[1,2]. Metal hydrides are efficient moderators (Fig. 1) and neutron shielding materials, and help to minimize the core shield volume[2]. Metal-clad yttrium hydride moderators capable of operation at 1000°C in air, uranium–zirconium hydride rods as a combination fuel–moderator element are examples,[3–5] and metal-clad zirconium hydride units as moderator elements for operation up to 600°C[6–10]. The hydrogen atom density in hydrides, N_H, the number of hydrogen atoms per cubic centimeter of hydride $\times 10^{-22}$, is calculated from the hydrogen-to-metal atom ratio, H/M, the density of the hydride ρ, and the molecular weight W by:

$$N_H = (H/M)(\rho)(60.23)/W \qquad (a)$$

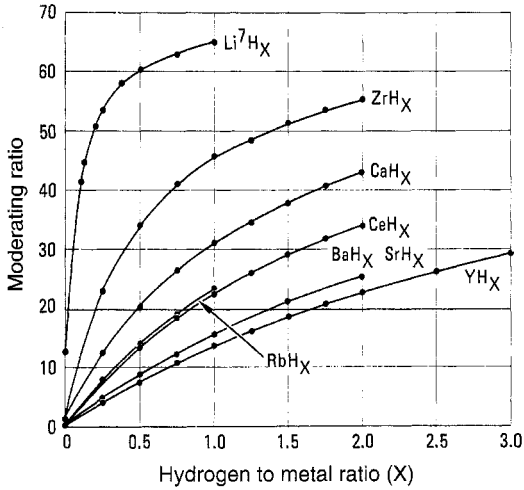

Figure 1. Moderating ratio vs. hydrogen content for selected hydrides. (After Ref. 1.)

The plateau pressures of the mono- and dihydrides of various metals are shown in Figure 2, which demonstrates their wide range of thermal stabilities. The 10^5 ρ_a (one-atmosphere) isobars in various stable metal hydrides are shown in Figure 3; isobars at higher pressures will be at larger N_H and higher temperatures. The isobars provide a measure of stabilities as a function of temperature and are useful for comparing the N_H parameter before consideration of other important criteria such as neutron-capture cross section, physical and mechanical properties, radiation stability, cost, and availability[11–15].

Metal hydrides for reactor shielding include zirconium hydride and mixed trap hydrides such as (ZrEu)H, (ZrHf)H, EuH, GdH, and ZrH–Eu_2O_3 or ZrH–B_4C mixtures. The absorption cross section of neutron absorbers increases with moderation in the neutron energy, so that the worth per unit volume of a mixed rod of $ZrH_{1.6}$ + Eu_2O_3 is comparable to that of a boron carbide rod 60% enriched in B-10, resulting in a considerable increase in the reactivity of the absorber. There is limited information on the preparation and properties of these hydrides except for zirconium hydride, which has a high N_H and good thermal stability and whose range of compositions extends to ZrH_2. At a composition having an N_H equivalent to that of H_2O (6.7), zirconium hydride can be used at 650°C.

The hydriding in a furnace of zirconium hydride moderator parts of 90 cm long by 10 cm in diameter (weighing ~ 27 kg)[2] lasts ~ 1 week[9]. The H/Zr ratio can be controlled to within ± 0.02, with a yield of 95%. In most cases, the hydrogen content is mostly 62–64 atom%. Stainless steel or nickel alloys are used for cladding zirconium hydride shielding elements.

Figure 4 plots the hydrogen density N_H versus the H/Zr ratio for zirconium hydride. The ZrH system is a simple eutectoid, containing at least four separate hydride phases in addition to the zirconium and allotropes (Fig. 5):

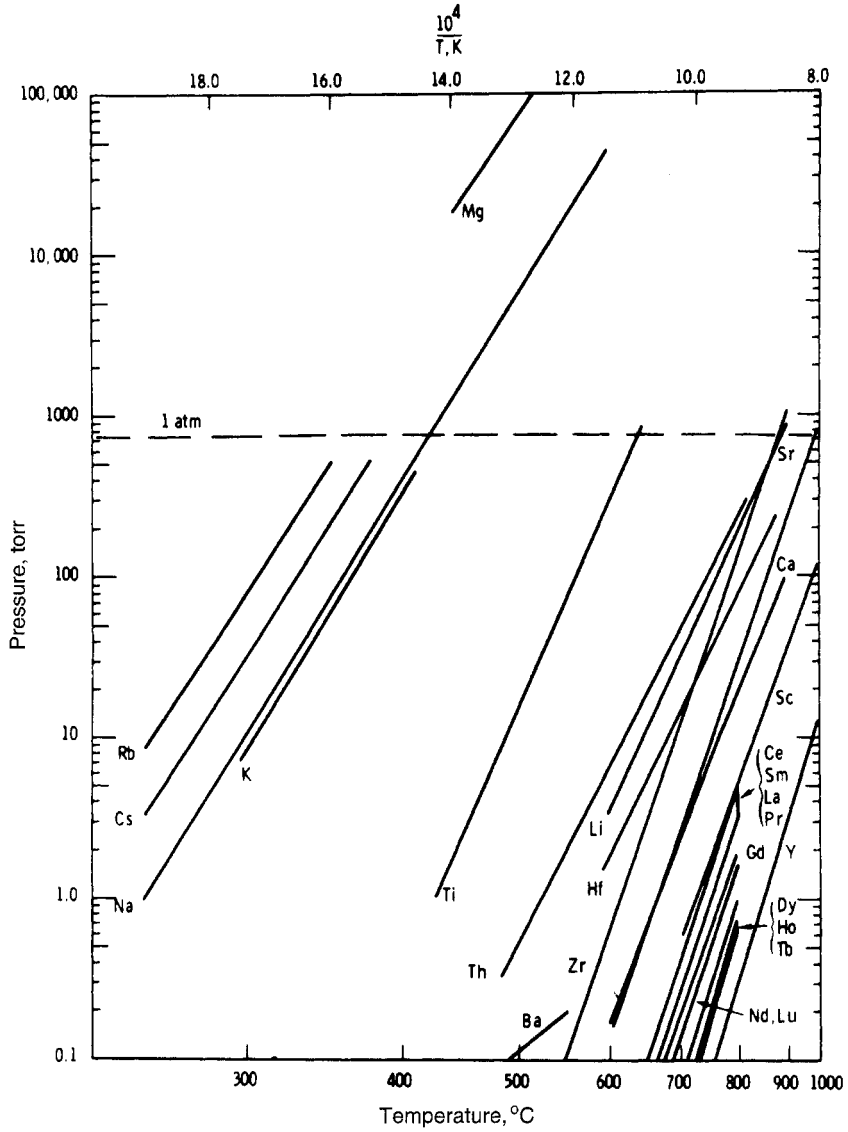

Figure 2. Plateau pressures of the monohydrides and dihydrides of various metals. (After Ref. 9.)

α phase: a low temperature terminal solid solution of H_2 in the hexagonal, close-packed, α-Zr lattice.

β phase: a solid solution of H_2 dissolved in the high temperature, body-centered cubic Zr phase.

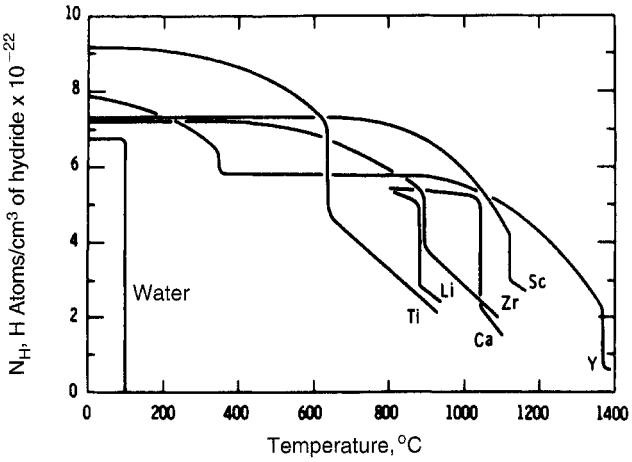

Figure 3. One-atmosphere isobars in various metal–hydrogen systems. (After Ref. 9.)

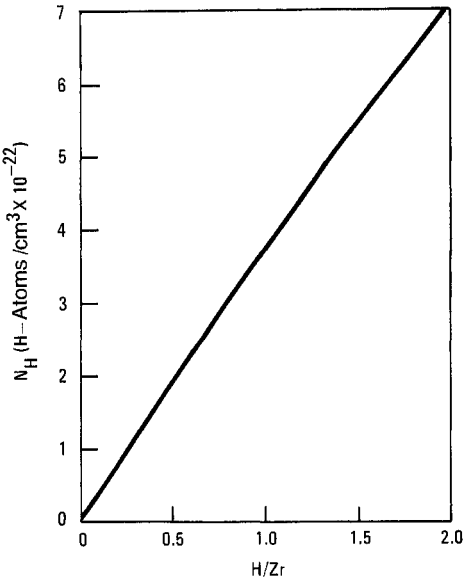

Figure 4. Hydrogen density (N_H) vs. H/Zr ratio for zirconium hydride at room temperature. (After Ref. 10.)

δ phase: a face-centered-cubic hydride phase; δ' phase is also formed below 240°C from the δ phase.

ε phase: a face-centered-tetragonal hydride phase with the ratio $c/a < 1$, extending beyond the δ phase to ZrH_2. The ε phase is not a true equilibrium phase, and it appears as a banded, twin structure.

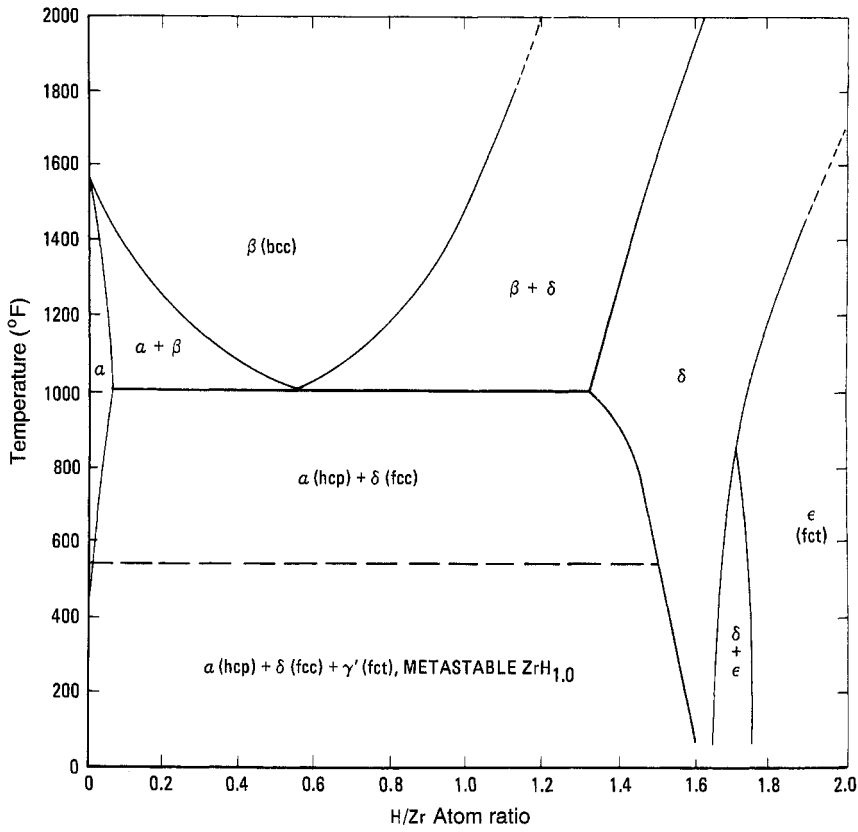

Figure 5. Zirconium hydride phase diagram, showing boundary determination. (After Ref. 11.)

The two-phase $\delta + \varepsilon$ region exists between $ZrH_{1.64}$ and $ZrH_{1.74}$ at room temperature, diminishes in width with increasing temperature, and closes at 455°C and $ZrH_{1.70}$. At higher temperatures, the δ and ε single-phase regions are separated by a single boundary sloping toward higher H/Zr ratios, reaching ZrH_2 at ~ 930°C. The transitions are first-order at the two-phase region and second-order at the single-phase region[11,12].

Oxygen concentrations of over 3.5 atom % in the hydride, shift the two-phase boundaries (δ plus ε) to lower H/Zr ratios, and the two-phase region becomes wider with increasing oxygen[11,12]. Reactor-grade zirconium contains 800–1000 ppm oxygen, and further oxygen contamination may occur during hydriding.

The heat of solution of hydrogen in the delta-hydrided phase decreases with increasing solute concentration[11] from -195 J/mol in δ of composition $ZrH_{1.4}$ to -158 J/mol in ε of composition $ZrH_{1.9}$. No discontinuity in the function occurs throughout the δ-to-ε range, involving H/Zr compositions of ~ 1.4–1.9. This is compatible with the transition from fcc-δ to fct-ε, involving a continuous anisotropic expansion

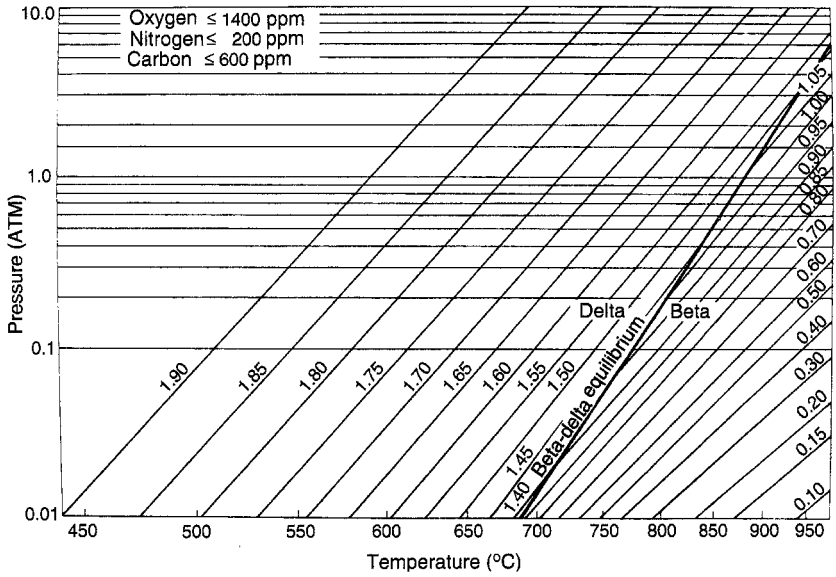

Figure 6. Dissociation pressure isochores of zirconium hydride (expressed as H/Zr atom ratios). (After Ref. 13.)

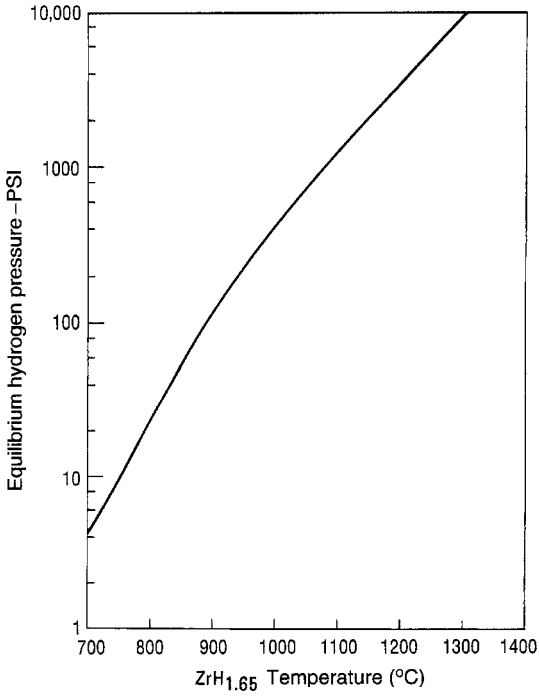

Figure 7. Equilibrium hydrogen pressure over $ZrH_{1.65}$ vs. temperature. (After Ref. 5.)

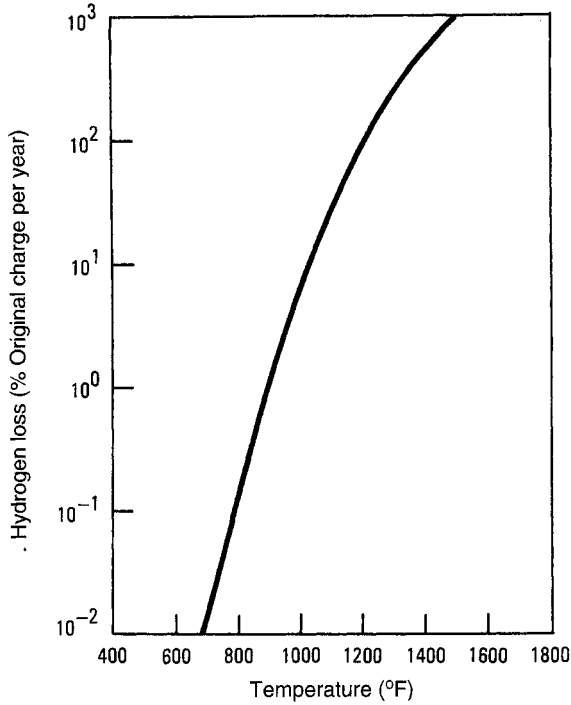

Figure 8. Hydrogen loss rate through 10 mil thick stainless steel moderator can. (After Ref. 10.)

of the cubic phase. The isochores of the δ and ε regions exhibit an increasing change in spacing with increasing hydrogen concentration. Any deviation from this progression is attributed to contamination (with oxygen, nitrogen, carbon, etc.) to form a ternary or higher order alloy system.

The higher hydride compositions (H/Zr > 1.5) are single phase (δ or ε) and are not subject to phase separation on thermal cycling. For a composition of $ZrH_{1.6}$, the equilibrium hydrogen dissociation pressure is 10^5 Pa at 760°C. The absence of a second phase in the higher hydrides eliminates large volume changes associated with phase transformations at ~ 540°C in the lower hydride compositions. Similarly, the absence of thermal diffusion of hydrogen in the higher hydrides precludes concomitant volume changes and cracking. The clad material of stainless steel or nickel alloys provides a diffusion barrier to H_2 at sustained cladding temperatures below ~ 300°C.

The equilibrium dissociation pressures in the H/Zr composition range of 1.55–1.7 at temperatures up to 1300°C agree closely with the values obtained from extrapolation of the reported data, which extend to 950°C[13,14]. However, for H/Zr of 1.4–1.5, hydrogen dissociation pressures are lower than the values extrapolated from below 950°C as a result of phase changes at the elevated temperatures[14].

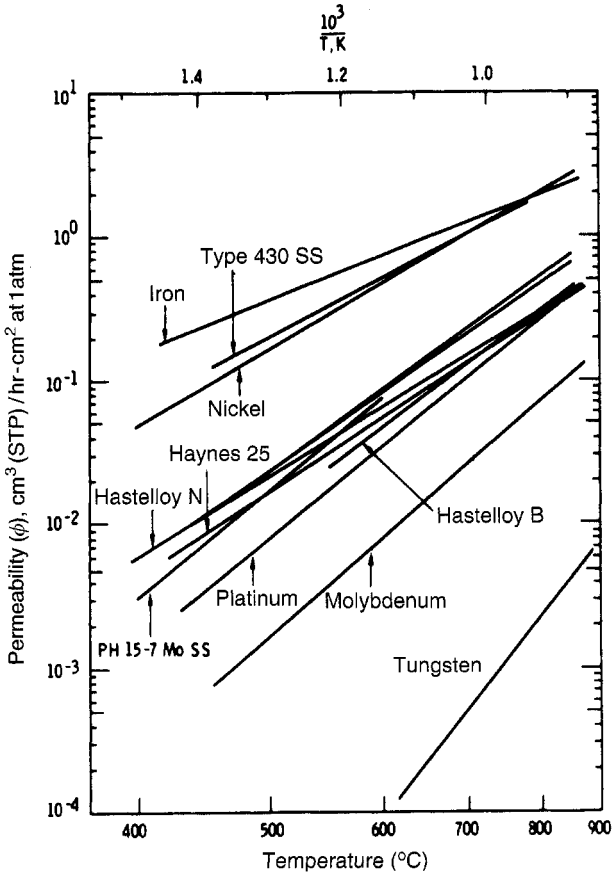

Figure 9. Permeability of various metals to hydrogen (1 mm thick metal). (After Ref. 9.)

Carbon raises the dissociation pressures of hydrogen in carbon-modified ZrH[15]:

$$P = K \exp\left(\frac{-\Delta H_a}{RT}\right) \tag{b}$$

where the value of K is governed by composition. The carbon is associated with Zr on a 1:1 ratio.

The hydrogen dissociation pressure for fuel with H/Zr ratios of 1.7–1.9 is:

$$\log P = 10.44(\mathrm{H/Zr}) - 10.47 - \frac{8538}{T} \tag{c}$$

where the dissociation pressure P is in atmospheres and the temperature T is in Kelvins[15].

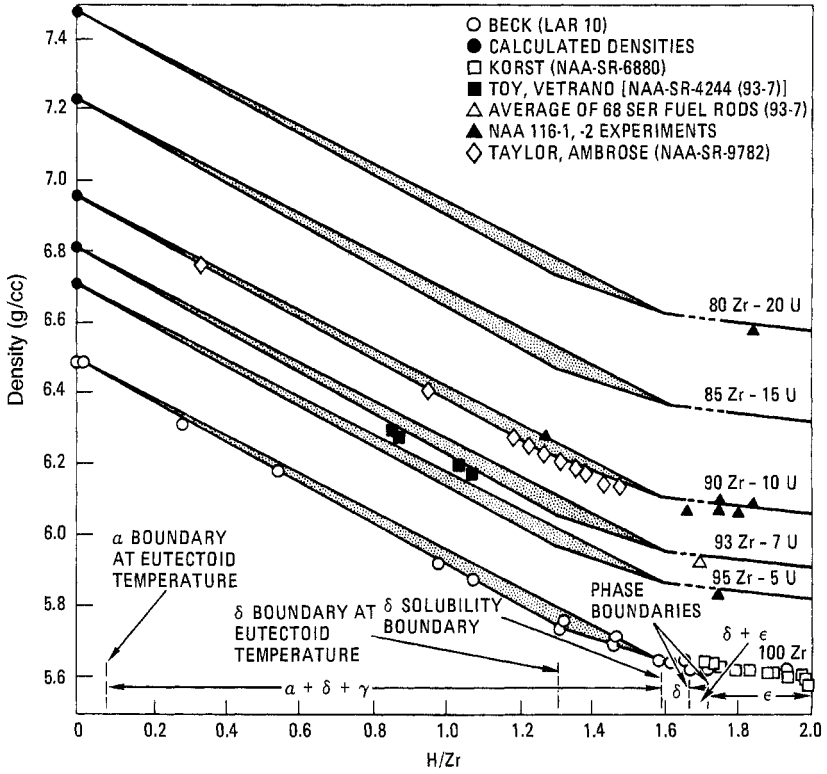

Figure 10. Density diagram. (After Refs. 4 and 5.)

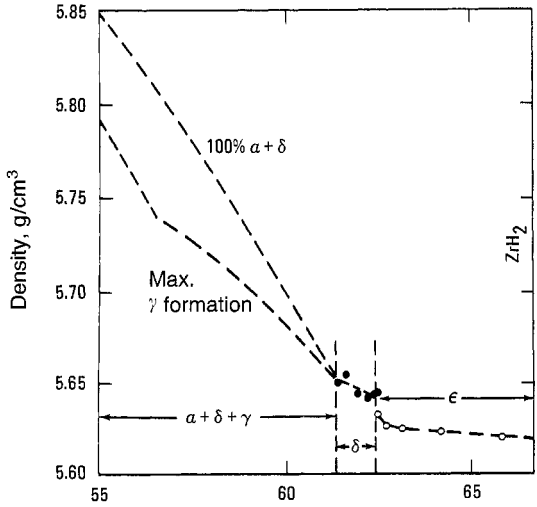

Figure 11. Density of δ and ε phases of zirconium hydride as determined by X-ray diffraction. (After Refs. 4 and 5.)

The hydride bodies should be clad to prevent loss of H_2 at elevated temperatures. The equilibrium dissociation pressure of H/Zr = 1.6 is about 1 Pa at 300°C. An oxide film or cladding may act as barrier to H_2 loss[10,14].

The rates of hydrogen loss through 250 μm thick stainless steel cladding are shown in Figure 8. A 1% loss of hydrogen per year occurs at ~500°C. The hydrogen permeabilities for a number of clean metals and alloys are shown in Figure 9. Metal cladding coated with glass–enamel (~76 μm thick glass coating) has low permeabilities (~10% of molybdenum) and is used at up to 700°C.

The density of ZrH decreases with an increase in the hydrogen content, as shown in Figures 10[16] and 11, up to the δ phase (H/Zr = 1.5) and then changes little.

(MASSOUD T. SIMNAD)

1. T. S. Lundy, E. E. Gross, *An Evaluation of Solid Moderating Materials*, U.S. AEC Report ORNL-2891, Oak Ridge National Laboratory, Oak Ridge, TN, April 1960.
2. W. M. Mueller, J. P. Blackledge, G.G. Libowitz, *Metal Hydrides*, Academic Press, New York, 1968.
3. A. F. Lillie, D. T. McClelland, W. J. Roberts, J. H. Walter, *Zirconium Hydride Fuel Element Performance Characteristics*, U.S. AEC Report AI-AEC-13084, Atomics International, Canoga Park, CA, June 1973.
4. M. T. Simnad, *Nucl. Eng. Design, 64*, 403 (1981).
5. M. T. Simnad, F. C. Foushee, G. G. West, *Nucl. Technol., 28*, 31 (1975).
6. R. Harde, K. W. Stoeher, in *Third Geneva Conference Proceedings*, Vol. 6, United Nations, Geneva, 1965, p. 353 (P/537).
7. G. A. Vasil'ev, A. P. Veselkin, V. I. Piskunov, *Vopr. Fiz. Zashch. Reaktorov, 5*, 91 (1972).
8. R. A. Andriyevskii, V. N. Bykov, V. N. Kumenkkov, in *Fourth Geneva Conference Proceedings*, Vol. 10, United Nations, Geneva, 1971, p. 383 (P/452).
9. J. B. Vetrano, *Nucl. Eng. Design, 14*, 390 (1970).
10. J. D. Gylfe, L. Bernath, *Evaluation of Zirconium Hydride as Moderator in Integral Boiling Water-Superheat Reactors*, U.S. AEC Report NAA-SR-5943, North American Aviation, Canoga Park, CA, 1962.
11. K. E. Moore, M. M. Nakata, *Phase Relationships in the Alpha-Plus-Delta Region of the Zr-H System*, U.S. AEC Report AI-AEC-12703, Atomics International, Canoga Park, CA, U.S. September 1986.
12. K. E. Moore, W. A. Young, *Phase Relationships at High Hydrogen Contents in the SNAP Fuel System*, U.S. AEC Report NAA-SR-12587, Atomics International, Canoga Park, CA, 1968.
13. J. W. Raymond, *Equilibrium Dissociation Pressures of the Delta and Epsilon Phases in the Zirconium-Hydrogen System*, U.S. AEC Report NAA-SR-9374, North American Aviation, Canoga Park, CA, 1964.
14. M. T. Simnad, J. B. Dee, in *Proc. IAEA Symp. Thermodynamics of Nuclear Materials*, September 1967, Vienna (SM-98136); International Atomic Energy Agency, Vienna, 1967, p. 513.
15. H. E. Johnson, *Hydrogen Dissociation Pressures of Modified SNAP Fuel*, Atomics International Report NAA-SR-9295, Canoga Park, CA, 1964.

17.3.12.2.3. Graphite.

The most stable graphites are the near-isotropic materials[1–3]. The effects of irradiation on the properties of graphite are governed by neutron energy, neutron fluence, temperature, temperature gradients, and structure and type of graphite used[1,2]. The effects of irradiation are dimensional changes, reduction in thermal conductivity, and enhancement of creep rates.

Graphite is manufactured from petroleum coke and coal tar pitch (Fig. 1), as cylindrical logs or articles or rectangular cross section in diameters up to 1.25 m (~50 in.).

Inorganic Reactions and Methods, Volume 18
Edited by J. J. Zuckerman, Jim D. Atwood

The hydride bodies should be clad to prevent loss of H_2 at elevated temperatures. The equilibrium dissociation pressure of H/Zr = 1.6 is about 1 Pa at 300°C. An oxide film or cladding may act as barrier to H_2 loss[10,14].

The rates of hydrogen loss through 250 μm thick stainless steel cladding are shown in Figure 8. A 1% loss of hydrogen per year occurs at ~500°C. The hydrogen permeabilities for a number of clean metals and alloys are shown in Figure 9. Metal cladding coated with glass–enamel (~76 μm thick glass coating) has low permeabilities (~10% of molybdenum) and is used at up to 700°C.

The density of ZrH decreases with an increase in the hydrogen content, as shown in Figures 10[16] and 11, up to the δ phase (H/Zr = 1.5) and then changes little.

(MASSOUD T. SIMNAD)

1. T. S. Lundy, E. E. Gross, *An Evaluation of Solid Moderating Materials*, U.S. AEC Report ORNL-2891, Oak Ridge National Laboratory, Oak Ridge, TN, April 1960.
2. W. M. Mueller, J. P. Blackledge, G.G. Libowitz, *Metal Hydrides*, Academic Press, New York, 1968.
3. A. F. Lillie, D. T. McClelland, W. J. Roberts, J. H. Walter, *Zirconium Hydride Fuel Element Performance Characteristics*, U.S. AEC Report AI-AEC-13084, Atomics International, Canoga Park, CA, June 1973.
4. M. T. Simnad, *Nucl. Eng. Design, 64*, 403 (1981).
5. M. T. Simnad, F. C. Foushee, G. G. West, *Nucl. Technol., 28*, 31 (1975).
6. R. Harde, K. W. Stoeher, in *Third Geneva Conference Proceedings*, Vol. 6, United Nations, Geneva, 1965, p. 353 (P/537).
7. G. A. Vasil'ev, A. P. Veselkin, V. I. Piskunov, *Vopr. Fiz. Zashch. Reaktorov, 5*, 91 (1972).
8. R. A. Andriyevskii, V. N. Bykov, V. N. Kumenkkov, in *Fourth Geneva Conference Proceedings*, Vol. 10, United Nations, Geneva, 1971, p. 383 (P/452).
9. J. B. Vetrano, *Nucl. Eng. Design, 14*, 390 (1970).
10. J. D. Gylfe, L. Bernath, *Evaluation of Zirconium Hydride as Moderator in Integral Boiling Water-Superheat Reactors*, U.S. AEC Report NAA-SR-5943, North American Aviation, Canoga Park, CA, 1962.
11. K. E. Moore, M. M. Nakata, *Phase Relationships in the Alpha-Plus-Delta Region of the Zr-H System*, U.S. AEC Report AI-AEC-12703, Atomics International, Canoga Park, CA, U.S. September 1986.
12. K. E. Moore, W. A. Young, *Phase Relationships at High Hydrogen Contents in the SNAP Fuel System*, U.S. AEC Report NAA-SR-12587, Atomics International, Canoga Park, CA, 1968.
13. J. W. Raymond, *Equilibrium Dissociation Pressures of the Delta and Epsilon Phases in the Zirconium-Hydrogen System*, U.S. AEC Report NAA-SR-9374, North American Aviation, Canoga Park, CA, 1964.
14. M. T. Simnad, J. B. Dee, in *Proc. IAEA Symp. Thermodynamics of Nuclear Materials*, September 1967, Vienna (SM-98136); International Atomic Energy Agency, Vienna, 1967, p. 513.
15. H. E. Johnson, *Hydrogen Dissociation Pressures of Modified SNAP Fuel*, Atomics International Report NAA-SR-9295, Canoga Park, CA, 1964.

17.3.12.2.3. Graphite.

The most stable graphites are the near-isotropic materials[1–3]. The effects of irradiation on the properties of graphite are governed by neutron energy, neutron fluence, temperature, temperature gradients, and structure and type of graphite used[1,2]. The effects of irradiation are dimensional changes, reduction in thermal conductivity, and enhancement of creep rates.

Graphite is manufactured from petroleum coke and coal tar pitch (Fig. 1), as cylindrical logs or articles or rectangular cross section in diameters up to 1.25 m (~50 in.).

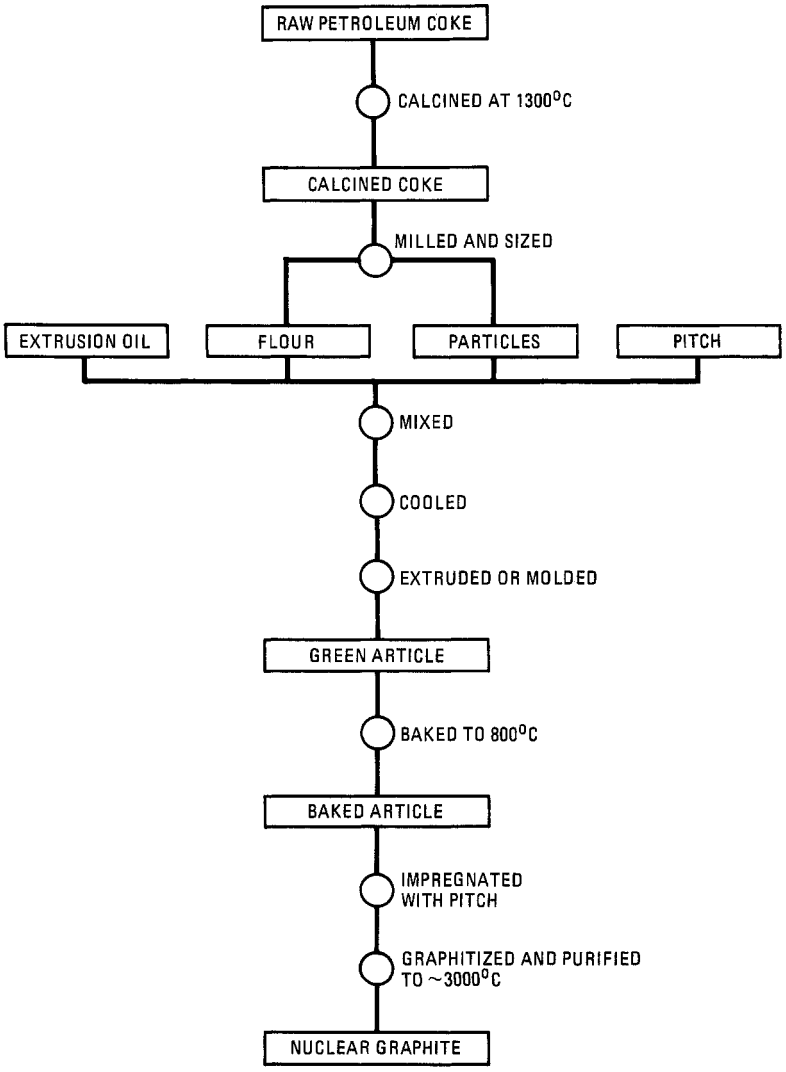

Figure 1. Flow diagram for manufacture of nuclear graphite.

For high strength and fine-grained materials, the calcination step is eliminated, the filler particles are reduced to the micrometer range, and isostatic molding at high pressures is substituted for conventional extrusion or molding. This limits the size of the product [to 250 mm (10 in.) diameter].

Purification during the graphitizing step can reduce ash to less than 100 ppm and metallic constituents such as Fe, Ti, and V that catalyze the oxidation reaction, to less than 50 ppm (see Tables 1 and 2)[3,4].

(MASSOUD T. SIMNAD)

TABLE 1. SUMMARY OF UNIRRADIATTED PROPERTIES OF NEAR-ISOTROPIC GRAPHITE (H-451)

Property	Mean Value	
	Axial	Radial
Log bulk density, Mg/m^3	1.72	
Ultimated tensile strength, MPa	16.4	13.4
Modulus of elasticity, GPa	8.4	7.3
Poisson's ratio	0.12	0.11
Flexural strength, MPa	21.5	20.1
Thermal expansion, $\times 10^6 K^{-1}$	4.15	4.58
Anisotropy factor, $\alpha_{radial}/\alpha_{axial}$	1.15	
Thermal conductivity at 1073 K, $W/m \cdot K$	64.9	62.8

TABLE 2. CANDIDATE GRAPHITES: FINE-GRAINED, HIGH STRENGTH (PHYSICAL AND MECHANICAL PROPERTIES OF POCO GRAPHITE)[a]

	AXF-50	AXF-80
Density, Mg/m^3	1.84	1.80
Compressive strength, MPa	131	
Flexural strength, MPa	83	
Tensile strength, MPa	62	
Modulus of elasticity in tension, GPa	11.7	11.9
Poisson's ratio	0.15	
Strain to failure in tension, %	0.82	
Coefficient of thermal expansion (25–1000°C), $°C^{-1}$	7.7×10^{-6}	7.5×10^{-6}
Thermal conductivity (25°C), $W/m \cdot K$	121	

[a]Ref. 4.

1. G. B. Engle, *Status of Graphite Technology and Requirements for HTGRs*, in *Proc. ANS National Topical Meeting on Gas-Cooled Reactors*, Gatlinburg, TN, May 1974 (TID-CONF-74051).
2. R. Nightingale, ed., *Nuclear Graphite*, Academic Press, New York, 1962.
3. A. L. Pinter, *Irradiation Effects on Graphite*, Report BNWL-SA-2468, Battelle Pacific Northwest Laboratories, Richland, WA, 1969.
4. Union PoCo Company, *Characteristics of Carbon and Graphite*, No. 10-1-73, Marketing brochure, Union PoCo, Decatur, TX.

17.3.12.3. Cladding

Graphite is used as cladding for nuclear fuel elements because of its low neutron-absorption cross section and good moderating properties, as well as its high temperature properties and high heat capacity.

The graphite cladding is fabricated by extrusion. The extruded and baked tubes are impregnated with pitch and furfuryl alcohol in a pressure autoclave and baked to achieve a low gas permeability (10^{-3} cm/s).

(MASSOUD T. SIMNAD)

Inorganic Reactions and Methods, Volume 18
Edited by J. J. Zuckerman, Jim D. Atwood

TABLE 1. SUMMARY OF UNIRRADIATTED PROPERTIES OF NEAR-ISOTROPIC GRAPHITE (H-451)

Property	Mean Value	
	Axial	Radial
Log bulk density, Mg/m^3	1.72	
Ultimated tensile strength, MPa	16.4	13.4
Modulus of elasticity, GPa	8.4	7.3
Poisson's ratio	0.12	0.11
Flexural strength, MPa	21.5	20.1
Thermal expansion, $\times 10^6 K^{-1}$	4.15	4.58
Anisotropy factor, $\alpha_{radial}/\alpha_{axial}$	1.15	
Thermal conductivity at 1073 K, $W/m \cdot K$	64.9	62.8

TABLE 2. CANDIDATE GRAPHITES: FINE-GRAINED, HIGH STRENGTH (PHYSICAL AND MECHANICAL PROPERTIES OF POCO GRAPHITE)[a]

	AXF-50	AXF-80
Density, Mg/m^3	1.84	1.80
Compressive strength, MPa	131	
Flexural strength, MPa	83	
Tensile strength, MPa	62	
Modulus of elasticity in tension, GPa	11.7	11.9
Poisson's ratio	0.15	
Strain to failure in tension, %	0.82	
Coefficient of thermal expansion (25–1000°C), $°C^{-1}$	7.7×10^{-6}	7.5×10^{-6}
Thermal conductivity (25°C), $W/m \cdot K$	121	

[a] Ref. 4.

1. G. B. Engle, *Status of Graphite Technology and Requirements for HTGRs*, in *Proc. ANS National Topical Meeting on Gas-Cooled Reactors*, Gatlinburg, TN, May 1974 (TID-CONF-74051).
2. R. Nightingale, ed., *Nuclear Graphite*, Academic Press, New York, 1962.
3. A. L. Pinter, *Irradiation Effects on Graphite*, Report BNWL-SA-2468, Battelle Pacific Northwest Laboratories, Richland, WA, 1969.
4. Union PoCo Company, *Characteristics of Carbon and Graphite*, No. 10-1-73, Marketing brochure, Union PoCo, Decatur, TX.

17.3.12.3. Cladding

Graphite is used as cladding for nuclear fuel elements because of its low neutron-absorption cross section and good moderating properties, as well as its high temperature properties and high heat capacity.

The graphite cladding is fabricated by extrusion. The extruded and baked tubes are impregnated with pitch and furfuryl alcohol in a pressure autoclave and baked to achieve a low gas permeability (10^{-3} cm/s).

(MASSOUD T. SIMNAD)

17.3.12.4. Control Rods

17.3.12.4.1. Boron Carbide.

Boron carbide is the control material used in thermal and fast reactors[1-12]. The absorption of neutrons by B-10 results in primary formation of Li-7, helium, tritium:

$$^{10}_{5}B + ^{1}_{0}n \longrightarrow ^{4}_{2}He + ^{7}_{3}Li + 2.3\ MeV \quad (a)$$

$$^{10}_{5}B + ^{1}_{0}n \longrightarrow ^{3}_{1}T + ^{4}_{2}He + ^{4}_{2}He \quad (b)$$

The fast-neutron-capture cross section of B-10 is greater than for any other isotope. Boron carbide has a boron concentration of 85% of that of elemental boron, and 19.8% of the boron is B-10, or 14.7% in boron carbide. The thermal neutron absorption cross section of B-10 is 4000 barns and of natural B_4CN 600 barns.

Boron carbide pellets and structures can be produced by cold pressing and sintering (70–80% density) or by hot pressing. In the latter the B_4C powder is first cold-pressed into pellet form and then hot-pressed in graphite dies at 2050–2300°C under 10.3 MPa (1500 psi). The density is controlled by varying the temperature and the pressure.

Boron carbide is rhombohedral ($a = 5.163$ Å; $\alpha = 65.59°$). The stoichiometric composition of boron carbide is $B_{13}C_2(B_{6.5}C)$, so that B_4C is a carbon-saturated solid solution. The phase diagram for the B–C system is shown in Figure 1. The density as a function of stoichiometry is shown in Figure 2.

Boron carbide is compatibile with stainless steel at 600–1000°C for up to 8600 h under pressure[8]. The interdiffusion is not influenced by irradiation, and the data fit the relation $R = 17.26 \times 10^9 \exp(-34{,}801/T)$, where R is the rate in mils/yr and T is the absolute temperature in °F (see Fig. 3).

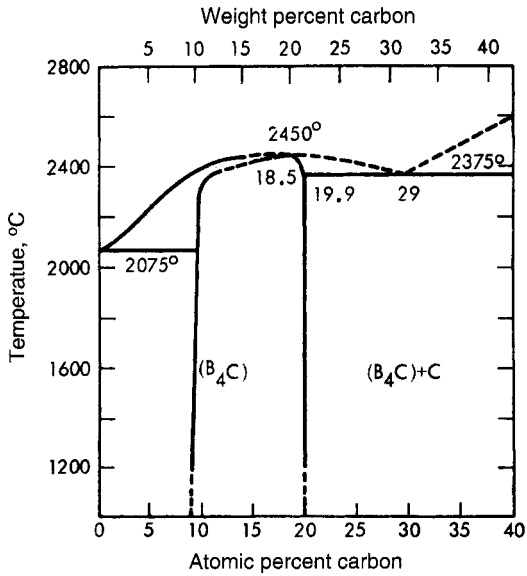

Figure 1. Boron–carbon equilibrium. (After Ref. 9.)

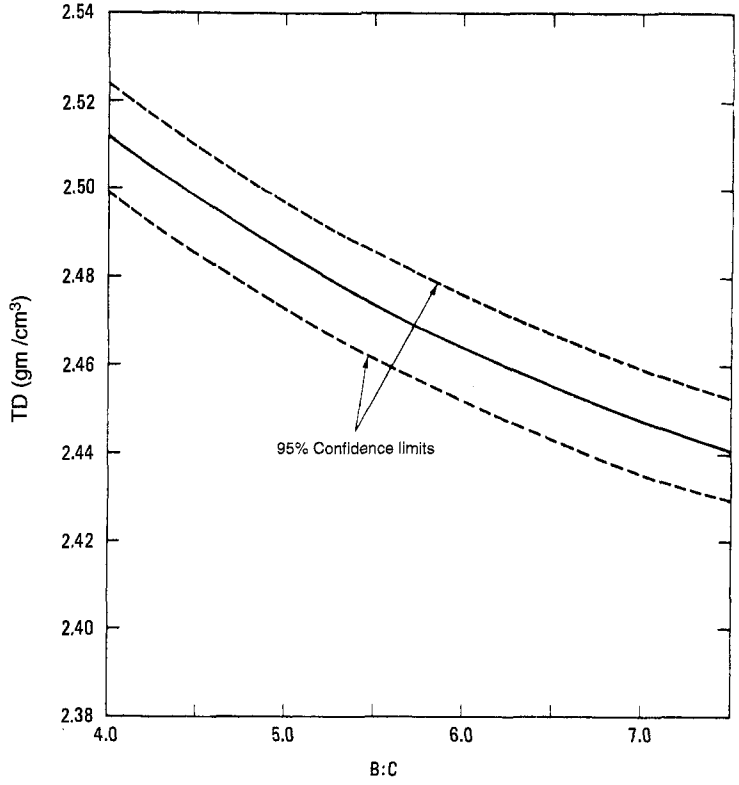

Figure 2. Theoretical density of natural boron carbide as a function of stoichiometry. (After Ref. 9.)

Irradiation of boronated graphites[13] containing 23–43 wt% boron as B_4C at 300–750°C in fast neutron fluences up to 7×10^{25} n/m^2 ($E > 29$ fJ) causes an anisotropic dimensional change related to the preferred orientation of the graphite crystallites in the matrix, a decrease in thermal conductivity, and an increase in thermal expansivity. The dimensional changes (< 2% change in dimensions at 300–750°C and 7×10^{25} n/m^2) are related to the fast neutron fluence and B-10 fission damage to the matrix. The damage increases with increasing B-10 isotope enrichment of the boron in the B_4C particles. Natural boron in the boronated graphite results in dimensional changes independent of the B-10 burnup gradient and correlated with the fast neutron fluence. The use of B-10-enriched B_4C leads to distortion directly related to the B-10 burnup gradient. The dimensional changes are not influenced by swelling of the B_4C particles during irradiation.

The boron carbide–graphite bodies are heat-treated to 2000°C after extrusion or warm pressing while protected from oxidation. Heat treatment is limited to below 2200°C to prevent migration of boron into the graphite crystals, which would enhance radiation swelling of the matrix.

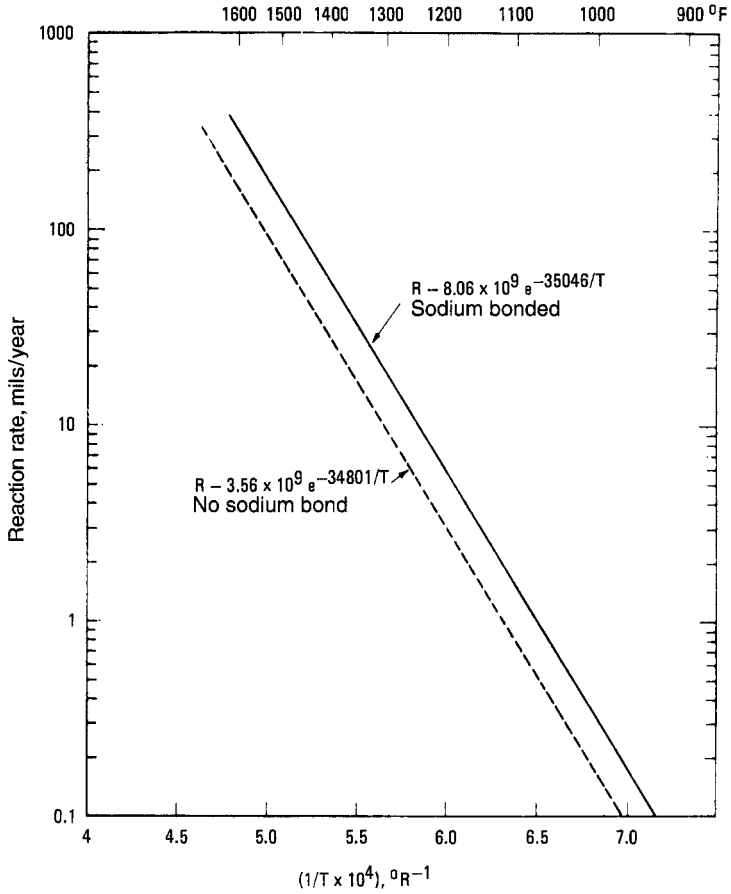

Figure 3. Interaction between boron carbide and type 316 stainless steel bonded by sodium. (After Ref. 9.)

At temperatures above 2000°C, the structural stability and strength of the boronated graphite materials degrade. Boron carbide melts at 2140–2450°C and reacts with the graphite matrix.

The rate of reaction of B_4C graphite bodies with metal cladding is appreciable only above 800°C[13].

(MASSOUD T. SIMNAD)

1. K. R. Birney, A. L., Pitner, R. D. Bourquin, *Trans. Am. Nucl. Soc., 26*, 173 (1977).
2. *Proc. ANS Topical Meeting on Reactor Materials Performance*, Richland, WA, April 1972; *Nucl. Technol., 16*, 208 (1972).
3. J. Bergonzi, ed., *Proc. 4th International Conference Reactor Shielding*, Paris, October 1972; Saclay, France, January 1974.

4. R. E. Dahl, Jr., J. W. Bennett, eds., *GFR Specialists Meeting on Absorbing Materials and Controls Rods for Fast Reactors*, Dimitrovgrad, USSR, June 1973; Report HEDL-TME-73-91, Hanford Engineering Development Laboratory, Richland, WA, 1973.
5. R. G. Brown, K. E. Gilchrist, *Some Physical and Mechanical Property Measurements on PFR Absorber Materials*, U.K. AEA Report TRG-Memo-6322, November 1973.
6. G. V. Samsonov, *Fiz. Met. Metalloved, 3*, 309 (1956).
7. J. P. Elliott, *The Boron–Carbide System*, U.S. AEC Report ARF-2200-12, Illinois Institute of Technology, Armour Research Foundation, Chicago, 1961.
8. *A Compilation of Boron Carbide Design Support Data for LMFBR Control Elements*, Report HEDL-TME-74-19, Hanford Engineering Development Laboratory, Richland, WA, 1975.
9. D. E. Mahagin, ed., *Neutron Absorber Development Programs*, Report HEDL-RRD, Hanford Engineering Development Laboratory, Richland, WA, 1974.
10. A. Lipp, *Boron Carbide: Production, Properties, Application*, Technische Rundschau Nos. 14, 28, and 33 (1965) and 7 (1966), Elektroschmelzwerk Kempten GmbH, Munich, 1966.
11. R. A. Murgatroyd, J. T. Bland, *Status of Studies on Boron Carbide Materials*, U. K. AEA Report TRG-Memo-6090, Harwell, England, March 1973.
12. R. L. Heestand, J. I. Federer, C. F. Leitten Jr., in *Compounds of Interest in Nuclear Reactor Technology*, J. T. Waber, P. Chiotti, W. N. Miner, eds., IMD Special Report No. 13, American Institute of Mining Engineers, New York, 1964, p. 539.
13. L. A. Beavan, *Control Materials in LHTGR Design*, General Atomic Report GA-AI3260, San Diego, CA, December 1974.

17.3.12.4.2. Europium Hexaboride.

Europium hexaboride is an alternate control material to B_4C[1–8]. It has a higher worth (by ~20%) than boron carbide and a higher volumetric worth and a lower volumetric cost than europium oxide. In hot pressing europium hexabonde, grade EB-2 power, an atmosphere other than vacuum could be used, since no carbon monoxide would be generated. Further, europium volatilization would be suppressed because volatile products would not be removed, and the vapor pressure of europium over EuB_6 in contact with graphite is lower than that of europium over Eu_2O_3 in contact with graphite. Hot pressing is conducted for about 2 h at 41.4 MPa (6000 psi) and 1900°C under 0.10 MPa (1 atm) of He[4].

(MASSOUD T. SIMNAD)

1. B. Weidenbaum, E. W. Hoyt, D. L. Zimmerman, W. V. Cummings, K. C. Anthony, in *Materials and Fuels for High-Temperature Nuclear Energy Applications*, M. T. Simnad, L. R. Zumwalt, eds., MIT Press, Cambridge, MA, 1964, p. 314.
2. A. E. Pasto, C. S. Morgan, *Status and Potential of Eu-Based Fast Neutron Absorber Materials*, Report ORNL-TM-5244, Oak Ridge National Laboratory, Oak Ridge, TN, February 1976.
3. A. E. Pasto, V. J. Tennery, *Trans. Am. Nucl. Soc., 26*, 176 (1977).
4. K. Schwerz, A. Lipp, *Atomwirtschaft, 18*, 531 (1973).
5. V. D. Klimov, *Tests on Absorbing Materials in BR-5 Reactor*, Report HEDL-TME-73-91, Hanford Engineering Development Laboratory, Richland, WA, 1973, p. 192.
6. S. A. Kuznetsov, *Control Rods for Fast Reactors with Sodium Collants*, Report HEDL-TME-73–91, Hanford Engineering Development Laboratory, Richland, WA, 1973, p. 214.
7. K. R. Birney, A. L. Pitner, R. D. Bourguin, *Trans. Am. Nucl. Soc., 26*, 173 (1977).
8. R. E. Dahl, Jr., J. W. Bennett, eds., *GFR Specialists Meeting on Absorbing Materials and Control Rods for Fast Reactors* (Dimitrovgrad, USSR, June 1973), Report HEDL-TME-73-91, Hanford Engineering Development Laboratory, Richland, WA, 1973.

17.3.12.4.3. Europium Oxide.

Use of europium oxide[1–7] as a neutron absorber in the control rods avoids gas generation under irradiation and gives a slower loss of reactivity with neutron exposure than boron carbide (10%). The main problems are obtaining adequate critical nuclear

Inorganic Reactions and Methods, Volume 18
Edited by J. J. Zuckerman, Jim D. Atwood

4. R. E. Dahl, Jr., J. W. Bennett, eds., *GFR Specialists Meeting on Absorbing Materials and Controls Rods for Fast Reactors*, Dimitrovgrad, USSR, June 1973; Report HEDL-TME-73-91, Hanford Engineering Development Laboratory, Richland, WA, 1973.
5. R. G. Brown, K. E. Gilchrist, *Some Physical and Mechanical Property Measurements on PFR Absorber Materials*, U.K. AEA Report TRG-Memo-6322, November 1973.
6. G. V. Samsonov, *Fiz. Met. Metalloved*, *3*, 309 (1956).
7. J. P. Elliott, *The Boron–Carbide System*, U.S. AEC Report ARF-2200-12, Illinois Institute of Technology, Armour Research Foundation, Chicago, 1961.
8. *A Compilation of Boron Carbide Design Support Data for LMFBR Control Elements*, Report HEDL-TME-74-19, Hanford Engineering Development Laboratory, Richland, WA, 1975.
9. D. E. Mahagin, ed., *Neutron Absorber Development Programs*, Report HEDL-RRD, Hanford Engineering Development Laboratory, Richland, WA, 1974.
10. A. Lipp, *Boron Carbide: Production, Properties, Application*, Technische Rundschau Nos. 14, 28, and 33 (1965) and 7 (1966), Elektroschmelzwerk Kempten GmbH, Munich, 1966.
11. R. A. Murgatroyd, J. T. Bland, *Status of Studies on Boron Carbide Materials*, U. K. AEA Report TRG-Memo-6090, Harwell, England, March 1973.
12. R. L. Heestand, J. I. Federer, C. F. Leitten Jr., in *Compounds of Interest in Nuclear Reactor Technology*, J. T. Waber, P. Chiotti, W. N. Miner, eds., IMD Special Report No. 13, American Institute of Mining Engineers, New York, 1964, p. 539.
13. L. A. Beavan, *Control Materials in LHTGR Design*, General Atomic Report GA-AI3260, San Diego, CA, December 1974.

17.3.12.4.2. Europium Hexaboride.

Europium hexaboride is an alternate control material to B_4C[1–8]. It has a higher worth (by ~20%) than boron carbide and a higher volumetric worth and a lower volumetric cost than europium oxide. In hot pressing europium hexabonde, grade EB-2 power, an atmosphere other than vacuum could be used, since no carbon monoxide would be generated. Further, europium volatilization would be suppressed because volatile products would not be removed, and the vapor pressure of europium over EuB_6 in contact with graphite is lower than that of europium over Eu_2O_3 in contact with graphite. Hot pressing is conducted for about 2 h at 41.4 MPa (6000 psi) and 1900°C under 0.10 MPa (1 atm) of He[4].

(MASSOUD T. SIMNAD)

1. B. Weidenbaum, E. W. Hoyt, D. L. Zimmerman, W. V. Cummings, K. C. Anthony, in *Materials and Fuels for High-Temperature Nuclear Energy Applications*, M. T. Simnad, L. R. Zumwalt, eds., MIT Press, Cambridge, MA, 1964, p. 314.
2. A. E. Pasto, C. S. Morgan, *Status and Potential of Eu-Based Fast Neutron Absorber Materials*, Report ORNL-TM-5244, Oak Ridge National Laboratory, Oak Ridge, TN, February 1976.
3. A. E. Pasto, V. J. Tennery, *Trans. Am. Nucl. Soc.*, *26*, 176 (1977).
4. K. Schwerz, A. Lipp, *Atomwirtschaft*, *18*, 531 (1973).
5. V. D. Klimov, *Tests on Absorbing Materials in BR-5 Reactor*, Report HEDL-TME-73-91, Hanford Engineering Development Laboratory, Richland, WA, 1973, p. 192.
6. S. A. Kuznetsov, *Control Rods for Fast Reactors with Sodium Collants*, Report HEDL-TME-73–91, Hanford Engineering Development Laboratory, Richland, WA, 1973, p. 214.
7. K. R. Birney, A. L. Pitner, R. D. Bourguin, *Trans. Am. Nucl. Soc.*, *26*, 173 (1977).
8. R. E. Dahl, Jr., J. W. Bennett, eds., *GFR Specialists Meeting on Absorbing Materials and Control Rods for Fast Reactors* (Dimitrovgrad, USSR, June 1973), Report HEDL-TME-73-91, Hanford Engineering Development Laboratory, Richland, WA, 1973.

17.3.12.4.3. Europium Oxide.

Use of europium oxide[1–7] as a neutron absorber in the control rods avoids gas generation under irradiation and gives a slower loss of reactivity with neutron exposure than boron carbide (10%). The main problems are obtaining adequate critical nuclear

Inorganic Reactions and Methods, Volume 18
Edited by J. J. Zuckerman, Jim D. Atwood

4. R. E. Dahl, Jr., J. W. Bennett, eds., *GFR Specialists Meeting on Absorbing Materials and Controls Rods for Fast Reactors*, Dimitrovgrad, USSR, June 1973; Report HEDL-TME-73-91, Hanford Engineering Development Laboratory, Richland, WA, 1973.
5. R. G. Brown, K. E. Gilchrist, *Some Physical and Mechanical Property Measurements on PFR Absorber Materials*, U.K. AEA Report TRG-Memo-6322, November 1973.
6. G. V. Samsonov, *Fiz. Met. Metalloved*, *3*, 309 (1956).
7. J. P. Elliott, *The Boron–Carbide System*, U.S. AEC Report ARF-2200-12, Illinois Institute of Technology, Armour Research Foundation, Chicago, 1961.
8. *A Compilation of Boron Carbide Design Support Data for LMFBR Control Elements*, Report HEDL-TME-74-19, Hanford Engineering Development Laboratory, Richland, WA, 1975.
9. D. E. Mahagin, ed., *Neutron Absorber Development Programs*, Report HEDL-RRD, Hanford Engineering Development Laboratory, Richland, WA, 1974.
10. A. Lipp, *Boron Carbide: Production, Properties, Application*, Technische Rundschau Nos. 14, 28, and 33 (1965) and 7 (1966), Elektroschmelzwerk Kempten GmbH, Munich, 1966.
11. R. A. Murgatroyd, J. T. Bland, *Status of Studies on Boron Carbide Materials*, U. K. AEA Report TRG-Memo-6090, Harwell, England, March 1973.
12. R. L. Heestand, J. I. Federer, C. F. Leitten Jr., in *Compounds of Interest in Nuclear Reactor Technology*, J. T. Waber, P. Chiotti, W. N. Miner, eds., IMD Special Report No. 13, American Institute of Mining Engineers, New York, 1964, p. 539.
13. L. A. Beavan, *Control Materials in LHTGR Design*, General Atomic Report GA-AI3260, San Diego, CA, December 1974.

17.3.12.4.2. Europium Hexaboride.

Europium hexaboride is an alternate control material to B_4C[1–8]. It has a higher worth (by $\sim$20%) than boron carbide and a higher volumetric worth and a lower volumetric cost than europium oxide. In hot pressing europium hexabonde, grade EB-2 power, an atmosphere other than vacuum could be used, since no carbon monoxide would be generated. Further, europium volatilization would be suppressed because volatile products would not be removed, and the vapor pressure of europium over EuB_6 in contact with graphite is lower than that of europium over Eu_2O_3 in contact with graphite. Hot pressing is conducted for about 2 h at 41.4 MPa (6000 psi) and 1900°C under 0.10 MPa (1 atm) of He[4].

(MASSOUD T. SIMNAD)

1. B. Weidenbaum, E. W. Hoyt, D. L. Zimmerman, W. V. Cummings, K. C. Anthony, in *Materials and Fuels for High-Temperature Nuclear Energy Applications*, M. T. Simnad, L. R. Zumwalt, eds., MIT Press, Cambridge, MA, 1964, p. 314.
2. A. E. Pasto, C. S. Morgan, *Status and Potential of Eu-Based Fast Neutron Absorber Materials*, Report ORNL-TM-5244, Oak Ridge National Laboratory, Oak Ridge, TN, February 1976.
3. A. E. Pasto, V. J. Tennery, *Trans. Am. Nucl. Soc.*, *26*, 176 (1977).
4. K. Schwerz, A. Lipp, *Atomwirtschaft*, *18*, 531 (1973).
5. V. D. Klimov, *Tests on Absorbing Materials in BR-5 Reactor*, Report HEDL-TME-73-91, Hanford Engineering Development Laboratory, Richland, WA, 1973, p. 192.
6. S. A. Kuznetsov, *Control Rods for Fast Reactors with Sodium Collants*, Report HEDL-TME-73–91, Hanford Engineering Development Laboratory, Richland, WA, 1973, p. 214.
7. K. R. Birney, A. L. Pitner, R. D. Bourguin, *Trans. Am. Nucl. Soc.*, *26*, 173 (1977).
8. R. E. Dahl, Jr., J. W. Bennett, eds., *GFR Specialists Meeting on Absorbing Materials and Control Rods for Fast Reactors* (Dimitrovgrad, USSR, June 1973), Report HEDL-TME-73-91, Hanford Engineering Development Laboratory, Richland, WA, 1973.

17.3.12.4.3. Europium Oxide.

Use of europium oxide[1–7] as a neutron absorber in the control rods avoids gas generation under irradiation and gives a slower loss of reactivity with neutron exposure than boron carbide (10%). The main problems are obtaining adequate critical nuclear

worths, maintaining pellet dimensional stability, and accommodating decay heating. But europium oxide with its (n, γ) reaction produces no helium and tritium; in addition, it has a long reactivity lifetime, radiation stability, and compatibility with cladding.

Europium is present in minor quantities in lanthanide minerals, particularly in monazite sand. The commercial oxide, which is sinterable to high density, is oxalate-derived and is in the cubic form. Dense pellets and rods can be produced both by cold pressing (40 MPa) and sintering (93–96% density) at 1650°C and by hot pressing (100% density). Sintering or hot pressing is carried out in vacuum above 1200°C to produce the monoclinic form and cooled slowly to prevent cracking. Hot pressing can be carried out at the cubic-to-monoclinic transformation temperature (1125°C) followed by heating at 1300°C for 1 h to produce 100%- dense monoclinic pellets.

Calcined Eu_2O_3 is body-centered-cubic (C-form) with a density of 7.28 g/cm^3 and an atom density of 2.49×10^{22} atoms Eu/cm^3. Conversion from cubic to monoclinic (B-form) takes place at ~1075°C. The monoclinic form lattice parameters and density are listed in Table 1. The reverse reaction (monoclinic-to-cubic) does not take place upon cooling to room temperature.

TABLE 1. COMPARISON OF STRUCTURE AND PROPERTIES OF Eu_2O_3 AND B_4C

	Eu_2O_3		
Structure or Property	Form I	Form II	B_4C
Structure type	Body-centered cubic	Monoclinic	Rhombohedral
Lattice parameter, pm	$a_0 = 10.866$	$a_0 = 14.1133$ $b_0 = 3.6025$ $c_0 = 8.8080$ $\beta = 100.026°$	$\alpha_R = 5.167$ $\alpha_R = 65.60°$
Theoretical density, g/cm^3	7.287	7.951	2.51
Absorber cation density, atoms/cm^3	2.49×10^{22}	2.72×10^{22}	2.17×10^{22}
Free eneergy of formation, kcal/mol			
At 25°C	− 374	− 372	− 12.55 (527°C)
At 727°C	− 322.7	− 322	− 8.68 (2227°C)
Melting point, °C		~ 2300	2350–2500
Specific heat, cal/mol (°C^{-1})			
0–800°C		33.3	16.6 (260°C)
Linear coefficient of thermal expansion, °C^{-1}			
At 30–840°C		10.5×10^{-6}	4.5×10^{-6} (25–800°C)
At 0–1000°C		10.35×10^{-6}	5.54×10^{-6} (25–1000°C)
At 0–1200°C		10.3×10^{-6}	6.02×10^{-6} (25–1500°C)
Thermal conductivity, W/m (°C^{-1})			
At 25°C		3.42	33.5 (25°C)
At 1000°C		2.38	12.6 (800°C)
Young's modulus, MPa at 25°C		31×10^3	450×10^3
Transformation rate[a]			
At 1100°C	Several days		
At 1300°C	< 1 h		

[a]Cubic → monoclinic, time to obtain 100% monoclinic form at given temperature).
Source: After Ref. 2.

At still higher temperatures, transformations to three other polymorphic forms occur: hexagonal (A-form) from 2040–2140°C, another hexagonal form (H-form) from 2140–2260°C, and an unknown structure (X-form) from 2260°C to the melting point (2330°C) (see Table 1).

The monoclinic form has a density of 8.18 g/cm^3, ~10% greater than that of the cubic form (7.287 g/cm^3). Hence, the monoclinic form will provide greater volumetric worth than the cubic form. However, the cubic form is more stable under irradiation.

Europium oxide pellets may be exposed to air for several weeks without damage. However, for long-term storage, a dry atmosphere is necessary; otherwise, the pellets will craze, crack, and swell by reaction with moisture[2].

Europium oxide interacts with stainless steel (grain boundary attack) above 500°C, to form europium silicate. No interaction occurs even at 1230°C when the silicon content of the steel is less than 58 ppm. Molybdenum or tungsten could be used as protective barriers, since these metals do not react with Eu_2O_3 at elevated temperatures[2].

Dispersion-type Eu_2O_3–stainless steel materials provide an advantage for reactors that require compact control rods[7]. The dispersions ($\leq$40% Eu_2O_3) are fabricated to the desired shapes by conventional powder-metallurgy techniques such as hot extrusion, coextrusion, and particularly hot roll-bonding. The addition of ~15 wt % MoO_3 to Eu_2O_3 results in formation of europium molybdate, which has a face-centered-cubic structure if cooled rapidly from above 1400°C and a rhombohedral structure if cooled slowly. The europium molybdate has good resistance to water corrosion. Also, its crystal structure is more resistant to radiation damage than monoclinic Eu_2O_3. Similarly, the titanate Eu_2O_3–$2TiO_2$ has better corrosion resistance and has been used in stainless steel dispersions as control material. However, the molybdate has a higher europium dispersion density.

(MASSOUD T. SIMNAD)

1. S. A. Kuznetsov, *Control Rods for Fast Reactors with Sodium Coolants*, Report HEDL-TME-73-91, Hanford Engineering Development Laboratory, Richland, WA, 1973, p. 214.
2. A. E. Paseo, *Europium Oxide as a Potential LMFBR Control Material*, Report ORNL-TM-4226, Oak Ridge National Laboratory, Oak Ridge, TN, September 1973.
3. H. Sperke, *Atomwirtschaft, 17*, 161 (1972).
4. W. K. Anderson, J. S. Theilacker, *Neutron Absorber Materials for Reactor Control*, U.S. AEC, Washington, DC, 1962, p. 534.
5. C. J. Leitten, R. J. Beaver, *Nucl. Appl., 4*, 439 (1968).
6. R. W. Knight, A. E. Richt, *Nucl. Technol., 15*, 384 (1972).
7. A. E. Richt, V. O. Haynes, *Inspection of Europium-Bearing Control Rod Absorber of SM-1 Reactor*, Report ORNL-TM-3637, Oak Ridge National Laboratory, Oak Ridge, TN, April 1972.

17.3.12.5. Other Nuclear Ceramics and Special Materials

Ceramic materials are also utilized in nuclear reactor components. Applications include insulation of pressure vessels with linings fabricated from silica and alumina-base ceramic bricks or fiber insulation; pressure vessels made of prestressed concrete structures that enclose the entire reactor and secondary system; wear-resistant surfaces produced by means of coatings such as chromium oxide or chromium carbide; and shielding applications, which include materials such as concrete, graphite, and leaded glass[1].

(MASSOUD T. SIMNAD)

1. *Proceedings of the Conference on Nuclear Applications of Non-Fissionable Ceramics*, May 9–11, 1966, Washington, DC, American Nuclear Society, LaGrange Park IL, 1967.

Inorganic Reactions and Methods, Volume 18
Edited by J. J. Zuckerman, Jim D. Atwood

At still higher temperatures, transformations to three other polymorphic forms occur: hexagonal (A-form) from 2040–2140°C, another hexagonal form (H-form) from 2140–2260°C, and an unknown structure (X-form) from 2260°C to the melting point (2330°C) (see Table 1).

The monoclinic form has a density of 8.18 g/cm^3, ~10% greater than that of the cubic form (7.287 g/cm^3). Hence, the monoclinic form will provide greater volumetric worth than the cubic form. However, the cubic form is more stable under irradiation.

Europium oxide pellets may be exposed to air for several weeks without damage. However, for long-term storage, a dry atmosphere is necessary; otherwise, the pellets will craze, crack, and swell by reaction with moisture[2].

Europium oxide interacts with stainless steel (grain boundary attack) above 500°C, to form europium silicate. No interaction occurs even at 1230°C when the silicon content of the steel is less than 58 ppm. Molybdenum or tungsten could be used as protective barriers, since these metals do not react with Eu_2O_3 at elevated temperatures[2].

Dispersion-type Eu_2O_3–stainless steel materials provide an advantage for reactors that require compact control rods[7]. The dispersions ($\leq$40% Eu_2O_3) are fabricated to the desired shapes by conventional powder-metallurgy techniques such as hot extrusion, coextrusion, and particularly hot roll-bonding. The addition of ~15 wt % MoO_3 to Eu_2O_3 results in formation of europium molybdate, which has a face-centered-cubic structure if cooled rapidly from above 1400°C and a rhombohedral structure if cooled slowly. The europium molybdate has good resistance to water corrosion. Also, its crystal structure is more resistant to radiation damage than monoclinic Eu_2O_3. Similarly, the titanate Eu_2O_3–$2TiO_2$ has better corrosion resistance and has been used in stainless steel dispersions as control material. However, the molybdate has a higher europium dispersion density.

(MASSOUD T. SIMNAD)

1. S. A. Kuznetsov, *Control Rods for Fast Reactors with Sodium Coolants*, Report HEDL-TME-73-91, Hanford Engineering Development Laboratory, Richland, WA, 1973, p. 214.
2. A. E. Paseo, *Europium Oxide as a Potential LMFBR Control Material*, Report ORNL-TM-4226, Oak Ridge National Laboratory, Oak Ridge, TN, September 1973.
3. H. Sperke, *Atomwirtschaft, 17*, 161 (1972).
4. W. K. Anderson, J. S. Theilacker, *Neutron Absorber Materials for Reactor Control*, U.S. AEC, Washington, DC, 1962, p. 534.
5. C. J. Leitten, R. J. Beaver, *Nucl. Appl., 4*, 439 (1968).
6. R. W. Knight, A. E. Richt, *Nucl. Technol., 15*, 384 (1972).
7. A. E. Richt, V. O. Haynes, *Inspection of Europium-Bearing Control Rod Absorber of SM-1 Reactor*, Report ORNL-TM-3637, Oak Ridge National Laboratory, Oak Ridge, TN, April 1972.

17.3.12.5. Other Nuclear Ceramics and Special Materials

Ceramic materials are also utilized in nuclear reactor components. Applications include insulation of pressure vessels with linings fabricated from silica and alumina-base ceramic bricks or fiber insulation; pressure vessels made of prestressed concrete structures that enclose the entire reactor and secondary system; wear-resistant surfaces produced by means of coatings such as chromium oxide or chromium carbide; and shielding applications, which include materials such as concrete, graphite, and leaded glass[1].

(MASSOUD T. SIMNAD)

1. *Proceedings of the Conference on Nuclear Applications of Non-Fissionable Ceramics*, May 9–11, 1966, Washington, DC, American Nuclear Society, LaGrange Park IL, 1967.

Inorganic Reactions and Methods, Volume 18
Edited by J. J. Zuckerman, Jim D. Atwood

Abbreviations

abs	absolute
a.c.	alternating current
Ac	acetyl, CH_3CO
acac	acetylacetonate anion
acacH	acetylacetone, $CH_2C(O)CH_2C(O)CH_3$
AcO	acetate anion, $CH_3C(O)O$
Ad	adamantyl
ads	adsorbed
AIBN	2,2′-azobis(isobutyronitrile), 2,2′-$[(CH_3)_2CCN]_2N_2$
Alk	alkyl
am	amine
amt	amount
Am	amyl, C_5H_{11}
amu	atomic mass unit
anhyd	anhydrous
aq	aqueous
Ar	aryl
asym	asymmetrical, asymmetric
at	atom (not atomic, except in atomic weight)
atm	atmosphere (not atmospheric)
av	average
BBN	9-Borabicyclo[3.3.1]nonane
bcc	body-centered cubic
BD	butadiene
BIMOP	6,6′-bis(diphenylphosphino)-3,3′-dimethoxy-2,2′,4,4′-tetramethyl-1,1′-biphenyl
BINAP	2,2′-bis(diphenylphosphino)-1,1′-binaphthyl
bipy	2,2′-bipyridyl
bipyH	protonated 2,2′-bipyridyl
BMPP	benzylmethylphenylphosphine, $(PhCH_2)(CH_3)PhP$
bp	boiling point
Bu	butyl, C_4H_9
Bz	benzyl, $C_6H_5CH_2$
c-	cyclo (used in formulas)
ca.	circa, about, approximately
catal	catalyst (not catalyzing, catalysis, catalyzed, etc.)
CDT	cyclododecatriene
cf.	compare
CFRP	carbon fiber reinforced plastics
Ch.	chapter
CHD	1,3-cycloheptadiene
Chx	cyclohexyl
ChxD	1,3-cyclohexadiene
CI	configuration interaction
Cob	cobalamine
COD	cycloctadiene

COE	cyclooctene
conc	concentrated (not concentration)
const.	constant
COT	*cyclooctariene*
COTe	cyclooctatetraene
Cp	cyclopentadienyl, C_5H_5
CPE	controlled-potential electrolysis
cpm	counts per minute
CRP	constant rate period
CT	charge-transfer
CV	cyclic voltammetry
CVD	chemical vapor deposition
CVI	chemical vapor infiltration
CW	continuous wave
Cy	cyclohexyl, C_6H_{11}
d	day, days
DABIP	N,N′-diisopropyl-1,4-diazabutadiene
DBA	dibenzylideneaccetone
d.c.	direct current
DCM	dicyclopentadienylmethane
DCME	$Cl_2CHC(O)CH_3$
DCP	1,3-dicyclopentadienylpropane
dct	*dithiocarbamato*, $[S_2CNR_2]^-$
DDT	dichlorodiphenyltrichloroethane, 1,1,1,′-trichloro-2,2-bis-(4-chlorophenyl)ethane
dec	decomposed
DED	1,1-bis(ethoxycarbonyl)ethene-2,2-dithiolate, $[(H_5C_2OC(O)]_2C{=}CS_2]^2$
depe	1,2-bis(diphenylphosphino)ethene, $(C_6H_5)_2PCH{=}CHP(C_6H_5)_2$
DIAD	diindenylanthracenyl
diars	1,2-bis(dimethylarsino)benzene, o-phenylenebis (dimethylarsine), $1,2\text{-}(CH_3)_2AsC_6H_4As(CH_3)_2$
dien	diethylenetriamine, $[H_2N(CH_2)_2]_2NH$
diglyme	diethyleneglycol dimethylether, $CH_3O(CH_2CH_2O)CH_2$
dil	dilute
diop	2,3-O-isopropylidene-2,3-dihydroxy-1,4-bis(diphenylphophino)butane, $(C_6H_5)_2PCH_2CH[OCH(CH_3){=}CH_2]CH[OCH(C_3){=}CH_2]CH_2P(C_6H_5)_2$
dipda	$p\text{-i-Pr}C_6H_4CH = CHC_6H_4\text{-c-p}$
diphos	1,2-bis(diphenylphosphino)benzene, $1,2\text{-}(C_6H_5)_2PC_6H_4P(C_6H_5)_2$
Div.	division
DMA	dimethylacetamide
dme	dropping mercury electrode
DME	1,2-dimethoxyethane, glyme, $CH_3O(CH_2)_2OCH_3$
DMF	N,N-dimethylformamide, $HC(O)N(CH_3)_2$
DMG	dimethylglyoxime, $CH_3C{=}NOH)C{=}NOH)CH_3$
dmgh	dimethylglyoximate anion
DMP	1,2-dimethoxybenzene, $1,2\text{-}(CH_3O)_2C_6H_4$
dmpe	1,2-bis(dimethylphosphino)ethane, $(CH_3)_2P(CH_2)_2P(CH_3)_2$

DMSO	dimethylsulfoxide, $(CH_3)_2SO$
dpam	bis(diphenylarsino)methane, $[(C_6H_5)_2As]_2CH_2$
dpav	*cis*-1,2-*bis*(diphenylarsino)ethane, $Ph_2AsCH{=}CHAsPh_2$
dpic	dipicolinate ion
DPP	differential pulse polarography
dppb	1,4-bis(diphenylphosphino)butane, 1,4-$(C_6H_5)_2P(CH_2)_4P(C_6H_5)_2$
dppbe	1,2-*bis*(diphenylphosphino)benzene, 1,2-$(Ph_2P)_2C_6H_4$
dppe	1,2-bis(diphenylphosphino)ethane, 1,2-$(C_6H_5)_2P(CH_2)_2P(C_6H_5)_2$
dppee	1,1-*bis*(diphenylphosphino)ethene, $H_2C{=}C(PPh_2)_2$
dppm	bis(diphenylphosphino)methane, $[(C_6H_5)_2P]_2CH_2$
dppoe	bis(diphenylphosphoryl)ethane
dppp	1,3-bis(diphenylphosphino)propane, 1,3-$(C_6H_5)_2P(CH_2)_3P(C_6H_5)_2$
dptpe	1,2-bis(di-p-tolylphosphino)ethane, 1,2-$(4\text{-}CH_3C_6H_4)_2P(CH_2)_2P(C_6H_4CH_3\text{-}4)_2$
DTA	differential thermal analysis
DTBQ	3,5-di-t-butyl-o-benzoquinone
DTH	1,6-dithiahexane, butane-1,4-dithiol, $1,4\text{-}HS(CH_2)_4SH$
DTS	dithiosquarate
ed.	edition, editor
eds.	editors
EDTA	ethylenediaminetetraacetic acid, $[HOC(O)]_2N(CH_2)_2N[C(O)OH]_2$
e.g.	exempli gratia, for example
EHMO	extended Hückel molecular orbital
emf	electromotive force
en	ethylenediamine, $H_2N(CH_2)_2NH_2$
enH	protonated ethylenediamine
EPR	electron paramagnetic resonance
equimol	equimolar
equiv	equivalent
EPR	electron paramagnetic resonance
Eq.	equation
ERF	effective reduction factor
ES	excited state
ESR	electron-spin resonance
esu	electrostatic unit
Et	ethyl, CH_3CH_2
etc.	et cetera, and so forth
Et_2O	diethyl ether, $(C_2H_5)_2O$
EtOH	ethanol, C_2H_5OH
et seq.	et sequentes, and the following
eu	entropy unit
fac	facial
Fc	ferrocenyl
fcc	face-centered cubic
FCVI	forced flow thermal gradient chemical vapor infiltration
ff.	following
Fig	figure
Fl	fluorenyl

Fp	η^5-$C_5H_5Fe(CO)_2$
fp	freezing point
FRP	falling rate period
g	gas
g-at	gram-atom
GLC	gas liquid chromatography
glyme	1,2-dimethoxyethane, $CH_3O(CH_2)_2OCH_3$
graph	graphite
GS	ground state
h	hour, hours
H-Cob	cobalamine
HD	1,5-hexadiene
hept	heptyl
Hex	hexyl
hfacac	1,1,1,5,5,5-hexafluoro-2,4-pentanedione anion, $CF_3C(=O)CHC(=O)CF_3^-$
HMDB	hexamethyl(Dewar benzene)
hmde	hanging mercury drop electrode
MHI	heptamethylindenyl
HMPA	hexamethylphosphoramide $[(CH_3)_2N]_3PO$
HOMO	highest occupied molecular orbital
HOPG	highly oriented pyrolytic graphite
HPLC	high-pressure liquid chromatography
HPPK	phenyl-2-pyriylketoxime
IBAD	Ion Beam Assisted Deposition
i.e.	id est, that is
ImH	imidazole
inter alia	among other things
IPC	isopinocamphylborane
IR	infrared
irrev	irreversible
ISC	intersystem crossing
isn	isonicotinamide
ivd	inside vapor-phase deposition
l	liquid
L	ligand
LC	ligand centered
LF	ligand field
LFER	linear free-energy relationship
liq	liquid
LMCT	ligand-to-metal charge transfer
Ln	lanthanides, rare earths
LPE	Liquid-Phase Epitaxy
LSV	linear-scan voltammetry
LUMO	lowest unoccupied molecular orbital
m	meta
max	maximum
M	metal
MC	metal centered
Me	methyl, CH_3
Me_2pn	2,2-dimethylpropane-1,3-diamine, $H_2NCH_2C(CH_3)_2CH_2NH_2$
Men	methyl

mes	mesitylene, 1,3,5-trimethylbenzene derivative
MeOH	methanol, CH_3OH
mer	meridional; the repeating unit of an oligomer or polymer
mhp	2-hydroxy-6-methylpyridine, 2-HO, 6-$CH_3C_5H_3N$
min	minimum, minute, minutes
MLCT	metal-to-ligand charge transfer
MO	molecular orbital
MOCVD	metal-organic chemical vapor deposition
mol	molar
mp	melting point
MV	methyl viologen, 1,1′-dimethyl-4,4′-bipyridinium dichloride
n.a.	not available
napy	naphthyridine
NASICON	sodium super ionic conductor
NBD	norbornadiene, [2.2.1]bicyclohepta-2,5-diene
neg	negative
nhe	normal hydrogen electrode
NMR	nuclear magnetic resonance
N,n′-Bz_2en	N,N′-dibenzylethylenediamine, $(C_6H_5CH_2)HNCH_2CH_2NH(CH_2C_6H_5)$
No.	number
np	tris-[2-diphenylphosphino)ethyl]amine, $N[CH_2CH_2P(C_6H_5)_2]_3$
Np	naphthyl
Nuc	nucleophile
NPP	normal pulse polarography
NQR	nuclear quadrupole resonance
NTA	nitrilotriacetate
o	ortho
obs	observed
Oct	octyl
oep	octaethylporphyrin
OEP	octaethylporphyrin
O_F	oxidation factor
O_h	octahedral
Oq	oxyquinolate
OMVPF	organometallic vapor phase epitaxy
ovd	outside vapor-phase deposition
ox.	oxidation
p	para
p.	page
P	pressure
Pat.	patent
pet.	petroleum
Ph	phenyl, C_6H_5
phen	1,10-phenanthroline
Ph_2PPy	2-(diphenylphosphino)pyridine, 2-$(C_6H_5)_2PC_5H_4N$
PID	proportional integral derivative
PPN	$[(Ph_3P)_2N]^+$
pip	piperidine, $C_5H_{10}N$
PMDT	pentamethyldiethylenetriamine, $(CH_3)_2N(CH_2)_2N(CH_3)(CH_2)_2N(CH_3)_2$

PMR	proton magnetic resonance
pn	propylene-1,3-diamine, $1,3\text{-}H_2NCH_2CH_2CH_2CH_2NH_2$
pos	positive
Po-tol_3	tri-o-tolylphosphine
pp.	pages
ppb	parts per billion
ppm	parts per million
ppn	bis(diphenylphosphino)amine, $[(C_6H_5)_2P]_2NH$
ppt	precipitate
Pr	propyl, C_3H_2
PSS	photostationary state
PVC	poly(vinyl chloride)
py	pyridine, C_5H_5N
pydac	pyridine-2,6-dicarboxylate
pyr	pyrazine
pzH	pyrazolyl
PZE	potential of zero charge
RABITS	rolling assisted biaxially textured substrates
rac	racemic mixture, racemate
R	organic group; universal gas constant
RDE	rotated disk electrode
RE	rare earths, lanthanides
red.	reduction
Redox	reduction-oxidation reactions
ref.	reference
rev	reversible
rf	radiofrequency
RF	reduction factor
R_F	R group with substituted F
rh	rhombohedral
rms	root mean square
rpm	revolutions per minutes
RT	room temperature
s	second, seconds; solid
sal	salicylaldehyde
salen	N,N′-*bis*(salicylidene)ethylenediamine
saldox	salicylaldoxime
sce	saturated calomel electrode
SCE	standard calomel electrode
sec	sescondary
SEM	scanning electron microscopy
Sep	sepulcrate, 1,3,6,8,10,13,16,19-octaazabicyclo[6.6.6]eicosane
Sia	Diisoamyl
SMAD	solvated metal-atom dispersed
soln	solution
solv	solvated
sp	specific
STP	standard temperature and pressure
subl	sublimes
Suppl.	supplement
sym	symmetrical, symmetric

t	time; tertiary
T	temperature
T_d	tetrahedral
TACN	1,4,7-triazacyclononane
TCNE	tetracyanoethylene
TEA	tetraethylammonium ion, $[(C_2H_5)_4N]^+$
TEM	transmission electron microscopy
terpy	2,2′2″-terpyridyl
tetraphos	$Ph_2PCH_2CH_2PPhCH_2CH_2PPhCH_2CH_2PPh_2$
TGA	thermogravimetric analysis
TGL	triethyleneglycol dimethylether
THF	tetrahydrofuran
THP	detrahydropyran
THT	tetrahydrothiophene
Thx	thexyl
TLC	thin-layer chromatography
TMED	N,N,N′,N′-tetramethylethylenediamine, $(CH_3)_2N(CH_2)_2N(CH_3)_2$
tmen	N,N,N′,N′-tetramethylethylenediamine
TMP	2,2,6,6-tetramythylpiperidyl
TMPH	2,2,6,6-tetramethylpiperidine, 2,2,6,6-$(CH_3)_4C_5H_7N$
TMPP	*tris*(2,4,6-trimethoxyphenyl)phosphine
Tol	tolyl, $C_6H_4CH_3$, p-tolyl
Tos	tosyl, tolylsulfonyl, 4-$CH_3C_6H_4SO_2$
TPA	tetraphenylarsonium ion, $[(C_6H_5)_4As]^+$
TPP	tetraphenylprophyrin
TPPO	triphenylphosphineoxide
tren	*tris*(*2-aminoethyl*)(*amine*, $N(CH_2CH_2NH_2)_3$
triars	*bis*-(dimethylarsino)phenyl]methylarsine, $[2\text{-}(CH_3)_2AsC_6H_4]_2AsCH_3$
triphos	1,1,1-tris(diphenylphosphinomethyl)ethane, $[(C_6H_5)_2PCH_2]_3CCH_3$
trien	triethylenetetraamine, $H_2N(CH_2)_2NH(CH_2)_2NH(CH_2)_2NH_2$
UV	ultraviolet
v	vicinal
V	volume
Vi	(E)-[2-$(CH_3)_2NHC_2C_6H_4$]C=C$(CH_3)C_6H_4CH_3$-4
viz.	videlical, that is to say, namely
vol., Vol.	volume
VPE	vapor-phase epitaxy
vs.	versus
wk.	week
wt	weight
X	halogen or pseudohalogen
xs	excess
Y	often useed for S, Se
yr.	year
§	section
η	hapto designator

Inorganic Reactions and Methods, Volume 18
Edited by J. J. Zuckerman, Jim D. Atwood

Author Index

The entries of this index were derived directly by computer program from the lists of references. The accuracy of the references was the sole responsibility of the authors. No editorial check, except for format and journal-title abbreviation, was applied. Consequently, errors occurring in authors' names in the references will recur in this index.
Each entry in the index refers to the appropriate section number.

B

E

I

J

K

N

O

P

Q

R

S

U

Z

Inorganic Reactions and Methods, Volume 18
Edited by J. J. Zuckerman, Jim D. Atwood

Compound Index

This index lists individual, fully specified compositions of matter that are mentioned in the text. It is an index of empirical formulas, ordered according to the following system: the elements within a given formula occur in alphabetical sequence except for C, or C and H if present, which always come first. The formulas are ordered alphanumerically without exception.

The index is augmented by successively permuted versions of all empirical formulas. As an example, $C_3H_3AlO_9$ will appear as such and, at the appropriate positions in the alphanumeric sequence, as $H_3{*}C_3AlO_9$, $Al{*}C_3H_3O_9$ and $O_9{*}C_3H_3Al$. The asterisk identifies a permuted formula and allows the original formula to be reconstructed by shifting to the front the elements that follow the asterisk.

Whenever an empirical formula does not show how the elements are combined in groups, it is followed by a linearized structural formula, which reveals the connectivity of the compound(s) underlying the empirical formula and serves to distinguish substances which are identical in composition but differ in the arrangement of elements.

The nonpermuted empirical formulas are followed by keywords. They describe the context in which the compounds represented by the empirical formulas are discussed. Section numbers direct the reader to relevant positions in the book.

Inorganic Reactions and Methods, Volume 18
Edited by J. J. Zuckerman, Jim D. Atwood

Subject Index

This index supplements the compound index and the table of contents by providing access to the text by way of methods, techniques, reaction conditions, properties, effects and other phenomena. Reactions of specific bonds and compound classes are noted when they are not accessed by the heading of the section in which they appear.
For multiple entries, additional keywords indicate contexts and thereby avoid the retrieval of information that is irrelevant to the user's need.
Section numbers are used to direct the reader to those positions in the volume where substantial information is to be found.